Florida Tech

Development and Testing of the Miniaturized Pavement Pressuremeter for Use in Unbound Pavement Layers

October 2018

FDOT Contract: BDV28-977-04

Principal Investigator:
Paul J. Cosentino, Ph.D., P.E.
Florida Tech
Department of Civil and Mechanical Engineering
150 West University Boulevard
Melbourne, Florida 32901
cosentin@fit.edu
321-674-7555 Direct
321-674-8048 Office
321-674-7565 Fax

Additional Authors:
Thaddeus J. Misilo III, Ph.D.
Alaa M. Shaban, Ph.D.
Jacob W. Jansen

DSR Contact: Carolyn Lockyer
Florida Tech
Office of Sponsored Programs
150 West University Boulevard
Melbourne, Florida 32901
clockyer@fit.edu
321-674-7490 Direct

Submitted to:
Project Manager: David Horhota, Ph.D., P.E.
Florida Department of Transportation
State Materials Office
5007 NE 39th Avenue
Gainesville, Florida 32609
David.Horhota@dot.state..us
352-955-2924 Direct

EN-569-1018

Disclaimer

The opinions, findings and conclusions expressed in this publications and those of the authors are not necessarily those of the State of Florida Department of Transportation.

Conversions to SI Units

Symbol	When you know	Multiply by	To find	Symbol
Length				
in	inches	25.4	millimeters	mm
ft	feet	0.305	meters	m
yd	yards	0.914	meters	m
mi	miles	1.61	kilometers	km
Area				
in^2	square inches	645.2	square millimeters	mm^2
ft^2	square feet	0.093	square meters	m^2
yd^2	square yards	0.836	square meters	m^2
ac	acres	0.405	hectares	ha
mi^2	square miles	2.59	square kilometers	km^2
Volume				
fl oz	fluid ounces	29.57	milliliters	mL
gal	gallons	3.785	liters	L
ft^3	cubic feet	0.028	cubic meters	m^3
yd^3	cubic yards	0.765	cubic meters	m^3
NOTE: volumes greater than 1 000 L shall be shown in m^3				
Mass				
oz	ounces	28.35	grams	g
lb	pounds	0.454	kilograms	kg
T	short tons (2,000 lb)	0.907	megagrams (or "metric ton")	Mg (or "t")
Temperature (exact degrees)				
°F	Fahrenheit	5 (F-32) / 9	Celsius	°C
Force and Pressure or Stress				
lbf	pound force	4.45	Newton's	N
lbf/in^2	pound force per square inch	6.89	kilopascals	kPa

*SI is the symbol for the International System of Units. Appropriate rounding should be make to comply with Section 4 of ASTM E380.

Technical Report Documentation Page

1. Report No.	2. Government Accession No.	3. Recipient's Catalog No.
FL/DOT/RMC/06650-7754		

4. Title and Subtitle	5. Report Date
Development and Testing of the Miniature Pavement Pressuremeter for Use in Unbound Pavement Layers: Final Report	September 1, 2018
	6. Performing Organization Code: Index 201949
7. Author's: P. J. Cosentino, Thaddeus J. Misilo III, Alaa M. Shaban, Jacob W. Janson	8. Performing Organization Report No.
9. Performing Organization Name and Address: Florida Institute of Technology (321) 674-7555 Civil Engineering Department 150 West University Blvd. Melbourne, FL 32901-6975	10. Work Unit No. (TRAIS)
	11. Contract or Grant No. Contract Number BDV 28 977-04
12. Sponsoring Agency Name and Address: Florida Department of Transportation 605 Suwannee Street Tallahassee, Florida 32399-0450	13. Type of Report and Period Covered: November 2015 to December 2018
	14. Sponsoring Agency Code: 99700-7601-119

15. Supplementary Notes

A small diameter pressuremeter (SDPMT) was developed, tested and used in numerous correlations at four testing sites on and near the campus of the Florida Institute of Technology. SDPMT probes were inserted directly in to the holes made with the drive pin used during nuclear density testing. SDPMT testing produced lift-off, and limit pressures along with elastic moduli that were all correlated to PENCEL PMT data. SDPMT data was acquired digitally using two types of strain-controlled tests; a conventional incremental volume injection test and a continuous volume injection test. Two probe lengths were developed and tested, one being 6-inches and a second being 12-inches long, to enable either 6- or 12-inch unbound pavement layers to be tested. Data from 159 SDPMT tests were correlated to stiffnesses from 96 Clegg Impact, and 141 Lightweight Deflectometer (LWD) tests, plus 107 dry densities from nuclear density testing. Finite element analyses were conducted so that SDPMT predicted deflections could be compared to LWD measured deflections at all four sites.

The SDPMT probes that were developed can be used and repaired much more efficiently than other PMT probes, making them very desirable. The continuous volume injection testing with data acquisition, using the Automated PMT software (APMT) was completed in less than a minute, making it a very useful engineering tool.

The correlations showed that both SDPMT stiffness and strength compare well to Clegg and LWD stiffnesses. They also showed a very strong correlation exists between the SDPMT strength and stiffness from the 12-inch SDPMT probe during incremental volume testing. The 12-inch SDPMT tests produced slightly more consistent results than the 6-inch SDPMT tests. The LWD measured and finite element SDPMT predicted deflections were similar, falling within about 10%.

In summary, both the incremental and continuous volume injection process for the 6-and 12-inch SDPMT were proven to be useful. These new pressuremeters are recommended for use in conjunction with nuclear density test data to thoroughly categorize the strength-stiffness and density information along any unbound pavement roadway section.

17. Key Words	18. Distribution Statement
Pressuremeter, Light Weight Deflectometer, Clegg Impact Hammer, Nuclear Density Gage, Pavement Evaluation	Document is available to the U.S. public through the National Technical Information Service, Springfield, Virginia 22161

19. Security Classif. (of this report)	20. Security Classif. (of this page)	21. No of Pages	22. Price
Unclassified	Unclassified	1048	

Form DOT 1700.7 (8-72)

Reproduction of completed page authorized

Acknowledgments

The research team would like to thank numerous individuals including: Dr. David Horhota, Jose Hernando, Glenn Johnson, Todd Britton, Kyle Sheppard from FDOT's State Materials Office who worked tirelessly both in the office/lab area and in the field during the testing. Also the cooperation of Jon M Hall at their Cypress Landing development enabled us to easily find and complete the field testing at a local site, while Granger Construction in conjunction with Brevard County Engineering, Ms. Rasha Riadh allowed us to easily test along the Saint John Heritage Parkway. Mr. Marcello Canitano, President and Owner of Spacecoast Precision, Inc., in Brevard County Florida, who also helped with the final probe design and components. The help from Alexandra Boggs, Quinn Duffy and Spencer Hinkley is also acknowledged in the completion of this work.

Executive Summary

Six inch and 12 inch (15 and 30 cm) long small diameter pressuremeter (i.e. SDPMT-6 and SDPMT-12) probes were developed and tested to determine in-situ stress-strain properties of unbound pavement layers. They were deployed in the same hole as the one made during nuclear density gage (NDG) testing. The stress-strain response of strain-controlled tests, run conventionally (with equal volume increments) and rapidly (with continuous volume increases), were evaluated at four sites in Brevard County, Florida. One test site consisted of A-1-b base material, three consisted of A-3 embankment quality materials.

The SDPMT tests were conducted by driving or drilling a hole 7 or 13 inches (17.5 or 32.5 cm) deep, and then inserting a 5/8 inch (15 mm) diameter, 6 or 12 inch (15 or 30 cm) long expandable cylindrical probe. Once the desired probe was in place, it was inflated with water as the soil stress-strain response was monitored and digitally recorded.

Field testing included 159 SDPMT tests, 107 NDG tests, 141 light weight deflectometer (LWD) tests, 96 Clegg impact hammer tests, and 36 dynamic cone penetrometer (DCP) tests. Lab testing included grain size, moisture-density, LBR and resilient modulus (Mr) tests.

The SDPMT results were compared with NDG dry unit weights (γ_{dry}), moduli from both Dynatest ($E_{0,Dynatest}$) and Zorn ($E_{d,Zorn}$) LWD's, impact values from Clegg impact tests, penetration index (PI) values from DCP tests, and Mr values from lab resilient modulus tests. A finite element analysis (FEA) was also conducted by comparing Zorn LWD deflections to predicted FEA deflections.

Five statistical models were used to evaluate the relationships between SDPMT parameters and the results from the other testing. The models produced linear, logarithmic and exponential correlations. Generally, the exponential models produced the best R^2 values. SDPMT initial moduli and limit pressures correlated very well to LWD stiffnesses and NDG dry densities.

The exponential relationship $\gamma_{dry} = 74(E_0)^{0.06354}$ produced R^2 of 0.85 from SDPMT-12 incremental testing. Both the SDPMT-6 and -12 incremental exponential models both produced R^2 values of 0.86, with the SDPMT-12 incremental equation being: $\gamma_{dry} = 82.69(p_L)^{0.07391}$.

Although both LWD's produced useful correlations, the Zorn LWD correlations were slightly better than those from the Dynatest LWD. Excellent linear and exponential correlations were developed between the Zorn LWD moduli ($E_{d,Zorn}$) and SDPMT E_0.

With both stiffnesses having units of kPa, SDPMT-6 continuous data produced the highest linear correlation ($R^2 = 0.83$) from the equation $E_{d,Zorn} = 1.816E_0 + 15,950$, and the highest exponential correlation ($R^2 = 0.87$) from the equation $E_{d,Zorn} = 75.77(E_0)^{0.6748}$.

SDPMT engineering parameters were consistent and comparable to published results. The rapid SDPMT testing was completed in less than 3-minutes and provided reliable data, indicating that with refinements in the data acquisition, calibration and data analysis, these test could compliment and possibly replace nuclear density testing as a compaction field control method.

The stress – strain response from SDPMT-6 and SDPMT-12 incremental and continuous tests, resembles those of the standard PENCEL pressuremeter curve. This study also demonstrates that SDPMT data match common PMT parameters for sands; however, p_0 is the least useful engineering parameter of those generated during testing.

By combining unload stress-strain results from SDPMT-6 and SDPMT-12 tests, with AASHTO T 307 Mr values, realistic strains for embankments, subbase/subgrade and base materials were found. This finding further validates the usefulness of SDPMT data for pavement design and analysis.

When SDPMT-6 and-12 unload stress-strain models were input into FEA analyses, they under predicted Zorn LWD deflections by 10 to 20 %, with SDPMT-12-inch data producing more accurate predictions than SDPMT-6 data.

SDPMT continuous testing needs refined to improve data acquisition, calibration procedures and the resulting analyses, especially in terms of initial moduli. Continuous tests were run very efficiently following NDG testing, producing data within one minute of the NDG tests. Surface tension cracks were observed during SDPMT testing, which may have an effect on the limit pressures, and should be studied further using surface surcharging evaluated as a method of mitigating these cracks.

Table of Contents

List of Figures

List of Tables

Chapter 1

Project Overview

1.1 Background

Currently, the most common methods for quality control of compacted materials are limited to the evaluation of moisture content and density from the sand cone and speedy moisture or the nuclear density gage (NDG). The results of these tests are compared to laboratory optimum moisture content and maximum dry density. In addition, minimum bearing requirements can be evaluated through the use of Limerock Bearing Ratio (LBR) or California Bearing Ratio (CBR) tests. The dynamic cone penetrometer (DCP) or a field CBR test produces in-situ estimates of the bearing strength, but do not provide stress-strain data. The CBR and LBR tests provide a stress deflection curve, but only report a ratio of bearing strength compared to a standard material.Engineers need better in-situ properties for pavement layers. A small diameter pressuremeter (SDPMT) test if performed quickly would provide a true in-situ stress-strain relationship of the compacted soil being tested. If the SDPMT could also be used in the NDG test hole, stress-strain information could quickly be related to moisture and density.

The current pavement field construction processes require contractors to place and compact the various unbound layers according to thickness and density specifications. FDOT's density specifications require testing the entire lift, typically using NDG equipment (Figure 1.1). The most common FDOT lift thicknesses are 6 and 12 inches (15 and 30 cm).

Although density is related to strength and stiffness neither are directly measured. The cost of operating NDG equipment is high simply due to the regulatory requirements.

The current recommended design methods for flexible and rigid pavements use the resilient modulus (M_r) as the design input parameter to determine pavement system layer thicknesses. The current recommended method of determining the M_r involves constructing a sample for testing in a triaxial cell and cyclically loading the specimen under prescribed confining and vertical stress conditions.

The development of a SDPMT test would allow critical engineering properties to be determined for a roadway. Engineering parameters that could be evaluated by using the

Figure 1.1: Typical Nuclear Density Equipment; including Carrying Case, Driving Rod, Template and Rod Remover, Calibration Block and Nuclear Density Device

SDPMT in conjunction with the NDG are limit pressure p_L, initial pressuremeter elastic modulus E_i, pressuremeter load unload modulus E_{lu}, pressuremeter unload secant modulus, and ratio of horizontal to vertical earth pressures (σ_h/σ_v) from the PMT and the NDG.

Briaud (1979) developed a smaller PMT, known as the PENCEL Pressuremeter (PPMT), specifically to test pavements. However because of its fixed 10 inches (25 cm) probe length, it was limited to testing pavement layers with this minimum thickness (Cosentino, 1987). Typical lifts of unbound pavement layers are six to 12 inches (15.3 to 30.5 cm), which makes a smaller PMT necessary. If this smaller probe could be used in conjunction with NDG testing the combination would produce strength and stiffness parameters at the in situ densities. If this process was followed long enough, the strength and stiffness information could replace the highly regulated NDG test.

A fast reliable in-situ test would enable both contractors and engineers to improve the pavement quality. A complex tri-cell PMT, was developed by Ménard in 1956. It is a unique soil-testing device that provides a complete stress-strain response of the soils tested. The data from this test can be used to determine at-rest soil pressures, elastic moduli and limit pressures. Figure 1.2 shows typical PMT output and the portions of

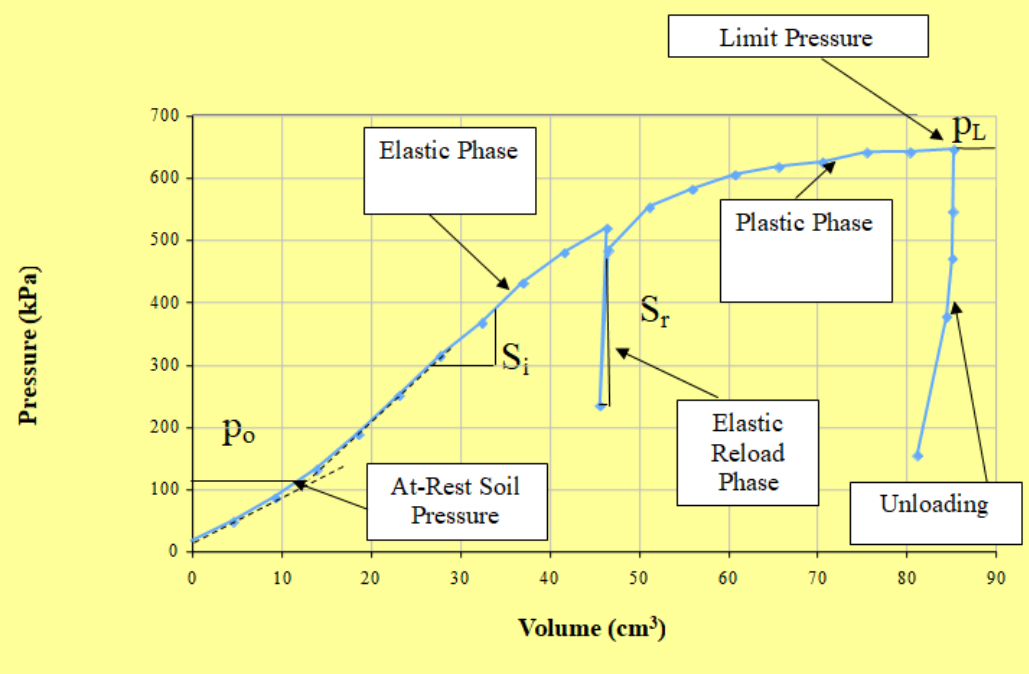

Figure 1.2: PMT Data Depicting At-rest Soil Pressure, Elastic portions, Plastic portions and Limit Pressure

the curve used for determining these various engineering strength and stiffness parameters.

Various size PMT's have been developed and used, including the stress-controlled tri-cell Ménard probe that is about 3-inches (75 mm) in diameter and 18-inches (450 mm) long; the strain-controlled mono-cell TEXAM probe of the same size and the smaller mono-cell strain controlled PPMT which is about 1.3-inches (32.5 mm) in diameter and 9-inches (22.5 cm) long (Figure 1.3). The PPMT was developed specifically to test airfield pavement layers. The main theoretical limitation for proper PMT testing is the length to diameter (L/D) ratio of the probe. As long as this ratio is 7:1 or longer, the theory applied to using the results for the expansion of an infinitely long cylindrical cavity is valid. The accuracy of the smaller probe and its associated control unit was significantly improved through instrumentation and data acquisition software developed under FDOT contract BD 658 by Cosentino et al. 2008 such that the reduced stress-strain curve is displayed on a laptop during testing. In addition to the real time data, the upgraded system allows more accurate stresses plus very small strains to be accurately determined. Digital pressures and volumes are recorded using a Labview® based data acquisition software interface called APMT for Automated Pressuremeter Testing. These small strains correlate to those produced during vehicle loading (i.e. 10^{-2} %) and allow accurate predictions of in-situ resilient moduli (Figure 1.4).

Many FDOT base, subbase/subgrade layers are either 6 or 12-inches (15 or 30 cm) enabling the widely accepted NDG to test these entire layers. A smaller diameter version of the PPMT that could rapidly test the entire lift would be desirable. The

(a) Closed Control Unit (b) Open Control Unit (c) Instrumentation

Figure 1.3: Roctest PENCEL Pressuremeter Control Unit with FIT Instrumentation Upgrades

diameter of the NDG driving rod (shown in Figure 1.1) is from 5/8th to 3/4th inches (15 to 19 mm), therefore; PMT probes should be developed that are 6 or 12 inches (15 or 30 cm) long with diameters in this range. The resulting stress-strain data would produce test results that can be used for compaction, which directly relates to design engineering properties (i.e., modulus).

1.2 Project Objective

The research objective is to develop and evaluate digital in-situ stress-strain responses for 6 and 12-inch long (15 to 30 cm) SDPMT probes using both incremental and rapid strain-controlled tests in 6 and 12 inch (15 and 30 cm) unbound pavement layers.

1.3 Approach and Supporting Tasks

Two SDPMT probes were developed that allowed for full depth testing of the two typical compacted layer thickness of highway pavement systems; one probe was six inches and the second probe was 12 inches (30 cm) long. The probes, that fit into a 3/4 inch (19 mm) diameter hole created by inserting the NDG drive pin into the ground were evaluated on their ability to produce reliable stress-strain information in tests that takes approximately five minutes. The following tasks were performed to accomplish the proposed research objective.

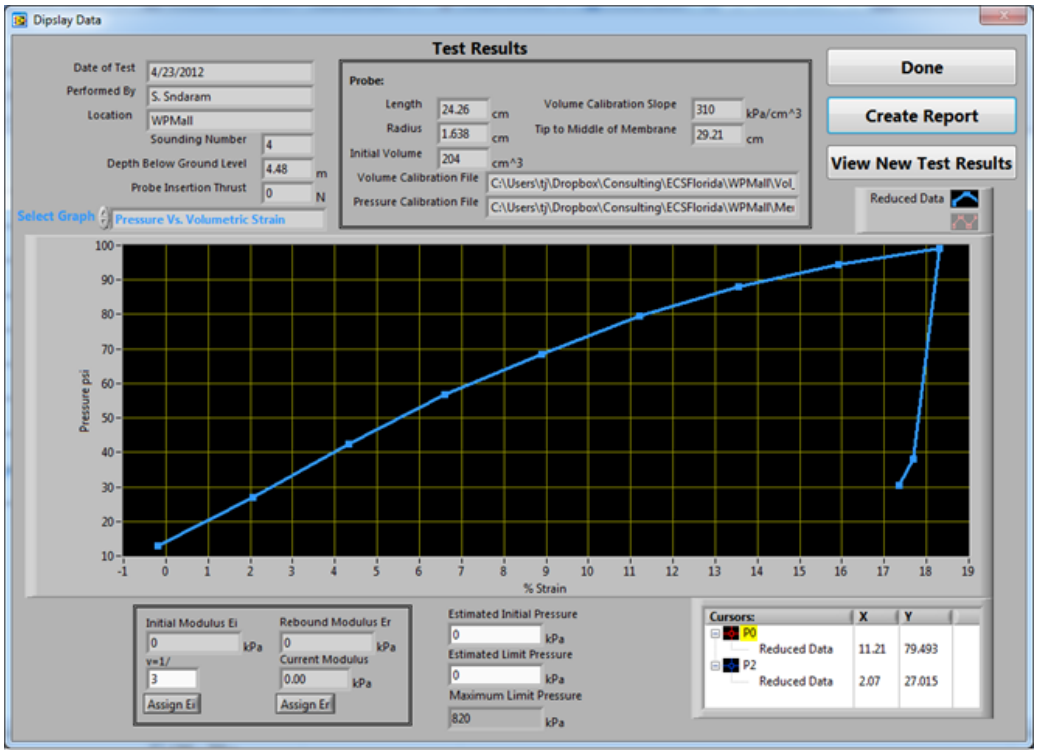

Figure 1.4: Typical Labview® APMT Screen Cosentino et al. (2008)

1.3.1 Task 1 Literature Search

The literature search is a summary of the current in-situ and laboratory unbound pavement layer tests. The advantages and disadvantages of each test were evaluated and are presented. This information includes the various types of pavement related pressuremeter tests, plus a review of several commonly used field tests that are being developed for design and construction. Nondestructive testing that was reviewed includes: a) the Clegg impact test (CIT), b) lightweight deflectometer (LWD), c) dynamic cone penetrometer (DCP), and d) falling weight deflectometer (FWD). Additionally, unbound pavement materials lab tests including, a) FDOT's modification of the California Bearing Ratio called the Limerock Bearing Ratio (LBR) and b) resilient modulus (M_r) test were reviewed. These tests were then used for the testing program to yield comparisons between SDPMT results and their relative outputs. The full literature review is presented in Chapter 2.

1.3.2 Task 2: Design and Construction of a SDPMT

The SDPMT diameter was a limiting factor of the probes design. This probe needed to fit into the hole used by the NGD approximately 0.875 inches (22 mm), without damaging the rubber membrane or having too small of a diameter. If the diameter is too small, the test results could be incomplete due to the limited amount of injectable water available during testing. Two probe lengths were developed and compared for use

in testing 6 and 12 inch (15 and 30 cm) compacted layers of unbound base and subbase materials.

The following several factors required design consideration:

- Probe Dimensions
- Probe Control Unit Connections
- Probe End Sealing System
- System Fluid
- Control Unit
- Testing Procedures

Once the overall dimensions of the probe were determined it was also necessary to determine elastic material to be used as the membrane for this probe. The membrane should not change elastic properties with continued cycles, and should not creep because of the cyclic nature of the testing.

Several parts needed to be developed to construct the SDPMT, including the probe body, membrane attachment fittings, and system expansion calibration sleeve. Different 3D fabrication methods were evaluated including traditional machining and additive manufacturing, which involves using layers to build 3D printed parts. The design of the probe is discussed in detail in Chapter 4.

1.3.3 Task 3: Evaluation of PMT Control Unit

The control unit was evaluated to determine if changes were necessary to accommodate the required testing. Evaluations included;

- what system fluid should be used, (i.e., water, hydraulic fluid, etc.),
- adding a different handle for injecting the fluid to allow for better control at the higher strengths associated with base materials and
- standardizing the tubing length from the control unit to the probe.

1.3.4 Task 4: Test Site(s) Selection

To develop sound conclusions about the SDPMT test results, a sufficient number of tests had to be conducted, at various locations with consistent strength-stiffness parameters, to a depth of at least 12-inches (30 cm). An area such as a roadbed under construction would be ideal, and the test site(s) for the validation study could be done along one travel lane approximately 300 feet (100 m) long. This site would permit 12 tests of each type to be performed every 25 feet (7.5 m). Testing that would be performed will include 6 and 12 inch (15 and 30 cm) SDPMT, continuous and incremental SDPMT tests, moisture density, LWD, DCP, and Clegg Impact tests (CIT). The description of the selected test sites is found in Chapter 3.

1.3.5 Task 5: Experimental Design

The experimental design was divided into two subtasks: preliminary testing to serve as a proof of concept, and the development of a MATLAB based data collection process to allow results from the statistical correlations to be outputted as the SDPMT and other engineering test data were compared.

1.3.5.1 Task 5a: Proof of Concept Data Collection

The goal of the proof of concept testing is to demonstrate that both the 6 and 12 inch (15 and 30 cm) SDPMT probes will produce consistent engineering results. Key parameters that will be evaluated are initial modulus and limit pressure. The lift-off pressure was excluded due to the inexact process used to determine it. If initial moduli are shown to be consistent, then any other moduli whether they be unload or second type moduli would also be consistent. Results of the preliminary testing are presented in Chapter 5.1.

1.3.5.2 Task 5b: Correlation Testing Data Collection

Once the PPMT and SDPMT probes are proven to provide consistent results, then testing can be transitioned into collecting the engineering data necessary for developing correlations between the SDPMT and other field compaction control methods. The typical in-situ parameters obtained from each comparison tests will be correlated the SDPMT data. The planned tests are:

- Field Moisture Content
- Field Density
- Clegg Impact Test
- Dynamic Cone Penetrometer
- Light Weight Deflectometer
- Incremental Injection SDPMT (6 inch (15 cm))
- Continuous Injection SDPMT (6 inch (15 cm))
- Incremental Injection SDPMT (12 inch (30 cm))
- Continuous Injection SDPMT (12 inch (30 cm))

Both the test site configuration and number of tests per location within each site will need to be developed. The number of tests per location along with the total number of tests should be sufficient to make conclusions to determine if PPMT and SDPMT are producing the consistent results under similar soil conditions.

Table 1.1: Proposed Correlation Testing by Site

	Cypress Landing	Olin Site	Heritage Parkway	Southgate Field
Nuclear Density Test	12	12	12	12
Incremental SDPMT-6		12	12	12
Continuous SDPMT-6		12	12	12
Incremental SDPMT-12	12	12	12	12
Continuous SDPMT-12	10	12	12	12
Lightweight Deflectometer - Dynatest	12	12	12	12
Lightweight Deflectometer - Zorn	12	12	12	12
Clegg Impact Test	12	12	12	12
Dynamic Cone Penetrometer	12	12	0	12
Resilient Modulus	6	6	6	6

The correlation testing plan shown in Table 1.1, has been developed to investigate the relationship between the SDPMT engineering parameters and acceptance tests (i.e. density and moisture content) and field/lab strength and deformation tests (i.e. DCP, CIT, LWD and M_r).

1.3.6 Task 6: Probe Construction

After a finalized probe design has been established it will need to be constructed. The probe body and sleeves will need to be machined, and the membrane material will need to be ordered.

1.3.7 Task 7: Software Development

Before field testing began, updates to the current Automated Pressuremeter (APMT) Software previously developed (Cosentino et al., 2006) will be made so that calibrations and data for the rapid continuous injection test can be recorded. The modifications to the APMT software are described in Appendix H.

1.3.8 Task 8: Testing Procedures

Testing for this task is separated into two major phases based on the experimental design from Task 5: phase one is validation testing and phase two is correlation testing. These phases are explained in detail below.

1.3.8.1 Phase 1: Validation Testing

Phase one testing will consist of evaluating the SDPMT probes at one location with consistent strength and stiffness properties. Data from the three PMT probes (i.e.,

PPMT, SDPMT-6, and SDPMT-12) will be compared. The constant strain, incremental volume injection testing procedure typically used during monocell PMT testing, will be used during testing with all three probes. The detailed procedure follows.

1.3.8.1.1 Standard PPMT Test

Standard PPMT tests will be conducted to create a baseline of data that can be used to compare the performance of the SDPMT probes. Prior to testing the soil the two typical calibrations (system expansion and membrane resistance) will be conducted. This data will be used to correct the raw data for the effects of the control system expansion and the membrane inertial resistance. The incremental strain controlled PPMT test will be conducted as 5 cm^3 increments of fluid are injected and the corresponding pressure is recorded. PPMT tests consisted of 26 points from an initial reading, then 5 cm^3 increments until either an injected volume of 90 cm^3 is achieved or 2500 kPa (360 psi) of probe pressure is reached. After the maximum injected volume or pressure is reached, unload readings will be taken at approximately 0.1, 0.2, 0.5, 1.0, 2.0, 4.0 and 8.0 cm^3, or until the reduced injected pressure reaches 0 kPa. This test sequence is based on the recommended procedure presented in Cosentino et al. (2006). This test sequence should provide an adequate number of data points to determine the pressuremeter parameters p_0, E_0, p_L and p_L^*. The unload sequence performed at the end of the test should provide data necessary to determine the relationship between differing strain levels and moduli.

1.3.8.1.2 SDPMT Incremental Strain Testing

Testing of the SDPMT in Phase I will consist an incremental strain test, with volumetric strain increments of approximately 2.5 cm^3. The incremental strain SDPMT test will consist of readings at 26 strain levels from 0 injected volume to approximately 15 cm^3 and 30 cm^3 for the 6 inch and 12 inch (15 and 30 cm) probes respectively. At the end of the test unload readings will be taken at the increments as the PPMT tests. Prior to SDPMT testing, the two conventional calibrations (system expansion and membrane resistance) will be conducted. This data will be used to reduce the effects of the system properties on the results.

This sequence was selected because it provides similar radial strains to the PPMT standard test. The test sequence should provide an adequate number of data points to determine the pressuremeter parameters p_0, E_0, p_L and p_L^*. The test sequence also includes an unload sequence at the end of the test to provide data to determine the relationship between differing strain level and moduli.

1.3.8.2 Phase 2: Field Correlation Testing

Phase II testing will consist of conducting a series of SDPMT tests along with the CIT, DCP , LWDs, moisture and density tests. A similar set of tests will be conducted at three different test sites for both base and subbase materials.

1.3.8.2.1 SDPMT Test

The test procedure for the Phase II testing of the SDPMT will be conducted the same as described in Section 1.3.8.1.2. This testing phase will consist of 12 tests per site for each probe length, producing 48 tests.

1.3.8.2.2 Continuous SDPMT Test

The continuous PMT test will be a strain-rate controlled test. The fluid will be injected into the probe from the control unit at a constant rate to be determined before testing. The APMT software will be modified to display an estimation of injection rate. During this test data will be recorded at a rate of four samples per second and displayed on the screen to the test operator. This test will consist of injecting fluid from 0 cm^3 to a maximum injected volume based on the size of the probe and the maximum pressure that the membrane can withstand, then removing fluid down to 0 cm^3, to complete the test.

The data collected will be analyzed to determine which points will be used to reduce the data. This testing will consist of 12 tests per site, per probe length, totaling 48 tests.

1.3.8.2.3 Moisture Density Testing

NDG equipment will be used to determine density and moisture content. The NDG moisture contents will be checked using lab samples obtained during NDG tests.

1.3.8.2.3.1 Nuclear Density Testing

Moisture content and density of the soil will be determined according to the Florida Method of Test (FM 1-T 238). NDG tests will be conduced at 6 and 12 inch (15 and 30 cm) depths at all 4 sites. However, an additional 12 tests will be conducted at a depth of 8 inches (20 cm), which is the thickness of the shoulder for Heritage Parkway. NDG tests for this research will total 108 tests, and will be conducted by staff from the Florida Department of Transportation (FDOT) State Materials Office (SMO).

1.3.8.2.4 Clegg Impact Hammer Testing

Clegg Impact Test (CIT) will be performed in the proximity of each test location, providing surface stiffness values. Twenty-four tests will be conducted at each of the 4 tests site totaling 96 tests.

1.3.8.2.5 Dynamic Cone Penetrometer Testing

DCP tests will be conducted at each test location in accordance with ASTM D6951-09, producing penetration index values versus depth. Twelve tests will be conducted at the Florida Tech Olin Complex, the Florida Tech Southgate Field and the Cypress Landing development, totaling 36 tests, however, the cemented coquina base at Heritage Parkway prevented DCP testing.

1.3.8.2.6 Resilient Modulus Testing

Disturbed samples will be obtained from each field testing site and transported to FDOT State Materials Office (SMO) to prepare samples for resilient modulus testing. Tests will be conducted in accordance with AASHTO T 307, Standard Method of Testing for Determining the Resilient Modulus of Soils and Aggregate Materials. The design resilient moduli from these tests will be compared to SDPMT results. Tests will be conducted dry of optimum, at optimum and wet of optimum moisture content to provide a range of values. A total of 26 design resilient moduli were obtained from this testing.

1.3.8.2.7 Testing Summary

The proposed tests to be conducted to develop working correlations for the SDPMTs are shown in Table 1.2.

1.3.9 Task 9: Data Reduction

Data reduction for Task 9 will also be split into two subtasks. The first, will be the probe validation, where the results of the three probe types (PPMT, SDPMT-6 and SDPMT-12) tests are compared. The second subtask will be where the Phase 2 Correlation Testing data will be evaluated so that key parameters can be compared and develop correlations. These subtasks are described below.

1.3.9.1 Phase 1: Validation Testings - Data Reduction

The test data from the incremental SDPMT and PPMT tests will be reduced from the raw data to provide engineering parameters for comparisons between the PPMT and the new SDPMT probes. Data reduction will include adjustments for the membrane resistance and volume or system expansion.

1.3.9.2 Phase 2: Correlation Testing - Data Reduction

The raw data collected from the various tests performed during the correlation testing will be reduced to their relevant engineering parameters to provide key results for further comparison. Such parameters include those calculated for the PMT tests in Phase 1, plus wet and dry density, estimated DCP penetration index, CIT, and LWD soil stiffnesses.

1.3.10 Task 10: Data Analysis

After the completion of each phase of testing the data will be analyzed, graphs and charts will be developed and a written description will be developed for the final report. The following sections describe the data analysis that will be completed for each phase of testing.

Table 1.2: Phase 2 Test Summary

Test	Length Inches	Olin Complex	Southgate Field	Cypress Landing	Heritage Parkway	Total Tests
SDPMT - Continuous Strain Rate	6	12	12	0	12	36
SDPMT - Continuous Strain Rate	12	12	12	12	12	48
SDPMT - Incremental Strain	6	12	12	0	12	36
SDPMT - Incremntal Strain	12	12	12	12	12	48
Moisture Density		24	24	24	36	108
Clegg Impact Test		24	24	24	24	96
Dynamic Cone Penetrometer		12	12	12	0	36
Lightweight Deflectometer		24	24	24	24	24
Resilient Modulus		6	6	6	8	28

1.3.10.1 Phase 1: Proof of Concept - Data Analysis

Results from the SDMPT and PPMT tests will be compared to determine if the new SDPMT probe produces results are similar to PPMT results. The shapes of the stress-strain curves along with the lift-off pressure (p_0), limit pressure (p_L), and initial moduli (E_0) will be compared.

1.3.10.2 Phase 2: Correlation Testing - Data Analysis

After the data is collected as proposed in Task 8 it will be analyzed to determine if any relationships can be developed between the different engineering properties reduced from the test data. Statistical correlations will be examined between the SDPMT's and the engineering properties from other testing.

Chapter 2

Literature Review of PMT and Field Pavement Evaluation Methods

2.1 Literature Review

2.1.1 Pressuremeter Development

In-situ strength and deformation characteristics are important aspects of the geotechnical engineering design and evaluation process. Field-testing reliance has arisen from the difficultly in extracting undisturbed soil samples to run complex laboratory tests. Therefore, researchers have developed in-situ testing techniques that can supplement or replace laboratory testing. One such in-situ testing technique is the pressuremeter (PMT) test, which was defined by Mair and Wood (1987) as "a cylindrical device designed to apply uniform pressure to the walls of a borehole by means of a flexible membrane". During a test the cylindrical probe is carefully inserted or hydraulically pushed to the desired in situ depth. The probe is connected by tubing to a control unit at the ground surface, which supplies a uniform pressure, hydraulic or gas, to expand the membrane. The pressure exerted on the membrane to the sides of the borehole causes redial deformation of the soil, resulting in a response in terms of applied pressure versus radial deformation. The soil response can be analyzed to obtain essential soil properties.

Kögler (1933) developed the initial concept of PMT testing in Germany, the idea was not developed further due to industrial restrictions limiting various synthetic rubbers Baguelin et al., 1978. In 1956, French engineer, Louis Ménard, successfully developed a pre-board pressuremeter device to determine in-situ soil characteristics. Since then, various PMT's have been developed and utilized. They include the stress-controlled Ménard PMT, consisting of a tri-cell probe that is about 3 inches (75mm) in diameter and 19 inches (475 mm) in length, the strain-controlled TEXAM PMT, consisting of a mono-cell probe at about 3 inches (75mm) in diameter and 18 inches (450 mm) in length, and a strain-controlled PENCEL PMT (PPMT), consisting of a mono-cell probe that is about 1.3 inches (33 mm) in diameter and 9 inches (225 mm)in length. Other

PPMT models are also available for specialty application where high pressure testing would be required. Figure 2.1 depicts the pressuremeter models. Strain-controlled testing produces more data and therefore, clearer stress-strain results than stress-controlled testing.

Figure 2.1: Pressuremeter Models: PPMT, Ménard PMT, and TEXAM PMT

2.1.2 Installation of PMT

The method of installation does affect the shape and quality of the PMT test stress-strain curve. Therefore, the method of installation should prevent excessive disturbance of the walls of the soil borehole. General installation guidelines are discussed below.

2.1.2.1 Installation of PBPMT

A pre-bored pressuremeter (PBPMT) test is one where the PMT probe is lowered into a slightly over-sized pre-formed hole. Pre-boring is the most common PMT installation process. In this case, the borehole can be created using an appropriate auger or rotary technique, based on the size of the PMT probe that will be employed, as well as the type of soil to be tested. When drilling the PMT hole, the primary objective is to minimize the soil disturbance while producing a uniformly circular hole (Clarke, 1996).

2.1.2.2 Installation of SBPMT

A self-boring pressuremeter (SBPMT) test involves the use of a probe with an internal bit located on the bottom of the probe, and is advanced into the ground by rotating internal rods. The rotating cutting head drills the borehole in clay soil. Soil cuttings are flushed to the surface through the rotating rods with the assistance of drilling mud. The disturbance of the borehole using this technique can be minimized by using a cutting head of similar size to the SBPMT probe, as well as using the minimum

pressure necessary to cycle the drilling mud. The pressure and deformation measurements recorded using the SBPMT represent the actual soil behavior and typically produce the best holes for testing. This technique is not preferable for use in sands because of the potential for borehole collapse during the drilling process (Clarke, 1996).

2.1.2.3 Installation of FDPMT

A full displacement pressuremeter (FDPMT) is a PPMT that is driven or pushed into the ground using a cone truck or other machine. The probe may or may not be fitted with a friction reducing ring to help preserve the membrane. During the installation process, the PMT probe is pushed into the ground at a constant speed (typically 2 cm/sec if CPT equipment is used), displacing the surrounding soil radially resulting in soil disturbance. The installation method of FDPMT may affect the PMT test results. Generally, this process can be carried out in differing soil types, including granular and fine-grained soils (Clarke, 1996). Cosentino et al. (2006) pushed PPMT's through sands and soft clays near Port Canaveral, Florida. They showed that the PPMT is resilient, and that the membrane would not fail if properly maintained.

2.1.2.4 General Installation Guidelines

With the insertion of any pressuremeter, the maximum difference between the borehole diameter and the probe diameter should be less than 10% ($D_{Hole}/D_{PMT} < 1.10$) (Mair and Wood, 1987). However, Briaud (2005) stated that this ratio could be < 1.20. There is currently no standard criterion for the size of the borehole.

2.1.3 Interpretation Methodology of PMT Data

As shown in Figure 2.2, the PMT stress-strain curve can be divided into three distinct phases:

- *Initial phase:* is a re-establishing curve portion at which the membrane moves into full contact with the walls of the borehole (from point A to point B),
- *Elastic phase:* is a straight-line portion during which the change in volumetric-strains of the membrane are assumed to be constant (from point B to point C),
- *Plastic phase:* is a nonlinear curve portion at which the stressed soil cavity increases significantly with little increase in applied pressure (from point C to point D).

The theoretical analysis of the PMT results are mainly based on an assumption that plane strains govern the behavior of soil response throughout the test. The analysis yields primary soil parameters including lift-off pressure (p_0), undrained shear strength

(S_u), shear modulus (G), initial elastic modulus (E_i), reload modulus (E_r), and ultimate or limit pressure (p_L). These analytical approaches are described below.

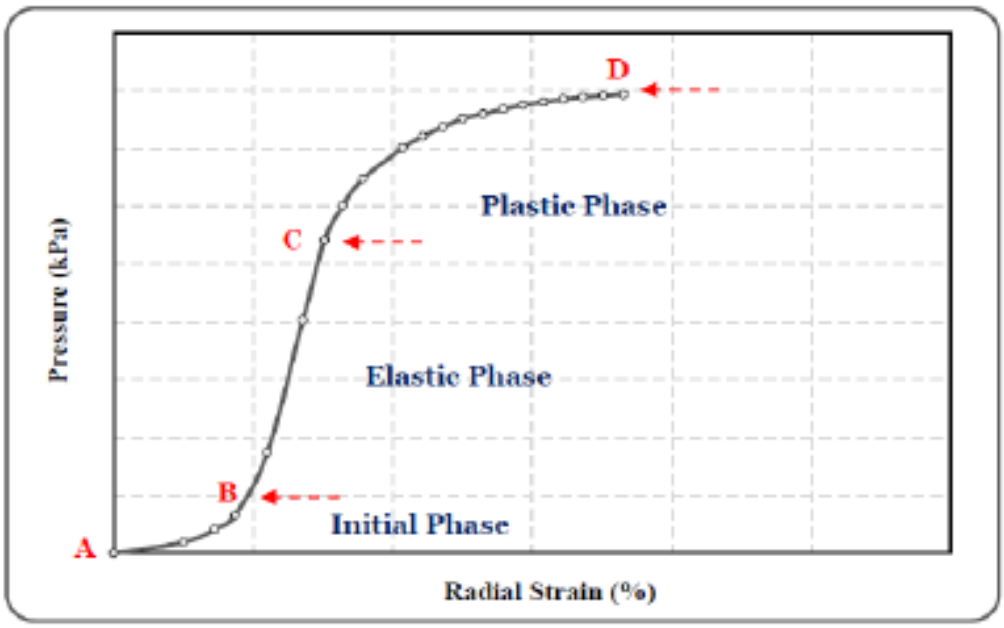

Figure 2.2: Typical Pressuremeter Test Curve

2.1.3.1 Lift-off Pressure

The lift-off pressure (p_0) is defined as an initial horizontal stress at which the slope of the PMT curve changes substantially. The determination of lift-off pressure depends mainly on visual selection of a single point from the test curve and therefore is subjective (Cunha, 1994). It generally represents the intersection point between the initial curve portion and linear elastic curve portion in the case of PBPMT. However, in the case of SBPMT's, the lift-off pressure represents the initial portion of the stress-strain data at which the soil cavity pressure is first observed. Figure 2.3 illustrate the selection methods for determining lift-off pressure in SBPMT (a) and PBPMT's (b) respectively.

Several studies have investigated the in-situ total horizontal stresses from the lift-off measurements of the PMT tests conducted in clays and sands. It was found the lift-off pressure obtained from SDPMT is approximately equal to field lateral stresses in the surrounding soils. However, it is not practical to predict in-situ horizontal stress from PBPMT lift-off pressure due to the considerable soil disturbance that occurs during the probe installation (Schnaid, 2009).

2.1.3.2 Deformation Modulus

The elastic deformation modulus of the soil can be calculated using linear elastic theory based on the expansion of a cylindrical cavity (Baguelin et al., 1978). Cylindrical

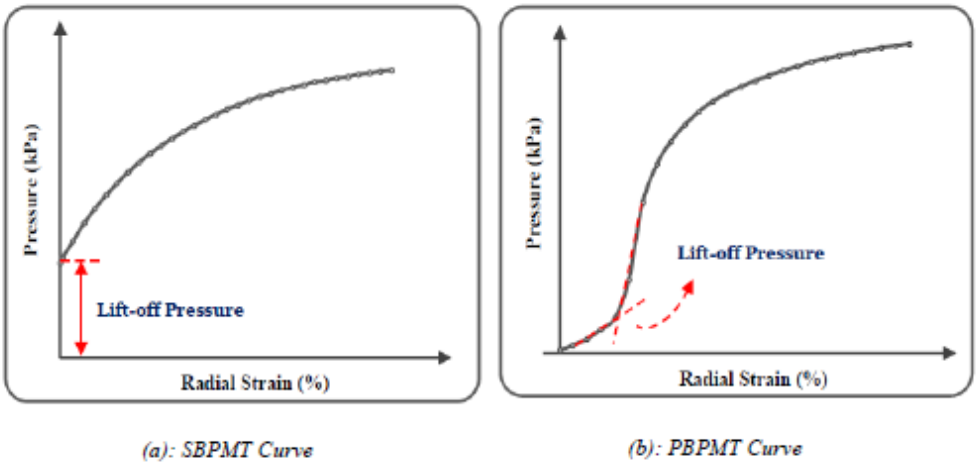

Figure 2.3: Estimation of Lift-off Pressure from SDPMT and PBPMT Curves (After: Mair and Wood, 1987)

cavity expansion theory assumes that the soil behaves elastically and the probe expands radially in an infinite elastic medium, under plane-strain conditions, which allows determining soil shear modulus (G) as follows:

$$G = V_m \left(\frac{\Delta P}{\Delta V} \right) \tag{2.1}$$

where:

V_0	Initial volume of the probe
V_m	Mean volume of the cylindrical cavity
ΔV	Change in volume the corresponding change in pressure, ΔP

The mean volume can be measured from the initial probe dimensions using the following equation:

$$V_m = V_0 + \left(\frac{\Delta V_f + \Delta V i}{2} \right) \tag{2.2}$$

where:

V_0	Initial volume of the probe
ΔV_i	Initial volume increment injected at a specific point
ΔV_f	Final volume increment injected at a specific point

Generally, the value of shear modulus, which is found from the elastic phase of the PMT curve, may be affected by soil disturbance from the probe installation. Therefore, it is often convenient to determine ground stiffness from an unloaded-reload cycle of the PMT test curve, see Figure 2.4. Two theoretical approaches have been developed to determine elasticity Equations 2.1 and 2.2, using the unload reload cycle. First, the average shear modulus is computed by fitting a line to all the data representing the cycle. As shown in Figure 2.4b, the average secant modulus is approximately equal to half of the slope of that line. Secondly, instead of using the whole cycle to determine

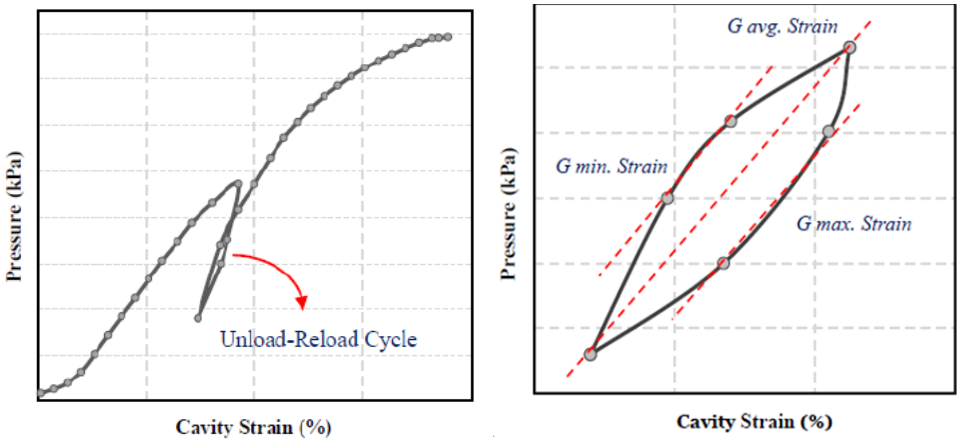

(a) PMT Curve (b) PMT Cycle

Figure 2.4: Determination of Soil Stiffness from Unload-Reload Cycle of PMT Curve (After: Clarke and Gambin, 1998)

shear modulus, a single line of unloading portion or reloading portion can be utilized to obtain soil stiffness over a specified strain range. However, it is more applicable to use minimum cavity strain of the reloading portion to determine soil modulus as this approach provides more consistent results Clarke and Gambin (1998).

The soil elastic constants, Young's Modulus (E) and Poisson's ratio, (ν), are related to the elastic shear modulus (G) using the expression:

$$G = \frac{E}{2\,(1+\nu)} \tag{2.3}$$

Therefore, Young's elastic modulus can be directly measured by substituting Equation 2.1 in Equation 2.3 as shown:

$$E = 2\,(1+\nu)\,V_m \left(\frac{\Delta P}{\Delta V}\right) \tag{2.4}$$

Briaud and Felio (1986) stated that presenting the data from the PMT test in terms of volumetric expansion (ΔV) is not practical, since different PMT probe dimensions had different total volumes. Therefore, it is helpful to plot PMT results as a function of either radial strain (ε_r) or hoop strain (ε_Θ), which are approximately equal but opposite in sign based on elastic theory.

$$\epsilon_r \approx -\epsilon_\Theta \tag{2.5}$$

Where ε_Θ is a function of cavity radius:

$$\epsilon_\Theta = \frac{2\pi R_f - 2\pi R_0}{2\pi R_0} = \frac{R_f - R_0}{R_0} = \frac{\Delta R}{R_0} \tag{2.6}$$

R_0: Initial cavity radius
R_f: Final cavity radius
ΔR: Change in cavity radius

Based on the previous equation, the soil elastic modulus can be calculated in terms of relative increase of the probe radius. The resulting elastic modulus equation format allows PMT moduli from different size probes to be compared:

$$E = (1+\nu)(P_2 - P_1)\frac{\left[\left(1+\frac{\Delta R_2}{R_0}\right)^2 + \left(1+\frac{\Delta R_1}{R_0}\right)^2\right]}{\left[\left(1+\frac{\Delta R_2}{R_0}\right)^2 - \left(1+\frac{\Delta R_1}{R_0}\right)^2\right]} \tag{2.7}$$

where:

R_0:	Initial cavity radius
ν:	Poisson's ratio
P_1:	Cavity radial stress at the beginning of the pressure increment
P_2:	Cavity radial stress at the end of the pressure increment
ΔR_1:	Increase in probe radius at the beginning of the pressure increment
ΔR_2:	Increase in probe radius at the end of the pressure increment

2.1.3.3 Limit Pressure

The limit pressure (p_L) represents the ultimate soil resistance at which strain deformations will increase continuously, without increasing applied radial pressure. Baguelin et al. (1978) indicated that the volume of the soil cavity must be inflated to twice its initial size to reach ultimate pressure. Therefore, the pressure corresponding to the point $(2V_0 + V_c)$ represents the limit pressure, p_L.

$$p_L \implies V_L = 2V_0 + V_c \tag{2.8}$$

where:

V_L:	Injected volume at p_L
V_0:	Initial volume of soil cavity
V_c:	Initial volume of the measuring cell (probe)

Briaud and Felio (1986) stated that the limit pressure can be predicted by extrapolating the injected pressure versus the radial strain curve. The limit pressure corresponds to a value of $\left(\frac{\Delta R}{R_0}\right)_L$ which relates to:

$$P_L \implies \text{P at} \left(\frac{\Delta R}{R_0}\right)_L = 0.41 + 1.41\left(\frac{\Delta R}{R_0}\right)_c \tag{2.9}$$

where:

$\left(\frac{\Delta R}{R_0}\right)_L$	Relative increase in probe radius at the limit pressure
$\left(\frac{\Delta R}{R_0}\right)_L$	Relative increase in probe radius at initial size of the soil cavity.

However, the radial deformations of the probe may not reach $\left(\frac{\Delta R}{R_0}\right)_L$ throughout the test. Therefore, the PMT testing curve should be extended manually to $\left(\frac{\Delta R}{R_0}\right)_L$ and read the limit pressure on the extrapolated curve.

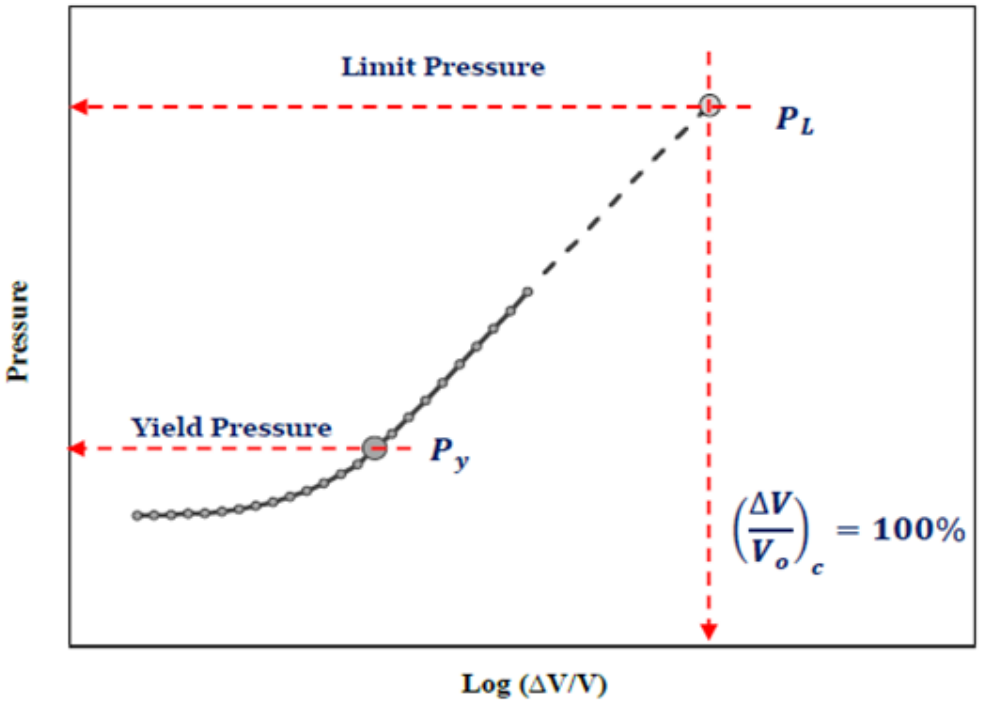

Figure 2.5: Limit Pressure Extrapolation for Ideal Elastic-Perfectly Plastic Soil (After: Mair and Wood, 1987)

Mair and Wood (1987) described an extrapolation technique which involves plotting PMT test on a pressure versus natural log of volumetric strain graph, as shown in Figure 2.5. The plot of pressure versus log-volume for the plastic phase results in a straight-line above the yield pressure (P_y). Thus, the limit pressure can be estimated by extending the obtained straight-line portion to a point that corresponds to a 100 percent volumetric cavity strain.

In geotechnical applications, the net limit pressure (P_L^*) is widely utilized to define soil strength for use in design and analysis procedures. This parameter can be estimated directly using the following expression:

$$P_L^* = P_L - P_0 \tag{2.10}$$

where:
P_L: Limit Pressure or p_L
P_0: Lift off pressure or p_0

2.1.3.4 Undrained Shear Strength

Four different methods have been proposed for estimating undrained shear strength of cohesive soils (S_u) using the PMT test curve including: 1) the limit pressure method, 2) the yield pressure method, 3) the Gibson-Anderson method, and 4) the sub-tangent method.

Table 2.1: Estimating Undrained Shear Strength from Limit Pressures (Adapted from: Clarke and Sadeeq (1996))

Undrained Shear Strength	Reference
$S_u = \frac{P_L - P_{ho}}{10} + 25$	Amar & Jezequel (1972)
$S_u = \frac{P_L - P_{ho}}{5.1}$	Lukas & Leclerc de Bussy (1972)
$S_u = \frac{P_L - P_{ho}}{2to5}$	Menard (1975)
$S_u = \frac{P_L - P_{ho}}{6.8}$	Marsland & Randolph (1977)
$S_u = \frac{P_L}{10} + 25$	Johnson (1986)
$S_u = \frac{P_L - P_{ho}}{10}$	Martin & Drahos (1986)

P_{ho} represents initial horizontal stress

The limit pressure method produces undrained shear strength as a function of ultimate soil strength, which is obtained from the latter portion of a PMT stress-strain curve. Various expressions to predict S_u from p_L have been developed, which subsequently were summarized by Clarke and Sadeeq (1996).

In addition, Briaud (2005) presented a more acceptable theoretical equation to predict in-situ shear strength of cohesive soils. This empirical equation, which was recommended by several investigators, depends on limit pressure and secant shear modulus of the soil:

$$P_L = P_o + S_u \left(1 + ln\frac{G}{S_u}\right) \tag{2.11}$$

Where S_u represents undrained shear strength of the cohesive soil. Equation 2.11 can be rearranged to:

$$S_u = \frac{P_L - P_0}{\left(1 + ln\frac{G}{S_u}\right)} = \frac{P_L^*}{\beta} \tag{2.12}$$

Where β represents a soil factor that relates the ratio of shear modulus to shear strength, which generally varies between 5.6 and 7.4 with an average recommended value of 6.5.

The second method considers the initial point of the plastic phase (i.e., the yield pressure P_y) as a critical input to assess undrained shear strength. It typically represents the difference between yield pressure and in-situ horizontal stress, as shown in Equation 2.13. However, it is not recommended to utilize this approach to estimate soil strength, since it tends to overestimates S_u (Briaud, 2005).

$$S_u = P_y - \sigma_{oh} \tag{2.13}$$

Paul (2004) described the third method of estimating undrained shear strength proposed by Gibson and Anderson (1961). This method depends on the theoretical expression derived from a semi-log plot of PMT data:

$$P = P_y + S_u ln\left[\frac{G}{S_u} \times \Delta\frac{V}{V_o}\right] \tag{2.14}$$

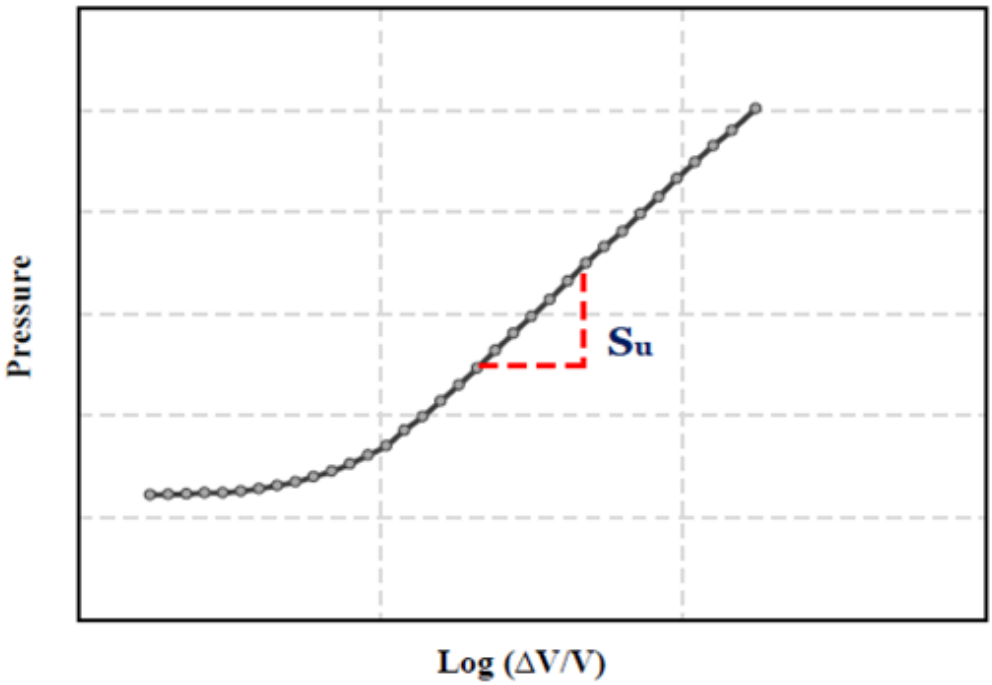

Figure 2.6: Yield Pressure Method to Estimate Shear Strength (After Paul, 2004)

where:

P: Applied pressure
P_y: Yield pressure
G: Secant shear modulus
S_u: Undrained shear strength
$\frac{\Delta V}{V_0}$: Relative increase in volumetric strain

It was found that for a constant G/Su ratio, the plot of pressure versus log cavity strain becomes a straight-line after the yield pressure (see Figure 2.6). The slope of this linear portion represents the undrained shear strength.

Finally, the sub-tangent method is determined from the graphical interpretation of the PMT shear stress-strain curve (see Figure 2.7). A tangent to PMT curve is drawn from a point at or just above the yield pressure to intersect the y-axis at point B, and a horizontal line is drawn from the point of tangency to the y-axis at point A. Subsequently, the vertical distance (AB) is equivalent to the maximum shear strength of the soil. Generally, this method is quite sensitive to soil disturbance; and therefore it is not preferred for estimating shear strength from pre-bored PMT results.

2.1.3.5 Friction and Dilation Angles

Hughes et al. (1977) originally presented an approach for determining the dilation and friction angle for sands. This method depends mainly on the slope of the linear part of a log of effective cavity pressure versus log of cavity strain plot. Figure 2.8 shows the determination of the slope of the log plot. Once the slope has been calculated, the

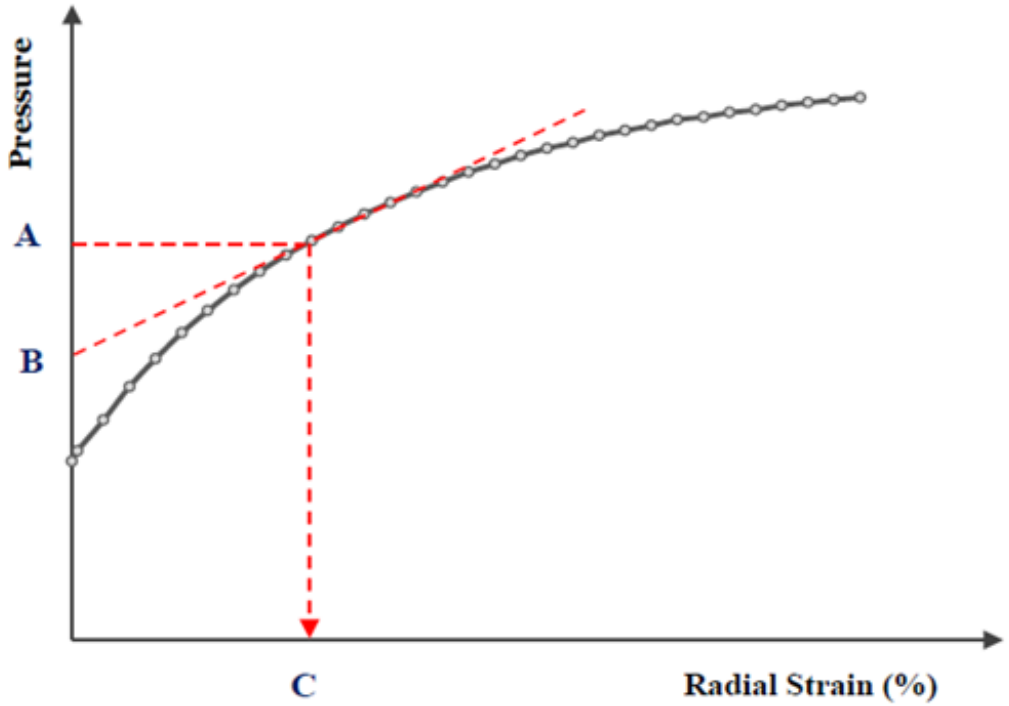

Figure 2.7: Sub-tangent Method to Estimate Shear Strength (After: Mair and Wood (1987))

friction and dilation angles can be calculated using the following equations:

$$\sin\phi' = \frac{S}{[1 + (1 - S)\sin\phi'_{CV}]} \tag{2.15}$$

$$\sin\psi = [S + (S - 1)\sin\phi'_{CV})] \tag{2.16}$$

where:

φ: Angle of shearing resistance
ψ: Dilation angle
S: Slope of log-log plot of PMT testing curve
ϕ'_{CV}: Angle of shearing resistance at constant volume

The angle of shearing resistance at a constant volume (ϕ'_{CV}) is termed a critical friction angle at which volumetric strain in the soil equals zero. Sands tend to decrease in volume if sheared below the critical friction angle ($\phi' < \phi'_{CV}$), and dilate if sheared above the critical friction angle ($\phi' > \phi'_{CV}$). Typically, this value can be deduced from the results of a drained triaxial test (Holtz and Kovacs, 1981). However, Mair and Wood (1987) indicated that this value can be assumed within an acceptable range ($30 < \phi'_{CV} < 35$), since it does not have a significant influence on determining a mobilized friction angle, φ. An uncertainty of 5° for ϕ'_{CV} results in an uncertainty of 2.5°in φ. Thus, Clarke and Sadeeq (1996) recommended 35°as a typical value of the critical friction angle in the absence of test results.

This methodology to identify the friction angle works very well with data obtained

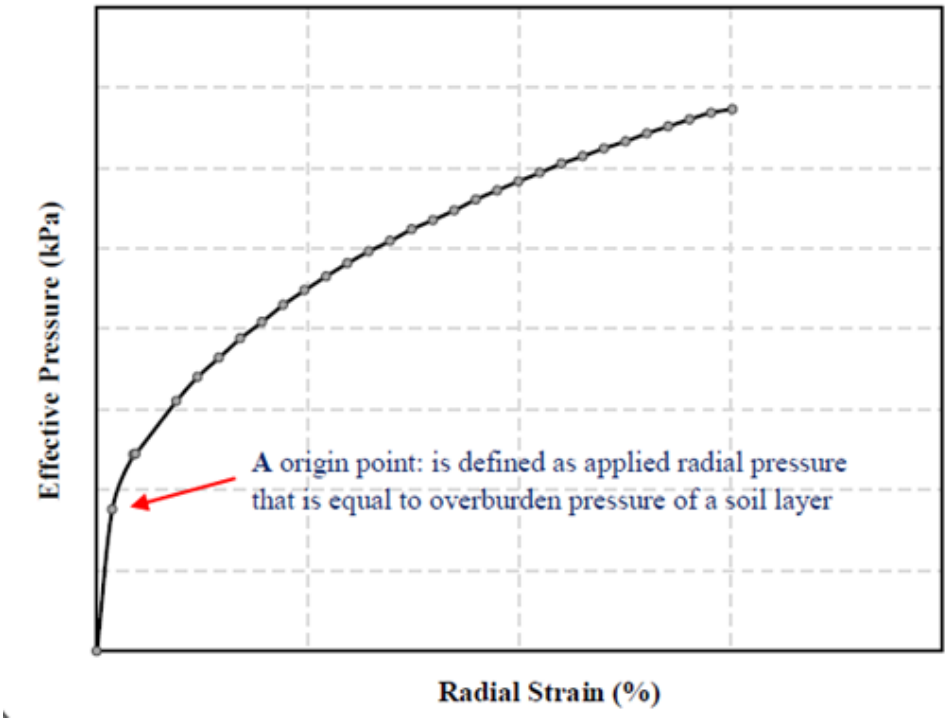

(a) Pressure vs. Strain

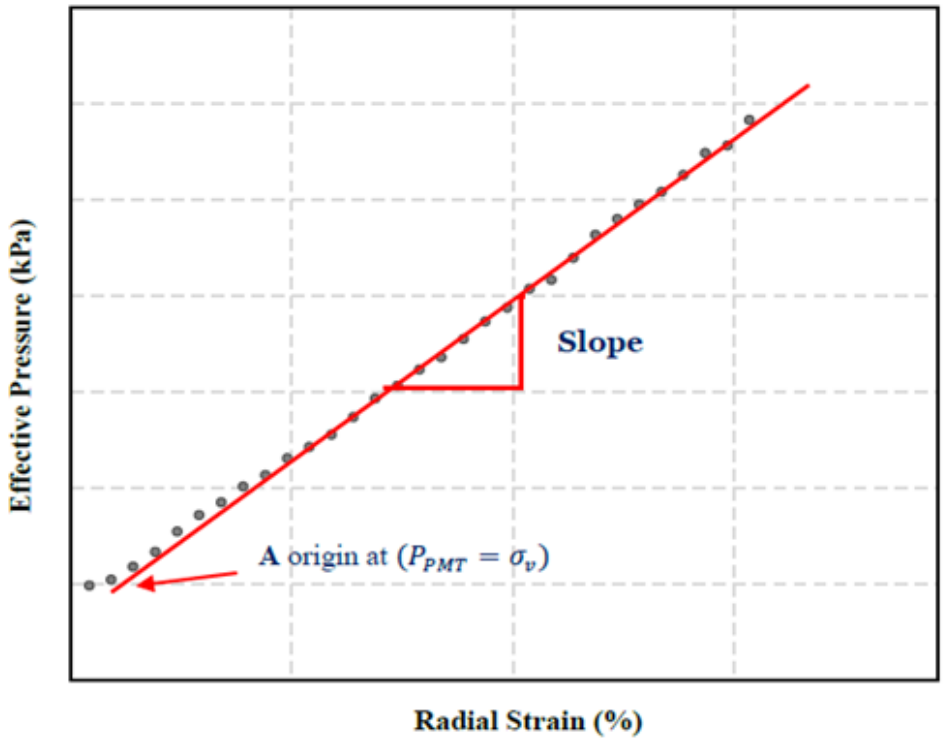

(b) Log pressure vs. Log strain

Figure 2.8: Determination of φ & ψ from Self-boring PMT Data (After: Mair and Wood (1987))

from self-boring PMT. However, several authors found that this technique does not yield consistent friction angles from pre-bored PMT data, due to large installation testing disturbance. Therefore, various improvements have been made to this approach in order to utilize it to interpret disturbed curves of pre-bored PMT, such as a trial-and-error method presented by Mair and Wood (1987). In this technique, several trials should be conducted to accurately determine a straight-line that covers large range of strains along the log-log plot for pre-bored PMT tests (see Figure 2.9).

2.1.4 Factors Affecting PMT Results

Three main factors can influence the results of a PMT test: installation disturbances, critical test depth, and slenderness ratio (L/D) of the PMT probe. The detailed descriptions of these factors are presented below.

2.1.4.1 Soil Disturbance

Inserting the PMT probe into the ground causes a soil disturbance. The amount of disturbance depends on several major factors, including method of PMT installation, strength and sensitivity of soil, and natural state of stress in the field (Prapaharan, 1987). The most critical of these is the soil disturbance. The disturbance of the annular zone around the probe can be reduced significantly by utilizing the self-boring PMT.

Several investigators have examined the effects of soil disturbance on the PMT elastic moduli and limit pressures. Aubeny et al. (2000), investigated the effects of installation disturbance on undrained shear strength measured from self-boring and full displacement PMT tests in clays. In this investigation, a strain path model was first developed for studying the changes in pore water pressure and effective stresses during the pile driving process. This model was also utilized to represent the effect of PMT probes disturbance on soil strength characteristics. During full displacement PMT tests in saturated clays, large pore water pressures will be generated. This pore water pressure increase results in 50% to 90% reduction in the clays undrained shear strength.

A parametric study was performed by Altschaeffl et al. (1990) to investigate the influence of the soils re-molded zone thickness. The authors conclusions were that; 1) undrained strength can be overestimated by as much as 100% at 1% of the initial unloaded strain, 2) soil deformation moduli are significantly influenced by the initial unloading condition from borehole preparation, producing an overestimation that ranges from 30 to 40%, and 3) that undrained soil strength is greatly affected by soil disturbances obtained from initial unloading of the soil cavity.

The in-situ lateral stress is also influenced by the degree of soil disturbance. The stress-strain curve of re-molded soils yields a 20% reduction in total horizontal stress resulting in an overestimation of 20 to 40% in undrained shear strength (Ladd et al., 1980).

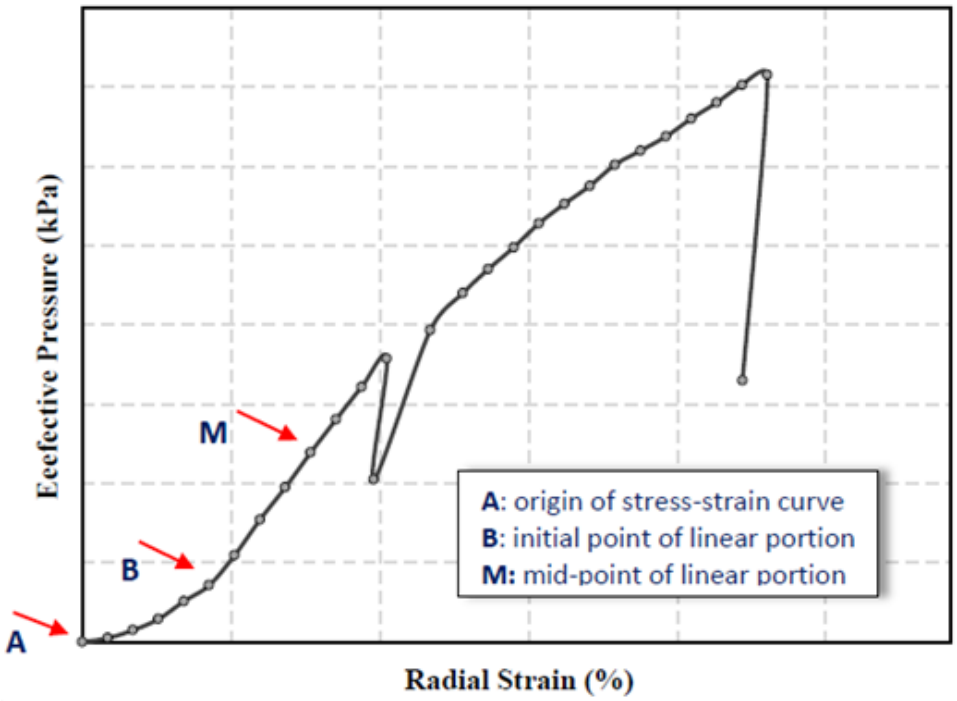

(a) Pressure vs. Strain

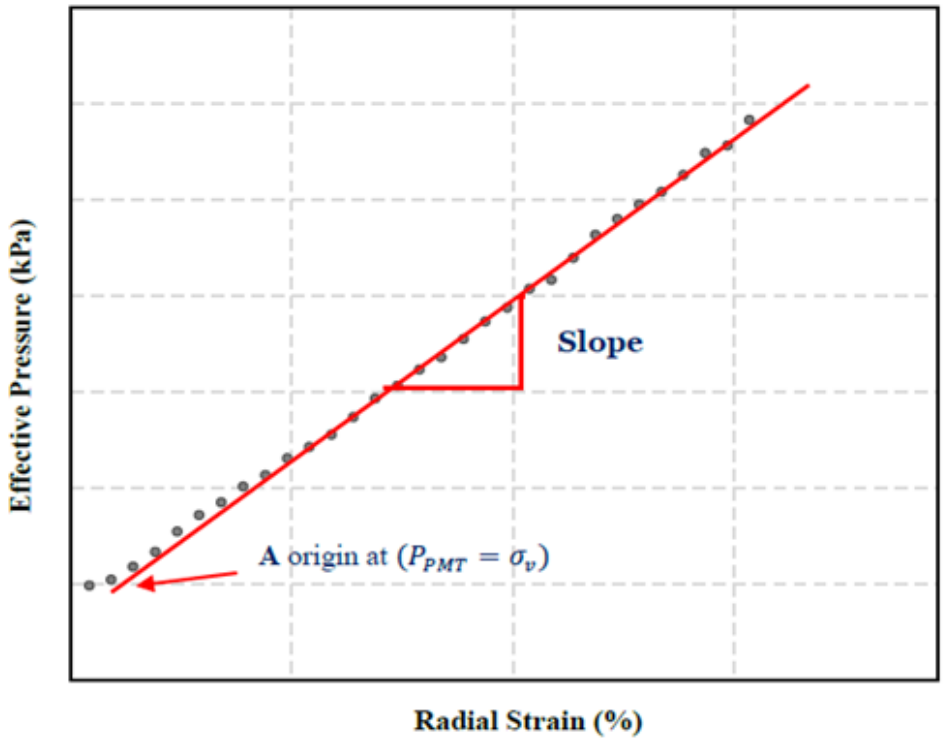

(b) Log pressure vs. Log strain

Figure 2.9: Determination of φ & ψ from Pre-bored PMT Data (After: Mair and Wood (1987))

2.1.4.2 Critical Depth

Conducting PMT tests near the ground surface results in considerable reduction of soil resistance because of the lack of vertical confinement. The depth of reduced lateral soil resistance is known as the critical depth. Baguelin et al. (1978) suggests that the critical depth is a function of the PMT probe diameter.

$$Z_c = 15 \times D_{PMT} \quad \text{for cohesive soil} \tag{2.17}$$

$$Z_c = 30 \times D_{PMT} \quad \text{for cohesionless soil} \tag{2.18}$$

where

Z_c : Critical depth

D_{PMT} : Diameter of PMT

For example the PPMT probe, with a 1.3 inch radius, would have a critical depth of approximately 1.63 feet in clay and 3.25 feet in sand. Briaud et al. (1983) conducted a comprehensive investigation to study the influence of the critical depth on lateral strain of expanded PMT's. In the study, a finite element model was developed to simulate the effect of shallow surface conditions on limit pressure and pressuremeter moduli obtained at small strains, see Figure 2.10. Based on the results of this theoretical model, it was found that the pressure developed from an inflated probe at shallow depths should be corrected as given in Equation 2.19

$$P_{\text{Corrected}} = \frac{P^*}{X} \tag{2.19}$$

where :

P^* :Net PMT pressure along curve$(p - P_0)$

X :Reduction factor estimated from Figure 2.10

Compaction of base and subbase/subgrade soils significantly affects the confinement and consequently the critical depth. As the compaction occurs, the vertical stresses are removed once the roller passes, however, the horizontal stresses remain. The soil confinement confinement in the horizontal direction increases with increasing degree of compaction. Therefore, the limits presented in Figure 2.10 may need to be reconsidered for PMT tests performed within pavement layers.

2.1.4.3 PMT Probe Slenderness Ratio

The effect of the slenderness or length-to-diameter ratio (L/D) on soil behavior during testing can be quantified by comparing theoretical equations of stress and displacement for spherical or cylindrical cavity expansions. Briaud and Felio (1986) performed a comprehensive analytical comparison to evaluate the maximum error that

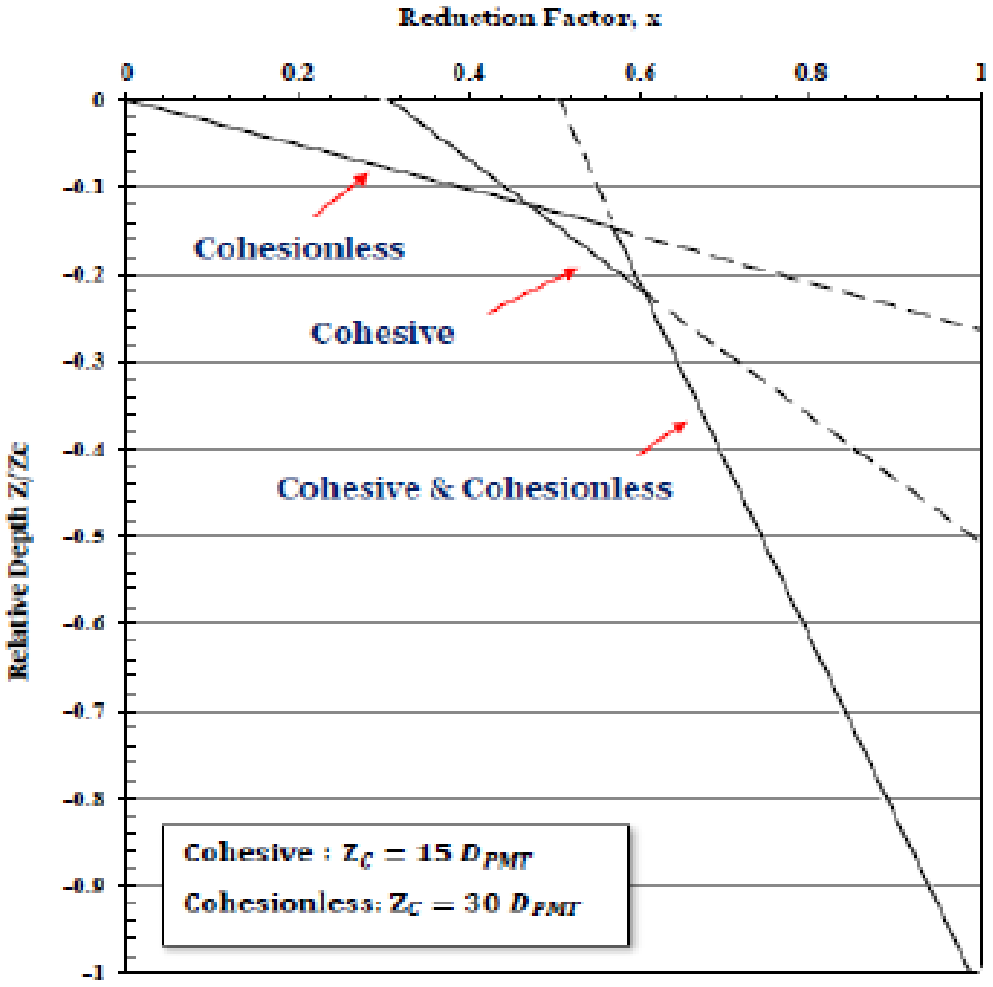

Figure 2.10: Proposed Reduction Factors of the PMT within the Critical Depth (After: Briaud et al., 1983)

would occur if a cylindrical expansion is used to determine limit pressure for a spherical measuring probe. The general theoretical relationships for cylindrical and spherical clay

cavities are:

$$p_{\text{L-spherical}} = p_0 \frac{4}{3} S_u \left(1 + \ln \frac{G_{\text{spherical}}}{S_u}\right) \tag{2.20}$$

$$p_{\text{L-cylindrical}} = p_0 \frac{4}{3} S_u \left(1 + \ln \frac{G_{\text{cylindrical}}}{S_u}\right) \tag{2.21}$$

where :

G :is the shear modulus,

p_0 :is the lift-off pressure,

p_L :is the limit pressure, and

S_u :is the undrained shear strength.

Referring to Equations 2.20 and 2.21, the ratio of spherical parameter to cylindrical parameters is approximately 1.33:1. In other words, the limit pressure for a probe with $L/D = 1$ compared to a probe with $L/D = \infty$ is 33% higher. However, for sands, the the following expressions can be used to show theoretically that the ratio of spherical to cylindrical limit pressure ranges from 3:1 for dense sands to 4:1 for loose sands.

$$p_{\text{L-spherical}} = p_0(1 + sin\phi) \left[\frac{G}{p_0 \sin\phi}\right]^{0.5(1-K_a)} \tag{2.22}$$

$$p_{\text{L-spherical}} = p_0 \left[\frac{a(1+\sin\phi)\cos\phi}{(a-\sin\phi)\sin\phi}\right] \left[\frac{G(a-\sin\phi)}{ap_0\sin\phi}\right]^{0.661(1-K_a)} \tag{2.23}$$

where :

ϕ : is the friction angle,

K_a : is the coefficient of active earth pressure,

G : is the shear modulus,

p_L : is the limit pressure, and

p_0 : is the lift-off pressure.

Lassourdiere and Zanier (1986) investigated the importance of the probe geometry on the PMT stress-strain curve. Numerical simulations of PMTs with slenderness ratios of 2, 4, and 6 were conducted. Figure 2.11 illustrates the simulated PMT in clays. It shows that as L/D approaches higher values, there is less variation in limit pressure. The slenderness ratio of the probe with $(L/D = 6)$ yields a maximum limit pressure of 190 kPa. The maximum limit pressure for the PMT test with a slenderness ratio of 4 $(L/D = 4)$ is 210 kPa. For the probe with a slenderness ratio of 2 $(L/D = 2)$, the maximum limit pressure was 240 kPa. Even though there are differences, once the slenderness ratio reaches 4, there is a relatively small change of about 11% in limit pressure.

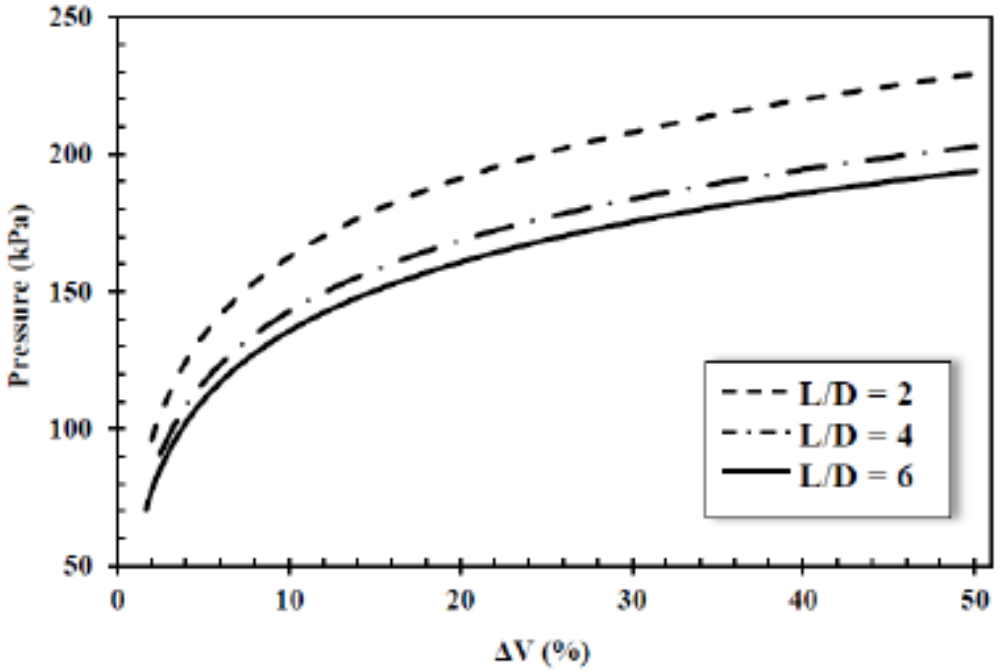

Figure 2.11: The Effect of Slenderness Ratio on Limit Pressure of Clay Soil (After Lassourdiere and Zanier, 1986)

Baguelin et al. (1986) carried out finite element analyses to evaluate the influence of slenderness ratio on undrained shear strength and shear moduli for clays. Again, three L/D ratios were considered 2, 4 and 6. Table 2.2 shows the results. Similar to other published studies, it was found that a probe with an $L/D = 2$ causes a significant overestimation of strength. These results show that the stiffness and strength are overestimated by about 20% at a ratio of 2, and less than 6% at a ratio of 6. Pore water pressures in clays are affected more than the strength and stiffness.

Table 2.2: Numerical Results of PMT Finite Length (Adapted from Baguelin et al., 1986)

Slenderness Ratio	$\left(\frac{L}{D}\right) = 2$	$\left(\frac{L}{D}\right) = 4$	$\left(\frac{L}{D}\right) = 6$
$\left(\frac{G}{G_\infty}\right)$	1.230	1.075	1.030
$\left(\frac{S_u}{S_{u\infty}}\right)$	1.220	1.110	1.065
u_{max}	2.04	1.75	1.64

An investigation into the effect of the slenderness ratio for self-boring PMT's was conducted by Houlsby and Yu (1990). In this study, a finite element analysis was utilized to simulate three probes for undrained tests in clays. Probes with L/D ratios of 4, 10 and 6 were chosen, with 4 representing the shortest, 10 longest and 6 the most practical, respectively. Simulated tests were carried out to predict shear strength (S_m) and shear

modulus (G_m). Predicted values for clays were then compared to the measured values of shear strength (S_a) and shear modulus (G_a). Table 2.3 lists the effects of slenderness ratios on stiffness and strength along with correction factors for each L/D ratio.

Table 2.3: Variation in Stiffness and Strength with L/D in Clay* (Adapted from Houlsby and Yu, 1990)

Slenderness Ratio	Predicted to Measured Correction Factors			
$\frac{L}{D}$	$\frac{G_a}{G_m}$	Stiffness Error (%)	$\frac{S_a}{S_m}$	Strength Error (%)
4	0.963	3.7	0.854	14.6
6	0.986	1.4	0.924	7.6
10	0.997	0.3	0.973	2.7
∞	1.000	0	1.000	0

* The measurement of S_m & G_m were determined based on the strain values at the center of the PMT probe.

The summary shown in Table 2.3, indicate that the predicted stiffness are lower than measured values by 3.7, 1.4 and 0.3% for L/D ratios of 4, 6 and 10 respectively. Likewise, the strength measurements for L/D ratios of 4, 6, and 10 are 14.6, 7.6 and 2.7% higher than the measured strength values. Therefore, strength is more critically affected by L/D than stiffness. Also the variations in stiffness are relatively small for the various L/D ratios used.

In summary, using a probe with a L/D ratio greater than or equal to 6 is acceptable unless pore water pressure measurements are required. L/D ratios less than 6 will affect strength more than stiffness.

2.1.5 Pavement Evaluation with PMT

A comprehensive literature search revealed limited experimental work with respect to utilization of PMT tests in pavement design and evaluation. Most of these investigations have focused on testing flexible airfield pavements, as summarized below.

Briaud (1979) first examined the possibility of utilizing PPMT for airport pavements in Canada. He suggested two theoretical methods to design airport pavements including the McCleod chart method and the multilayer elastic method. In the first approach, a series of PPMT and McCleod plate bearing tests were conducted in airport subgrades. The results indicated that there was a linear relationship between average subgrade stiffness obtained from McCleod plate bearing tests and equivalent pavement PPMT reload modulus (E_{ero}). The equivalent modulus is found by conducting PPMT tests

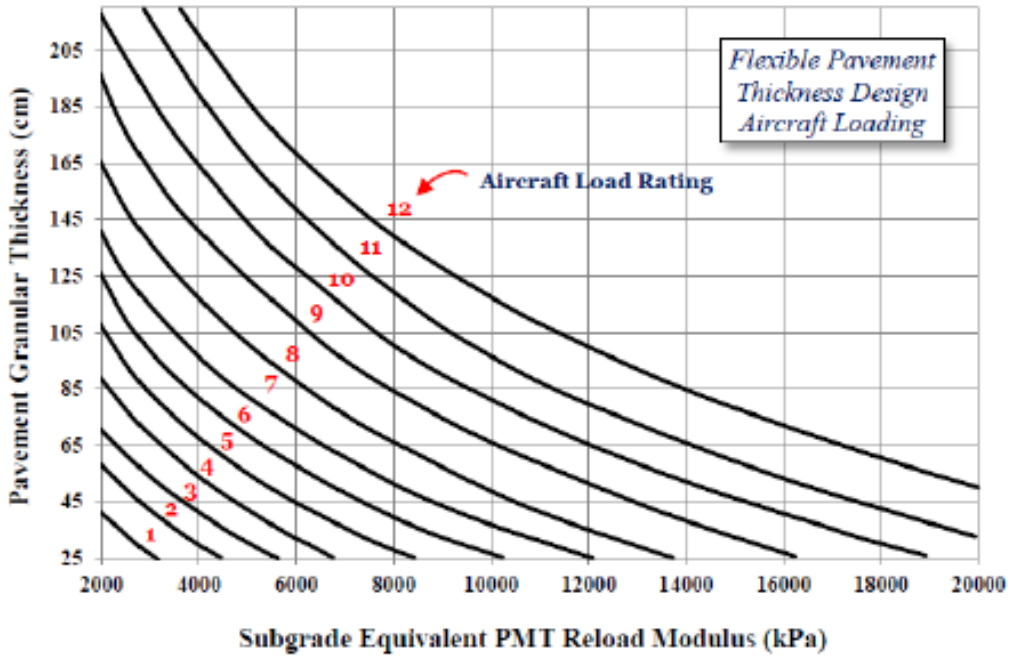

Figure 2.12: Airfield Pavement Design Chart Method Based on PMT Modulus (After: Briaud, 1979)

every 300 mm down to depth of 1500 mm below surface course pavement according to:

$$\frac{1}{E_{ero}} = 0.01\left(\frac{22.1}{E_1} + \frac{33.5}{E_2} + \frac{24.6}{E_3} + \frac{14.8}{E_4} + \frac{5}{E_5}\right) \tag{2.24}$$

where :

E_1 : is the PPMT reloaded modulus determined at the first 300 mm depth and E_2, E_3, E_4, E_5 : are measured in the next four 300 mm increments.

The overall required granular thickness for the runway can be directly identified from the chart presented in Figure 2.12 based on the values of aircraft load rating and subgrade characteristics in terms of PPMT reload modulus. The aircraft load rating (ALR) is an index number representing the weight of a plane in the airport design procedure. The number ranges from 1 to 12. The ALR for a Boeing 747 is 12, while the ALR for a small aircraft is 1 (Airport Structural Guidelines (ASG-19), 1992).

In the second approach, a multilayer elastic computer program known as BISAR - Bitumen Stress Analysis in Roads, was used to evaluate stress-strain conditions in airfield pavement layers. The multilayer elastic theory is a mechanistic analysis procedure which is typically used to investigate two types of structural failures in pavement layers: cracking, which results from excessive horizontal tensile strain at the bottom surface course layer, and rutting, which results from excessive vertical

compressive strength at the top of the subgrade layer. The key BISAR input parameter is the subgrade modulus. Therefore, the modulus obtained from PPMT tests was input into BISAR, to evaluate the layers of selected airports. Three main parameters were determined: the maximum horizontal strain at the bottom of the surface course, the maximum vertical strain at the top of the subgrade, and maximum vertical deflection at the pavement surface. These computed quantities were compared with allowable values reported in the airport design manual (Airport Structural Guidelines (ASG-19), 1992). When BISAR's predicted strains are greater than the allowable strains, airport pavement designers should consider an increase in asphalt pavement thickness. If the computer strains are lower than the allowable strains, the pavement design is satisfactory.

Cosentino (1987) performed a comparative study between data from the PPMT, the falling weight deflectometer (FWD), and the cyclic triaxial (CT) at three airfield pavements in Texas. Kondner's (1963) strain level model was used with unloading stress-strain data from PPMT tests. Two comparisons were made between the results of the tests in this experimental work. First, PPMT moduli were compared directly to CT moduli and backcalculated FWD moduli. Second, measured FWD deflections were compared with predicted FWD deflections determined as a function of PPMT and CT moduli. The predicted deflections were obtained using ILLI-Pave and ILLI-Salb, two Finite element software packages from the University of Illinois. It was concluded that PPMT moduli measured as a function of Kondner's (1963) hyperbolic model (i.e. strain level model) yielded the best prediction of surface FWD deflections for sand and clay soils, respectively.

Sanders (1991) examined the use of a special PMT known as the PENCEL Shear Pavement Pressuremeter (PSPPMT) for pavement rehabilitation and design applications. The apparatus, PSPPMT, was first developed in South Africa based on the original concept from two existing pieces of equipment: the PENCEL pavement PMT and the Handy Borehole Shear Tester. In this investigation, PSPPMT testing was performed in conjunction with Heavy Vehicle Simulator (HVS) testing to investigate the elastic modulus of subgrade granular materials of specific roads. A strong correlation was observed between predicted elastic PSPPMT moduli and back-calculated moduli from the HVS, with values being within 10%. In conclusion, the elastic subgrade moduli derived from the PSPPMT test can be directly utilized in mechanistic design approach instead of back-calculating it from HVS tests.

Erbland (1993) investigated the determination of subgrade moduli over low strain levels. In this investigation, three PMT probes with different slenderness ratios were used: The TEXAM PMT ($L/D = 6.6$ and $D = 2.75$ inches), the standard PPMT ($L/D = 7.2$ and $D = 1.30$ inches), and modified PPMT (L/D = 9.5 and D=1.30 inches). Increasing the membrane length of the standard PPMT probe from 9.5 inches to 12.5 inches was done to evaluate the L/D ratio during PPMT tests.

In each PMT test, thirty unload-reload cycles were conducted at three stress levels in order to evaluate the dependency of PMT results on the L/D ratio, see Figure 2.13. From each of these tests, thirty reload elastic moduli were determined along with limit pressure, initial elastic modulus and lift-off pressure. The results indicate that using a probe with a larger slenderness ratio (i.e. L/D = 9.5) yielded higher reload elastic

moduli, but showed lower estimations of limit pressures and initial moduli, thereby, matching other literature findings.

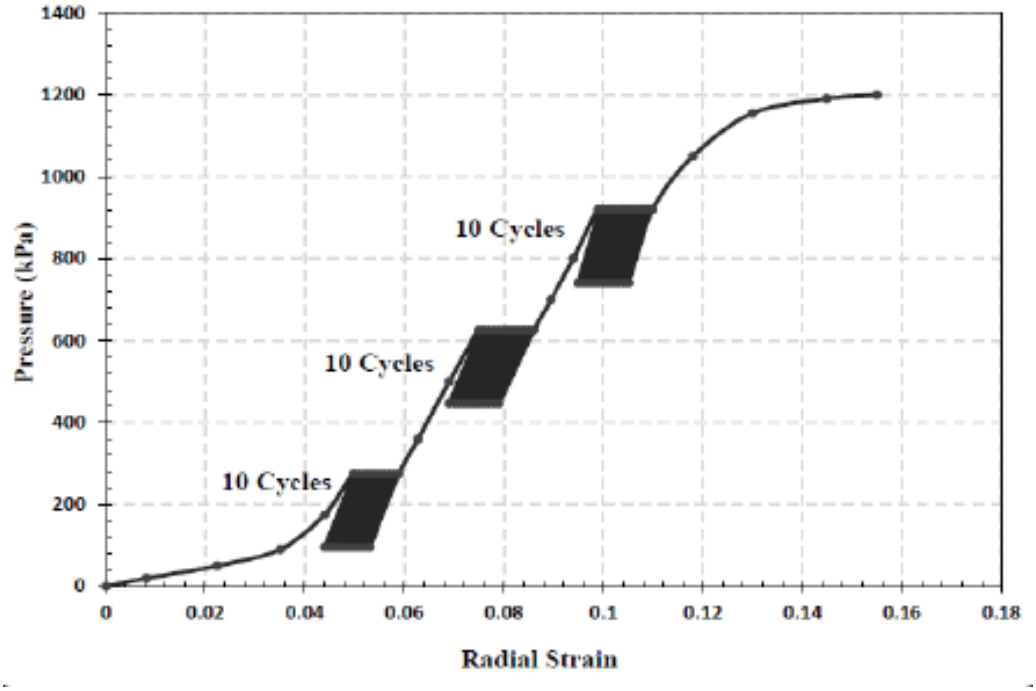

Figure 2.13: Typical Cyclic PPPMT Test (After: Erbland, 1993)

Erbland (1993) also investigated the PPMT reload elastic moduli found from small volume increments (i.e. 0.2 and 0.5 cm^3). These moduli were compared with small strain elastic moduli from a seismic testing method known as Spectral Analysis of Surface Waves (SASW). The results showed that the modified PPMT probe can give reasonable moduli values. In the SASW test, a small hammer was dropped onto a soil surface generating different wave frequencies, which were received by two geophones and transmitted to a waveform analyzer. The velocity of stress waves computed using the waveform analyzer was used to determine subgrade elastic moduli.

2.1.6 Flexible Pavement Evaluation Methods

2.1.6.1 Pavement Assessment Using LWD

The lightweight deflectometer (LWD) is a portable nondestructive device used for evaluating unbound pavement layers. It produces a stiffness (i.e., vertical dynamic modulus (E_{LWD})) and surface deflection (δ of the desired pavement materials under dynamic impulse loads. There are several known LWD manufacturers, with the two most common being the Zorn and Dynatest® models. During this research the Zorn Type ZFG 3.0 and Dynatest® Model 3031 were used. Zorn LWD's are manufactured by KSE Testing Inc. These two models differ, with the Zorn producing deflection versus impulse load time based on an assumed contact force based on dropping the 22-pound

mass 3.8 feet onto the 12-inch (30 cm) diameter loading plate. The Dynatest® produces measured load and deflection data as it contains a load cell at the contact point one the plate.

The surface deflections are determined by double integrating impulse acceleration readings from an accelerometer fixed inside a circular loading plate (Fleming et al., 2007). These vertical deflections are used to determine E_{vd} based on Boussinesq's elastic half-space theory. The Boussinesq, (1885) elastic theory, which relates to soil displacements with applied dynamic pressure for a rigid or flexible base, can be represented by the following expression:

$$E_{LWD} = \frac{(1-\nu^2)\sigma_o a}{\delta} f \tag{2.25}$$

$where:$

E_{LWD} : is dynamic soil stiffness in MPa,

δ : is soil surface deflection in mm,

σ_o : is the applied dynamic stress in (MPa),

a : is this radius of the loading plate in mm,

f : is the plate rigidity factor, and

ν : is Poisson's ratio.

The following sections are a review of the methods available for using LWD in pavement assessment. They include published relationships between LWD dynamic stiffness and the other laboratory and field engineering parameters.

Hossain et al. (2010) evaluated the possibility of using LWD as an in-situ test to evaluate unbound pavement materials for Virgina's roads, instead of using conventional moisture and density. They observed that the E_{LWD} increases with increasing density and that as moisture content increases E_{LWD} decreases.

Mohammad et al. (2009) performed a comparative testing program between LWD tests and laboratory cyclic triaxial tests, with a goal of predicting laboratory resilient moduli for subgrade soils (M_{rsub}) in terms of E_{LWD}. Statistical analyses were carried out on the data. The results were presented using two models. The first model relates M_{rsub} with E_{LWD}. The statistical coefficients obtained from the model including coefficient of determination (R^2) and square root of the mean square error (RMSE) were 0.54 and 9.66 MPa, respectively. The resulting model equation is given as:

$$M_{rsub} = 27.75 \times {E_{LWD}}^{0.18} \tag{2.26}$$

Due to the weakness of the correlation between the data, several physical properties of the soils were included in a second model to produce a better correlation ($R^2 = 0.7$ & $RSME = 7$ MPa). The soil property model predicts resilient modulus of subgrades in

terms of dynamic LWD soil moduli and moisture content (w) of the soil as expressed below:

$$M_{rs} = 11.23 + 12.46(E_{LWD})^{0.2} + 242.32\left(\frac{1}{w}\right) \tag{2.27}$$

where:

M_{rs} : Subgrade resilient modulus

E_{LWD} : Dynamic modulus

Fleming et al. (2007) carried out a comparative investigation between LWD and FWD. The authors reported no significant correlation exists between FWD and LWD moduli due to the different loading rates and levels used in the two testing procedures. However, the test results indicated that the ratio of soil stiffness between LWD and FWD typically ranged from 0.8 to 1.21, while R^2 varied from 0.5 to 0.9.

The relationship between the strength of laterite subgrade soils from laboratory CBR tests and LWD elastic soil modulus was explored in experimental work conducted by Rao et al. (2008). They found that the CBR values correlated well to the LWD moduli for laterite subgrade soils according to the following linear model which produced an R^2 of 0.96 and a standard error of 2.47 MPa. Laterite is a reddish soil, rich in iron and aluminum found in India.

$$CBR = -2.7543 + 0.2867E_{LWD} \tag{2.28}$$

where:

E_{LWD} : Dynamic LWD soil modulus

In 2006, the Minnesota Department of Transportation (MnDOT) conducted a series of LWD tests on various laboratory soil specimens as part of the Local Road Research Board (LRRB 2006-20) investigation. In this work, a standard LWD testing procedure was developed. It was found that utilizing a 200 mm LWD loading plate with 10 kg of weight dropped from a 500 mm height provides an adequate influence depth for a lift of compacted materials. Also, it was recommended to place the loading plate at a depth of 15 cm below the desired surface as well as preform three pre-loading seating drops before starting the field test measurements (i.e. three loading drops) in order to eliminate the effects of plastic deformation of loose or rutted surface materials (Davich et al., 2006).

Steinert et al. (2005) examined the suitability of utilizing LWD to assess compaction adequacy of unbound granular pavement layers based on LWD soil stiffness measured at optimum moisture content (OMC). In this study, two major testing approaches were performed in 12 selected sections located in New England: (1) LWD to determine soil modulus and (2) nuclear density gauge to measure in-situ soil density with field moisture content. It was concluded that both moisture content and degree of compaction have a unique influence on unbound modulus. As summarized in Table 2.4, the authors relate degree of compaction of pavement granular materials in New England

Table 2.4: Relationship Between Degree of Compaction and LWD Moduli (Adapted from: Steinert et al., 2005)

Degree of Compaction (%) (AASHTO T-180)	LWD Soil Modulus (psi) (ASTM D4120)
90	92
95	115
98	130
100	139

with composite soil modulus obtained from in-situ LWD test at OMC for base and subbase pavement layers.

2.1.6.2 Pavement Assessment Using DCP

The dynamic cone penetrometer (DCP), which was first manufactured in the 1960's in South Africa, is utilized for in-situ evaluation of unbound pavement materials in several states including Florida, Louisiana, Minnesota, and Ohio. As shown in Figure 2.14, this equipment provides continuous measurements of soil properties with the depth.

DCP testing includes dropping an 8 kg weight from a height of 575 mm to drive a 16 mm diameter steel rod into a granular base or underlying subgrade soil while measuring penetration depth per blow. DCP data can be expressed in several ways. The most common is the penetration index (PI_{dcp}). The PI_{dcp} represents the ratio of penetration depth in mm to the number of blows (N). Another index, known as the Dynamic Cone Penetration Index (DCPI), is the slope of the plot of DCP readings versus depth at any point. The DCPI, also termed penetration rate (PR), provides an indication about granular pavement materials resistance with higher values indicating lower soil stiffness, and the opposite for lower values. (National Cooperative Highway Research Program, 2009).

MnDOT conducted a study to use DCP as a construction quality assurance test for evaluating in-situ pavements materials. Based on the results of this study, a DCP specification was developed in 1998 for utilization on aggregate base. Several modifications have been added to the specification including moisture content and gradation in order to cover a wide range of granular materials characteristics (Siekmeier, 2009).

Due to the complexity involved in determining resilient moduli from lab testing, a group of correlations have been proposed between Mr and DCPI. Table 2.5 is a list of the published regression models relating these variables.

Many experimental correlations were developed by federal agencies to predict CBR of unbound material in terms of DCPI. Table 2.6 summarizes these equations along with their associated references.

Table 2.5: Summary of Correlations between M_r and DCPI

Proposed Relationship	Soil Type	Reference
$M_r = 7013.056 - 2040.783 \ln(DCPI)$	Fine Grained	Hassan, 1996
$\log M_r = 3.04785 - 1.0616 \log(DCPI)$	Fine Grained	South Africa, 2000
$M_r = a_0 \left(\frac{DCPI}{\log C_u}\right)^{a_1} (W^{a_2} + {\gamma_d}^{a_3})$	Coarse Grained	George and Uddin 2000
$M_r = a_0 (DCPI)^{a_1} \left(\gamma_d^{a_2} + \left(\frac{L.L}{w}\right)^{a_3}\right)$	Fine Grained	George and Uddin 2000
$M_r = 357.87 \times (DCPI)^{-0.6445}$	Fine Grained	Pandey et al. 2003
$M_r = 78.05 \times (DCPI)^{-0.6645}$	Coarse Grained	Chen et al. 2005
$M_r = \frac{1045.9}{DCPI^{1.096}}$	Fine Grained	Mohammad et al. 2009
$M_r = 3.86 + 2020.2 \left(\frac{1}{DCPI^{1.46}}\right) + 619.4 \left(\frac{1}{w^{1.27}}\right)$	Fine Grained	Mohammad et al. 2009
$M_r = 2555 \left(\frac{292}{DPCI^{1.12}}\right)^{0.64}$	Coarse Grained	Ho et al. 2012

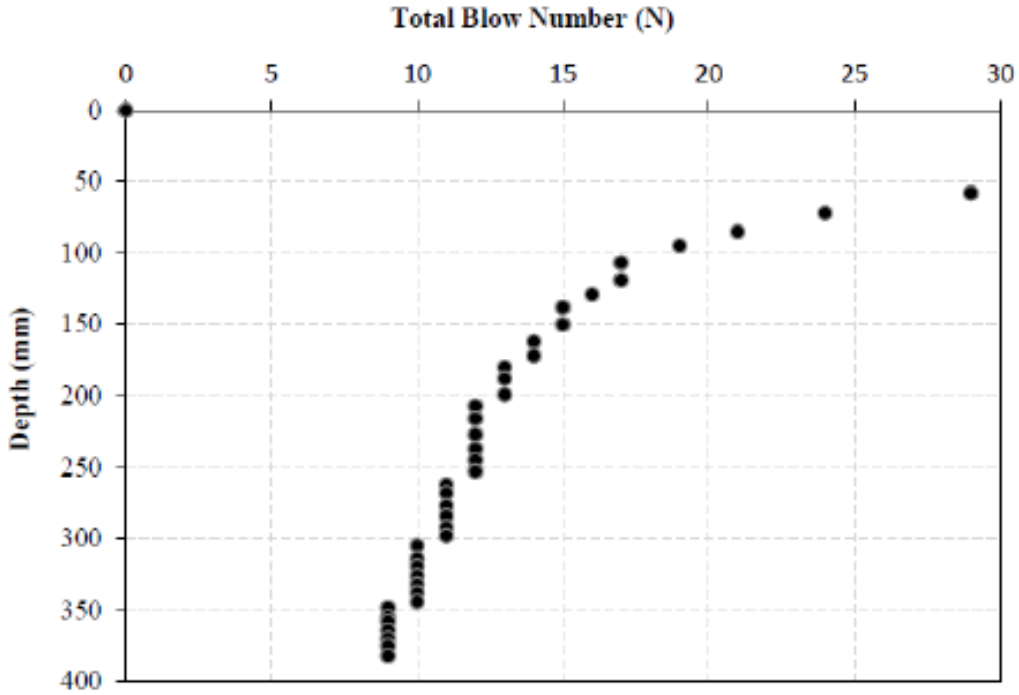

Figure 2.14: Typical DCP Results

Table 2.6: Summary of Correlations Between CBR and DCPI (Adapted from: Dai and Kermer, 2006)

Proposed Relationship	Reference
$\log(CBR) = 2.62 - 1.27\log(PR)$	Kleyn, 1975
$\log(CBR) = 2.56 - 1.15\log(PR)$	McElvancy, 1991
$\log(CBR) = 2.20 - 0.7\,(\log(PR))^{1.5}$	Livneh et al, 1987
$\log(CBR) = 2.81 - 1.32\log(PR)$	Harison, 1989
$\log(CBR) = 2.61 - 1.27\log(PR)$	Kleyn, 1992
$\log(CBR) = 2.465 - 1.12\log(PR)$	USACE, 1992
$CBR = \frac{292}{DCPI^{1.12}}$	Webster et al, 1994
$\log(CBR) = 2.669 - 1.065\log(PR)$	Ese et al, 1994
$\log(CBR) = 2.53 - 1.144\log(PR)$	Coonse, 1999
$\log(CBR) = 1.40 - 0.55\log(PR)$	Gaber, 2000
$\log(CBR) = \frac{2559.44}{(DCPI^{1.84} - 7.35) - 1.41}$	Nazzal, 2003
$CBR = \frac{5.1}{PR^{0.2} - 1.41}$	Abu-Frasakh et al., 2004
$\log(CBR) = 67.898 - 17.483\ln(PR)$	Sahoo & Reddy, 2009

2.1.6.3 Pavement Assessment Using FWD

The falling weight deflectometer (FWD) is a nondestructive testing device, which has been utilized since 1980 to evaluate in-situ conditions of highway and airfield pavements. This device is a trailer-mounted apparatus capable of applying dynamic impulse loads to a pavement surface, simulating the duration and force of various wheel loads. The duration of the impulse load varies between 25 and 30 µsec (Dean et al., 2006).

The general procedure for conducting FWD tests is described in ASTM D4694-09. A typical FWD unit is positioned at any desired test location. The FWD consists of a circular loading plate and up to seven geophones (i.e. velocity transducers) suspended from a trailing arm mounted to the trailer. During testing, the vehicle is driven to the desired location and stopped, the geophones are lowered onto the location, then the specified mass is hydraulically raised to the proper height and released to provide the required impulse force to the pavement. The surface deflections generated from the dropped weight are determined using the geophones. The vertical deflections recorded by the sensors can be used to estimate elastic moduli of pavement layers based on iterative back-calculation methods. Generally, four different loading levels, with weights dropped from four heights, are performed at each location. This test can be completed in less than 2 minutes, allowing numerous locations to be tested daily.

Several computer programs are currently available to handle the sophisticated iterative back-calculation analysis including: ELSYM5 (developed by the University of California, Berkeley), EVERSTRESS (developed by the Washington State DOT), and KENLAYER (developed by the University of Kentucky, Lexington). These software packages allow the user to input to varying elastic moduli of pavement materials in an iterative process until a match to the observed pavement deflection is satisfied.

FDOT carried out a FWD research project to assess the suitability of using FWD data for pavement design purposes. In this study, FWD surface deflections were compared with those measured from the Dynaflect to validate the accuracy of FWD data. The Dynaflect is an older nondestructive testing device, capable of producing pavements deflections caused by an oscillating load produced from a dynamic force. It has a limitation of only being able to apply one set of sinusoidal loads. The results indicate a strong correlation between soils moduli measured from these devices with R^2 of 0.88:

$$E_{Dyn} = 3.3863 \left(E_{FWD}^{0.898}\right) \tag{2.29}$$

where:

E_{Dyn}: Predicted Dynaflect soil modulus

E_{FWD}: Soil modulus measured based on FWD data

It was found that the following power model yields the most appropriate in-situ soil moduli from FWD for designing structural pavement layers Choubane and McNamara (2000).

$$E_{FWD} = 0.03764 \left(\frac{P}{d_r}\right)^{0.898} \tag{2.30}$$

where:

P: Applied load (lbs)

d_r Deflection measured at radial distance of 36 inches

FDOT also studied the feasibility of using nondestructive testing techniques for pavement evaluation. The pavement material responses at low strain levels were measured using FWD and the Seismic Pavement Analyzer (SPA). Based on 22 pavement sites, it was concluded that the surface deflection produced from SPA is lower than the surface deflection obtained from FWD testing. An exponential model has been suggested to predict modulus of asphalt pavement Tawfiq et al. (2000). This model is presented as:

$$\begin{aligned} E_n &= E_{max} \exp^{-\beta x} \\ \beta &= 4.67 + 0.004t \end{aligned} \tag{2.31}$$

where:

E_n: Asphalt pavement modulus at any deflection level (MPa)

E_{max}: Maximum pavement modulus at deflection level $\leq 10^{-3}$ mm

β: Factor depends on pavement layer thickness (mm^{-1})

t: Asphalt pavement thickness (mm)

x: Maximum surface deflection at point load (mm)

Tanyu et al. (2003) implemented a comparison between resilient moduli measured from conventional laboratory testing methods with elastic moduli determined from a large-scale model experiment (LSME) and FWD. The schematic cross section of the LSWE is shown in Figure 2.15

The testing program was performed on a granular base course and two industrial byproduct materials utilized as subbase. The results of this investigation indicated that the laboratory resilient modulus of the industrial byproduct materials (slag and fly ash) tend to be lower than those obtained from LSME and FWD tests by a factor ranging from 1.5 to 4. Also, it was found that the bulk stress (Θ) estimated from in-situ field tests might be much lower than the bulk stress inferred from laboratory tests. The bulk stress determined from field tests ranged from 13 to 104 kPa, while those measured from triaxial laboratory test ranged from 84 to 718 kPa.

Thottempudi (2010) studied the difference between laboratory resilient moduli and FWD back-calculated elastic moduli for various unbound pavement layers. It was concluded that on average, the back-calculated resilient modulus measured from FWD pavement surface deflections is four times larger than laboratory resilient modulus.

Two nondestructive testing techniques including FWD and Portable Seismic Pavement Analyzer (PSPA) have been used to evaluate and compare asphalt concrete (AC) pavement moduli with those obtained from laboratory dynamic modulus tests. The results produced a good statistical correlation among the moduli of asphalt concrete pavement measured from FWD, PSPA, and laboratory dynamic tests at corresponding temperatures and load frequencies (Ho et al., 2012). These correlations are expressed as:

$$E_{FWD} = 0.882 E_{DM} \tag{2.32}$$

$$E_{PSPA} = 0.978 E_{DM} \tag{2.33}$$

$$E_{FWD} = 0.868 E_{PSPA} \tag{2.34}$$

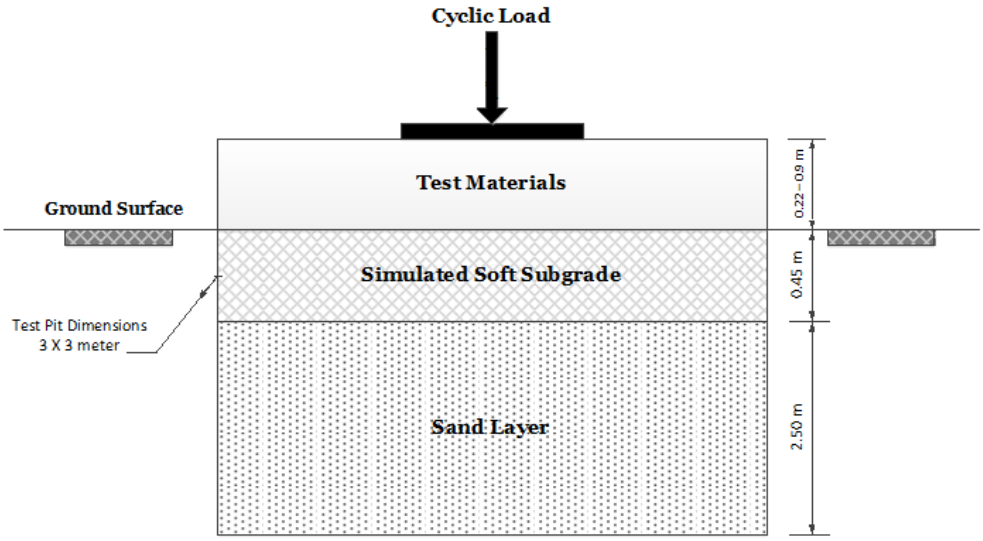

Figure 2.15: Schematic Cross Section of the LSME (After: Tanyu et al. (2003))

where: E_{FWD}: FWD back-calculated modulus
E_{PSPA}: PASPA modulus of asphalt concrete
E_{DM}: Laboratory dynamic modulus of asphalt concrete

Texas Department of Transportation (TxDOT) in cooperation with FDOT carried out an investigation to compare laboratory resilient moduli of unbound pavement materials with in-situ pavement moduli back-calculated from FWD data. In this research, the mechanistic-pavement design (M-E PDG) approach for determining resilient modulus was followed. The M-E PDG incorporates the effect of moisture content, bulk stress, and octahedral shear stress on resilient moduli as given by:

$$M_r = k_1 P_a \left[\frac{\Theta - 3k_4}{Pa}\right]^{k_2} \left[\frac{\tau_{oct}}{Pa} + 1\right]^{k_3} \tag{2.35}$$

where:

Θ	Bulk stress
T_{oct}	Octahedral shear stress
P_a	Atmospheric pressure
k_1, k_2, k_3	Model coefficients
k_4	Effect of moisture variation on the magnitude of bulk stress

Using Equation 2.35, the resilient modulus was determined based on the field stress conditions (i.e. bulk and octahedral shear stresses) developed under the influence of FWD load level. Based on comparison results, the researchers established different empirical factors (i.e. conversion factors- CFs) to convert FWD back-calculated modulus to resilient modulus. The results indicated that the CFs (CF = in-situ M_r/ FWD-M_r) ranged from 0.25 to 0.40, and these factors fit well FWD modulus data in a power regression model (Ho et al., 2012).

Ping et al. (2001) conducted a study to evaluate in-situ bearing behavior of different types of Florida pavements. In this study, the pavement layers properties were

characterized using the falling weight deflectometer (FWD), the plate bearing test (PLT), and the nuclear density gauge (NDG). In addition, disturbed soil samples were collected from the same pavements layers, and these samples were utilized to determine resilient modulus at both optimum and field moisture content, and at different stress states.

The results showed that the in-situ pavement moduli back-calculated from FWD are higher than resilient moduli obtained from laboratory triaxial test (CT). The ratio of FWD modulus to laboratory resilient modulus ($M_{r,FWD}/M_{r,CT}$) ranged from 1.5 to 1.9. It was also found that resilient modulus values measured at field moisture content are better correlated with in-situ FWD modulus values than resilient moduli measured at optimum moisture content.

2.1.6.4 Pavement Assessment Using NDG

The NDG is widely utilized to evaluate in situ unit weight and moisture content. Although NDG testing simple and fast, this nuclear device regulatory requirements are very cumbersome. Therefore, many agencies have investigated alternative testing methods to assess pavement layer quality.

The Virginia Department of Transportation (VDOT) examined the suitability of using LWD, the soil stiffness gauge (SSG), and DCP to monitor unbound base and the underlying subgrade soils instead of NDG. The SSG is a nondestructive device, which applies small dynamic forces at frequencies between 100 to 200 Hz, while measuring surface deflections that are converted to soil stifness. The data indicated that there was high spatial variability, thus no significant correlations were found. The results also showed that NDG water content had an unique effect on layers moduli determined by all three devices, particularly the LWD (Hossain et al., 2010).

Salgado and Yoon (2003) conducted a research project which was sponsored by the Indiana Department of Transportation (INDOT) to investigate the possibility of utilizing DPC as an alternative non-nuclear field test for evaluating compacted subgrade soils. Several construction sites were tested using DCP and NDG, allowing a comparison between density and moisture content and dynamic penetration index (DPI). The results indicated that DPI decreases with increasing dry unit weight of the soil and slightly increases with decreasing water content. An empirical equation was derived from the results of field-testing that can be used to predict dry unit weight of clayey sand subgrade as a function of DPI:

$$\gamma_d = \left(10^{1.5} \times PI^{-0.14} \times \sqrt{\acute{\sigma_v}/P_a}\right)^{0.5} \times \gamma_w \tag{2.36}$$

where:

PI :Penetration index (mm/blow)

$\acute{\sigma_v}$:Vertical Overburden Pressure (kPa)

γ_w :Water Unit Weight (9.81 kN/m^3)

TXDOT implemented a field-testing program to explore the possibility of establishing an empirical correlation between NDG density and SSG stiffness. SSG and NDG tests were conducted at six road construction sites. It was found that soil stiffness generally increases as soil unit weight increases, however, a very weak correlation with coefficient of determination ($R^2 = 0.35$) was identified. In summary, NDG density is much less sensitive to the quality of unbound granular materials than SSG stiffness (Chen et al., 1999).

2.1.6.5 Pavement Assessment Using CBR

Laboratory CBR testing conducted in accordance with ASTM standard specification D1883 and Florida's version of the bearing test, the LBR conducted in accordance with State Materials Office (2000) FM 5-515, 2000 are similar and therefore related in several ways. The simplest relationship has the LBR being equivalent to 1.25*CBR. FDOT suggests the following correlation between CBR and Mr, which can be used to predict design subgrade resilient modulus Ho (1992).

$$M_r\,[psi] = 10^{0.7365 \log LBR} \times 809 \tag{2.37}$$

The results of this study yielded a correlation between LBR and soil support value (SSV). The latter parameter, is defined by AASHTO as "an index number which expresses the relative ability of a soil or aggregate mixture to support traffic loads through a flexible pavement structures". The following equation presents the model proposed by Ho (1992):

$$SSV = 4.596 \log LBR - 0.576 \tag{2.38}$$

Substituting Equation 2.37 into Equation 2.38 yields the general correlation model presented in Equation 2.39. This model can be used to estimate the design Mr. However, it is not recommended to use the Mr-prediction model with LBR values greater than 40 (FDOT 625-10, 2008):

$$SSV = 6.24 \log (M_r) - 18.76 \tag{2.39}$$

In 1986, the AASHTO guide for pavement design suggested using regression models to predict laboratory resilient modulus based on CBR values. Many studies have been conducted correlating the two parameters. Table 2.7 provides a list of prediction models.

2.1.6.6 Pavement Assessment Using Resilient Modulus Testing

Cyclic triaxial equipment is used in accordance with AASHTO T 307 resilient modulus testing to produce design resilient moduli (M_r) of unbound pavement materials. The stress-strain data of each cycle is recorded, and then the resilient modulus is measured by dividing applied deviator stress by the recoverable axial strain as shown in Figure 2.16.

$$M_r = \frac{\sigma_d}{\epsilon_r} \tag{2.40}$$

Table 2.7: Summary of Correlations between Mr and CBR

Proposed Relationship	Reference
M_r[ksi] = 1.42 ×CBR	Heukelom and Klomp (1962)
M_r[ksi] = 5.409 ×$CBR^{0.711}$	Green and Hall (1975)
M_r[ksi] = 2.554 ×$CBR^{0.64}$	Powell et al (1984)
M_r[ksi] = 3.116 ×$CBR^{0.47797}$	Webb and Campbell (1986)
M_r[ksi]=$k_1\sigma_d^{k_2}$	Lofti et al (1988)
$k_1=10^{(1.0016+0.043CBR)}$	
$k_2 = -\left(\frac{1.9577}{CBR} + 0.1705\right)$	
M_r[ksi] = 3 ×$CBR^{0.65}$	South African Council (1995)
M_r [ksi] = 1.5 ×CBR (Fine Grained)	Virginia DOT (2003)
M_r [ksi] = 3 ×CBR^0.65 (Course Grained)	
M_r [ksi] = 1.2 ×CBR	Ohio DOT (2008)

where:
σ_d: Applied deviator stress
ε_r: Resilient strain
AASHTO T307 is very sophisticated and time-consuming. Therefore, the highway agencies tend to predict resilient modulus values from simple conventional test methods. Based on the state of stresses induced during the test, various M_r models have been developed. Song (2009) summarizes more than 12 models, which have been developed over the last 60 years, as shown in Table 2.8. They range from simple to much more complex power models. FDOT uses the bulk stress (Θ) model proposed by Seed et al (1967). Note that many of the model stress terms are normalized with atmospheric pressure (p_a) and that the model coefficients are: k_1, k_2, k_3, k_4 α, and β.

2.1.7 Other Small Diameter Probes

A search of additional small diameter PMT probes was conducted. The results of this research are presented here.

2.1.7.1 Purdue University Model Pressuremeter

Huang (1986) developed a calibration chamber that included a model PMT to test cohesive soils, (see Figure 2.17). The model PMT was 4.73 inches (111 mm) in length and 0.473 inches (11.1 mm) in diameter, which yields an L/D ratio of 10. The author found that the model pressuremeter produced agreeable undrained shear strength results with corresponding triaxial tests at strain rates between 0.1 and 0.73% per minute. The author also determined that borehole disturbance can cause significant variations in the lateral earth pressure and initial shear modulus, which affects the interpretation of undrained shear strength.

Table 2.8: Summary of current prediction models for M_r (Adapted from: Song (2009))

Model (M_r)	Reference	Remark
M_r=k$_1$ P_a $(\sigma_3/P_a)^{(k_2)}$	Dunlap (1963)	k_1 and k_2: Model constants
$M_r = k_1 (\Theta)^{k_2}$	Seed et al (1967)	$\Theta = \sigma_1 + \sigma_2 + \sigma_3$
$M_r = k_1 P_a \left(\frac{\Theta}{P_a}\right)^{k_2}$	Seed et al. (1967)	P_a: Atmospheric pressure
$M_r = k_1 \sigma_1 \sigma_{oct}^{k_2} \tau_{oct}^{k_3}$	Shackel (1973)	$\sigma_{oct} = \Theta/3$
$M_r = k_1 P_a \left(\frac{\Theta}{P_a}\right)^{k_2} \left(\frac{\sigma_d}{P_a}\right)^{k_3}$	Uzan (1895)	$\sigma_d = \sigma_1 - \sigma_3$
$M_r = k_1 P_a \left(\frac{\Theta}{P_a}\right)^{k_2} \left(\frac{\tau_{oct}}{P_a}\right)^{k_3}$	Witczak and Uzan (1988)	$\Theta = \sigma_1 + \sigma_2 + \sigma_3$
$M_r = k_1 P_a \left(\frac{\sigma_3}{P_a}\right)^{k_2} \left(\frac{\sigma_d}{P_a}\right)^{k_3}$	Ni et al. (1993)	σ_3: Minor principle stress
$M_r = A (n_{max} - n) P_a \left(\frac{\Theta}{P_a}\right)^{0.5}$	Kolisoja (1997)	n: Porosity of aggregate
$M_r = k_1 P_a \left(1 + \frac{\sigma_3}{P_a}\right)^{k_2} \times \left(1 + \frac{\sigma_d}{P_a}\right)^{k_3}$	Ni et al. (2002)	σ_1: Major principle stress
$M_r = k_1 P_a \left(1 + \frac{\Theta}{P_a}^{k_2}\right) \times \left(1 + \frac{\sigma_d}{P_a}\right)^{k^3}$	Ooi et al. (2004)	σ_2: Intermediate stress
$M_r = k_1 P_a \left(1 + \frac{\Theta}{P_a}\right)^{k_2} \times \left(1 + \frac{\tau_{oct}}{P_a}\right)^{k_3}$	Ooi et al. (2004)	$\tau_{oct} = \sqrt{\frac{2\sigma_d}{3}}$
$M_r = k_1 P_a \left(\frac{\Theta}{P_a}\right)^{k_2} \left(1 + \frac{\tau_{oct}}{P_a}\right)^{k_3}$	ARA Inc. (2006)	k_1, k_2 and k_3: Model constants
$M_r = k_1 P_a \left(\frac{\sigma_b - 3k_6}{P_a}\right)^{k_2} \times \left(k_7 + \frac{\tau_{oct}}{P_a}\right)^{k_3} + \alpha_1 (u_a - u_w)^{\beta_1}$	Gupta et al. (2007)	α_1&β_1 Regression constants

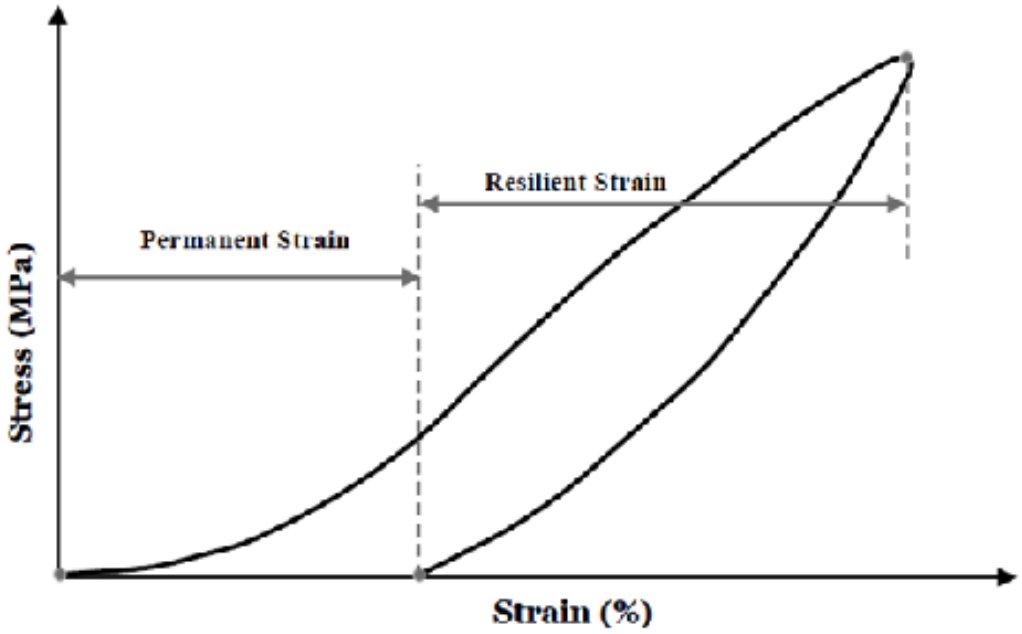

Figure 2.16: Granular Materials Response under One Cycle Loading (After AASHTO T307)

2.1.8 Test Chamber for PMT Tests

Jewell et al. (1980) used the Cambridge Self-Boring PMT in a large triaxial cell with a soil sample approximately 3.28 ft (1 m) in diameter and 3.28 ft (1 m) high. This test setup allowed a full-sized PMT to be placed in the soil with a probe length of 19.69 inches (500 mm) and a diameter of 3.17 inches (80.4 mm) with a L/D ratio of 6.22. Figure 2.18 shows the chamber setup used. The authors evaluated effective friction angle (ϕ') and Poisson's ratio (ν), and found them to compare with other published results obtained from a Simple Shear Apparatus.

2.1.9 FDOT Specification for QC of Base Courses

FDOT (2018) Standard Specifications for Road and Bridge Construction Section 200-7 covers the QC criteria that must be achieved for a base course. According to Section 120-8 a lot is a single lift of finished base course not exceeding 500 feet (152.4 meters). The Specification minimum frequency for density testing is that each lot check must be performed by QC and every 4 lots must be verified by the third party Verification.

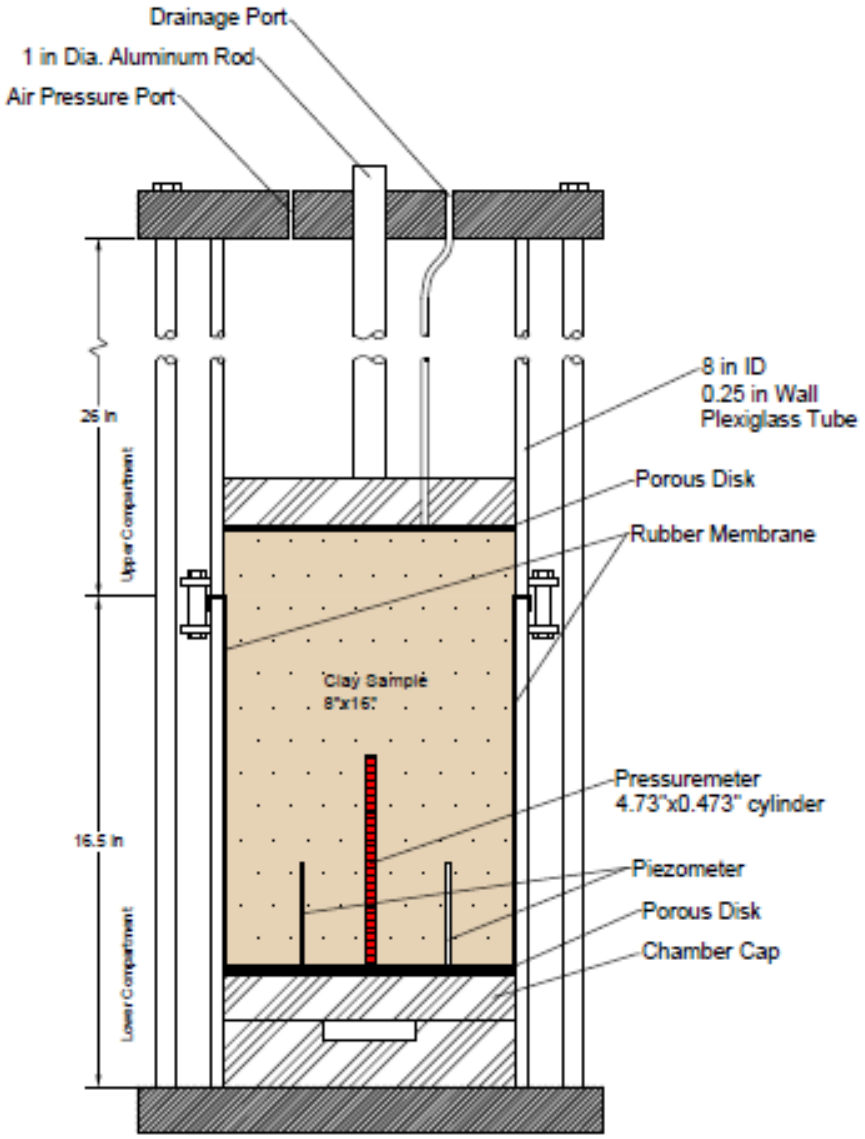

Figure 2.17: Triaxial Chamber with PMT (After: Huang, 1986)

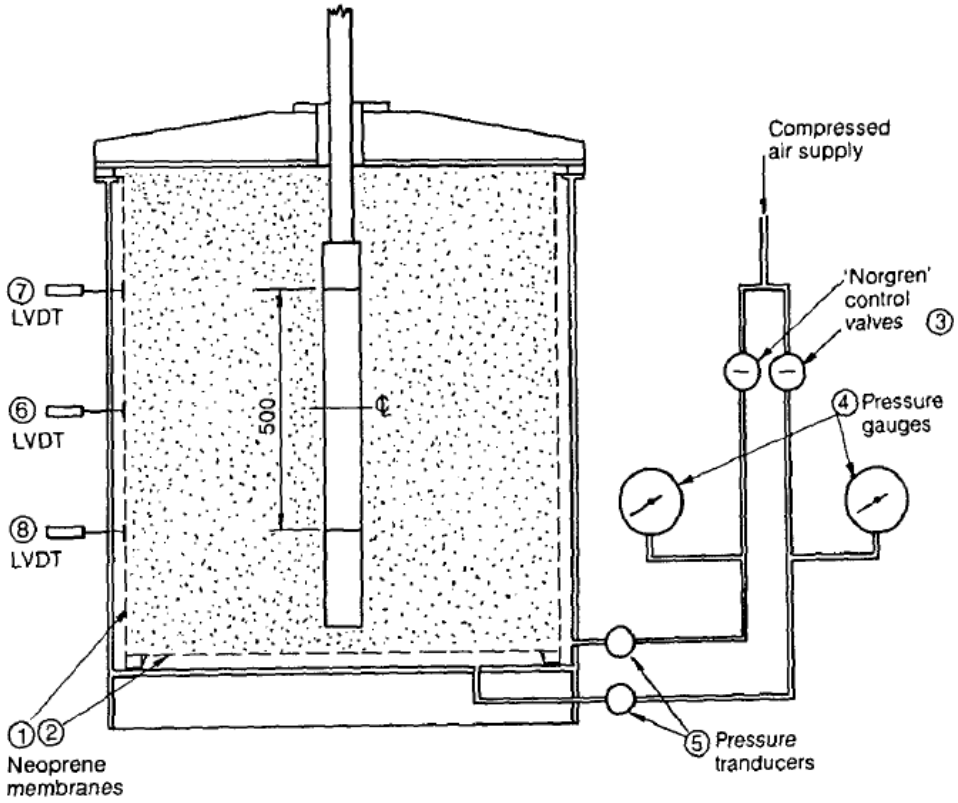

Figure 2.18: PMT Test Chamber (From Jewell et al., 1980)

2.1.10 Instrumentation of PMT Testing

2.1.10.1 Fully Automated PMT Test

Law (1984) presents the implementation of computer and servo-controlled self-bored Cambridge pressuremeter testing. The author's system is capable of four different tests: stress controlled test, strain rate controlled test, strain level controlled test, and cyclic test. They developed an automated control system which used a compressed gas cylinder to provide the applied pressure to the pressuremeter, a schematic of the system is shown in Figure 2.19. This nitrogen based control system was capable of cyclic testing as fast as 15 seconds per cycle (0.067 Hz) and test soils at pressures up to 87 psi (600 kPa).

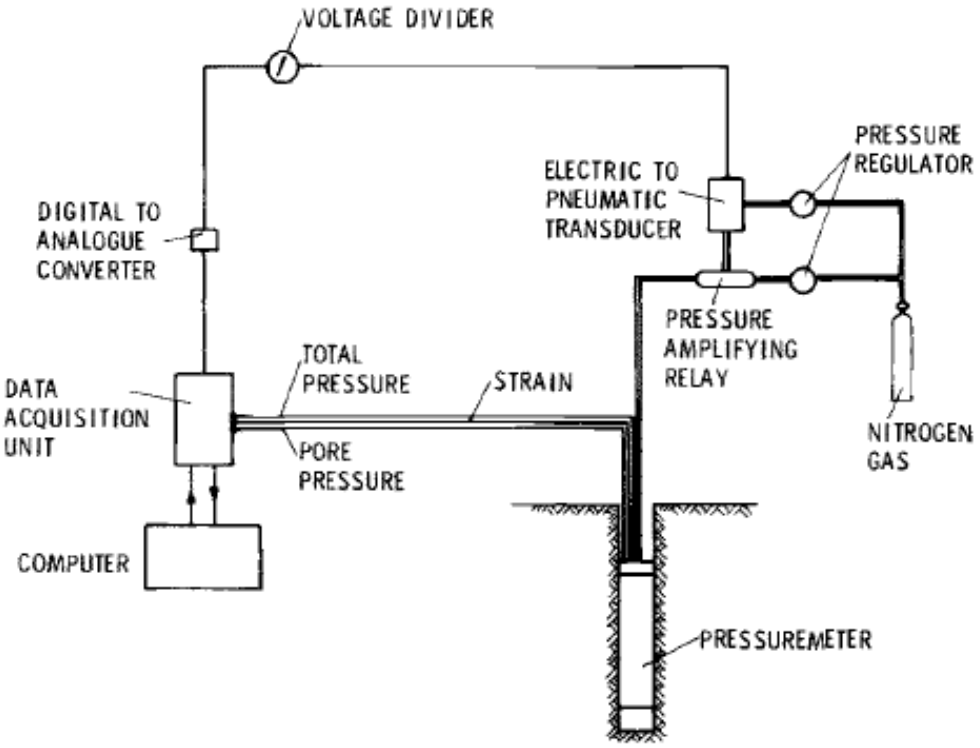

Figure 2.19: Schematic of Computer Controlled PMT Testing and Data Acquisition System

Chapter 3

Description and Basic Soil Properties of Test Sites

3.1 Test Site Locations

Four sites within 30 minutes of the FIT campus were selected to conduct the testing program. Two were on the campus and two were in the surrounding areas as shown in Figure 3.1 . Soil samples from these sites were collected and transported to the lab in order to determine their basic engineering properties. The following lab testing was completed.

- Grain-size analyses with Atterberg limits.
- Moisture-density testing.
- Limerock bearing ratio (LBR) testing.
- Resilient modulus (M_r) testing.

The lab test results were utilized to validate the quality of the materials. The resilient moduli results will be presented separately. Field tests were conducted at four sites in Brevard County, Florida. The sites were:

- Florida Tech's Olin Complex Overflow Parking Area,
- Florida Tech's Southgate Field,
- Cypress Landing Development's Potenza Drive in West Melbourne and
- Heritage Parkway in Melbourne.

Field samples were collected and tested at the SMO. The site descriptions and results from these tests are presented in the following sections.

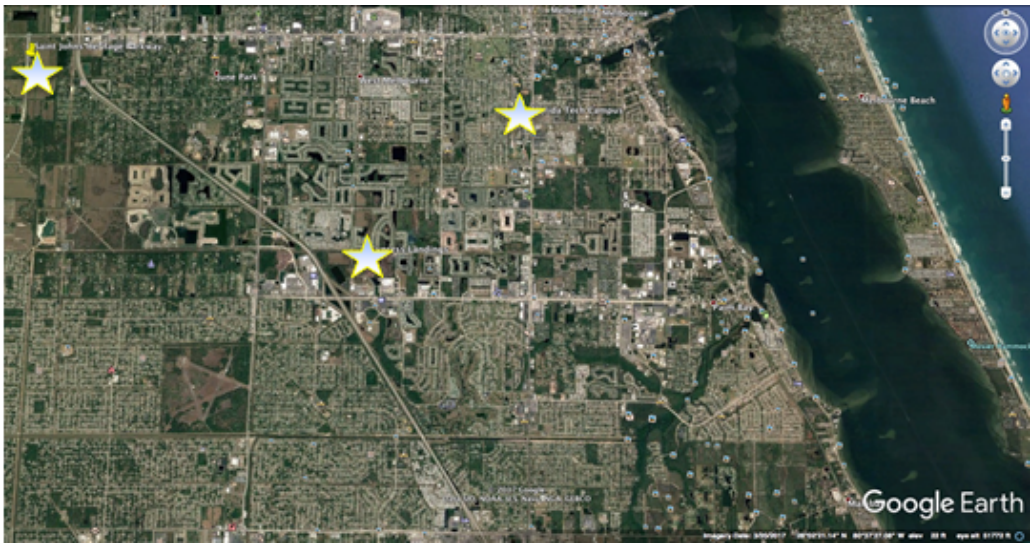

Figure 3.1: Google Earth Image showing relative location of test sites

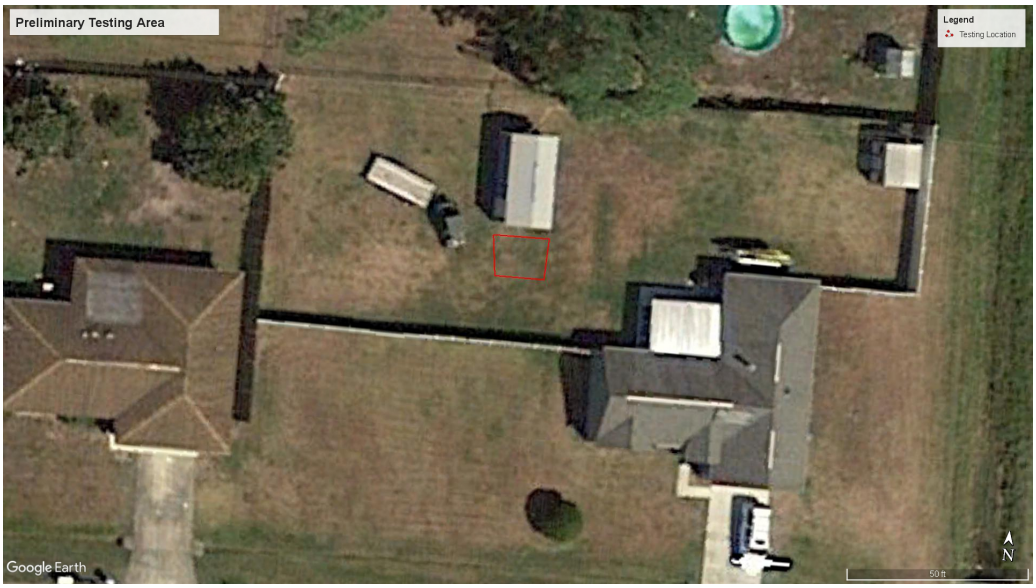

Figure 3.2: Aerial Image of Preliminary Testing Area

3.1.1 Preliminary Test Site

A grassy area located at (N 28° 1' 53.076", W 80° 41' 0.326") and shown in Figure 3.2 was used to conduct testing for the two preliminary probe designs. Note that the red box marks the area where testing occurred. This site is an undeveloped lot that was covered with fill and grass lawn.

Figure 3.3: Satellite Map of Testing Area in the Florida Tech Southgate Athletic Field

3.1.2 Florida Tech Southgate Athletic Field

Florida Tech's Southgate Field is a recreational field located on the campus, between Babcock Street (SR 507), University Boulevard, and Albemarle Street (Jansen, 2017). This grass-covered field consists of subgrade type sand with a layer thickness of at least 3 feet. Twelve test locations, running east to west and 25 feet apart, were selected to produce a 300 foot long testing path. Figure 3.5 shows a satellite view of the test site; tests were conducted along the red line indicated on the image. Figure 3.4 shows a generalized schematic view of each test location across the site. Table 3.1 shows the types and number of tests conducted on this site. Testing at each location included SDPMT, NDG, LWD, CIT and DCP tests. Both the Zorn and Dynatest LWD's were used during testing. SDPMT and NDG tests were performed at depths of 6 and 12 inches below the ground surface. LWD, CIT and DCP tests were carried out within 3 feet of the SDPMT tests.

Disturbed soil samples were collected and transported to the SMO lab for testing to identify basic index properties. Figure 3.6 shows the grain size analysis for this soil. The soil classified as a poorly graded sand (SP) according to the USCS; and A-3 sand according to AASHTO. Atterberg limit testing indicates that the soil is non-plastic. Figure 3.7 shows the results of modified Proctor tests, showing that the sand has a maximum dry unit weight of 100 lb/ft^3 (15.7 kN/m^3) and an optimum moisture content of 12%. LBR testing produced a value of 7. These basic physical properties are summarized in Table 3.2.

Table 3.1: Number of Tests per Location at the Florida Tech Southgate Athletic Field Site

Test Location	Offset Distance [ft]	SDPMT-6 Tests	SDPMT-12 Tests	Nuclear Density Tests [6/12 in]	Clegg Impact Hammer	LWD Zorn	LWD Dynatest	DCP Tests
401	0	2	2	1/1	2	1	1	1
402	25	2	2	1/1	2	1	1	1
403	50	2	2	1/1	2	1	1	1
404	75	2	2	1/1	2	1	1	1
405	100	2	2	1/1	2	1	1	1
406	125	2	2	1/1	2	1	1	1
407	150	2	2	1/1	2	1	1	1
408	175	2	2	1/1	2	1	1	1
409	200	2	2	1/1	2	1	1	1
410	225	2	2	1/1	2	1	1	1
411	250	2	2	1/1	2	1	1	1
412	275	2	2	1/1	2	1	1	1
Total:		24	24	12/12	24	12	12	12

Table 3.2: Average Index properties of Subgrade Soil at Southgate Field

Property	Test Results	Comments
Max Dry Unit Weight	100.0 lb/ft^3	
Optimum Moisture Content	12.0%	
Field Dry Unit Weight	91.5 lb/ft^3	RC=91.5%
Field Moisture Content	4.6%	
Uniformity Coefficient	2.60	
Curvature Coefficient	1.03	
Gravel Fraction	Zero	
Fine Content	1%	
Soil Classifications	A-3	AASHTO
	SP - Poorly Graded Sand	USCS
Atterberg Limits	NP	
LBR (Lab Soaked)	7	
CBR* (Field Unsoaked)	7	

*: Field CBR was predicted from DCP test as a function of dynamic penetration index value.

3.1.3 Florida Tech Olin Complex Overflow Parking

Florida Tech's Overflow parking is located at the southwest corner of the Olin Complex, at the southern end of of Country Club Road (Jansen, 2017). Testing was conducted in the south west corner of the Olin Complex in an area between the overflow parking lot and the retention pond. Twelve test locations were selected running south to north, every 25 feet across the site. A satellite view of the site is shown in Figure 3.8; the tests were conducted along the red line. Figure 3.9 is a photo of the flagged test locations at this site, and Figure 3.10 shows a generalized schematic of test points at each test location. At each location, SDPMT, LWD, CIT, DCP and NDG tests were performed. Both the Zorn and Dynatest LWD's were used during testing. Table 3.3 summarizes the types and number of tests conducted on the site. Samples were collected across the test site to determine the index properties of the soil. Figure 3.11 illustrates the grain size data which was used to determine that the subgrade soil classified as poorly graded sand (SP) according to USCS and A-3 according to AASHTO.
Figure 3.12 shows the modified Proctor results, which produced a maximum dry density of 111.1 lb/ft^3 at an optimum moisture content of 10.5%. The LBR of this soil was 10, and Atteberg limits indicated that the soil is non-plastic. A summary of these properties is shown in Table 3.4.

3.1.4 Cypress Landing Subgrade

Cypress Landing is a new residential development located at the southeast corner of Imagine Way and Litchfield Drive, which is located west of Hollywood Boulevard and

Table 3.3: Number of Test per Location at the Florida Tech Olin Complex

Test Location	Offset Distance [ft]	SDPMT-6 Tests	SDPMT-12 Tests	Nuclear Density Tests [6/12 in]	Clegg Impact Test	LWD Zorn	LWD Dynatest	DCP Tests
201	0	2	2	1/1	2	1	1	1
202	25	2	2	1/1	2	1	1	1
203	50	2	2	1/1	2	1	1	1
204	75	2	2	1/1	2	1	0	1
205	100	2	2	1/1	2	1	1	1
206	125	2	2	1/1	2	1	1	1
207	150	2	2	1/1	2	1	1	1
208	175	2	2	1/1	2	1	1	1
209	200	2	2	1/1	2	1	0	1
210	225	2	2	1/1	2	1	1	1
211	250	2	2	1/1	2	1	1	1
212	275	*	*	1/1	2	1	0	1
Total:		24	24	12/12	24	12	9	12

* - Untestable Due to Construction in Area

Table 3.4: Average Index properties of Subgrade Soil at FIT Olin Complex

Property	Test Results	Comments
Max Dry Unit Weight	111.1 lb/ft^3	
Optimum Moisture Content	10.5%	
Field Dry Unit Weight	105.8 lb/ft^3	RC=95%
Field Moisture Content	1.6%	
Uniformity Coefficient	2.42	
Curvature Coefficient	1.38	
Gravel Fraction	Zero	
Fine Content	1%	
Soil Classifications	A-3	AASHTO
	SP - Poorly Graded Sand	USCS
Atterberg Limits	NP	
LBR (Lab Soaked)	10	
CBR* (Field Unsoaked)	39	

*: Field CBR was predicted from DCP test as a function of dynamic penetration index value.

north of Palm Bay Road (CR 516), in West Melbourne Florida (Jansen, 2017). Twelve test locations were tested along the north side of Potenza Drive, extending west to east. Figure 3.15 shows the generalized test points at each location across the site. The soil at this test site was a poorly graded subgrade sand that was 12 inches thick. At each location SDPMT-12, NDG, CIT, LWD (Zorn and Dynatest), and DCP tests were conducted. An aerial view is shown in Figure 3.13, and Figure 3.9 shows the flagged test locations across the site.

Tests were conducted on April 19, 2017. Rainfall levels in the region prior to testing were much lower than normal, producing very dry conditions. Fieldwork began approximately 8:00 AM. The temperatures ranged from 70 to about 80°F, and a 10-minute thunderstorm occurred at approximately 2:00 PM causing the surface soils to become moist to a depth of about 2 inches (7.5 cm). Soil samples were collected and tested to obtain index properties. The sieve analysis produced the gradation shown in Figure 3.16. According to USCS it classified as poorly graded sand (SP) and AASHTO as an A-3 soil. As show in Figure 3.17, the modified Proctor optimum moisture content is 10%, at a maximum dry unit weight of 117.2 lb/ft^3 (18.4 kN/m^3). Atterberg limit results indicated that the soil is non-plastic, bearing ratio testing produced an LBR equal to 6. These results are summarized in Table 3.5.

3.1.5 Heritage Parkway

St. John Heritage Parkway includes 5.6 miles of two-lane access road located between the western most portions of Malabar Road in Palm Bay, Florida and US 192 just west of Interstate 95, in unincorporated Brevard County, Florida (Misilo III, 2018). The

Table 3.5: Average Index properties of Subgrade at Cypress Landing

Property	Test Results	Comments
Max Dry Unit Weight	117.2 lb/ft^3	
Optimum Moisture Content	10.0%	
Field Dry Unit Weight	112.0 lb/ft^3	RC=96%
Field Moisture Content	8.3%	
Uniformity Coefficient	2.72	
Curvature Coefficient	1.08	
Gravel Fraction	Zero	
Fine Content	2%	
Soil Classifications	A-3	AASHTO
	SP - Poorly Graded Sand	USCS
Atterberg Limits	NP	
LBR (Lab Soaked)	6	
CBR* (Field Unsoaked)	11	

*: Field CBR was predicted from DCP test as a function of dynamic penetration index value.

aerial view of the of the test site is shown in Figure 3.18 Testing was conducted in the East of the roadway near the edge of the base layer of pavement and the shoulder. Twelve test locations were selected, running north to south, every 50 feet down the site, which is indicated by the red line in Figure 3.18, and Figure 3.19 shows a schematic of the test points at each test location. Heritage Parkway consists of an 8 inch (20 cm) base course of untreated cemented coquina over the natural subgrade sand. Evaluating the NDG results at 6, 8, and 12 inch test depths (15, 20 and 30 cm), it was determined that approximately 12 inches (30 cm) of the base/subgrade material was uniformly compacted with similar densities allowing the testing of both 6 and 12 inch probes at this site.

Testing was conducted over 12 test locations along a 600 feet of roadway shoulder. In-situ tests including SDPMT, NDG, LWD, CIT were conducted every 50 feet on the unpaved shoulder within 3 feet of the edge of the paved section.

The results of the grain size analysis for the base materials are presented in Figure 3.20. It classified as a well-graded sand (SW) according to USCS, and an A-1-b according to AASHTO. Figure 3.21 displays modified Proctor tests results showing a maximum dry densities of 127.5 lb/ft^3 (19.5 kN/m^3) at the optimum moisture content of 7.4%. The basic physical properties of tested materials are summarized in Table 3.6.

Table 3.6: Average Index properties of Base Course at Heritage Parkway

Property	Test Results	Comments
Max Dry Unit Weight	127.5 lb/ft^3	
Optimum Moisture Content	7.4%	
Field Dry Unit Weight	127.5 lb/ft^3	RC=100.0%
Field Moisture Content	3.8%	
Uniformity Coefficient	10.45	
Curvature Coefficient	0.48	
Gravel Fraction	22%	
Fine Content	2%	
Soil Classifications	A-1-b	AASHTO
	SW - Well Graded Sand	USCS
Atterberg Limits	NP	
LBR (Lab Soaked)	99	
CBR* (Field Unsoaked)	N/A	

*: Field CBR was predicted from DCP test as a function of dynamic penetration index value.

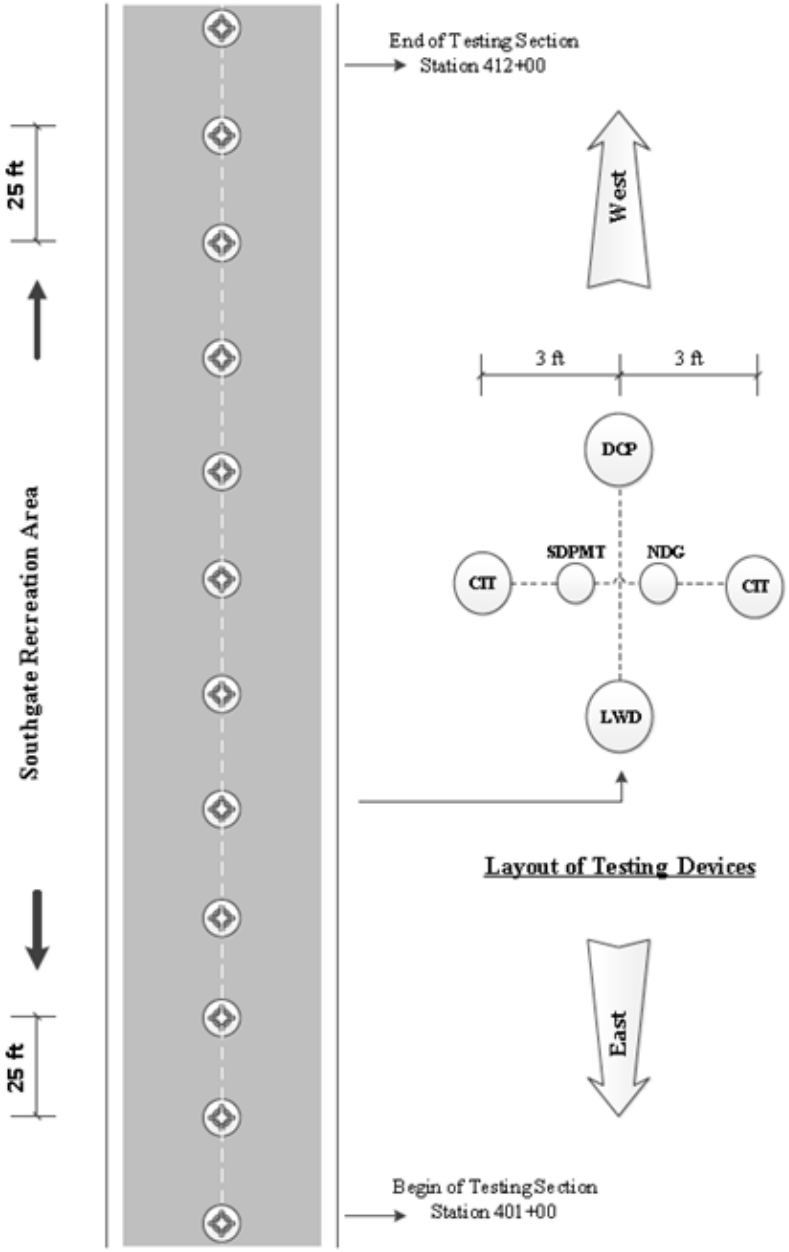

Figure 3.4: Schematic Diagram of Field Testing Locations Florida Tech Southgate Field

Figure 3.5: Satellite Map of Testing Area within the Florida Tech Southgate Athletic Field

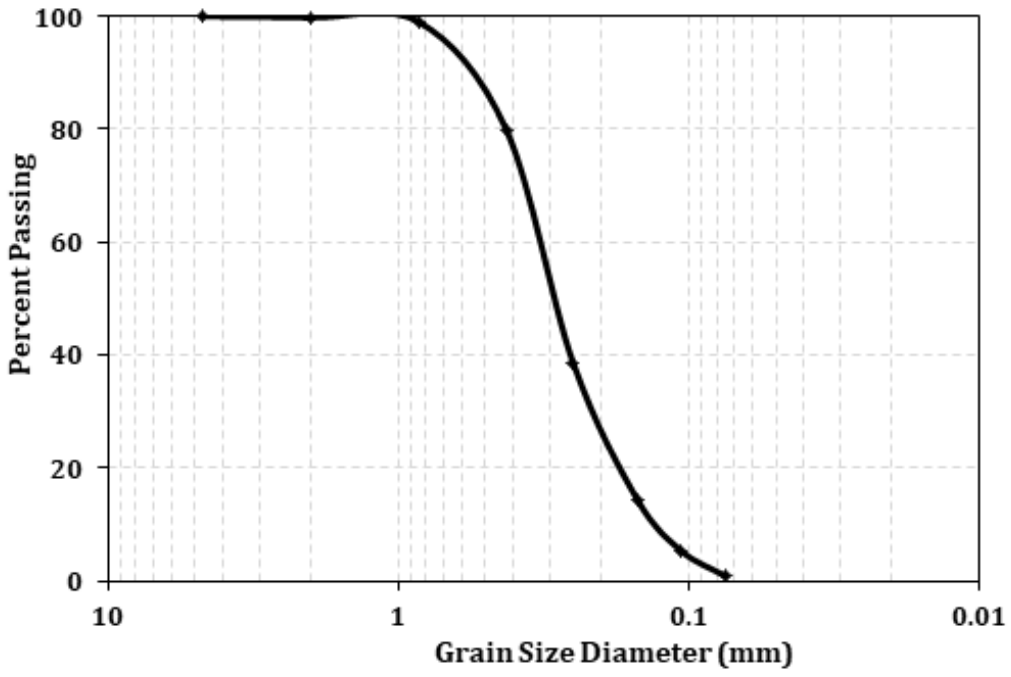

Figure 3.6: Grain Size Distribution for Subgrade Soil at Southgate Field

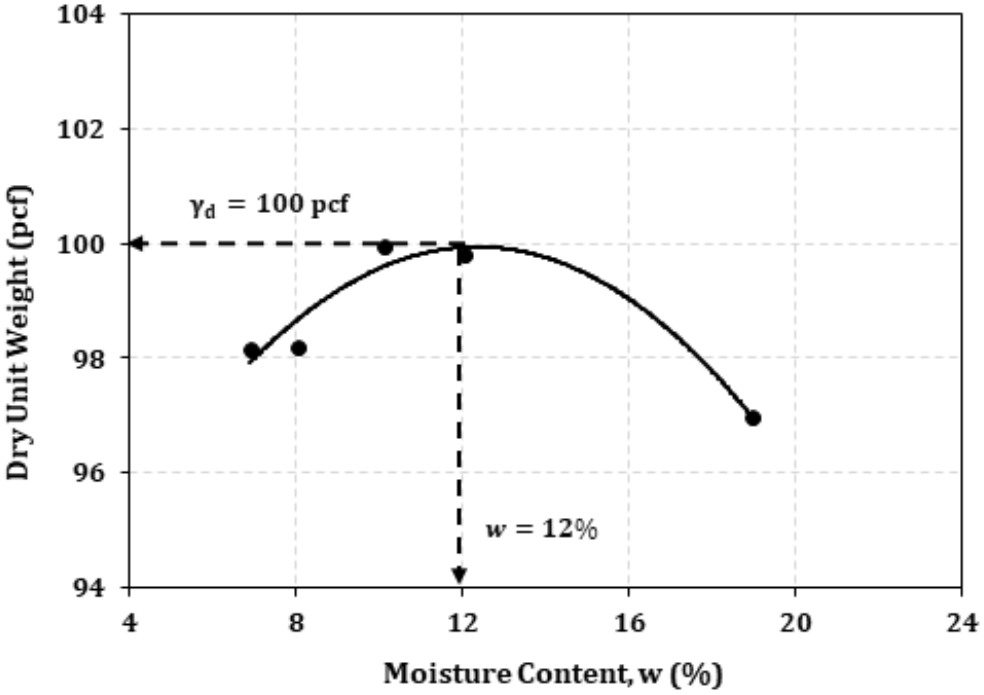

Figure 3.7: Modified Proctor Results for Subgrade Soil at Southgate Field

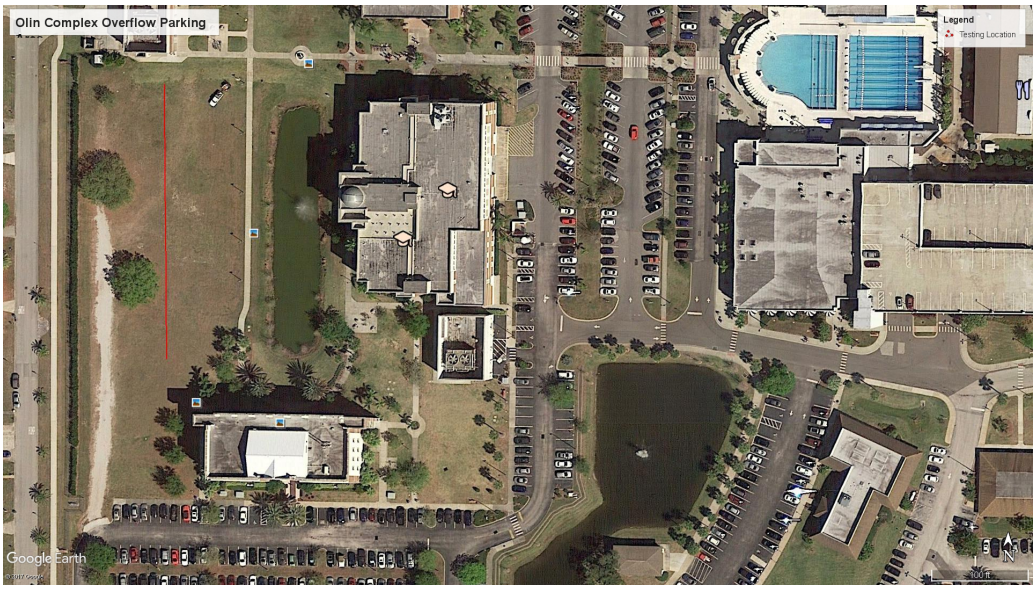

Figure 3.8: Aerial Image of Testing Area at the Olin Complex

Figure 3.9: FIT Overflow Parking Flagged Testing Locations

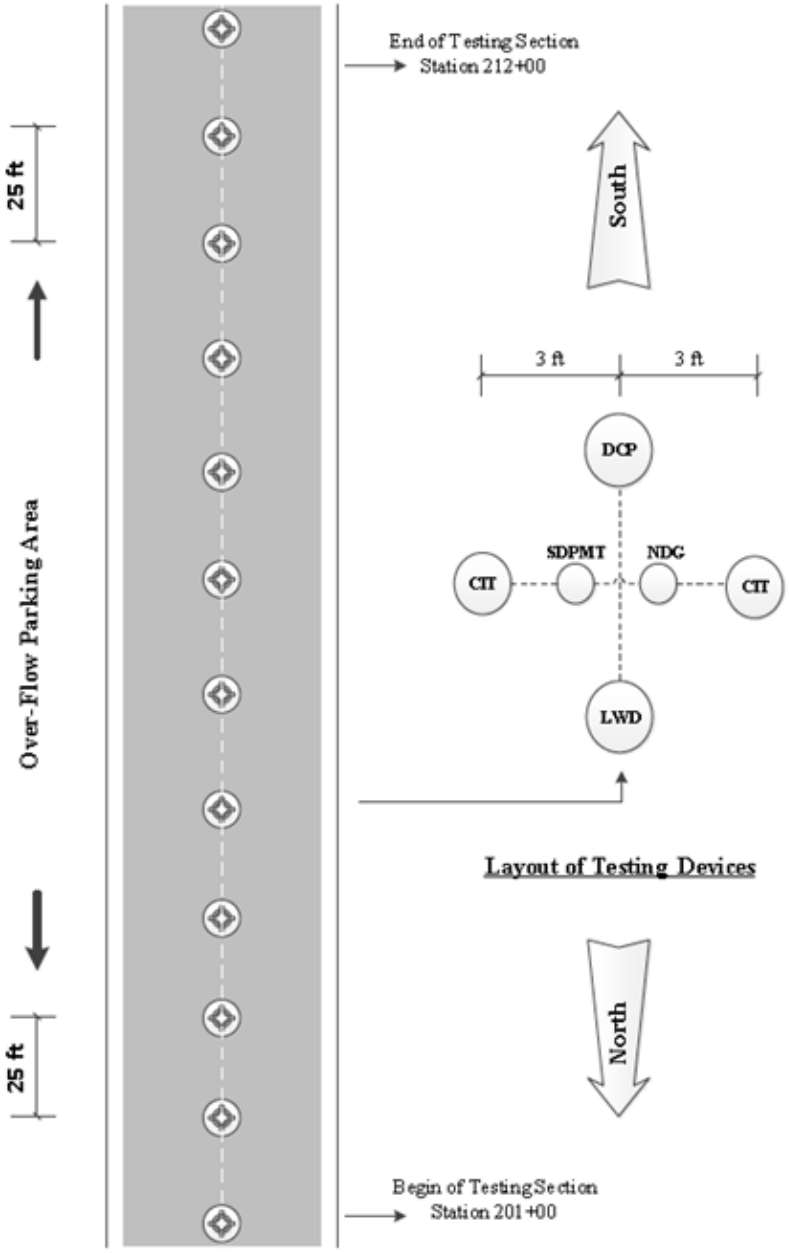

Figure 3.10: Schematic Diagram of Field Testing Locations – FIT Overflow Parking Lot

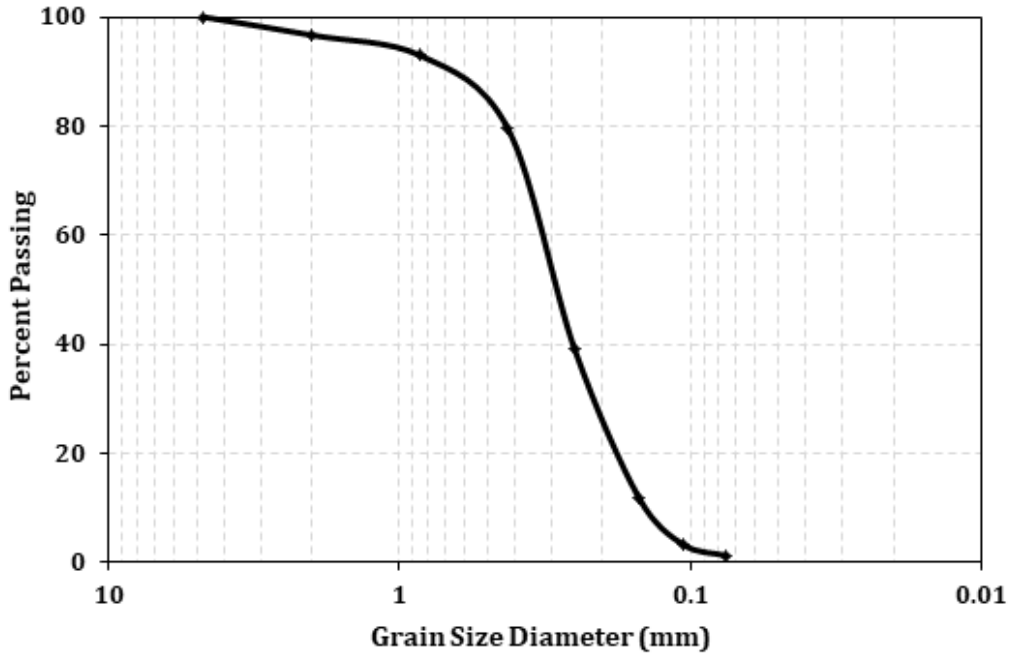

Figure 3.11: Grain Size Distribution for Subgrade Soil at FIT Olin Complex

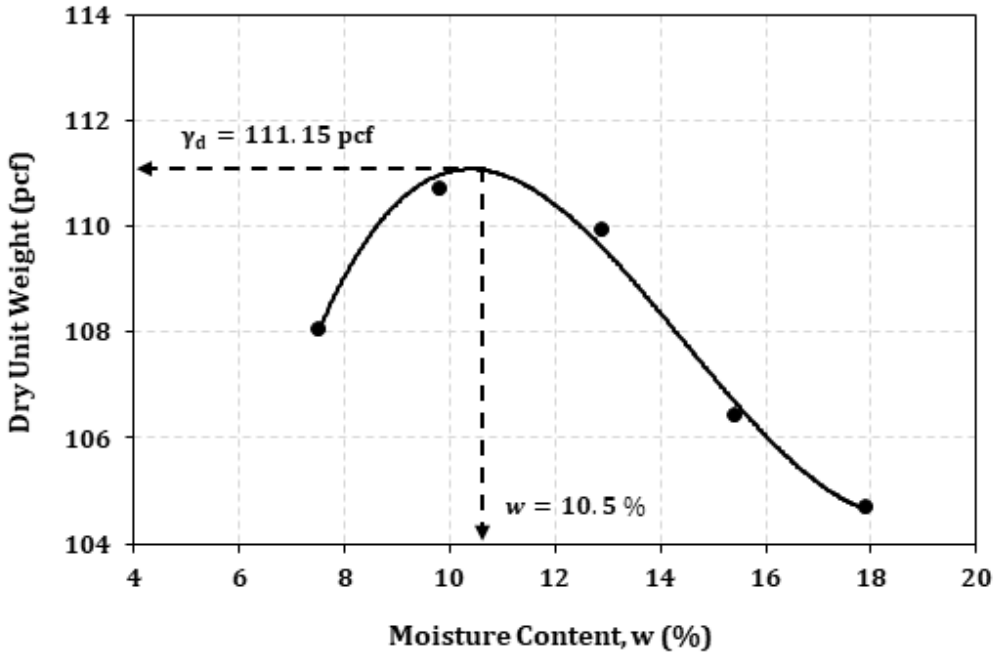

Figure 3.12: Modified Proctor Results for Subgrade Soil at FIT Olin Complex

Figure 3.13: Satellite Map of Testing area in the Cypress Landing Development

Figure 3.14: Potenza Drive Subgrade Testing Site with Orange Flags at Testing Locations

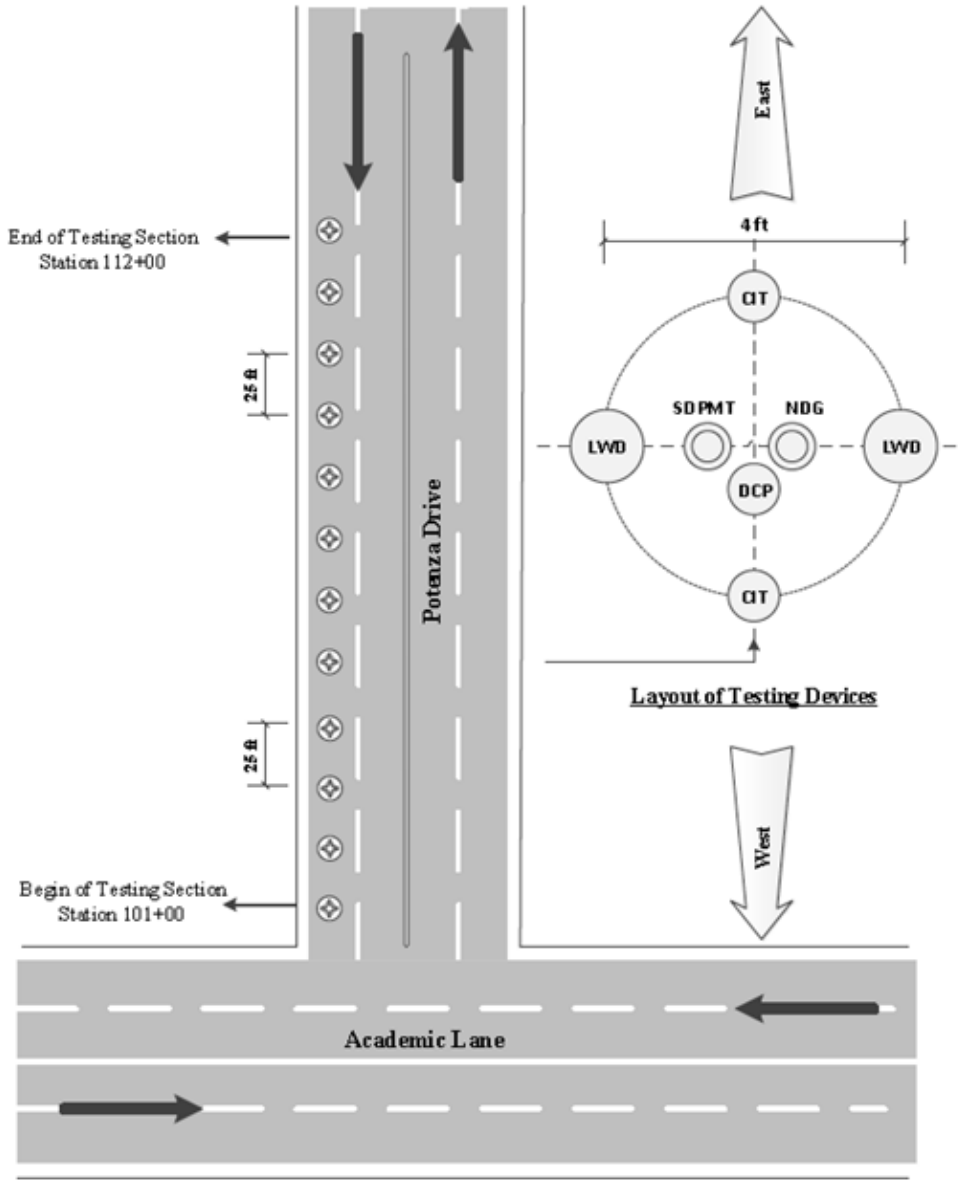

Figure 3.15: Schematic Diagram of Field-Testing Location – Potenza Drive within Cypress Landing

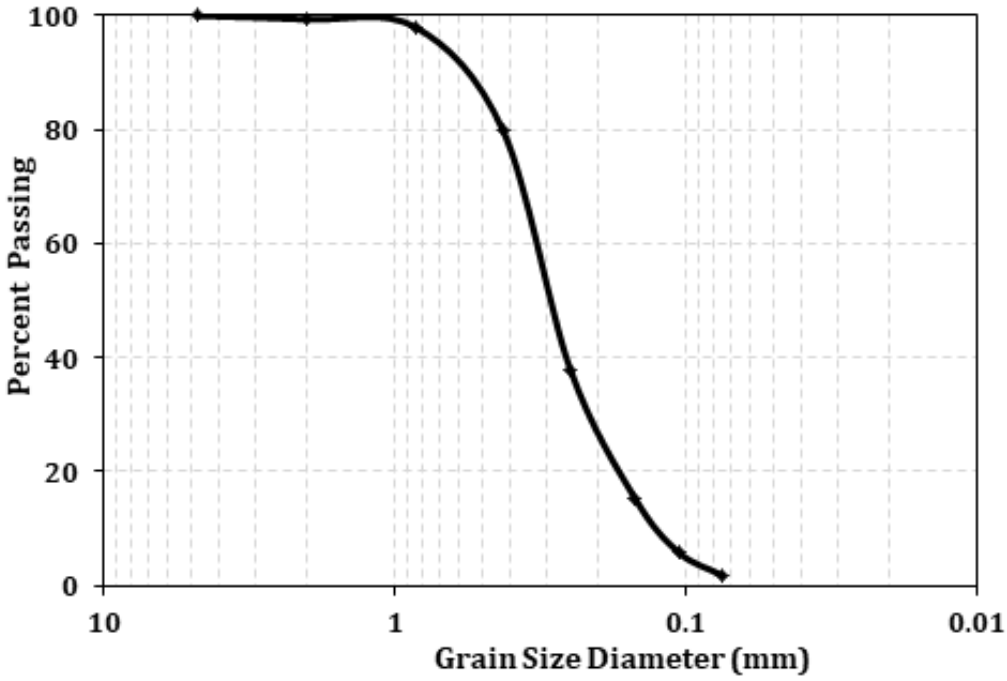

Figure 3.16: Grain Size Distribution for Subgrade at Cypress Landing

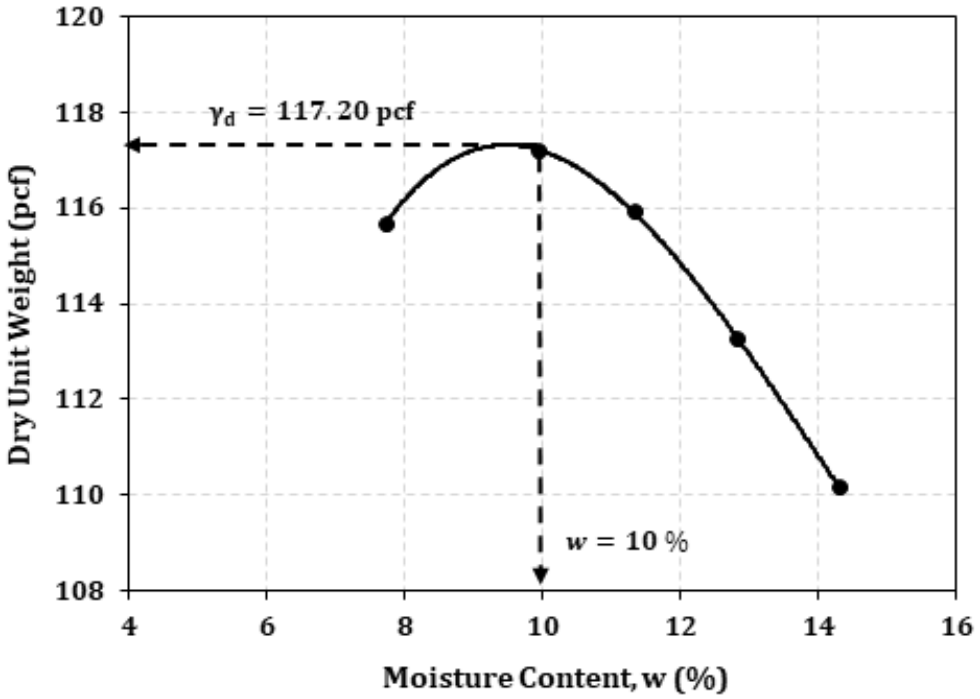

Figure 3.17: Modified Proctor Results for Subgrade at Cypress Landing

Figure 3.18: Map of Heritage Parkway Testing Area

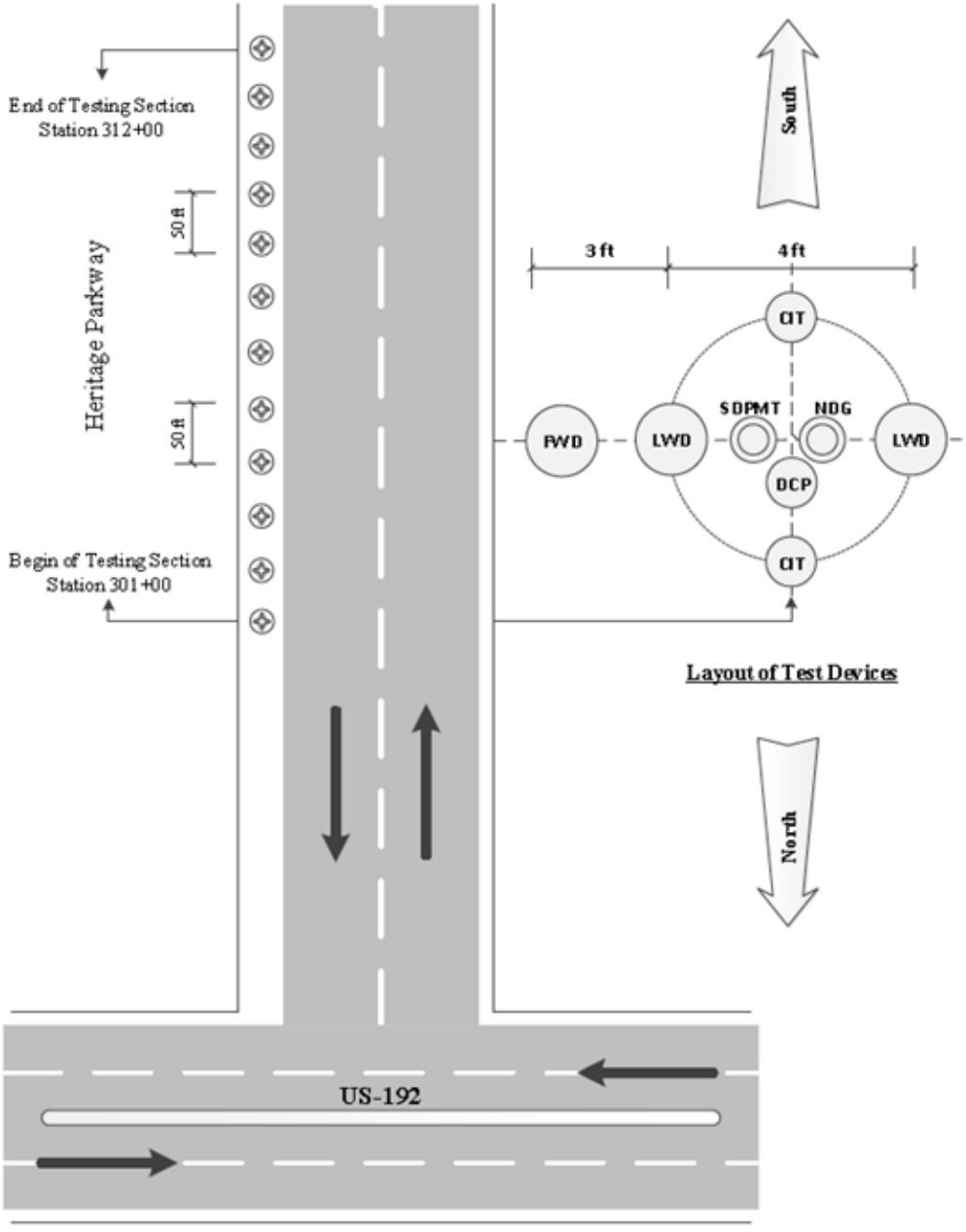

Figure 3.19: Schematic Diagram of Field Testing Locations – St. John Heritage Parkway

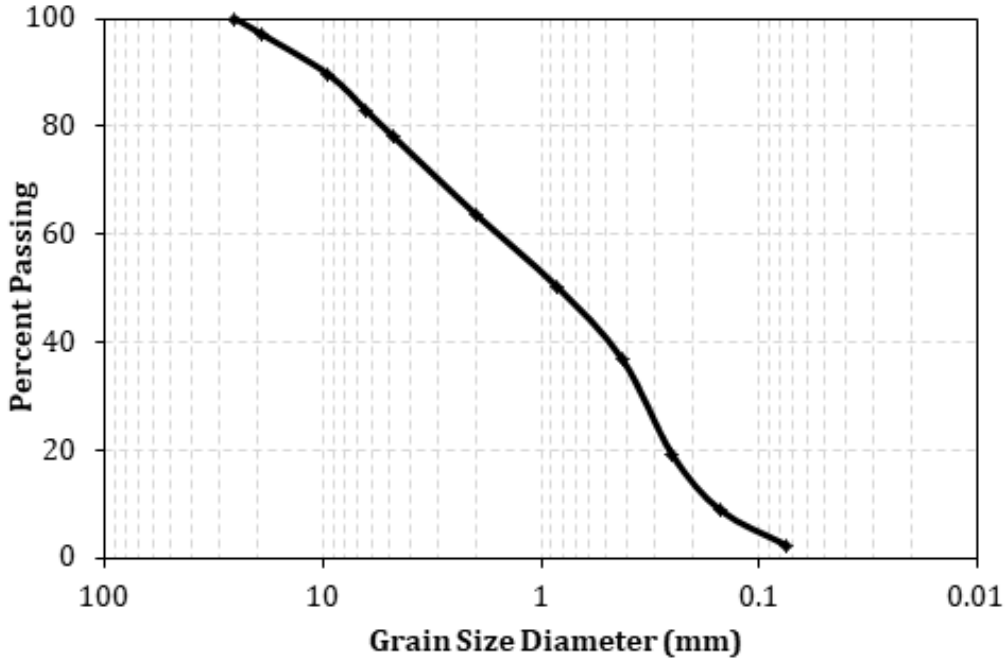

Figure 3.20: Grain Size Distribution for Base Course at Heritage Parkway

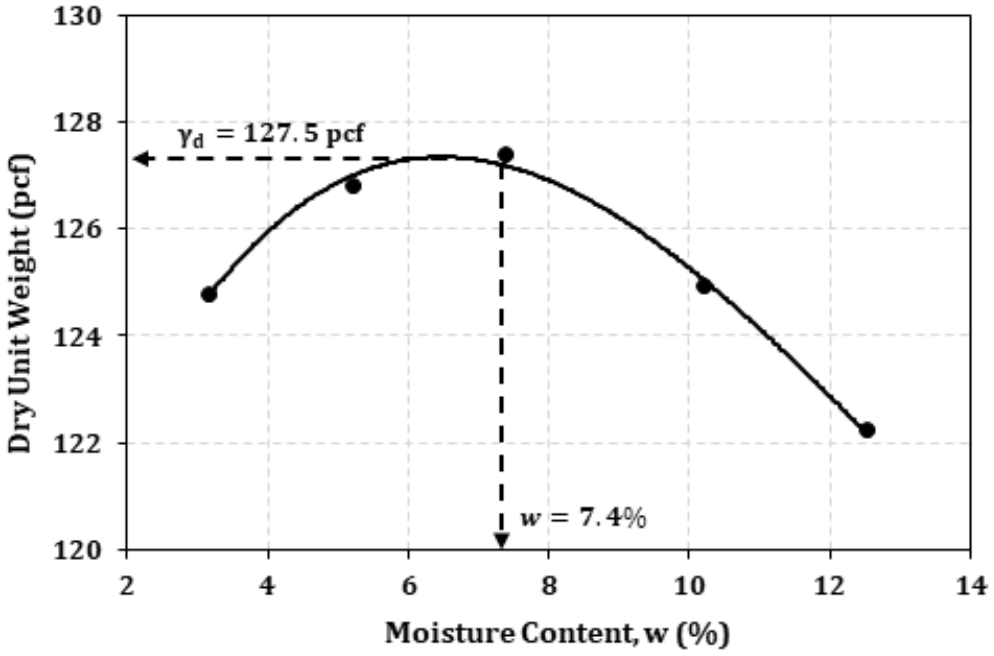

Figure 3.21: Modified Proctor Results for Base Course at Heritage Parkway

Chapter 4

Probe Development and Design

Several probe body styles were designed and fabricated. The probes ranged from 1/8 inch (3 mm) diameter galvanized pipe to several plastic probes to copper and aluminum probes. The effective testing length of the probe varied from 4.5 to 12 inches (112 to 300 mm). The probe bodies were covered with rubber membranes for evaluation. A summary of observations related to the different test probes are described in Table 4.2 (Misilo III, 2018).

4.1 Galvanized Pipe Body Probes

4.1.1 Galvanized Pipe with Replaceable Steel Crimp Rings

A 4.3 inch x 0.625 inch (107 mm x 15 mm) hollow probe constructed with 1/8 inch (3 mm) galvanized pipe and replaceable steel crimp rings was developed as a first iteration design to help visualize the possibility of making a probe the size needed based on the design requirements. Figure 4.1 shows this probe partially inflated. The membrane used on this probe was a section of readily available air hose tubing with an inside diameter of 0.375 inches (9 mm) and an outside diameter of 0.625 inches (15 mm) (Misilo III, 2018).

Testing with this probe produced two inherent problems that made it undesirable for this research. First, the steel crimps used to attach the membrane to the probe body have tabs extending outside the probe diameter; making the resulting outer diameter wider than the maximum performed insertion hole diameter. These crimps are shown in Figure 4.1 near the 68 and 80 cm (2.4 and 3.1 inch) locations along the scale. The second problem is that assembly of the probe was difficult. The threaded pipe necessitated the use of two pipe wrenches to assemble the probe body. It was difficult to move the rubber membrane enough to make a space necessary to place one pipe wrench on the probe body during assembly. The assembly time required for this probe was approximately 45 minutes (Misilo III, 2018).

Figure 4.1: 1/8 inch Galvanized Pipe with Steel PEX Crimp Ring, partially inflated, Testing Dimensions: 4.4 inch x 0.625 inch (Misilo III, 2018)

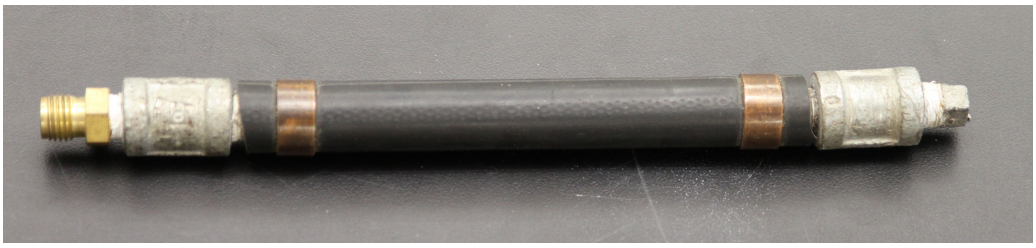

Figure 4.2: 1/8 inch Diameter Galvanized Pipe with Copper Crimp Ring Covered with Rubber Membrane, Testing Dimensions: 4.3 inch x 0.625 inch (Misilo III, 2018)

4.1.2 Galvanized Pipe with Copper Crimp Ring

A second iteration using the 4.3 inch x 0.625 inch (107 to 15 mm) galvanized pipe body probe was developed where the steel crimps were replaced with copper crimping rings. This design is shown in Figure 4.2. The copper crimping rings decreased the overall diameter of the probe assembly such that it would fit into the insertion hole. However, other problems with this design became evident when pressure tests were completed. First, the seal would not withstand high pressures and second, long assembly times were still required. An undesirable characteristic of galvanized pipe is that is has a rough exterior, which permits water seepage when under pressure. Because of the assembly and seepage problems, this probe design was not pursued further (Misilo III, 2018).

4.2 Polylatic Acid

Florida Tech's College of Engineering has several 3D printers, one of which uses polylatic acid (PLA). 3D printed probes could be very cost effective if found feasible. PLA is a biodegradable thermo plastic that is melted to build the part. A 3D AutoCAD file was generated and converted to the required 3D printer format. The resulting printed PLA thermo plastic probe is shown in Figure 4.3. This probe had one major problem - when cutting the threads into the part, the PLA chipped and consequently would not thread. The chipping problem prevented this material from being used for the

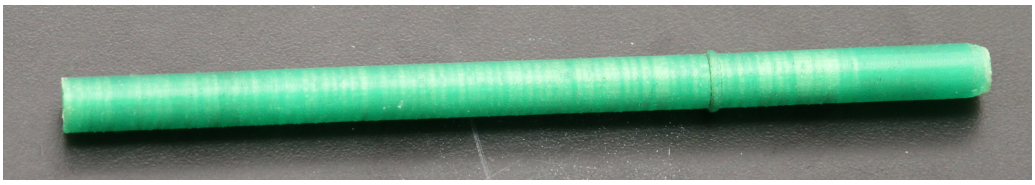

Figure 4.3: 3D Printed PLA Probe 3/8 Diameter (Misilo III, 2018)

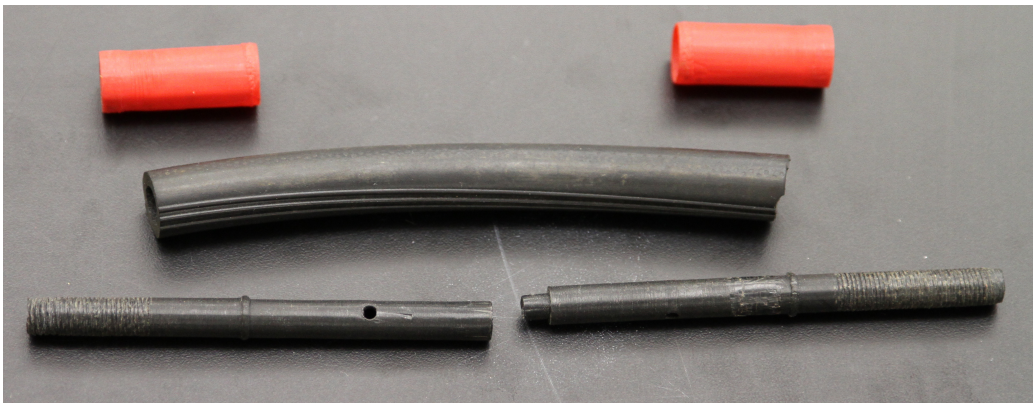

Figure 4.4: 3D Printed ABS Probe Parts (black) and Sleeves (red) (Misilo III, 2018)

construction of the probe (Misilo III, 2018).

4.3 Acrylonitrile Butadiene Styrene Plastic

A second 3D probe design was developed and printed using Acrylonitrile Butadiene Styrene (ABS) Plastic. This probe is shown in Figure 4.4. It consists of a two-piece ABS body and two sleeves. The sleeves were secured with standard zinc plated hardware. This design was based on a preliminary design requirement of the probes ability of be placed into a 0.625 inch (15.9 mm) diameter hole, but it was later discovered that the probe would have to be sized to fit into a 0.75 inch (19 mm) diameter hole (Misilo III, 2018).

The probe manufacturing method had some advantages over the PLA version, most importantly the ABS plastic is a more machinable material. A disadvantage of this probe was that because of the 3D printer model used, the probe body was unable to be fabricated in one piece. This material and design has potential once final dimensions were developed. When final dimensions were determined, this material and process were used to make a probe. A major leaking problem occurred while pressure testing this probe, because many layers were used to print it; therefore, it was difficult to thread resulting in leaks between the printed layers (Misilo III, 2018).

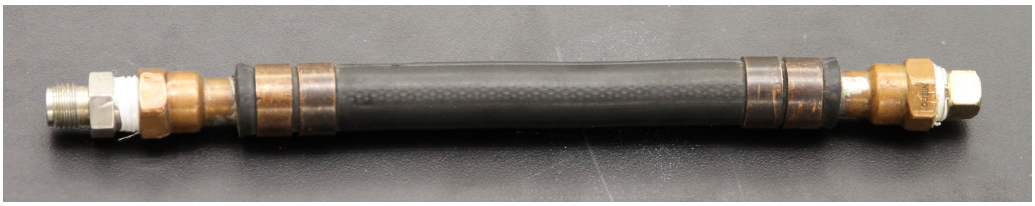

Figure 4.5: 5/8 inch diameter Copper Probe 4 inch (19.1 mm) long

4.4 3/8 Diameter Copper Tubbing Probe

A copper tubing probe design was developed because of the flexibility in obtaining and cutting copper pipe lengths. This tubing could be cut to any reasonable length. A 0.325 inch (8.1 mm) diameter probe body, covered with a 0.625 inch (16.2 mm) outside diameter membrane was constructed with an overall length of 6.5 inches (16.2 cm). Once the copper crimps were placed over the rubber, the testing length was 4 inches (10.16 cm), as shown in Figure 4.5. This preliminary probe length was developed to keep the L/D ratio consistent with the PPMT probe. This probe design was successfully tested to a pressure in excess of 500 psi (3500 kPa) (Misilo III, 2018).

This probe design has some concerns. One is that the fittings used on the ends of the pipe extend beyond the diameter of the probe body, and cannot be dissembled easily to replace the membrane. A second design challenge observed was that in order to assemble the probe a lubricant is necessary to allow the membrane to slide onto the probe body. The lubricant produced a film under the membrane that prevents it from sealing for about 24 hours (Misilo III, 2018).

Following preliminary testing of this probe it was observed that the membrane material used has a significantly higher resistance to expansion, ten times greater, than a standard PPMT probe membrane. Note that it required approximately 145 psi (1000 kPa) compared to 14.5 psi (100 kPa) during membrane calibration testing. This excessive membrane resistance would severely limit the soil strength that could be evaluated (Misilo III, 2018).

4.5 Machined Aluminum Probe Body

Based on testing to date an aluminum probe design was developed. Aluminum was machined using a Computer Numerically Controlled (CNC) lathe to address the leakage and sizing problems associated with the previous designs. A key feature of this design was the addition of an integrated O-ring to help create a seal at the ends of the probe. This probe design includes machined sleeves to create a pressure seal between the probe body and the membrane. Also the connectors that attach the tubing to the probe are threaded directly into the body of the probe allowing a simplified process to remove and replace the membrane. Addressing concerns of membrane resistance a new rubber material was tested that was 0.125 inches larger in internal diameter (Misilo III, 2018).

Pressure testing with this probe showed that it could withstand the requirements of

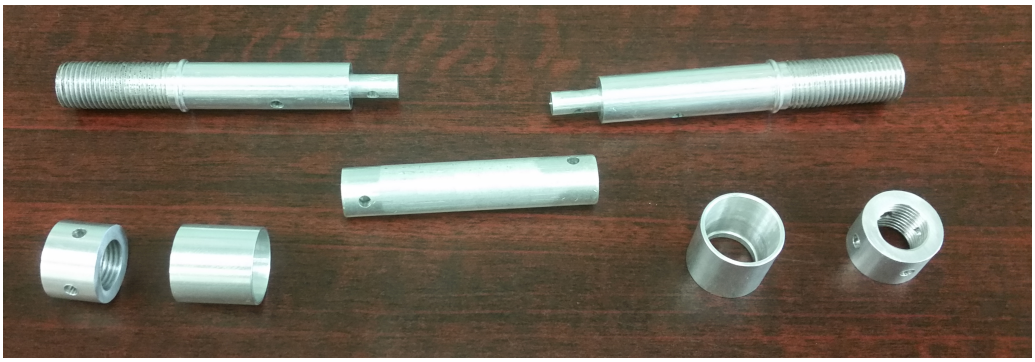

Figure 4.6: Unassembled Prototype SDPMT-6 Aluminum Probe, Testing Dimensions: 5.5 inch x 0.625 inch (137 mm x 15 mm), probe ends (2 each), Probe Center, Nuts (2 each), and Sleeves (2 each) (Misilo III, 2018)

Figure 4.7: Fully Assembled Prototype SDPMT-6 Aluminum Probe, Testing Dimensions: 5.5 inch x 0.625 inch (137 mm x 15 mm) (Misilo III, 2018)

testing of base course materials; therefore, it was selected for continued testing with this project. This probe is designated as a small diameter pressuremeter probe or SDPMT. Figures 4.6 and 4.7 show an unassembled and fully assembled aluminum probe with a testing zone measuring 5.5 inches x 0.625 inches (137 mm x 15 mm) and an overall length of 10.5 inches (26.2 cm) fully assembled. Figures 4.8 and 4.9 show a partial and fully assembled aluminum probe measuring 11.5 inches x 0.625 inches (287 mm x 15 mm) and overall length of 16.5 inches (41.2 cm) fully assembled (Misilo III, 2018).

Figure 4.8: Partially Assembled Prototype SDPMT-12 Aluminum Probe Testing Dimensions: 11.5 inch x 0.625 inch (287 mm x 15 mm), probe ends (2 each), Probe Center, Nuts (2 each), and Sleeves (2 each) (Misilo III, 2018)

Figure 4.9: Fully Assembled Prototype SDPMT-12, Aluminum Probe Testing Dimensions: 11.5 inch x 0.625 inch (287 mm x 15 mm) (Misilo III, 2018)

Table 4.1: Probe L/D Ratios for a 0.625 inch Probe of Varying Lengths

Length inch	L/D Ratio
3	4.8
4	6.4
5	8.0
6	9.6
7	11.2
8	12.8
9	14.4
10	16.0
11	17.6
12	19.2

4.5.1 Probe Profile Lengths

Base and subgrade soil lifts can vary from approximately three to 12 inches. Based on this information and the preliminary design probe diameter, Table 4.1 was developed. It shows that with a 5/8 inch (15 mm) diameter probe the L/D ratio varies from 4.8 to 19.2 when the probe length is varied from 3 to 12 inches (75 to 300 mm), respectively. Based on the FDOT research project requirements the 6 and 12 inch (150 to 300 mm) probes were evaluated. Hartman (1974) presents a parametric analysis comparing L/D ratio to variations in the injected volume to the theoretical cylindrical expansion. Hartman shows that when the L/D ratio is at least 6 the % error is within 5%, giving a reasonable minimum L/D ratio for reliability of results (Misilo III, 2018).

In summary, Table 4.2 shows the basic prototype designs and the major observations from preliminary lab testing with these probes. The SDPMT aluminum design was able to be 1) used without leaking, 2) assembled in a very timely manner and 3) constructed at a very reasonable cost. A 3D CNC parts company in Brevard County, Spacecoast Precision, Inc., was used to complete the machining. Six, eight, ten and 12-inch (15, 20, 25 and 30 cm) long probes were produced (Misilo III, 2018).

Table 4.2: Preliminary Comparison of Probe Designs

Probe Design	**Observations**
1/8 inch Galvanized Pipe A	To large for NDG hole
1/8 inch Galvanized Pipe B	$\tilde{3}$50 psi (2400 kPa)
Polylatic Acid (PLA) Thermoplastic	Will not thread reliably
Acrylonitrile Butadiene Styrene (ABS) Plastic	Multiple Parts
3/8 inch Copper 4 inch	> 435 psi (3500 kPa)
3/8 inch Copper 6 inch	> 435 psi (3500 kPa)
5/8 inch Aluminum 6 & 12 inch w/ crimp rings	Could not Install clamping
5/8 inch Aluminum 6 & 12 inch w/ sleeves	Selected Design

Note: 1-inch=25.4 mm

4.6 Preliminary Probe Design Test Plan

4.6.1 Preliminary Test Test Location

A grassy area located at (N 28°1' 53.076" W 80°41' 0.236") a.k.a. The Misilo House, was used to test the capabilities of the designed probes. This location was selected because it gave easy access to tools needed to assemble the probe, and make changes as necessary. Tests were conducted using the 6 inch and 12 inch (150 and 300 mm) SDPMT probe designs and the results were compared to PPMT tests conducted in the same area. Four PMT tests with each probe were conducted in a grassy area 15 ft by 8 ft (4.5 m by 2.5 m), producing 12 tests. The test soundings were organized into four columns and three rows. The testing layout is shown in Figure 4.10, with the first number per location being the sounding number and the following acronym being the probe type designation (Misilo III, 2018).

4.6.2 Bore Hole Preparation

The holes for the SDPMT probes were created by driving a 0.875 inch x 20 inch (2.1 cm by 50 cm) drill rod, manufactured by Humboldt Scientific for their NDG, through a scraper plate / drill rod guide to a depth of 17 inches (45 cm). SDPMT-6 and SDPMT-12 probes were placed at the bottom of the hole for testing (Misilo III, 2018).

The holes for the PPMT tests were formed using a hollow 1.375 inch (34 mm) outside diameter and 1.25 inch (31 mm) inside diameter steel tube with a beveled edge driven into the ground to a depth of 24 inches (60 cm). The PPMT probe was placed at the bottom of the hole for testing (Misilo III, 2018).

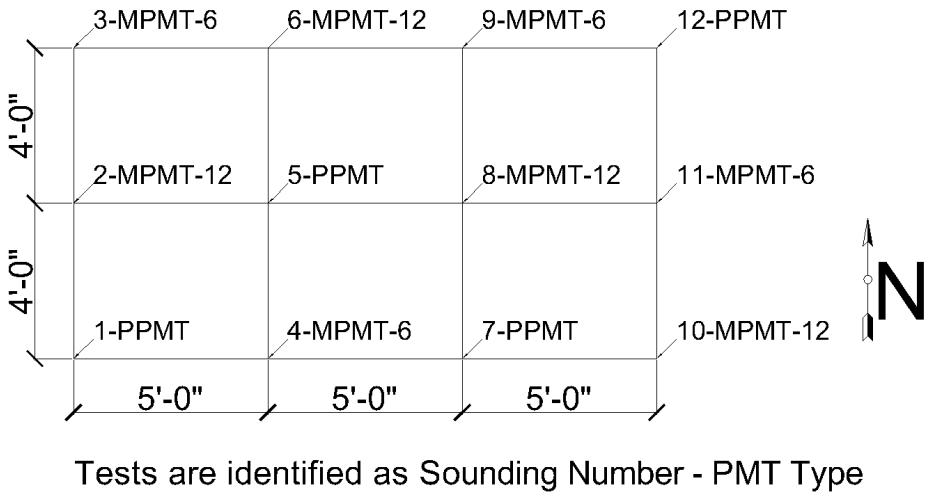

Figure 4.10: Preliminary Testing Layout for SDPMT-6, -12 and PPMT Evaluation (Misilo III, 2018)

4.6.3 Testing Procedure

SDPMT tests consisted of inserting the probe to the desired test depth (17 inches) and running a strain controlled test. Readings were taken at 0 cm^3 injected volume, and at 2 cm^3 increments until it was obvious that the limit pressure could be determined or 30 cm^3 of fluid had been injected. Once the maximum volume was injected into the probe, unload readings were taken. During unloading, readings were taken after 0.1 cm^3, 0.3 cm^3, 1 cm^3. No unload-reload loop readings were taken during this testing (Misilo III, 2018).

PPMT testing consisted of inserting the probe to the desired test depth (24 inches) and running a strain controlled test. Readings were taken at 0 cm^3 injected volume, and at 5 cm^3 increments until it was obvious that the limit pressure could be determined or 90 cm^3 of fluid had been injected. Once the maximum volume to be injected into the probe for the test unload readings were taken. During unloading, readings were taken after 0.1 cm^3, 1 cm^3, 1 cm^3, 3 cm^3. No unload-reload loop readings were taken during this testing (Misilo III, 2018).

4.7 Selected Probe Design Drawings

4.7.1 SDPMT Probe Body

Based on the scope of FDOT research, (i.e. the need to fully test 6 and 12 inch (15 and 30 cm) pavement layers), two probe lengths were designed for testing these thicknesses. The aluminum SDPMT prototype manufactured for this preliminary testing was slightly shorter than desired. This small design error resulted in each probe being

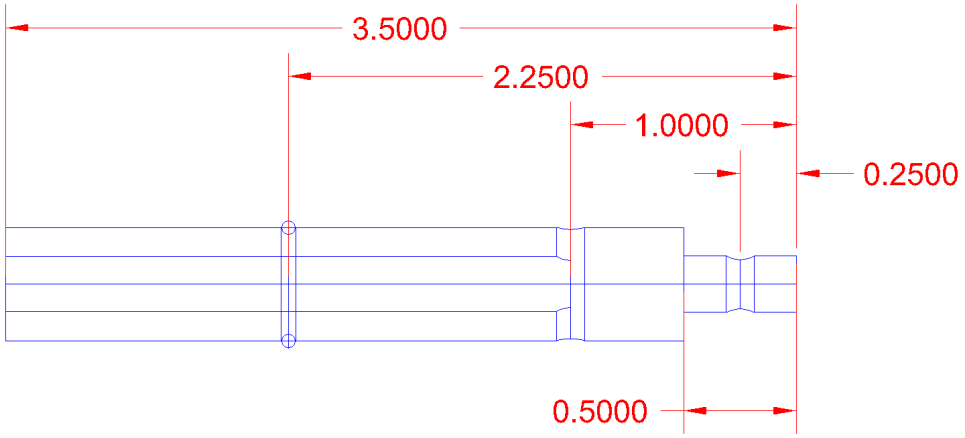

Figure 4.11: Probe Body End, Linear Dimensions in inches (Misilo III, 2018)

0.5 inches (12 mm) shorter than expected. This small error did not affect testing at this point of the research and was corrected for the remaining work. It was easily corrected by increasing the center section of the probe for the future prototypes (Misilo III, 2018).

The SDPMT probe body consists two parts: the two identical probe ends and an adjustable length probe center. As the center length is changed the overall length of the probe changes (Misilo III, 2018).

4.7.1.1 Probe End

Each end of the assembled probe is threaded on: a) the inside with 1/16-inch National Pipe Thread (NPT) to allow the fluid hose to be secured to the probe, and b) on the outside using 1/2-20 Unified National Thread Course (UNC) to secure the sleeves to the probe body, creating a water tight seal with the membrane. The linear dimensions in inches of the probe end are shown in Figure 4.11, and the radial dimensions in inches are show in Figure 4.12 (Misilo III, 2018).

4.7.1.2 Probe Center

The length of the probes' center section can be changed to set the desired length of the exposed membrane. The overall length of the center section is determined by subtracting 3 inches (75 mm) from the desired overall probe length (Misilo III, 2018).

The 6 inch probe has a center section with an overall length of 3 inches, and is detailed in Figure 4.13. The SDPMT-12 probe has a center section with an overall length of 9 inches (22.5 cm), and is detailed in Figure 4.14 (Misilo III, 2018).

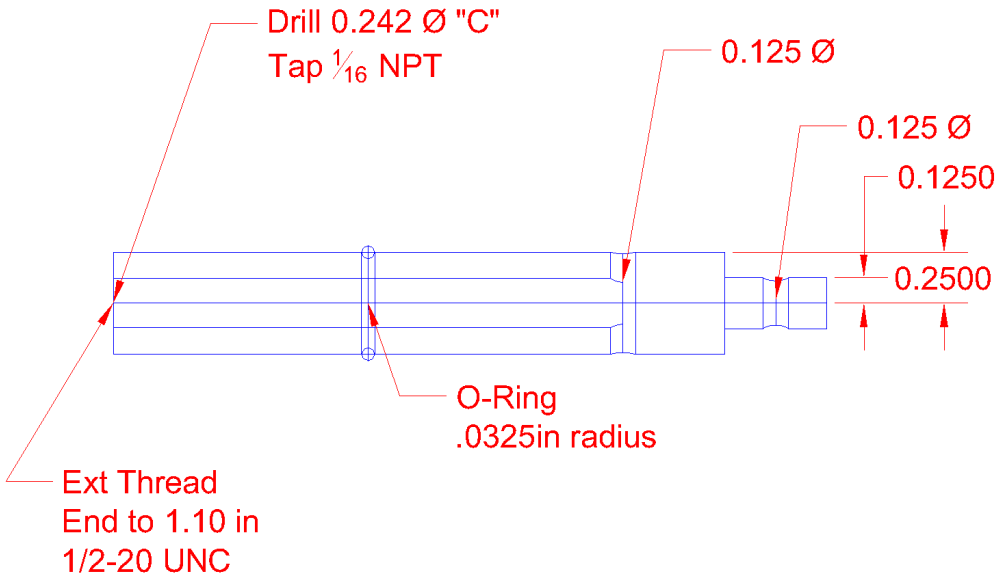

Figure 4.12: Probe Body End, Radial Dimensions in inches (Misilo III, 2018)

4.7.2 Probe Sleeves

Each probe has two identical sleeves which slide over the end of the probe body and the membrane to create a pressure and water seal that allows the membrane to expand when fluid is injected from the control unit. The inside sleeve thickness tapers from its minimum of 0.04 inches to the maximum of 0.1072 inches (2.7 mm) to create the seal. Each sleeve was machined from aluminum as shown in Figure 4.15 (Misilo III, 2018).

4.7.3 Probe Retaining Nuts

Each probe has two aluminum retaining nuts, which when tightened force the sleeves over the membrane to secure the membrane and sleeves in place. Figure 4.16 shows the retaining nut face and Figure 4.17 shows a side view (Misilo III, 2018).

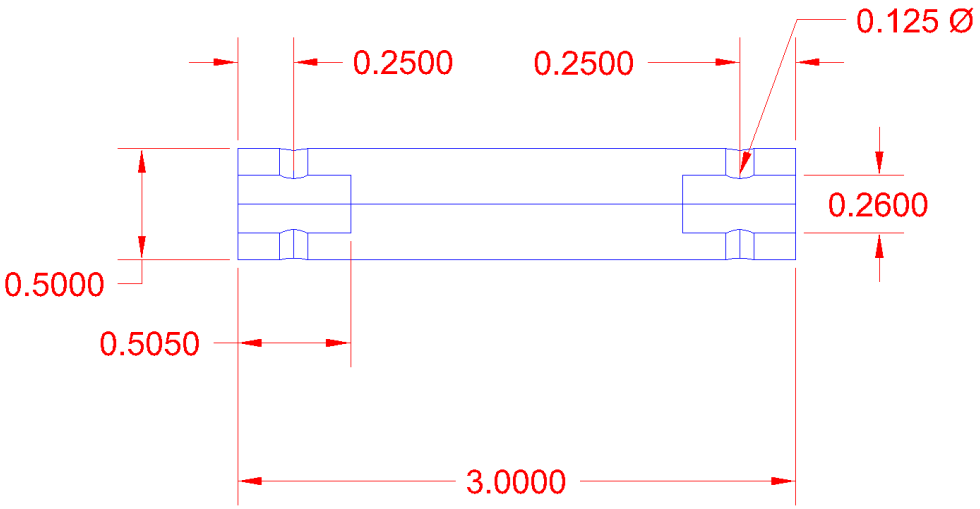

Figure 4.13: Center Section SDPMT-6 Inch, Dimensions in inches (Misilo III, 2018)

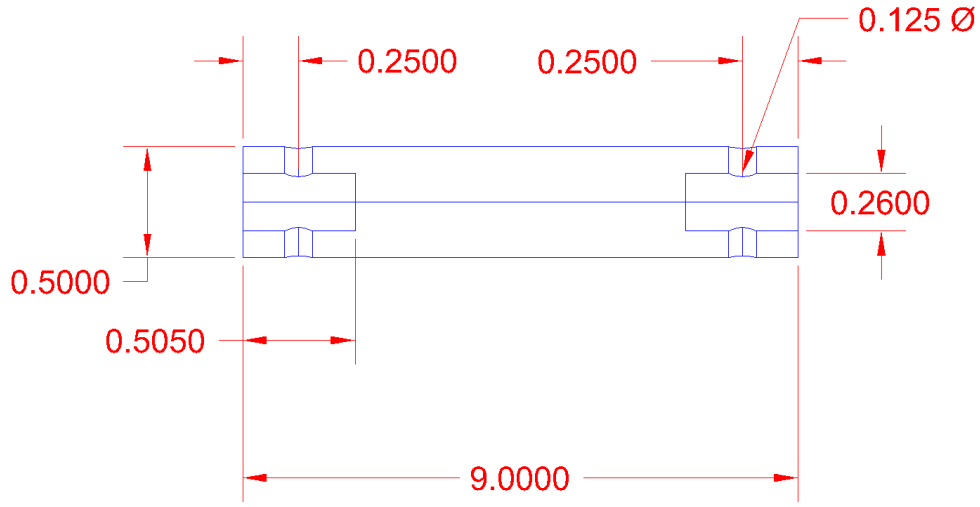

Figure 4.14: Center Section SDPMT-12 Probe, Dimensions in inches (Misilo III, 2018)

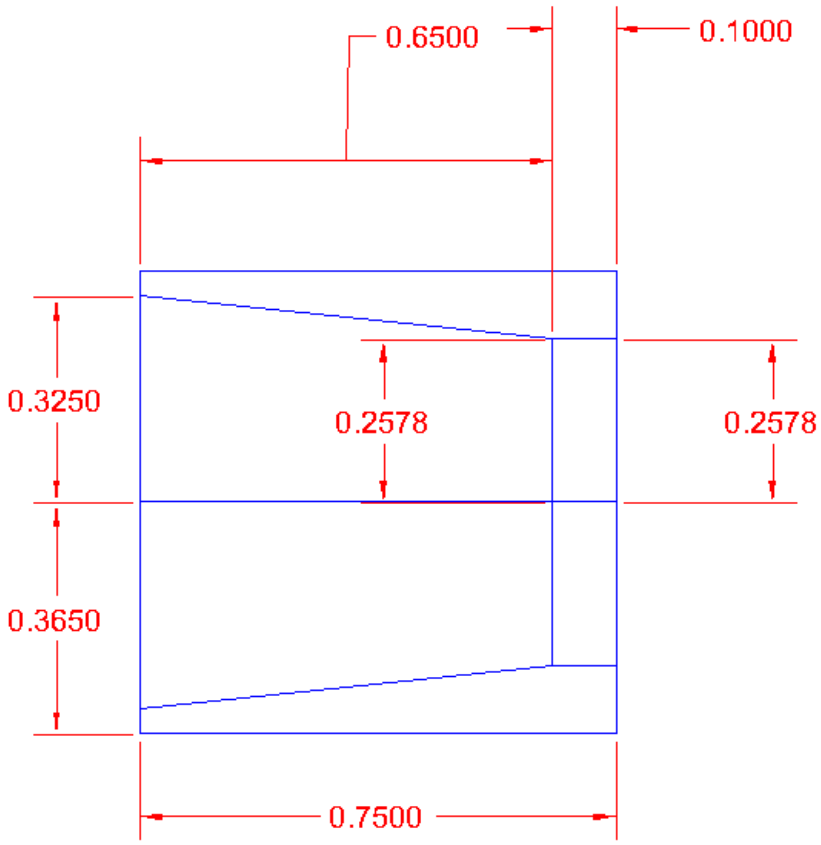

Figure 4.15: Aluminum Sleeve Side View, Dimensions in inches (Misilo III, 2018)

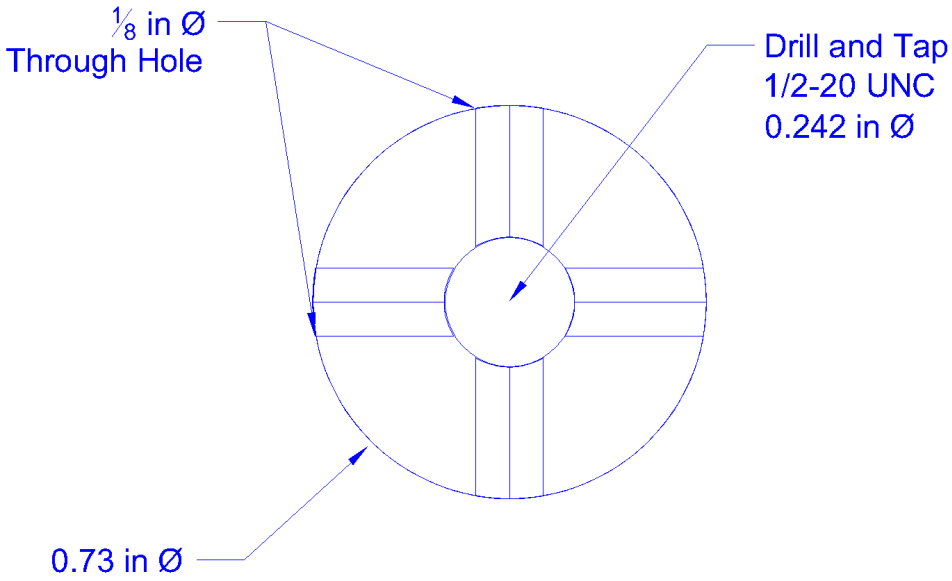

Figure 4.16: Aluminum Retaining Nut Face View, Dimensions in inches (Misilo III, 2018)

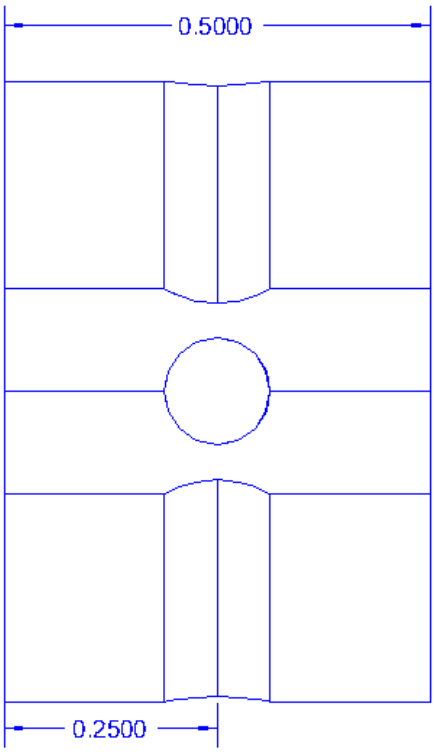

Figure 4.17: Aluminum Retaining Nut Side View, Dimensions in inches (Misilo III, 2018)

Chapter 5

Field Test Results

This chapter contains the field testing results. It is separated into three main sections: preliminary testing results, SDPMT testing observations and correlation testing results.

5.1 Preliminary Testing

Twelve preliminary PMT validation tests were conducted within an 8 by 15 foot grass test site in Palm Bay, Florida to evaluate how the two proposed probes compared to the standard PPMT. Standard PPMT and the 6- and 12-inch SDPMT results were compared to each other and are presented below. Test locations are referred to as soundings because they produce engineering data without producing any soil samples.

5.1.1 PPMT Test Results

Four PPMT tests were conducted using the 11 inch long probe with a diameter of 1.25 in. One test was conducted in soundings 1, 5, 7, and 12. Each test was conducted in holes 0.61 m or 24 inches deep, with the center of the membrane set at 10.75 inches below the ground surface.

PPMT in sounding 1 required approximately 20 cm^3 of fluid to be injected before the probe contacted the side of the hole. To complete this test, an additional 55 cm^3 of fluid was injected, in 5 cm^3 increments, up to a total of approximately 75 cm^3. The reduced data was used to determine E_0, p_0 and p_L which resulted in 346.8 psi (2391 kPa), 0 psi (0 kPa) and 32.6 psi (225 kPa), respectively. The raw and reduced data from sounding 1 is presented in Figure 5.1. The engineering properties are presented in Table 5.2.

PPMT in sounding 5 required approximately 15 cm^3 of fluid to be injected before the probe contacted the side of the hole. To complete the test, an additional 50 cm^3 of fluid was injected, in 5 cm^3 increments, up to a total of approximately 65 cm^3. The reduced data was used to determine E_0, p_0, and p_L which was 419.1 psi (2889 kPa), 1.3 psi (9 kPa) and 32.6 psi (225 kPa), respectively. Raw and reduced data from sounding 5 is presented in Figure 5.2, and the engineering properties are presented in Table 5.2.

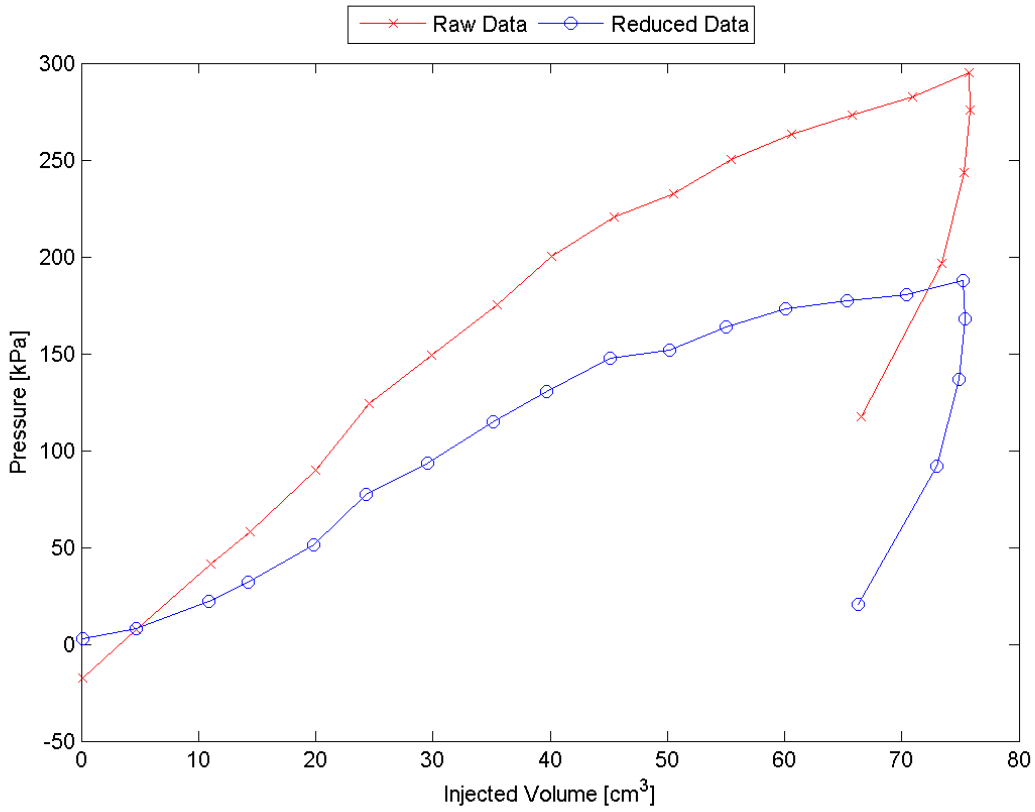

Figure 5.1: Raw and Reduced Data, Sounding 1, 0.61m, PPMT

PPMT in sounding 7 required approximately 10 cm^3 of fluid to be injected before the probe contacted the side of the hole. To complete the test, an additional 80 cm^3 of fluid was injected, in 5 cm^3 increments, up to a total of approximately 90 cm^3. The reduced data was used to determine E_0 (402.3 psi or 2774 kPa), p_0 (2.9 psi or 20 kPa) and p_L (33.7 psi or 260 kPa). The raw and reduced data from sounding 7 is presented in Figure 5.3, and the engineering properties are presented in Table 5.2.

PPMT in sounding 12 required approximately 10 cm^3 of fluid to be injected before the probe contacted the side of the hole. To complete the testing, additional 70 cm^3 of fluid was injected, in 5 cm^3 increments, up to a total of approximately 80 cm^3. The reduced data was used to determine E_0 (367.0 psi or 2530 kPa), p_0 (1.1 psi or 8 kPa) and p_L (29.0 psi or 200 kPa). The raw and reduced data from sounding 12 is presented in Figure 5.4. The engineering properties are presented in Table 5.2.

5.1.2 SDPMT-6 Test Results

Four tests were conducted with SDPMT-6; the 5.5 inch probe with a diameter of 0.625 in. One test was conducted in soundings 3, 4, 9 and 11. Each test was conducted

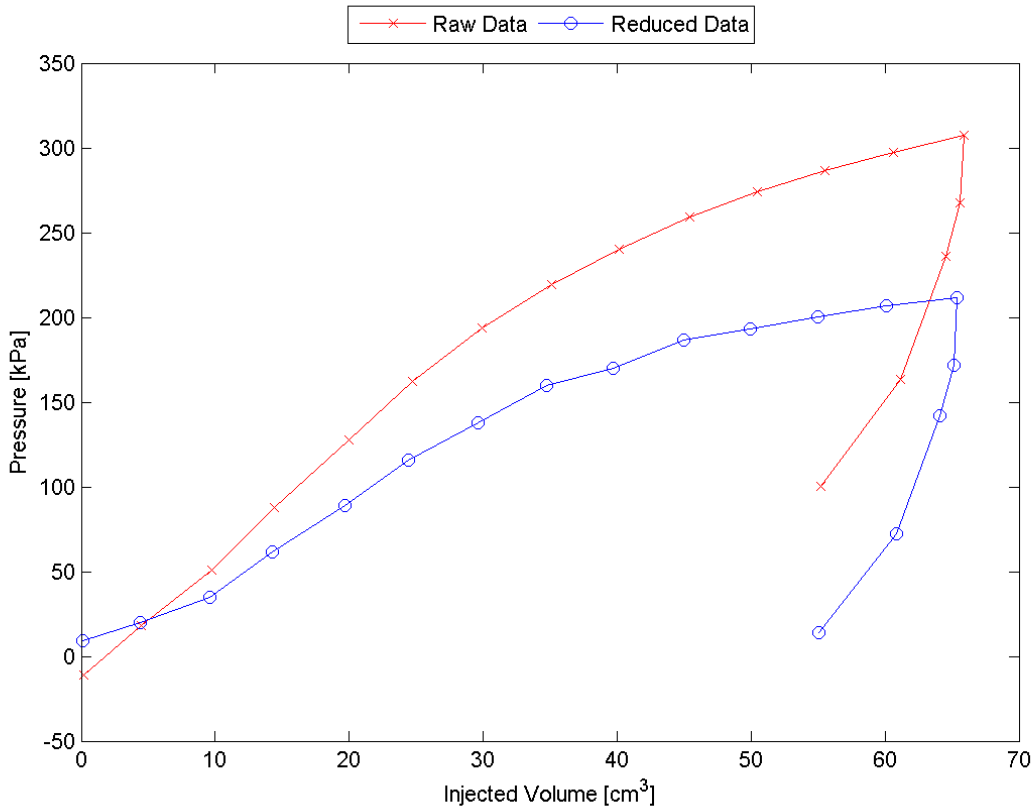

Figure 5.2: Raw and Reduced Data, Sounding 5, 0.61m, PPMT

in holes 0.43 m or 17 inches deep, with the center of the membrane located at 11.67 inches.

SDPMT-6 in sounding 3 required approximately 17 cm^3 of fluid to be injected before the probe contacted the side of the hole. To complete this test, an additional fluid was injected up to approximately 30 cm^3. Based on the reduced data estimations for E_0 (707.9 psi or 4881 kPa), p_0 (2.0 psi or 13 kPa), and p_L (65.3 psi or 450 kPa) were determined. The raw and reduced data from sounding 3 is presented in Figure 5.5. The engineering properties are presented in Table 5.2.

SDPMT-6 in sounding 4 required approximately 17 cm^3 of fluid to be injected before the probe contacted the side of the hole. To complete this test, an additional 13 cm^3 of fluid was injected to a total of approximately 30 cm^3. Based on the reduced data, E_0 was 468.3 psi (3229 kPa), p_0 was estimated at 0 psi (0 kPa) and the p_L for this test was 43.5 psi (300 kPa). The raw and reduced data from sounding 4 is presented in Figure 5.6. The engineering properties are presented in Table 5.2.

SDPMT-6 in sounding 9 required approximately 17 cm^3 of fluid to be injected before the probe contacted the side of the hole. To complete this test, an additional 13 cm^3 of fluid was injected to a total of approximately 30 cm^3. The reduced data from this test

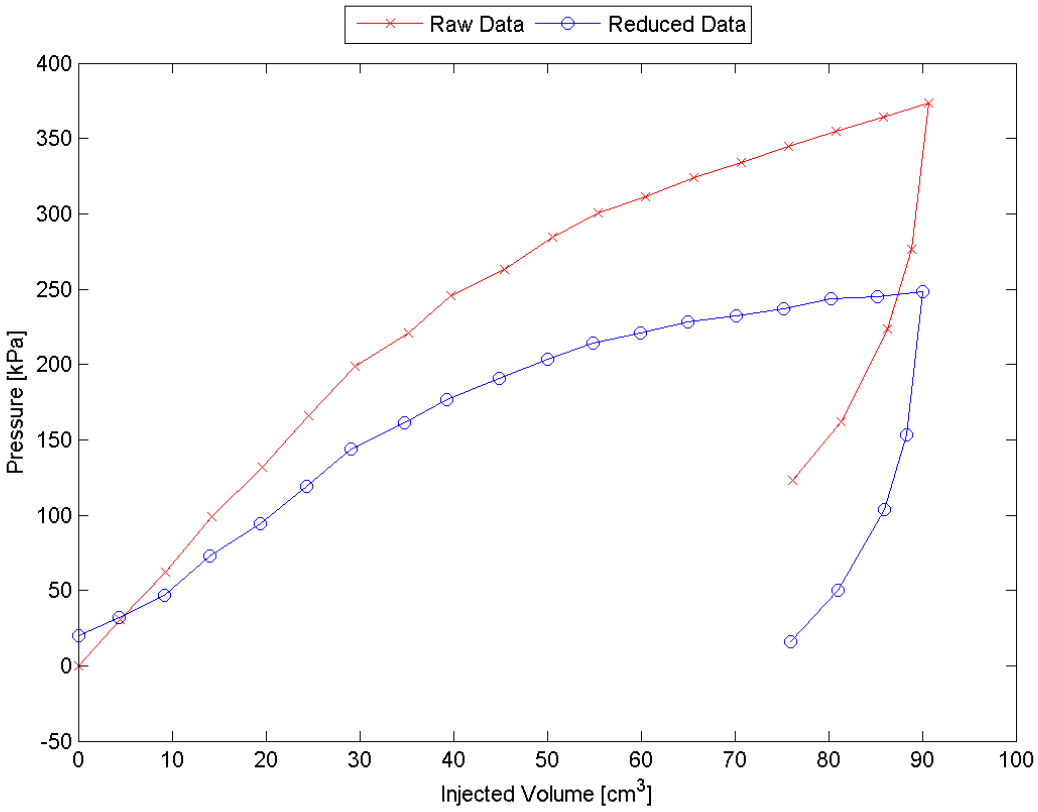

Figure 5.3: Raw and Reduced Data, Sounding 7, 0.61m, PPMT

was used to determine E_0 (566.1 psi or 3903 kPa), p_0 (0 psi or 0 kPa) and p_L (50.8 psi or 350 kPa). The raw and reduced data from sounding 9 is presented in Figure 5.7, and the engineering properties are presented in Table 5.2.

SDPMT-6 in sounding 11 required approximately 15 cm^3 of fluid to be injected before the probe contacted the side of the hole. To complete this test, an additional 15 cm^3 of fluid was injected to a total of approximately 30 cm^3. The reduced data from this test was used to determine E_0 to be 302.3 psi (1395 kPa), p_0 was estimated at 0 psi (0 kPa) and the p_L to be 29.0 psi (200 kPa). The raw and reduced data from sounding 11 is presented in Figure 5.8. The engineering properties are presented in Table 5.2.

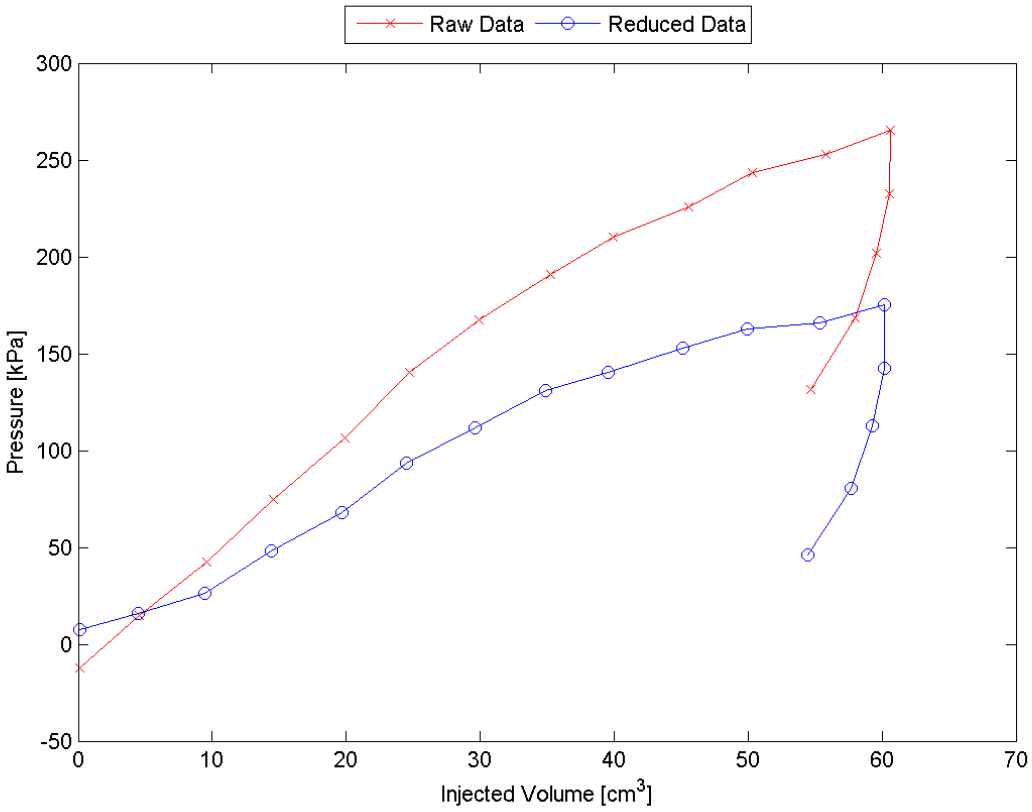

Figure 5.4: Raw and Reduced Data, Sounding 12, 0.61m, PPMT

5.1.3 SDPMT-12 Test Results

Four tests were conducted with the SDPMT-12; the 11.5 inch probe with a diameter of 0.625 in. Because this probe was sized large[1], as shown in Figure 5.9, less water had to be injected into it before it would reach the sides of the 3/4" diameter test hole. One test was performed in each of the soundings 2, 6, 8 and 10. Each test was conducted in holes 17 inches or 0.43 m deep, with the center of the membrane located at 8.92 inches.

SDMPT-12 in sounding 2 required approximately 15 cm^3 of fluid to be injected before the probe contacted the side of the hole. To complete this test, an additional 15 cm^3 of fluid was injected to a total of approximately 30 cm^3 during the test. The reduced data was used to determine E_0 as 357.3 psi (2464 kPa), p_0 was estimated at -2.9 psi (20 kPa) and p_L was 21.8 psi (150 kPa). The raw and reduced data from sounding 2 is presented in Figure 5.9. The engineering properties are presented in Table 5.2.

[1]Note: the initial volume of the monocell pressuremeters can be increased or decreased slightly to improve the test quality. In this testing a large initial size improved the testing.

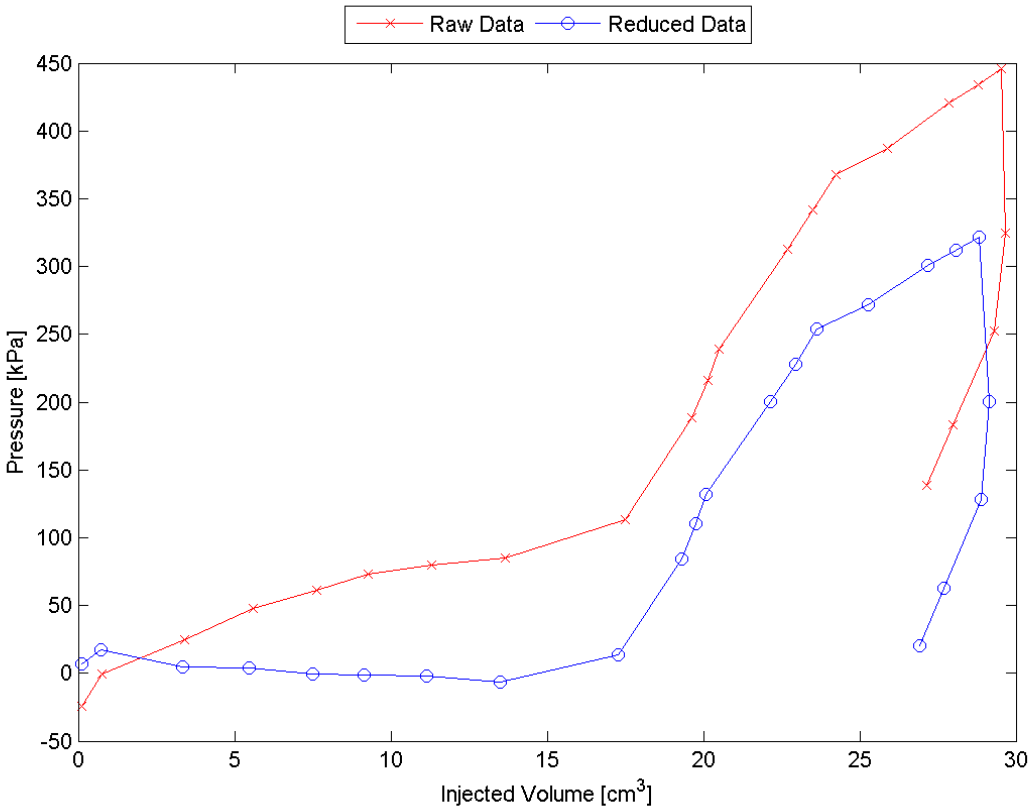

Figure 5.5: Raw and Reduced Data, Sounding 3, 0.43m, SDPMT-6

SDMPT-12 in sounding 6 required approximately 6 cm^3 of fluid to be injected before the probe contacted the side of the hole. To complete this test, an additional 24 cm^3 of fluid was injected to produce a total of approximately 30 cm^3 for the test. The reduced data was used to determine E_0 (451.4 psi or 3112 kPa), p_0 (-2.3 psi or -16 kPa) and p_L (36.3 psi 250 kPa) for this test. The raw and reduced data from sounding 6 is presented in Figure 5.10. The engineering properties are presented in Table 5.2.

SDPMT-12 in sounding 8 required approximately 7 cm^3 of fluid to be injected before the probe contacted the side of the hole. To complete this test, an additional 23 cm^3 of fluid was injected to a total of approximately 30 cm^3. The reduced data was used to determine that E_0 was 442.4 psi (3050 kPa), p_0 was estimated at 0.2 psi (2 kPa) and the p_L was 32.6 psi (225 kPa). The raw and reduced data from sounding 8 is presented in Figure 5.11. The engineering properties are presented in Table 5.2.

SDPMT-12 in sounding 10 required approximately 10 cm^3 of fluid to be injected before the probe contacted the side of the hole. To complete this test, an additional 20 cm^3 of fluid was injected to a total of approximately 30 cm^3. The reduced data was used to determine that E_0 was 637.5 psi (4396 kPa), p_0 was estimated at 3.4 psi (23 kPa) and the p_L was 36.3 psi (250 kPa). The raw and reduced data from sounding

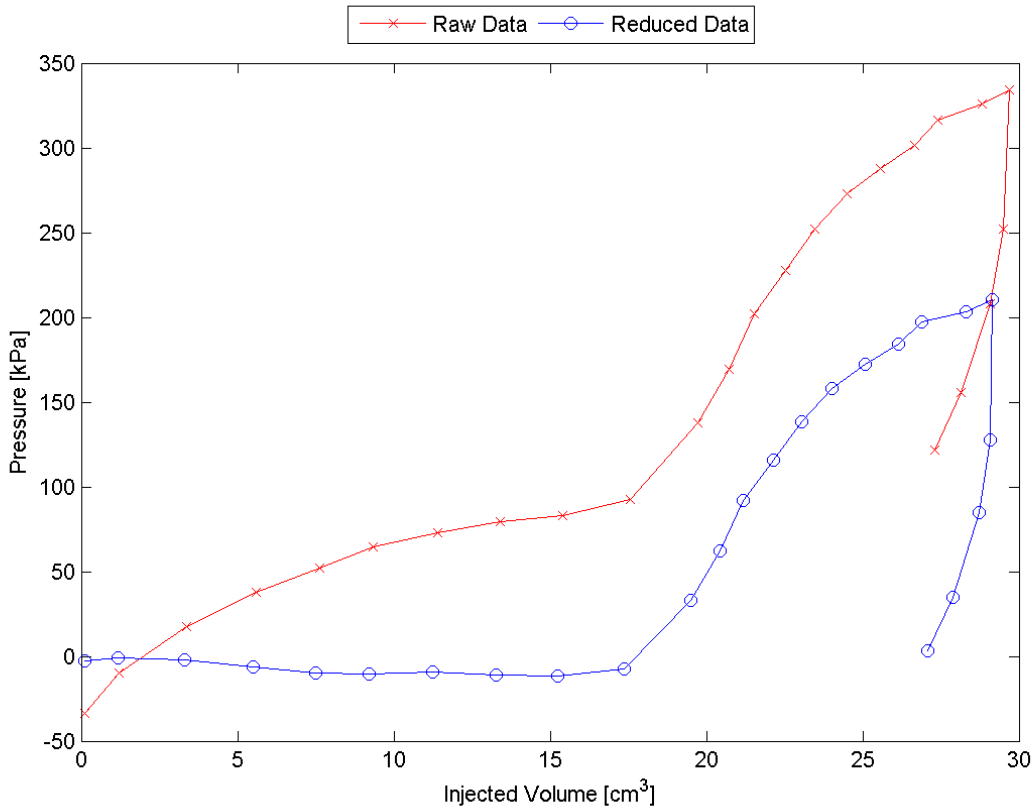

Figure 5.6: Raw and Reduced Data, Sounding 4, 0.43m, SDPMT-6

Table 5.1: Approximate Common PMT Parameters for Sands, After Briaud (2005)

Soil Type	Loose	Compact	Dense	Very Dense
p_L^* (kPa)	0 - 500	500 - 1,500	1,500 - 2,500	>2,500
E_0 (kPa)	0 - 3,500	3,500 - 12,000	12,000 - 22,500	>22,500

10 is presented in Figure 5.12. The engineering properties are presented in Table 5.2.

5.1.4 Preliminary Testing Results

Two engineering soil properties were determined using the APMT software during testing (E_0, p_L). Briaud (2005) proposed a relationship between soil type and typical ranges of p_L and E_0. Based on Briaud's (2005) the recommended values for sands, shown in Table 5.1, the soil type and visual consistency were determined from the data collected with the three PMT probes.

The moduli calculated from SDPMT-6 tests ranged from 202.3 psi to 707 psi with an average modulus of 486.2 psi. SDPMT-12 testing produced moduli ranging from

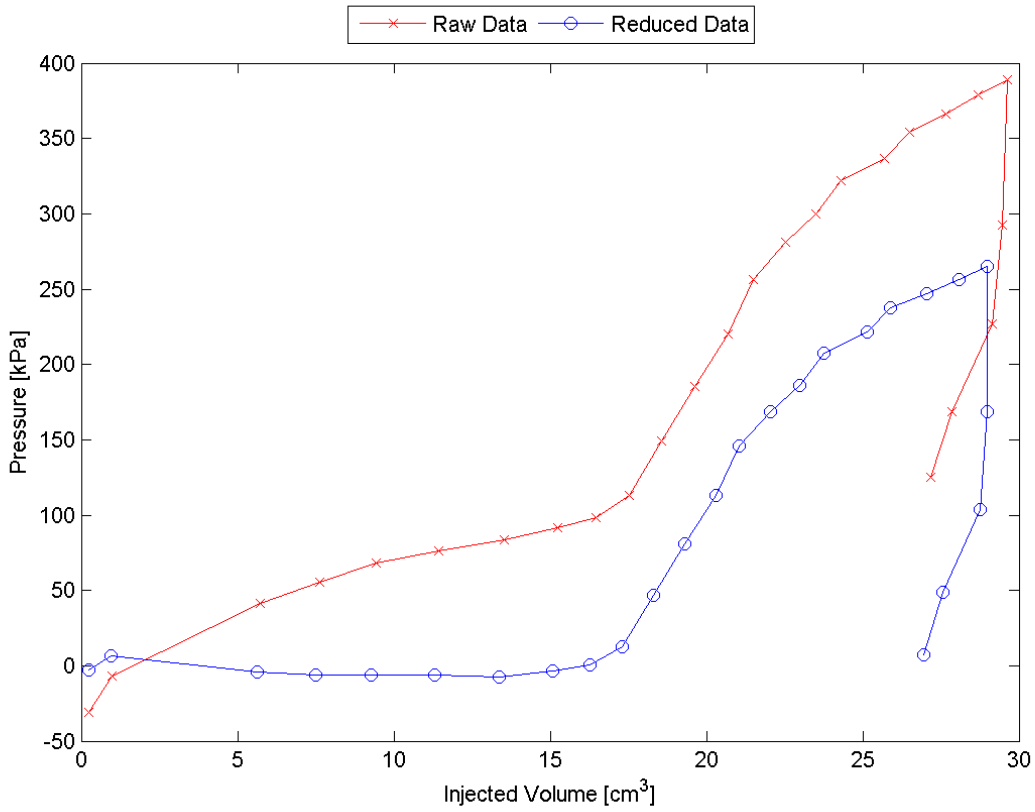

Figure 5.7: Raw and Reduced Data, Sounding 9, 0.43m, SDPMT-6

357.3 psi to 637.5 psi with an average of 472.2 psi. The PPMT produced a moduli ranging from 346.8 psi to 419.1 psi with an average of 383.8 psi. The average initial modulus for all 12 tests is 447.4 psi. The E_0 and p_L data are summarized in Table 5.2. In general, these values are similar. The p_l values from the SDPMT-12 and PPMT are very similar, while the SDPMT-6 values are higher but still within the loose rage cited by Briaud (2005). There is more variability in E_0, therefore they are all considered similar and within the loose category according to Briaud (2005).

An intensity plot showing the variation of E_0 across the site is shown in Figure 5.13. Moduli from 250 to 800 psi are depicted. The plot indicates some variation across the site, with higher moduli at the opposite sides of the test site, i.e., soundings 3 and 10 and the lowest moduli at soundings 11 and 12.

The limit pressures determined from SDPMT-6 testing ranged from 29.0 psi to 65.3 psi with an average of 47.1 psi. SDPMT-12 produced limit pressures ranging from 21.8 psi to 36.3 psi, with an average of 31.7 psi. The PPMT produced limit pressures ranging from 29.0 psi to 36.3 psi, with an average 33.5 psi. The average limit pressure of all 12 tests is 37.5 psi. The limit pressure data is summarized in Table 5.2. In summary, the limit pressures are similar for the SDPMT-12 and PPMT, but the SDPMT-6

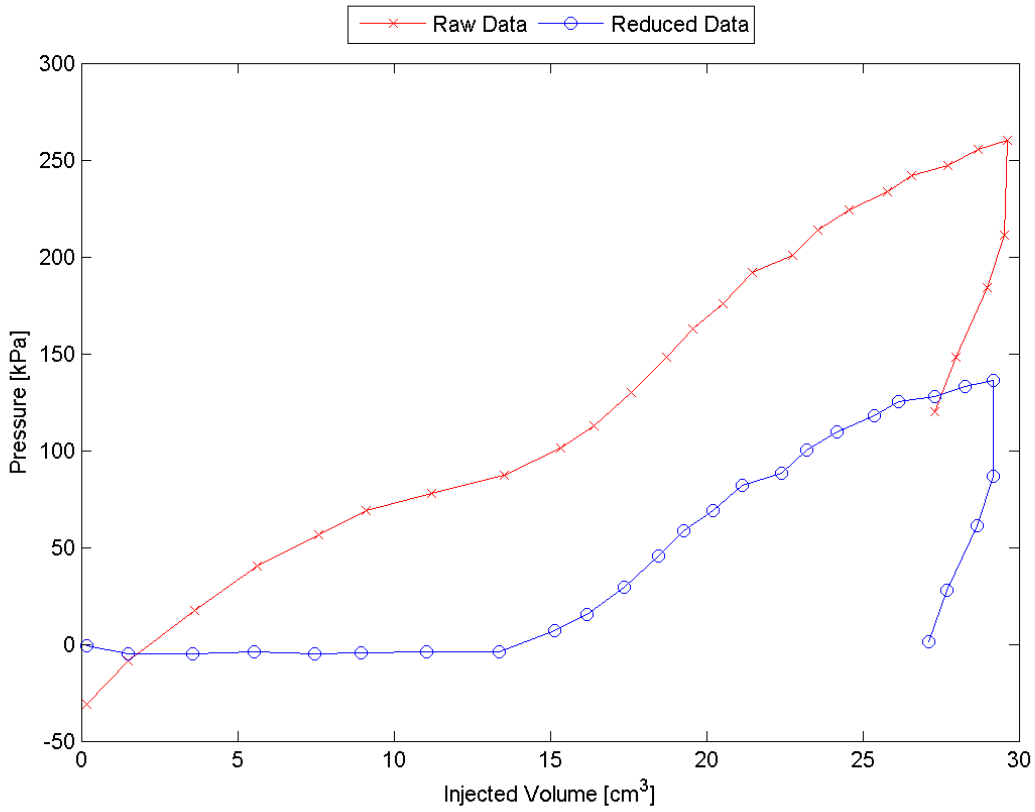

Figure 5.8: Raw and Reduced Data, Sounding 11, 0.43m, SDPMT-6

produced higher values. The variation across this site was expected, because it was a general fill area for residential construction.

A second intensity plot showing the variation of p_L across the site is shown in Figure 5.14. Limit pressures from 25 to 65 psi are depicted. The plot shows some variation across the site, however it is more consistent than the E_0 intensity plot. The limit pressure is highest at sounding 3, but generally is between 24 and 45 psi.

All soils were visually classified as sands, therefore Briaud's relationship for sands was used and is shown in Figure 5.1. Based on the tests results the moduli and limit pressures indicate that sands varied from loose to medium dense.

5.2 SDPMT Testing Observations

Three observations were made throughout the testing with the SDPMT probe at the four sites. These observations concern the probe insertion technique in cemented coquina base, surface cracking due to the low confinement during testing and slippage of the rubber membrane during testing.

Table 5.2: Summary of Preliminary Engineering Properties

Probe Type	Test Number	Sounding Number	E0		P0		Pl		Soil Type & Visual Consistency
			psi	kPa	psi	kPa	psi	kPa	
Mini-PMT 6in	1	3	707.9	4881	2.0	13	65.3	450	Med. Dense Sand
	2	4	468.3	3229	0	0	43.5	300	Loose Sand
	3	9	566.1	3903	0	0	50.8	350	Loose to Med. Dense Sand
	4	11	202.3	1395	0	0	29.0	200	Loose Sand
		Average	486.2	3352	0.5	3	47.1	325	
Mini-PMT 12in	5	2	357.3	2464	0	0	21.8	150	Loose Sand
	6	6	451.4	3112	0	0	36.3	250	Loose Sand
	7	8	442.4	3050	0.2	2	32.6	225	Loose Sand
	8	10	637.5	4396	3.4	23	36.3	250	Loose to Med. Dense Sand
		Average	472.2	3255	0.9	6.25	31.7	219	
PPMT	9	1	346.8	2391	0	0.0	32.6	225	Loose Sand
	10	5	419.1	2889	1.3	9	32.6	225	Loose Sand
	11	7	402.3	2774	2.9	20	33.7	260	Loose Sand
	12	12	367.0	2530	1.1	8	29.0	200	Loose Sand
		Average	383.8	2646	1.3	9	33.0	228	

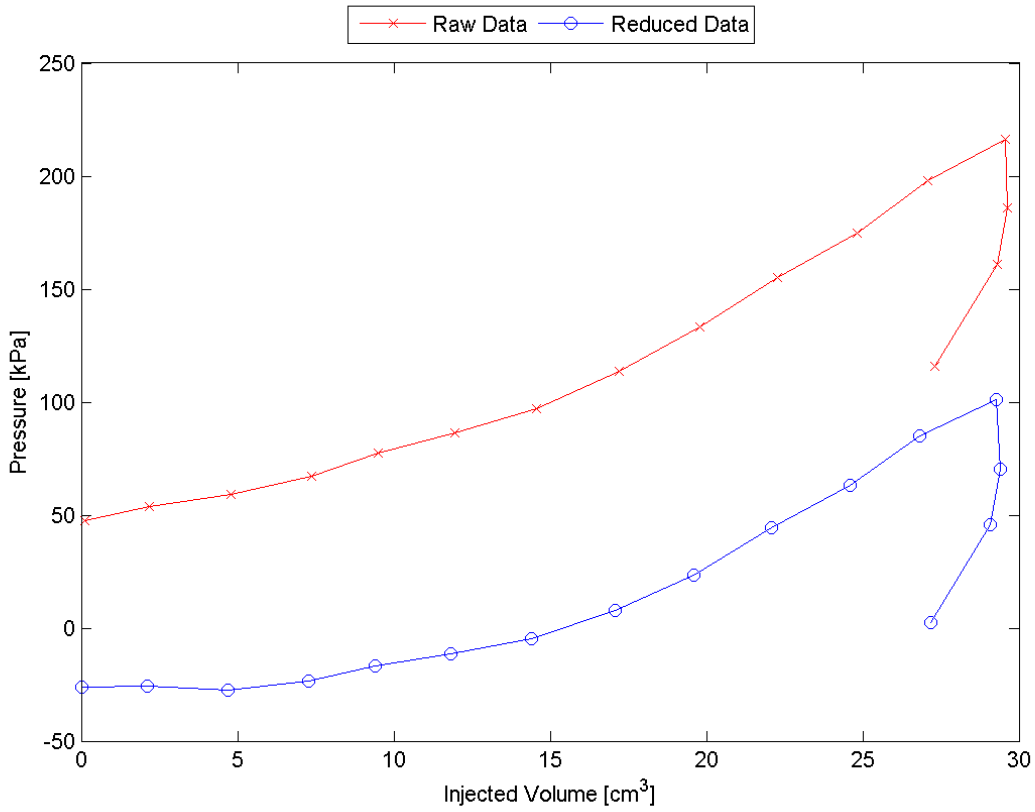

Figure 5.9: Raw and Reduced Data, Sounding 2, 0.43m, SDPMT-12

5.2.1 Rotary Hammer Drill in Base Material

The St. Johns Heritage Parkway test site proved to be a difficult site for installing SDPMT probes. The cemented coquina base was tested in mid-summer during a very dry period. Cemented coquina stiffens significantly during dry weather. The resulting very dense dry cemented coquina, made it very difficult to drive the NDG pin into the soil, which decreased productivity.

To address this issue, an alternative insertion method was developed (Figure 5.15). It involved first making a pilot hole through the NDG template using a 5/8 inch (15 mm) masonry bit and hammer drill. This pilot hole was 2 inches (50 mm) deeper than the depth required for the SDPMT probe to allow for the probe ends to rest in the soil and the rubber testing section to be set for either the 6 or 12-inch tests. After completing the pilot hole, the modified 3/4 inch (19 mm) diameter NDG pin was driven to the base of the pilot hole. It was then removed, while ensuring that the hole was clean. Finally, the probe was inserted for testing. This two-step process significantly improved the insertion time in this base material. The resulting time per test was approximately four minutes, which was a significant decrease from the 30 minutes required without the pilot hole.

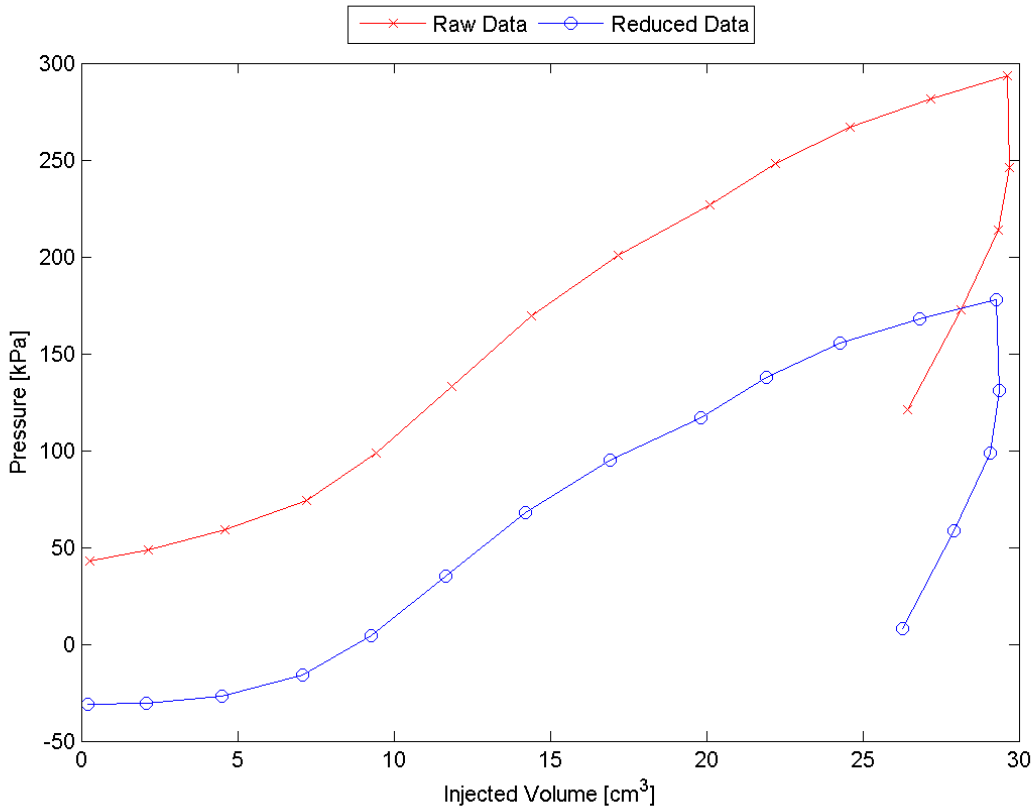

Figure 5.10: Raw and Reduced Data, Sounding 6, 0.43m, SDPMT-12

5.2.2 Surface Cracking

During SDPMT testing, occasionally surface cracks were observed during the probe the inflation process. These cracks were observed when testing with both 6 and 12 inch probes and during incremental and rapid tests. Although it was difficult to determine which injected volumes produced these cracks, they tended to form in the very dry cemented coquina at Heritage Parkway. An example of these cracks is illustrated in Figure 5.16. Figure 5.17 illustrates a typical continuous test where surface cracks were observed. The cracking produced a drop in pressure from about 2,100 kPa to 1,800 kPa (305 to 261 psi) between injected volumes of 25 and 30 cm^3.

The surface cracking is most likely due to stresses applied to the soil by the SDPMT reaching the unconfined surface. A possible way to mitigate this problem would be to use surcharge plates over the test location to help constrain the stresses to the tested layer. Surcharge plates are used during field CBR tests. Weights were not used during this phase of the research.

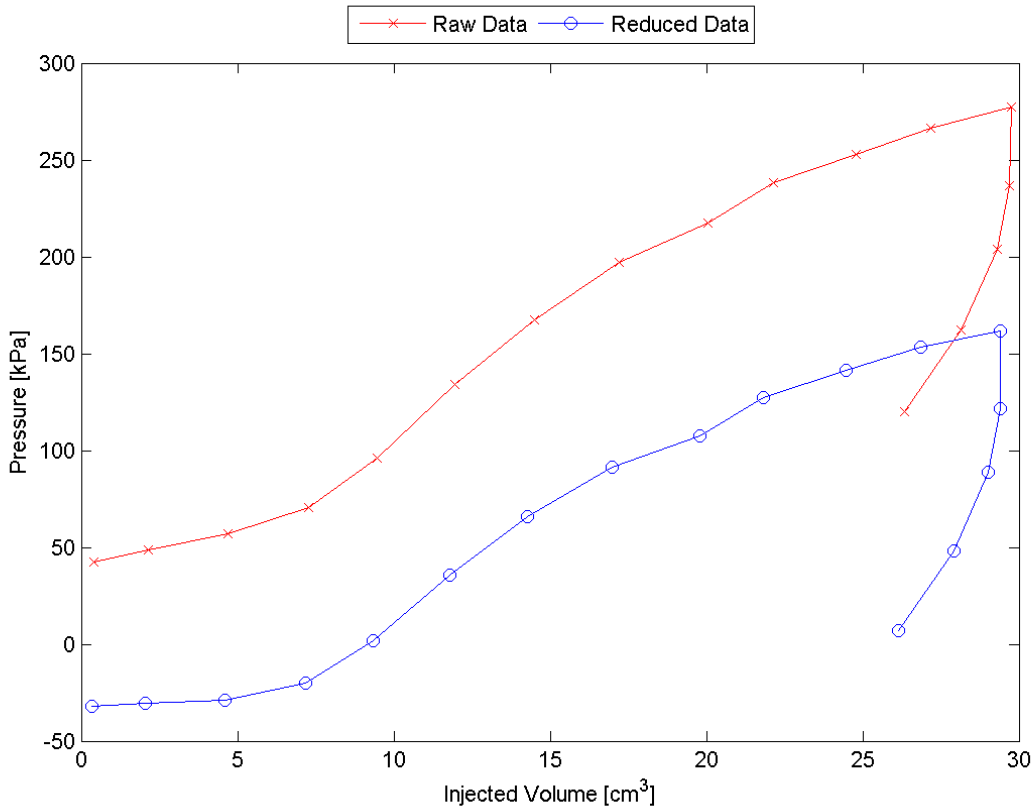

Figure 5.11: Raw and Reduced Data, Sounding 8, 0.43m, SDPMT-12

5.2.3 Membrane Slipping

During testing with SDPMT probes, the membrane would randomly slide causing it to move either within or completely out of the aluminum sleeve (Figure 5.18). This sleeve is designed to prevent leaks by securing the membrane to the probe body. The right side of the probe in Figure 5.18 illustrates an example, which occurred during testing of the membrane slippage. The operator should adjust the equipment as needed if this occurs.

5.3 Correlation Testing

Testing was conducted at the four test sites to compile a statistically reliable set of data. These data were used to develop correlations between basic engineering parameters obtained from SDPMT testing and those obtained from the other unbound pavement layer testing techniques. The results from this testing are presented in the following sections.

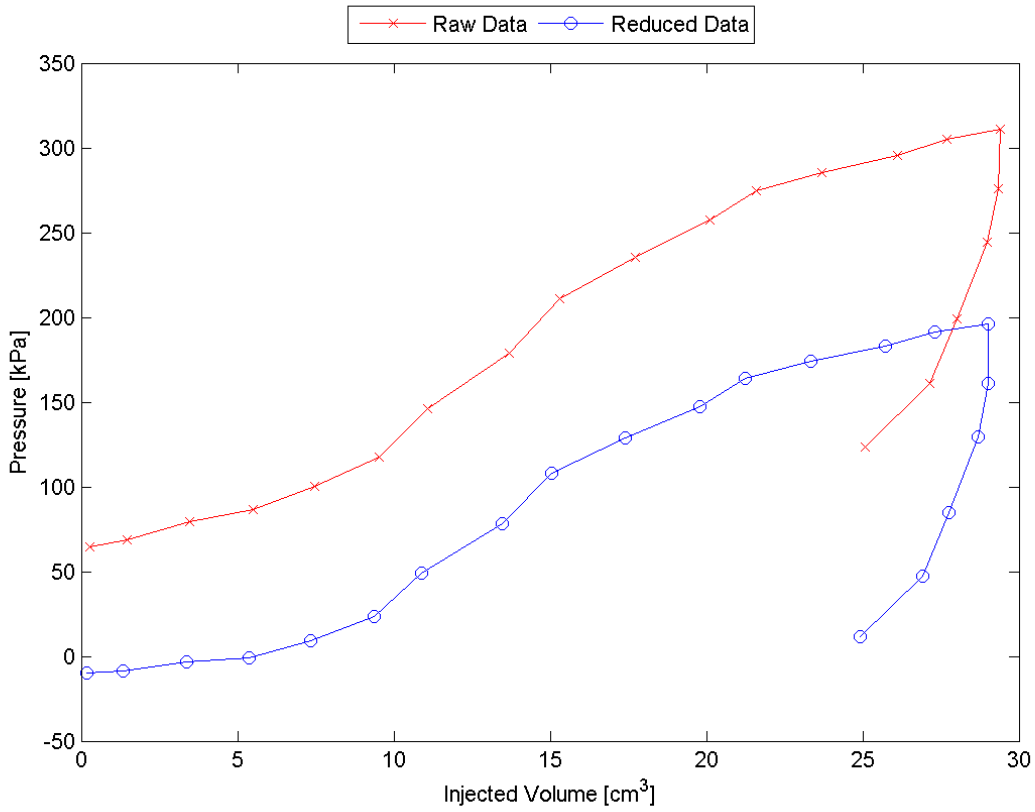

Figure 5.12: Raw and Reduced Data, Sounding 10, 0.43m, SDPMT-12

5.3.1 Site 1: Cypress Landing

Testing at the Cypress Landing test site included SDPMT-12 tests, NDG tests, LWD tests using both with the Zorn and Dynatest models. Tests were also conducted with the CIT device and DCP. Samples of the subgrade soil were also collected and transported to the FDOT SMO to run index testing along with resilient modulus tests. The results of these tests are summarized below.

5.3.1.1 PMT Test Results

Twenty-six SDPMT-12 tests were conducted at Cypress Landing. Table 5.3 indicates which test types were performed at each location. Test locations were spaced 25 feet apart along the residential street (i.e., Potenza Drive), which was under construction during testing. SDPMT-12 tests were categorized as follows: a) incremental tests; b) continuous tests, c) tests in the same hole as the NDG test and d) tests performed in a separate hole.

Eleven incremental tests were conducted with the 12 inch SDPMT probe. The test categories are summarized in Table 5.3. The X's shown in this table indicate the type of

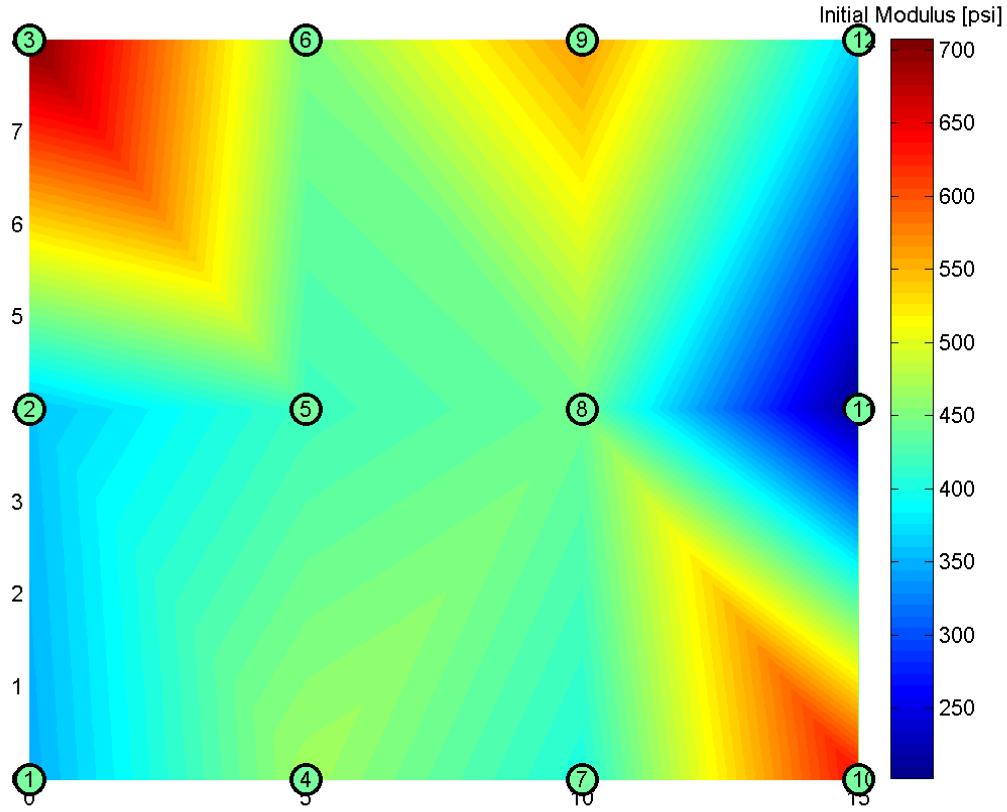

Figure 5.13: Variation of E_0 Across Preliminary Test Area, Based on all Three Test Types with sounding numbers shown in circles

test conducted at a particular location, while the bottom row in the table indicates the appendix location that the resulting plots can be found. Four tests were conducted in the same hole as the NDG tests, and results of the tests are shown in Section C.1. Seven tests were conducted in a separately driven hole, and the results of these test are shown in Section C.3. A total of ten SDPMT tests were conducted using the continuous SDPMT test method. Five SDPMT tests were conducted with the SDPMT-6 probe in the same hole as the NDG test, and these results are shown in Section C.4. Five continuous tests were conducted in separate holes adjacent to the NDG tests. The results are shown in Section C.2.

5.3.1.1.1 SDPMT-12 Incremental Results

The engineering parameters obtained from the 11 incremental SDPMT-12 tests are summarized in Table 5.4. Positive lift-off pressures were determined from 7 of the eleven tests. Negative lift-off pressures, shown from four of the tests, imply soil is experiencing tension, which are not realistic. The lift-off pressure has not been a consistent property

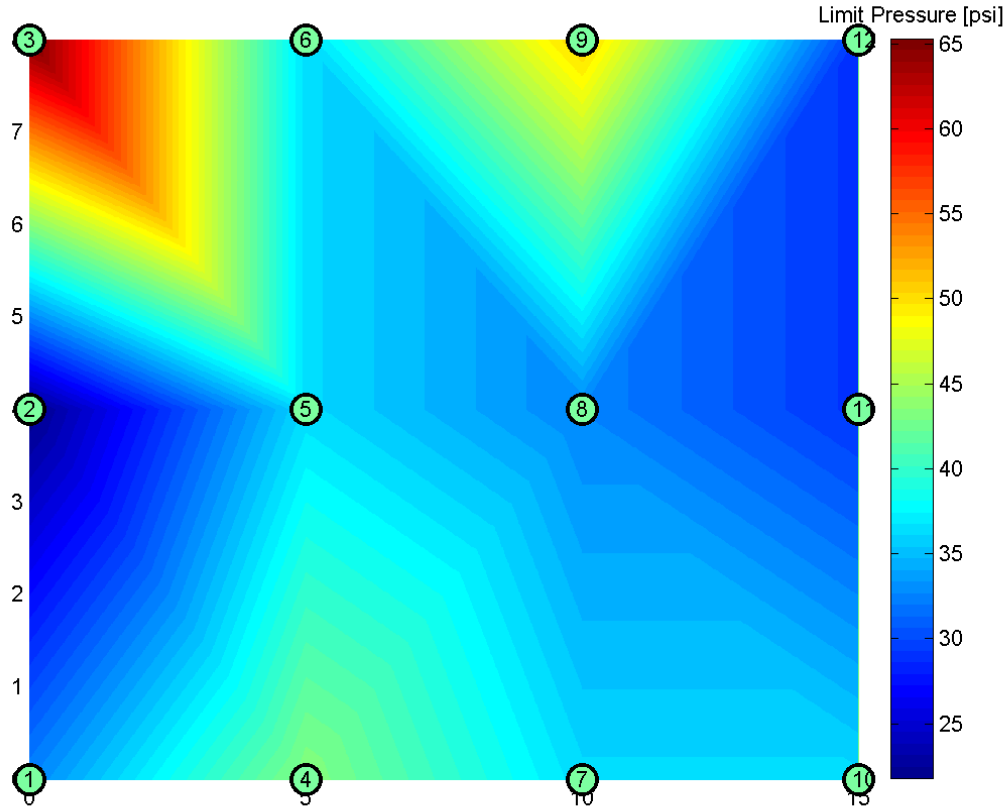

Figure 5.14: Variation of p_L Across Test Area, Based on all Three Test Types with sounding numbers show in circles

and therefore, is not typically used by geotechnical engineers in either design or analysis. Values ranged from 1.4 to 14.0 kPa (0.2 to 2.0 psi) producing an average of 6.7 kPa (1 psi) and a standard deviation of 4.5 kPa (0.7 psi). The limit pressure of the soil ranged from 330.0 to 740.0 kPa (47.9 to 107.3 psi) with an average of 480.0 kPa (69.6 psi) and a standard deviation of 150.0 kPa (21.8 psi). Initial moduli ranged from 2865 to 8758 kPa (415.5 to 1270.2 psi) with an average of 5486 kPa (795.6 psi) and a standard deviation of 1994 kPa (289.2 psi).

5.3.1.1.2 SDPMT-12 Continuous Results

Ten SDPMT-12 continuous tests were conducted; however, due to over-sized boreholes, four tests did not produce results that could be analyzed. The engineering parameters obtained from the remaining 6 tests are summarized in Table 5.5. Positive lift-off pressures were able to be determined from 3 of the 6 tests (i.e., the remaining three produced negative lift-off pressures, which are not realistic in sands). These values ranged from 25.7 to 87.4 kPa (3.7 to 12.7 psi) producing an average of 63.3 kPa (9.1

Table 5.3: Summary of Cypress Landing SDPMT Test Locations and Procedure

Location Number	Separate Hole		NDG Hole	
	Incremental	Continuous	Incremental	Continuous
101	X	X		
102	X	X		
103	X			
104			X	X
105	X	X		
106			X	X
107	X			
108	X			
109		X	X	X
110	X			
111		X	X	X
112	X			X
Appendix	C.1	C.2	C.3	C.4

Table 5.4: SDPMT-12 inch Incremental Test Results for Cypress Landing

Location Number	Lift-off Pressure p_0 [kPa]	Limit Pressure p_L [kPa]	Initial PMT Modulus E_0 [kPa]
101	14.0	380.0	3211
103	4.0	330.0	4740
104	4.3	345.0	2856
105	6.5	610.0	8758
106	11.4	725.0	8004
107	−0.1	740.0	8311
108	5.2	415.0	4905
109	1.4	335.0	4745
110	−6.2	470.0	4536
111	−0.8	420.0	4967
112	−5.8	510.0	5315
Average	3.1	480.0	5486
Standard Dev.	6.3	150.0	1994

Figure 5.15: Drilling 5/8 Diameter Hole for SDPMT Testing

psi) with a standard deviation of 33.0 kPa (47.9 psi). The limit pressure ranged from 160.0 to 725.0 kPa (23.2 to 105.1 psi) with an average of 448.3 kPa (65.0 psi) and a standard deviation of 205.0 kPa (29.7 psi). Initial moduli ranged from 2,479 to 11,929 kPa (359.5 to 1730.1 psi) with an average of 5,642 kPa (818.3 psi) and a standard deviation of 3,403 kPa (2479 psi).

5.3.1.2 NDG Results

Twenty-four NDG tests were conducted at both 6 and 12 inch depths across the Cypress Landing test site. The dry densities from the 12 NDG tests at the six inch depth ranged from 106.0 to 115.2 lb/ft^3 (16.6 to 18.1 kN/m^3)with an average of 112.3 lb/ft^3 (17.6 kN/m^3), and a standard deviation of 2.9 lb/ft^3 (0.5 kN/m^3). These results are summarized in Table 5.6. The dry densities from the 12 inch deep tests ranged from 103.8 to 114.6 lb/ft^3 (16.3 to 17.9 kN/m^3) with an average of 111.9 lb/ft^3 (17.6 kN/m^3),

Figure 5.16: Observed Surface Cracks in Dry Cemented Coquina, 3/4 inch hole

and a standard deviation of 3.3 lb/ft^3 (0.5 kN/m^3). The results from the 12 NDG 12 inch tests are summarized in Table 5.7. With the exception of the values at location 104, which are well below the average,the densities along the testing locations are consistent.

5.3.1.3 Zorn LWD Results

Twenty-four LWD tests, two at each location, were conducted with the Zorn LWD device at the Cypress Landing test site. Surface deflections and elastic moduli were measured with the apparatus. Surface deflections ranged from 0.45 to 3.84 mm (0.2 to 0.15 inch) and elastic deformation moduli (E_d) ranged from 5.9 to 50.3 MPa (885.0 to 7293.0 psi). The test data is summarized in Table 5.8 and illustrated in Figure 5.19. The moduli values are calculated using software within the control unit after three drops of the weight.

5.3.1.4 Dynatest LWD Results

Twenty-four LWD tests, two at each location, were conducted with the Dynatest LWD at the Cypress Landing test site. Elastic moduli measured with the apparatus ranged from 32.3 to 174.7 MPa (468.5 to 2533.7 psi). The test data is summarized in Table 5.9.

5.3.1.5 CIT Results

Twenty-four CITs were performed at the Cypress Landing test site, two at each location, with Clegg impact values ranging from 4.6 to 10.9 g's. The test data is summarized in Table 5.10 and illustrated in Figure 5.20.

Table 5.5: SDPMT-12 inch Continuous Test Results for Cypress Landing

Location Number	Lift-off Pressure p_0 [kPa]	Limit Pressure p_L [kPa]	Initial PMT Modulus E_0 [kPa]
101	−82.5	410.0	2808
102		†	
105	−80.7	315.0	5122
105	−52.9	625.0	5886
107	25.7	725.0	11929
108		†	
109		†	
110	87.4	160.0	2479
111		†	
112	77.0	455.0	5626
Average	−4.3	448.3	5642
Standard Dev.	77.7	205.0	3403

†: Borehole to large for reliable results.
Note: 1 KPa = 14.5 psi

Table 5.6: Nuclear Density Test Results for Cypress Landing, 6 inch test depth

Location	Density Dry [lb/ft^3]	Density Wet [lb/ft^3]	Moisture Content [%]
101	109.1	120.3	10.3
102	114.0	123.3	8.2
103	109.7	116.1	5.9
104	106.0	113.0	6.6
105	112.8	118.8	5.3
106	115.0	121.8	5.9
107	114.4	121.6	6.3
108	115.2	123.0	6.8
109	111.6	122.8	10.1
110	110.9	121.4	9.5
111	114.1	127.0	11.3
112	114.5	124.6	8.8
Average :	112.3	121.1	7.9
Std. Dev. :	2.9	3.8	2.0

1 lb/ft^3 = 0.157 kN/m^3

Table 5.7: Nuclear Density Test Results for Cypress Landing, 12-inch test depth

Location	Density Dry [lb/ft^3]	Density Wet [lb/ft^3]	Moisture Content [%]
101	109.1	120.3	10.3
102	114.0	123.3	8.2
103	109.7	116.1	5.9
104	106.0	113.0	6.6
105	112.8	118.8	5.3
106	115.0	121.8	5.9
107	114.4	121.6	6.3
108	115.2	123.0	6.8
109	111.6	122.8	10.1
110	110.9	121.4	9.5
111	114.1	127.0	11.3
112	114.5	124.6	8.8
Average :	112.3	121.1	7.9
Std. Dev. :	2.9	3.8	2.0

l lb/ft^3 = 0.157 kN/m^3

Table 5.8: Cypress Landing Zorn LWD Testing Summary

Location	Test 1 Sd [mm]	Test 1 Ed [MPa]	Test 2 Sd [mm]	Test 2 Ed [MPa]	Average Sd [mm]	Average Ed [MPa]
101	1.26	17.8	0.87	25.8	1.07	21.8
102	0.74	30.5	0.82	27.4	0.78	29.0
103	1.74	13.0	1.03	21.8	1.38	17.4
104	3.84	5.9	3.75	6.0	3.79	5.9
105	0.74	30.4	0.53	42.7	0.63	36.5
106	0.62	36.4	0.73	31.0	0.67	33.7
107	0.79	28.3	0.67	33.6	0.73	31.0
108	0.91	24.8	0.82	27.3	0.87	26.0
109	0.58	38.8	0.55	41.1	0.56	39.9
110	0.55	41.2	0.52	43.4	0.53	42.3
111	0.63	35.9	0.45	50.3	0.54	43.1
112	0.48	46.8	0.52	42.9	0.50	44.9
Average	1.07	29.1	0.94	32.8	1.01	31.0
Std. Dev.	0.94	12.1	0.90	12.2	0.91	11.7

Note: 25 mm = 1 inch, 1 MPa = 145 psi

Table 5.9: Cypress Landing Dynatest LWD Testing Summary

	Test 1	Test 2	Average
Location	E0 [MPa]	E0 [MPa]	E0 [MPa]
101	37.3	32.3	34.8
102	72.3	62.6	67.5
103	51.3	46.7	49.0
104	21.3	24.7	23.0
105	174.7	95.7	135.2
106	74.0	90.3	82.2
107	60.7	59.7	60.2
108	92.3	67.0	79.7
109	55.0	85.3	70.2
110	82.0	112.0	97.0
111	96.3	120.7	108.5
112	95.3	108.3	101.8
Average	76.0	75.4	75.7
Std. Dev.	38.9	31.5	32.1

Note: 1 MPa = 145 psi

Table 5.10: Cypress Landing Clegg Impact Test Results

Location	Test1 [g's]	Test2 [g's]	Average [g's]
101	8.1	6.8	7.5
102	6.1	4.6	5.4
103	5.5	5.3	5.4
104	6.5	5.3	5.9
105	10.0	9.6	9.8
106	8.7	9.1	8.9
107	10.4	10.9	10.7
108	5.5	7.0	6.3
109	8.7	7.2	8.0
110	10.0	7.6	8.8
111	6.5	7.4	7.0
112	5.9	5.0	5.5
Average	7.7	7.2	7.4
Std. Dev.	1.9	2.0	1.8

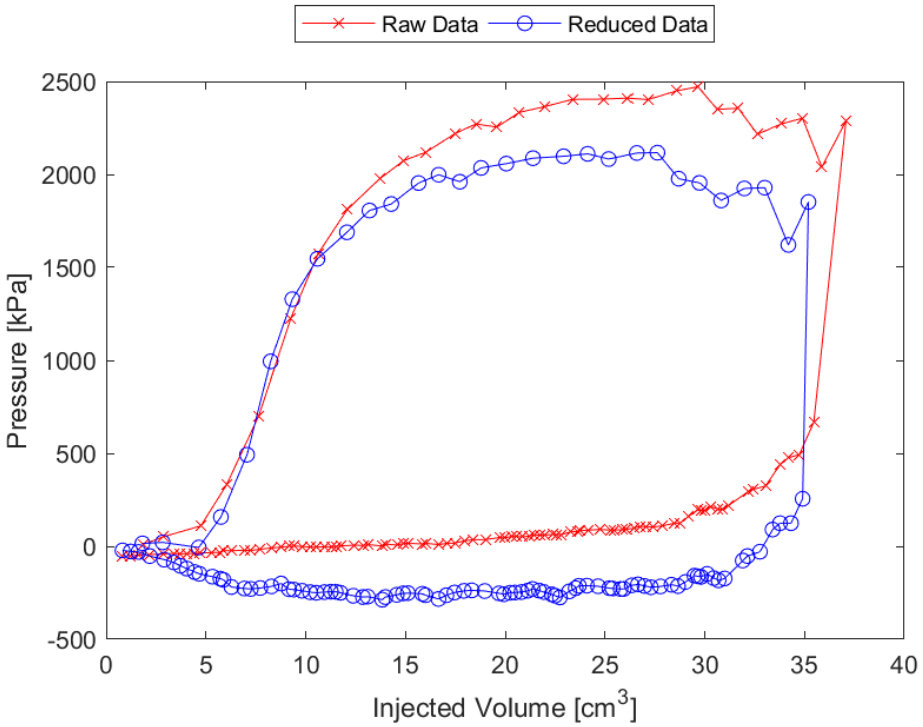

Figure 5.17: Example of Typical Test Data of Observed Surface Cracks

5.3.1.6 DCP Test Results

Twelve DCP tests, one at each test location, were conducted at the Cypress Landing site. DCP tests were conducted to a depth of 12 inches. A typical set of plots is contained in Figure 5.21. The data from each test is presented in Figures I.25 through I.36. Each figure includes two plots; one with total penetration versus total number of blows, and a second with penetration depth versus penetration per blow. Note the both the imperial (i.e. English) and international units are displayed on the y-axes.

5.3.1.6.1 DCP Data Reduction

The data collected from each DCP test was further analyzed to determine an average 6 and 12 inch (15 and 30 cm) penetration per blow or penetration index (DCP PI). The average DCP index was compared with SDPMT engineering parameters.

Table 5.11 summarizes the penetration rate for the Cypress Landing DCP tests. The 6 inch (15 cm) averages ranged from 20.0 to 35.2 mm/blow (0.8 to 1.4 inches/blow) with an overall average and standard deviation of 27.3 and 4.8 mm/blow, (1.1 to 0.2 inches/blow)respectively. The 12 inch (30 cm) averages ranged from 14.8 to 24.5 mm/blow (0.6 to 1.0 inches/blow) with an overall average an standard deviation of 20.8 and 3.4 mm/blow (0.8 to 0.1 inches/blow), respectively. The small standard deviations for the DCP PI is an indication that the properties are consistent across of

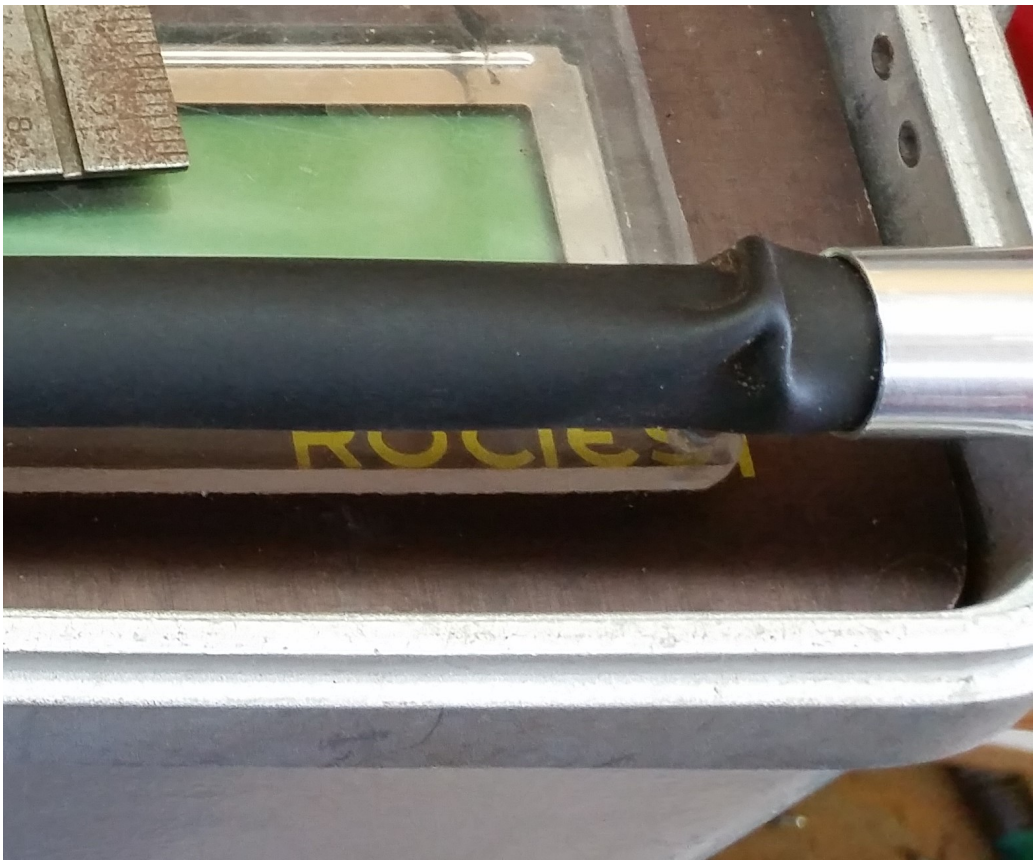

Figure 5.18: Example of Membrane Slipping Observed During Testing

the site.

5.3.1.7 Resilient Modulus Results

FDOT SMO laboratory performed eight resilient modulus tests according to AASHTO T-307 on the soil collected from Cypress Landing. As part of the testing, SMO determined that the maximum density from AASHTO T99 was 117.2 lb/ft^3 (18.4 kN/m^3), with an optimum moisture content of 10%. Resilient modulus test samples were compacted to the following target moisture contents; dry of optimum (3 and 6%), optimum (10%), and wet of optimum (12%). Moduli at a bulk stress of 11 psi ranged from 10,869 to 16,988 psi (1576 to 2462 kPa). In general, the moduli decreased with increasing water content. The largest decrease occurs below the optimum moisture content. The results of this testing are summarized in Table 5.12.

The two resilient modulus tests, from samples compacted at the optimum moisture content, were used to estimate an average strain and resilient modulus for the soil at the Olin Overflow Parking site. This data is shown in Table 5.13. As the moisture content increased from 6 to 12 percent, the resilient moduli from each test decreased. The average strain, from the 15 loading sequences conducted during the resilient modulus test, was 3.10x10^{-2} %, and the average moduli was 16,471 psi (2389 kPa). These data

Table 5.11: Summary of DCP Indices for 6 and 12 inch Penetrations at Cypress Landing

Location Number	6 inch Average Blows to 153 mm [blows]	6 inch Average Total Penetration [mm]	6 inch Average Penetration per blow [mm/blow]	12 inch Average Blows to 305 mm [blows]	12 inch Average Total Penetration [mm]	12 inch Average Penetration per blow [mm/blow]
101	6	163	27.2	15	323	21.5
102	6	166	27.7	14	324	23.1
103	6	175	29.2	13	309	23.8
104	5	162	32.4	13	319	24.5
105	7	162	23.1	17	312	18.4
106	8	160	20.0	20	308	15.4
107	8	161	20.1	18	319	17.7
108	6	165	27.5	14	320	22.9
109	7	170	24.3	21	310	14.8
110	6	168	28.0	15	310	20.7
111	5	163	32.6	14	319	22.8
112	5	176	35.2	13	313	24.1
Average			27.3			20.8
Std. Dev.			4.8			3.4

Note: 25 mm = 1 inch

Table 5.12: Resilient Modulus Test Results Dry, Wet and at Optimum Moisture from Cypress Landing Subgrade

	Target Moisture [%]	Max † Density [lb/ft^3]	Compacted Density [lb/ft^3]	Compacted Moisture [%]	Percent of Optimum [%]	K1	K2	Resilient Modulus ($\theta = 11$ psi) [psi]
Dry 1	6	117.2	114.2	5.9	97.5	5629.6	0.4283	15,722
Dry 2	6	117.2	114.4	5.9	97.8	6304.1	0.4134	16,988
Dry 3	8	117.2	115.3	7.7	98.6	4752.9	0.4359	13,518
Dry 4	8	117.2	115.0	7.9	98.2	4886.8	0.4445	14,189
Opt 1	10	117.2	117.0	10.0	99.8	3749.3	0.5253	13,212
Opt 2	10	117.2	117.0	10.0	99.8	3177.3	0.5851	12,923
Wet 1	12	117.2	114.2	12.0	97.4	3487.5	0.4951	11,468
Wet 2	12	117.2	114.0	12.2	97.2	3098.5	0.5246	10,869

† AASHTO T99 Results

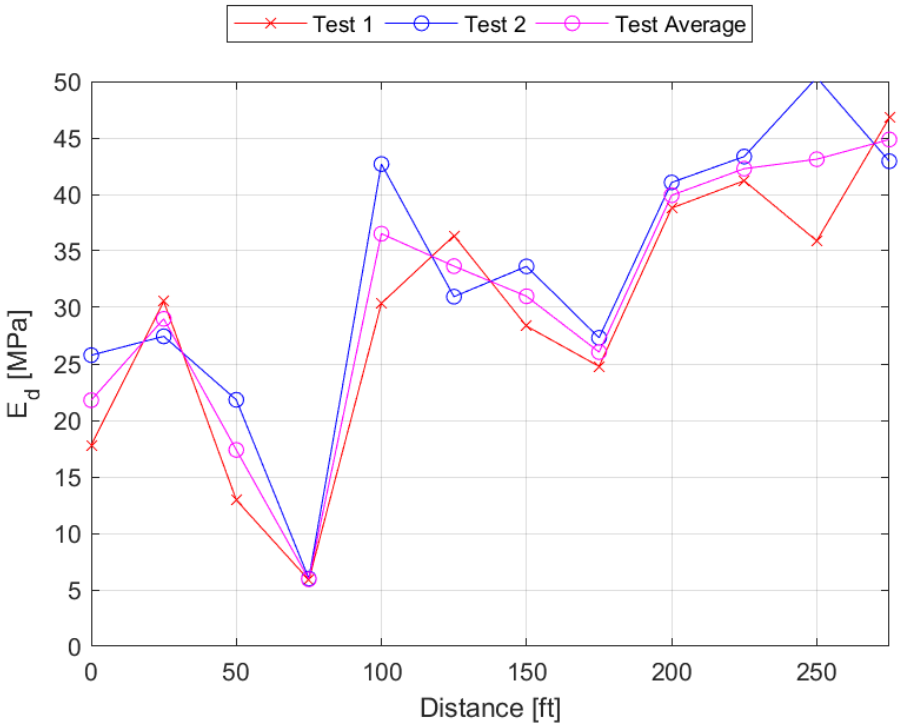

Figure 5.19: LWD Zorn E_d Along the Cypress Landing Test Site

were compared with moduli obtained from the SDPMT unload data.

Table 5.13: Summary of Resilient Modulus Sequence Data for Cypress Landing

Sequence	Chamber Confining Pressure	Nominal Maximum Axial Stress	Nominal Bulk Stress	Test 1		Test 2		Average	
				Resilient Strain	Resilient Modulus	Resilient Strain	Resilient Modulus	Resilient Strain	Resilient Modulus
	σ_3 [psi]	σ_3 [psi]	θ [psi]	ϵ_r [in/in]	M_r [psi]	ϵ_r [in/in]	M_r [psi]	ϵ_r [in/in]	M_r [psi]
1	6	2	20	0.000093	18473	0.000092	18480	0.00009	18476
2	6	4	22	0.000177	19726	0.000174	19924	0.00018	19825
3	6	6	24	0.000260	20013	0.000255	20454	0.00026	20233
4	6	8	26	0.000343	20352	0.000331	21047	0.00034	20699
5	6	10	28	0.000420	20842	0.000404	21716	0.00041	21279
6	4	2	14	0.000110	15220	0.000112	14949	0.00011	15084
7	4	4	16	0.000215	15784	0.000217	15555	0.00022	15669
8	4	6	18	0.000312	16449	0.000312	16433	0.00031	16441
9	4	8	20	0.000395	17474	0.000393	17589	0.00039	17531
10	4	10	22	0.000475	18229	0.000463	18767	0.00047	18498
11	2	2	8	0.000140	11436	0.000144	11042	0.00014	11239
12	2	4	10	0.000269	12119	0.000276	11665	0.00027	11892
13	2	6	12	0.000379	13141	0.000390	12678	0.00038	12909
14	2	8	14	0.000479	13719	0.000486	13698	0.00048	13708
15	2	10	16	0.000597	13483	0.000598	13678	0.00060	13581
							Average:	0.000310	16471

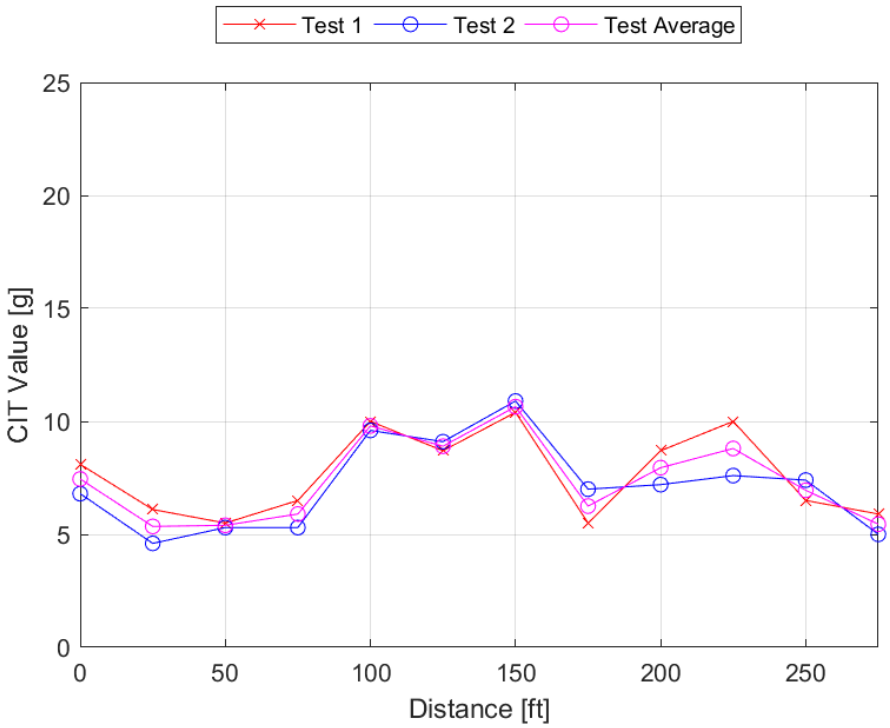

Figure 5.20: CIT Values Across the Cypress Landing Test Site

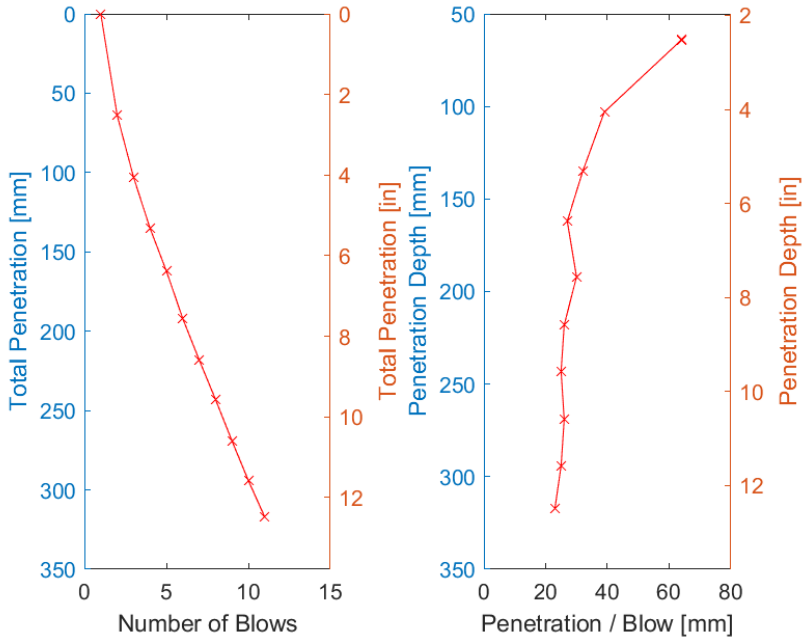

Figure 5.21: Typical DCP Results from this Research

Table 5.14: Summary of Florida Tech Olin Overflow Complex SDPMT Test Locations

Location Number	Incremental		Continuous	
	SDPMT-6	SDPMT-12	SDPMT-6	SDPMT-12
201	X	X	X	X
202	X	X	X	X
203	X	X	X	X
204	X	X	X	X
205	X	X	X	X
206	X	X	X	X
207	X	X	X	X
208	X	X	X	X
209	X	X	X	X
210	X	X	X	X
211	X	X	†	X
212	†	†	†	†
Appendix	A.1	A.3	A.2	A.4

†: No test conducted

5.3.2 Site 2: Florida Tech Olin Overflow Parking

5.3.2.1 SDPMT Test Results

Forty-three SDPMT tests were conducted across the Florida Tech Olin Overflow Parking site at eleven different locations. Test locations were set 25 feet apart along a 300 foot (90 m) long traverse, located near the approximate center of the grass area east of the temporary parking zone.

Tests included both SDPMT-6 and SDPMT-12 incremental and continuous tests. Twenty-two incremental tests were conducted, with eleven of SDPMT-6 and eleven SDPMT-12 tests. Twenty-one continuous tests were conducted with ten of the SDPMT-6 tests and eleven of the SDPMT-12 tests. No SDPMT tests were conducted at location 212 because that area was being used as a staging area for a university construction project. The SDPMT-6 continuous test was not completed at location 211 because the hole collapsed.

A summary of where SDPMT tests were conducted, along with the Appendix section where the test data is included, is presented in Table 5.14. The X's shown in this table indicate the type of test conducted at a particular location, while the bottom row in the table indicates the appendix location where the plots can be found.

5.3.2.1.1 SDPMT-6 Incremental Results

The engineering parameters obtained from the 11 incremental SDPMT tests are summarized in Table 5.15. Positive lift-off pressures were able to be determined from two of the eleven tests and values ranged from 4.6 to 8.3 kPa (0.7 to 1.2 psi) with an

Table 5.15: SDPMT-6 inch Incremental Test Results for Florida Tech Olin Overflow Parking Complex

Location Number	Lift-off Pressure p_0 [kPa]	Limit Pressure p_L [kPa]	Initial PMT Modulus E_0 [kPa]
201	4.6	310.0	3950
202	−10.7	350.0	3793
203	−15.7	300.0	2905
204	−22.1	350.0	4126
205	−13.3	350.0	3326
206	−13.6	450.0	4609
207	−18.8	550.0	4438
208	−19.8	675.0	8463
209	8.3	285.0	3907
210	−21.1	325.0	3710
211	−23.4	370.0	5500
Average	−13.2	392.3	4430
Standard Dev.	10.6	120.5	1500

average of 6.5 kPa (0.9 psi) and a standard deviation of 2.6 kPa (0.4 psi). Negative lift-off pressures are not possible in soils since they imply that the soil experiences tension. The limit pressures ranged from 285.0 to 675.9 kPa (41.3 to98.0 psi) producing an average of 392.3 kPa (56.9 psi) with a standard deviation of 120.5 kPa (18.0 psi). Initial moduli ranged from 2905 to 8463 kPa (421 to1227 psi) with an average of 4430 kPa (643 psi) and a standard deviation of 1500 kPa (218 psi).

5.3.2.1.2 SDPMT-6 Continuous Results

The results of the 10 continuous SDPMT-6 inch tests are summarized in Table 5.16. Positive lift-off pressures were able to be determined from 4 of the 10 tests. Values ranged from 4.2 to 23.4 kPa (0.6 to 3.4 psi) producing an average of 23.9 kPa (3.5 psi) with a standard deviation of 8.2 kPa (1.2 psi). The limit pressure of the soil ranged from 150.0 to 300 kPa (22 to 44 psi) with an average of 199.5 kPa (28.9 psi) and a standard deviation of 61.5 kPa (8.9 psi). Initial moduli ranged from 2182 to 9035 kPa (316 to 1310 psi) with an average of 5602 kPa (812 psi) and a standard deviation of 1993 kPa (289 psi).

5.3.2.1.3 SDPMT-12 Incremental Results

The results of the 11 incremental SDPMT tests are summarized in Table 5.17. Positive lift-off pressures were determined for seven of the eleven tests. Values ranged from 1.0 to 16.4 kPa (0.1 to 2.4 psi) producing an average of 5.5 kPa (0.8 psi) with a

Table 5.16: SDPMT-6 inch Continuous Test Results for Florida Tech Olin Overflow Parking Complex

Location Number	Lift-off Pressure p_0 [kPa]	Limit Pressure p_L [kPa]	Initial PMT Modulus E_0 [kPa]
201	23.4	200.0	7359
202	−18.2	300.0	6103
203	−22.7	170.0	3860
204	−9.6	150.0	4121
205	−25.5	150.0	2182
206	−4.6	175.0	5703
207	9.3	150.0	4623
208	14.6	250.0	9035
209	−49.0	150.0	7251
210	4.2	300.0	5786
Average	−7.8	199.5	5602
Standard Dev.	21.8	61.5	1993

standard deviation of 5.6 kPa (0.8 psi). The limit pressure ranged from 200.0 to 450.0 kPa (29.0 to 65.3 psi) with an average of 355.5 kPa (51.6 psi) and a standard deviation of 69.4 kPa (10.1 psi). Initial moduli ranged from 2,562 to 8,265 kPa (371 to 1,199 psi) with an average of 5,091 kPa (738 psi) and a standard deviation of 1,587 kPa (230 psi).

5.3.2.1.4 SDPMT-12 Continuous Results

The results of the 11 continuous SDPMT-12 inch tests are summarized in Table 5.18. Only one lift-off pressure was determined for the eleven tests and had a value of 38.4 kPa (5.6 psi). The limit pressure ranged from 125.0 to 375.0 kPa (18.1 to 54.4 psi) with an average of 205.3 kPa (29.8 psi) and a standard deviation of 74.8 kPa (10.8 psi). Initial moduli ranged from 3,044 to 10,167 kPa (441 to 1,475 psi) with an average of 6,821 kPa (989 psi) and a standard deviation of 2,337 kPa (339 psi) for 10 of the 11 tests.

5.3.2.2 NDG Results

Twenty-four NDG tests, two at each location, were conducted along the 300-foot transect at the Florida Tech Olin Overflow Parking Complex site. Densities were recorded using both 6 and 12 inch test depths. Table 5.19 and Table 5.20 summarize the 6 and 12 inch results, respectively. Moisture content, wet and dry densities were recorded during each NDG test. The six inch dry densities ranged from 101.1 to 108.4 lb/ft^3 (15.9 to 17.0 kN/m^3), and 12 inch dry densities ranged from 104.2 to 109.7 lb/ft^3 (16.3 to 17.3 kN/m^3). Densities were relatively consistent along this site.

Table 5.17: SDPMT-12 inch Incremental Test Results for Florida Tech Olin Overflow Parking Complex

Location Number	Lift-off Pressure p_0 [kPa]	Limit Pressure p_L [kPa]	Initial PMT Modulus E_0 [kPa]
201	4.6	200.0	2562
202	−6.7	350.0	5090
203	16.4	350.0	4837
204	−5.0	450.0	4846
205	−0.0	400.0	4779
206	1.7	350.0	3432
207	1.0	280.0	4163
208	9.6	425.0	6300
209	3.0	405.0	8265
210	2.1	350.0	4809
211	−3.4	350.0	6916
Average	2.1	355.5	5091
Standard Dev.	6.6	69.4	1587

Table 5.18: SDPMT-12 inch Continuous Test Results for Florida Tech Olin Overflow Parking Complex

Location Number	Lift-off Pressure p_0 [kPa]	Limit Pressure p_L [kPa]	Initial PMT Modulus E_0 [kPa]
201	−53.5	185.0	4439
202	−56.6	150.0	5084
203	−58.3	148.0	6059
204	−33.0	140.0	3044
205	−34.4	165.0	8555
206	−43.7	250.0	6753
207	−54.9	225.0	6032
208	−29.7	375.0	8357
209	−43.8	125.0	‡
210	38.4	280.0	9723
211	−18.0	215.0	10167
Average	−35.2	205.3	6821
Standard Dev.	27.6	74.8	2337

‡: Value could not be determined.

Table 5.19: Nuclear Density Test Results for Florida Tech Olin Overflow Complex, 6 inch depth

	Density		Moisture
	Dry	Wet	Content
Location	[lb/ft^3]	[lb/ft^3]	[%]
201	103.2	105.1	1.9
202	105.8	107.0	1.2
203	107.0	108.5	1.4
204	105.2	106.7	1.4
205	103.8	105.4	1.5
206	101.1	103.0	1.8
207	105.8	107.5	1.6
208	106.6	108.7	1.5
209	106.4	108.1	1.6
210	108.4	110.4	1.9
211	106.4	107.5	1.1
212	102.9	105.2	2.2
Average :	105.2	106.9	1.6
Std. Dev. :	2.1	2.0	0.3

Table 5.20: Nuclear Density Test Results for Florida Tech Olin Overflow Complex, 12 inch depth

	Density		Moisture
	Dry	Wet	Content
Location	[lb/ft^3]	[lb/ft^3]	[%]
201	103.2	105.1	1.9
202	105.8	107.0	1.2
203	107.0	108.5	1.4
204	105.2	106.7	1.4
205	103.8	105.4	1.5
206	101.1	103.0	1.8
207	105.8	107.5	1.6
208	106.6	108.7	1.5
209	106.4	108.1	1.6
210	108.4	110.4	1.9
211	106.4	107.5	1.1
212	102.9	105.2	2.2
Average :	105.2	106.9	1.6
Std. Dev. :	2.1	2.0	0.3

Table 5.21: Laboratory Moisture Contents from Florida Tech Olin Overflow Parking Complex at the Time of SDPMT-6 and SDPMT-12 Incremental Testing

Location	NDG Dry Unit Weight [lb/ft^3]	Wet Mass [g]	Dry Mass [g]	Moisture Content [g]	Moisture Content [%]	Wet Unit Weight [lb/ft^3]
201	109.1	82.7	81.3	1.4	1.8	111.0
202	114.0	78.9	76.3	2.6	3.5	118.0
203	109.7	90.0	88.2	1.8	2.1	112.0
204	106.0	78.1	76.6	1.5	2.0	108.1
205	112.8	83.6	81.6	2.0	2.5	115.6
206	115.0	80.7	77.7	3.0	4.0	119.5
207	114.4	73.4	71.6	1.8	2.6	117.4
208	115.2	70.2	67.7	2.5	3.8	119.6
209	111.6	77.4	76.0	1.4	1.9	113.7
210	110.9	59.3	55.4	3.9	7.3	119.0
211	114.1	74.7	71.8	2.9	4.1	118.8
212	114.5	†	†	†	†	†

†: Test was not performed because of ongoing construction
Note: Moisture content cans were all 1.8 g mass.

5.3.2.3 Moisture Content Results

Because of temporary construction at the Florida Tech Olin Complex, it was not possible to perform SDPMT tests at the same time as NDG tests. Therefore, moisture content samples were obtained during SDPMT testing, and it was assumed that densities did not change between SDPMT and NDG testing. These moisture contents were used with NDG dry densities to determine wet densities associated with the time of SDPMT testing. Since this process was performed both during incremental and continuous testing two sets of 11 moisture contents were obtained. One set from 6- and 12-inch (15 and 30 cm) incremental testing and the second set from the 6- and 12-inch (15 and 30 cm) continuous testing. The incremental moisture contents are summarized in Table 5.21 and the continuous results are summarized in Table 5.22.

5.3.2.4 Zorn LWD Results

One LWD test with the Zorn apparatus was conducted at each test location, producing a maximum surface deflection (S_d) and elastic moduli (E_d). Surface deflections ranged from 0.49 to 1.22 mm (0.02 to 0.05 inches) with an average of 0.82 mm (0.03 inches) and standard deviation of 0.21 mm (0.01 inches). Elastic moduli ranged from 18.5 to 46.1 MPa (2,682.5 to 6,684.5 psi) with an average of 29.4 MPa (4,263.0 psi) and a standard deviation of 8.1 MPa (1,174.5 psi). This data is summarized in Table 5.23.

Table 5.22: Laboratory Moisture Contents from Florida Tech Olin Overflow Parking Complex at the Time of SDPMT-6 and SDPMT-12 Continuous Testing

Location	NDG Dry Unit Weight [lb/ft^3]	Wet Mass [g]	Dry Mass [g]	Moisture Content [g]	Moisture Content [%]	Wet Unit Weight [lb/ft^3]
201	109.1	76.5	73.8	2.7	3.8	113.2
202	114.0	77.0	73.4	3.6	5.0	119.7
203	109.7	73.9	70.8	3.1	4.5	114.6
204	106.0	69.1	65.7	3.4	5.3	111.6
205	112.8	72.8	69.3	3.5	5.2	118.6
206	115.0	79.7	76.0	3.7	5.0	120.7
207	114.4	65.3	61.9	3.4	5.7	120.9
208	115.2	64.4	61.2	3.2	5.4	121.4
209	111.6	54.0	51.1	2.9	5.9	118.2
210	110.9	71.1	68.0	3.1	4.7	116.1
211	114.1	75.0	71.0	4.0	5.8	120.7
212	113.9	†	†	†	†	†

†: Test was not conducted because of ongoing construction

Table 5.23: Florida Tech Olin Overflow Parking Complex Zorn LWD Testing Results

	Test 1	
Location	Sd [mm]	Ed [MPa]
201	0.88	25.7
202	0.78	28.7
203	0.85	26.4
204	1.01	22.4
205	1.22	18.5
206	1.02	22.1
207	0.55	41.1
208	0.90	24.9
209	0.49	46.1
210	0.64	35.2
211	0.68	33.0
212	0.79	28.5
Average	0.82	29.4
Std. Dev.	0.21	8.1

25 mm = 1 inch 1 MPa = 145 psi

Table 5.24: FIT Olin Complex Dynatest LWD Results

	Test 1
Location	E0 [MPa]
201	104.7
202	96.7
203	93.7
204	‡
205	138.3
206	186.3
207	175.3
208	106.0
209	‡
210	156.7
211	164.3
212	‡
Average	135.8
Std. Dev.	36.3

‡ - Reading was not taken because of dead battery in LWD.

5.3.2.5 Dynatest LWD Results

Dynatest's LWD tests were conducted at nine of the 12 test locations. Tests were not conducted at locations 204, 209 and 212 because the unit lost battery power while testing. The elastic modulus from the Dynatest LWD ranged from 93.7 to 186.3 MPa (13,587 to 27,014 psi), with an average of 135.8 MPa (19,691 psi) and a standard deviation of 36.3 MPa (5,264 psi). The results of these tests are summarized in Table 5.24.

5.3.2.6 CIT Results

Twenty-four CITs were conducted across the FIT Olin Complex site. Clegg Impact Values (CIV) ranged from 8.7 to 23.2 g's. The results of the CITs are summarized in Table 5.25.

5.3.2.7 DCP Test Results

Twelve DCP test were conducted to a depth of 12 inches (30 cm) along the Florida Tech Olin Overflow Parking Complex test site. The data from each test is presented in Figures I.13 through I.24. Each figure includes two plots; one with total penetration versus total number of blows, and a second with penetration depth versus penetration

Table 5.25: FIT Olin Complex CIT Results

Location	Clegg Impact Value Test1 [g's]	Test2 [g's]	Average [g's]
201	9.4	10.0	9.7
202	11.3	13.3	12.3
203	11.7	10.2	11.0
204	10.2	12.6	11.4
205	9.4	12.2	10.8
206	8.7	9.6	9.2
207	20.8	21.7	21.3
208	14.3	14.1	14.2
209	21.3	23.2	22.3
210	17.2	12.4	14.8
211	17.8	16.7	17.3
212	14.5	14.6	14.6
Average	13.9	14.2	14.1
Std Dev.	4.5	4.4	4.3

per blow. Note the both the imperial (i.e. English) and international units are displayed on the y-axes.

5.3.2.7.1 DCP Data Reduction

The data for each DCP test was further analyzed to determine an average penetration per blow or penetration index (DCP PI) for 6 and 12 inches (15 to 30 cm) of penetration. The average DCP index was compared with SDPMT engineering parameters.

Table 5.26 summarizes the penetration rate for the DCP tests at the Florida Tech Olin Overflow Parking Complex. The 6 inch averages ranged from 5.3 to 15.9 mm/blow with an average and standard deviation of 9.4 and 3.5 mm/blow respectively. The 12 inch averages ranged from 3.7 to 14.1 mm/blow with an average and standard deviation of 8.1 and 3.2 mm/blow respectively. The small standard deviations for the penetration rates is an indication of the consistent properties across of the site.

5.3.2.8 Resilient Modulus Results

FDOT SMO laboratory performed six resilient modulus tests in accordance with AASHTO T-307 on the soil collected at the Olin Complex site. The maximum density from AASHTO T99 was 111.2 lb/ft^3 (17.4 kN/m^3), with an optimum moisture content of 10.5%. The modulus samples were compacted at two target moisture contents dry of optimum (3 and 6%), at optimum (10.5%), and wet of optimum (12%). The resulting

Table 5.26: Summary of DCP Indices for 6 and 12-inch Penetrations at Florida Tech Olin Overflow Parking Complex

	6 inch Average			12 inch Average		
Location Number	Blows to 153 mm [blows]	Total Penetration [mm]	Penetration per blow [mm/blow]	Blows to 305 mm [blows]	Total Penetration [mm]	Penetration per blow [mm/blow]
201	11	157	14.3	27	307	11.4
202	15	160	10.7	23	324	14.1
203	10	159	15.9	26	313	12.0
204	16	156	9.8	51	306	6.0
205	17	157	9.2	41	306	7.5
206	12	155	12.9	30	305	10.2
207	23	154	6.7	41	305	7.4
208	18	162	9.0	35	305	8.7
209	29	154	5.3	82	305	3.7
210	27	154	5.7	54	305	5.6
211	25	157	6.3	55	307	5.6
212	22	156	7.1	66	305	4.6
Average			9.4			8.1
Std. Dev.			3.5			3.2

moduli determined at the bulk stress of 11 psi ranged from 12,710 to 40,079 psi. The results of this testing are summarized in Table 5.27.

The two resilient modulus tests at optimum were used to estimate an average strain and resilient modulus for the soil at the Olin Complex site, and this data is shown in Table 5.28. The average strain for the 15 loading sequences conducted during the resilient modulus test was $9.12 \text{x} 10^{-3}$ %, and the corresponding average modulus was 18,403 psi (2,669 kPa). This data was compared with moduli from the SDPMT unload data.

Table 5.27: Resilient Modulus Test Results Dry, Wet and at Optimum Moisture for Florida Tech Olin Overflow Parking Complex Soil

	Target Moisture [%]	Max Density [lb/ft^3]	Compacted Density [lb/ft^3]	Compacted Moisture [%]	Percent of Optimum [%]	K1	K2	Resilient Modulus ($\theta = 11$ psi) [psi]
Dry 1	3	111.2	110.5	2.9	99.3	19386.5	0.3029	40,079
Dry 2	3	111.2	110.9	3.2	99.8	13711.3	0.3508	31,801
Dry 3	6	111.2	111.0	6.1	99.8	6369.6	0.4766	19,974
Dry 4	6	111.2	111.0	6.2	99.8	8353.2	0.3367	18,727
Opt 1	10.5	111.2	111.0	10.5	99.8	3956.3	0.5002	13,129
Opt 2	10.5	111.2	111.1	10.7	99.9	4006.5	0.4815	12,710
Wet 1	12	111.2	109.6	12.1	98.5	4324.5	0.4701	13,351
Wet 2	12	111.2	110.3	12.0	99.2	3923.6	0.4965	12,906

Table 5.28: Summary of Resilient Modulus Sequence Data for Florida Tech Olin Overflow Parking Complex

Sequence	Chamber Confining Pressure	Nominal Maximum Axial Stress	Nominal Bulk Stress	Test 1		Test 2		Average	
				Resilient Strain	Resilient Modulus	Resilient Strain	Resilient Modulus	Resilient Strain	Resilient Modulus
	σ_3 [psi]	σ_3 [psi]	θ [psi]	ϵ_r [in/in]	M_r [psi]	ϵ_r [in/in]	M_r [psi]	ϵ_r [in/in]	M_r [psi]
1	6	2	20	0.000091	18403	0.000095	17239	0.000093	17821
2	6	4	22	0.000179	18985	0.000186	18007	0.000182	18496
3	6	6	24	0.000267	19201	0.000275	18376	0.000271	18788
4	6	8	26	0.000350	19544	0.000362	18702	0.000356	19123
5	6	10	28	0.000430	19999	0.000443	19163	0.000437	19581
6	4	2	14	0.000107	15201	0.000109	14668	0.000108	14934
7	4	4	16	0.000213	15529	0.000217	14981	0.000215	15255
8	4	6	18	0.000311	16148	0.000319	15553	0.000315	15850
9	4	8	20	0.000398	16952	0.000411	16259	0.000405	16606
10	4	10	22	0.000480	17680	0.000494	16963	0.000487	17321
11	2	2	8	0.000137	11194	0.000139	10957	0.000138	11075
12	2	4	10	0.000266	11804	0.000270	11492	0.000268	11648
13	2	6	12	0.000380	12704	0.000387	12287	0.000384	12495
14	2	8	14	0.000474	13815	0.000487	13211	0.000480	13513
15	2	10	16	0.000574	14276	0.000596	13515	0.000585	13896
							Average:	0.000091	18403

Table 5.29: Summary of SDPMT Test Locations at the Heritage Parkway Test Site

Location Number	Incremental		Continuous	
	SDPMT-6	SDPMT-12	SDPMT-6	SDPMT-12
301	X	X	X	X
302	X	X	X	X
303	X	X	X	X
304	X	X	X	X
305	X	X	X	X
306	X	X	X	X
307	X	X	X	X
308	X	X	X	X
309	X	X	X	X
310	X	X	X	X
311	X	X	X	X
312	X	X	X	X
Appendix	D.1	D.3	D.2	D.4

5.3.3 Site 3: Heritage Parkway

5.3.3.1 PMT Test Results

Forty-eight SDPMT tests were conducted at the Heritage Parkway test site. Test locations were 50 feet (15 m) apart, and located along the westbound shoulder. A summary of where SDPMT tests were conducted, along with the appendix section where the test data located, is summarized in Table 5.29. Each of the four SDPMT test types were conducted at each test location, that is 12 of each: incremental SDPMT-6 and SDPMT-12 tests and continuous SDPMT-6 and SDPMT-12 tests. The X's shown in this table indicate the type of test conducted at a particular location, while the bottom row in the table indicates the appendix location that the plots can be found.

5.3.3.1.1 SDPMT-6 Incremental Results

The engineering parameters obtained from the 12 incremental SDPMT-6 tests are summarized in Table 5.30. Lift-off pressures were determined for 5 of the 12 tests and values ranged from 6.9 to 17.7 kPa (1 to 2.5 kPa) with and average of 10.9 kPa (1.6 psi) and a standard deviation of 4.2 kPa. The limit pressure ranged from 1,140.0 to 9,526.0 kPa (165 to 1382 kPa) with an average of 5,265.9 kPa (764 psi) and a standard deviation of 2,392.7 kPa (347 psi). The variation across the site is illustrated in Figure 5.22. Initial moduli ranged from 14,405 to 183,145 kPa (2089 to 26562 psi) with an average of 85,001 kPa (12,328 psi) and a standard deviation of 55,877 kPa (8,104 psi). The variation across the site is illustrated in Figure 5.23.

Table 5.30: SDPMT-6 inch Incremental Test Results for Heritage Parkway

Location Number	Lift-off Pressure p_0 [kPa]	Limit Pressure p_L [kPa]	Initial PMT Modulus E_0 [kPa]
301	−29.2	2135.0	24726
302	8.3	2750.0	52207
303	17.7	5000.0	92683
304	−12.2	5000.0	122484
305	−39.7	4700.0	52584
306	6.9	6425.0	99175
307	11.9	5560.0	183145
308	−48.0	1140.0	14405
309	−0.7	9526.0	18831
310	9.9	6275.0	172445
311	−19.8	7620.0	101725
312	−15.9	7060.0	85599
Average	−9.2	5265.9	85001
Standard Dev.	21.7	2392.7	55877

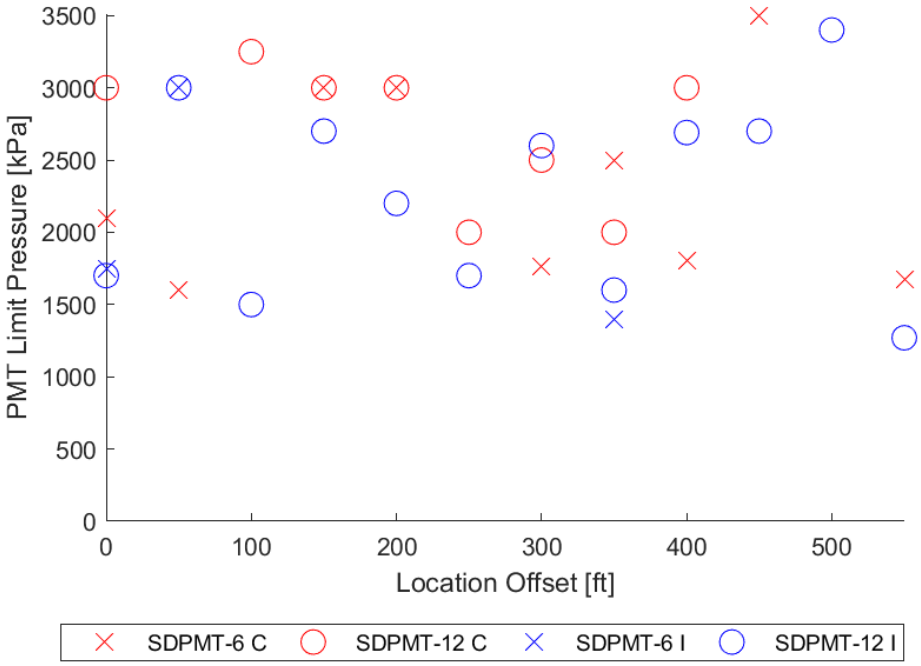

Figure 5.22: Heritage Parkway SDPMT p_L Across Site

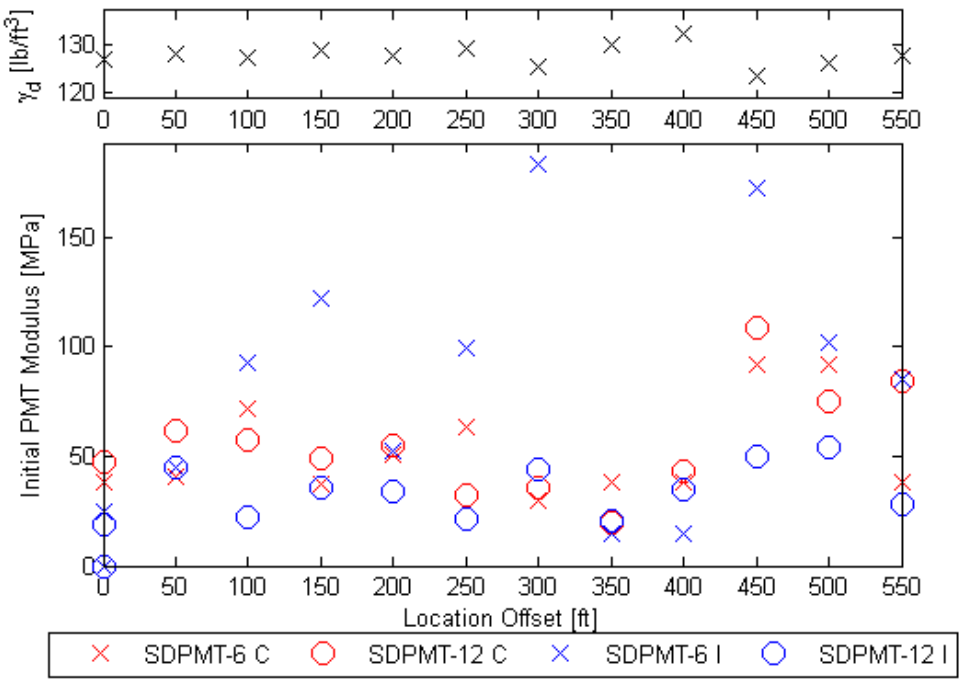

Figure 5.23: Heritage Parkway SDPMT E_0 Across Site

5.3.3.1.2 SDPMT-6 Continuous Results

The engineering parameters obtained from the 12 continuous SDPMT-6 inch tests are summarized in Table 5.31. Lift-off pressures were determined for 11 of the 12 tests and values ranged from 12.4 to 156.2 kPa (1.8 to 22.7 psi) with and average of 68.2 kPa (10 psi) and a standard deviation of 47.0 kPa (7 kPa). The limit pressure of the soil ranged from 1,840.0 to 3,700.0 kPa (267 to 536 psi) with an average of 2,427.9 kPa (352 psi) and a standard deviation of 508.2 kPa (74 psi). The variation across the site is illustrated in Figure 5.22. Initial moduli ranged from 29,505 to 92,018 kPa (4,298 to 13,346 psi) with an average of 52,645 kPa (7,635 psi) and a standard deviation of 20,637 kPa (2,993 kPa). The variation across the site is illustrated in Figure 5.23.

5.3.3.1.3 SDPMT-12 Incremental Results

The engineering parameters obtained from the 12 incremental SDPMT tests are summarized in Table 5.32. Lift-off pressures ranged from 2.0 to 57.6 kPa (0.3 to 8.4 psi) with an average of 29.2 kPa (4.2 psi) and a standard deviation of 15.9 kPa (2.3 psi). The limit pressure ranged from 1,510.0 to 3,425.0 kPa (219 to 497 psi) with an average of 2370.4 kPa (343 psi) and a standard deviation of 657.7 kPa (95 psi). The variation across the site is illustrated in Figure 5.22. Initial moduli ranged from 18,917 to 54,542 kPa (7,910 psi) with an average of 33,589 kPa (4,872 psi) and a standard

Table 5.31: SDPMT-6 inch Continuous Test Results for Heritage Parkway

Location Number	Lift-off Pressure p_0 [kPa]	Limit Pressure p_L [kPa]	Initial PMT Modulus E_0 [kPa]
301	−6.4	2200.0	43441
302	24.8	1965.0	40682
303	46.9	2500.0	61178
304	37.6	2500.0	37607
305	37.7	2500.0	50523
306	73.4	2250.0	63069
307	108.0	2050.0	29505
308	133.0	2500.0	42017
309	156.2	1840.0	41682
310	12.4	3000.0	91656
311	36.8	3700.0	92018
312	83.3	2130.0	38365
Average	62.0	2427.9	52645
Standard Dev.	49.7	508.2	20637

deviation of 11,546 kPa (1.675 psi). The variation across the site is illustrated if Figure 5.23.

5.3.3.1.4 SDPMT-12 Continuous Results

The engineering parameters obtained from the 12 continuous SDPMT-12 inch tests are summarized in Table 5.33. Positive lift-off pressures were determined for 10 of the 12 tests and values ranged from 23.1 to 177.8 kPac (3.4 to 25.8 psi) with and average of 67.7 kPa (9.9 psi) and a standard deviation of 46.5 kPa (6.7 psi). Two lift-off pressures were determined to be negative and excluded from further analyses. The limit pressure of the soil ranged from 1,860.0 to 3,780.0 kPa (270 to 548 psi) with an average of 2,710.8 kPa (393 psi) and a standard deviation of 522.4 kPa (76 psi). The variation across the site is illustrated in Figure 5.22. Initial moduli ranged from 16,248 to 115,021 kPa (2,356 to 16,682 psi) with an average of 59,773 kPa (8,669 psi) and a standard deviation of 29,846 kPa (4,329 psi). The variation across the site is illustrated in Figure 5.23.

5.3.3.2 NDG Results

Thirty-five NDG tests were conducted along the Heritage Parkway test site. NDG tests were conducted at 6, 8 and as close to 12 inch (15, 20 and 30 cm) depths; results are tabulated in Tables 5.34, 5.35 and 5.36 respectively. The very hard and dry base

Table 5.32: SDPMT-12 inch Incremental Test Results for Heritage Parkway

Location Number	Lift-off Pressure p_0 [kPa]	Limit Pressure p_L [kPa]	Initial PMT Modulus E_0 [kPa]
301	2.0	1720.0	18917
302	14.2	3340.0	45159
303	18.5	1510.0	21435
304	23.6	2750.0	35326
305	32.2	2350.0	38603
306	44.7	1765.0	21564
307	15.8	2635.0	43980
308	57.6	1595.0	20508
309	24.1	2690.0	35065
310	45.9	2700.0	40151
311	40.8	3425.0	54542
312	30.8	1965.0	27812
Average	29.2	2370.4	33589
Standard Dev.	15.9	658.7	11546

Table 5.33: SDPMT-12 inch Continuous Test Results for Heritage Parkway

Location Number	Lift-off Pressure p_0 [kPa]	Limit Pressure p_L [kPa]	Initial PMT Modulus E_0 [kPa]
301	177.8	2665.0	48079
302	114.5	2790.0	61962
303	53.5	2500.0	57689
304	76.8	2500.0	48942
305	23.1	3780.0	63413
306	46.3	2000.0	32733
307	−19.4	2660.0	36066
308	43.5	1860.0	16248
309	72.1	3275.0	43658
310	50.5	2500.0	108785
311	−18.9	3000.0	115021
312	29.2	3000.0	84678
Average	54.1	2710.8	59773
Standard Dev.	54.2	522.4	29846

Table 5.34: Heritage Parkway NDG Data 6 inch Depth

Location	Density Dry [lb/ft^3]	Density Wet [lb/ft^3]	Moisture Content [%]
301	126.3	134.8	6.7
302	125.3	130.0	3.8
303	127.4	131.6	3.3
304	127.7	132.1	3.5
305	128.4	132.3	3.0
306	127.7	132.3	3.6
307	123.5	127.4	3.2
308	127.2	134.3	5.5
309	131.3	135.6	3.2
310	124.4	128.5	3.3
311	125.5	129.1	2.9
312	127.2	131.4	3.3
Average :	126.8	131.6	3.8
Std. Dev. :	2.0	2.5	1.1

material caused one location test hole to collapse, and prevented the 12-inch (30 cm) test from being completed. The dry unit weights across the site are illustrated in Figure 5.24.

5.3.3.3 Moisture Content Results

Because of logistics at the Heritage Parkway site, it was not possible to preform the testing with the SDPMT probes at the same time as the NDG tests. To obtain moisture contents, disturbed samples were collected at the time of SDPMT testing. It was assumed that NDG dry unit weights could be used along with the moisture contents obtained during SDPMT testing to predict total or wet unit weights during SDPMT testing.

Forty-two moisture content samples were retrieved when SDPMT testing was conducted. Samples were taken after each test except for SDPMT-6 continuous test, where the conditions had not changed since the NDG test at that location was conducted. The twelve moisture content tests, conducted after the 6 inch incremental tests, are summarized in Table 5.37. Moisture content samples taken after the 12 inch SDPMT tests are summarized in Table 5.38. Results of the six inch continuous moisture content samples taken after the SDPMT-6 continuous tests are summarized in Table 5.39. The 12 moisture content samples taken after the SDPMT-12 continuous tests are summarized in Table 5.40.

Table 5.35: Heritage Parkway NDG Data 8 inch Depth

Location	Density Dry [lb/ft^3]	Density Wet [lb/ft^3]	Moisture Content [%]
301	127.1	135.0	6.2
302	128.0	132.6	3.6
303	127.5	132.1	3.6
304	129.0	133.1	3.2
305	127.6	131.8	3.3
306	129.4	133.6	3.3
307	125.6	129.4	3.0
308	129.9	136.3	5.7
309	132.2	137.0	3.6
310	123.7	128.0	3.4
311	126.2	129.7	2.8
312	127.9	132.6	3.7
Average :	127.8	132.6	3.8
Std. Dev. :	2.2	2.7	1.1

5.3.3.4 Zorn LWD Results

Twenty-four Zorn LWD tests were conducted, with two at each of the 12 locations at the Heritage Parkway site. The modulus E_d ranged from 84.0 to 166.7 MPa (12,180 to 24,172 psi). The surface deflections ranged from 0.14 to 0.27 mm (0.006 to 0.011 inches). The results from the 24 tests are summarized in Table 5.41 and illustrated in Figure 5.25.

5.3.3.5 Dynatest LWD Results

Two tests at each location were performed with the Dynatest LWD device, producing a total of 24 tests. The moduli ranged from 260.0 to 1,795.0 MPa (37,700 to 260,275 psi) and averaged 808.5 MPa (117,233 psi) with a standard deviation of 335.9 MPa (48,706 psi). The Dynatest LWD testing produced a wide variation of results across the test site. The data collected with the Dynatest LWD device are summarized in Table 5.42 and illustrated in Figure 5.26.

5.3.3.6 CIT Results

Two CITs were conducted at each of the 12 testing locations. The CIVs results ranged from 12 to 66.9 g's. The results from the CIT testing are summarized in Table 5.43 and illustrated in Figure 5.27.

Table 5.36: Heritage Parkway NDG Data 12 inch Depth

Location	Density Dry [lb/ft^3]	Density Wet [lb/ft^3]	Moisture Content [%]
301	128.0	136.5	6.6
302	128.2	132.8	3.5
303	127.7	132.0	3.3
304	128.0	131.8	3.0
305	127.7	131.6	3.1
306	129.3	133.9	3.6
307	125.2	129.0	3.0
308	129.9	136.7	5.2
309	132.3	137.0	3.5
310	124.7	128.7	3.3
311	124.0	127.8	3.1
312		†	
Average :	127.7	132.5	3.7
Std. Dev. :	2.4	3.3	1.1

†: No test conducted at depth

5.3.3.7 DCP Test Results

Testing with the DCP could not be conducted because the stiffness of the base material did not allow penetration of the probe, and would have damaged the instrument. As a result no DCP tests were conducted at the Heritage Parkway site.

5.3.3.8 Resilient Modulus Results

FDOT SMO laboratory performed six resilient modulus tests according to AASHTO T-307 on the soil collected from a stockpile of base material at the Heritage Parkway site. The maximum density from the AASHTO T99 test was 127.5 lb/ft^3 (19.9 kN/m^3), with an optimum moisture content of 7.4%. The modulus samples were compacted to target moisture contents dry of optimum (3 and 6 %), at optimum (7.4%), and wet of optimum (9%). The 11 psi (2 kPa) bulk stress resilient moduli ranged from 9,006 to 30,617 psi (1306 to 4440 kPa) at moisture contents of 9.3 to 2.9%, respectively. The results of this testing are summarized in Table 5.44

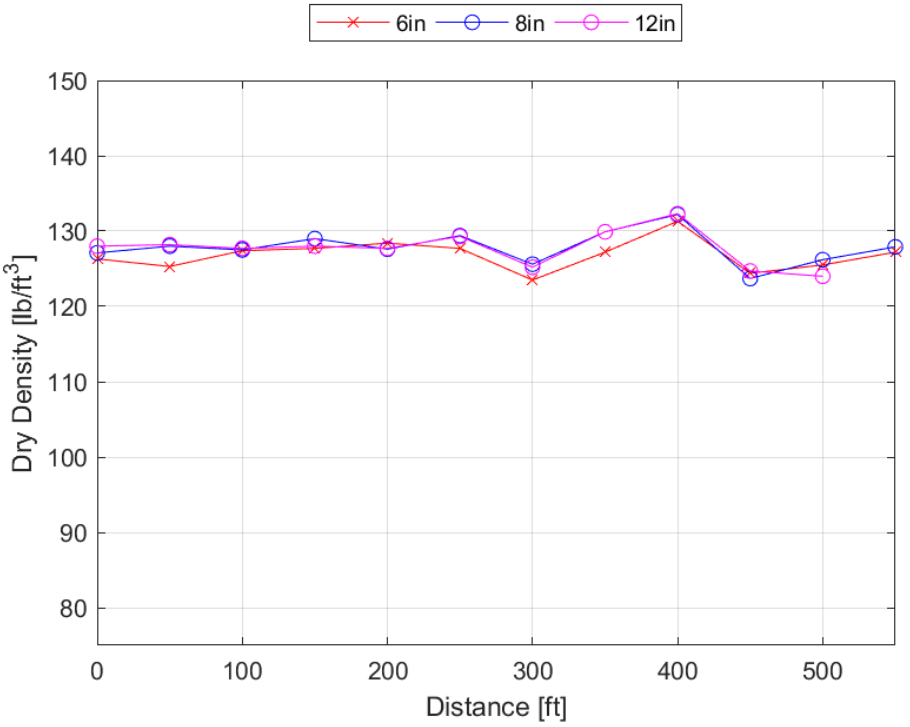

Figure 5.24: Heritage Parkway NDG Dry Unit Weight (γ_d) Across Site

Table 5.37: Summary of Additional Moisture Content Samples at Heritage Parkway at the Time of SDPMT-6 Incremental Testing

Location	NDG Dry Unit Weight [lb/ft^3]	Wet Mass [g]	Dry Mass [g]	Moisture Content [g]	Moisture Content [%]	Wet Unit Weight [lb/ft^3]
301	126.3	94.8	91.2	3.6	4.0	131.4
302	125.3	90.0	86.9	3.1	3.6	129.9
303	127.4	82.0	79.3	2.7	3.5	131.8
304	127.7	101.7	98.2	3.5	3.6	132.3
305	128.4	95.6	91.7	3.9	4.3	134.0
306	127.7	105.7	101.9	3.8	3.8	132.5
307	123.5	103.1	100.2	2.9	2.9	127.1
308	127.2	97.1	93.2	3.9	4.3	132.6
309	131.3	109.2	105.8	3.4	3.3	135.6
310	124.4	115.5	112.0	3.5	3.2	128.4
311	125.5	98.9	95.5	3.4	3.6	130.1
312	127.2	110.1	106.5	3.6	3.4	131.6

†: Test was not performed because of ongoing construction
Note: Moisture content cans were all of a standard 1.8 g mass.

Table 5.38: Summary of Additional Moisture Content Samples at Heritage Parkway at the Time of SDPMT-12 Incremental Testing

Location	NDG Dry Unit Weight [lb/ft^3]	Wet Mass [g]	Dry Mass [g]	Moisture Content [g]	Moisture Content [%]	Wet Unit Weight [lb/ft^3]
301	128.0	86.5	80.6	5.9	7.5	137.6
302	128.2	90.6	85.9	4.7	5.6	135.4
303	127.7	95.1	89.9	5.2	5.9	135.2
304	128.0	109.5	104.5	5.0	4.9	134.2
305	127.7	88.1	84.1	4.0	4.9	133.9
306	129.3	98.0	93.7	4.3	4.7	135.3
307	125.2	107.3	102.8	4.5	4.5	130.8
308	129.9	111.5	106.2	5.3	5.1	136.5
309	132.3	108.1	103.4	4.7	4.6	138.4
310	124.7	92.6	88.7	3.9	4.5	130.3
311	124.0	94.9	81.1	13.8	17.4	145.6
312	127.9	92.3	87.7	4.6	5.4	134.7

†: Test was not performed because of ongoing construction
Note: Moisture content cans were all of a standard 1.8 g mass.

Table 5.39: Summary of Additional Moisture Content Samples at Heritage Parkway at the Time of SDPMT-6 Continuous Testing

Location	NDG Dry Unit Weight [lb/ft^3]	Wet Mass [g]	Dry Mass [g]	Moisture Content [g]	Moisture Content [%]	Wet Unit Weight [lb/ft^3]
301	126.3	†	†	†	†	†
302	125.3	†	†	†	†	†
303	127.4	†	†	†	†	†
304	127.7	†	†	†	†	†
305	128.4	†	†	†	†	†
306	127.7	†	†	†	†	†
307	123.5	100.8	95.4	5.4	5.8	130.6
308	127.2	111.4	102.5	8.9	8.8	138.4
309	131.3	78.2	73.9	4.3	6.0	139.1
310	124.4	102.2	97.0	5.2	5.5	131.2
311	125.5	96.6	91.9	4.7	5.2	132.0
312	127.2	108.0	102.0	6.0	6.0	134.8

†: Test was not conducted because of ongoing construction
Note: Moisture content cans were all of a standard 1.8 g mass.

Table 5.40: Summary of Additional Moisture Content Samples at Heritage Parkway at the Time of SDPMT-12 Continuous Testing

Location	NDG Dry Unit Weight [lb/ft^3]	Wet Mass [g]	Dry Mass [g]	Moisture Content [g]	Moisture Content [%]	Wet Unit Weight [lb/ft^3]
301	128.0	90.4	87.4	3.0	3.5	132.5
302	128.2	101.0	98.6	2.4	2.5	131.4
303	127.7	117.3	113.0	4.3	3.9	132.6
304	128.0	103.4	99.7	3.7	3.8	132.8
305	127.7	84.1	81.0	3.1	3.9	132.7
306	129.3	96.9	92.9	4.0	4.4	135.0
307	125.2	98.6	95.2	3.4	3.6	129.8
308	129.9	80.1	74.8	5.3	7.3	139.3
309	132.3	89.3	86.1	3.2	3.8	137.3
310	124.7	95.4	92.2	3.2	3.5	129.1
311	124.0	114.9	111.8	3.1	2.8	127.5
312	127.9	112.4	109.0	3.4	3.2	132.0

†: Test was not conducted because of ongoing construction
Note: Moisture content cans were all of a standard 1.8 g mass.

Table 5.41: Heritage Parkway Zorn LWD Results

	Test 1		Test 2		Average	
Location	Sd [mm]	Ed [MPa]	Sd [mm]	Ed [MPa]	Sd [mm]	Ed [MPa]
301	0.20	112.5	0.20	115.4	0.20	113.9
302	0.20	113.6	0.20	113.1	0.20	113.4
303	0.14	161.9	0.15	152.0	0.14	157.0
304	0.26	87.2	0.16	137.2	0.21	112.2
305	0.14	157.3	0.22	101.4	0.18	129.3
306	0.16	138.9	0.23	99.1	0.19	119.0
307	0.17	134.0	0.27	84.0	0.22	109.0
308	0.25	91.1	0.25	91.5	0.25	91.3
309	0.16	143.3	0.22	104.2	0.19	123.7
310	0.14	166.7	0.18	122.3	0.16	144.5
311	0.18	125.0	0.15	149.0	0.17	137.0
312	0.20	112.5	0.17	135.5	0.18	124.0
Average	0.18	128.7	0.20	117.0	0.19	122.9
Std. Dev.	0.04	26.3	0.04	22.4	0.03	17.5

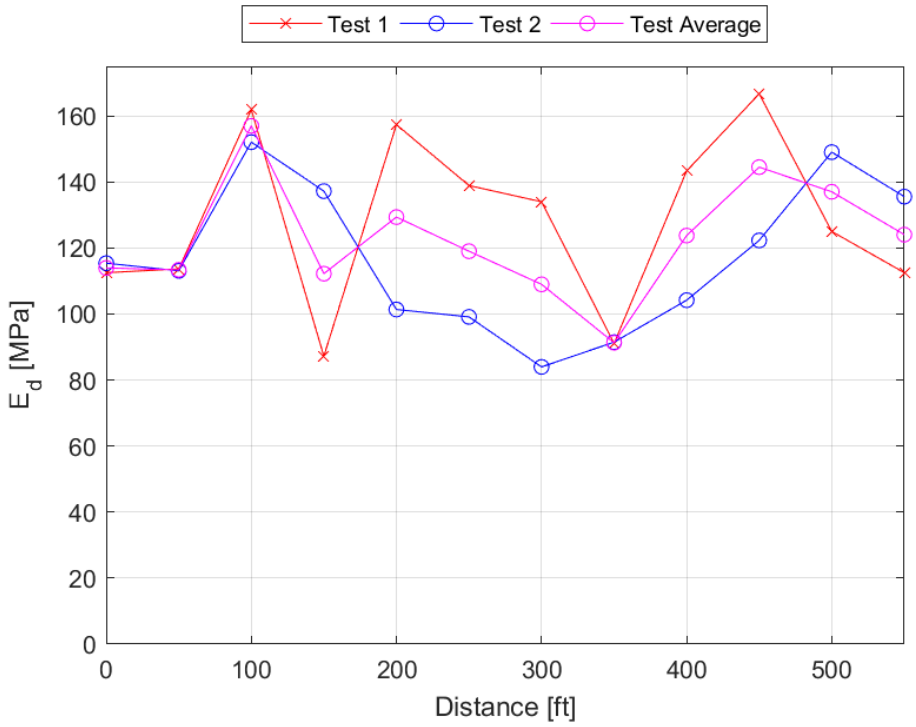

Figure 5.25: Heritage Parkway LWD Zorn Modulus Values Across Site

Table 5.42: Heritage Parkway Dynatest LWD Results

Location	Test 1 E0 [MPa]	Test 2 E0 [MPa]	Average E0 [MPa]
301	442.0	598.0	520.0
302	323.0	617.0	470.0
303	522.0	817.0	669.5
304	885.6	582.3	734.0
305	816.3	530.0	673.2
306	950.3	1148.3	1049.3
307	710.0	584.6	647.3
308	609.3	260.0	434.7
309	638.3	838.0	738.2
310	773.6	1199.7	986.7
311	1795.0	1341.7	1568.4
312	1231.0	1191.7	1211.4
Average	808.0	809.0	808.5
Std. Dev.	394.2	338.6	335.9

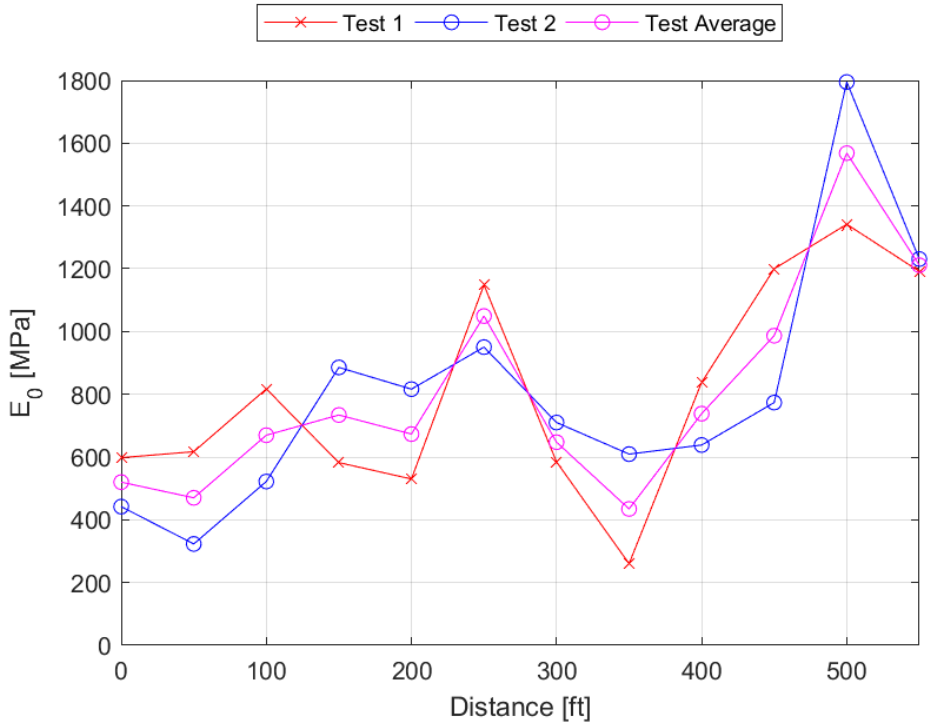

Figure 5.26: Heritage Parkway LWD Dynatest Modulus Values Across Site

Table 5.43: Heritage Parkway CIV Results Summary

	CIV		
Location	Test1 [g's]	Test2 [g's]	Average [g's]
301	12.0	39.2	25.6
302	26.0	35.3	30.7
303	37.3	46.6	42.0
304	31.6	48.5	40.1
305	50.0	31.2	40.6
306	51.4	30.6	41.0
307	66.9	44.4	55.7
308	20.0	43.6	31.8
309	47.6	22.8	35.2
310	57.6	30.1	43.9
311	65.0	32.5	48.8
312	64.8	29.1	47.0
Average	44.2	36.2	40.2
Std Dev.	18.6	8.1	8.4

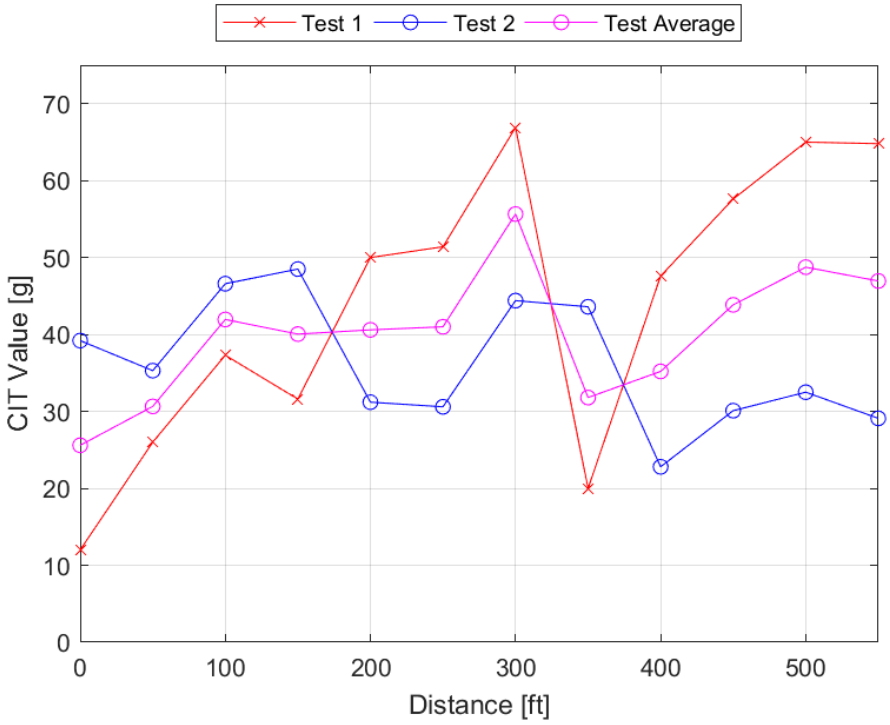

Figure 5.27: Heritage Parkway CIV Results Across Site

Table 5.44: Resilient Modulus Test Results for Heritage Parkway Base Course Soil Dry, Wet and at Optimum Moisture

	Target Moisture [%]	Max Density [lb/ft^3]	Compacted Density [lb/ft^3]	Compacted Moisture [%]	Percent of Optimum [%]	K1	K2	Resilient Modulus ($\theta = 11$ psi) [psi]
Dry 1	3.0	127.5	127.0	2.9	99.6	10238.7	0.3458	23,463
Dry 2	3.0	127.5	127.1	2.9	99.7	18241.0	0.2160	30,617
Dry 3	6.0	127.5	126.9	5.8	99.5	3434.3	0.5580	13,090
Dry 4	6.0	127.5	127.3	5.9	99.9	3599.9	0.5570	13,688
Opt 1	7.4	127.5	126.9	7.4	99.6	2938.1	0.5755	11,679
Opt 2	7.4	127.5	127.0	7.4	99.6	3037.8	0.5551	11,499
Wet 1	9.0	127.5	126.1	8.9	98.9	2248.0	0.6279	10,133
Wet 2	9.0	127.5	125.9	9.1	98.8	1753.2	0.6825	9,006

The two resilient modulus tests performed on samples compacted at optimum moisture content were used to estimate an average strain and resilient modulus for the soil at Heritage Parkway. This data is shown in Table 5.45. The average strain for the 15 loading sequences conducted during the resilient modulus test was $1.88\text{x}10^{-2}$ %, and the corresponding average modulus was 12,354 psi (1792 kPa). This data was compared with moduli from the SDPMT unload data.

Table 5.45: Summary of Resilient Modulus Sequence Data for Heritage Parkway

Sequence	Chamber Confining Pressure	Nominal Maximum Axial Stress	Nominal Bulk Stress	Test 1		Test 2		Average	
				Resilient Strain	Resilient Modulus	Resilient Strain	Resilient Modulus	Resilient Strain	Resilient Modulus
	σ_3 [psi]	σ_3 [psi]	θ [psi]	ϵ_r [in/in]	M_r [psi]	ϵ_r [in/in]	M_r [psi]	ϵ_r [in/in]	M_r [psi]
1	3	3	12	0.000188	12354	0.000186	12317	0.000187	12336
2	3	6	15	0.000376	12740	0.000379	12518	0.000377	12629
3	3	9	18	0.000530	13998	0.000537	13660	0.000533	13829
4	5	5	20	0.000241	17224	0.000247	16627	0.000244	16925
5	5	10	25	0.000475	17940	0.000491	17212	0.000483	17576
6	5	15	30	0.000690	18778	0.000708	18197	0.000699	18488
7	10	10	40	0.000339	25880	0.000357	24434	0.000348	25157
8	10	20	50	0.000668	26658	0.000694	25614	0.000681	26136
9	10	30	60	0.000958	28003	0.000976	27454	0.000967	27728
10	15	10	55	0.000289	30899	0.000309	28640	0.000299	29769
11	15	15	60	0.000430	31248	0.000460	29021	0.000445	30135
12	15	30	75	0.000813	33352	0.000834	32432	0.000823	32892
13	20	15	75	0.000376	36132	0.000408	33167	0.000392	34650
14	20	20	80	0.000495	36791	0.000528	34278	0.000512	35534
15	20	40	100	0.000919	39554	0.000938	38778	0.000928	39166
							Average:	0.000188	12354

Table 5.46: Summary of SDPMT Test Locations at the Southgate Field Test Site

Location Number	Incremental		Continuous	
	SDPMT-6	SDPMT-12	SDPMT-6	SDPMT-12
401	X	X	X	X
402	X	X	X	X
403	X	X	X	X
404	X	X	X	X
405	X	X	X	X
406	X	X	X	X
407	X	X	X	X
408	X	X	X	X
409	X	X	X	
410	X	X	X	X
411	X	X	X	X
412		X	X	X
Appendix	B.1	B.3	B.2	B.4

5.3.4 Site 4: FIT Southgate Field

5.3.4.1 PMT Test Results

Forty-six SDPMT tests were conducted at the Southgate Field test site. A summary of where SDPMT tests were conducted, along with the appendix section where the test data can be found, is summarized in Table 5.46. The X's shown in this table indicate the type of test conducted at a particular location, while the bottom row in the table indicates the appendix location where the plots can be found. Each of the four SDPMT test types were conducted at each test location with the exception of locations 409 and 412. The SDPMT-12 continuous test at location 409 could not be conducted because the soil was very loose and the test hole would not stay open to allow for the full insertion of the probe. The SDPMT-6 incremental test at location 412 was unable to be completed because the membrane broke at the end of the test. A total of 23 incremental tests were conducted at this site, eleven SDPMT-6's and twelve SDPMT-12's. Twenty three continuous tests were conducted at this test site, twelve SDPMT-6 tests and eleven SDPMT-12 tests.

5.3.4.1.1 SDPMT-6 Incremental Results

The engineering parameters obtained from the 12 incremental SDPMT-6 tests are summarized in Table 5.47. Lift-off pressures were determined for 5 of the 12 tests and values ranged from 2.1 to 16.3 kPa (0.3 to 2.3 psi) with and average of 8.8 kPa (1.3 psi) and a standard deviation of 5.3 kPa (0.8 psi). The limit pressure of the soil ranged from 200.0 to 320.0 kPa (29 to 47 psi) with an average of 262.5 kPa (38 psi) and a standard deviation of 40.1 kPa (5.8 psi). Initial moduli ranged from 1,218 to 2,516 kPa (177 to

Table 5.47: SDPMT-6 inch Incremental Test Results for Southgate Field

Location Number	Lift-off Pressure p_0 [kPa]	Limit Pressure p_L [kPa]	Initial PMT Modulus E_0 [kPa]
401	6.7	300.0	1488
402	10.7	320.0	2431
403	16.3	280.0	2516
404	2.1	300.0	1638
405	−0.0	200.0	1218
406	−7.1	200.0	1454
407	8.0	300.0	2098
408	−17.0	275.0	1783
409	−6.4	250.0	1452
410	−1.9	250.0	1562
411	−11.0	225.0	2356
412	−4.5	250.0	2176
Average	−0.3	262.5	1848
Standard Dev.	9.6	40.1	446

365 psi) with an average of 1,848 kPa (268 psi) and a standard deviation of 446 kPa (65 psi).

5.3.4.1.2 SDPMT-6 Continuous Results

Twelve SDPMT-6 continuous tests were attempted and 11 provided engineering parameters that are summarized in Table 5.47. Lift-off pressures were determined for 5 of the 11 tests and values ranged from 6.7 to 51.5 kPa (1.0 to 7.5 psi) with and average of 19.1 kPa (2.8 psi)and a standard deviation of 17.3 kPa (2.5 psi). The limit pressure of the soil ranged from 350.0 to 600.0 kPa (51 to 87 psi) with an average of 446.4 kPa (64.7 psi) and a standard deviation of 82.9 kPa (12.9 psi). Initial moduli ranged from 4,355 to 12,060 kPa (632 to 1749 psi) with an average of 7,623 kPa (1,106 psi) and a standard deviation of 2,665 kPa (387 psi).

5.3.4.1.3 SDPMT-12 Incremental Results

The engineering parameters obtained from the 12 incremental SDPMT-6 inch tests are summarized in Table 5.47. Lift-off pressures were determined for one test at location 405 and had a value of 6.1 kPa (0.9 psi). The limit pressure of the soil ranged from 145.0 to 295.0 kPa (21 to 43 psi) with an average of 222.5 kPa (32.3 psi) and a standard deviation of 52.0 kPa (7.5 psi). Initial moduli ranged from 1,019 to 3,044 kPa (148 to 442 psi) with an average of 1,999 kPa (290 psi) and a standard deviation of 705 kPa (102 psi).

Table 5.48: SDPMT-6 inch Continuous Test Results for Southgate Field

Location Number	Lift-off Pressure p_0 [kPa]	Limit Pressure p_L [kPa]	Initial PMT Modulus E_0 [kPa]
401	−9.9	350.0	6169
402	−29.4	400.0	6347
403	9.6	350.0	9046
404	51.5	400.0	6217
405	−8.0	500.0	8538
406	−15.5	500.0	4355
407	6.7	400.0	5716
408	9.9	380.0	4487
409		†	
410	−4.2	600.0	12060
411	25.8	530.0	11577
412	10.9	500.0	9339
Average	4.3	446.4	7623
Standard Dev.	21.8	82.9	2665

†: Borehole to large for reliable results.

Table 5.49: SDPMT-12 inch Incremental Test Results for Southgate Field

Location Number	Lift-off Pressure p_0 [kPa]	Limit Pressure p_L [kPa]	Initial PMT Modulus E_0 [kPa]
401	−7.7	250.0	1511
402	−11.7	275.0	3044
403	−2.8	295.0	2760
404	−2.8	225.0	1420
405	−0.3	270.0	1325
406	−9.0	185.0	2788
407	6.1	280.0	1684
408	−15.4	215.0	1556
409	−14.4	145.0	1019
410	−19.6	160.0	1689
411	−12.7	210.0	2808
412	−5.8	160.0	2381
Average	−8.0	222.5	1999
Standard Dev.	7.3	52.0	705

Table 5.50: SDPMT-12 inch Continuous Test Results for Southgate Field

Location Number	Lift-off Pressure p_0 [kPa]	Limit Pressure p_L [kPa]	Initial PMT Modulus E_0 [kPa]
401	−11.7	300.0	5371
402	−1.3	200.0	826
403	0.6	300.0	5372
404	−40.3	300.0	5320
405	13.1	400.0	4685
406	−3.4	300.0	3074
407	26.1	500.0	8633
408	−1.4	200.0	3186
410	3.5	500.0	8741
411	−27.2	500.0	7319
412	−11.9	300.0	4159
Average	−4.9	345.5	5153
Standard Dev.	18.0	112.8	2406

5.3.4.1.4 SDPMT-12 Continuous Results

The engineering parameters obtained from the 11 continuous SDPMT-12 inch tests are summarized in Table 5.49. Positive lift-off pressures were determined for 4 of the 11 tests, from locations 403, 405, 407, and 410; the values ranged from 0.6 to 26.1 kPa (0.1 to 3.8 psi) with and average of 10.8 kPa (1.6 psi) and a standard deviation of 11.5 kPa (1.7 psi). The limit pressure of the soil ranged from 200.0 to 500.0 kPa (29 to 73 psi) with an average of 345.5 kPa (50 psi) and a standard deviation of 111.8 kPa (16.2 psi). Initial moduli ranged from 826 to 8,741 kPa (120 to 1,268 psi) with an average of 5,153 kPa (747 psi) and a standard deviation of 2,406 kPa (349 psi).

5.3.4.2 NDG Results

Twenty-four NDG tests were conducted at the FIT Southgate Field test site, with twelve tests each at 6 and 12 inch depths. The results from the NDG tests are summarized in Table 5.51. The dry densities ranged from 85.8 to 95.4 lb/ft^3 (13.3 to 14.9 kN/m^3) with a standard deviation of 2.4 lb/ft^3 (0.4 kN/m^3) at a depth of 6 inches (15 cm). The 12 inch (30 cm) depth NDG dry densities ranged from 86.9 to 94.7 lb/ft^3 (13.6 to 14.9 kN/m^3) with a standard deviation of 2.3 lb/ft^3 (0.4 kN/m^3).

5.3.4.3 Moisture Content Results

Because of logistics at the FIT Southgate Field it, was not possible to conduct the SDPMT tests at the same time as the NDG tests. To obtain moisture contents,

Table 5.51: FIT Southgate Field NDG Test Result Summary

Location	Depth [in]	Density Dry $\left[\frac{lb}{ft^3}\right]$	Density Wet $\left[\frac{lb}{ft^3}\right]$	Moisture Content [%]	Depth [in]	Density Dry $\left[\frac{lb}{ft^3}\right]$	Density Wet $\left[\frac{lb}{ft^3}\right]$	Moisture Content [%]
401	6	91.7	96.0	4.7	12	91.9	96.3	4.8
402	6	92.2	95.5	3.7	12	92.3	95.9	3.9
403	6	91.1	94.9	4.1	12	89.9	93.8	4.4
404	6	85.8	90.7	5.8	12	86.9	91.8	5.7
405	6	92.8	97.1	4.7	12	89.5	94.0	5.0
406	6	92.3	96.1	4.2	12	91.6	95.2	3.9
407	6	91.1	95.6	4.9	12	89.5	94.1	5.1
408	6	95.4	97.6	2.3	12	94.7	97.0	2.4
409	6	92.9	94.5	1.7	12	94.1	95.7	1.7
410	6	95.2	99.5	4.4	12	92.9	97.3	4.7
411	6	91.4	96.6	5.7	12	89.3	94.9	6.2
412	6	91.4	98.1	7.3	12	90.1	96.8	7.4
Average:		91.9	96.0	4.5		91.1	95.2	4.6
Std. Dev.:		2.4	2.2	1.5		2.3	1.6	1.5

disturbed samples were collected at the time of SDPMT testing. These results were used to determine the wet unit weight at the time of SDPMT testing.

At the time of conducting the incremental SDPMT-6 and SDPMT-12 tests, twelve disturbed samples were collected and dried in the lab to determine field moisture contents, which were then used to determine the wet unit weight. The moisture content results are summarized in Table 5.52.

The results of the moisture content samples taken at the time of the continuous testing are summarized in Table 5.53. At the time of conducting the continuous SDPMT-6 and SDPMT-12 tests, twelve additional moisture content disturbed samples were collected and dried in the lab to determine the wet unit weight of the soil at the time of testing.

5.3.4.4 Zorn LWD Results

Twelve Zorn LWD tests were conducted, with one at each location, across the site. The test results are summarized in Table 5.54. Surface deflections ranged from 0.86 to 2.19 mm (0.03 to 0.09 inch) averaging 1.61 mm (0.06 inch) with a standard deviation of 0.4 mm (0.1 inch). The moduli (E_d) ranged from 10.3 to 26.1 MPa (1,493 to 3,785 psi), with an average 15.0 MPa (2,175 psi) and a standard deviation of 4.4 MPa (638 psi).

Table 5.52: Summary of Additional Moisture Content Samples at FIT Southgate Field at the Time of SDPMT-6 and SDPMT-12 Incremental Testing

Location	NDG Dry Unit Weight [lb/ft^3]	Wet Mass [g]	Dry Mass [g]	Moisture Content [g]	Moisture Content [%]	Wet Unit Weight [lb/ft^3]
401	103.2	61.1	58.1	3.0	5.3	108.7
402	105.8	56.4	52.6	3.8	7.5	113.7
403	107.0	62.7	61.9	0.8	1.3	108.4
404	105.2	51.0	47.5	3.5	7.7	113.3
405	103.8	42.7	39.0	3.7	9.9	114.1
406	101.1	60.1	56.7	3.4	6.2	107.4
407	105.8	64.7	63.3	1.4	2.3	108.2
408	106.6	78.7	78.1	0.6	0.8	107.4
409	106.4	56.4	54.3	2.1	4.0	110.7
410	108.4	59.5	56.6	2.9	5.3	114.1
411	106.4	59.1	56.7	2.4	4.4	111.1
412	102.9	63.9	61.7	2.2	3.7	106.7

Note: Moisture content cans were all of a standard 1.8 g mass.

Table 5.53: Summary of Additional Moisture Content Samples at FIT Southgate Field at the Time of SDPMT-6 and SDPMT-12 Continuous Testing

Location	NDG Dry Unit Weight [lb/ft^3]	Wet Mass [g]	Dry Mass [g]	Moisture Content [g]	Moisture Content [%]	Wet Unit Weight [lb/ft^3]
401	103.2	64.3	63.7	0.6	1.0	104.2
402	105.8	62.0	61.5	0.5	0.8	106.7
403	107.0	60.7	60.0	0.7	1.2	108.3
404	105.2	70.1	69.3	0.8	1.2	106.4
405	103.8	61.2	60.5	0.7	1.2	105.0
406	101.1	67.4	66.7	0.7	1.1	102.2
407	105.8	53.1	52.0	1.1	2.2	108.1
408	106.6	65.7	64.2	1.5	2.4	109.2
409	106.4	59.9	59.1	0.8	1.4	107.9
410	108.4	48.7	47.4	1.3	2.9	111.5
411	106.4	55.5	54.0	1.5	2.9	109.5
412	102.9	54.4	53.5	0.9	1.7	104.7

Note: Moisture content cans were all of a standard 1.8 g mass.

Table 5.54: FIT Southgate Field Zorn LWD Results

	Test 1	
Location	S_d [mm]	E_d [MPa]
401	2.11	10.7
402	1.76	12.8
403	1.32	17.0
404	1.76	12.8
405	1.98	11.3
406	1.37	16.4
407	1.69	13.3
408	0.86	26.1
409	1.27	17.7
410	1.25	18.0
411	1.70	13.3
412	2.19	10.3
Average	1.61	15.0
Std. Dev.	0.40	4.4

5.3.4.5 Dynatest LWD Results

Twelve Dynatest LWD tests were conducted across the Southgate Field test site, with one at each location. The results are summarized in Table 5.55. The moduli (E_0) values range from 18.0 to 112.3 MPa (2,610 to 16,283 psi), with an average of 67.7 MPa (9,817 psi) and a standard deviation of 26.2 MPa (3,799 psi).

5.3.4.6 CIT Results

Twenty-four CITs were conducted across the Southgate Field test site, with two at each location. The CIVs ranged from 4.6 to 8.5 g's, and average of 6.4 g's and a standard deviation of 0.8 g's. The test results are summarized in Table 5.56.

5.3.4.7 DCP Test Results

Twelve DCP tests were conducted at the Southgate Field test site, with one at each test location to a depth of 12 inches. The data from each test is presented in Figures I.1 through I.12. Each figure includes two plots; one with total penetration versus total number of blows, and a second with penetration depth versus penetration per blow. Note the both the imperial (i.e. English) and international units are displayed on the y-axes.

Table 5.55: FIT Southgate Field Dynatest LWD Test Data

Location	Test 1 E0 [MPa]
401	42.0
402	61.6
403	55.3
404	18.0
405	68.6
406	112.3
407	72.3
408	85.3
409	53.3
410	89.3
411	100.3
412	54.3
Average	67.7
Std. Dev.	26.2

Table 5.56: Clegg Impact Values for Southgate Field

Location	Test 1 [g's]	Test 2 [g's]	Average [g's]
401	5.3	4.6	5.0
402	4.6	5.9	5.3
403	7.0	5.5	6.3
404	5.5	7.0	6.3
405	6.1	6.1	6.1
406	6.1	6.6	6.4
407	8.5	6.1	7.3
408	8.5	7.6	8.1
409	7.6	5.7	6.7
410	6.1	7.4	6.8
411	5.9	6.1	6.0
412	5.2	7.9	6.6
Average	6.4	6.4	6.4
Std Dev.	1.3	1.0	0.8

5.3.4.7.1 DCP Data Reduction

The data for each DCP test was further analyzed to determine an average penetration per blow or penetration index (DCP PI) for 6 and 12 inches (15 and 30 cm) of penetration. The average DCP index will be used to compare with SDPMT parameters.

Table 5.57 summarizes the penetration rate for the DCP tests at Southgate Field. The 6 inch averages ranged from 31.6 to 52.7 mm/blow (1.2 to 2.1 in/blow)with an average and standard deviation of 37.7 and 6.3 mm/blow (1.5 to 0.25 in/blow) respectively. The 12 inch (30 cm) averages ranged from 23.3 to 46.6 mm/blow (0.9 to 1.8 in/blow)with an average and standard deviation of 30.5 and 6.9 mm/blow (1.2 to 0.3 in/blow) respectively.

5.3.4.8 Resilient Modulus Results

FDOT SMO laboratory performed six resilient modulus tests according to AASHTO T-307 on the soil collected at the Southgate Field site. The maximum density from AASHTO T99 was 100 lb/ft^3 (15.7 kN/m^3), with an optimum moisture content of 10%. The modulus samples were compacted to target moisture contents at dry of optimum (5%), at optimum (10%), and wet of optimum (12%). The 11 psi (2 kPa) bulk stress moduli ranged from 10,289 to 16,730 psi (1,492 to 1,878 kPa). The results of this testing are summarized in Table 5.58

The two resilient modulus tests performed on samples prepared at optimum moisture content were used to estimate an average strain and resilient modulus for the soil at Southgate Field. This data is shown in Table 5.45. The average strain for the 15 loading sequences conducted during the resilient modulus test was 3.74x10^{-2} %, and the corresponding average modulus was 12,948 psi (1,878 kPa). This data was compared with moduli from the SDPMT unload data.

Table 5.57: Summary of DCP Indexes for 6 and 12 inch Penetrations at FIT Southgate Field

Location Number	6 inch Average Blows to 153 mm [blows]	6 inch Average Total Penetration [mm]	6 inch Average Penetration per blow [mm/blow]	12 inch Average Blows to 305 mm [blows]	12 inch Average Total Penetration [mm]	12 inch Average Penetration per blow [mm/blow]
401	5	185	37.0	10	308	30.8
402	4	162	40.5	10	317	31.7
403	4	166	41.5	10	312	31.2
404	4	162	40.5	11	310	28.2
405	5	172	34.4	12	328	27.3
406	5	165	33.0	13	320	24.6
407	5	158	31.6	12	305	25.4
408	5	158	31.6	14	325	23.2
409	3	158	52.7	7	326	46.6
410	5	161	32.2	11	308	28.0
411	5	170	34.0	12	326	27.2
412	4	173	43.3	8	333	41.6
Average			37.7			30.5
Std. Dev.			6.3			6.9

Table 5.58: Resilient Modulus Test Results for Southgate Field Soil Dry, Wet and at Optimum Moisture

	Target Moisture [%]	Max Density [lb/ft^3]	Compacted Density [lb/ft^3]	Compacted Moisture [%]	Percent of Optimum [%]	K1	K2	Resilient Modulus ($\theta = 11$ psi) [psi]
Dry 1	5	100.0	101.0	4.7	101.0	7937.0	0.3110	16,730
Dry 2	5	100.0	100.0	4.7	100.0	5388.7	0.3724	13,162
Opt 1	10	100.0	100.5	10.3	100.5	2644.1	0.5667	10,289
Opt 2	10	100.0	99.8	10.0	99.8	2758.5	0.5544	12,380
Wet 1	12	100.0	100.9	12.0	100.9	2468.0	0.6942	13,039
Wet 2	12	100.0	100.8	12.1	100.8	2784.6	0.6671	13,786

Table 5.59: Summary of Resilient Modulus Sequence Data for Southgate Field

Sequence	Chamber Confining Pressure	Nominal Maximum Axial Stress	Nominal Bulk Stress	Test 1		Test 2		Average	
				Resilient Strain	Resilient Modulus	Resilient Strain	Resilient Modulus	Resilient Strain	Resilient Modulus
	σ_3 [psi]	σ_3 [psi]	θ [psi]	ϵ_r [in/in]	M_r [psi]	ϵ_r [in/in]	M_r [psi]	ϵ_r [in/in]	M_r [psi]
1	6	2	20	0.000105	15487	0.000104	15685	0.000104	15586
2	6	4	22	0.000209	15663	0.000208	15778	0.000208	15721
3	6	6	24	0.000312	15796	0.000312	15853	0.000312	15824
4	6	8	26	0.000413	15978	0.000412	16037	0.000412	16007
5	6	10	28	0.000510	16249	0.000509	16344	0.000509	16297
6	4	2	14	0.000126	12591	0.000124	12675	0.000125	12633
7	4	4	16	0.000251	12685	0.000250	12725	0.000251	12705
8	4	6	18	0.000366	13185	0.000367	13179	0.000366	13182
9	4	8	20	0.000473	13709	0.000474	13703	0.000474	13706
10	4	10	22	0.000577	14085	0.000578	14081	0.000578	14083
11	2	2	8	0.000166	8647	0.000165	8710	0.000166	8679
12	2	4	10	0.000324	9108	0.000318	9294	0.000321	9201
13	2	6	12	0.000464	9806	0.000455	9954	0.000459	9880
14	2	8	14	0.000596	10283	0.000581	10568	0.000588	10425
15	2	10	16	0.000748	10187	0.000733	10396	0.000741	10292
							Average:	0.0.000374	12948

Chapter 6

Data Analysis

6.1 SDPMT Stress-Strain Analysis

Before any complex analyses were conducted, the basic stress-strain relationships from the SDPMT-6 and SDPMT-12 digital data for the incremental and continuous tests were compared to determine if the data quality was acceptable. The critical portions of a high quality PMT curve are identified in Figure 6.1. The testing sequence associated with generating the elastic reload slope was not conducted for this research because PMT unloading data can be used to estimate elastic moduli. The parameters evaluated for this PMT data quality evaluation were: at-rest or lift-off soil pressure (p_0), slope of elastic phase (S_i), beginning of plastic phase, the limit pressure (p_L) and the unloading portion.

A group of SDPMT curves were visually evaluated. Figure 6.2 illustrates four typical SDPMT-6 and SDPMT-12 incremental and continuous SDPMT curves. Visually, each plot shows reduced data that would allow engineers to find lift-off pressures, elastic slopes, plastic ranges, limit pressures, and unloading regions. The preliminary conclusion was that the digitally recorded SDPMT data is producing typical and high quality PMT stress-strain curves; and therefore, the research with these probes and testing processes should continue (Misilo III, 2018).

6.2 Basic Statistical Regression Analysis

Five statistical regression models were chosen to evaluate the data from the various tests. Each model will be used to determine if any relationships exist between the key parameters. The analysis consisted of linear, non-linear logarithmic and exponential regression models (Misilo III, 2018).

For each comparison a table will be presented showing: a) the statistical relationship developed between the independent and dependent test variables, b) the coefficient of determination (R^2), c) the regression model, and d) the figure number where the model and data are presented.

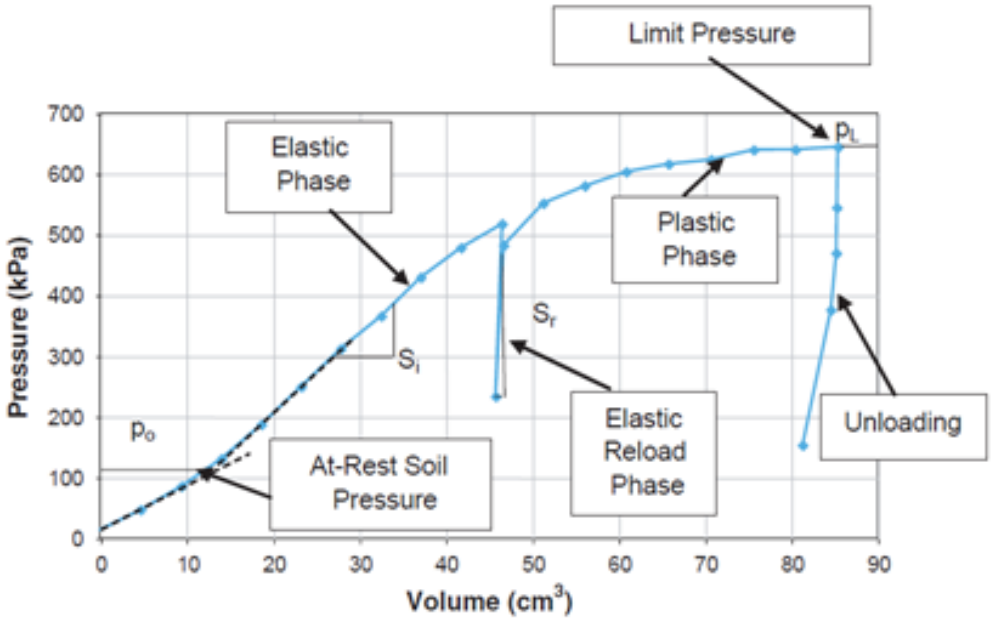

Figure 6.1: Typical PMT Stress Strain Curve

The five models use X as the independent variable and Y as the dependent variable, plus A and B as the statistical regression coefficients. The general form of the arithmetic linear - linear model to be evaluated is shown in Equation 6.1. Three logarithmic models will be evaluated for each relationship; log versus linear, linear versus log, and log versus log. The general forms of these models are described in Equations 6.2, 6.3, and 6.4 respectively. An exponential relationship will also be evaluated for each comparison and its general form is described in Equation 6.5.

$$Y = A \times X + B \tag{6.1}$$
$$\log_{10}(Y) = A \times X + B \tag{6.2}$$
$$Y = A \times \log_{10}(X) + B \tag{6.3}$$
$$\log_{10}(Y) = A \times \log_{10}(X) + B \tag{6.4}$$
$$Y = A \times (X)^B \tag{6.5}$$

Appendix E contains all the plots from these analyses. Only the conventional arithmetic plot for each case, however, is shown within the corresponding section. Its purpose is to allow the reader to see the overall the quality of the comparison.

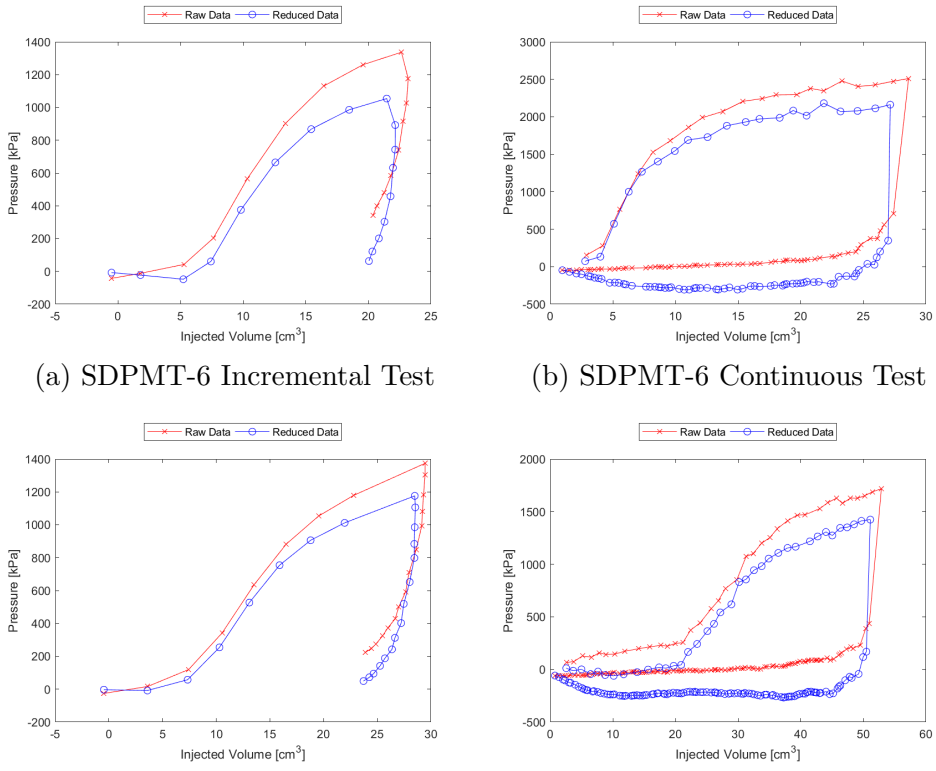

(a) SDPMT-6 Incremental Test

(b) SDPMT-6 Continuous Test

(c) SDPMT-12 Incremental Test

(d) SDPMT-12 Continuous Test

Figure 6.2: Typical SDPMT Curves

6.3 Regression Models from SDPMT Parameters, All Sites

Engineering parameters from the four types of SDPMT tests conduced were compared with each other, and five regression models were developed and evaluated. This process produced 20 comparison equations for dependent and independent variable. Data from all four SDPMT test types were used to determine the acceptability of the different regression models (Misilo III, 2018).

6.3.1 Regression Models of p_0 versus E_0

A soils inherent lift-off or at-rest pressure should be a relatively small value that may vary from zero to 35 kPa (5 psi). Correlations with p_0, therefore, should be difficult to obtain. Regardless of this fact, correlations were attempted.

Twenty p_0 versus E_0 regression models were evaluated. The results are summarized in Table 6.1. Between 12 and 27 datasets were analyzed.

In these analyses, data points where $p_0 < 0$ are ignored for the analysis because; a) these values do not make physical sense in soils, and b) the lift-off pressure graphical construction process is not easily applied to data from pre-bored holes.

Table 6.1: Models of E_0 (kPa) versus p_0 (kPa), All Sites

Relationship x	Relationship y	R^2	Model	# of Tests	Figure
			SDPMT-6 Incremental		
Linear	Linear	0.10	E_0=4806 p_0 +6798	12	E.1
Linear	Log10	0.12	$\log_{10}(E_0)$=0.06814 p_0 +3.439	12	E.193
Log10	Linear	0.13	E_0=9.979E+04 $\log_{10}(p_0)$ -3.968E+04	12	E.97
Log10	Log10	0.16	$\log_{10}(E_0)$=1.416 $\log_{10}(p_0)$ +2.779	12	E.289
Exponential Model		0.10	E_0=1.034E+04 $(p_0)^{0.7394}$	12	E.385
			SDPMT-6 Continuous		
Linear	Linear	0.09	E_0=191.5 p_0 +2.315E+04	21	E.2
Linear	Log10	0.24	$\log_{10}(E_0)$=0.005153 p_0 +4.068	21	E.194
Log10	Linear	0.19	E_0=2.726E+04 $\log_{10}(p_0)$ -7590	21	E.98
Log10	Log10	0.39	$\log_{10}(E_0)$=0.6481 $\log_{10}(p_0)$ +3.363	21	E.290
Exponential Model		0.16	E_0=1.118E+04 $(p_0)^{0.3032}$	21	E.386
			SDPMT-12 Incremental		
Linear	Linear	0.42	E_0=666.4 p_0 +6758	27	E.3
Linear	Log10	0.47	$\log_{10}(E_0)$=0.01992 p_0 +3.702	27	E.195
Log10	Linear	0.46	E_0=2.155E+04 $\log_{10}(p_0)$ -3179	27	E.99
Log10	Log10	0.47	$\log_{10}(E_0)$=0.6234 $\log_{10}(p_0)$ +3.425	27	E.291
Exponential Model		0.48	E_0=4256 $(p_0)^{0.5591}$	27	E.387
			SDPMT-12 Continuous		
Linear	Linear	0.06	E_0=178.2 p_0 +2.514E+04	18	E.4
Linear	Log10	0.09	$\log_{10}(E_0)$=0.003434 p_0 +4.125	18	E.196
Log10	Linear	0.12	E_0=1.907E+04 $\log_{10}(p_0)$ +5730	18	E.100
Log10	Log10	0.16	$\log_{10}(E_0)$=0.3486 $\log_{10}(p_0)$ +3.78	18	E.292
Exponential Model		0.11	E_0=1.317E+04 $(p_0)^{0.265}$	18	E.388

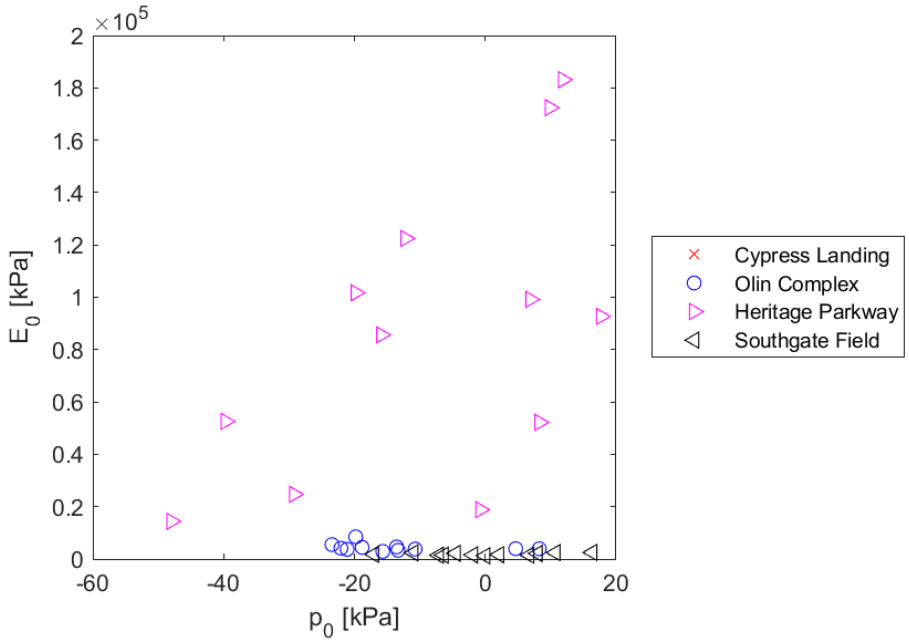

Figure 6.3: SDPMT-6 Incremental, E_0 versus p_0, All Sites

6.3.1.1 Regression models from SDPMT-6 Incremental Tests, E_0 versus p_0

Table 6.1 shows the five regression models developed and analyzed for the SDPMT-6 incremental tests. All the p_0 and E_0 data from the SDPMT-6 incremental tests data is shown in Figure 6.3. The data, excluding the negative p_0 values used to develop the models, is illustrated in Figure 6.4. Examination of this figure shows no logical trends. It also shows a very limited number of data points (i.e. 12). The models produced R^2 values ranging from 0.10 to 0.16, which substantiate the belief that correlations with p_0 are difficult.

6.3.1.2 Regression Models from SDPMT-6 Continuous Tests, E_0 versus p_0

Table 6.1 shows the five regression models developed and analyzed for the SDPMT-6 continuous tests. Figure 6.5 shows all the data points relating p_0 and E_0 for the SDPMT-6 continuous tests. Note that p_0 values as low as zero and high as 170 kPa (25 psi) are shown for the cemented coquina at Heritage Parkway. These maximum values seem unrealistically high. They are much higher than those found from SDPMT-6 incremental testing. Using the values of p_0 greater or equal to zero, the models produced R^2 values ranging from 0.09 to 0.39. The data used to develop the models is illustrated in Figure 6.5. The log-log relationship had the best R^2 value of 0.39, indicating a weak relationship between p_0 and E_0, (see Figure E.290), which makes the correlation unreliable.

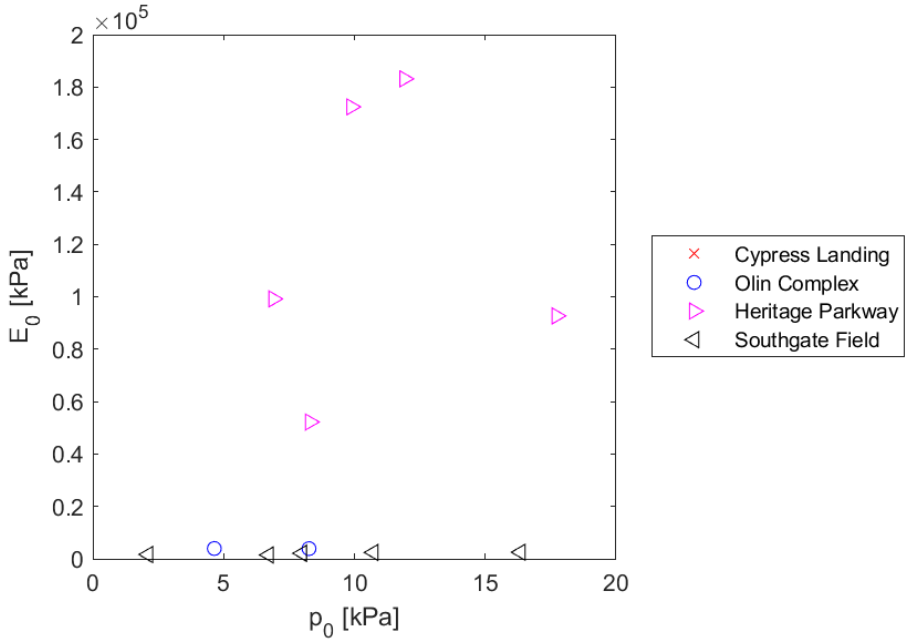

Figure 6.4: SDPMT-6 Incremental, E_0 versus p_0, All Sites, Negative values of p_0 removed

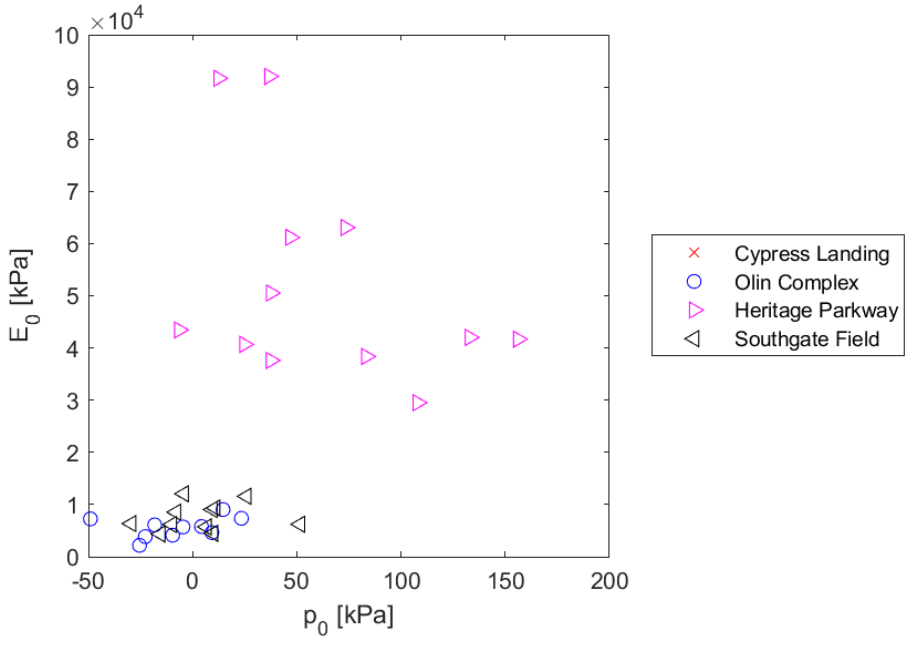

Figure 6.5: SDPMT-6 Continuous, E_0 versus p_0, All Sites

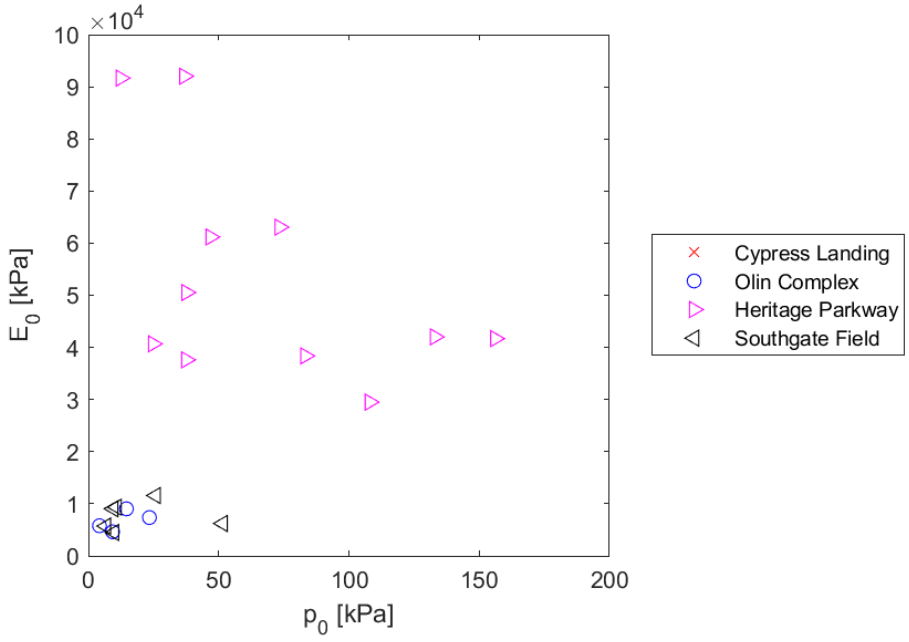

Figure 6.6: SDPMT-6 Continuous, E_0 versus p_0, All Sites, Negative values of p_0 removed

6.3.1.3 Regression Models from SDPMT-12 Incremental Tests, E_0 versus p_0

Table 6.1 shows the five regression models developed and evaluated for the SDPMT-12 incremental tests. Figure 6.7 shows all the data points collected relating p_0 to E_0. Using values of p_0 greater or equal to zero, the models produced R^2 values ranging from 0.42 to 0.47. The data used to develop the models is illustrated in Figure 6.8, with negative p_0 values removed from the model development. All models illustrate a weak relationship between p_0 and E_0, with a high dispersement of data, making the correlations unreliable.

6.3.1.4 Regression Models from SDPMT-12 Continuous Tests, E_0 versus p_0

Table 6.1 show the five regression models developed and analyzed for the SDPMT-12 continuous tests and Figure 6.9 shows all the data points collected relating p_0 to E_0. Note that these continuous tests produced p_0 values nearing 180 kPa (26 psi). Using the non-negative p_0 values, the models produced R^2 values ranging from 0.06 to 0.16. The measured data used to develop the models is illustrated in Figure 6.10. None of these models showed a strong relationship between p_0 and E_0 for SDPMT-12 continuous tests.

6.3.1.5 Summary of E_0 versus p_0 regression models

All statistical regressions evaluated between p_0 and E_0 produced weak correlations. The SDPMT-12 incremental produced better results than the other tests. This outcome

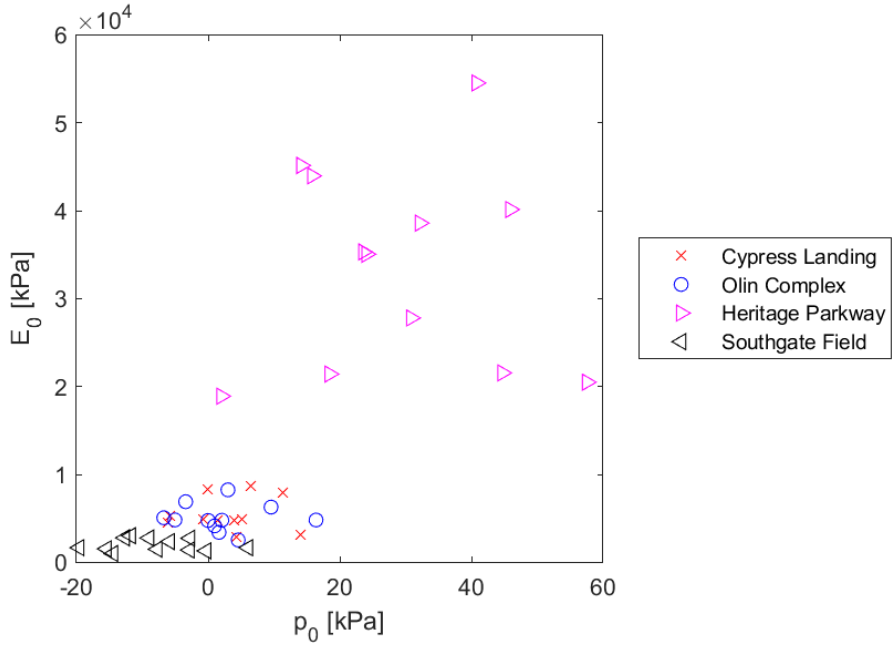

Figure 6.7: SDPMT-12 Incremental, E_0 versus p_0, All Sites

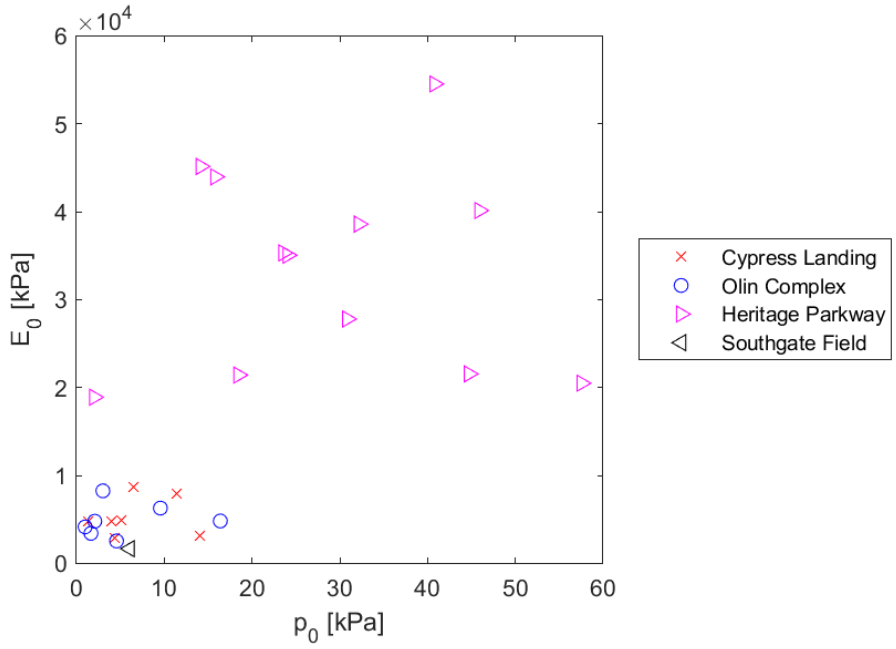

Figure 6.8: SDPMT-12 Incremental, E_0 versus p_0, All Sites, Negative values of p_0 removed

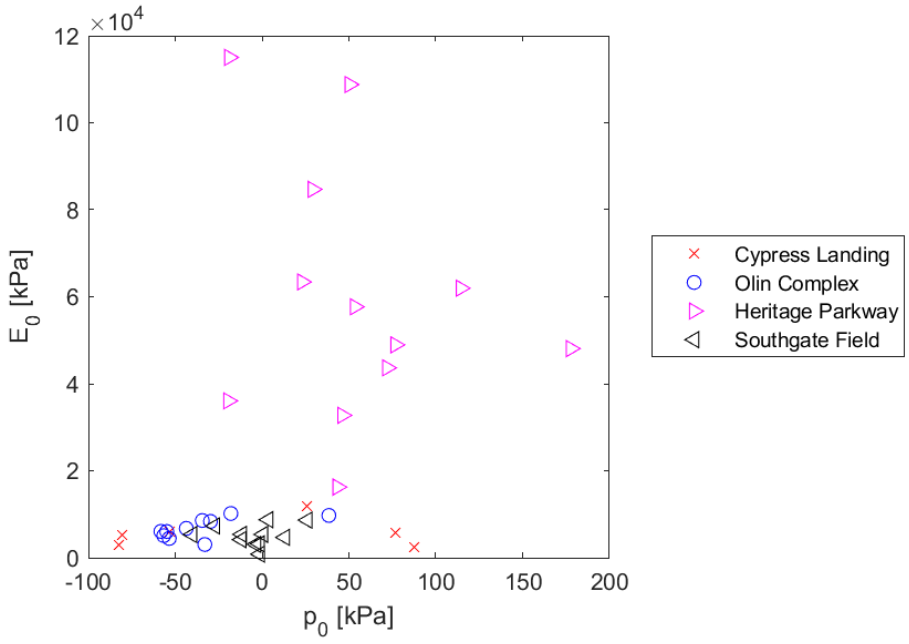

Figure 6.9: SDPMT-12 Continuous, E_0 versus p_0, All Sites

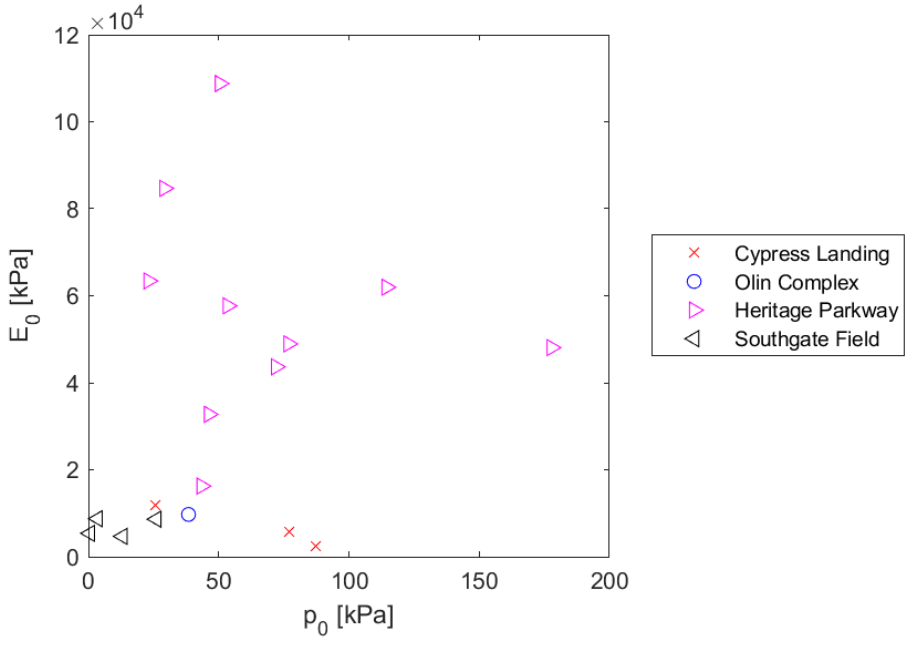

Figure 6.10: SDPMT-12 Continuous, E_0 versus p_0, All Sites, Negative values of p_0 removed

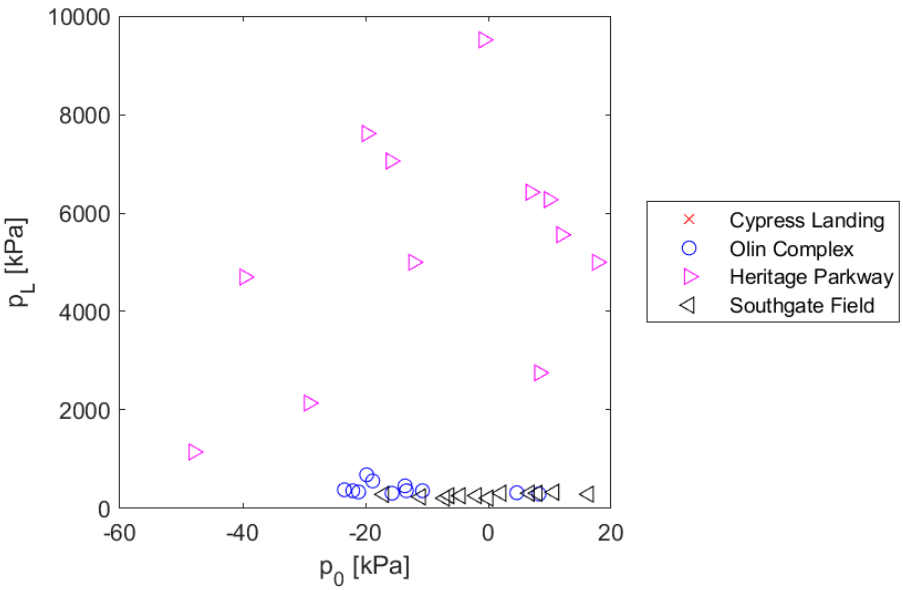

Figure 6.11: SDPMT-6 Incremental, p_L versus p_0, All Sites

is most likely due to both the inexact graphical process used to estimate p_0 and the method used to make the boreholes. The continuous SDPMT tests produced p_0 values that are unrealistically high.

6.3.2 Regression Models of p_L versus p_0

Twenty p_L versus p_0 regression models were evaluated. The results are summarized in Table 6.2. The reliability of determining p_0 is a contributing factor to the limited confidence in these models, since many data points where $p_0 < 0$ had to be omitted. Regression coefficients ranged from 0.09 to 0.5, indicating that p_L and p_0 may not be related. The SDPMT-12 incremental testing produced the highest correlation coefficients.

6.3.2.1 Comparison of SDPMT-6 Incremental Tests, p_L versus p_0

Table 6.2 show the five regression models tested for SDPMT-6 incremental tests. The data collected relating p_0 to p_L is shown in Figure 6.11. The models developed produced very weak R^2 values ranging from 0.09 to 0.13. The data used to develop the models is illustrated in Figure 6.12; and it is noted that negative values of p_0 were removed for model development. None of these models showed a strong relation between p_0 and p_L for SDPMT-6 incremental tests. The limited number of data points (12) available to build this model has significantly decreased its reliability.

Table 6.2: Models of p_L (kPa) versus p_0 (kPa), All Sites

Relationship x	Relationship y	R^2	Model	# of Tests	Figure
			SDPMT-6 Incremental		
Linear	Linear	0.09	p_L=181.1 p_0 +658.8	12	E.21
Linear	Log10	0.10	$\log_{10}(p_L)$=0.04584 p_0 +2.559	12	E.213
Log10	Linear	0.12	p_L=3692 $\log_{10}(p_0)$ -1030	12	E.117
Log10	Log10	0.13	$\log_{10}(p_L)$=0.9276 $\log_{10}(p_0)$ +2.138	12	E.309
Exponential Model		0.10	p_L=572.3 $(p_0)^{0.6487}$	12	E.405
			SDPMT-6 Continuous		
Linear	Linear	0.20	p_L=11.8 p_0 +932.6	21	E.22
Linear	Log10	0.29	$\log_{10}(p_L)$=0.005757 p_0 +2.715	21	E.214
Log10	Linear	0.34	p_L=1496 $\log_{10}(p_0)$ -698.1	21	E.118
Log10	Log10	0.43	$\log_{10}(p_L)$=0.6839 $\log_{10}(p_0)$ +1.986	21	E.310
Exponential Model		0.29	p_L=400.7 $(p_0)^{0.3724}$	21	E.406
			SDPMT-12 Incremental		
Linear	Linear	0.43	p_L=44.97 p_0 +533.1	27	E.23
Linear	Log10	0.50	$\log_{10}(p_L)$=0.01853 p_0 +2.616	27	E.215
Log10	Linear	0.47	p_L=1453 $\log_{10}(p_0)$ -136.7	27	E.119
Log10	Log10	0.53	$\log_{10}(p_L)$=0.5928 $\log_{10}(p_0)$ +2.345	27	E.311
Exponential Model		0.49	p_L=330.7 $(p_0)^{0.5301}$	27	E.407
			SDPMT-12 Continuous		
Linear	Linear	0.12	p_L=9.957 p_0 +1147	18	E.24
Linear	Log10	0.10	$\log_{10}(p_L)$=0.003368 p_0 +2.868	18	E.216
Log10	Linear	0.19	p_L=918.7 $\log_{10}(p_0)$ +284.9	18	E.120
Log10	Log10	0.18	$\log_{10}(p_L)$=0.3326 $\log_{10}(p_0)$ +2.543	18	E.312
Exponential Model		0.18	p_L=586.4 $(p_0)^{0.2863}$	18	E.408

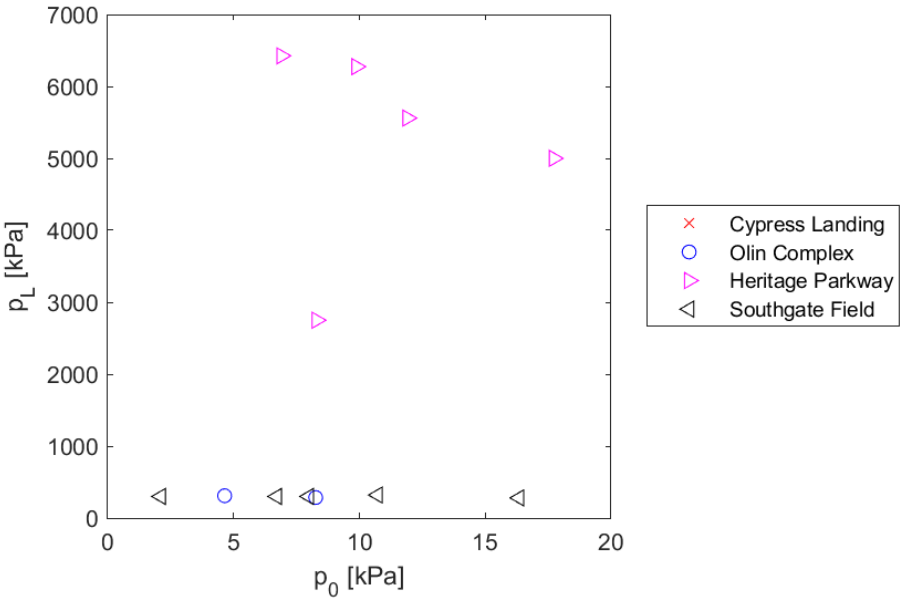

Figure 6.12: SDPMT-6 Incremental, p_L versus p_0, All Sites, Negative values of p_0 removed

6.3.2.2 Comparison of SDPMT-6 Continuous Tests, p_L versus p_0

Table 6.2 show the five regression models tested for SDPMT-6 continuous tests. All the data collected that relates p_0 to p_L is shown in Figure 6.13. The models produced relatively weak R^2 values ranging from 0.29 to 0.43. The data used to develop the models is illustrated in Figure 6.14, and only points where $p_0 > 0$ (21 data points) were used. Note the unrealistically high p_0 values in this plot. None of these models showed a strong relation between p_0 and p_L for SDPMT-6 continuous tests. This finding is attributed to the imprecise method of determining p_0.

6.3.2.3 Comparison of SDPMT-12 Incremental Tests, p_L versus p_0

Table 6.2 show the five regression models tested for SDPMT-12 incremental tests. All data relates p_0 to p_L is shown in Figure 6.15. The models produced relatively weak R^2 values ranging from 0.43 to 0.53, based on 27 data points. The measured data used to develop the models is illustrated in Figure 6.16; with the negative p_0 values removed for model development. The log - log model had the highest R^2 of 0.53. This model is described by the Equation 6.6. The log-log model is marginally acceptable for relating p_0 and p_L.

$$log_{10}(p_L) = 5.928 \times 10^{-1} log_{10}(p_0) + 2.345 \tag{6.6}$$

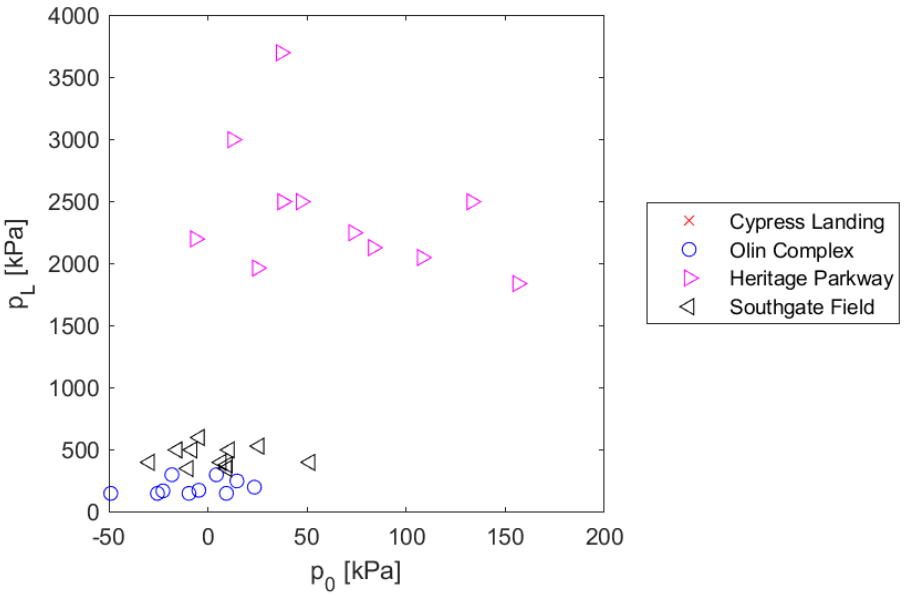

Figure 6.13: SDPMT-6 Continuous, p_L versus p_0, All Sites

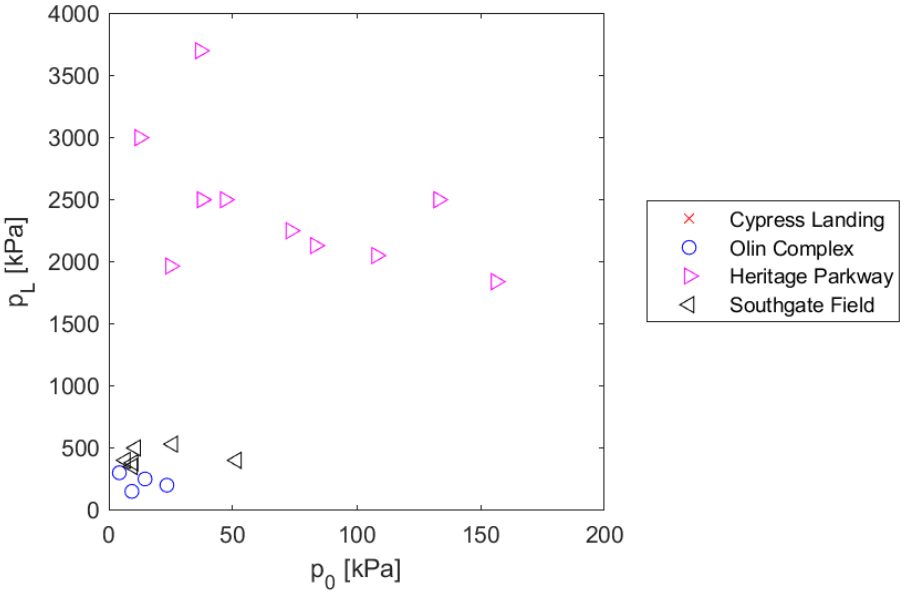

Figure 6.14: SDPMT-6 Continuous, p_L versus p_0, All Sites, Negative values of p_0 removed

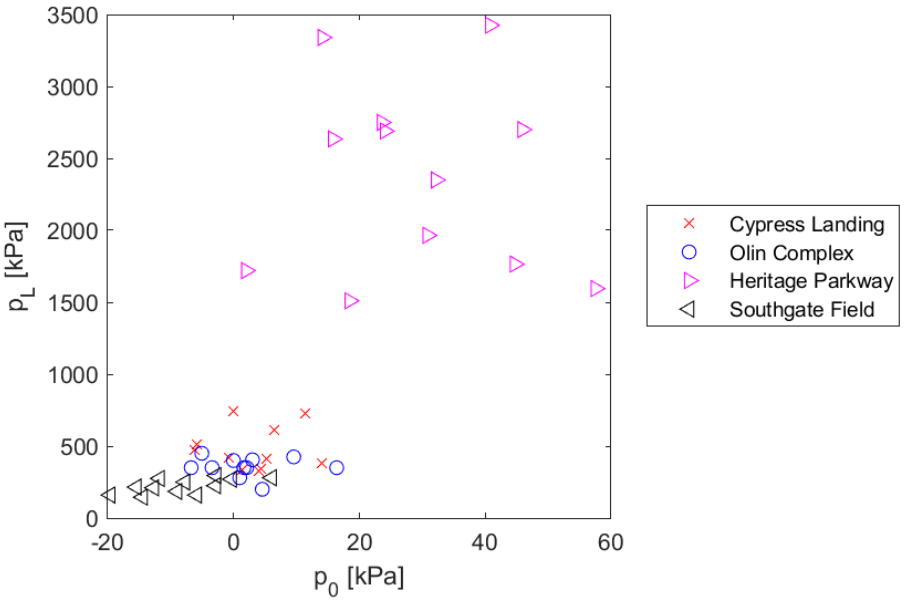

Figure 6.15: SDPMT-12 Incremental, p_L versus p_0, All Sites

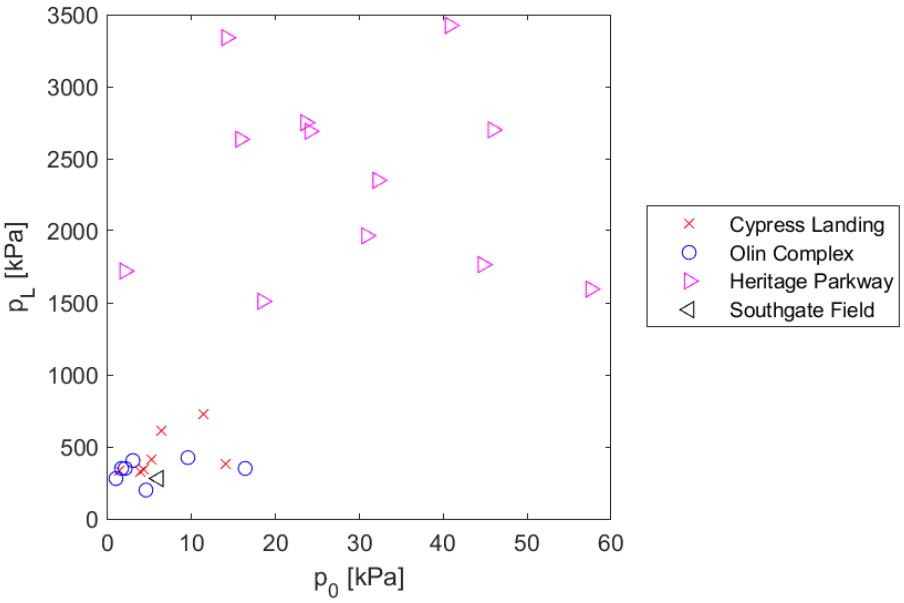

Figure 6.16: SDPMT-12 Incremental, p_L versus p_0, All Sites, Negative values of p_0 removed

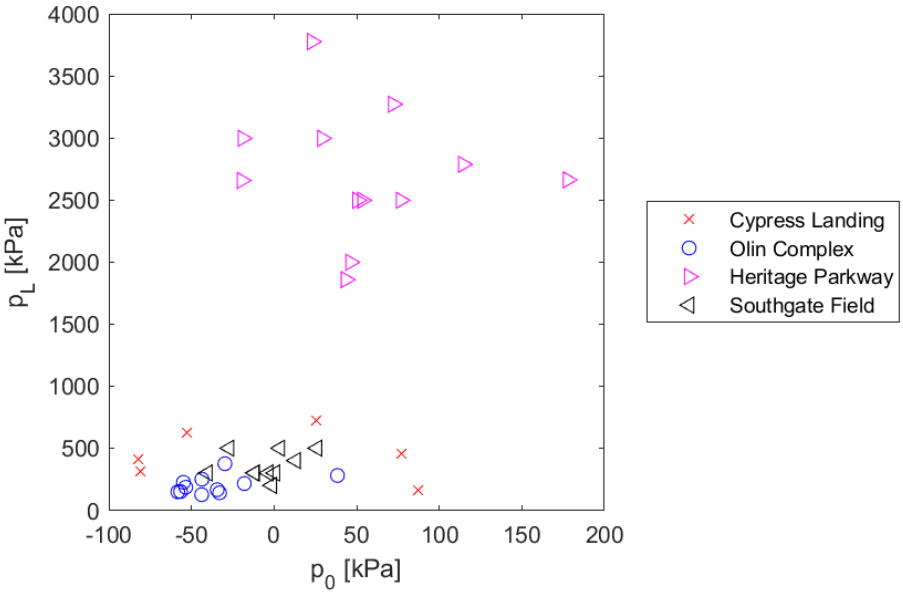

Figure 6.17: SDPMT-12 Continuous, p_L versus p_0, All Sites

6.3.2.4 Comparison of SDPMT-12 Continuous Tests, p_L versus p_0

Table 6.2 shows the five regression models for SDPMT-12 continuous tests. All data collected that relates p_0 to p_L is illustrated in Figure 6.17. The models produced weak R^2 values ranging from 0.10 to 0.19. The data used to develop the models is illustrated in Figure 6.18. The negative p_0 values have been removed from the model development. Note there are unrealistically high p_0 values in this plot. None of these models showed a strong relation between p_0 and p_L for SDPMT-12 continuous tests.

6.3.2.5 Summary of p_L versus p_0 regression models

The statistical regression models developed between p_0 and p_L showed very weak to marginal correlations. The SDPMT-12 incremental testing produced the best results for this comparison. Similar to the p_0 versus E_0 results, these poor correlations may be attributed to the inexact graphical construction process used to estimate p_0. Note that both SDPMT continuous tests produced unrealistically high p_0 values, indicating that the testing and calibration process needs further evaluation.

6.3.3 Regression Models of p_L versus E_0

Twenty p_L versus E_0 regression models were evaluated and are summarized in Table 6.3. All testing produced useful correlation coefficients. The best correlations were produced by the SDPMT-12 incremental data. The poorest correlations were produced

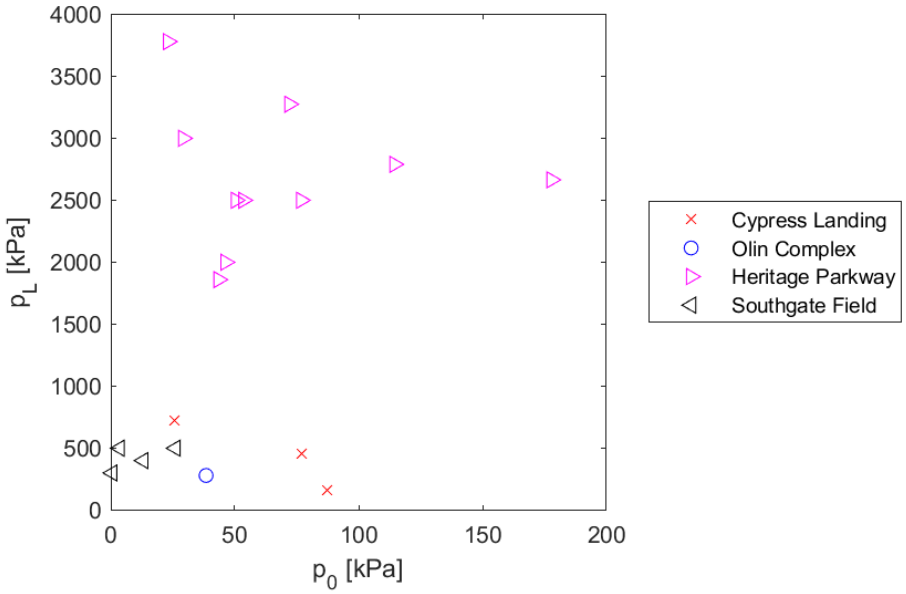

Figure 6.18: SDPMT-12 Continuous, p_L versus p_0, All Sites, Negative values of p_0 removed

by the SDPMT-6 incremental data. Cosentino et al. (2008) also showed excellent correlations between p_L and E_0.

6.3.3.1 Comparison of SDPMT-6 Incremental Tests, p_L versus E_0

Figure 6.19 shows all data points collected from SDPMT-6 incremental tests. Visually, there seems to be a linear trend up to about 4,000 kPa. Estimated p_L values greater than 6,000 kPa produced a large amount of scatter, which is associated with the upper limit of existing pressure gage used during testing. This gage has an upper limit of 5,000 kPa, therefore, any tests on materials where pressures approach 5,000 kPa would be reaching the limits of the equipment. Also note, the handle used to push water along the cylinder in the control during testing becomes very difficult to turn as pressures exceed 2,000 kPa. These factors would significantly contribute to the high scatter. The high strengths of the Heritage Parkway base material resulted in more variability in p_L. A summary of models developed for SDPMT-6 tests are noted in Table 6.3. Coefficients of determination for these models ranged from 0.60 to a very promising upper value of 0.91. The model that best correlates with the data from SDPMT-6 incremental tests is the log-log model described in Equation 6.7. It is shown in Figure E.301. This testing indicates that there is a relationship between p_L and E_0 based on SDPMT-6 incremental testing at the four sites.

$$\log(p_L) = 0.7872 \log(E_0) - 0.1816 \tag{6.7}$$

Table 6.3: Models of p_L (kPa) versus E_0 (kPa), All Sites

Relationship x	Relationship y	R^2	Model	# of Tests	Figure
			SDPMT-6 Incremental		
Linear	Linear	0.60	p_L=0.04187 E_0 +713.7	35	E.13
Linear	Log10	0.67	$\log_{10}(p_L)$=9.577E-06 E_0 +2.595	35	E.205
Log10	Linear	0.74	p_L=3276 $\log_{10}(E_0)$ -1.078E+04	35	E.109
Log10	Log10	0.91	$\log_{10}(p_L)$=0.7872 $\log_{10}(E_0)$ -0.1816	35	E.301
Exponential Model		0.70	p_L=13 $(E_0)^{0.5243}$	35	E.397
			SDPMT-6 Continuous		
Linear	Linear	0.91	p_L=0.03997 E_0 +157.4	33	E.14
Linear	Log10	0.76	$\log_{10}(p_L)$=1.621E-05 E_0 +2.422	33	E.206
Log10	Linear	0.91	p_L=2176 $\log_{10}(E_0)$ -7875	33	E.110
Log10	Log10	0.90	$\log_{10}(p_L)$=0.9551 $\log_{10}(E_0)$ -1.134	33	E.302
Exponential Model		0.93	p_L=0.4816 $(E_0)^{0.7804}$	33	E.398
			SDPMT-12 Incremental		
Linear	Linear	0.98	p_L=0.06609 E_0 +95.51	46	E.15
Linear	Log10	0.86	$\log_{10}(p_L)$=2.656E-05 E_0 +2.417	46	E.207
Log10	Linear	0.84	p_L=1831 $\log_{10}(E_0)$ -6080	46	E.111
Log10	Log10	0.93	$\log_{10}(p_L)$=0.8246 $\log_{10}(E_0)$ -0.4019	46	E.303
Exponential Model		0.98	p_L=0.2475 $(E_0)^{0.8785}$	46	E.399
			SDPMT-12 Continuous		
Linear	Linear	0.75	p_L=0.03354 E_0 +301.8	39	E.16
Linear	Log10	0.67	$\log_{10}(p_L)$=1.322E-05 E_0 +2.46	39	E.208
Log10	Linear	0.83	p_L=2005 $\log_{10}(E_0)$ -7018	39	E.112
Log10	Log10	0.81	$\log_{10}(p_L)$=0.8263 $\log_{10}(E_0)$ -0.5705	39	E.304
Exponential Model		0.83	p_L=2.025 $(E_0)^{0.6465}$	39	E.400

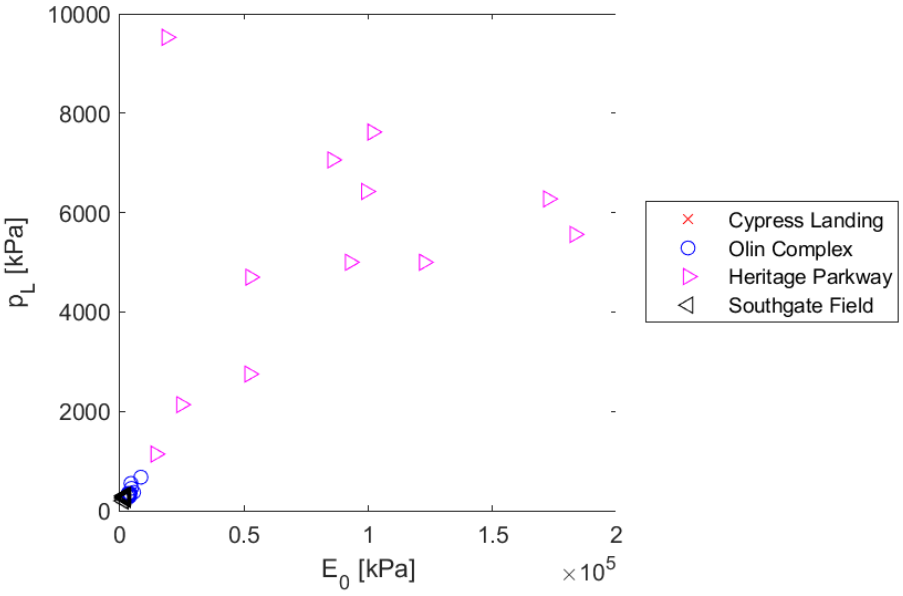

Figure 6.19: SDPMT-6 Incremental, p_L versus E_0, All Sites

6.3.3.2 Comparison of SDPMT-6 Continuous Tests, p_L versus E_0

Figure 6.20 shows all data points collected from SDPMT-6 continuous tests for the parameters E_0 and p_L. Visually, this figure shows that there might be a correlation between these two variables; however, there are gaps in the data below p_L of 1,800 kPa and a large scatter in data above p_L of 1,800 kPa. A summary of models developed for SDPMT-6 tests are noted in Table 6.3. Coefficients of determination for these models were fairly good, ranging from 0.76 to 0.93. The model that best correlates with the collected data from SDPMT-6 continuous tests is the log-linear model as described in Equation 6.8. This model is shown in Figure E.110. Note, this model produced $R^2 = 0.91$, which is lower than the exponential model, but shows a better fit. This testing indicates that there is a relationship between p_L and E_0 based on SDPMT-6 continuous testing at the four sites.

$$p_L = 2176 \log(E_0) - 7875 \tag{6.8}$$

6.3.3.3 Comparison of SDPMT-12 Incremental Tests, p_L versus E_0

Figure 6.21 shows all data points collected from SDPMT-12 incremental tests for E_0 and p_L. Visually, there seems to be a clear linear relationship between these two variables. A summary of models developed for SDPMT-12 incremental tests are shown in Table 6.3. Coefficients of determination for these models were all excellent, ranging

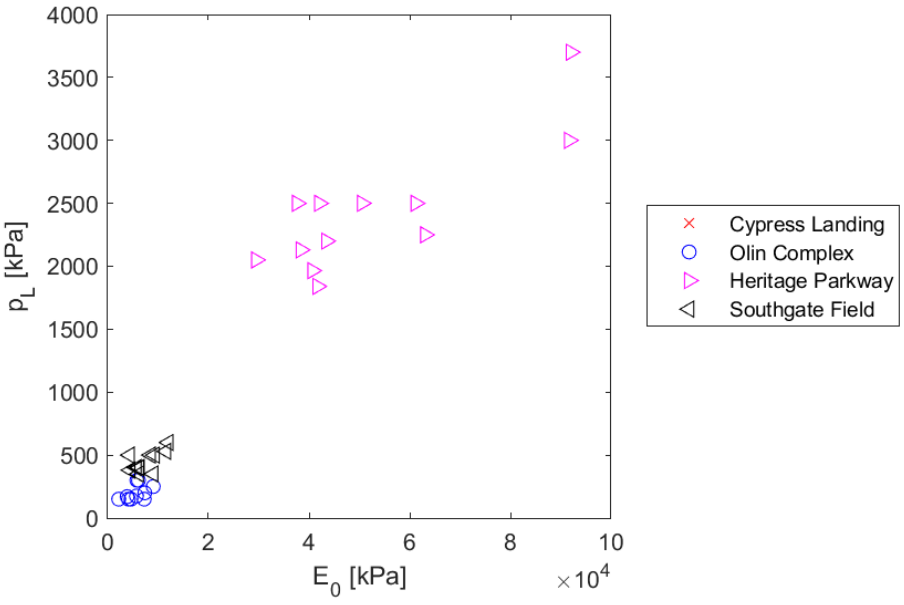

Figure 6.20: SDPMT-6 Continuous, p_L versus E_0, All Sites

from 0.84 to 0.98. Both the linear-linear model and exponential models produced $R^2 = 0.98$. The model chosen to best correlate with the SDPMT-12 incremental tests is the exponential model described in Equation 6.9. This proposed model plotted against the collected data is shown in Figure E.399.

This testing indicates that there is a very promising relationship between p_L and E_0 based on SDPMT-12 incremental testing at the four sites. It may be possible to predict p_L values from E_0 values and visa-versa, which has broader applications. It may be possible to correlate cone penetrometer point resistances to p_L values and then correlate them to E_0 values.

$$p_L = 0.2475(E_0)^{0.7875} \tag{6.9}$$

$$p_L = 0.066069E_0 + 95.51 \tag{6.10}$$

6.3.3.4 Comparison of SDPMT-12 Continuous Tests, p_L versus E_0

Figure 6.22 shows all data points collected from SDPMT-12 continuous tests. Visually, there seems to be a nonlinear relationship between these variables. There is more scatter in this data than for the SDPMT-12 incremental p_L versus E_0 data. A summary of models developed for SDPMT-12 tests are presented in Table 6.3. Coefficients of determination for these models were promising, ranging from 0.67 to 0.83. The model that best correlates with the collected data from SDPMT-12 continuous tests is the log-linear model as described in Equation 6.11. This proposed model is shown in Figure E.112. As was the case for the SDPMT-6 continuous p_L versus E_0 correlation,

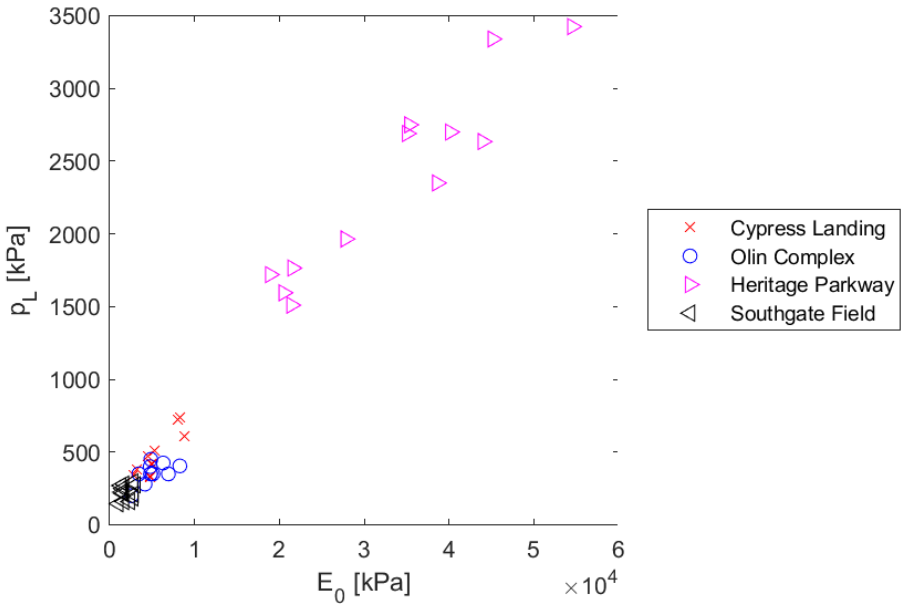

Figure 6.21: SDPMT-12 Incremental, p_L versus E_0, All Sites

there is more scatter and weaker correlations than for the incremental comparison. This data indicates that more research needs to be conducted on the continuous testing so that the p_L versus E_0 correlations become more reliable.

$$\log(E_0) = 4.128 \times 10^{-4} P_L + 3.581 \tag{6.11}$$

6.3.4 Summary of p_L versus E_0 regression models

There are several key observations from analyzing p_L versus E_0. First, there is a very promising set of correlations for the SDPMT-12 incremental tests. There is a need to improve the accuracy of the testing when high strength base materials are tested and the SDPMT continuous testing needs further work on the testing process, including data acquisition and calibrations. A final examination of the test data also shows that the continuous tests produced approximately twice the initial modulus as the incremental tests, indicating that the rate of loading must be considered when using this data.

6.3.5 Test Quality Indicator E_0 / p_L

The test quality indicator E_0/p_L ratio for the incremental SDPMT tests show that the average ratio ranged from 7.0 to 16.1 for both 6 and 12 inch probes. This finding is similar to Briaud's (2005) published relationship of 7 to 12; therefore, the test data is acceptable. The test quality indicator E_0/p_L ratio for rapid or continuous SDPMT tests

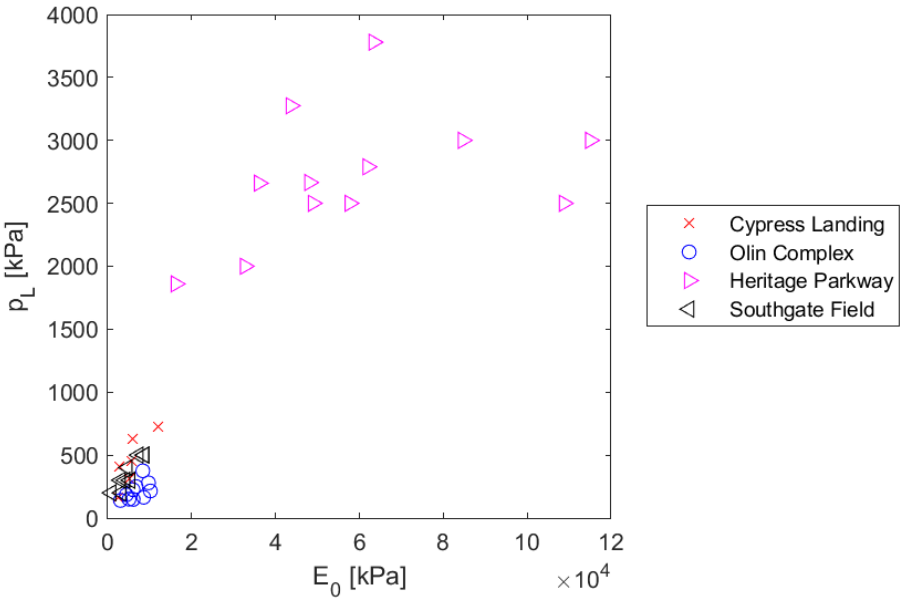

Figure 6.22: SDPMT-12 Continuous, p_L versus E_0, All Sites

ranged from 10.9 to 33.2 for the 6 and 12 inch probes. Although this is higher than the upper range of 12; the tests are still of good quality. The higher values are due to the increased strain-rate applied to the soil compared to the incremental test.

The ratio of p_L/E_0 for incremental tests ranged from 0.142 to 0.62 Comparing these values to the Briaud's (2005) estimated ratio of 0.125 and the Cosentino et al. (2008) ratio of 0.079 places the data from these tests within the same general range. The lower values recorded are expected because of the stiffer material tested. Therefore the developed probes measure realistic stress – strain response of the unbound pavement layers. The high R^2 from SDPMT-12 incremental testing imply that engineers may be able to predict p_L from E_0 for if they encounter poor quality SDPMT data.

6.4 Comparisons with SDPMT E_0 and Other Tests

Comparisons were made with E_0 from the SDPMT probes. E_0 values were compared with γ_{dry}, elastic moduli from the Zorn and Dynatest LWD's, CIV's and DCP index values. The results of this analyses are described in the following sections (Misilo III, 2018).

6.4.1 Dry Unit Weight versus SDPMT E_0

Twenty γ_{dry} versus E_0 regression models were evaluated. The results are summarized in Table 6.4. Between 35 and 46 tests produced data for these correlations. The regression coefficients ranged from 0.46 to 0.85, with the nonlinear models producing higher R^2 values than the linear models. Correlations obtained from SDPMT-12 incremental data, which were developed from the most data (i.e., 46 tests), were the best of the four PMT's.

6.4.1.1 SDPMT-6 Incremental Comparisons

Table 6.4 shows the five regression models developed from SDPMT-6 incremental testing. Figure 6.23 shows the data used to develop the models. Visually, the plot shows γ_{dry} varies from 100 to 115 lbs/ft^3 at the lowest moduli associated with the three sandy sites, and E_o varies significantly when densities ranged from 125 to 132 lbs/ft^3, which corresponds to the cemented coquina base at Heritage. These models produced R^2 values ranging from 0.46 to 0.83, based on 35 data points. Three of the five models produced $R^2 > 0.80$. The exponential model R^2 of 0.81 (Figure E.421 and described by Equation 6.12) shows good agreement at lower E_0 values and more scatter as E_0 increases. The log-linear model (Figure E.133 and described by Equation 6.13) has a consistent fit to the data. The second model with a R^2 of 0.83 was the log-log model shown in Figure E.325 and described by Equation 6.14. Both the log-linear and log-log plots both show similar trend lines with the data. Overall, the 6-inch incremental SDPMT E_0 versus γ_{dry} correlations vary from poor to good, while the data visually indicates that there may be two separate relationships between E_0 and γ_{dry}.

$$\gamma_{dry} = 83.89(E_0)^{0.04405} \tag{6.12}$$

$$\gamma_{dry} = 12.12 \log_{10}(E_0) + 77.61 \tag{6.13}$$

$$\log_{10}(\gamma_{dry}) = 0.4535 \log_{10}(E_0) + 1.919 \tag{6.14}$$

6.4.1.2 SDPMT-6 Continuous Comparisons

Table 6.4 shows the five regression models developed from SDPMT-6 continuous testing. Figure 6.24 shows the data used to develop the models. Its data show trends similar to Figure 6.23. At low moduli there is a relatively large range of densities (100 to 115 pcf) and at densiteis between 123 and 133 pcf there is a large scatter in E_0. The models produced R^2 values ranging from 0.63 to 0.73, using 33 data points. All five models show weak agreement between the data and the models, as would be expected from inspection of the plot. This data also visually indicates that there may be two separate relationships between E_0 and γ_{dry}.

Table 6.4: Correlation Coefficients, γ_{dry} (lbs/ft^3) versus E_0 (kPa), All Sites

Relationship x	Relationship y	R^2	Model	# of Tests	Figure
			SDPMT-6 Incremental		
Linear	Linear	0.46	γ_{dry}=0.0008865 E_0 +110.8	35	E.37
Linear	Log10	0.46	$\log_{10}(\gamma_{dry})$=3.311E-06 E_0 +2.044	35	E.229
Log10	Linear	0.83	γ_{dry}=12.12 $\log_{10}(E_0)$ +77.61	35	E.133
Log10	Log10	0.83	$\log_{10}(\gamma_{dry})$=0.04535 $\log_{10}(E_0)$ +1.919	35	E.325
Exponential Model		0.81	γ_{dry}=83.89 $(E_0)^{0.04405}$	35	E.421
			SDPMT-6 Continuous		
Linear	Linear	0.64	γ_{dry}=0.002091 E_0 +108	33	E.38
Linear	Log10	0.63	$\log_{10}(\gamma_{dry})$=7.779E-06 E_0 +2.033	33	E.230
Log10	Linear	0.72	γ_{dry}=17.54 $\log_{10}(E_0)$ +57.48	33	E.134
Log10	Log10	0.71	$\log_{10}(\gamma_{dry})$=0.06513 $\log_{10}(E_0)$ +1.846	33	E.326
Exponential Model		0.73	γ_{dry}=69.79 $(E_0)^{0.06583}$	33	E.422
			SDPMT-12 Incremental		
Linear	Linear	0.69	γ_{dry}=0.003536 E_0 +108.3	46	E.39
Linear	Log10	0.68	$\log_{10}(\gamma_{dry})$=1.309E-05 E_0 +2.035	46	E.231
Log10	Linear	0.85	γ_{dry}=17 $\log_{10}(E_0)$ +64.06	46	E.135
Log10	Log10	0.85	$\log_{10}(\gamma_{dry})$=0.06335 $\log_{10}(E_0)$ +1.87	46	E.327
Exponential Model		0.85	γ_{dry}=74 $(E_0)^{0.06354}$	46	E.423
			SDPMT-12 Continuous		
Linear	Linear	0.54	γ_{dry}=0.001592 E_0 +109.8	39	E.40
Linear	Log10	0.54	$\log_{10}(\gamma_{dry})$=5.905E-06 E_0 +2.04	39	E.232
Log10	Linear	0.74	γ_{dry}=15.4 $\log_{10}(E_0)$ +65.89	39	E.136
Log10	Log10	0.74	$\log_{10}(\gamma_{dry})$=0.05719 $\log_{10}(E_0)$ +1.877	39	E.328
Exponential Model		0.75	γ_{dry}=75.33 $(E_0)^{0.0573}$	39	E.424

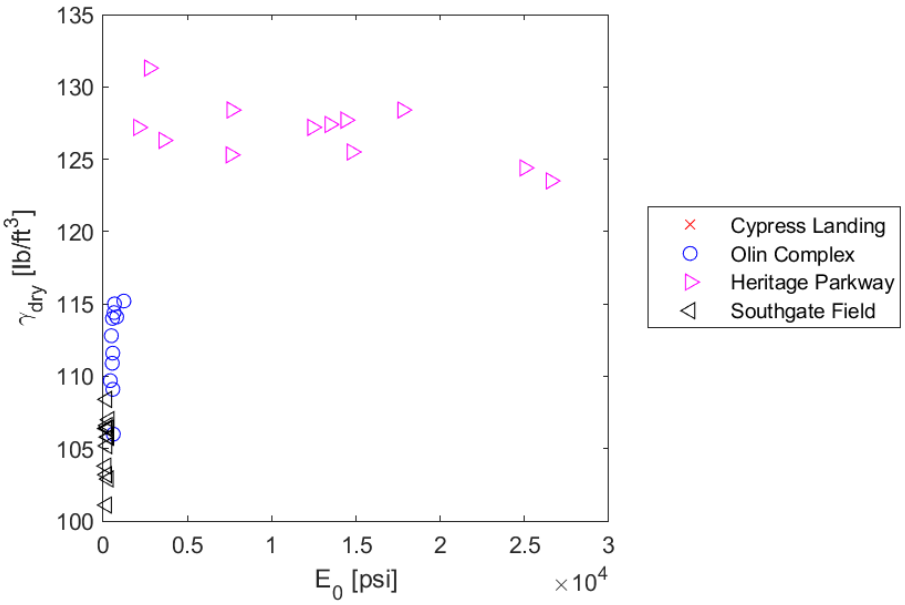

Figure 6.23: SDPMT-6 Incremental, γ_{dry} versus E_0, All Sites

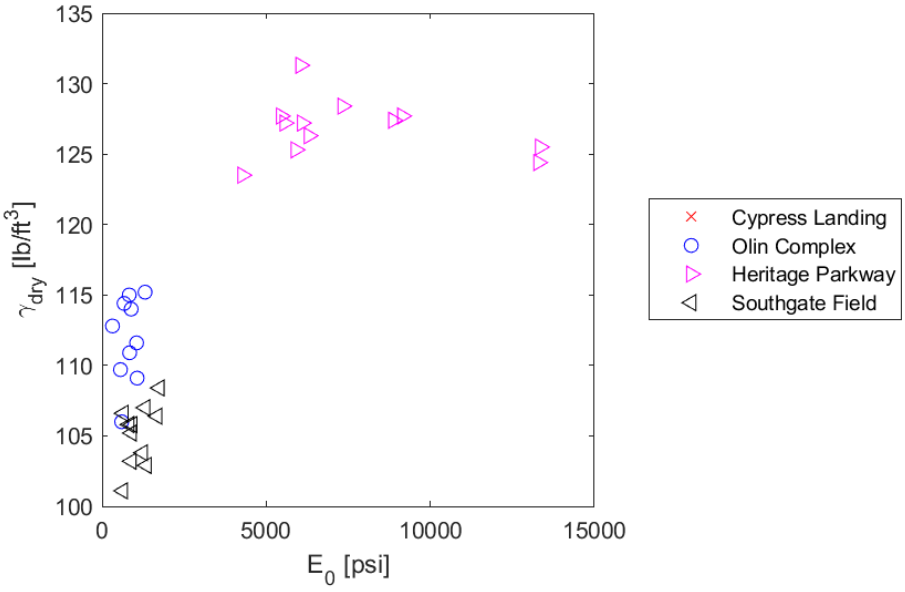

Figure 6.24: SDPMT-6 Continuous, γ_{dry} versus E_0, All Sites

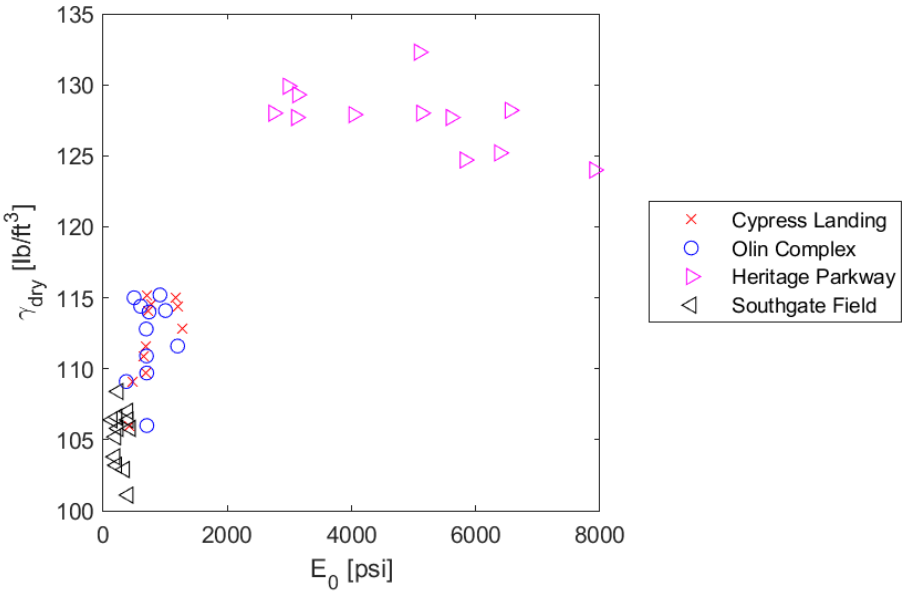

Figure 6.25: SDPMT-12 Incremental, γ_{dry} versus E_0, All Sites

6.4.1.3 SDPMT-12 Incremental Comparisons

Table 6.4 shows the five regression models developed from SDPMT-12 incremental testing. Figure 6.25 shows the data used to develop the models. Visually, again there are two zones of data, as were evident from both SDPMT-6 plots; however, there does appear to be a possible nonlinear relationship. These R^2 values were the highest of the four options, with values ranging from 0.68 to 0.85, based on 46 data points. Three of the five models produced R^2 values of 0.85. The log-linear model is described by Equation 6.16 and shown in Figure E.135. This model shows general agreement with the data. The second model that produced a R^2 value of 0.85 was the log-log model shown in Figure E.327 and described by Equation 6.16. It shows good general agreement with the data. The third model with a R^2 value of 0.85 was the exponential model described by Equation 6.17 (see Figure E.423). This model shows good agreement at the lower E_0 values (less than 2,000 psi) but has more variability at higher E_0 values. The log-linear and log-log models both show better agreement with the data than the exponential model.

$$\gamma_{dry} = 17 \log_{10}(E_0) + 46.06 \tag{6.15}$$

$$\log_{10}(\gamma_{dry}) = 0.6335 \log_{10}(E_0) + 1.87 \tag{6.16}$$

$$\gamma_{dry} = 74(E_0)^{0.06354} \tag{6.17}$$

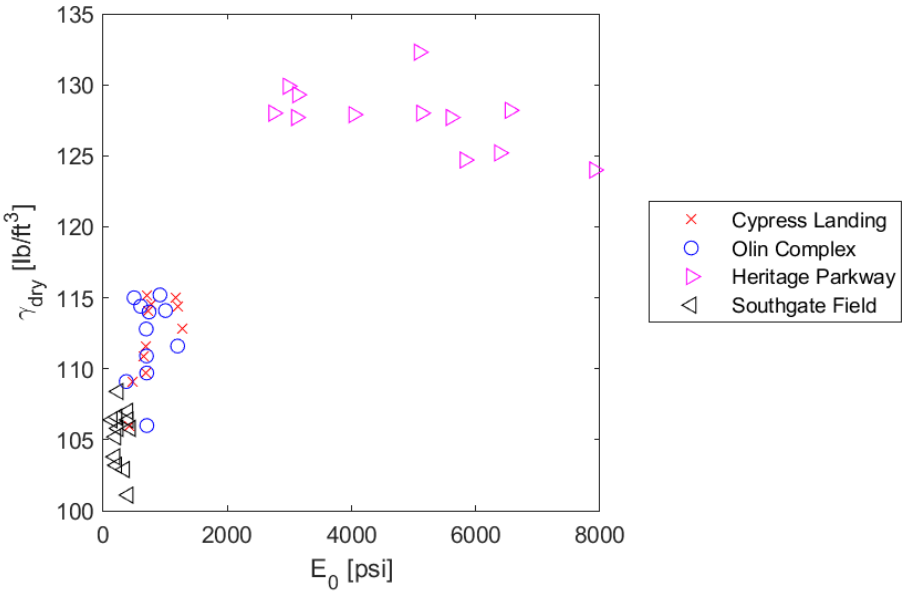

Figure 6.26: SDPMT-12 Continuous, γ_{dry} versus E_0, All Sites

6.4.1.4 SDPMT-12 Continuous Comparisons

Table 6.4 shows the five regression models developed from SDPMT-12 continuous testing. Figure 6.26 shows the data used to develop the models. Visually, again there are two zones of data as were evident from both SDPMT-6 plots; however, there does appear to be a possible nonlinear relationship, similar to that shown in the SDPMT-12 data. The models produced R^2 values ranging from 0.54 to 0.75, based on 39 data points. Three of the models produced R^2 values greater than 0.74. The log-linear and log-log modes both produced a R^2 value of 0.47. The modes are described by Equations 6.18 and 6.19, and shown in Figures E.136 and E.328 for the log-linear and log-log models respectively. The log-linear model shows a general fit to the data. The log-log model appears to show a tight fit, but because of the log-log is such a compressed scale it is difficult to visually see disagreements with the model and data. The exponential model produced R^2 of 0.75, and is described by Equation 6.20 and shown in Figure E.424. The exponential model shows good agreement for $E_0 < 500$ psi, but the data diverges more as E_0 increases.

$$\gamma_{dry} = 15.4 \log_{10}(E_0) + 65.89 \tag{6.18}$$

$$\log_{10}(\gamma_{dry}) = 0.5719 \log_{10}(E_0) + 1.87 \tag{6.19}$$

$$\gamma_{dry} = 75.33(E_0)^{0.0573} \tag{6.20}$$

6.4.1.5 Summary of γ_{dry} versus E_0 Regression Models

In conclusion, all four analyses indicate that two separate relationship zones may exit, one for γ_{dry} from 100 to 115 lbs/ft^3 and a second for densities from 125 to 132 lbs/ft^3. More data needs to be evaluated to improve these correlations. The SDPMT-6 continuous data and SDPMT-12 incremental produced the best statistical correlations between γ_{dry} and E_0. The four log-linear A and B coefficients were similar, with A values ranging from 12.2 to 17.5 and B values ranging from 57.5 to 77.61 while R^2 values were between 0.72 and 0.85. This consistency suggests that log-linear models may be the most useful for relating γ_{dry} to E_0.

6.4.2 Zorn E_D versus SDPMT E_0

Twenty $E_{d,Zorn}$ versus E_0 regression models were evaluated. Between 35 and 46 sets of data were analyzed and R^2 ranged from 0.55 to 0.87. In general, the linear-log models produced the lowest R^2 values, while the exponential models produced the highest R^2 values. The results are summarized in Table 6.5.

6.4.2.1 SDPMT-6 Incremental Comparisons

Table 6.5 shows the five regression models developed from SDPMT-6 incremental testing. Figure 6.27 shows the data used to develop the models. As was evident with the E_o versus γ_{dry} data, two zones exist; one for lower moduli with data from the subgrade sands of Olin Cypress and Southgate, and a second for the cemented coquina at Heritage Parkway. There is a distinct gap in moduli obtained from the Zorn LWD between 50,000 and 90,000 kPa, which corresponds to the distinction in soil types from subgrade sands to cemented coquina base.

The resulting models produced R^2 values ranging from 0.55 to 0.89, based on 35 data points. The proposed log-linear model along with the accompanying data is shown in Figure E.157. This model produced the best R^2 value of 0.89 indicating a strong relationship between $E_{d,Zorn}$ and E_0 of the SDPMT-6 incremental test. The log-linear model is described by Equation 6.21.

$$E_{d,Zorn} = 6.611 \times 10^4 \log_{10}(E_0) - 2.017 \times 10^5 \tag{6.21}$$

6.4.2.2 SDPMT-6 Continuous Comparisons

Table 6.5 shows the five regression models developed from SDPMT-6 continuous testing. Figure 6.28 shows the data used to develop the models. These produced R^2 values ranging from 0.69 to 0.87, based on 33 data points. The proposed exponential model (Equation 6.22) produced the highest R^2 of 0.87, and the equation and associated plot are shown in Figure E.446.

$$E_{d,Zorn} = 75.77(E_0)^{0.6748} \tag{6.22}$$

Table 6.5: Correlation Coefficients, $E_{d,Zorn}$ (kPa) versus E_0 (kPa), All Sites

Relationship x	Relationship y	R^2	Model	# of Tests	Figure
			SDPMT-6 Incremental		
Linear	Linear	0.63	$E_{d,Zorn}$=0.7879 E_0 +3.196E+04	35	E.61
Linear	Log10	0.55	$\log_{10}(E_{d,Zorn})$=5.995E-06 E_0 +4.383	35	E.253
Log10	Linear	0.89	$E_{d,Zorn}$=6.611E+04 $\log_{10}(E_0)$ -2.017E+05	35	E.157
Log10	Log10	0.86	$\log_{10}(E_{d,Zorn})$=0.5288 $\log_{10}(E_0)$ +2.504	35	E.349
Exponential Model		0.82	$E_{d,Zorn}$=1426 $(E_0)^{0.3885}$	35	E.445
			SDPMT-6 Continuous		
Linear	Linear	0.83	$E_{d,Zorn}$=1.816 E_0 +1.595E+04	33	E.62
Linear	Log10	0.69	$\log_{10}(E_{d,Zorn})$=1.358E-05 E_0 +4.264	33	E.254
Log10	Linear	0.85	$E_{d,Zorn}$=1.002E+05 $\log_{10}(E_0)$ -3.542E+05	33	E.158
Log10	Log10	0.72	$\log_{10}(E_{d,Zorn})$=0.7545 $\log_{10}(E_0)$ +1.472	33	E.350
Exponential Model		0.87	$E_{d,Zorn}$=75.77 $(E_0)^{0.6748}$	33	E.446
			SDPMT-12 Incremental		
Linear	Linear	0.81	$E_{d,Zorn}$=2.846 E_0 +1.683E+04	46	E.63
Linear	Log10	0.70	$\log_{10}(E_{d,Zorn})$=2.203E-05 E_0 +4.279	46	E.255
Log10	Linear	0.83	$E_{d,Zorn}$=8.609E+04 $\log_{10}(E_0)$ -2.766E+05	46	E.159
Log10	Log10	0.83	$\log_{10}(E_{d,Zorn})$=0.7196 $\log_{10}(E_0)$ +1.806	46	E.351
Exponential Model		0.86	$E_{d,Zorn}$=148.3 $(E_0)^{0.6391}$	46	E.447
			SDPMT-12 Continuous		
Linear	Linear	0.78	$E_{d,Zorn}$=1.41 E_0 +2.287E+04	39	E.64
Linear	Log10	0.63	$\log_{10}(E_{d,Zorn})$=1.024E-05 E_0 +4.341	39	E.256
Log10	Linear	0.82	$E_{d,Zorn}$=8.251E+04 $\log_{10}(E_0)$ -2.777E+05	39	E.160
Log10	Log10	0.73	$\log_{10}(E_{d,Zorn})$=0.6246 $\log_{10}(E_0)$ +2.056	39	E.352
Exponential Model		0.86	$E_{d,Zorn}$=230.8 $(E_0)^{0.5655}$	39	E.448

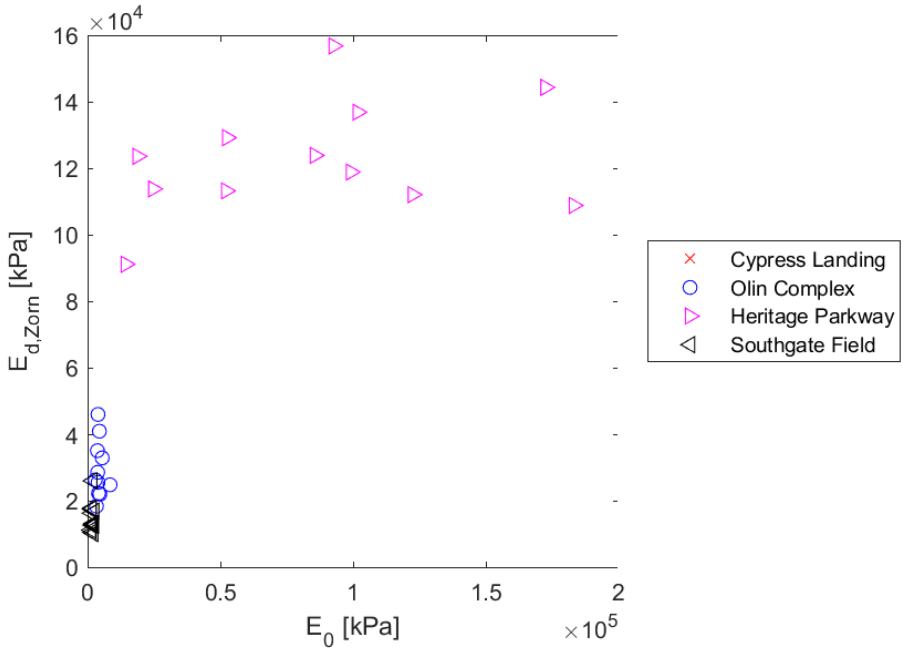

Figure 6.27: SDPMT-6 Incremental, E_0 versus $E_{d,Zorn}$, All Sites

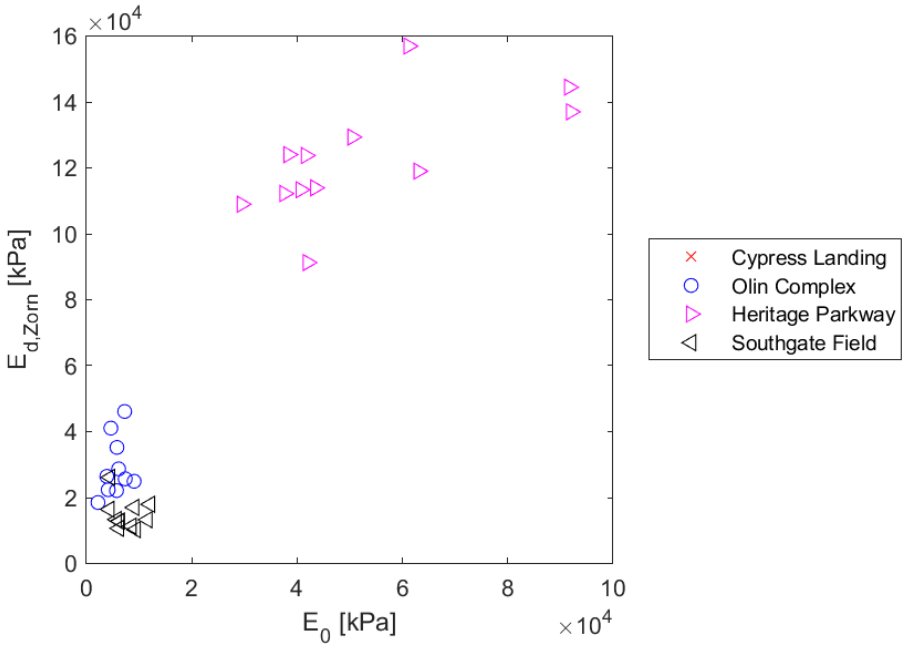

Figure 6.28: SDPMT-6 Continuous, E_0 versus $E_{d,Zorn}$, All Sites

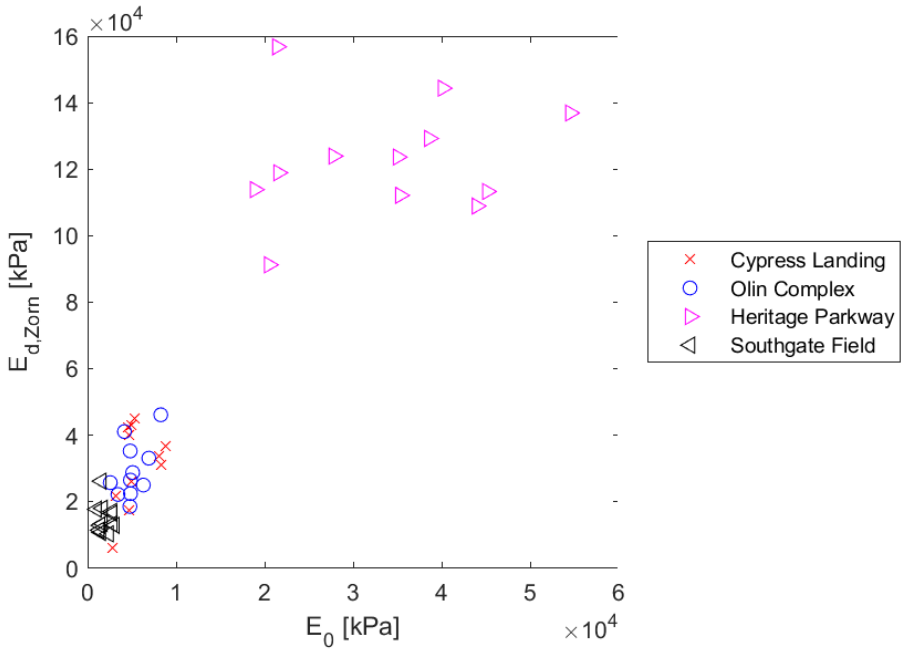

Figure 6.29: SDPMT-12 Incremental, E_0 versus $E_{d,Zorn}$, All Sites

6.4.2.3 SDPMT-12 Incremental Comparisons

Table 6.5 shows the five regression models developed from SDPMT-12 incremental testing. Figure 6.29 shows the data used to develop the models. It has the strongest correlations of the four options, showing a possible relationship could exist between the Zorn LWD and SDPMT-12 stiffnesses. These models produced R^2 ranging from 0.70 to 0.86, based on 46 data points. The proposed exponential model (Equation 6.23) produced the highest R^2 values of 0.86, and is shown in Figure E.447.

$$E_{d,Zorn} = 148.3(E_0)^{0.6391} \tag{6.23}$$

6.4.2.4 SDPMT-12 Continuous Comparisons

Table 6.5 shows the five regression models developed from SDPMT-12 continuous testing. Figure 6.30 shows the data used to develop the models. The developed models had R^2 ranging from 0.63 to 0.86, using 39 data points. The proposed exponential model (Equation 6.24 and Figure E.448) had the greatest R^2 value of 0.86, but diverges within the Heritage Parkway base data. The log-linear model produced the best apparent correlation that follows the trend better, but produced a slightly lower R^2 of 0.82. The model relationship is described in Equation 6.25, and the plotted in Figure E.160.

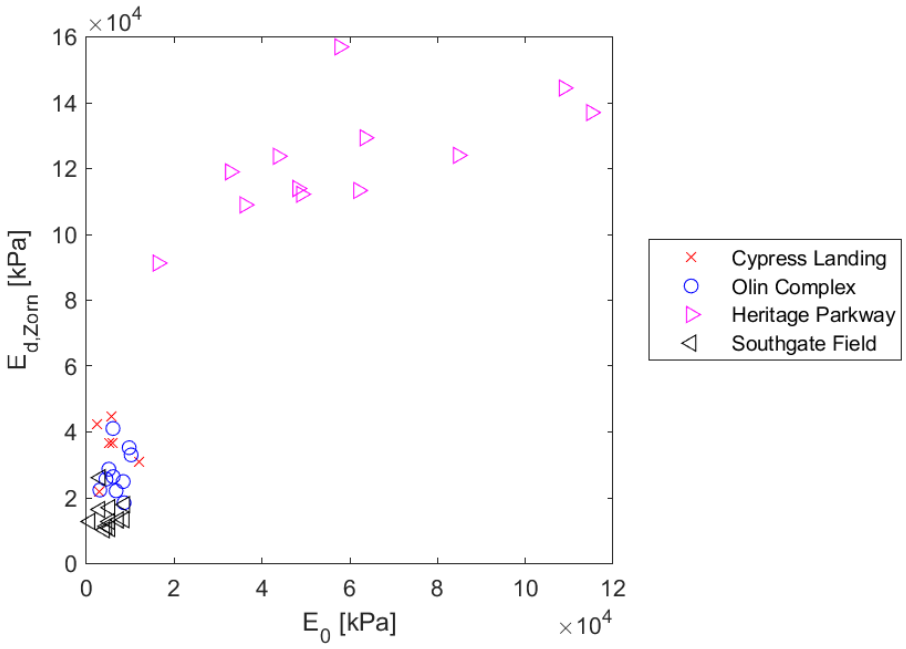

Figure 6.30: SDPMT-12 Continuous, E_0 versus $E_{d,Zorn}$, All Sites

$$E_{d,Zorn} = 230.8(E_0)^{0.5655} \tag{6.24}$$

$$E_{d,Zorn} = 8.251 \times 10^4 \log_{10}(E_0) - 2.777 \times 10^5 \tag{6.25}$$

6.4.2.5 Summary of $E_{d,Zorn}$ versus E_0 Regression Models

The SDPMT-6 continuous and SDPMT-12 incremental data produced the best statistical correlations between $E_{d,Zorn}$ and E_0. The distinct gap in moduli obtained from the Zorn LWD between 50,000 and 90,000 kPa corresponds to the distinction in soil types from subgrade sands to cemented coquina base. The most consistent model for the relationship between E_0 and $E_{d,Zorn}$ is the log-linear model.

6.4.3 Dynatest E_0 versus SDPMT E_0

Twenty $E_{0,Dynatest}$ versus E_0 regression models were evaluated. Between 33 and 44 sets of data were analyzed and R^2 ranged from 0.58 to 0.85. This range is similar to the range from the $E_{0,Zorn}$ versus E_0 regressions. In three of the four cases, the linear-log models produced the lowest R^2 values. The results are summarized in Table 6.6.

Table 6.6: Correlation Coefficients, $E_{0,Dyndatest}$ versus E_0, All Sites

Relationship x	Relationship y	R^2	Model	# of Tests	Figure
			SDPMT-6 Incremental		
Linear	Linear	0.62	$E_{0,Dynatest}$=6.096 E_0 +1.556E+05	33	E.73
Linear	Log10	0.58	$\log_{10}(E_{0,Dynatest})$=7.487E-06 E_0 +5.03	33	E.265
Log10	Linear	0.78	$E_{0,Dynatest}$=4.822E+05 $\log_{10}(E_0)$ -1.537E+06	33	E.169
Log10	Log10	0.86	$\log_{10}(E_{0,Dynatest})$=0.6402 $\log_{10}(E_0)$ +2.762	33	E.361
Exponential Model		0.75	$E_{0,Dynatest}$=3936 $(E_0)^{0.4675}$	33	E.457
			SDPMT-6 Continuous		
Linear	Linear	0.82	$E_{0,Dynatest}$=14.24 E_0 +2.233E+04	31	E.74
Linear	Log10	0.72	$\log_{10}(E_{0,Dynatest})$=1.683E-05 E_0 +4.882	31	E.266
Log10	Linear	0.74	$E_{0,Dynatest}$=7.39E+05 $\log_{10}(E_0)$ -2.691E+06	31	E.170
Log10	Log10	0.72	$\log_{10}(E_{0,Dynatest})$=0.9192 $\log_{10}(E_0)$ +1.485	31	E.362
Exponential Model		0.82	$E_{0,Dynatest}$=43.55 $(E_0)^{0.9012}$	31	E.458
			SDPMT-12 Incremental		
Linear	Linear	0.77	$E_{0,Dynatest}$=21.93 E_0 +2.161E+04	44	E.75
Linear	Log10	0.74	$\log_{10}(E_{0,Dynatest})$=2.877E-05 E_0 +4.819	44	E.267
Log10	Linear	0.68	$E_{0,Dynatest}$=6.173E+05 $\log_{10}(E_0)$ -2.059E+06	44	E.171
Log10	Log10	0.78	$\log_{10}(E_{0,Dynatest})$=0.8848 $\log_{10}(E_0)$ +1.805	44	E.363
Exponential Model		0.77	$E_{0,Dynatest}$=81.48 $(E_0)^{0.8778}$	44	E.459
			SDPMT-12 Continuous		
Linear	Linear	0.84	$E_{0,Dynatest}$=11.67 E_0 +5.427E+04	38	E.76
Linear	Log10	0.70	$\log_{10}(E_{0,Dynatest})$=1.354E-05 E_0 +4.924	38	E.268
Log10	Linear	0.75	$E_{0,Dynatest}$=6.311E+05 $\log_{10}(E_0)$ -2.228E+06	38	E.172
Log10	Log10	0.77	$\log_{10}(E_{0,Dynatest})$=0.8179 $\log_{10}(E_0)$ +1.93	38	E.364
Exponential Model		0.85	$E_{0,Dynatest}$=120.7 $(E_0)^{0.7981}$	38	E.460

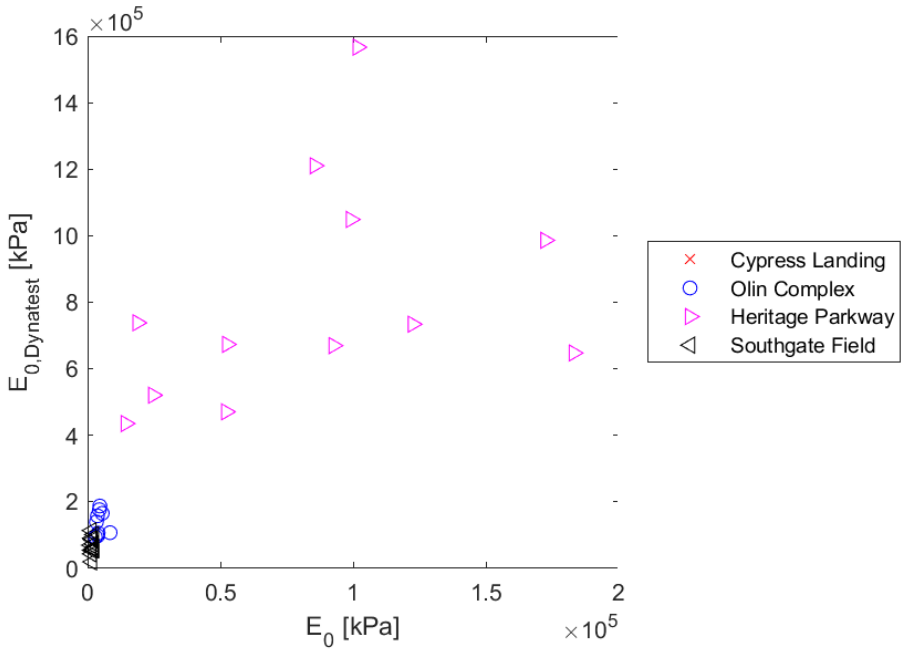

Figure 6.31: SDPMT-6 Incremental, $E_{0,Dyatest}$ versus E_0, All Sites

6.4.3.1 SDPMT-6 Incremental Comparisons

Table 6.6 shows the five regression models for SDPMT-6 incremental tests. Figure 6.31 shows the data used to develop the models. The models developed produced R^2 values ranging from 0.58 to 0.86, using 33 data points. The proposed log-log model (Figure E.361) produced the highest R^2 of 0.86 and is described by Equation 6.26.

$$\log_{10}(E_{0,Dynatest}) = 0.6402 \log_{10}(E_0) + 2.762 \tag{6.26}$$

6.4.3.2 SDPMT-6 Continuous Comparisons

Table 6.6 shows the five regression models for SDPMT-6 continuous tests. Figure 6.32 showed the data used to develop the models. The models developed produced R^2 values ranging from 0.72 to 0.82, using 31 data points. Two of the developed models produced R^2 values of 0.82; the a) linear-linear as shown in Figure E.74 and described by Equation 6.27, b) exponential model as shown in Figure E.458 and described by Equation 6.28. Both models appear to give a similar fit to the data.

$$E_{0,Dynatest} = 14.24 E_0 + 2.233 \times 10^4 \tag{6.27}$$

$$E_{0,Dynatest} = 43.55 (E_0)^{0.9012} \tag{6.28}$$

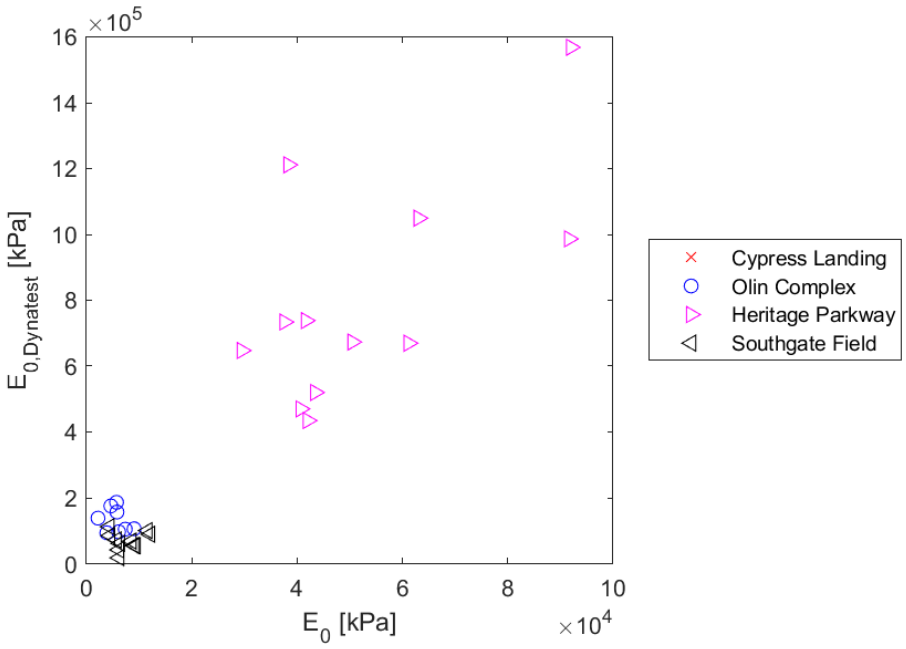

Figure 6.32: SDPMT-6 Continuous, $E_{0,Dyatest}$ versus E_0, All Sites

6.4.3.3 SDPMT-12 Incremental Comparisons

Table 6.6 shows the five regression models for SDPMT-12 incremental tests. Figure 6.34 showed the data used to develop the models. The models developed produced R^2 values ranging from 0.68 to 0.78, using 44 data points. The log-log model produced the best R^2 value of 0.78. The model is shown in Figure E.363 and described by Equation 6.29. This model showed a good correlation between E_0 of the SDPMT-12 incremental test and E_0 of the Dynatest LWD device.

$$\log_{10}(E_{0,Dynatest}) = 0.8848 \log_{10}(E_0) + 1.805 \tag{6.29}$$

6.4.3.4 SDPMT-12 Continuous Comparisons

Table 6.6 shows the five regression models for SDPMT-12 continuous tests. Figure 6.34 showed the data used to develop the models. The models developed produced R^2 values ranging from 0.70 to 0.85, using 38 data points. The linear-linear and exponential models produced similar R^2 values, 0.84 and 0.85 respectively. The linear-linear model is shown in Figure E.76 and represented by Equation 6.30. The exponential model is shown in Figure E.460 and represented by Equation 6.31. Both models produced a similar fit, and this is due to the variation of data with the Heritage Parkway site.

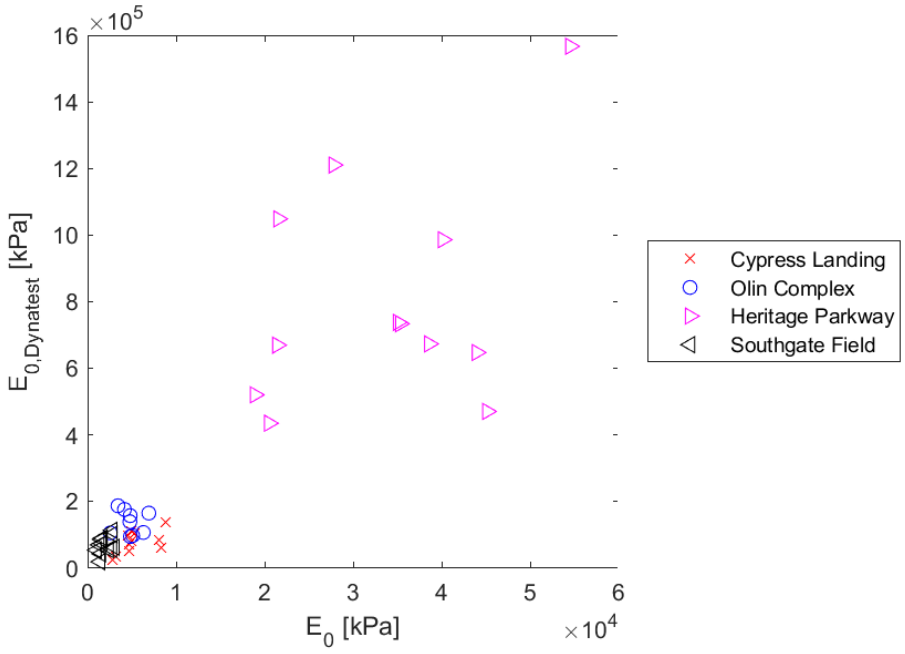

Figure 6.33: SDPMT-12 Incremental, $E_{0,Dyatest}$ versus E_0, All Sites

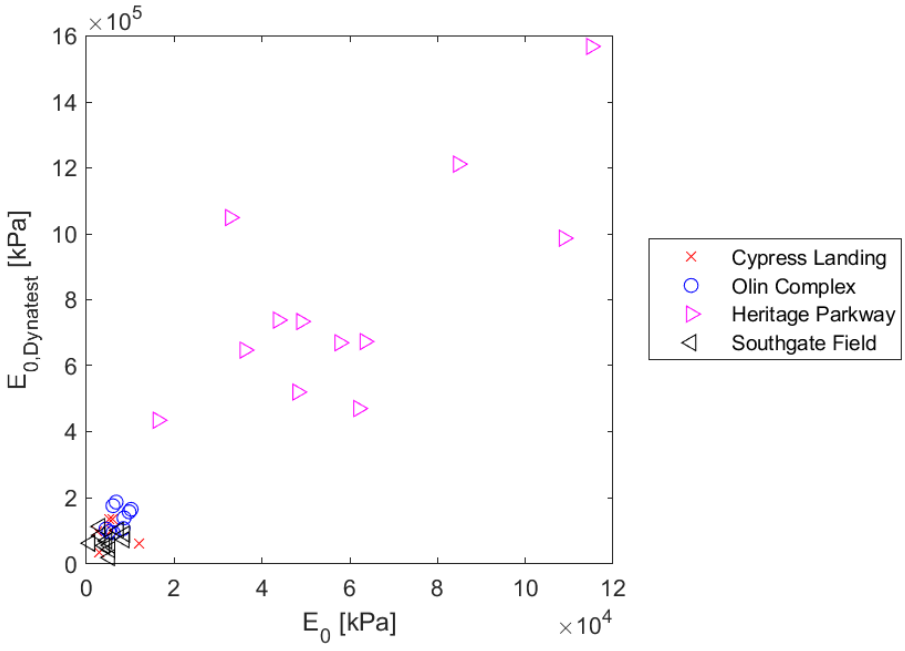

Figure 6.34: SDPMT-12 Continuous, $E_{0,Dyatest}$ versus E_0, All Sites

$$E_{0,Dynatest} = 11.76(E_0) + 5.427 \times 10^4 \quad (6.30)$$

$$E_{0,Dynatest} = 120.7(E_0)^{0.7981} \quad (6.31)$$

6.4.3.5 Summary of $E_{0,Dynatest}$ versus E_0 Regression Models

A large amount of variation exists in these models because of the higher moduli at the Heritage Parkway site. These moduli are two to three times higher than those from to the other three sites.

6.4.4 CIT Number versus SDPMT E_0

Twenty CIV versus E_0 regression models were evaluated. Between 35 and 46 sets of data were used to developed the correlations. R^2 values ranged from 0.59 to 0.90, with the linear-log models producing the lowest values for all four options. Linear-linear models produced acceptable R^2 values for all four cases, ranging from 0.70 to 0.83. In general, the correlations are promising. The results are summarized in Table 6.7.

6.4.4.1 SDPMT-6 Incremental Comparisons

Table 6.7 shows the five regression models developed from SDPMT-6 incremental data. Figure 6.35 shows the data used to develop the models. Visually, it shows a relatively non-linear relationship between CIV and E_0. These models produced R^2 values ranging from 0.59 to 0.93, based on 35 data points. The proposed log-linear model (Figure E.181) produced the highest R^2 of 0.93 and is described by Equation 6.32. Note that E_0 values are represented on the log scale. The log-linear model shows a strong relationship between E_0 and CIV for SDPMT-6 incremental tests.

$$CIV = 0.0002715 \log_{10}(E_0) + 11.9 \quad (6.32)$$

6.4.4.2 SDPMT-6 Continuous Comparisons

Table 6.7 shows the five regression models developed from SDPMT-6 continuous data. Figure 6.36 shows the data used to develop the models. They produced R^2 values ranging from 0.63 to 0.75, based on 33 data points. The exponential model produced the highest R^2 of 0.75 as shown in Figure E.470, and is described by Equation 6.33. The log-linear model (Figure E.182) produced the second highest R^2 of 0.73 and is described by Equation 6.34. Both the exponential and log-linear models show a good relationship between E_0 and CIV for SDPMT-6 continuous tests.

$$CIV = 0.0.08184 \log_{10}(E_0)^{0.565} \quad (6.33)$$

$$CIV = 29.19 \log_{10}(E_0) - 99.42 \quad (6.34)$$

Table 6.7: Correlation Coefficients, CIV versus E_0, All Sites

Relationship x	Relationship y	R^2	Model	# of Tests	Figure
			SDPMT-6 Incremental		
Linear	Linear	0.76	CIV=0.0002715 E_0 +11.9	35	E.85
Linear	Log10	0.59	$\log_{10}$(CIV)=5.297E-06 E_0 +1.011	35	E.277
Log10	Linear	0.93	CIV=21.19 $\log_{10}(E_0)$ -62.42	35	E.181
Log10	Log10	0.88	$\log_{10}$(CIV)=0.4542 $\log_{10}(E_0)$ -0.5987	35	E.373
Exponential Model		0.90	CIV=0.5934 $(E_0)^{0.3724}$	35	E.469
			SDPMT-6 Continuous		
Linear	Linear	0.70	CIV=0.0005263 E_0 +8.562	33	E.86
Linear	Log10	0.63	$\log_{10}$(CIV)=1.093E-05 E_0 +0.9289	33	E.278
Log10	Linear	0.73	CIV=29.19 $\log_{10}(E_0)$ -99.42	33	E.182
Log10	Log10	0.65	$\log_{10}$(CIV)=0.603 $\log_{10}(E_0)$ -1.3	33	E.374
Exponential Model		0.75	CIV=0.08194 $(E_0)^{0.565}$	33	E.470
			SDPMT-12 Incremental		
Linear	Linear	0.83	CIV=0.0009394 E_0 +6.209	46	E.87
Linear	Log10	0.75	$\log_{10}$(CIV)=2.004E-05 E_0 +0.8657	46	E.279
Log10	Linear	0.80	CIV=27.57 $\log_{10}(E_0)$ -87.4	46	E.183
Log10	Log10	0.81	$\log_{10}$(CIV)=0.6252 $\log_{10}(E_0)$ -1.272	46	E.375
Exponential Model		0.86	CIV=0.05477 $(E_0)^{0.63}$	46	E.471
			SDPMT-12 Continuous		
Linear	Linear	0.72	CIV=0.0004374 E_0 +9.038	39	E.88
Linear	Log10	0.64	$\log_{10}$(CIV)=9.073E-06 E_0 +0.9383	39	E.280
Log10	Linear	0.79	CIV=26.05 $\log_{10}(E_0)$ -86.01	39	E.184
Log10	Log10	0.78	$\log_{10}$(CIV)=0.5673 $\log_{10}(E_0)$ -1.142	39	E.376
Exponential Model		0.80	CIV=0.1309 $(E_0)^{0.5161}$	39	E.472

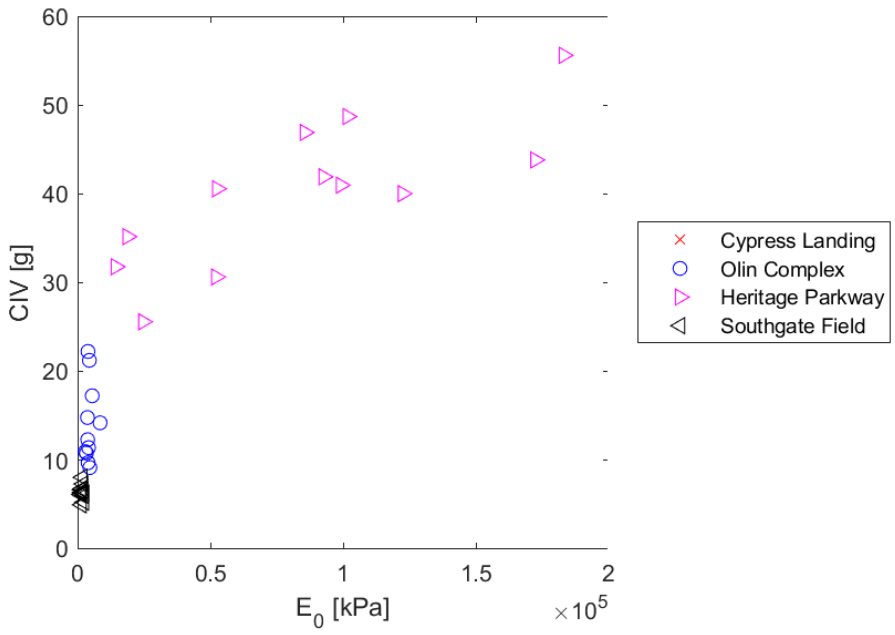

Figure 6.35: SDPMT-6 Incremental, CIV versus E_0, All Sites

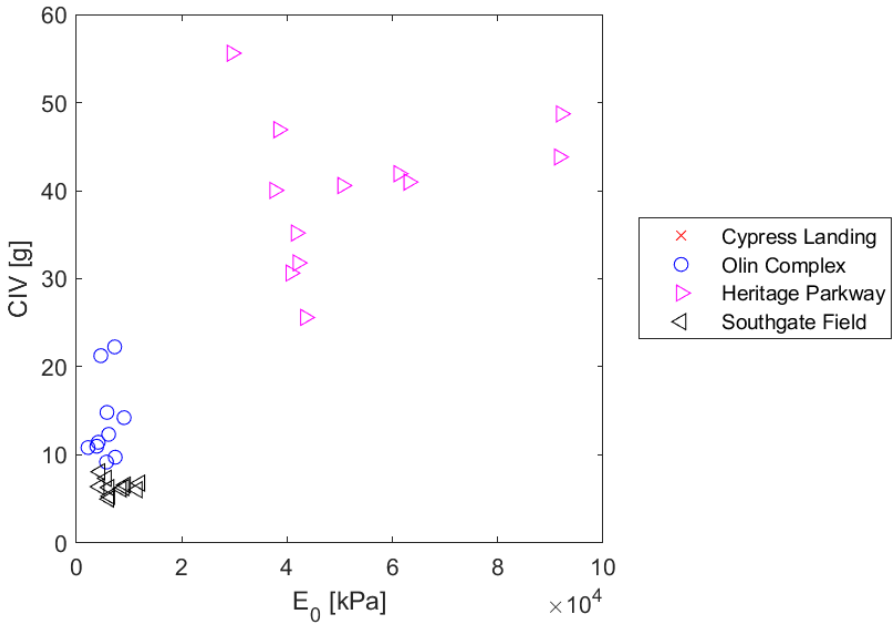

Figure 6.36: SDPMT-6 Continuous, CIV versus E_0, All Sites

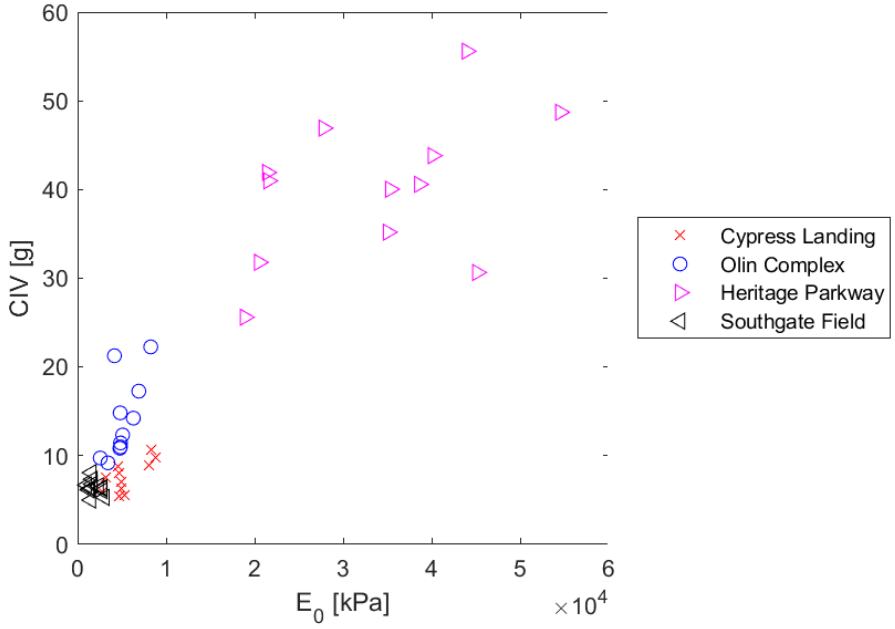

Figure 6.37: SDPMT-12 Incremental, CIV versus E_0, All Sites

6.4.4.3 SDPMT-12 Incremental Comparisons

Table 6.7 shows the five regression models developed from SDPMT-12 incremental data. Figure 6.37 shows the data used to develop the models. Visually, the plot indicates a probable relationship could exit between these variables. These models produced R^2 values ranging from 0.75 to 0.86, using 46 data points. Four of the five models have $R^2 \geq$ of 0.8. The log-linear model, as described by Equation 6.35 (see Figure E.183) which produced R^2 of 0.80, shows good agreement with the data; although, there does seem to be some variability at the lower bounds of the model. The log-log model described by Equation 6.36 (see Figure E.375) produced R^2 of 0.81, indicating a relatively good correlation. The linear-linear model produced R^2 of 0.83 as described by Equation 6.37, and also shows a good correlation between the model and the data, (see FigureE.87). The exponential model described by Equation 6.38 produced R^2 of 0.86, which indicates a very good relationship, as shown in Figure E.471.

$$CIV = 27.57 \log_{10}(E_0) - 87.4 \tag{6.35}$$

$$\log_{10}(CIV) = 0.6252 \log_{10}(E_0) - 1.272 \tag{6.36}$$

$$CIV = 0.0009394(E_0) + 6.209 \tag{6.37}$$

$$CIV = 0.05477(E_0)^{0.63} \tag{6.38}$$

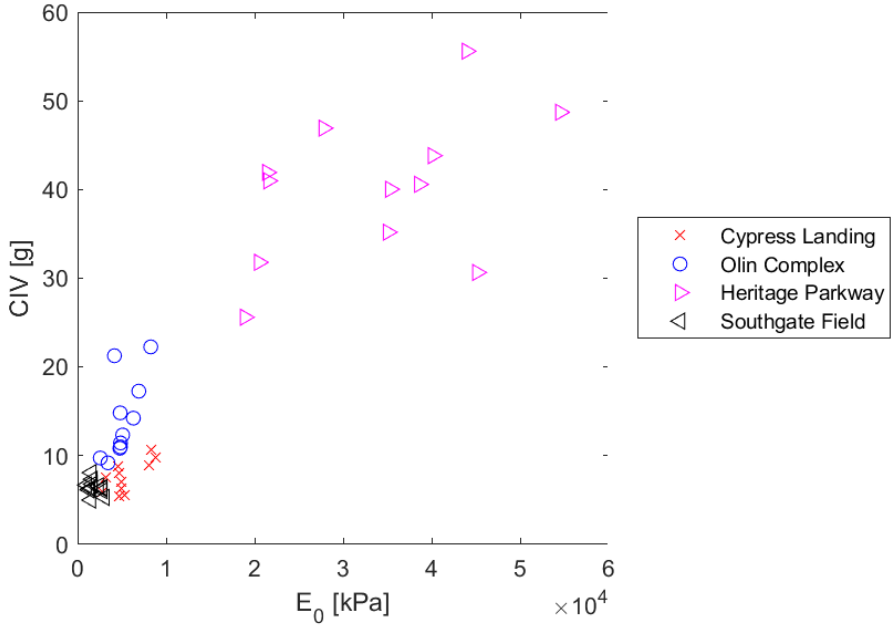

Figure 6.38: SDPMT-12 Continuous, CIV versus E_0, All Sites

6.4.4.4 SDPMT-12 Continuous Comparisons

Table 6.7 shows the five regression models developed from SDPMT-12 continuous data. Figure 6.38 shows the data used to develop the models. Visually, this plot also indicates a probable relationship could exit between these variables. The models produced R^2 values ranging from 0.64 to 0.80, based on 39 data points. Three of the five models produced $R^2 \geq 0.78$, and show good agreement between the data and model. The log-log model as described by Equation 6.39 produced R^2 of 0.78. Figure E.376 shows good agreement between the data and model. The log-linear model produced a R^2 value of 0.79 and is described by Equation 6.40. Figure E.184 shows the good agreement between the data model. The exponential model described by Equation 6.41 produced R^2 of 0.80 and Figure E.472 shows good agreement between the model and the data.

$$\log_{10}(CIV) = 0.5673 \log_{10}(E_0) = 1.142 \tag{6.39}$$

$$CIV = 26.05 \log_{10}(E_0) - 86.01 \tag{6.40}$$

$$CIV = 0.1309(E_0)^{0.5161} \tag{6.41}$$

6.4.4.5 Summary of CIV versus E_0 Regression Models

In general, it was concluded that these two variables are statistically related. The log-linear models for the four SDPMT test types showed a good consistent fit to the

data, where SDPMT E_0 values were plotted on the log of the x-axis and CIV values on the y-axis. The A coefficients of the log-linear models ranged from 21.2 to 29.2.

6.4.5 DCP Penetration Index versus SDPMT E_0

Twenty DCP Penetration Index (PI) versus E_0 regression models were evaluated. Higher DCP PI values occur in softer or weaker soils; therefore, an inverse relationship between it and E_0 would be expected. The results are summarized in Table 6.8. Between 21 and 34 sets of data were used to develop these models. R^2 values ranged from 0.12 to 0.69, with the highest values corresponding to the SDPMT-6 incremental tests. The high strength and density of the cemented coquina base would have damaged the DCP; equipment therefore, no DCP tests were conducted at Heritage Parkway. Only DCP data from the subgrade sands were evaluated; therefore, limiting the soils evaluated. Due to construction logistics, SDPMT-6 tests were unable to be conducted at Cypress Landing, and consequently, not used in the development of the E_0 and DCP PI SDPMT-6 models.

6.4.5.1 SDPMT-6 Incremental Comparisons

Table 6.8 shows the five regression models developed from SDPMT-6 incremental testing. Figure 6.39 shows the data used to develop the models. They produced R^2 values ranging from 0.57 to 0.69, based on 23 data points. Three of the five models produced $R^2 \geq 0.65$. The exponential model described by Equation 6.42 and shown in Figure E.433 illustrates a weak agreement between the model and data. The log-linear model described by Equation 6.43 produced an R^2 value of 0.69. The relationship between this model and data is shown in Figure E.145. The log-log model described by Equation 6.44 produced an R^2 value of 0.69. Figure E.337 shows the relationship between this model and data. These models generally produced somewhat promising R^2 values.

$$DCPPI = 4.708 \times 10^{-0.9696} \tag{6.42}$$

$$DCPPI = -56.88 \log_{10} + 219.6 \tag{6.43}$$

$$\log_{10}(DCPPI) = -1.267 \log_{10} + 5.626 \tag{6.44}$$

6.4.5.2 SDPMT-6 Continuous Comparisons

Figure 6.40 shows the data used to develop the E_0 versus DCP PI models. Visually, it shows that no correlations may be expected as higher PI's did not relate to lower moduli. Table 6.8 shows the five regression models developed from SDPMT-6 continuous data. They produced R^2 values ranging from 0.13 to 0.16, based on 21 data points. These low R^2 values confirm that SDPMT-6 testing produced no promising E_0 versus DCP PI correlations.

Table 6.8: Correlation Coefficients, DCP PI versus E_0, All Sites

Relationship x	Relationship y	R^2	Model	# of Tests	Figure
			SDPMT-6 Incremental		
Linear	Linear	0.57	DCP PI=-0.006772 E_0 +45.13	23	E.49
Linear	Log10	0.58	$\log_{10}$(DCP PI)=-0.0001511 E_0 +1.742	23	E.241
Log10	Linear	0.68	DCP PI=-56.88 $\log_{10}(E_0)$ +219.6	23	E.145
Log10	Log10	0.69	$\log_{10}$(DCP PI)=-1.267 $\log_{10}(E_0)$ +5.626	23	E.337
Exponential Model		0.65	DCP PI=4.708E+04 $(E_0)^{-0.9696}$	23	E.433
			SDPMT-6 Continuous		
Linear	Linear	0.16	DCP PI=0.002214 E_0 +9.013	21	E.50
Linear	Log10	0.13	$\log_{10}$(DCP PI)=4.641E-05 E_0 +0.969	21	E.242
Log10	Linear	0.16	DCP PI=32.47 $\log_{10}(E_0)$ -99.38	21	E.146
Log10	Log10	0.13	$\log_{10}$(DCP PI)=0.6639 $\log_{10}(E_0)$ -1.239	21	E.338
Exponential Model		0.16	DCP PI=0.1129 $(E_0)^{0.6096}$	21	E.434
			SDPMT-12 Incremental		
Linear	Linear	0.38	DCP PI=-0.002968 E_0 +32.38	34	E.51
Linear	Log10	0.34	$\log_{10}$(DCP PI)=-7.374E-05 E_0 +1.537	34	E.243
Log10	Linear	0.47	DCP PI=-28 $\log_{10}(E_0)$ +119.5	34	E.147
Log10	Log10	0.38	$\log_{10}$(DCP PI)=-0.6713 $\log_{10}(E_0)$ +3.616	34	E.339
Exponential Model		0.48	DCP PI=2091 $(E_0)^{-0.5749}$	34	E.435
			SDPMT-12 Continuous		
Linear	Linear	0.14	DCP PI=-0.001381 E_0 +27.69	27	E.52
Linear	Log10	0.15	$\log_{10}$(DCP PI)=-3.843E-05 E_0 +1.452	27	E.244
Log10	Linear	0.13	DCP PI=-14.68 $\log_{10}(E_0)$ +74.15	27	E.148
Log10	Log10	0.13	$\log_{10}$(DCP PI)=-0.3927 $\log_{10}(E_0)$ +2.685	27	E.340
Exponential Model		0.12	DCP PI=201.7 $(E_0)^{-0.2738}$	27	E.436

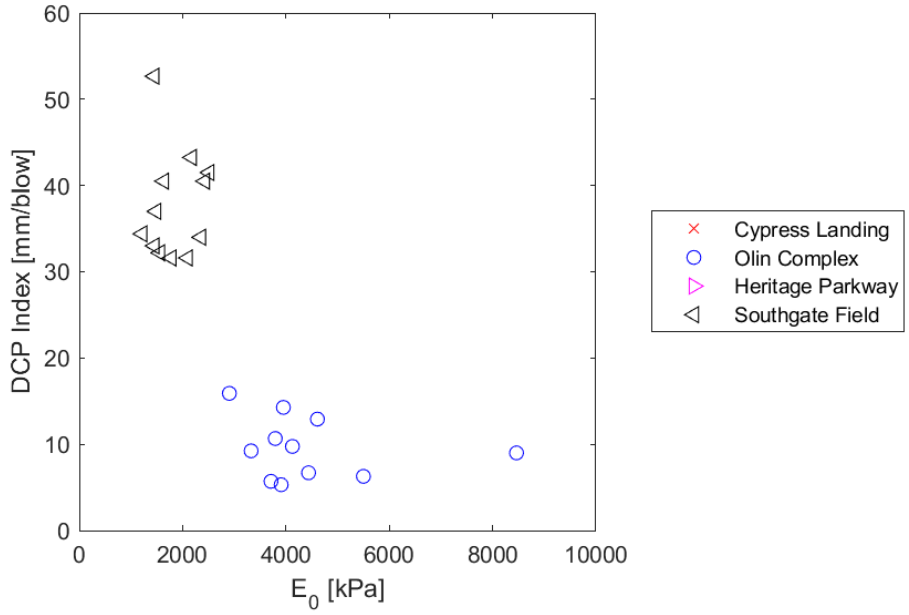

Figure 6.39: SDPMT-6 Incremental, DCP PI versus E_0, All Sites

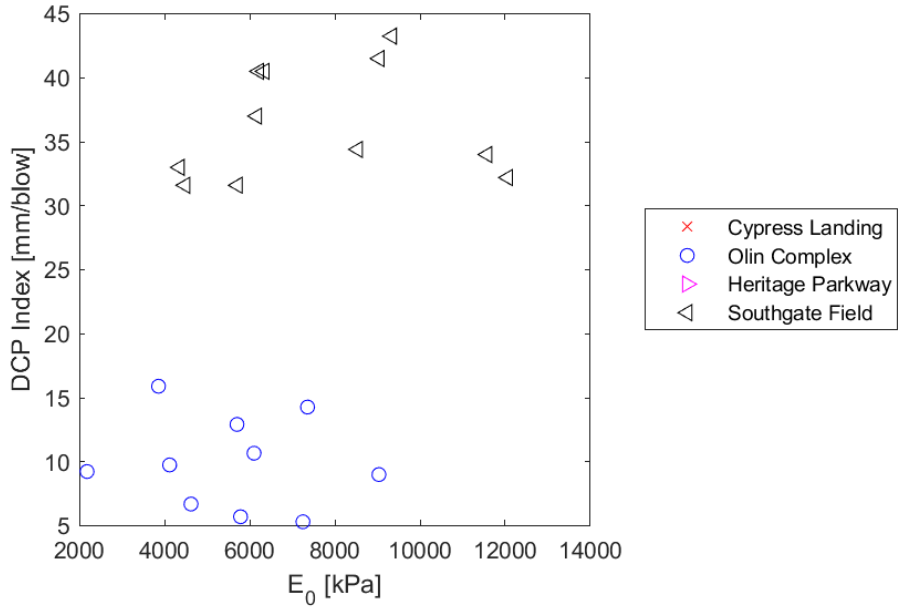

Figure 6.40: SDPMT-6 Continuous, DCP PI versus E_0, All Sites

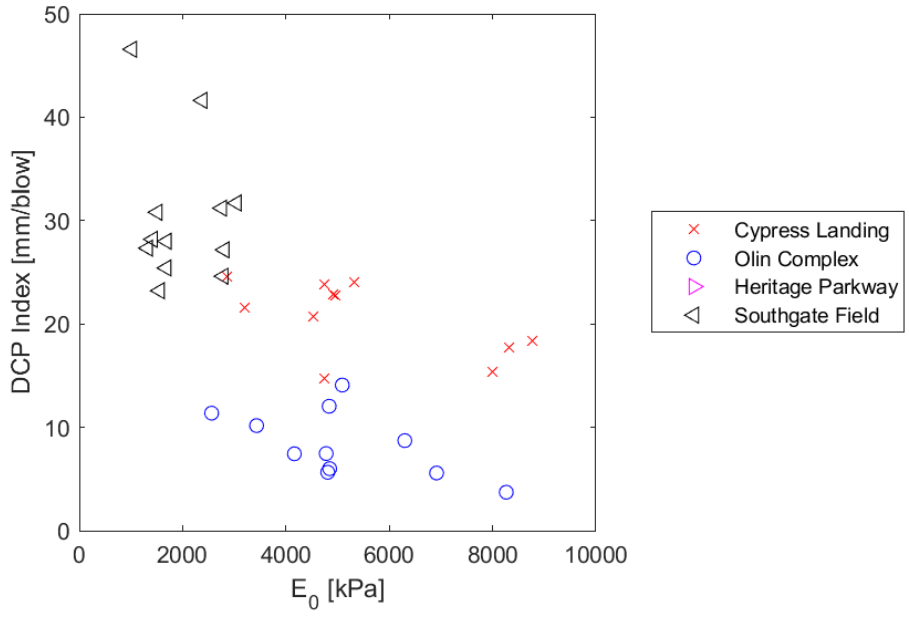

Figure 6.41: SDPMT-12 Incremental, DCP PI versus E_0, All Sites

6.4.5.3 SDPMT-12 Incremental Comparisons

Table 6.8 shows the five regression models developed from SDPMT-12 incremental testing. Figure 6.41 shows the data used to develop the models. Visually, it shows that correlations could be possible as higher PI's relate to lower moduli. The models produced R^2 values ranging from 0.34 to 0.48, based on 34 data points. Although the data in the figure show a possible trend, the R^2 values do not support this. Additional data is needed to improve these correlations.

6.4.5.4 SDPMT-12 Continuous Comparisons

Table 6.8 shows the five regression models developed from SDPMT-12 continuous testing. Figure 6.42 shows the data used to develop the models. Visually, it is similar to Figure 6.41; however, much more scatter exists at the higher DCP Indices. As a result of this scatter, the models developed produced very low R^2 values ranging from 0.12 to 0.15, using 27 data points. In conclusion, there are no correlations evident from this comparison.

6.4.5.5 Summary of DCP PI versus E_0 Regression Models

All SDPMT test types, except the SDPMT-6 incremental, show that as SDPMT E_0 increases the DCP PI decreases. The statistical models produced poor correlations at

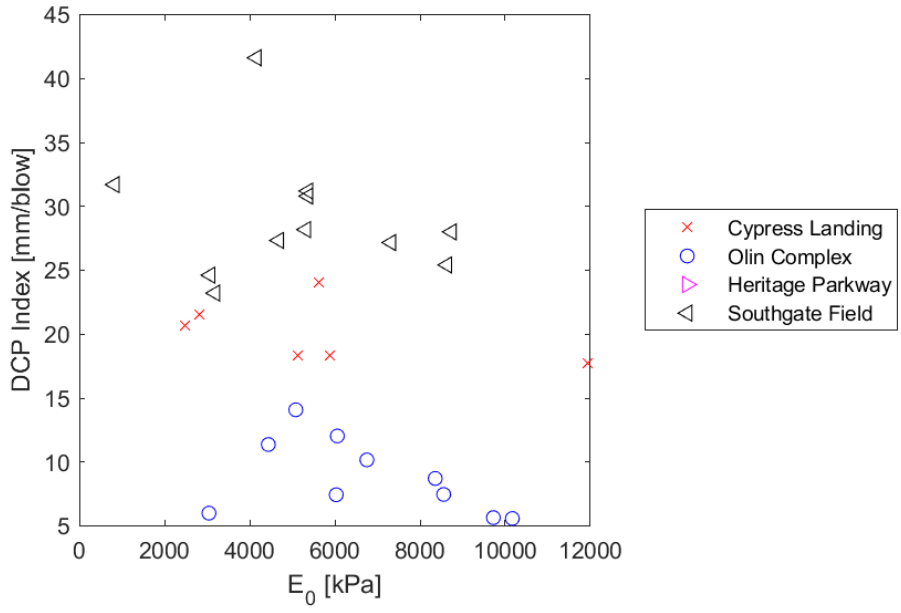

Figure 6.42: SDPMT-12 Continuous, DCP PI versus E_0, All Sites

best. Only sandy subgrade soils were tested; therefore, additional soil types must be tested to develop better correlations.

6.5 Comparisons with SDPMT p_0

Comparisons were made between p_0 from the SDPMT probes to; γ_{dry}, elastic moduli from the Zorn and Dynatest LWD's, CIV's and DCP index values. The results of this analyses are described in the following sections (Misilo III, 2018).

6.5.1 Dry Unit Weight versus SDPMT p_0

Twenty γ_{dry} versus p_0 regression models were evaluated. Between 12 and 27 sets of data were analyzed producing R^2 values from 0.11 to 0.47. These values generally indicate poor to no correlations exist. The most likely reasons for these poor correlations are the fact that p_0 falls within a limited range of stresses (0 to 35 kPa) and the difficulties associated with choosing p_0.

The results are summarized in Table 6.9. Because the original values of unit weight are reported as lb/ft^3, it was decided to develop the models using p_0 using psi instead of kPa to simplify the use of the relationships.

Table 6.9: Correlation Coefficients, γ_{dry} versus p_0, All Sites

Relationship x	Relationship y	R^2	Model	# of Tests	Figure
			SDPMT-6 Incremental		
Linear	Linear	0.11	γ_{dry}=5.216 p_0 +107.6	12	E.45
Linear	Log10	0.11	$\log_{10}(\gamma_{dry})$=0.01961 p_0 +2.032	12	E.237
Log10	Linear	0.14	γ_{dry}=15.34 $\log_{10}(p_0)$ +113.5	12	E.141
Log10	Log10	0.14	$\log_{10}(\gamma_{dry})$=0.05785 $\log_{10}(p_0)$ +2.054	12	E.333
Exponential Model		0.14	γ_{dry}=113.5 $(p_0)^{0.05858}$	12	E.429
			SDPMT-6 Continuous		
Linear	Linear	0.38	γ_{dry}=0.9706 p_0 +111.9	21	E.46
Linear	Log10	0.37	$\log_{10}(\gamma_{dry})$=0.003569 p_0 +2.048	21	E.238
Log10	Linear	0.46	γ_{dry}=15.17 $\log_{10}(p_0)$ +109	21	E.142
Log10	Log10	0.45	$\log_{10}(\gamma_{dry})$=0.05587 $\log_{10}(p_0)$ +2.037	21	E.334
Exponential Model		0.46	γ_{dry}=109.2 $(p_0)^{0.05573}$	21	E.430
			SDPMT-12 Incremental		
Linear	Linear	0.47	γ_{dry}=2.57 p_0 +112.6	27	E.47
Linear	Log10	0.46	$\log_{10}(\gamma_{dry})$=0.009359 p_0 +2.051	27	E.239
Log10	Linear	0.40	γ_{dry}=10.72 $\log_{10}(p_0)$ +117.3	27	E.143
Log10	Log10	0.40	$\log_{10}(\gamma_{dry})$=0.03894 $\log_{10}(p_0)$ +2.068	27	E.335
Exponential Model		0.41	γ_{dry}=117.1 $(p_0)^{0.04037}$	27	E.431
			SDPMT-12 Continuous		
Linear	Linear	0.22	γ_{dry}=0.7448 p_0 +114.2	18	E.48
Linear	Log10	0.22	$\log_{10}(\gamma_{dry})$=0.002766 p_0 +2.056	18	E.240
Log10	Linear	0.33	γ_{dry}=9.916 $\log_{10}(p_0)$ +113.3	18	E.144
Log10	Log10	0.33	$\log_{10}(\gamma_{dry})$=0.03684 $\log_{10}(p_0)$ +2.053	18	E.336
Exponential Model		0.33	γ_{dry}=112.9 $(p_0)^{0.03789}$	18	E.432

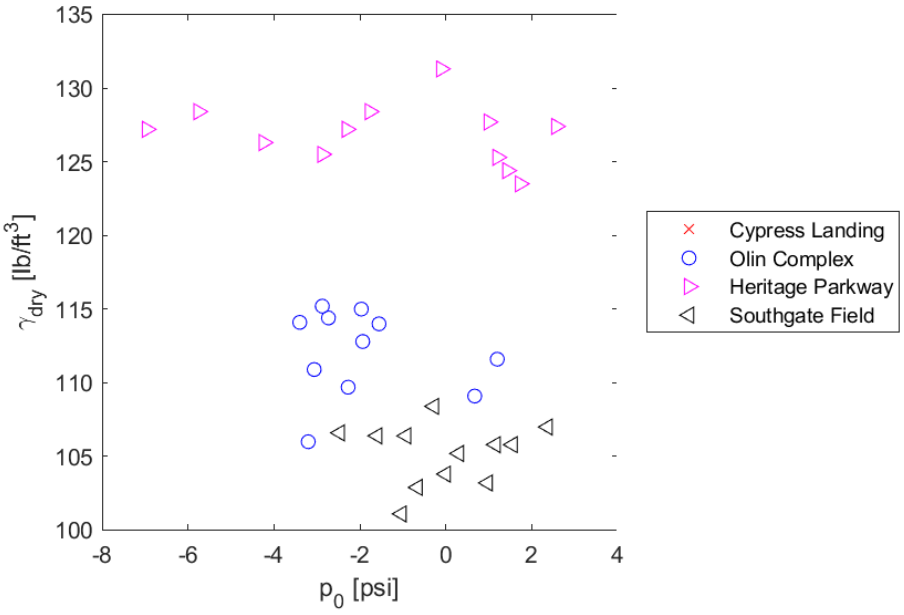

Figure 6.43: SDPMT-6 Incremental, γ_{dry} versus p_0, All Sites

6.5.1.1 SDPMT-6 Incremental Comparisons

Table 6.9 shows the five regression models developed from SDPMT-6 incremental data. Figure 6.43 shows all data relating γ_{dry} and p_0. Figure 6.44 shows the data used to develop the models, with negative values of p_0 removed. These models, based on Figure 6.44, produced R^2 values ranging from 0.11 to 0.14, using 12 data points. These low values along with the limited number of data points indicate that these two variables are not correlated.

6.5.1.2 SDPMT-6 Continuous Comparisons

Table 6.9 shows the five regression models developed from SDPMT-6 continuous data. Figure 6.45 show all data relating γ_{dry} to p_0. Figure 6.46 shows the data used to develop the models, with the negative p_0 values having been removed. These models produced R^2 values ranging from 0.38 to 0.46, based on 21 data points. A weak correlation may exist between p_0 and γ_{dry}; however, more data is needed to help define it.

6.5.1.3 SDPMT-12 Incremental Comparisons

Table 6.9 shows the five regression models developed from SDPMT-12 incremental data. Figure 6.47 shows test data relating γ_{dry} to p_0. Figure 6.48 shows the data used to develop the models, with the negative values of p_0 removed for the analysis. The resulting models produced R^2 values ranging from 0.40 to 0.47, based on 27 data points.

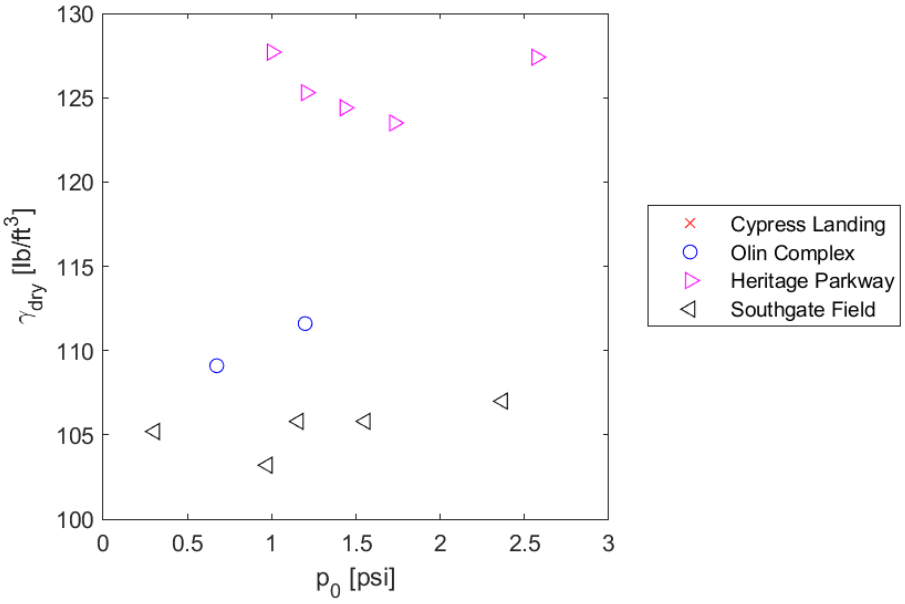

Figure 6.44: SDPMT-6 Incremental, γ_{dry} versus p_0, All Sites, Negative values of p_0 removed

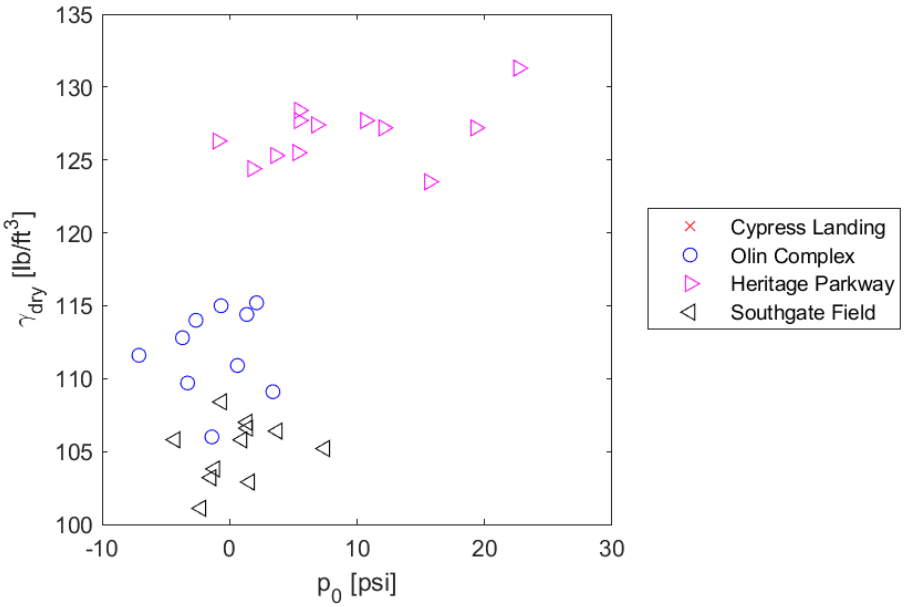

Figure 6.45: SDPMT-6 Continuous, γ_{dry} versus p_0, All Sites

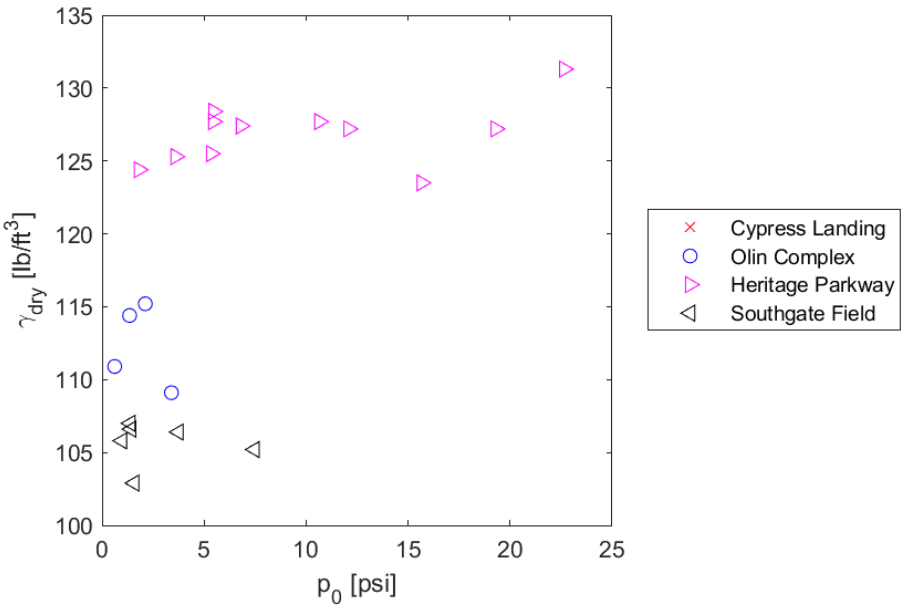

Figure 6.46: SDPMT-6 Continuous, γ_{dry} versus p_0, All Sites, Negative values of p_0 removed

As was the case with the 6-inch incremental data, a weak correlation may exist between p_0 and γ_{dry}; however, more data is needed to help define it.

6.5.1.4 SDPMT-12 Continuous Comparisons

Table 6.9 shows the five regression models developed from SDPMT-12 continuous data. Figure 6.49 shows all test data relating γ_{dry} to p_0. Figure 6.50 shows the data used to develop the models, with negative values of p_0 removed from the dataset and not used in model development. The models developed produced R^2 values ranging from 0.22 to 0.33, based on 18 data points. A general trend may exist between p_0 and γ_{dry}, but not enough data was able to be obtained to support this finding.

6.5.1.5 Summary of γ_{dry} versus p_0 Regression Models

Since graphics graphical construction methods to estimate p_0 can produce negative lift-off or at-rest stresses, many of data points had to be discarded from the analyses. This process, combined with the limited range of p_0 values resulted in poor γ_{dry} versus p_0 correlations.

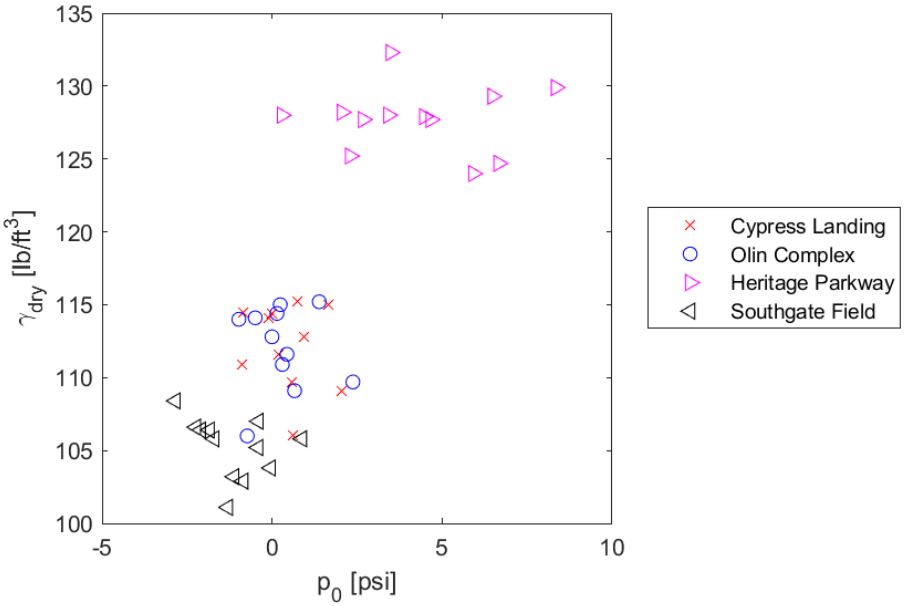

Figure 6.47: SDPMT-12 Incremental, γ_{dry} versus p_0, All Sites

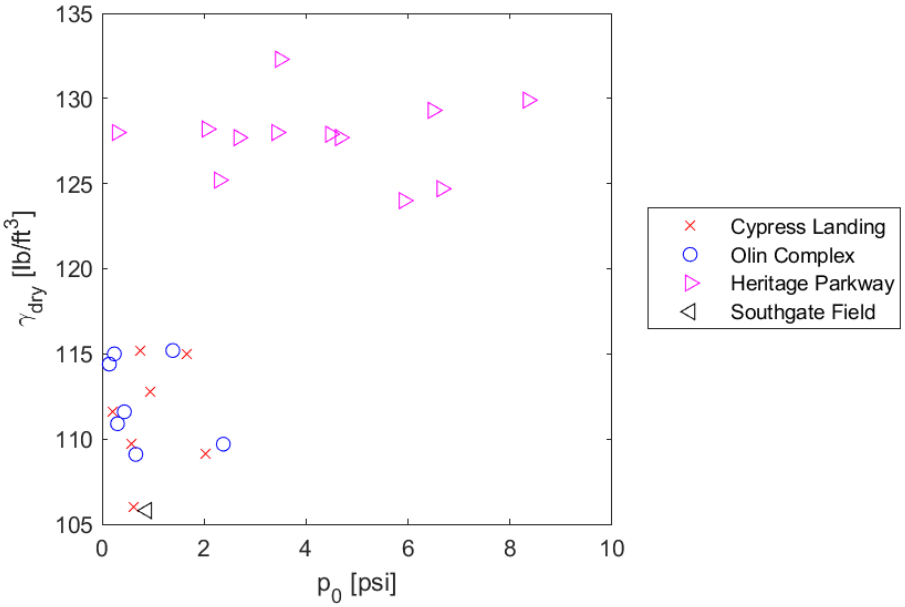

Figure 6.48: SDPMT-12 Incremental, γ_{dry} versus p_0, All Sites, Negative values of p_0 removed

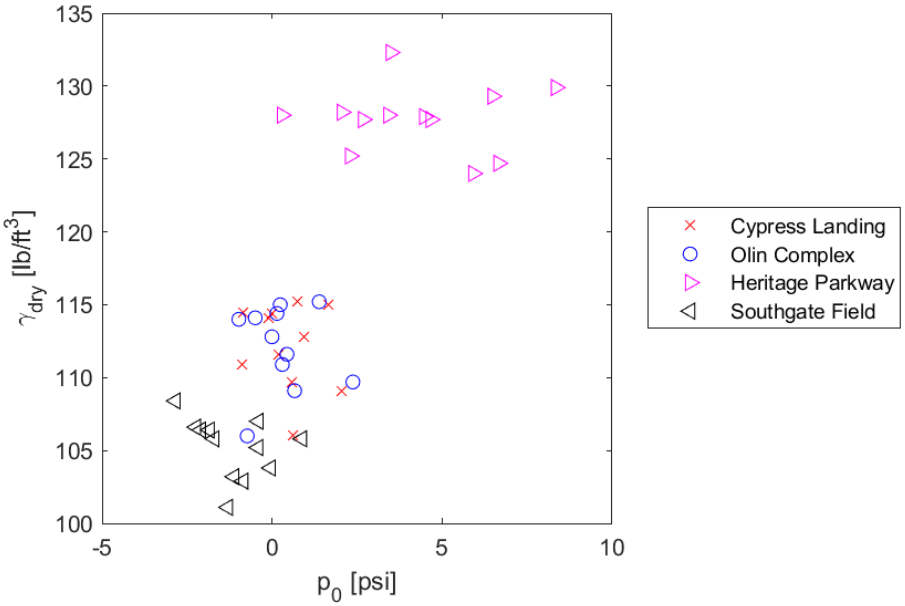

Figure 6.49: SDPMT-12 Continuous, γ_{dry} versus p_0, All Sites

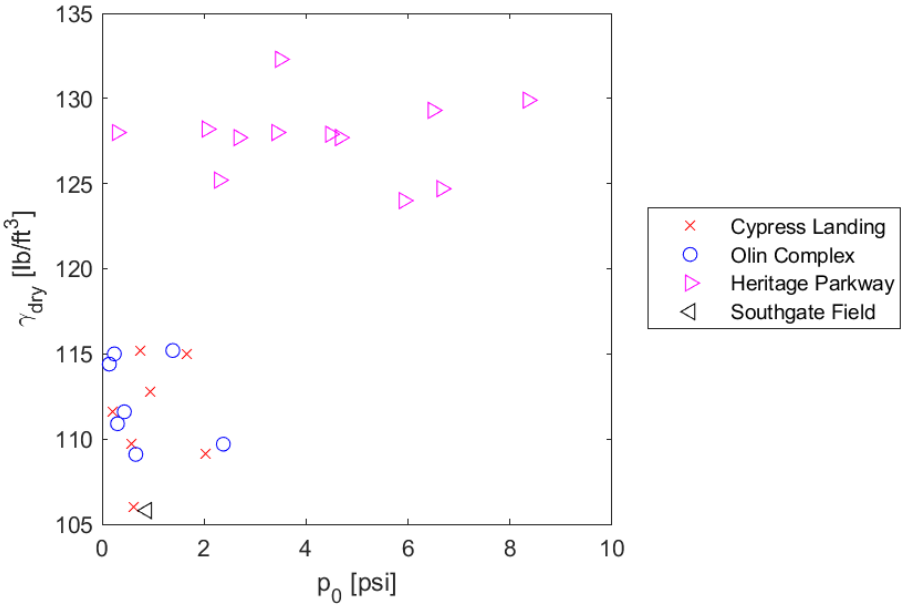

Figure 6.50: SDPMT-12 Continuous, γ_{dry} versus p_0, All Sites, Negative values of p_0 removed

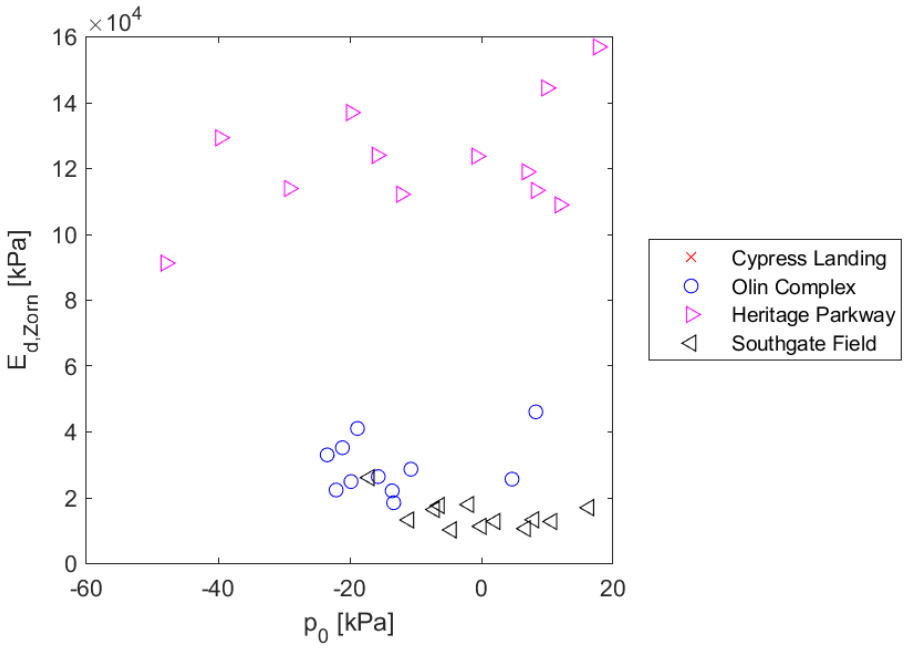

Figure 6.51: SDPMT-6 Incremental, $E_{d,Zorn}$ versus p_0, All Sites

6.5.2 Zorn E_d versus SDPMT p_0

Twenty $E_{d,Zorn}$ versus p_0 regression models were evaluated. Between 12 and 27 sets of data were analyzed, producing R^2 values from 0.12 to 0.47. The results are summarized in Table 6.10.

6.5.2.1 SDPMT-6 Incremental Comparisons

Table 6.10 shows the five regression models developed from SDPMT-6 incremental testing. Figure 6.51 shows all SDPMT-6 incremental p_0 (kPa) versus $E_{d,Zorn}$ (kPa) data. Figure 6.52 shows the data used to develop the models, with the negative p_0 values removed. The resulting models produced very poor R^2 values ranging from 0.12 to 0.17, based on 12 data points, validating the belief that the lift-off pressures are difficult to use in correlations.

6.5.2.2 SDPMT-6 Continuous Comparisons

Table 6.10 shows the five regression models developed from SDPMT-6 continuous testing. Figure 6.53 shows all data in kPa, relating p_0 and $E_{d,Zorn}$. Figure 6.54 shows the data used to develop the models, with negative p_0 values removed. Note the unrealistically high values of p_0 from this continuous testing will affect the correlations. The models produced R^2 values ranging from 0.23 to 0.35, based on 21 data points,

Table 6.10: Correlation Coefficients, $E_{d,Zorn}$ (kPa) versus p_0 (kPa), All Sites

Relationship x	Relationship y	R^2	Model	# of Tests	Figure
			SDPMT-6 Incremental		
Linear	Linear	0.16	$E_{d,Zorn}$=5160 p_0 +1.714E+04	12	E.69
Linear	Log10	0.12	$\log_{10}(E_{d,Zorn})$=0.03671 p_0 +4.258	12	E.261
Log10	Linear	0.17	$E_{d,Zorn}$=9.827E+04 $\log_{10}(p_0)$ -2.466E+04	12	E.165
Log10	Log10	0.15	$\log_{10}(E_{d,Zorn})$=0.757 $\log_{10}(p_0)$ +3.908	12	E.357
Exponential Model		0.17	$E_{d,Zorn}$=1.458E+04 $(p_0)^{0.6851}$	12	E.453
			SDPMT-6 Continuous		
Linear	Linear	0.23	$E_{d,Zorn}$=597.7 p_0 +4.916E+04	21	E.70
Linear	Log10	0.25	$\log_{10}(E_{d,Zorn})$=0.004961 p_0 +4.495	21	E.262
Log10	Linear	0.35	$E_{d,Zorn}$=7.143E+04 $\log_{10}(p_0)$ -2.718E+04	21	E.166
Log10	Log10	0.33	$\log_{10}(E_{d,Zorn})$=0.5532 $\log_{10}(p_0)$ +3.919	21	E.358
Exponential Model		0.32	$E_{d,Zorn}$=2.154E+04 $(p_0)^{0.3618}$	21	E.454
			SDPMT-12 Incremental		
Linear	Linear	0.47	$E_{d,Zorn}$=2154 p_0 +3.483E+04	27	E.71
Linear	Log10	0.41	$\log_{10}(E_{d,Zorn})$=0.01555 p_0 +4.45	27	E.263
Log10	Linear	0.43	$E_{d,Zorn}$=6.349E+04 $\log_{10}(p_0)$ +8656	27	E.167
Log10	Log10	0.34	$\log_{10}(E_{d,Zorn})$=0.4351 $\log_{10}(p_0)$ +4.283	27	E.359
Exponential Model		0.50	$E_{d,Zorn}$=2.09E+04 $(p_0)^{0.4758}$	27	E.455
			SDPMT-12 Continuous		
Linear	Linear	0.17	$E_{d,Zorn}$=486.6 p_0 +5.415E+04	18	E.72
Linear	Log10	0.25	$\log_{10}(E_{d,Zorn})$=0.004556 p_0 +4.526	18	E.264
Log10	Linear	0.29	$E_{d,Zorn}$=4.756E+04 $\log_{10}(p_0)$ +7984	18	E.168
Log10	Log10	0.39	$\log_{10}(E_{d,Zorn})$=0.4256 $\log_{10}(p_0)$ +4.123	18	E.360
Exponential Model		0.28	$E_{d,Zorn}$=2.564E+04 $(p_0)^{0.3097}$	18	E.456

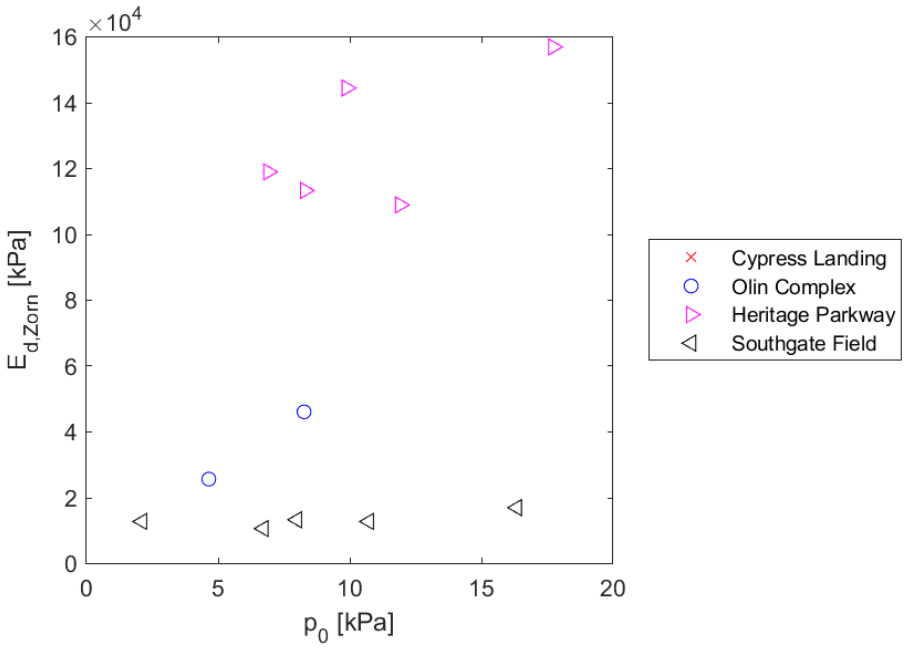

Figure 6.52: SDPMT-6 Incremental, $E_{d,Zorn}$ versus p_0, All Sites, Negative values of p_0 removed

which again validate the belief that the lift-off pressures are difficult to use in correlations.

6.5.2.3 SDPMT-12 Incremental Comparisons

Table 6.10 shows the five regression models developed from SDPMT-12 incremental testing. Figure 6.55 shows all data in kPa, relating p_0 and $E_{d,Zorn}$ for the SDPMT-12 incremental tests. Figure 6.56 shows the data used to develop the models. The models developed produced R^2 values ranging from 0.34 to 0.50, using 27 data points. Because of the imprecise method of determining p_0 it difficult to get an accurate value, making correlations of the data difficult to determine.

6.5.2.4 SDPMT-12 Continuous Comparisons

Table 6.10 shows the five regression models developed from SDPMT-12 continuous testing. Figure 6.57 shows all the data in kPa, relating p_0 to $E_{d,Zorn}$. Figure 6.58 shows the data used to develop the models, with negative p_0 values removed from the model development. Note the unrealistically high values of p_0 from this continuous testing will affect the correlations. The models developed produced R^2 values ranging from 0.17 to 0.39, using 18 data points. A general trend was observed between p_0 and $E_{d,Zorn}$, but not enough data was obtained to strengthen this relationship.

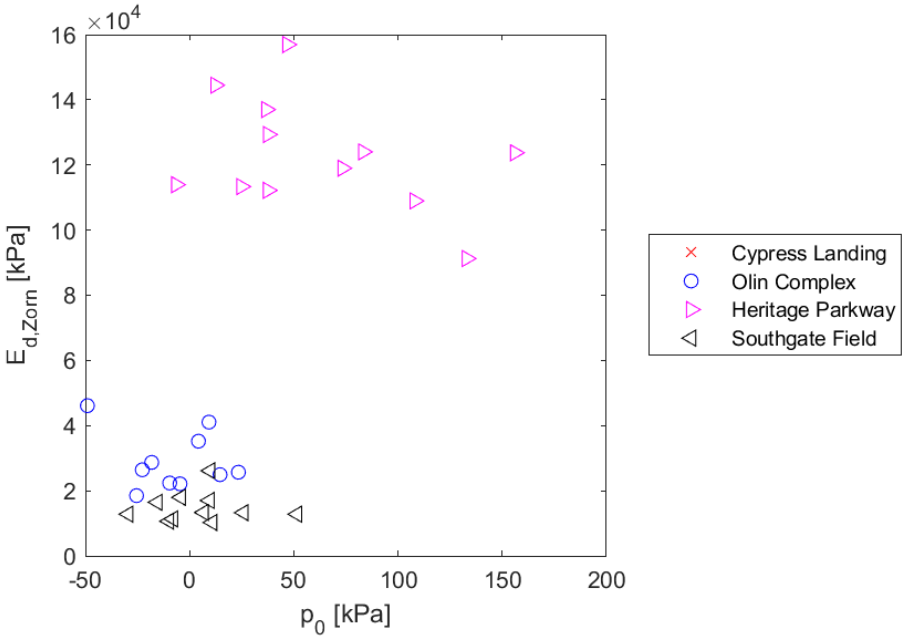

Figure 6.53: SDPMT-6 Continuous, $E_{d,Zorn}$ versus p_0, All Sites

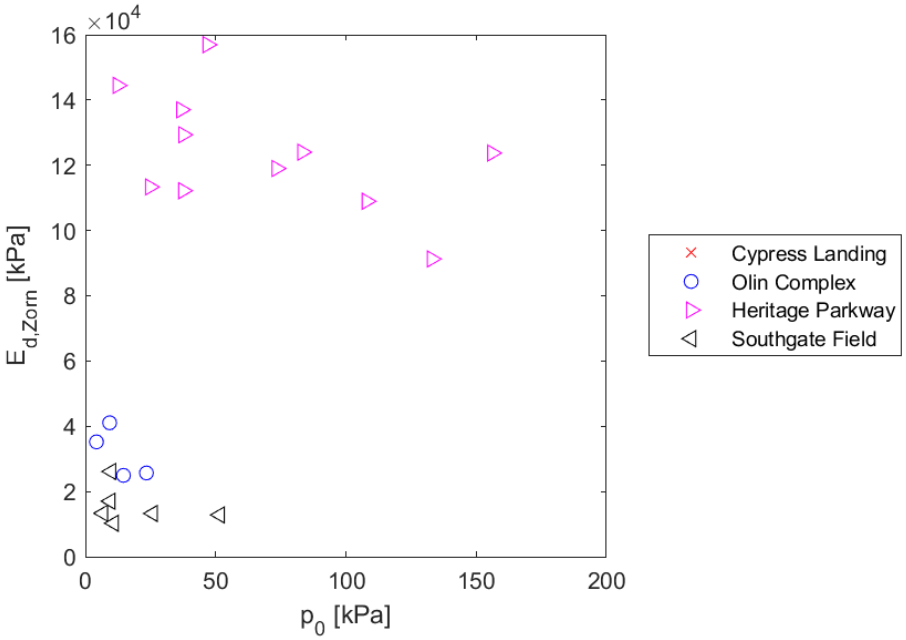

Figure 6.54: SDPMT-6 Continuous, $E_{d,Zorn}$ versus p_0, All Sites, Negative values of p_0 removed

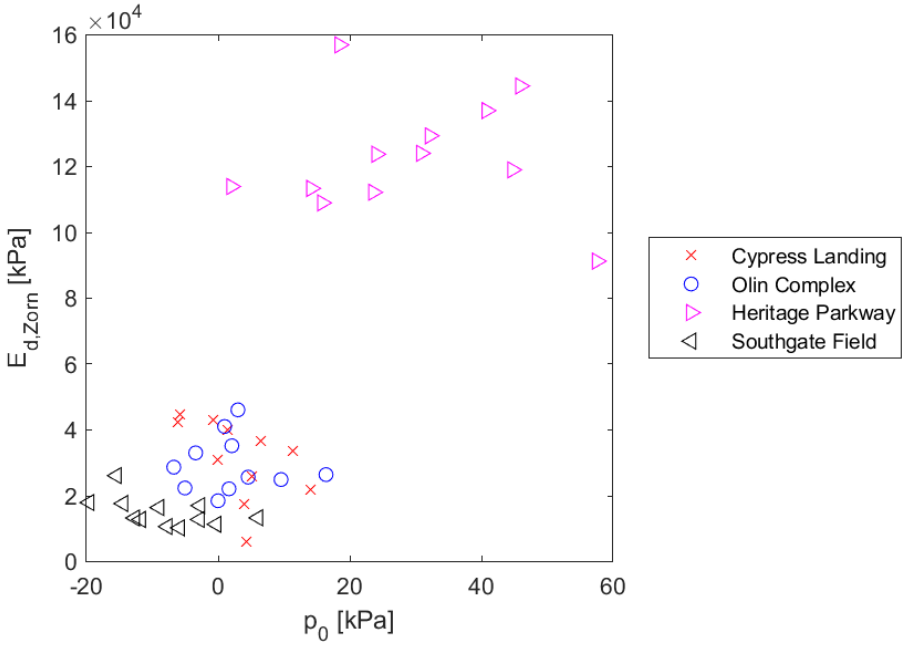

Figure 6.55: SDPMT-12 Incremental, $E_{d,Zorn}$ versus p_0, All Sites

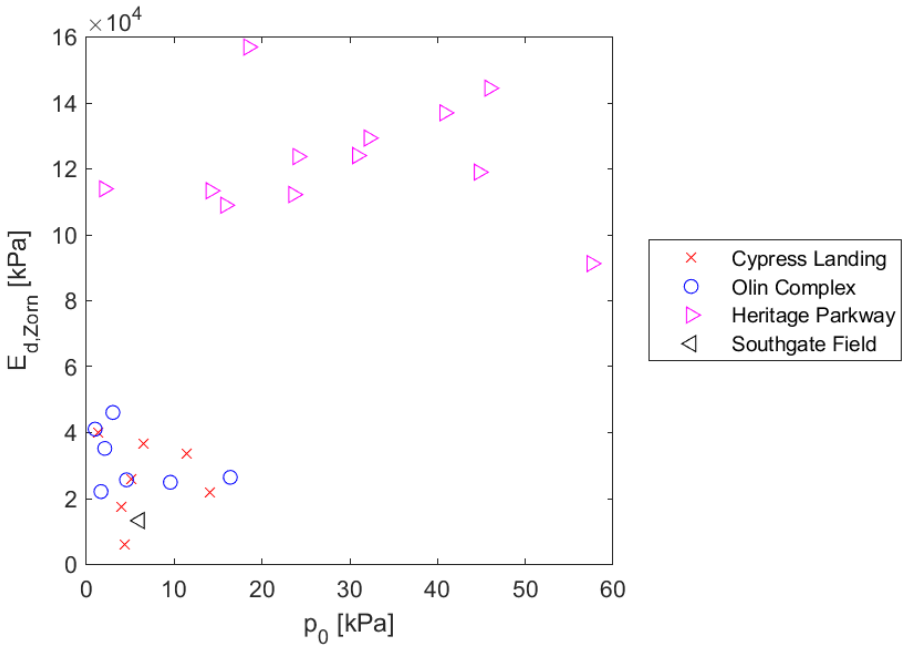

Figure 6.56: SDPMT-12 Incremental, $E_{d,Zorn}$ versus p_0, All Sites, Negative values of p_0 removed

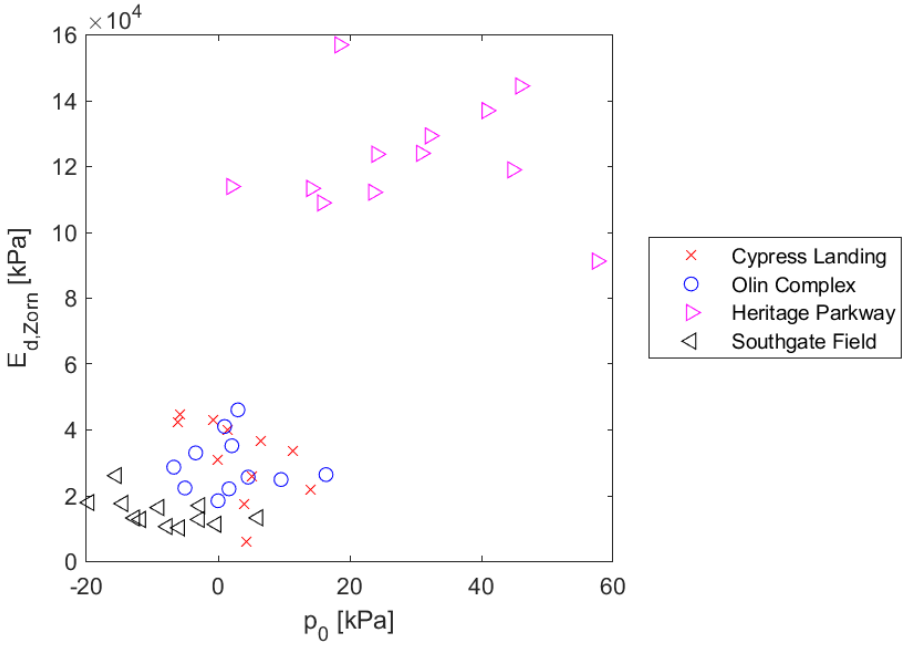

Figure 6.57: SDPMT-12 Continuous, $E_{d,Zorn}$ versus p_0, All Sites

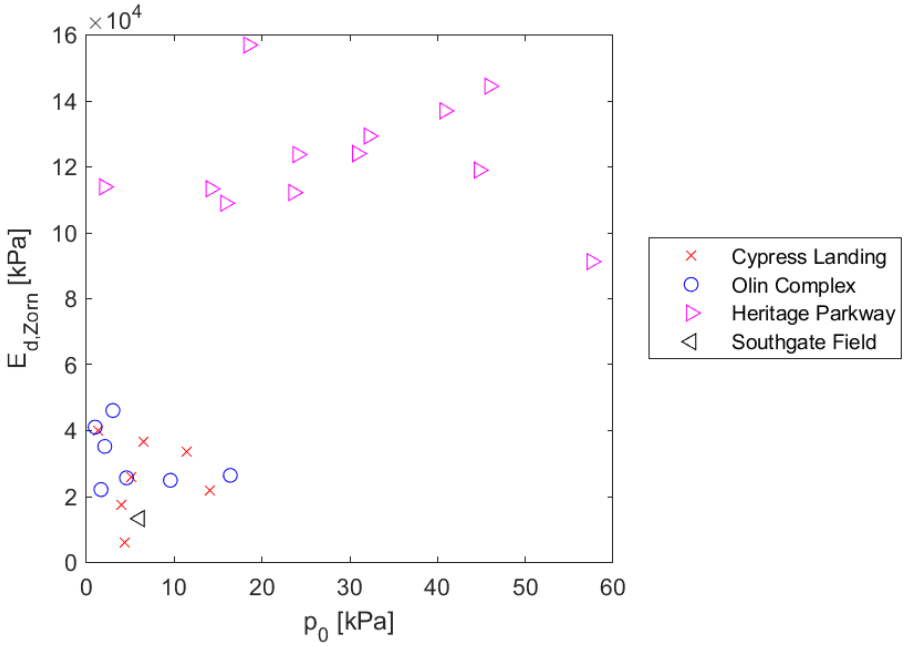

Figure 6.58: SDPMT-12 Continuous, $E_{d,Zorn}$ versus p_0, All Sites, Negative values of p_0 removed

6.5.2.5 Summary of $E_{d,Zorn}$ versus p_0 Regression Models

Several factors contribute the unreliability of the models produced from the SDPMT p_0 and Zorn E_d. Estimating SDPMT p_0 from the graphical construction method is not precise, plus p_0 falls within a limited range, and finally p_0 values were unrealistically high from both continuous tests, indicating that this testing procedure needs further improvements.

6.5.3 Dynatest E_0 versus SDPMT p_0

Twenty $E_{0,Dynatest}$ versus p_0 regression models were evaluated. The results are summarized in Table 6.11. Between 11 and 26 sets of data were used to develop the correlations, which produced R^2 values ranging from 0.03 to 0.56. Once again the inherent variability associated with estimating p_0 produced very poor correlations.

6.5.3.1 SDPMT-6 Incremental Comparisons

Table 6.11 shows the five regression models developed from SDPMT-6 incremental data. Figure 6.59 shows all data relating p_0 and $E_{0,Dynatest}$ for SDPMT-6 incremental tests. Figure 6.60 shows the data used to develop the models. The models produced R^2 values ranging from 0.05. to 0.23, using 11 data points. Even though the correlations are very poor, there is not enough data to make a conclusion about the relationship between p_0 and $E_{0,Dynatest}$ for SDPMT-6 incremental tests.

6.5.3.2 SDPMT-6 Continuous Comparisons

Table 6.11 shows the five regression models developed from SDPMT-6 continuous data. Figure 6.61 shows all the data relating p_0 and $E_{0,Dynatest}$ for SDPMT-6 continuous tests. Figure 6.62 shows the data used to develop the models, with the negative p_0 values removed for model development. The models produced R^2 values ranging from 0.16 to 0.28, based on 21 data points. The large scatter across the plot lead to very low R^2 values and the conclusion that the relationship between p_0 and $E_{0,Dynatest}$ for SDPMT-6 continuous tests is very poor.

6.5.3.3 SDPMT-12 Incremental Comparisons

Table 6.11 shows the five regression models developed from SDPMT-12 incremental data. Figure 6.63 shows all data relating p_0 and $E_{0,Dynatest}$ for the SDPMT-12 incremental tests. Figure 6.64 shows the data used to develop the models, with the negative values removed. The models produced R^2 values ranging from 0.36 to 0.56, using 26 data points. There a large scatter of data plus not enough data to make a conclusion about the relationship between p_0 and $E_{0,Dynatest}$ for SDPMT-12 incremental tests.

Table 6.11: Correlation Coefficients, $E_{0,Dynatest}$ versus p_0, All Sites

Relationship x	Relationship y	R^2	Model	# of Tests	Figure
			SDPMT-6 Incremental		
Linear	Linear	0.05	$E_{0,Dynatest}$=1.933E+04 p_0 +1.982E+05	11	E.81
Linear	Log10	0.13	$\log_{10}(E_{0,Dynatest})$=0.04866 p_0 +4.781	11	E.273
Log10	Linear	0.10	$E_{0,Dynatest}$=4.772E+05 $\log_{10}(p_0)$ -5.606E+04	11	E.177
Log10	Log10	0.23	$\log_{10}(E_{0,Dynatest})$=1.172 $\log_{10}(p_0)$ +4.168	11	E.369
Exponential Model		0.07	$E_{0,Dynatest}$=1.448E+05 $(p_0)^{0.4487}$	11	E.465
			SDPMT-6 Continuous		
Linear	Linear	0.16	$E_{0,Dynatest}$=4182 p_0 +2.99E+05	21	E.82
Linear	Log10	0.21	$\log_{10}(E_{0,Dynatest})$=0.005897 p_0 +5.162	21	E.274
Log10	Linear	0.28	$E_{0,Dynatest}$=5.328E+05 $\log_{10}(p_0)$ -2.825E+05	21	E.178
Log10	Log10	0.28	$\log_{10}(E_{0,Dynatest})$=0.6576 $\log_{10}(p_0)$ +4.477	21	E.370
Exponential Model		0.24	$E_{0,Dynatest}$=1.231E+05 $(p_0)^{0.3947}$	21	E.466
			SDPMT-12 Incremental		
Linear	Linear	0.54	$E_{0,Dynatest}$=1.952E+04 p_0 +9.696E+04	26	E.83
Linear	Log10	0.47	$\log_{10}(E_{0,Dynatest})$=0.02256 p_0 +4.985	26	E.275
Log10	Linear	0.45	$E_{0,Dynatest}$=5.539E+05 $\log_{10}(p_0)$ -1.199E+05	26	E.179
Log10	Log10	0.36	$\log_{10}(E_{0,Dynatest})$=0.6157 $\log_{10}(p_0)$ +4.758	26	E.371
Exponential Model		0.56	$E_{0,Dynatest}$=5.98E+04 $(p_0)^{0.7284}$	26	E.467
			SDPMT-12 Continuous		
Linear	Linear	0.03	$E_{0,Dynatest}$=1577 p_0 +3.709E+05	18	E.84
Linear	Log10	0.12	$\log_{10}(E_{0,Dynatest})$=0.004025 p_0 +5.223	18	E.276
Log10	Linear	0.13	$E_{0,Dynatest}$=2.438E+05 $\log_{10}(p_0)$ +8.536E+04	18	E.180
Log10	Log10	0.27	$\log_{10}(E_{0,Dynatest})$=0.4407 $\log_{10}(p_0)$ +4.769	18	E.372
Exponential Model		0.11	$E_{0,Dynatest}$=2.004E+05 $(p_0)^{0.2269}$	18	E.468

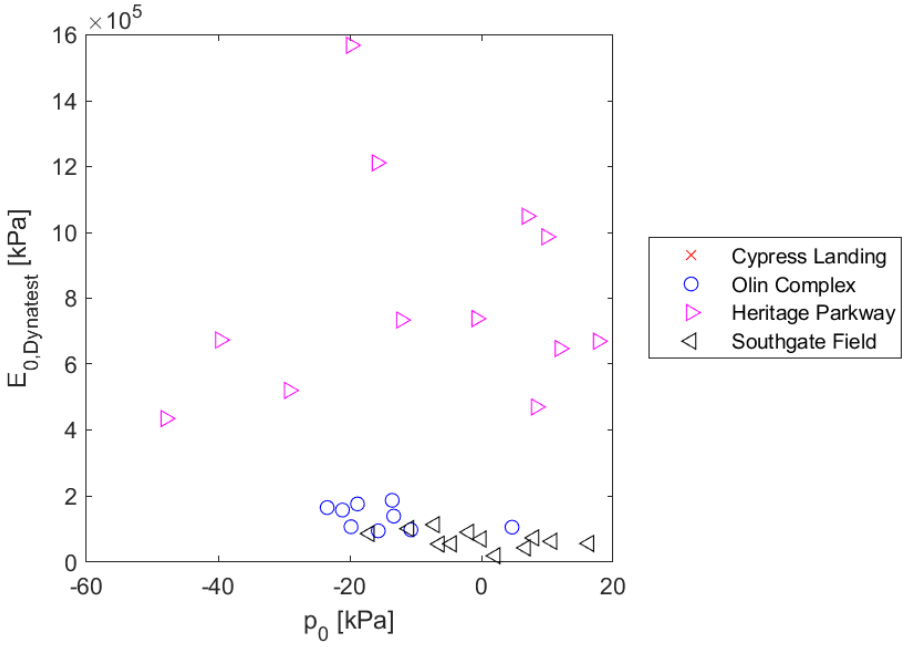

Figure 6.59: SDPMT-6 Incremental, $E_{0,Dynatest}$ versus p_0, All Sites

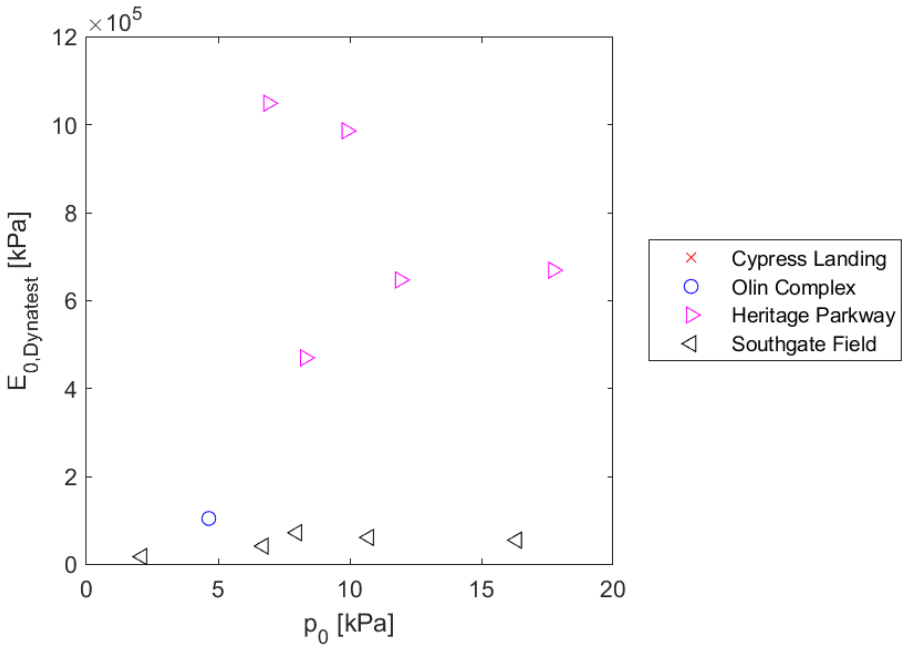

Figure 6.60: SDPMT-6 Incremental, $E_{0,Dynatest}$ versus p_0, All Sites, Negative values of p_0 removed

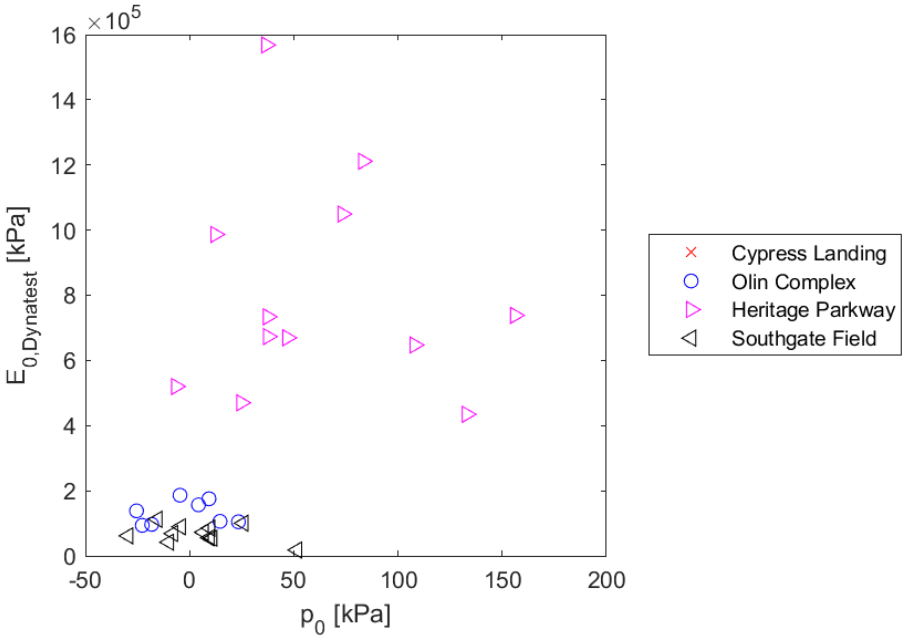

Figure 6.61: SDPMT-6 Continuous, $E_{0,Dynatest}$ versus p_0, All Sites

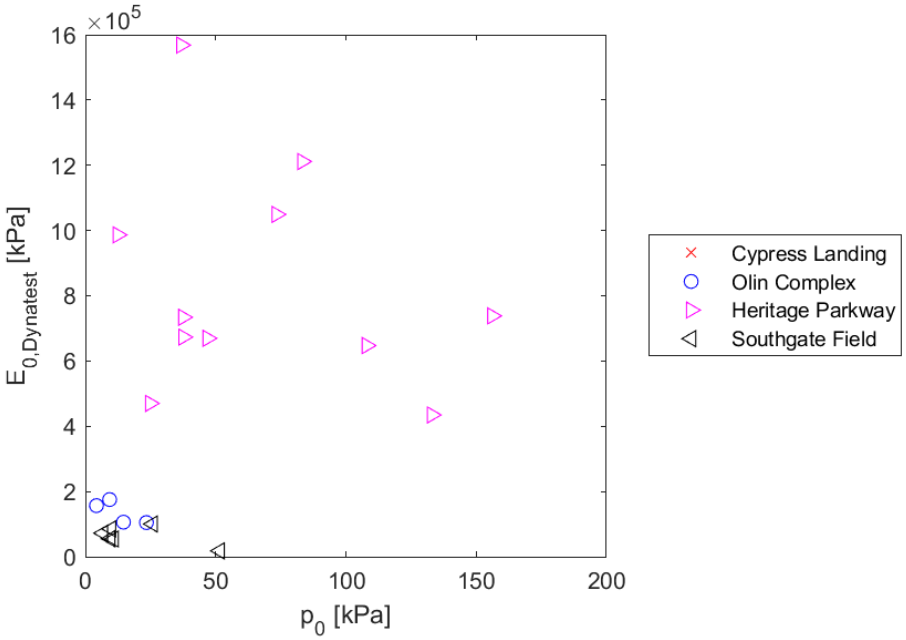

Figure 6.62: SDPMT-6 Continuous, $E_{0,Dynatest}$ versus p_0, All Sites, Negative values of p_0 removed

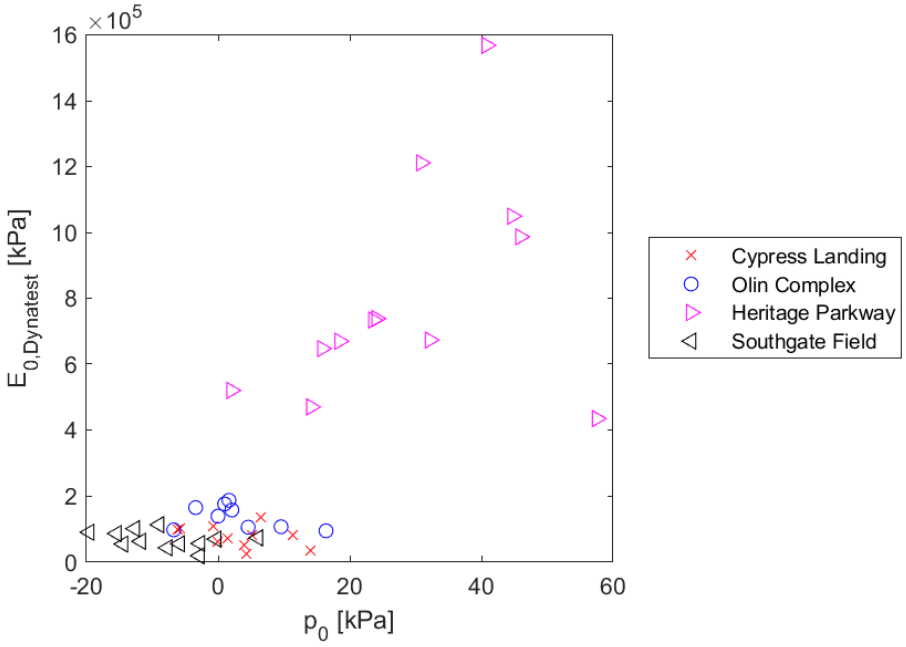

Figure 6.63: SDPMT-12 Incremental, $E_{0,Dynatest}$ versus p_0, All Sites

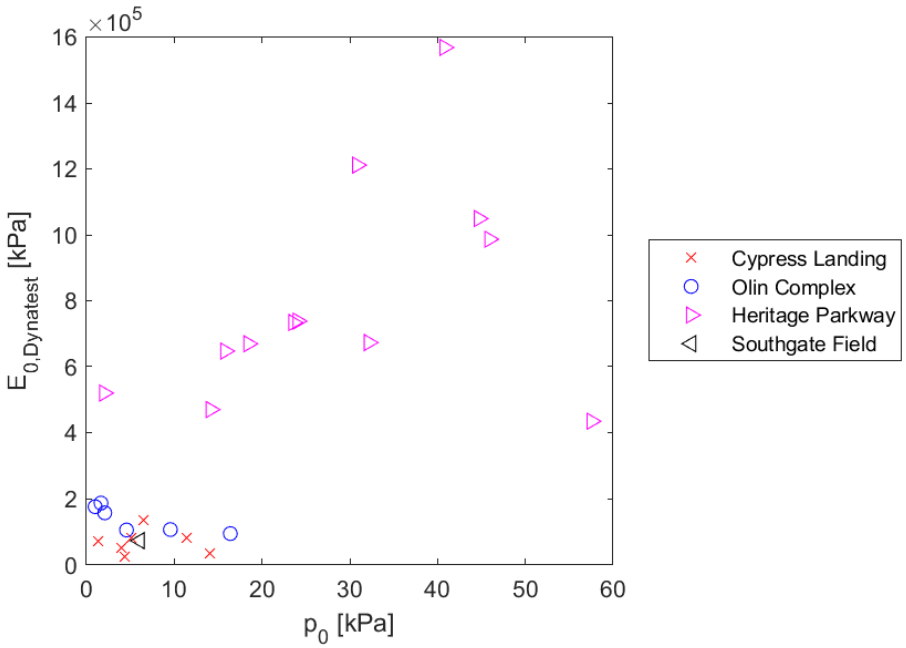

Figure 6.64: SDPMT-12 Incremental, $E_{0,Dynatest}$ versus p_0, All Sites, Negative values of p_0 removed

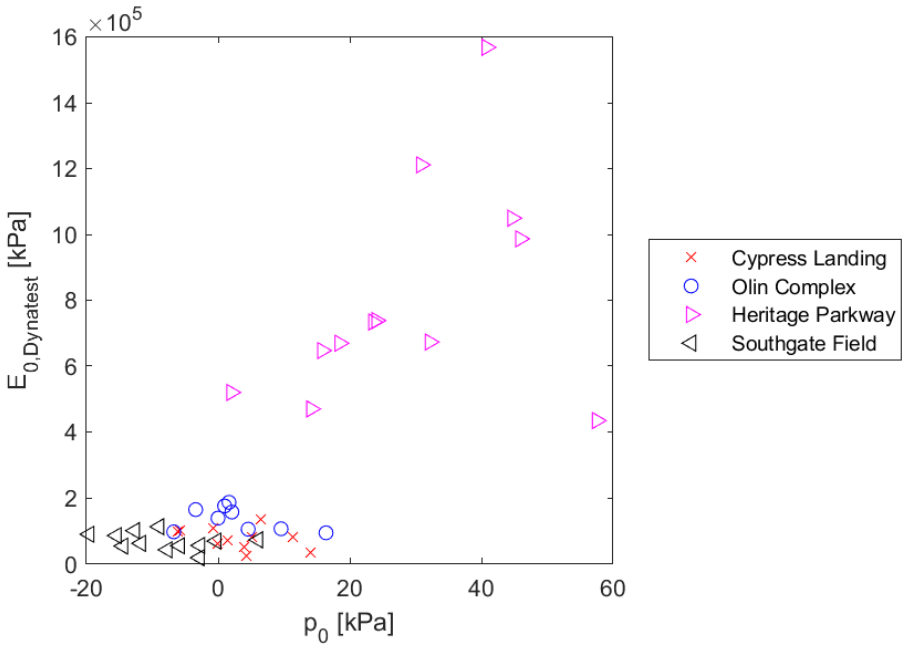

Figure 6.65: SDPMT-12 Continuous, $E_{0,Dynatest}$ versus p_0, All Sites

6.5.3.4 SDPMT-12 Continuous Comparisons

Table 6.11 shows the five regression models developed from SDPMT-12 continuous data. Figure 6.65 shows all data relating p_0 and $E_{0,Dynatest}$. Figure 6.66 shows the data used to develop the models, with negative values of p_0 removed. The models produced very poor R^2 values ranging from 0.03 to 0.27, based on 18 data points, indicating no correlations exits between these variables. There is limited data used to make this conclusion.

6.5.3.5 Summary of $E_{0,Dynatest}$ versus p_0 Regression Models

There is visual evidence that some limited relationships exist between SDPMT p_0 and Dynatest LWD E_0 values. Once again the methods used to determine p_0 must be improved, especially from continuous tests, plus negative p_0 values must also be addressed.

6.5.4 CIV versus SDPMT p_0

Twenty CIV versus p_0 regression models were evaluated. Between 12 and 27 sets of data were used to develop R^2 values ranging from 0.04 to 0.51. Once again the inherent variability associated with estimating p_0 produced very poor correlations. SDPMT-12 incremental testing yielded the highest R^2 values and also included the largest number of data points. The results are summarized in Table 6.12.

Table 6.12: Correlation Coefficients, CIV versus p_0, All Sites

Relationship x	Relationship y	R^2	Model	# of Tests	Figure
			SDPMT-6 Incremental		
Linear	Linear	0.12	CIV=1.428 p_0 +9.644	12	E.93
Linear	Log10	0.08	$\log_{10}$(CIV)=0.02703 p_0 +0.9415	12	E.285
Log10	Linear	0.15	CIV=29.61 $\log_{10}(p_0)$ -4.123	12	E.189
Log10	Log10	0.12	$\log_{10}$(CIV)=0.5947 $\log_{10}(p_0)$ +0.6496	12	E.381
Exponential Model		0.14	CIV=7.137 $(p_0)^{0.5392}$	12	E.477
			SDPMT-6 Continuous		
Linear	Linear	0.28	CIV=0.209 p_0 +17.4	21	E.94
Linear	Log10	0.26	$\log_{10}$(CIV)=0.004276 p_0 +1.114	21	E.286
Log10	Linear	0.39	CIV=24.03 $\log_{10}(p_0)$ -7.939	21	E.190
Log10	Log10	0.34	$\log_{10}$(CIV)=0.4695 $\log_{10}(p_0)$ +0.6279	21	E.382
Exponential Model		0.37	CIV=7.629 $(p_0)^{0.3597}$	21	E.478
			SDPMT-12 Incremental		
Linear	Linear	0.49	CIV=0.7115 p_0 +12.2	27	E.95
Linear	Log10	0.45	$\log_{10}$(CIV)=0.01432 p_0 +1.025	27	E.287
Log10	Linear	0.44	CIV=21.04 $\log_{10}(p_0)$ +3.489	27	E.191
Log10	Log10	0.37	$\log_{10}$(CIV)=0.403 $\log_{10}(p_0)$ +0.8697	27	E.383
Exponential Model		0.51	CIV=7.412 $(p_0)^{0.4611}$	27	E.479
			SDPMT-12 Continuous		
Linear	Linear	0.04	CIV=0.07497 p_0 +20.66	18	E.96
Linear	Log10	0.09	$\log_{10}$(CIV)=0.002485 p_0 +1.137	18	E.288
Log10	Linear	0.17	CIV=11.48 $\log_{10}(p_0)$ +7.259	18	E.192
Log10	Log10	0.24	$\log_{10}$(CIV)=0.3068 $\log_{10}(p_0)$ +0.8048	18	E.384
Exponential Model		0.15	CIV=11.85 $(p_0)^{0.203}$	18	E.480

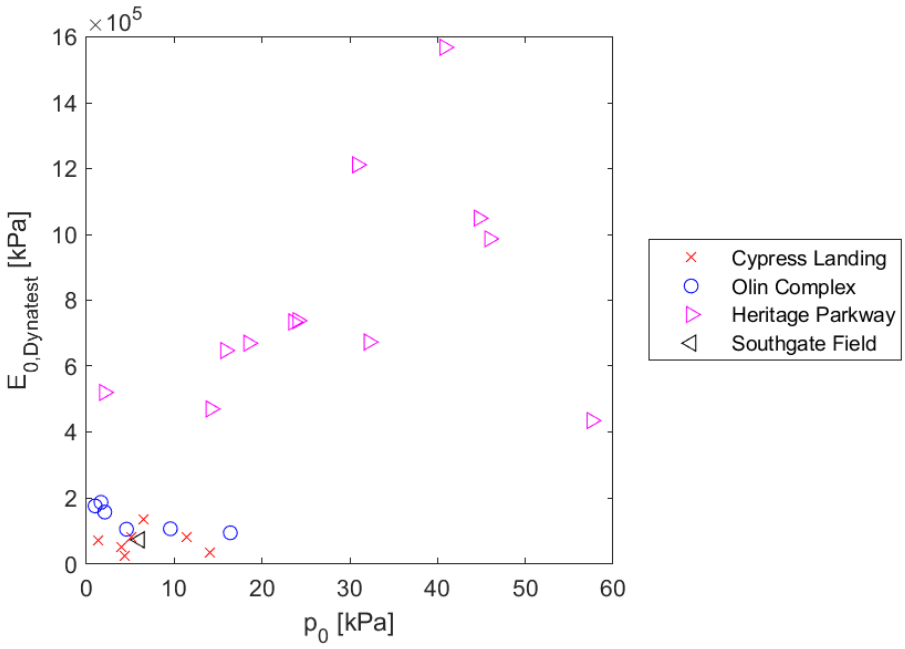

Figure 6.66: SDPMT-12 Continuous, $E_{0,Dynatest}$ versus p_0, All Sites, Negative values of p_0 removed

6.5.4.1 SDPMT-6 Incremental Comparisons

Table 6.12 shows the five regression models developed from SDPMT-6 incremental data. Figure 6.67 shows the data from testing. Figure 6.68, used to develop the models, shows the data with values of p_0 less than zero removed. The models produced R^2 values ranging from 0.08 to 0.15, based on 12 data points. There is insufficient data available to make a conclusion about the relationship between p_0 and CIV for SDPMT-6 incremental tests.

6.5.4.2 SDPMT-6 Continuous Comparisons

Table 6.12 shows the five regression models developed from SDPMT-6 continuous data. Figure 6.69 shows the data relating p_0 to the CIV for SDPMT-6 continuous tests. Figure 6.70 shows the data used to develop the models, with the negative p_0 values removed. These models produced R^2 values ranging from 0.26 to 0.39, based on 21 data points. There are several very high p_0 values along with a large scatter of the p_0 values associated with the Heritage Parkway cemented coquina (i.e. 10 to 170 kPa). In general, a very poor correlation resulted for these variables.

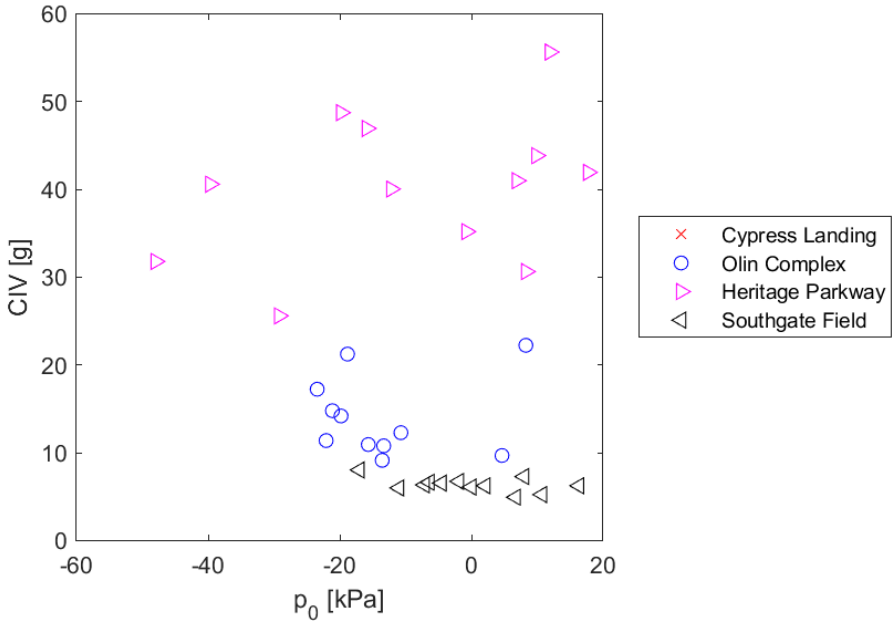

Figure 6.67: SDPMT-6 Incremental, CIV versus p_0, All Sites

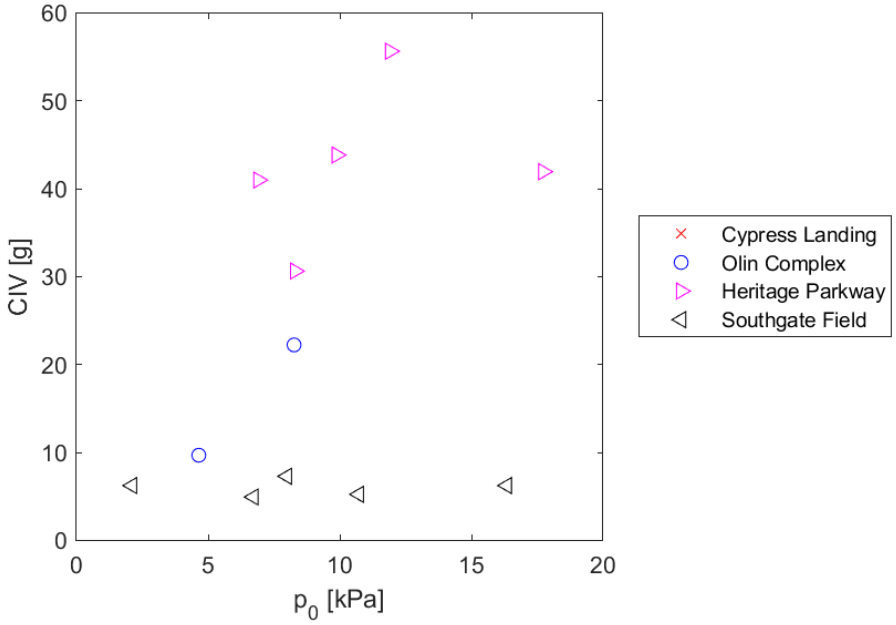

Figure 6.68: SDPMT-6 Incremental, CIV versus p_0, All Sites, Negative Values of p_0 Removed

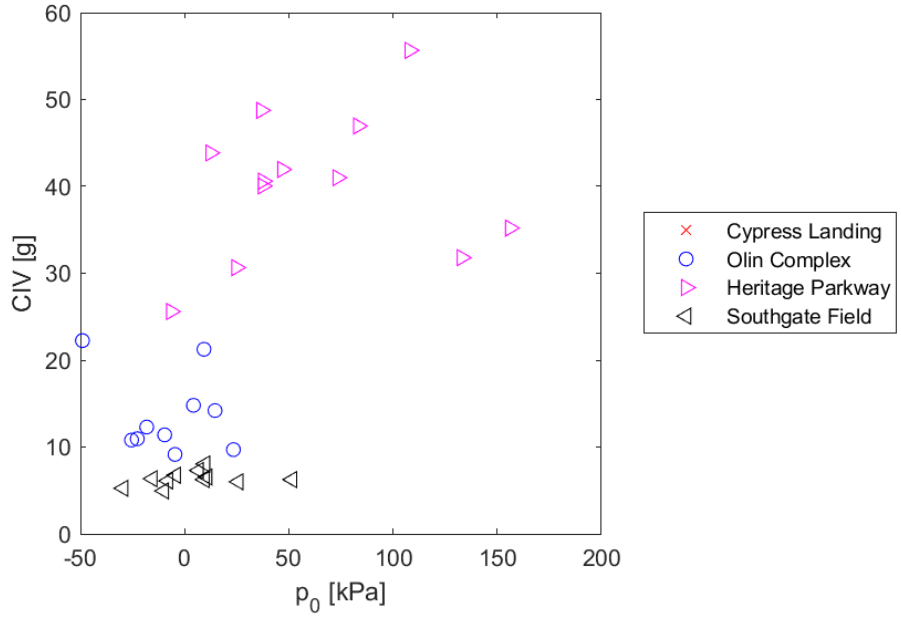

Figure 6.69: SDPMT-6 Continuous, CIV versus p_0, All Sites

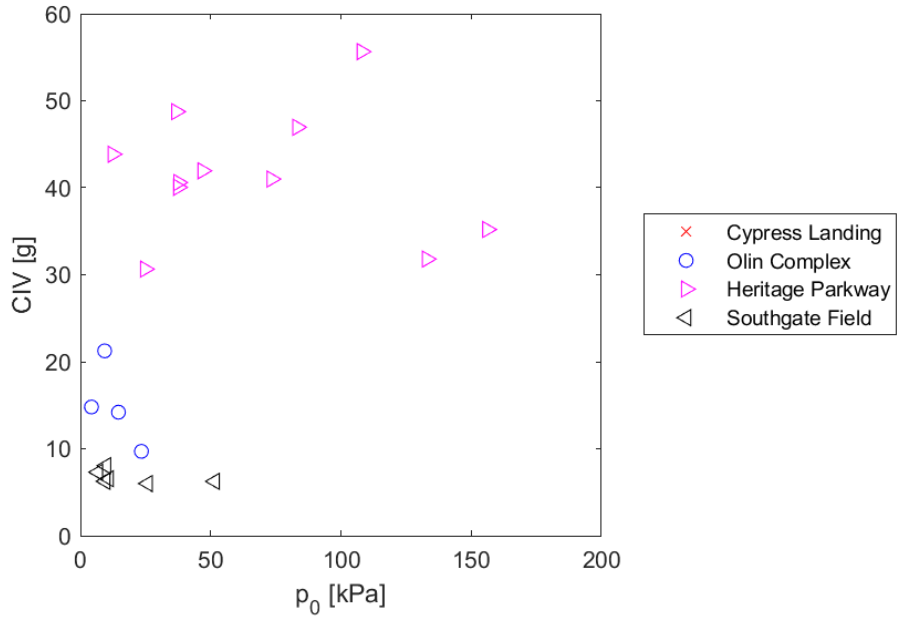

Figure 6.70: SDPMT-6 Continuous, CIV versus p_0, All Sites, Negative values of p_0 removed

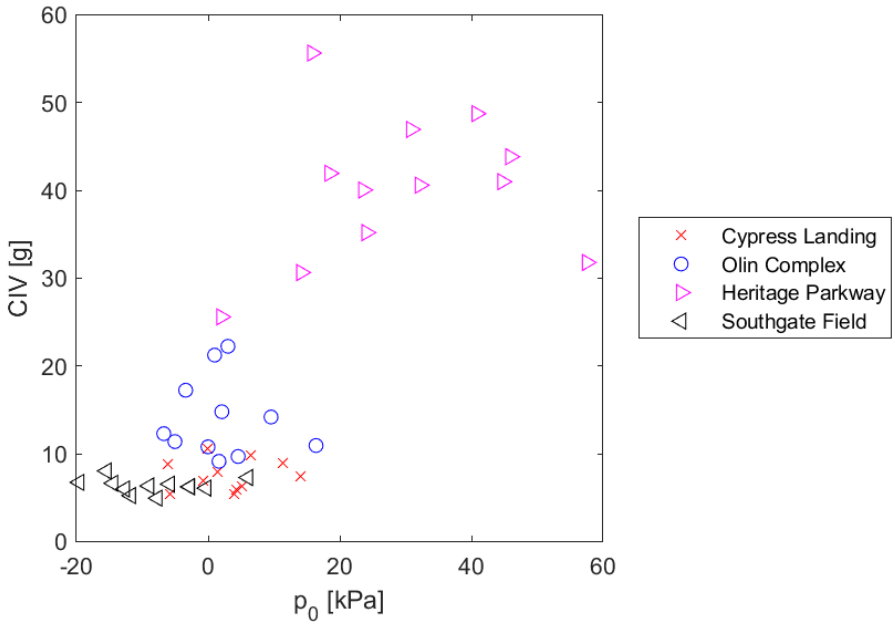

Figure 6.71: SDPMT-12 Incremental, CIV versus p_0, All Sites

6.5.4.3 SDPMT-12 Incremental Comparisons

Table 6.12 shows the five regression models developed from SDPMT-12 incremental data. Figure 6.71 shows the data relating p_0 and CIV. Figure 6.72 shows the data used to develop the models, with the negative p_0 values removed. The models produced R^2 values ranging from 0.37 to 0.51, based on 27 data points. In conclusion there is a weak relationship between p_0 from SDPMT-12 incremental tests and CIV.

6.5.4.4 SDPMT-12 Continuous Comparisons

Table 6.12 shows the five regression models developed from SDPMT-12 continuous data. Figure 6.73 shows the corresponding data relating p_0 and CIV. Figure 6.74 shows the data used to develop the models, with negative p_0 values removed. These models produced very low R^2 values ranging from 0.04 to 0.24, based on 18 data points. There is very wide range of scatter associated with p_0 for Heritage Parkway that produces these poor results. Additional data is necessary to improve or validate this correlation.

6.5.4.5 Summary of CIV versus p_0 Regression Models

No acceptable correlations were obtained from the p_0 and CIV analyses, because of the various concerns over the p_0 values.

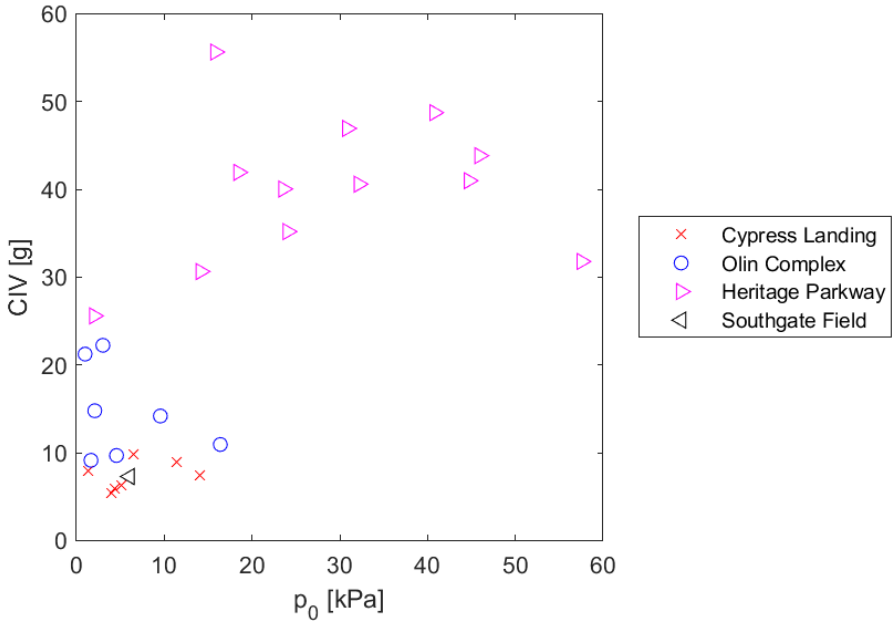

Figure 6.72: SDPMT-12 Incremental, CIV versus p_0, All Sites, Negative values of p_0 removed

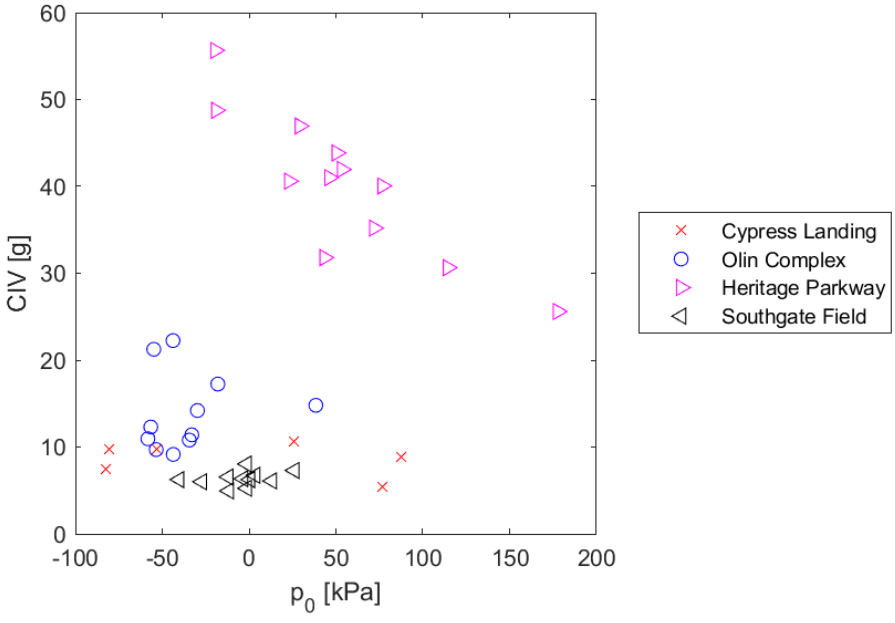

Figure 6.73: SDPMT-12 Continuous, CIV versus p_0, All Sites

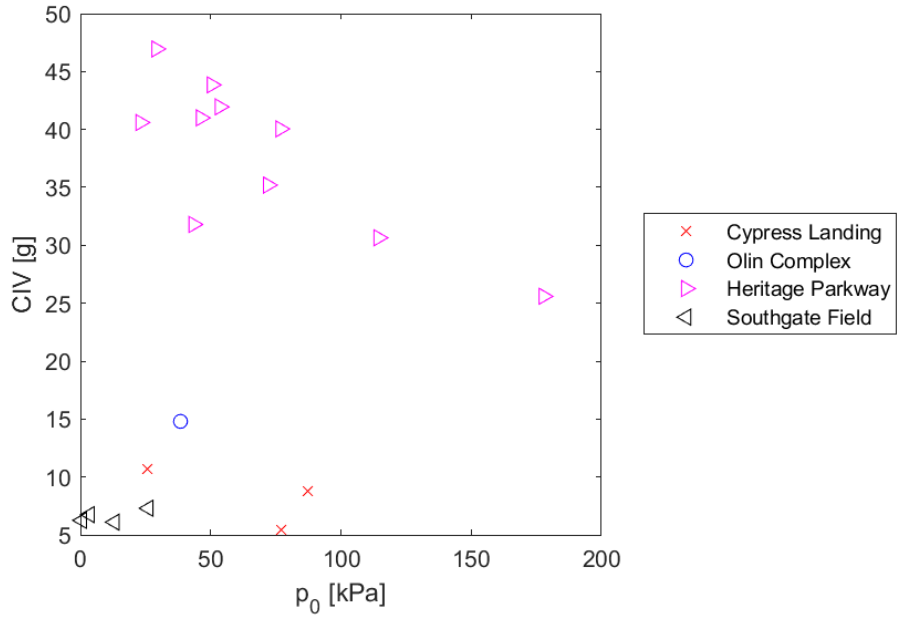

Figure 6.74: SDPMT-12 Continuous, CIV versus p_0, All Sites, Negative values of p_0 removed

6.5.5 DCP Penetration Index versus SDPMT p_0

Twenty DCP PI versus p_0 regression models were evaluated. Higher DCP PI's result from softer or weaker soils, while p_0 from SDPMT testing has proven to be inconsistent. Therefore, very weak correlations were expected.

The results are summarized in Table 6.13. Between 7 and 15 sets of data were used to develop these models. The resulting very low R^2 values ranged from 0.00 to 0.33. The high strength and density of the cemented coquina base would have damaged the DCP; therefore, DCP tests were not conducted at Heritage Parkway. The results from the other three sites limited the soil types evaluated. Due to construction logistics, SDPMT-6 test were unable to be conducted at Cypress Landing, and consequently, not used in these comparisons.

6.5.5.1 SDPMT-6 Incremental Comparisons

Table 6.13 shows the five regression models developed from SDPMT-6 incremental data. Figure 6.75 shows the data relating p_0 and DCP PI. Figure 6.76, with negative p_0 values removed, shows the data used to develop the models. The models produced R^2 values ranging from 0.00 to 0.06, based only on 7 data points. Even though R^2 values are unacceptable, there is insufficient data to make a conclusion about the relationship between p_0 from SDPMT-6 incremental data and DCP PI.

Table 6.13: Correlation Coefficients, DCP PI versus p_0, All Sites

Relationship x	Relationship y	R^2	Model	# of Tests	Figure
			SDPMT-6 Incremental		
Linear	Linear	0.06	DCP PI=0.8023 p_0 +23.59	7	E.57
Linear	Log10	0.03	$\log_{10}$(DCP PI)=0.01281 p_0 +1.293	7	E.249
Log10	Linear	0.00	DCP PI=3.551 $\log_{10}(p_0)$ +27.11	7	E.153
Log10	Log10	0.00	$\log_{10}$(DCP PI)=0.01774 $\log_{10}(p_0)$ +1.382	7	E.345
Exponential Model		0.01	DCP PI=25.96 $(p_0)^{0.07566}$	7	E.441
			SDPMT-6 Continuous		
Linear	Linear	0.10	DCP PI=0.3495 p_0 +20.01	10	E.58
Linear	Log10	0.12	$\log_{10}$(DCP PI)=0.008543 p_0 +1.167	10	E.250
Log10	Linear	0.11	DCP PI=15.9 $\log_{10}(p_0)$ +8.17	10	E.154
Log10	Log10	0.15	$\log_{10}$(DCP PI)=0.4287 $\log_{10}(p_0)$ +0.8326	10	E.346
Exponential Model		0.11	DCP PI=13.41 $(p_0)^{0.2505}$	10	E.442
			SDPMT-12 Incremental		
Linear	Linear	0.04	DCP PI=0.3139 p_0 +13.15	15	E.59
Linear	Log10	0.08	$\log_{10}$(DCP PI)=0.01472 p_0 +1.028	15	E.251
Log10	Linear	0.13	DCP PI=7.144 $\log_{10}(p_0)$ +10.41	15	E.155
Log10	Log10	0.15	$\log_{10}$(DCP PI)=0.2684 $\log_{10}(p_0)$ +0.9432	15	E.347
Exponential Model		0.11	DCP PI=11.43 $(p_0)^{0.178}$	15	E.443
			SDPMT-12 Continuous		
Linear	Linear	0.13	DCP PI=-0.08831 p_0 +25.51	8	E.60
Linear	Log10	0.05	$\log_{10}$(DCP PI)=-0.001683 p_0 +1.367	8	E.252
Log10	Linear	0.33	DCP PI=-6.284 $\log_{10}(p_0)$ +30.1	8	E.156
Log10	Log10	0.18	$\log_{10}$(DCP PI)=-0.138 $\log_{10}(p_0)$ +1.477	8	E.348
Exponential Model		0.33	DCP PI=30.22 $(p_0)^{-0.1118}$	8	E.444

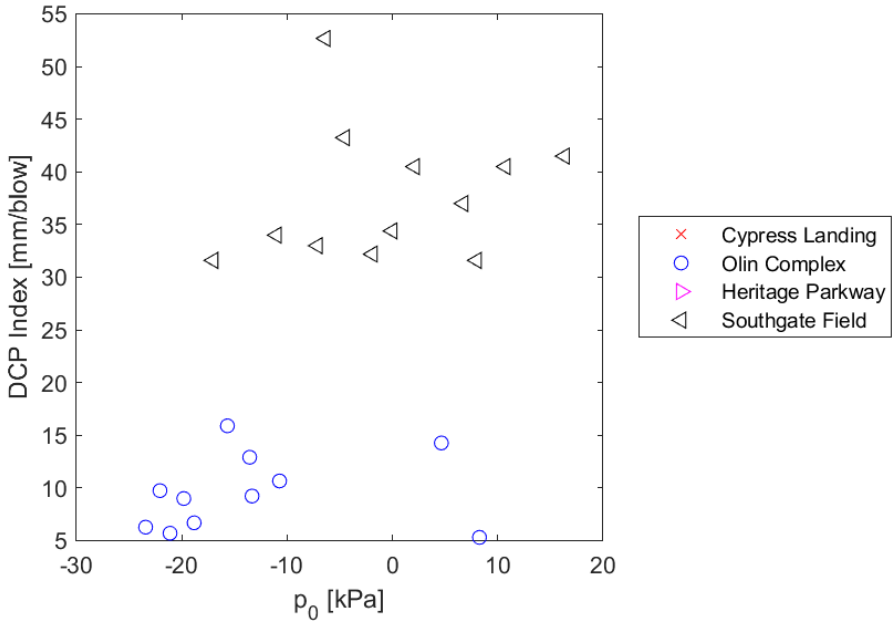

Figure 6.75: SDPMT-6 Incremental, DCP PI versus p_0, All Sites

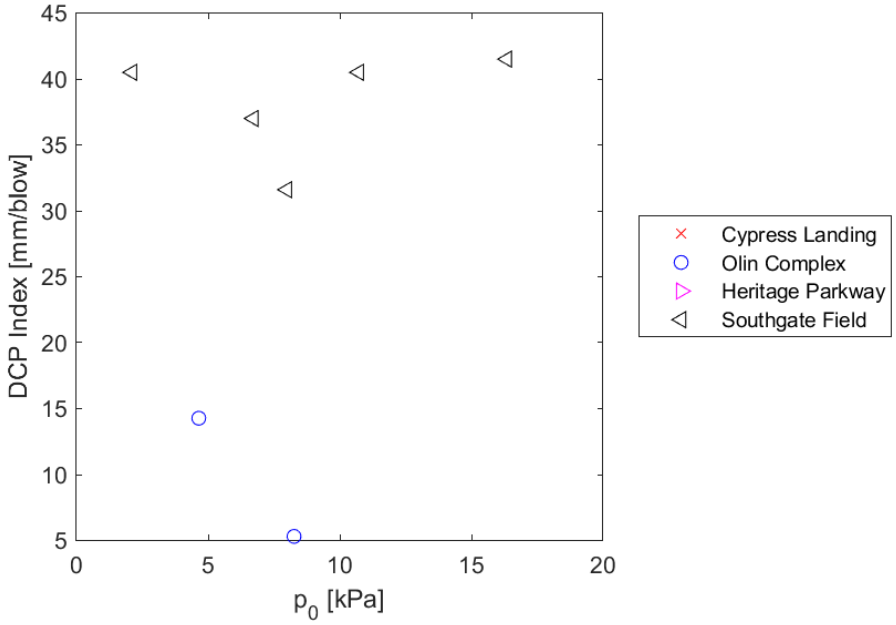

Figure 6.76: SDPMT-6 Incremental, DCP PI versus p_0, All Sites, Negative values of p_0 removed

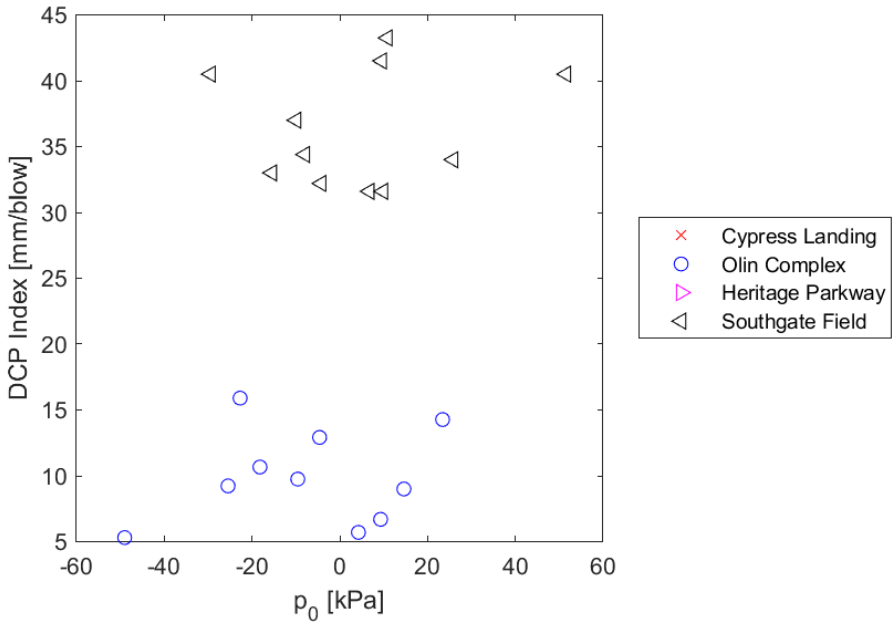

Figure 6.77: SDPMT-6 Continuous, DCP PI versus p_0, All Sites

6.5.5.2 SDPMT-6 Continuous Comparisons

Table 6.13 shows the five regression models developed from SDPMT-6 continuous data. Figure 6.77 shows all data that relate p_0 to the DCP index for SDPMT-6 continuous tests. Figure 6.78, with negative p_0 values removed, shows the data used to develop the models. The models produced R^2 values ranging from 0.10 to 0.15, based on only 10 data points. Again, even though R^2 values are unacceptable, there is insufficient data to make a conclusion about the relationship between p_0 from SDPMT-6 continuous tests and DCP PI.

6.5.5.3 SDPMT-12 Incremental Comparisons

Table 6.13 shows the five regression models developed from SDPMT-12 incremental data. Figure 6.75 shows all data points relating p_0 to the DCP index for SDPMT-12 incremental tests. Figure 6.76, with negative p_0 values removed, shows the data used to develop the models. The models developed produced R^2 values ranging from 0.04 to 0.15, using 15 data points. Again, even though R^2 values are unacceptable, there is insufficient data to make a conclusion about the relationship between p_0 from SDPMT-12 incremental tests and DCP PI .

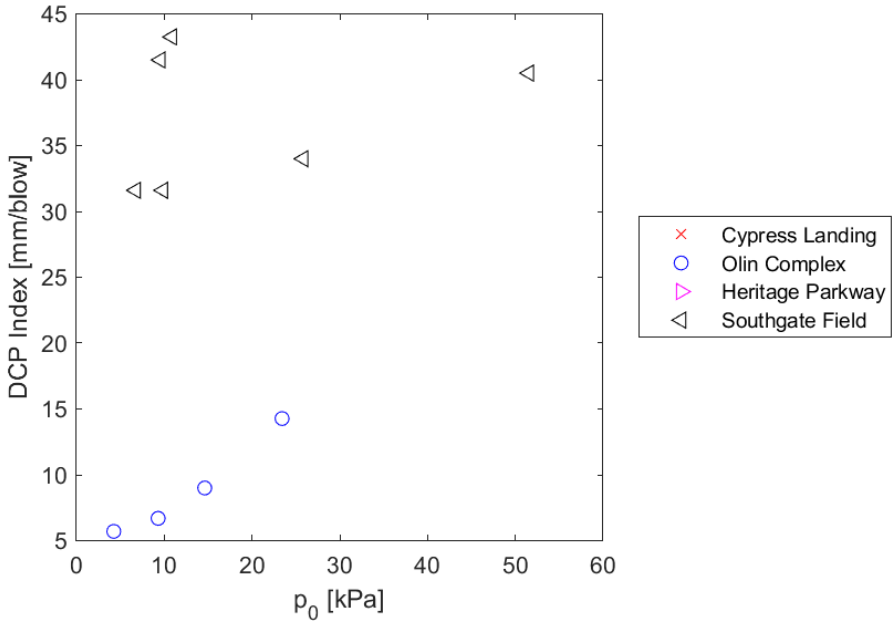

Figure 6.78: SDPMT-6 Continuous, DCP PI versus p_0, All Sites, Negative values p_0 removed

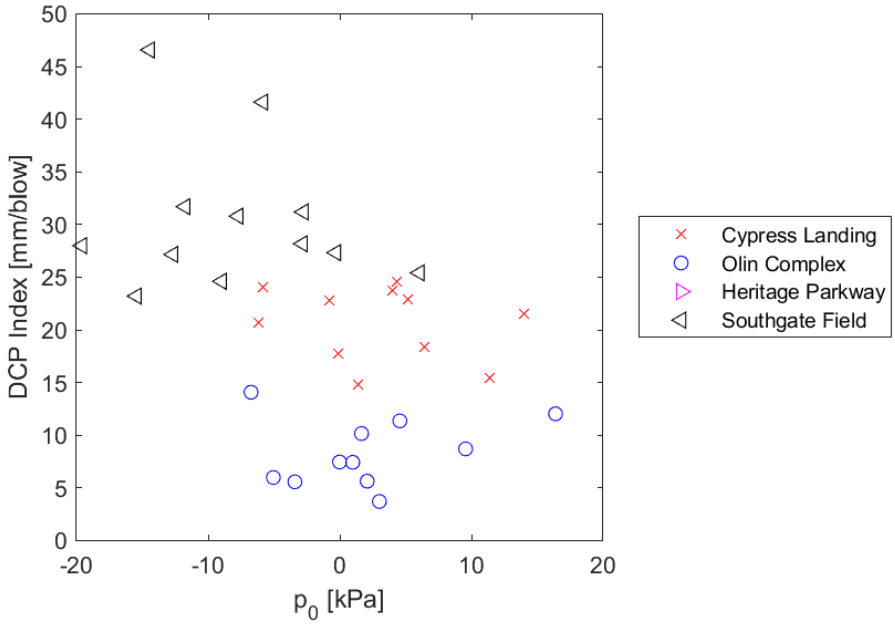

Figure 6.79: SDPMT-12 Incremental, DCP PI versus p_0, All Sites

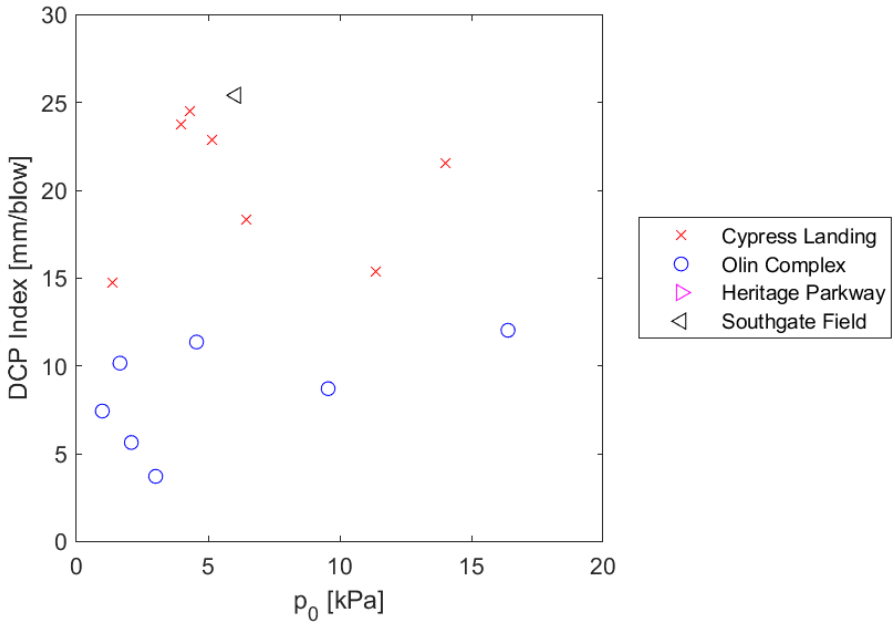

Figure 6.80: SDPMT-12 Incremental, DCP PI versus p_0, All Sites, Negative values of p_0 removed

6.5.5.4 SDPMT-12 Continuous Comparisons

Table 6.13 shows the five regression models developed from SDPMT-12 continuous data. Figure 6.81 shows all data points relating p_0 to the DCP index. Figure 6.82, with negative p_0 values removed, shows the data used to develop the models. The models developed produced R^2 values ranging from 0.05 to 0.33, based on 8 data points. Again, even though R^2 values are unacceptable, there is insufficient data to make a conclusion about the relationship between p_0 from SDPMT-12 continuous tests and DCP PI.

6.5.5.5 Summary of DCP PI versus p_0 Regression Models

Due to the limited number of tests and types of soils tested, plus the inherent variability in p_0, the anticipated results of not being able to develop any correlations between the DCP PI and p_0 were confirmed. If DCP testing can be performed on cemented coquina base immediately following compaction, then additional data could be added to this analysis, resulting in a larger dataset.

6.6 Comparisons with SDPMT p_L

Comparisons were made between p_L from the SDPMT probes to; γ_{dry}, elastic moduli from the Zorn and Dynatest LWD's, CIV's and DCP index values. The results of this

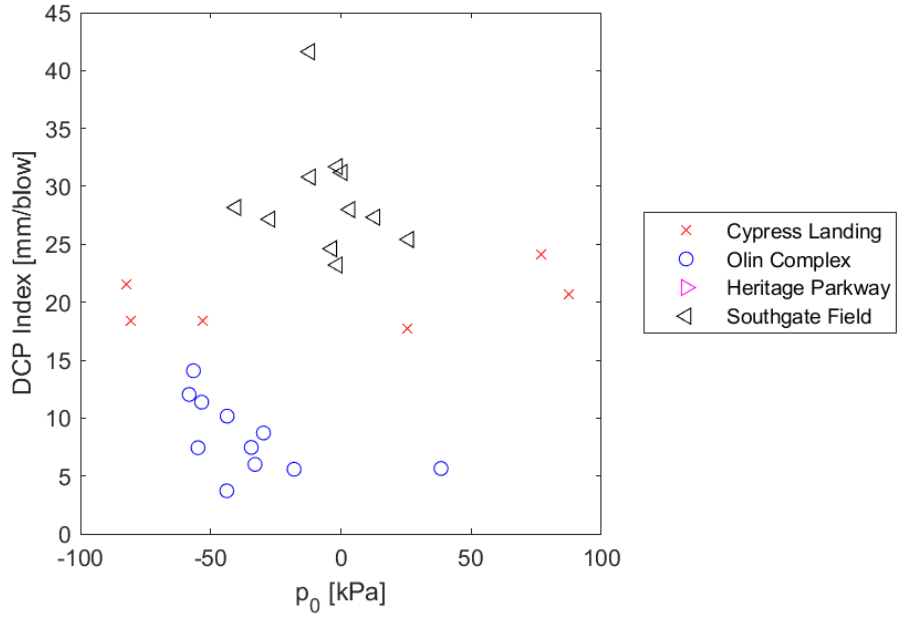

Figure 6.81: SDPMT-12 Continuous, DCP PI versus p_0, All Sites

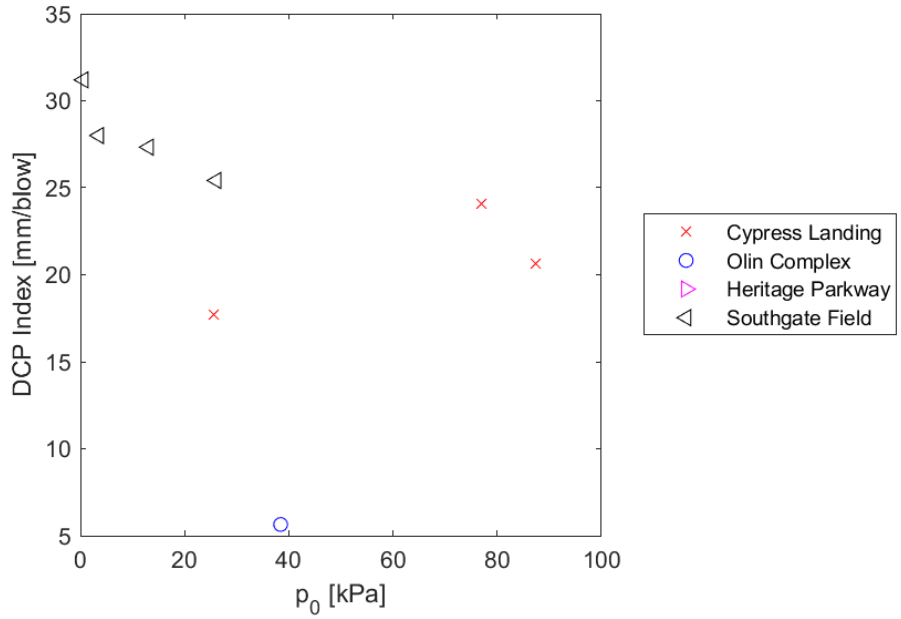

Figure 6.82: SDPMT-12 Continuous, DCP PI versus p_0, All Sites, Negative values of p_0 removed

analyses are described in the following sections (Misilo III, 2018).

6.6.1 Dry Unit Weight versus SDPMT p_L

Twenty γ_{dry} versus p_L regression models were evaluated. The results are summarized in Table 6.14. Between 33 and 46 sets of data were used and R^2 ranged from 0.61 to 0.86. SDPMT-12 incremental testing produced the best correlations. Both sets of linear-linear continuous tests produced the highest R^2 values.

6.6.1.1 SDPMT-6 Incremental Comparisons

Table 6.14 shows the five regression models developed from SDPMT-6 incremental data. Figure 6.83 shows the data used to develop the models. Visually, there seems to be a nonlinear relationship. Dry units weights ranged from 100 to 115 pcf and then 123 to 133 pcf. The gap in these values may affect the resulting correlations. The models produced R^2 values ranging from 0.67 to 0.87, based on 35 data points. Three of the five models have R^2 greater than 0.86. The log-log and exponential models both produced $R^2 = 0.86$. The log-log model is shown in Figure E.329 and described by Equation 6.45. It shows a good agreement between the data and equation. The exponential model is described by Equation 6.46 and is shown in Figure E.425. This model shows a good agreement between the data and the equation. It appears best at lower limit pressures (< 250 psi), and has more scatter at higher limit pressures. The log-linear model produced an R^2 value of 0.87 and is shown in Figure E.137 and described by Equation 6.47. This models produced a good overall agreement throughout the data. When viewing these specific plots it become apparent that the gap in data must be addressed to improve these models.

$$\log_{10}(\gamma_{dry}) = 0.05628 \log_{10}(p_L) + 1.943 \tag{6.45}$$

$$\gamma_{dry} = 88.17(p_L)^{0.05519} \tag{6.46}$$

$$\gamma_{dry} = 15.12 \log_{10}(p_L) + 88.73 \tag{6.47}$$

6.6.1.2 SDPMT-6 Continuous Comparisons

Table 6.14 shows the five regression models developed from SDPMT-6 continuous data. Figure 6.84 shows the data used to develop the models. This data shows gaps for both unit weight and p_L, which will affect the correlations. They produced R^2 values ranging from 0.59 to 0.73, based on 33 data points. The highest R^2 value corresponds with the linear-linear model; however, the figure shows a large scatter for the lower range of values, and a large gap in data before the upper range occurs (i.e. cemented coquina from Heritage Parkway). If additional tests are conducted they should be in soils that have unit weights between 115 and 125 pcf to improve these correlations.

Table 6.14: Correlation Coefficients, γ_{dry} versus p_L, All Sites

Relationship x	Relationship y	R^2	Model	# of Tests	Figure
			SDPMT-6 Incremental		
Linear	Linear	0.69	γ_{dry}=0.01997 p_L +109	35	E.41
Linear	Log10	0.67	$\log_{10}(\gamma_{dry})$=7.401E-05 p_L +2.037	35	E.233
Log10	Linear	0.87	γ_{dry}=15.12 $\log_{10}(p_L)$ +83.73	35	E.137
Log10	Log10	0.86	$\log_{10}(\gamma_{dry})$=0.05628 $\log_{10}(p_L)$ +1.943	35	E.329
Exponential Model		0.86	γ_{dry}=88.17 $(p_L)^{0.05519}$	35	E.425
			SDPMT-6 Continuous		
Linear	Linear	0.73	γ_{dry}=0.05315 p_L +106.6	33	E.42
Linear	Log10	0.71	$\log_{10}(\gamma_{dry})$=0.0001973 p_L +2.028	33	E.234
Log10	Linear	0.61	γ_{dry}=15.98 $\log_{10}(p_L)$ +83.7	33	E.138
Log10	Log10	0.59	$\log_{10}(\gamma_{dry})$=0.05893 $\log_{10}(p_L)$ +1.944	33	E.330
Exponential Model		0.63	γ_{dry}=86.98 $(p_L)^{0.06141}$	33	E.426
			SDPMT-12 Incremental		
Linear	Linear	0.74	γ_{dry}=0.05469 p_L +107.4	46	E.43
Linear	Log10	0.73	$\log_{10}(\gamma_{dry})$=0.0002021 p_L +2.031	46	E.235
Log10	Linear	0.86	γ_{dry}=20 $\log_{10}(p_L)$ +76.54	46	E.139
Log10	Log10	0.85	$\log_{10}(\gamma_{dry})$=0.07429 $\log_{10}(p_L)$ +1.917	46	E.331
Exponential Model		0.86	γ_{dry}=82.69 $(p_L)^{0.07391}$	46	E.427
			SDPMT-12 Continuous		
Linear	Linear	0.78	γ_{dry}=0.049 p_L +107.6	40	E.44
Linear	Log10	0.76	$\log_{10}(\gamma_{dry})$=0.0001805 p_L +2.032	40	E.236
Log10	Linear	0.71	γ_{dry}=16.07 $\log_{10}(p_L)$ +84.36	40	E.140
Log10	Log10	0.70	$\log_{10}(\gamma_{dry})$=0.05913 $\log_{10}(p_L)$ +1.947	40	E.332
Exponential Model		0.73	γ_{dry}=87.9 $(p_L)^{0.06067}$	40	E.428

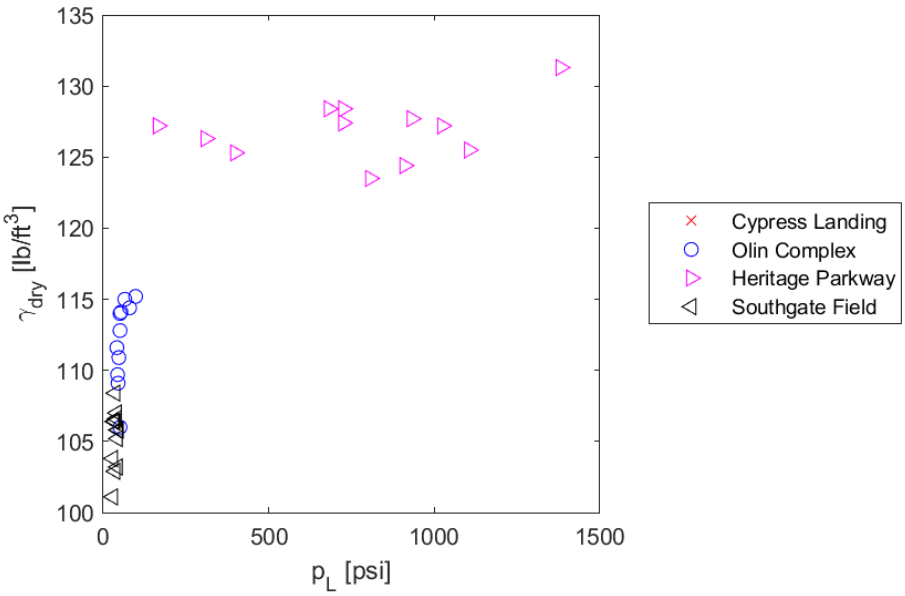

Figure 6.83: SDPMT-6 Incremental, γ_{dry} versus p_L, All Sites

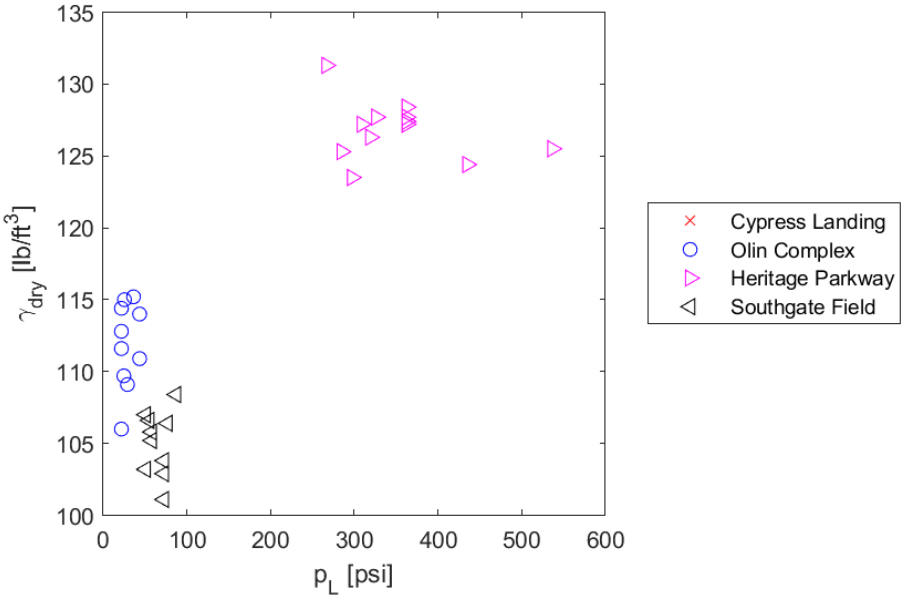

Figure 6.84: SDPMT-6 Continuous, γ_{dry} versus p_L, All Sites

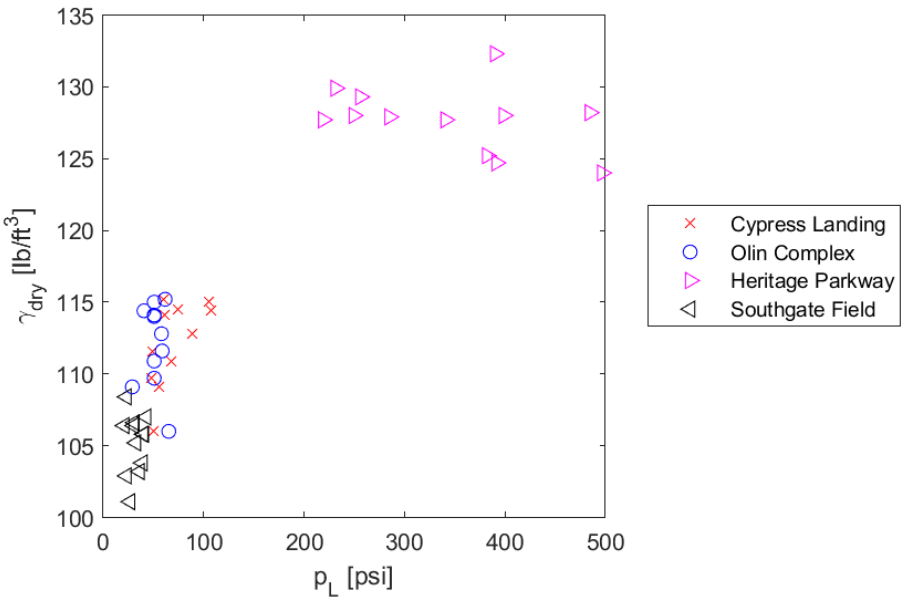

Figure 6.85: SDPMT-12 Incremental, γ_{dry} versus p_L, All Sites

6.6.1.3 SDPMT-12 Incremental Comparisons

Table 6.14 shows the five regression models developed from SDPMT-12 incremental data. Figure 6.85 shows the data used to develop the models. Again, there are gaps in both unit weight and p_L values. The models produced R^2 values ranging from 0.73 to 0.86, based on 46 data points. Three of the five models produced $R^2 > 0.85$. They were the log-linear, log-log, and exponential models. The log-log model produced R^2 of 0.85, and described by Equation 6.48 and shown in Figure E.331. This model shows good agreement with the data. The log-linear and exponential models both produced R^2 of 0.86. The log-linear model shows good agreement with the data (see Figure E.139) and is described by Equation 6.49. The exponential model also produced an R^2 value of 0.86 as shown in Figure E.427 and described by Equation 6.50. This model shows a relatively good agreement when p_L is below 150 psi and its data generally follows the shape of the equation at higher values of p_L.

$$\log_{10}(\gamma_{dry}) = 0.07429 \log_{10}(p_L) + 1.917 \tag{6.48}$$

$$\gamma_{dry} = 20 \log_{10}(p_L) + 76.54 \tag{6.49}$$

$$\gamma_{dry} = 82.69(p_L)^{0.07391} \tag{6.50}$$

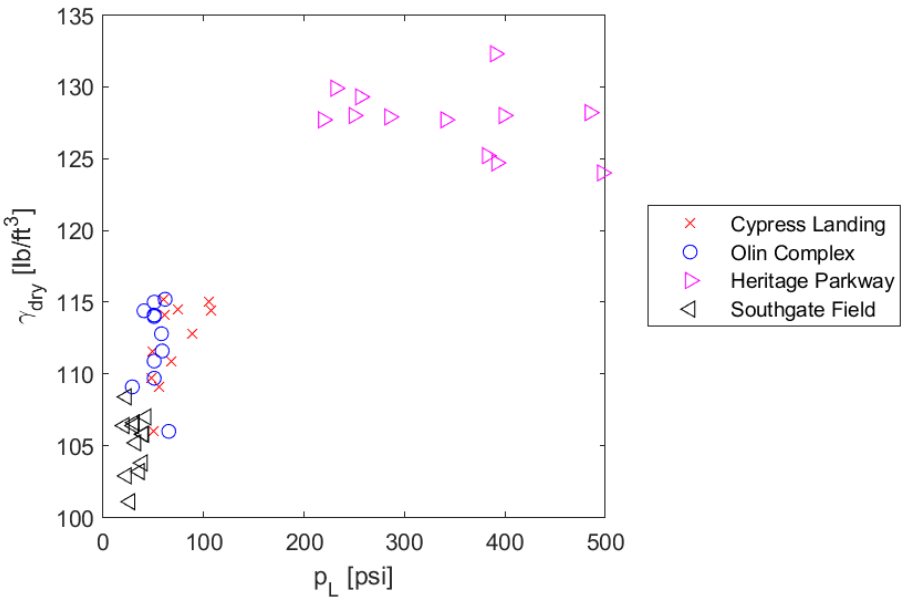

Figure 6.86: SDPMT-12 Continuous, γ_{dry} versus p_L, All Sites

6.6.1.4 SDPMT-12 Continuous Comparisons

Table 6.14 shows the five regression models developed from SDPMT-12 continuous data. Figure 6.86 shows the data used to develop the models. The models produced R^2 values ranging from 0.70 to 0.78, based on 40 data points. Although the linear-linear and linear-log models produced the two highest R^2 values 0.78 and 0.76, both of these models do not have good agreement below 100 psi; see Figures E.43 and E.235. The other three models visually fit the dataset better. For the SDPMT-12 continuous data, there is a large variation in the data; making a reliable correlation with the models difficult.

6.6.1.5 Summary of γ_{dry} versus p_L Regression Models

There are gaps between the lower and higher dry unit weights and the corresponding lower and higher p_L values, that can affect the analyses. Additional data within this range should be added to validate and improve these correlations. The nonlinear nature of this data can best be modeled using log-linear models.

6.6.2 Zorn E_d versus SDPMT p_L

Twenty $E_{d,Zorn}$ versus p_L regression models were evaluated. Between 33 and 46 sets of data were analyzed, producing R^2 values from 0.64 to 0.93. The R^2 values from all four types of tests were similar. The results are summarized in Table 6.15.

Table 6.15: Correlation Coefficients, $E_{d,Zorn}$ versus p_L, All Sites

Relationship x	Relationship y	R^2	Model	# of Tests	Figure
			SDPMT-6 Incremental		
Linear	Linear	0.79	$E_{d,Zorn}$=16.3 p_L +2.362E+04	35	E.65
Linear	Log10	0.69	$\log_{10}(E_{d,Zorn})$=0.0001238 p_L +4.32	35	E.257
Log10	Linear	0.93	$E_{d,Zorn}$=8.185E+04 $\log_{10}(p_L)$ -1.803E+05	35	E.161
Log10	Log10	0.86	$\log_{10}(E_{d,Zorn})$=0.6401 $\log_{10}(p_L)$ +2.717	35	E.353
Exponential Model		0.88	$E_{d,Zorn}$=1540 $(p_L)^{0.5066}$	35	E.449
			SDPMT-6 Continuous		
Linear	Linear	0.88	$E_{d,Zorn}$=44.6 p_L +9696	33	E.66
Linear	Log10	0.75	$\log_{10}(E_{d,Zorn})$=0.0003378 p_L +4.212	33	E.258
Log10	Linear	0.76	$E_{d,Zorn}$=9.409E+04 $\log_{10}(p_L)$ -2.052E+05	33	E.162
Log10	Log10	0.61	$\log_{10}(E_{d,Zorn})$=0.6857 $\log_{10}(p_L)$ +2.66	33	E.354
Exponential Model		0.88	$E_{d,Zorn}$=211.5 $(p_L)^{0.8124}$	33	E.450
			SDPMT-12 Incremental		
Linear	Linear	0.83	$E_{d,Zorn}$=43.01 p_L +1.276E+04	46	E.67
Linear	Log10	0.71	$\log_{10}(E_{d,Zorn})$=0.000332 p_L +4.248	46	E.259
Log10	Linear	0.86	$E_{d,Zorn}$=1.022E+05 $\log_{10}(p_L)$ -2.287E+05	46	E.163
Log10	Log10	0.80	$\log_{10}(E_{d,Zorn})$=0.8245 $\log_{10}(p_L)$ +2.288	46	E.355
Exponential Model		0.86	$E_{d,Zorn}$=438.5 $(p_L)^{0.7182}$	46	E.451
			SDPMT-12 Continuous		
Linear	Linear	0.88	$E_{d,Zorn}$=38.48 p_L +1.462E+04	40	E.68
Linear	Log10	0.74	$\log_{10}(E_{d,Zorn})$=0.0002845 p_L +4.28	40	E.260
Log10	Linear	0.79	$E_{d,Zorn}$=8.578E+04 $\log_{10}(p_L)$ -1.807E+05	40	E.164
Log10	Log10	0.64	$\log_{10}(E_{d,Zorn})$=0.6229 $\log_{10}(p_L)$ +2.866	40	E.356
Exponential Model		0.88	$E_{d,Zorn}$=453.4 $(p_L)^{0.7057}$	40	E.452

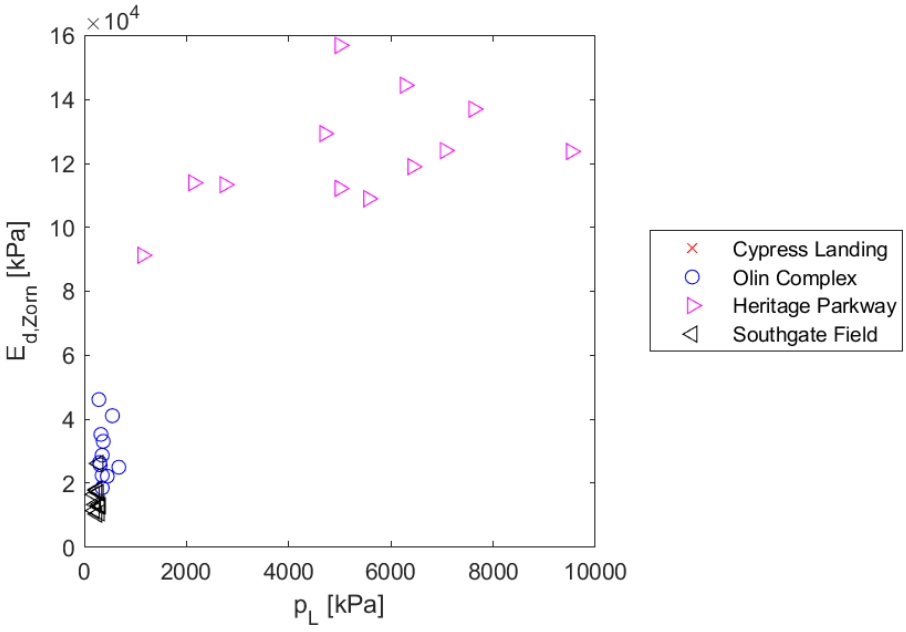

Figure 6.87: SDPMT-6 Incremental, $E_{d,Zorn}$ versus p_L, All Sites

6.6.2.1 SDPMT-6 Incremental Comparisons

Table 6.15 shows the five regression models developed from SDPMT-6 incremental data. Figure 6.87 shows the data, which has a nonlinear type relationship, used to develop the models. The gaps in Zorn stiffnesses exist between 5 and 9 kPa and may affect the analyses. The models developed produced R^2 values ranging from 0.69 to 0.93, based on 35 data points. The proposed log-linear model, shown in Figure E.161, produced the highest R^2 of 0.93 and is described by Equation 6.51. The log-linear model produced a strong relationship between p_L from SDPMT-6 incremental tests and $E_{d,Zorn}$.

$$E_{d,Zorn} = 25.34 \log_{10}(E_0) - 52.98 \tag{6.51}$$

6.6.2.2 SDPMT-6 Continuous Comparisons

Table 6.15 shows the five regression models developed from SDPMT-6 continuous data. Figure 6.88 shows the data used to develop the models. It has significant scatter at the lower boundaries and a nonlinear type relationship. The models produced R^2 values ranging from 0.61 to 0.88, based on 33 data points. Both the linear-linear and exponential models produced R^2 of 0.88. Figure E.66 shows the linear-linear model, which is described by Equation 6.52. The exponential model, is described by Equation 6.53 and shown in Figure E.450. Both of these SDPMT-6 continuous test data models show strong agreement with the data.

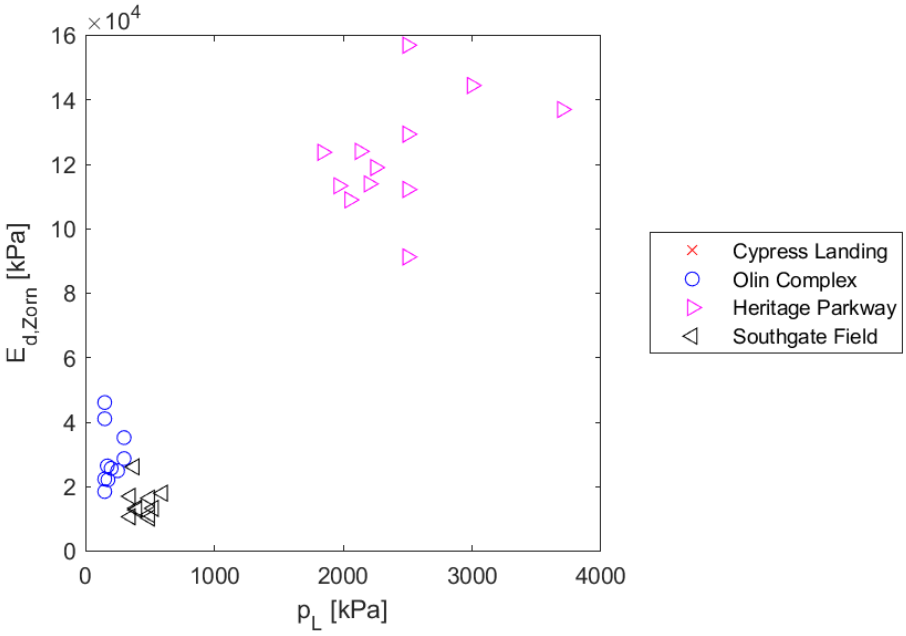

Figure 6.88: SDPMT-6 Continuous, $E_{d,Zorn}$ versus p_L, All Sites

$$E_{d,Zorn} = 44.6p_L + 9696 \tag{6.52}$$

$$E_{d,Zorn} = 211.5(p_L)^{0.8124} \tag{6.53}$$

6.6.2.3 SDPMT-12 Incremental Comparisons

Table 6.15 shows the five regression models developed from SDPMT-12 incremental data. Figure 6.89 shows the data used to develop the models. It displays a nonlinear type relationship and scatter in the upper ranges. The models produced R^2 values ranging from 0.71 to 0.86, from 46 data points. Four of the five models produced R^2 values over 0.80, indicating good agreement between the models and the data. The two models that produced the highest R^2 of 0.86 were the log-linear and exponential models. Figure E.163 shows the log-linear model, which is described by Equation 6.54. The exponential model is described by Equation 6.55 and shown in Figure E.451. The log-linear and exponential SDPMT-12 incremental models, produced strong correlations with the data.

$$E_{d,Zorn} = 1.022 \times 10^5 p_L + 2.278 \times 10^5 \tag{6.54}$$

$$E_{d,Zorn} = 438.5(E_0)^{0.7182} \tag{6.55}$$

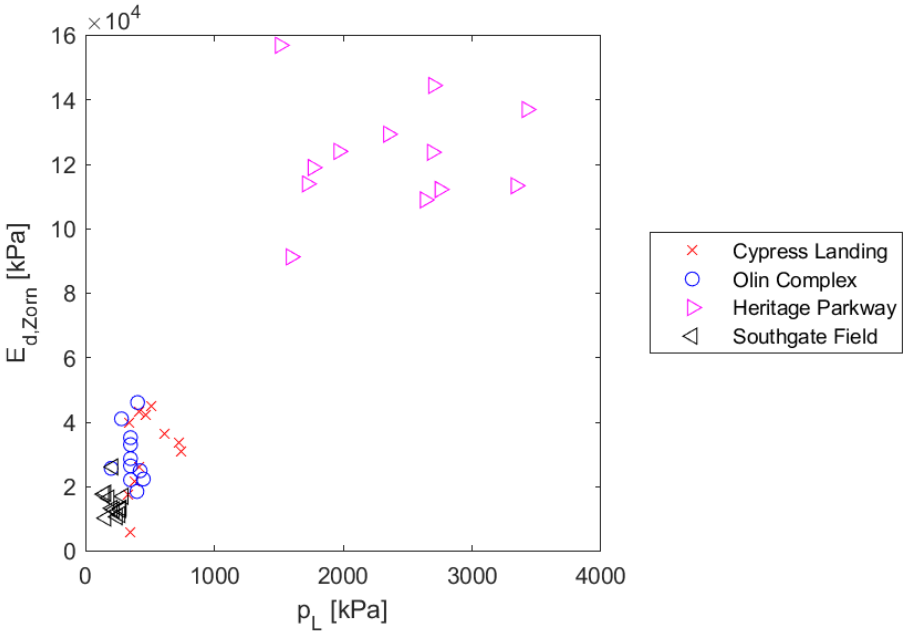

Figure 6.89: SDPMT-12 Incremental, $E_{d,Zorn}$ versus p_L, All Sites

6.6.2.4 SDPMT-12 Continuous Comparisons

Table 6.15 shows the five regression models developed from SDPMT-12 continuous data. Figure 6.90 shows the data used to develop the models. Again, this figure displays a nonlinear type relationship and scatter in the upper ranges. The models developed produced R^2 values ranging from 0.64 to 0.88, using 40 data points. Two of the five models produced R^2 values of 0.88, the linear-linear and exponential models. The linear-linear model is described by Equation 6.56 and shown in Figure E.68. The exponential model is shown in Figure E.452 and expressed by Equation 6.57. The linear-linear and exponential models produced strong correlations from the data.

$$E_{d,Zorn} = 38.48 p_L + 1.462 \times 10^4 \tag{6.56}$$

$$E_{d,Zorn} = 453.4 (E_0)^{0.7057} \tag{6.57}$$

6.6.2.5 Summary of $E_{d,Zorn}$ versus p_L Regression Models

The developed models shows good agreement with the test data, with the linear-linear and exponential models producing the strongest correlations. The gaps in the data should be addressed to strengthen these models. Testing should include E_d values ranging from 60,000 to 100,000 kPa.

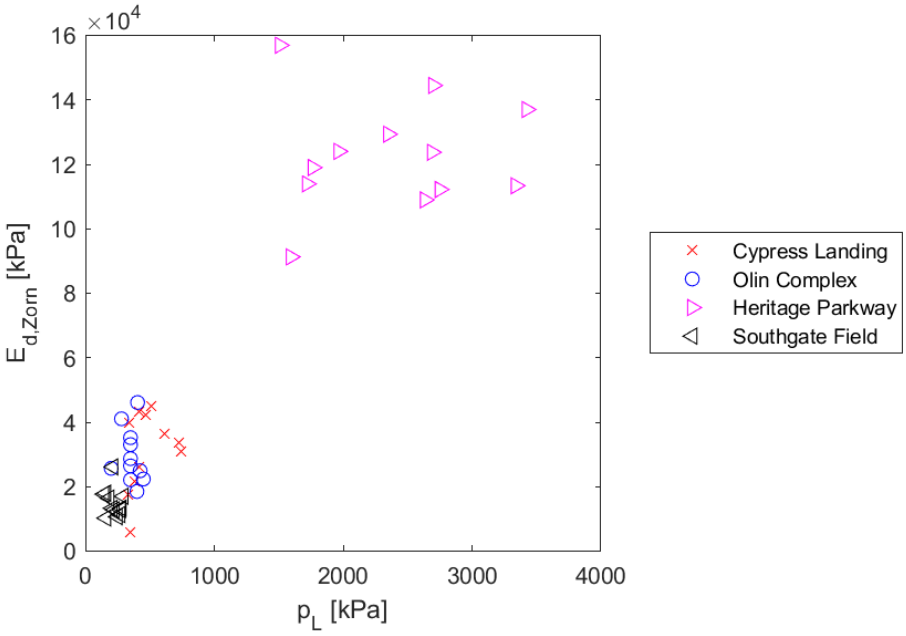

Figure 6.90: SDPMT-12 Continuous, $E_{d,Zorn}$ versus p_L, All Sites

6.6.3 Dynatest E_0 versus SDPMT p_L

Twenty $E_{0,Dynatest}$ versus p_L regression models were evaluated. Between 33 and 44 sets of data were analyzed, producing R^2 values from 0.61 to 0.93. In general, the correlations show promise, with nearly all R^2 values exceeding 0.70. The results are summarized in Table 6.16.

6.6.3.1 SDPMT-6 Incremental Comparisons

Table 6.16 shows the five regression models developed from SDPMT-6 incremental data. Figure 6.91 shows the data used to develop the models. There is a gap in moduli between 2 and 4 kPa, but the gap is not as pronounced as the one from the Zorn LWD testing. The models produced R^2 values ranging from 0.75 to 0.86, from 33 data points. Four of the five models had $R^2 \geq 0.85$. The linear-linear and log-linear models both produced an R^2 value of 0.84. They are described by Equation 6.58 and 6.59 respectively. The log-log and exponential models both produced R^2 values of 0.86, and are described by Equations 6.60 and 6.61 respectively.

Table 6.16: Correlation Coefficients, $E_{0,Dynatest}$ versus p_L, All Sites

Relationship x	Relationship y	R^2	Model	# of Tests	Figure
			SDPMT-6 Incremental		
Linear	Linear	0.84	$E_{0,Dynatest}$=132 p_L +7.556E+04	33	E.77
Linear	Log10	0.75	$\log_{10}(E_{0,Dynatest})$=0.0001573 p_L +4.942	33	E.269
Log10	Linear	0.84	$E_{0,Dynatest}$=6.118E+05 $\log_{10}(p_L)$ -1.43E+06	33	E.173
Log10	Log10	0.86	$\log_{10}(E_{0,Dynatest})$=0.7843 $\log_{10}(p_L)$ +2.987	33	E.365
Exponential Model		0.86	$E_{0,Dynatest}$=2132 $(p_L)^{0.6933}$	33	E.461
			SDPMT-6 Continuous		
Linear	Linear	0.82	$E_{0,Dynatest}$=343.3 p_L -2.426E+04	31	E.78
Linear	Log10	0.78	$\log_{10}(E_{0,Dynatest})$=0.0004219 p_L +4.809	31	E.270
Log10	Linear	0.68	$E_{0,Dynatest}$=7.305E+05 $\log_{10}(p_L)$ -1.704E+06	31	E.174
Log10	Log10	0.65	$\log_{10}(E_{0,Dynatest})$=0.9007 $\log_{10}(p_L)$ +2.736	31	E.366
Exponential Model		0.83	$E_{0,Dynatest}$=39.42 $(p_L)^{1.273}$	31	E.462
			SDPMT-12 Incremental		
Linear	Linear	0.76	$E_{0,Dynatest}$=326.2 p_L -6571	44	E.79
Linear	Log10	0.74	$\log_{10}(E_{0,Dynatest})$=0.0004308 p_L +4.779	44	E.271
Log10	Linear	0.70	$E_{0,Dynatest}$=7.334E+05 $\log_{10}(p_L)$ -1.72E+06	44	E.175
Log10	Log10	0.74	$\log_{10}(E_{0,Dynatest})$=1.007 $\log_{10}(p_L)$ +2.411	44	E.367
Exponential Model		0.76	$E_{0,Dynatest}$=396.5 $(p_L)^{0.9735}$	44	E.463
			SDPMT-12 Continuous		
Linear	Linear	0.74	$E_{0,Dynatest}$=282.1 p_L +1.786E+04	38	E.80
Linear	Log10	0.76	$\log_{10}(E_{0,Dynatest})$=0.0003657 p_L +4.841	38	E.272
Log10	Linear	0.67	$E_{0,Dynatest}$=6.554E+05 $\log_{10}(p_L)$ -1.495E+06	38	E.176
Log10	Log10	0.67	$\log_{10}(E_{0,Dynatest})$=0.8398 $\log_{10}(p_L)$ +2.907	38	E.368
Exponential Model		0.74	$E_{0,Dynatest}$=576.1 $(p_L)^{0.9128}$	38	E.464

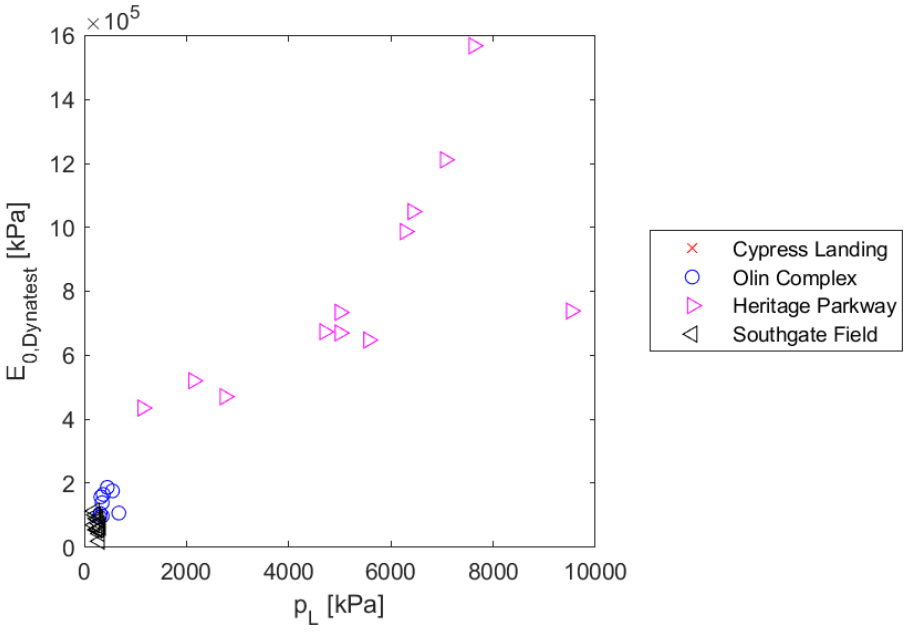

Figure 6.91: SDPMT-6 Incremental, $E_{0,Dynatest}$ versus p_L, All Sites

$$E_{0,Dynatest} = 132pL + 7.556 \times 10^4 \tag{6.58}$$

$$E_{0,Dynatest} = 6.118 \times 10^5 \log_{10}(p_L) - 1.43 \times 10^6 \tag{6.59}$$

$$\log_{10}(E_{0,Dynatest}) = 0.7843 \log_{10}(p_L) + 2.987 \times 10^6 \tag{6.60}$$

$$E_{0,Dynatest} = 2132 p_L^{0.6933} \tag{6.61}$$

6.6.3.2 SDPMT-6 Continuous Comparisons

Table 6.16 shows the five regression models developed from SDPMT-6 continuous data. Figure 6.92 shows the data used to develop the models. The models produced R^2 values ranging from 0.65 to 0.83, from 31 data points. Two models produced R^2 values greater than 0.80. The linear-linear model produced R^2 of 0.82 as shown in Figure E.78, and described by Equation 6.62. The exponential model produced R^2 of 0.83 as described by Equation 6.63 and shown in Figure E.462. Both models show promise as their trends fit the corresponding data fairly well.

$$E_{0,Dynatest} = 343.3 p_L + 2.426 \times 10^4 \tag{6.62}$$

$$E_{0,Dynatest} = 39.42 (p_L)^{1.273} \tag{6.63}$$

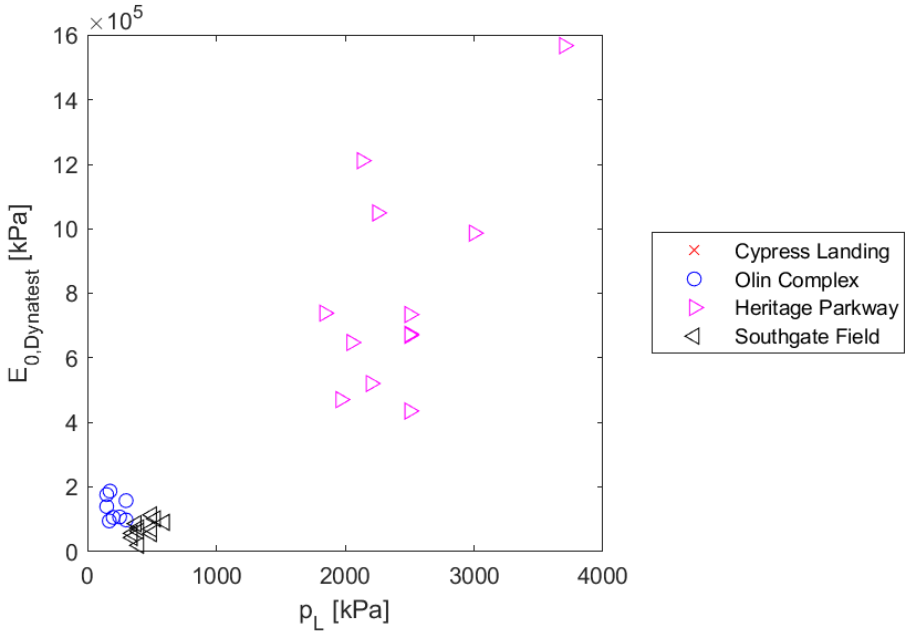

Figure 6.92: SDPMT-6 Continuous, $E_{0,Dynatest}$ versus p_L, All Sites

6.6.3.3 SDPMT-12 Incremental Comparisons

Table 6.16 shows the five regression models developed from SDPMT-12 incremental data. Figure 6.93 shows the data used to develop the models. Gaps in stiffnesses range from 2 to 4 kPa and gaps in p_L ranged from about 800 to 1,700 kPa. The models produced R^2 values ranging from 0.70 to 0.76, based on 44 data points. All five models show a general agreement with the data. Additional data from tests in medium-dense materials would help validate the models.

6.6.3.4 SDPMT-12 Continuous Comparisons

Table 6.16 shows the five regression models developed from SDPMT-12 continuous data. Figure 6.94 shows the data used to develop the models. The models produced R^2 values ranging from 0.67 to 0.76, based on 38 data points. All five models produced $R^2 \geq 0.70$. The linear-linear and exponential models both produced R^2 values of 0.74, these models are described by Equations 6.64 and 6.65 respectively. Figures E.80 and E.464 show the data and the linear-linear and exponential models respectively. The log-linear model produced the best R^2 from the SDPMT-12 incremental data, and is described by Equation 6.66 and shown in Figure E.272.

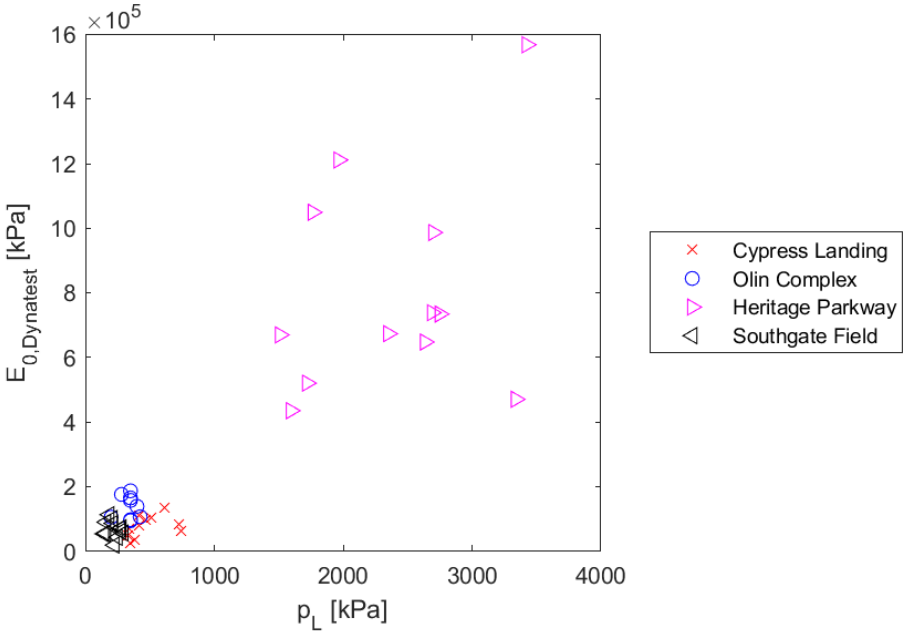

Figure 6.93: SDPMT-12 Incremental, $E_{0,Dynatest}$ versus p_L, All Sites

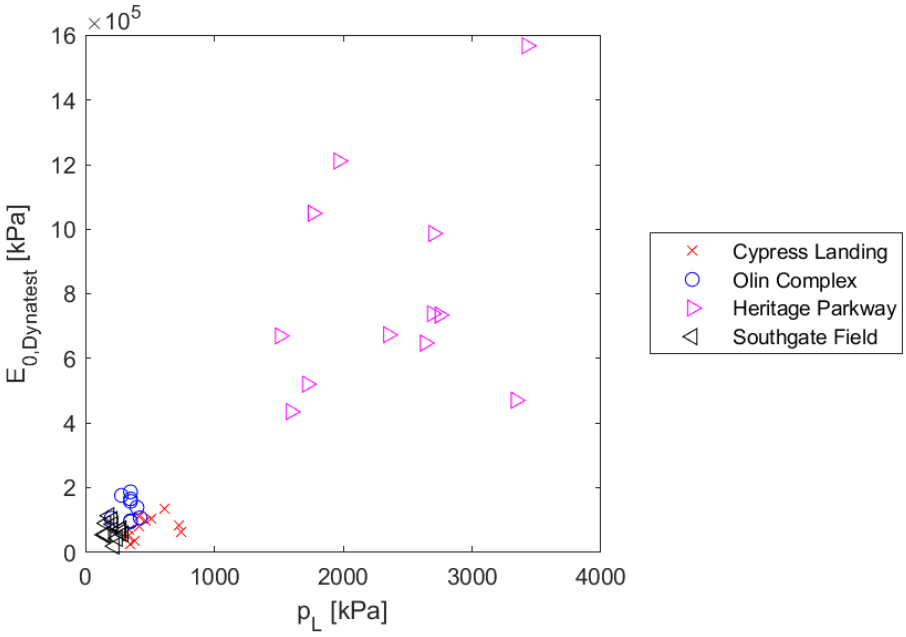

Figure 6.94: SDPMT-12 Continuous, $E_{0,Dynatest}$ versus p_L, All Sites

$$E_{0,Dynatest} = 212.1 p_L - 1.786 \times 10^4 \quad (6.64)$$

$$E_{0,Dynatest} = 576.1 (E_0)^{0.9128} \quad (6.65)$$

$$\log_{10}(E_{0,Dynatest}) = 0.0003657 p_L + 4.841 \quad (6.66)$$

6.6.3.5 Summary of $E_{0,Dynatest}$ versus p_L Regression Models

There is good general agreement with both probe sizes and test types between E_0 of the Dynatest LWD device and the SDPMT p_L. In general, there seems to be good agreement between the linear-linear and exponential models and the data. Additional tests in soil where the SDPMT p_L ranges from 1,000 to 2,000 kPa would help validate the models as there are some gaps in the data.

6.6.4 CIV versus SDPMT p_L

Twenty CIV versus p_L regression models were evaluated. Between 33 and 46 sets of data were analyzed, producing R^2 values from 0.52 to 0.90. The linear-linear regressions produced the most consistent R^2 values, ranging from 0.77 to 0.82. The results are summarized in Table 6.17.

6.6.4.1 SDPMT-6 Incremental Comparisons

Table 6.17 shows the five regression models developed from SDPMT-6 incremental data. Figure 6.95 shows the data used to develop them. They produced R^2 values ranging from 0.67 to 0.90, based on 35 data points. The log-linear model (Figure E.185) produced the highest R^2 of 0.90 and is described by Equation 6.67. The log-linear model produced a strong relationship between p_L from SDPMT-6 incremental tests and CIV.

$$CIV = 25.34 \log_{10}(E_0) - 52.98 \quad (6.67)$$

6.6.4.2 SDPMT-6 Continuous Comparisons

Table 6.17 shows the five regression models developed from SDPMT-6 continuous data. Figure 6.96 shows the data used to develop them. An obvious gap in p_L exists between 800 and 2,000 kPa. The models produced R^2 values ranging from 0.52 to 0.79, based on 33 data points. The linear-linear model produced the highest R^2 value of 0.79 as shown in Figure E.90, and as described by Equation 6.68.

$$CIV = 0.01332 E_0 + 6.321 \quad (6.68)$$

Table 6.17: Correlation Coefficients, CIV versus p_L, All Sites

Relationship x	Relationship y	R^2	Model	# of Tests	Figure
			SDPMT-6 Incremental		
Linear	Linear	0.78	CIV=0.005103 p_L +10.06	35	E.89
Linear	Log10	0.67	$\log_{10}$(CIV)=0.000104 p_L +0.9657	35	E.281
Log10	Linear	0.90	CIV=25.34 $\log_{10}(p_L)$ -52.98	35	E.185
Log10	Log10	0.83	$\log_{10}$(CIV)=0.5372 $\log_{10}(p_L)$ -0.3789	35	E.377
Exponential Model		0.87	CIV=0.8335 $(p_L)^{0.4515}$	35	E.473
			SDPMT-6 Continuous		
Linear	Linear	0.79	CIV=0.01332 p_L +6.321	33	E.90
Linear	Log10	0.69	$\log_{10}$(CIV)=0.0002738 p_L +0.8855	33	E.282
Log10	Linear	0.65	CIV=27.35 $\log_{10}(p_L)$ -55.73	33	E.186
Log10	Log10	0.52	$\log_{10}$(CIV)=0.5374 $\log_{10}(p_L)$ -0.3208	33	E.378
Exponential Model		0.77	CIV=0.1949 $(p_L)^{0.6803}$	33	E.474
			SDPMT-12 Incremental		
Linear	Linear	0.80	CIV=0.01376 p_L +5.252	46	E.91
Linear	Log10	0.73	$\log_{10}$(CIV)=0.0002958 p_L +0.8433	46	E.283
Log10	Linear	0.79	CIV=31.98 $\log_{10}(p_L)$ -70.01	46	E.187
Log10	Log10	0.76	$\log_{10}$(CIV)=0.7081 $\log_{10}(p_L)$ -0.831	46	E.379
Exponential Model		0.82	CIV=0.1832 $(p_L)^{0.6882}$	46	E.475
			SDPMT-12 Continuous		
Linear	Linear	0.79	CIV=0.01176 p_L +6.811	40	E.92
Linear	Log10	0.71	$\log_{10}$(CIV)=0.0002447 p_L +0.8947	40	E.284
Log10	Linear	0.68	CIV=25.77 $\log_{10}(p_L)$ -51.67	40	E.188
Log10	Log10	0.58	$\log_{10}$(CIV)=0.5214 $\log_{10}(p_L)$ -0.2815	40	E.380
Exponential Model		0.78	CIV=0.2906 $(p_L)^{0.6199}$	40	E.476

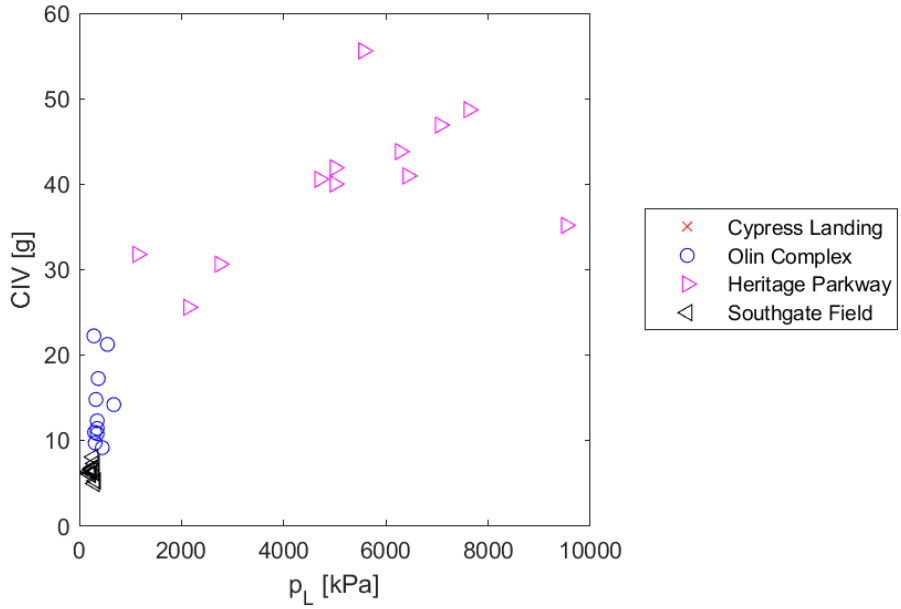

Figure 6.95: SDPMT-6 Incremental, CIV versus p_L, All Sites

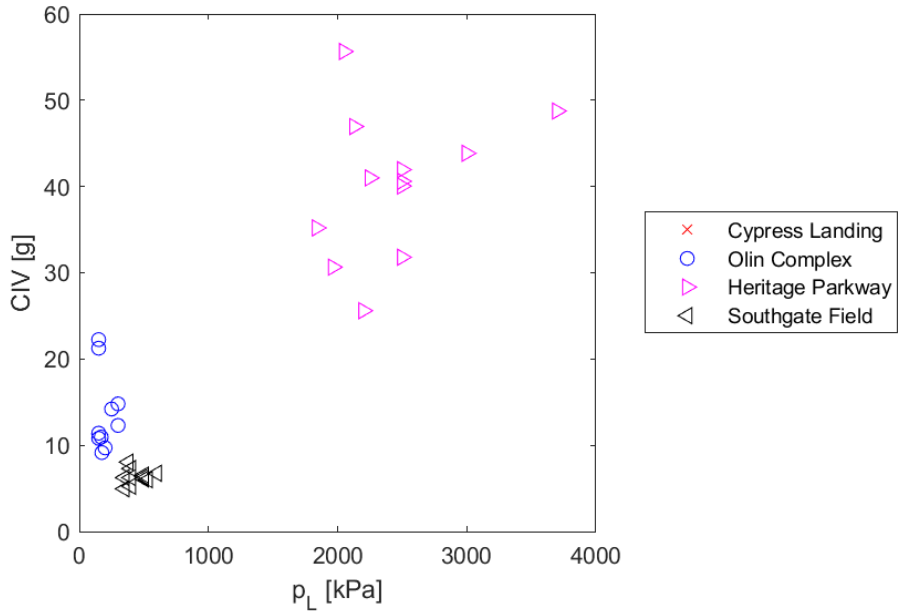

Figure 6.96: SDPMT-6 Continuous, CIV versus p_L, All Sites

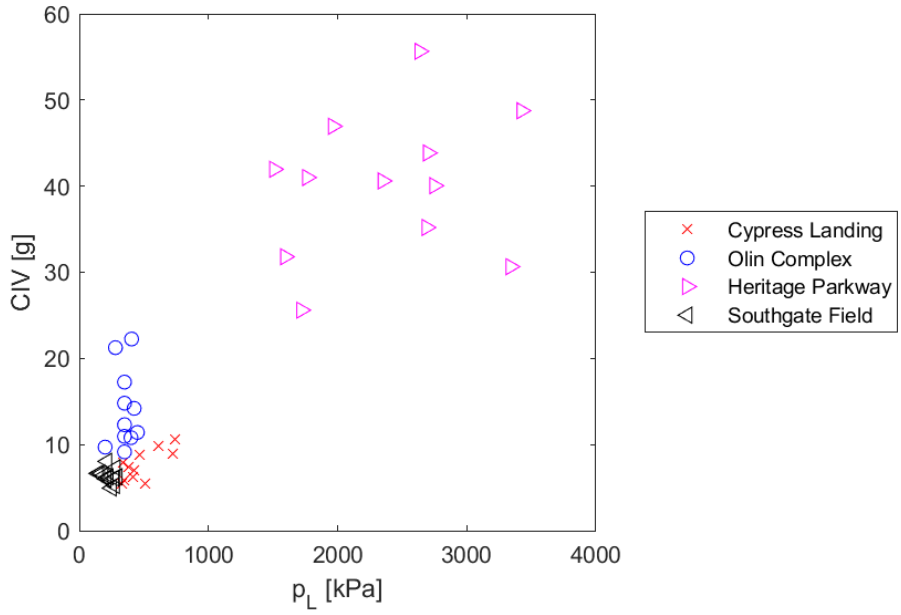

Figure 6.97: SDPMT-12 Incremental, CIV versus p_L, All Sites

6.6.4.3 SDPMT-12 Incremental Comparisons

Table 6.17 shows the five regression models developed from SDPMT-12 incremental data. Figure 6.97 shows the data used to develop these models. The gap in p_L between 800 and 2,000 kPa again exists. These models produced R^2 values ranging from 0.73 to 0.82, based on 46 data points. Two of the five models produced $R^2 \geq 0.8$. The linear-linear model described by Equation 6.69 (see Figure E.91) produced R^2 of 0.80 and shows good agreement with the data. There does seem to be some discrepancy between the equation and the data at the lower bounds of the model. The exponential model described by Equation 6.70 produced R^2 of 0.82 and indicates good agreement between the model and data, as shown in Figure E.475.

$$CIV = 0.01376E_0 + 5.252 \tag{6.69}$$

$$CIV = 0.1832(E_0)^{0.6882} \tag{6.70}$$

6.6.4.4 SDPMT-12 Continuous Comparisons

Table 6.17 shows the five regression models developed from SDPMT-12 continuous data. Figure 6.98 shows the data used to develop the models. The same gap in p_L exists between 800 and 2,000 kPa. The models produced R^2 values ranging from 0.58 to 0.79, based on 40 data points. Two of the five models produced $R^2 \geq 0.75$, indicating relatively good agreement between the data and model. The exponential model

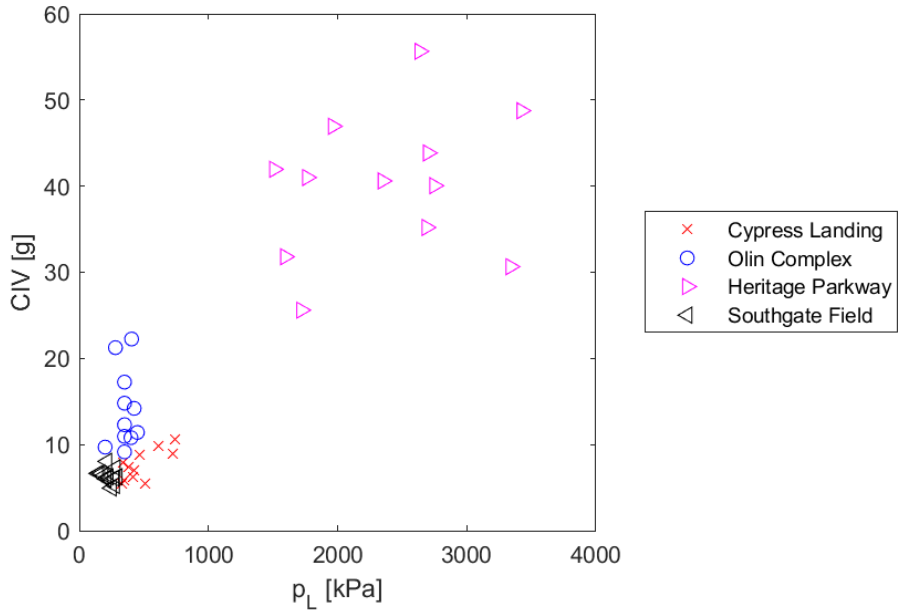

Figure 6.98: SDPMT-12 Continuous, CIV versus p_L, All Sites

described by Equation 6.71 produced R^2 of 0.78. Figure E.476 shows that there is good agreement between this model and the data. The linear-linear model, described by Equation 6.72 produced R^2 of 0.79. Correspondingly, Figure E.92 shows there is good agreement between the data and this linear-linear model.

$$CIV = 0.1309(E_0)^{0.5161} \tag{6.71}$$

$$CIV = 0.01176 p_L + 6.811 \tag{6.72}$$

6.6.4.5 Summary of CIV versus p_L Regression Models

Additional tests in subgrade soils with the SDPMT probes would help to fill in the gaps in the model data. The general trend of the relationship between CIV and p_L is either a positive linear one or an exponential one. Additional test data in the range of 1,000 to 2,000 kPa for p_L would strengthen the models.

6.6.5 DCP Penetration Index vs SDPMT p_L

Twenty DCP PI versus p_L regression models were evaluated. Between 21 and 34 sets of data were analyzed, producing R^2 values from 0.10 to 0.64. The results are summarized in Table 6.18.

Higher DCP PI values correspond to softer soils; therefore, an inverse relationship is expected from these correlations. The high strength and density of the cemented

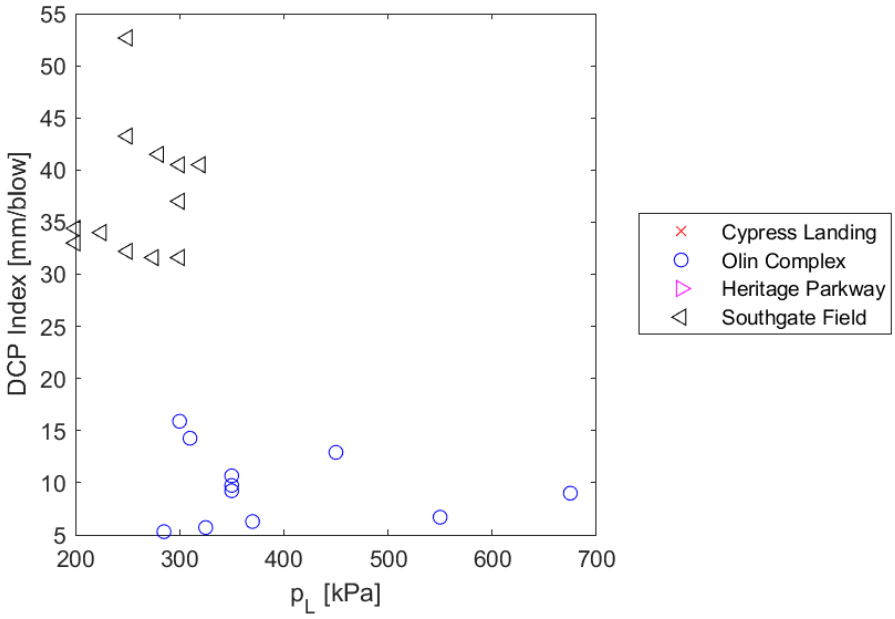

Figure 6.99: SDPMT-6 Incremental, DCP PI versus p_L, All Sites

coquina base would have damaged the DCP; therefore, no DCP tests were conducted at Heritage Parkway, and they were not used in these comparisons. As a result, only DCP data from subgrade sands were evaluated, limiting the type of soils evaluated. Due to construction logistics, SDPMT-6 tests were unable to be conducted at Cypress Landing, and consequently, were not used in the development of the E_0 SDPMT-6 and DCP PI models.

6.6.5.1 SDPMT-6 Incremental Comparisons

Table 6.18 shows the five regression models developed from SDPMT-6 incremental test data. Figure 6.99 shows the data used to develop the models. The models produced R^2 values ranging from 0.34 to 0.40, based on 23 data points. These models show signs of a correlation between p_L and the DCP PI, but there is a high degree of variability. Collecting additional data could strengthen these correlations.

6.6.5.2 SDPMT-6 Continuous Comparisons

Table 6.18 shows the five regression models developed from SDPMT-6 continuous test data. Figure 6.100 shows the data used to develop the models. The models produced R^2 values ranging from 0.62 to 0.67, based on 21 data points. However, this relationship can not be realistic, because the plot shows DCP PI increasing with p_L values. This plot highlights the need for additional data to improve this relationship.

Table 6.18: Correlation Coefficients, DCP PI versus p_L, All Sites

Relationship x	Relationship y	R^2	Model	# of Tests	Figure
			SDPMT-6 Incremental		
Linear	Linear	0.34	DCP PI=-0.08126 p_L +50.63	23	E.53
Linear	Log10	0.34	$\log_{10}$(DCP PI)=-0.001799 p_L +1.86	23	E.245
Log10	Linear	0.39	DCP PI=-76.45 $\log_{10}(p_L)$ +214.8	23	E.149
Log10	Log10	0.40	$\log_{10}$(DCP PI)=-1.698 $\log_{10}(p_L)$ +5.509	23	E.341
Exponential Model		0.39	DCP PI=9.232E+04 $(p_L)^{-1.448}$	23	E.437
			SDPMT-6 Continuous		
Linear	Linear	0.64	DCP PI=0.0776 p_L -1.754	21	E.54
Linear	Log10	0.62	$\log_{10}$(DCP PI)=0.001745 p_L +0.7044	21	E.246
Log10	Linear	0.67	DCP PI=55.02 $\log_{10}(p_L)$ -112.2	21	E.150
Log10	Log10	0.65	$\log_{10}$(DCP PI)=1.233 $\log_{10}(p_L)$ -1.77	21	E.342
Exponential Model		0.64	DCP PI=0.07144 $(p_L)^{1.004}$	21	E.438
			SDPMT-12 Incremental		
Linear	Linear	0.19	DCP PI=-0.03117 p_L +31	34	E.55
Linear	Log10	0.10	$\log_{10}$(DCP PI)=-0.0006036 p_L +1.443	34	E.247
Log10	Linear	0.29	DCP PI=-31.92 $\log_{10}(p_L)$ +100.2	34	E.151
Log10	Log10	0.17	$\log_{10}$(DCP PI)=-0.6491 $\log_{10}(p_L)$ +2.861	34	E.343
Exponential Model		0.36	DCP PI=2052 $(p_L)^{-0.8109}$	34	E.439
			SDPMT-12 Continuous		
Linear	Linear	0.13	DCP PI=0.02312 p_L +11.78	28	E.56
Linear	Log10	0.18	$\log_{10}$(DCP PI)=0.000792 p_L +0.9548	28	E.248
Log10	Linear	0.20	DCP PI=21.43 $\log_{10}(p_L)$ -33.41	28	E.152
Log10	Log10	0.26	$\log_{10}$(DCP PI)=0.6949 $\log_{10}(p_L)$ -0.4977	28	E.344
Exponential Model		0.17	DCP PI=1.891 $(p_L)^{0.4071}$	28	E.440

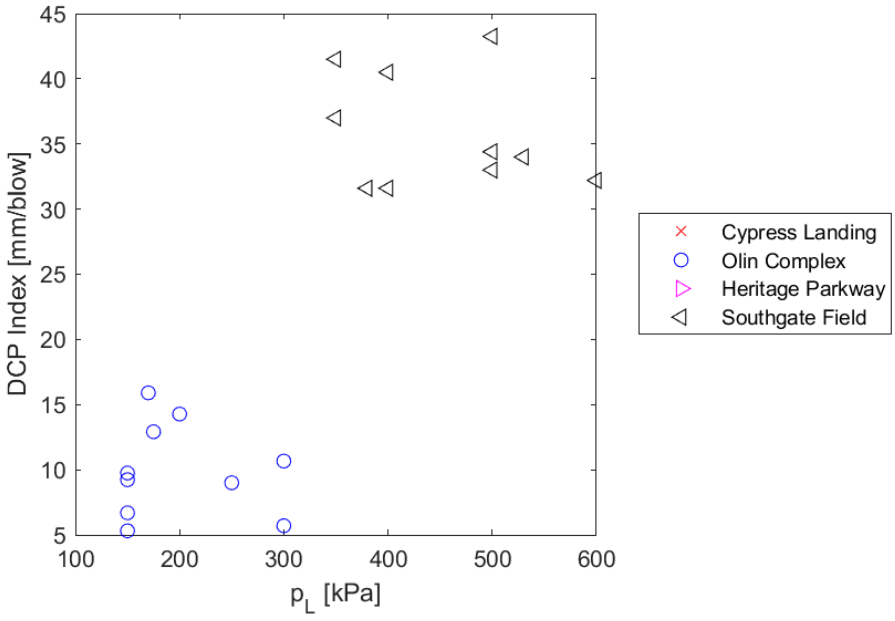

Figure 6.100: SDPMT-6 Continuous, DCP PI versus p_L, All Sites

6.6.5.3 SDPMT-12 Incremental Comparisons

Table 6.18 shows the five regression models developed from SDPMT-12 incremental test data. Figure 6.99 shows the data used to develop the models. The models produced R^2 values ranging from 0.10 to 0.36, based on 34 data points. These models show signs of a correlation existing between p_L and the DCP PI, as there is a general decrease in DCP PI with increasing p_L. The extremely low R^2 values indicate that more data should be collected to the strengthen these correlations.

6.6.5.4 SDPMT-12 Continuous Comparisons

Table 6.18 shows the five regression models developed from SDPMT-12 continuous test data. Figure 6.102 shows the data used to develop the models. Visually, there is no obvious trend shown. The models produced R^2 values ranging from 0.13 to 0.26, based on 28 data points. There is too much scatter in the data and no apparent correlation between DCP PI and p_L.

6.6.5.5 Summary of DCP PI versus p_L Regression Models

Because of the limitations of the DCP, only a limited amount of data could be obtained. DCP testing on high quality base must be performed immediately after compaction and that was not possible at Heritage Parkway. If more data could be

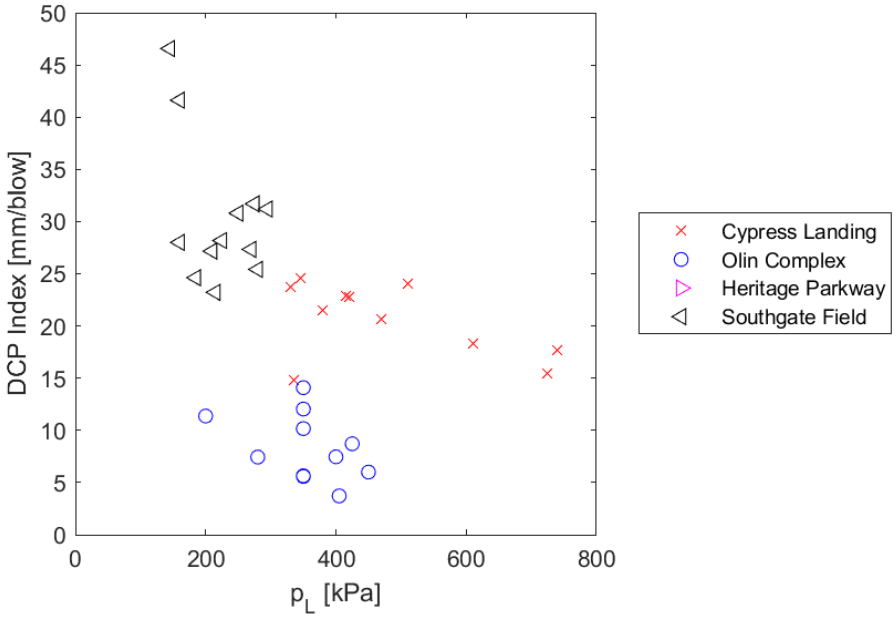

Figure 6.101: SDPMT-12 Incremental, DCP PI versus p_L, All Sites

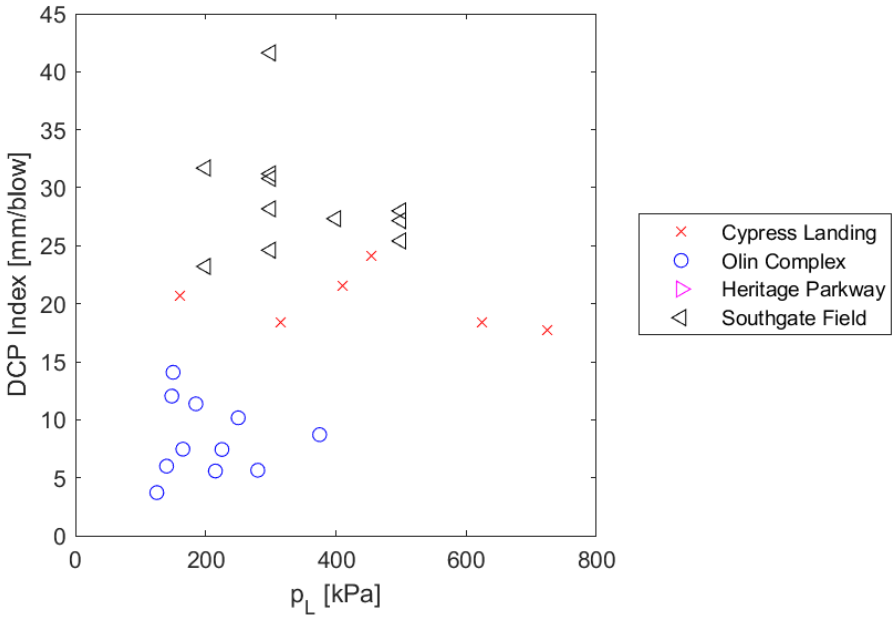

Figure 6.102: SDPMT-12 Continuous, DCP PI versus p_L, All Sites

collected from embankments, subbase/subgrade and high quality bases materials, better statistical models could be developed.

6.7 Comparisons with SDPMT E_{ul}

6.8 Comparisons Between Finite Element Deflections Predicted Based on SDPMT Data and Zorn LWD Field Deflections

6.8.1 Introduction

A comparison between predicted and measured surface deflections of the base/subgrade materials from the four field sites was conducted. SDPMT stress-strain data was input into finite element analyses (FEA) software to produce predicted deflections. Zorn LWD test results were used as the corresponding measured surface deflections. All soils exhibit nonlinear stress-strain behavior when loaded.

To conduct the comparisons, LWD and SDPMT data from each of the 12 locations at each site was used. Results from both tests at each location was obtained and then averaged for input into the FEA model.

The index properties from the four sites are summarized in Table 6.19. Three of the four sites contained poorly graded sands (SP or A-3) with minimal fines and compacted to about 95 % of the modified Proctor maximum dry density. These three sites are embankment quality materials, since their LBR values are 10 or less. The fourth site (Heritage Parkway) is a well graded sand with over 20 % gravel compacted to 100 % of the modified Proctor maximum density. It has an LBR of nearly 100 and is considered a base material.

6.8.2 Finite Element Model

6.8.2.1 Geometry and Boundary Conditions

A finite element program called ADINA (Automatic Dynamic Incremental Nonlinear Analysis) was used for this analysis to simulate pavement layers. This software provides a powerful tool for analyzing behavior of 2D and 3D complex structures subjected to various loading conditions, including; acceleration, prescribed displacements, static and dynamic loads, changes in temperature, etc.

An axisymmetric finite element formulation was utilized in modeling the geometry of the pavement layer. The 2D-axisymmetric model is often employed for representing circular loading problems at which stress and strain conditions are presumed to be congruent in any radial direction (Cho et al., 2000). Therefore, it provides appropriate numerical simulation for the pavement system under the contact pressure of wheel loadings.

Property	FIT Southgate Results	FIT Overflow Results	Potenza Drive Results	Heritage Parkway Results
Max. Dry Unit Weight	100.0 lb/ft^3	111.1 lb/ft^3	117.2 lb/ft^3	127.5 lb/ft^3
Optimum Moisture Content	12%	10.50%	10%	7.40%
Field Dry Unit Weight	91.5 lb/ft^3	105.8 lb/ft^3	112 lb/ft^3	127.5 lb/ft^3
Field Moisture Content	4.6%	1.6%	8.3%	3.8%
Relative Compaction	91.5%	95.2%	95.6%	100.0%
Uniformity Coefficient	2.6	2.42	2.72	10.45
Curvature Coefficient	1.03	1.38	1.08	0.48
Gravel Fraction	0%	0%	0%	22%
Fine Content	1%	1%	2%	2%
Soil Classification	A-3	A-3	A-3	A-1-b
	SP – poody graded sand	SP – poody graded sand	SP – poody graded sand	SW – well graded sand
Atterberg Limits	NP	NP	NP	NP
$LBR_{(lab\text{-}soaked)}$	7	10	6	99

Table 6.19: Summary of Index Properties

The size and geometry of the finite element model was a function of the LWD contact plate radius. Shaban (2016) stated that the optimum size of finite element pavement model should be greater than or equal to 35 times radius of the loading area in the vertical direction, and 25 times radius of the loading area in the horizontal direction. Therefore, the domain size of the model is specified as 6m (>5.25 m) deep, and 4m (>3.75 m) wide.

Figure 6.103 illustrates size and type of the finite element formulation. The large size of the model helps to minimize the influence of external boundary conditions on the magnitude of predicted surface deflections, as well as preventing undesirable wave reflections propagated from LWD dynamic loads (Stamp and Mooney, 2013).

A schematic illustration of the geometry and boundary conditions for the finite element model is presented in Figure 6.104. The boundary conditions were defined at the bottom and along the sides of the model. A fixed support was applied at the bottom of the model to prevent movement and rotation in all directions. A x-translation support, which allows for the elements to move only in the vertical direction, was assigned to the inner and outer vertical boundaries.

Since the geometry and boundary conditions are symmetric, only half of the model was evaluated during the finite element simulation. Therefore, the right-side of the geometry was modeled in order to minimize the computational time.

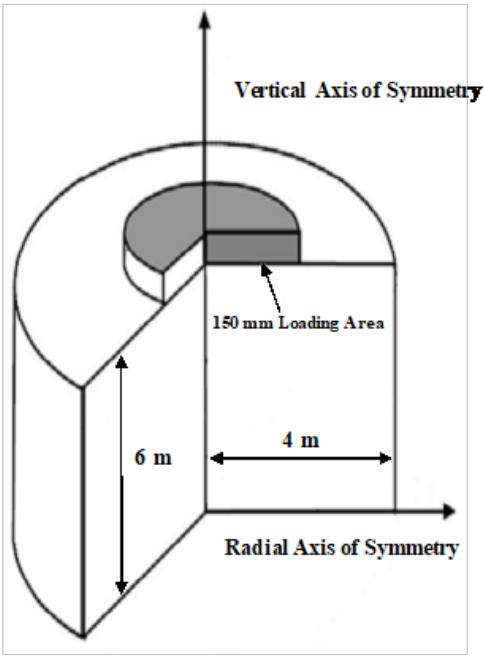

Figure 6.103: Axisymmetric Finite Element Pavement Model with Loading Plate

6.8.2.2 Mesh and Loading Configurations

The axisymmetric 2D model was meshed using quadrilateral 9-node 2-D solid elements as shown in Figure 6.105. Quadrilateral elements allow higher order shape functions to be used for analyses. The finite element mesh shown in Figure 6.105 was generated using various mesh sizes. Point A is the node that was used in the predicted deflection versus time plots. It is the node directly under the center of the simulated loading. To optimize the mesh coarseness and minimize computational errors, a local mesh refinement was developed underneath the loading area. The mesh coarseness was increased as the distance from the loading zone increased. Half of the model was simulated in FE analysis due to geometric and boundary symmetry.

The loading condition from the Zorn LWD was used for the numerical simulation. The Zorn-LWD load simulates a truck axle moving at 80 Km/hour over the 300 mm diameter loading plate. The simulation produces a dynamic impact pressure with 100

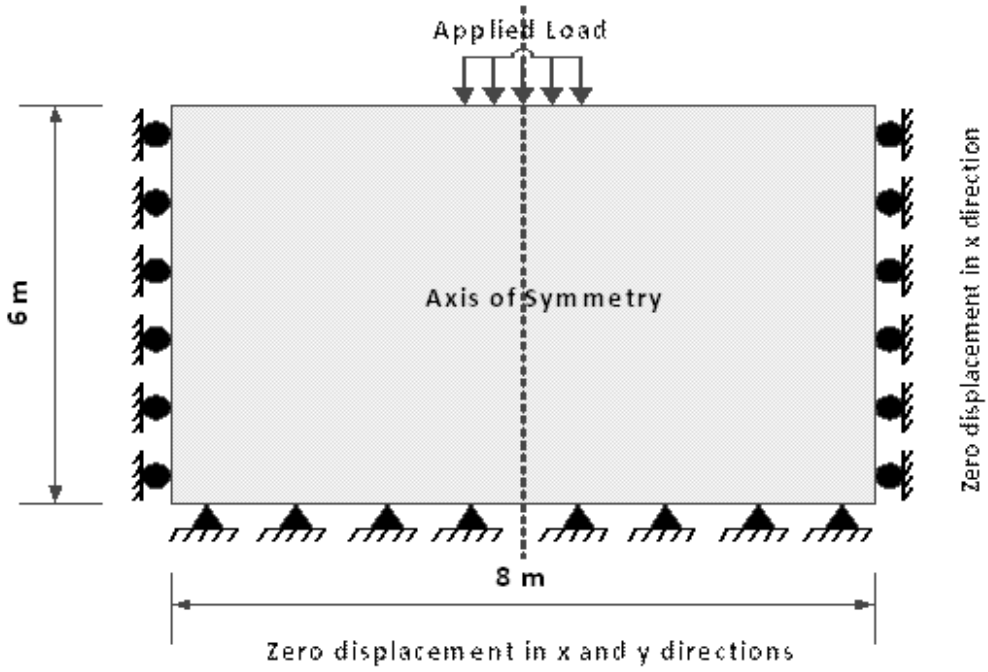

Figure 6.104: Schematic Illustration of Geometry and Boundary Conditions of the Model

kPa peak magnitude and a duration of 0.018 second. Figure 6.106 illustrates this time-dependent LWD haversine impulse.

6.8.2.3 Finite Element Numerical Formulations

Anisotropic stress-strain soil behavior can be appropriately represented using several nonlinear finite element formulations. However, for simplicity, linear finite element formulations are commonly utilized since they decrease computational analysis time, as well as eliminate the necessity for using several nonlinear material inputs.

Based on the results of finite element studies by Pandey et al. (2003), Tang et al. (2013), and Shaban and Cosentino (2017) it was found that using linear elastic analyses for modeling base course and subgrade layers produces structural pavement responses with a reasonable degree of accuracy. Under typical traffic loads, the unbound layers are often subjected to low strain conditions which lie within the elastic range of the pavement strains. Additionally, the pavement response from a moving wheel load (i.e. dynamic impact load) can be very different from applying a static wheel load. Therefore, a linear elastic-dynamic finite element model was adopted in the numerical simulation. The basic theory for the linear elastic-dynamic analysis of a soil mass subjected to an impact load is presented based on equilibrium of forces (F(t)) and Newton's second law of motion:

$$F(t) - (R_{sta.} + Rdyn.) = m \times a \tag{6.73}$$

The internal static and dynamic forces ($R_{sta.}$ and R_{dya}) acting on a volume at a specific

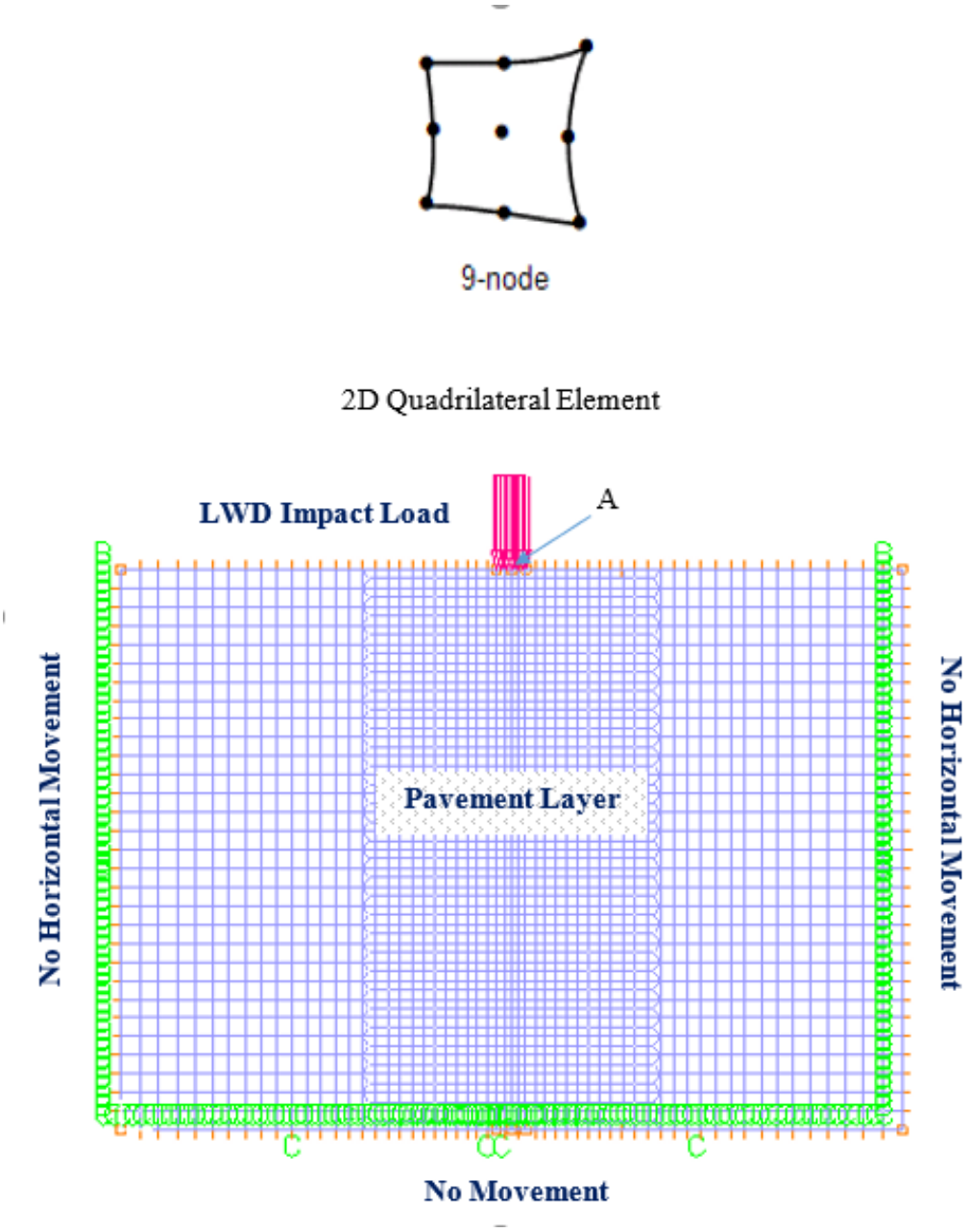

Figure 6.105: 2D Axisymmetric Finite Element Model Meshed with Quadrilateral Elements

time are related to the stiffness (K) and displacement (U) and the damping (C) and U, respectively:

$$R_{(sta.)} = K \times U \tag{6.74}$$

$$R_{(dyn.)} = C \times U \tag{6.75}$$

Substituting Equations 6.74 and 6.75 into Equation 6.73 produces the governing

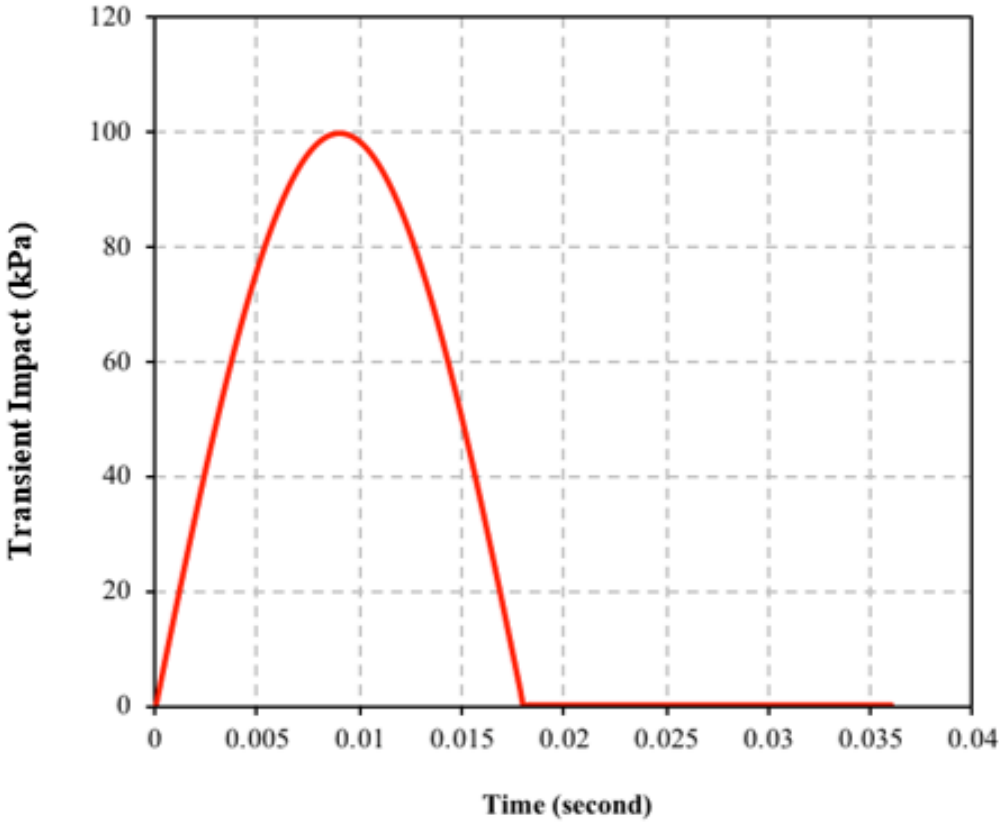

Figure 6.106: Typical LWD-Zorn Transient Impact versus Time Impulse

equation for dynamic behavior:

$$F(t) = K \times U + C \times \dot{U} + M \times \ddot{U} \tag{6.76}$$

where:

F(t) is the stiffness matrix
U is the displacement vector at the nodal point,
C is the damping matrix,
$\dot{U}$ is the velocity vector at the nodal point,
M is the mass matrix, and
$\ddot{U}$ is the acceleration vector at the nodal point.

The system of dynamic equilibrium equations can be solved using either of two mathematical methods: (1) direct integration, or (2) mode superposition (Bathe, 2014). The direct integration technique was used, which is based on Newmark's implicit time integration method (Newmark, 1959). The Newmark integration scheme, which produces displacement and velocity, is based on the following equations:

$$U(t + \Delta t) = U(t) + \dot{U} \times \Delta t + \left[\left(\frac{1}{2} - \alpha\right) \times \ddot{U}(t) + \alpha \times \ddot{U}(t + \Delta t)\right] \tag{6.77}$$

$$\dot{U}(t+\Delta t) = \dot{U}(t) + \left[(1-\delta) \times \ddot{U}(t) + \delta \times \ddot{U}(t+\Delta t\right] \times \Delta t \tag{6.78}$$

where: Δt is the time step, α and δ are the Newmark integration parameters (Newmark, 1959). The average values used for α and δ were 0.25 and 0.50. Newmark's integration scheme produces a reliable calculation process with a stable solution.

6.8.2.4 FEA Material Properties

The stiffness matrix (K) in Equation 6.76 is a function of each elements engineering properties (i.e., soil's modulus, Poisson's ratio, and density). The nonlinear stress-strain response, typical of soils, produces hyperbolic shaped curves. Kondner (1963) recognized that these shapes can be simplified mathematically. Kondner's strain level model, allows the stress at any strain level to be determined using a hyperbolic function:

$$\sigma = \frac{\epsilon}{a + b\epsilon} \tag{6.79}$$

where: σ is the deviator stress, and ϵ is the axial strain. The hyperbolic model can be re-written in terms of modulus E to produce a straight-line relationship between 1/E and strain as follows:

$$\frac{1}{E} = a + b\epsilon \tag{6.80}$$

where: E is a secant modulus obtained from a stress-strain curve, a is the y-aixs intercept and b is the slope of the plot. Figure 6.107 illustrates a typical stress-strain level model with secant moduli determined at various strains, while Figure 6.108 illustrates Kondner's model based on Equation 6.80.

In this work, the radial stress σ_r and radial strain ϵ_r measured from the unloading portion of the SDPMT stress-strain curve were used to determine the strain level parameters. Using SDPMT elastic moduli and corresponding strains, obtained from the unloading pressuremeter data Kondner's (1963) the strain level model parameters were used in the numerical simulation. Modeling was done by plotting the data of inverse soil moduli versus corresponding strain levels, and then fitting the best regression straight line through these data points.

After determining the strain model parameters, the in-situ average strain levels determined from LWD tests were substituted in the models to produce a predicted set of SDPMT moduli. The strain levels were calculated by dividing LWD surface deflections by thickness of tested soil layer. The SDPMT moduli were input into the finite element model to define soil stiffness.

Due to the small influence of Poisson's ratio (ν) of unbound pavement materials on finite element results and complicated laboratory testing procedure involved in determining Poisson's ratio, this parameter was assumed within the ranges listed in Table 6.20.

The final required FE input, density, was determined from NDG tests. The total field unit weight obtained from field NDG measurements was input in the numerical simulation.

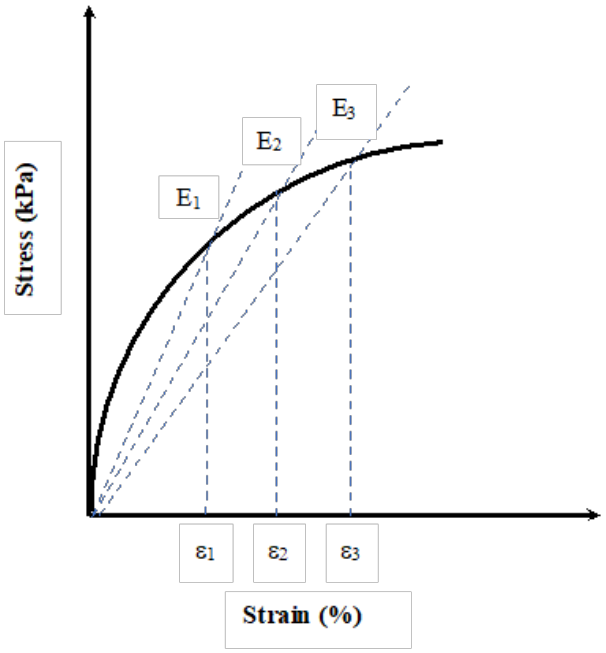

Figure 6.107: Typical Hyperbolic Stress-Strain Curve with Secant Moduli at Various Strains

6.8.3 Strain Level Model Parameters

The unloading SDPMT stress-strain data were reduced and analyzed to determine the parameters for the strain level model described in Equation 6.80. The strain level plots and their regression data are presented in Appendix F. The following subsections are summaries of the results for strain level parameters for each testing site. The SDPMT strain level testing shows that the FIT Southgate Field site is the least stiff site, followed by the FIT Overflow Parking, Potenza Drive and finally Heritage Parkway. Therefore, the data will be presented with the sites in this order.

6.8.3.1 FIT Southgate Field

For the embankment soils at FIT's Southgate Field, 6- and 12-inch SDPMT tests were performed at each location. The soil layer tested was approximately 3 feet thick. Table 6.21 is a summary of FIT's Southgate Field strain level model constants from the 6- and 12-inch SDPMT tests. The results from the 6-inch SDPMT test indicated that the constant (a in equation 6.80) varied from 2.20×10^{-5} to 5.69×10^{-5}, and the slope

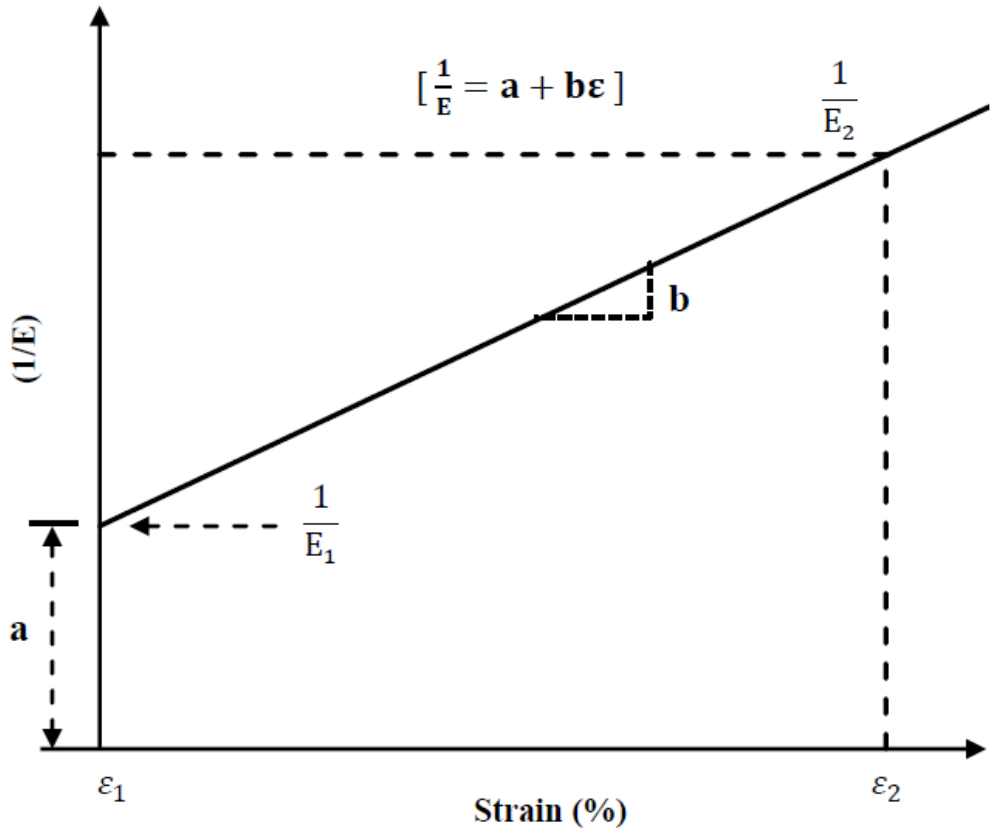

Figure 6.108: Kondner's (1963) Typical Strain Level Model

Pavement Material	Poisson's Ratio
Bituminous Concrete	0.50 for E <500,000 psi 0.30 for E >500,000 psi
Unbound Granular Base and Subbase	0.30
Chemically Stabilized Soils	0.20
Cohesive Subgrade Soils	0.40
Cohesionless Subgrade Soils	0.30

Table 6.20: Typical Poisson's Ratio for Various Soils

(b) ranged from 1.44×10^{-3} to 2.40×10^{-3} (1/kPa). The average values of (a) and (b) were 3.82×10^{-5} and 1.86×10^{-3}, respectively. The results from the 12-inch SDPMT test showed that (a) varied from 1.73×10^{-5} to $6.05 \times 10{-}5$, and the slope (b) ranged from 1.49×10^{-3} to 5.61×10^{-3} (1/kPa). The average values of (a) and (b) were 3.77×10^{-5} and 2.66×10^{-3}, respectively.

Table 6.21: Strain Model Parameters for the Subgrade at FIT's Southgate Field

Station No.	Strain Level Model: $\left[\frac{1}{E} = a + b\varepsilon\right]$					
	PMT Testing Mode – 6 inch			PMT Testing Mode – 12 inch		
	$a \times 10^{-5}$	$b \times 10^{-3}$	R^2	$a \times 10^{-5}$	$b \times 10^{-3}$	R^2
401	5.69	1.44	0.99	5.52	1.71	0.83
402	2.20	1.68	0.97	4.26	1.55	0.91
403	3.59	1.65	0.94	2.98	2.02	0.98
404	3.51	1.64	0.97	6.05	1.69	0.77
405	2.90	2.23	0.94	3.72	3.00	0.92
406	4.10	2.40	0.99	3.50	1.49	0.94
407	2.88	1.64	0.99	2.31	2.86	0.97
408	3.87	2.03	0.97	4.88	2.08	0.92
409	5.30	1.62	0.99	4.49	4.01	0.92
410	3.52	1.90	0.97	1.73	5.61	0.99
411	3.66	2.33	0.97	2.32	2.73	0.93
412	4.66	1.73	0.99	3.44	3.21	0.97
Average	**3.82**	**1.86**	**0.97**	**3.77**	**2.66**	**0.92**

6.8.3.2 FIT Olin Complex

For the embankment soils tested at the FIT Overflow Parking Lot, SDPMT-6 and 12 testing depths were conducted at each location. Table 6.22 is a summary of resulting strain level model constants from this site. The soil layer tested was approximately 3 feet thick. The results from the 6-inch SDPMT test showed that strain level model intercept (a) ranged from $0.96 \times 10 - 5$ to 3.05×10^{-5}, and the slope (b) ranged from 0.92×10^{-3} to 2.69×10^{-3} (1/kPa). The average values of (a) and (b) were 2.03×10^{-5} and 1.59×10^{-3}, respectively. The results from the 12-inch SDPMT test indicated that the strain level intercept (a) varied between $1.38 \times 10{-}5$ and 3.81×10^{-5}, and the slope (b) varied between 1.24×10^{-3} and $3.59 \times 10{-}3$ (1/kPa). The average values of (a) and (b) were 2.48×10^{-5} and 1.94×10^{-3}, respectively.

6.8.3.3 Cypress Landing

For the 12-inch thick recompacted embankment soils tested at Potenza Drive in Cypress Landing (See Table 6.23), SDPMT-12 testing produced strain level model

Table 6.22: Strain Level Model Parameters for the Subgrade at FIT's Overflow Parking Lot

Station No.	Strain Level Model: $\left[\frac{1}{E} = a + b\varepsilon\right]$					
	PMT Testing Mode – 6 inch			PMT Testing Mode – 12 inch		
	$a \times 10^{-5}$	$b \times 10^{-3}$	R^2	$a \times 10^{-5}$	$b \times 10^{-3}$	R^2
201	1.49	1.87	0.98	2.62	3.59	0.88
202	2.98	1.50	0.98	1.59	1.87	0.97
203	2.10	1.38	0.99	2.99	1.38	0.81
204	2.41	1.69	0.96	1.98	1.60	0.97
205	3.05	1.62	0.97	1.38	3.37	0.82
206	1.76	1.33	0.98	3.17	1.87	0.97
207	1.46	1.12	0.99	3.81	1.90	0.90
208	9.63	0.92	0.98	2.39	1.24	0.96
209	2.54	2.69	0.97	1.83	1.58	0.98
210	2.50	1.52	0.93	2.32	1.34	0.93
211	1.03	1.83	0.94	3.17	1.65	0.93
212	NA		/	NA		/
Average	**2.03**	**1.59**	**0.97**	**2.48**	**1.94**	**0.92**

intercept (a) values that varied between 0.71×10^{-5} and 5.83×10^{-5} (1/kPa) and slopes (b) that ranged from 2.38×10^{-3} to 7.79×10^{-3} (1/kPa). The average values of (a) and (b) were 2.12×10^{-5} and 4.50×10^{-3}, respectively. Due to construction constraints, the 6-inch SDPMT tests could not be conducted at this site.

6.8.3.4 Heritage Parkway

For the base course at Heritage Parkway-Phase II, both SDPMT-6 and SDPMT-12 tests were conducted at all 12 locations. The base material was reported to be 8-inches (20 cm) thick; however, NDG testing indicated that the upper 12-inches (30 cm) was compacted to approximately the same densities along the entire site. Table 6.24 is a summary of Heritage Parkway's strain level model constants for SDPMT-6 and SDPMT-12 tests. The results from the SDPMT-6 tests indicated that the strain level model intercept (a) varied from 0.87×10^{-6} to 7.59×10^{-6}, and the slope (b) ranged from 1.76×10^{-4} to 5.51×10^{-4} (1/kPa). The average values of (a) and (b) were

Table 6.23: Strain Level Model Parameters for Subgrade for Potenza Drive in Cypress Landing

Location	Strain Level Model: $\left[\frac{1}{E} = a + b\varepsilon\right]$		Regression Coefficient R^2
	$a \times 10^{-5}$	$b \times 10^{-3}$	
101	1.02	4.54	0.71
102	N/A		/
103	1.18	4.88	0.99
104	2.79	4.04	0.87
105	1.02	3.59	0.94
106	0.71	2.38	0.99
107	3.66	3.68	0.74
108	1.73	2.71	0.95
109	2.59	6.64	0.91
110	5.83	7.79	0.94
111	1.24	3.22	0.99
112	1.53	6.07	0.93
Average	**2.12**	**4.50**	**0.91**

2.38×10^{-6} and 2.98×10^{-4}, respectively. The results from the 12-inch SDPMT tests showed that (a) varied from 2.80×10^{-6} to 8.85×10^{-6}, and the slope (b) ranged from 2.32×10^{-4} to 5.87×10^{-4} (1/kPa). The average values of (a) and (b) were 4.79×10^{-6} and 3.97×10^{-4}, respectively.

6.8.3.5 Typical Strain Level Model Parameters

The strain level parameters obtained from SDPMT-6 and SDPMT-12 testing modes fall within typical values reported by Briaud et al. (1983), Terry (2016), Cosentino (1987), and Shaban (2016) as shown in Table 6.25. These parameters show a wide range of values for both constants determined from performing the PMT tests on different materials. These materials ranged from a granular aggregate to a loose sand to a high plasticity clay.

6.8.4 Finite Element Results

The axisymmetric finite element model was utilized to simulate LWD impact load-time pavement layer response. ADINA model's inputs were determined using field

Table 6.24: Strain Level Model Parameters for the Base Course at Heritage Parkway

Location	Strain Level Model: $\left[\frac{1}{E} = a + b\varepsilon\right]$		Regression Coefficient R^2
	$a \times 10^{-5}$	$b \times 10^{-3}$	
101	1.02	4.54	0.71
102	N/A		/
103	1.18	4.88	0.99
104	2.79	4.04	0.87
105	1.02	3.59	0.94
106	0.71	2.38	0.99
107	3.66	3.68	0.74
108	1.73	2.71	0.95
109	2.59	6.64	0.91
110	5.83	7.79	0.94
111	1.24	3.22	0.99
112	1.53	6.07	0.93
Average	**2.12**	**4.50**	**0.91**

Table 6.25: Typical Strain Level Model Parameters (Briaud et al., 1983, Terry, 2016, Cosentino, 1987, Shaban, 2016)

Type of Material	α [1/kPa]	b [1/kPa]
Clay	2.0×10^{-6} to 3.0×10^{-5}	2.0×10^{-5} to 3.0×10^{-3}
Sand	5.0×10^{-6} to 1.0×10^{-4}	4.0×10^{-4} to 7.0×10^{-3}
Aggregate	1.0×10^{-6} to 9.0×10^{-6}	1.0×10^{-3} to 5.0×10^{-3}

measurements from the SDPMT and LWD tests. SDPMT unload stress-strain data were used to determine elastic moduli from the strain level equations. Average strains were calculated from the LWD maximum surface deflection divided by the pavement layer thickness. These strains were then used to calculate the modulus from Equation 6.80.

At each location, simulated plots of displacement versus time were developed and compared to the measured LWD plots, using the average of three LWD tests at each drop location. They included measured data and predicted deflections over about 0.02 seconds. The measured and predicted deflection-time plots from all four sites are given in Appendix G.

A review of the Appendix G results show that the finite element results showed a

reasonable agreement between predicted and measured pavement surface deflections. The following subsections present the comparison between measured and predicted surface deflections for each testing site.

6.8.4.1 FIT Southgate Field LWD and FEA Comparisons

For the FIT Southgate Field embankment sand, the results showed that the predicted surface deflections based on 6-inch SDPMT data are 22% lower than measured deflections from the LWD measurements, while those predicted based on 12-inch SDPMT testing data are 14% lower than measured deflections. Table 6.26 is a summary of predicted and measured deflections data collected at each testing location. The results indicated that predicted deflections ranged from 0.827 to 1.830 mm, while those measured from the LWD tests varied from 0.861 to 2.193 mm. The results also revealed that both 6-inch SDPMT and 12-inch SDPMT data produce acceptable results; however, the deflection basin estimated from 12-inch SDPMT moduli compare well with the actual deflection basin obtained from the LWD test. Figure 6.109 presents a comparison between average measured and average predicted surface deflections. Figure 6.110 displays a comparison between average measured and predicted time-deflection basin. Figure 6.111 illustrates the FEA distribution of vertical deformations in meters for location 405 (shown in red). The magnitude of vertical displacement decreases with increasing depth. The maximum deflection shown is 0.001344 m or 1.344 mm. The highest deflections occur under the simulated LWD plate and decrease nonlinearly with distance from the loading plate. In conclusion, the SDPMT results from the FIT Southgate Site embankment sands were successfully used to predict LWD deflection-time data.

6.8.4.2 FIT Overflow Parking LWD and FEA Comparisons

For the FIT Overflow Parking Lot embankment sand, the predicted surface deflections based on SDPMT-6 data are 20% lower than LWD measured deflections, while those predicted based on SDPMT-12 data are less than 1% lower than measured deflections. Table 6.27 lists FEA predicted and LWD measured deflections at each testing location. These were determined based on the strain level moduli calculated from an average strain calculated by dividing the surface deflection by the corresponding layer thickness. Figure 6.112 shows the comparison between average LWD measured and SDPMT FEA predicted deflections. The predicted deflections ranged from 0.323 to 1.084 mm, while those measured from the LWD tests varied from 0.488 to 1.216 mm. Figure 6.113 displays the distribution of vertical deformations from the finite element simulations. The highest deflections occur under the simulated LWD plate (i.e. 0.0008667 or 0.8667 mm). They decrease nonlinearly as the distance from the loading plate increases. As shown in Figure 6.113, both SDPMT-6 and SDPMT-12 data yield acceptable results; however, the deflection basin estimated based on SDPMT-12 moduli compare well with the actual deflection basin obtained from the LWD test. In conclusion, the SDPMT results were successfully used to predict LWD deflection-time

Table 6.26: Summary of Modulus and Deflection Data for SP Sands - FIT Southgate Field

Location	SDPMT Testing Mode – 6 inch			SDPMT Testing Mode – 12 inch		
	Strain Level Modulus (kPa) [1]	Measured Deflections (mm) [3]	Predicted Deflections (mm)	Strain Level Modulus (kPa) [2]	Measured Deflections (mm)	Predicted Deflections (mm)
401	14950	2.111	1.744	14925	2.111	1.747
402	31551	1.757	0.827	19396	1.757	1.344
403	23240	1.323	1.122	25956	1.323	1.005
404	22449	1.756	1.162	14246	1.756	1.830
405	**22990**	**1.984**	**1.134**	**17621**	**1.984**	**1.480**
406	19316	1.369	1.350	24014	1.369	1.086
407	26378	1.688	0.989	25668	1.688	1.016
408	22501	0.861	1.159	18295	0.861	1.425
409	16744	1.274	1.557	16226	1.274	1.607
410	23273	1.253	1.120	24784	1.253	1.052
411	20166	1.696	1.293	26079	1.696	1.000
412	16947	2.193	1.539	17394	2.193	1.499
Average	**20814**	**1.605**	**1.250**	**20473**	**1.605**	**1.375**

1) Strain level moduli were determined using average LWD strains from 6-inch SDPMT test.
2) Strain level moduli were determined using average LWD strains from 12-inch SDPMT test.
3) Measured deflection was obtained from performing one LWD test at each testing location.

data in the embankment sands tested at the FIT Overflow Parking Site.

6.8.4.3 Potenza Drive within Cypress Landing Results

The results from Potenza Drive within Cypress Landing, where two sets of LWD test were analyzed (A & B), indicated that the FEA predicted deflections are from 4 to 11% lower than LWD measured deflections. Several studies including Cosentino (1987) and Shaban (2016) reported that ± 25% is an acceptable difference between measured and predicted deflections. As shown in Table 7, the predicted deflections ranged from 0.310 to 2.052 mm, while those measured from the LWD tests varied from 0.447 to 3.836 mm. The FE outputs also showed that the SDPMT strain level moduli yield acceptable results in which a higher soil modulus produces lower deflection. Figure 6.115 displays the comparison between average measured and predicted surface deflections, whereas average difference is about 11% and 4% for the dataset No.1, and dataset No.2, respectively.

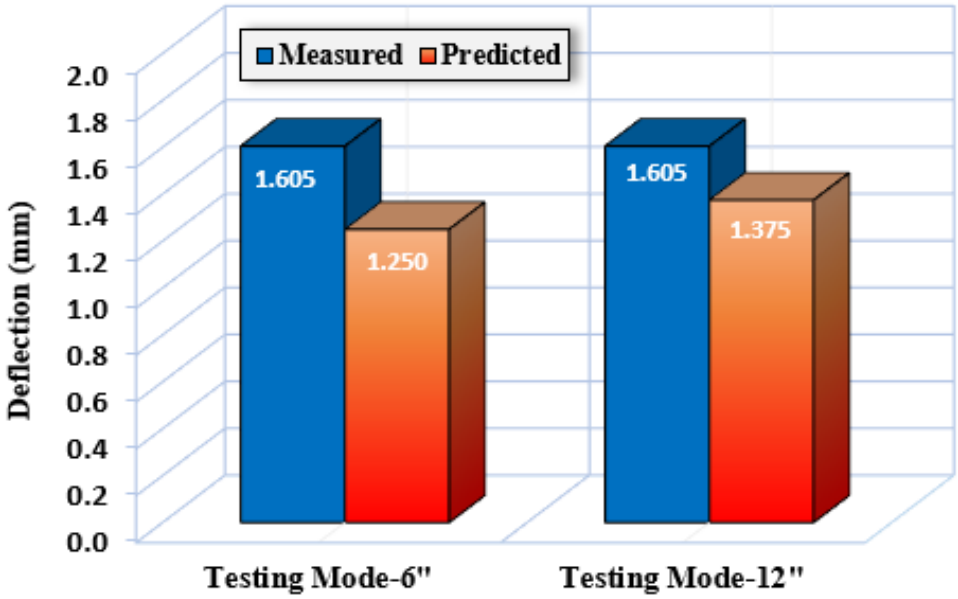

Figure 6.109: Average Surface Deflection Data - FIT Southgate Field

Using the average values from the 12 sets of Potenza Drive tests, the SDPMT strain level model predicted distribution of vertical displacements is shown in Figure 6.117. The highest deflections occur under the simulated LWD plate (i.e. 0.000975 mm). They decrease nonlinearly as the distance from the loading plate increases. The deformations gradually diminished near the bottom and the edges of the model. Figure 6.116 presents average time-deflection curves obtained from the FEA simulation and LWD tests.

In general, the results from Table 6.28 show relatively good agreement between measured and predicted deflections. The results in Figure 6.116 show excellent agreement between measured and predicted LWD deflections. In conclusion, the SDPMT results were successfully used to predict LWD deflection time data in the embankment soils tested at Potenza Drive within Cypress Landing.

6.8.4.4 Heritage Parkway LWD and FEA Comparisons

For the Heritage Parkway base course, SDPMT-6 and SDPMT-12 plus two LWD tests (A & B) were conducted at each testing location. Table 6.29 is a summary of the moduli and deflection data collected at each testing location. FEA results based on the SDPMT-6 data showed that the average predicted deflections ranged from 19% to 26% lower than the measured deflections, while those based on SDPMT-12 data indicated that the average predicted deflections ranged from 14% to 5% lower than the measured deflections (see Table 6.29). Of the four sites tested this set of 12-inch measured versus predicted were the only ones in which the predicted defections exceeded the measured deflections. The FEA predictions indicate that the deflection basins predicted based on

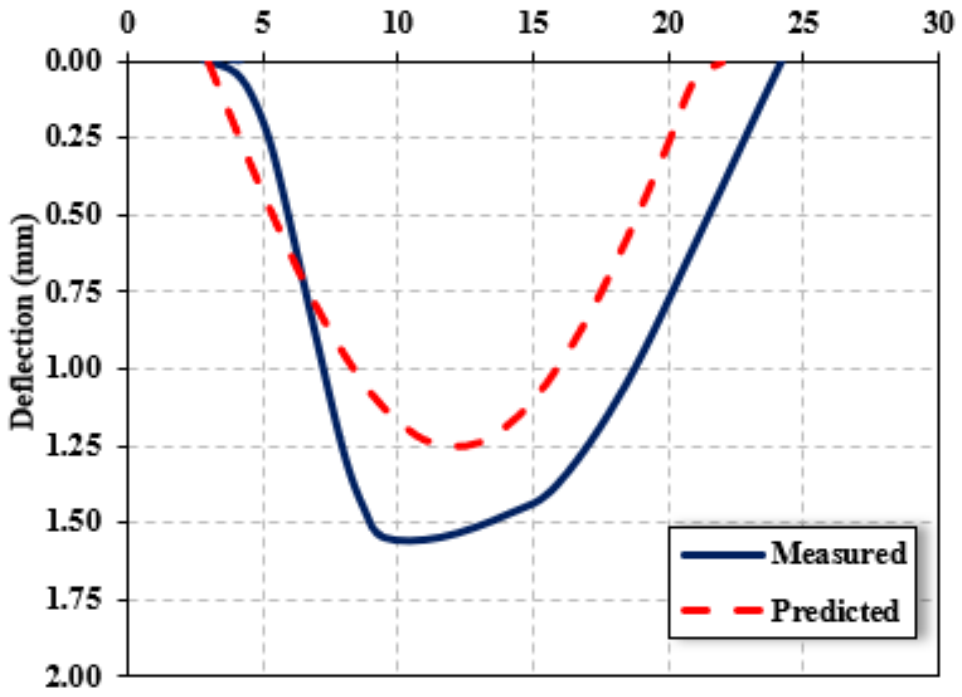

6-inch Average SDPMT Comparison

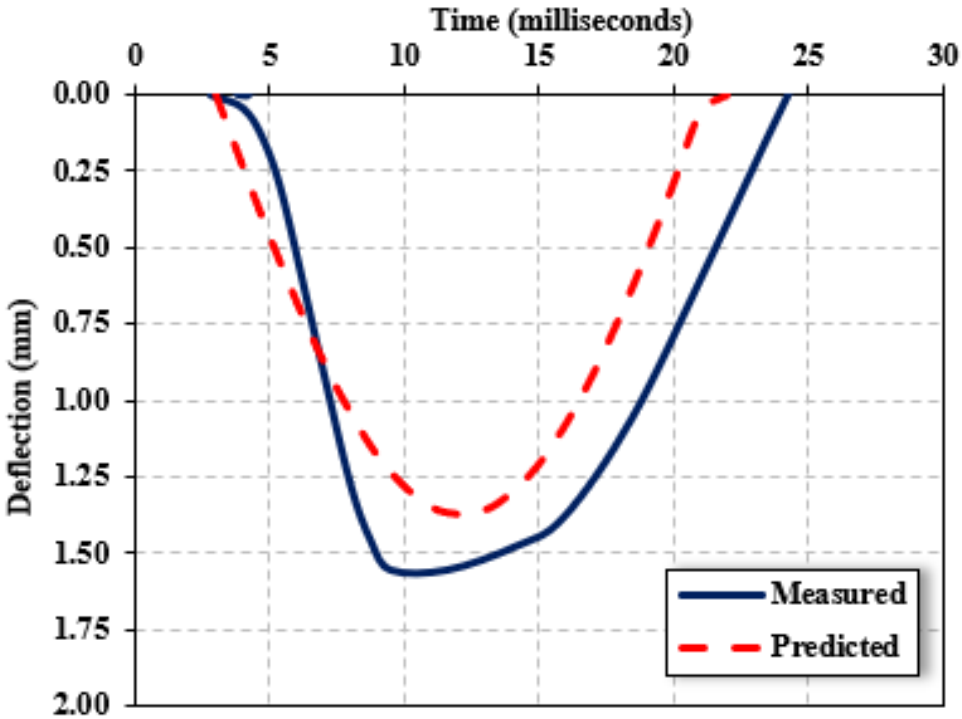

12-inch Average SDPMT Comparison

Figure 6.110: Time-Deflection Comparison between Measured and Predicted Soil Response FIT Southgate Field

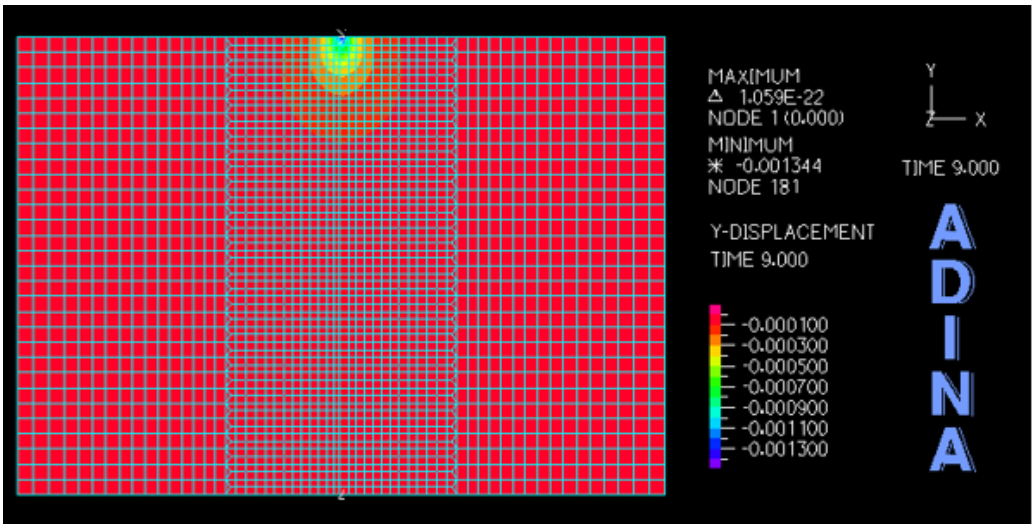

Figure 6.111: Location 405 FEA Displacements in meters - FIT Southgate Field

SDPMT-6 and SDPMT-12 data compare well with the actual deflection basins obtained from LWD measurements.

Figure 6.118, Figure 6.119, and Figure 6.120 show that the SDPMT-12 data produce better deflection estimates than the SDPMT-6 data. This result was expected since the zone of influence of the LWD is much larger than 6-inches (15 cm) and most likely 24-inches (60 cm) deep. Therefore, SDPMT-12 data should more closely match the behavior throughout the zone of influence than the SDPMT-6 results. As shown in Figure 6.121 the distribution of vertical displacements from the finite element model decreases with depth and completely dissipates at the external boundaries of the model. The highest deflections occur under the simulated LWD plate (i.e. 0.000156 m or 0.156 mm). They decrease nonlinearly as the distance from the loading plate increases. In conclusion, the SDPMT results were successfully used to predict LWD deflection-time data for the cemented coquina base tested at Heritage Parkway.

6.8.5 FEA Conclusions

In general, the measured deflections based on averages from three LWD drops per testing point exceeded the FEA predicted deflections at the center node under the loaded area. The FEA predictions based on SDPMT-12 strain level moduli were more accurate (5 to 14%) than the SDPMT-6 (19 to 26%) predictions. These results indicate that the SDPMT data can be used to evaluate pavement materials and that SDPMT-12 data is more effective than SDPMT-6 data.

Table 6.27: Summary of Modulus and Deflection Data for SP Sands - FIT Overflow Parking Lot

Location	SDPMT Testing Mode – 6 inch			SDPMT Testing Mode – 12 inch		
	Strain Level Modulus (kPa) (1)	Measured Deflections (mm) (3)	Predicted Deflections (mm)	Strain Level Modulus (kPa) (2)	Measured Deflections (mm)	Predicted Deflections (mm)
201	49087	0.876	0.531	27267	0.876	0.956
202	29678	0.784	0.879	48141	0.784	0.542
203	40172	0.851	0.649	29557	0.851	0.882
204	33554	1.006	0.777	39669	1.006	0.657
205	26961	1.216	0.967	36468	1.216	0.715
206	45313	1.017	0.576	26281	1.017	0.992
207	59924	0.548	0.435	24065	0.548	1.084
208	80778	0.902	0.323	36257	0.902	0.719
209	33611	0.488	0.776	47900	0.488	0.544
210	35469	0.639	0.735	38452	0.639	0.678
211	69067	0.681	0.531	28205	0.681	0.925
212	NA	0.790	NA	NA	0.790	NA
Average	**45783**	**0.817**	**0.653**	**34751**	**0.817**	**0.815**

1) Strain level moduli were determined from average LWD strains on 6-inch SDPMT test.
2) Strain level moduli were determined from average LWD strains 12-inch SDPMT test.
3) Measured deflection was obtained from performing one LWD test at each testing location.

6.9 Relating Resilient Moduli to SDPMT Moduli

6.9.1 Analytical Approach

Using the data from 30 resilient moduli tests run in accordance with AASHTO T 307, Mr values for base, subbase/subgrade materials and embankment materials were input into the hyperbolic equation, $1/E=a+b\epsilon$, developed by Kondner (1963) to estimate strains. Table 6.30 presents a summary of the strains. They were estimated by first using the average a and b parameters obtained from the SDPMT unloading stress-strain data and then inputing the Mr-values obtained from resilient modulus testing. Strains were estimated using three bulk stresses (Θ) ranging from 11 psi

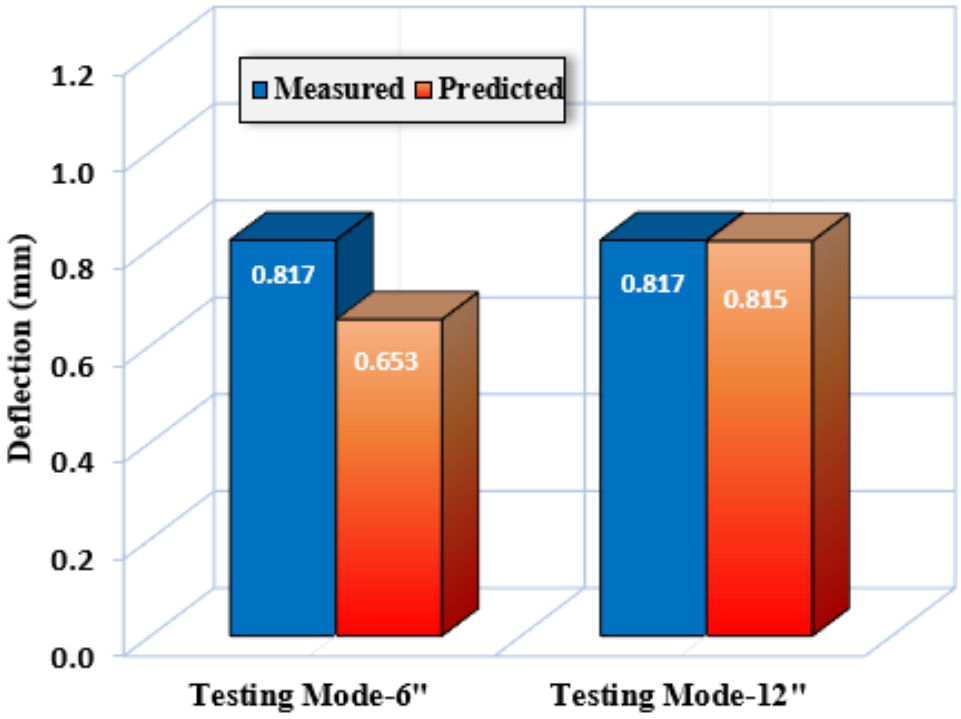

Figure 6.112: Average Surface Deflection Data for FIT Overflow Parking Lot

(1.5 kPa) to simulate embankment stresses, to 17 psi (2 kPa) to simulate subbase/subgrade stresses and finally 30 psi (4 kPa) to simulate base course stresses.

6.9.2 SDPMT and Mr Conclusions

The percent strains ranged from a minimum of 0.0034 % to a maximum of 0.28 %. The first three sites shown in Table 6.30 are embankment materials, and the fourth site is Heritage Parkway base. Typical strains decrease from 0.1 percent in base materials to 0.01 % in subbase/subgrade layers to 0.0001 % in embankments. The first three sites produced strains that are typical of subbase/subgrade strains, ranging from 0.0034 to 0.0302 %. The base material produced strains between 0.1104 and 0.2890 %.

In conclusion, applying the Kondner (1963) model to the unload stress-strain SDPMT data produced realistic strains for unbound pavement layers and embankments.

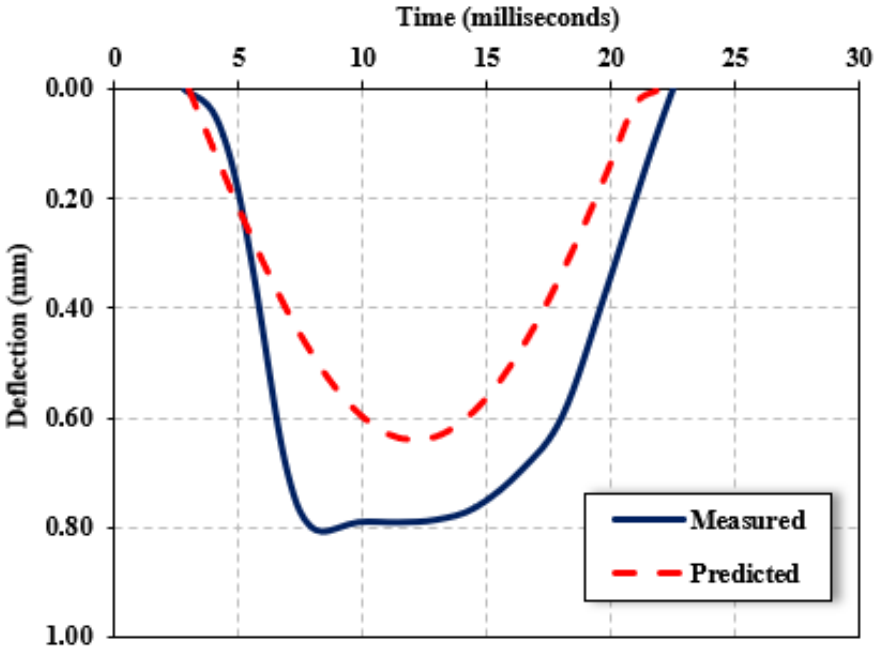

6-inch Average SDPMT Comparison

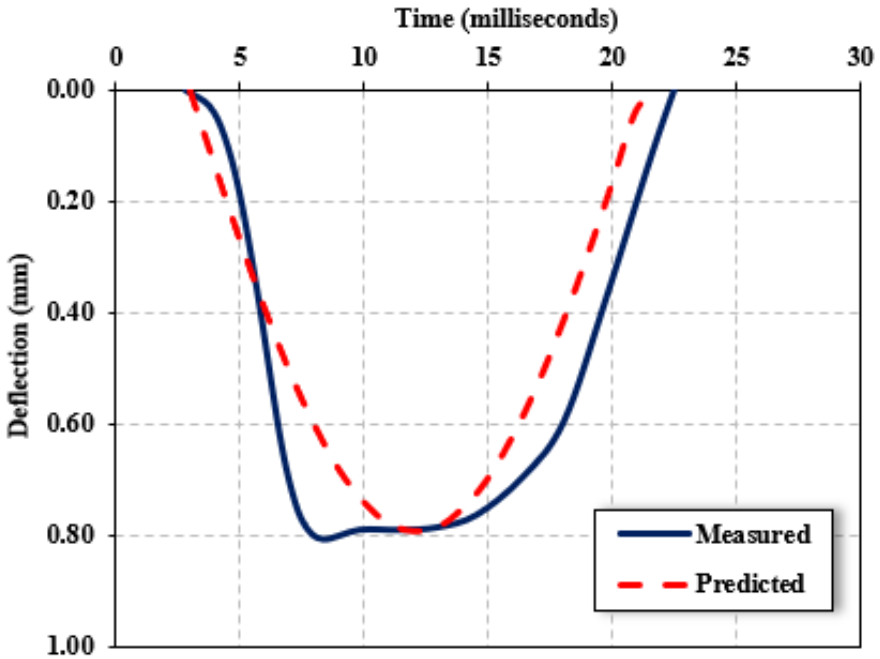

12-inch Average SDPMT Comparison

Figure 6.113: Time-Deflection Comparison between Measured and Predicted Soil Response FIT Overflow Parking Lot

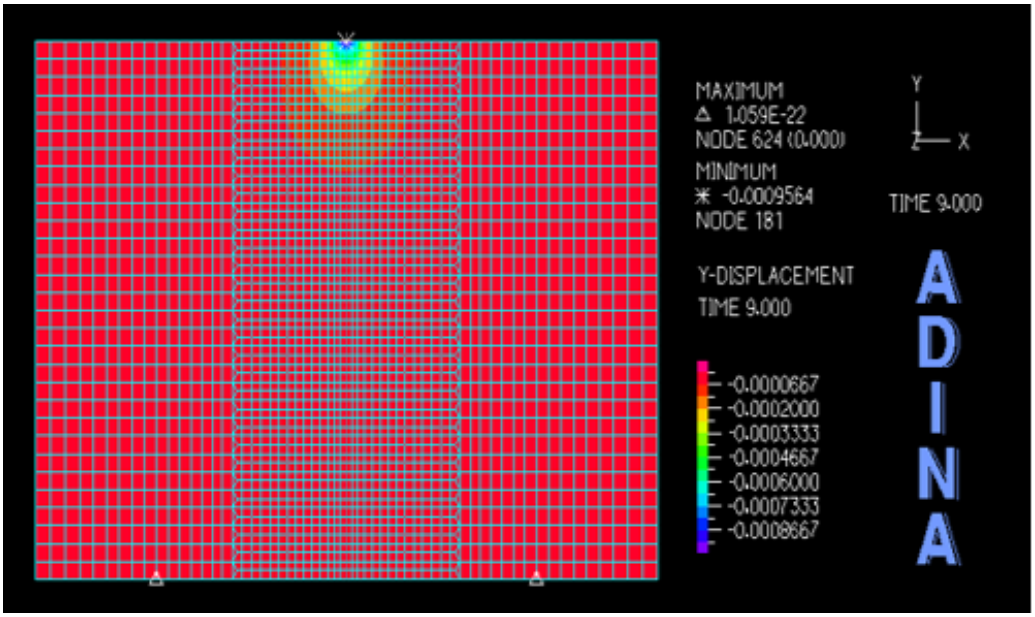

Figure 6.114: Location 201 FEA Displacements in meters - FIT Overflow Parking Lot

Table 6.28: Modulus and Deflection Summary for SP Sand Subgrade - Potenza Drive Cypress Landing

Location	Strain Level Modulus (1) (kPa)		Measured Deflections (2) (mm)		Predicted Deflections (mm)	
	Test A	Test B	Test A	Test B	Test A	Test B
101	34490	43140	1.264	0.873	0.756	0.605
102	NA		0.737	0.820	NA	
103	**25248**	**35352**	**1.738**	**1.031**	**1.033**	**0.738**
104	12708	12899	3.836	3.748	2.052	2.022
105	52877	61013	0.741	0.527	0.493	0.427
106	84065	78498	0.619	0.727	0.310	0.332
107	21652	22383	0.794	0.669	1.204	1.165
108	39425	40619	0.908	0.824	0.661	0.642
109	25954	26432	0.580	0.548	1.005	0.987
110	13849	13983	0.546	0.519	1.883	1.865
111	52617	58458	0.627	0.447	0.496	0.446
112	40286	38943	0.481	0.524	0.647	0.670
Average	**36652**	**39247**	**1.073**	**0.938**	**0.958**	**0.900**

1) Strain level moduli were determined from average LWD strains based on the 12-inch SDPMT stress-strain data.
2) Two LWD tests were performed at each testing location (Testing No.1, and Testing No.2).

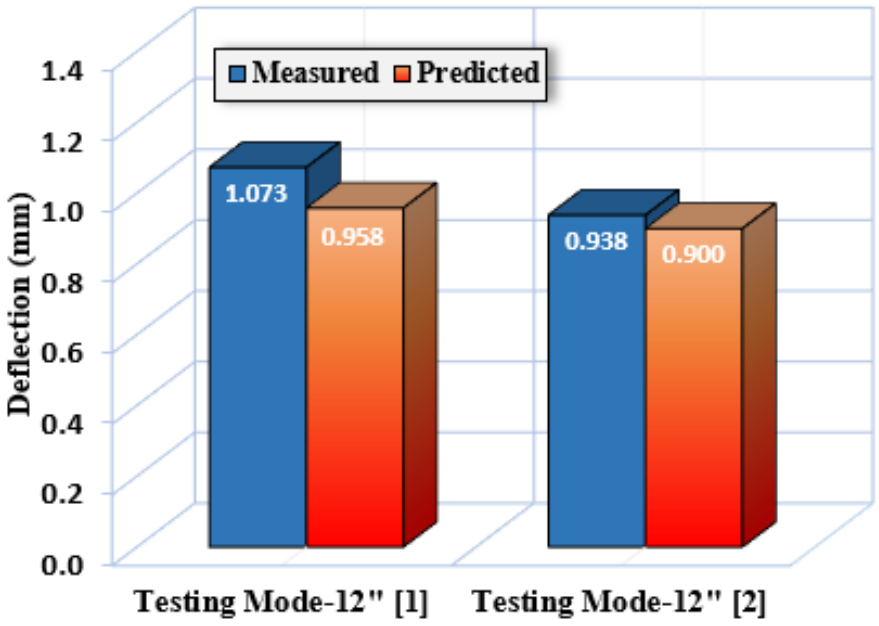

Figure 6.115: Average Surface Deflection Data for Potenza Drive in Cypress Landing

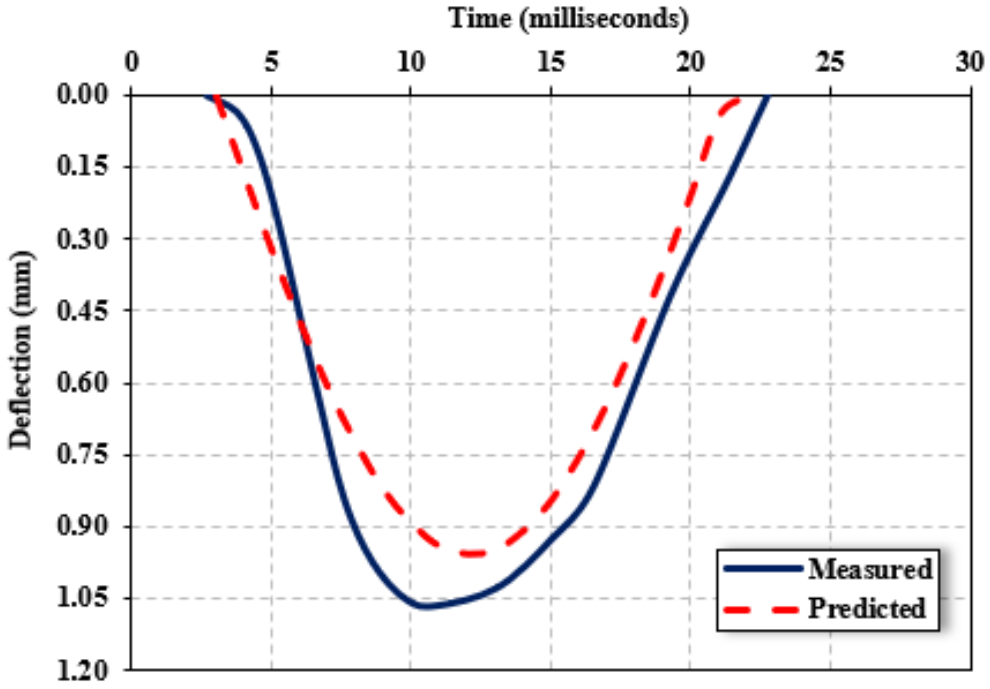

12-inch Average SDPMT Comparison Test A

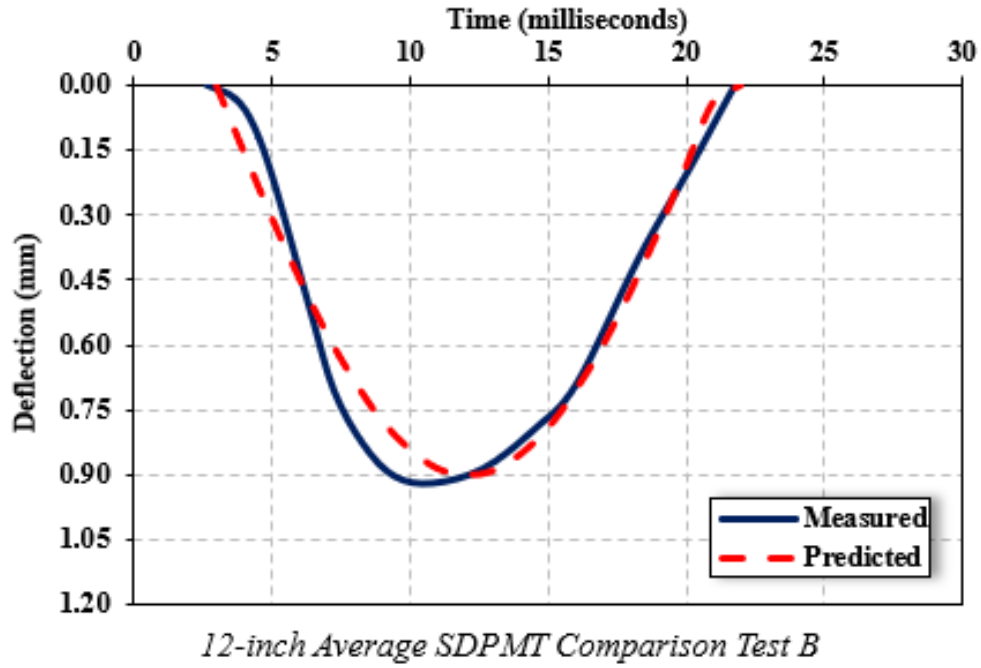

12-inch Average SDPMT Comparison Test B

Figure 6.116: Time-Deflection Comparisons between Average Measured and Predicted Soil Response Potenza Drive within Cypress Landing

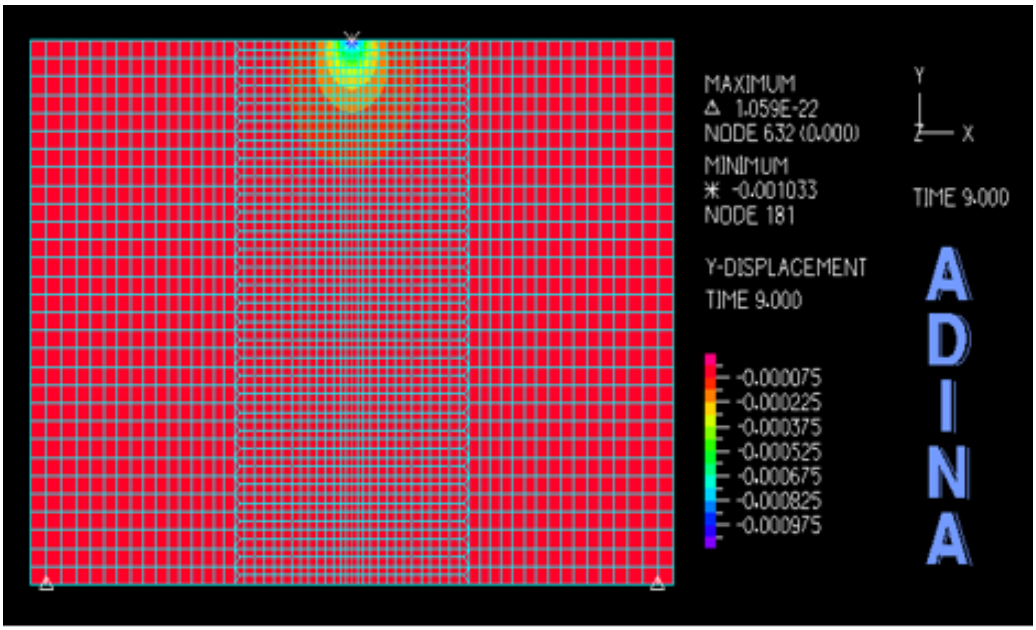

Figure 6.117: Location 103 FEA Displacements in meters - Potenza Drive Cypress Landing

Table 6.29: Summary of Modulus and Deflection Data of Base Materials - Heritage Parkway

Location	LWD Test		SDPMT Testing Mode – 6 inch				SDPMT Testing Mode – 12 inch			
	Measured (1) Deflection (mm)		Strain Level Modulus (kPa)		Predicted (2) Deflection (mm)		Strain Level Modulus (kPa)		Predicted Deflection (mm)	
	A	B	A	B	A	B	A	B	A	B
301	0.200	0.195	306661	307205	0.170	0.170	157661	157856	0.236	0.236
302	0.198	0.199	293906	293839	0.173	0.173	282731	282656	0.176	0.176
303	0.139	0.148	537368	535302	0.132	0.133	160833	160386	0.234	0.234
304	0.258	0.164	734652	789872	0.116	0.113	248779	255011	0.188	0.185
305	0.143	0.222	252527	248369	0.186	0.188	191106	187684	0.214	0.216
306	0.162	0.227	683511	650841	0.120	0.122	225317	220372	0.197	0.199
307	0.168	0.268	470212	457820	0.140	0.142	300543	290799	0.172	0.174
308	0.247	0.246	124440	124468	0.269	0.269	107893	107913	0.292	0.292
309	0.157	0.216	648789	630148	0.122	0.124	296740	290902	0.173	0.174
310	0.135	0.184	980647	931027	0.103	0.105	199885	198405	0.209	0.210
311	0.180	0.151	909069	935094	0.106	0.106	335561	338860	0.163	0.163
312	0.200	0.166	598706	607377	0.126	0.126	151123	152443	0.242	0.241
Ave.	**0.182**	**0.199**	**545041**	**542614**	**0.147**	**0.148**	**221514**	**214603**	**0.208**	**0.208**

1) Measured deflections were obtained from performing two LWD tests at each testing location.
2) Predicted deflections were determined from strain level models using average LWD strains for 6-inch and 12-inch SDPMT tests.

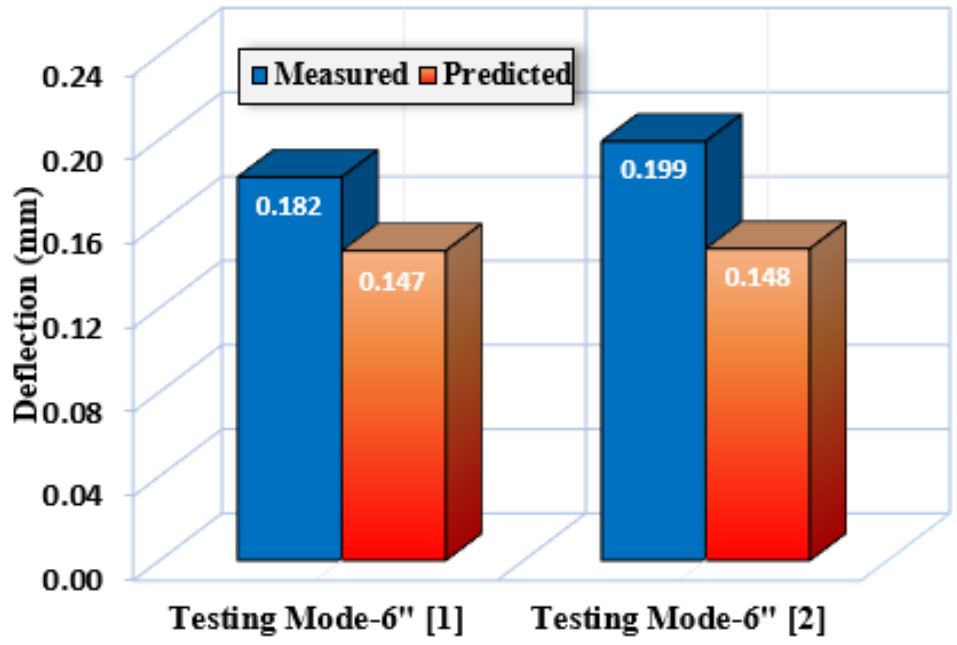

Predicted Deflections based on 6-inch SDPMT Test

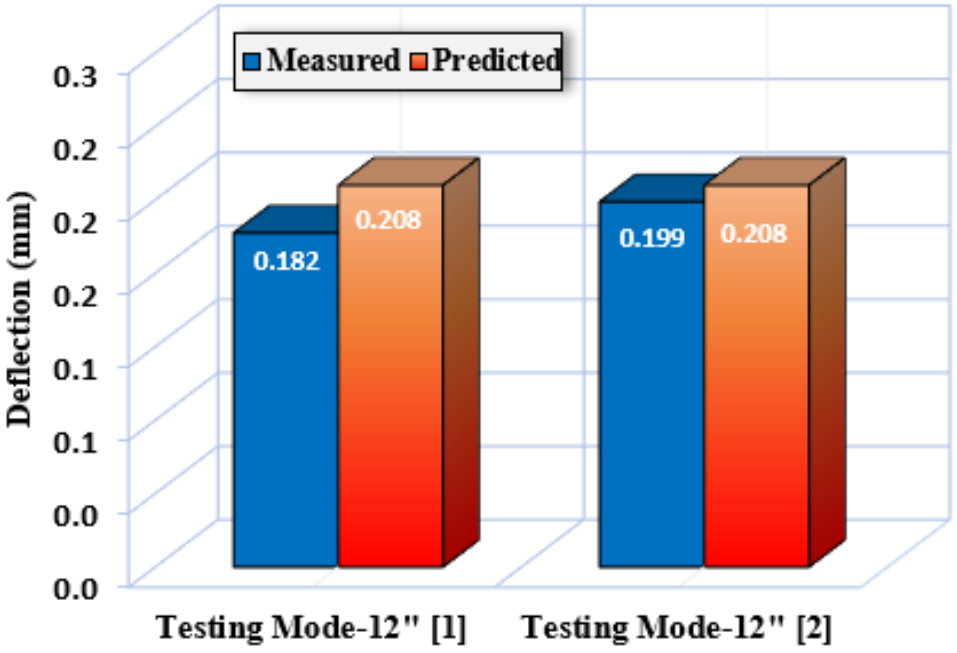

Predicted Deflections based on 12-inch SDPMT Test

Figure 6.118: Average Surface Deflection Data - Heritage Parkway

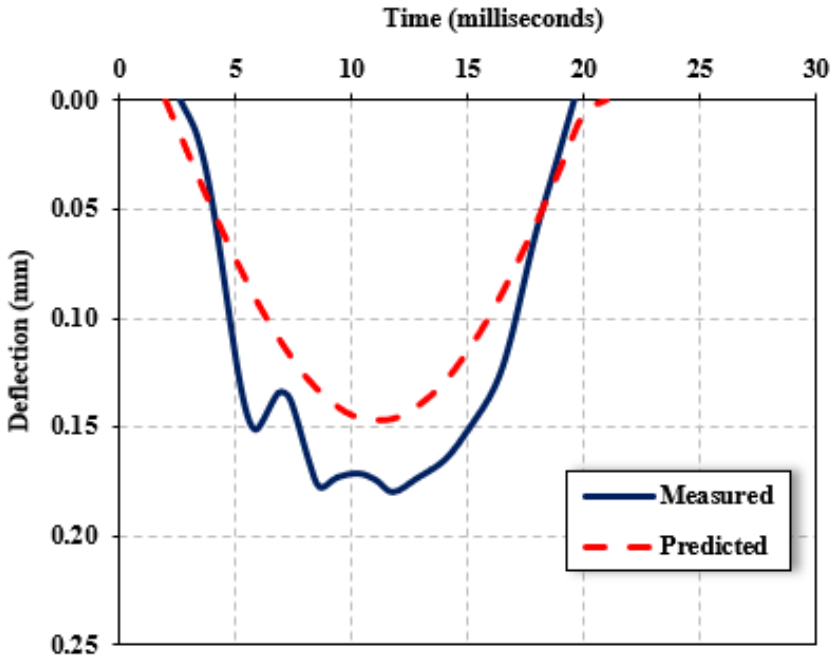

6-inch Average SDPMT Comparison Test No.1

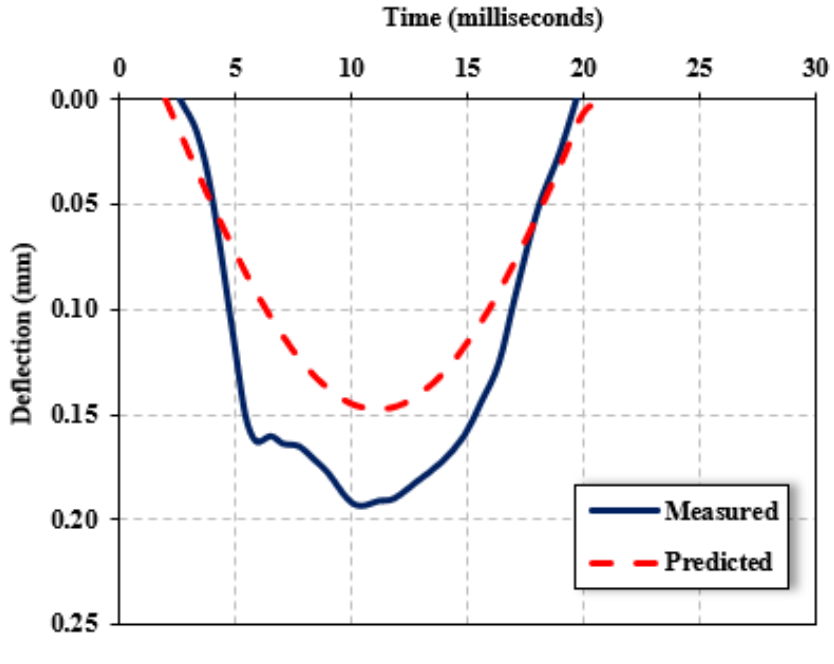

6-inch Average SDPMT Comparison Test No.2

Figure 6.119: Time-Deflection Comparison between Measured and Predicted Soil Response Heritage Parkway - SDPMT-6 Testing Mode

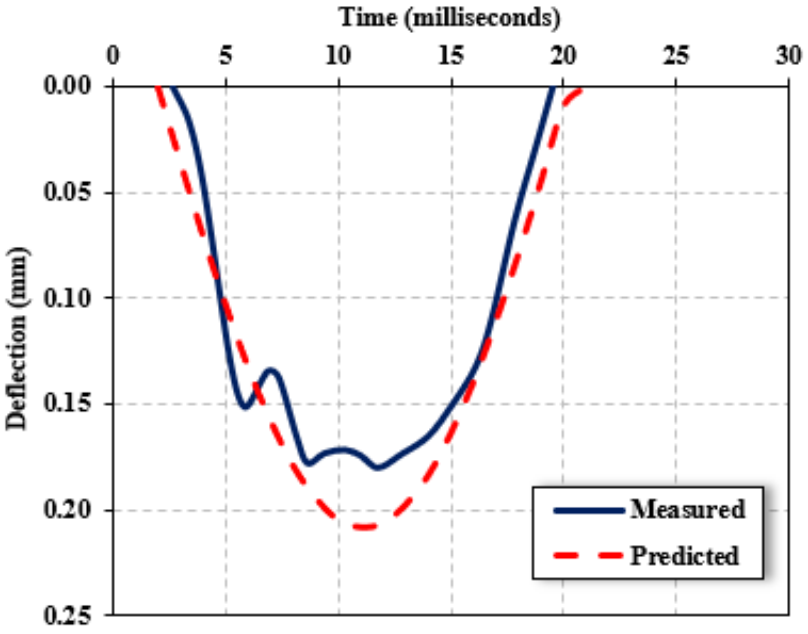

12-inch Average SDPMT Comparison Test No.1

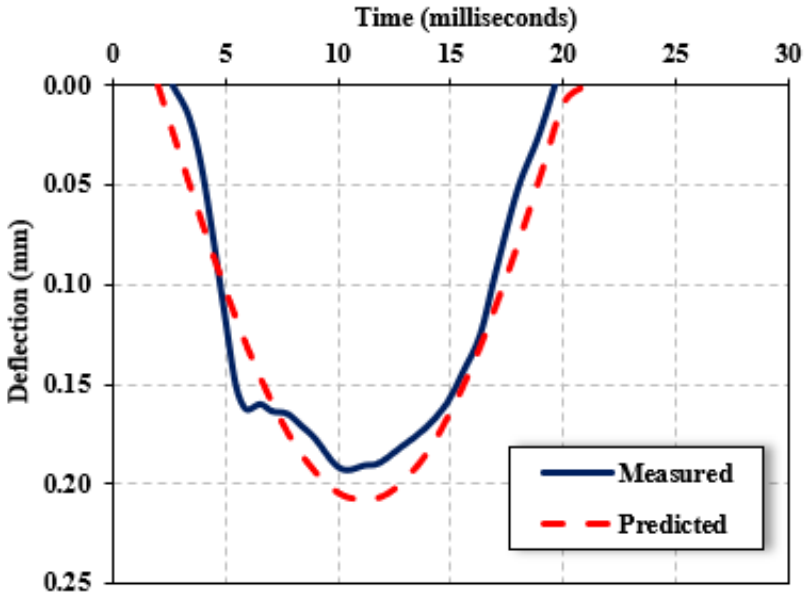

12-inch Average SDPMT Comparison Test No.2

Figure 6.120: Time-Deflection Comparison between Measured and Predicted Soil Response Heritage Parkway - SDPMT-12 Test

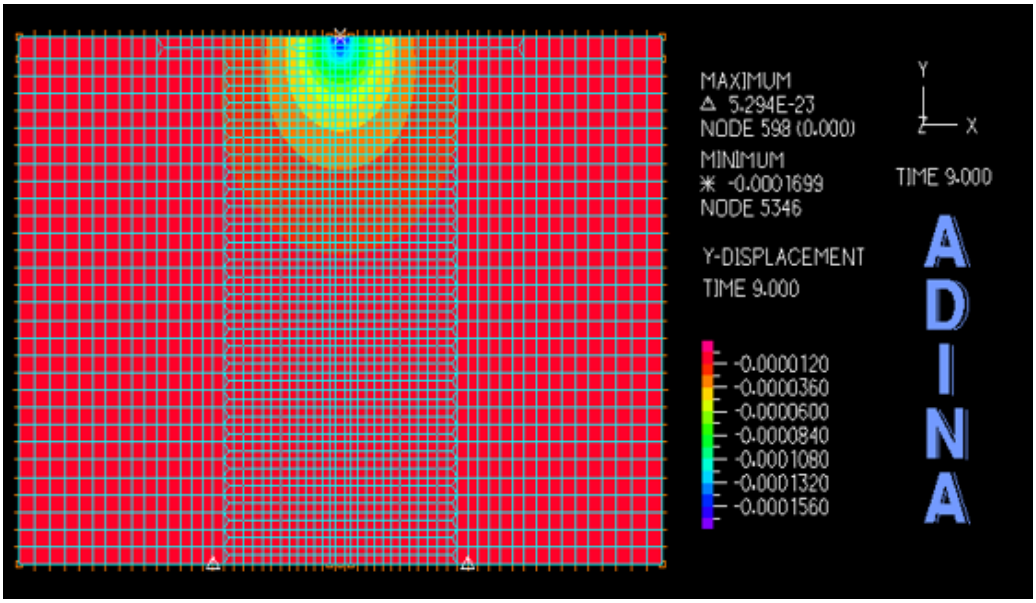

Figure 6.121: Location 301 FEA Displacements in meters - Heritage Parkway

Site	SDPMT Test	Bulk Stress (psi) 11	17	30
Southgate Field	6-inch	0.0221	0.0142	0.0046
	12-inch	0.0157	0.0101	0.0034
Cypress Landing	6-inch	N/A	N/A	N/A
	12-inch	0.0001	0.0070	0.0055
Overflow Parking	6-inch	0.0302	0.0183	0.0141
	12-inch	0.0224	0.0127	0.0110
Heritage Parkway	6-inch	0.2890	0.1759	0.1551
	12-inch	0.2108	0.1259	0.1104

Table 6.30: Unbound Base and Subbase/Subgrade Strains (%) Predicted from SDPMT Unload Data

Chapter 7

Conclusions and Recommendations

7.1 Conclusions

Based on the data acquired digitally from 159 SDPMT tests conducted with an instrumented control unit at four test sites, it is concluded that both SDPMT-6 and SDPMT-12 probes produce useful pavement engineering properties. Numerous correlations were developed between SDPMT engineering parameters indicating that the SDPMT stiffness E_0 and limit pressure or strength p_L produce the best correlations and that the lift-off pressure p_0 yielded the weakest correlations. Of the four SDPMT probe/test types conducted, correlations were strongest with SDPMT-12 probes and weakest with the continuous or rapid tests. These data were obtained in the NDG drive hole immediately following NDG testing, indicating that SDPMT testing could replace the NDG testing. SDPMT and NGD testing times were comparable.

Both E_0 and p_L produced excellent correlations with LWD and Clegg impact data, indicating that field devices which produce stiffnesses can be correlated with SDPMT E_0 and p_L. NDG γ_{dry} correlated well to both E_0 and p_L, although there is a gap in the dataset of the density ranges tested, but still indicating that reliable correlations can be developed.

Continuous or rapid testing must be evaluated further because: a) data from SDPMT continuous tests showed more scatter, b) p_0 values were unrealistically high, and c) elastic moduli from the continuous tests were approximately two times those from the incremental tests.

7.1.1 SDPMT Stress - Strain Conclusions

The stress – strain responses from the SDPMT incremental and continuous, 6 and 12 inch tests resembles those obtained from incremental PPMT testing.

The E_0/p_L ratio from incremental SDPMT tests ranged from 7.0 to 16.1 for both 6 and 12 inch probes, which is similar to Briaud's (2005) published relationship of 7 to 12, proving that SDPMT test data quality is acceptable.

The E_0/p_L ratio for rapid or continuous SDPMT tests ranged from 10.9 to 33.2 for the 6 and 12 inch probes. Although, the upper values are higher than 12, the tests are still of good quality, because the higher values are due to the increased strain-rate applied to the soil compared to the incremental test strain-rate.

7.1.1.1 p_L versus E_0

Excellent correlations were found between p_L and E_0, using units of kPa. SDPMT-12 incremental data produced both the linear and exponential equations (i.e., $E_0 = 14.77p_L - 1127$ and $E_0 = 5.68(p_L)^{1.281}$) with $R^2 = 0.98$, suggesting that engineers my be able to predict p_L from E_0. This finding would be beneficial for SDPMT tests with questionable p_L values. These p_L and E_0 correlations were very similar to those found by Cosentino et al. (2008) and Briaud (2005).

7.1.1.2 p_0 versus E_0 and p_L

Poor correlations between p_0, E_0 or p_L were observed with the 6 inch and 12 inch probes for both incremental and continuous tests.

7.1.2 SDPMT - Density Conclusions

7.1.2.1 γ_{dry} versus E_0

Data collected during this research shows a good correlation between γ_{dry} and SDPMT E_0 for all test configurations. The exponential relationship $\gamma_{dry}(pcf) = 74(E_0)(kPa)^{0.06354}$ produced R^2 of 0.85 as did the log-linear and log-log correlations from SDPMT-12 incremental testing.

7.1.2.2 γ_{dry} versus p_L

Even though there was a gap in the dataset of unit weights, γ_{dry}, and p_L data produced promising correlations for all test configurations. The SDPMT-6 and -12 incremental exponential models both produced R^2 values of 0.86, with the SDPMT-12 incremental equation being: $\gamma_{dry}(pcf) = 82.69(p_L(kPa))^{0.07391}$.

7.1.3 LWD Stiffness-SDPMT E_0 and p_L Conclusions

Moduli correlations from SDPMT and LWD data were stronger based on Zorn LWD data than Dynatest LWD data. Nearly all R^2 values exceeded 0.70, indicating good to excellent stiffness correlations exist between SDPMT moduli and LWD moduli from both devices. Generally, either linear-linear or exponential models produced the highest R^2 values.

7.1.3.1 Zorn LWD versus SDPMT

Excellent linear-linear and exponential correlations were developed between $E_{d,Zorn}$ and SDPMT E_0. Both stiffnesses having units of kPa for the correlations. SDPMT-6 continuous data produced the highest linear-linear correlation ($R^2 = 0.83$) based on $E_{d,Zorn} = 1.816E_0 + 15,950$, and the highest exponential correlation ($R^2 = 0.87$) based on $E_{d,Zorn} = 75.77(E_0)^{0.6748}$.

$E_{d,Zorn}$ and SDPMT p_L correlations produced slightly higher R^2 values than $E_{d,Zorn}$ and SDPMT E_0 correlations. Again the correlations were developed based on units of kPa. Both the SDPMT-6 and -12 continuous data produced R^2 values of 0.88 for the linear-linear and exponential models, while the log-linear SDPMT-6 incremental data produced R^2 of 0.93. The exponential model is $E_{d,Zorn} = 453.4(p_L)^{0.7057}$ (See Table 6.15).

7.1.3.2 Dynatest LWD versus SDPMT

Generally, the Dynatest LWD moduli ($E_{0,Dynatest}$) and SDPMT E_0 data produced good linear-linear and exponential correlations, as shown in Table 6.6. The highest R^2 value of 0.85 resulted from the SDPMT-12 continuous exponential model, according to the equation being $E_{0,Dynatest}(kPa) = 120.7(E_0(kPa))^{0.7981}$.

Generally, the Dynatest LWD moduli ($E_{0,Dynatest}$) and SDPMT p_L data produced good correlations; however, they were lower than the corresponding Zorn correlations (See Table 6.16). The exponential model $E_{0,Dynatest} = 2132(p_L)^{0.6933}$ produced the highest R^2 value of 0.86, when units of kPa were used.

7.1.4 CIV Conclusions

Stiffnesses in kPa from SDPMT testing correlated well to CIV values in g's from Clegg impact hammer testing. Good exponential correlations were developed between CIV and SDPMT incremental initial moduli, with R^2 values ranging from 0.75 to 0.90. The equation $CIV = 0.5934(E_0)^{0.3724}$, developed from SDPMT-6 incremental data, resulted in a R^2 value of 0.90.

Good exponential correlations were also developed between CIV and SDPMT p_L data in kPa, with R^2 values ranging from 0.75 to 0.90. The equation $CIV = 0.8335(p_L)^{0.4515}$, developed from SDPMT-6 incremental data, resulted in a R^2 value of 0.87.

7.1.5 Conclusions from DCP PI Evaluation

Based on the data collected, no useful correlations could be developed between the DCP PI and SDPMT p_0, p_L or E_0 data.

7.1.6 Resilient Moduli Conclusions

Combining SDPMT unload stress-strain results from 6- and 12-inch with AASHTO T 307 M_r values produced realistic strains for subbase/subgrade and base materials. This

finding further validates the usefulness of SDPMT data for pavement design and analysis.

7.1.7 SDPMT and LWD FEA Predicted-Measured Conclusions

When SDPMT-6 and -12 unload stress-strain results were input into FEA analyses, they slightly under predicted Zorn LWD deflections (i.e., in the 10 to 20 % range), with SDPMT-12 data producing more accurate predictions than SDPMT 6-inch data.

7.2 Recommendations

There are promising correlations between SDPMT data, LWD stiffnesses and NDG dry unit weights, recommended for trial use by pilot projects. The strongest correlations which were based on incremental SDPMT testing are recommended at this time. The use of these correlations is the first step in replacing NDG specifications. As industry becomes more accustomed to using SDPMT data, NDG testing may be phased out.

The following are possible areas of additional research:

- Using the strong correlations from the 12-inch SDPMT, additional tests should be performed to determine how accurately limit pressures can be predicted from initial moduli. Once this is completed, data from the LWD and Clegg impact tests should be evaluated to determine how accurately SDPMT limit pressures can be estimated from these tests.
- The time savings from using a rotary hammer drill and masonry drill bit to produce holes for testing in the dry cemented coquina base is recommend in stiff materials to optimize the testing procedure. Although, a study is needed to compare densities in base rock when using the hammer drill-masonry bit hole preparation compared with standard drive pin method.
- Surface cracking affects the quality of the SDPMT test; therefore, an investigation should be conducted to evaluate the benefits of using surcharge weights at the soil surface, and how they affect the surface cracking and the pressuremeter parameters.
- The unloading portion of the SDPMT tests should be used to estimate elastic moduli at various strains, and can be related to the lab resilient modulus.
- Use of a 5,000 kPa PMT control unit is warranted for base materials which display limit pressures in excess of 3,500 kPa.
- Modify the existing SDPMT probe ends to properly control any membrane slipping.
- An automated pressuremeter control unit should be developed to make continuous testing more consistent.

- Because only SP embankment soils and a very dry cemented coquina were tested, more soils must be tested to validate and strengthen these correlations.
- The existing correlations between NGD γ_d and both SDPMT E_0 and p_L showed promise but must be validated by including tests with unit weights from 115 to 125 pcf (which was the range missing from this dataset).

References

Airport Structural Guidelines (ASG-19). "Pavement Structural Design." Report AK-68-12, Transport Canada, Ottawa, 1992.

Altschaeffl, A. G., Prapaharan, S., Holtz, R. D., and Chameau, J.L. "Effect of Disturbance on Pressuremeter Results in Clays." *Journal of Geotechnical Engineering* 116 (1990).1: 35–53. ID: 5711438291.

ARA Inc. "Guide for Mechanistic-Empirical Design of New and Rehabilitated Pavement Structures." Final report, National Cooperative Highway Research Program (NCHRP) Project 1-37A, 2006.

Aubeny, C. P., Whittle, A. J., and Ladd, C.C. "Effects of Disturbance on Undrained Strengths Interpreted from Pressuremeter Tests." *Journal of Geotechnical and Geoenvironmental Engineering* 126 (2000): 1133–1144. ID: 201402334.

Baguelin, F., Jézéquel, J. F., and Shields, D. H. *The pressuremeter and foundation engineering*. Series on rock and soil mechanics ;. Clausthal, Germany: Aedermannsdorf, Switzerland: Trans Tech Publications; Distributed by Trans Tech S.A., 1978, 1st ed.

Baguelin, G.J., Frank, R.A., and Nahra, R. "A Theoretical Study of the Pore Pressure Generation and Dissipation Around the Pressuremeter." *The Pressuremeter and its Marine Applications*. 1986, 169–186.

Bathe, K. *Finite Element Procedures*. Prentice Hall and Pearson Education, Inc., 2014, 2nd ed.

Briaud, Jean-Louis. *The Pressuremeter: Application to Pavement Design*. Ph.D. thesis, University of Ottawa, Ottawa, Canada, 1979.

———. *The Pressuremeter*. A.A. Balkema, 2005, 2nd ed.

Briaud, J.L. and Felio, G.Y. "Conventional Parameters from Pressuremeter Test Data: Review of Existing Methods." *The Pressuremeter and its Marine Applications*. 1986, 265–282.

Briaud, J.L., Tucker, L., and Smith, T. "Pressuremeter Design of Laterally Loaded Piles." Report 340-3, State Department of Highway and Public Transportation, Federal Highway Administration, Texas, USA, 1983.

Chen, Dar-Hao, Wu, Wei, He, Rong, Bilyeu, John, and Arrelano, Mike. "Evaluation of in-situ resilient modulus testing techniques." *Geotechnical Special Publication. ASCE* 86 (1999): 1–11.

Chen, DH, Lin, DF, Liau, PH, and Bilyen, J. "A correlation between dynamic cone penetrometer values and pavement layer moduli." *Geotechnical Testing Journal* 28 (2005).1: 1. Doi: 10.1520/GTJ12312 pmid:.

Cho, Y., McCullough, B. F., and Weissmann, J. "Considerations on Finite Element Method Application in Pavement Structural Analysis." *Transportation Research Record: Journal of the Transportation Research Board* 1539 (2000): 96–101.

Choubane, B. and McNamara, R.J. "A Practical Approach to Predicting Flexible Pavement Embankment Moduli Using Falling Weight Deflectometer (FWD) Data." Report FL/DOT/SMO/00-442, State Materials Office, Tallahassee, FL, 2000.

Clarke, B. G. and Sadeeq, J. A. "A Practical Guide to the Derivation of Undrained Shear Strength from Pressuremeter Tests." *Advances in Site Investigation Practice*. Institution of Civil Engineers, London, UK: Thomas Telford, 1996, 559–570.

Clarke, B.G. "Pressuremeter Testing in Ground Investigation. Part 1-Site Operations." *Proceeding of the Institution of Civil Engineers: Geotechnical Engineering*. vol. 119(2). 1996, 96–108.

Clarke, B.G. and Gambin, M.P. "Pressuremter Testing in onshoure ground investigations: A report by the ISSMGE Committee TC16." Tech. rep., 1998.

Cosentino, Paul J. *Pressuremeter Moduli for Airport Pavement Design*. Ph.D. thesis, Texas A&M University, Austin, TX, 1987.

Cosentino, Paul J, Kalajian, Edward, Messaoud, Farid, Sundaram, Sunil, Misilo, Thaddeus J, and Horhota, David J. "Correlations between PENCEL pressuremeter, cone penetrometer, and dilatometer parameters." *Transportation Research Record: Journal of the Transportation Research Board* 2053 (2008).1: 65–71.

Cosentino, Paul J, Kalajian, Edward, Stansifer, Ryan, Anderson, J Brian, Kattamuri, Kishore, Sundaram, Sunil, Messaoud, Farid, Misilo, Thaddeus J, and Cottingham, Marcus A. "Standardizing the Pressuremeter Test for Determining py Curves for Laterally Loaded Piles." Final report, Florida Department of Transportation, 2006.

Cunha, Renato Pinto da. *Interpretation of selfboring pressuremeter tests in sand*. Ph.D. thesis, University of British Columbia, Canada, 1994.

Dai, S. and Kermer, C. "Improvement and Validation of Mn/DOT DCP Specifications for Aggregate Base Materials and Select Granulars." Report MN/RC-2005-32, Minnesota Department of Transportation, U.S.A., 2006.

Davich, Peter, Camargo, Felipe, Larsen, Brett, Roberson, Ruth, and Siekmeier, John. "Validation of DCP and LWD Moisture Specifications for Granular Materials." Tech. rep., Minnesota Department of Transportation, 2006.

Dean, S.W., Choubane, B., Gokhale, A., and Nazef, A. "Assessing the Precision of Falling Weight Deflectometer for Field Measurements." *Journal of ASTM International* (2006).

Erbland, Phillip James. *Modifying the Pavement Pressuremeter to Enable Low Strain Level Resilient Moduli Determination.* Master's thesis, Florida Institute of Technology, Melbourne, FL, 1993.

FDOT. *Standard Specifications for Road and Bridge Construction.* Florida Department of Transportation, 2018.
URL `http://www.fdot.gov/programmanagement/Implemented/SpecBooks/January2018/Files/118eBook.pdf`

Fleming, Paul, Frost, Matthew, and Lambert, John. "Review of lightweight deflectometer for routine in situ assessment of pavement material stiffness." *Transportation research record: journal of the Transportation Research Board* (2007).2004: 80–87.

for Testing, American Society and Materials. "Standard Test Method for Deflections with a Falling-Weight-Type Impulse Load Device." Standard D4694-09, ASTM, 2009.

George, K.P. and Uddin, W. "Subgrade Characterization for Highway Pavement Design." Report FHWA/MS-DOT-RD-00-131, Mississippi Department of Transportation, USA, 2000.

Gibson, R.E. and Anderson, W.F. "In-situ Measurements of Soil Properties with the Pressuremete." *Civil Engineering and Public Works Review* 56 (1961).658: 615–618.

Gupta, S., Ranaivoson, A., Edil, T., Benson, C., and Sawangsuriya, A. "Pavement Design Using Unsaturated Soil Technology." Rerpot no. mn/rc-2007-11, University of Minisota, Minneapolis, 2007.

Hartman, John Paul. *Finite Element Parametric Study of Vertical Strain Influence Factors and the Pressuremter Test to Estimate the Settlement of Footings in Sand.* Ph.D. thesis, University of Florida, Gainesville, Florida, 1974.

Hassan, Azmi Bin. *The effects of material parameters on Dynamic Cone Penetrometer results for fine-grained soils and granular materials.* Ph.D. thesis, Oklahoma State University Stillwater, Oklahoma, 1996.

Ho, Jeong Ho, Fernando, E. G., and Holzschuher C., Horhota D. "Comparison of resilient modulus values for Florida flexible mechanistic-empirical pavement design." *International Journal of Pavement Engineering* 13 (2012).5: 472–484.

Ho, R. K. H. "Memorandum to W.N. Lofroos." Memorandum State Pavement Design Engineer, 1992.

Holtz, R. D. and Kovacs, W. D. *An Introduction to Geotechnical Engineering*. New Jersey, USA: Prentice-Hall, Inc.,, 1981.

Hossain, M. Shabbir, Apeagyei, Alex K., Virginia., Department of Transportation., United States., Federal Highway Administration., and Council., Virginia Transportation Research. "Evaluation of the lightweight deflectometer for in-situ determination of pavement layer moduli." Tech. rep., Virginia Transportation Research Council (VTRC), Charlottesville, Va., 2010. ID: 607347538.

Houlsby, GT and Yu, HS. "Finite Element Analysis of the Cone-Pressuremeter Test." *Pressuremeters proceedings of the Third International Symposium on Pressuremeters, organised by the British Geotechnical Society and held at Oxford University, 2-6 April 1990*. 1990, 221–230.

Huang, An-Bin. *LABORATORY PRESSUREMETER EXPERIMENTS IN CLAY SOILS*. Ph.D. thesis, Purdue University, 1986. Copyright - Copyright UMI - Dissertations Publishing 1986; Last updated - 2015-08-25; First page - n/a. URL `http://search.proquest.com.portal.lib.fit.edu/docview/303529147?accountid=27313`

Hughes, M. O., Worth, C. P., and Windle, D. "Pressuremeter Tests in Sands." *Geotechnique Journal* (1977).27(4): 455–477.

Jansen, Jacob W. *Correlating Strength and Stiffness Data of the PENCEL Pressuremeter and Triaxial Compression Tests in Florida Sands*. Master's thesis, Florida Institute of Technology, Melbourne, FL, 2017.

Jewell, R.J., Fahey, M., and Worth, C.P. "Laboratory Studies of the Pressuremeter Test in Sand." *Géotechnique* 30 (1980).4: 507–531.

Kögler, F. "Discussions of soil mechanics research." *Am. Soc. Civ. Engrs. Transact* 98 (1933): 299–301.

Kolisoja, P. *Resilient Deformation Characteristics of Granular Materials*. Ph.D. thesis, Tampere University of Technology, Finland, 1997. Publication No 223.

Kondner, RL. "Hyperbolic Stress-Strain Response: Cohesive Soils." *Journal of the Soil Mechanics and Foundations Division* 89 (1963).1: 115–144.

Ladd, C.C., Germaine, JJT, Baligh, M.M., and Lacasse, S.M. "Evaluation of Self-Boring Pressuremeter Test in the Boston Blue Clay." Intrm report, Urban Mass Transportation Administration, 1980.

Lassourdiere, F.M. and Zanier, F.B. "Numerical Analysis of Pressuremeter Tests by the Finite Element Method." *The Pressuremeter and its Marine Applications*. 1986, 121–136.

Law, K.T. "Computer-Aided Pressuremeter Test." *Geotechnical Testing Journal, GTJODJ* 7 (1984).2: 99–103.

Mair, RJ and Wood, DM. "Pressuremeter testing: methods and interpretation." *Construction Industry Research and Information Association* (1987).

Misilo III, T.J. *Development of a Small Diameter Rapid Pressuremeter Test for Unbound Pavement Layer Evaluations*. Ph.D. thesis, Florida Institute of Technology, Melbourne, Florida, 2018.

Mohammad, Louay N, Nazzal, Munir D, Abu-Farsakh, Murad Y, and Alshibli, Khalid. "Estimation of subgrade soils resilient modulus from in-situ devices test results." *Journal of Testing and Evaluation* 37 (2009).3: 245–253.

National Cooperative Highway Research Program. "NDT Technology for Quality Assurance of HMA Pavement Construction." Report 626, Transportation Research Board, Washington, D.C., 2009.

Newmark, N.M. "A method of computation for structural dynamics." *Journal of Engineering Mechanics* 85 (1959).EM3: 67 – 94.

Ni, B., Hopkins, T.C., Sun, L., and Beckham, T.L. "A General Method of Reporting Resilient Modulus Test of Soils: A Pavement Engineer's Point of View." *72nd Annual Meeting of the Transportation Research Board*. Washington, D.C., 1993.

———. "Modeling the Resilient Modulus of Soils." *Proceedings of the 6th International Conference on the Bearing Capacity of Roads, Railways, and Airfields*. vol. 2. Rotterdam, Netherlands: Balkema Publishers, 2002, 1131–1142.

Ooi, P.S.K., Archilla, A.R., and Sandefur, K.G. "Resilient Modulus for Compacted Choesive Soils." *Transportation Research Record: Journal of the Transportation Research Board* 1874 (2004): 115–124.

Pandey, B.B., Srinivasa, K.R., and Sudhakar, R.K. "Regression Models for Estimation of In-Situ Subgrade Moduli from DCP Tets." *Indian Roads Congress* 31 (2003).7: 5–19.

Paul, J. B. "In-Situ Rock Modulus Apparatus." Tech. Rep. Rep. No.4910-4504-721-12, FDOT, 2004.

Ping, W.V, Yang, Z., Liu, C., and Dietrich, B. "Measuring Resilient Modulus of Granular Materials in Flexible Pavements." *Transportation Research Record: Journal of the Transportation Research Board* (2001): 81–90.

Prapaharan, Sinnadurai. *Effects of disturbance, strain rate, and partial drainage on pressuremeter test results in clay*. Ph.D. thesis, Purdue University, 1987. ID: 57718380.

Rao, Ch Nageshwar, George, Varghese, and Shivashankar, R. "PFWD, CBR and DCP evaluation of lateritic subgrades of Dakshina Kannada, India." *The 12th International Conference of International Association for Computer Methods and Advances in Geomechanics. Goa: Indian Institute of Technology*. 2008, 4417–4423.

Salgado, Rodrigo and Yoon, Sungmin. "Dynamic cone penetration test (DCPT) for subgrade assessment." Report FHWA/IN/JTRP-2002/30, Joint Transportation Research Program, 2003.

Sanders, P.J. "Mechanistic Pavement Design Using a PENCEL Pressuremeter." *Proceedings of the Tenth Regional Conference for Africa Soil Mechanics and Foundation Engineering*. eds. A.A. Balkema, Rotterdam, and Brookfield. Africa, 1991, 177–185.

Schnaid, Fernando. *In Situ Testing in Geomechanics: The Main Tests*. New York: Taylor and Francis, 2009.

Seed, H.B., Mitry, F.G., Monismith, C.L., and Chan, C.K. "Factors Influencing the Resilient Deformations of Untreated Aggregate Base into Tow Layer Pavements Subjected to Repeated Loading." *Highway Research Record* 190 (1967): 19–55.

Shaban, A. M. *Evaluation of Unbound Pavement Layer Moduli Using the Miniaturized Pressuremeter Test*. Ph.D. thesis, Florida Institute of Technology, Melbourne, Florida, 2016.

Shaban, A.M. and Cosentino, P.J. "Characterizing Structural Performance of Unbound Pavement Materials Using Miniaturized Pressuremeter and California Bearing Ratio Tests." *Journal of Testing and Evaluation* 45 (2017).3: 818–834.

Shackel, B. "Repeated Loading of Soils - A Review." *Australian Road Research* 5 (1973).3: 22–49.

Siekmeier, John. "Using the dynamic cone penetrometer and light weight deflectometer for construction quality assurance." Tech. rep., Minnesota Department of Transportation, St. Paul, Minn.; [Springfield, Va.], 2009. ID: 441875986.

Song, Y. *Testing and Analysis of Recycled Materials for Highway Projects*. Ph.D. thesis, University of Hawaii, Hawaii, 2009.

Stamp, D.H. and Mooney, M.A. "Influence of Lightweight Deflectometer Characteristics on Deflection Measurement." *Geotechnical Testing Journal* 36 (2013).22: 216–226.

State Materials Office. *The Florida Sampling and Testing Methods (FM).* Florida Department of Transportation, 2000.

Steinert, Bryan C., Humphrey, Dana Norman., and Kestler, Maureen A. "Portable falling weight deflectometer study." Tech. rep., University of Maine at Orono, Storrs, CT; [Springfield, Va.], 2005. ID: 61233176.

Tang, X., Stoffels, S. M., and Palomino, A. M. "Evaluation of Pavement Layer Moduli Using Instrumentation Measurements." *International Journal of Pavement Research and Technology* 6 (2013): 755–764.

Tanyu, B. F., Kim, W. H., Edil, T. B., and Benson, C. H. "Comparison of Laboratory Resilient Modulus with Back-Calculated Elastic Moduli from Large- Scale Model Experiments and FWD Tests on Granular Materials." *Resilient Modulus Testing for Pavement Components, ASTM STP 1437.* eds. G. N. Durham, W.A. Marr, and W. L. De Groff. ASTM International, 2003, 191–208.

Tawfiq, K., Armaghani, J., and Sobanjo, J. "Seismic Pavement Analyzer vs. Falling Weight Deflectometer for Pavement Evaluation: Comparative Study." *Nondestructive Testing of Pavements and Back-calculation of Moduli: Third Volume, ASTM STP 1375.* eds. D. Tayabji and E. O. Lukanen. American Society for Testing and Materials, 2000, 191–208.

Terry, T.A. *Soil Properties from Preboring and Driven Pressuremeters.* Master's thesis, Texas A&M University, College Station, Texas, 2016.

Thottempudi, K.A. *Back-calculation of Layer Moduli of Granular Layers for Both Rigid and Flexible Pavements.* Ph.D. thesis, Michigan State University, Michigan, USA, 2010.

Uzan, J. "Characterization of Granular Material." *Transportation Research Record: Journal of the Transportation Research Board* 1022 (1895): 52–59.

Witczak, M.W. and Uzan, J. "The Universal Airport Pavement Design System." Report 1 of 4 granular material characterization, College Park, 1988.

Appendix A

Southgate Field Pressuremeter Test Results

A.1 SDPMT-6 Incremental Test Data

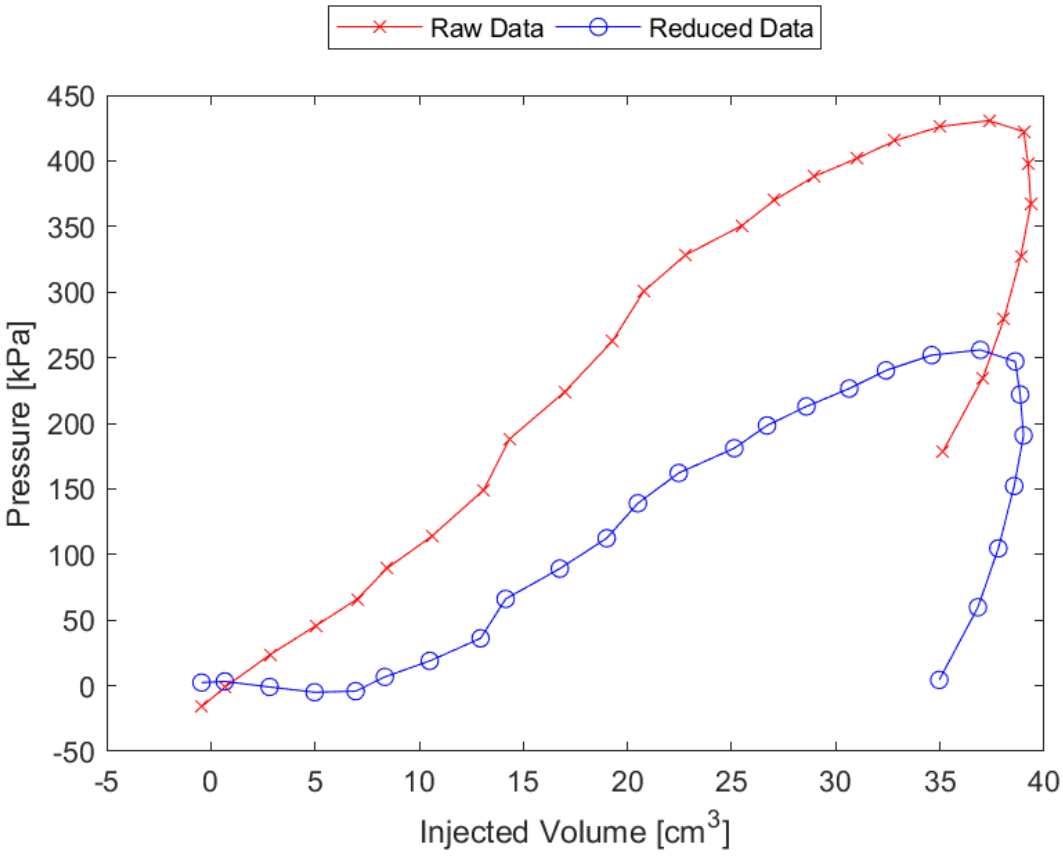

Figure A.1: Sounding 401, SDPMT-6 Incremental Test, Membrane O.D. 0.625m, Depth 0.25 m, Raw and Reduced Data

Table A.1: Sounding 401, SDPMT-6 Incremental Test, Result Summary

Parameter				
Lift-Off Pressure (p_0)	6.7	kPa	0.97	psi
Contact Volume (V_c)	8.4	cm^3	0.51	in^3
Limit Pressure (p_L)	300.0	kPa	43.51	psi
Assumed ν		0.33		
Initial Modulus (E_0)	1488.0	kPa	215.82	psi
Dry Unit Weight (γ_{dry})	1653.1	kg/m^3	103.2	lb/ft^3
Wet Unit Weight (γ_{wet})	1741.2	kg/m^3	108.7	lb/ft^3

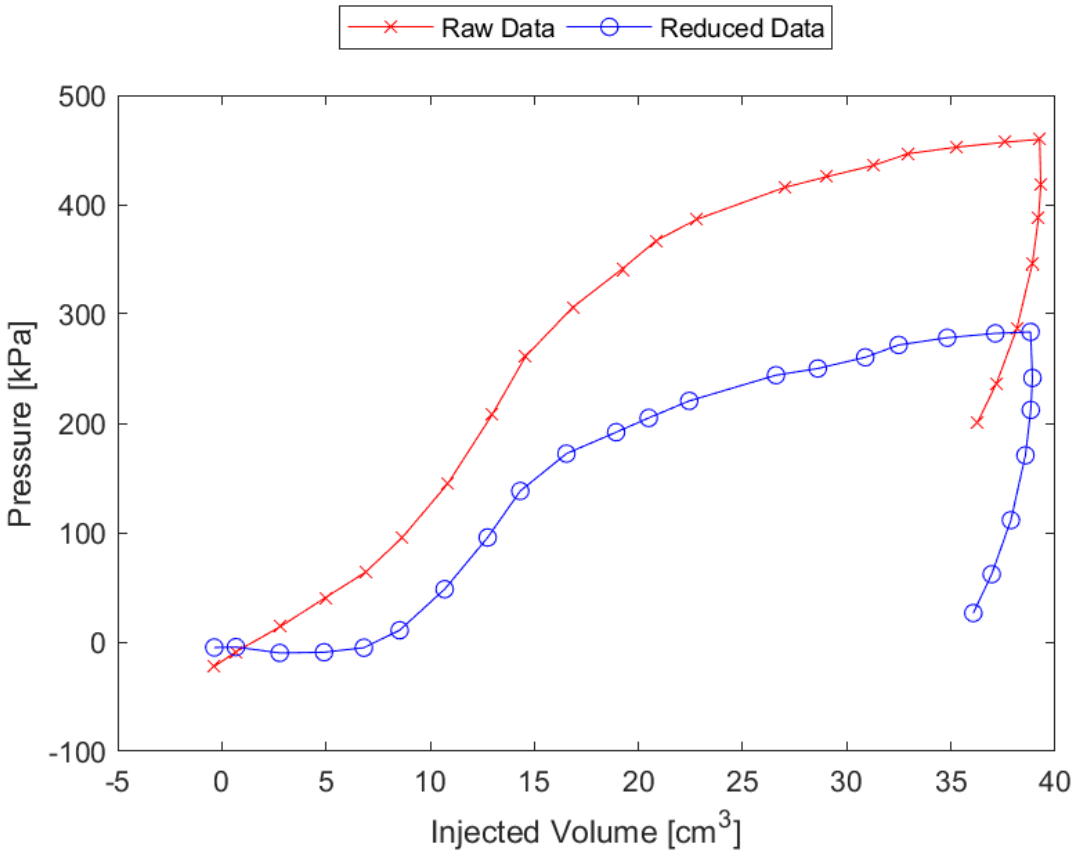

Figure A.2: Sounding 402, SDPMT-6 Incremental Test, Membrane O.D. 0.625m, Depth 0.25 m, Raw and Reduced Data

Table A.2: Sounding 402, SDPMT-6 Incremental Test, Result Summary

Parameter				
Lift-Off Pressure (p_0)	10.7	kPa	1.56	psi
Contact Volume (V_c)	8.5	cm^3	0.52	in^3
Limit Pressure (p_L)	320.0	kPa	46.41	psi
Assumed ν		0.33		
Initial Modulus (E_0)	2431.1	kPa	352.60	psi
Dry Unit Weight (γ_{dry})	1694.8	kg/m^3	105.8	lb/ft^3
Wet Unit Weight (γ_{wet})	1821.3	kg/m^3	113.7	lb/ft^3

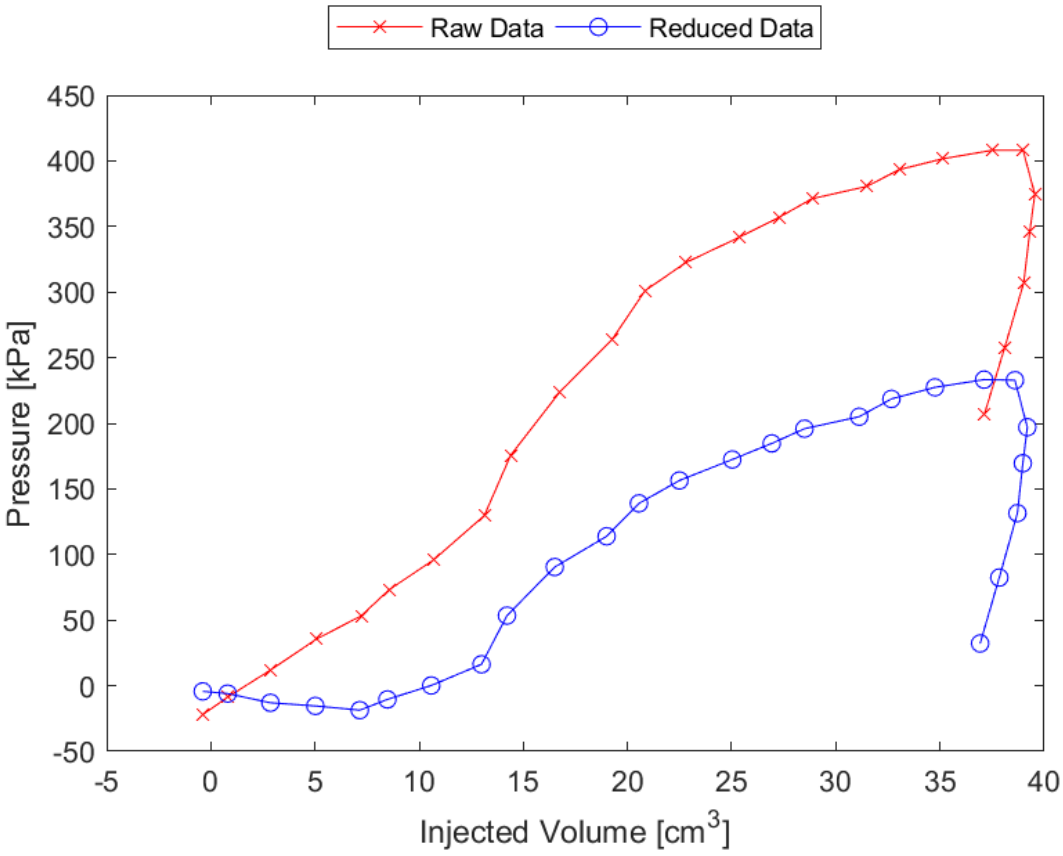

Figure A.3: Sounding 403, SDPMT-6 Incremental Test, Membrane O.D. 0.625m, Depth 0.25 m, Raw and Reduced Data

Table A.3: Sounding 403, SDPMT-6 Incremental Test, Result Summary

Parameter				
Lift-Off Pressure (p_0)	16.3	kPa	2.37	psi
Contact Volume (V_c)	13.0	cm^3	0.79	in^3
Limit Pressure (p_L)	280.0	kPa	40.61	psi
Assumed ν		0.33		
Initial Modulus (E_0)	2516.0	kPa	364.91	psi
Dry Unit Weight (γ_{dry})	1714.0	kg/m^3	107.0	lb/ft^3
Wet Unit Weight (γ_{wet})	1736.4	kg/m^3	108.4	lb/ft^3

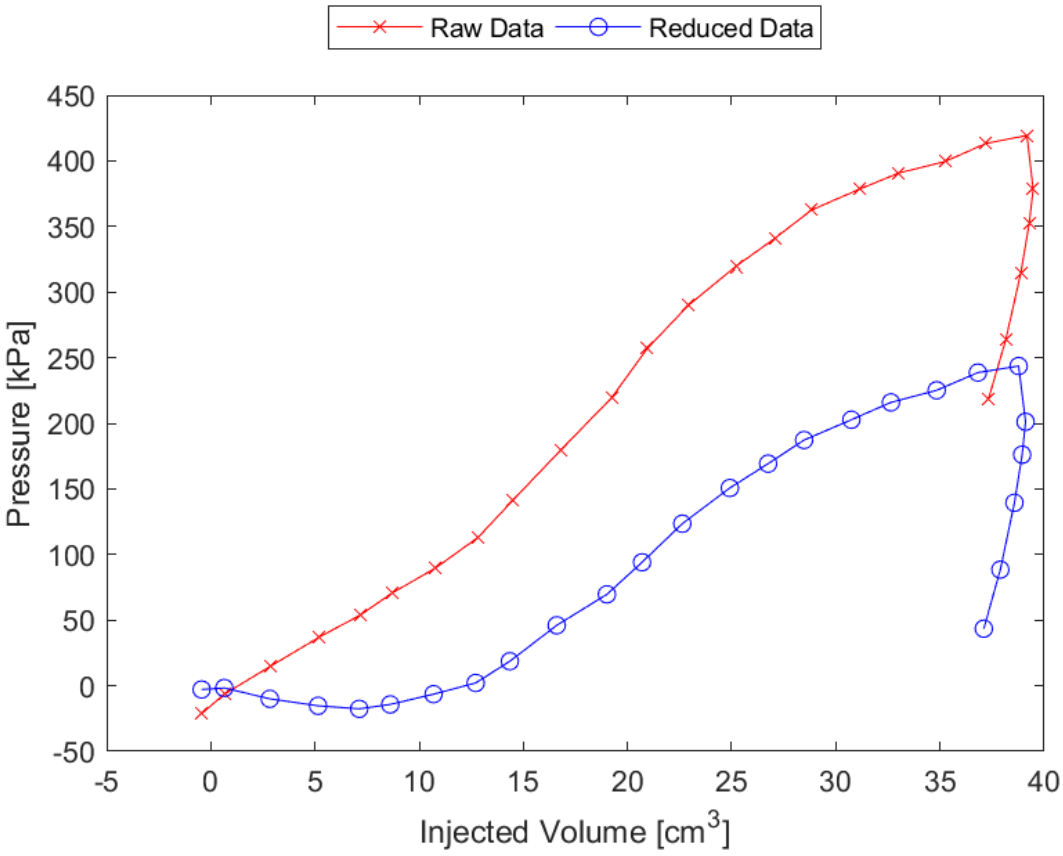

Figure A.4: Sounding 404, SDPMT-6 Incremental Test, Membrane O.D. 0.625m, Depth 0.25 m, Raw and Reduced Data

Table A.4: Sounding 404, SDPMT-6 Incremental Test, Result Summary

Parameter				
Lift-Off Pressure (p_0)	2.1	kPa	0.31	psi
Contact Volume (V_c)	12.7	cm^3	0.78	in^3
Limit Pressure (p_L)	300.0	kPa	43.51	psi
Assumed ν		0.33		
Initial Modulus (E_0)	1637.7	kPa	237.54	psi
Dry Unit Weight (γ_{dry})	1685.1	kg/m^3	105.2	lb/ft^3
Wet Unit Weight (γ_{wet})	1814.9	kg/m^3	113.3	lb/ft^3

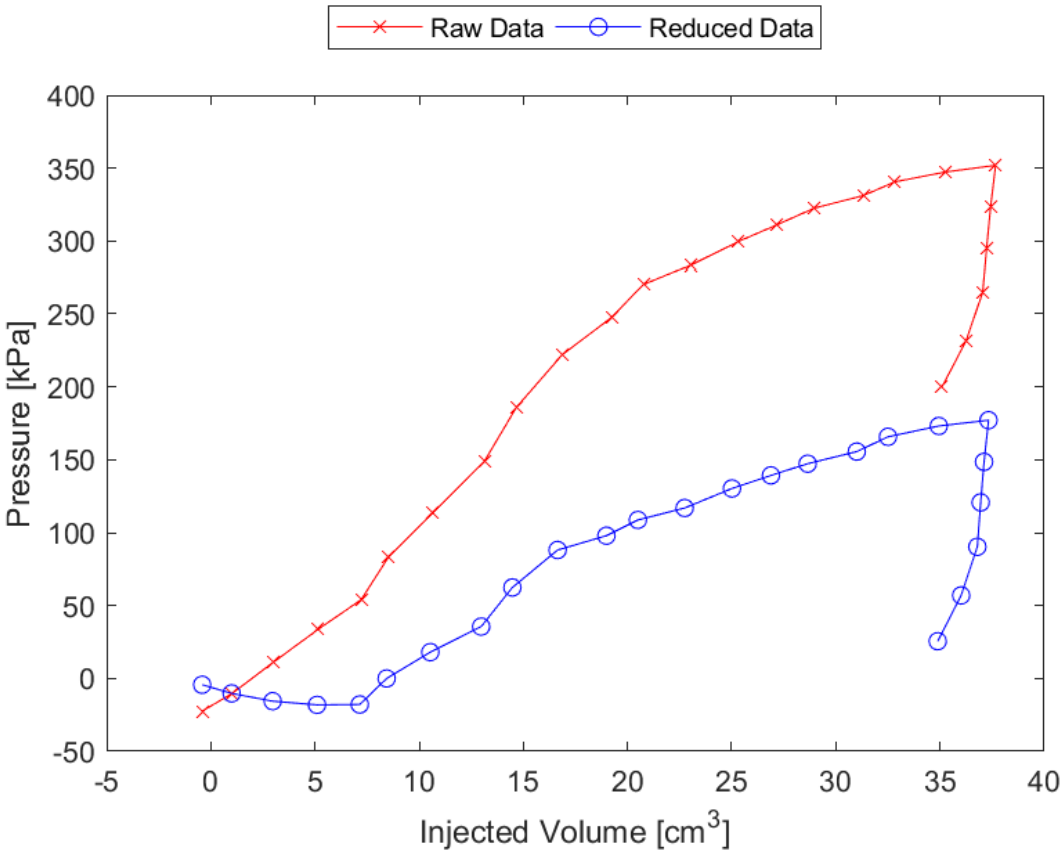

Figure A.5: Sounding 405, SDPMT-6 Incremental Test, Membrane O.D. 0.625m, Depth 0.25 m, Raw and Reduced Data

Table A.5: Sounding 405, SDPMT-6 Incremental Test, Result Summary

Parameter				
Lift-Off Pressure (p_0)	−0.0	kPa	−0.00	psi
Contact Volume (V_c)	8.4	cm^3	0.52	in^3
Limit Pressure (p_L)	200.0	kPa	29.01	psi
Assumed ν		0.33		
Initial Modulus (E_0)	1218.0	kPa	176.66	psi
Dry Unit Weight (γ_{dry})	1662.7	kg/m^3	103.8	lb/ft^3
Wet Unit Weight (γ_{wet})	1827.7	kg/m^3	114.1	lb/ft^3

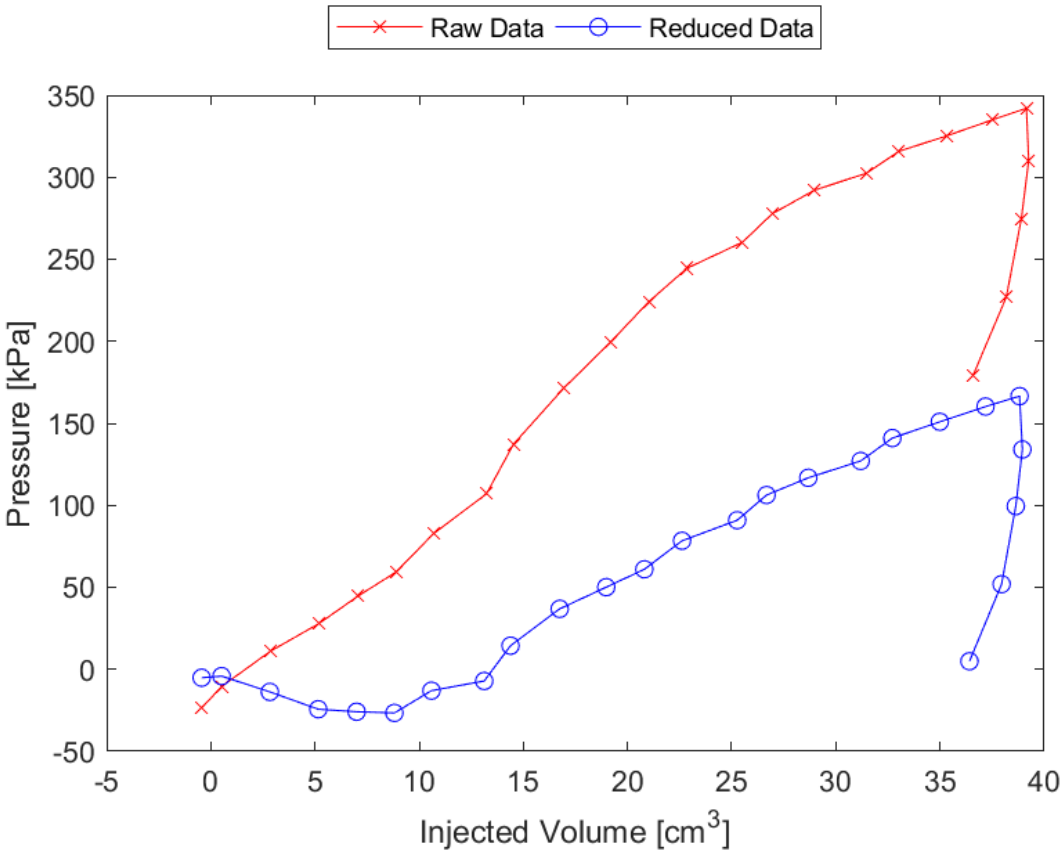

Figure A.6: Sounding 406, SDPMT-6 Incremental Test, Membrane O.D. 0.625m, Depth 0.25 m, Raw and Reduced Data

Table A.6: Sounding 406, SDPMT-6 Incremental Test, Result Summary

Parameter				
Lift-Off Pressure (p_0)	−7.1	kPa	−1.03	psi
Contact Volume (V_c)	13.1	cm^3	0.80	in^3
Limit Pressure (p_L)	200.0	kPa	29.01	psi
Assumed ν		0.33		
Initial Modulus (E_0)	1454.3	kPa	210.93	psi
Dry Unit Weight (γ_{dry})	1619.5	kg/m^3	101.1	lb/ft^3
Wet Unit Weight (γ_{wet})	1720.4	kg/m^3	107.4	lb/ft^3

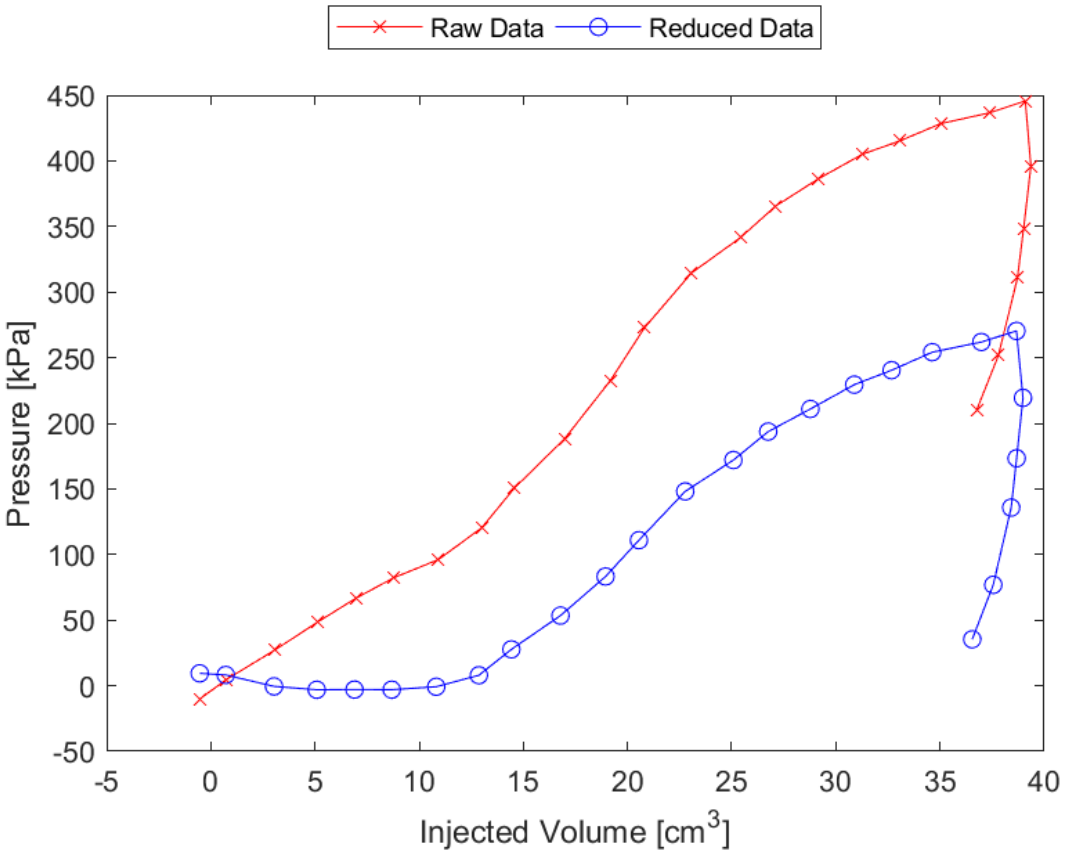

Figure A.7: Sounding 407, SDPMT-6 Incremental Test, Membrane O.D. 0.625m, Depth 0.25 m, Raw and Reduced Data

Table A.7: Sounding 407, SDPMT-6 Incremental Test, Result Summary

Parameter				
Lift-Off Pressure (p_0)	8.0	kPa	1.16	psi
Contact Volume (V_c)	12.9	cm^3	0.79	in^3
Limit Pressure (p_L)	300.0	kPa	43.51	psi
Assumed ν		0.33		
Initial Modulus (E_0)	2098.5	kPa	304.36	psi
Dry Unit Weight (γ_{dry})	1694.8	kg/m^3	105.8	lb/ft^3
Wet Unit Weight (γ_{wet})	1733.2	kg/m^3	108.2	lb/ft^3

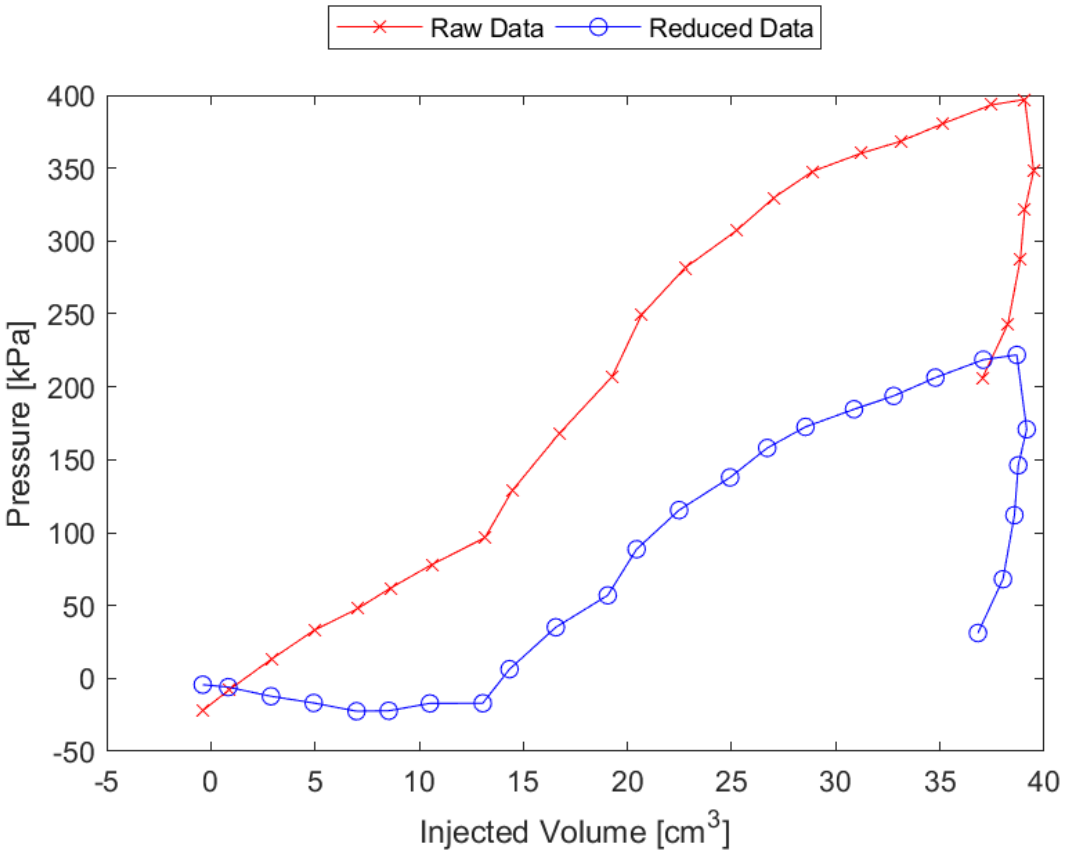

Figure A.8: Sounding 408, SDPMT-6 Incremental Test, Membrane O.D. 0.625m, Depth 0.25 m, Raw and Reduced Data

Table A.8: Sounding 408, SDPMT-6 Incremental Test, Result Summary

Parameter				
Lift-Off Pressure (p_0)	−17.0	kPa	−2.47	psi
Contact Volume (V_c)	13.1	cm^3	0.80	in^3
Limit Pressure (p_L)	275.0	kPa	39.89	psi
Assumed ν		0.33		
Initial Modulus (E_0)	1782.7	kPa	258.56	psi
Dry Unit Weight (γ_{dry})	1707.6	kg/m^3	106.6	lb/ft^3
Wet Unit Weight (γ_{wet})	1720.4	kg/m^3	107.4	lb/ft^3

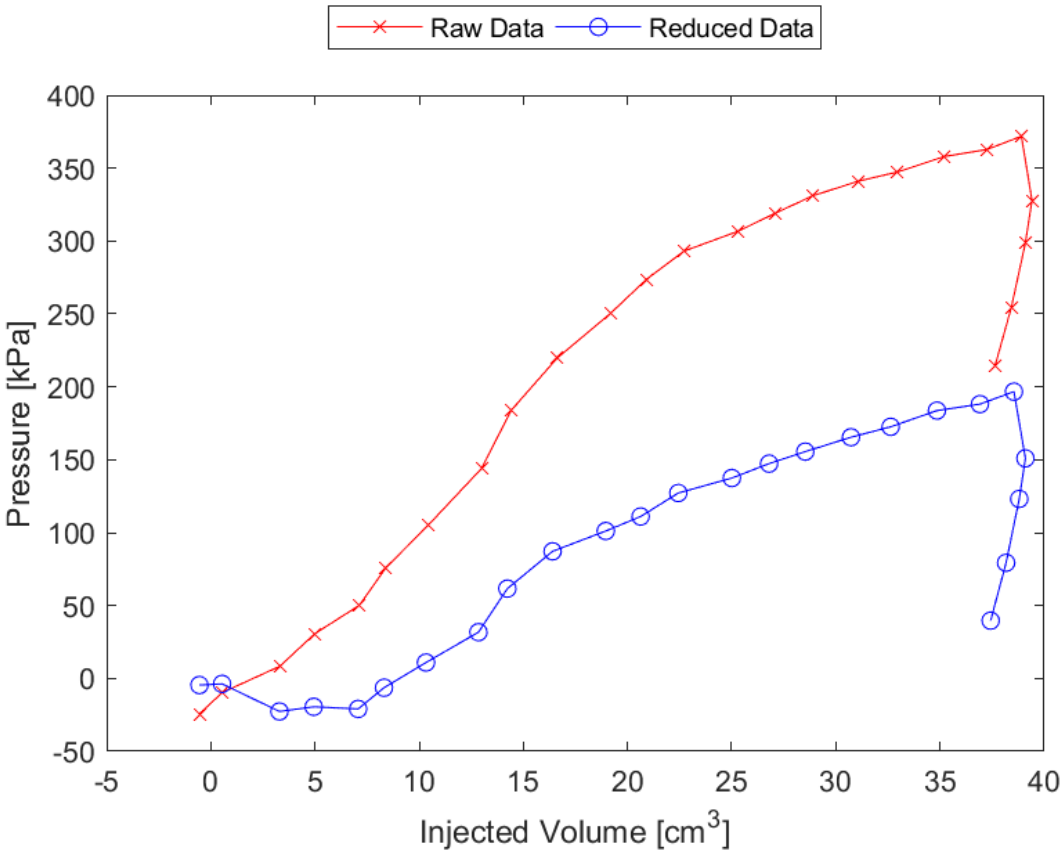

Figure A.9: Sounding 409, SDPMT-6 Incremental Test, Membrane O.D. 0.625m, Depth 0.25 m, Raw and Reduced Data

Table A.9: Sounding 409, SDPMT-6 Incremental Test, Result Summary

Parameter				
Lift-Off Pressure (p_0)	−6.4	kPa	−0.92	psi
Contact Volume (V_c)	8.3	cm^3	0.51	in^3
Limit Pressure (p_L)	250.0	kPa	36.26	psi
Assumed ν		0.33		
Initial Modulus (E_0)	1451.7	kPa	210.55	psi
Dry Unit Weight (γ_{dry})	1704.4	kg/m^3	106.4	lb/ft^3
Wet Unit Weight (γ_{wet})	1773.2	kg/m^3	110.7	lb/ft^3

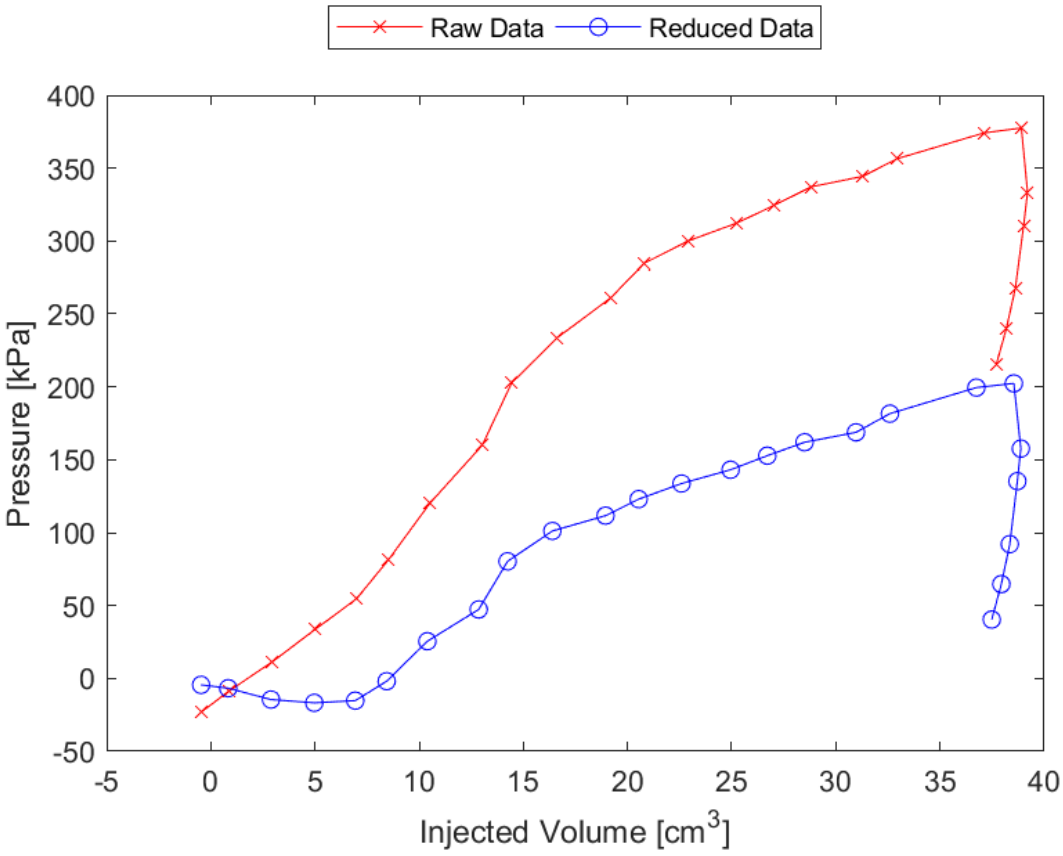

Figure A.10: Sounding 410, SDPMT-6 Incremental Test, Membrane O.D. 0.625m, Depth 0.25 m, Raw and Reduced Data

Table A.10: Sounding 410, SDPMT-6 Incremental Test, Result Summary

Parameter				
Lift-Off Pressure (p_0)	−1.9	kPa	−0.27	psi
Contact Volume (V_c)	8.4	cm^3	0.52	in^3
Limit Pressure (p_L)	250.0	kPa	36.26	psi
Assumed ν		0.33		
Initial Modulus (E_0)	1562.1	kPa	226.57	psi
Dry Unit Weight (γ_{dry})	1736.4	kg/m^3	108.4	lb/ft^3
Wet Unit Weight (γ_{wet})	1827.7	kg/m^3	114.1	lb/ft^3

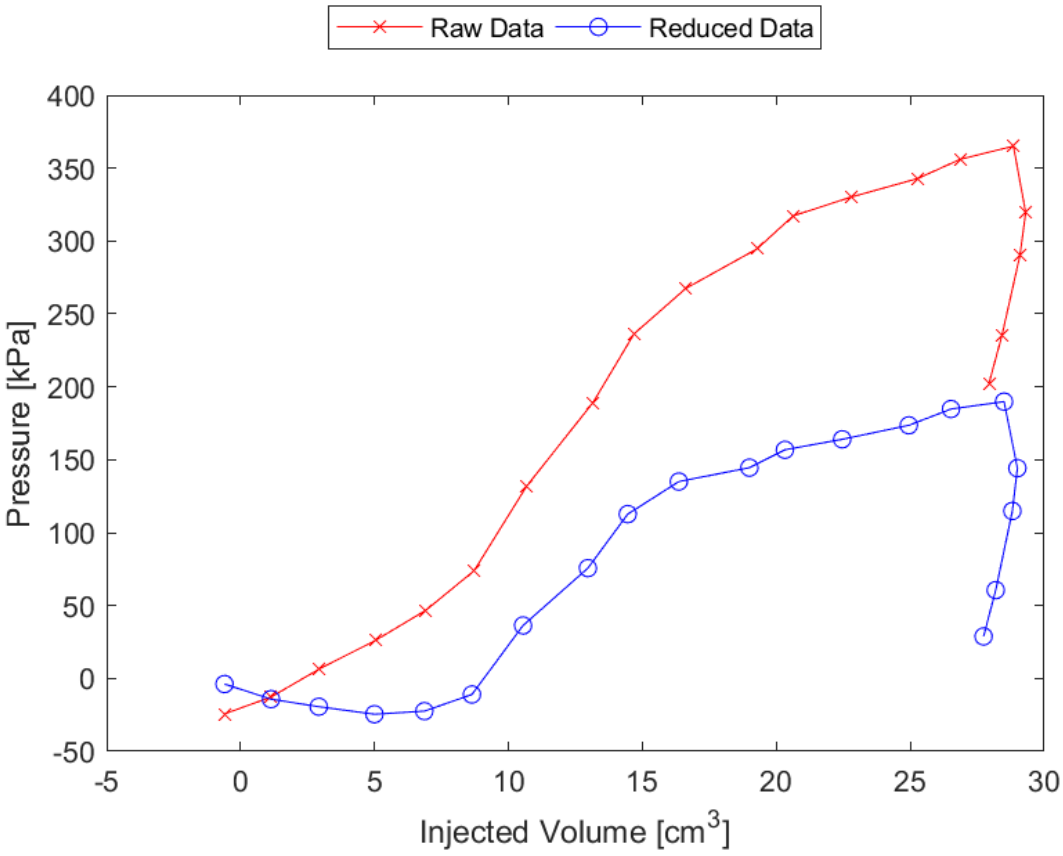

Figure A.11: Sounding 411, SDPMT-6 Incremental Test, Membrane O.D. 0.625m, Depth 0.25 m, Raw and Reduced Data

Table A.11: Sounding 411, SDPMT-6 Incremental Test, Result Summary

Parameter				
Lift-Off Pressure (p_0)	−11.0	kPa	−1.60	psi
Contact Volume (V_c)	8.6	cm^3	0.53	in^3
Limit Pressure (p_L)	225.0	kPa	32.63	psi
Assumed ν		0.33		
Initial Modulus (E_0)	2356.0	kPa	341.71	psi
Dry Unit Weight (γ_{dry})	1704.4	kg/m^3	106.4	lb/ft^3
Wet Unit Weight (γ_{wet})	1779.7	kg/m^3	111.1	lb/ft^3

A.2 SDPMT-6 Continuous Test Data

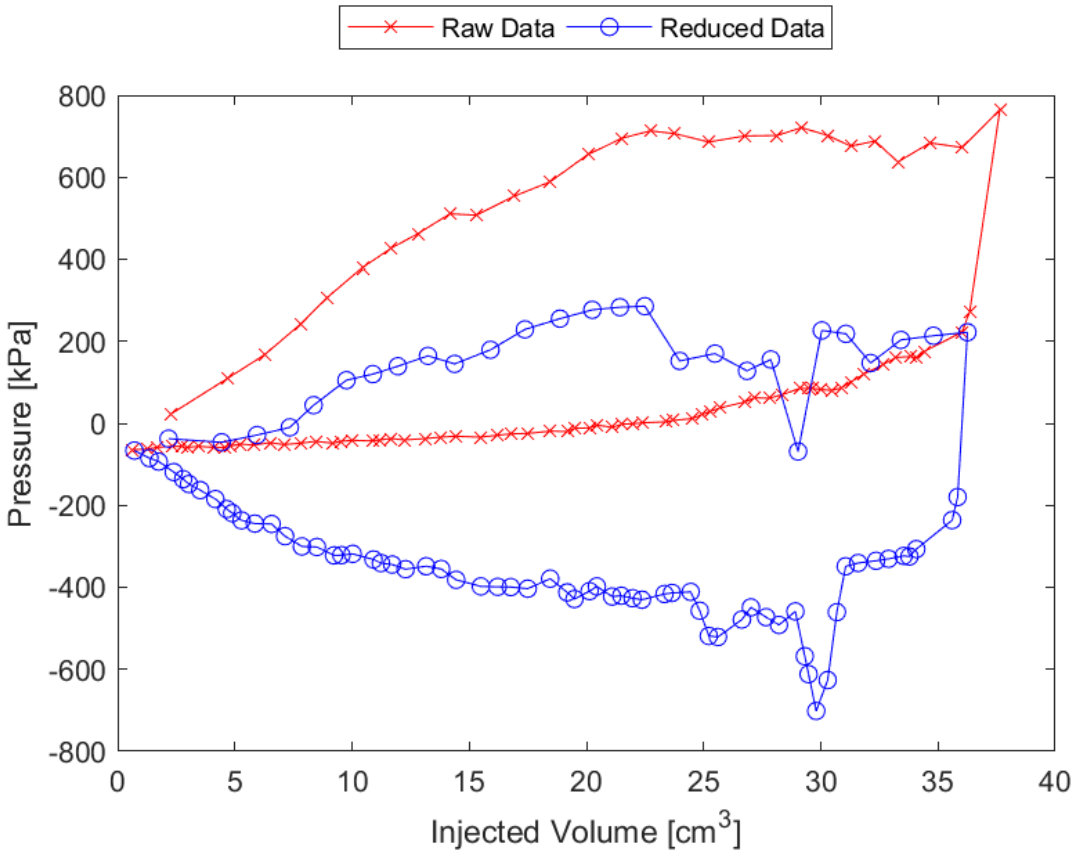

Figure A.12: Sounding 401, SDPMT-6 Continuous Test, Membrane O.D. 0.6875m, Depth 0.25 m, Raw and Reduced Data

Table A.12: Sounding 401, SDPMT-6 Continuous Test, Result Summary

Parameter				
Lift-Off Pressure (p_0)	−9.9	kPa	−1.44	psi
Contact Volume (V_c)	7.3	cm^3	0.45	in^3
Limit Pressure (p_L)	350.0	kPa	50.76	psi
Assumed ν		0.33		
Initial Modulus (E_0)	6168.8	kPa	894.71	psi
Dry Unit Weight (γ_{dry})	1653.1	kg/m^3	103.2	lb/ft^3
Wet Unit Weight (γ_{wet})	1669.1	kg/m^3	104.2	lb/ft^3

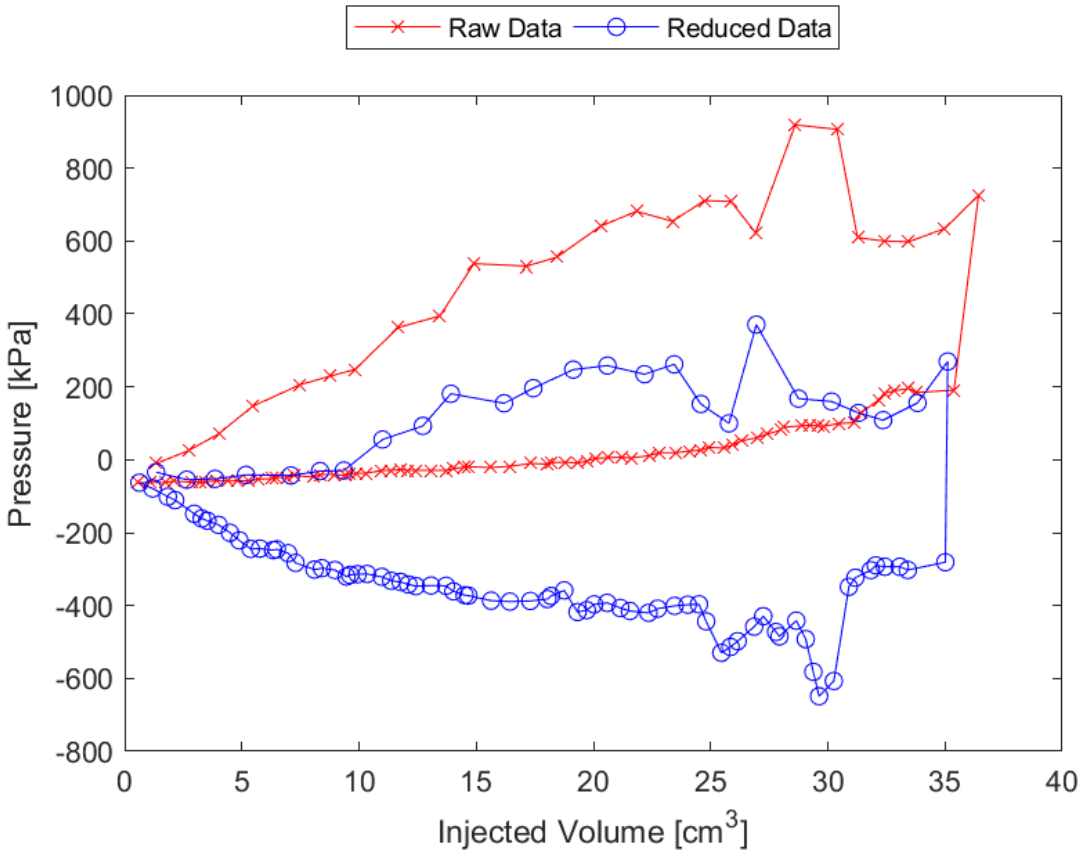

Figure A.13: Sounding 402, SDPMT-6 Continuous Test, Membrane O.D. 0.6875m, Depth 0.25 m, Raw and Reduced Data

Table A.13: Sounding 402, SDPMT-6 Continuous Test, Result Summary

Parameter				
Lift-Off Pressure (p_0)	−29.4	kPa	−4.27	psi
Contact Volume (V_c)	9.4	cm^3	0.57	in^3
Limit Pressure (p_L)	400.0	kPa	58.02	psi
Assumed ν		0.33		
Initial Modulus (E_0)	6346.6	kPa	920.50	psi
Dry Unit Weight (γ_{dry})	1694.8	kg/m^3	105.8	lb/ft^3
Wet Unit Weight (γ_{wet})	1709.2	kg/m^3	106.7	lb/ft^3

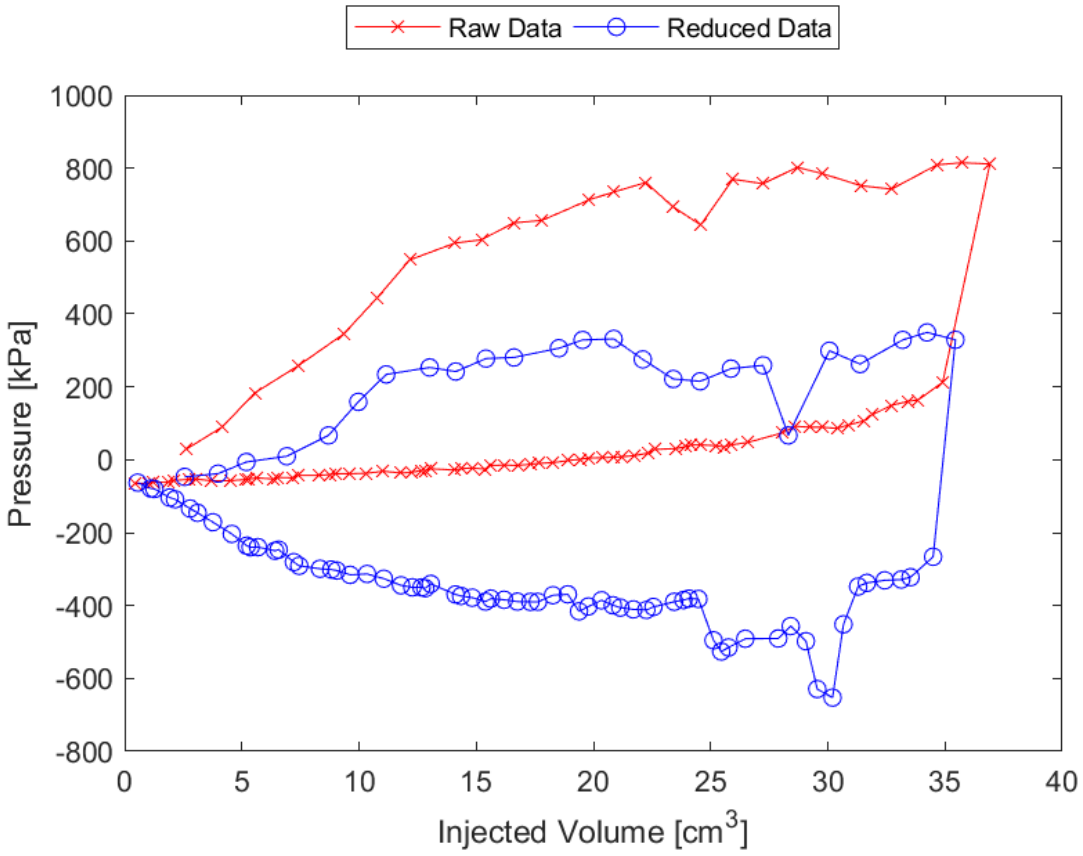

Figure A.14: Sounding 403, SDPMT-6 Continuous Test, Membrane O.D. 0.6875m, Depth 0.25 m, Raw and Reduced Data

Table A.14: Sounding 403, SDPMT-6 Continuous Test, Result Summary

Parameter				
Lift-Off Pressure (p_0)	9.6	kPa	1.39	psi
Contact Volume (V_c)	6.9	cm^3	0.42	in^3
Limit Pressure (p_L)	350.0	kPa	50.76	psi
Assumed ν		0.33		
Initial Modulus (E_0)	9045.9	kPa	1312.00	psi
Dry Unit Weight (γ_{dry})	1714.0	kg/m^3	107.0	lb/ft^3
Wet Unit Weight (γ_{wet})	1734.8	kg/m^3	108.3	lb/ft^3

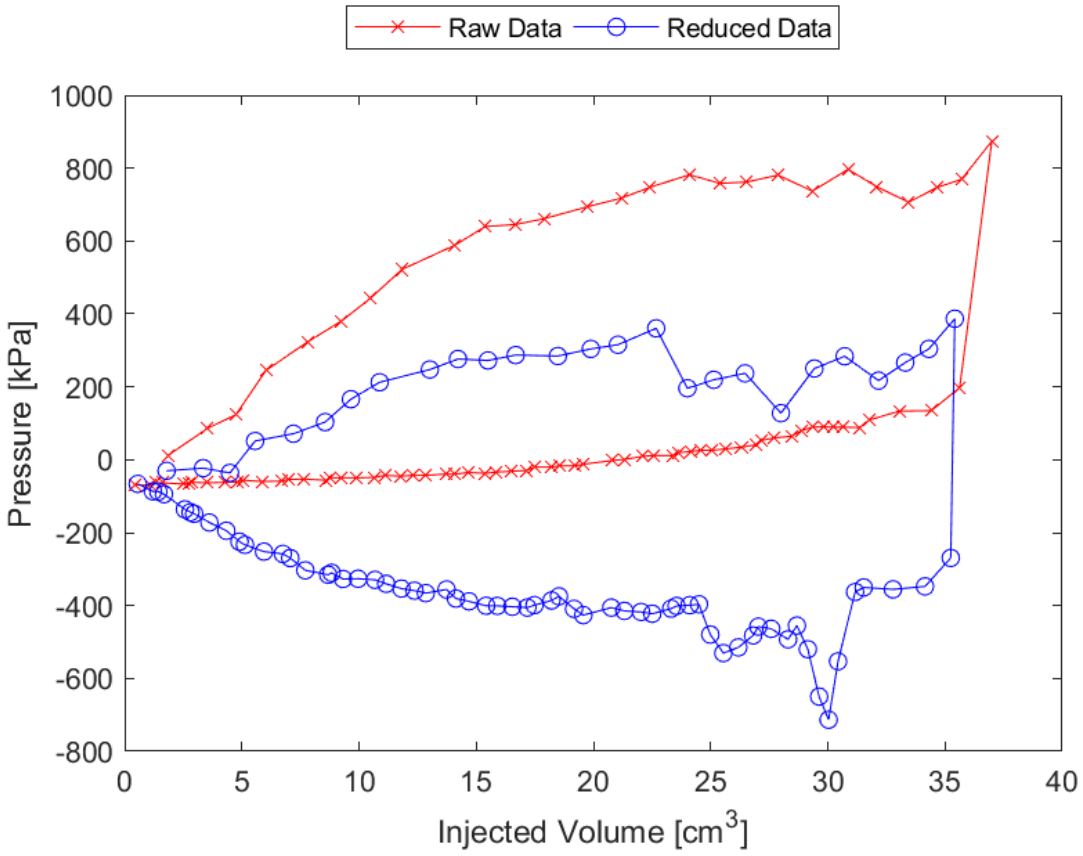

Figure A.15: Sounding 404, SDPMT-6 Continuous Test, Membrane O.D. 0.6875m, Depth 0.25 m, Raw and Reduced Data

Table A.15: Sounding 404, SDPMT-6 Continuous Test, Result Summary

Parameter				
Lift-Off Pressure (p_0)	51.5	kPa	7.48	psi
Contact Volume (V_c)	5.6	cm^3	0.34	in^3
Limit Pressure (p_L)	400.0	kPa	58.02	psi
Assumed ν		0.33		
Initial Modulus (E_0)	6217.2	kPa	901.73	psi
Dry Unit Weight (γ_{dry})	1685.1	kg/m^3	105.2	lb/ft^3
Wet Unit Weight (γ_{wet})	1704.4	kg/m^3	106.4	lb/ft^3

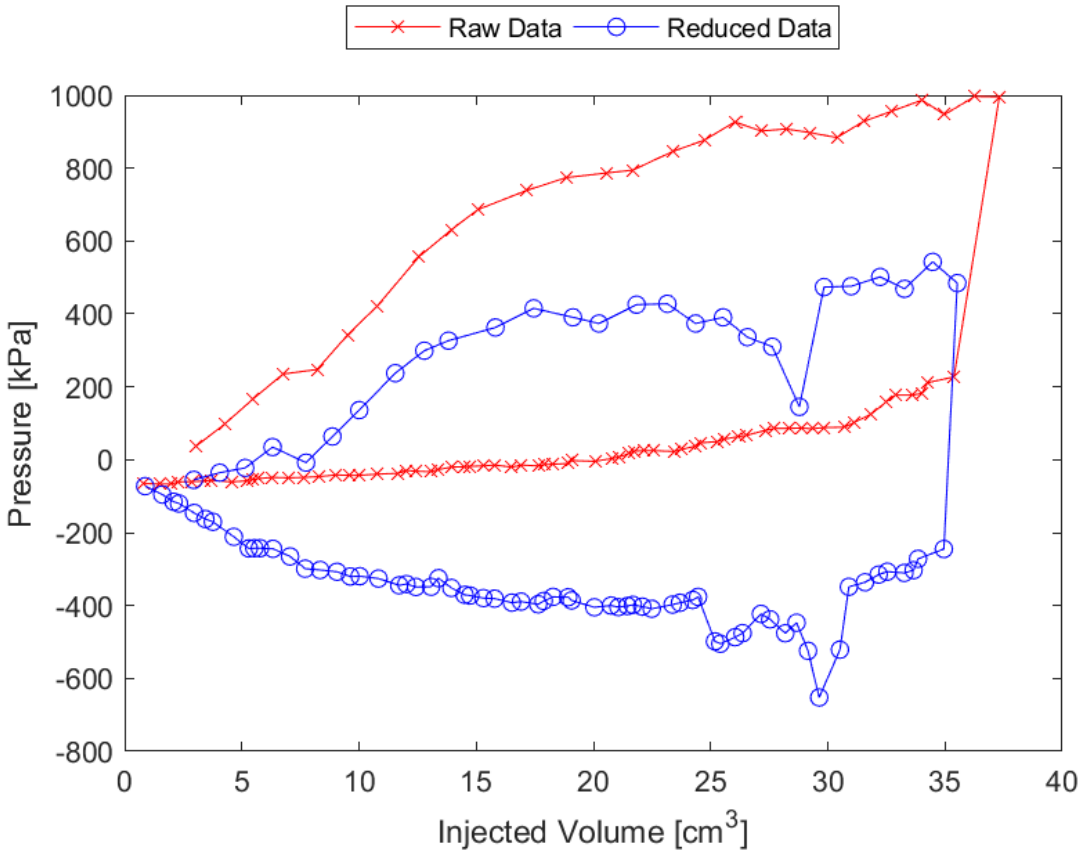

Figure A.16: Sounding 405, SDPMT-6 Continuous Test, Membrane O.D. 0.6875m, Depth 0.25 m, Raw and Reduced Data

Table A.16: Sounding 405, SDPMT-6 Continuous Test, Result Summary

Parameter				
Lift-Off Pressure (p_0)	−8.0	kPa	−1.15	psi
Contact Volume (V_c)	7.7	cm^3	0.47	in^3
Limit Pressure (p_L)	500.0	kPa	72.52	psi
Assumed ν		0.33		
Initial Modulus (E_0)	8537.9	kPa	1238.33	psi
Dry Unit Weight (γ_{dry})	1662.7	kg/m^3	103.8	lb/ft^3
Wet Unit Weight (γ_{wet})	1681.9	kg/m^3	105.0	lb/ft^3

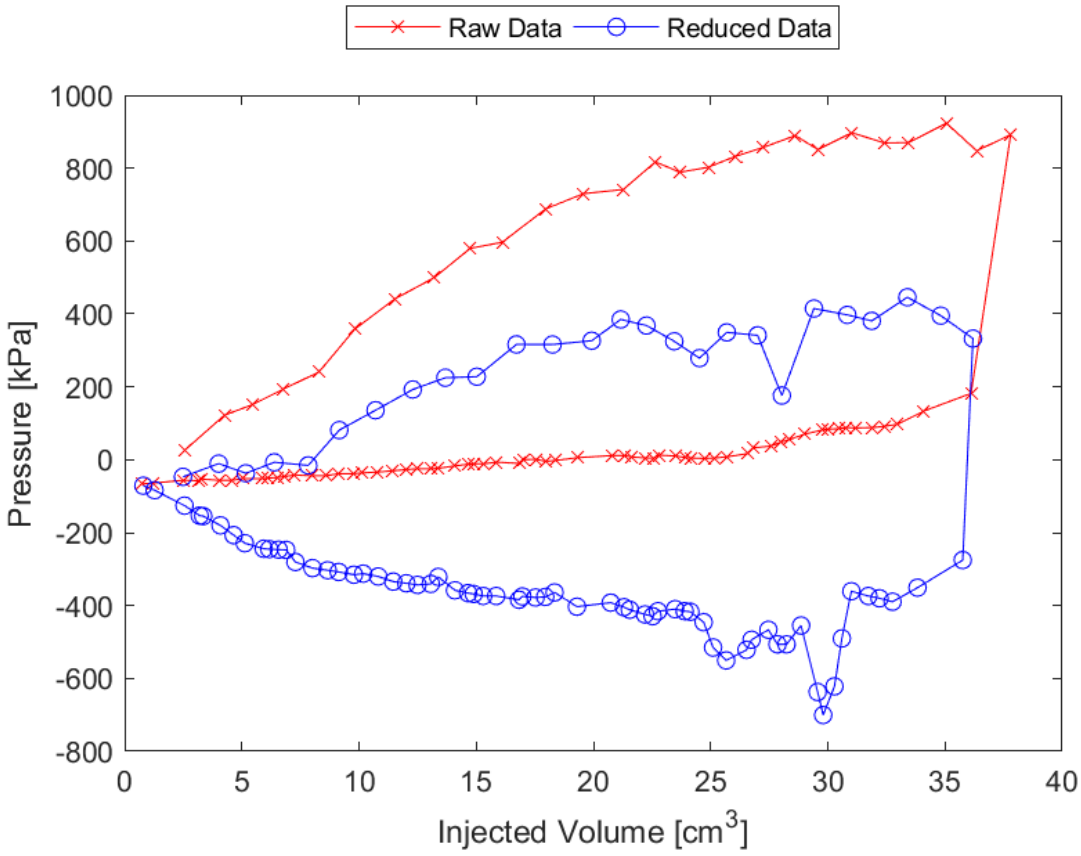

Figure A.17: Sounding 406, SDPMT-6 Continuous Test, Membrane O.D. 0.6875m, Depth 0.25 m, Raw and Reduced Data

Table A.17: Sounding 406, SDPMT-6 Continuous Test, Result Summary

Parameter				
Lift-Off Pressure (p_0)	−15.5	kPa	−2.24	psi
Contact Volume (V_c)	7.8	cm^3	0.48	in^3
Limit Pressure (p_L)	500.0	kPa	72.52	psi
Assumed ν		0.33		
Initial Modulus (E_0)	4354.8	kPa	631.62	psi
Dry Unit Weight (γ_{dry})	1619.5	kg/m^3	101.1	lb/ft^3
Wet Unit Weight (γ_{wet})	1637.1	kg/m^3	102.2	lb/ft^3

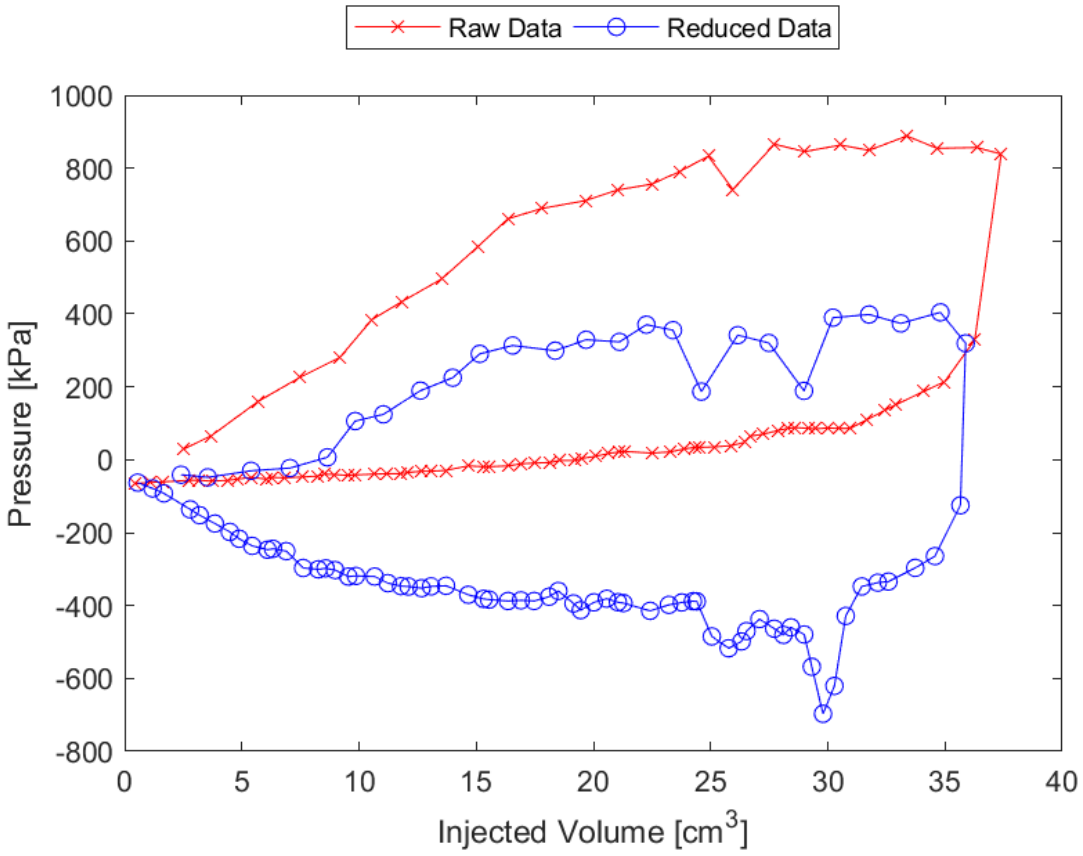

Figure A.18: Sounding 407, SDPMT-6 Continuous Test, Membrane O.D. 0.6875m, Depth 0.25 m, Raw and Reduced Data

Table A.18: Sounding 407, SDPMT-6 Continuous Test, Result Summary

Parameter				
Lift-Off Pressure (p_0)	6.7	kPa	0.98	psi
Contact Volume (V_c)	8.6	cm^3	0.53	in^3
Limit Pressure (p_L)	400.0	kPa	58.02	psi
Assumed ν		0.33		
Initial Modulus (E_0)	5716.0	kPa	829.03	psi
Dry Unit Weight (γ_{dry})	1694.8	kg/m^3	105.8	lb/ft^3
Wet Unit Weight (γ_{wet})	1731.6	kg/m^3	108.1	lb/ft^3

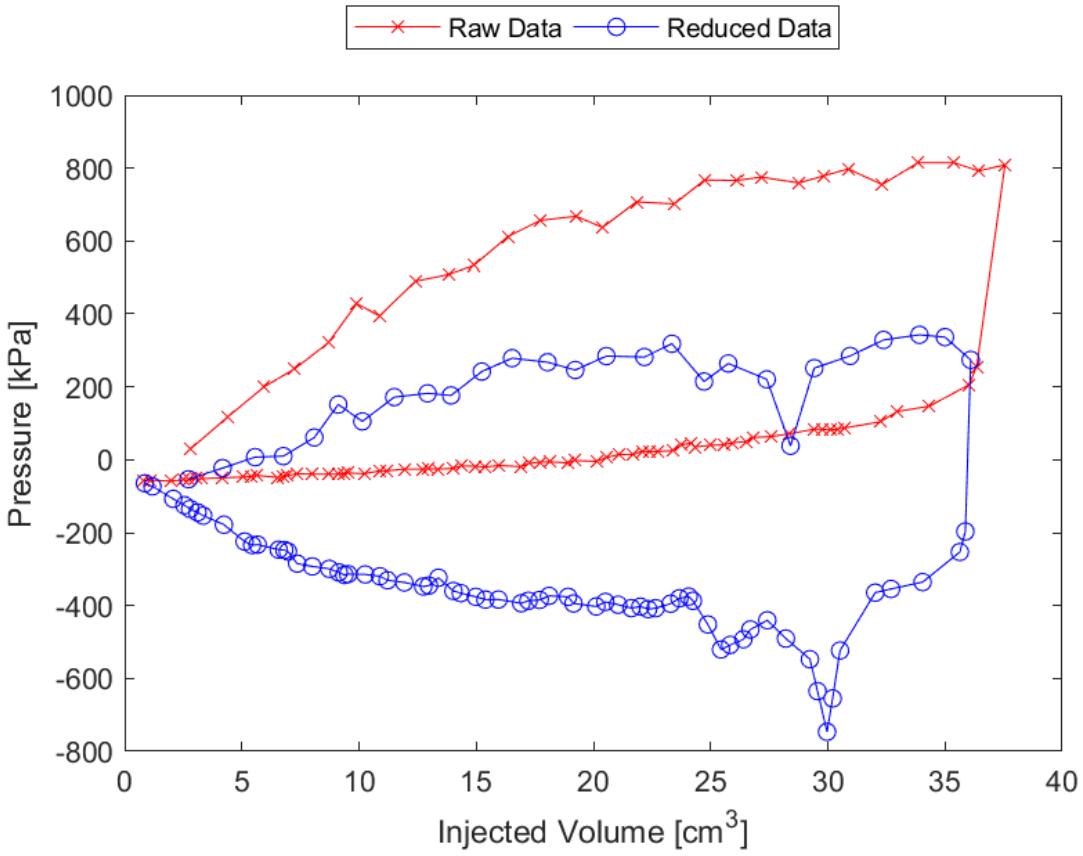

Figure A.19: Sounding 408, SDPMT-6 Continuous Test, Membrane O.D. 0.6875m, Depth 0.25 m, Raw and Reduced Data

Table A.19: Sounding 408, SDPMT-6 Continuous Test, Result Summary

Parameter				
Lift-Off Pressure (p_0)	9.9	kPa	1.43	psi
Contact Volume (V_c)	6.8	cm^3	0.41	in^3
Limit Pressure (p_L)	380.0	kPa	55.11	psi
Assumed ν		0.33		
Initial Modulus (E_0)	4486.6	kPa	650.72	psi
Dry Unit Weight (γ_{dry})	1707.6	kg/m^3	106.6	lb/ft^3
Wet Unit Weight (γ_{wet})	1749.2	kg/m^3	109.2	lb/ft^3

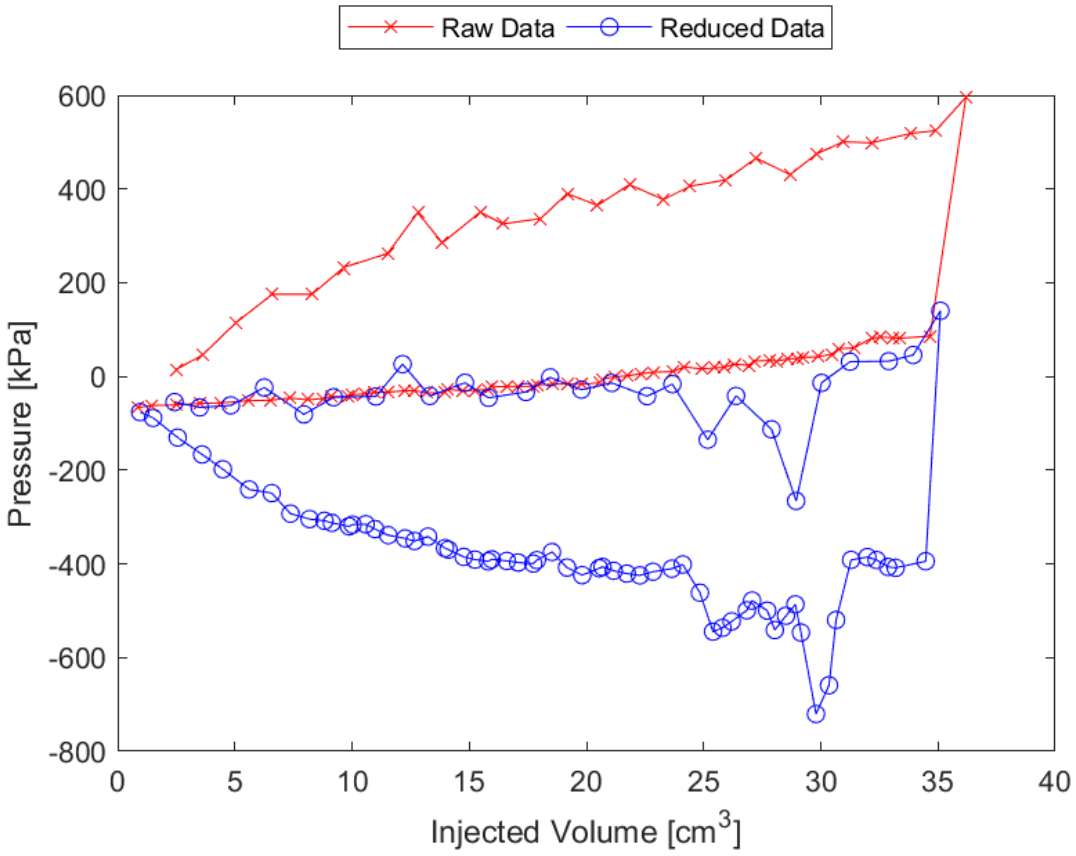

Figure A.20: Sounding 409, SDPMT-6 Continuous Test, Membrane O.D. 0.6875m, Depth 0.25 m, Raw and Reduced Data

Table A.20: Sounding 409, SDPMT-6 Continuous Test, Result Summary

Parameter				
Lift-Off Pressure (p_0)	NaN	kPa	NaN	psi
Contact Volume (V_c)	NaN	cm^3	NaN	in^3
Limit Pressure (p_L)	NaN	kPa	NaN	psi
Assumed ν		0.33		
Initial Modulus (E_0)	NaN	kPa	NaN	psi
Dry Unit Weight (γ_{dry})	1704.4	kg/m^3	106.4	lb/ft^3
Wet Unit Weight (γ_{wet})	1728.4	kg/m^3	107.9	lb/ft^3

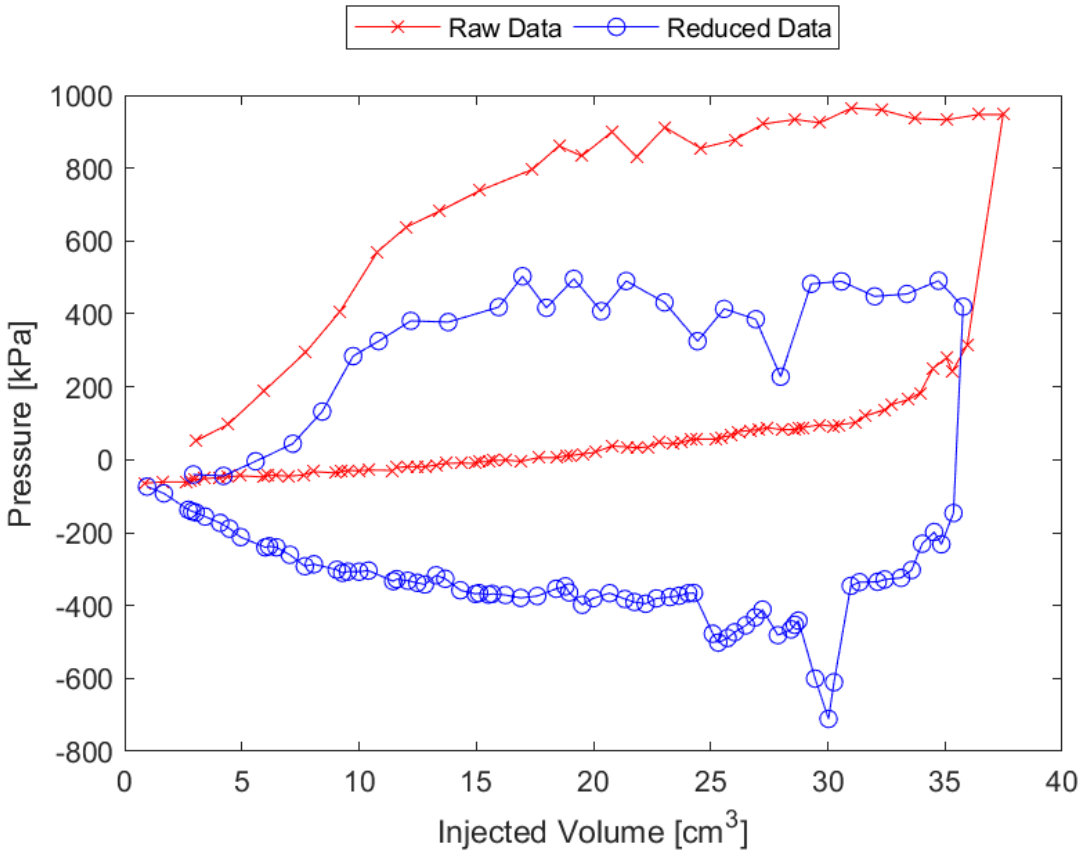

Figure A.21: Sounding 410, SDPMT-6 Continuous Test, Membrane O.D. 0.6875m, Depth 0.25 m, Raw and Reduced Data

Table A.21: Sounding 410, SDPMT-6 Continuous Test, Result Summary

Parameter				
Lift-Off Pressure (p_0)	−4.2	kPa	−0.61	psi
Contact Volume (V_c)	5.6	cm^3	0.34	in^3
Limit Pressure (p_L)	600.0	kPa	87.02	psi
Assumed ν		0.33		
Initial Modulus (E_0)	12060.2	kPa	1749.18	psi
Dry Unit Weight (γ_{dry})	1736.4	kg/m^3	108.4	lb/ft^3
Wet Unit Weight (γ_{wet})	1786.1	kg/m^3	111.5	lb/ft^3

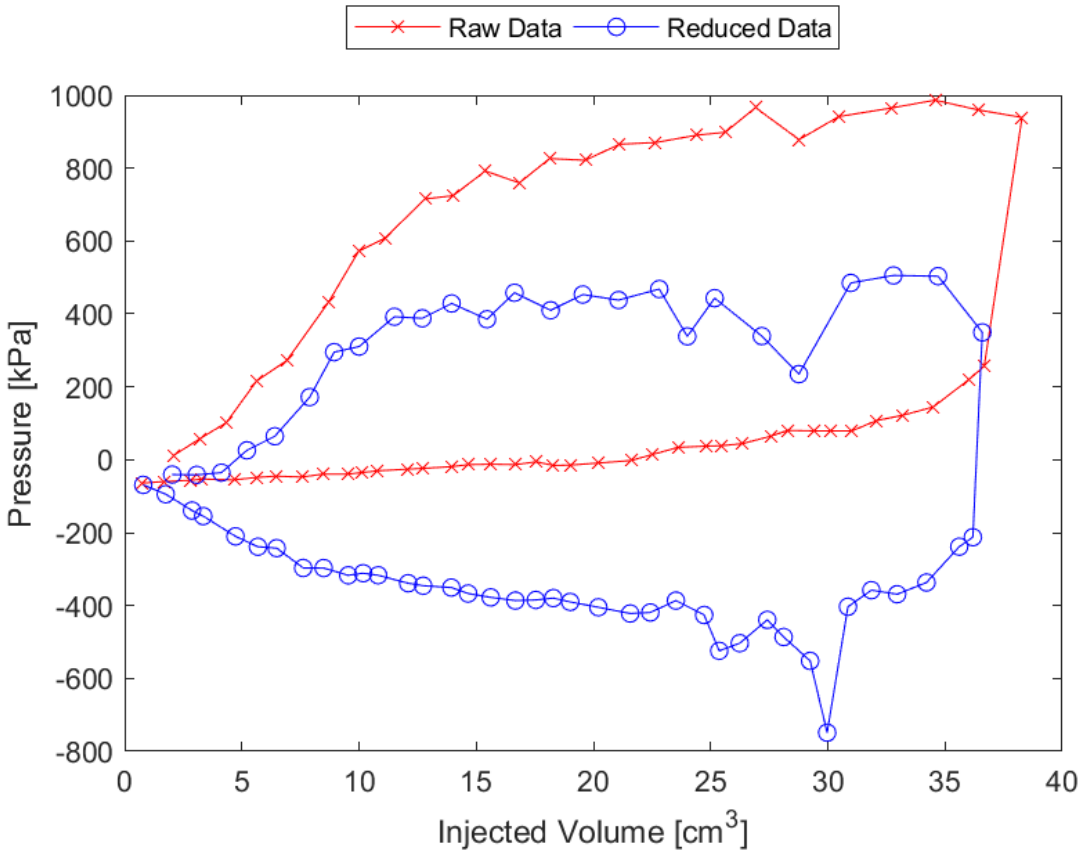

Figure A.22: Sounding 411, SDPMT-6 Continuous Test, Membrane O.D. 0.6875m, Depth 0.25 m, Raw and Reduced Data

Table A.22: Sounding 411, SDPMT-6 Continuous Test, Result Summary

Parameter				
Lift-Off Pressure (p_0)	25.8	kPa	3.75	psi
Contact Volume (V_c)	5.2	cm^3	0.32	in^3
Limit Pressure (p_L)	530.0	kPa	76.87	psi
Assumed ν		0.33		
Initial Modulus (E_0)	11577.5	kPa	1679.17	psi
Dry Unit Weight (γ_{dry})	1704.4	kg/m^3	106.4	lb/ft^3
Wet Unit Weight (γ_{wet})	1754.0	kg/m^3	109.5	lb/ft^3

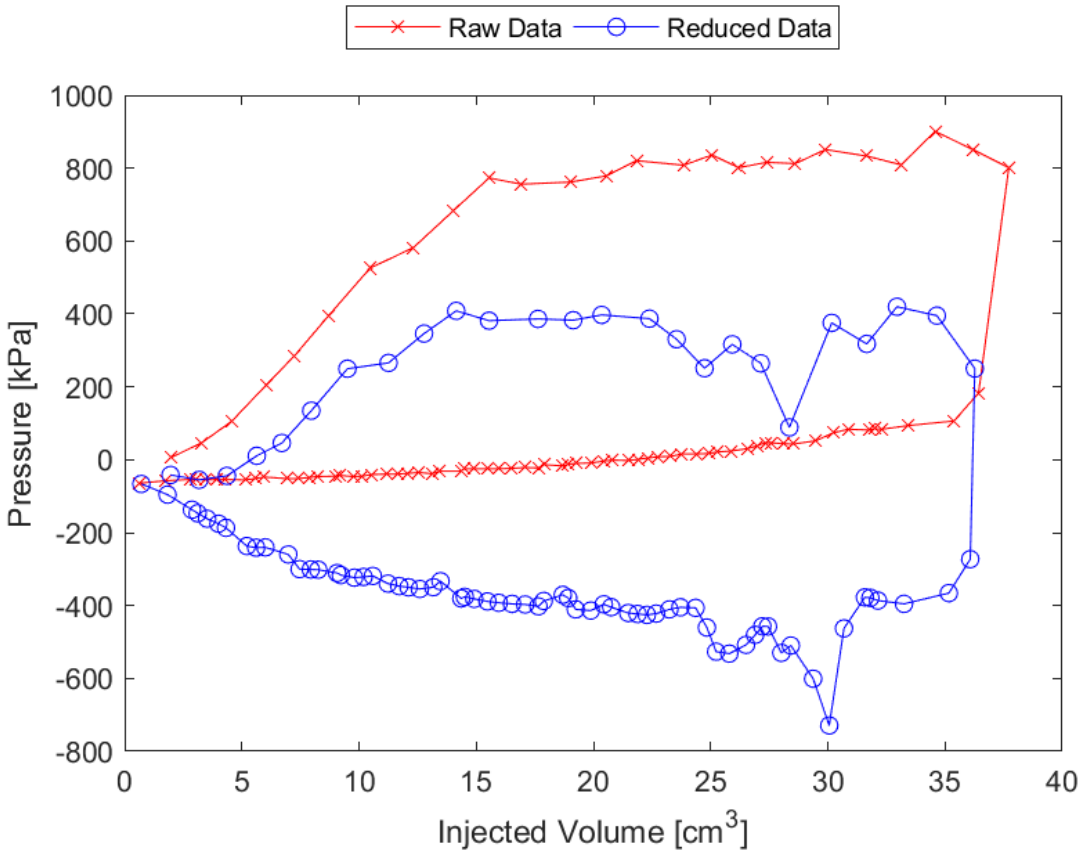

Figure A.23: Sounding 412, SDPMT-6 Continuous Test, Membrane O.D. 0.6875m, Depth 0.25 m, Raw and Reduced Data

Table A.23: Sounding 412, SDPMT-6 Continuous Test, Result Summary

Parameter				
Lift-Off Pressure (p_0)	10.9	kPa	1.58	psi
Contact Volume (V_c)	5.6	cm^3	0.34	in^3
Limit Pressure (p_L)	500.0	kPa	72.52	psi
Assumed ν		0.33		
Initial Modulus (E_0)	9338.6	kPa	1354.45	psi
Dry Unit Weight (γ_{dry})	1648.3	kg/m^3	102.9	lb/ft^3
Wet Unit Weight (γ_{wet})	1677.1	kg/m^3	104.7	lb/ft^3

A.3 SDPMT-12 Incremental Test Data

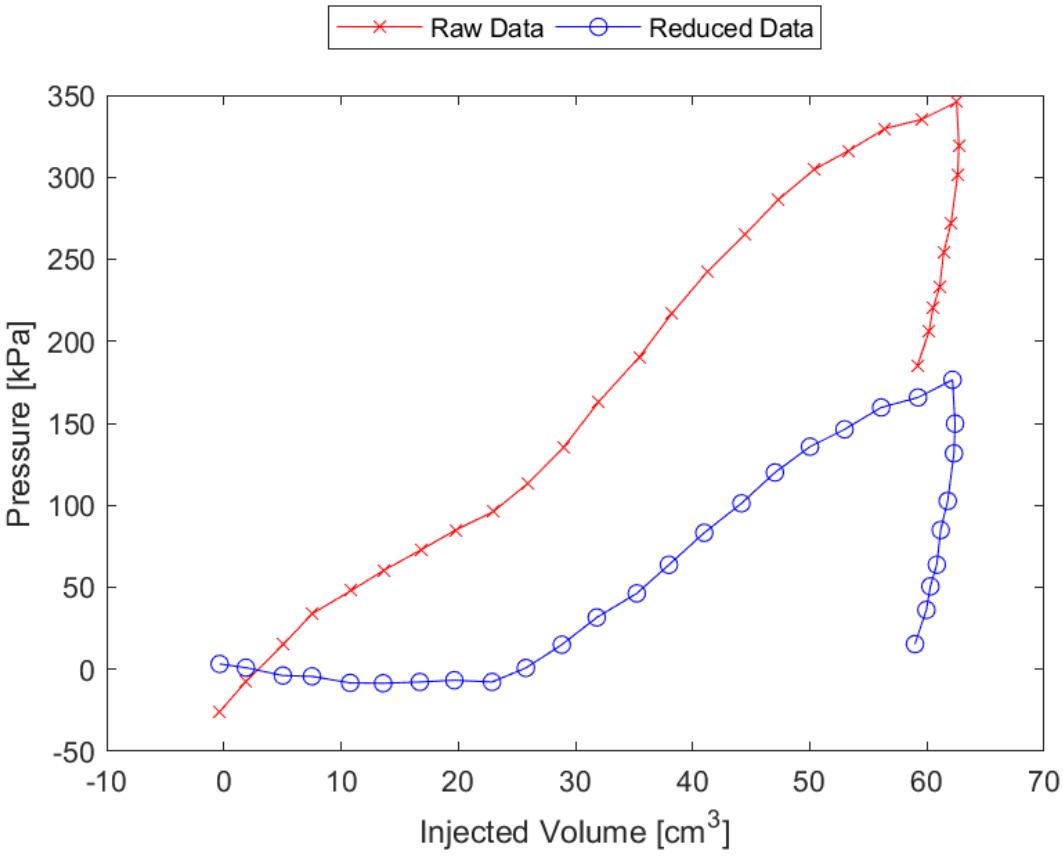

Figure A.24: Sounding 401, SDPMT-12 Incremental Test, Membrane O.D. 0.625m, Depth 0.33 m, Raw and Reduced Data

Table A.24: Sounding 401, SDPMT-12 Incremental Test, Result Summary

Parameter				
Lift-Off Pressure (p_0)	−7.7	kPa	−1.12	psi
Contact Volume (V_c)	61482.7	cm^3	3751.90	in^3
Limit Pressure (p_L)	250.0	kPa	36.26	psi
Assumed ν		0.33		
Initial Modulus (E_0)	1511.5	kPa	219.22	psi
Dry Unit Weight (γ_{dry})	1653.1	kg/m^3	103.2	lb/ft^3
Wet Unit Weight (γ_{wet})	1741.2	kg/m^3	108.7	lb/ft^3

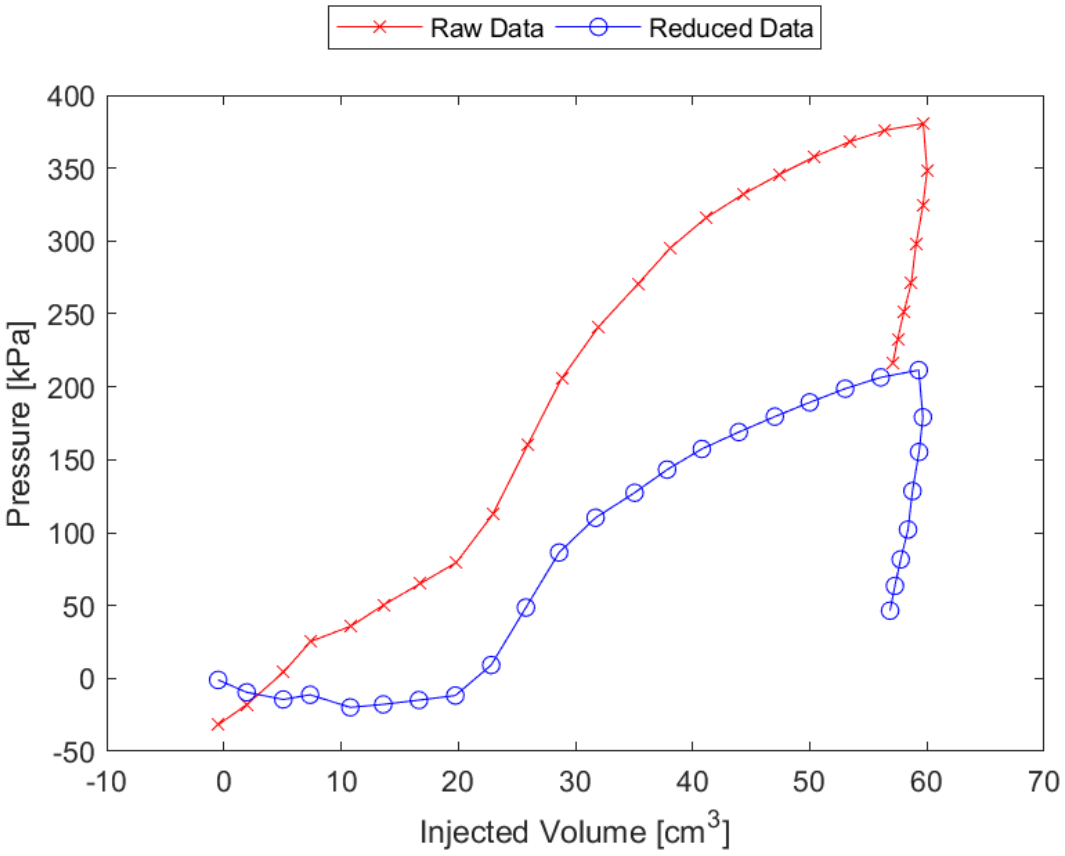

Figure A.25: Sounding 402, SDPMT-12 Incremental Test, Membrane O.D. 0.625m, Depth 0.38 m, Raw and Reduced Data

Table A.25: Sounding 402, SDPMT-12 Incremental Test, Result Summary

Parameter				
Lift-Off Pressure (p_0)	−11.7	kPa	−1.70	psi
Contact Volume (V_c)	19.8	cm^3	1.21	in^3
Limit Pressure (p_L)	275.0	kPa	39.89	psi
Assumed ν		0.33		
Initial Modulus (E_0)	3043.8	kPa	441.47	psi
Dry Unit Weight (γ_{dry})	1694.8	kg/m^3	105.8	lb/ft^3
Wet Unit Weight (γ_{wet})	1821.3	kg/m^3	113.7	lb/ft^3

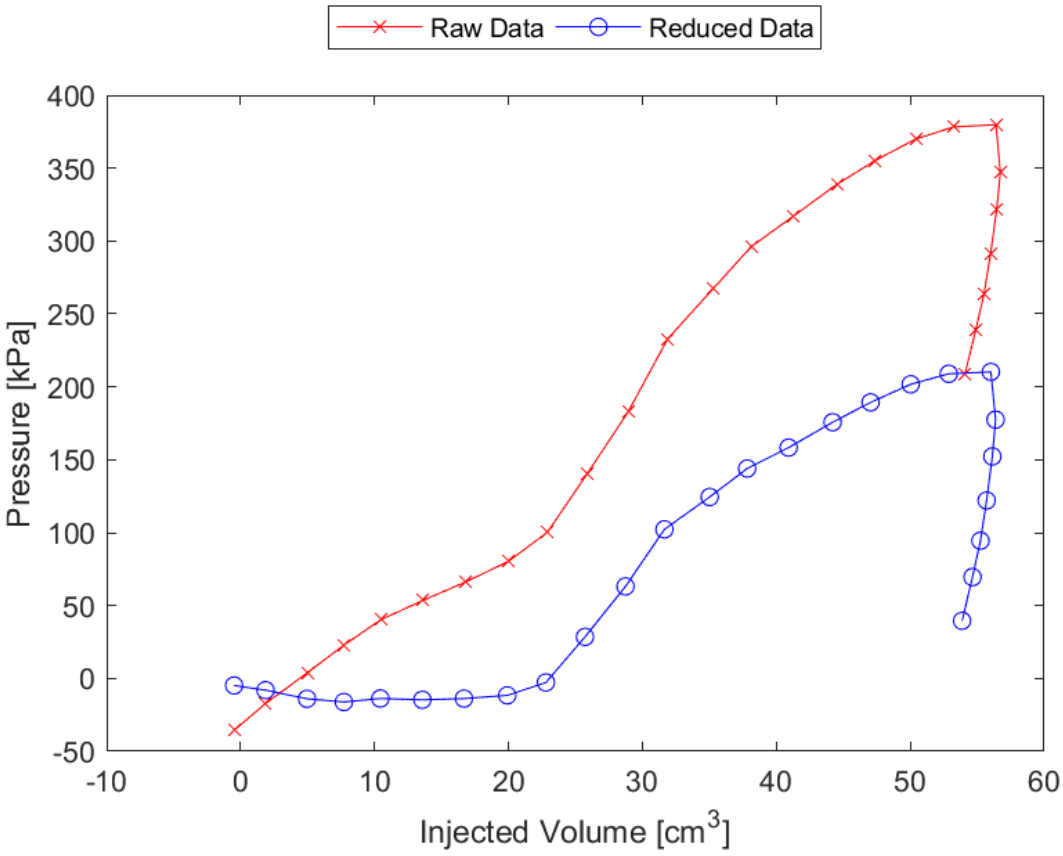

Figure A.26: Sounding 403, SDPMT-12 Incremental Test, Membrane O.D. 0.625m, Depth 0.38 m, Raw and Reduced Data

Table A.26: Sounding 403, SDPMT-12 Incremental Test, Result Summary

Parameter				
Lift-Off Pressure (p_0)	−2.8	kPa	−0.40	psi
Contact Volume (V_c)	22.8	cm^3	1.39	in^3
Limit Pressure (p_L)	295.0	kPa	42.79	psi
Assumed ν		0.33		
Initial Modulus (E_0)	2759.7	kPa	400.26	psi
Dry Unit Weight (γ_{dry})	1714.0	kg/m^3	107.0	lb/ft^3
Wet Unit Weight (γ_{wet})	1736.4	kg/m^3	108.4	lb/ft^3

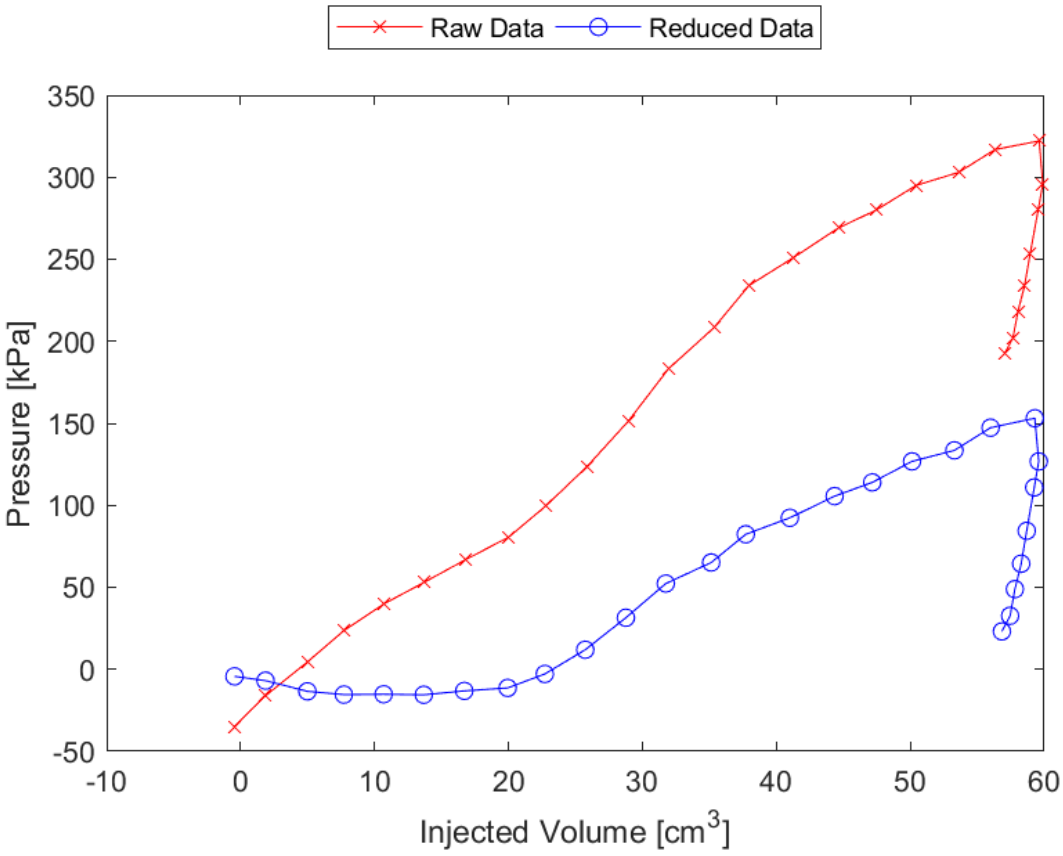

Figure A.27: Sounding 404, SDPMT-12 Incremental Test, Membrane O.D. 0.625m, Depth 0.38 m, Raw and Reduced Data

Table A.27: Sounding 404, SDPMT-12 Incremental Test, Result Summary

Parameter				
Lift-Off Pressure (p_0)	−2.8	kPa	−0.41	psi
Contact Volume (V_c)	22.7	cm^3	1.39	in^3
Limit Pressure (p_L)	225.0	kPa	32.63	psi
Assumed ν		0.33		
Initial Modulus (E_0)	1420.1	kPa	205.96	psi
Dry Unit Weight (γ_{dry})	1685.1	kg/m^3	105.2	lb/ft^3
Wet Unit Weight (γ_{wet})	1814.9	kg/m^3	113.3	lb/ft^3

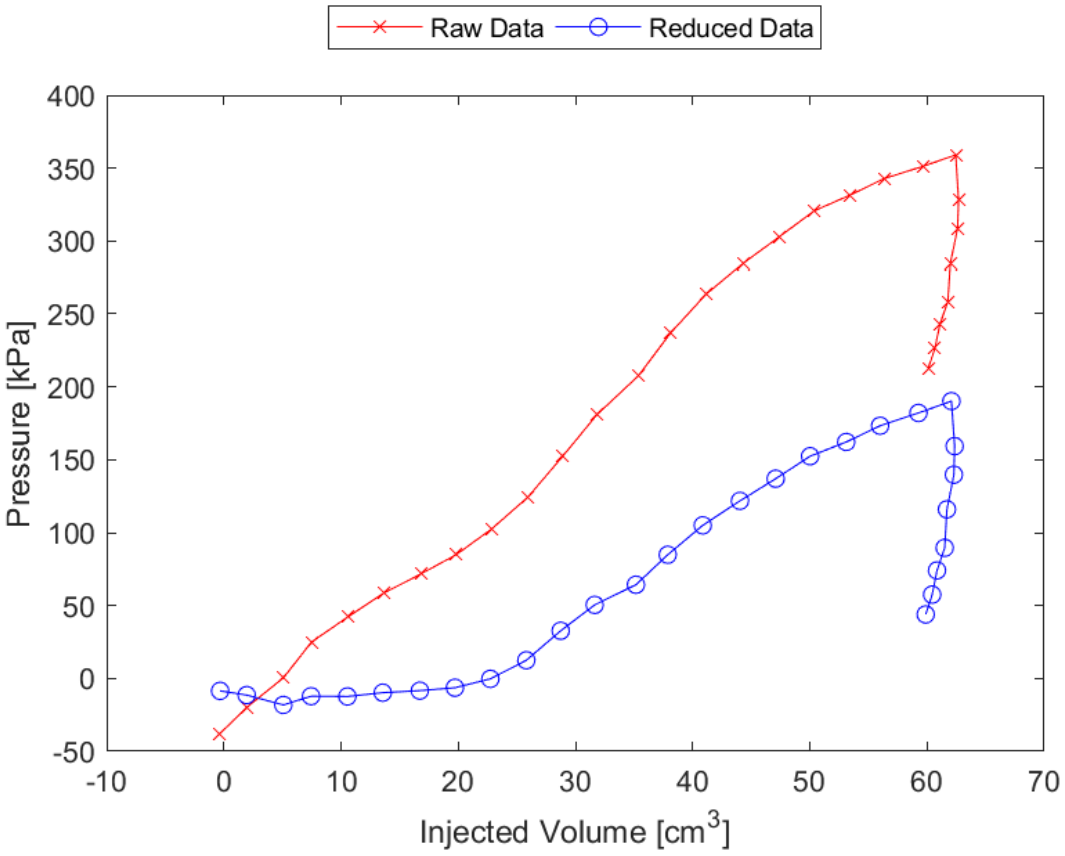

Figure A.28: Sounding 405, SDPMT-12 Incremental Test, Membrane O.D. 0.625m, Depth 0.38 m, Raw and Reduced Data

Table A.28: Sounding 405, SDPMT-12 Incremental Test, Result Summary

Parameter				
Lift-Off Pressure (p_0)	−0.3	kPa	−0.04	psi
Contact Volume (V_c)	22.7	cm^3	1.39	in^3
Limit Pressure (p_L)	270.0	kPa	39.16	psi
Assumed ν		0.33		
Initial Modulus (E_0)	1325.5	kPa	192.25	psi
Dry Unit Weight (γ_{dry})	1662.7	kg/m^3	103.8	lb/ft^3
Wet Unit Weight (γ_{wet})	1827.7	kg/m^3	114.1	lb/ft^3

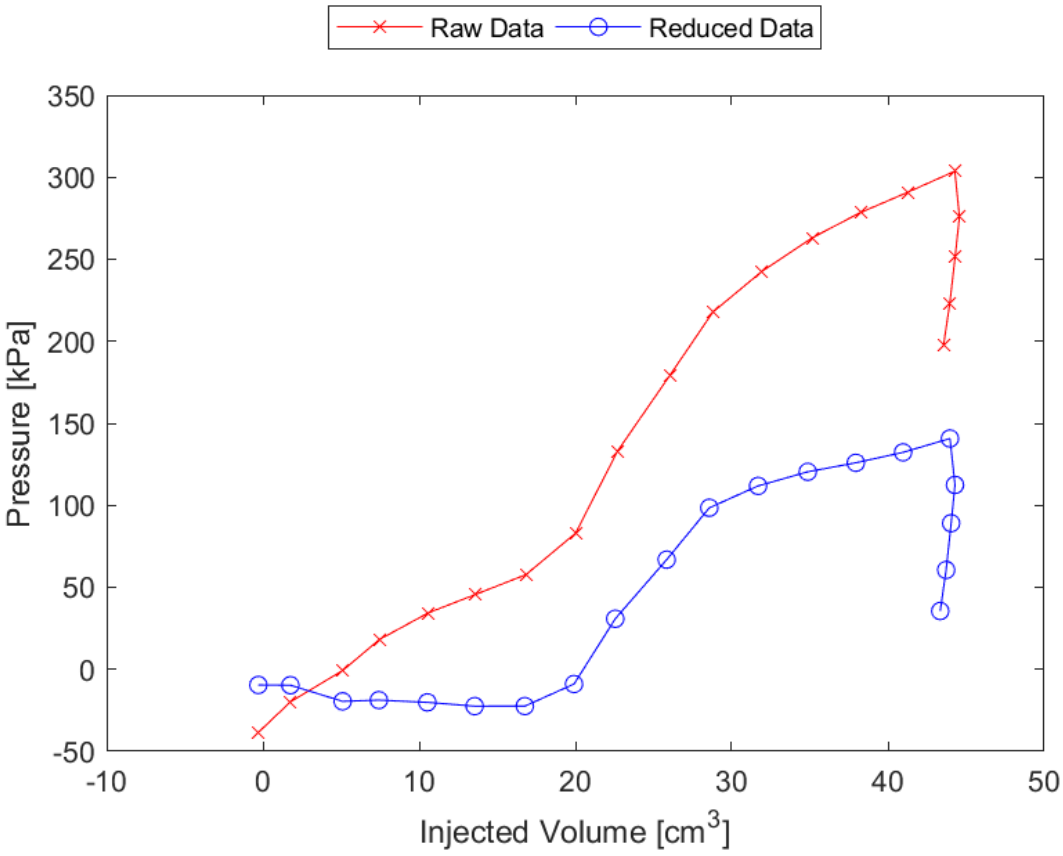

Figure A.29: Sounding 406, SDPMT-12 Incremental Test, Membrane O.D. 0.625m, Depth 0.38 m, Raw and Reduced Data

Table A.29: Sounding 406, SDPMT-12 Incremental Test, Result Summary

Parameter				
Lift-Off Pressure (p_0)	−9.0	kPa	−1.30	psi
Contact Volume (V_c)	19.9	cm^3	1.22	in^3
Limit Pressure (p_L)	185.0	kPa	26.83	psi
Assumed ν		0.33		
Initial Modulus (E_0)	2788.3	kPa	404.41	psi
Dry Unit Weight (γ_{dry})	1619.5	kg/m^3	101.1	lb/ft^3
Wet Unit Weight (γ_{wet})	1720.4	kg/m^3	107.4	lb/ft^3

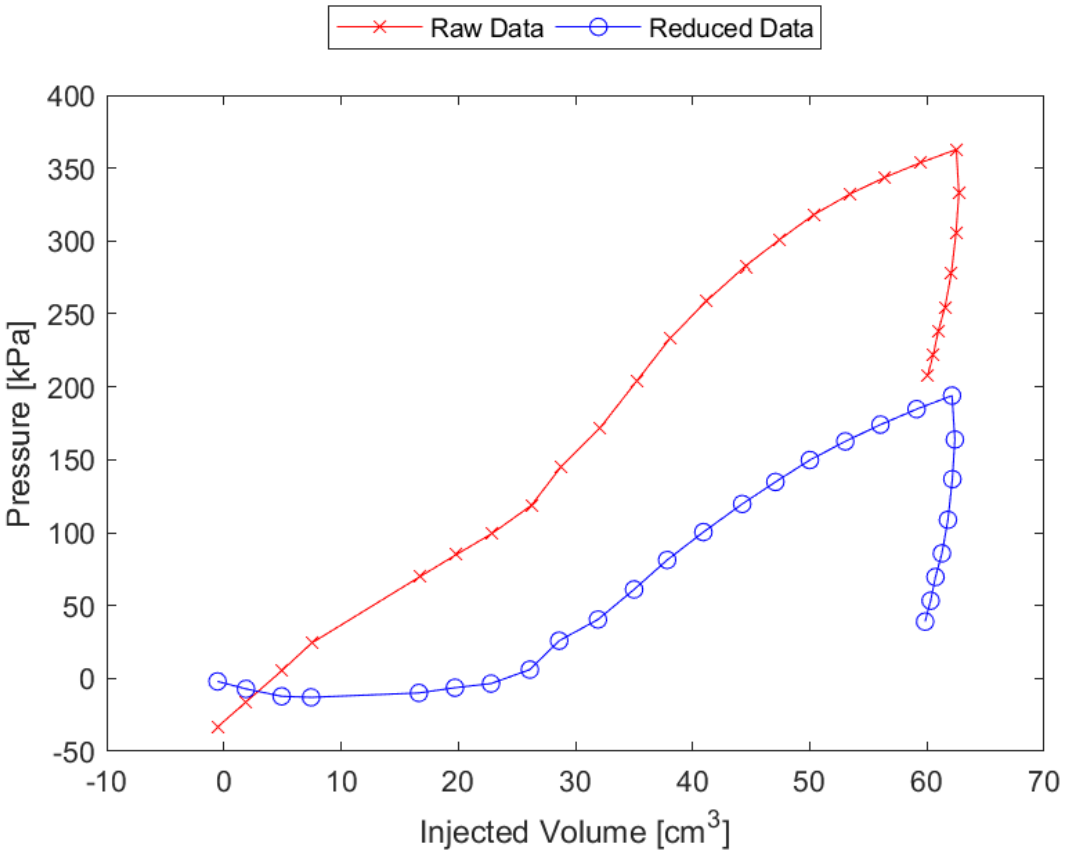

Figure A.30: Sounding 407, SDPMT-12 Incremental Test, Membrane O.D. 0.625m, Depth 0.38 m, Raw and Reduced Data

Table A.30: Sounding 407, SDPMT-12 Incremental Test, Result Summary

Parameter				
Lift-Off Pressure (p_0)	6.1	kPa	0.88	psi
Contact Volume (V_c)	26.1	cm^3	1.59	in^3
Limit Pressure (p_L)	280.0	kPa	40.61	psi
Assumed ν		0.33		
Initial Modulus (E_0)	1683.9	kPa	244.23	psi
Dry Unit Weight (γ_{dry})	1694.8	kg/m^3	105.8	lb/ft^3
Wet Unit Weight (γ_{wet})	1733.2	kg/m^3	108.2	lb/ft^3

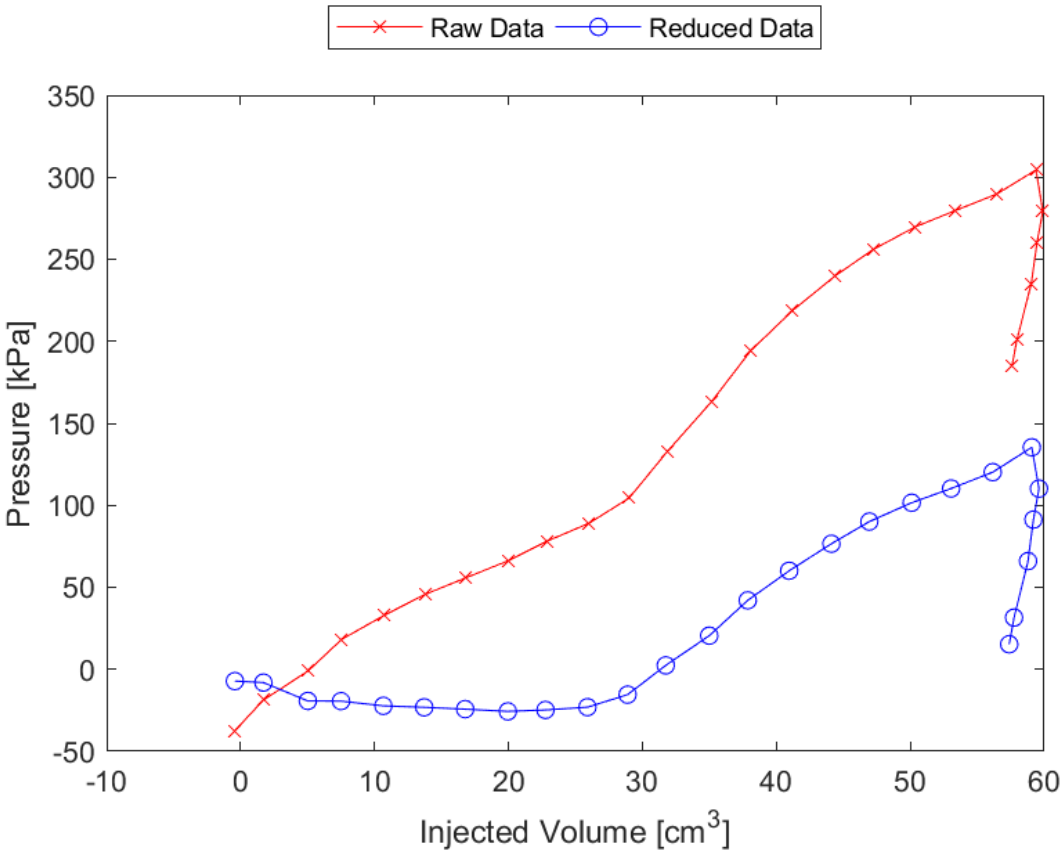

Figure A.31: Sounding 408, SDPMT-12 Incremental Test, Membrane O.D. 0.625m, Depth 0.38 m, Raw and Reduced Data

Table A.31: Sounding 408, SDPMT-12 Incremental Test, Result Summary

Parameter				
Lift-Off Pressure (p_0)	−15.4	kPa	−2.24	psi
Contact Volume (V_c)	28.9	cm^3	1.76	in^3
Limit Pressure (p_L)	215.0	kPa	31.18	psi
Assumed ν		0.33		
Initial Modulus (E_0)	1556.0	kPa	225.69	psi
Dry Unit Weight (γ_{dry})	1707.6	kg/m^3	106.6	lb/ft^3
Wet Unit Weight (γ_{wet})	1720.4	kg/m^3	107.4	lb/ft^3

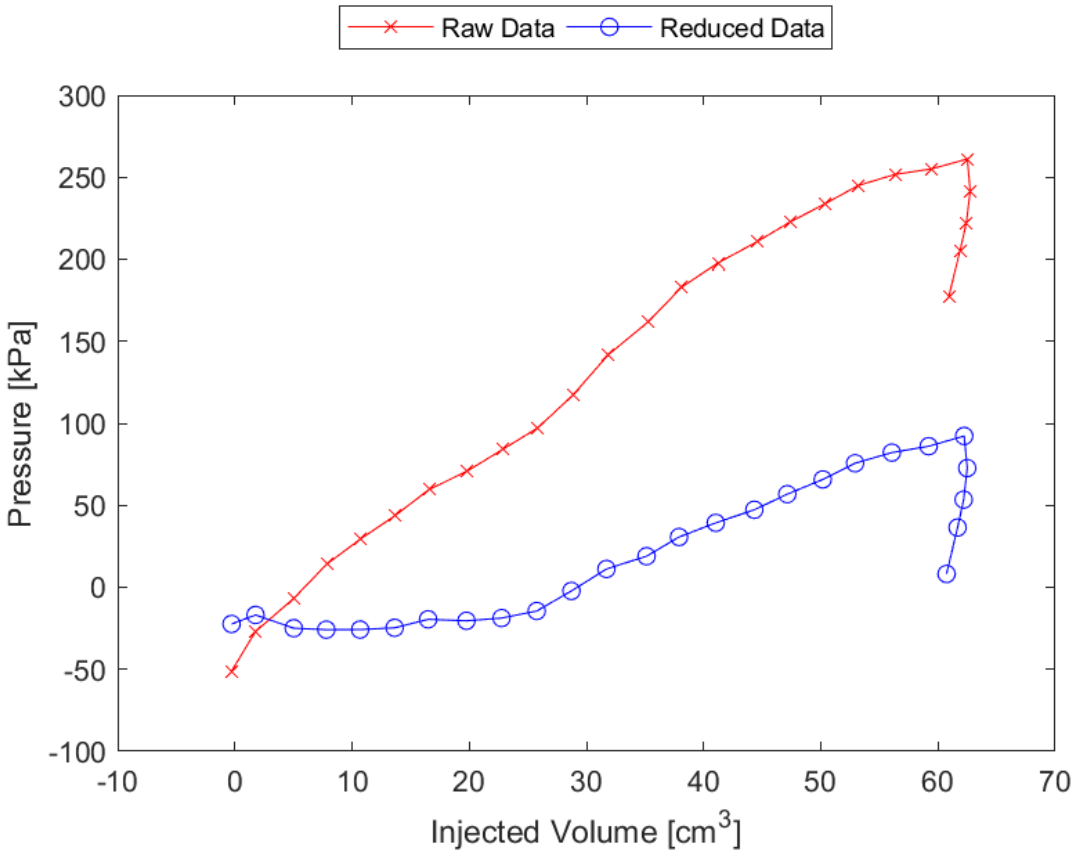

Figure A.32: Sounding 409, SDPMT-12 Incremental Test, Membrane O.D. 0.625m, Depth 0.38 m, Raw and Reduced Data

Table A.32: Sounding 409, SDPMT-12 Incremental Test, Result Summary

Parameter				
Lift-Off Pressure (p_0)	−14.4	kPa	−2.09	psi
Contact Volume (V_c)	25.8	cm^3	1.57	in^3
Limit Pressure (p_L)	145.0	kPa	21.03	psi
Assumed ν		0.33		
Initial Modulus (E_0)	1018.6	kPa	147.74	psi
Dry Unit Weight (γ_{dry})	1704.4	kg/m^3	106.4	lb/ft^3
Wet Unit Weight (γ_{wet})	1773.2	kg/m^3	110.7	lb/ft^3

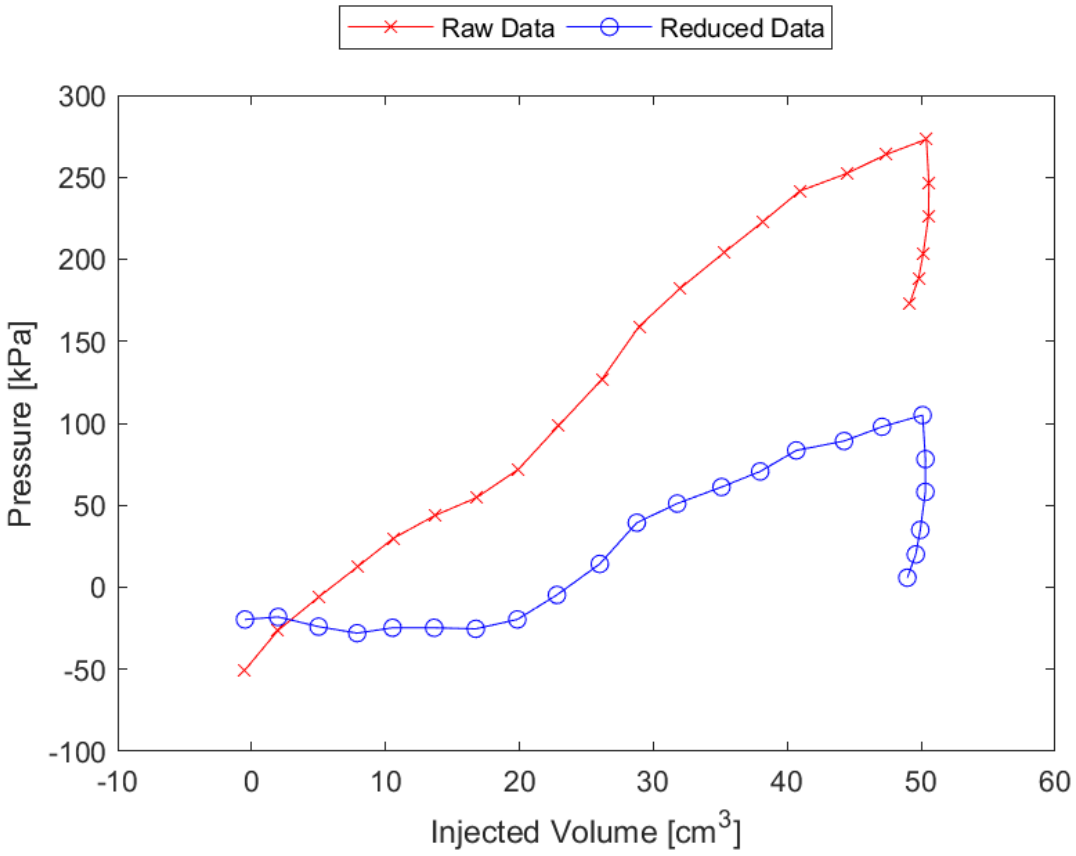

Figure A.33: Sounding 410, SDPMT-12 Incremental Test, Membrane O.D. 0.625m, Depth 0.38 m, Raw and Reduced Data

Table A.33: Sounding 410, SDPMT-12 Incremental Test, Result Summary

Parameter				
Lift-Off Pressure (p_0)	−19.6	kPa	−2.84	psi
Contact Volume (V_c)	19.8	cm^3	1.21	in^3
Limit Pressure (p_L)	160.0	kPa	23.21	psi
Assumed ν		0.33		
Initial Modulus (E_0)	1689.4	kPa	245.02	psi
Dry Unit Weight (γ_{dry})	1736.4	kg/m^3	108.4	lb/ft^3
Wet Unit Weight (γ_{wet})	1827.7	kg/m^3	114.1	lb/ft^3

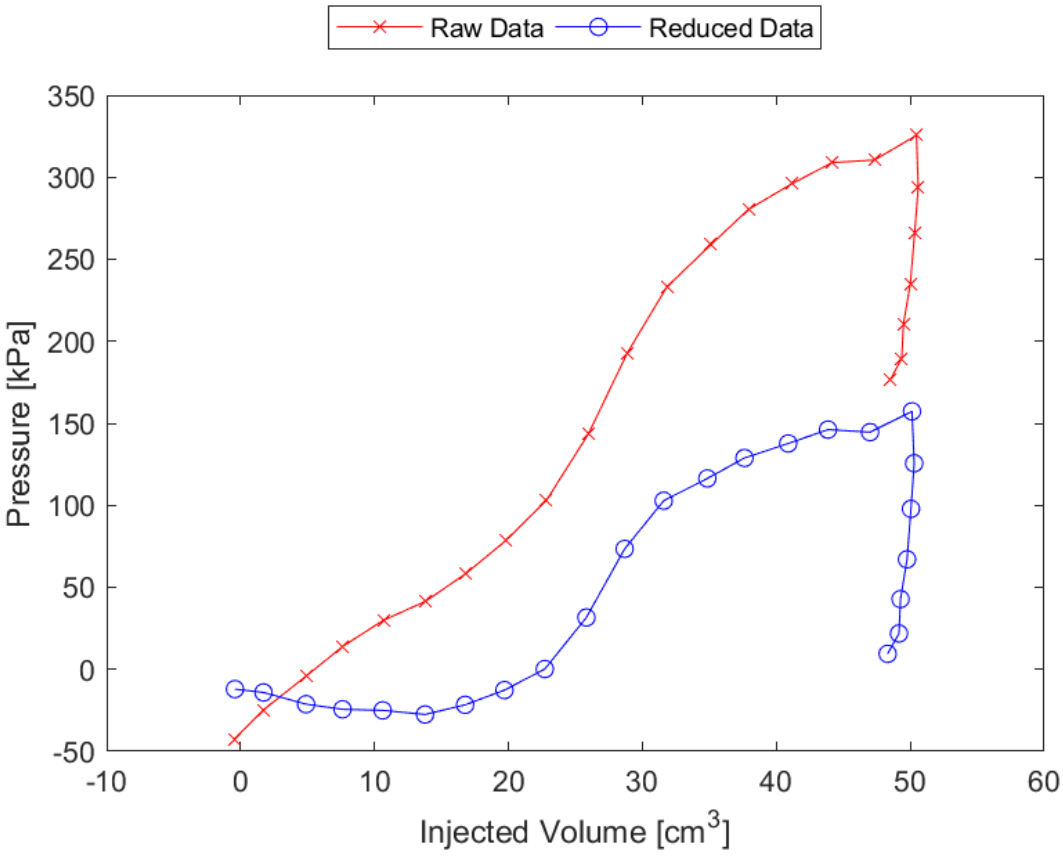

Figure A.34: Sounding 411, SDPMT-12 Incremental Test, Membrane O.D. 0.625m, Depth 0.38 m, Raw and Reduced Data

Table A.34: Sounding 411, SDPMT-12 Incremental Test, Result Summary

Parameter				
Lift-Off Pressure (p_0)	−12.7	kPa	−1.84	psi
Contact Volume (V_c)	19.7	cm^3	1.20	in^3
Limit Pressure (p_L)	210.0	kPa	30.46	psi
Assumed ν		0.33		
Initial Modulus (E_0)	2808.1	kPa	407.29	psi
Dry Unit Weight (γ_{dry})	1704.4	kg/m^3	106.4	lb/ft^3
Wet Unit Weight (γ_{wet})	1779.7	kg/m^3	111.1	lb/ft^3

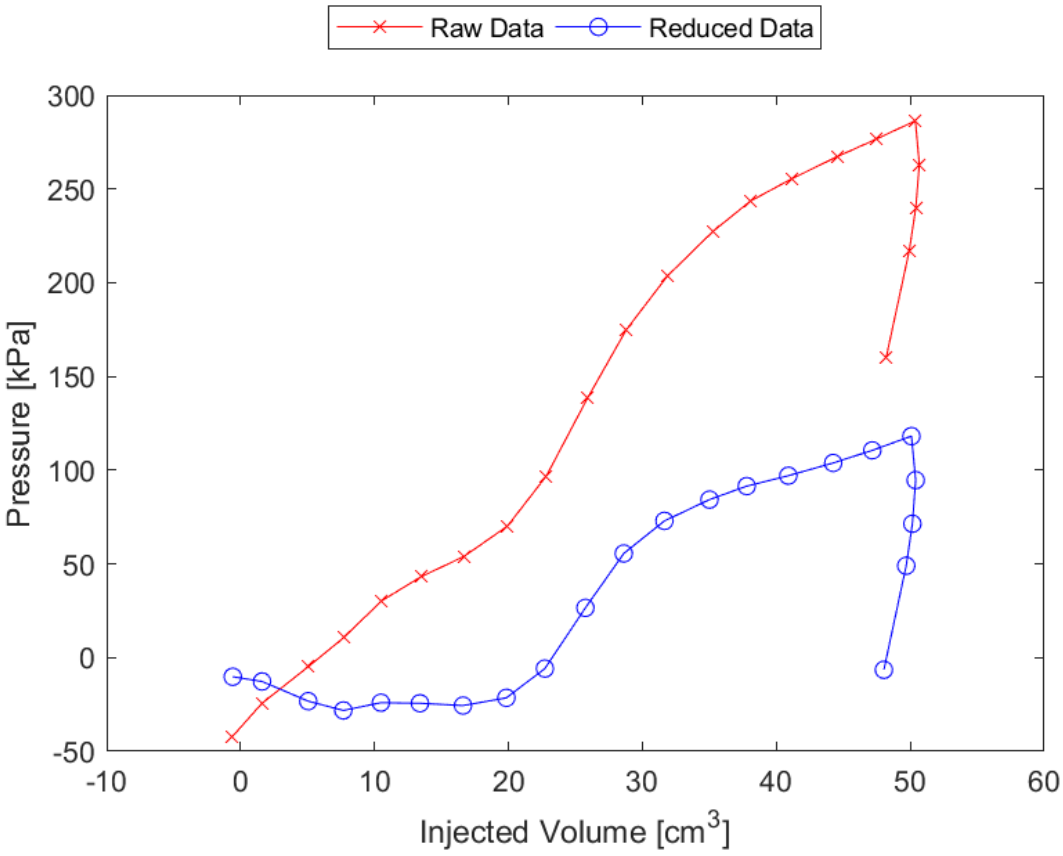

Figure A.35: Sounding 412, SDPMT-12 Incremental Test, Membrane O.D. 0.625m, Depth 0.38 m, Raw and Reduced Data

Table A.35: Sounding 412, SDPMT-12 Incremental Test, Result Summary

Parameter				
Lift-Off Pressure (p_0)	−5.8	kPa	−0.85	psi
Contact Volume (V_c)	22.7	cm^3	1.39	in^3
Limit Pressure (p_L)	160.0	kPa	23.21	psi
Assumed ν		0.33		
Initial Modulus (E_0)	2380.8	kPa	345.30	psi
Dry Unit Weight (γ_{dry})	1648.3	kg/m^3	102.9	lb/ft^3
Wet Unit Weight (γ_{wet})	1709.2	kg/m^3	106.7	lb/ft^3

A.4 SDPMT-12 Continuous Test Data

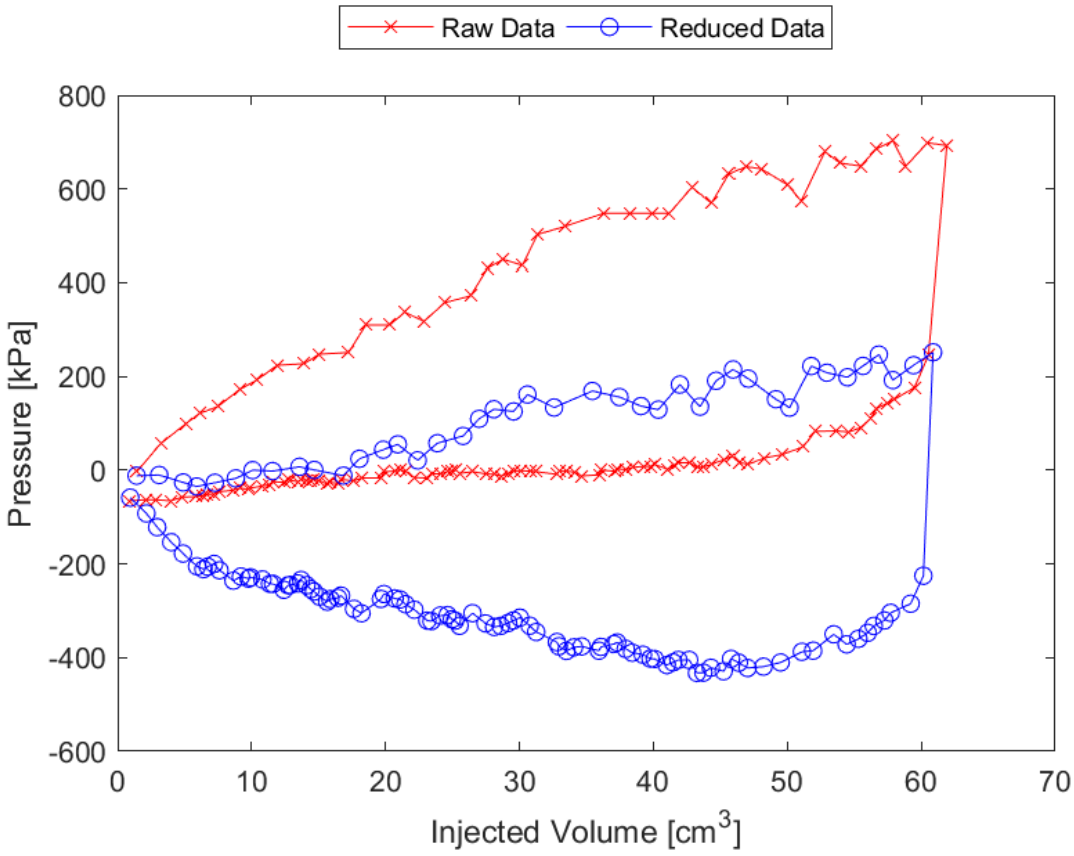

Figure A.36: Sounding 401, SDPMT-12 Continuous Test, Membrane O.D. 0.6875m, Depth 0.41 m, Raw and Reduced Data

Table A.36: Sounding 401, SDPMT-12 Continuous Test, Result Summary

Parameter				
Lift-Off Pressure (p_0)	−11.7	kPa	−1.69	psi
Contact Volume (V_c)	16.8	cm^3	1.03	in^3
Limit Pressure (p_L)	300.0	kPa	43.51	psi
Assumed ν		0.33		
Initial Modulus (E_0)	5371.2	kPa	779.03	psi
Dry Unit Weight (γ_{dry})	1653.1	kg/m^3	103.2	lb/ft^3
Wet Unit Weight (γ_{wet})	1669.1	kg/m^3	104.2	lb/ft^3

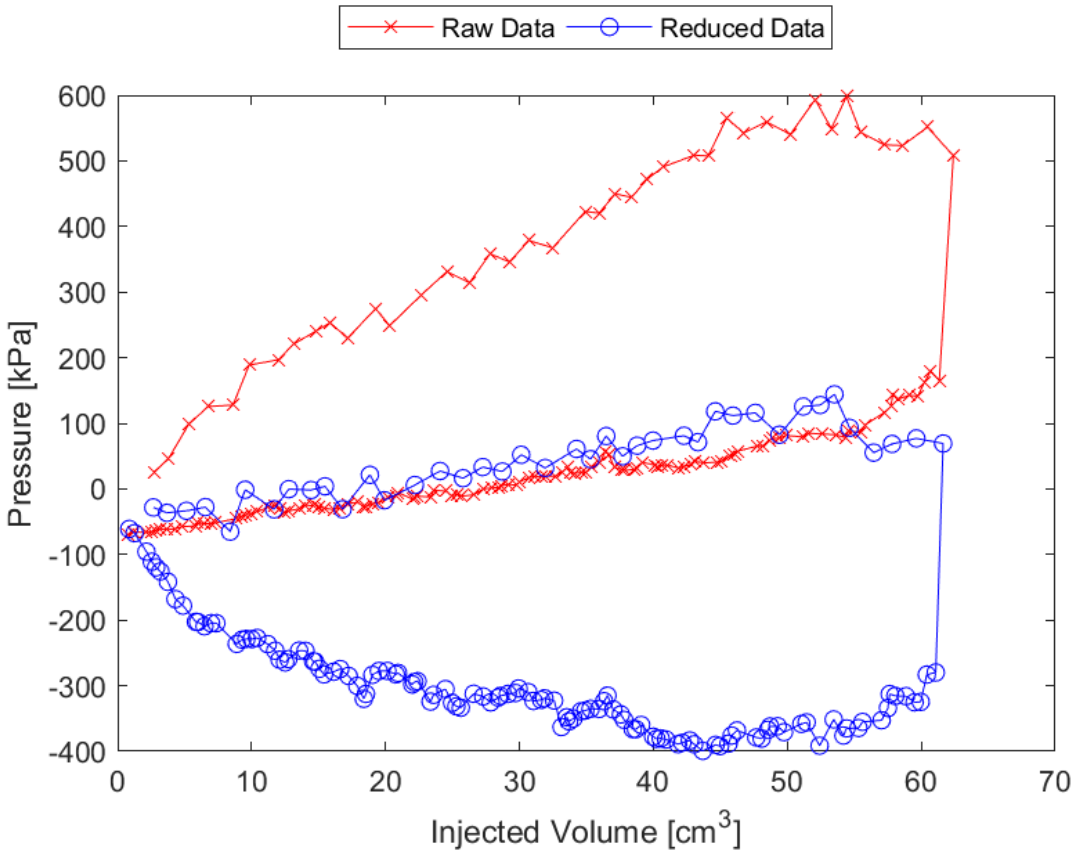

Figure A.37: Sounding 402, SDPMT-12 Continuous Test, Membrane O.D. 0.6875m, Depth 0.41 m, Raw and Reduced Data

Table A.37: Sounding 402, SDPMT-12 Continuous Test, Result Summary

Parameter				
Lift-Off Pressure (p_0)	−1.3	kPa	−0.19	psi
Contact Volume (V_c)	9.5	cm^3	0.58	in^3
Limit Pressure (p_L)	200.0	kPa	29.01	psi
Assumed ν		0.33		
Initial Modulus (E_0)	826.3	kPa	119.85	psi
Dry Unit Weight (γ_{dry})	1694.8	kg/m^3	105.8	lb/ft^3
Wet Unit Weight (γ_{wet})	1709.2	kg/m^3	106.7	lb/ft^3

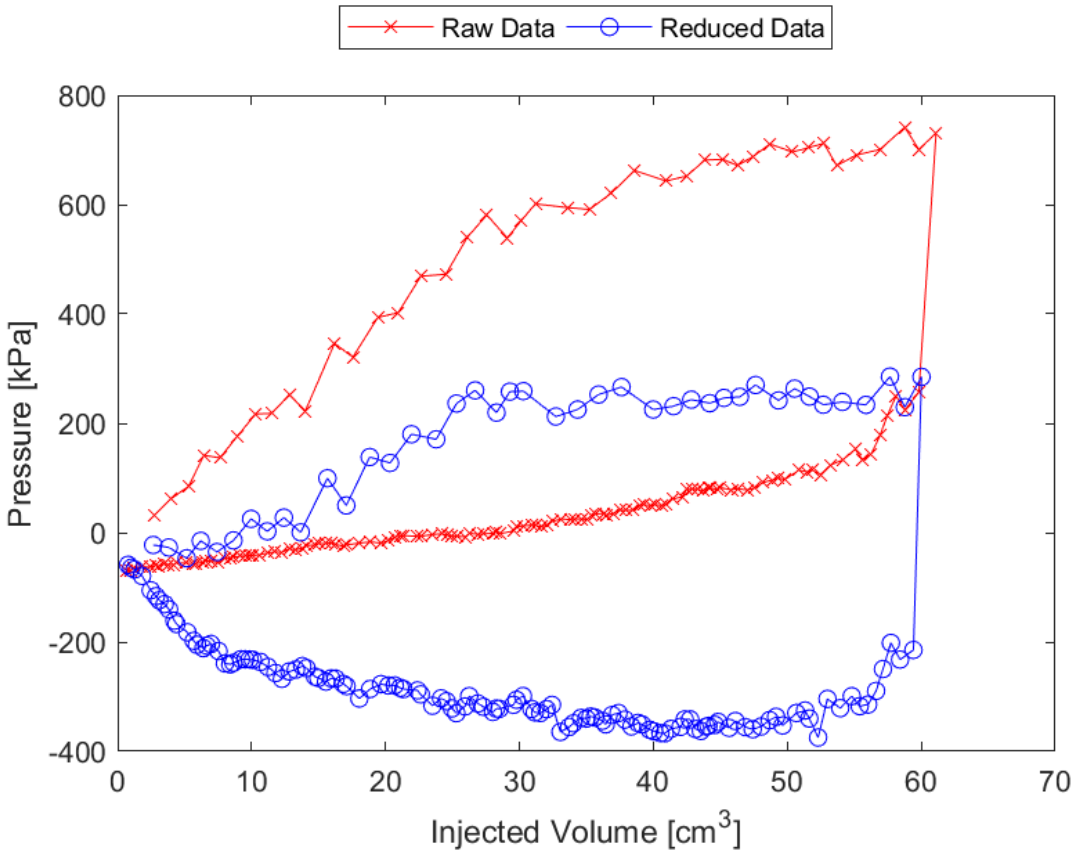

Figure A.38: Sounding 403, SDPMT-12 Continuous Test, Membrane O.D. 0.6875m, Depth 0.41 m, Raw and Reduced Data

Table A.38: Sounding 403, SDPMT-12 Continuous Test, Result Summary

Parameter				
Lift-Off Pressure (p_0)	0.6	kPa	0.08	psi
Contact Volume (V_c)	13.7	cm^3	0.83	in^3
Limit Pressure (p_L)	300.0	kPa	43.51	psi
Assumed ν		0.33		
Initial Modulus (E_0)	5372.2	kPa	779.18	psi
Dry Unit Weight (γ_{dry})	1714.0	kg/m^3	107.0	lb/ft^3
Wet Unit Weight (γ_{wet})	1734.8	kg/m^3	108.3	lb/ft^3

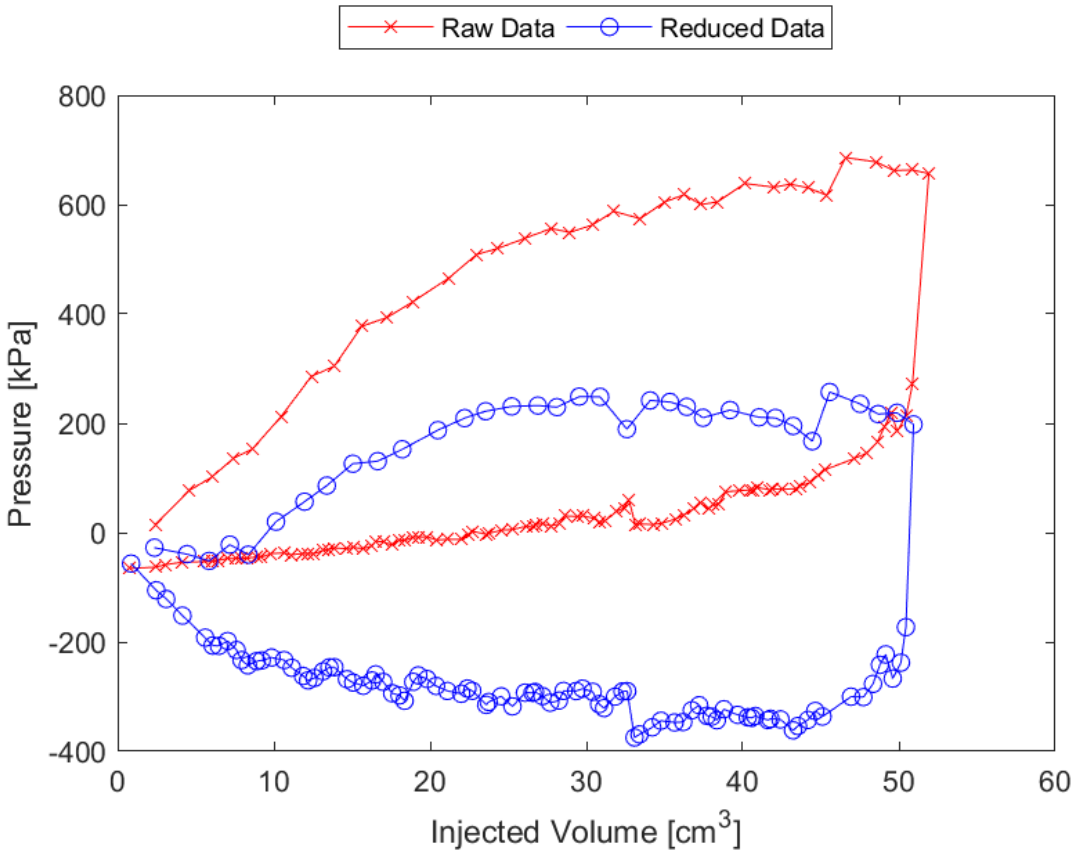

Figure A.39: Sounding 404, SDPMT-12 Continuous Test, Membrane O.D. 0.6875m, Depth 0.41 m, Raw and Reduced Data

Table A.39: Sounding 404, SDPMT-12 Continuous Test, Result Summary

Parameter				
Lift-Off Pressure (p_0)	−40.3	kPa	−5.84	psi
Contact Volume (V_c)	8.4	cm^3	0.51	in^3
Limit Pressure (p_L)	300.0	kPa	43.51	psi
Assumed ν		0.33		
Initial Modulus (E_0)	5320.0	kPa	771.61	psi
Dry Unit Weight (γ_{dry})	1685.1	kg/m^3	105.2	lb/ft^3
Wet Unit Weight (γ_{wet})	1704.4	kg/m^3	106.4	lb/ft^3

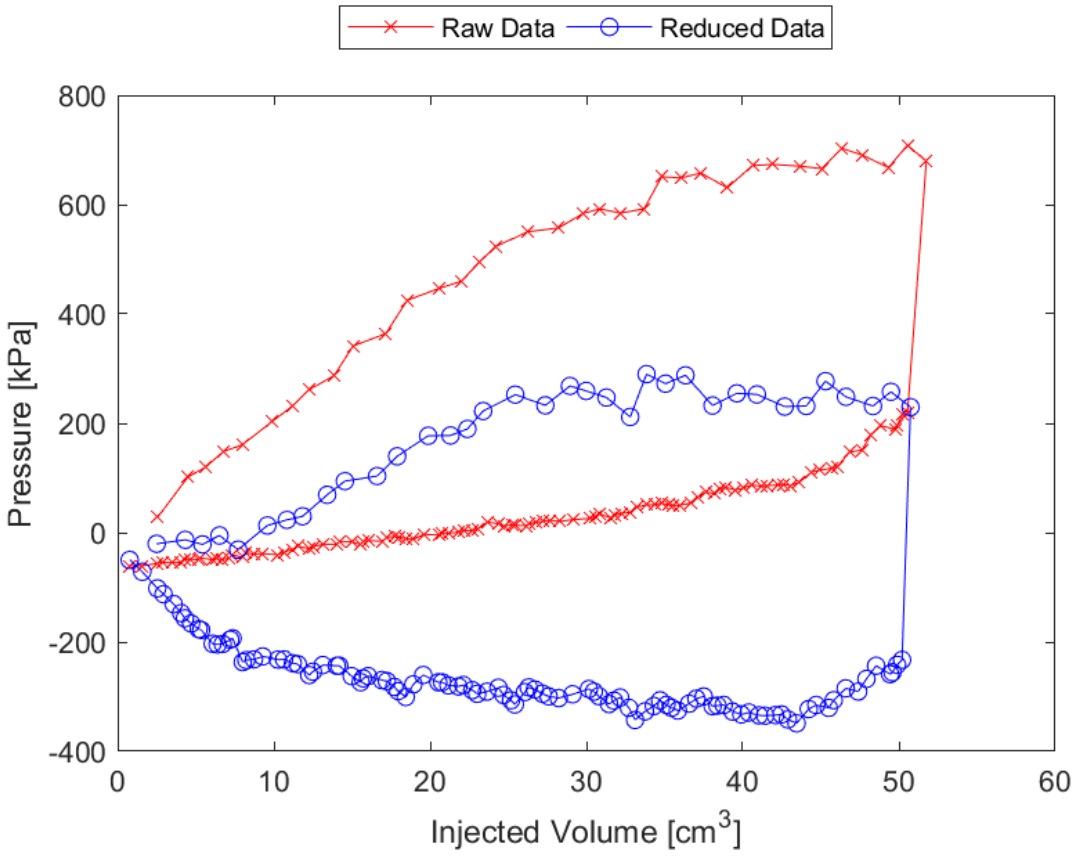

Figure A.40: Sounding 405, SDPMT-12 Continuous Test, Membrane O.D. 0.6875m, Depth 0.41 m, Raw and Reduced Data

Table A.40: Sounding 405, SDPMT-12 Continuous Test, Result Summary

Parameter				
Lift-Off Pressure (p_0)	13.1	kPa	1.90	psi
Contact Volume (V_c)	9.6	cm^3	0.58	in^3
Limit Pressure (p_L)	400.0	kPa	58.02	psi
Assumed ν		0.33		
Initial Modulus (E_0)	4685.4	kPa	679.57	psi
Dry Unit Weight (γ_{dry})	1662.7	kg/m^3	103.8	lb/ft^3
Wet Unit Weight (γ_{wet})	1681.9	kg/m^3	105.0	lb/ft^3

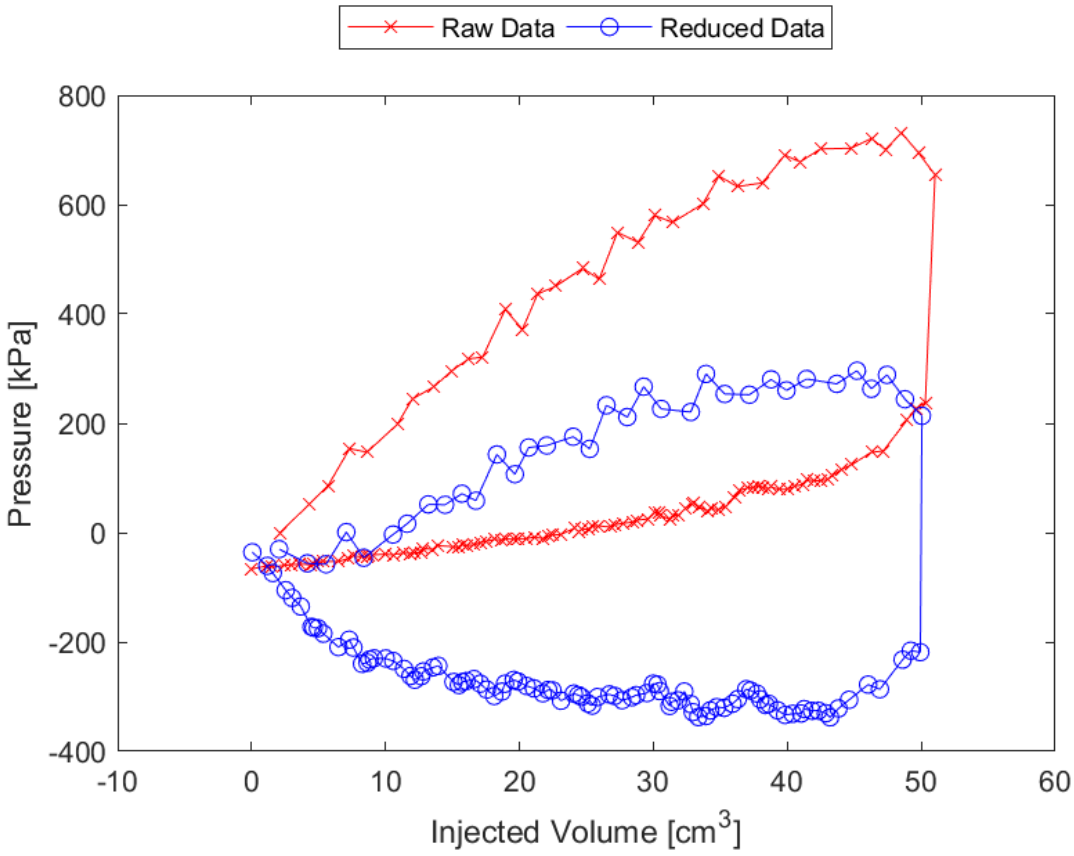

Figure A.41: Sounding 406, SDPMT-12 Continuous Test, Membrane O.D. 0.6875m, Depth 0.41 m, Raw and Reduced Data

Table A.41: Sounding 406, SDPMT-12 Continuous Test, Result Summary

Parameter				
Lift-Off Pressure (p_0)	−3.4	kPa	−0.50	psi
Contact Volume (V_c)	10.6	cm^3	0.64	in^3
Limit Pressure (p_L)	300.0	kPa	43.51	psi
Assumed ν		0.33		
Initial Modulus (E_0)	3074.1	kPa	445.86	psi
Dry Unit Weight (γ_{dry})	1619.5	kg/m^3	101.1	lb/ft^3
Wet Unit Weight (γ_{wet})	1637.1	kg/m^3	102.2	lb/ft^3

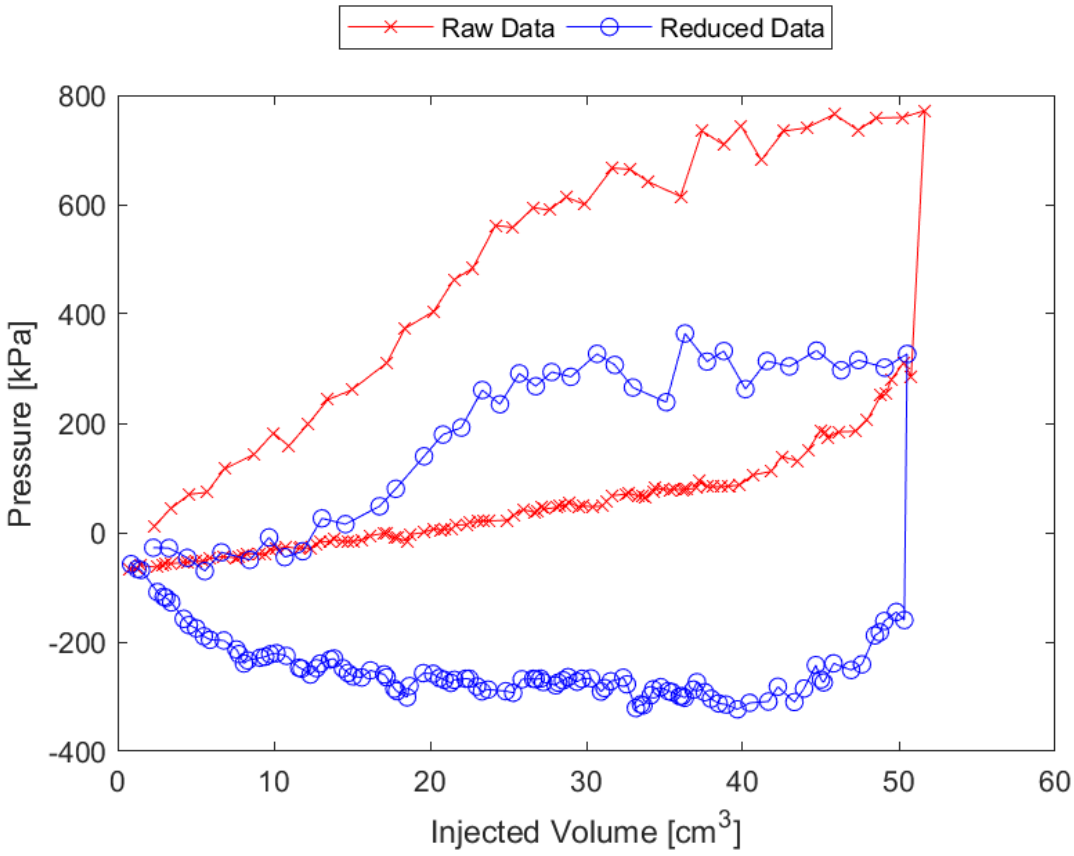

Figure A.42: Sounding 407, SDPMT-12 Continuous Test, Membrane O.D. 0.6875m, Depth 0.41 m, Raw and Reduced Data

Table A.42: Sounding 407, SDPMT-12 Continuous Test, Result Summary

Parameter				
Lift-Off Pressure (p_0)	26.1	kPa	3.78	psi
Contact Volume (V_c)	13.1	cm^3	0.80	in^3
Limit Pressure (p_L)	500.0	kPa	72.52	psi
Assumed ν		0.33		
Initial Modulus (E_0)	8632.7	kPa	1252.06	psi
Dry Unit Weight (γ_{dry})	1694.8	kg/m^3	105.8	lb/ft^3
Wet Unit Weight (γ_{wet})	1731.6	kg/m^3	108.1	lb/ft^3

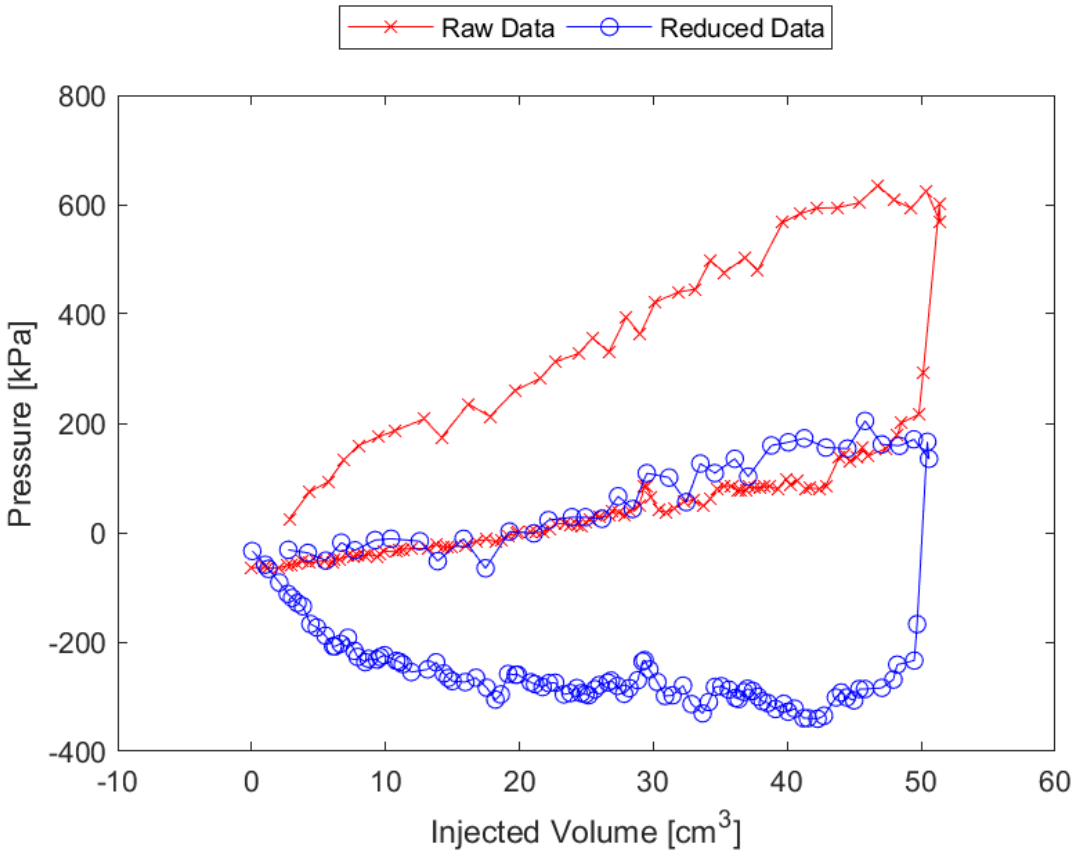

Figure A.43: Sounding 408, SDPMT-12 Continuous Test, Membrane O.D. 0.6875m, Depth 0.41 m, Raw and Reduced Data

Table A.43: Sounding 408, SDPMT-12 Continuous Test, Result Summary

Parameter				
Lift-Off Pressure (p_0)	−1.4	kPa	−0.20	psi
Contact Volume (V_c)	21.1	cm^3	1.29	in^3
Limit Pressure (p_L)	200.0	kPa	29.01	psi
Assumed ν		0.33		
Initial Modulus (E_0)	3186.2	kPa	462.13	psi
Dry Unit Weight (γ_{dry})	1707.6	kg/m^3	106.6	lb/ft^3
Wet Unit Weight (γ_{wet})	1749.2	kg/m^3	109.2	lb/ft^3

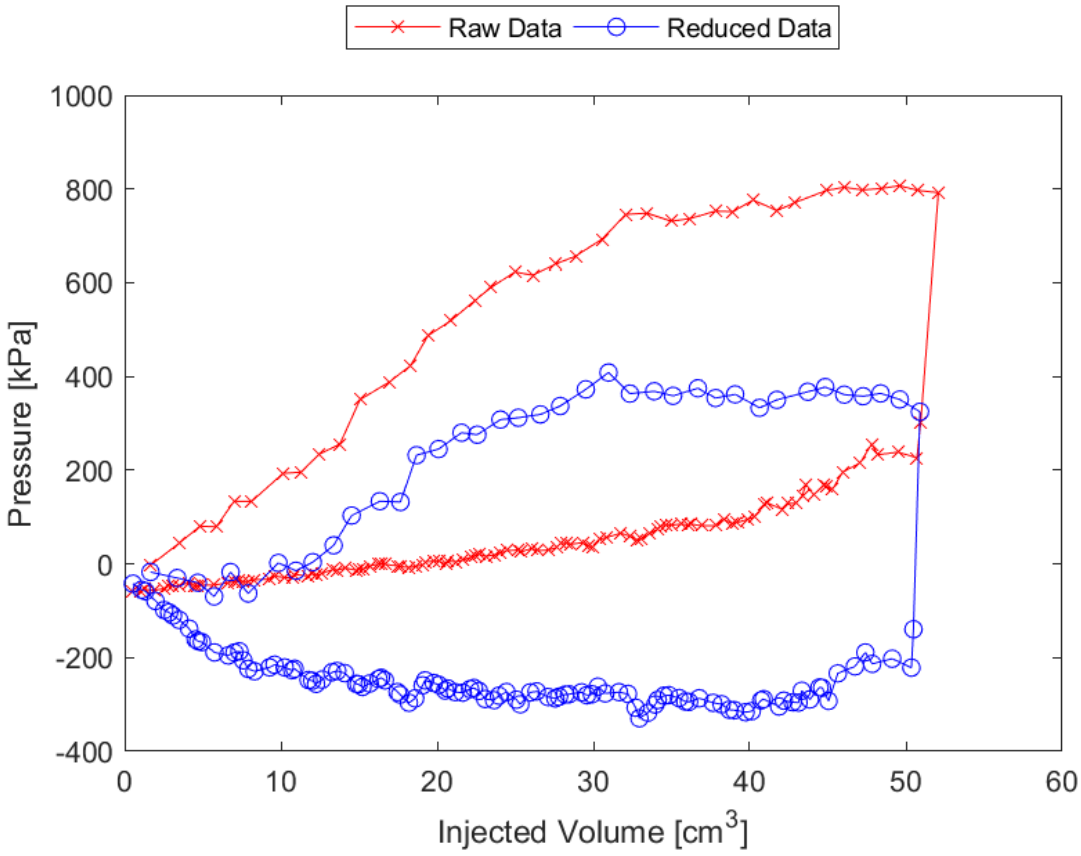

Figure A.44: Sounding 410, SDPMT-12 Continuous Test, Membrane O.D. 0.6875m, Depth 0.41 m, Raw and Reduced Data

Table A.44: Sounding 410, SDPMT-12 Continuous Test, Result Summary

Parameter				
Lift-Off Pressure (p_0)	3.5	kPa	0.51	psi
Contact Volume (V_c)	12.0	cm^3	0.73	in^3
Limit Pressure (p_L)	500.0	kPa	72.52	psi
Assumed ν		0.33		
Initial Modulus (E_0)	8740.8	kPa	1267.75	psi
Dry Unit Weight (γ_{dry})	1736.4	kg/m^3	108.4	lb/ft^3
Wet Unit Weight (γ_{wet})	1786.1	kg/m^3	111.5	lb/ft^3

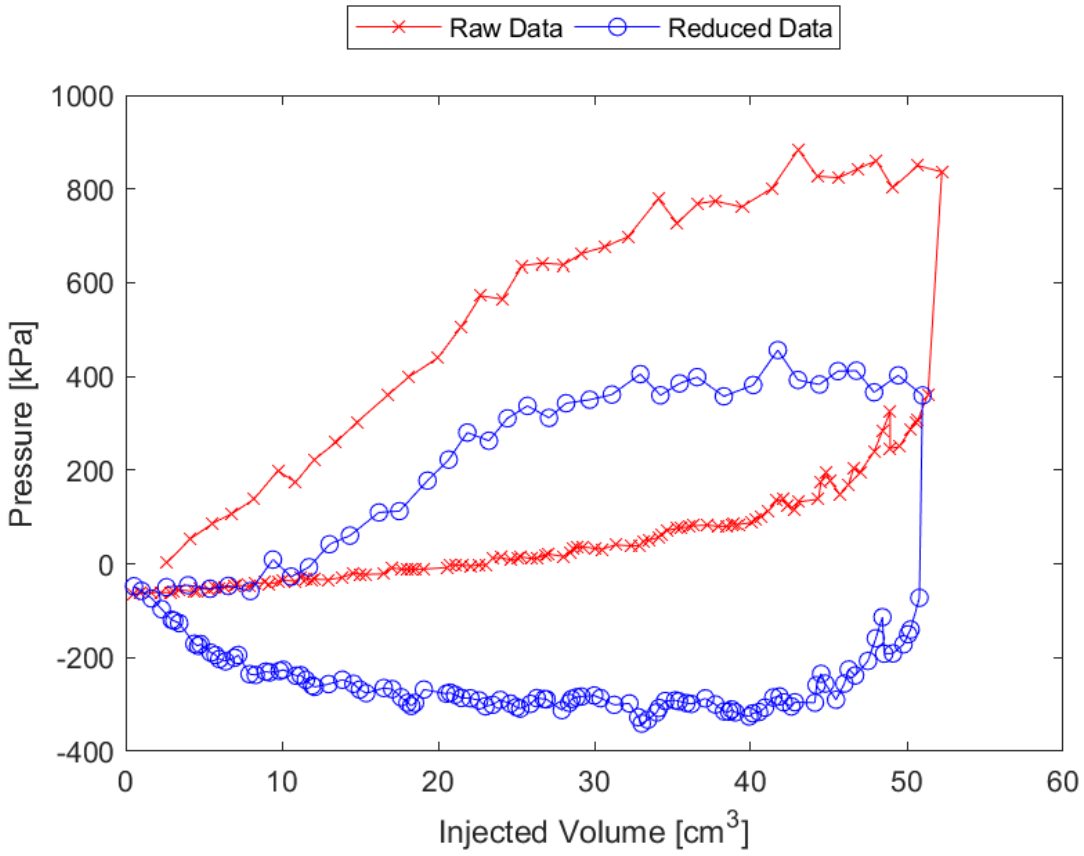

Figure A.45: Sounding 411, SDPMT-12 Continuous Test, Membrane O.D. 0.6875m, Depth 0.41 m, Raw and Reduced Data

Table A.45: Sounding 411, SDPMT-12 Continuous Test, Result Summary

Parameter				
Lift-Off Pressure (p_0)	−27.2	kPa	−3.94	psi
Contact Volume (V_c)	10.6	cm^3	0.65	in^3
Limit Pressure (p_L)	500.0	kPa	72.52	psi
Assumed ν		0.33		
Initial Modulus (E_0)	7319.1	kPa	1061.54	psi
Dry Unit Weight (γ_{dry})	1704.4	kg/m^3	106.4	lb/ft^3
Wet Unit Weight (γ_{wet})	1754.0	kg/m^3	109.5	lb/ft^3

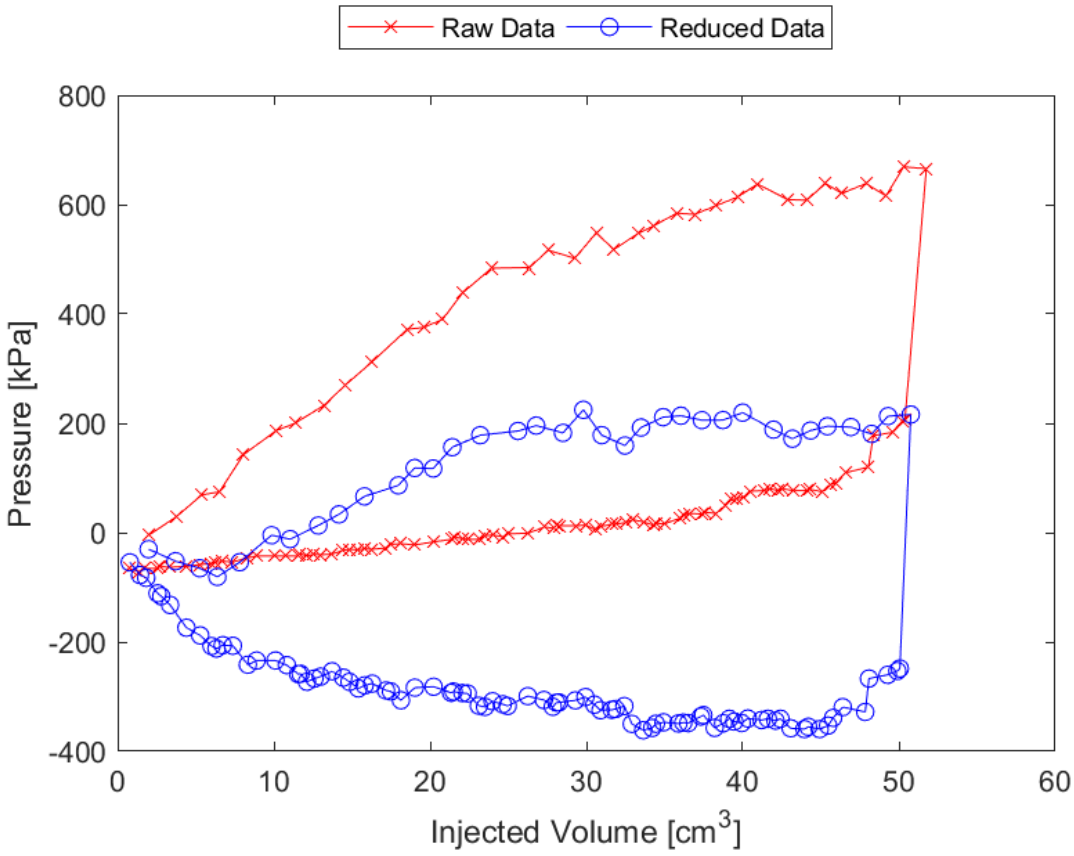

Figure A.46: Sounding 412, SDPMT-12 Continuous Test, Membrane O.D. 0.6875m, Depth 0.41 m, Raw and Reduced Data

Table A.46: Sounding 412, SDPMT-12 Continuous Test, Result Summary

Parameter				
Lift-Off Pressure (p_0)	−11.9	kPa	−1.73	psi
Contact Volume (V_c)	11.0	cm^3	0.67	in^3
Limit Pressure (p_L)	300.0	kPa	43.51	psi
Assumed ν		0.33		
Initial Modulus (E_0)	4159.5	kPa	603.28	psi
Dry Unit Weight (γ_{dry})	1648.3	kg/m^3	102.9	lb/ft^3
Wet Unit Weight (γ_{wet})	1677.1	kg/m^3	104.7	lb/ft^3

Appendix B

Olin Complex Pressuremeter Test Data

B.1 SDPMT-6 Incremental Test Data

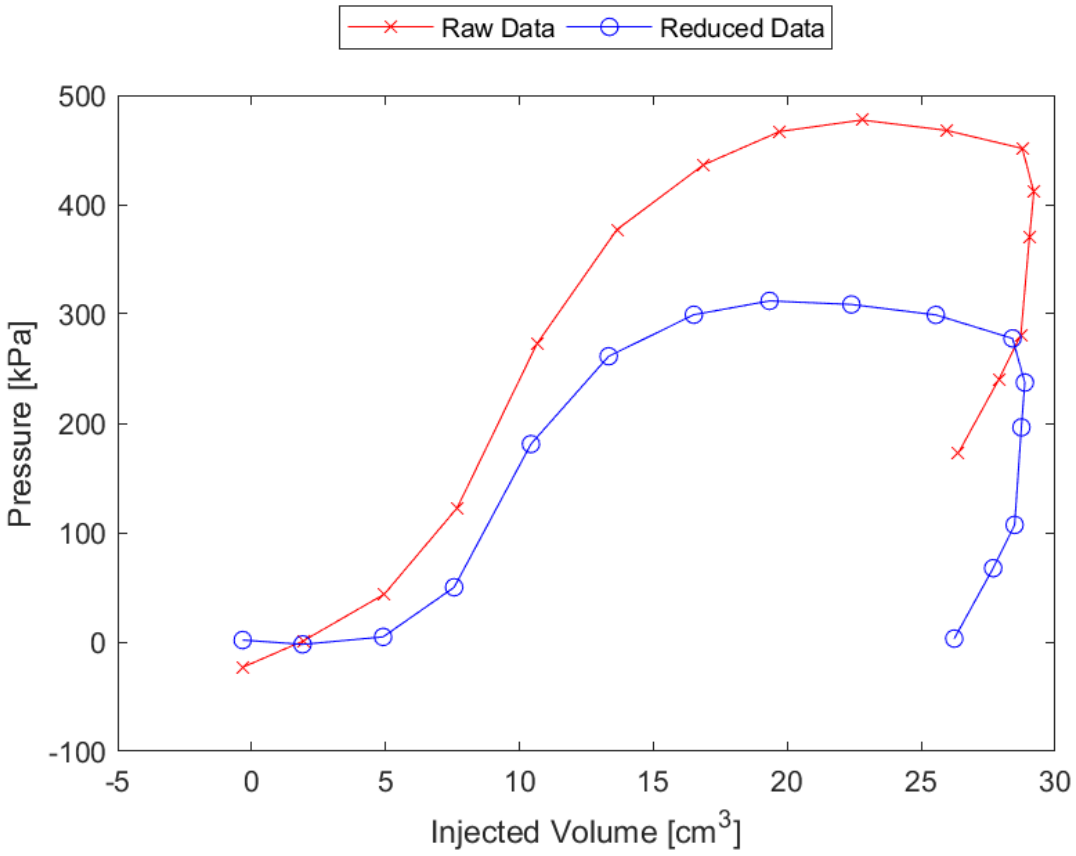

Figure B.1: Sounding 201, SDPMT-6 Incremental Test, Membrane O.D. 0.625m, Depth 0.25 m, Raw and Reduced Data

Table B.1: Sounding 201, SDPMT-6 Incremental Test, Result Summary

Parameter				
Lift-Off Pressure (p_0)	4.6	kPa	0.67	psi
Contact Volume (V_c)	4.9	cm^3	0.30	in^3
Limit Pressure (p_L)	310.0	kPa	44.96	psi
Assumed ν		0.33		
Initial Modulus (E_0)	3950.3	kPa	572.95	psi
Dry Unit Weight (γ_{dry})	1747.6	kg/m^3	109.1	lb/ft^3
Wet Unit Weight (γ_{wet})	1778.0	kg/m^3	111.0	lb/ft^3

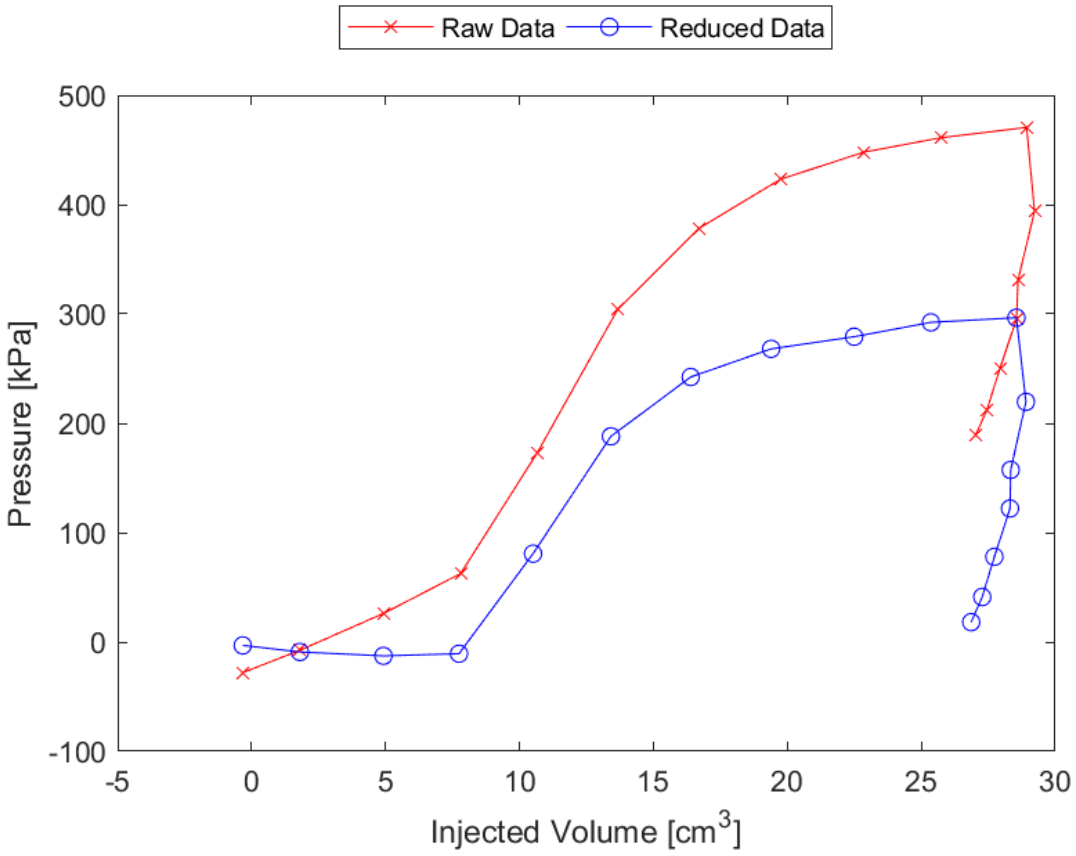

Figure B.2: Sounding 202, SDPMT-6 Incremental Test, Membrane O.D. 0.625m, Depth 0.25 m, Raw and Reduced Data

Table B.2: Sounding 202, SDPMT-6 Incremental Test, Result Summary

Parameter				
Lift-Off Pressure (p_0)	−10.7	kPa	−1.55	psi
Contact Volume (V_c)	7.7	cm^3	0.47	in^3
Limit Pressure (p_L)	350.0	kPa	50.76	psi
Assumed ν		0.33		
Initial Modulus (E_0)	3792.9	kPa	550.12	psi
Dry Unit Weight (γ_{dry})	1826.1	kg/m^3	114.0	lb/ft^3
Wet Unit Weight (γ_{wet})	1890.2	kg/m^3	118.0	lb/ft^3

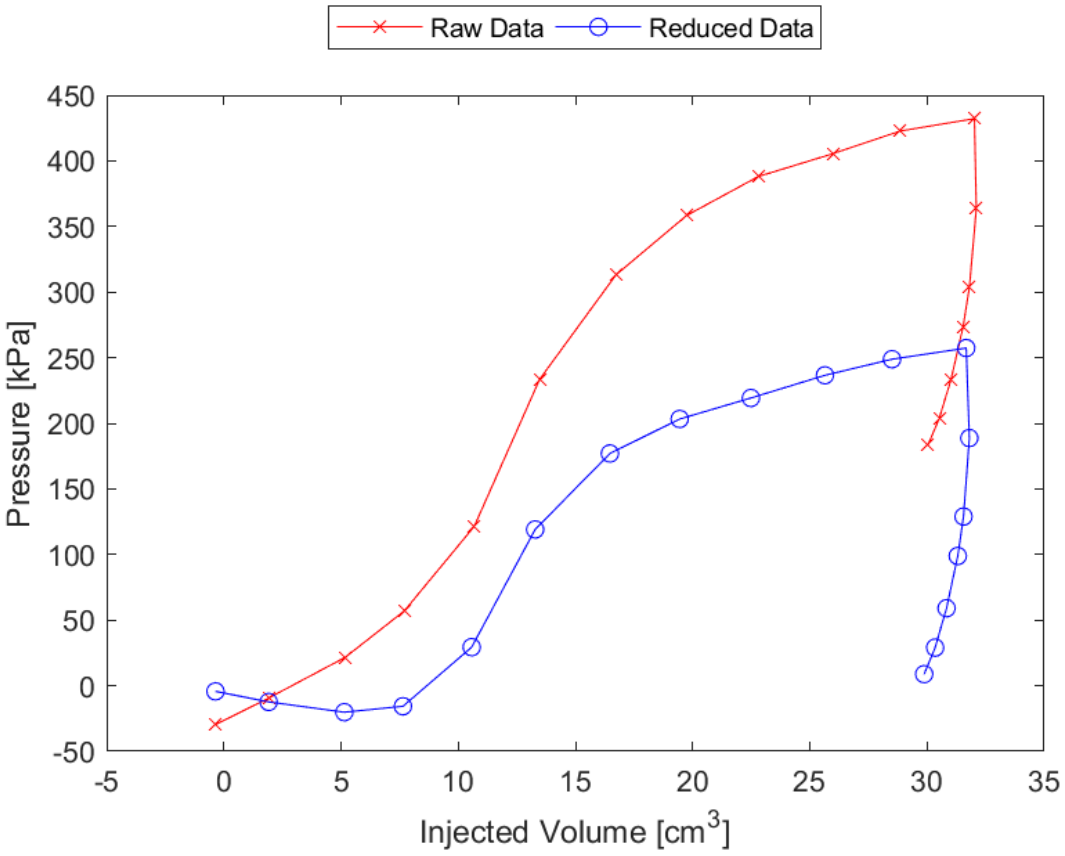

Figure B.3: Sounding 203, SDPMT-6 Incremental Test, Membrane O.D. 0.625m, Depth 0.25 m, Raw and Reduced Data

Table B.3: Sounding 203, SDPMT-6 Incremental Test, Result Summary

Parameter				
Lift-Off Pressure (p_0)	−15.7	kPa	−2.27	psi
Contact Volume (V_c)	7.6	cm^3	0.47	in^3
Limit Pressure (p_L)	300.0	kPa	43.51	psi
Assumed ν		0.33		
Initial Modulus (E_0)	2904.9	kPa	421.32	psi
Dry Unit Weight (γ_{dry})	1757.2	kg/m^3	109.7	lb/ft^3
Wet Unit Weight (γ_{wet})	1794.1	kg/m^3	112.0	lb/ft^3

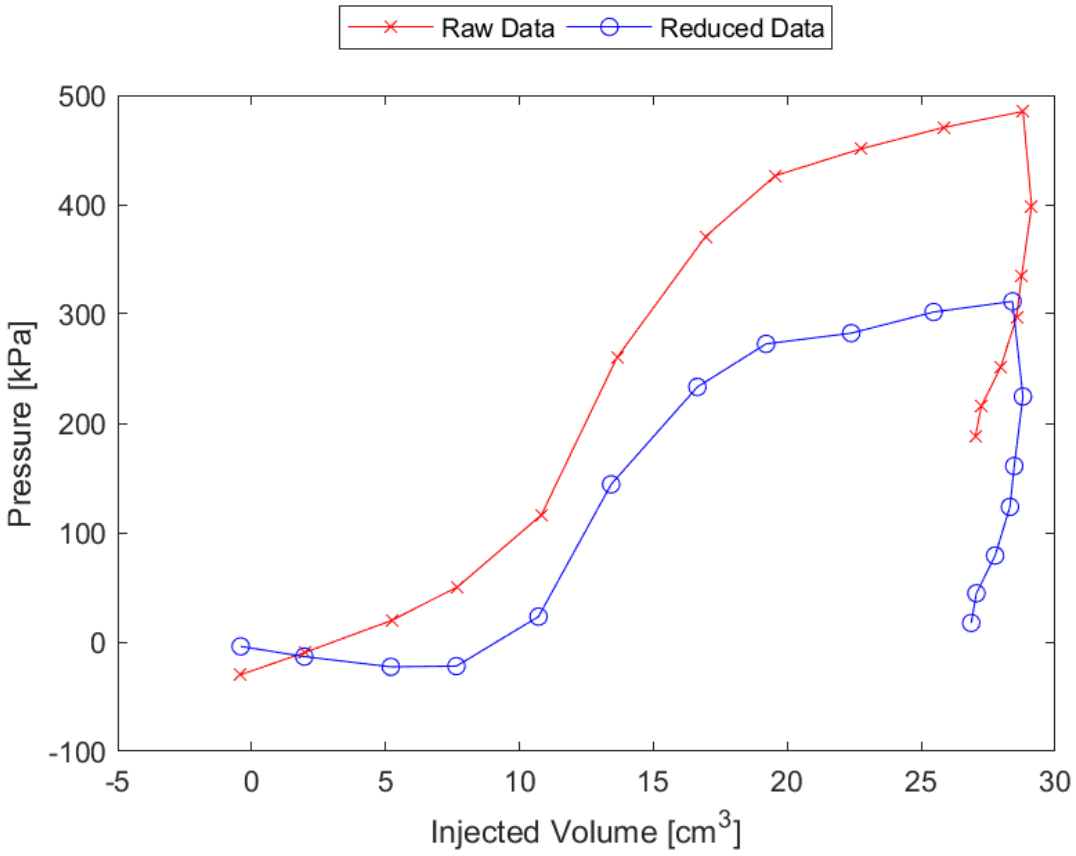

Figure B.4: Sounding 204, SDPMT-6 Incremental Test, Membrane O.D. 0.625m, Depth 0.25 m, Raw and Reduced Data

Table B.4: Sounding 204, SDPMT-6 Incremental Test, Result Summary

Parameter				
Lift-Off Pressure (p_0)	−22.1	kPa	−3.20	psi
Contact Volume (V_c)	7.6	cm^3	0.47	in^3
Limit Pressure (p_L)	350.0	kPa	50.76	psi
Assumed ν		0.33		
Initial Modulus (E_0)	4125.5	kPa	598.36	psi
Dry Unit Weight (γ_{dry})	1698.0	kg/m^3	106.0	lb/ft^3
Wet Unit Weight (γ_{wet})	1731.6	kg/m^3	108.1	lb/ft^3

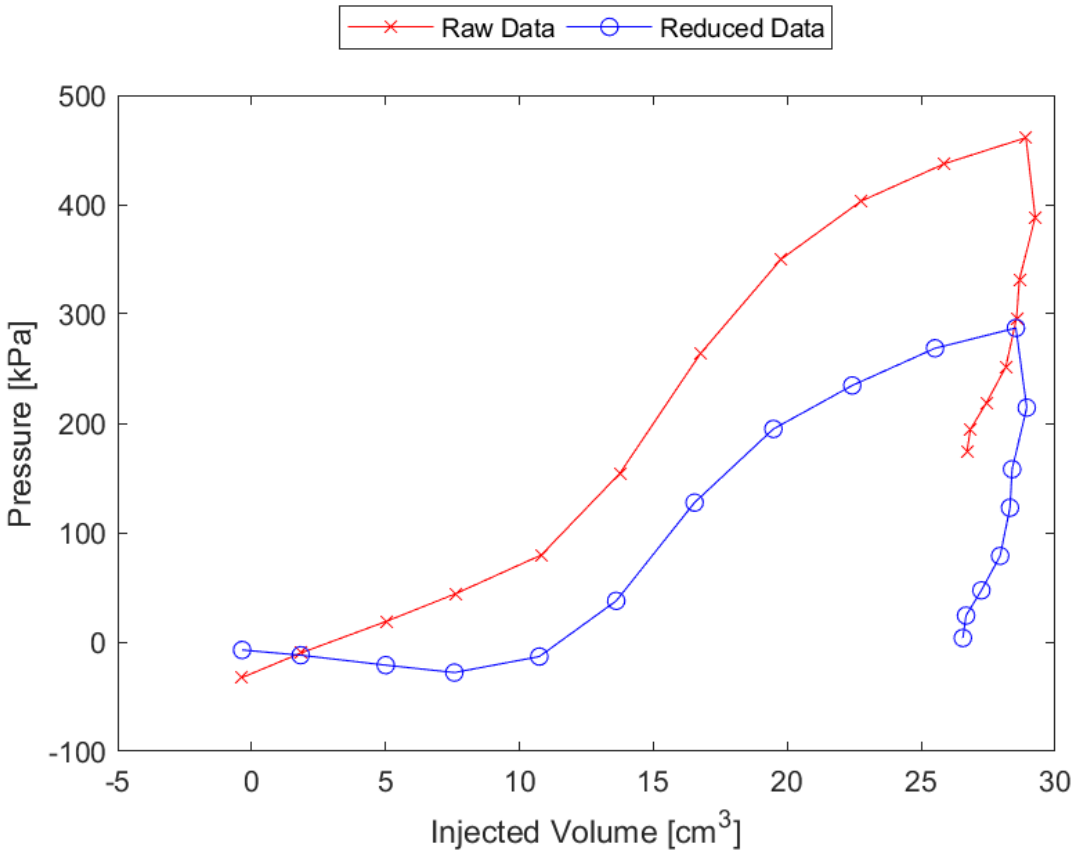

Figure B.5: Sounding 205, SDPMT-6 Incremental Test, Membrane O.D. 0.625m, Depth 0.25 m, Raw and Reduced Data

Table B.5: Sounding 205, SDPMT-6 Incremental Test, Result Summary

Parameter				
Lift-Off Pressure (p_0)	−13.3	kPa	−1.93	psi
Contact Volume (V_c)	−13.3	cm^3	−0.81	in^3
Limit Pressure (p_L)	350.0	kPa	50.76	psi
Assumed ν		0.33		
Initial Modulus (E_0)	3325.6	kPa	482.33	psi
Dry Unit Weight (γ_{dry})	1806.9	kg/m^3	112.8	lb/ft^3
Wet Unit Weight (γ_{wet})	1851.7	kg/m^3	115.6	lb/ft^3

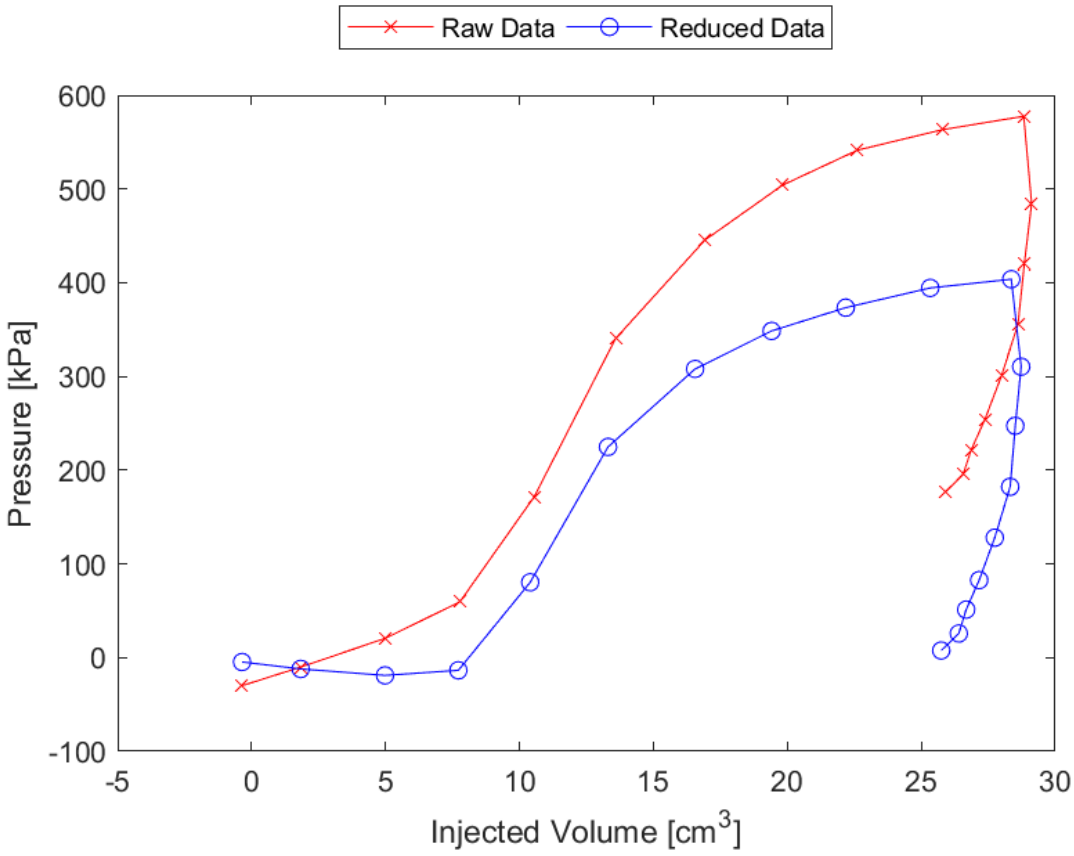

Figure B.6: Sounding 206, SDPMT-6 Incremental Test, Membrane O.D. 0.625m, Depth 0.25 m, Raw and Reduced Data

Table B.6: Sounding 206, SDPMT-6 Incremental Test, Result Summary

Parameter				
Lift-Off Pressure (p_0)	−13.6	kPa	−1.97	psi
Contact Volume (V_c)	7.7	cm^3	0.47	in^3
Limit Pressure (p_L)	450.0	kPa	65.27	psi
Assumed ν		0.33		
Initial Modulus (E_0)	4609.3	kPa	668.52	psi
Dry Unit Weight (γ_{dry})	1842.1	kg/m^3	115.0	lb/ft^3
Wet Unit Weight (γ_{wet})	1914.2	kg/m^3	119.5	lb/ft^3

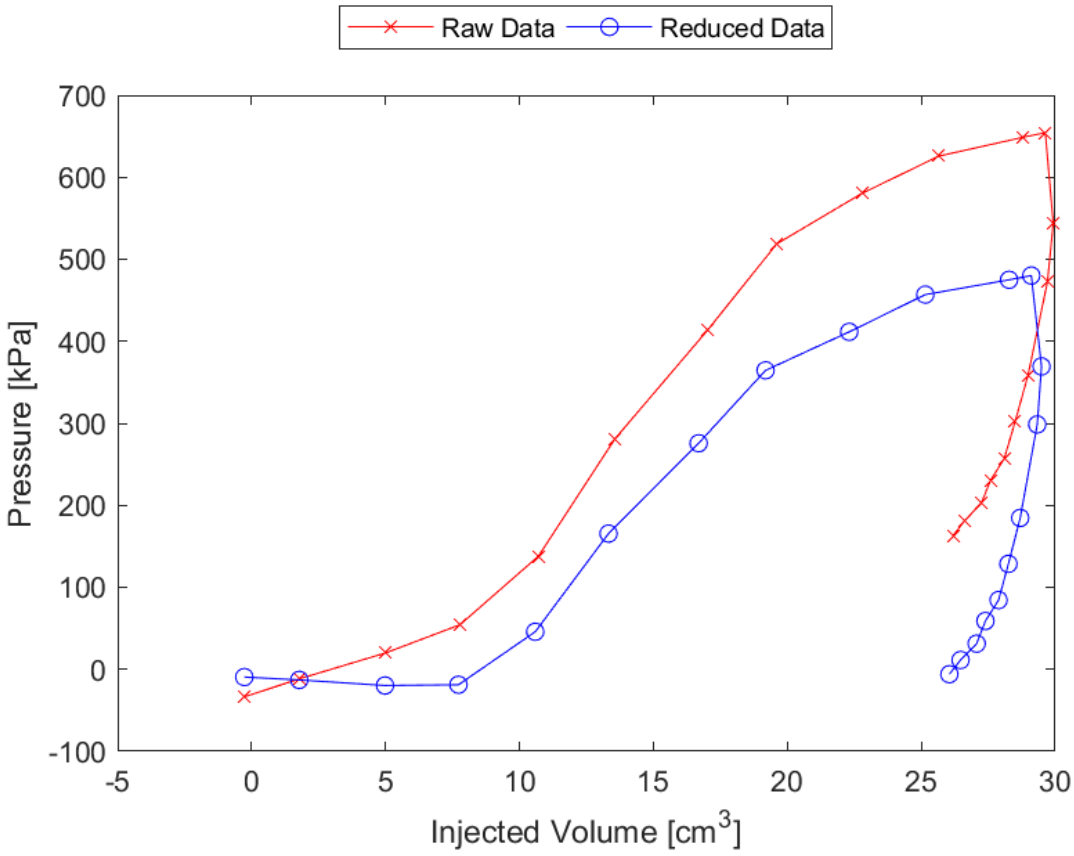

Figure B.7: Sounding 207, SDPMT-6 Incremental Test, Membrane O.D. 0.625m, Depth 0.25 m, Raw and Reduced Data

Table B.7: Sounding 207, SDPMT-6 Incremental Test, Result Summary

Parameter				
Lift-Off Pressure (p_0)	−18.8	kPa	−2.73	psi
Contact Volume (V_c)	7.7	cm^3	0.47	in^3
Limit Pressure (p_L)	550.0	kPa	79.77	psi
Assumed ν		0.33		
Initial Modulus (E_0)	4437.5	kPa	643.61	psi
Dry Unit Weight (γ_{dry})	1832.5	kg/m^3	114.4	lb/ft^3
Wet Unit Weight (γ_{wet})	1880.6	kg/m^3	117.4	lb/ft^3

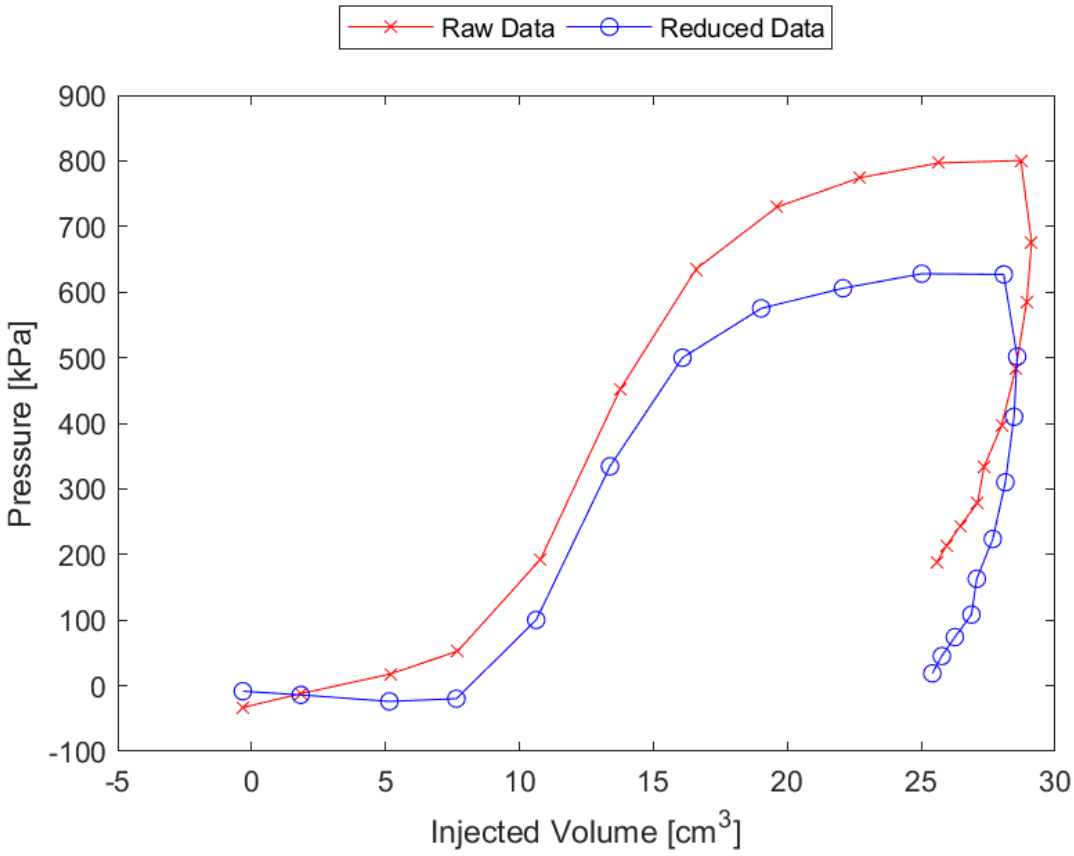

Figure B.8: Sounding 208, SDPMT-6 Incremental Test, Membrane O.D. 0.625m, Depth 0.25 m, Raw and Reduced Data

Table B.8: Sounding 208, SDPMT-6 Incremental Test, Result Summary

Parameter				
Lift-Off Pressure (p_0)	−19.8	kPa	−2.87	psi
Contact Volume (V_c)	7.6	cm^3	0.47	in^3
Limit Pressure (p_L)	675.0	kPa	97.90	psi
Assumed ν		0.33		
Initial Modulus (E_0)	8462.9	kPa	1227.45	psi
Dry Unit Weight (γ_{dry})	1845.3	kg/m^3	115.2	lb/ft^3
Wet Unit Weight (γ_{wet})	1915.8	kg/m^3	119.6	lb/ft^3

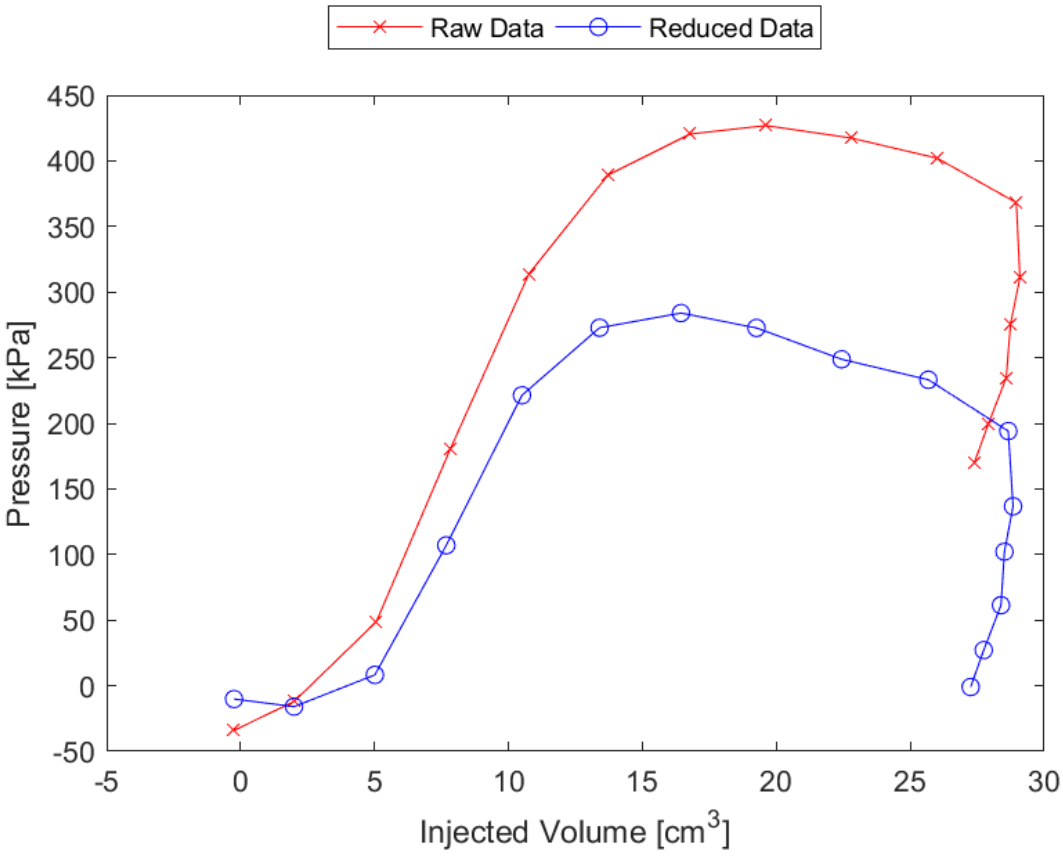

Figure B.9: Sounding 209, SDPMT-6 Incremental Test, Membrane O.D. 0.625m, Depth 0.25 m, Raw and Reduced Data

Table B.9: Sounding 209, SDPMT-6 Incremental Test, Result Summary

Parameter				
Lift-Off Pressure (p_0)	8.3	kPa	1.20	psi
Contact Volume (V_c)	5.0	cm^3	0.31	in^3
Limit Pressure (p_L)	285.0	kPa	41.34	psi
Assumed ν		0.33		
Initial Modulus (E_0)	3907.4	kPa	566.72	psi
Dry Unit Weight (γ_{dry})	1787.7	kg/m^3	111.6	lb/ft^3
Wet Unit Weight (γ_{wet})	1821.3	kg/m^3	113.7	lb/ft^3

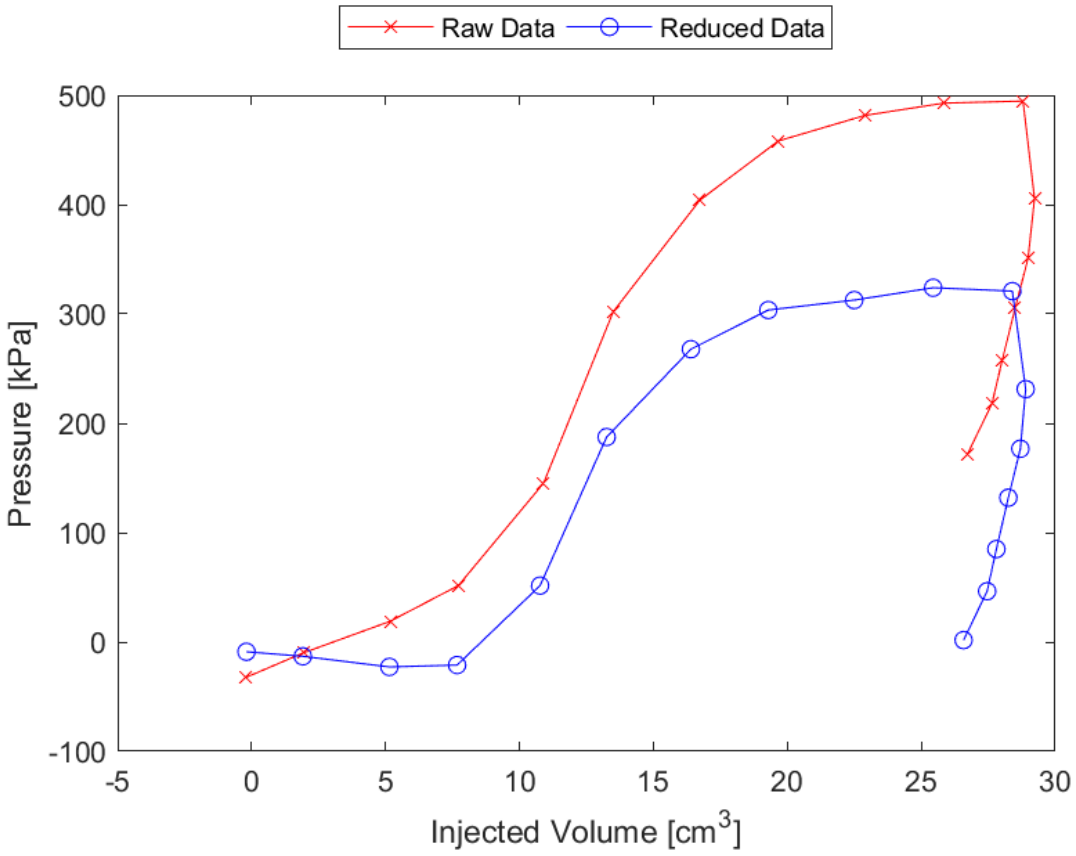

Figure B.10: Sounding 210, SDPMT-6 Incremental Test, Membrane O.D. 0.625m, Depth 0.25 m, Raw and Reduced Data

Table B.10: Sounding 210, SDPMT-6 Incremental Test, Result Summary

Parameter				
Lift-Off Pressure (p_0)	−21.1	kPa	−3.06	psi
Contact Volume (V_c)	7.7	cm^3	0.47	in^3
Limit Pressure (p_L)	325.0	kPa	47.14	psi
Assumed ν		0.33		
Initial Modulus (E_0)	3710.0	kPa	538.10	psi
Dry Unit Weight (γ_{dry})	1776.4	kg/m^3	110.9	lb/ft^3
Wet Unit Weight (γ_{wet})	1906.2	kg/m^3	119.0	lb/ft^3

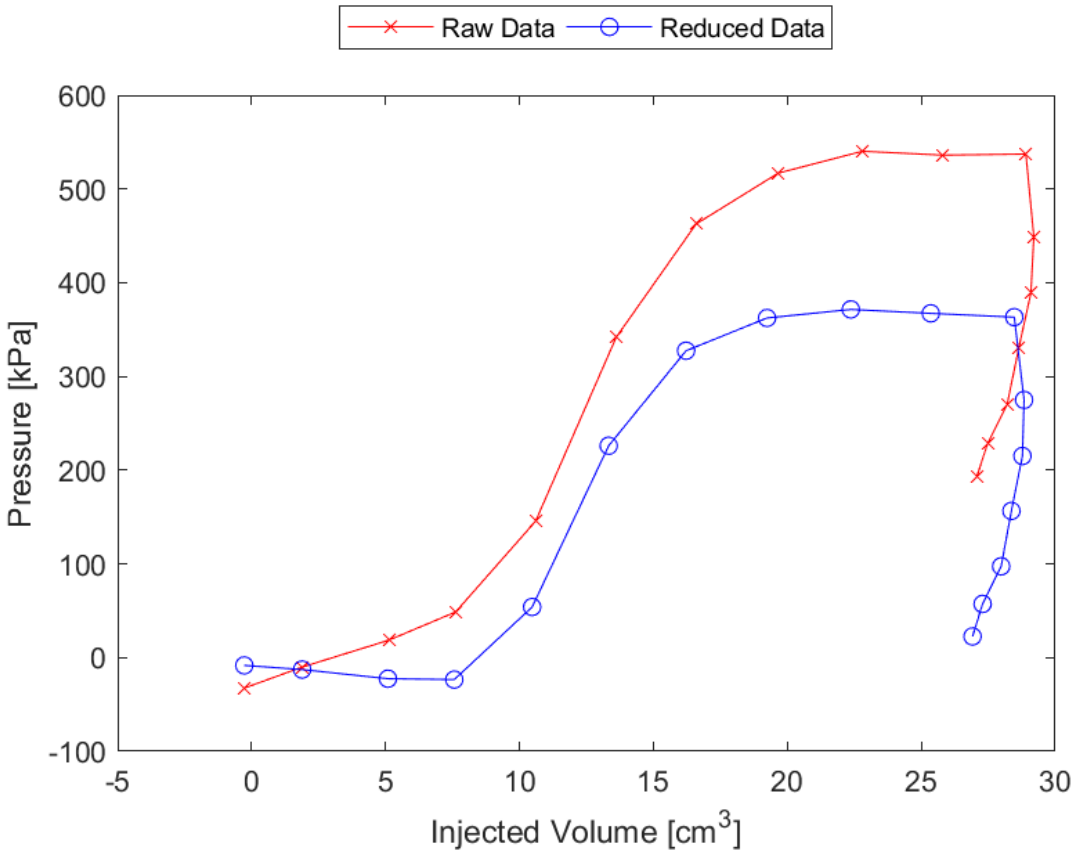

Figure B.11: Sounding 211, SDPMT-6 Incremental Test, Membrane O.D. 0.625m, Depth 0.25 m, Raw and Reduced Data

Table B.11: Sounding 211, SDPMT-6 Incremental Test, Result Summary

Parameter				
Lift-Off Pressure (p_0)	−23.4	kPa	−3.40	psi
Contact Volume (V_c)	7.6	cm^3	0.46	in^3
Limit Pressure (p_L)	370.0	kPa	53.66	psi
Assumed ν		0.33		
Initial Modulus (E_0)	5500.1	kPa	797.73	psi
Dry Unit Weight (γ_{dry})	1827.7	kg/m^3	114.1	lb/ft^3
Wet Unit Weight (γ_{wet})	1903.0	kg/m^3	118.8	lb/ft^3

B.2 SDPMT-6 Continuous Test Data

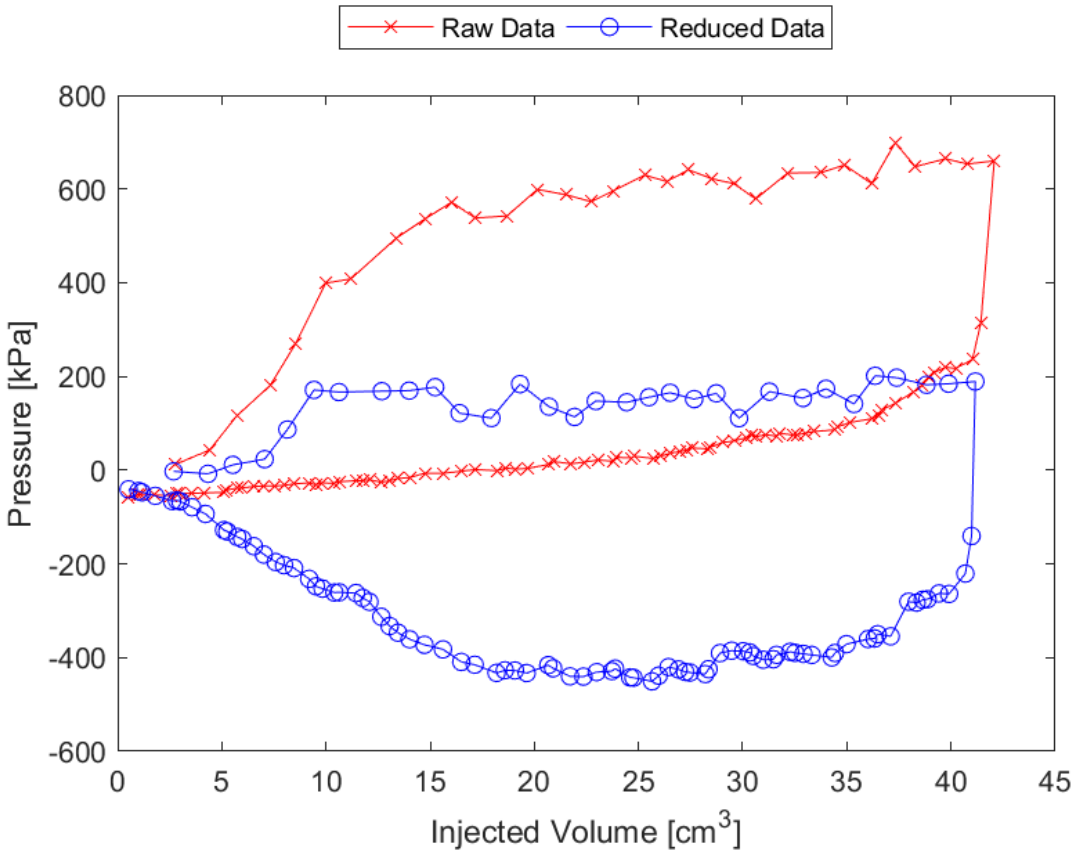

Figure B.12: Sounding 201, SDPMT-6 Continuous Test, Membrane O.D. 0.6875m, Depth 0.25 m, Raw and Reduced Data

Table B.12: Sounding 201, SDPMT-6 Continuous Test, Result Summary

Parameter				
Lift-Off Pressure (p_0)	23.4	kPa	3.40	psi
Contact Volume (V_c)	7.1	cm^3	0.43	in^3
Limit Pressure (p_L)	200.0	kPa	29.01	psi
Assumed ν		0.33		
Initial Modulus (E_0)	7359.0	kPa	1067.34	psi
Dry Unit Weight (γ_{dry})	1747.6	kg/m^3	109.1	lb/ft^3
Wet Unit Weight (γ_{wet})	1813.3	kg/m^3	113.2	lb/ft^3

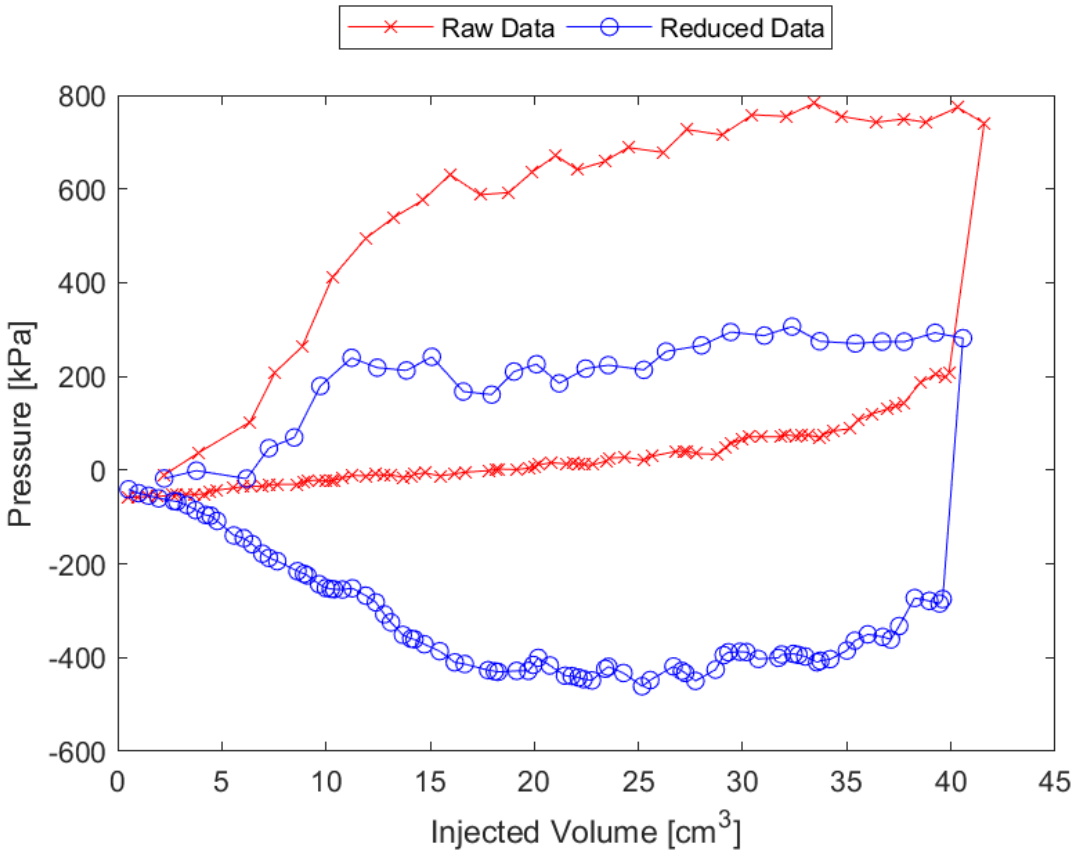

Figure B.13: Sounding 202, SDPMT-6 Continuous Test, Membrane O.D. 0.6875m, Depth 0.25 m, Raw and Reduced Data

Table B.13: Sounding 202, SDPMT-6 Continuous Test, Result Summary

Parameter				
Lift-Off Pressure (p_0)	−18.2	kPa	−2.64	psi
Contact Volume (V_c)	6.2	cm^3	0.38	in^3
Limit Pressure (p_L)	300.0	kPa	43.51	psi
Assumed ν		0.33		
Initial Modulus (E_0)	6102.7	kPa	885.13	psi
Dry Unit Weight (γ_{dry})	1826.1	kg/m^3	114.0	lb/ft^3
Wet Unit Weight (γ_{wet})	1917.4	kg/m^3	119.7	lb/ft^3

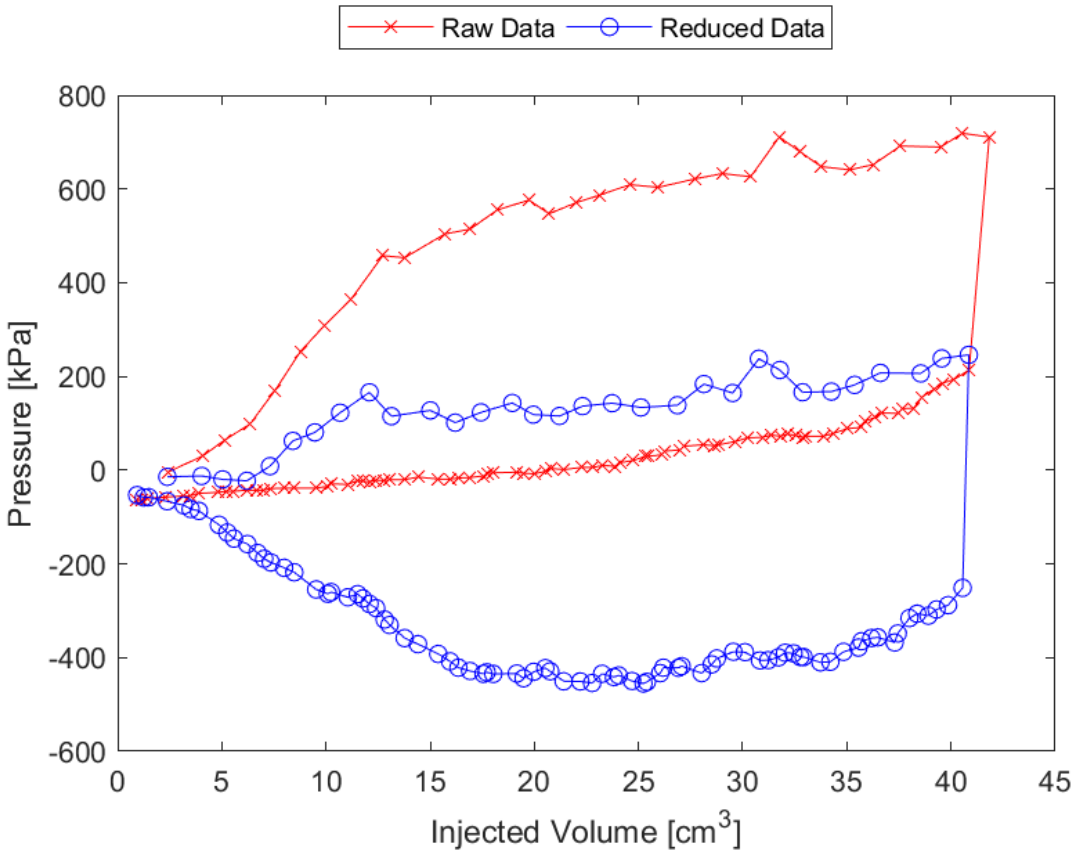

Figure B.14: Sounding 203, SDPMT-6 Continuous Test, Membrane O.D. 0.6875m, Depth 0.25 m, Raw and Reduced Data

Table B.14: Sounding 203, SDPMT-6 Continuous Test, Result Summary

Parameter				
Lift-Off Pressure (p_0)	−22.7	kPa	−3.29	psi
Contact Volume (V_c)	6.2	cm^3	0.38	in^3
Limit Pressure (p_L)	170.0	kPa	24.66	psi
Assumed ν		0.33		
Initial Modulus (E_0)	3860.3	kPa	559.90	psi
Dry Unit Weight (γ_{dry})	1757.2	kg/m^3	109.7	lb/ft^3
Wet Unit Weight (γ_{wet})	1835.7	kg/m^3	114.6	lb/ft^3

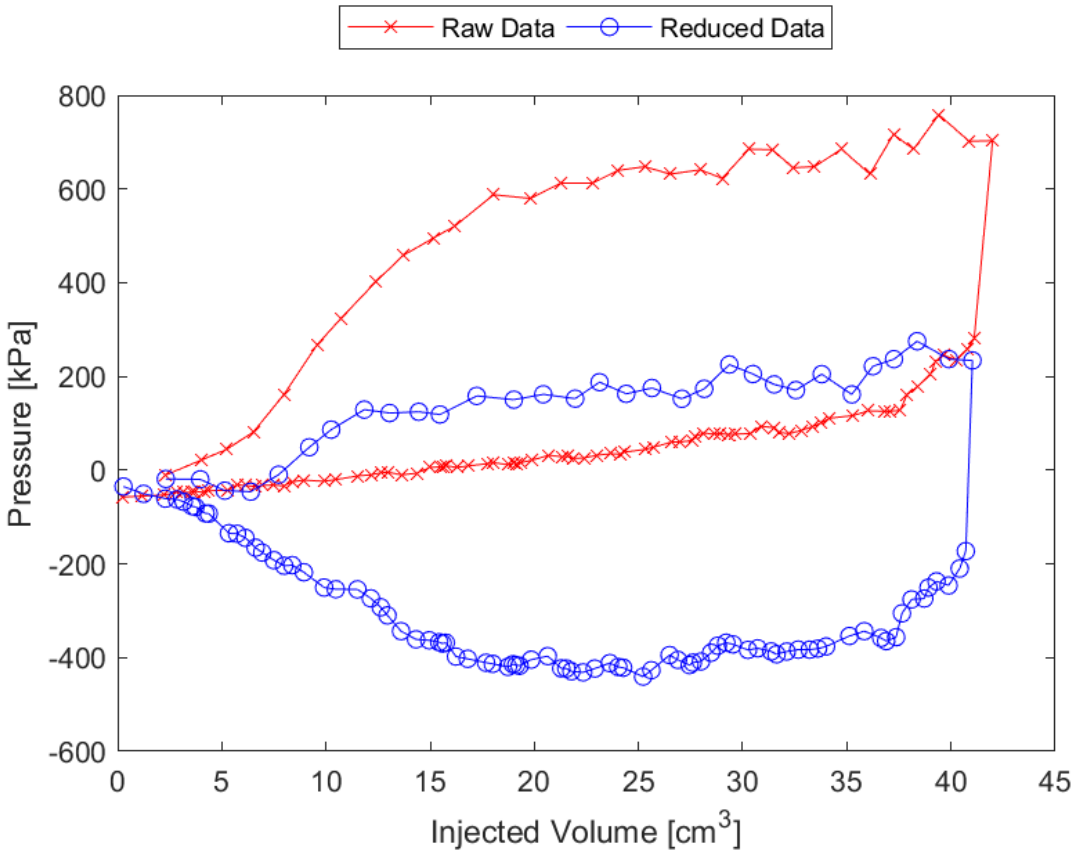

Figure B.15: Sounding 204, SDPMT-6 Continuous Test, Membrane O.D. 0.6875m, Depth 0.25 m, Raw and Reduced Data

Table B.15: Sounding 204, SDPMT-6 Continuous Test, Result Summary

Parameter				
Lift-Off Pressure (p_0)	−9.6	kPa	−1.39	psi
Contact Volume (V_c)	7.7	cm^3	0.47	in^3
Limit Pressure (p_L)	150.0	kPa	21.76	psi
Assumed ν		0.33		
Initial Modulus (E_0)	4121.3	kPa	597.74	psi
Dry Unit Weight (γ_{dry})	1698.0	kg/m^3	106.0	lb/ft^3
Wet Unit Weight (γ_{wet})	1787.7	kg/m^3	111.6	lb/ft^3

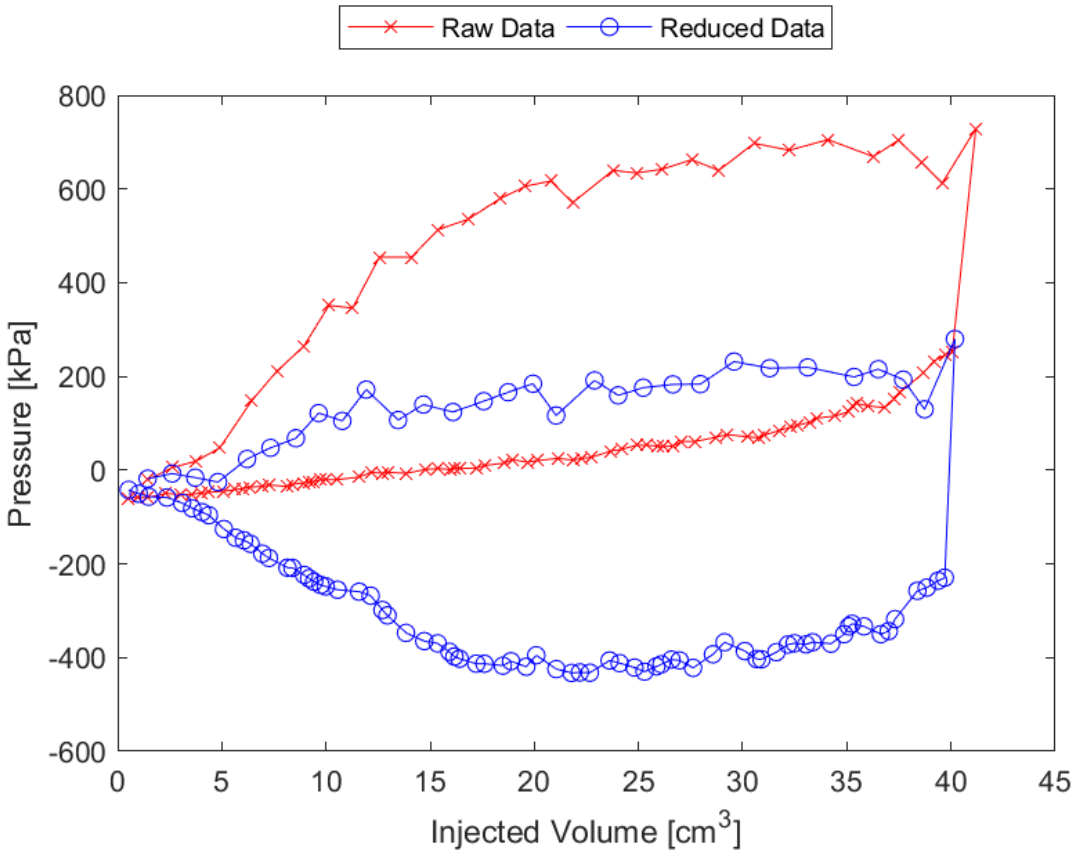

Figure B.16: Sounding 205, SDPMT-6 Continuous Test, Membrane O.D. 0.6875m, Depth 0.25 m, Raw and Reduced Data

Table B.16: Sounding 205, SDPMT-6 Continuous Test, Result Summary

Parameter				
Lift-Off Pressure (p_0)	−25.5	kPa	−3.69	psi
Contact Volume (V_c)	4.8	cm^3	0.29	in^3
Limit Pressure (p_L)	150.0	kPa	21.76	psi
Assumed ν		0.33		
Initial Modulus (E_0)	2182.4	kPa	316.53	psi
Dry Unit Weight (γ_{dry})	1806.9	kg/m^3	112.8	lb/ft^3
Wet Unit Weight (γ_{wet})	1899.8	kg/m^3	118.6	lb/ft^3

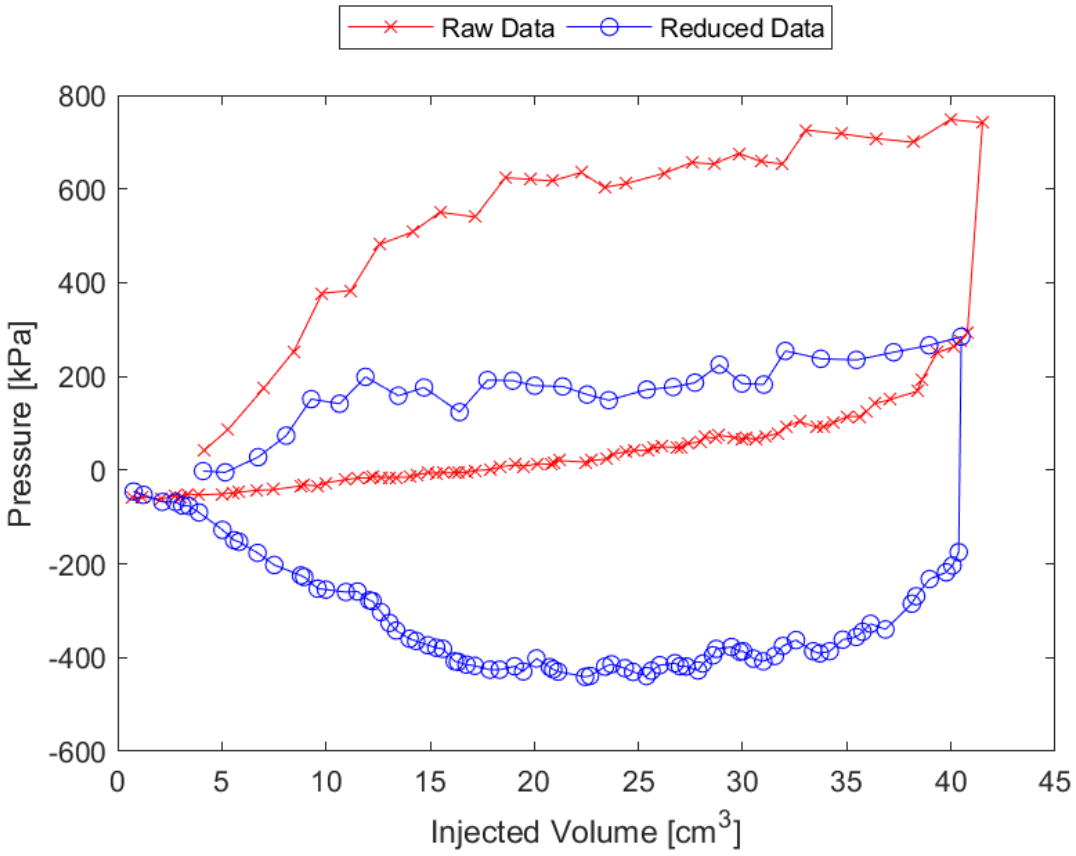

Figure B.17: Sounding 206, SDPMT-6 Continuous Test, Membrane O.D. 0.6875m, Depth 0.25 m, Raw and Reduced Data

Table B.17: Sounding 206, SDPMT-6 Continuous Test, Result Summary

Parameter				
Lift-Off Pressure (p_0)	−4.6	kPa	−0.67	psi
Contact Volume (V_c)	5.2	cm^3	0.32	in^3
Limit Pressure (p_L)	175.0	kPa	25.38	psi
Assumed ν		0.33		
Initial Modulus (E_0)	5702.7	kPa	827.11	psi
Dry Unit Weight (γ_{dry})	1842.1	kg/m^3	115.0	lb/ft^3
Wet Unit Weight (γ_{wet})	1933.4	kg/m^3	120.7	lb/ft^3

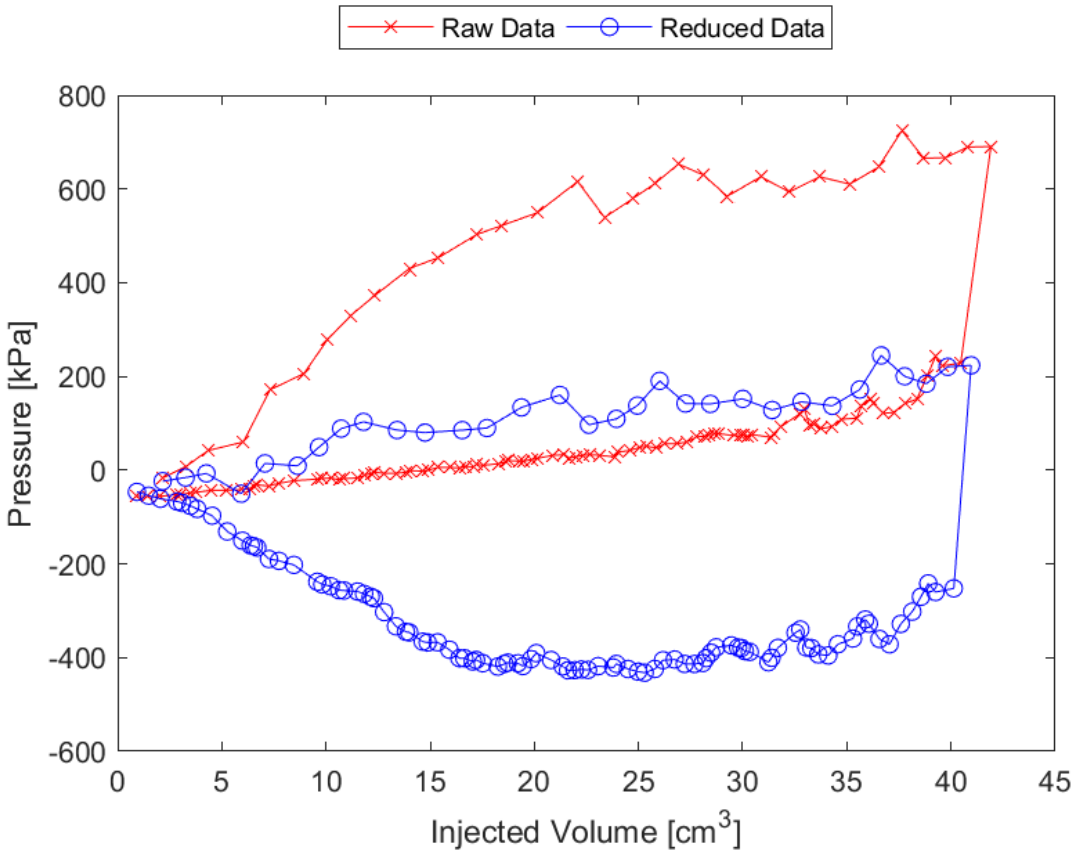

Figure B.18: Sounding 207, SDPMT-6 Continuous Test, Membrane O.D. 0.6875m, Depth 0.25 m, Raw and Reduced Data

Table B.18: Sounding 207, SDPMT-6 Continuous Test, Result Summary

Parameter				
Lift-Off Pressure (p_0)	9.3	kPa	1.35	psi
Contact Volume (V_c)	8.6	cm^3	0.53	in^3
Limit Pressure (p_L)	150.0	kPa	21.76	psi
Assumed ν		0.33		
Initial Modulus (E_0)	4623.3	kPa	670.55	psi
Dry Unit Weight (γ_{dry})	1832.5	kg/m^3	114.4	lb/ft^3
Wet Unit Weight (γ_{wet})	1936.6	kg/m^3	120.9	lb/ft^3

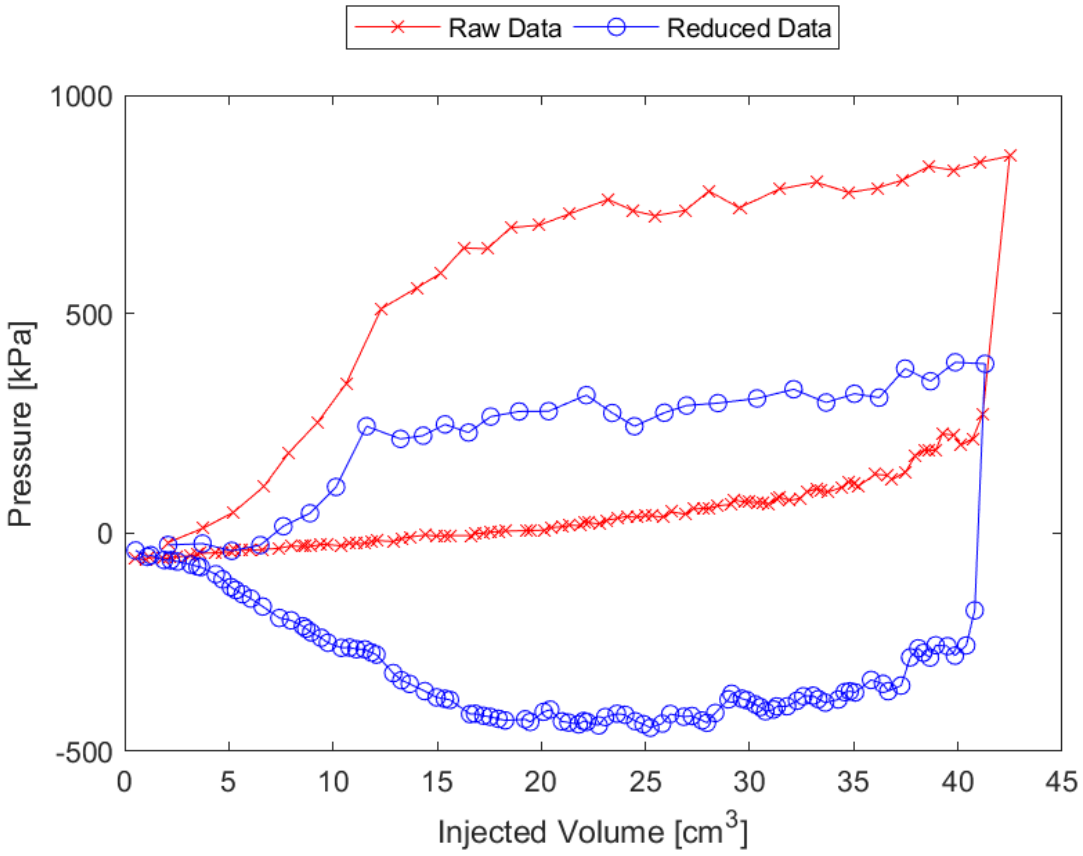

Figure B.19: Sounding 208, SDPMT-6 Continuous Test, Membrane O.D. 0.6875m, Depth 0.25 m, Raw and Reduced Data

Table B.19: Sounding 208, SDPMT-6 Continuous Test, Result Summary

Parameter				
Lift-Off Pressure (p_0)	14.6	kPa	2.12	psi
Contact Volume (V_c)	7.6	cm^3	0.46	in^3
Limit Pressure (p_L)	250.0	kPa	36.26	psi
Assumed ν		0.33		
Initial Modulus (E_0)	9035.4	kPa	1310.48	psi
Dry Unit Weight (γ_{dry})	1845.3	kg/m^3	115.2	lb/ft^3
Wet Unit Weight (γ_{wet})	1944.6	kg/m^3	121.4	lb/ft^3

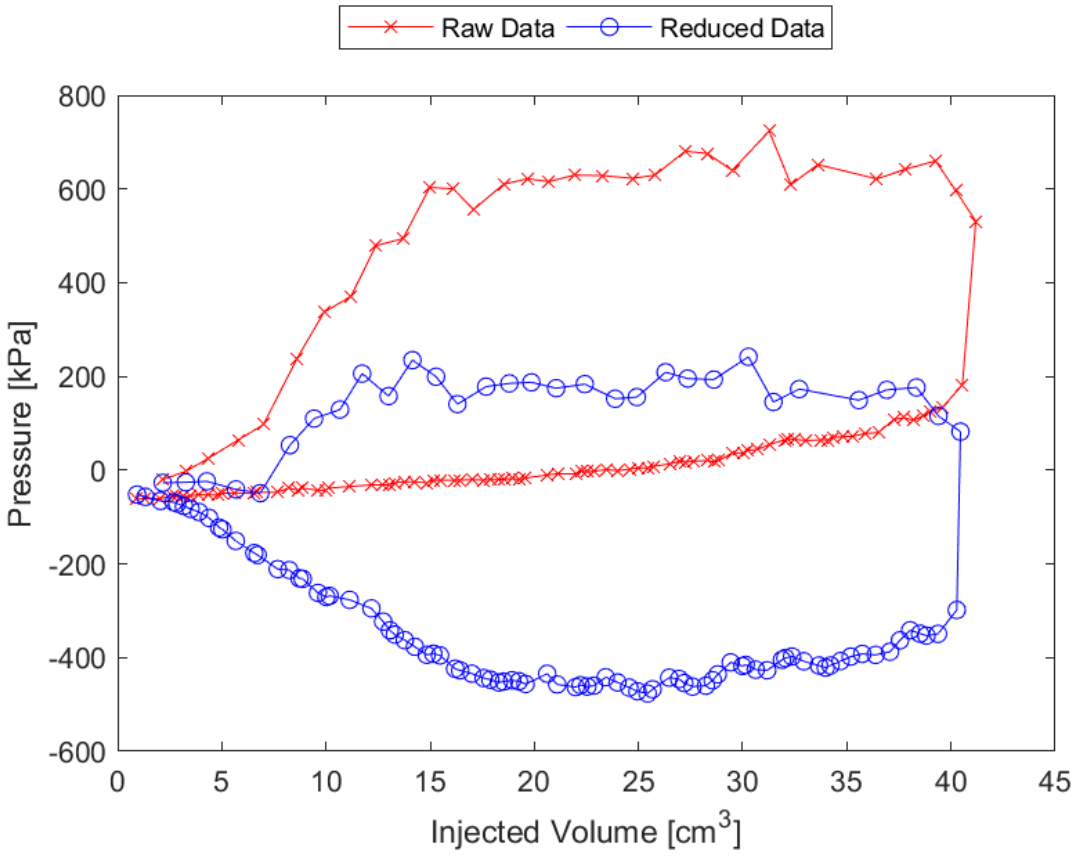

Figure B.20: Sounding 209, SDPMT-6 Continuous Test, Membrane O.D. 0.6875m, Depth 0.25 m, Raw and Reduced Data

Table B.20: Sounding 209, SDPMT-6 Continuous Test, Result Summary

Parameter				
Lift-Off Pressure (p_0)	−49.0	kPa	−7.11	psi
Contact Volume (V_c)	6.8	cm^3	0.42	in^3
Limit Pressure (p_L)	150.0	kPa	21.76	psi
Assumed ν		0.33		
Initial Modulus (E_0)	7250.8	kPa	1051.64	psi
Dry Unit Weight (γ_{dry})	1787.7	kg/m^3	111.6	lb/ft^3
Wet Unit Weight (γ_{wet})	1893.4	kg/m^3	118.2	lb/ft^3

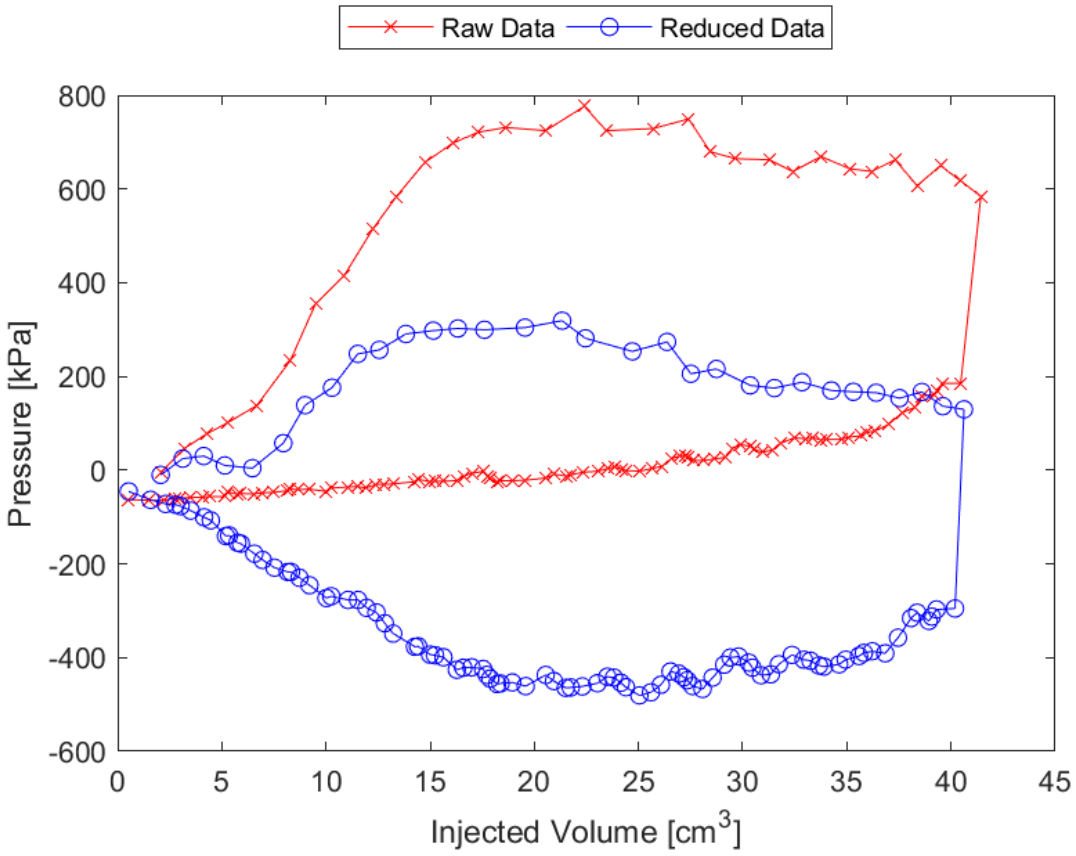

Figure B.21: Sounding 210, SDPMT-6 Continuous Test, Membrane O.D. 0.6875m, Depth 0.25 m, Raw and Reduced Data

Table B.21: Sounding 210, SDPMT-6 Continuous Test, Result Summary

Parameter				
Lift-Off Pressure (p_0)	4.2	kPa	0.62	psi
Contact Volume (V_c)	6.5	cm^3	0.39	in^3
Limit Pressure (p_L)	300.0	kPa	43.51	psi
Assumed ν		0.33		
Initial Modulus (E_0)	5785.9	kPa	839.18	psi
Dry Unit Weight (γ_{dry})	1776.4	kg/m^3	110.9	lb/ft^3
Wet Unit Weight (γ_{wet})	1859.7	kg/m^3	116.1	lb/ft^3

B.3 SDPMT-12 Incremental Test Data

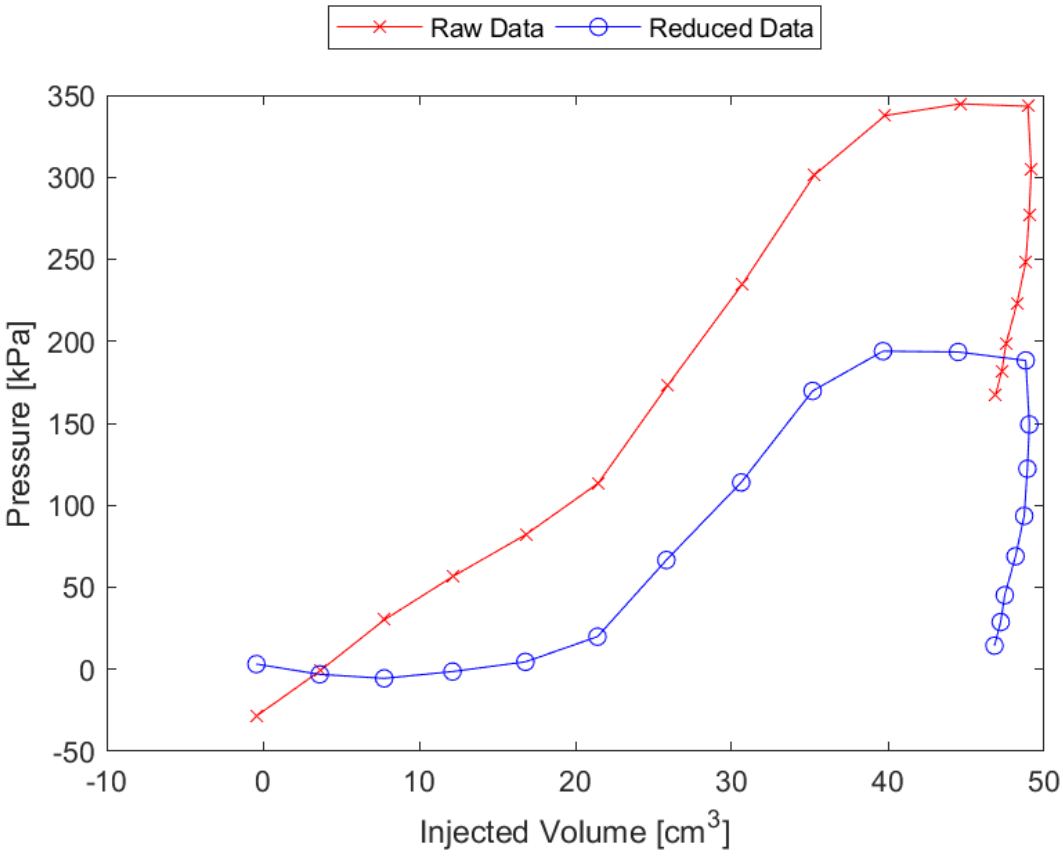

Figure B.22: Sounding 201, SDPMT-12 Incremental Test, Membrane O.D. 0.625m, Depth 0.41 m, Raw and Reduced Data

Table B.22: Sounding 201, SDPMT-12 Incremental Test, Result Summary

Parameter				
Lift-Off Pressure (p_0)	4.6	kPa	0.66	psi
Contact Volume (V_c)	16.8	cm^3	1.03	in^3
Limit Pressure (p_L)	200.0	kPa	29.01	psi
Assumed ν		0.33		
Initial Modulus (E_0)	2561.6	kPa	371.53	psi
Dry Unit Weight (γ_{dry})	1747.6	kg/m^3	109.1	lb/ft^3
Wet Unit Weight (γ_{wet})	1778.0	kg/m^3	111.0	lb/ft^3

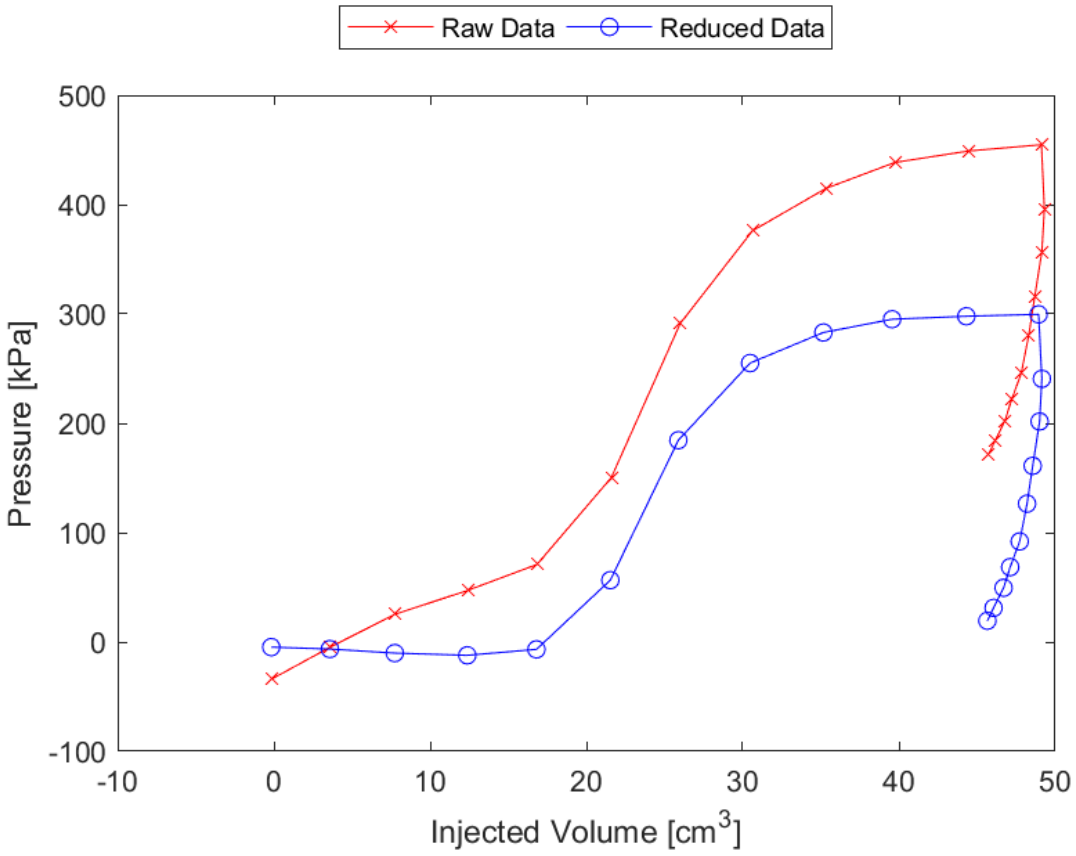

Figure B.23: Sounding 202, SDPMT-12 Incremental Test, Membrane O.D. 0.625m, Depth 0.41 m, Raw and Reduced Data

Table B.23: Sounding 202, SDPMT-12 Incremental Test, Result Summary

Parameter				
Lift-Off Pressure (p_0)	−6.7	kPa	−0.98	psi
Contact Volume (V_c)	16.8	cm^3	1.03	in^3
Limit Pressure (p_L)	350.0	kPa	50.76	psi
Assumed ν		0.33		
Initial Modulus (E_0)	5090.3	kPa	738.28	psi
Dry Unit Weight (γ_{dry})	1826.1	kg/m^3	114.0	lb/ft^3
Wet Unit Weight (γ_{wet})	1890.2	kg/m^3	118.0	lb/ft^3

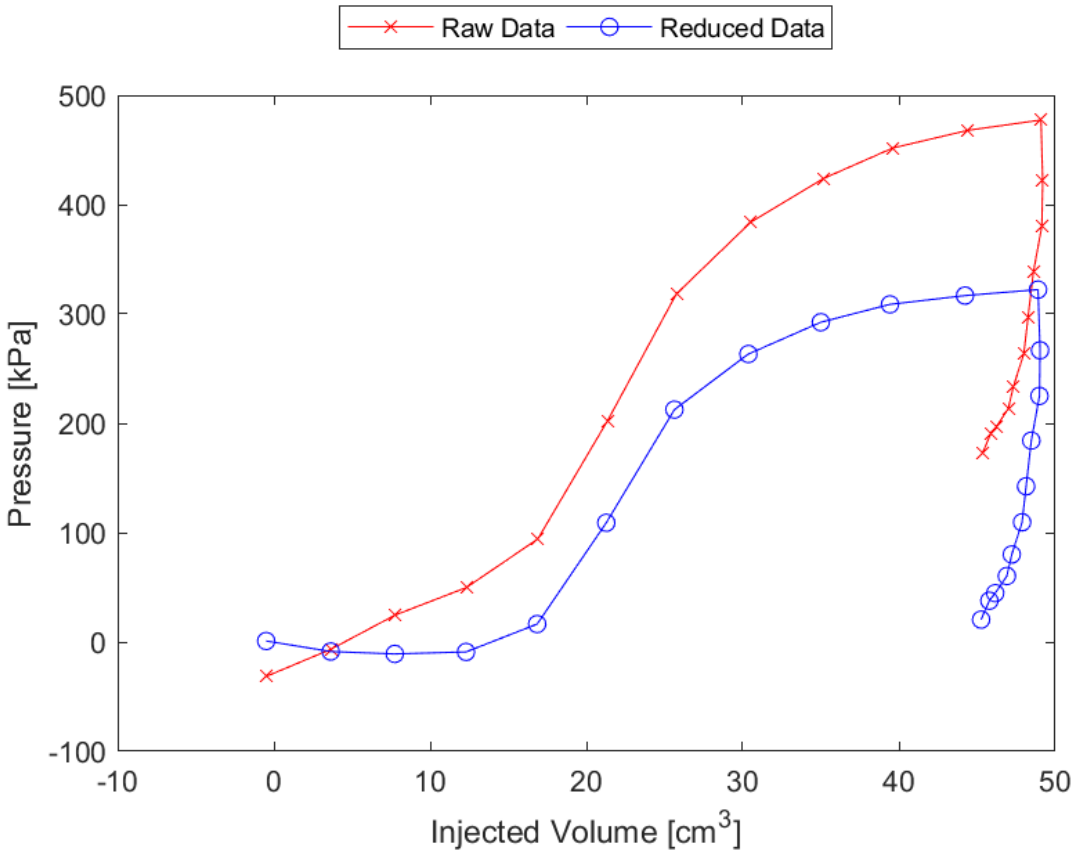

Figure B.24: Sounding 203, SDPMT-12 Incremental Test, Membrane O.D. 0.625m, Depth 0.41 m, Raw and Reduced Data

Table B.24: Sounding 203, SDPMT-12 Incremental Test, Result Summary

Parameter				
Lift-Off Pressure (p_0)	16.4	kPa	2.38	psi
Contact Volume (V_c)	16.8	cm^3	1.03	in^3
Limit Pressure (p_L)	350.0	kPa	50.76	psi
Assumed ν		0.33		
Initial Modulus (E_0)	4836.7	kPa	701.51	psi
Dry Unit Weight (γ_{dry})	1757.2	kg/m^3	109.7	lb/ft^3
Wet Unit Weight (γ_{wet})	1794.1	kg/m^3	112.0	lb/ft^3

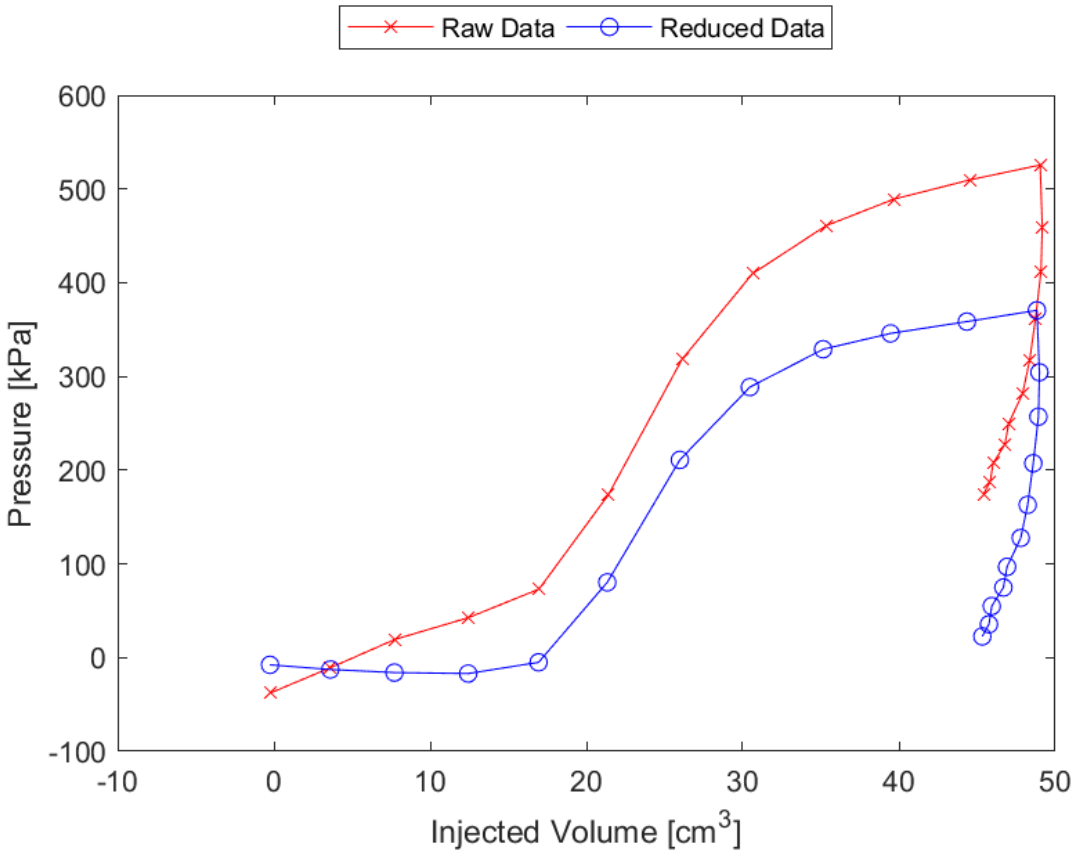

Figure B.25: Sounding 204, SDPMT-12 Incremental Test, Membrane O.D. 0.625m, Depth 0.41 m, Raw and Reduced Data

Table B.25: Sounding 204, SDPMT-12 Incremental Test, Result Summary

Parameter				
Lift-Off Pressure (p_0)	−5.0	kPa	−0.73	psi
Contact Volume (V_c)	16.9	cm^3	1.03	in^3
Limit Pressure (p_L)	450.0	kPa	65.27	psi
Assumed ν		0.33		
Initial Modulus (E_0)	4846.1	kPa	702.87	psi
Dry Unit Weight (γ_{dry})	1698.0	kg/m^3	106.0	lb/ft^3
Wet Unit Weight (γ_{wet})	1731.6	kg/m^3	108.1	lb/ft^3

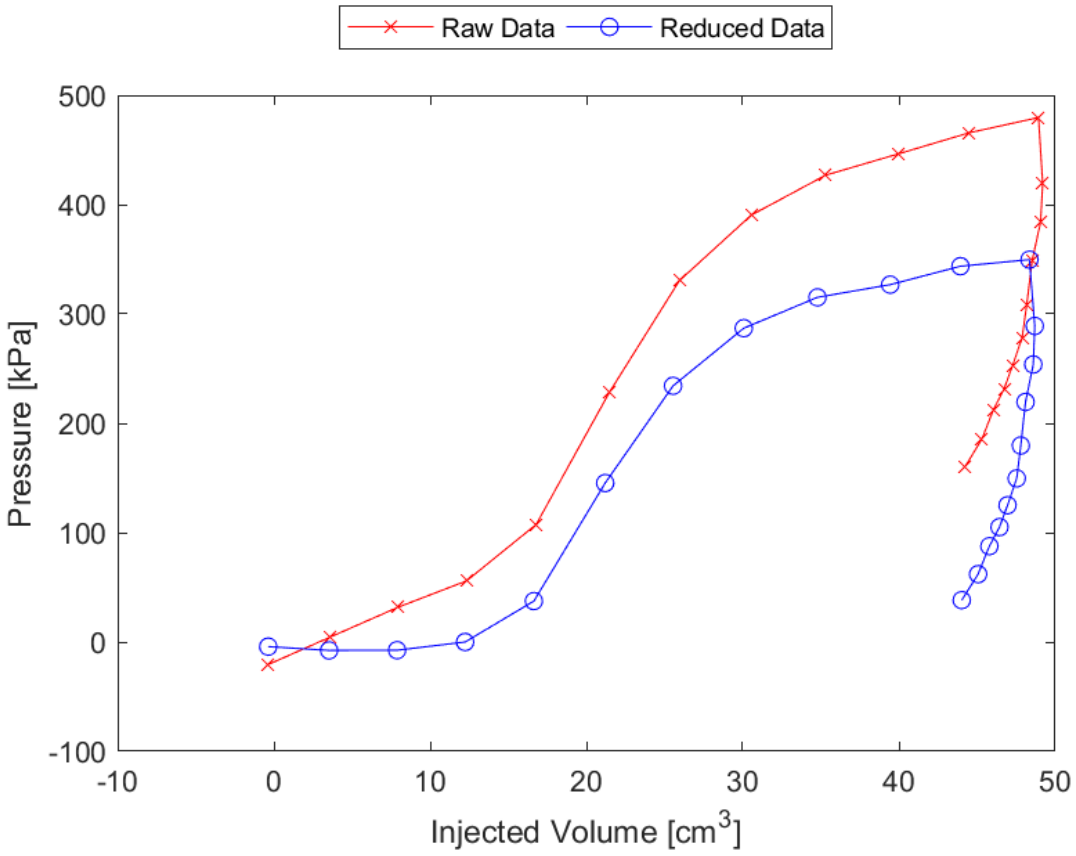

Figure B.26: Sounding 205, SDPMT-12 Incremental Test, Membrane O.D. 0.625m, Depth 0.41 m, Raw and Reduced Data

Table B.26: Sounding 205, SDPMT-12 Incremental Test, Result Summary

Parameter				
Lift-Off Pressure (p_0)	−0.0	kPa	−0.00	psi
Contact Volume (V_c)	−0.0	cm^3	−0.00	in^3
Limit Pressure (p_L)	400.0	kPa	58.02	psi
Assumed ν		0.33		
Initial Modulus (E_0)	4778.7	kPa	693.09	psi
Dry Unit Weight (γ_{dry})	1806.9	kg/m^3	112.8	lb/ft^3
Wet Unit Weight (γ_{wet})	1851.7	kg/m^3	115.6	lb/ft^3

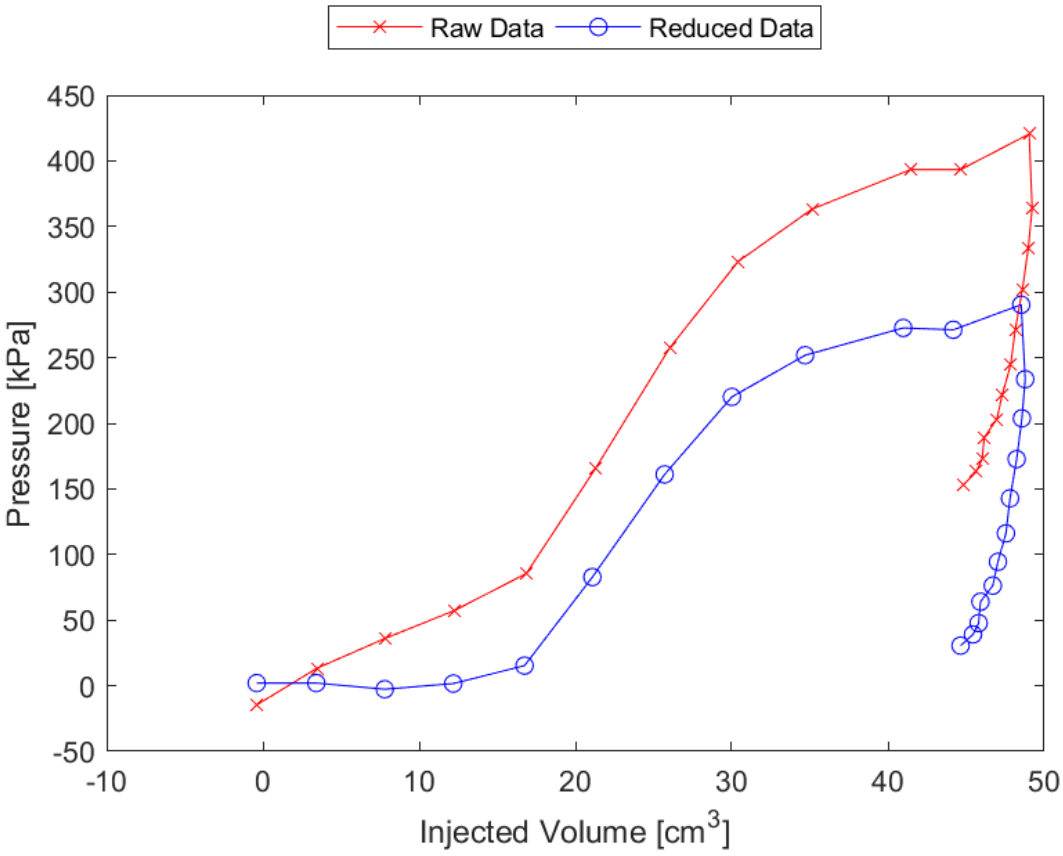

Figure B.27: Sounding 206, SDPMT-12 Incremental Test, Membrane O.D. 0.625m, Depth 0.41 m, Raw and Reduced Data

Table B.27: Sounding 206, SDPMT-12 Incremental Test, Result Summary

Parameter				
Lift-Off Pressure (p_0)	1.7	kPa	0.24	psi
Contact Volume (V_c)	12.2	cm^3	0.74	in^3
Limit Pressure (p_L)	350.0	kPa	50.76	psi
Assumed ν		0.33		
Initial Modulus (E_0)	3431.7	kPa	497.73	psi
Dry Unit Weight (γ_{dry})	1842.1	kg/m^3	115.0	lb/ft^3
Wet Unit Weight (γ_{wet})	1914.2	kg/m^3	119.5	lb/ft^3

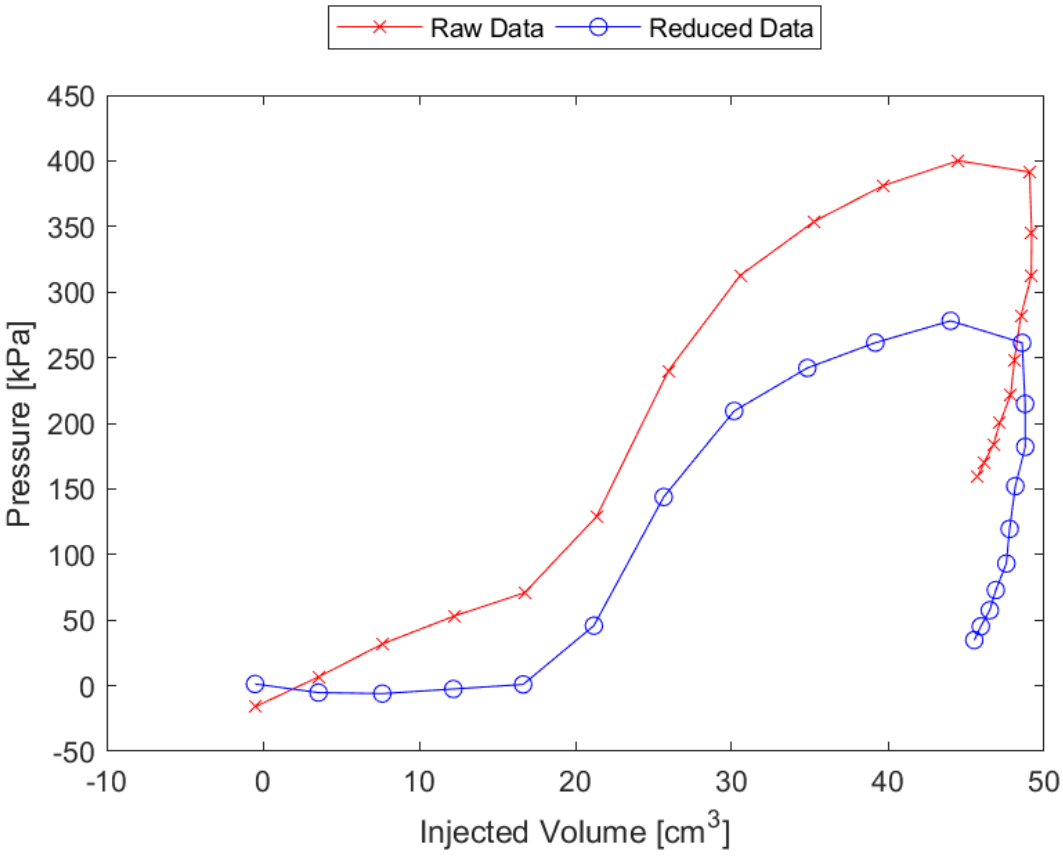

Figure B.28: Sounding 207, SDPMT-12 Incremental Test, Membrane O.D. 0.625m, Depth 0.41 m, Raw and Reduced Data

Table B.28: Sounding 207, SDPMT-12 Incremental Test, Result Summary

Parameter				
Lift-Off Pressure (p_0)	1.0	kPa	0.14	psi
Contact Volume (V_c)	16.7	cm^3	1.02	in^3
Limit Pressure (p_L)	280.0	kPa	40.61	psi
Assumed ν		0.33		
Initial Modulus (E_0)	4163.3	kPa	603.84	psi
Dry Unit Weight (γ_{dry})	1832.5	kg/m^3	114.4	lb/ft^3
Wet Unit Weight (γ_{wet})	1880.6	kg/m^3	117.4	lb/ft^3

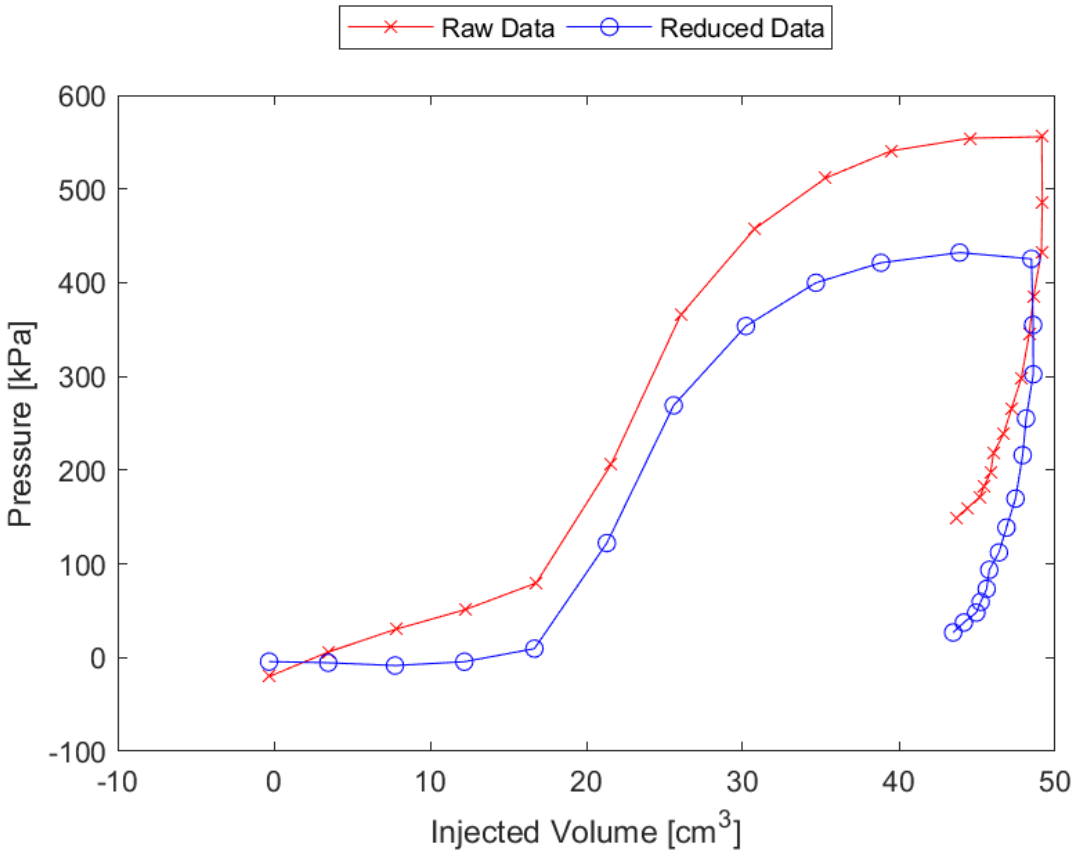

Figure B.29: Sounding 208, SDPMT-12 Incremental Test, Membrane O.D. 0.625m, Depth 0.41 m, Raw and Reduced Data

Table B.29: Sounding 208, SDPMT-12 Incremental Test, Result Summary

Parameter				
Lift-Off Pressure (p_0)	9.6	kPa	1.39	psi
Contact Volume (V_c)	16.7	cm^3	1.02	in^3
Limit Pressure (p_L)	425.0	kPa	61.64	psi
Assumed ν		0.33		
Initial Modulus (E_0)	6300.3	kPa	913.78	psi
Dry Unit Weight (γ_{dry})	1845.3	kg/m^3	115.2	lb/ft^3
Wet Unit Weight (γ_{wet})	1915.8	kg/m^3	119.6	lb/ft^3

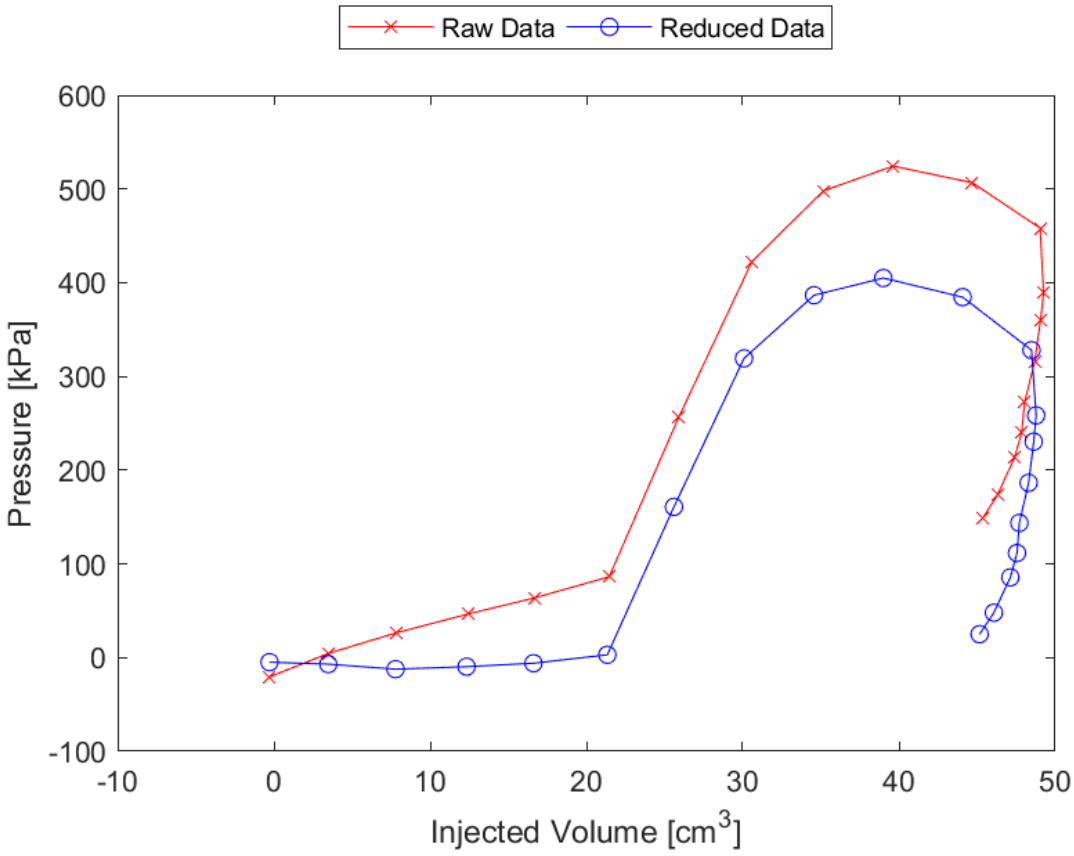

Figure B.30: Sounding 209, SDPMT-12 Incremental Test, Membrane O.D. 0.625m, Depth 0.41 m, Raw and Reduced Data

Table B.30: Sounding 209, SDPMT-12 Incremental Test, Result Summary

Parameter				
Lift-Off Pressure (p_0)	3.0	kPa	0.44	psi
Contact Volume (V_c)	21.3	cm^3	1.30	in^3
Limit Pressure (p_L)	405.0	kPa	58.74	psi
Assumed ν		0.33		
Initial Modulus (E_0)	8264.7	kPa	1198.70	psi
Dry Unit Weight (γ_{dry})	1787.7	kg/m^3	111.6	lb/ft^3
Wet Unit Weight (γ_{wet})	1821.3	kg/m^3	113.7	lb/ft^3

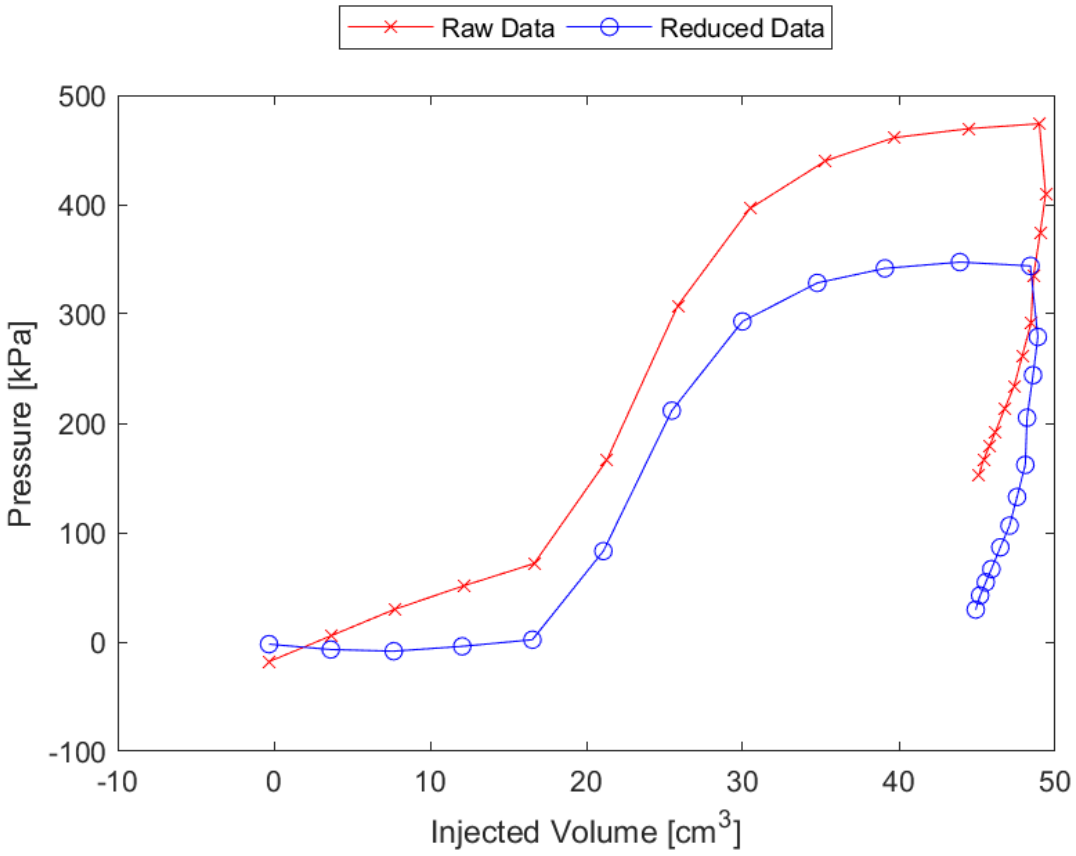

Figure B.31: Sounding 210, SDPMT-12 Incremental Test, Membrane O.D. 0.625m, Depth 0.41 m, Raw and Reduced Data

Table B.31: Sounding 210, SDPMT-12 Incremental Test, Result Summary

Parameter				
Lift-Off Pressure (p_0)	2.1	kPa	0.30	psi
Contact Volume (V_c)	16.5	cm^3	1.01	in^3
Limit Pressure (p_L)	350.0	kPa	50.76	psi
Assumed ν		0.33		
Initial Modulus (E_0)	4809.1	kPa	697.50	psi
Dry Unit Weight (γ_{dry})	1776.4	kg/m^3	110.9	lb/ft^3
Wet Unit Weight (γ_{wet})	1906.2	kg/m^3	119.0	lb/ft^3

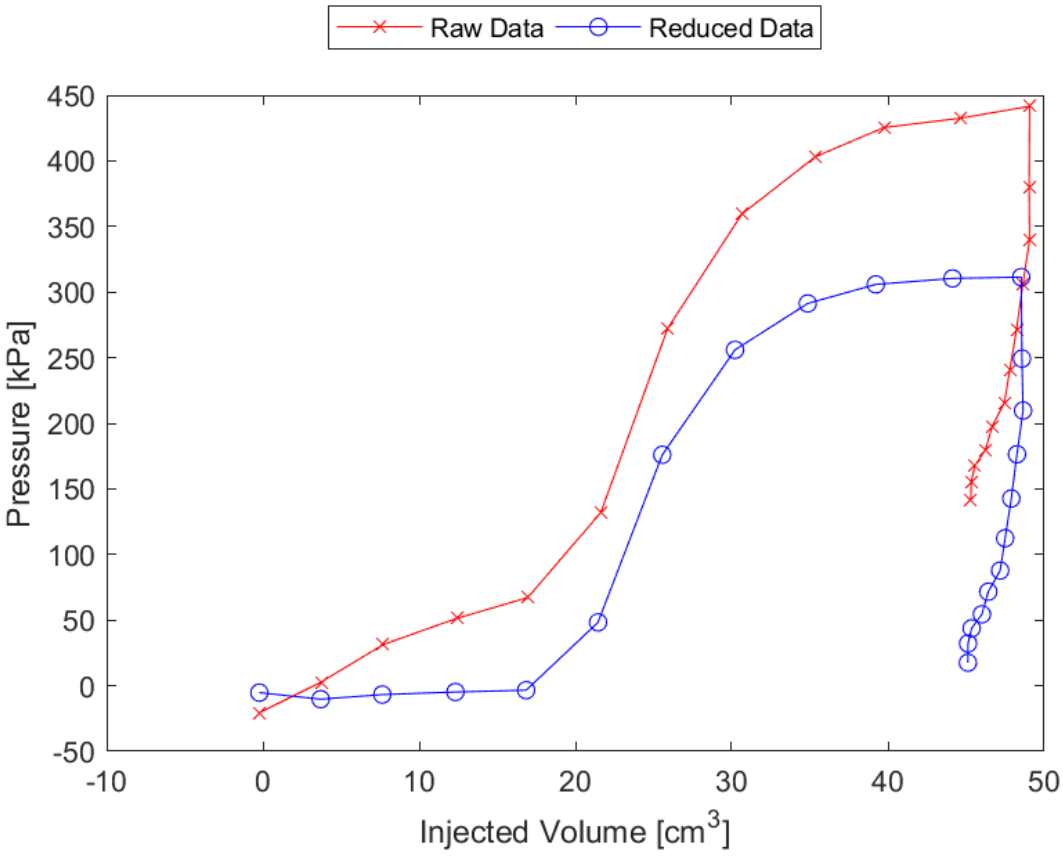

Figure B.32: Sounding 211, SDPMT-12 Incremental Test, Membrane O.D. 0.625m, Depth 0.41 m, Raw and Reduced Data

Table B.32: Sounding 211, SDPMT-12 Incremental Test, Result Summary

Parameter				
Lift-Off Pressure (p_0)	−3.4	kPa	−0.49	psi
Contact Volume (V_c)	16.8	cm^3	1.03	in^3
Limit Pressure (p_L)	350.0	kPa	50.76	psi
Assumed ν		0.33		
Initial Modulus (E_0)	6916.2	kPa	1003.11	psi
Dry Unit Weight (γ_{dry})	1827.7	kg/m^3	114.1	lb/ft^3
Wet Unit Weight (γ_{wet})	1903.0	kg/m^3	118.8	lb/ft^3

B.4 SDPMT-12 Continuous Test Data

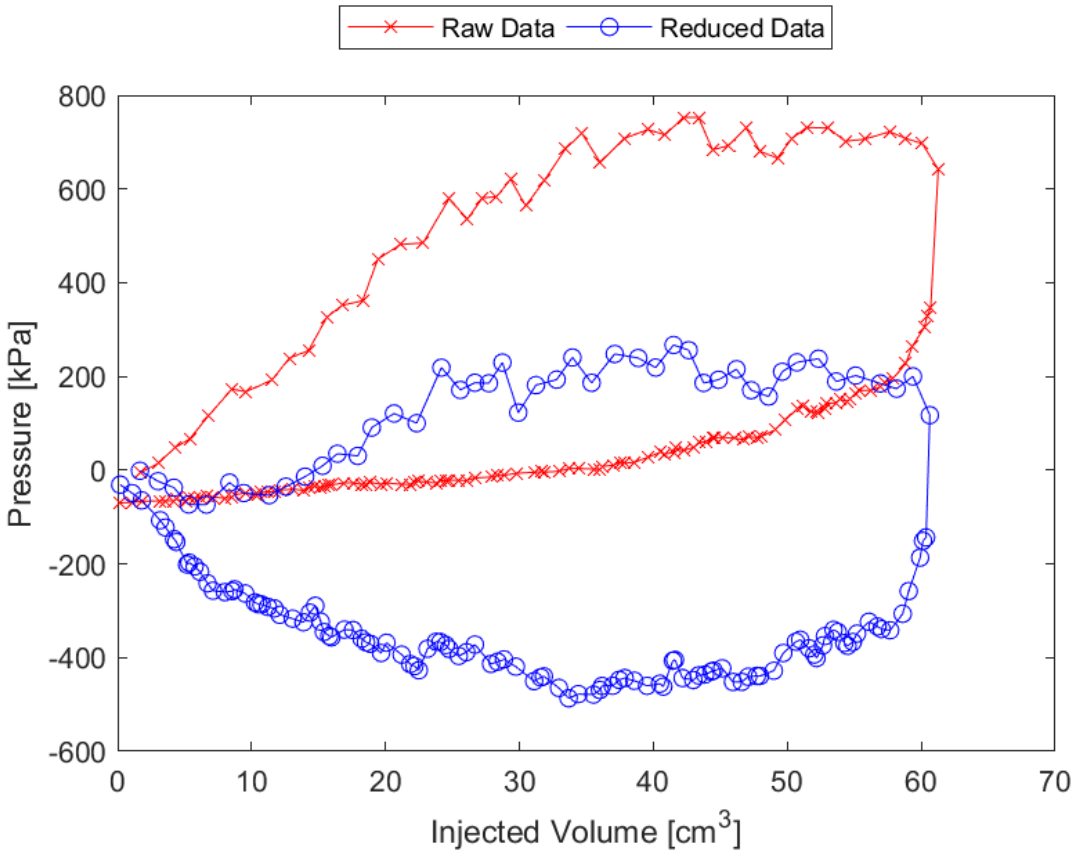

Figure B.33: Sounding 201, SDPMT-12 Continuous Test, Membrane O.D. 0.6875m, Depth 0.41 m, Raw and Reduced Data

Table B.33: Sounding 201, SDPMT-12 Continuous Test, Result Summary

Parameter				
Lift-Off Pressure (p_0)	−53.5	kPa	−7.75	psi
Contact Volume (V_c)	11.3	cm^3	0.69	in^3
Limit Pressure (p_L)	185.0	kPa	26.83	psi
Assumed ν		0.33		
Initial Modulus (E_0)	4438.6	kPa	643.77	psi
Dry Unit Weight (γ_{dry})	1747.6	kg/m^3	109.1	lb/ft^3
Wet Unit Weight (γ_{wet})	1813.3	kg/m^3	113.2	lb/ft^3

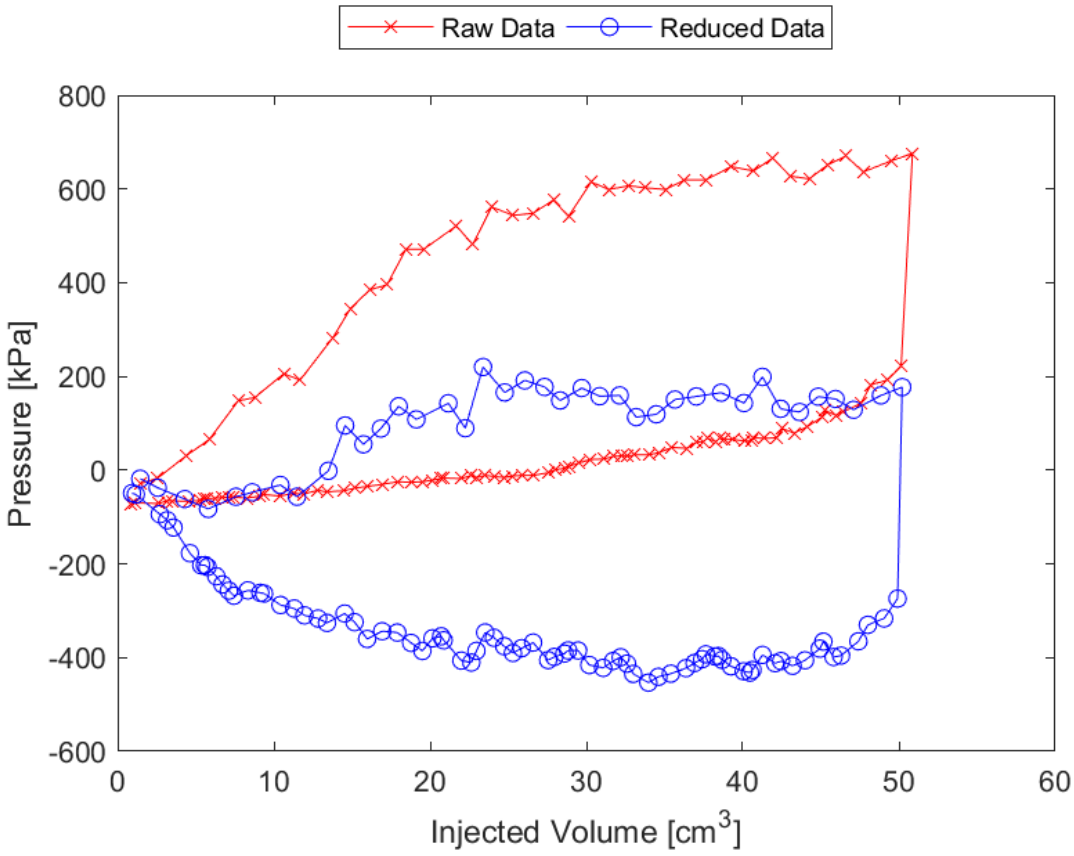

Figure B.34: Sounding 202, SDPMT-12 Continuous Test, Membrane O.D. 0.6875m, Depth 0.41 m, Raw and Reduced Data

Table B.34: Sounding 202, SDPMT-12 Continuous Test, Result Summary

Parameter				
Lift-Off Pressure (p_0)	−56.6	kPa	−8.21	psi
Contact Volume (V_c)	11.5	cm^3	0.70	in^3
Limit Pressure (p_L)	150.0	kPa	21.76	psi
Assumed ν		0.33		
Initial Modulus (E_0)	5083.5	kPa	737.30	psi
Dry Unit Weight (γ_{dry})	1826.1	kg/m^3	114.0	lb/ft^3
Wet Unit Weight (γ_{wet})	1917.4	kg/m^3	119.7	lb/ft^3

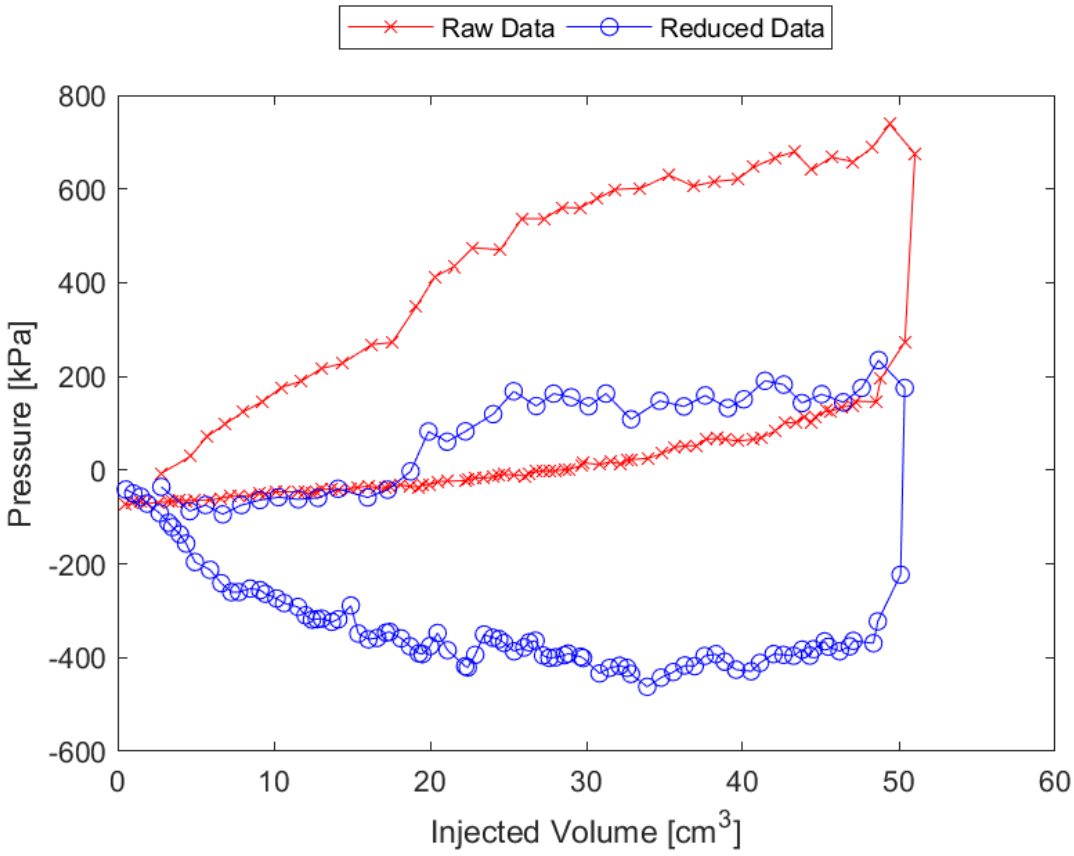

Figure B.35: Sounding 203, SDPMT-12 Continuous Test, Membrane O.D. 0.6875m, Depth 0.41 m, Raw and Reduced Data

Table B.35: Sounding 203, SDPMT-12 Continuous Test, Result Summary

Parameter				
Lift-Off Pressure (p_0)	−58.3	kPa	−8.45	psi
Contact Volume (V_c)	16.0	cm^3	0.98	in^3
Limit Pressure (p_L)	148.0	kPa	21.47	psi
Assumed ν		0.33		
Initial Modulus (E_0)	6059.2	kPa	878.81	psi
Dry Unit Weight (γ_{dry})	1757.2	kg/m^3	109.7	lb/ft^3
Wet Unit Weight (γ_{wet})	1835.7	kg/m^3	114.6	lb/ft^3

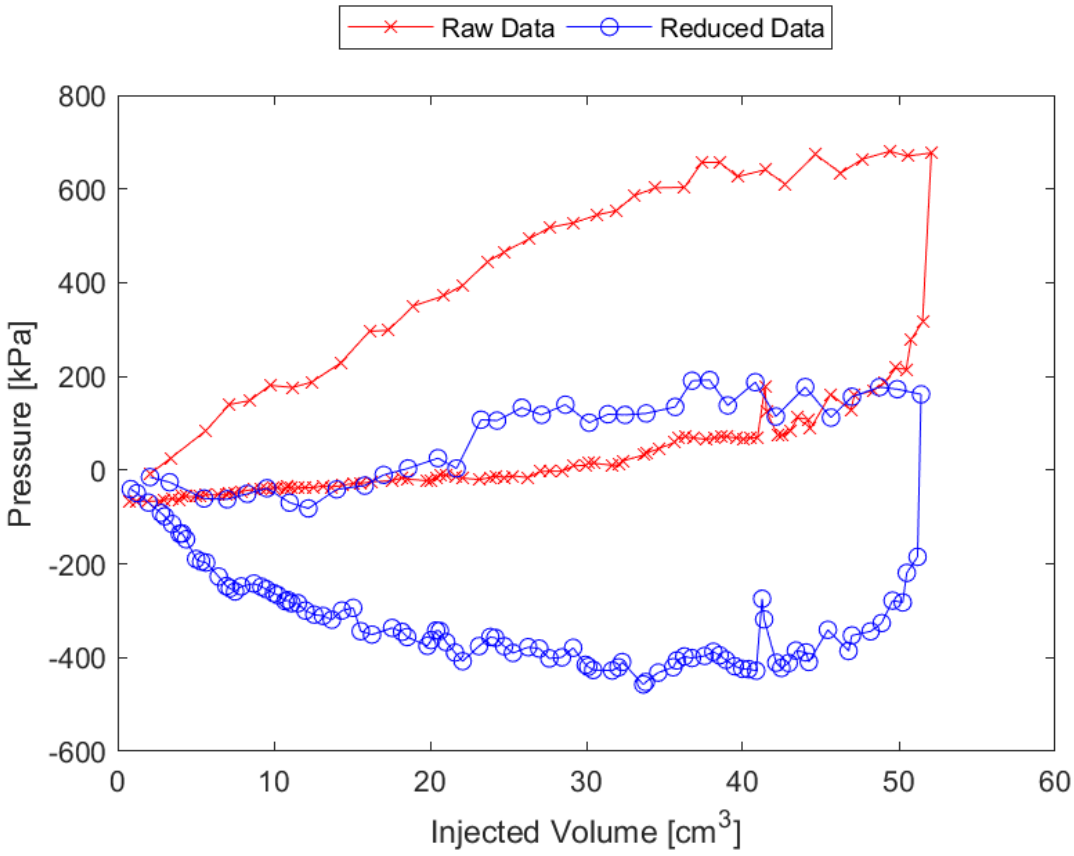

Figure B.36: Sounding 204, SDPMT-12 Continuous Test, Membrane O.D. 0.6875m, Depth 0.41 m, Raw and Reduced Data

Table B.36: Sounding 204, SDPMT-12 Continuous Test, Result Summary

Parameter				
Lift-Off Pressure (p_0)	−33.0	kPa	−4.78	psi
Contact Volume (V_c)	15.8	cm^3	0.96	in^3
Limit Pressure (p_L)	140.0	kPa	20.31	psi
Assumed ν		0.33		
Initial Modulus (E_0)	3044.4	kPa	441.55	psi
Dry Unit Weight (γ_{dry})	1698.0	kg/m^3	106.0	lb/ft^3
Wet Unit Weight (γ_{wet})	1787.7	kg/m^3	111.6	lb/ft^3

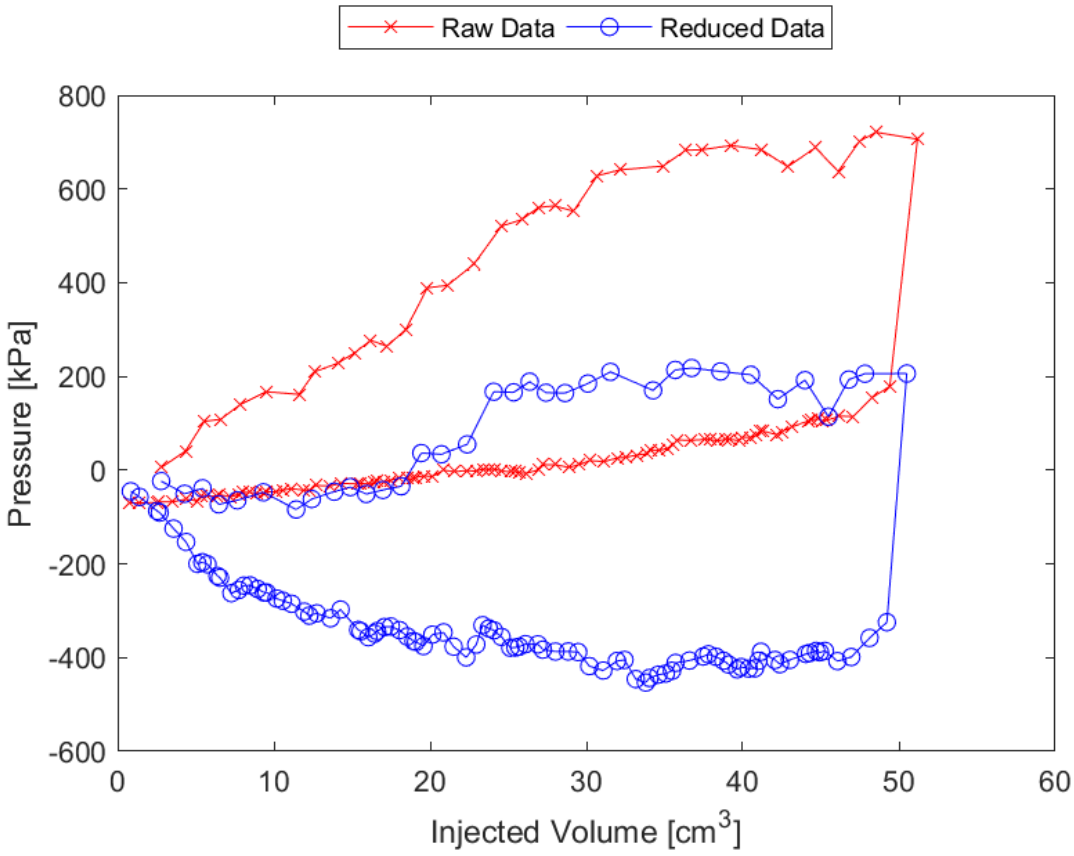

Figure B.37: Sounding 205, SDPMT-12 Continuous Test, Membrane O.D. 0.6875m, Depth 0.41 m, Raw and Reduced Data

Table B.37: Sounding 205, SDPMT-12 Continuous Test, Result Summary

Parameter				
Lift-Off Pressure (p_0)	−34.4	kPa	−4.99	psi
Contact Volume (V_c)	18.1	cm^3	1.11	in^3
Limit Pressure (p_L)	165.0	kPa	23.93	psi
Assumed ν		0.33		
Initial Modulus (E_0)	8555.0	kPa	1240.81	psi
Dry Unit Weight (γ_{dry})	1806.9	kg/m^3	112.8	lb/ft^3
Wet Unit Weight (γ_{wet})	1899.8	kg/m^3	118.6	lb/ft^3

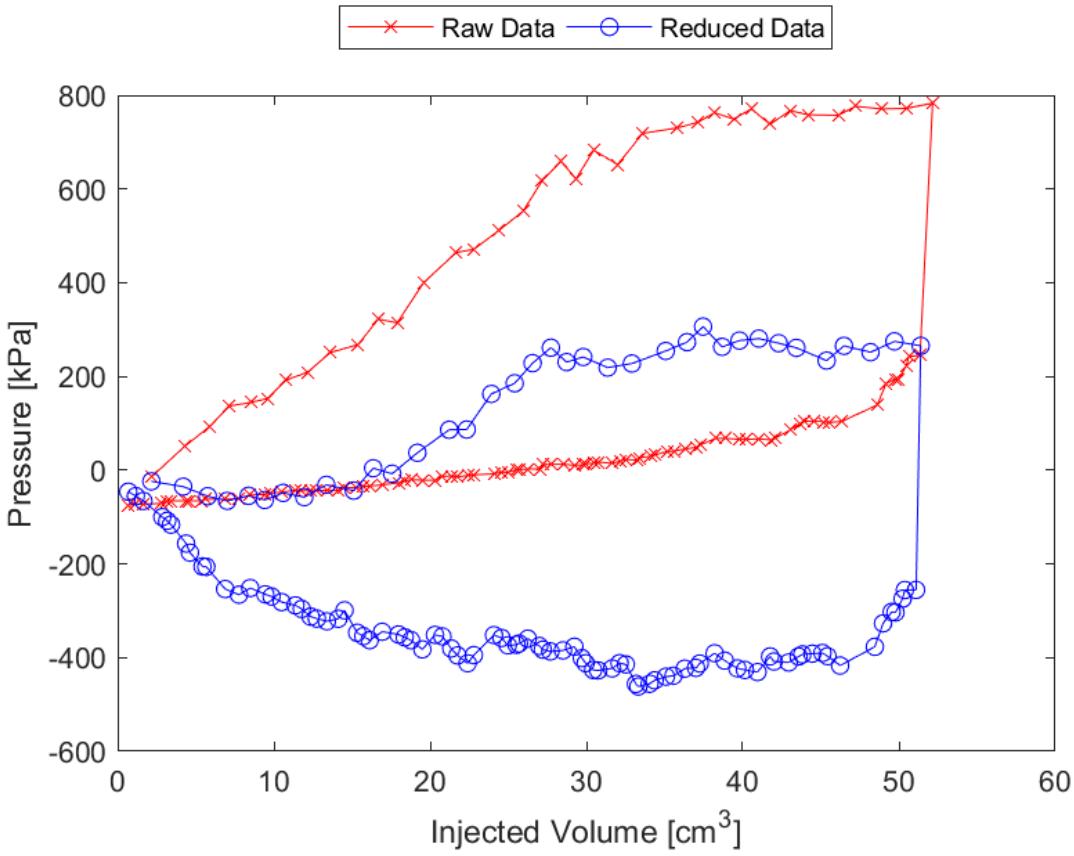

Figure B.38: Sounding 206, SDPMT-12 Continuous Test, Membrane O.D. 0.6875m, Depth 0.41 m, Raw and Reduced Data

Table B.38: Sounding 206, SDPMT-12 Continuous Test, Result Summary

Parameter				
Lift-Off Pressure (p_0)	−43.7	kPa	−6.33	psi
Contact Volume (V_c)	15.1	cm^3	0.92	in^3
Limit Pressure (p_L)	250.0	kPa	36.26	psi
Assumed ν		0.33		
Initial Modulus (E_0)	6753.2	kPa	979.47	psi
Dry Unit Weight (γ_{dry})	1842.1	kg/m^3	115.0	lb/ft^3
Wet Unit Weight (γ_{wet})	1933.4	kg/m^3	120.7	lb/ft^3

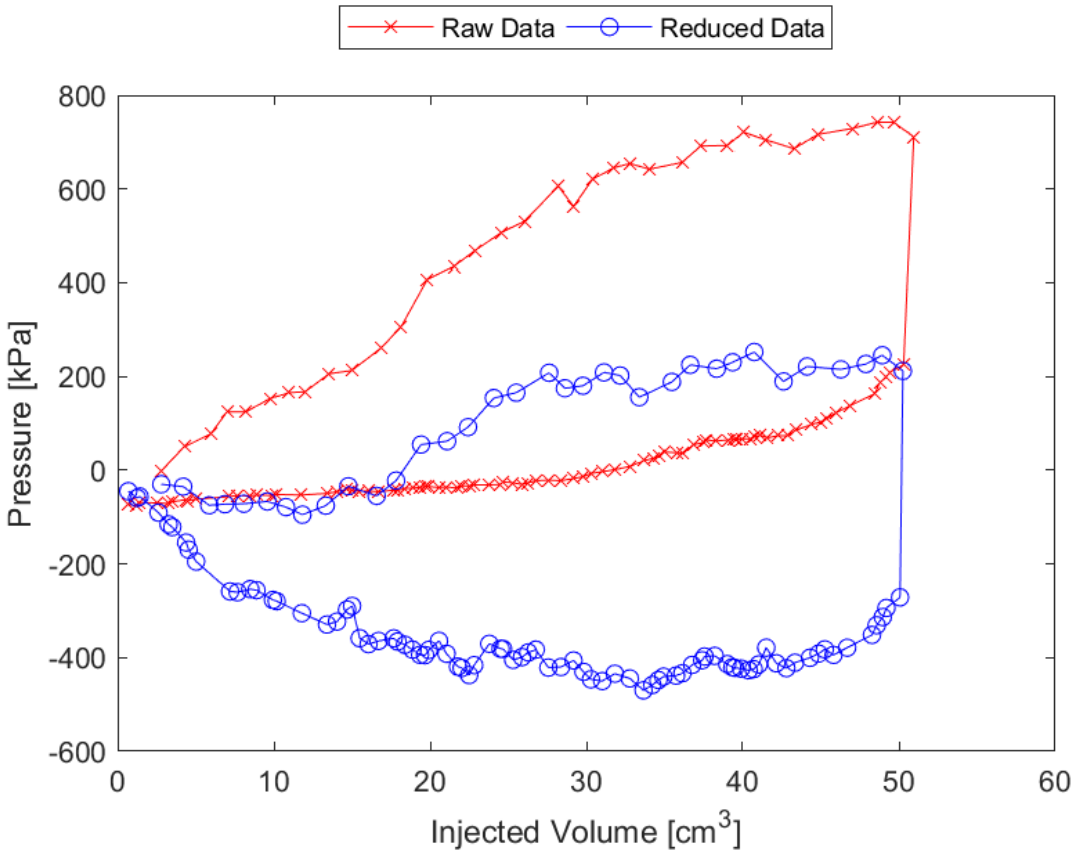

Figure B.39: Sounding 207, SDPMT-12 Continuous Test, Membrane O.D. 0.6875m, Depth 0.41 m, Raw and Reduced Data

Table B.39: Sounding 207, SDPMT-12 Continuous Test, Result Summary

Parameter				
Lift-Off Pressure (p_0)	−54.9	kPa	−7.96	psi
Contact Volume (V_c)	16.6	cm^3	1.01	in^3
Limit Pressure (p_L)	225.0	kPa	32.63	psi
Assumed ν		0.33		
Initial Modulus (E_0)	6032.4	kPa	874.92	psi
Dry Unit Weight (γ_{dry})	1832.5	kg/m^3	114.4	lb/ft^3
Wet Unit Weight (γ_{wet})	1936.6	kg/m^3	120.9	lb/ft^3

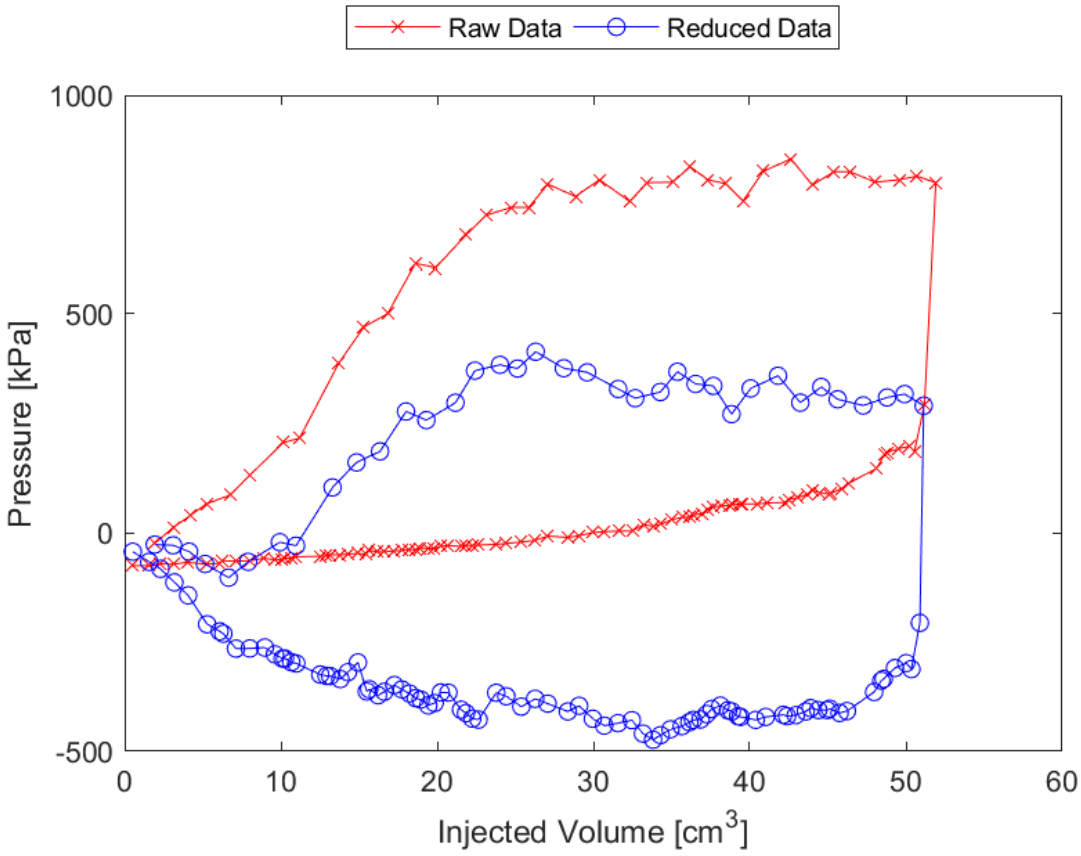

Figure B.40: Sounding 208, SDPMT-12 Continuous Test, Membrane O.D. 0.6875m, Depth 0.41 m, Raw and Reduced Data

Table B.40: Sounding 208, SDPMT-12 Continuous Test, Result Summary

Parameter				
Lift-Off Pressure (p_0)	−29.7	kPa	−4.31	psi
Contact Volume (V_c)	11.0	cm^3	0.67	in^3
Limit Pressure (p_L)	375.0	kPa	54.39	psi
Assumed ν		0.33		
Initial Modulus (E_0)	8357.4	kPa	1212.14	psi
Dry Unit Weight (γ_{dry})	1845.3	kg/m^3	115.2	lb/ft^3
Wet Unit Weight (γ_{wet})	1944.6	kg/m^3	121.4	lb/ft^3

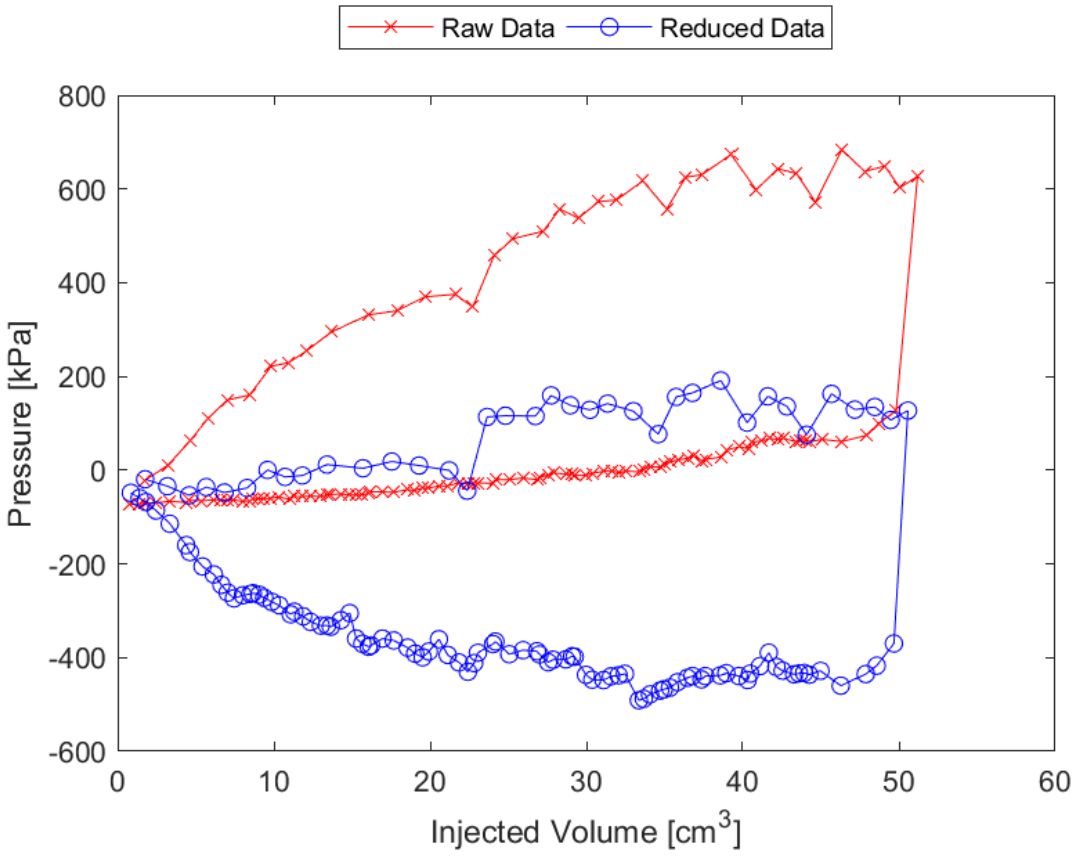

Figure B.41: Sounding 209, SDPMT-12 Continuous Test, Membrane O.D. 0.6875m, Depth 0.41 m, Raw and Reduced Data

Table B.41: Sounding 209, SDPMT-12 Continuous Test, Result Summary

Parameter				
Lift-Off Pressure (p_0)	−43.8	kPa	−6.35	psi
Contact Volume (V_c)	22.4	cm^3	1.37	in^3
Limit Pressure (p_L)	125.0	kPa	18.13	psi
Assumed ν		0.33		
Initial Modulus (E_0)	NaN	kPa	NaN	psi
Dry Unit Weight (γ_{dry})	1787.7	kg/m^3	111.6	lb/ft^3
Wet Unit Weight (γ_{wet})	1893.4	kg/m^3	118.2	lb/ft^3

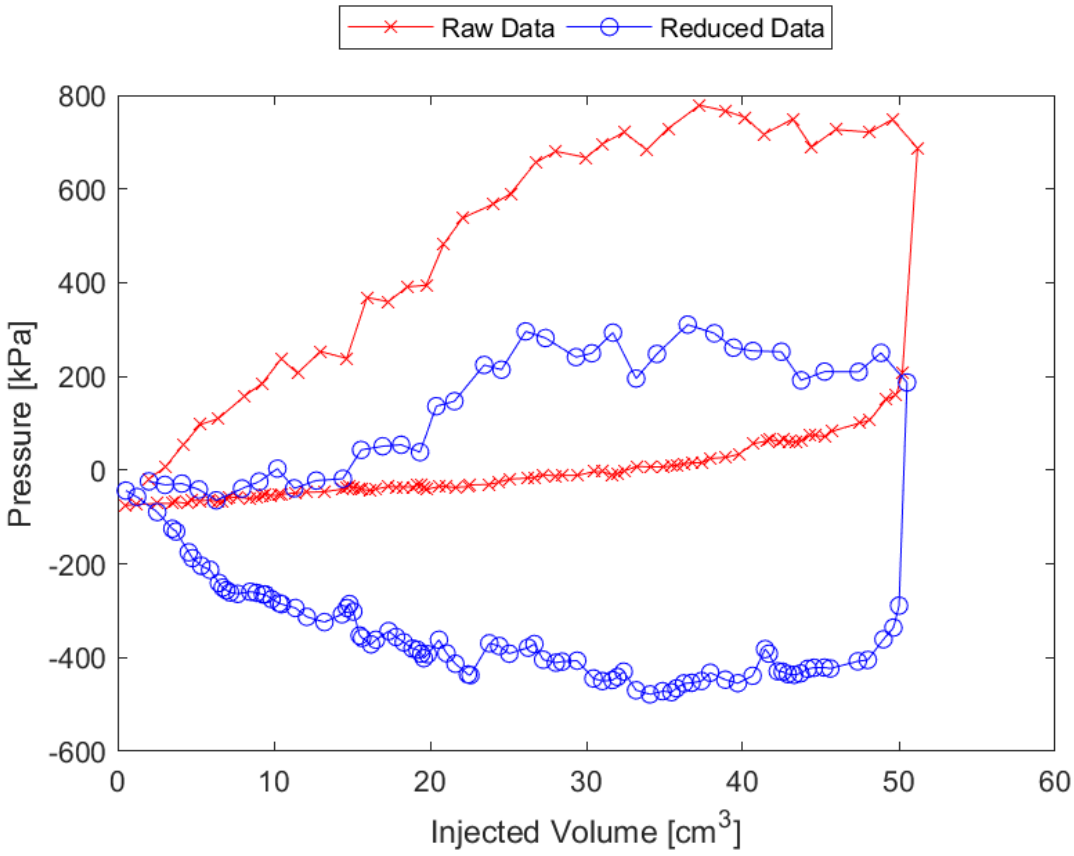

Figure B.42: Sounding 210, SDPMT-12 Continuous Test, Membrane O.D. 0.6875m, Depth 0.41 m, Raw and Reduced Data

Table B.42: Sounding 210, SDPMT-12 Continuous Test, Result Summary

Parameter				
Lift-Off Pressure (p_0)	38.4	kPa	5.57	psi
Contact Volume (V_c)	19.3	cm^3	1.18	in^3
Limit Pressure (p_L)	280.0	kPa	40.61	psi
Assumed ν		0.33		
Initial Modulus (E_0)	9722.5	kPa	1410.14	psi
Dry Unit Weight (γ_{dry})	1776.4	kg/m^3	110.9	lb/ft^3
Wet Unit Weight (γ_{wet})	1859.7	kg/m^3	116.1	lb/ft^3

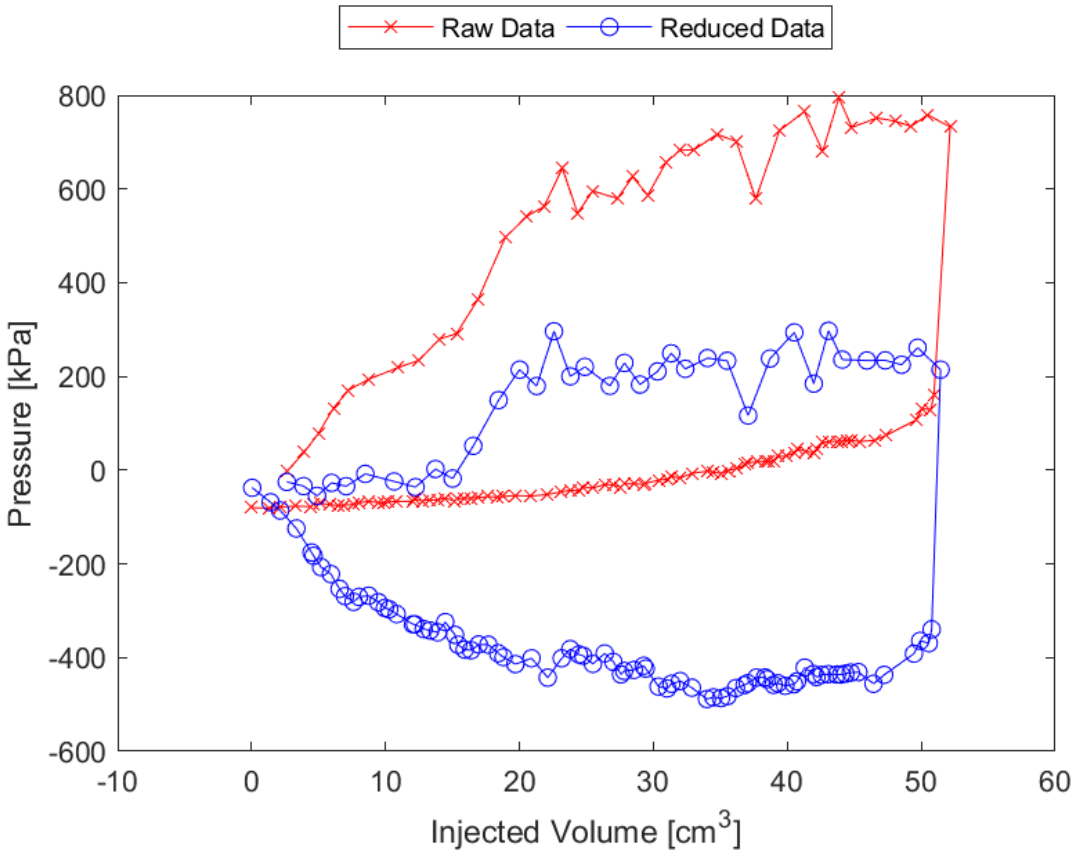

Figure B.43: Sounding 211, SDPMT-12 Continuous Test, Membrane O.D. 0.6875m, Depth 0.41 m, Raw and Reduced Data

Table B.43: Sounding 211, SDPMT-12 Continuous Test, Result Summary

Parameter				
Lift-Off Pressure (p_0)	−18.0	kPa	−2.61	psi
Contact Volume (V_c)	15.0	cm^3	0.92	in^3
Limit Pressure (p_L)	215.0	kPa	31.18	psi
Assumed ν		0.33		
Initial Modulus (E_0)	10167.0	kPa	1474.61	psi
Dry Unit Weight (γ_{dry})	1827.7	kg/m^3	114.1	lb/ft^3
Wet Unit Weight (γ_{wet})	1933.4	kg/m^3	120.7	lb/ft^3

Appendix C

Cypress Landing Pressuremeter Test Results

C.1 SDPMT-12 Incremental Test Separate Hole Data

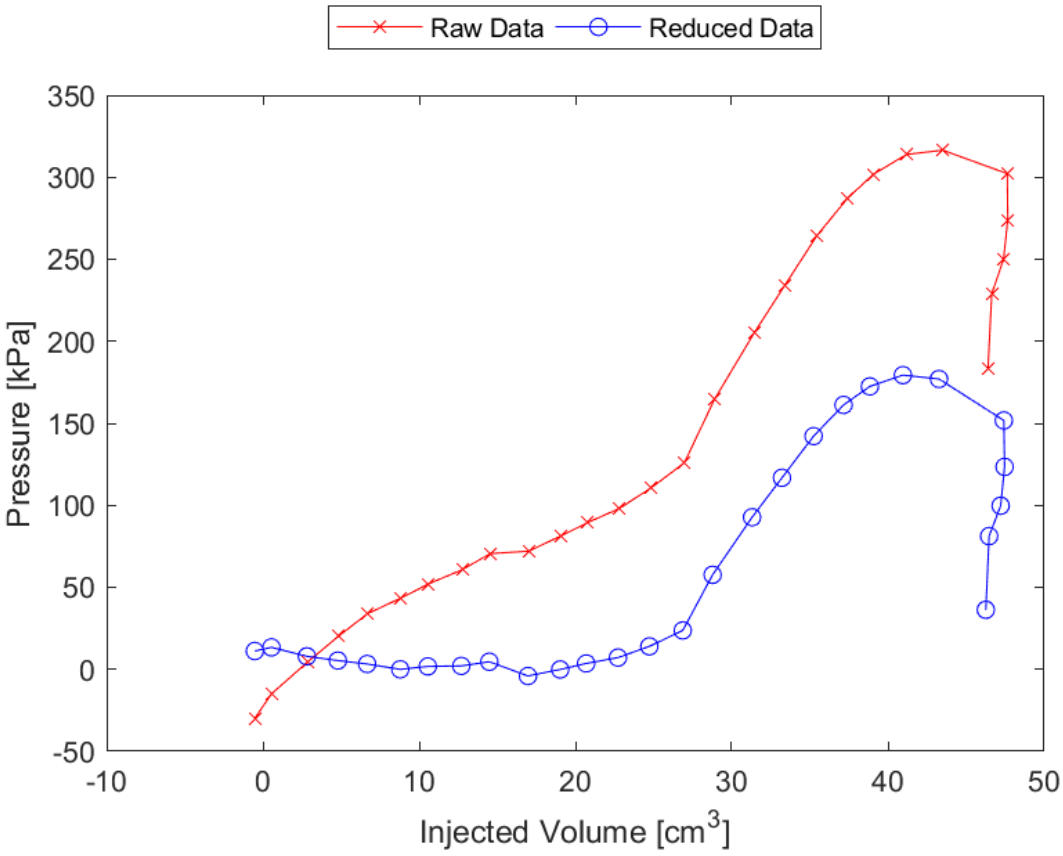

Figure C.1: Sounding 101, SDPMT-12 Incremental Test, Membrane O.D. 0.625m, Depth 0.38 m, Raw and Reduced Data

Table C.1: Sounding 101, SDPMT-12 Incremental Test, Result Summary

Parameter				
Lift-Off Pressure (p_0)	14.0	kPa	2.03	psi
Contact Volume (V_c)	24.7	cm^3	1.51	in^3
Limit Pressure (p_L)	380.0	kPa	55.11	psi
Assumed ν		0.33		
Initial Modulus (E_0)	3210.6	kPa	465.66	psi
Dry Unit Weight (γ_{dry})	1747.6	kg/m^3	109.1	lb/ft^3
Wet Unit Weight (γ_{wet})	1927.0	kg/m^3	120.3	lb/ft^3

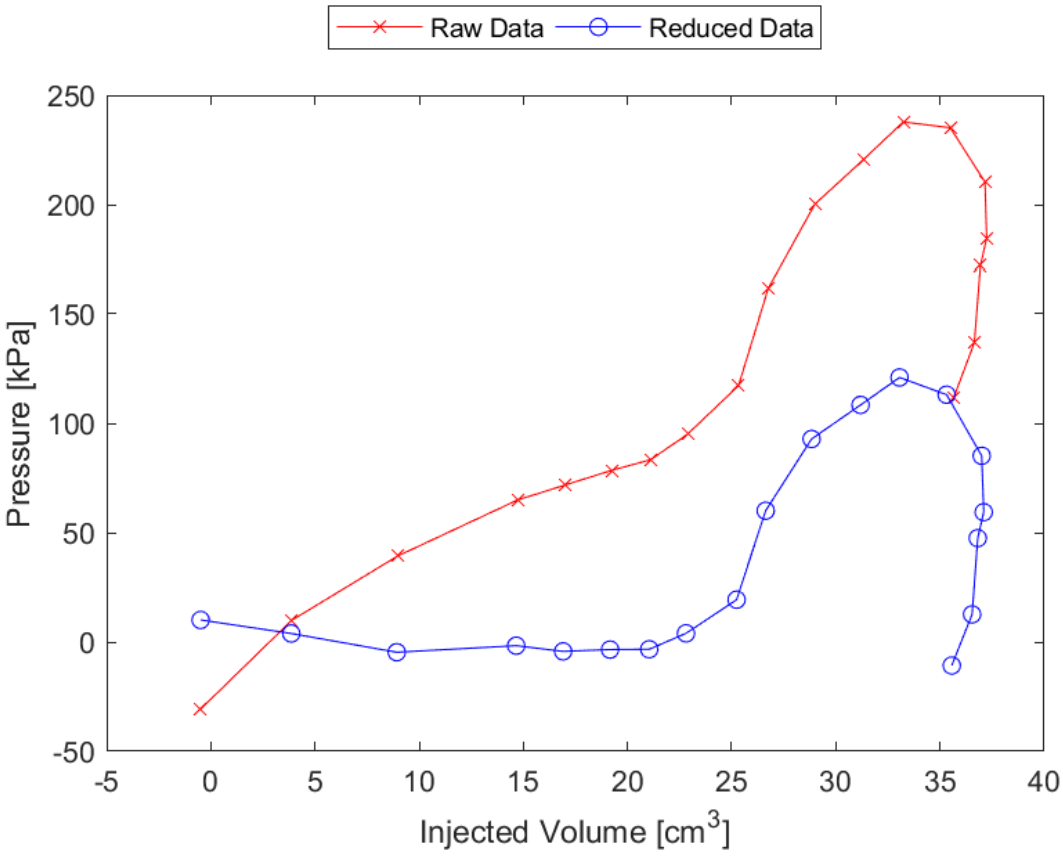

Figure C.2: Sounding 103, SDPMT-12 Incremental Test, Membrane O.D. 0.625m, Depth 0.38 m, Raw and Reduced Data

Table C.2: Sounding 103, SDPMT-12 Incremental Test, Result Summary

Parameter				
Lift-Off Pressure (p_0)	4.0	kPa	0.57	psi
Contact Volume (V_c)	22.8	cm^3	1.39	in^3
Limit Pressure (p_L)	330.0	kPa	47.86	psi
Assumed ν		0.33		
Initial Modulus (E_0)	4740.3	kPa	687.52	psi
Dry Unit Weight (γ_{dry})	1757.2	kg/m^3	109.7	lb/ft^3
Wet Unit Weight (γ_{wet})	1859.7	kg/m^3	116.1	lb/ft^3

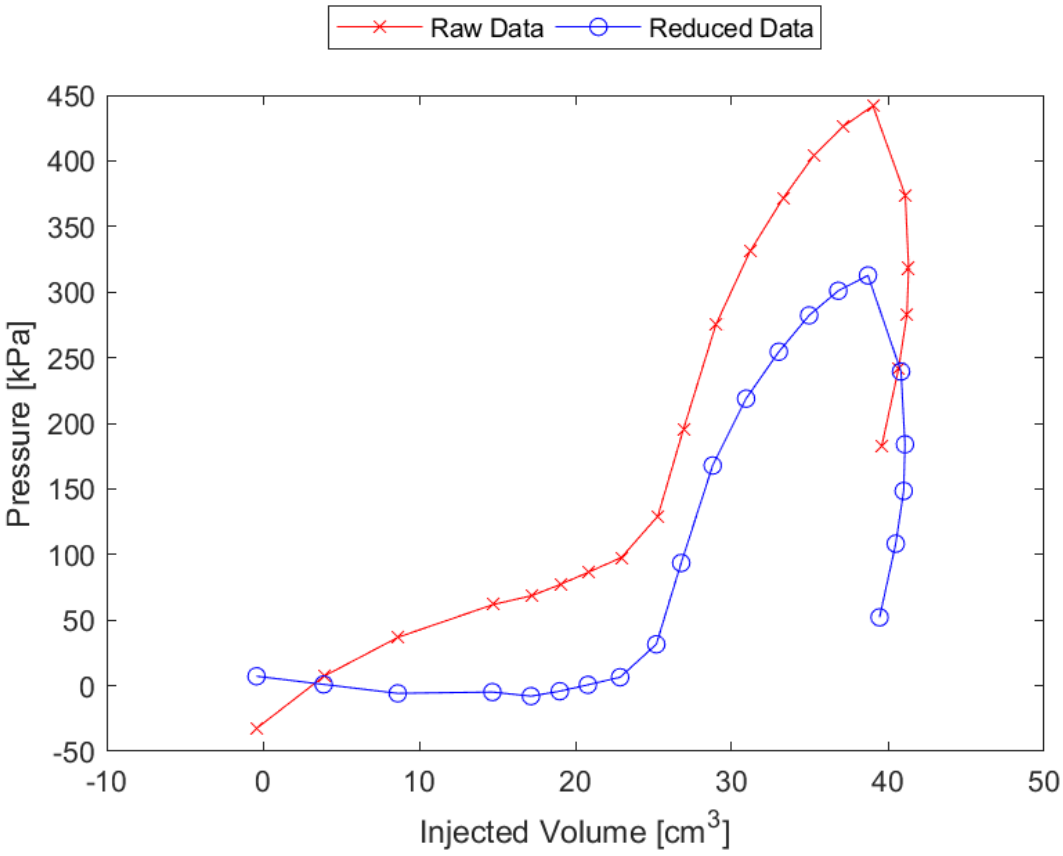

Figure C.3: Sounding 105, SDPMT-12 Incremental Test, Membrane O.D. 0.625m, Depth 0.38 m, Raw and Reduced Data

Table C.3: Sounding 105, SDPMT-12 Incremental Test, Result Summary

Parameter				
Lift-Off Pressure (p_0)	6.5	kPa	0.94	psi
Contact Volume (V_c)	22.9	cm^3	1.39	in^3
Limit Pressure (p_L)	610.0	kPa	88.47	psi
Assumed ν		0.33		
Initial Modulus (E_0)	8758.2	kPa	1270.27	psi
Dry Unit Weight (γ_{dry})	1806.9	kg/m^3	112.8	lb/ft^3
Wet Unit Weight (γ_{wet})	1903.0	kg/m^3	118.8	lb/ft^3

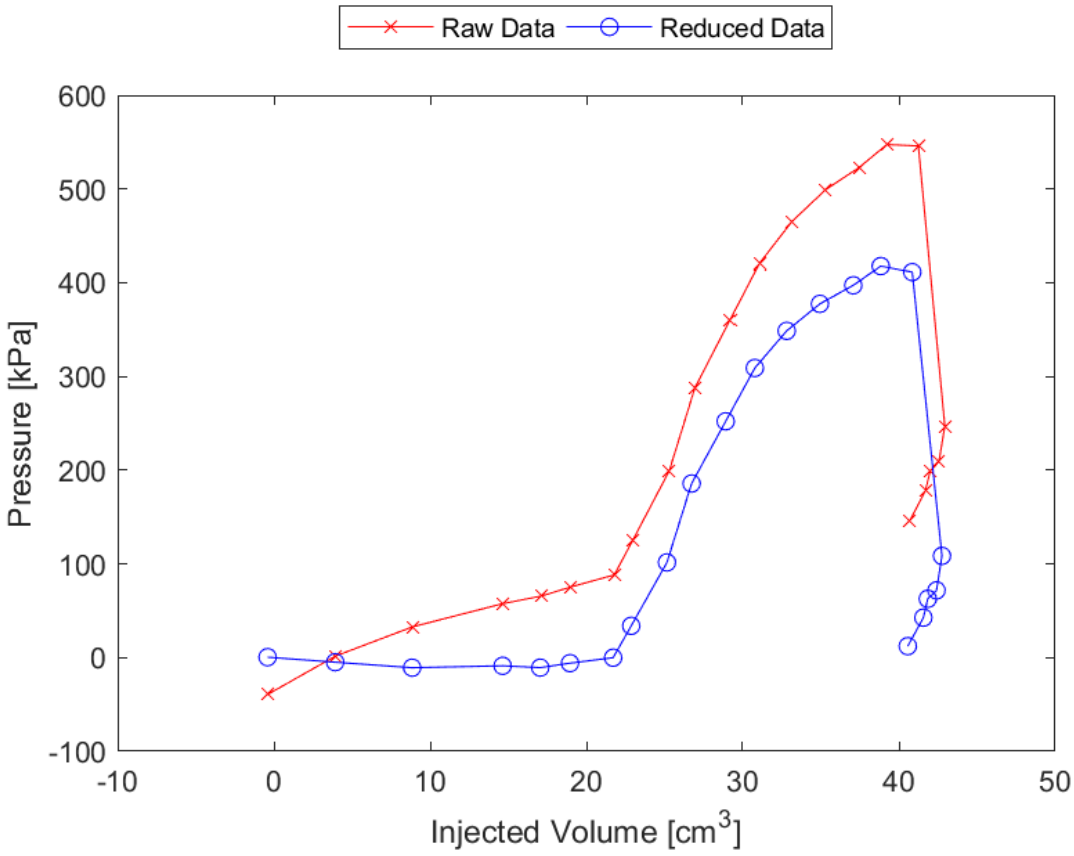

Figure C.4: Sounding 107, SDPMT-12 Incremental Test, Membrane O.D. 0.625m, Depth 0.38 m, Raw and Reduced Data

Table C.4: Sounding 107, SDPMT-12 Incremental Test, Result Summary

Parameter				
Lift-Off Pressure (p_0)	−0.1	kPa	−0.01	psi
Contact Volume (V_c)	21.7	cm^3	1.32	in^3
Limit Pressure (p_L)	740.0	kPa	107.33	psi
Assumed ν		0.33		
Initial Modulus (E_0)	8310.6	kPa	1205.36	psi
Dry Unit Weight (γ_{dry})	1832.5	kg/m^3	114.4	lb/ft^3
Wet Unit Weight (γ_{wet})	1947.8	kg/m^3	121.6	lb/ft^3

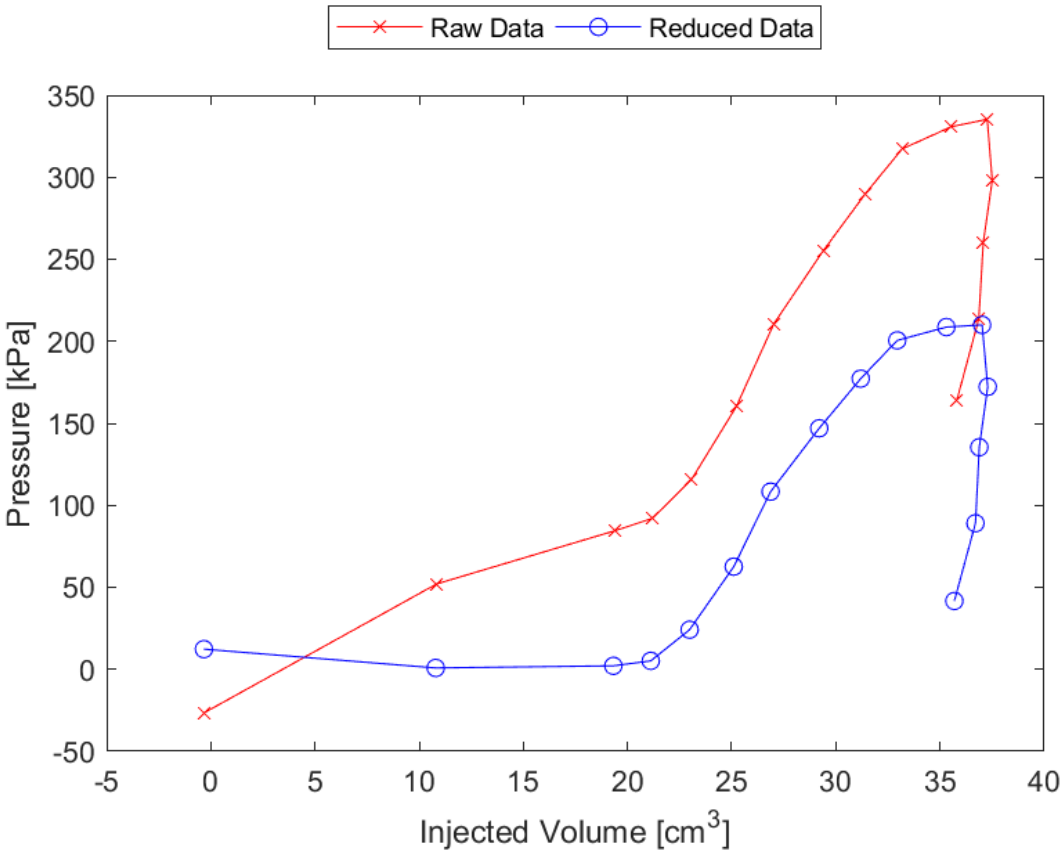

Figure C.5: Sounding 108, SDPMT-12 Incremental Test, Membrane O.D. 0.625m, Depth 0.38 m, Raw and Reduced Data

Table C.5: Sounding 108, SDPMT-12 Incremental Test, Result Summary

Parameter				
Lift-Off Pressure (p_0)	5.2	kPa	0.75	psi
Contact Volume (V_c)	21.1	cm^3	1.29	in^3
Limit Pressure (p_L)	415.0	kPa	60.19	psi
Assumed ν		0.33		
Initial Modulus (E_0)	4904.7	kPa	711.37	psi
Dry Unit Weight (γ_{dry})	1845.3	kg/m^3	115.2	lb/ft^3
Wet Unit Weight (γ_{wet})	1970.3	kg/m^3	123.0	lb/ft^3

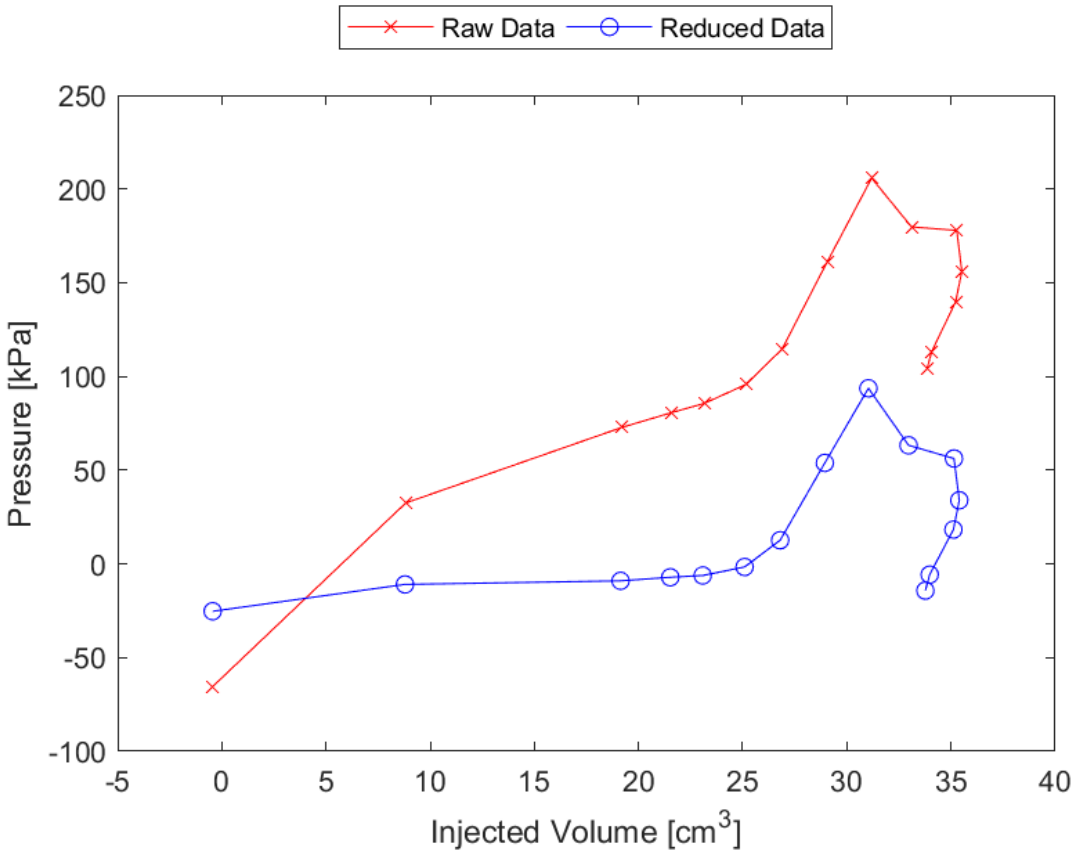

Figure C.6: Sounding 110, SDPMT-12 Incremental Test, Membrane O.D. 0.625m, Depth 0.38 m, Raw and Reduced Data

Table C.6: Sounding 110, SDPMT-12 Incremental Test, Result Summary

Parameter				
Lift-Off Pressure (p_0)	−6.2	kPa	−0.90	psi
Contact Volume (V_c)	23.1	cm^3	1.41	in^3
Limit Pressure (p_L)	470.0	kPa	68.17	psi
Assumed ν		0.33		
Initial Modulus (E_0)	4536.1	kPa	657.91	psi
Dry Unit Weight (γ_{dry})	1776.4	kg/m^3	110.9	lb/ft^3
Wet Unit Weight (γ_{wet})	1944.6	kg/m^3	121.4	lb/ft^3

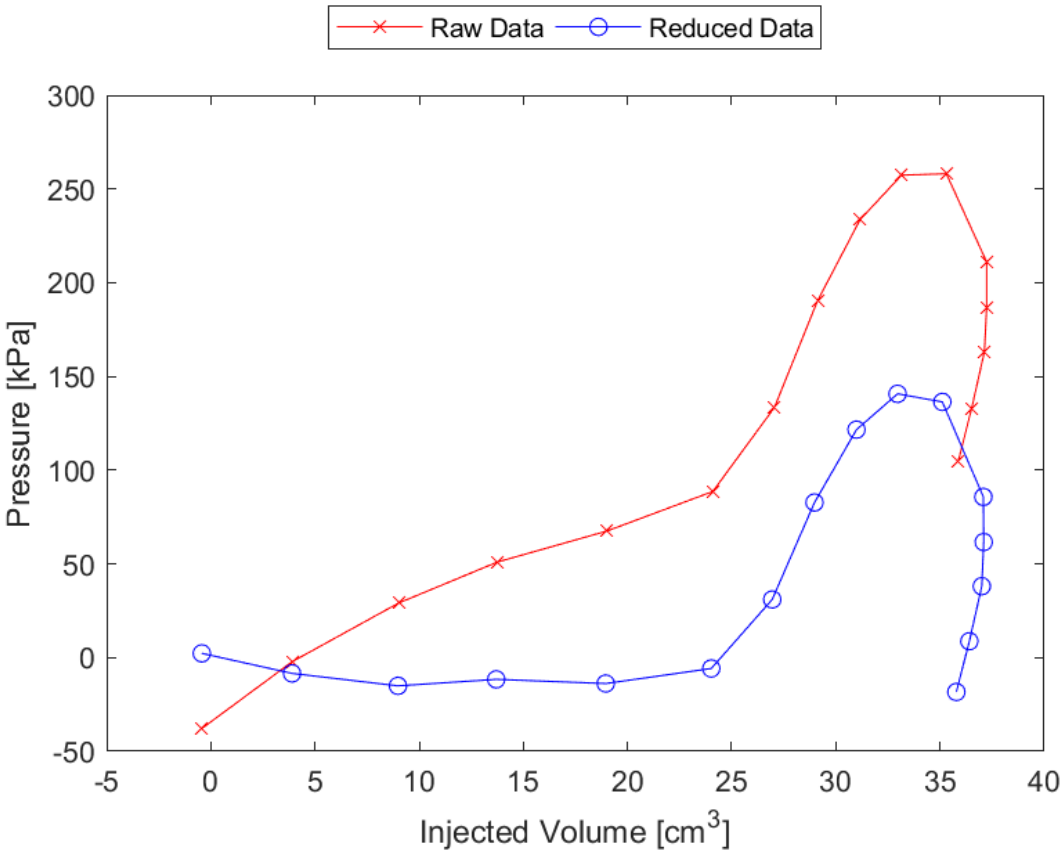

Figure C.7: Sounding 112, SDPMT-12 Incremental Test, Membrane O.D. 0.625m, Depth 0.38 m, Raw and Reduced Data

Table C.7: Sounding 112, SDPMT-12 Incremental Test, Result Summary

Parameter				
Lift-Off Pressure (p_0)	−5.8	kPa	−0.84	psi
Contact Volume (V_c)	24.0	cm^3	1.47	in^3
Limit Pressure (p_L)	510.0	kPa	73.97	psi
Assumed ν		0.33		
Initial Modulus (E_0)	5314.9	kPa	770.86	psi
Dry Unit Weight (γ_{dry})	1834.1	kg/m^3	114.5	lb/ft^3
Wet Unit Weight (γ_{wet})	1995.9	kg/m^3	124.6	lb/ft^3

C.2 SDPMT-12 Continuous Test Separate Hole Data

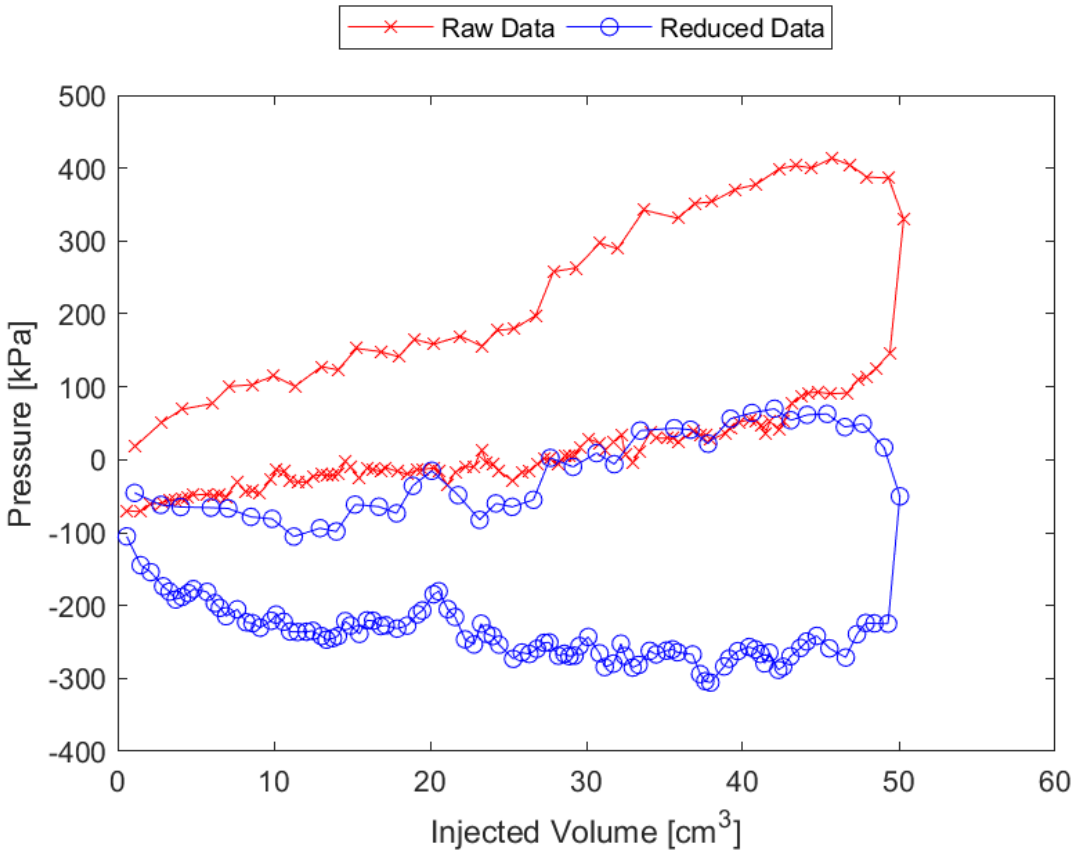

Figure C.8: Sounding 101, SDPMT-12 Continuous Test, Membrane O.D. 0.625m, Depth 0.38 m, Raw and Reduced Data

Table C.8: Sounding 101, SDPMT-12 Continuous Test, Result Summary

Parameter				
Lift-Off Pressure (p_0)	−82.5	kPa	−11.97	psi
Contact Volume (V_c)	49.1	cm^3	2.99	in^3
Limit Pressure (p_L)	410.0	kPa	59.47	psi
Assumed ν		0.33		
Initial Modulus (E_0)	2807.6	kPa	407.20	psi
Dry Unit Weight (γ_{dry})	1747.6	kg/m^3	109.1	lb/ft^3
Wet Unit Weight (γ_{wet})	1927.0	kg/m^3	120.3	lb/ft^3

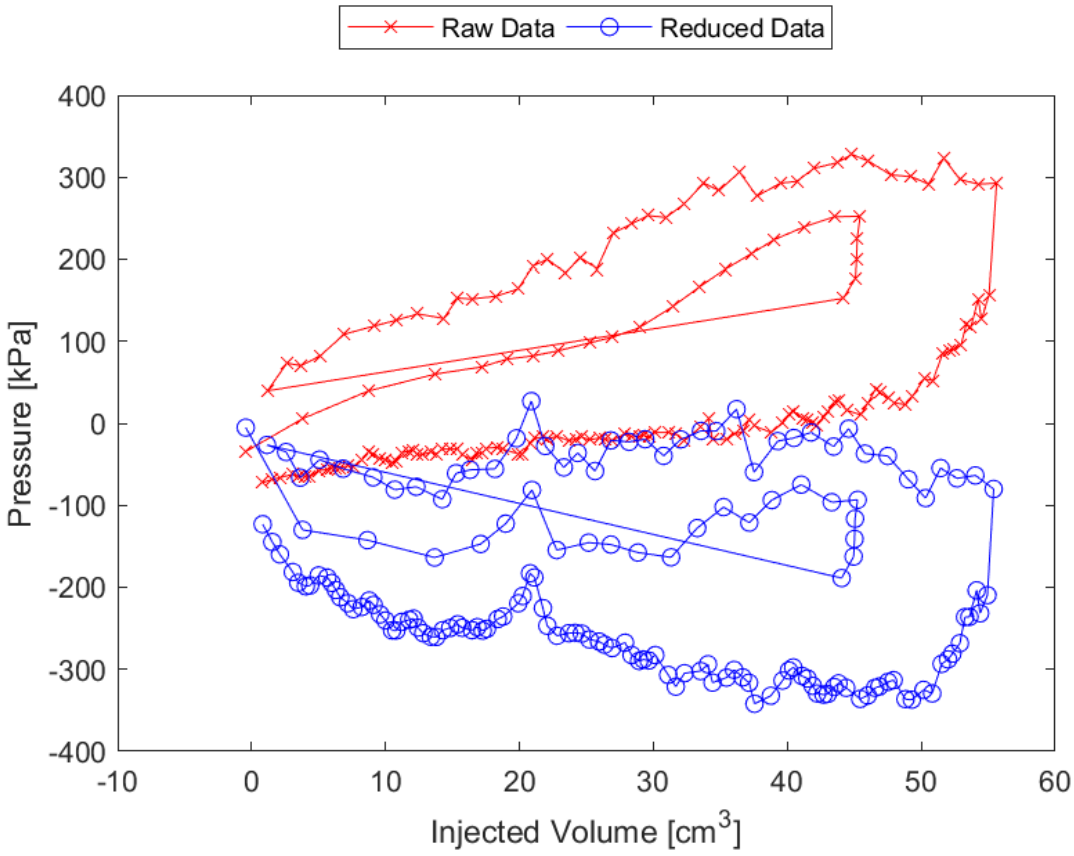

Figure C.9: Sounding 102, SDPMT-12 Continuous Test, Membrane O.D. 0.625m, Depth 0.38 m, Raw and Reduced Data

Table C.9: Sounding 102, SDPMT-12 Continuous Test, Result Summary

Parameter				
Lift-Off Pressure (p_0)	NaN	kPa	NaN	psi
Contact Volume (V_c)	NaN	cm^3	NaN	in^3
Limit Pressure (p_L)	NaN	kPa	NaN	psi
Assumed ν		0.33		
Initial Modulus (E_0)	NaN	kPa	NaN	psi
Dry Unit Weight (γ_{dry})	1826.1	kg/m^3	114.0	lb/ft^3
Wet Unit Weight (γ_{wet})	1975.1	kg/m^3	123.3	lb/ft^3

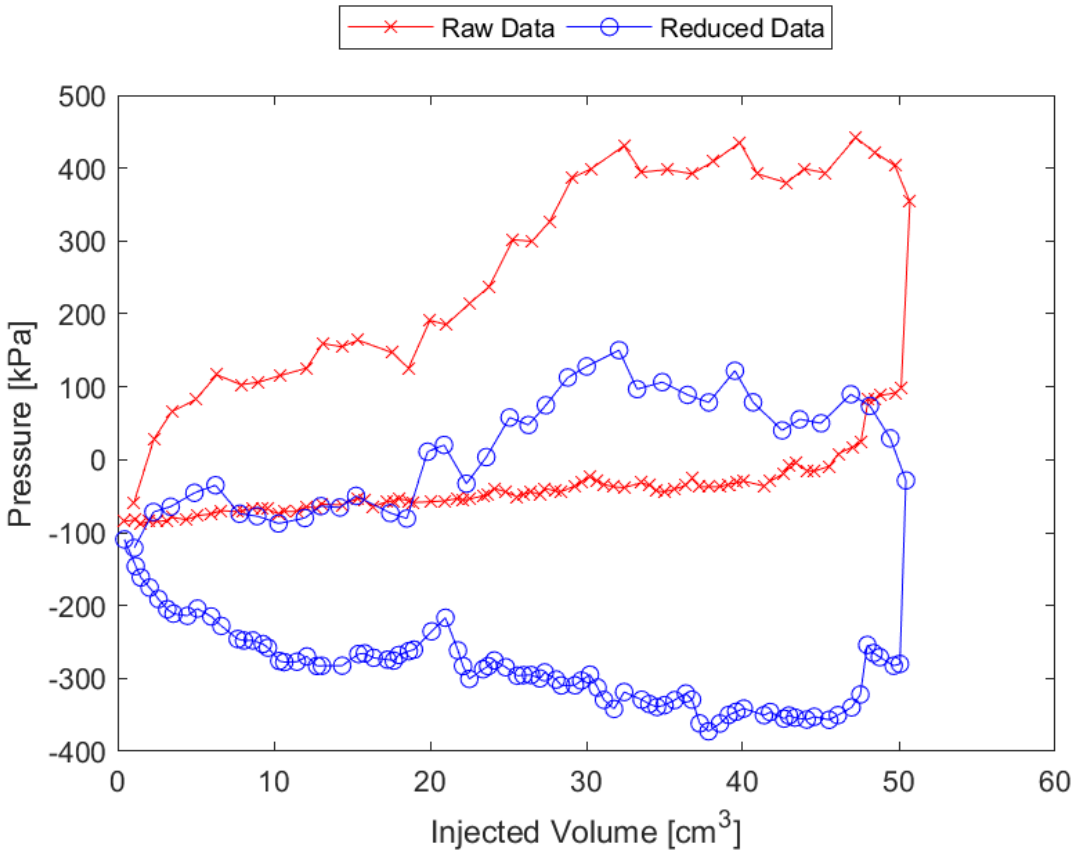

Figure C.10: Sounding 105, SDPMT-12 Continuous Test, Membrane O.D. 0.625m, Depth 0.38 m, Raw and Reduced Data

Table C.10: Sounding 105, SDPMT-12 Continuous Test, Result Summary

Parameter				
Lift-Off Pressure (p_0)	−80.7	kPa	−11.70	psi
Contact Volume (V_c)	18.5	cm^3	1.13	in^3
Limit Pressure (p_L)	315.0	kPa	45.69	psi
Assumed ν		0.33		
Initial Modulus (E_0)	5121.8	kPa	742.86	psi
Dry Unit Weight (γ_{dry})	1806.9	kg/m^3	112.8	lb/ft^3
Wet Unit Weight (γ_{wet})	1903.0	kg/m^3	118.8	lb/ft^3

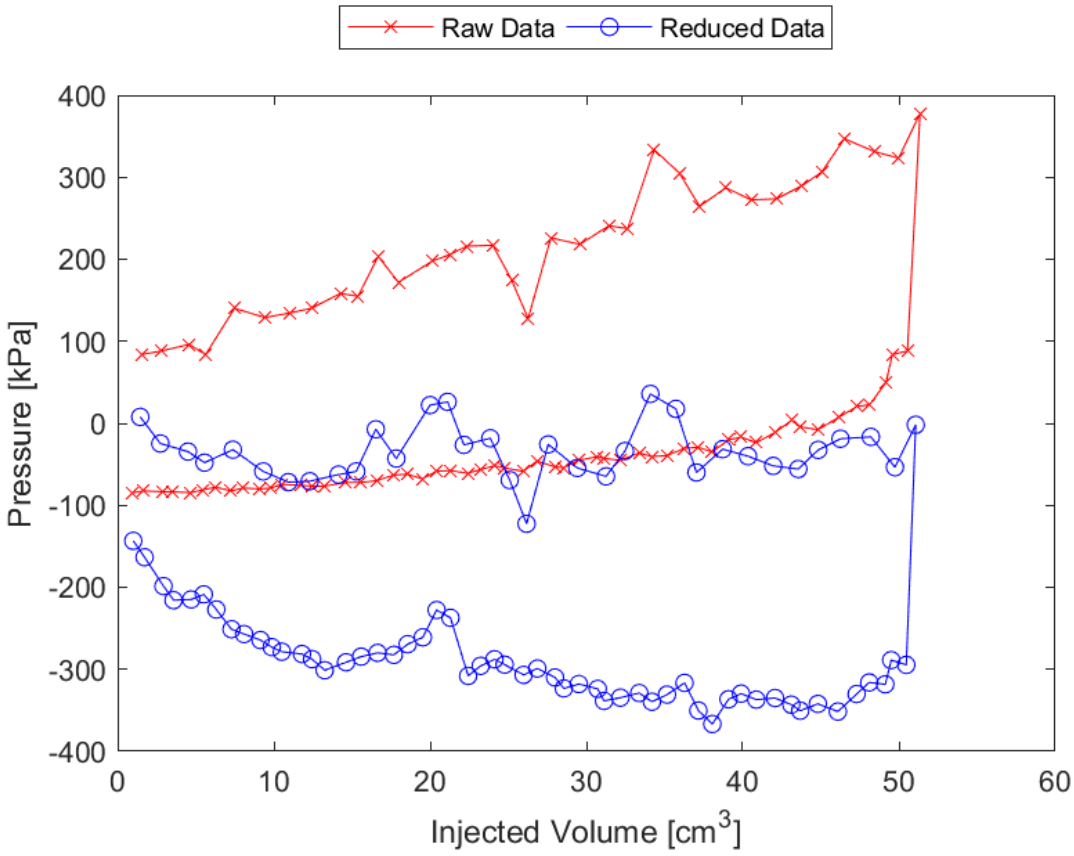

Figure C.11: Sounding 109, SDPMT-12 Continuous Test, Membrane O.D. 0.625m, Depth 0.38 m, Raw and Reduced Data

Table C.11: Sounding 109, SDPMT-12 Continuous Test, Result Summary

Parameter				
Lift-Off Pressure (p_0)	NaN	kPa	NaN	psi
Contact Volume (V_c)	NaN	cm^3	NaN	in^3
Limit Pressure (p_L)	NaN	kPa	NaN	psi
Assumed ν		0.33		
Initial Modulus (E_0)	NaN	kPa	NaN	psi
Dry Unit Weight (γ_{dry})	1787.7	kg/m^3	111.6	lb/ft^3
Wet Unit Weight (γ_{wet})	1967.1	kg/m^3	122.8	lb/ft^3

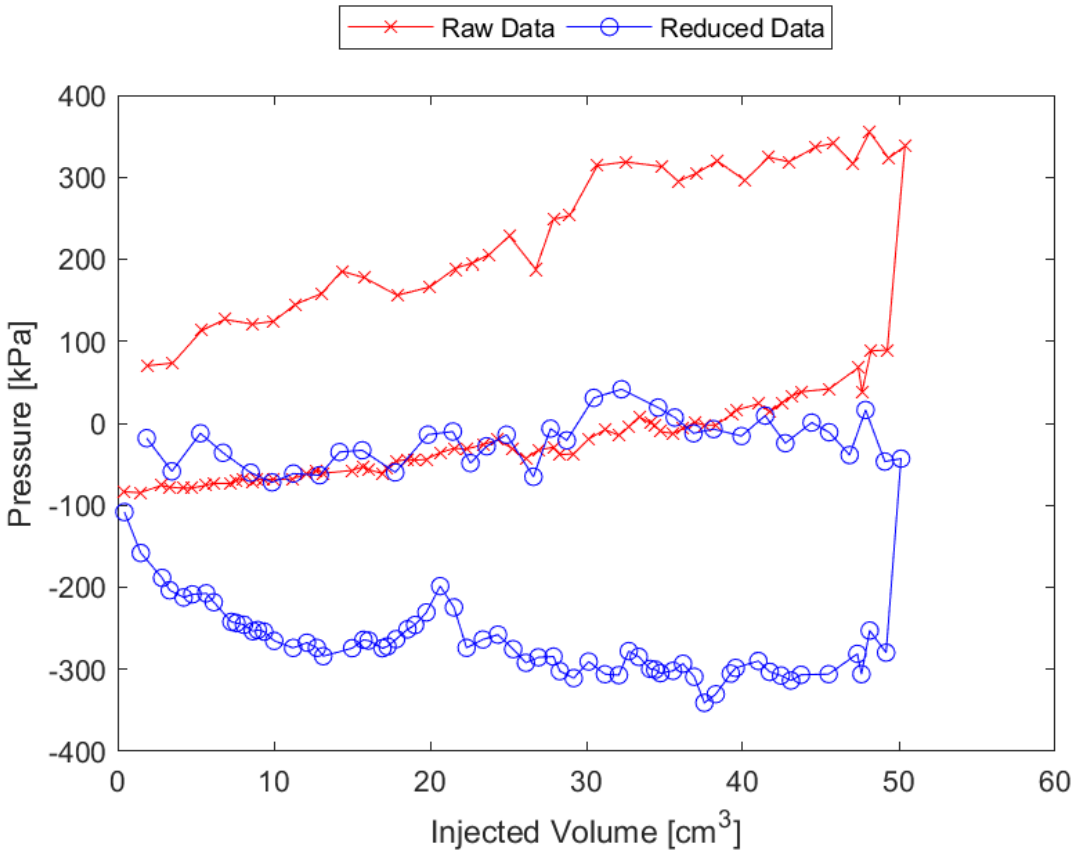

Figure C.12: Sounding 111, SDPMT-12 Continuous Test, Membrane O.D. 0.625m, Depth 0.38 m, Raw and Reduced Data

Table C.12: Sounding 111, SDPMT-12 Continuous Test, Result Summary

Parameter				
Lift-Off Pressure (p_0)	NaN	kPa	NaN	psi
Contact Volume (V_c)	NaN	cm^3	NaN	in^3
Limit Pressure (p_L)	NaN	kPa	NaN	psi
Assumed ν		0.33		
Initial Modulus (E_0)	NaN	kPa	NaN	psi
Dry Unit Weight (γ_{dry})	1827.7	kg/m^3	114.1	lb/ft^3
Wet Unit Weight (γ_{wet})	2034.3	kg/m^3	127.0	lb/ft^3

C.3 SDPMT-12 Incremental Test NDG Hole Data

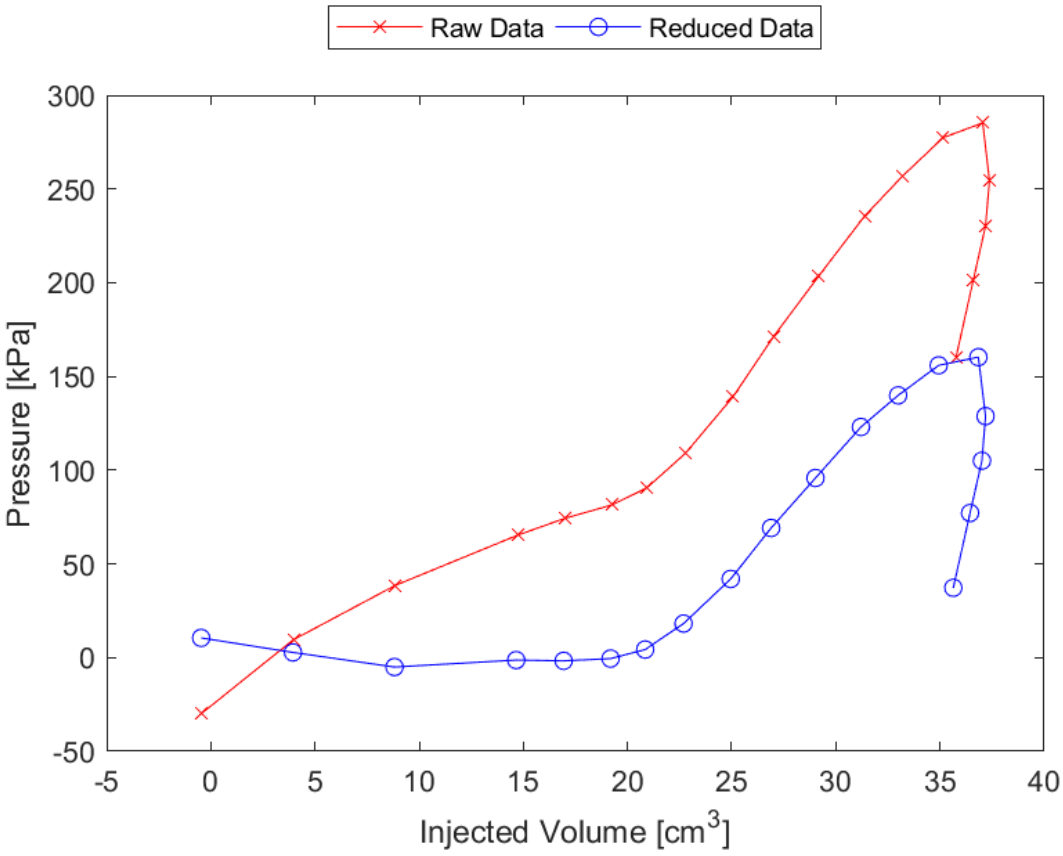

Figure C.13: Sounding 104, SDPMT-12 Incremental Test, Membrane O.D. 0.625m, Depth 0.38 m, Raw and Reduced Data

Table C.13: Sounding 104, SDPMT-12 Incremental Test, Result Summary

Parameter				
Lift-Off Pressure (p_0)	4.3	kPa	0.63	psi
Contact Volume (V_c)	20.8	cm^3	1.27	in^3
Limit Pressure (p_L)	345.0	kPa	50.04	psi
Assumed ν		0.33		
Initial Modulus (E_0)	2855.9	kPa	414.21	psi
Dry Unit Weight (γ_{dry})	1698.0	kg/m^3	106.0	lb/ft^3
Wet Unit Weight (γ_{wet})	1810.1	kg/m^3	113.0	lb/ft^3

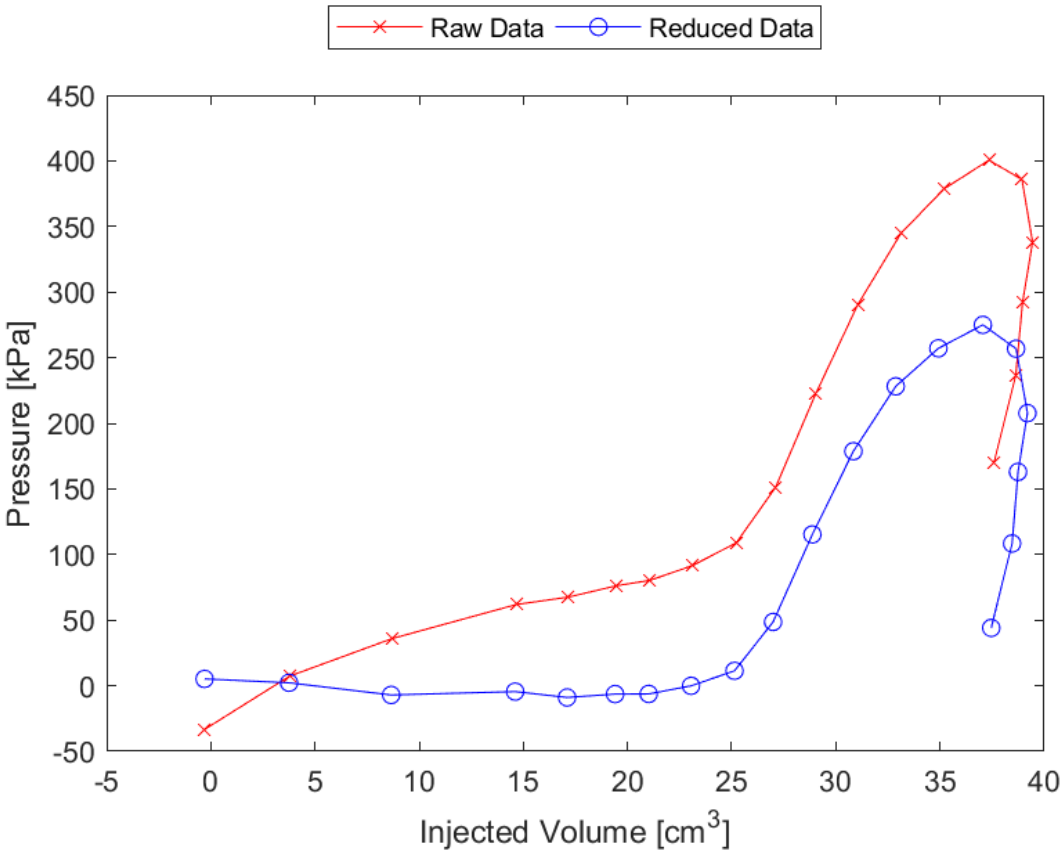

Figure C.14: Sounding 106, SDPMT-12 Incremental Test, Membrane O.D. 0.625m, Depth 0.38 m, Raw and Reduced Data

Table C.14: Sounding 106, SDPMT-12 Incremental Test, Result Summary

Parameter				
Lift-Off Pressure (p_0)	11.4	kPa	1.65	psi
Contact Volume (V_c)	25.1	cm^3	1.53	in^3
Limit Pressure (p_L)	725.0	kPa	105.15	psi
Assumed ν		0.33		
Initial Modulus (E_0)	8004.1	kPa	1160.90	psi
Dry Unit Weight (γ_{dry})	1842.1	kg/m^3	115.0	lb/ft^3
Wet Unit Weight (γ_{wet})	1951.0	kg/m^3	121.8	lb/ft^3

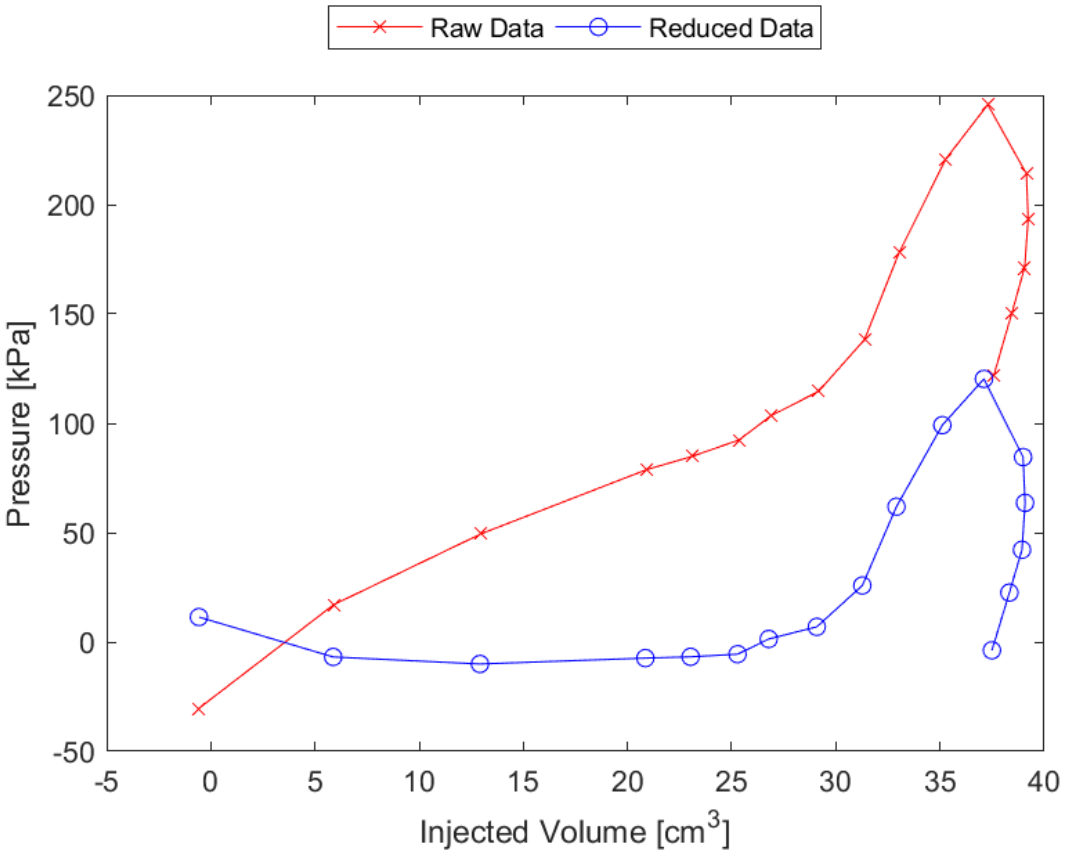

Figure C.15: Sounding 109, SDPMT-12 Incremental Test, Membrane O.D. 0.625m, Depth 0.38 m, Raw and Reduced Data

Table C.15: Sounding 109, SDPMT-12 Incremental Test, Result Summary

Parameter				
Lift-Off Pressure (p_0)	1.4	kPa	0.20	psi
Contact Volume (V_c)	26.8	cm^3	1.63	in^3
Limit Pressure (p_L)	335.0	kPa	48.59	psi
Assumed ν		0.33		
Initial Modulus (E_0)	4745.1	kPa	688.22	psi
Dry Unit Weight (γ_{dry})	1787.7	kg/m^3	111.6	lb/ft^3
Wet Unit Weight (γ_{wet})	1967.1	kg/m^3	122.8	lb/ft^3

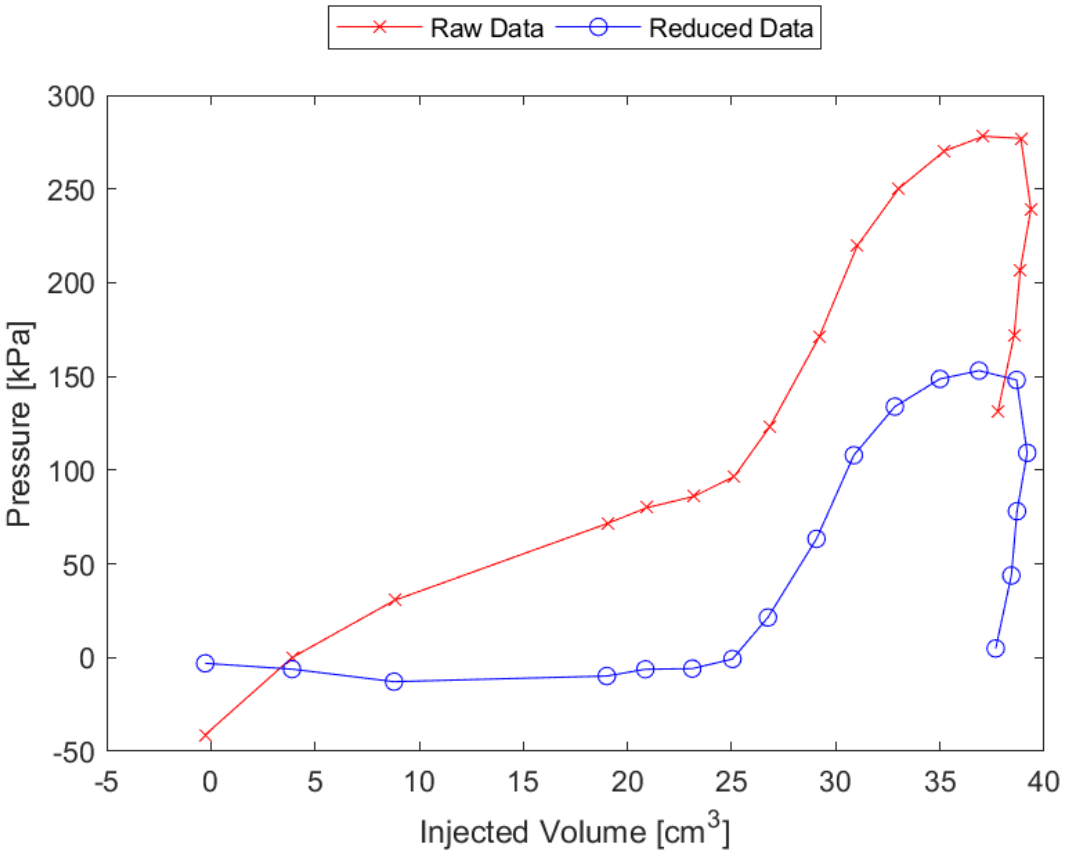

Figure C.16: Sounding 111, SDPMT-12 Incremental Test, Membrane O.D. 0.625m, Depth 0.38 m, Raw and Reduced Data

Table C.16: Sounding 111, SDPMT-12 Incremental Test, Result Summary

Parameter				
Lift-Off Pressure (p_0)	−0.8	kPa	−0.11	psi
Contact Volume (V_c)	25.0	cm^3	1.53	in^3
Limit Pressure (p_L)	420.0	kPa	60.92	psi
Assumed ν		0.33		
Initial Modulus (E_0)	4967.4	kPa	720.46	psi
Dry Unit Weight (γ_{dry})	1827.7	kg/m^3	114.1	lb/ft^3
Wet Unit Weight (γ_{wet})	2034.3	kg/m^3	127.0	lb/ft^3

C.4 SDPMT-12 Continuous Test NDG Hole Data

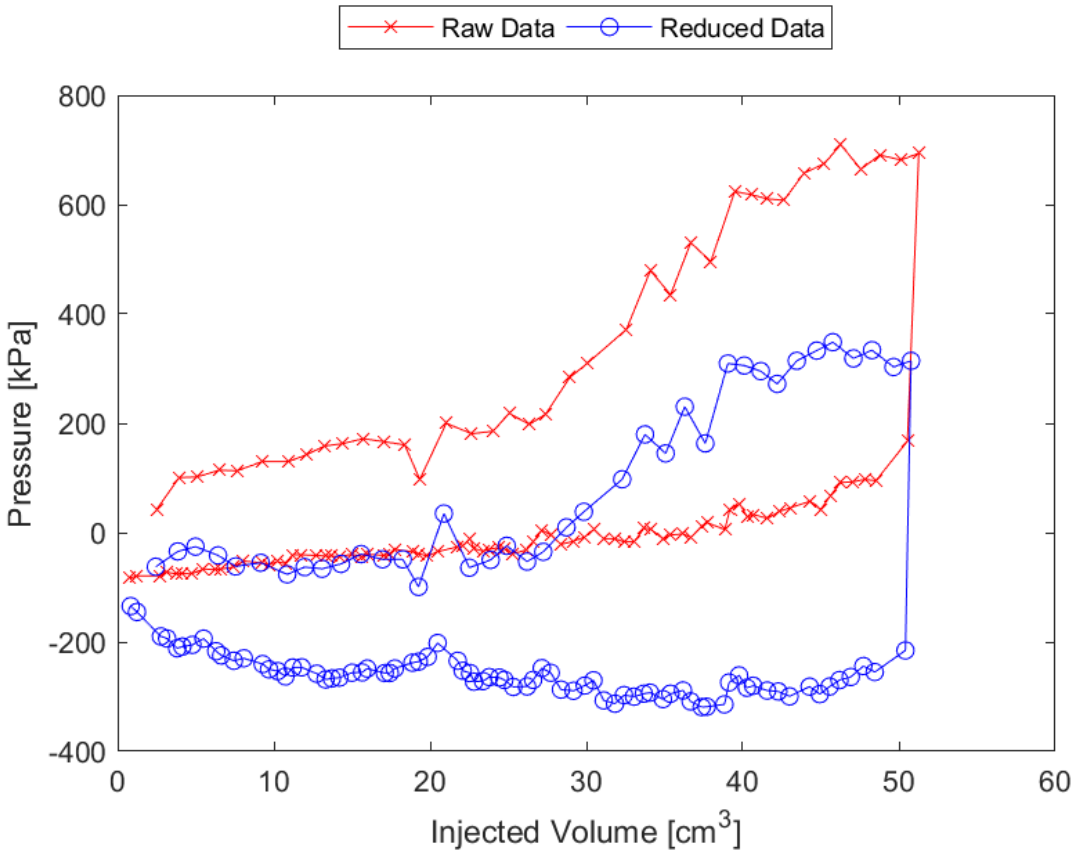

Figure C.17: Sounding 104, SDPMT-12 Continuous Test, Membrane O.D. 0.625m, Depth 0.38 m, Raw and Reduced Data

Table C.17: Sounding 104, SDPMT-12 Continuous Test, Result Summary

Parameter				
Lift-Off Pressure (p_0)	−52.9	kPa	−7.68	psi
Contact Volume (V_c)	26.2	cm^3	1.60	in^3
Limit Pressure (p_L)	625.0	kPa	90.65	psi
Assumed ν		0.33		
Initial Modulus (E_0)	5886.5	kPa	853.76	psi
Dry Unit Weight (γ_{dry})	1806.9	kg/m^3	112.8	lb/ft^3
Wet Unit Weight (γ_{wet})	1903.0	kg/m^3	118.8	lb/ft^3

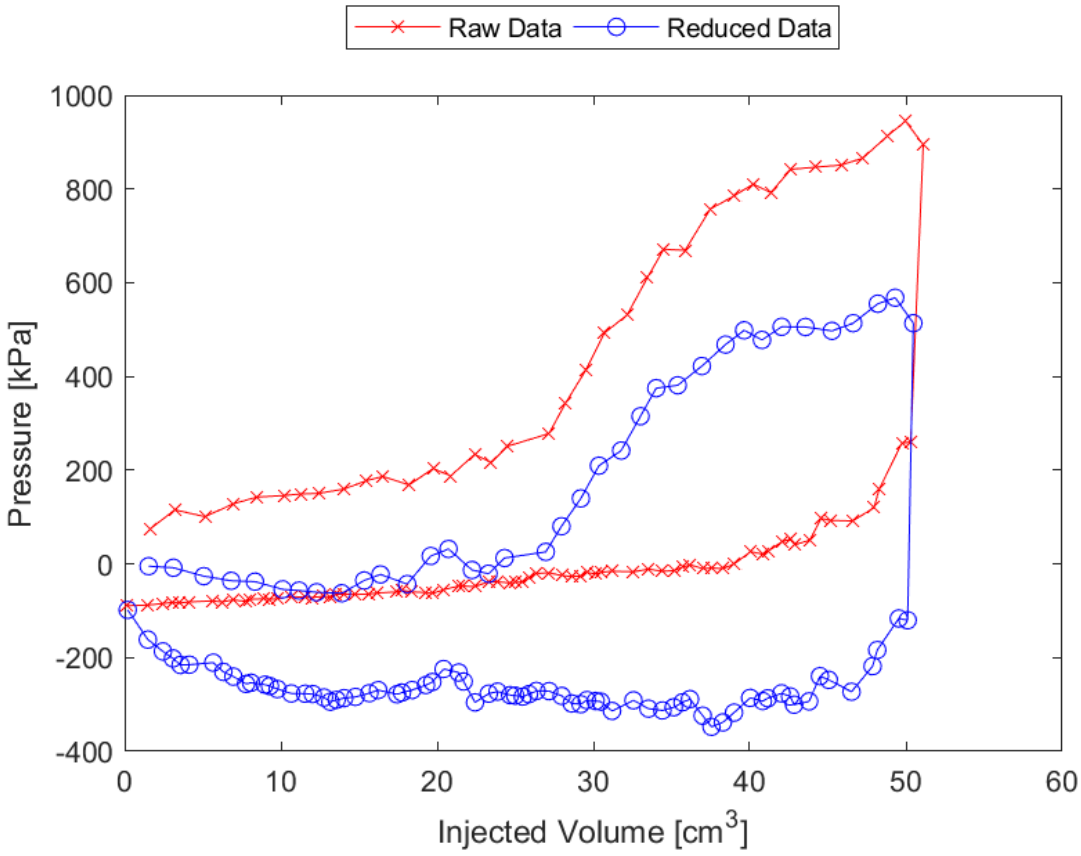

Figure C.18: Sounding 106, SDPMT-12 Continuous Test, Membrane O.D. 0.625m, Depth 0.38 m, Raw and Reduced Data

Table C.18: Sounding 106, SDPMT-12 Continuous Test, Result Summary

Parameter				
Lift-Off Pressure (p_0)	25.7	kPa	3.72	psi
Contact Volume (V_c)	27.0	cm^3	1.64	in^3
Limit Pressure (p_L)	725.0	kPa	105.15	psi
Assumed ν		0.33		
Initial Modulus (E_0)	11929.2	kPa	1730.18	psi
Dry Unit Weight (γ_{dry})	1832.5	kg/m^3	114.4	lb/ft^3
Wet Unit Weight (γ_{wet})	1947.8	kg/m^3	121.6	lb/ft^3

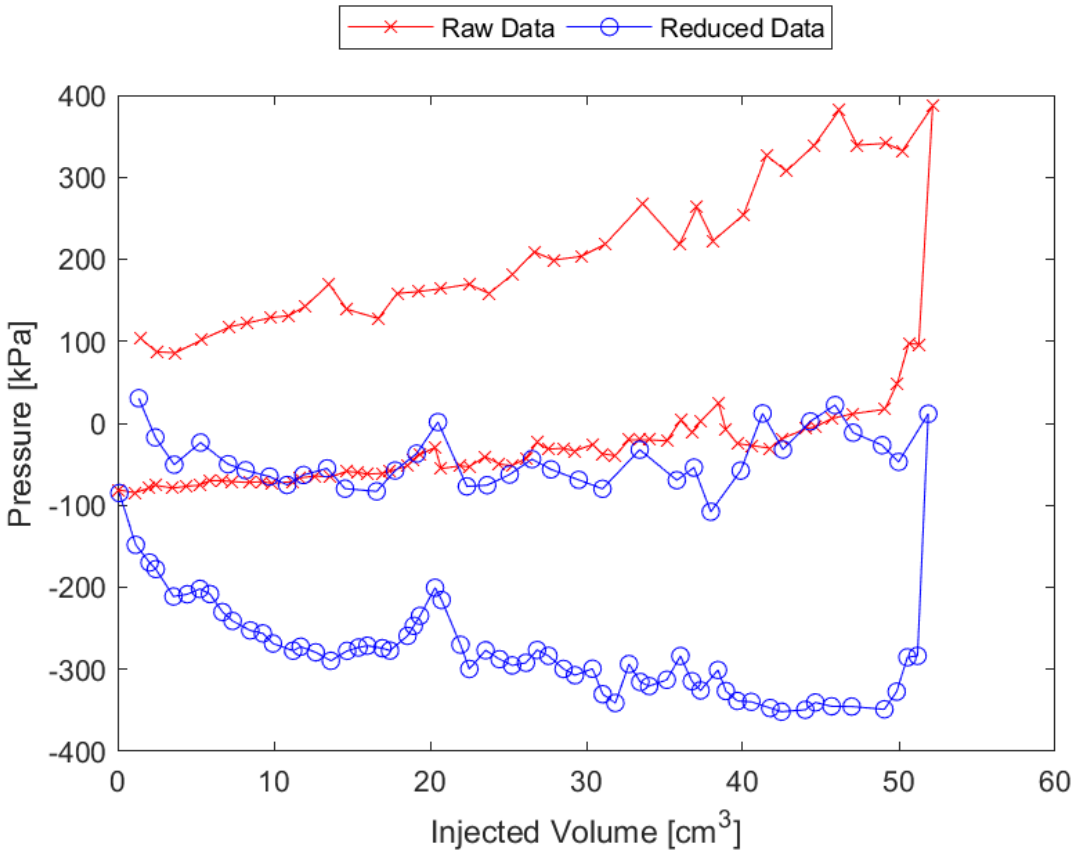

Figure C.19: Sounding 109, SDPMT-12 Continuous Test, Membrane O.D. 0.625m, Depth 0.38 m, Raw and Reduced Data

Table C.19: Sounding 109, SDPMT-12 Continuous Test, Result Summary

Parameter				
Lift-Off Pressure (p_0)	NaN	kPa	NaN	psi
Contact Volume (V_c)	NaN	cm^3	NaN	in^3
Limit Pressure (p_L)	NaN	kPa	NaN	psi
Assumed ν		0.33		
Initial Modulus (E_0)	NaN	kPa	NaN	psi
Dry Unit Weight (γ_{dry})	1845.3	kg/m^3	115.2	lb/ft^3
Wet Unit Weight (γ_{wet})	1970.3	kg/m^3	123.0	lb/ft^3

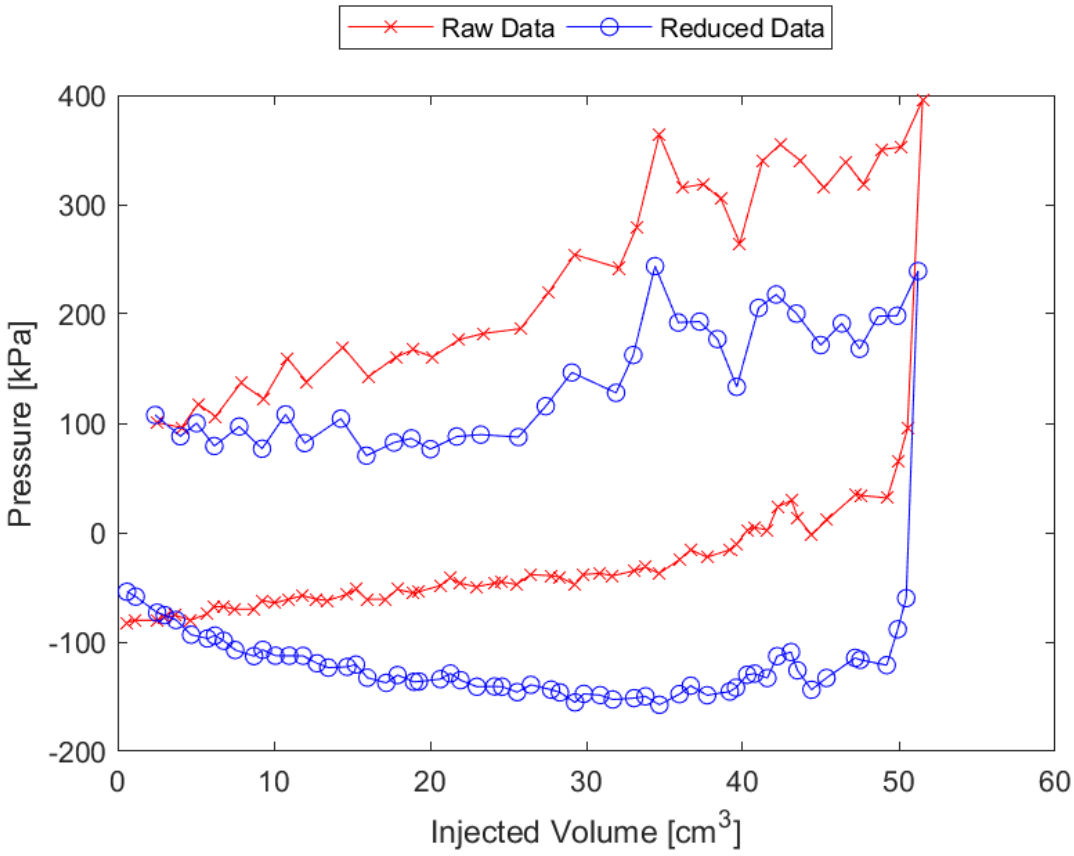

Figure C.20: Sounding 111, SDPMT-12 Continuous Test, Membrane O.D. 0.625m, Depth 0.38 m, Raw and Reduced Data

Table C.20: Sounding 111, SDPMT-12 Continuous Test, Result Summary

Parameter				
Lift-Off Pressure (p_0)	87.4	kPa	12.67	psi
Contact Volume (V_c)	25.6	cm^3	1.57	in^3
Limit Pressure (p_L)	160.0	kPa	23.21	psi
Assumed ν		0.33		
Initial Modulus (E_0)	2478.6	kPa	359.49	psi
Dry Unit Weight (γ_{dry})	1776.4	kg/m^3	110.9	lb/ft^3
Wet Unit Weight (γ_{wet})	1944.6	kg/m^3	121.4	lb/ft^3

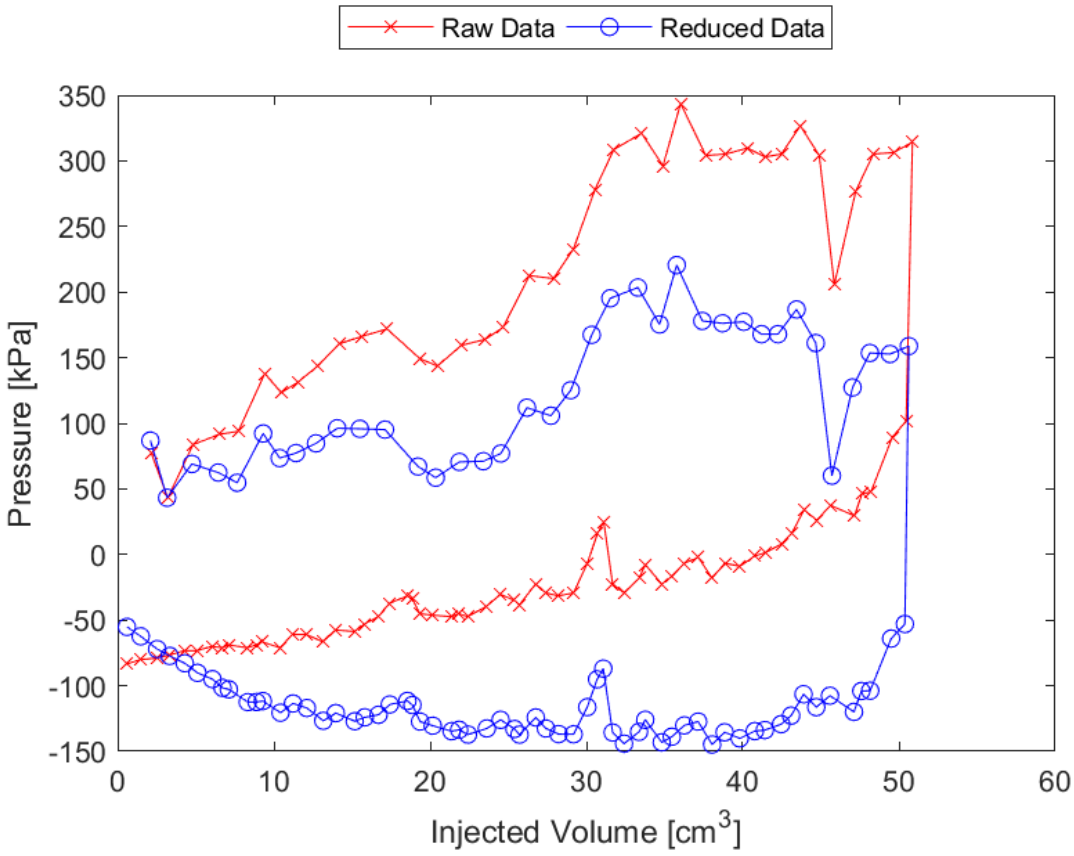

Figure C.21: Sounding 112, SDPMT-12 Continuous Test, Membrane O.D. 0.625m, Depth 0.38 m, Raw and Reduced Data

Table C.21: Sounding 112, SDPMT-12 Continuous Test, Result Summary

Parameter				
Lift-Off Pressure (p_0)	77.0	kPa	11.16	psi
Contact Volume (V_c)	24.5	cm^3	1.50	in^3
Limit Pressure (p_L)	455.0	kPa	65.99	psi
Assumed ν		0.33		
Initial Modulus (E_0)	5625.8	kPa	815.96	psi
Dry Unit Weight (γ_{dry})	1834.1	kg/m^3	114.5	lb/ft^3
Wet Unit Weight (γ_{wet})	1995.9	kg/m^3	124.6	lb/ft^3

Appendix D

Heritage Parkway Pressuremeter Test Results

D.1 SDPMT-6 Incremental Test Data

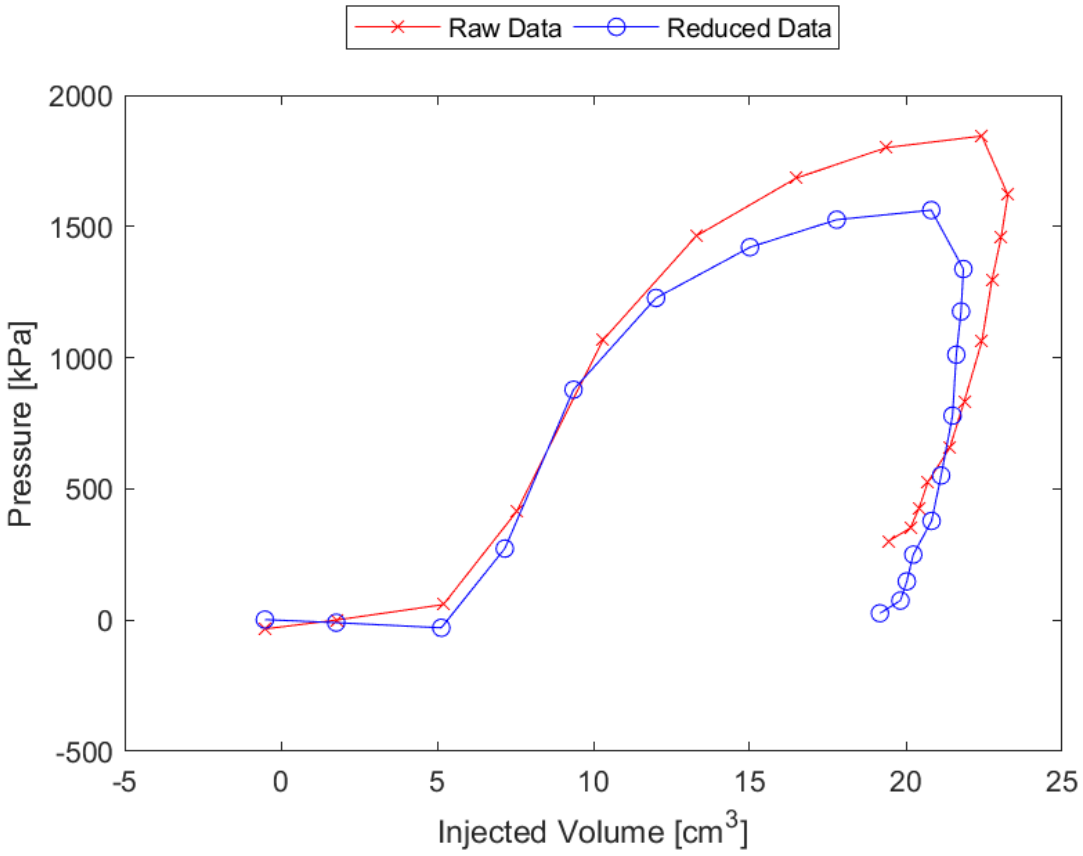

Figure D.1: Sounding 301, SDPMT-6 Incremental Test, Membrane O.D. 0.6875m, Depth 0.25 m, Raw and Reduced Data

Table D.1: Sounding 301, SDPMT-6 Incremental Test, Result Summary

Parameter				
Lift-Off Pressure (p_0)	−29.2	kPa	−4.24	psi
Contact Volume (V_c)	5.1	cm^3	0.31	in^3
Limit Pressure (p_L)	2135.0	kPa	309.66	psi
Assumed ν		0.33		
Initial Modulus (E_0)	24726.0	kPa	3586.21	psi
Dry Unit Weight (γ_{dry})	2023.1	kg/m^3	126.3	lb/ft^3
Wet Unit Weight (γ_{wet})	2104.8	kg/m^3	131.4	lb/ft^3

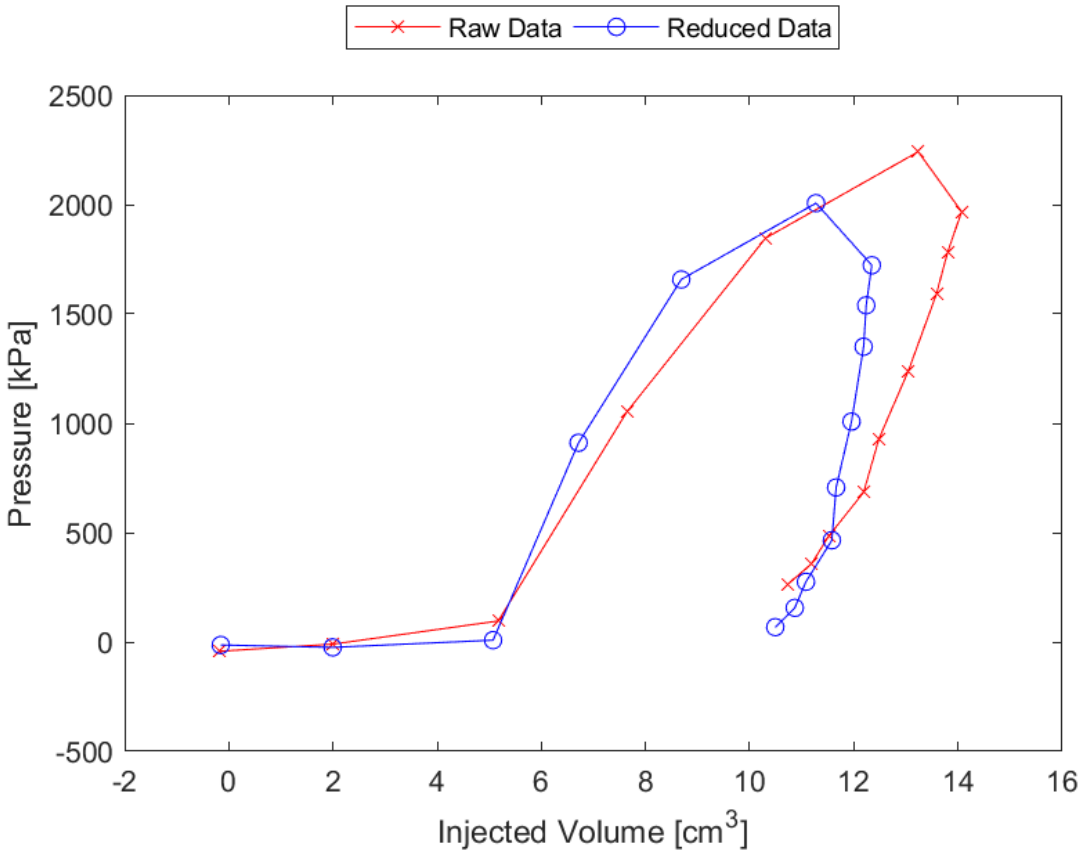

Figure D.2: Sounding 302, SDPMT-6 Incremental Test, Membrane O.D. 0.6875m, Depth 0.25 m, Raw and Reduced Data

Table D.2: Sounding 302, SDPMT-6 Incremental Test, Result Summary

Parameter				
Lift-Off Pressure (p_0)	8.3	kPa	1.20	psi
Contact Volume (V_c)	5.1	cm^3	0.31	in^3
Limit Pressure (p_L)	2750.0	kPa	398.85	psi
Assumed ν		0.33		
Initial Modulus (E_0)	52207.3	kPa	7572.04	psi
Dry Unit Weight (γ_{dry})	2007.1	kg/m^3	125.3	lb/ft^3
Wet Unit Weight (γ_{wet})	2080.8	kg/m^3	129.9	lb/ft^3

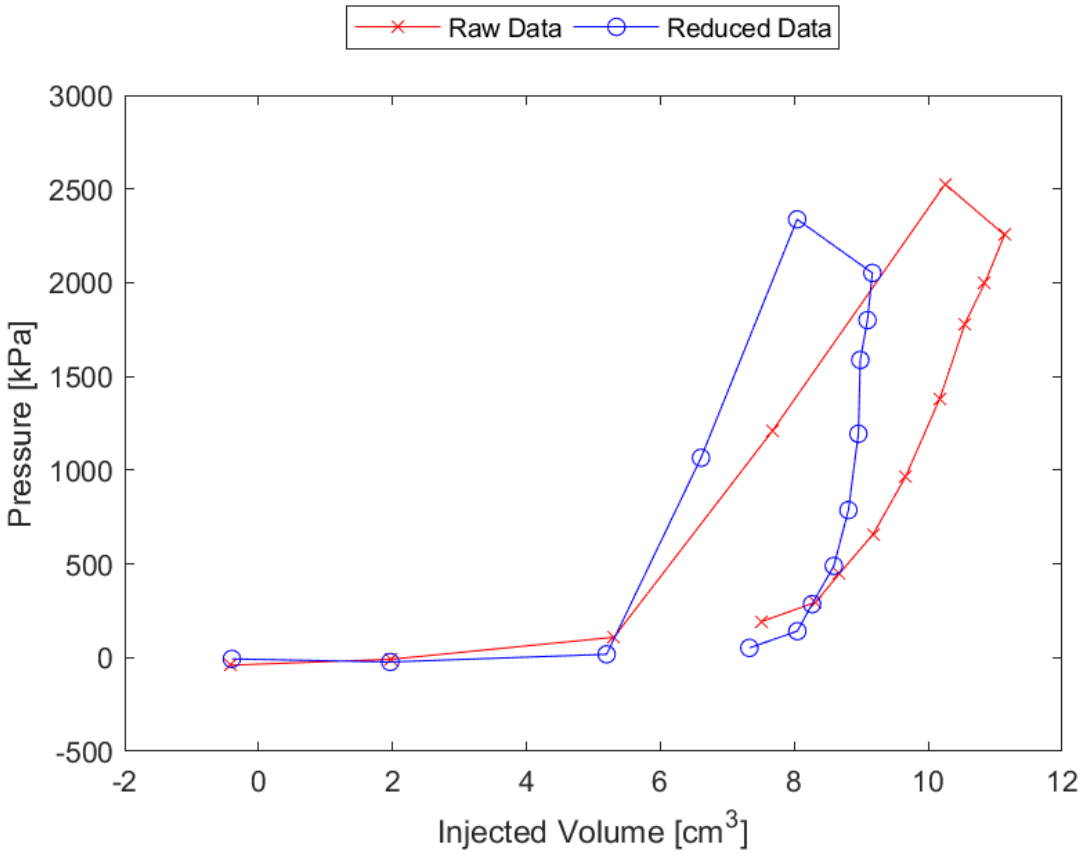

Figure D.3: Sounding 303, SDPMT-6 Incremental Test, Membrane O.D. 0.6875m, Depth 0.25 m, Raw and Reduced Data

Table D.3: Sounding 303, SDPMT-6 Incremental Test, Result Summary

Parameter				
Lift-Off Pressure (p_0)	17.7	kPa	2.57	psi
Contact Volume (V_c)	5.2	cm^3	0.32	in^3
Limit Pressure (p_L)	5000.0	kPa	725.19	psi
Assumed ν		0.33		
Initial Modulus (E_0)	92682.9	kPa	13442.55	psi
Dry Unit Weight (γ_{dry})	2040.8	kg/m^3	127.4	lb/ft^3
Wet Unit Weight (γ_{wet})	2111.2	kg/m^3	131.8	lb/ft^3

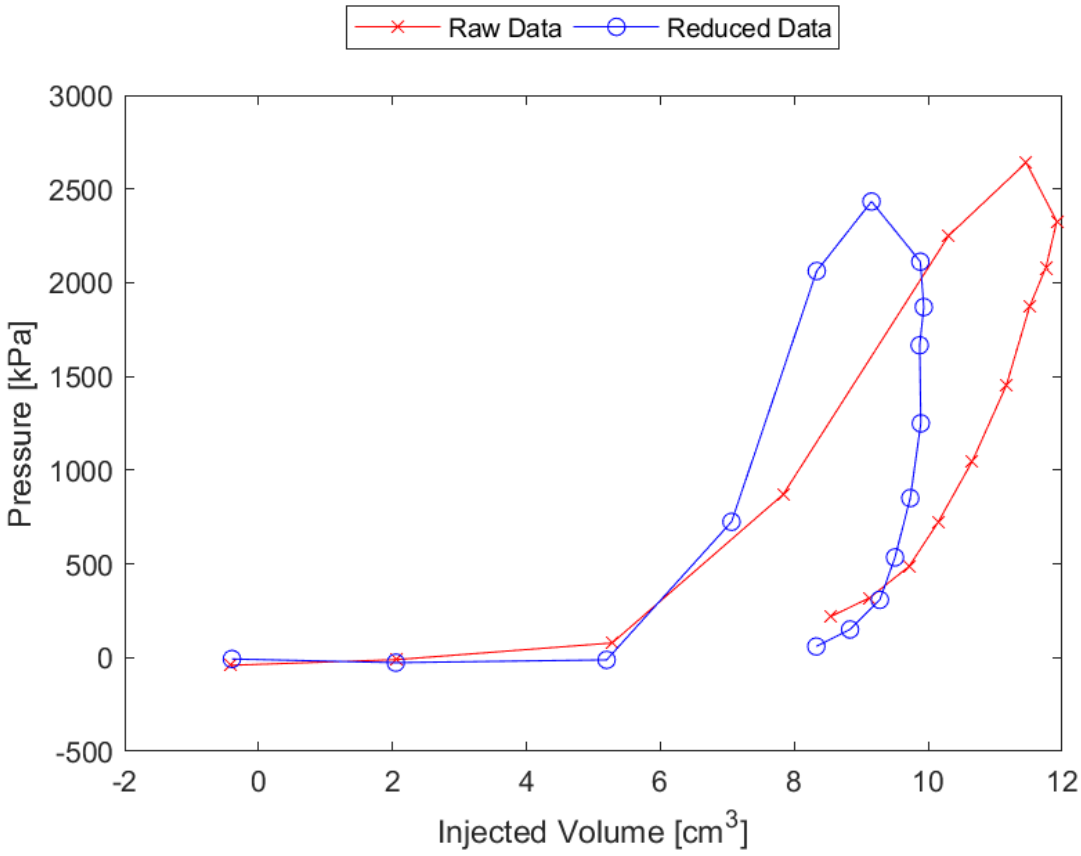

Figure D.4: Sounding 304, SDPMT-6 Incremental Test, Membrane O.D. 0.6875m, Depth 0.25 m, Raw and Reduced Data

Table D.4: Sounding 304, SDPMT-6 Incremental Test, Result Summary

Parameter				
Lift-Off Pressure (p_0)	−12.2	kPa	−1.77	psi
Contact Volume (V_c)	5.2	cm^3	0.32	in^3
Limit Pressure (p_L)	5000.0	kPa	725.19	psi
Assumed ν		0.33		
Initial Modulus (E_0)	122484.0	kPa	17764.83	psi
Dry Unit Weight (γ_{dry})	2056.8	kg/m^3	128.4	lb/ft^3
Wet Unit Weight (γ_{wet})	2119.2	kg/m^3	132.3	lb/ft^3

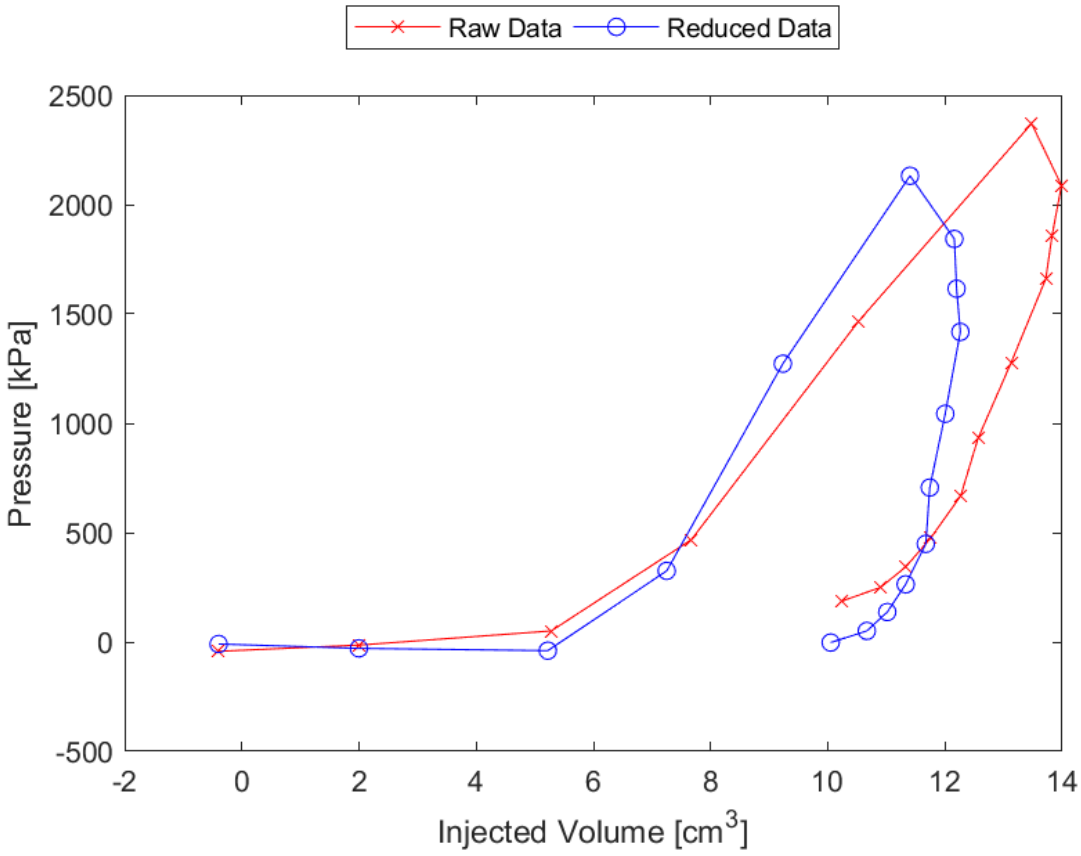

Figure D.5: Sounding 305, SDPMT-6 Incremental Test, Membrane O.D. 0.6875m, Depth 0.25 m, Raw and Reduced Data

Table D.5: Sounding 305, SDPMT-6 Incremental Test, Result Summary

Parameter				
Lift-Off Pressure (p_0)	−39.7	kPa	−5.75	psi
Contact Volume (V_c)	5.2	cm^3	0.32	in^3
Limit Pressure (p_L)	4700.0	kPa	681.68	psi
Assumed ν		0.33		
Initial Modulus (E_0)	52583.6	kPa	7626.61	psi
Dry Unit Weight (γ_{dry})	2056.8	kg/m^3	128.4	lb/ft^3
Wet Unit Weight (γ_{wet})	2146.5	kg/m^3	134.0	lb/ft^3

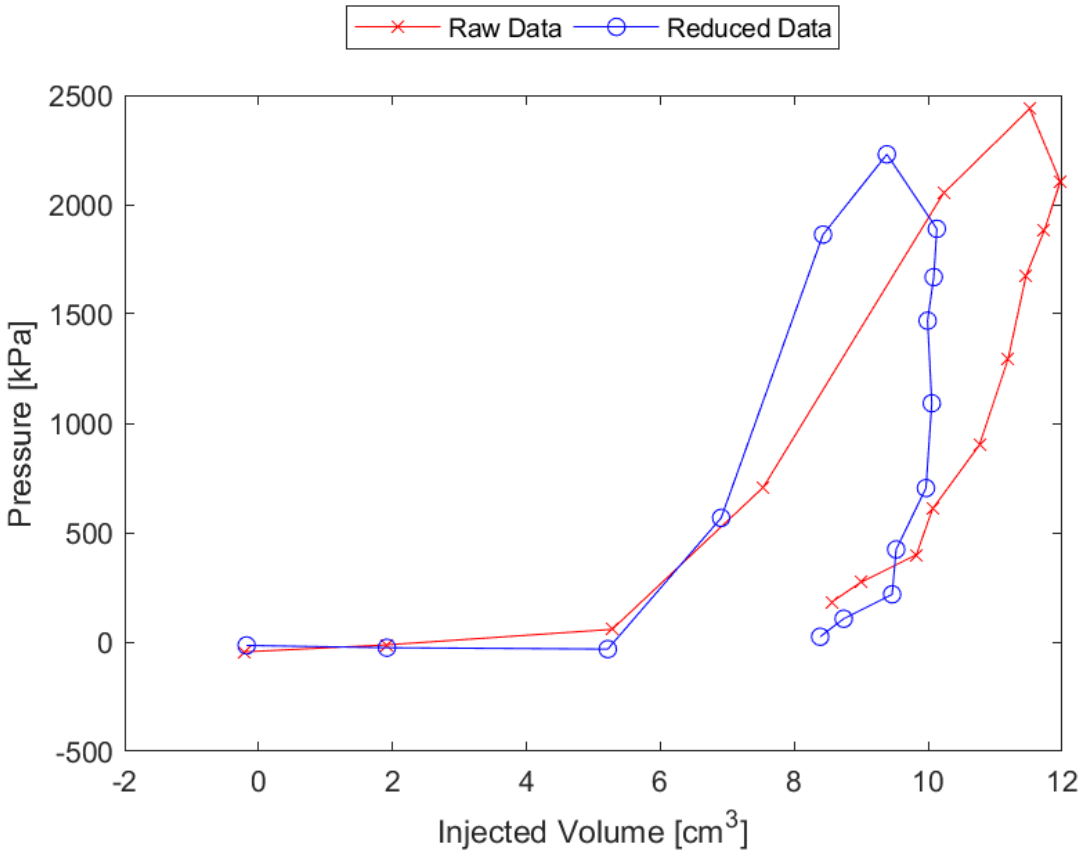

Figure D.6: Sounding 306, SDPMT-6 Incremental Test, Membrane O.D. 0.6875m, Depth 0.25 m, Raw and Reduced Data

Table D.6: Sounding 306, SDPMT-6 Incremental Test, Result Summary

Parameter				
Lift-Off Pressure (p_0)	6.9	kPa	1.00	psi
Contact Volume (V_c)	5.2	cm^3	0.32	in^3
Limit Pressure (p_L)	6425.0	kPa	931.87	psi
Assumed ν		0.33		
Initial Modulus (E_0)	99175.1	kPa	14384.15	psi
Dry Unit Weight (γ_{dry})	2045.6	kg/m^3	127.7	lb/ft^3
Wet Unit Weight (γ_{wet})	2122.4	kg/m^3	132.5	lb/ft^3

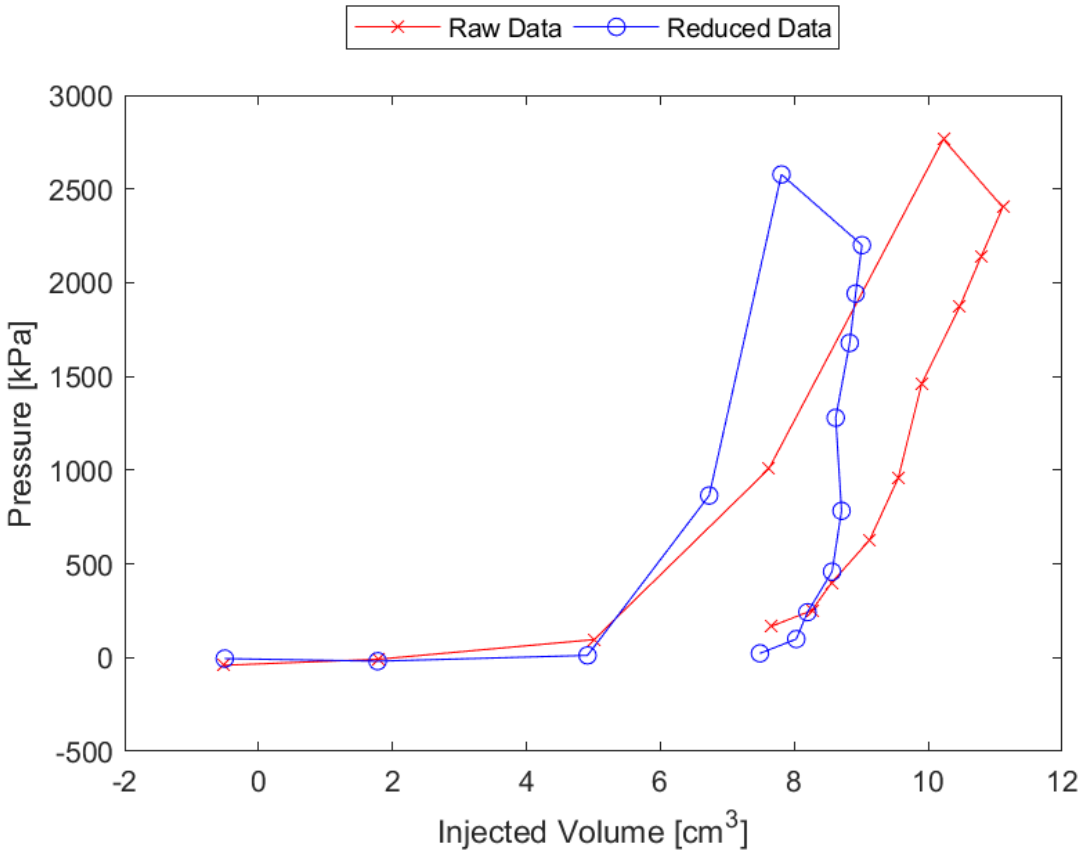

Figure D.7: Sounding 307, SDPMT-6 Incremental Test, Membrane O.D. 0.6875m, Depth 0.25 m, Raw and Reduced Data

Table D.7: Sounding 307, SDPMT-6 Incremental Test, Result Summary

Parameter				
Lift-Off Pressure (p_0)	11.9	kPa	1.73	psi
Contact Volume (V_c)	4.9	cm^3	0.30	in^3
Limit Pressure (p_L)	5560.0	kPa	806.41	psi
Assumed ν		0.33		
Initial Modulus (E_0)	183144.8	kPa	26562.96	psi
Dry Unit Weight (γ_{dry})	1978.3	kg/m^3	123.5	lb/ft^3
Wet Unit Weight (γ_{wet})	2035.9	kg/m^3	127.1	lb/ft^3

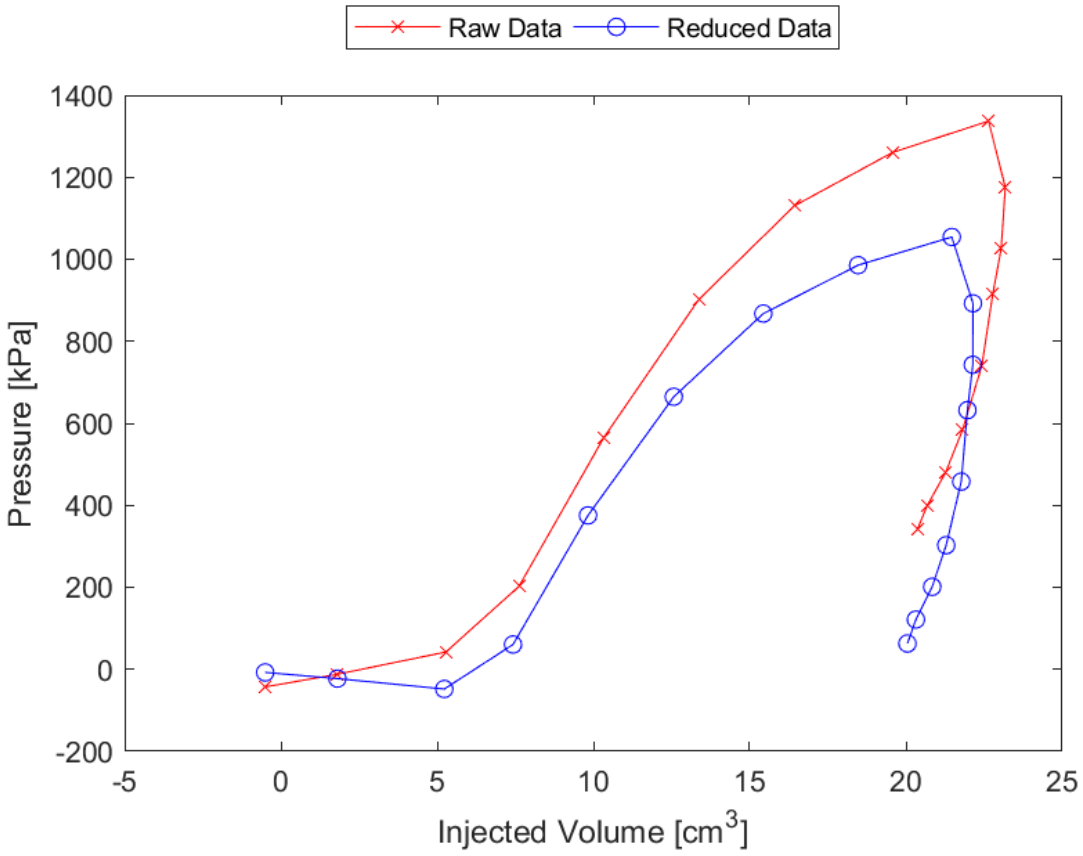

Figure D.8: Sounding 308, SDPMT-6 Incremental Test, Membrane O.D. 0.6875m, Depth 0.25 m, Raw and Reduced Data

Table D.8: Sounding 308, SDPMT-6 Incremental Test, Result Summary

Parameter				
Lift-Off Pressure (p_0)	−48.0	kPa	−6.96	psi
Contact Volume (V_c)	5.2	cm^3	0.32	in^3
Limit Pressure (p_L)	1140.0	kPa	165.34	psi
Assumed ν		0.33		
Initial Modulus (E_0)	14404.9	kPa	2089.25	psi
Dry Unit Weight (γ_{dry})	2037.5	kg/m^3	127.2	lb/ft^3
Wet Unit Weight (γ_{wet})	2124.0	kg/m^3	132.6	lb/ft^3

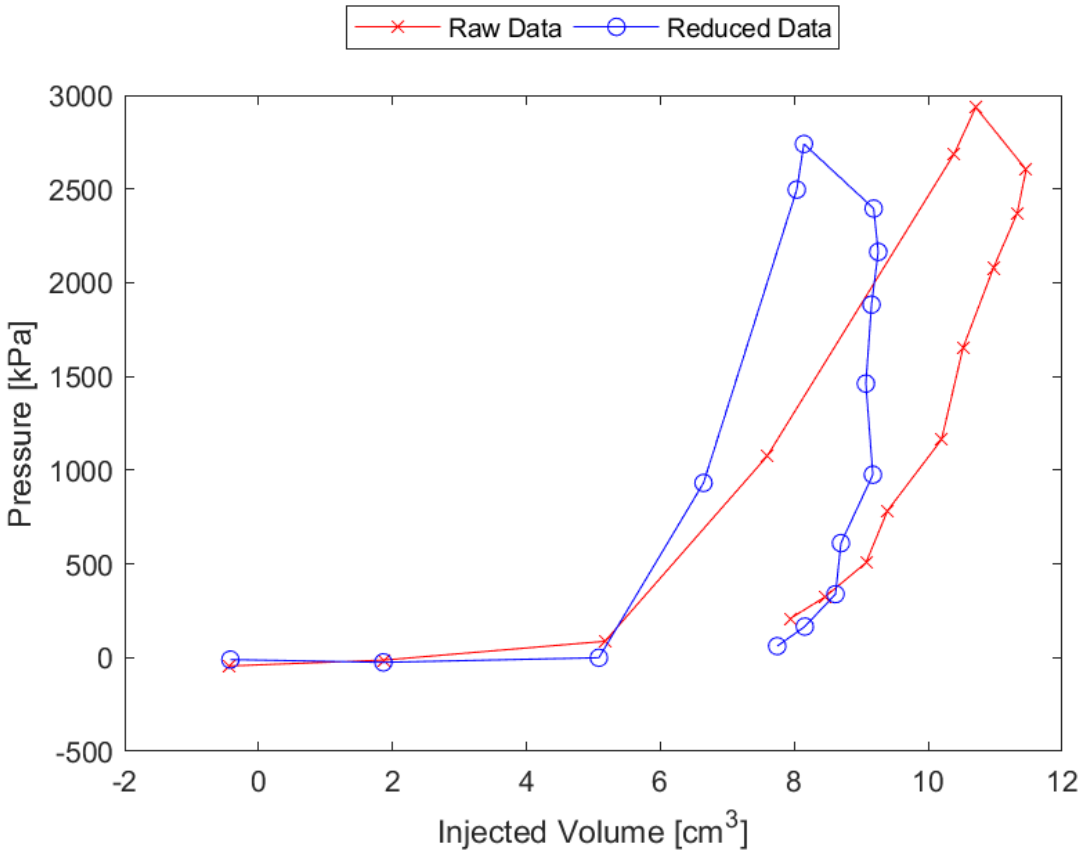

Figure D.9: Sounding 309, SDPMT-6 Incremental Test, Membrane O.D. 0.6875m, Depth 0.25 m, Raw and Reduced Data

Table D.9: Sounding 309, SDPMT-6 Incremental Test, Result Summary

Parameter				
Lift-Off Pressure (p_0)	−0.7	kPa	−0.11	psi
Contact Volume (V_c)	5.1	cm^3	0.31	in^3
Limit Pressure (p_L)	9526.0	kPa	1381.63	psi
Assumed ν		0.33		
Initial Modulus (E_0)	18830.9	kPa	2731.20	psi
Dry Unit Weight (γ_{dry})	2103.2	kg/m^3	131.3	lb/ft^3
Wet Unit Weight (γ_{wet})	2172.1	kg/m^3	135.6	lb/ft^3

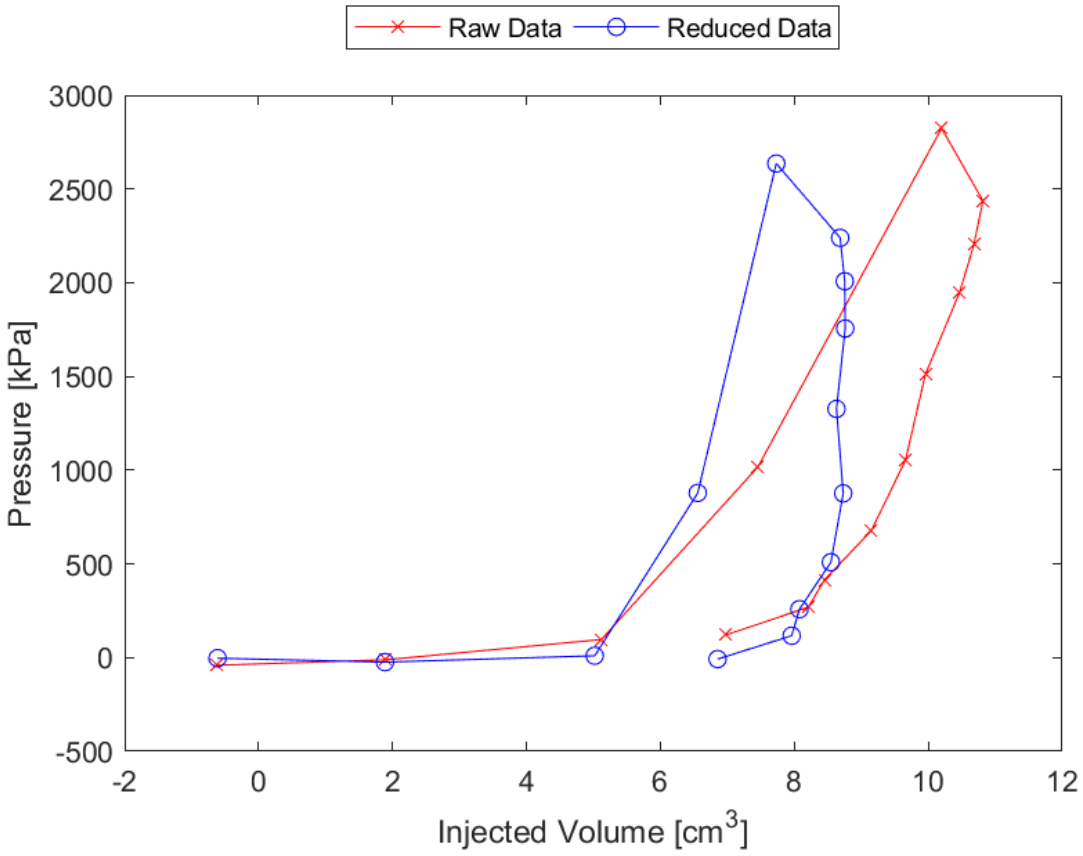

Figure D.10: Sounding 310, SDPMT-6 Incremental Test, Membrane O.D. 0.6875m, Depth 0.25 m, Raw and Reduced Data

Table D.10: Sounding 310, SDPMT-6 Incremental Test, Result Summary

Parameter				
Lift-Off Pressure (p_0)	9.9	kPa	1.43	psi
Contact Volume (V_c)	5.0	cm^3	0.31	in^3
Limit Pressure (p_L)	6275.0	kPa	910.11	psi
Assumed ν		0.33		
Initial Modulus (E_0)	172444.7	kPa	25011.04	psi
Dry Unit Weight (γ_{dry})	1992.7	kg/m^3	124.4	lb/ft^3
Wet Unit Weight (γ_{wet})	2056.8	kg/m^3	128.4	lb/ft^3

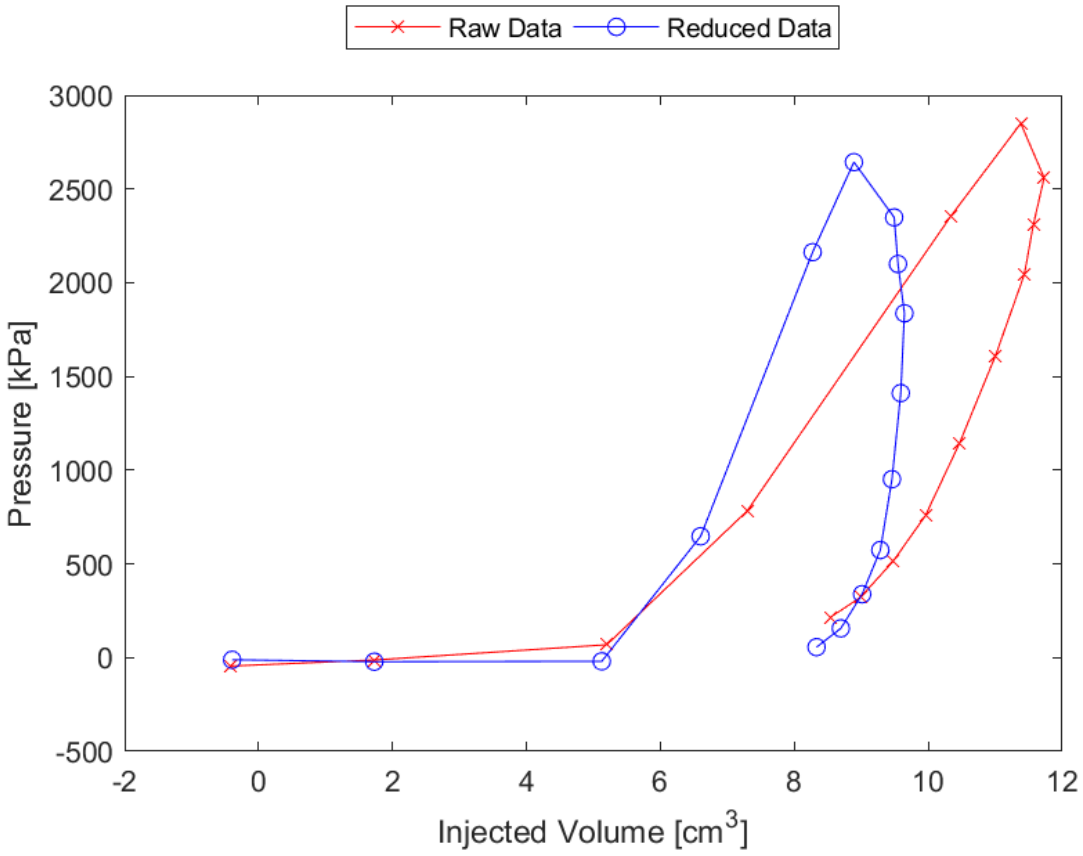

Figure D.11: Sounding 311, SDPMT-6 Incremental Test, Membrane O.D. 0.6875m, Depth 0.25 m, Raw and Reduced Data

Table D.11: Sounding 311, SDPMT-6 Incremental Test, Result Summary

Parameter				
Lift-Off Pressure (p_0)	−19.8	kPa	−2.87	psi
Contact Volume (V_c)	5.1	cm^3	0.31	in^3
Limit Pressure (p_L)	7620.0	kPa	1105.19	psi
Assumed ν		0.33		
Initial Modulus (E_0)	101724.7	kPa	14753.94	psi
Dry Unit Weight (γ_{dry})	2010.3	kg/m^3	125.5	lb/ft^3
Wet Unit Weight (γ_{wet})	2084.0	kg/m^3	130.1	lb/ft^3

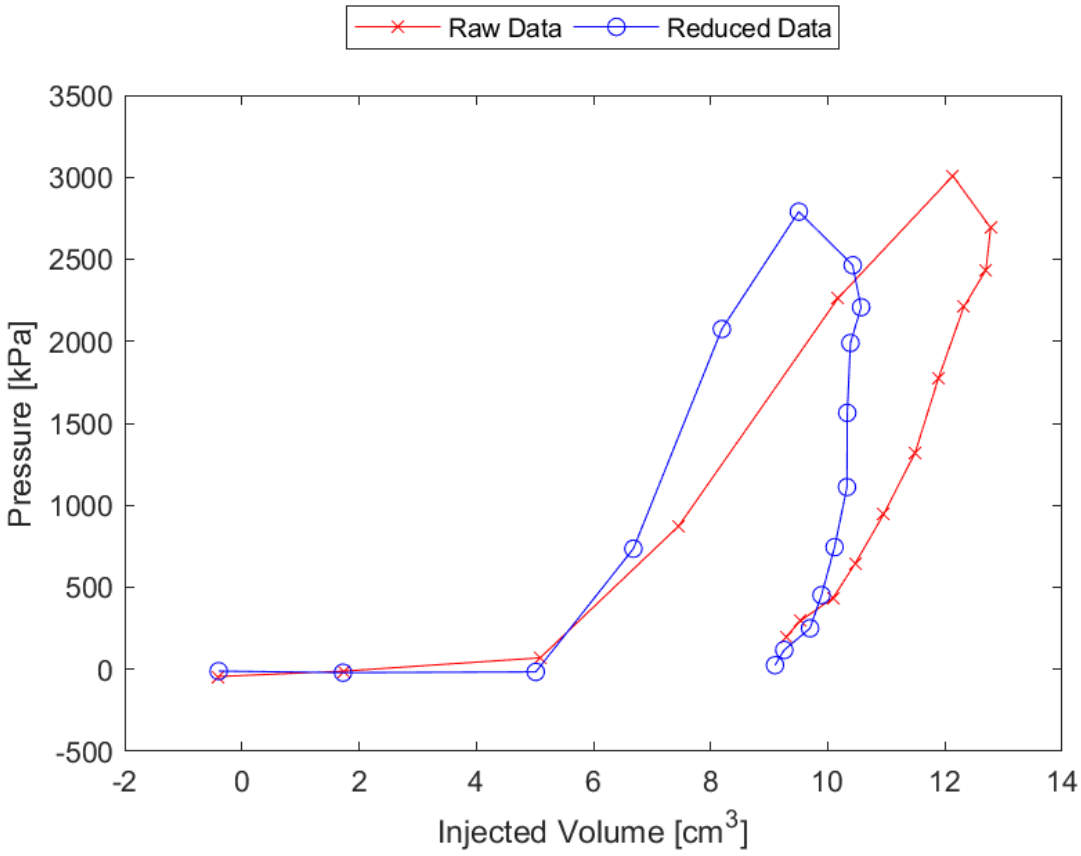

Figure D.12: Sounding 312, SDPMT-6 Incremental Test, Membrane O.D. 0.6875m, Depth 0.25 m, Raw and Reduced Data

Table D.12: Sounding 312, SDPMT-6 Incremental Test, Result Summary

Parameter				
Lift-Off Pressure (p_0)	−15.9	kPa	−2.30	psi
Contact Volume (V_c)	5.0	cm^3	0.31	in^3
Limit Pressure (p_L)	7060.0	kPa	1023.97	psi
Assumed ν		0.33		
Initial Modulus (E_0)	85598.7	kPa	12415.07	psi
Dry Unit Weight (γ_{dry})	2037.5	kg/m^3	127.2	lb/ft^3
Wet Unit Weight (γ_{wet})	2108.0	kg/m^3	131.6	lb/ft^3

D.2 SDPMT-6 Continuous Test Data

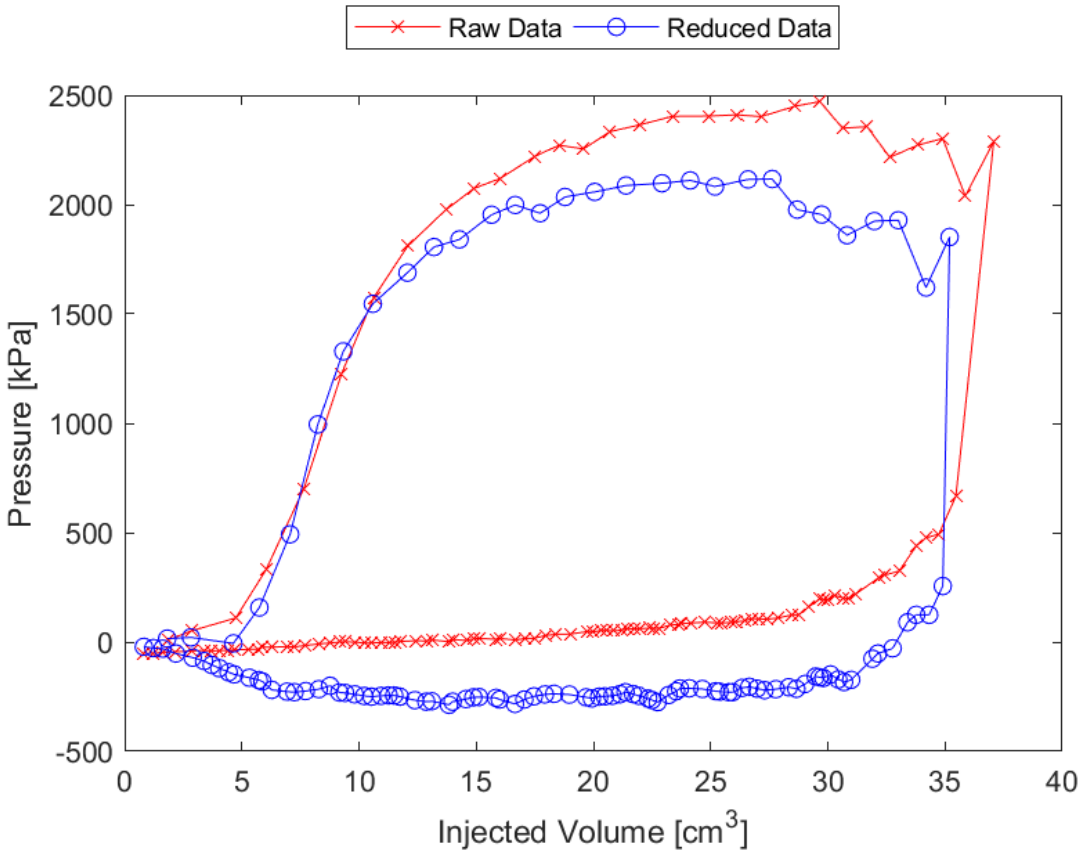

Figure D.13: Sounding 301, SDPMT-6 Continuous Test, Membrane O.D. 0.6875m, Depth 0.25 m, Raw and Reduced Data

Table D.13: Sounding 301, SDPMT-6 Continuous Test, Result Summary

Parameter				
Lift-Off Pressure (p_0)	−6.4	kPa	−0.93	psi
Contact Volume (V_c)	4.6	cm^3	0.28	in^3
Limit Pressure (p_L)	2200.0	kPa	319.08	psi
Assumed ν		0.33		
Initial Modulus (E_0)	43440.8	kPa	6300.56	psi
Dry Unit Weight (γ_{dry})	2023.1	kg/m^3	126.3	lb/ft^3
Wet Unit Weight (γ_{wet})	2159.3	kg/m^3	134.8	lb/ft^3

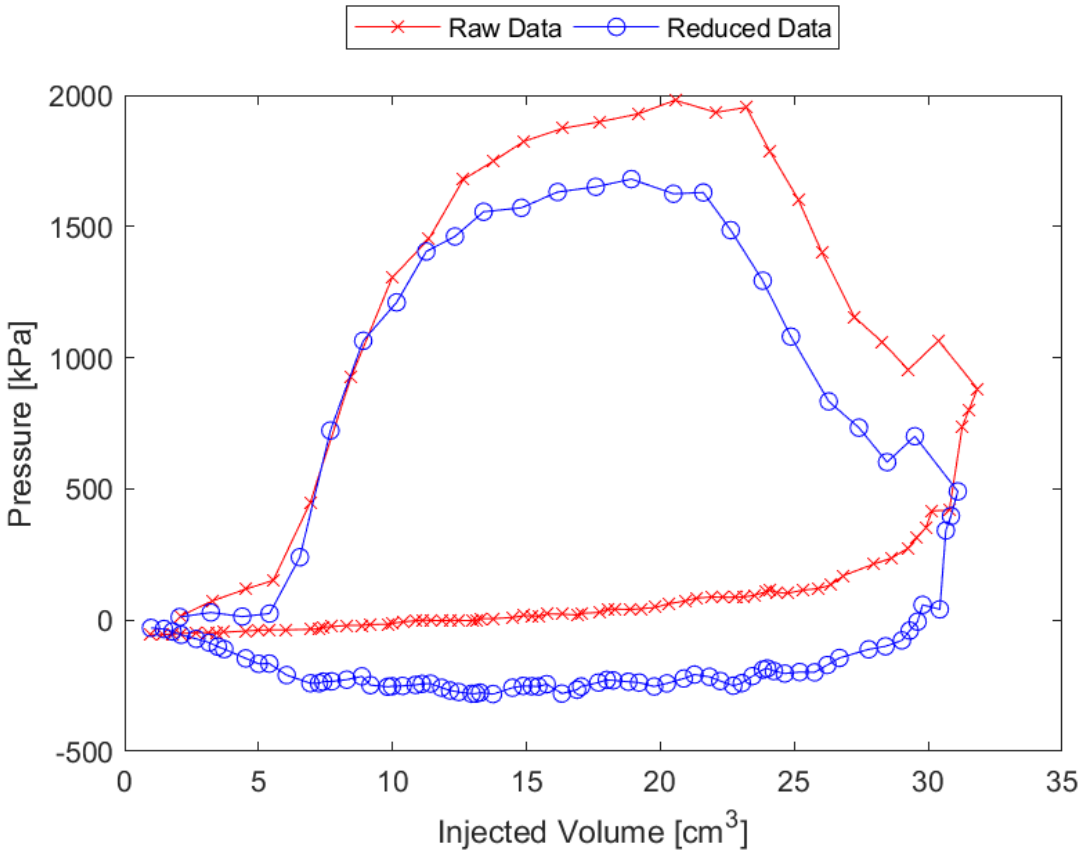

Figure D.14: Sounding 302, SDPMT-6 Continuous Test, Membrane O.D. 0.6875m, Depth 0.25 m, Raw and Reduced Data

Table D.14: Sounding 302, SDPMT-6 Continuous Test, Result Summary

Parameter				
Lift-Off Pressure (p_0)	24.8	kPa	3.60	psi
Contact Volume (V_c)	24.8	cm^3	1.52	in^3
Limit Pressure (p_L)	1965.0	kPa	285.00	psi
Assumed ν		0.33		
Initial Modulus (E_0)	40681.8	kPa	5900.41	psi
Dry Unit Weight (γ_{dry})	2007.1	kg/m^3	125.3	lb/ft^3
Wet Unit Weight (γ_{wet})	2082.4	kg/m^3	130.0	lb/ft^3

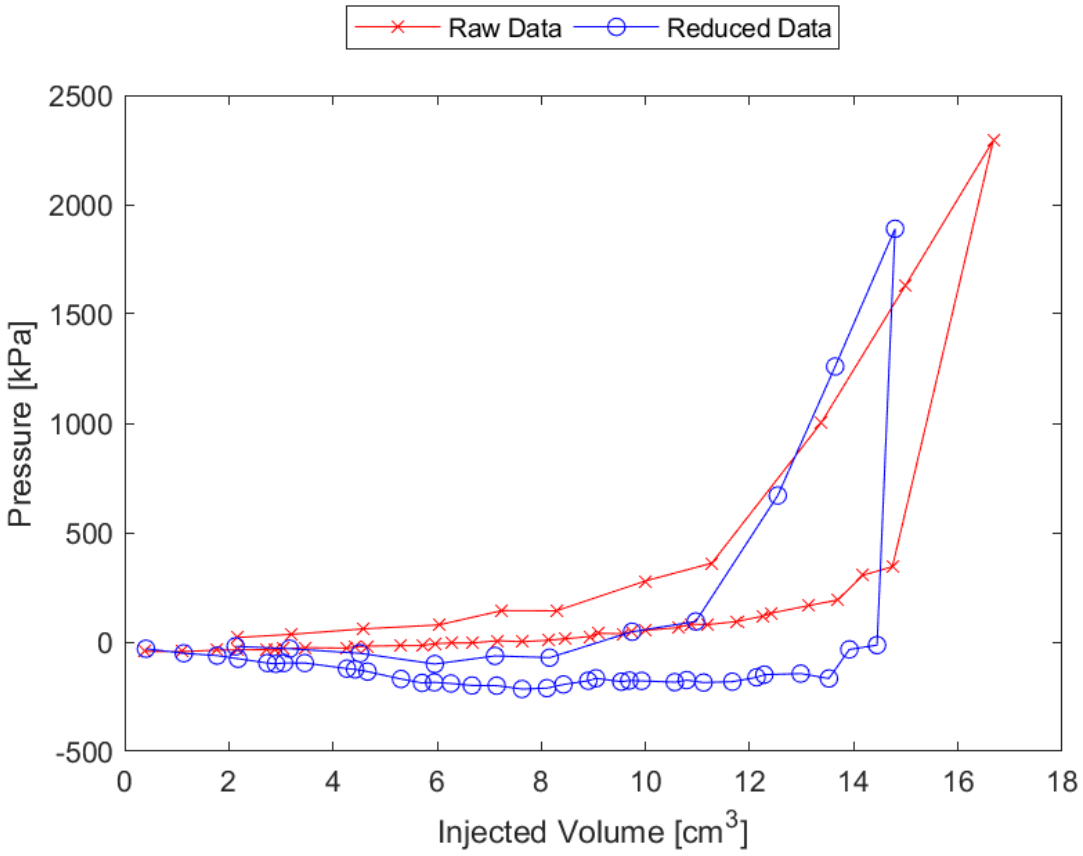

Figure D.15: Sounding 303, SDPMT-6 Continuous Test, Membrane O.D. 0.6875m, Depth 0.25 m, Raw and Reduced Data

Table D.15: Sounding 303, SDPMT-6 Continuous Test, Result Summary

Parameter				
Lift-Off Pressure (p_0)	46.9	kPa	6.81	psi
Contact Volume (V_c)	9.7	cm^3	0.59	in^3
Limit Pressure (p_L)	2500.0	kPa	362.60	psi
Assumed ν		0.33		
Initial Modulus (E_0)	61178.1	kPa	8873.15	psi
Dry Unit Weight (γ_{dry})	2040.8	kg/m^3	127.4	lb/ft^3
Wet Unit Weight (γ_{wet})	2108.0	kg/m^3	131.6	lb/ft^3

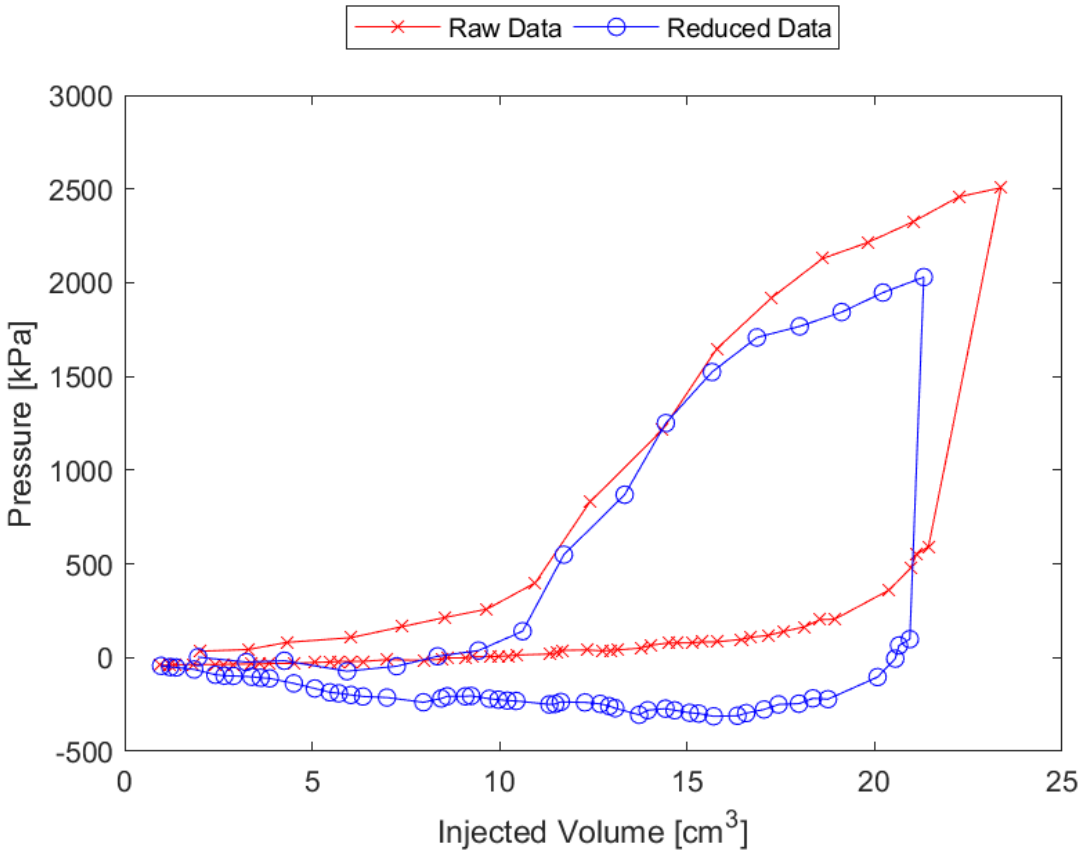

Figure D.16: Sounding 304, SDPMT-6 Continuous Test, Membrane O.D. 0.6875m, Depth 0.25 m, Raw and Reduced Data

Table D.16: Sounding 304, SDPMT-6 Continuous Test, Result Summary

Parameter				
Lift-Off Pressure (p_0)	37.6	kPa	5.45	psi
Contact Volume (V_c)	9.4	cm^3	0.58	in^3
Limit Pressure (p_L)	2500.0	kPa	362.60	psi
Assumed ν		0.33		
Initial Modulus (E_0)	37606.7	kPa	5454.40	psi
Dry Unit Weight (γ_{dry})	2045.6	kg/m^3	127.7	lb/ft^3
Wet Unit Weight (γ_{wet})	2116.0	kg/m^3	132.1	lb/ft^3

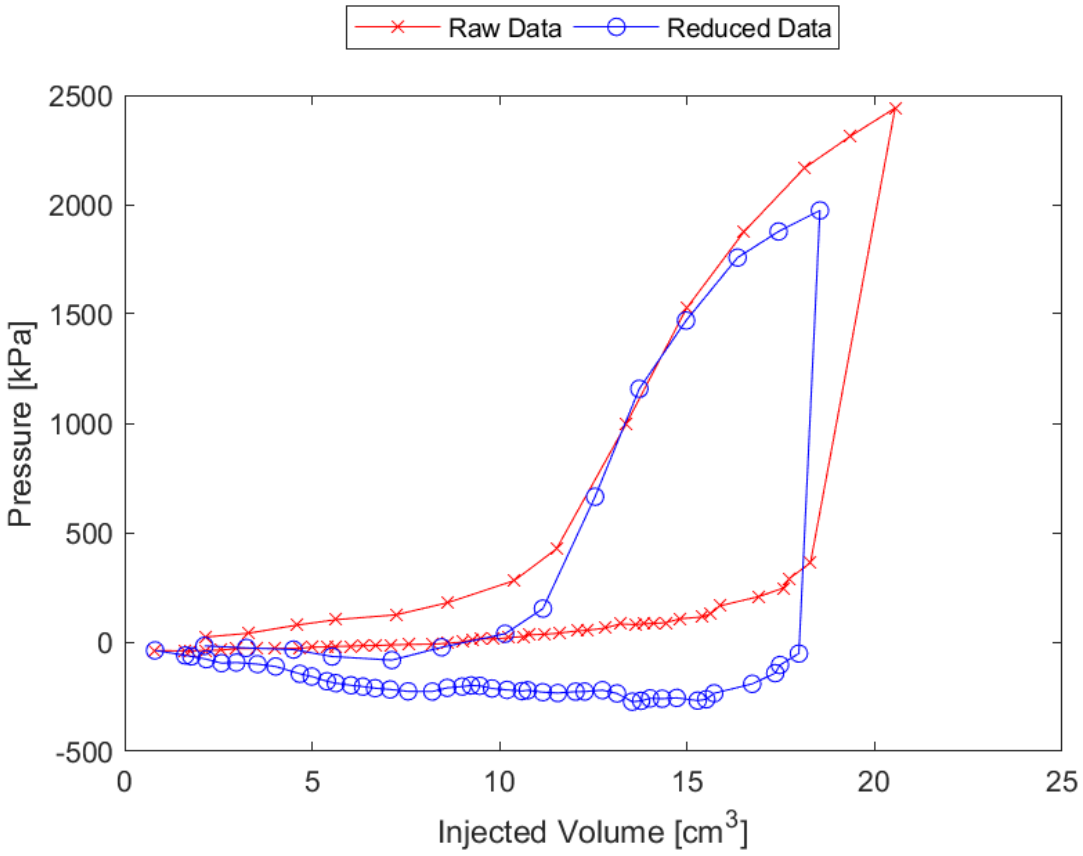

Figure D.17: Sounding 305, SDPMT-6 Continuous Test, Membrane O.D. 0.6875m, Depth 0.25 m, Raw and Reduced Data

Table D.17: Sounding 305, SDPMT-6 Continuous Test, Result Summary

Parameter				
Lift-Off Pressure (p_0)	37.7	kPa	5.46	psi
Contact Volume (V_c)	10.1	cm^3	0.62	in^3
Limit Pressure (p_L)	2500.0	kPa	362.60	psi
Assumed ν		0.33		
Initial Modulus (E_0)	50522.7	kPa	7327.71	psi
Dry Unit Weight (γ_{dry})	2056.8	kg/m^3	128.4	lb/ft^3
Wet Unit Weight (γ_{wet})	2119.2	kg/m^3	132.3	lb/ft^3

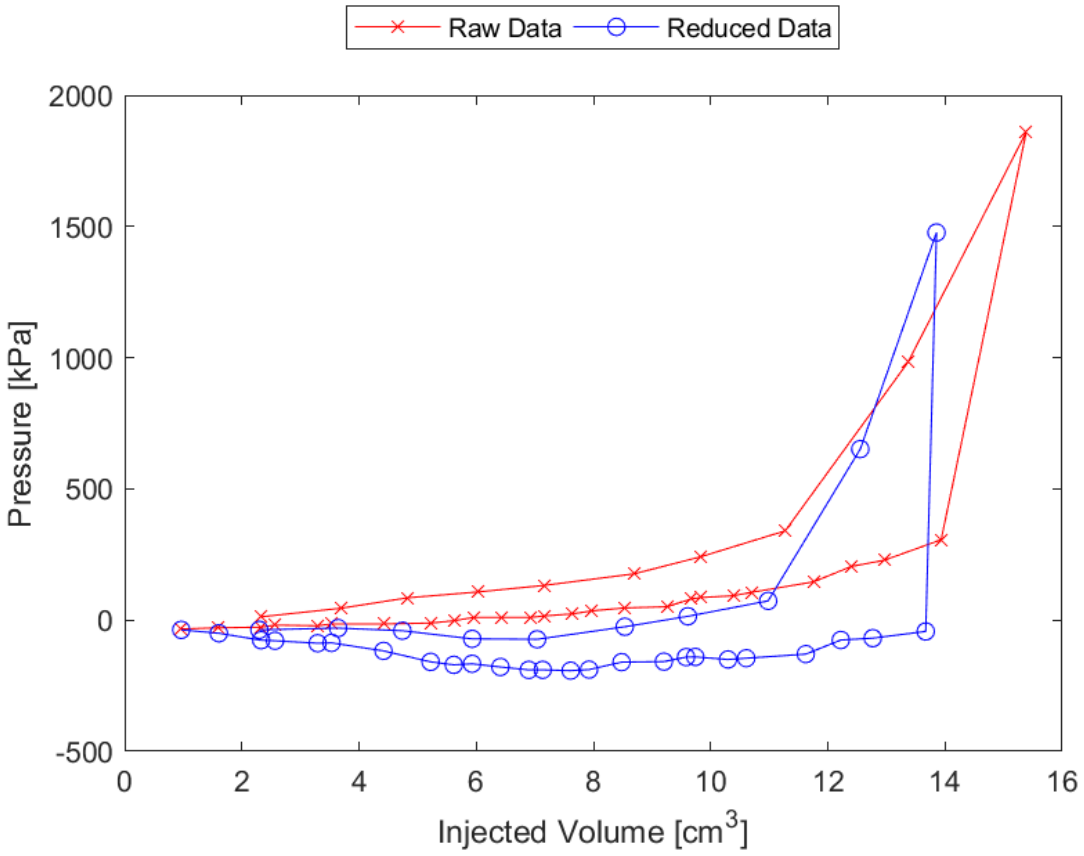

Figure D.18: Sounding 306, SDPMT-6 Continuous Test, Membrane O.D. 0.6875m, Depth 0.25 m, Raw and Reduced Data

Table D.18: Sounding 306, SDPMT-6 Continuous Test, Result Summary

Parameter				
Lift-Off Pressure (p_0)	73.4	kPa	10.65	psi
Contact Volume (V_c)	11.0	cm^3	0.67	in^3
Limit Pressure (p_L)	2250.0	kPa	326.34	psi
Assumed ν		0.33		
Initial Modulus (E_0)	63069.2	kPa	9147.43	psi
Dry Unit Weight (γ_{dry})	2045.6	kg/m^3	127.7	lb/ft^3
Wet Unit Weight (γ_{wet})	2119.2	kg/m^3	132.3	lb/ft^3

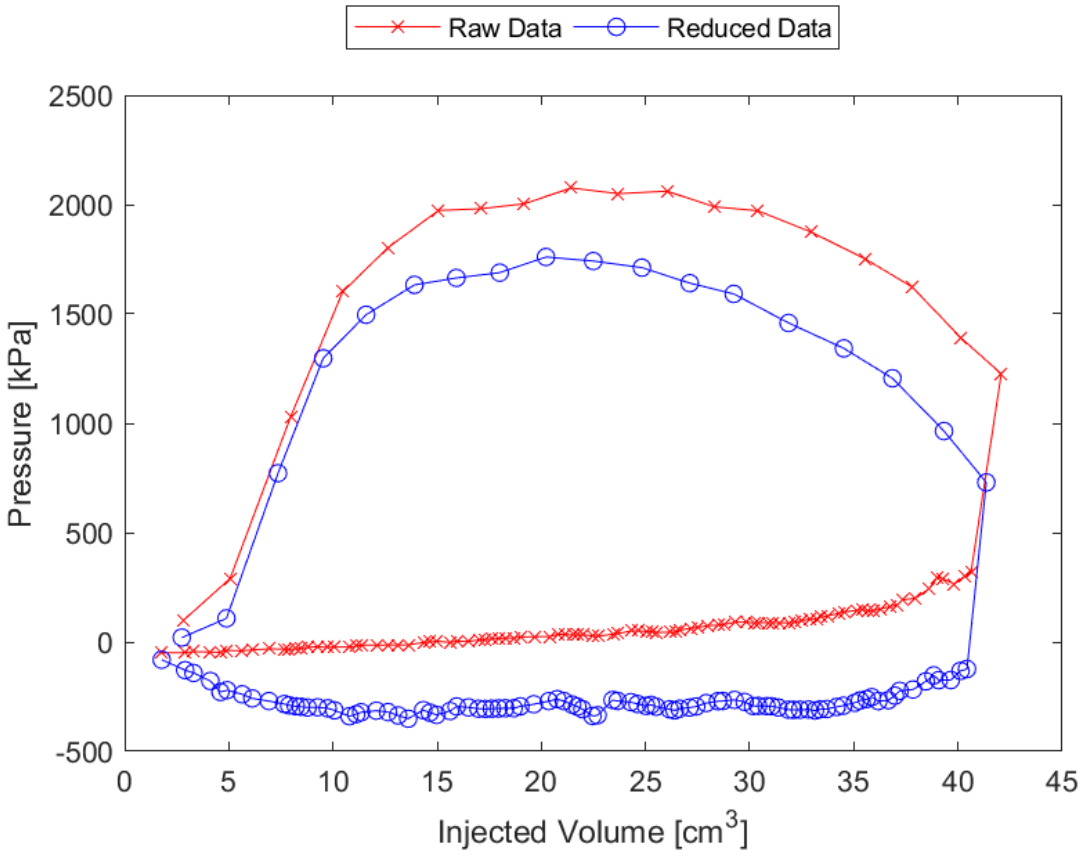

Figure D.19: Sounding 307, SDPMT-6 Continuous Test, Membrane O.D. 0.6875m, Depth 0.25 m, Raw and Reduced Data

Table D.19: Sounding 307, SDPMT-6 Continuous Test, Result Summary

Parameter				
Lift-Off Pressure (p_0)	108.0	kPa	15.67	psi
Contact Volume (V_c)	4.9	cm^3	0.30	in^3
Limit Pressure (p_L)	2050.0	kPa	297.33	psi
Assumed ν		0.33		
Initial Modulus (E_0)	29505.2	kPa	4279.37	psi
Dry Unit Weight (γ_{dry})	1978.3	kg/m^3	123.5	lb/ft^3
Wet Unit Weight (γ_{wet})	2092.0	kg/m^3	130.6	lb/ft^3

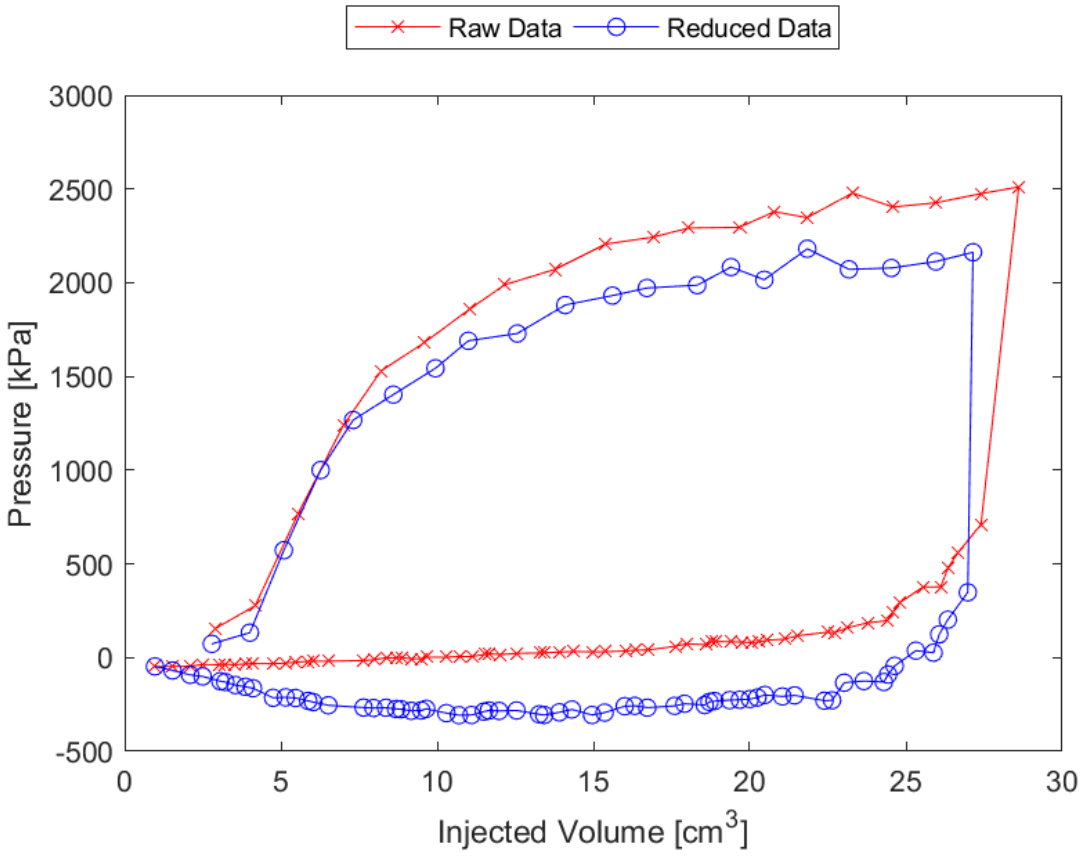

Figure D.20: Sounding 308, SDPMT-6 Continuous Test, Membrane O.D. 0.6875m, Depth 0.25 m, Raw and Reduced Data

Table D.20: Sounding 308, SDPMT-6 Continuous Test, Result Summary

Parameter				
Lift-Off Pressure (p_0)	133.0	kPa	19.29	psi
Contact Volume (V_c)	4.0	cm^3	0.24	in^3
Limit Pressure (p_L)	2500.0	kPa	362.60	psi
Assumed ν		0.33		
Initial Modulus (E_0)	42017.0	kPa	6094.07	psi
Dry Unit Weight (γ_{dry})	2037.5	kg/m^3	127.2	lb/ft^3
Wet Unit Weight (γ_{wet})	2217.0	kg/m^3	138.4	lb/ft^3

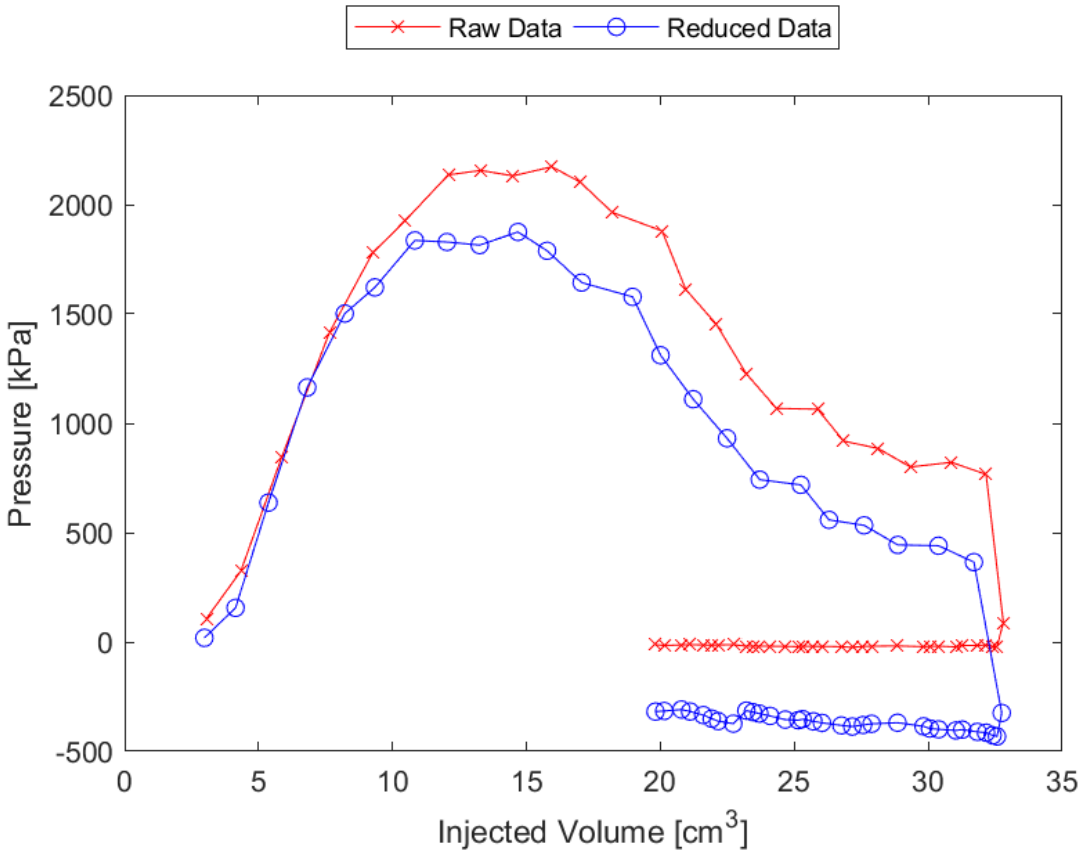

Figure D.21: Sounding 309, SDPMT-6 Continuous Test, Membrane O.D. 0.6875m, Depth 0.25 m, Raw and Reduced Data

Table D.21: Sounding 309, SDPMT-6 Continuous Test, Result Summary

Parameter				
Lift-Off Pressure (p_0)	156.2	kPa	22.65	psi
Contact Volume (V_c)	4.1	cm^3	0.25	in^3
Limit Pressure (p_L)	1840.0	kPa	266.87	psi
Assumed ν		0.33		
Initial Modulus (E_0)	41681.9	kPa	6045.45	psi
Dry Unit Weight (γ_{dry})	2103.2	kg/m^3	131.3	lb/ft^3
Wet Unit Weight (γ_{wet})	2228.2	kg/m^3	139.1	lb/ft^3

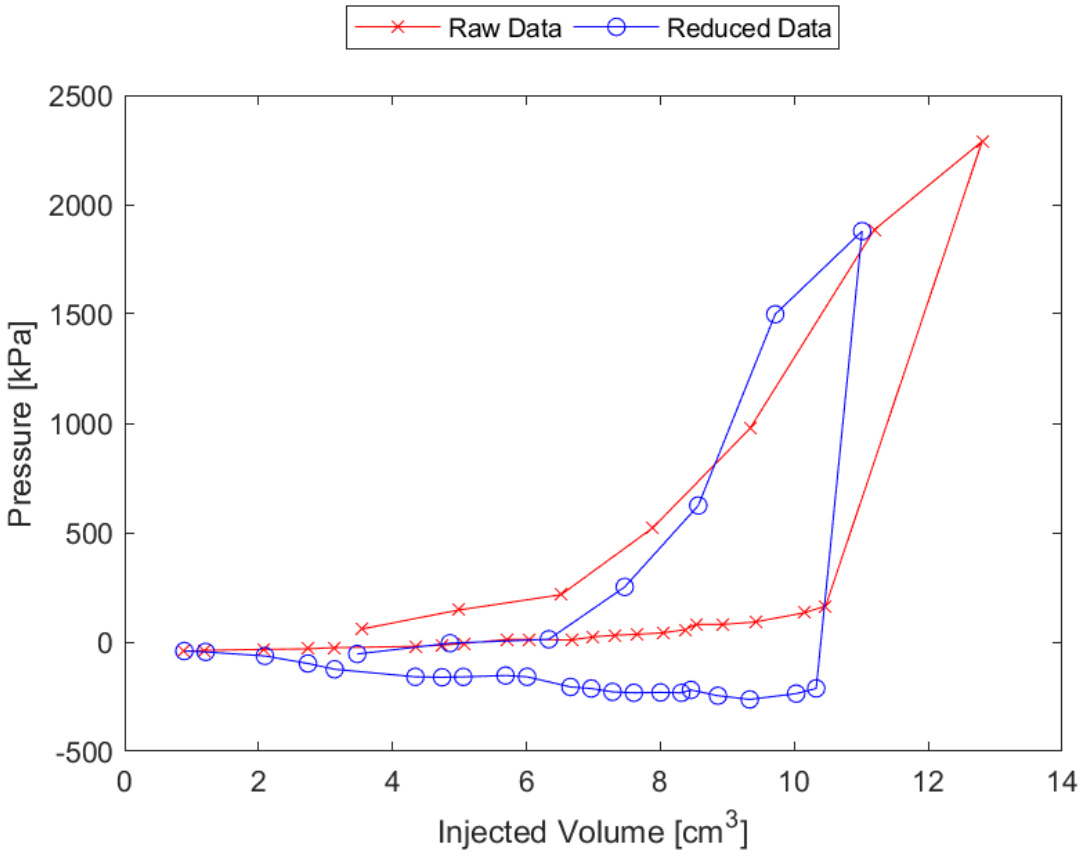

Figure D.22: Sounding 310, SDPMT-6 Continuous Test, Membrane O.D. 0.6875m, Depth 0.25 m, Raw and Reduced Data

Table D.22: Sounding 310, SDPMT-6 Continuous Test, Result Summary

Parameter				
Lift-Off Pressure (p_0)	12.4	kPa	1.80	psi
Contact Volume (V_c)	6.3	cm^3	0.39	in^3
Limit Pressure (p_L)	3000.0	kPa	435.11	psi
Assumed ν		0.33		
Initial Modulus (E_0)	91656.0	kPa	13293.60	psi
Dry Unit Weight (γ_{dry})	1992.7	kg/m^3	124.4	lb/ft^3
Wet Unit Weight (γ_{wet})	2101.6	kg/m^3	131.2	lb/ft^3

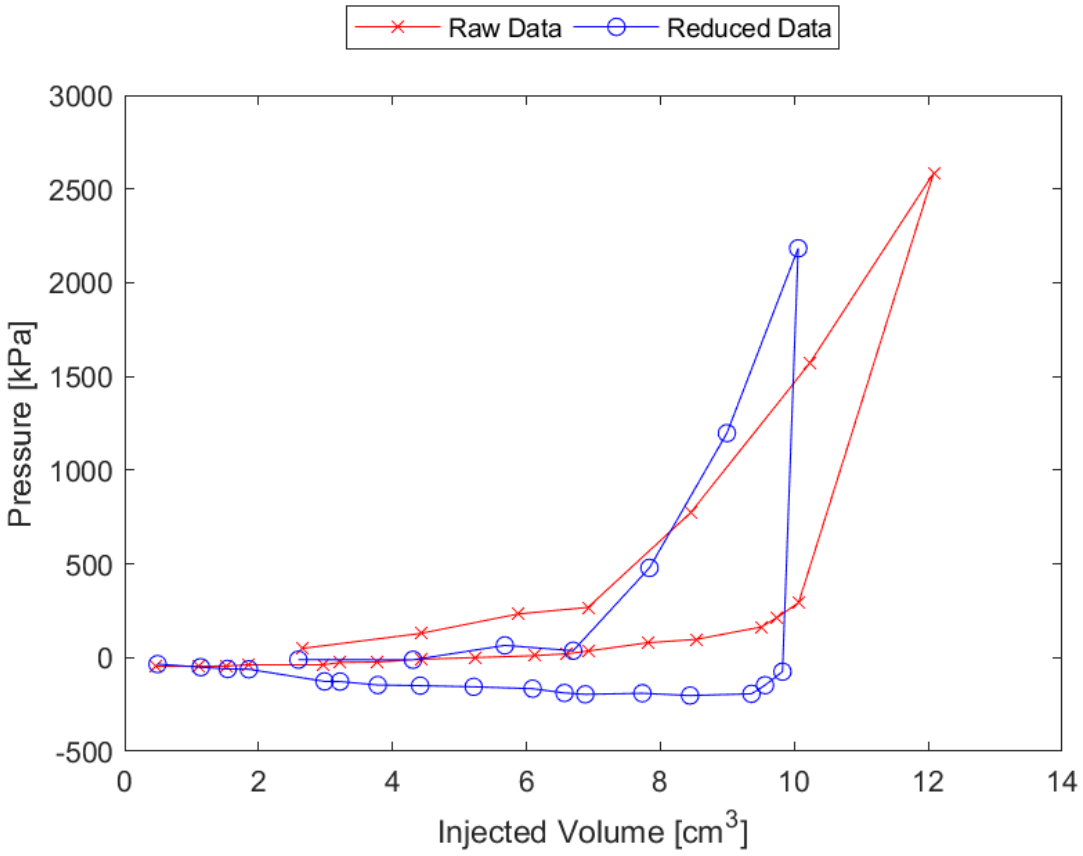

Figure D.23: Sounding 311, SDPMT-6 Continuous Test, Membrane O.D. 0.6875m, Depth 0.25 m, Raw and Reduced Data

Table D.23: Sounding 311, SDPMT-6 Continuous Test, Result Summary

Parameter				
Lift-Off Pressure (p_0)	36.8	kPa	5.34	psi
Contact Volume (V_c)	6.7	cm^3	0.41	in^3
Limit Pressure (p_L)	3700.0	kPa	536.64	psi
Assumed ν		0.33		
Initial Modulus (E_0)	92017.8	kPa	13346.08	psi
Dry Unit Weight (γ_{dry})	2010.3	kg/m^3	125.5	lb/ft^3
Wet Unit Weight (γ_{wet})	2114.4	kg/m^3	132.0	lb/ft^3

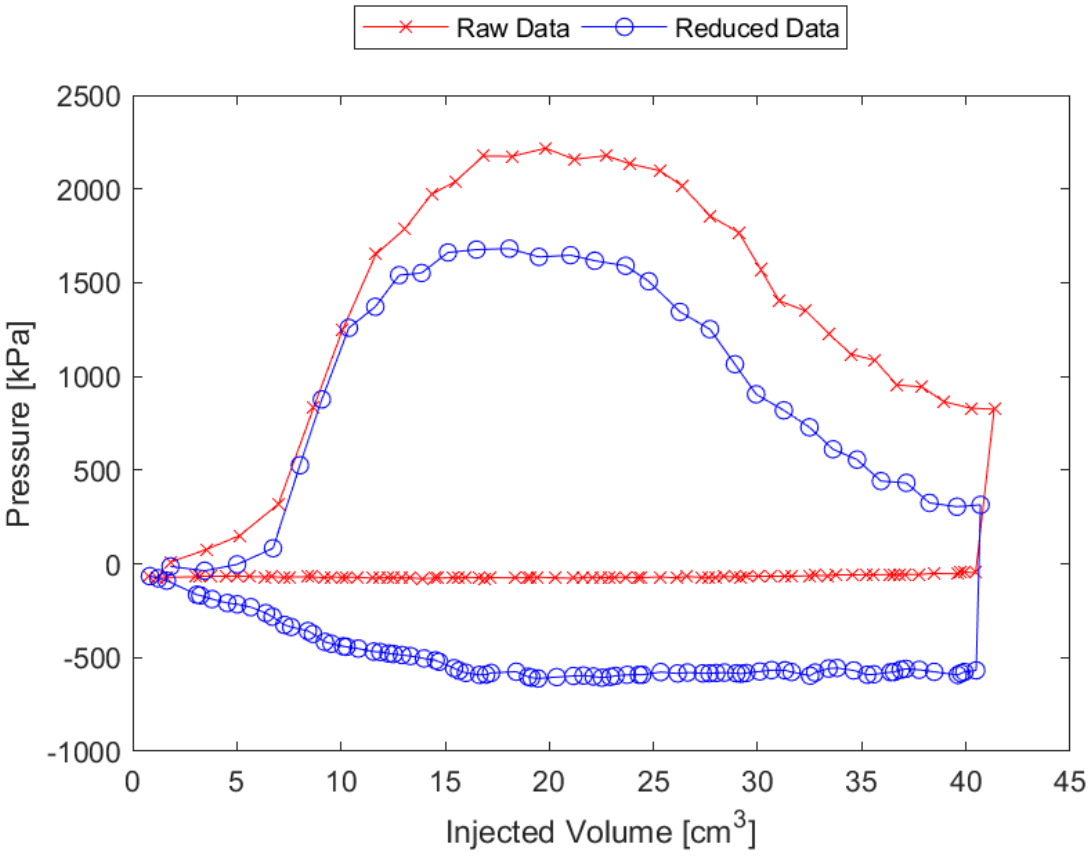

Figure D.24: Sounding 312, SDPMT-6 Continuous Test, Membrane O.D. 0.6875m, Depth 0.25 m, Raw and Reduced Data

Table D.24: Sounding 312, SDPMT-6 Continuous Test, Result Summary

Parameter				
Lift-Off Pressure (p_0)	83.3	kPa	12.08	psi
Contact Volume (V_c)	6.7	cm^3	0.41	in^3
Limit Pressure (p_L)	2130.0	kPa	308.93	psi
Assumed ν		0.33		
Initial Modulus (E_0)	38364.8	kPa	5564.35	psi
Dry Unit Weight (γ_{dry})	2037.5	kg/m^3	127.2	lb/ft^3
Wet Unit Weight (γ_{wet})	2159.3	kg/m^3	134.8	lb/ft^3

D.3 SDPMT-12 Incremental Test Data

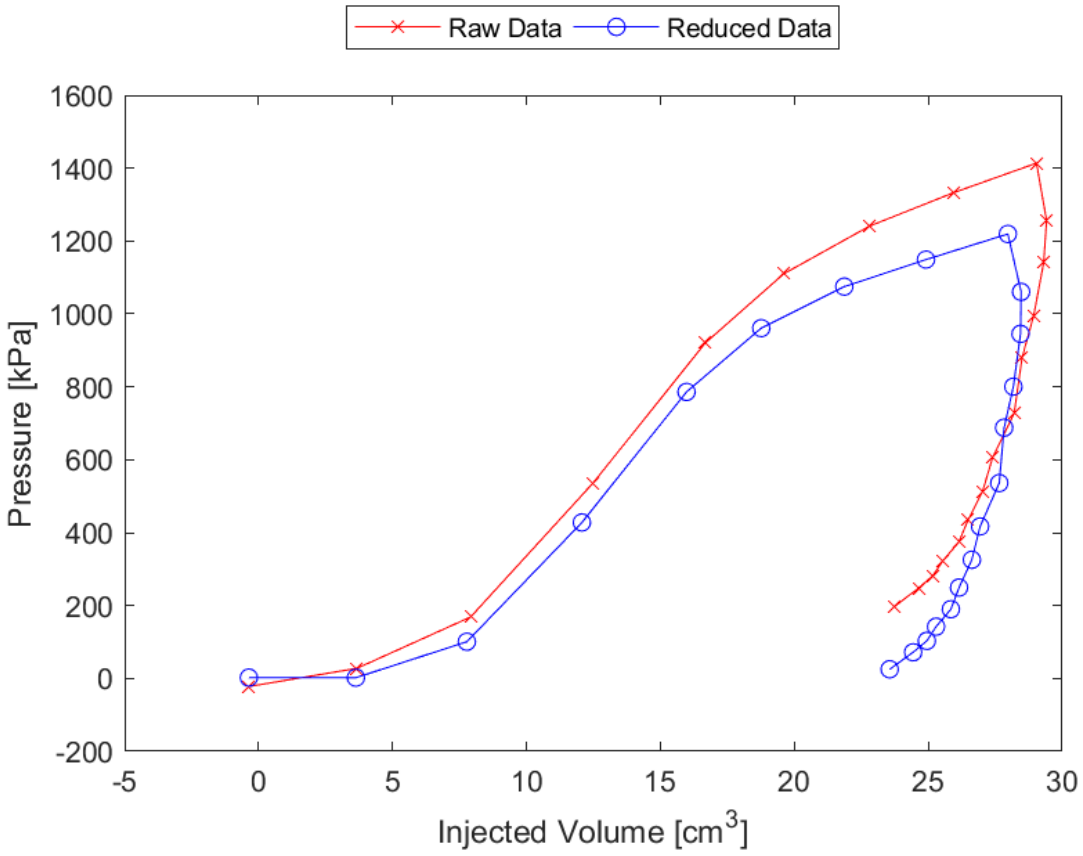

Figure D.25: Sounding 301, SDPMT-12 Continuous Test, Membrane O.D. 0.6875m, Depth 0.41 m, Raw and Reduced Data

Table D.25: Sounding 301, SDPMT-12 Continuous Test, Result Summary

Parameter				
Lift-Off Pressure (p_0)	2.0	kPa	0.29	psi
Contact Volume (V_c)	3.6	cm^3	0.22	in^3
Limit Pressure (p_L)	1720.0	kPa	249.47	psi
Assumed ν		0.33		
Initial Modulus (E_0)	18916.6	kPa	2743.62	psi
Dry Unit Weight (γ_{dry})	2050.4	kg/m^3	128.0	lb/ft^3
Wet Unit Weight (γ_{wet})	2204.1	kg/m^3	137.6	lb/ft^3

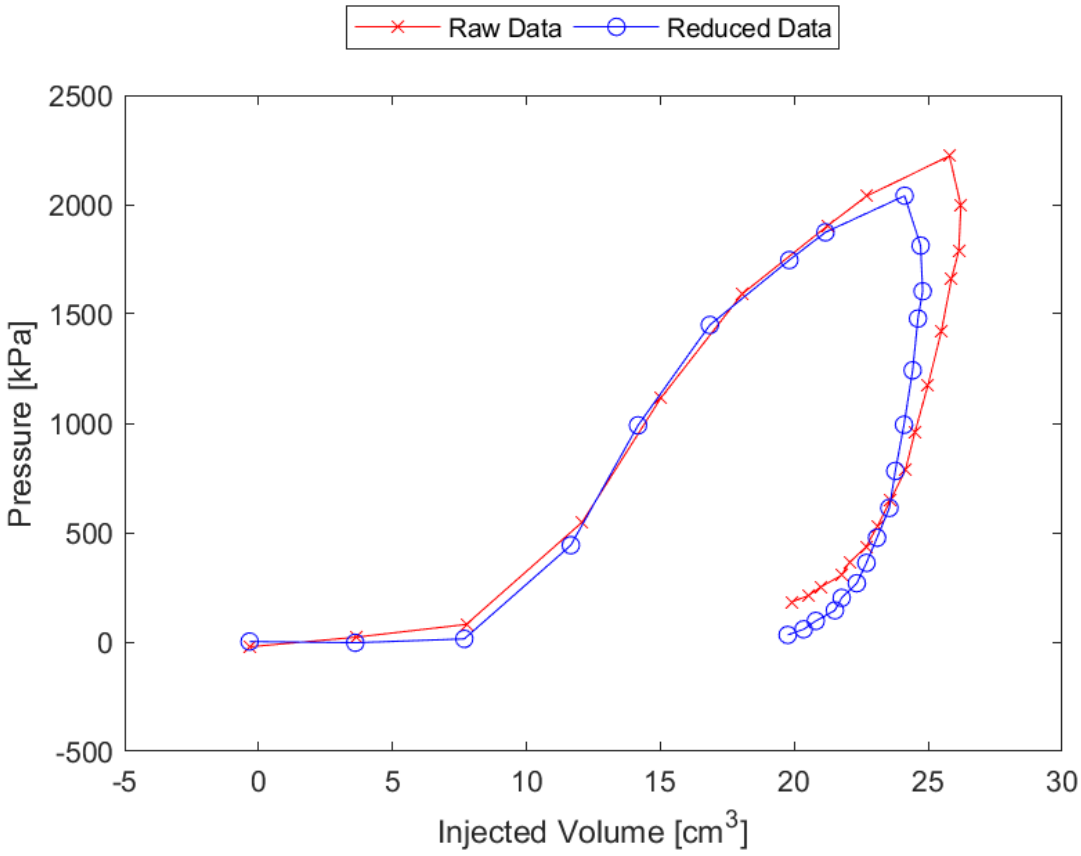

Figure D.26: Sounding 302, SDPMT-12 Continuous Test, Membrane O.D. 0.6875m, Depth 0.41 m, Raw and Reduced Data

Table D.26: Sounding 302, SDPMT-12 Continuous Test, Result Summary

Parameter				
Lift-Off Pressure (p_0)	14.2	kPa	2.05	psi
Contact Volume (V_c)	7.7	cm^3	0.47	in^3
Limit Pressure (p_L)	3340.0	kPa	484.43	psi
Assumed ν		0.33		
Initial Modulus (E_0)	45159.3	kPa	6549.82	psi
Dry Unit Weight (γ_{dry})	2053.6	kg/m^3	128.2	lb/ft^3
Wet Unit Weight (γ_{wet})	2168.9	kg/m^3	135.4	lb/ft^3

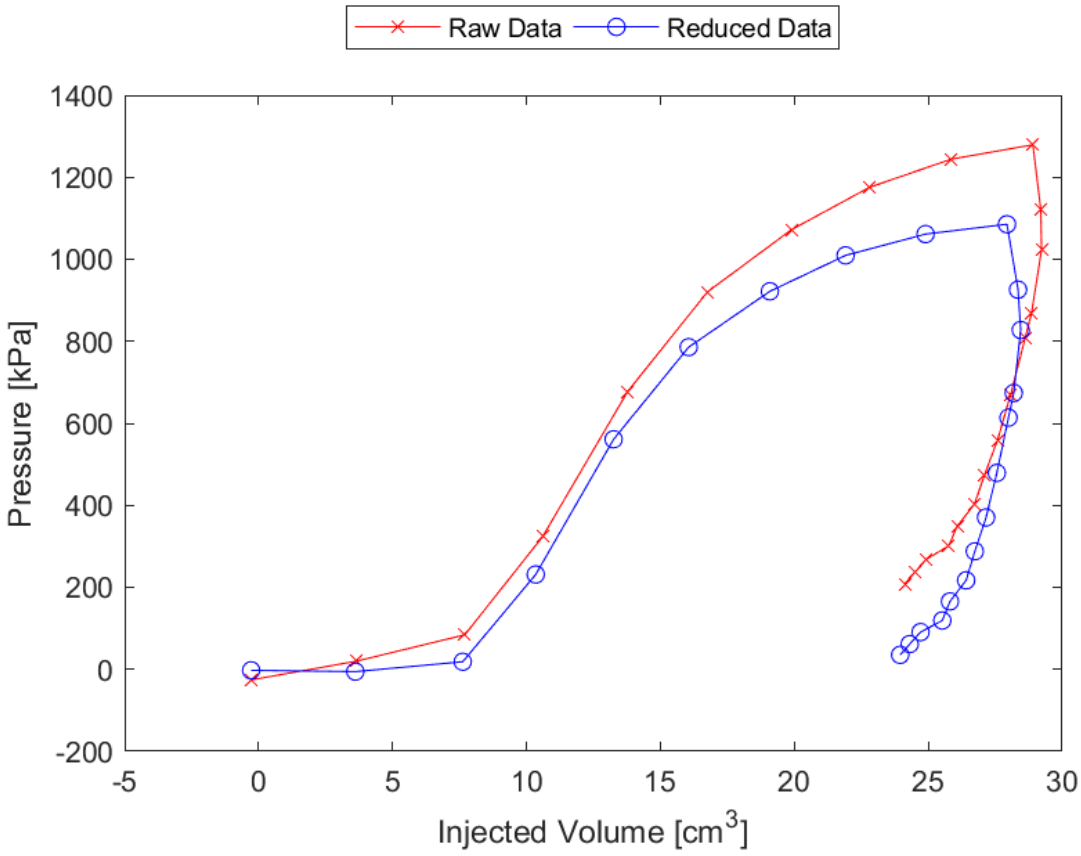

Figure D.27: Sounding 303, SDPMT-12 Continuous Test, Membrane O.D. 0.6875m, Depth 0.41 m, Raw and Reduced Data

Table D.27: Sounding 303, SDPMT-12 Continuous Test, Result Summary

Parameter				
Lift-Off Pressure (p_0)	18.5	kPa	2.68	psi
Contact Volume (V_c)	7.6	cm^3	0.47	in^3
Limit Pressure (p_L)	1510.0	kPa	219.01	psi
Assumed ν		0.33		
Initial Modulus (E_0)	21434.8	kPa	3108.87	psi
Dry Unit Weight (γ_{dry})	2045.6	kg/m^3	127.7	lb/ft^3
Wet Unit Weight (γ_{wet})	2165.7	kg/m^3	135.2	lb/ft^3

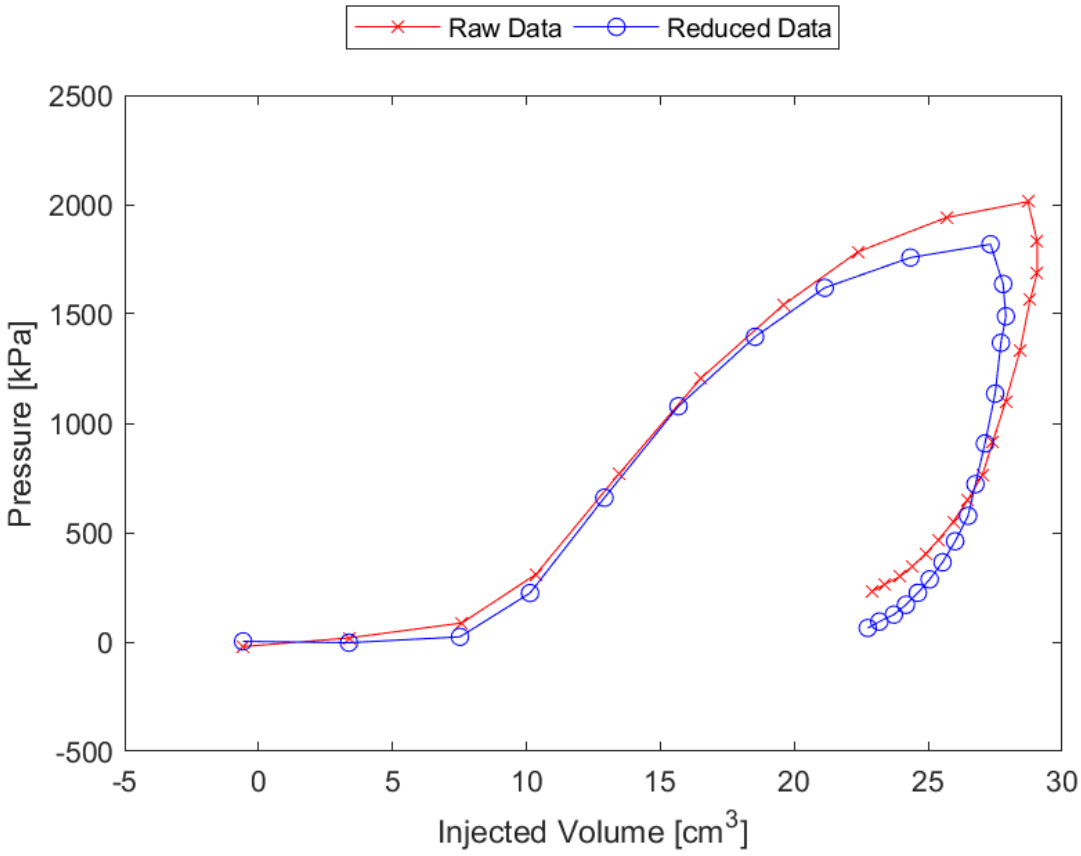

Figure D.28: Sounding 304, SDPMT-12 Continuous Test, Membrane O.D. 0.6875m, Depth 0.41 m, Raw and Reduced Data

Table D.28: Sounding 304, SDPMT-12 Continuous Test, Result Summary

Parameter				
Lift-Off Pressure (p_0)	23.6	kPa	3.42	psi
Contact Volume (V_c)	7.5	cm^3	0.46	in^3
Limit Pressure (p_L)	2750.0	kPa	398.85	psi
Assumed ν		0.33		
Initial Modulus (E_0)	35326.3	kPa	5123.66	psi
Dry Unit Weight (γ_{dry})	2050.4	kg/m^3	128.0	lb/ft^3
Wet Unit Weight (γ_{wet})	2149.7	kg/m^3	134.2	lb/ft^3

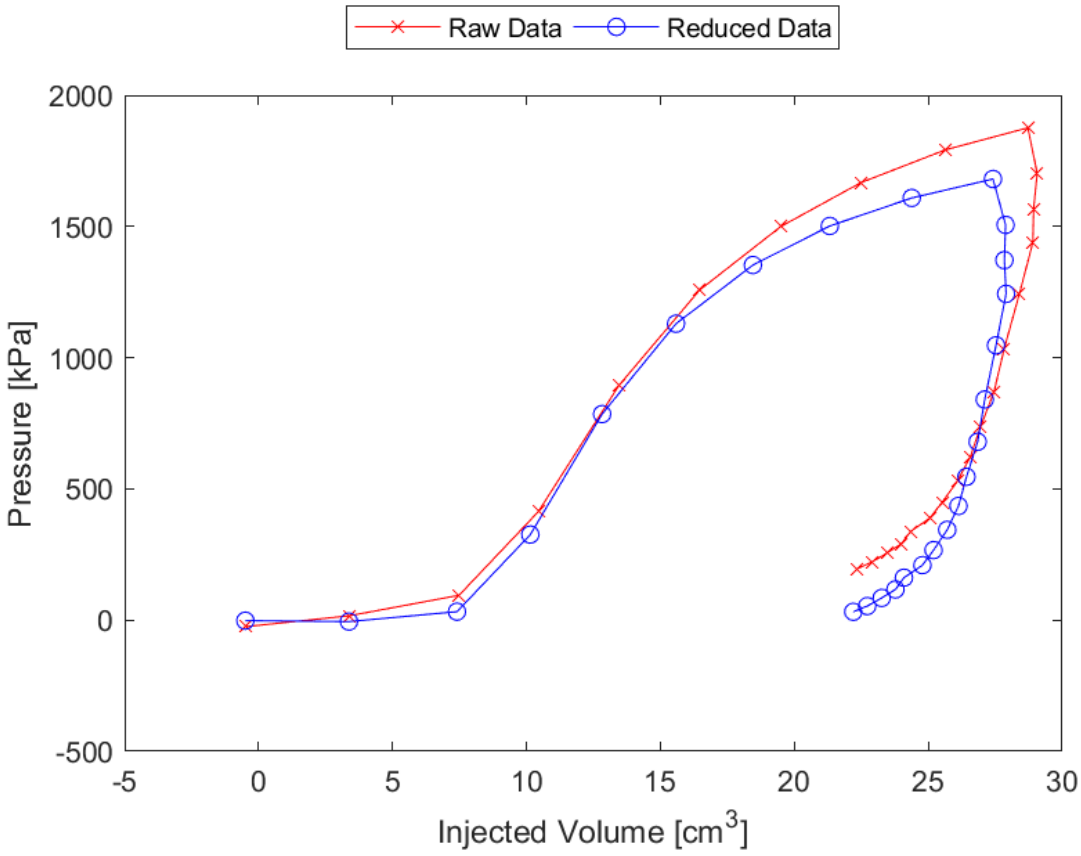

Figure D.29: Sounding 305, SDPMT-12 Continuous Test, Membrane O.D. 0.6875m, Depth 0.41 m, Raw and Reduced Data

Table D.29: Sounding 305, SDPMT-12 Continuous Test, Result Summary

Parameter				
Lift-Off Pressure (p_0)	32.2	kPa	4.67	psi
Contact Volume (V_c)	7.4	cm^3	0.45	in^3
Limit Pressure (p_L)	2350.0	kPa	340.84	psi
Assumed ν		0.33		
Initial Modulus (E_0)	38603.5	kPa	5598.97	psi
Dry Unit Weight (γ_{dry})	2045.6	kg/m^3	127.7	lb/ft^3
Wet Unit Weight (γ_{wet})	2144.9	kg/m^3	133.9	lb/ft^3

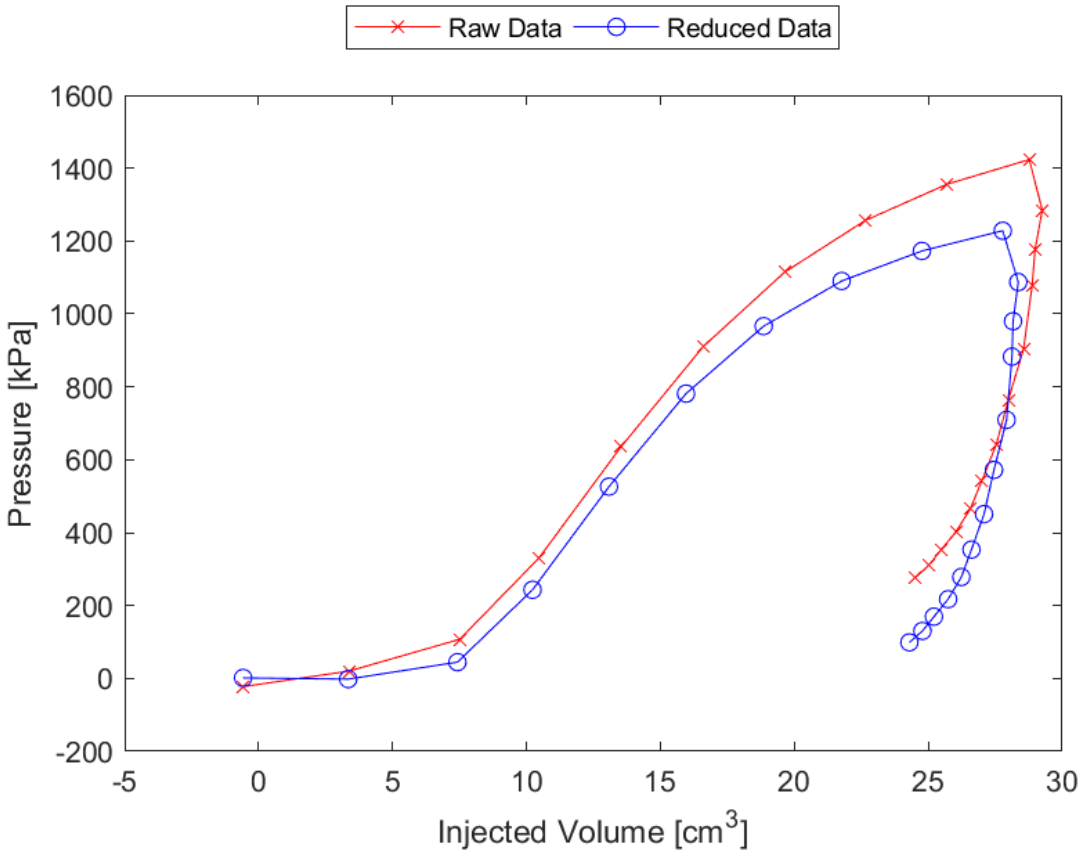

Figure D.30: Sounding 306, SDPMT-12 Continuous Test, Membrane O.D. 0.6875m, Depth 0.41 m, Raw and Reduced Data

Table D.30: Sounding 306, SDPMT-12 Continuous Test, Result Summary

Parameter				
Lift-Off Pressure (p_0)	44.7	kPa	6.49	psi
Contact Volume (V_c)	7.4	cm^3	0.45	in^3
Limit Pressure (p_L)	1765.0	kPa	255.99	psi
Assumed ν		0.33		
Initial Modulus (E_0)	21564.3	kPa	3127.65	psi
Dry Unit Weight (γ_{dry})	2071.2	kg/m^3	129.3	lb/ft^3
Wet Unit Weight (γ_{wet})	2167.3	kg/m^3	135.3	lb/ft^3

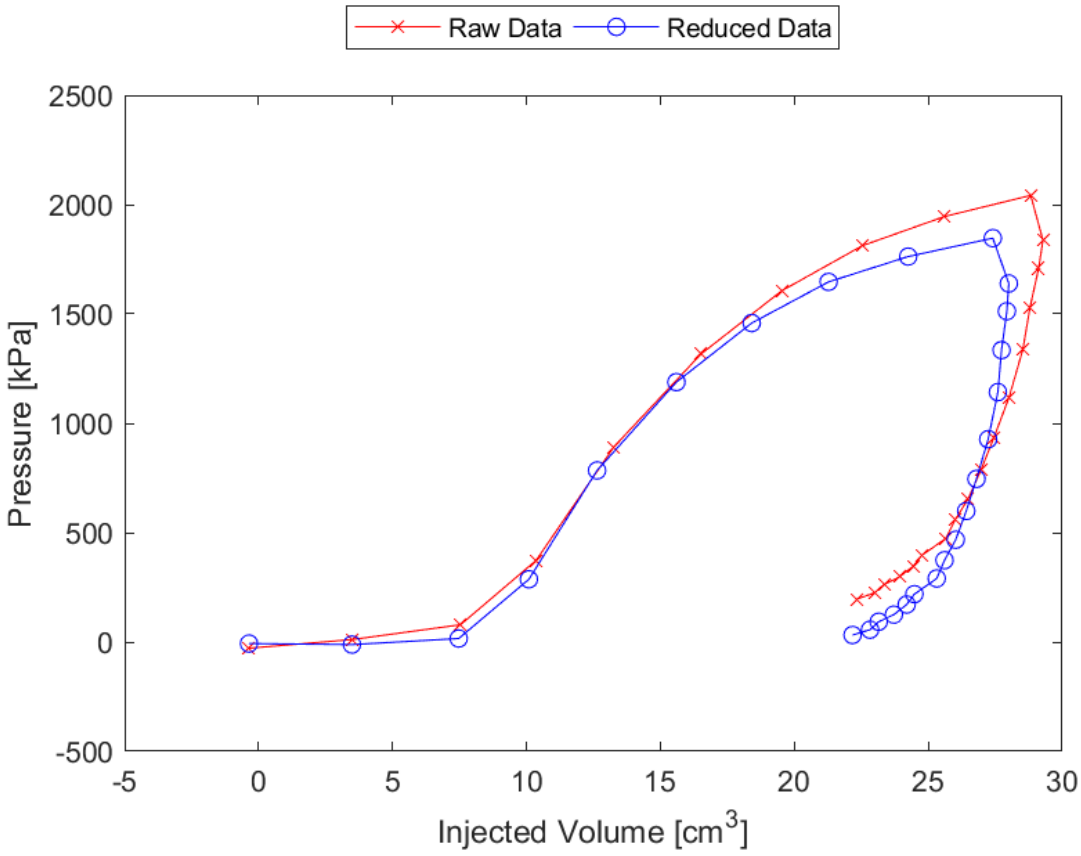

Figure D.31: Sounding 307, SDPMT-12 Continuous Test, Membrane O.D. 0.6875m, Depth 0.41 m, Raw and Reduced Data

Table D.31: Sounding 307, SDPMT-12 Continuous Test, Result Summary

Parameter				
Lift-Off Pressure (p_0)	15.8	kPa	2.29	psi
Contact Volume (V_c)	7.5	cm^3	0.46	in^3
Limit Pressure (p_L)	2635.0	kPa	382.18	psi
Assumed ν		0.33		
Initial Modulus (E_0)	43980.2	kPa	6378.80	psi
Dry Unit Weight (γ_{dry})	2005.5	kg/m^3	125.2	lb/ft^3
Wet Unit Weight (γ_{wet})	2095.2	kg/m^3	130.8	lb/ft^3

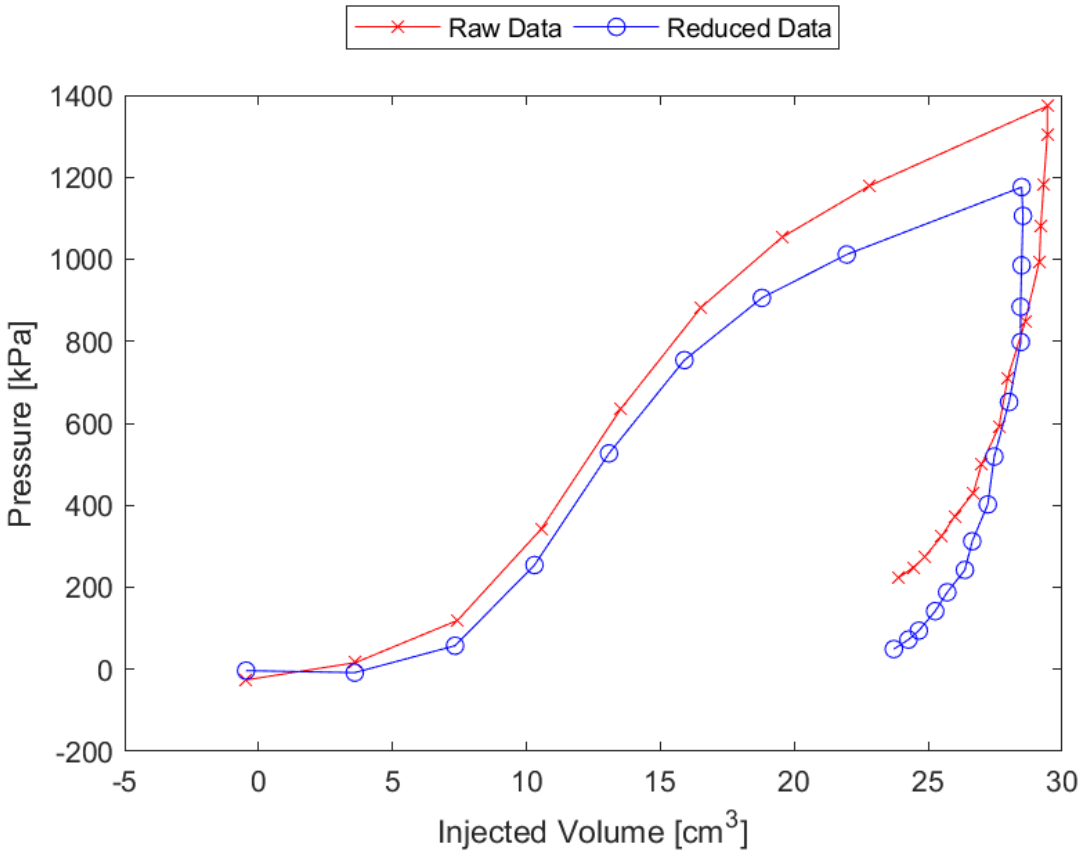

Figure D.32: Sounding 308, SDPMT-12 Continuous Test, Membrane O.D. 0.6875m, Depth 0.41 m, Raw and Reduced Data

Table D.32: Sounding 308, SDPMT-12 Continuous Test, Result Summary

Parameter				
Lift-Off Pressure (p_0)	57.6	kPa	8.35	psi
Contact Volume (V_c)	7.3	cm^3	0.45	in^3
Limit Pressure (p_L)	1595.0	kPa	231.34	psi
Assumed ν		0.33		
Initial Modulus (E_0)	20507.8	kPa	2974.41	psi
Dry Unit Weight (γ_{dry})	2080.8	kg/m^3	129.9	lb/ft^3
Wet Unit Weight (γ_{wet})	2186.5	kg/m^3	136.5	lb/ft^3

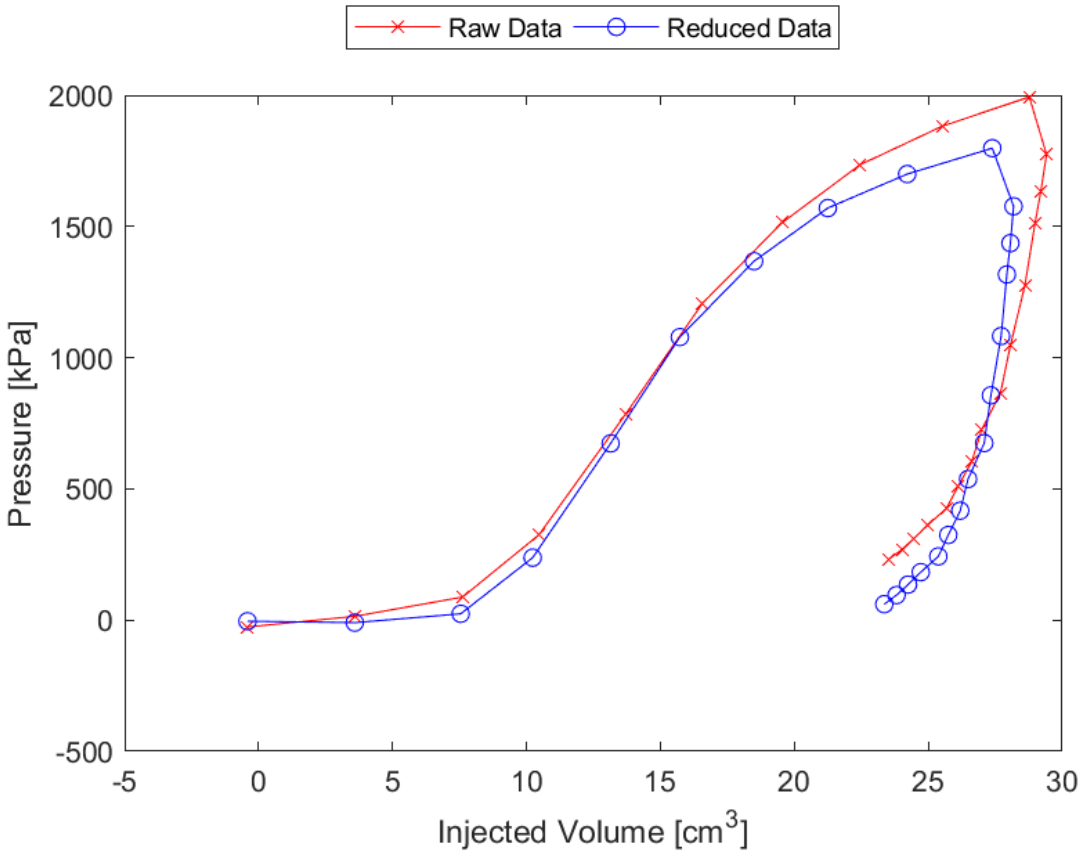

Figure D.33: Sounding 309, SDPMT-12 Continuous Test, Membrane O.D. 0.6875m, Depth 0.41 m, Raw and Reduced Data

Table D.33: Sounding 309, SDPMT-12 Continuous Test, Result Summary

Parameter				
Lift-Off Pressure (p_0)	24.1	kPa	3.49	psi
Contact Volume (V_c)	7.5	cm^3	0.46	in^3
Limit Pressure (p_L)	2690.0	kPa	390.15	psi
Assumed ν		0.33		
Initial Modulus (E_0)	35065.3	kPa	5085.79	psi
Dry Unit Weight (γ_{dry})	2119.2	kg/m^3	132.3	lb/ft^3
Wet Unit Weight (γ_{wet})	2217.0	kg/m^3	138.4	lb/ft^3

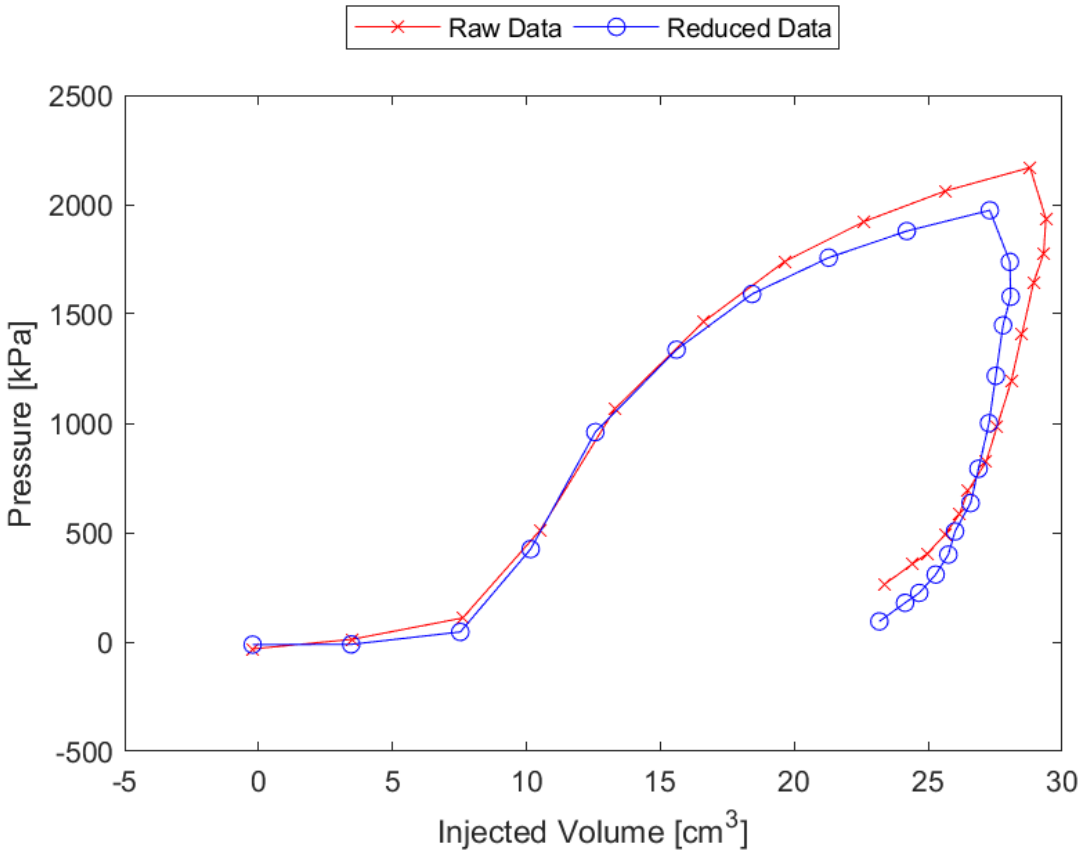

Figure D.34: Sounding 310, SDPMT-12 Continuous Test, Membrane O.D. 0.6875m, Depth 0.41 m, Raw and Reduced Data

Table D.34: Sounding 310, SDPMT-12 Continuous Test, Result Summary

Parameter				
Lift-Off Pressure (p_0)	45.9	kPa	6.66	psi
Contact Volume (V_c)	7.5	cm^3	0.46	in^3
Limit Pressure (p_L)	2700.0	kPa	391.60	psi
Assumed ν		0.33		
Initial Modulus (E_0)	40150.6	kPa	5823.37	psi
Dry Unit Weight (γ_{dry})	1997.5	kg/m^3	124.7	lb/ft^3
Wet Unit Weight (γ_{wet})	2087.2	kg/m^3	130.3	lb/ft^3

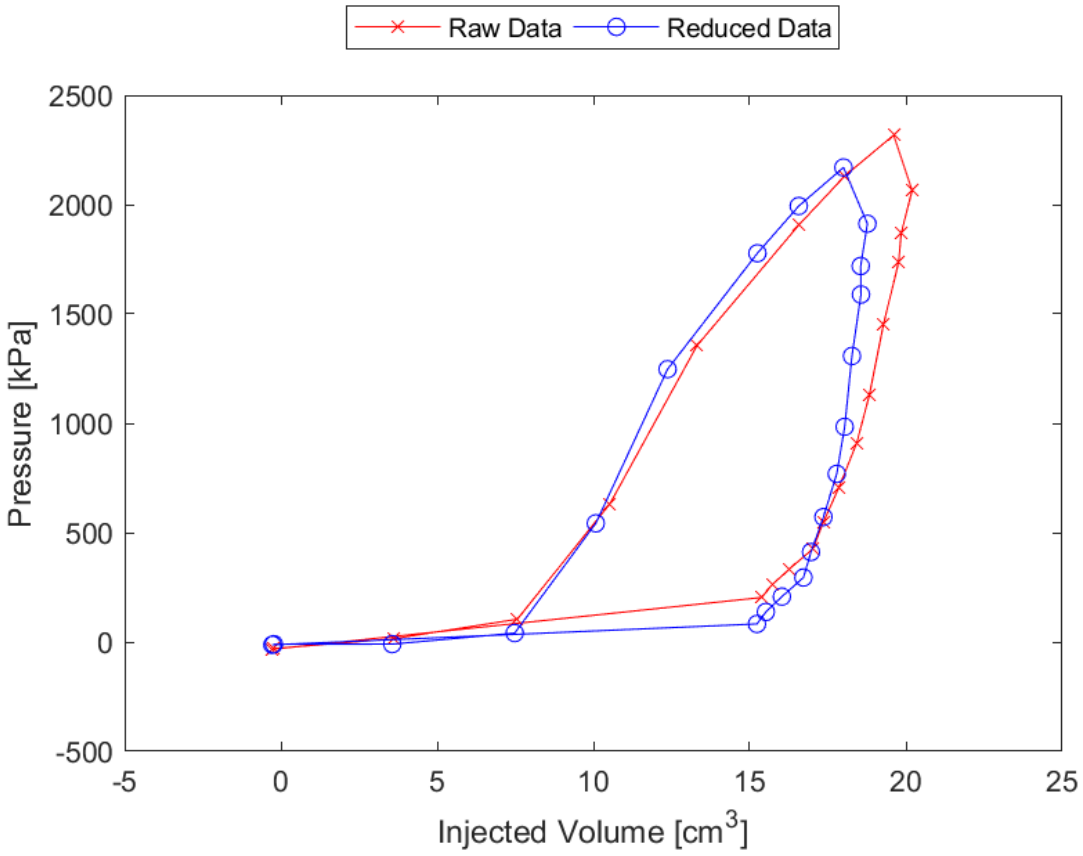

Figure D.35: Sounding 311, SDPMT-12 Continuous Test, Membrane O.D. 0.6875m, Depth 0.41 m, Raw and Reduced Data

Table D.35: Sounding 311, SDPMT-12 Continuous Test, Result Summary

Parameter				
Lift-Off Pressure (p_0)	40.8	kPa	5.92	psi
Contact Volume (V_c)	7.5	cm^3	0.46	in^3
Limit Pressure (p_L)	3425.0	kPa	496.76	psi
Assumed ν		0.33		
Initial Modulus (E_0)	54542.0	kPa	7910.66	psi
Dry Unit Weight (γ_{dry})	1986.3	kg/m^3	124.0	lb/ft^3
Wet Unit Weight (γ_{wet})	2332.3	kg/m^3	145.6	lb/ft^3

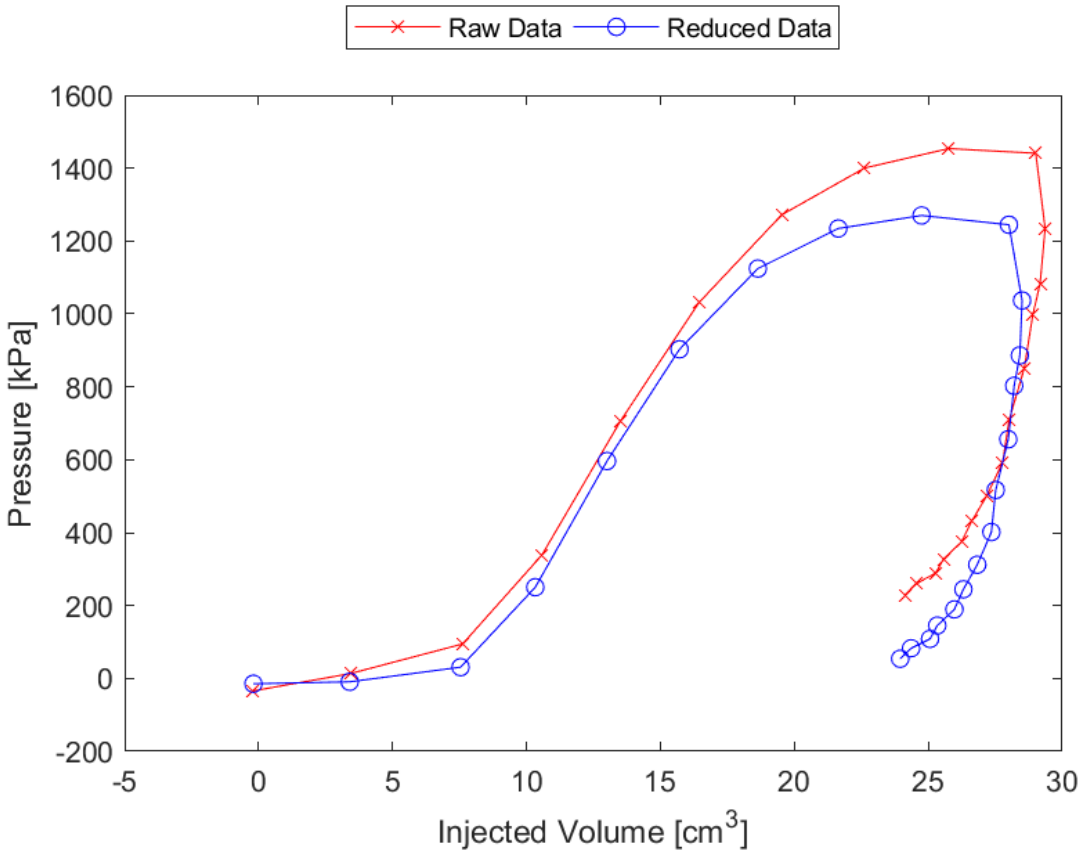

Figure D.36: Sounding 312, SDPMT-12 Continuous Test, Membrane O.D. 0.6875m, Depth 0.41 m, Raw and Reduced Data

Table D.36: Sounding 312, SDPMT-12 Continuous Test, Result Summary

Parameter				
Lift-Off Pressure (p_0)	30.8	kPa	4.47	psi
Contact Volume (V_c)	7.5	cm^3	0.46	in^3
Limit Pressure (p_L)	1965.0	kPa	285.00	psi
Assumed ν		0.33		
Initial Modulus (E_0)	27811.7	kPa	4033.75	psi
Dry Unit Weight (γ_{dry})	2048.8	kg/m^3	127.9	lb/ft^3
Wet Unit Weight (γ_{wet})	2157.7	kg/m^3	134.7	lb/ft^3

D.4 SDPMT-12 Continuous Test Data

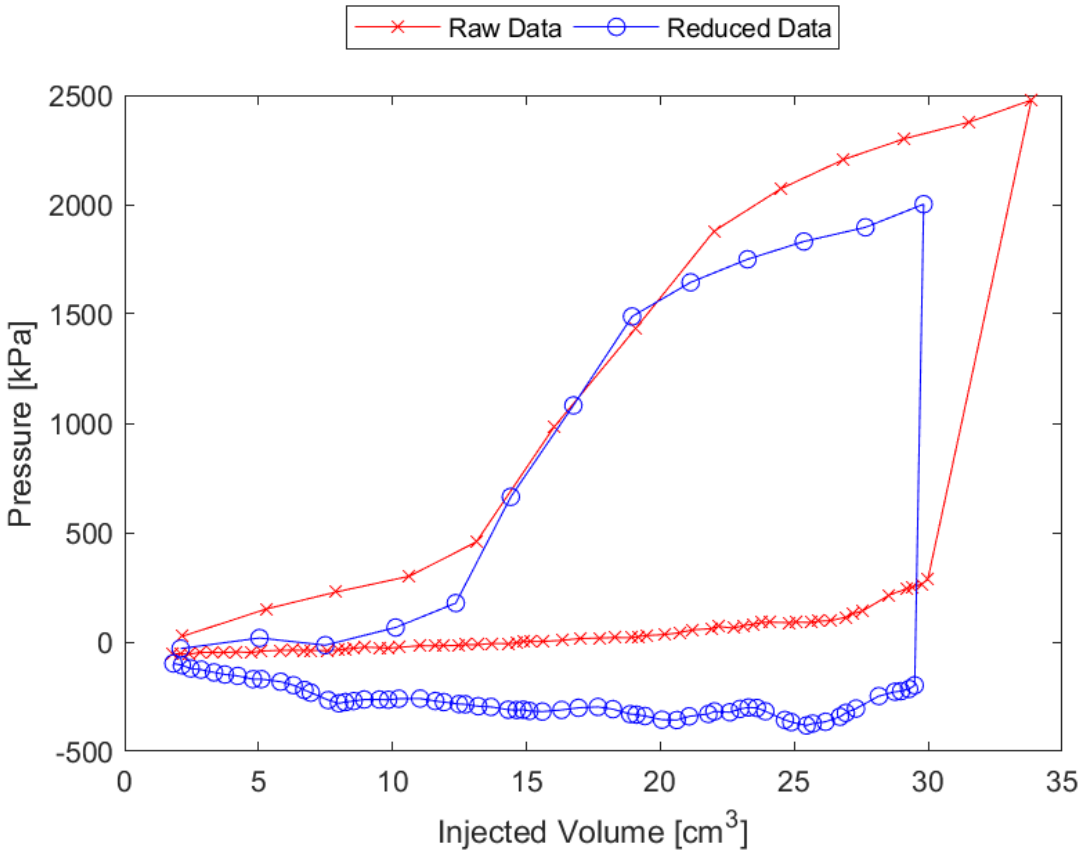

Figure D.37: Sounding 301, SDPMT-12 Continuous Test, Membrane O.D. 0.625m, Depth 0.41 m, Raw and Reduced Data

Table D.37: Sounding 301, SDPMT-12 Continuous Test, Result Summary

Parameter				
Lift-Off Pressure (p_0)	177.8	kPa	25.79	psi
Contact Volume (V_c)	12.4	cm^3	0.75	in^3
Limit Pressure (p_L)	2665.0	kPa	386.53	psi
Assumed ν		0.33		
Initial Modulus (E_0)	48079.0	kPa	6973.28	psi
Dry Unit Weight (γ_{dry})	2050.4	kg/m^3	128.0	lb/ft^3
Wet Unit Weight (γ_{wet})	2122.4	kg/m^3	132.5	lb/ft^3

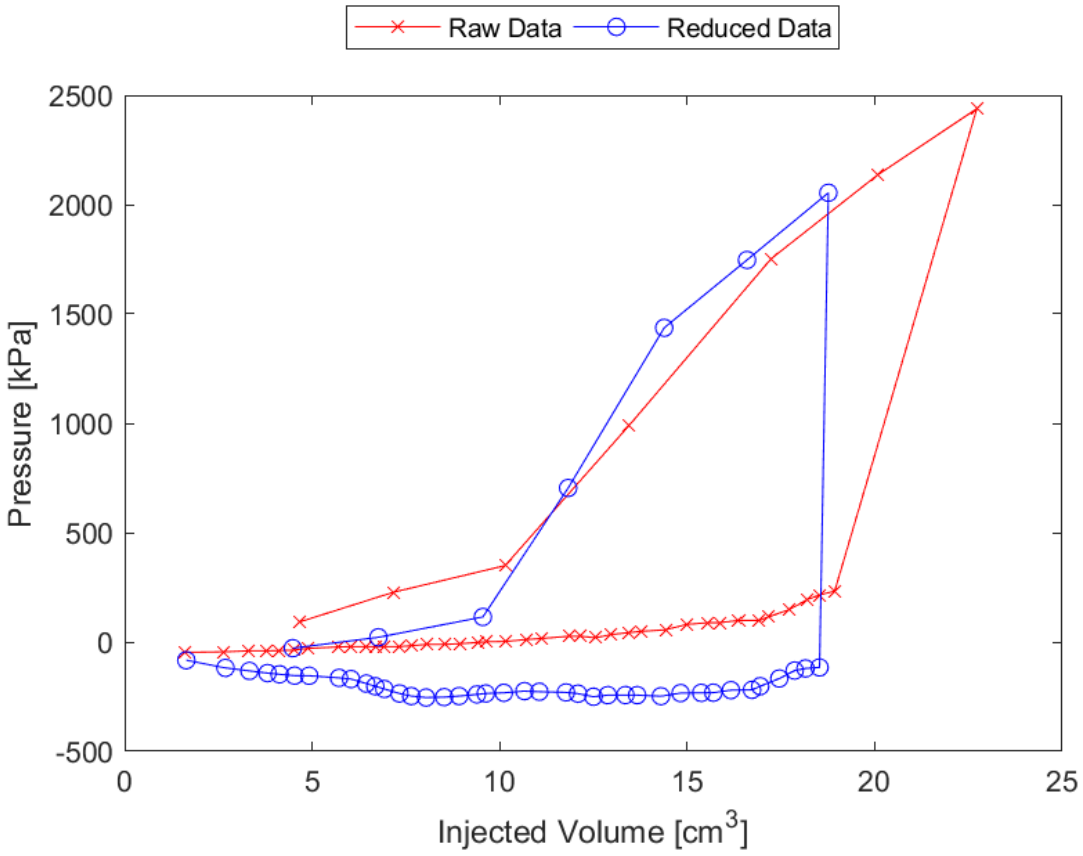

Figure D.38: Sounding 302, SDPMT-12 Continuous Test, Membrane O.D. 0.625m, Depth 0.41 m, Raw and Reduced Data

Table D.38: Sounding 302, SDPMT-12 Continuous Test, Result Summary

Parameter				
Lift-Off Pressure (p_0)	114.5	kPa	16.60	psi
Contact Volume (V_c)	9.6	cm^3	0.58	in^3
Limit Pressure (p_L)	2790.0	kPa	404.66	psi
Assumed ν		0.33		
Initial Modulus (E_0)	61962.1	kPa	8986.86	psi
Dry Unit Weight (γ_{dry})	2053.6	kg/m^3	128.2	lb/ft^3
Wet Unit Weight (γ_{wet})	2104.8	kg/m^3	131.4	lb/ft^3

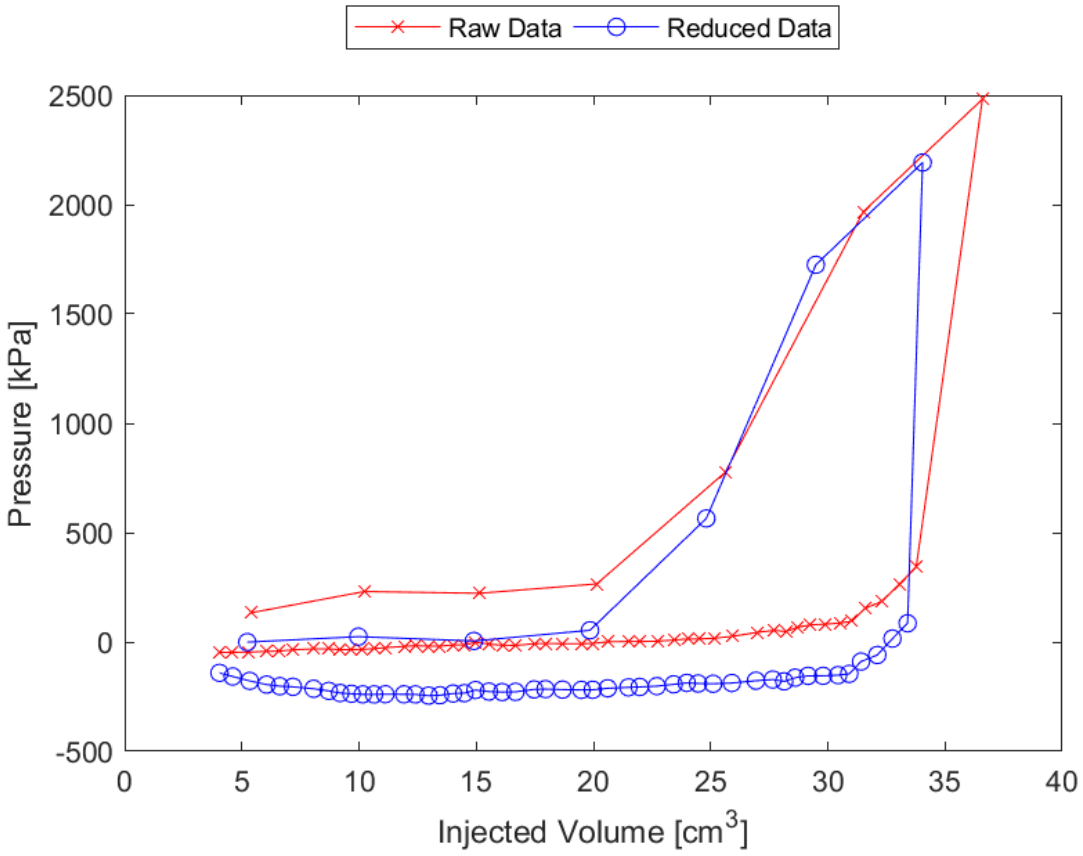

Figure D.39: Sounding 303, SDPMT-12 Continuous Test, Membrane O.D. 0.625m, Depth 0.41 m, Raw and Reduced Data

Table D.39: Sounding 303, SDPMT-12 Continuous Test, Result Summary

Parameter				
Lift-Off Pressure (p_0)	53.5	kPa	7.76	psi
Contact Volume (V_c)	19.9	cm^3	1.21	in^3
Limit Pressure (p_L)	2500.0	kPa	362.60	psi
Assumed ν		0.33		
Initial Modulus (E_0)	57688.6	kPa	8367.05	psi
Dry Unit Weight (γ_{dry})	2045.6	kg/m^3	127.7	lb/ft^3
Wet Unit Weight (γ_{wet})	2124.0	kg/m^3	132.6	lb/ft^3

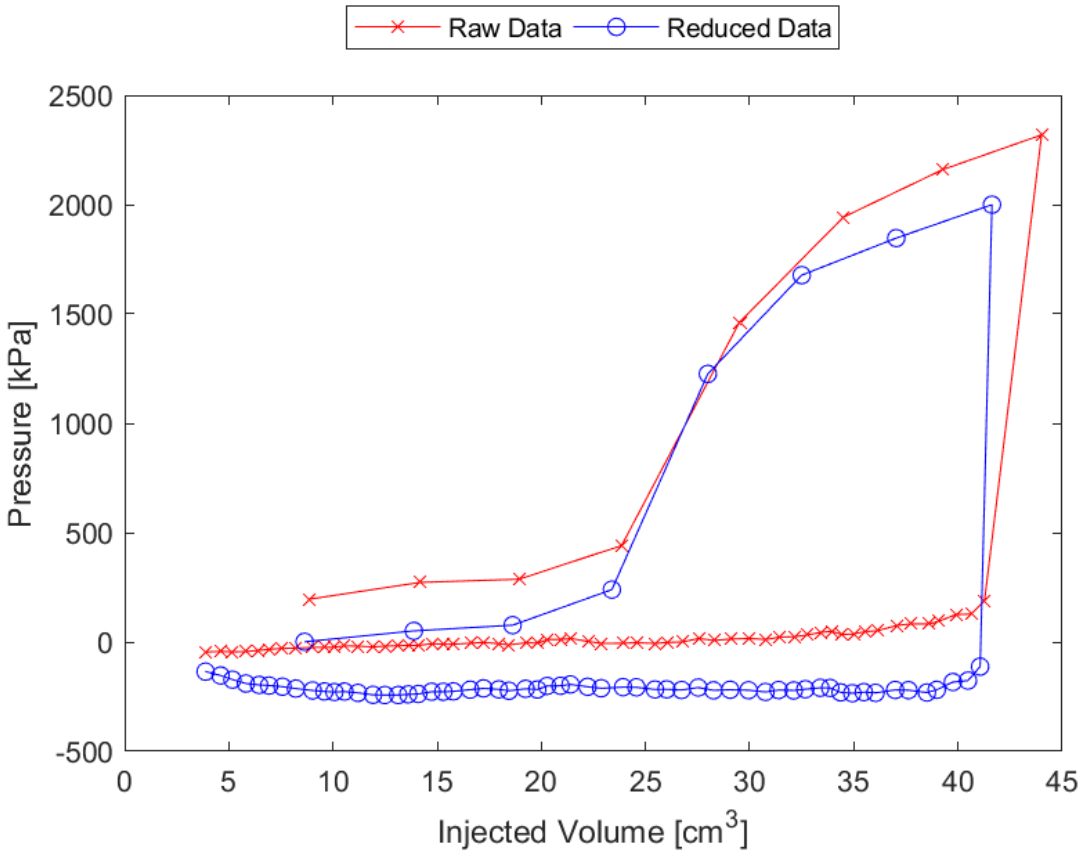

Figure D.40: Sounding 304, SDPMT-12 Continuous Test, Membrane O.D. 0.625m, Depth 0.41 m, Raw and Reduced Data

Table D.40: Sounding 304, SDPMT-12 Continuous Test, Result Summary

Parameter				
Lift-Off Pressure (p_0)	76.8	kPa	11.14	psi
Contact Volume (V_c)	18.6	cm^3	1.14	in^3
Limit Pressure (p_L)	2500.0	kPa	362.60	psi
Assumed ν		0.33		
Initial Modulus (E_0)	48941.9	kPa	7098.44	psi
Dry Unit Weight (γ_{dry})	2050.4	kg/m^3	128.0	lb/ft^3
Wet Unit Weight (γ_{wet})	2127.3	kg/m^3	132.8	lb/ft^3

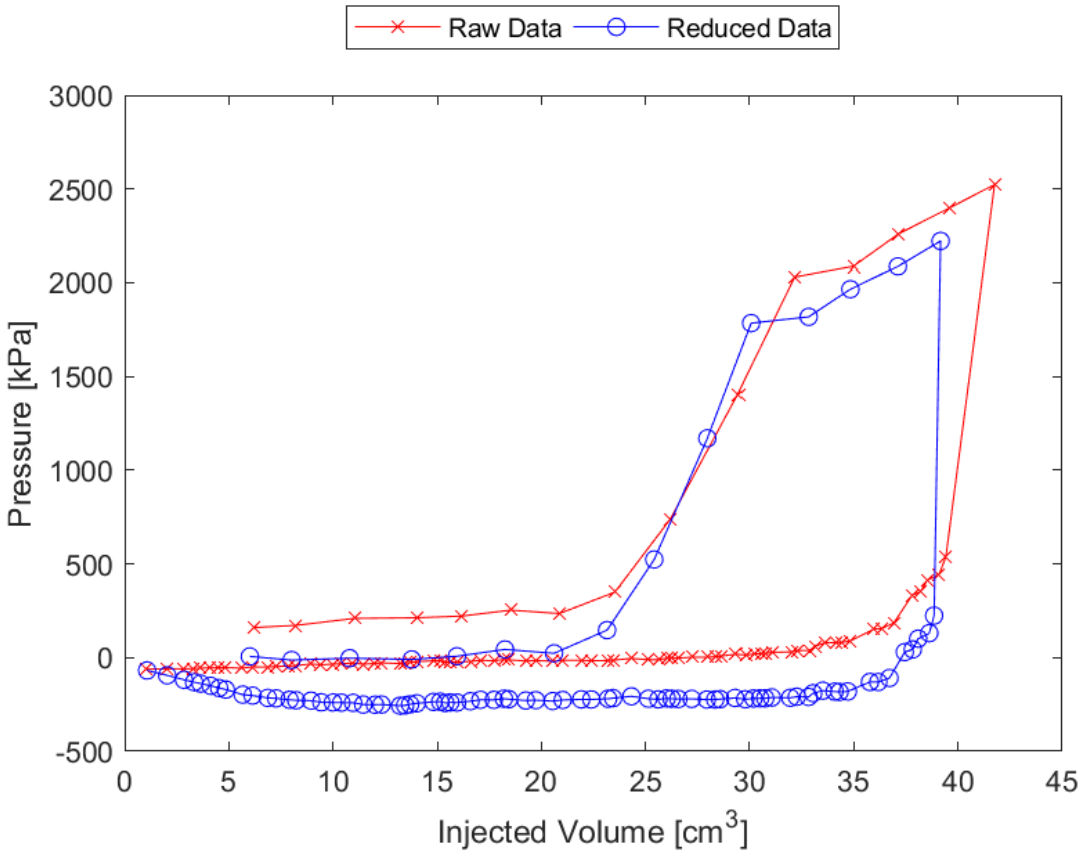

Figure D.41: Sounding 305, SDPMT-12 Continuous Test, Membrane O.D. 0.625m, Depth 0.41 m, Raw and Reduced Data

Table D.41: Sounding 305, SDPMT-12 Continuous Test, Result Summary

Parameter				
Lift-Off Pressure (p_0)	23.1	kPa	3.35	psi
Contact Volume (V_c)	20.6	cm^3	1.26	in^3
Limit Pressure (p_L)	3780.0	kPa	548.24	psi
Assumed ν		0.33		
Initial Modulus (E_0)	63413.2	kPa	9197.32	psi
Dry Unit Weight (γ_{dry})	2045.6	kg/m^3	127.7	lb/ft^3
Wet Unit Weight (γ_{wet})	2125.7	kg/m^3	132.7	lb/ft^3

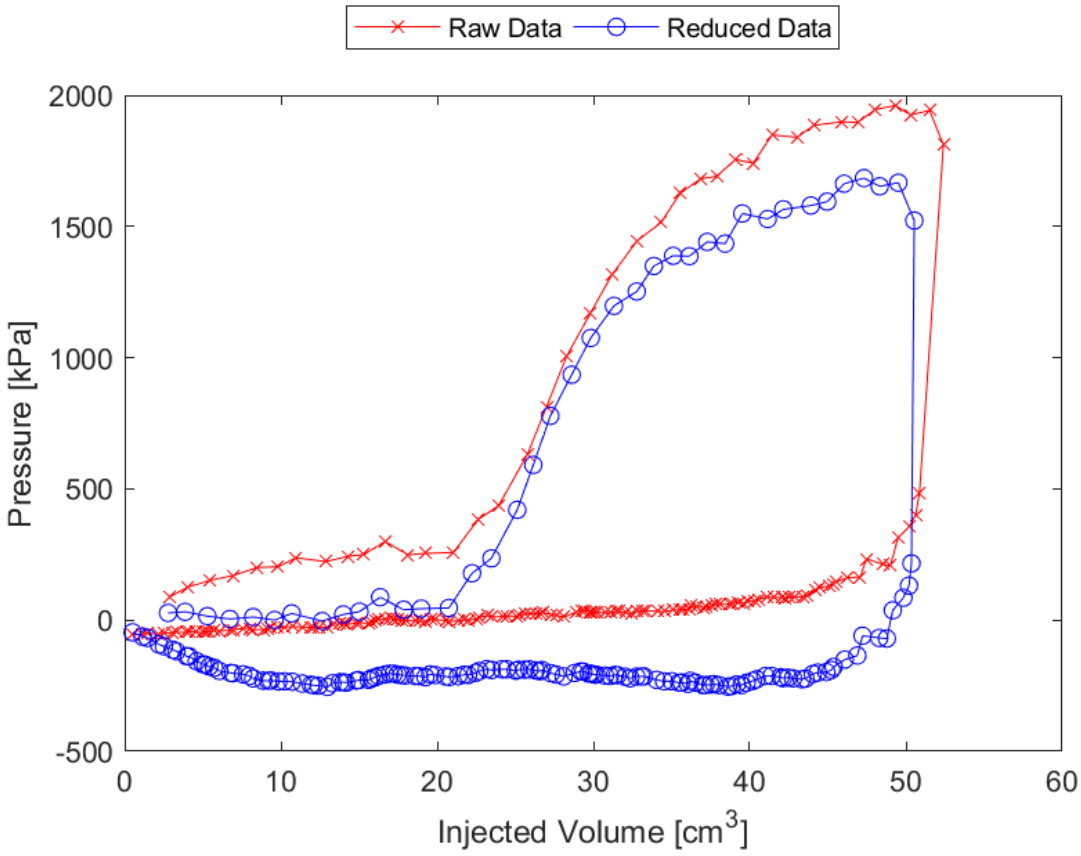

Figure D.42: Sounding 306, SDPMT-12 Continuous Test, Membrane O.D. 0.625m, Depth 0.41 m, Raw and Reduced Data

Table D.42: Sounding 306, SDPMT-12 Continuous Test, Result Summary

Parameter				
Lift-Off Pressure (p_0)	46.3	kPa	6.71	psi
Contact Volume (V_c)	20.7	cm^3	1.27	in^3
Limit Pressure (p_L)	2000.0	kPa	290.08	psi
Assumed ν		0.33		
Initial Modulus (E_0)	32733.1	kPa	4747.54	psi
Dry Unit Weight (γ_{dry})	2071.2	kg/m^3	129.3	lb/ft^3
Wet Unit Weight (γ_{wet})	2162.5	kg/m^3	135.0	lb/ft^3

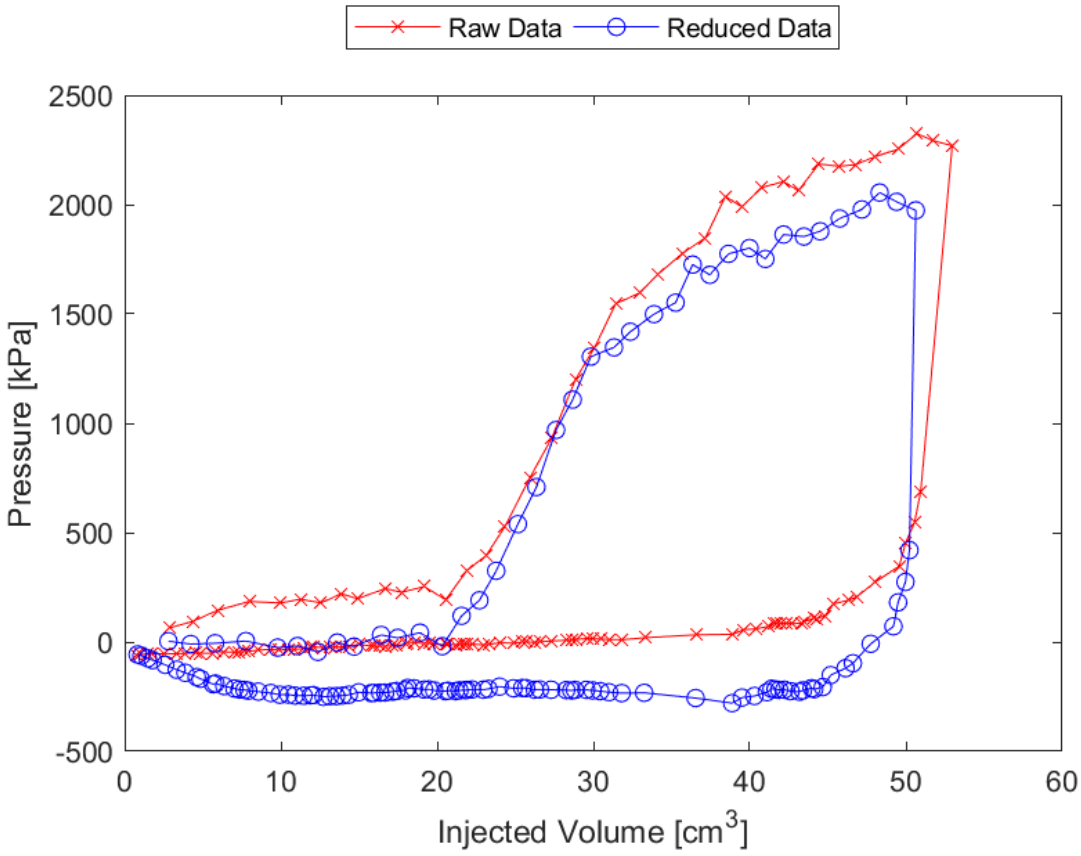

Figure D.43: Sounding 307, SDPMT-12 Continuous Test, Membrane O.D. 0.625m, Depth 0.41 m, Raw and Reduced Data

Table D.43: Sounding 307, SDPMT-12 Continuous Test, Result Summary

Parameter				
Lift-Off Pressure (p_0)	−19.4	kPa	−2.82	psi
Contact Volume (V_c)	20.3	cm^3	1.24	in^3
Limit Pressure (p_L)	2660.0	kPa	385.80	psi
Assumed ν		0.33		
Initial Modulus (E_0)	36066.1	kPa	5230.95	psi
Dry Unit Weight (γ_{dry})	2005.5	kg/m^3	125.2	lb/ft^3
Wet Unit Weight (γ_{wet})	2079.2	kg/m^3	129.8	lb/ft^3

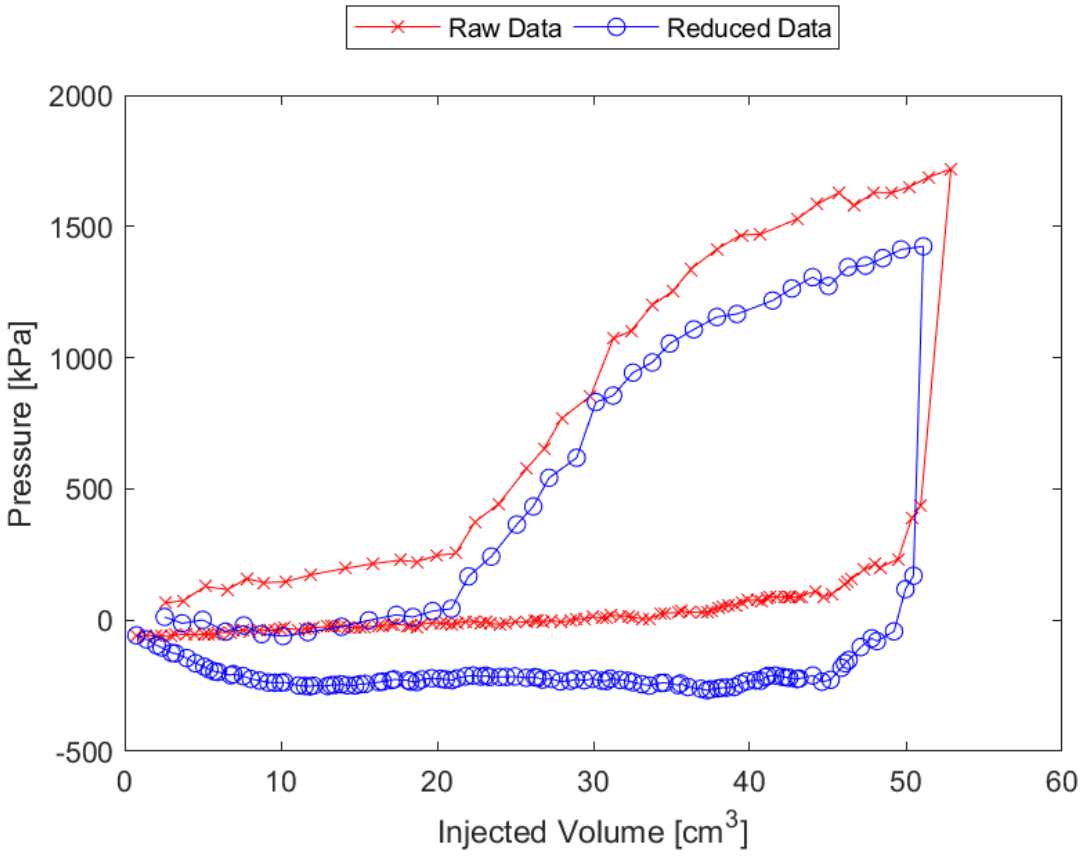

Figure D.44: Sounding 308, SDPMT-12 Continuous Test, Membrane O.D. 0.625m, Depth 0.41 m, Raw and Reduced Data

Table D.44: Sounding 308, SDPMT-12 Continuous Test, Result Summary

Parameter				
Lift-Off Pressure (p_0)	43.5	kPa	6.30	psi
Contact Volume (V_c)	20.9	cm^3	1.28	in^3
Limit Pressure (p_L)	1860.0	kPa	269.77	psi
Assumed ν		0.33		
Initial Modulus (E_0)	16247.5	kPa	2356.51	psi
Dry Unit Weight (γ_{dry})	2080.8	kg/m^3	129.9	lb/ft^3
Wet Unit Weight (γ_{wet})	2231.4	kg/m^3	139.3	lb/ft^3

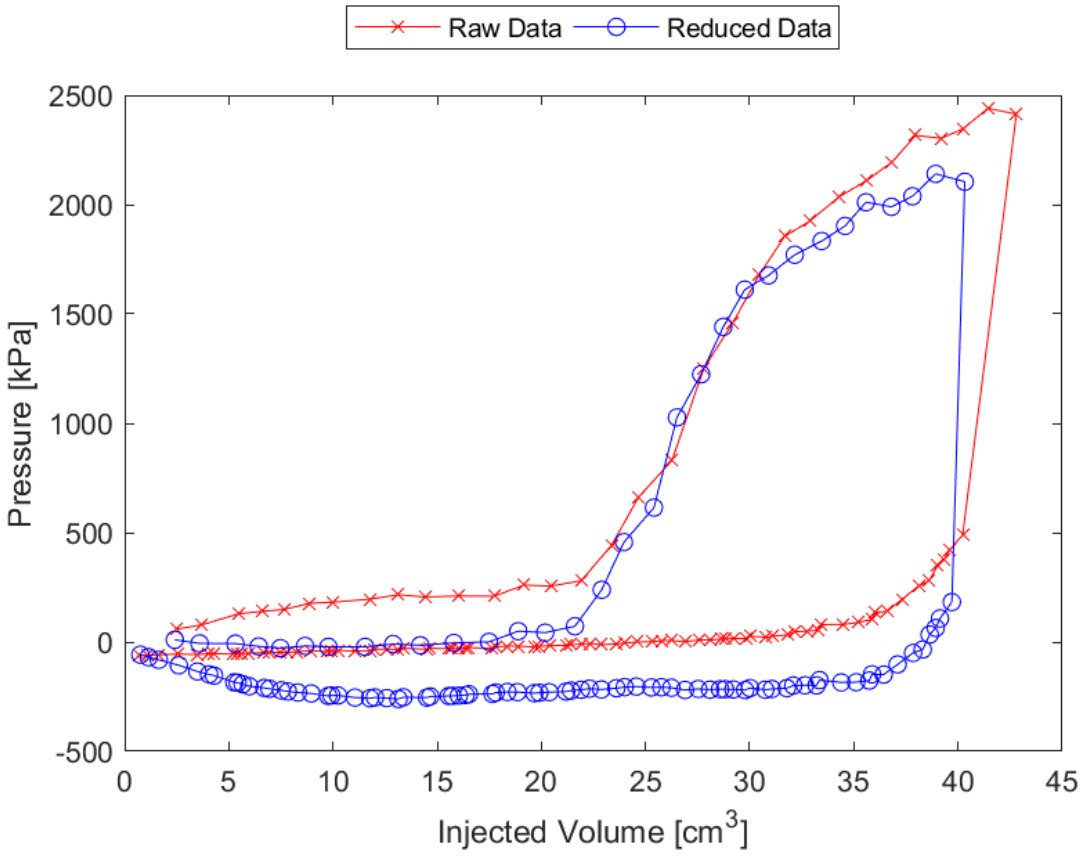

Figure D.45: Sounding 309, SDPMT-12 Continuous Test, Membrane O.D. 0.625m, Depth 0.41 m, Raw and Reduced Data

Table D.45: Sounding 309, SDPMT-12 Continuous Test, Result Summary

Parameter				
Lift-Off Pressure (p_0)	72.1	kPa	10.45	psi
Contact Volume (V_c)	21.6	cm^3	1.32	in^3
Limit Pressure (p_L)	3275.0	kPa	475.00	psi
Assumed ν		0.33		
Initial Modulus (E_0)	43657.7	kPa	6332.03	psi
Dry Unit Weight (γ_{dry})	2119.2	kg/m^3	132.3	lb/ft^3
Wet Unit Weight (γ_{wet})	2199.3	kg/m^3	137.3	lb/ft^3

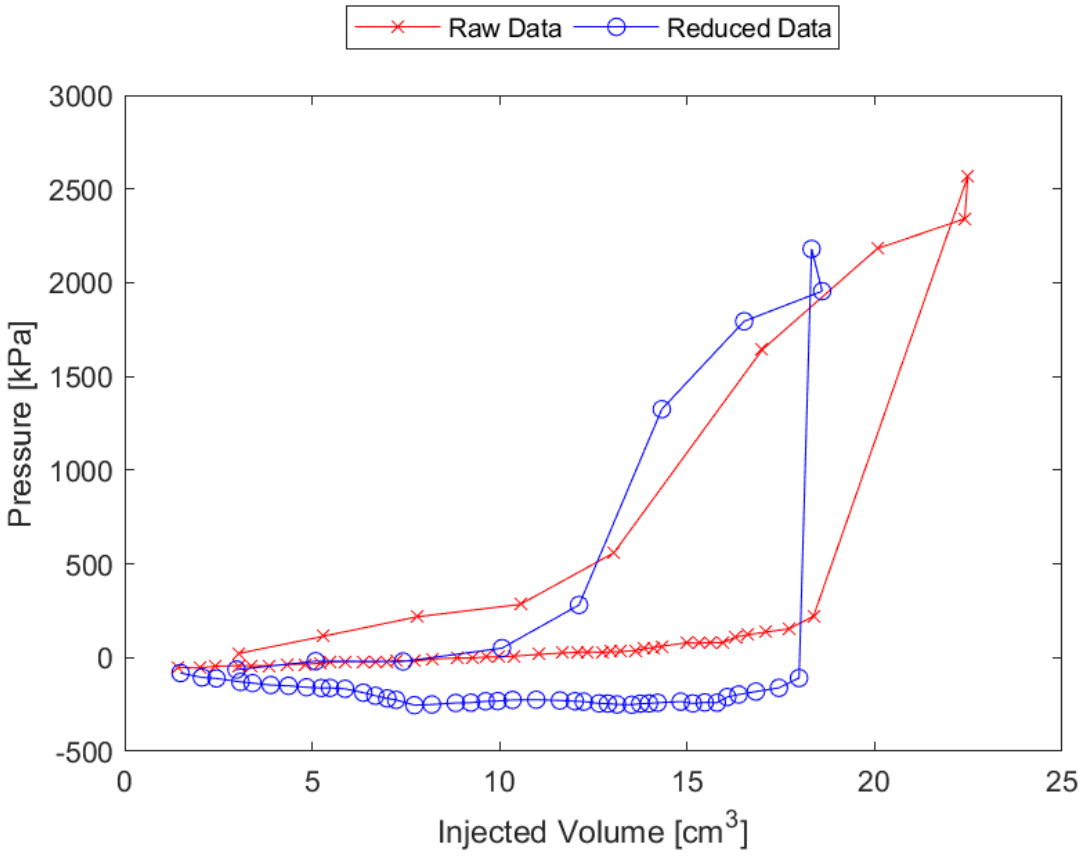

Figure D.46: Sounding 310, SDPMT-12 Continuous Test, Membrane O.D. 0.625m, Depth 0.41 m, Raw and Reduced Data

Table D.46: Sounding 310, SDPMT-12 Continuous Test, Result Summary

Parameter				
Lift-Off Pressure (p_0)	50.5	kPa	7.32	psi
Contact Volume (V_c)	10.1	cm^3	0.61	in^3
Limit Pressure (p_L)	2500.0	kPa	362.60	psi
Assumed ν		0.33		
Initial Modulus (E_0)	108785.3	kPa	15778.01	psi
Dry Unit Weight (γ_{dry})	1997.5	kg/m^3	124.7	lb/ft^3
Wet Unit Weight (γ_{wet})	2068.0	kg/m^3	129.1	lb/ft^3

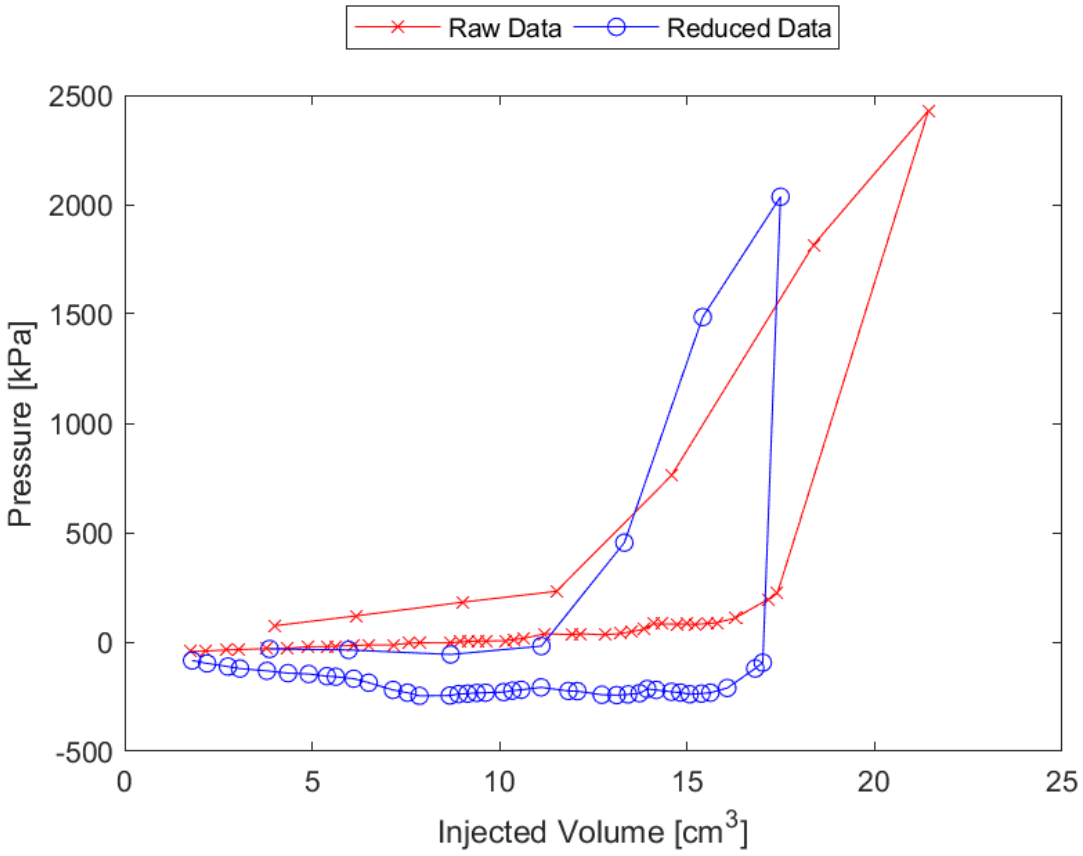

Figure D.47: Sounding 311, SDPMT-12 Continuous Test, Membrane O.D. 0.625m, Depth 0.41 m, Raw and Reduced Data

Table D.47: Sounding 311, SDPMT-12 Continuous Test, Result Summary

Parameter				
Lift-Off Pressure (p_0)	−18.9	kPa	−2.74	psi
Contact Volume (V_c)	11.1	cm^3	0.68	in^3
Limit Pressure (p_L)	3000.0	kPa	435.11	psi
Assumed ν		0.33		
Initial Modulus (E_0)	115021.3	kPa	16682.46	psi
Dry Unit Weight (γ_{dry})	1986.3	kg/m^3	124.0	lb/ft^3
Wet Unit Weight (γ_{wet})	2042.4	kg/m^3	127.5	lb/ft^3

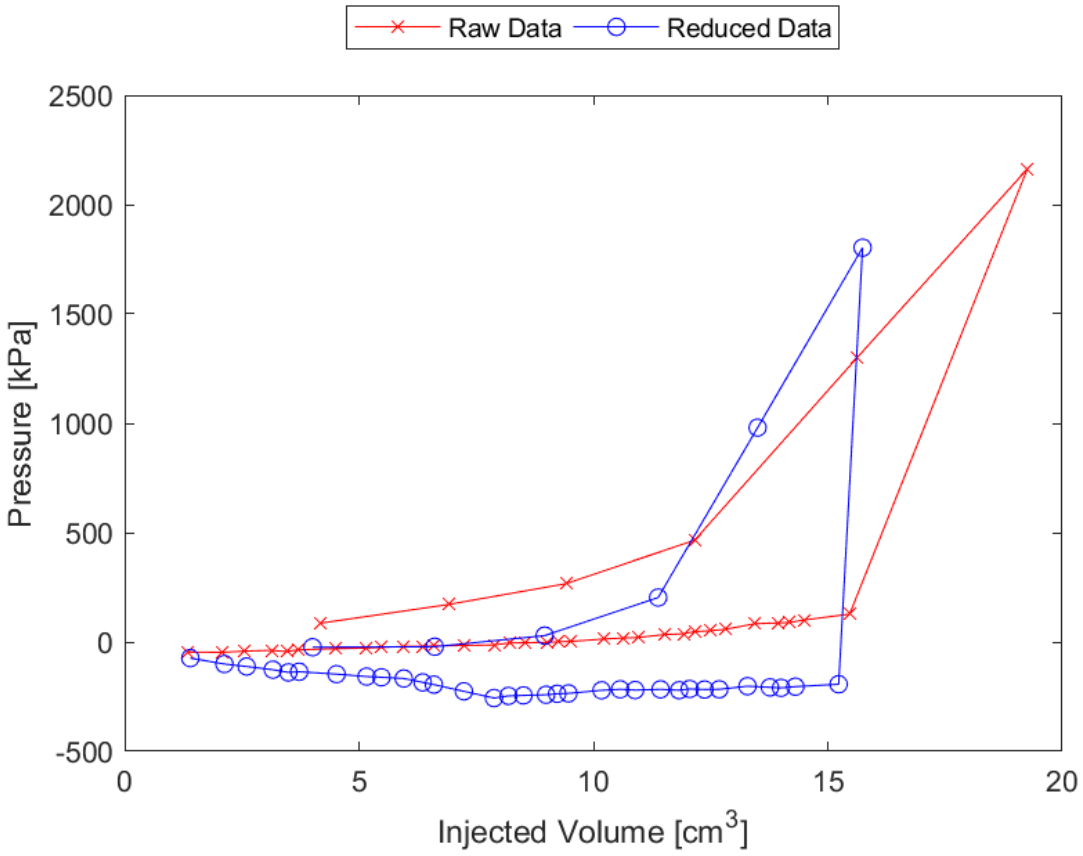

Figure D.48: Sounding 312, SDPMT-12 Continuous Test, Membrane O.D. 0.625m, Depth 0.41 m, Raw and Reduced Data

Table D.48: Sounding 312, SDPMT-12 Continuous Test, Result Summary

Parameter				
Lift-Off Pressure (p_0)	29.2	kPa	4.24	psi
Contact Volume (V_c)	9.0	cm^3	0.55	in^3
Limit Pressure (p_L)	3000.0	kPa	435.11	psi
Assumed ν		0.33		
Initial Modulus (E_0)	84678.5	kPa	12281.59	psi
Dry Unit Weight (γ_{dry})	2048.8	kg/m^3	127.9	lb/ft^3
Wet Unit Weight (γ_{wet})	2114.4	kg/m^3	132.0	lb/ft^3

Appendix E

Model Graphs

E.1 Linear - Liner Models

E.1.1 SDPMT E_0 versus p_0

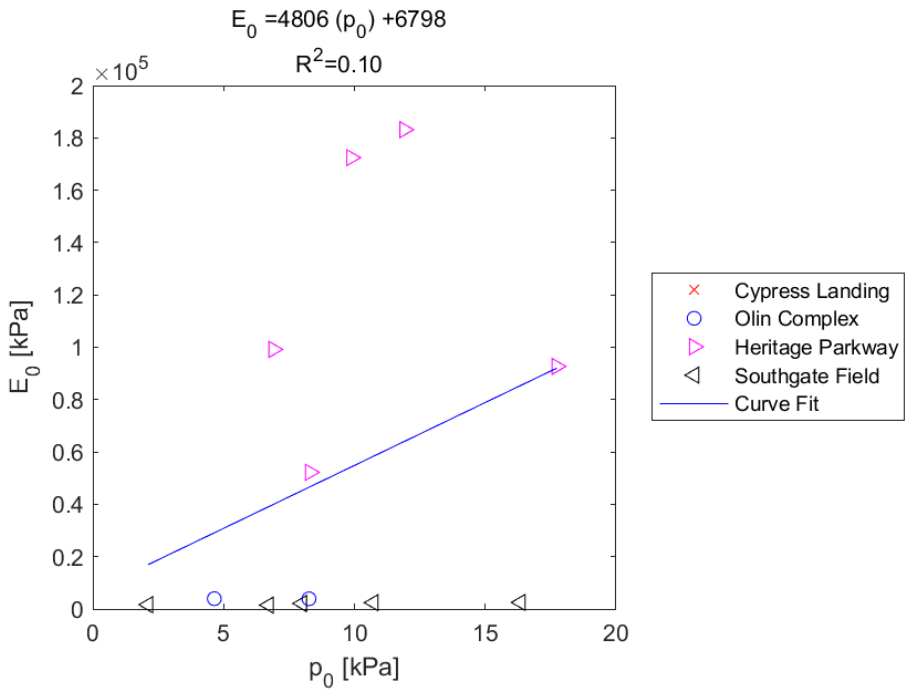

Figure E.1: Linear - Linear Model of E_0 versus p_0 for SDPMT-6 Incremental Tests, All Sites

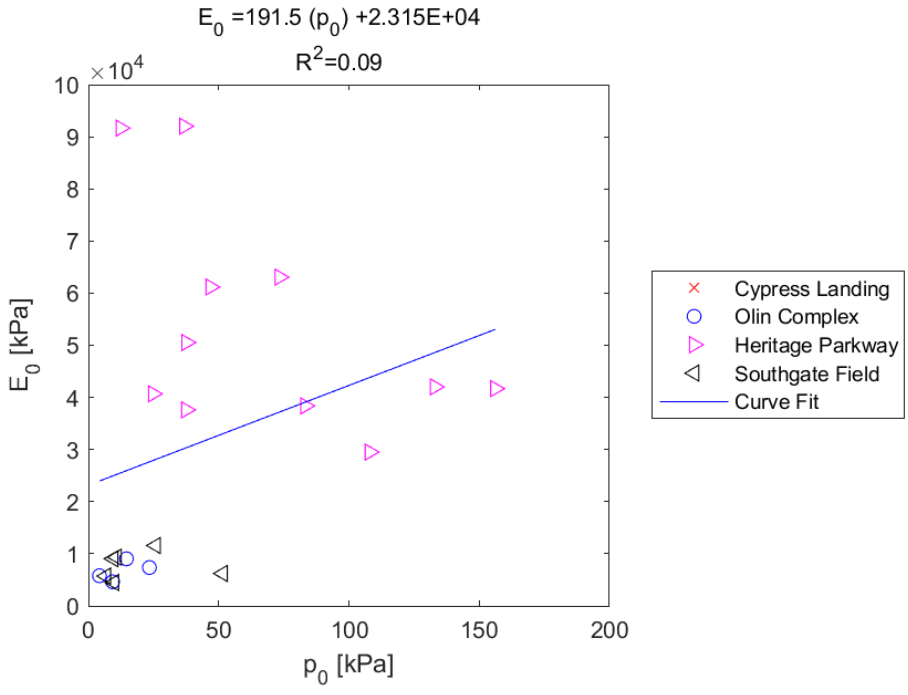

Figure E.2: Linear - Linear Model of E_0 versus p_0 for SDPMT-6 Continuous Tests, All Sites

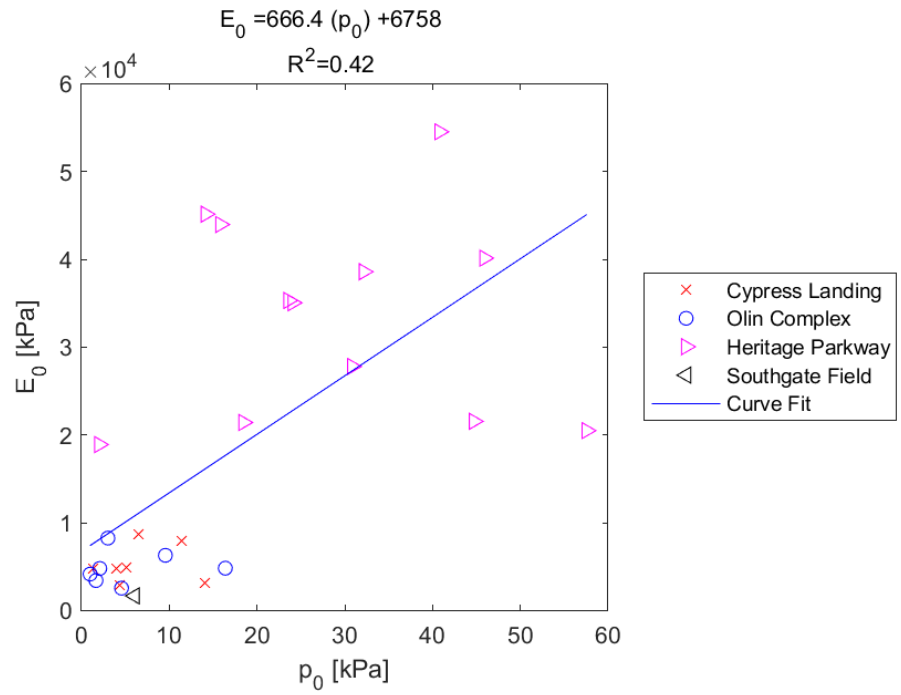

Figure E.3: Linear - Linear Model of E_0 versus p_0 for SDPMT-12 Incremental Tests, All Sites

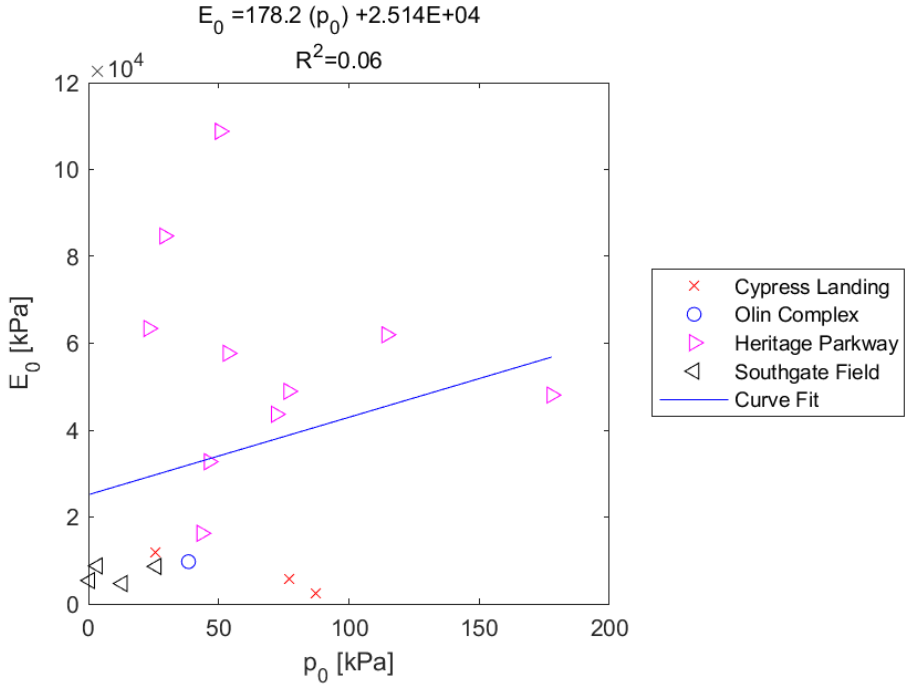

Figure E.4: Linear - Linear Model of E_0 versus p_0 for SDPMT-12 Continuous Tests, All Sites

E.1.2 SDPMT p_0 versus E_0

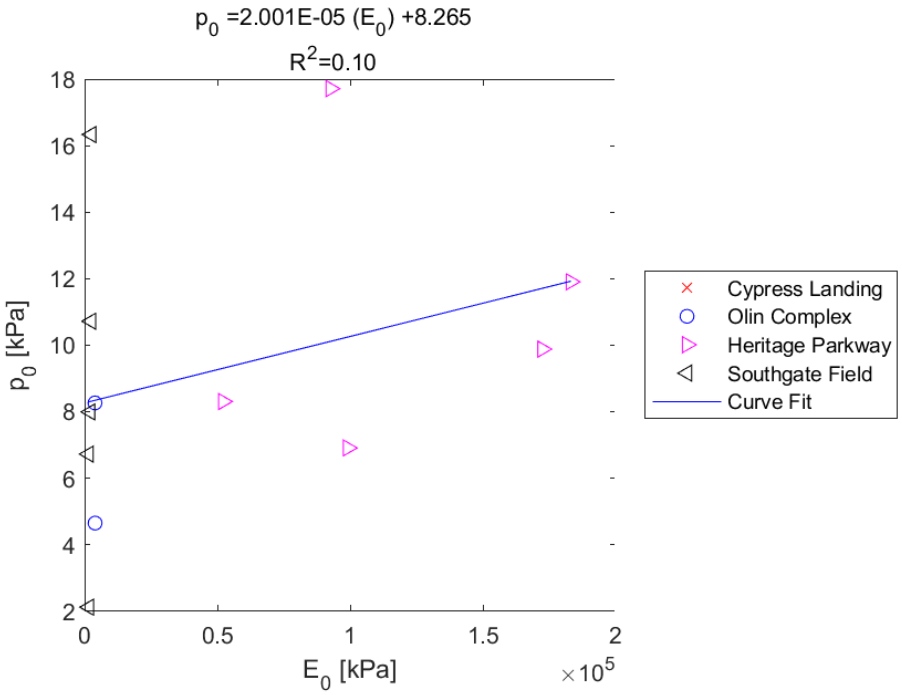

Figure E.5: Linear - Linear Model of p_0 versus E_0 for SDPMT-6 Incremental Tests, All Sites

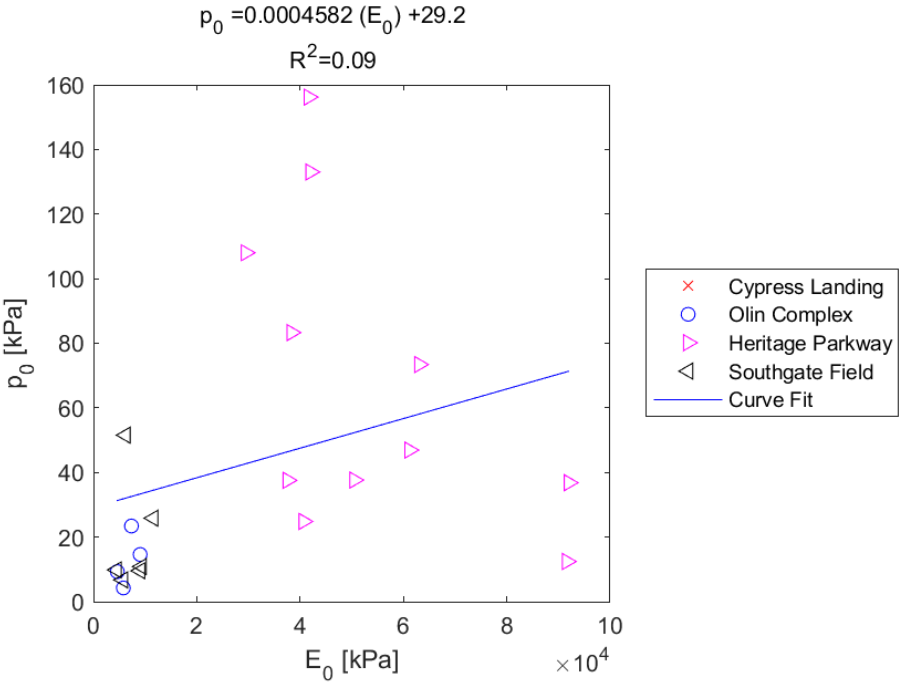

Figure E.6: Linear - Linear Model of p_0 versus E_0 for SDPMT-6 Continuous Tests, All Sites

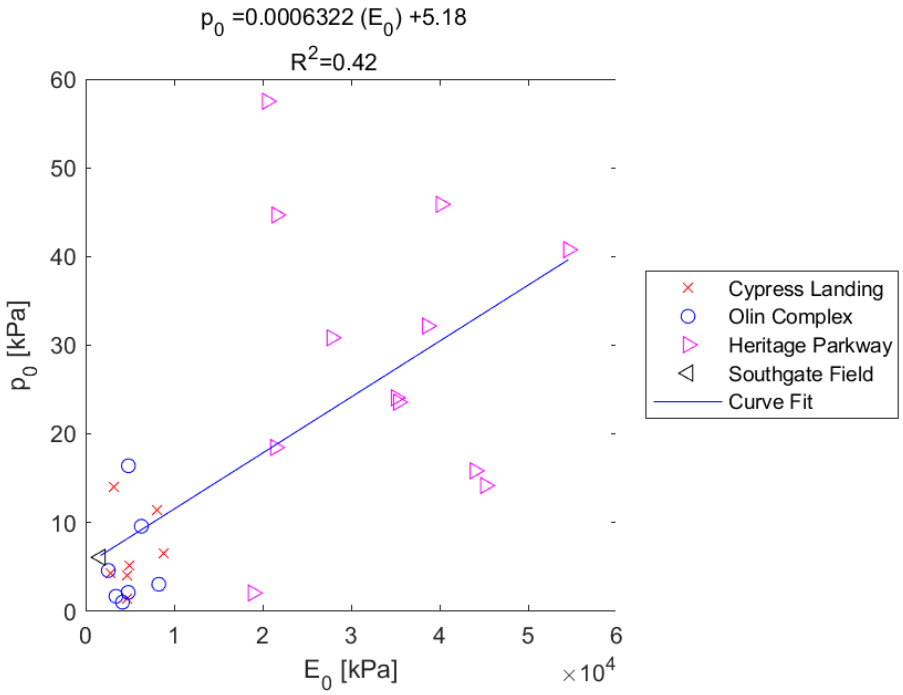

Figure E.7: Linear - Linear Model of p_0 versus E_0 for SDPMT-12 Incremental Tests, All Sites

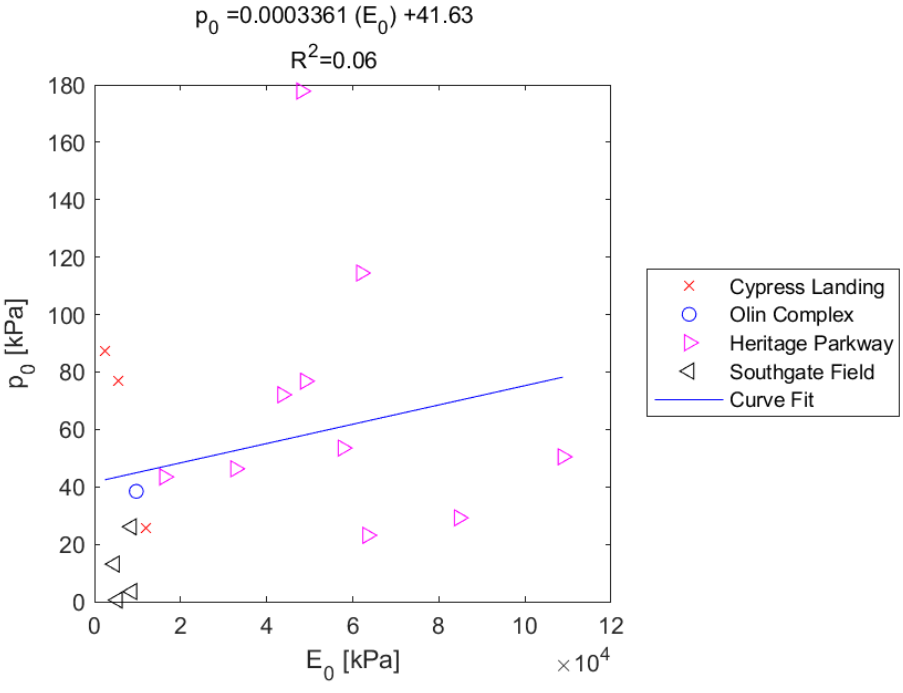

Figure E.8: Linear - Linear Model of p_0 versus E_0 for SDPMT-12 Continuous Tests, All Sites

E.1.3 SDPMT $\mathbf{E}_0$ versus $\mathbf{p}_L$

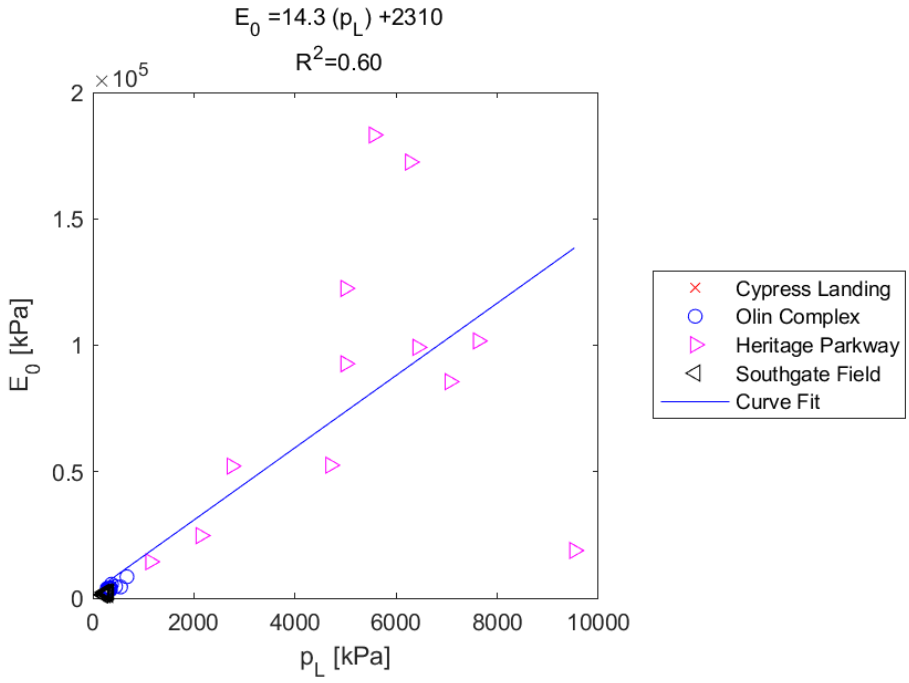

Figure E.9: Linear - Linear Model of E_0 versus p_L for SDPMT-6 Incremental Tests, All Sites

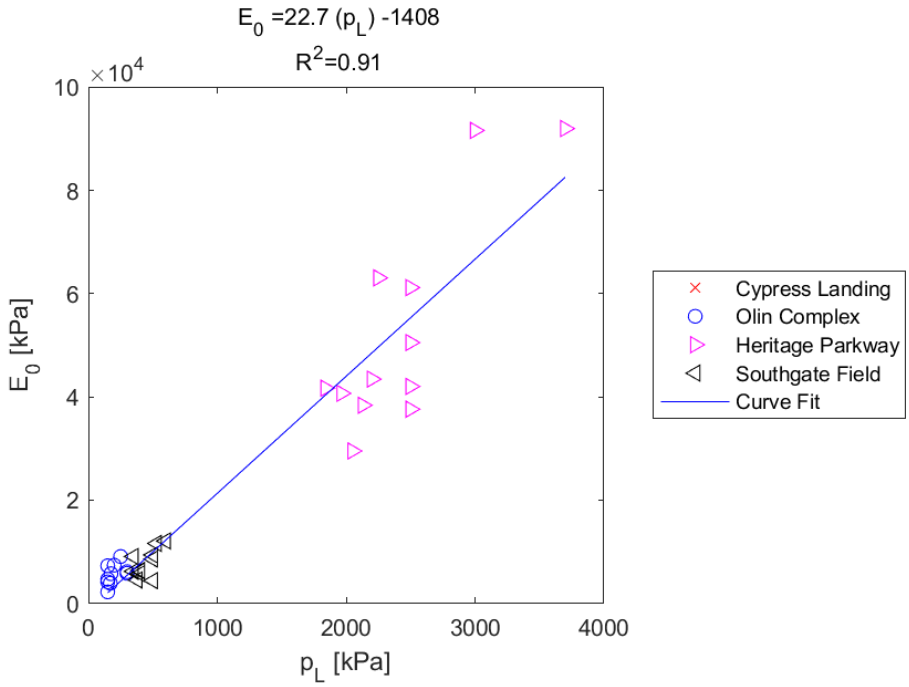

Figure E.10: Linear - Linear Model of E_0 versus p_L for SDPMT-6 Continuous Tests, All Sites

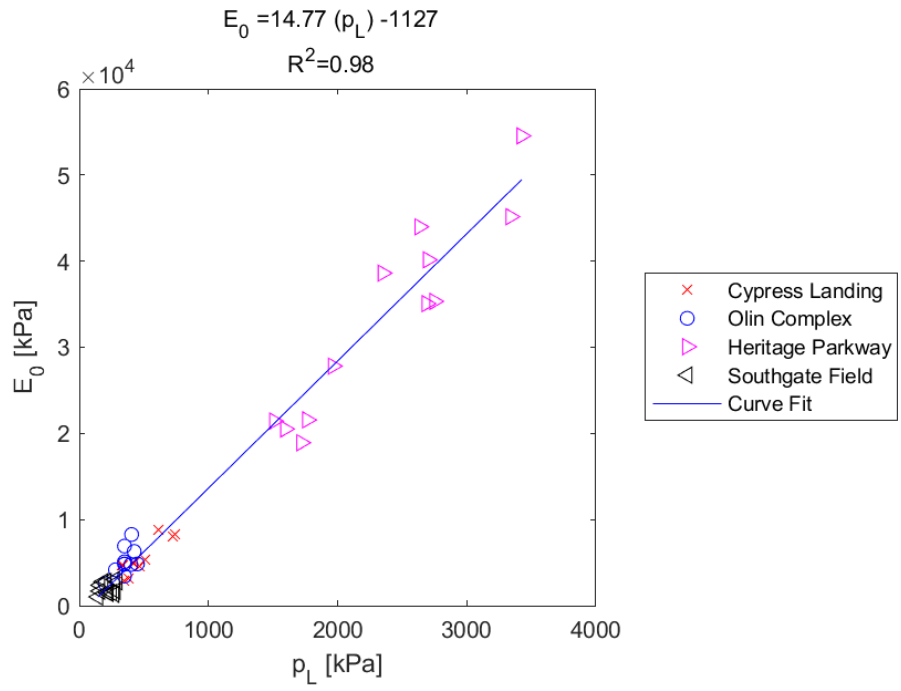

Figure E.11: Linear - Linear Model of E_0 versus p_L for SDPMT-12 Incremental Tests, All Sites

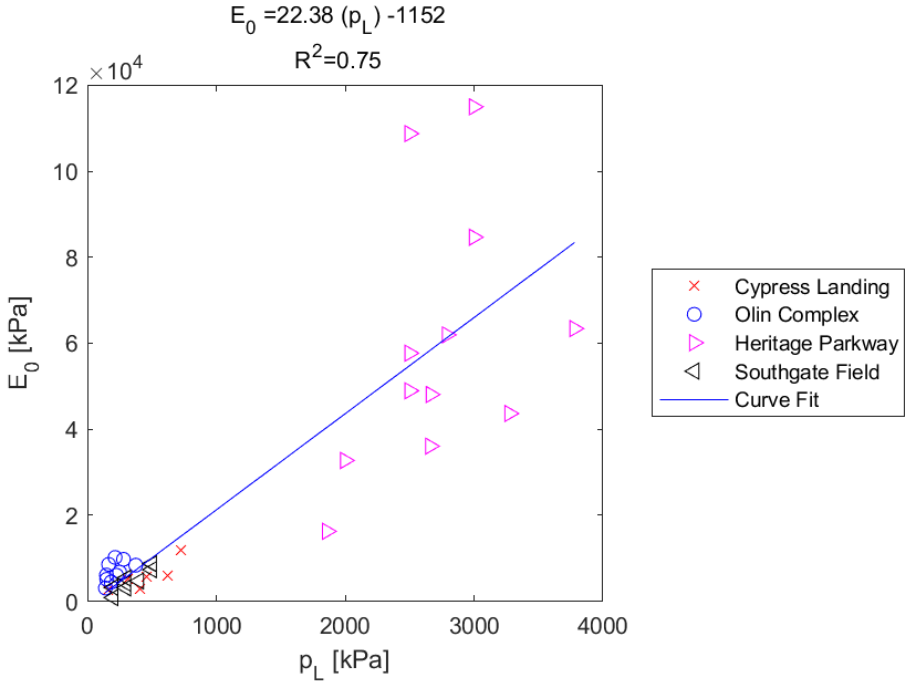

Figure E.12: Linear - Linear Model of E_0 versus p_L for SDPMT-12 Continuous Tests, All Sites

E.1.4 SDPMT $\mathbf{p}_L$ versus $\mathbf{E}_0$

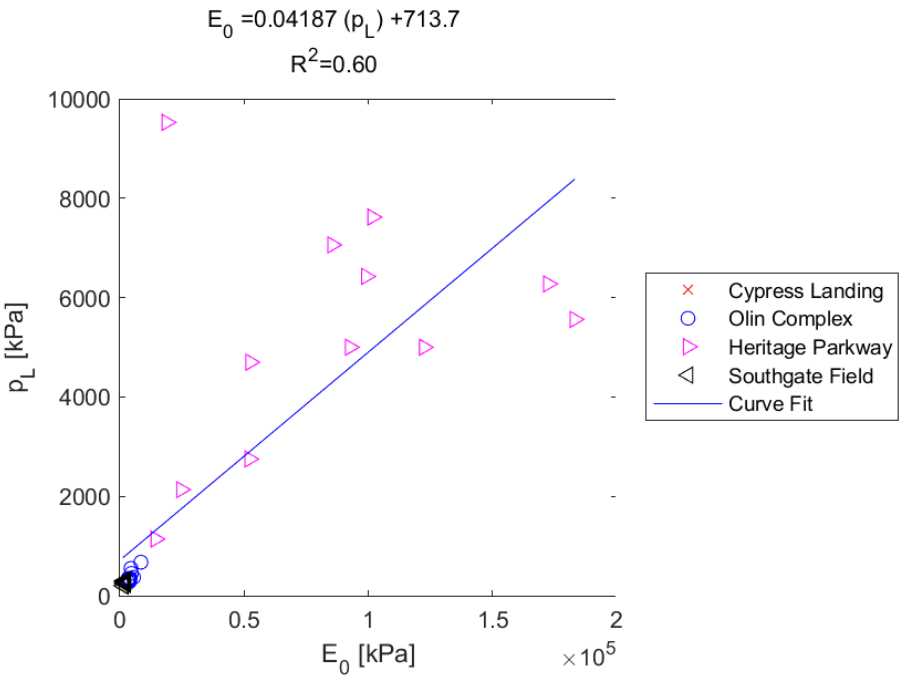

Figure E.13: Linear - Linear Model of p_L versus E_0 for SDPMT-6 Incremental Tests, All Sites

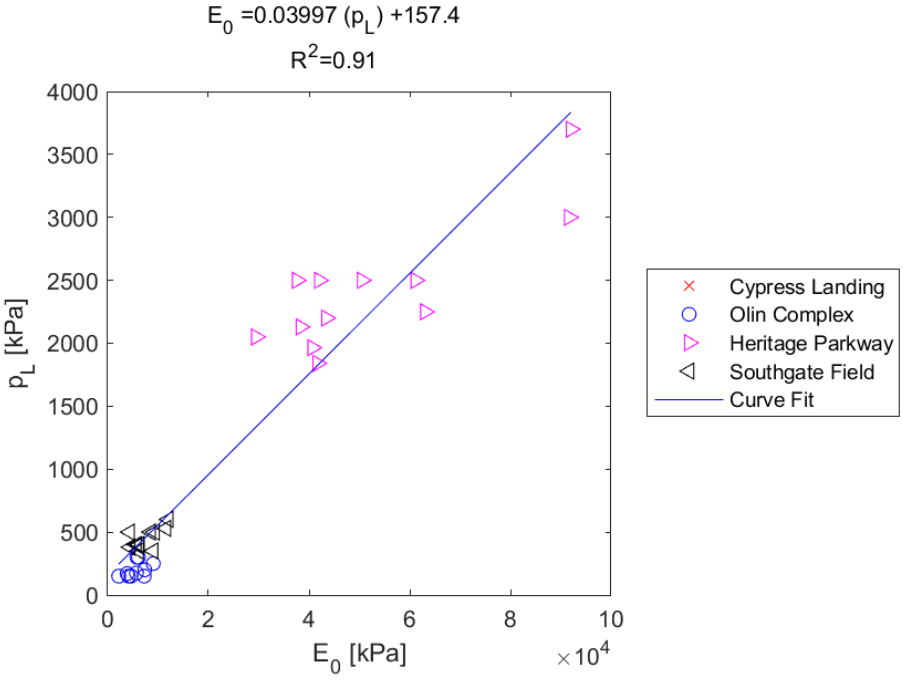

Figure E.14: Linear - Linear Model of p_L versus E_0 for SDPMT-6 Continuous Tests, All Sites

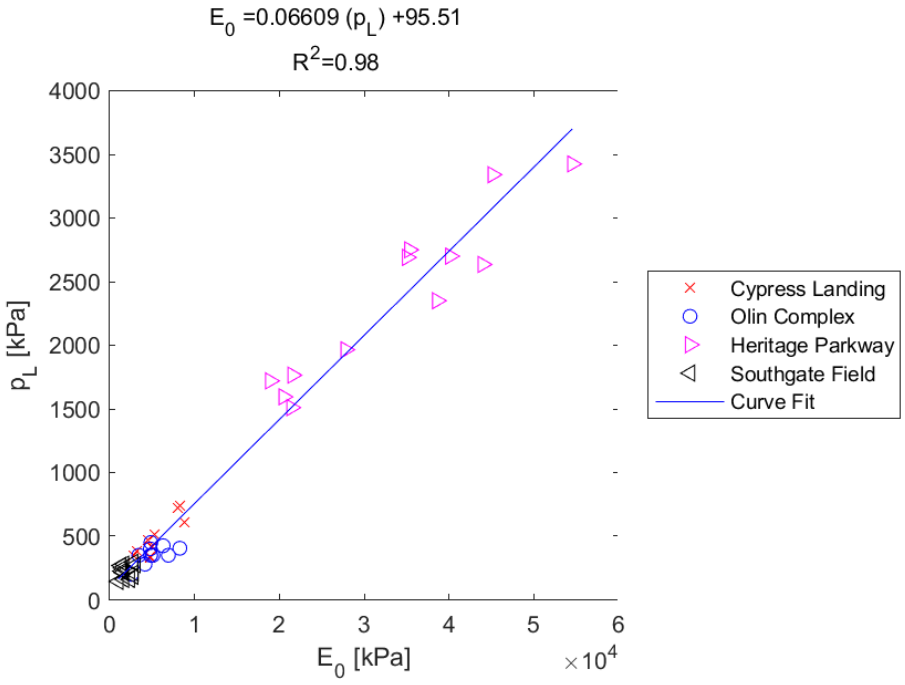

Figure E.15: Linear - Linear Model of p_L versus E_0 for SDPMT-12 Incremental Tests, All Sites

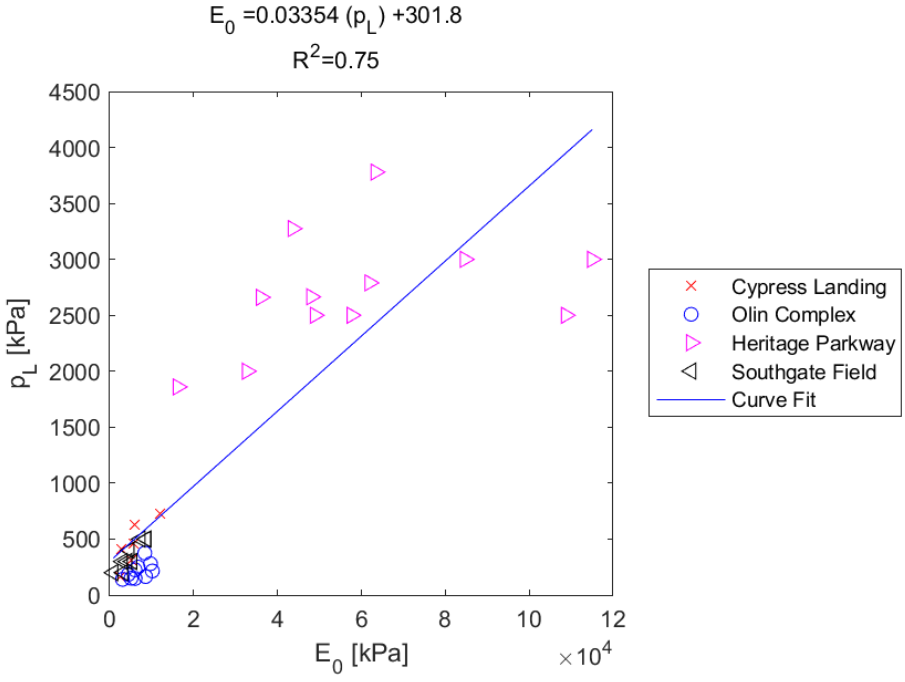

Figure E.16: Linear - Linear Model of p_L versus E_0 for SDPMT-12 Continuous Tests, All Sites

E.1.5 SDPMT $\mathbf{p}_0$ versus $\mathbf{p}_L$

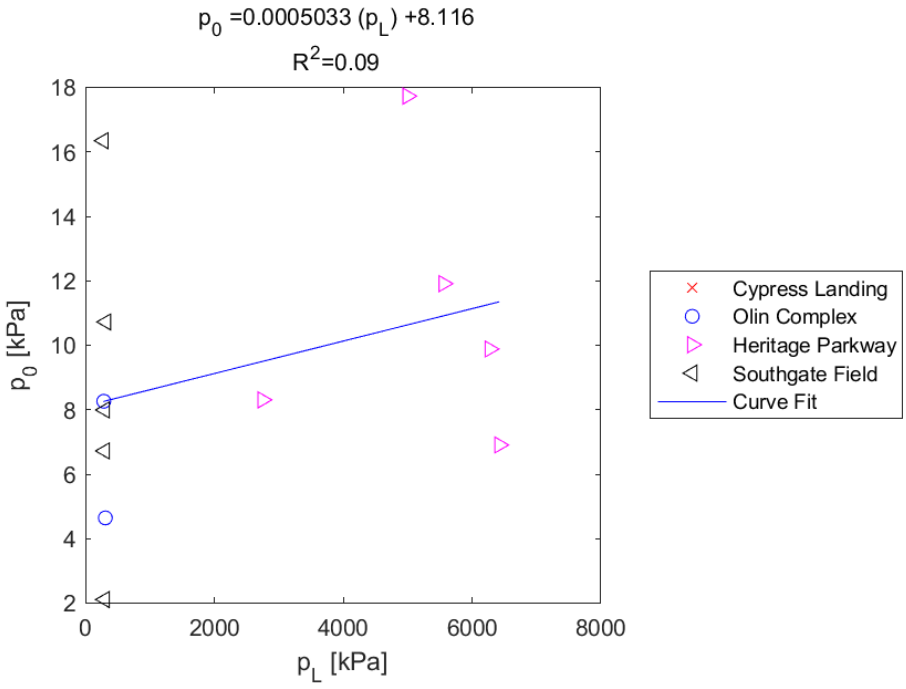

Figure E.17: Linear - Linear Model of p_0 versus p_L for SDPMT-6 Incremental Tests, All Sites

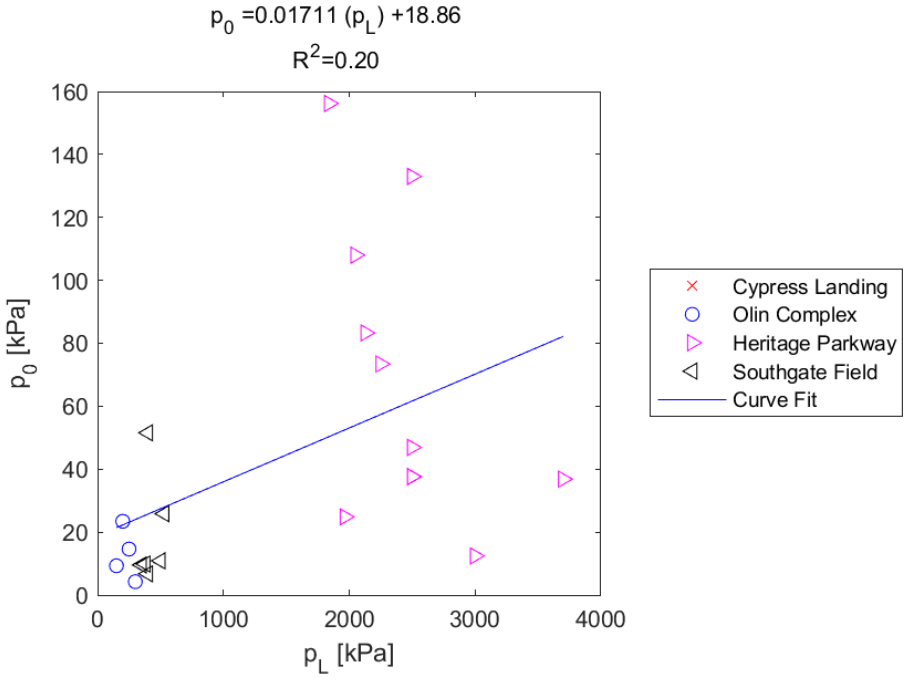

Figure E.18: Linear - Linear Model of p_0 versus p_L for SDPMT-6 Continuous Tests, All Sites

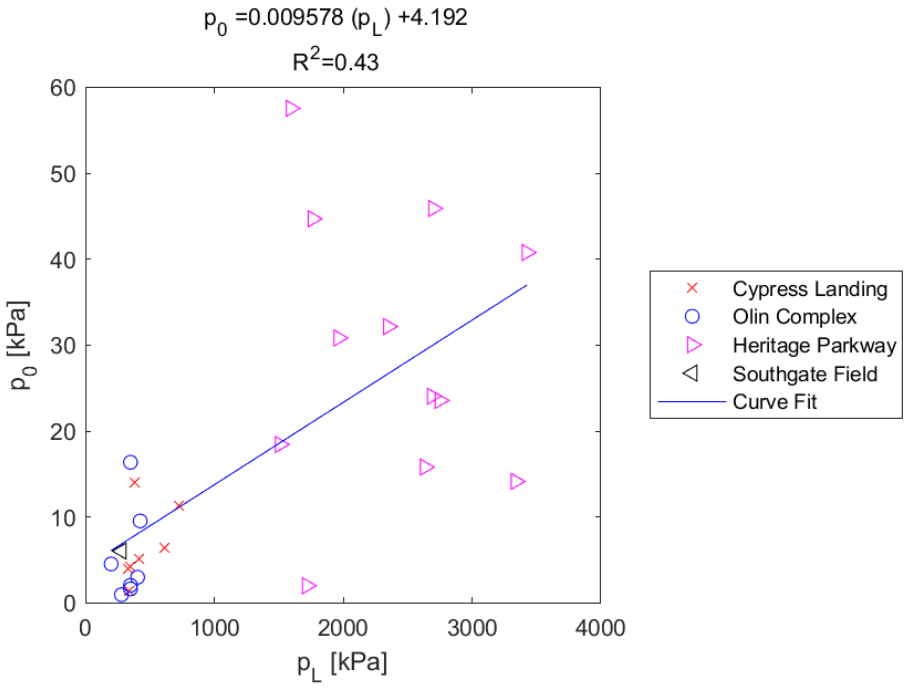

Figure E.19: Linear - Linear Model of p_0 versus p_L for SDPMT-12 Incremental Tests, All Sites

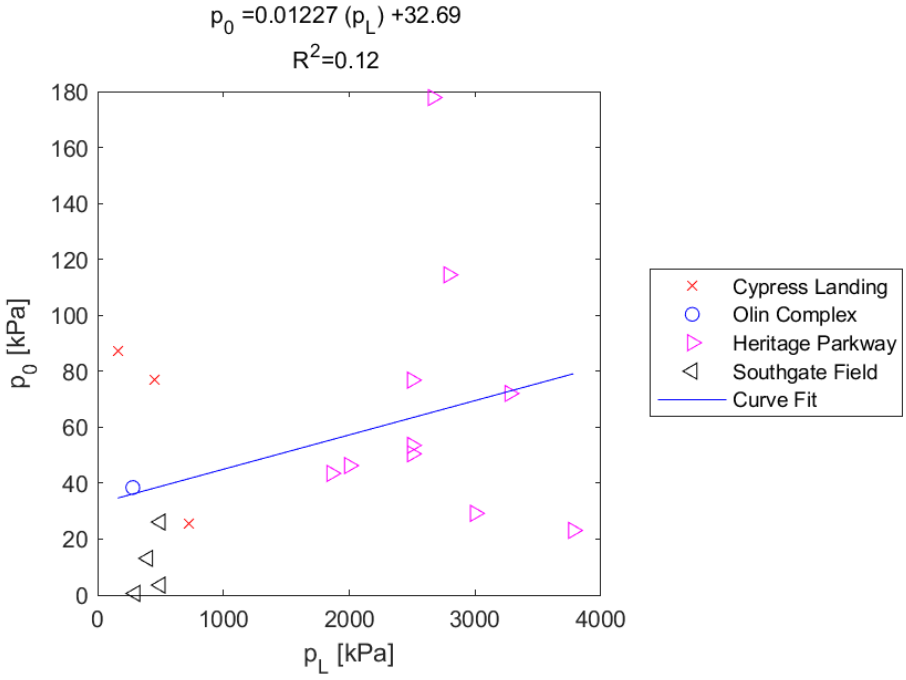

Figure E.20: Linear - Linear Model of p_0 versus p_L for SDPMT-12 Continuous Tests, All Sites

E.1.6 SDPMT $\mathbf{p}_L$ versus $\mathbf{p}_0$

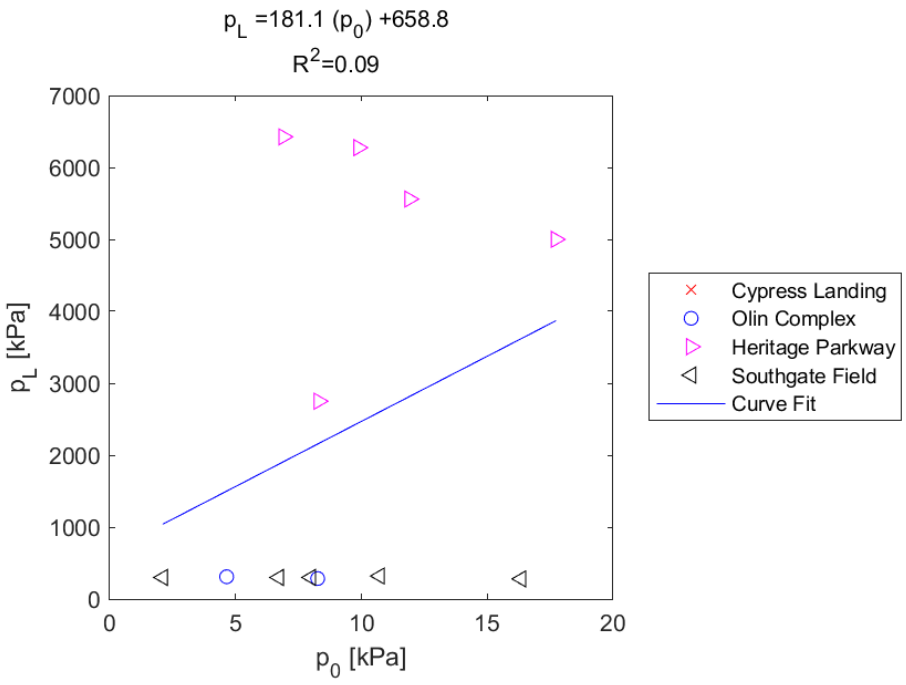

Figure E.21: Linear - Linear Model of p_L versus p_0 for SDPMT-6 Incremental Tests, All Sites

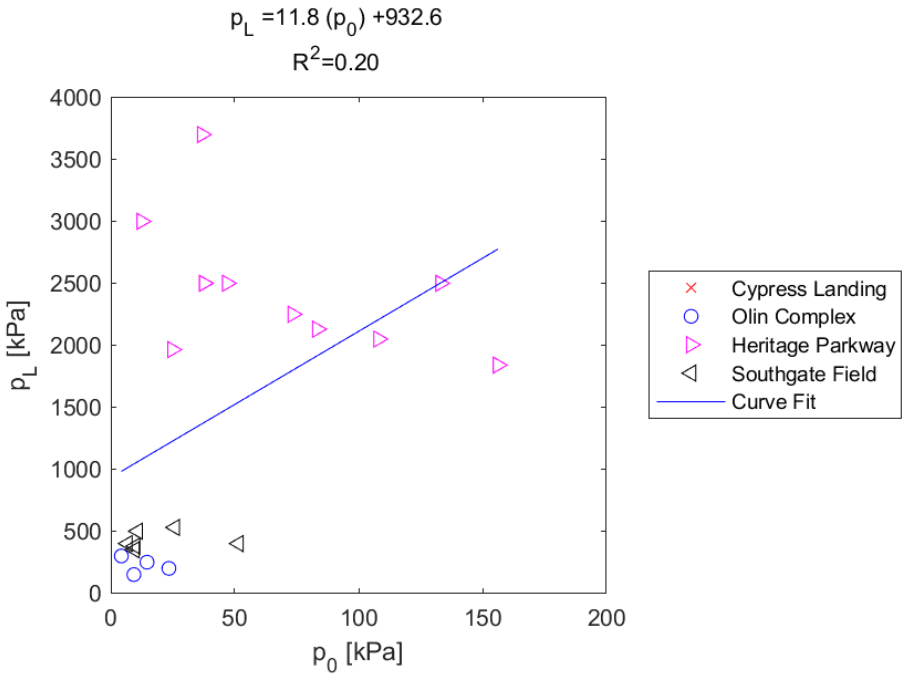

Figure E.22: Linear - Linear Model of p_L versus p_0 for SDPMT-6 Continuous Tests, All Sites

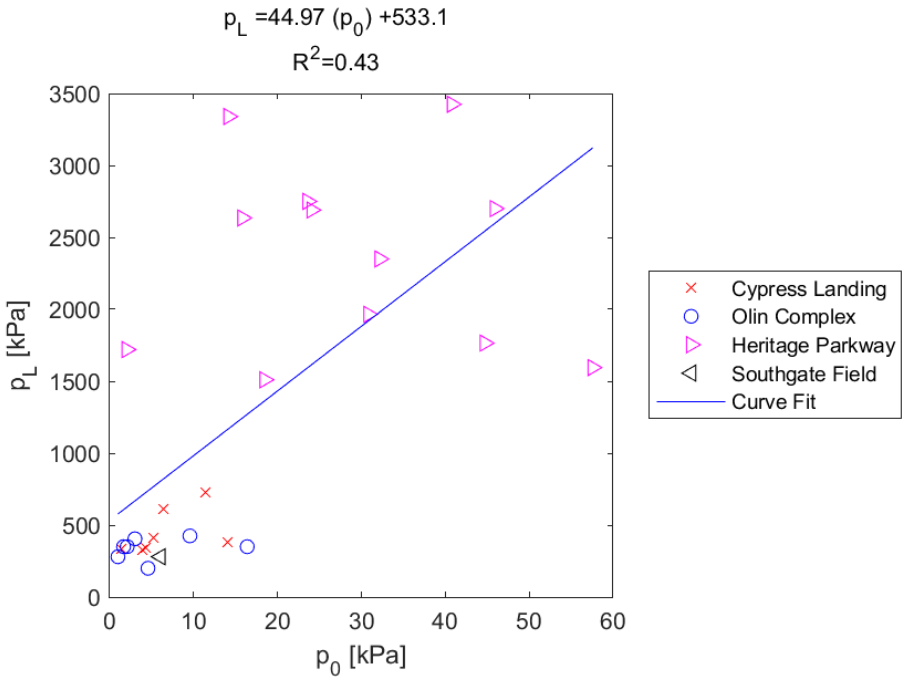

Figure E.23: Linear - Linear Model of p_L versus p_0 for SDPMT-12 Incremental Tests, All Sites

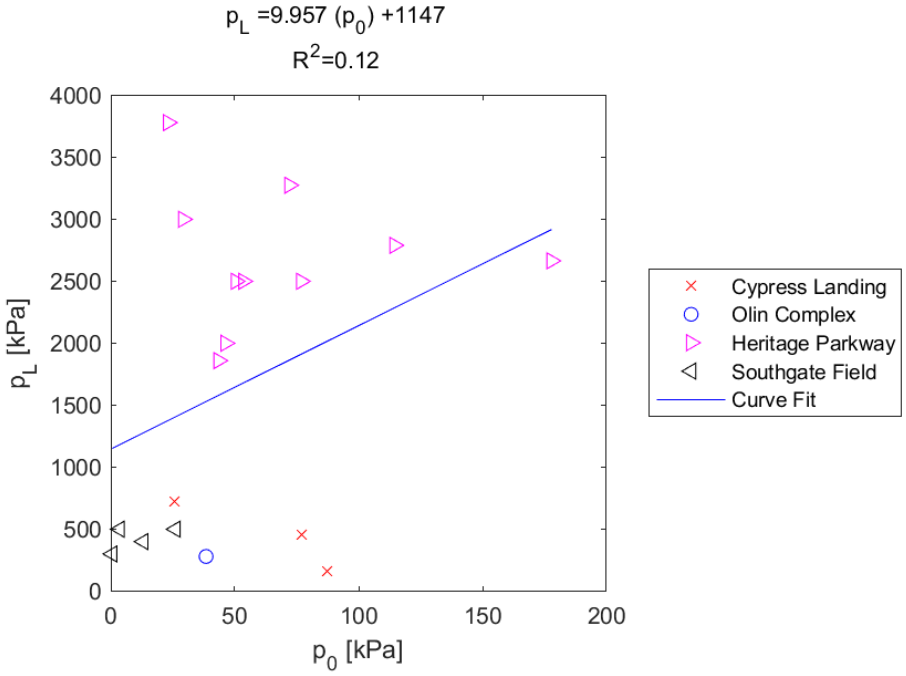

Figure E.24: Linear - Linear Model of p_L versus p_0 for SDPMT-12 Continuous Tests, All Sites

E.1.7 γ_{wet} versus $\mathbf{E}_0$

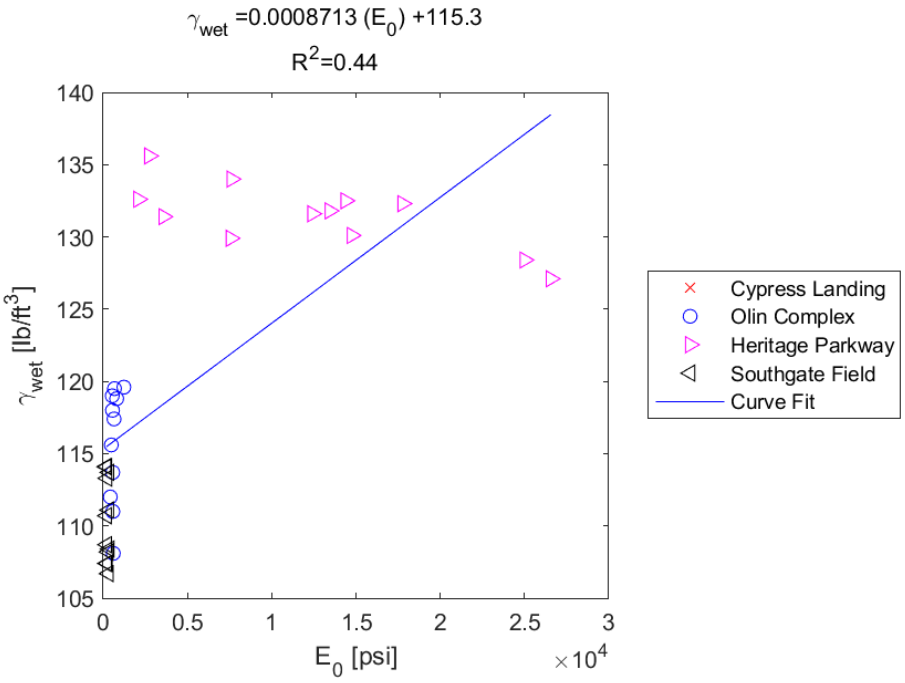

Figure E.25: Linear - Linear Model of γ_{wet} versus E_0 for SDPMT-6 Incremental Tests, All Sites

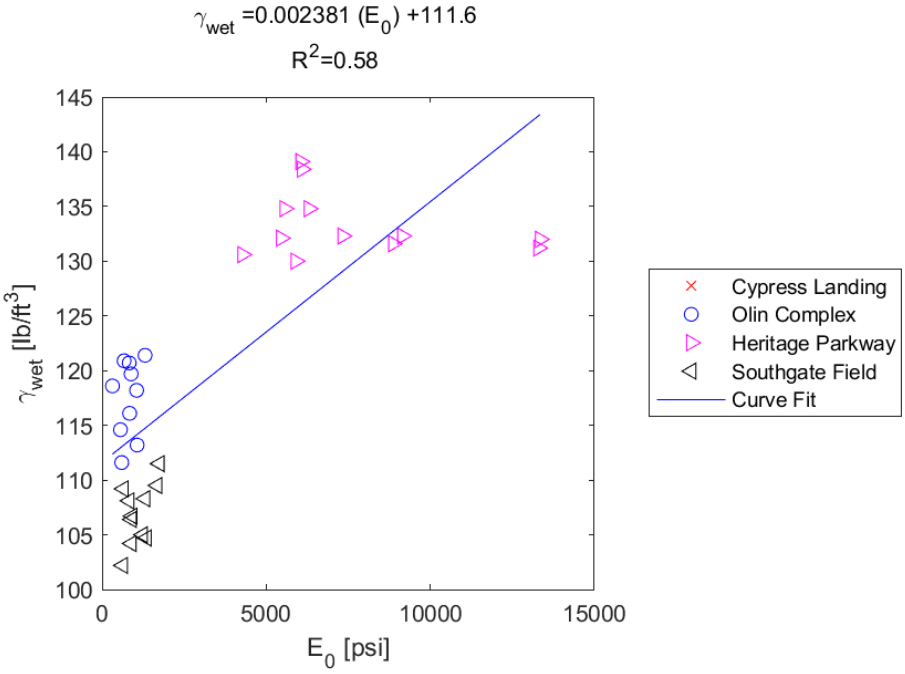

Figure E.26: Linear - Linear Model of γ_{wet} versus E_0 for SDPMT-6 Continuous Tests, All Sites

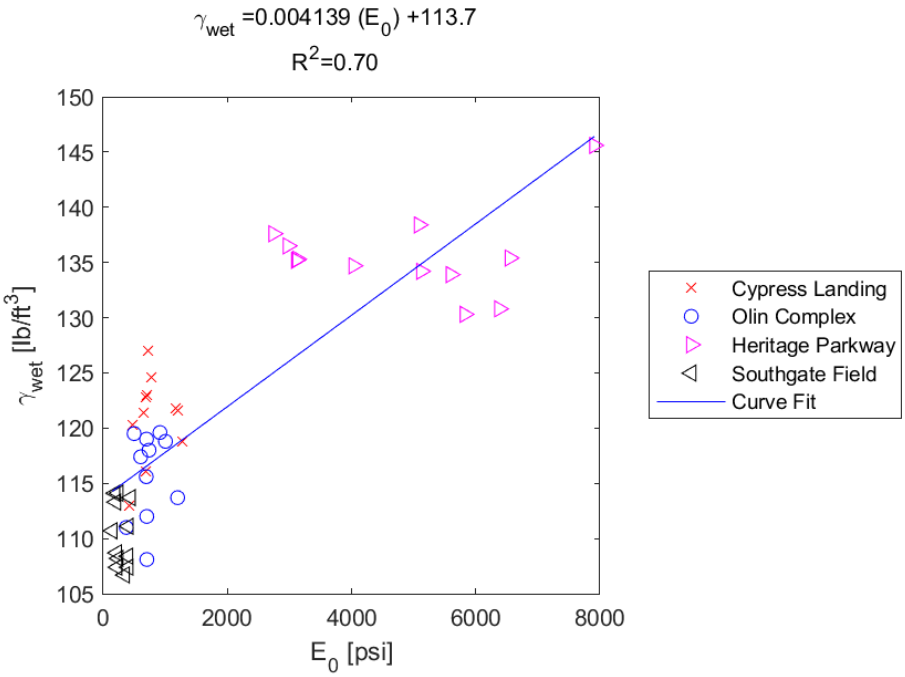

Figure E.27: Linear - Linear Model of γ_{wet} versus E_0 for SDPMT-12 Incremental Tests, All Sites

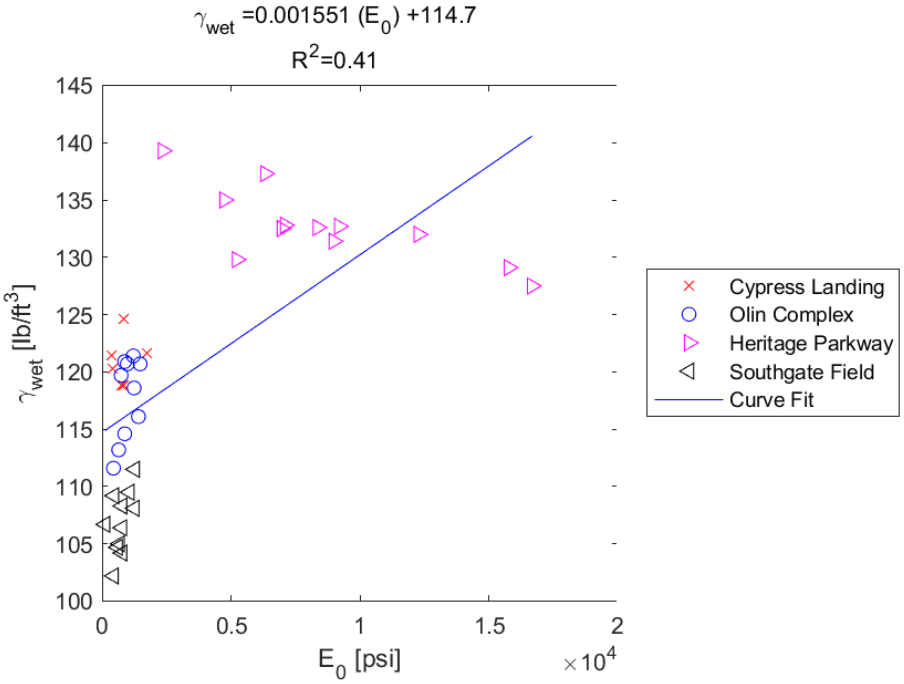

Figure E.28: Linear - Linear Model of γ_{wet} versus E_0 for SDPMT-12 Continuous Tests, All Sites

E.1.8 γ_{wet} versus $\mathbf{p}_L$

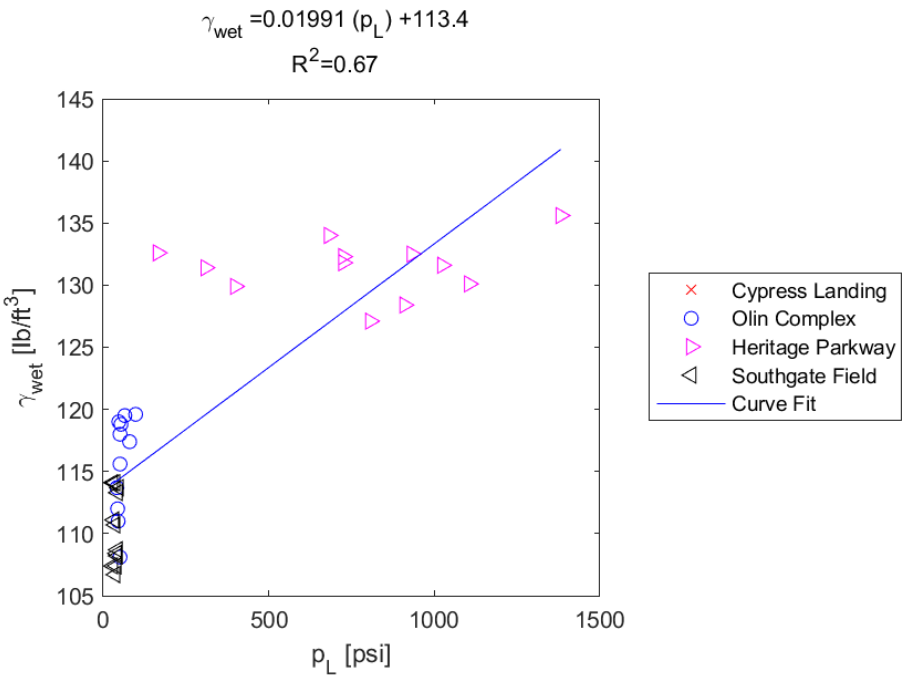

Figure E.29: Linear - Linear Model of γ_{wet} versus p_L for SDPMT-6 Incremental Tests, All Sites

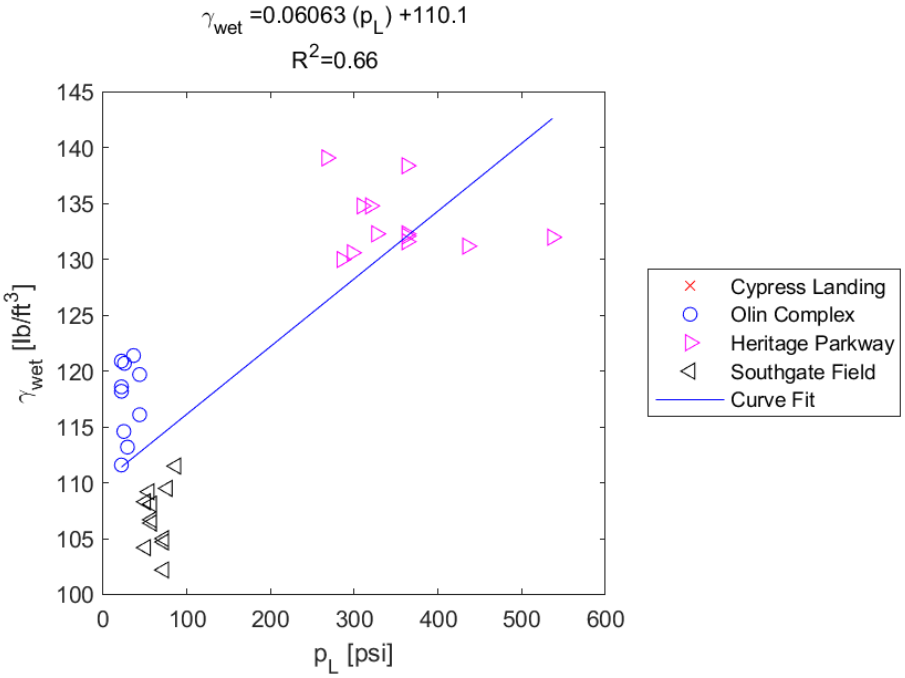

Figure E.30: Linear - Linear Model of γ_{wet} versus p_L for SDPMT-6 Continuous Tests, All Sites

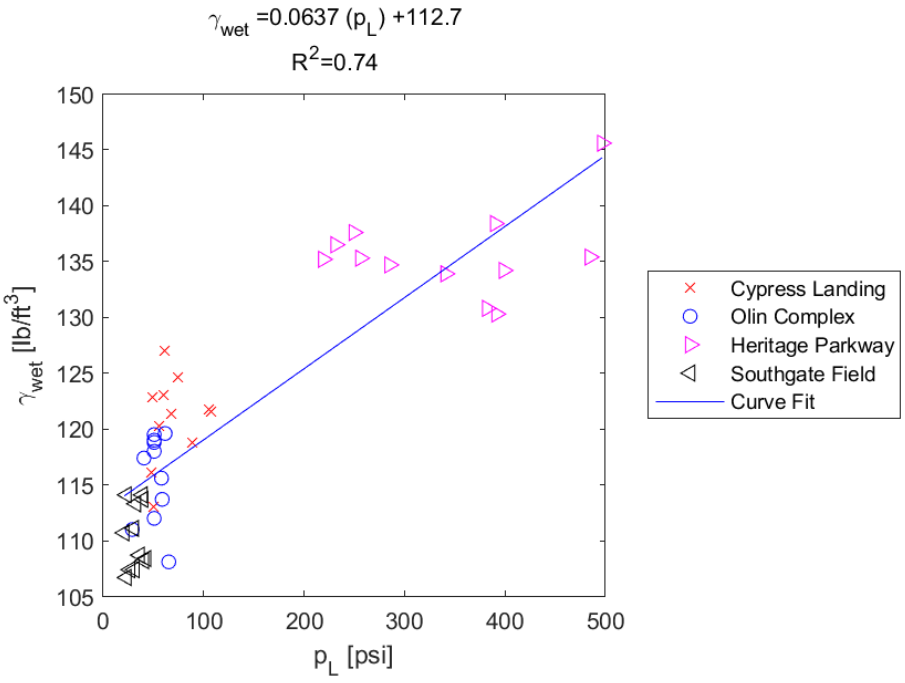

Figure E.31: Linear - Linear Model of γ_{wet} versus p_L for SDPMT-12 Incremental Tests, All Sites

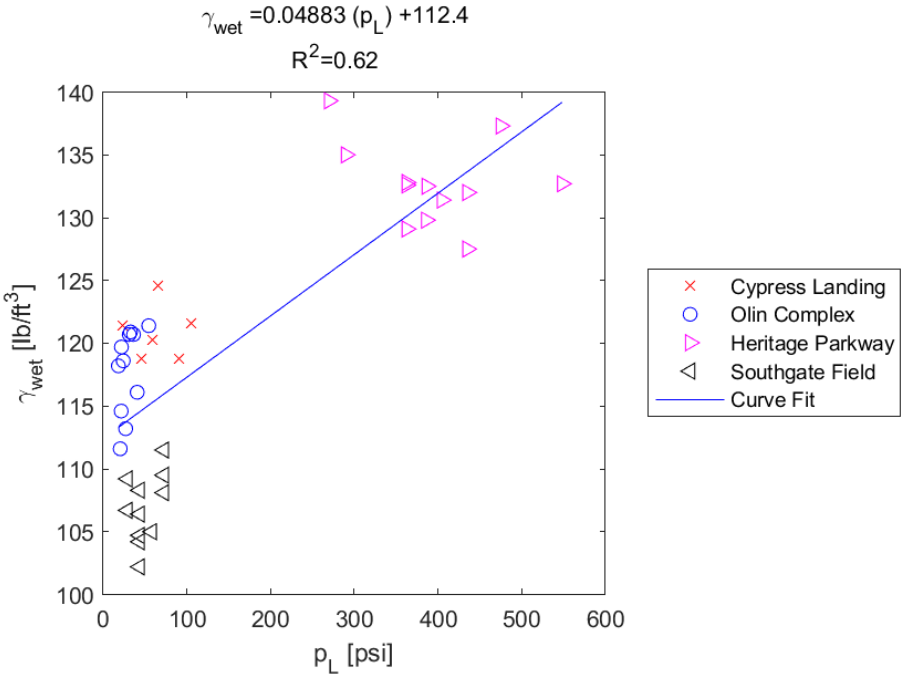

Figure E.32: Linear - Linear Model of γ_{wet} versus p_L for SDPMT-12 Continuous Tests, All Sites

E.1.9 γ_{wet} versus $\mathbf{p}_0$

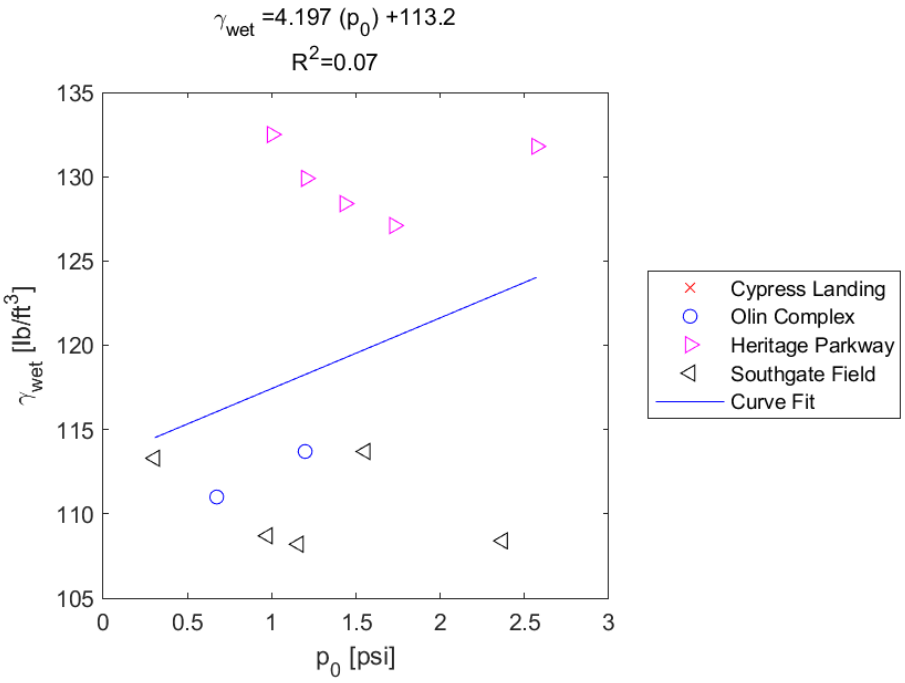

Figure E.33: Linear - Linear Model of γ_{wet} versus p_0 for SDPMT-6 Incremental Tests, All Sites

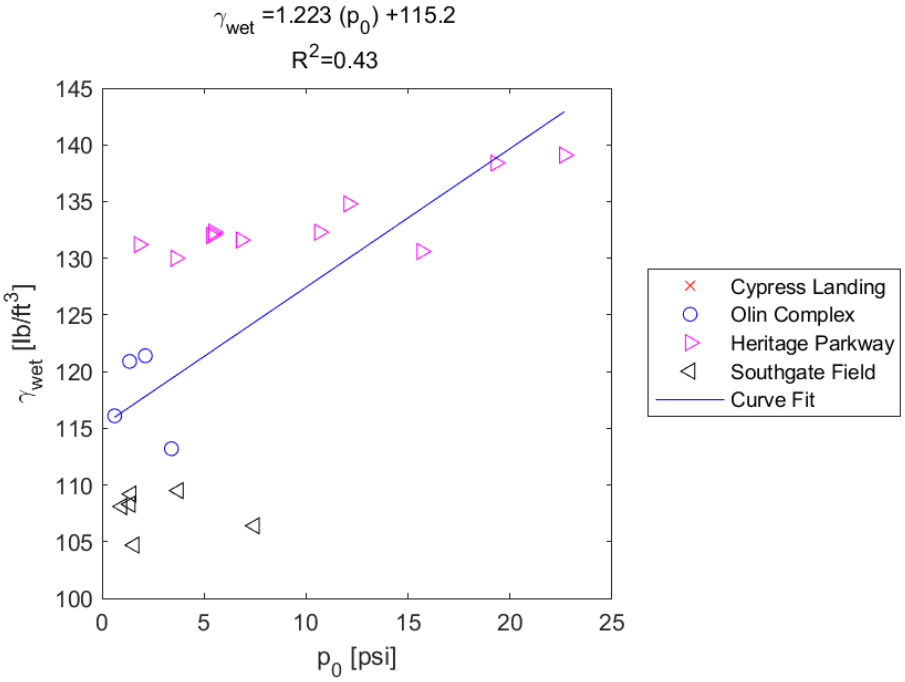

Figure E.34: Linear - Linear Model of γ_{wet} versus p_0 for SDPMT-6 Continuous Tests, All Sites

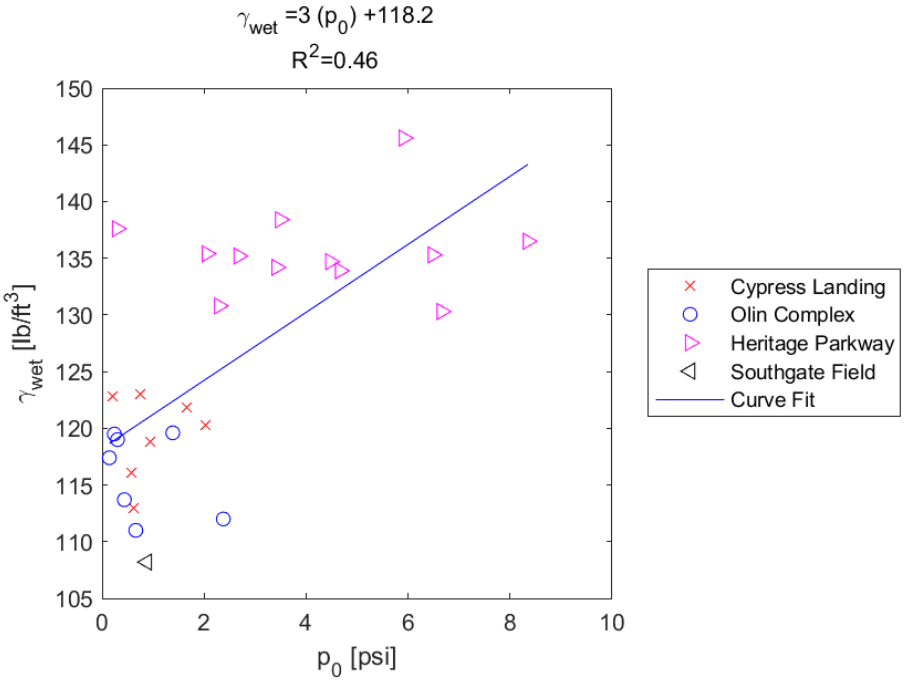

Figure E.35: Linear - Linear Model of γ_{wet} versus p_0 for SDPMT-12 Incremental Tests, All Sites

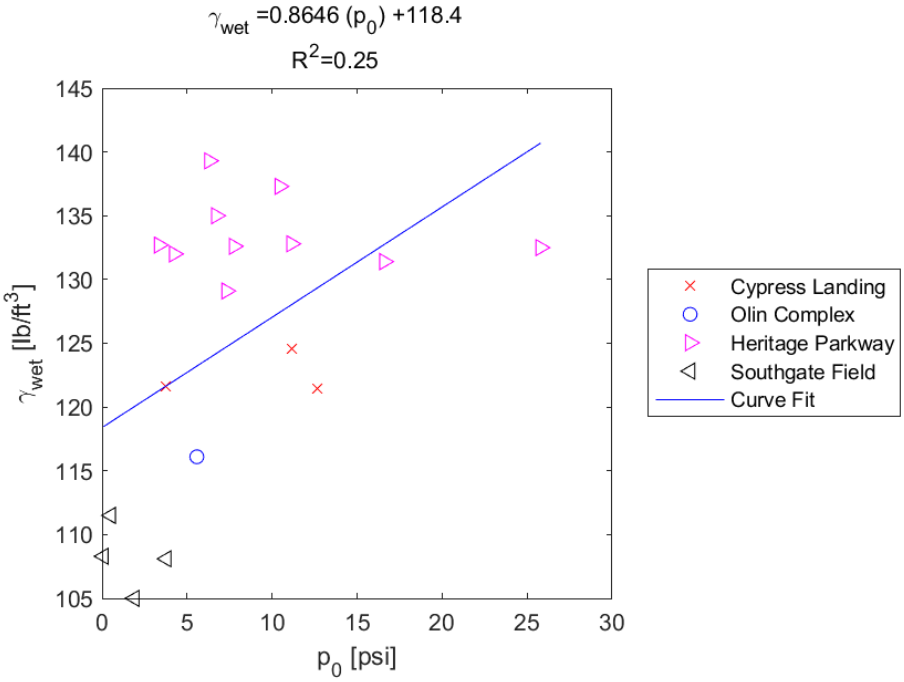

Figure E.36: Linear - Linear Model of γ_{wet} versus p_0 for SDPMT-12 Continuous Tests, All Sites

E.1.10 γ_{dry} versus $\mathbf{E}_0$

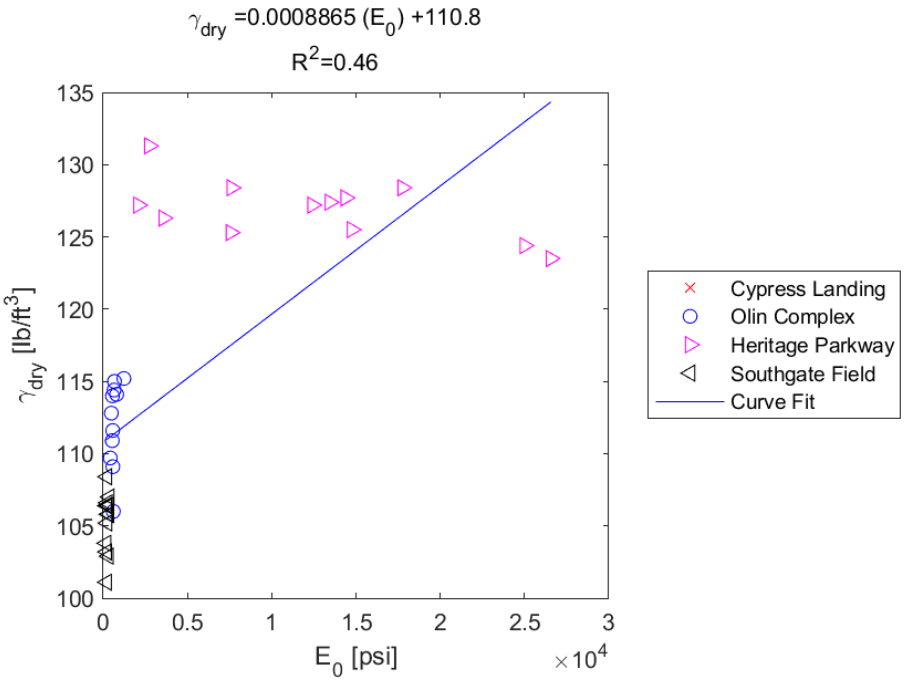

Figure E.37: Linear - Linear Model of γ_{dry} versus E_0 for SDPMT-6 Incremental Tests, All Sites

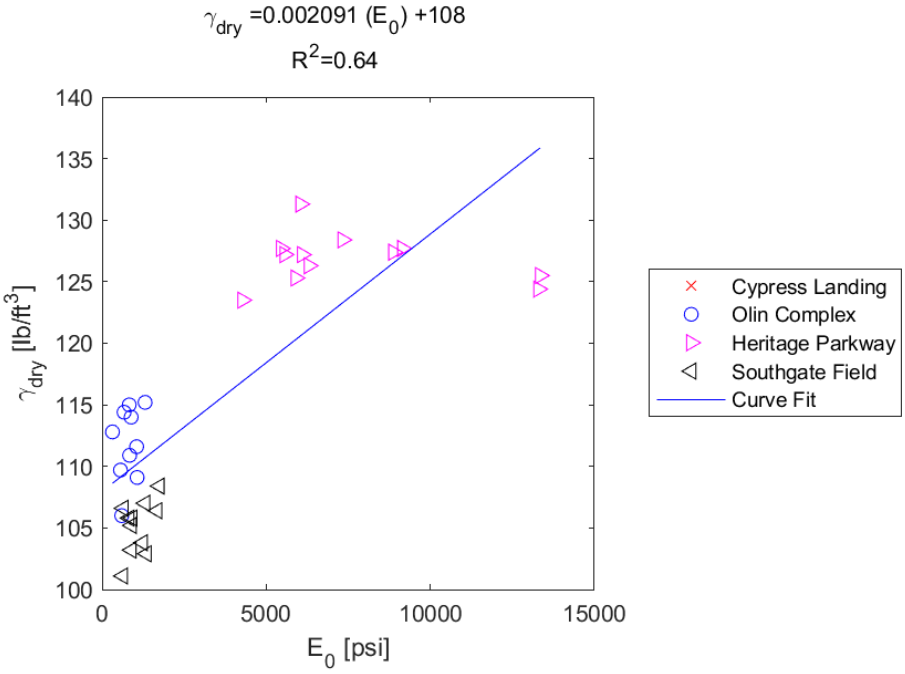

Figure E.38: Linear - Linear Model of γ_{dry} versus E_0 for SDPMT-6 Continuous Tests, All Sites

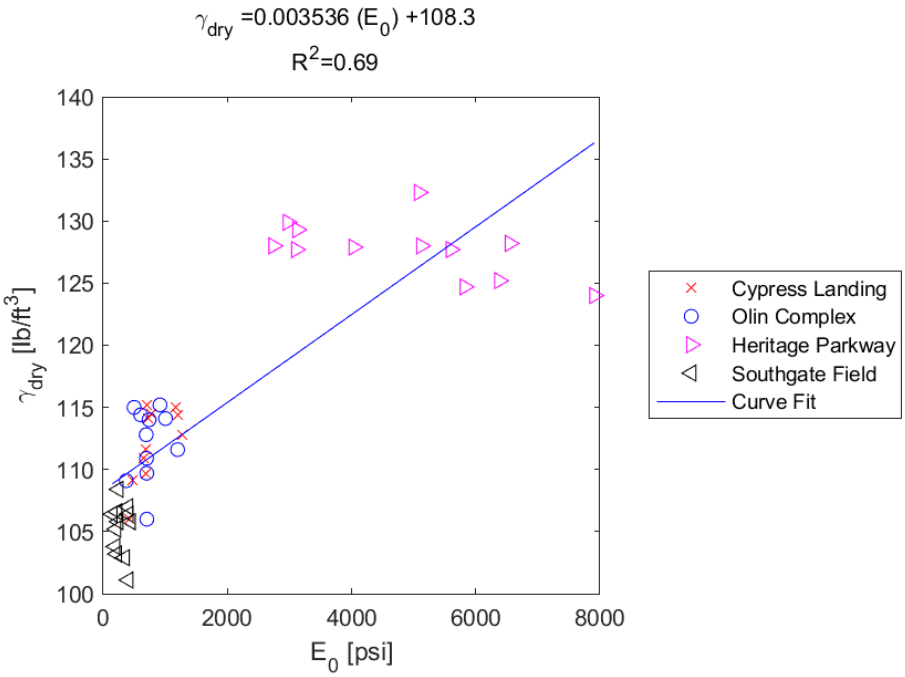

Figure E.39: Linear - Linear Model of γ_{dry} versus E_0 for SDPMT-12 Incremental Tests, All Sites

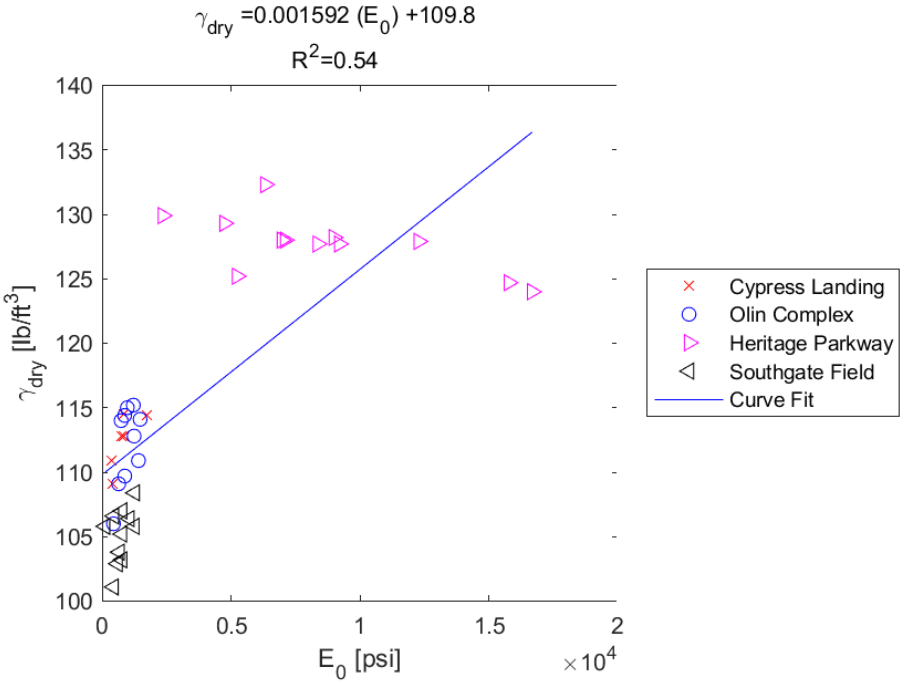

Figure E.40: Linear - Linear Model of γ_{dry} versus E_0 for SDPMT-12 Continuous Tests, All Sites

E.1.11 γ_{dry} versus $\mathbf{p}_L$

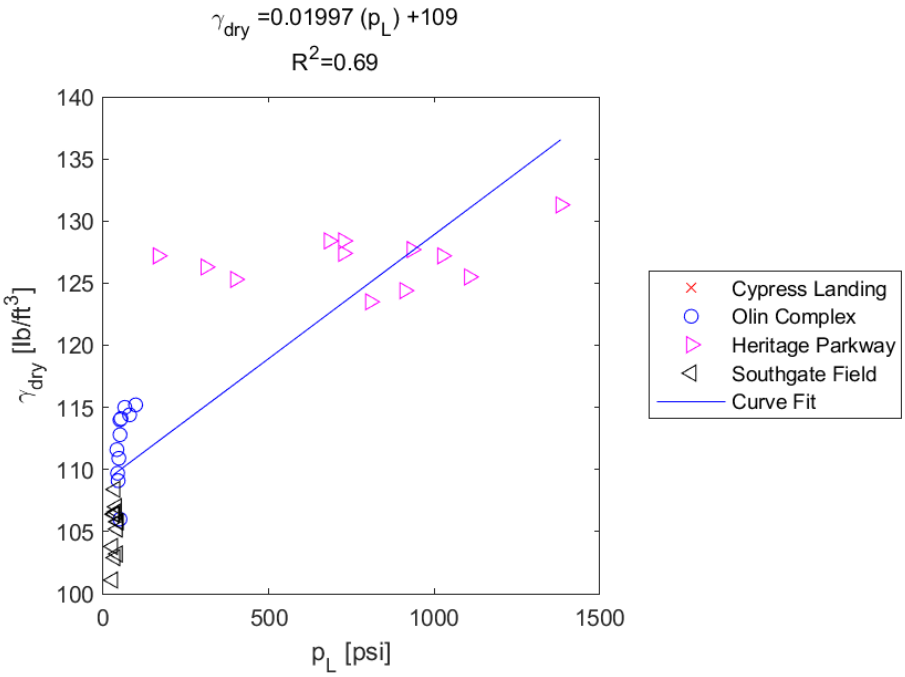

Figure E.41: Linear - Linear Model of γ_{dry} versus p_L for SDPMT-6 Incremental Tests, All Sites

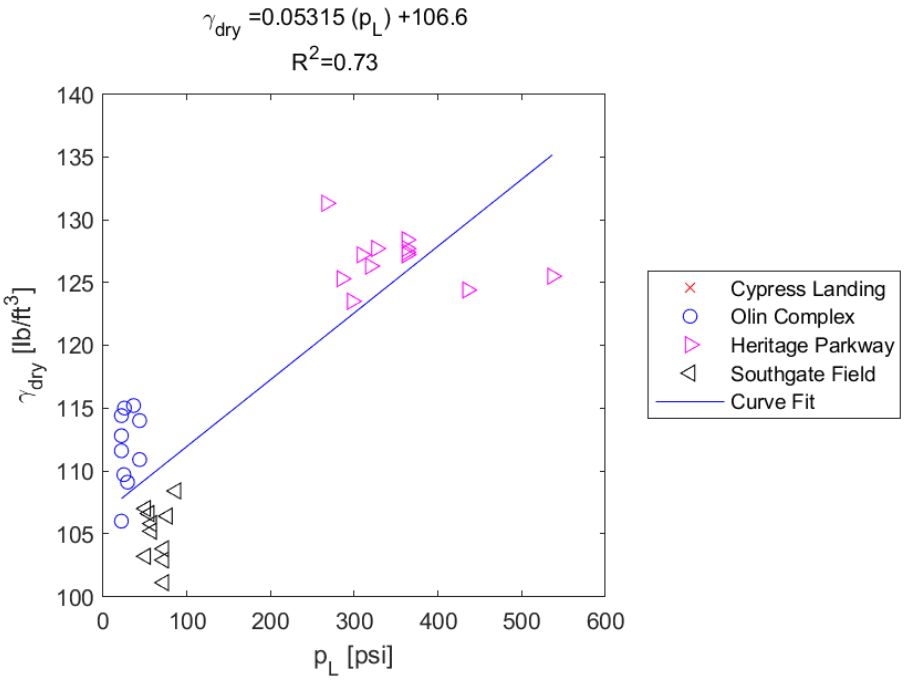

Figure E.42: Linear - Linear Model of γ_{dry} versus p_L for SDPMT-6 Continuous Tests, All Sites

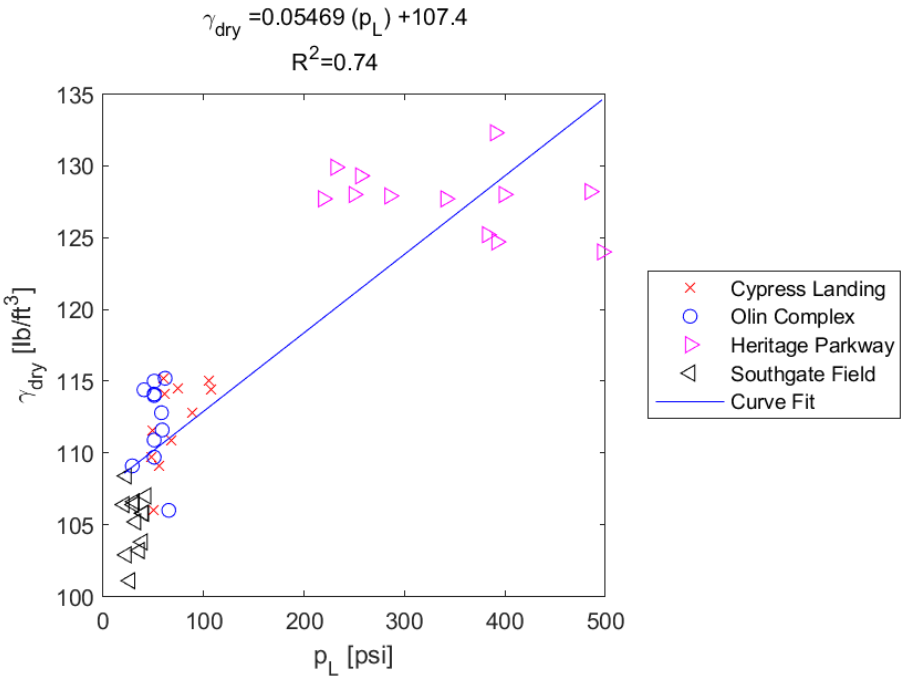

Figure E.43: Linear - Linear Model of γ_{dry} versus p_L for SDPMT-12 Incremental Tests, All Sites

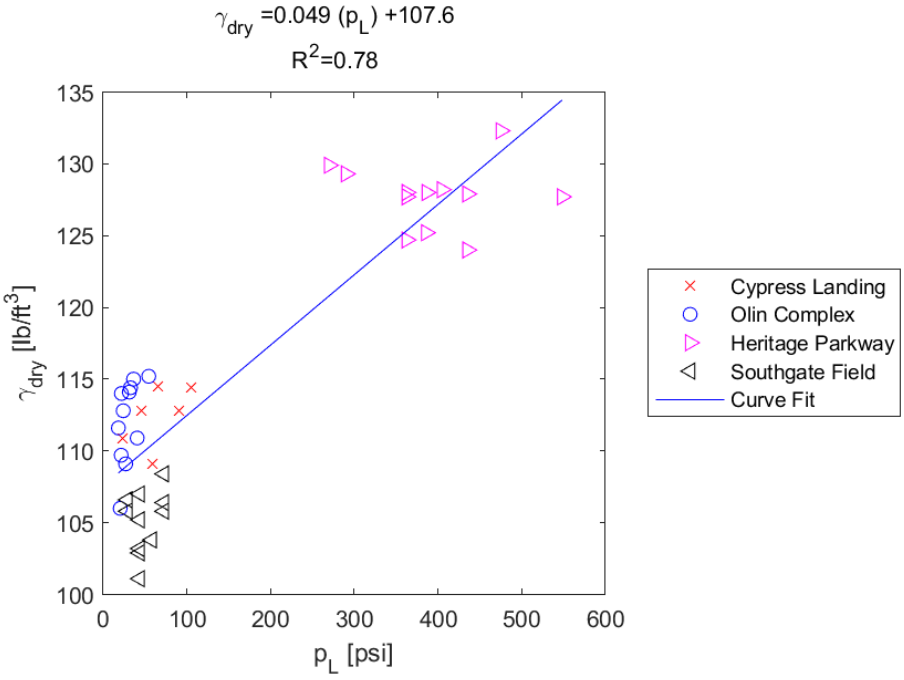

Figure E.44: Linear - Linear Model of γ_{dry} versus p_L for SDPMT-12 Continuous Tests, All Sites

E.1.12 γ_{dry} versus $\mathbf{p}_0$

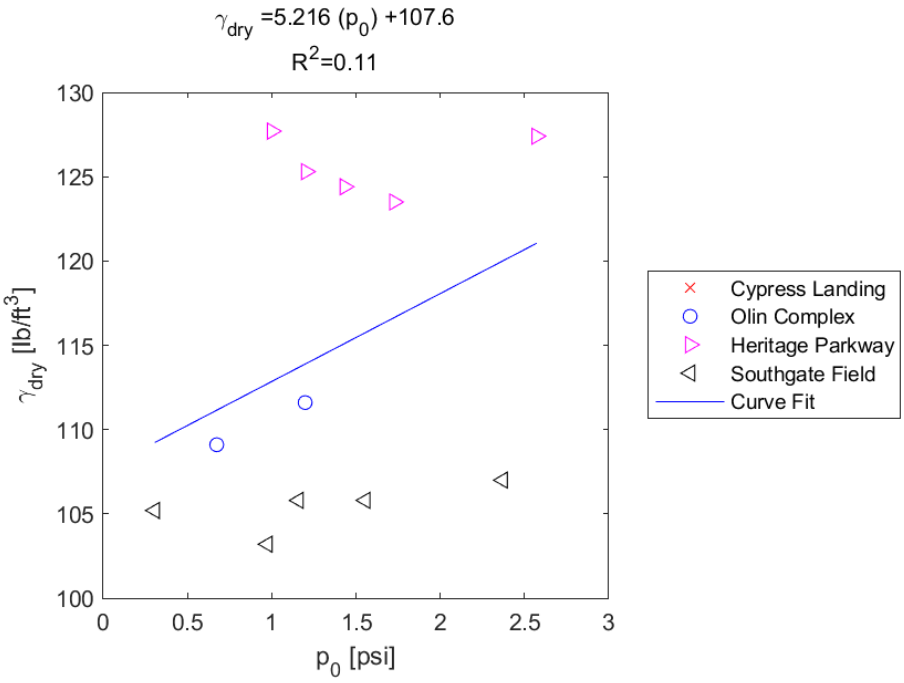

Figure E.45: Linear - Linear Model of γ_{dry} versus p_0 for SDPMT-6 Incremental Tests, All Sites

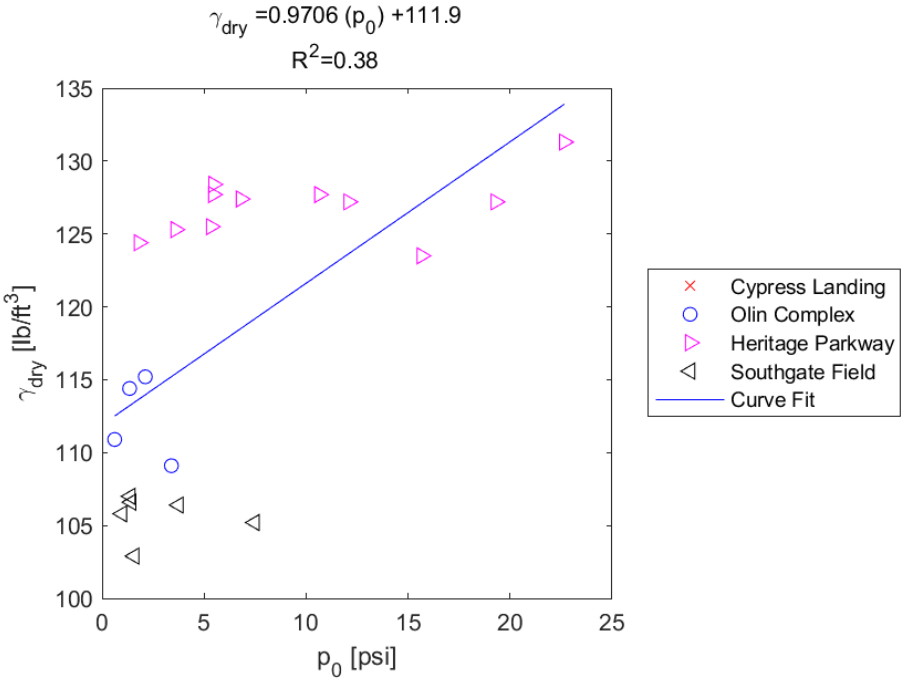

Figure E.46: Linear - Linear Model of γ_{dry} versus p_0 for SDPMT-6 Continuous Tests, All Sites

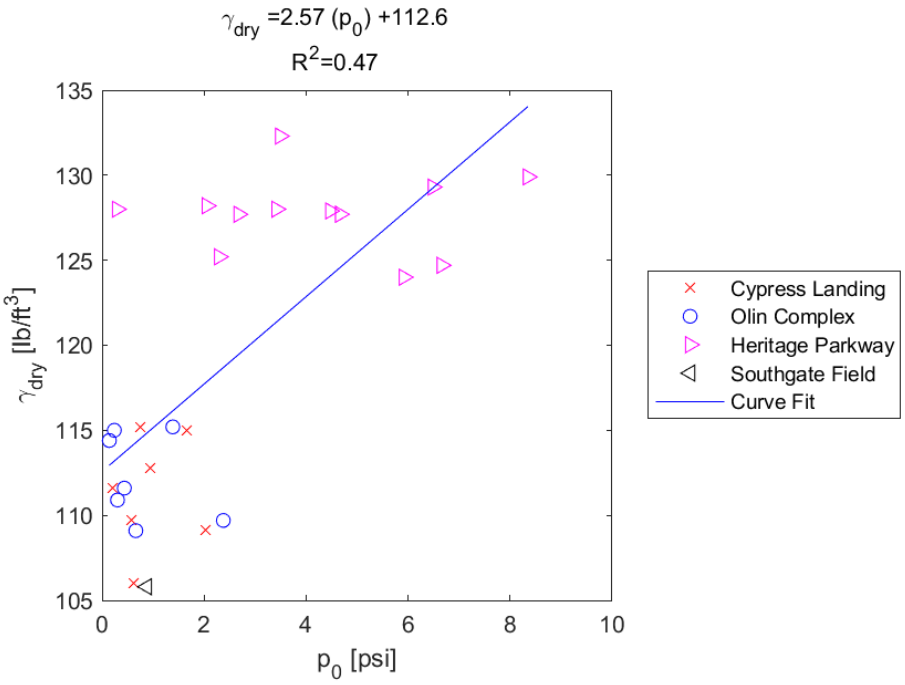

Figure E.47: Linear - Linear Model of γ_{dry} versus p_0 for SDPMT-12 Incremental Tests, All Sites

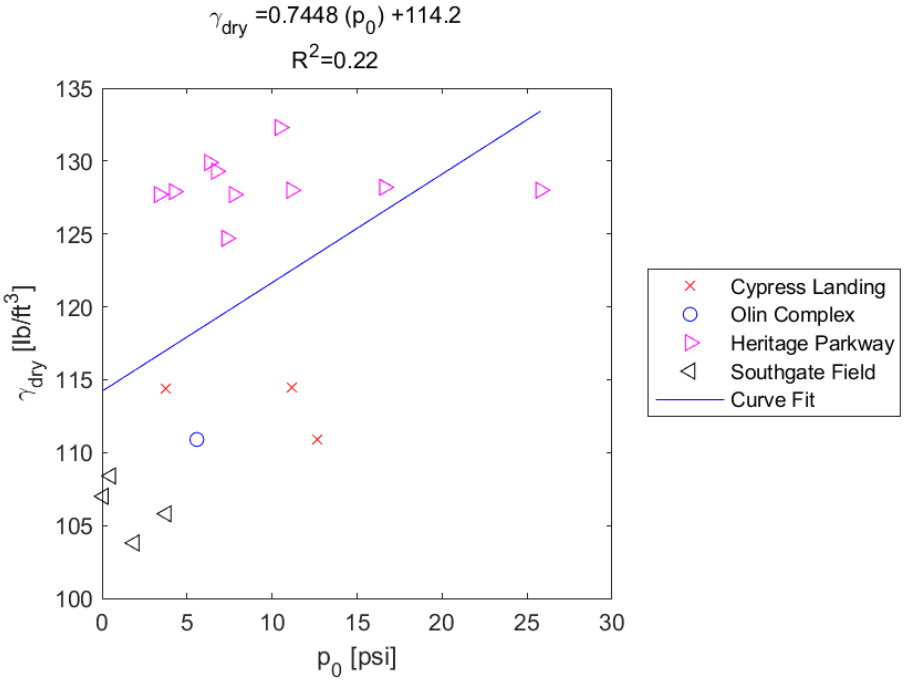

Figure E.48: Linear - Linear Model of γ_{dry} versus p_0 for SDPMT-12 Continuous Tests, All Sites

E.1.13 DCP PI versus E_0

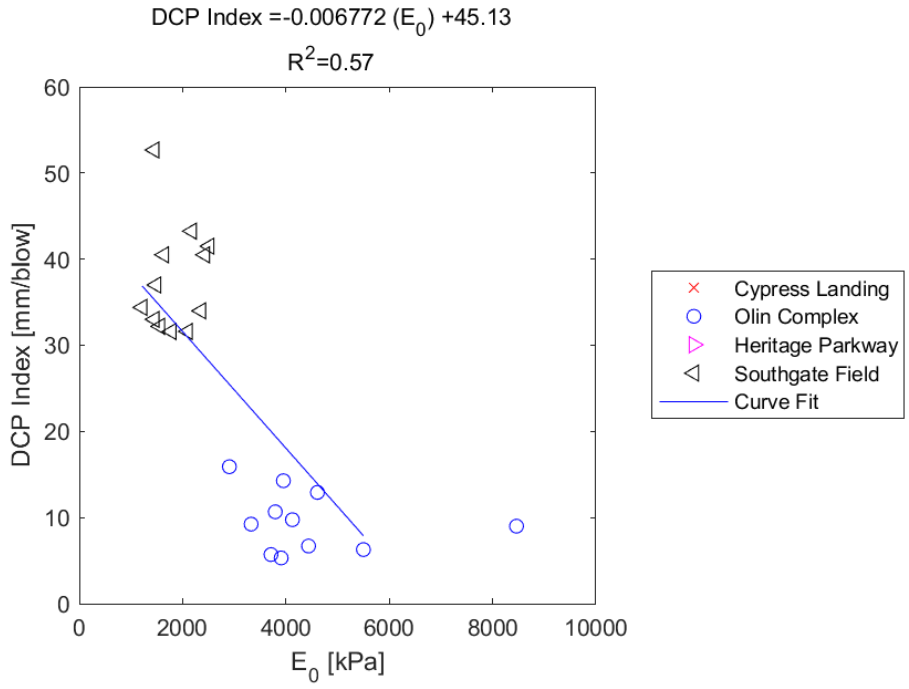

Figure E.49: Linear - Linear Model of DCP PI versus E_0 for SDPMT-6 Incremental Tests, All Sites

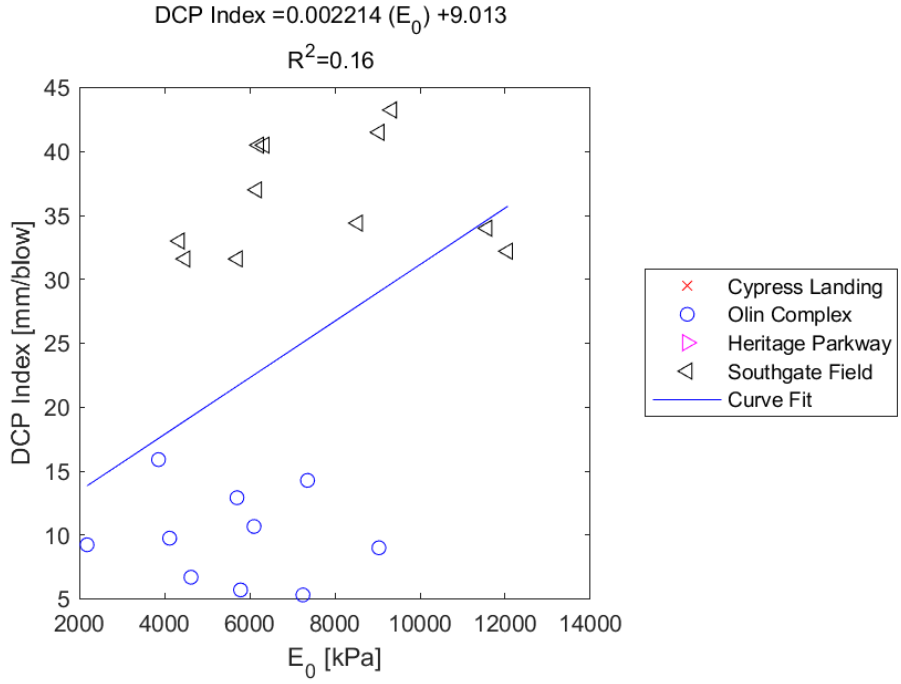

Figure E.50: Linear - Linear Model of DCP PI versus E_0 for SDPMT-6 Continuous Tests, All Sites

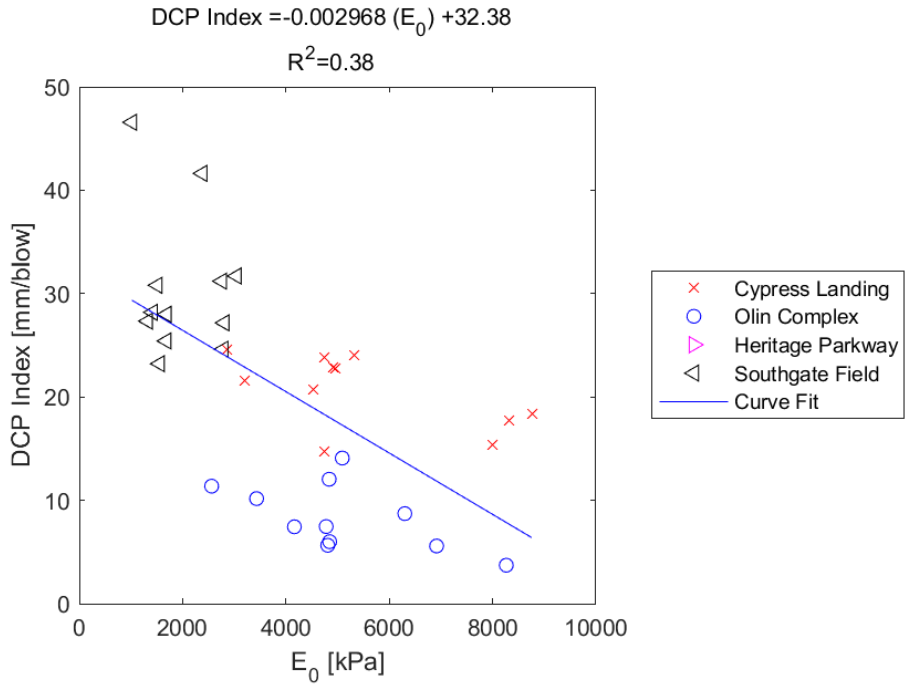

Figure E.51: Linear - Linear Model of DCP PI versus E_0 for SDPMT-12 Incremental Tests, All Sites

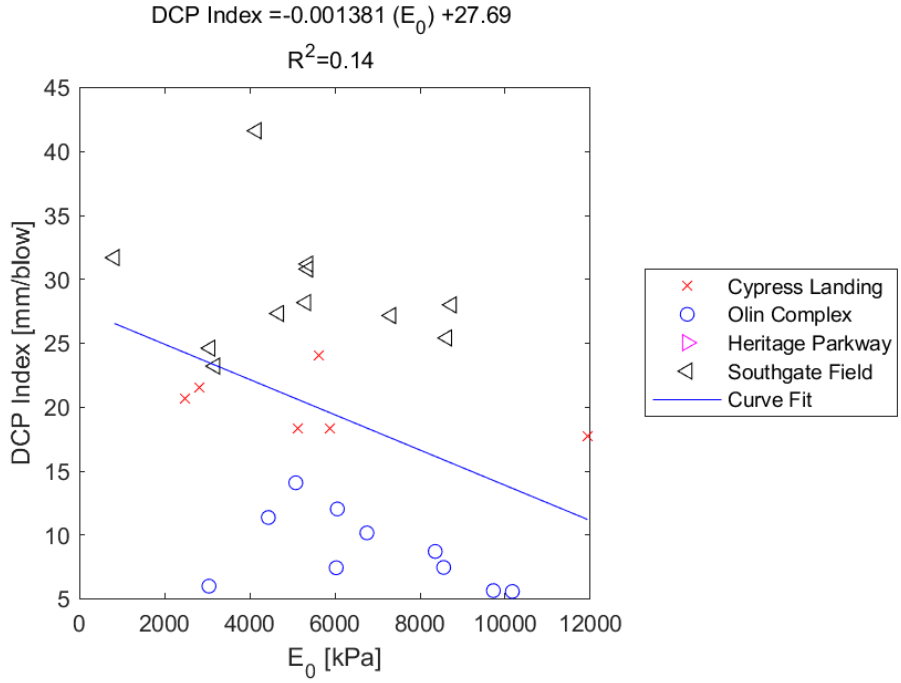

Figure E.52: Linear - Linear Model of DCP PI versus E_0 for SDPMT-12 Continuous Tests, All Sites

E.1.14 DCP PI versus $\mathbf{p}_L$

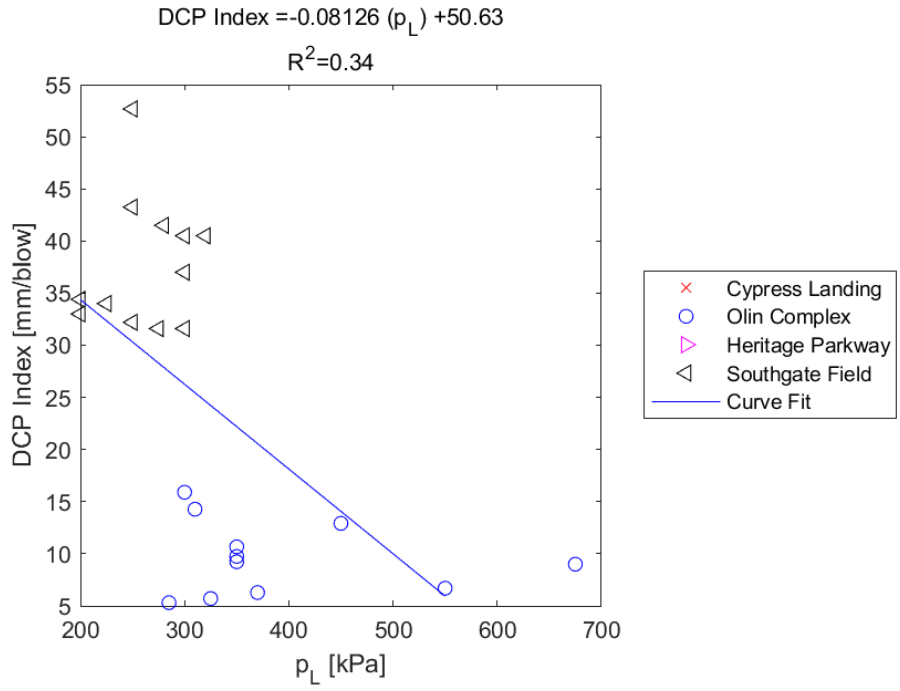

Figure E.53: Linear - Linear Model of DCP PI versus p_L for SDPMT-6 Incremental Tests, All Sites

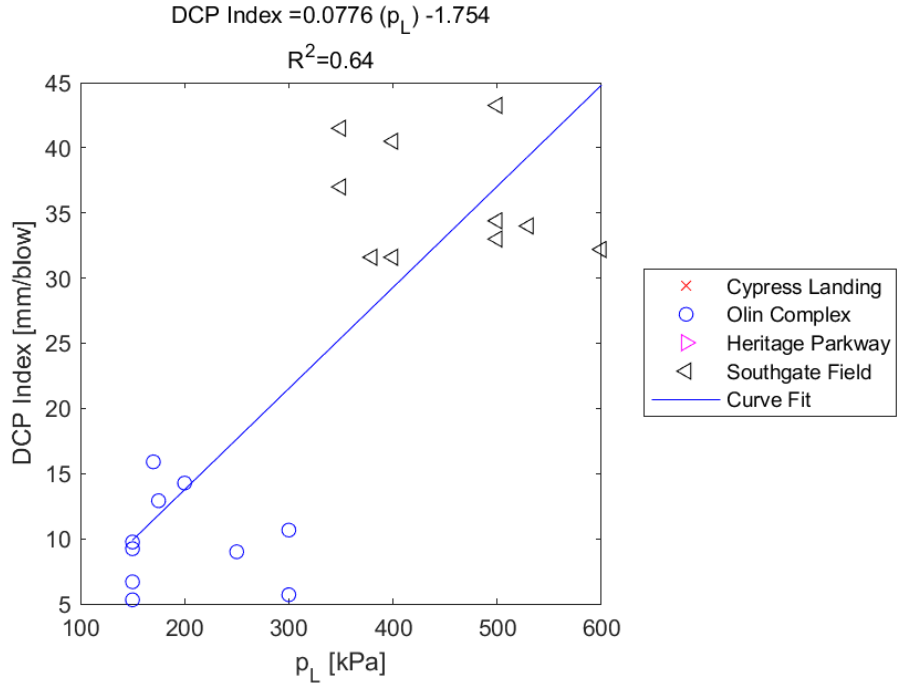

Figure E.54: Linear - Linear Model of DCP PI versus p_L for SDPMT-6 Continuous Tests, All Sites

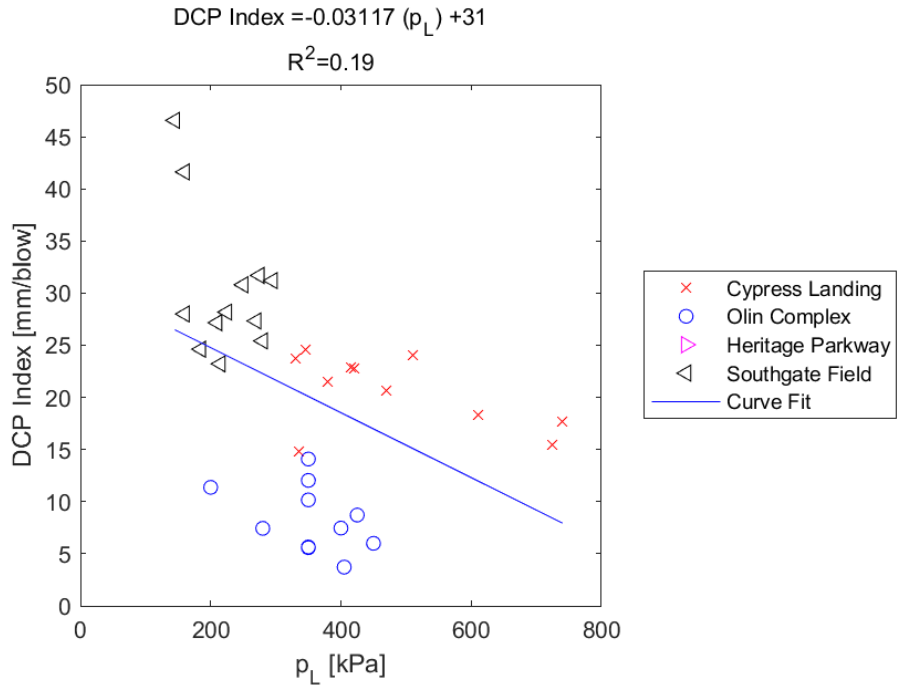

Figure E.55: Linear - Linear Model of DCP PI versus p_L for SDPMT-12 Incremental Tests, All Sites

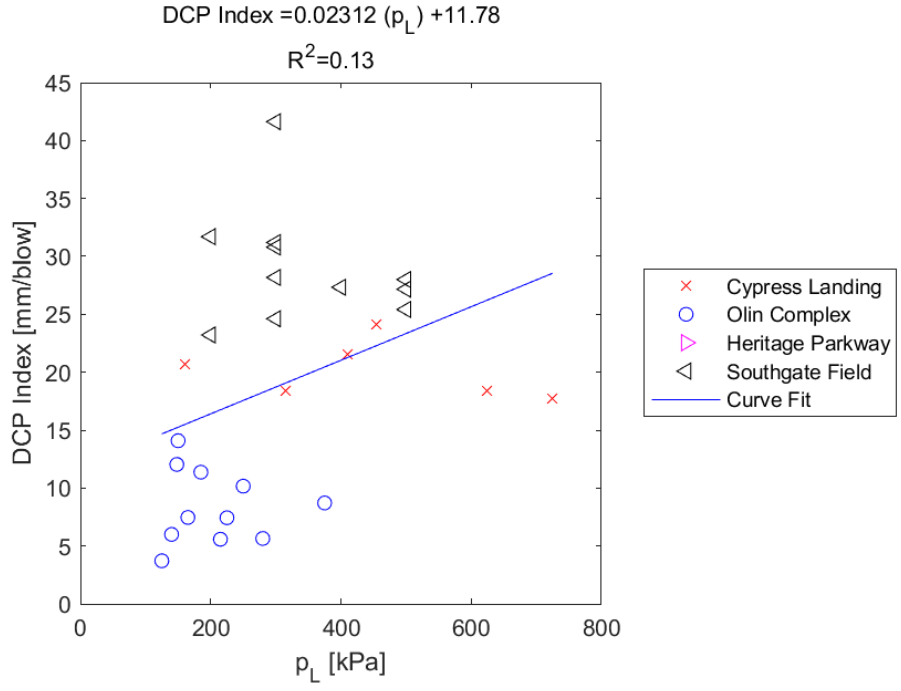

Figure E.56: Linear - Linear Model of DCP PI versus p_L for SDPMT-12 Continuous Tests, All Sites

E.1.15 DCP PI versus $\mathbf{p}_0$

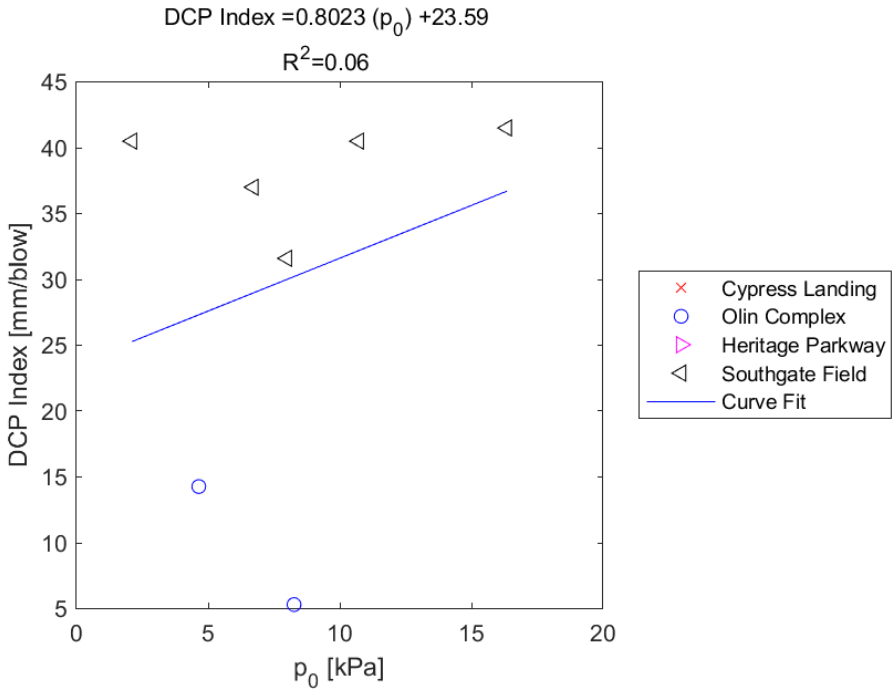

Figure E.57: Linear - Linear Model of DCP PI versus p_0 for SDPMT-6 Incremental Tests, All Sites

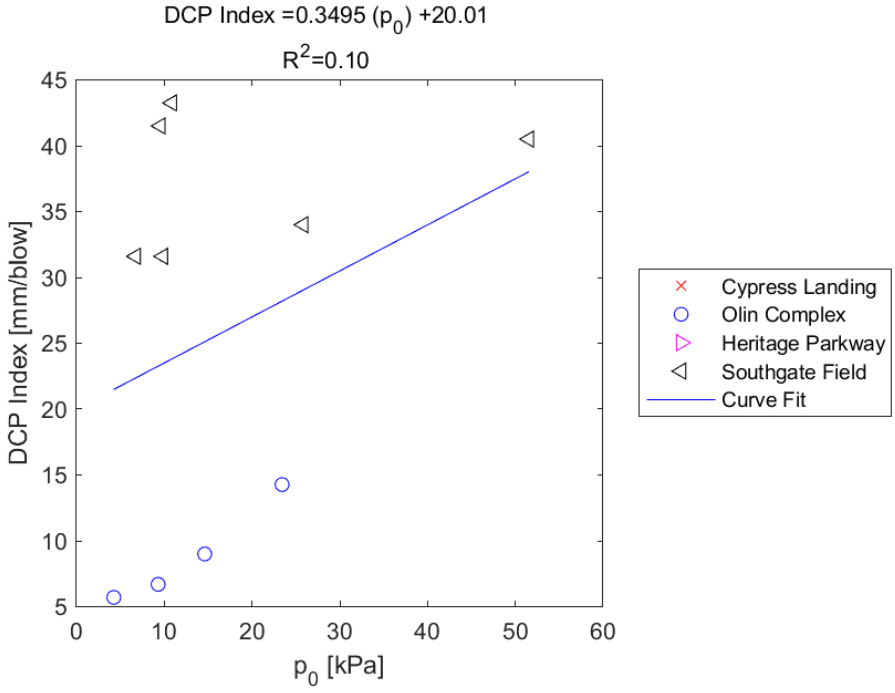

Figure E.58: Linear - Linear Model of DCP PI versus p_0 for SDPMT-6 Continuous Tests, All Sites

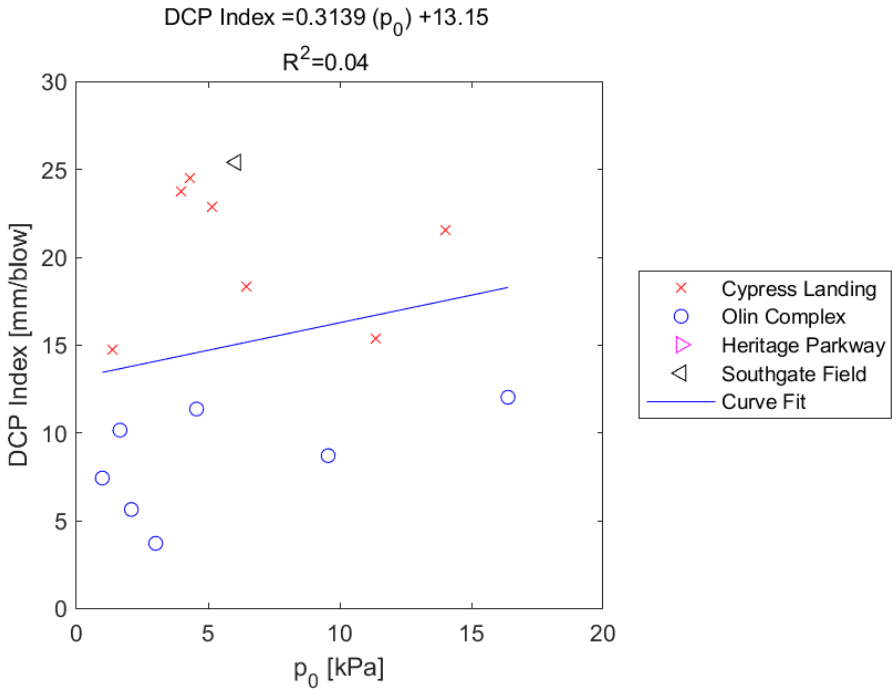

Figure E.59: Linear - Linear Model of DCP PI versus p_0 for SDPMT-12 Incremental Tests, All Sites

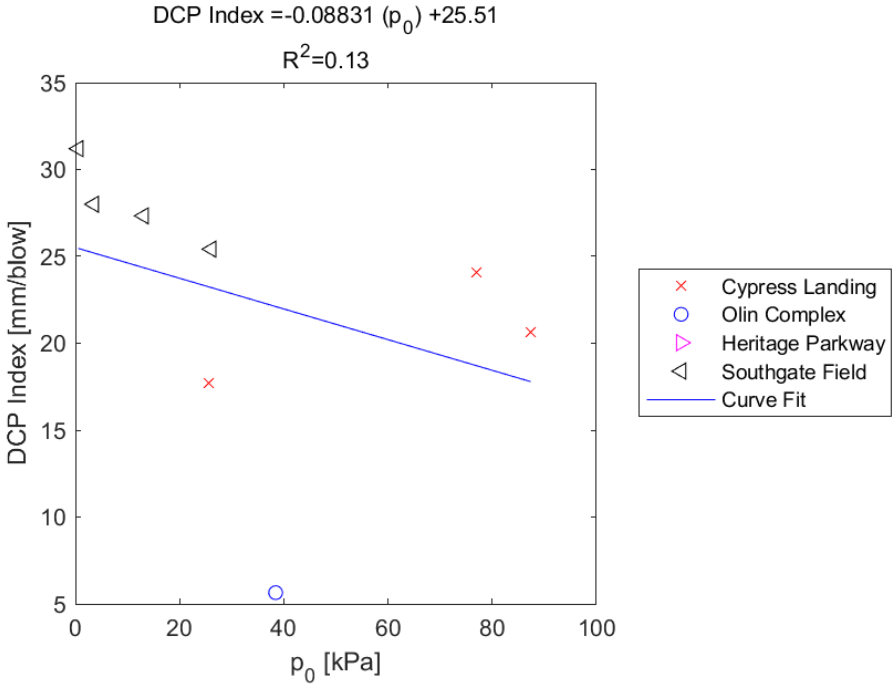

Figure E.60: Linear - Linear Model of DCP PI versus p_0 for SDPMT-12 Continuous Tests, All Sites

E.1.16 $\mathbf{E}_{d,zorn}$ versus $\mathbf{E}_0$

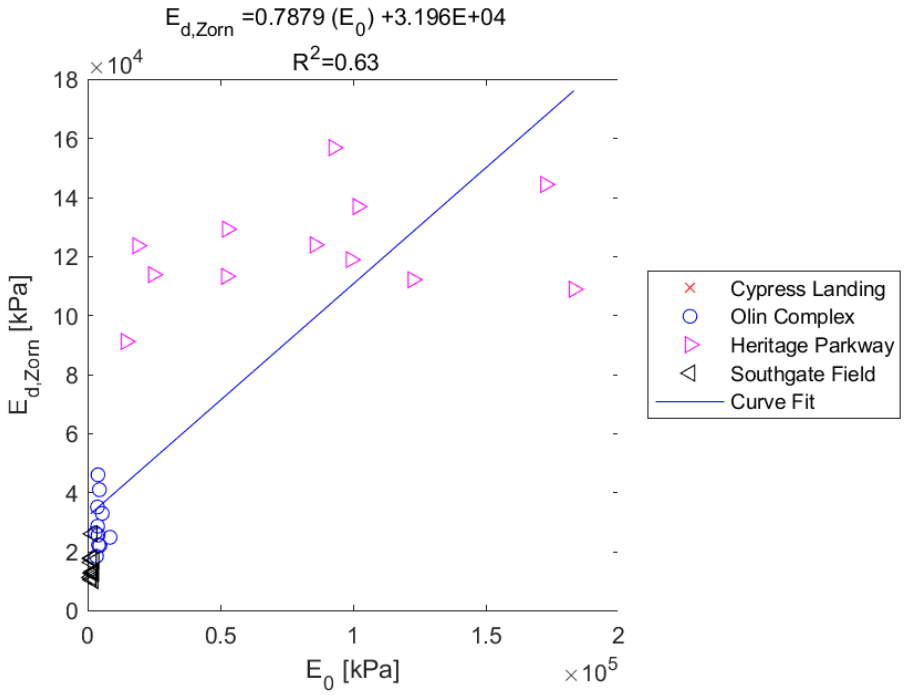

Figure E.61: Linear - Linear Model of $E_{d,zorn}$ versus E_0 for SDPMT-6 Incremental Tests, All Sites

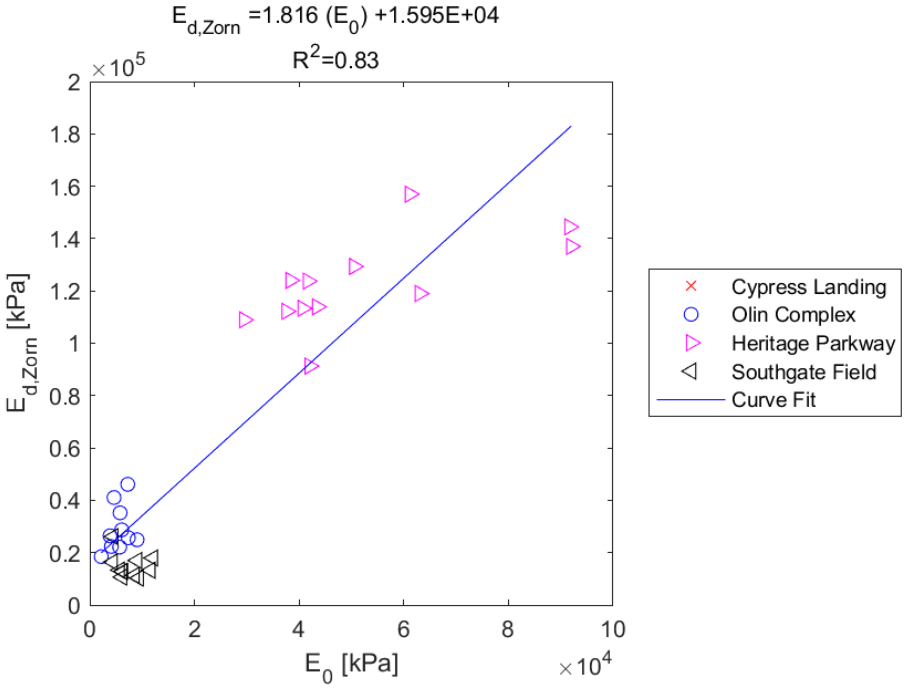

Figure E.62: Linear - Linear Model of $E_{d,zorn}$ versus E_0 for SDPMT-6 Continuous Tests, All Sites

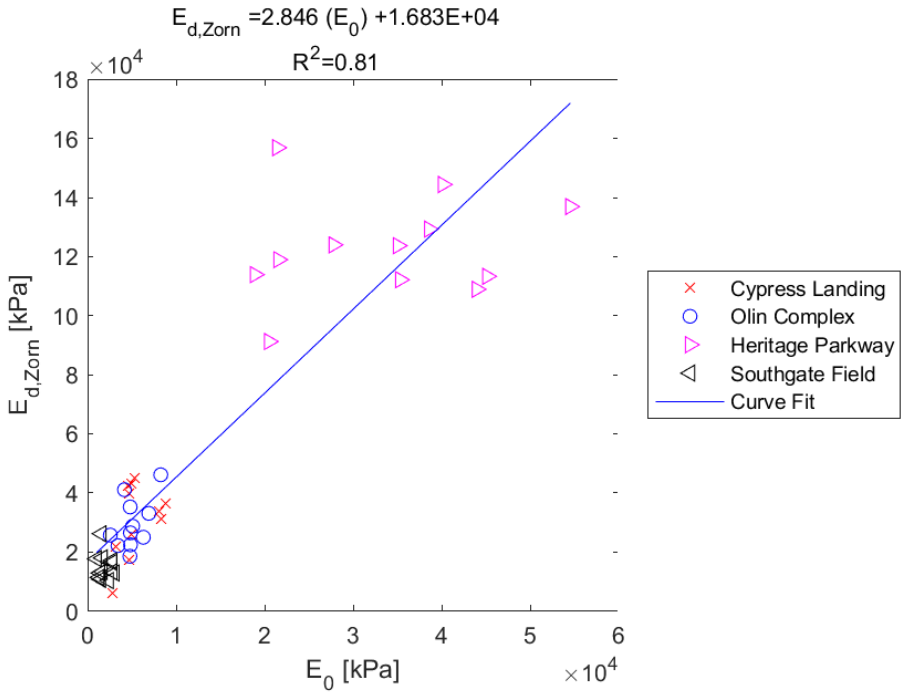

Figure E.63: Linear - Linear Model of $E_{d,zorn}$ versus E_0 for SDPMT-12 Incremental Tests, All Sites

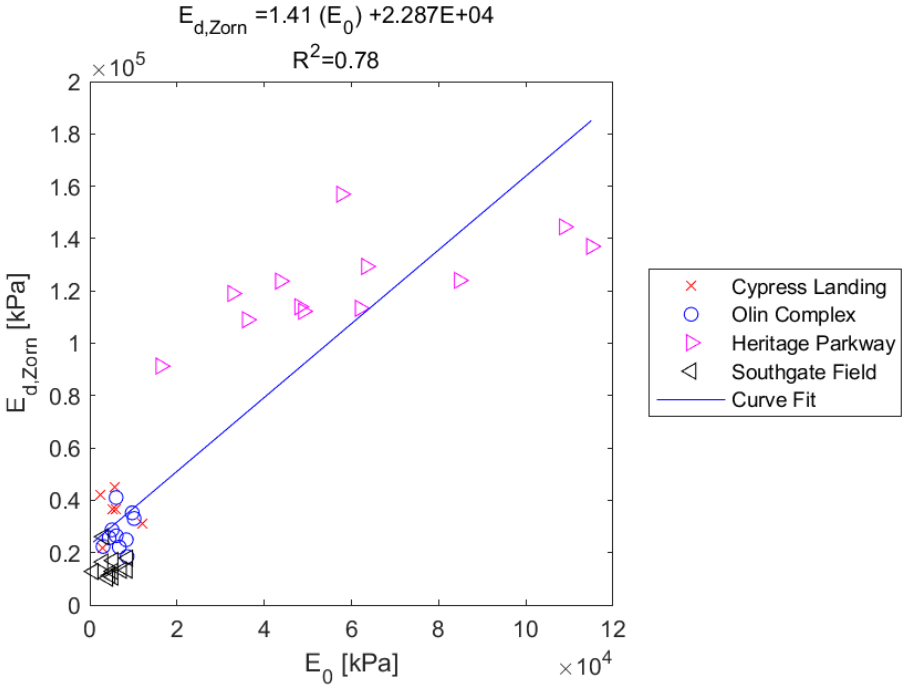

Figure E.64: Linear - Linear Model of $E_{d,zorn}$ versus E_0 for SDPMT-12 Continuous Tests, All Sites

E.1.17 $\mathbf{E}_{d,zorn}$ versus $\mathbf{p}_L$

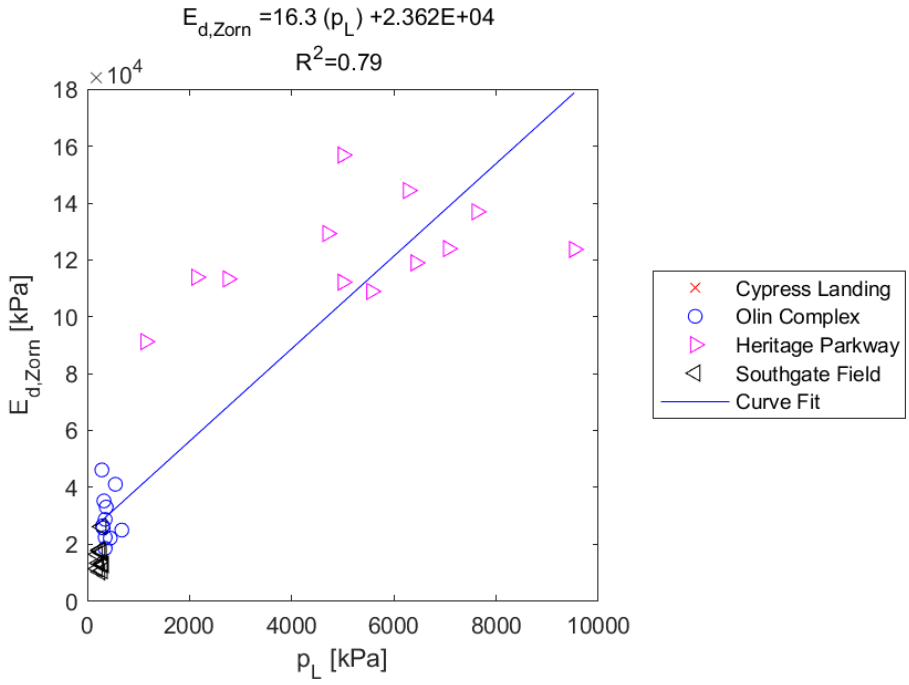

Figure E.65: Linear - Linear Model of $E_{d,zorn}$ versus p_L for SDPMT-6 Incremental Tests, All Sites

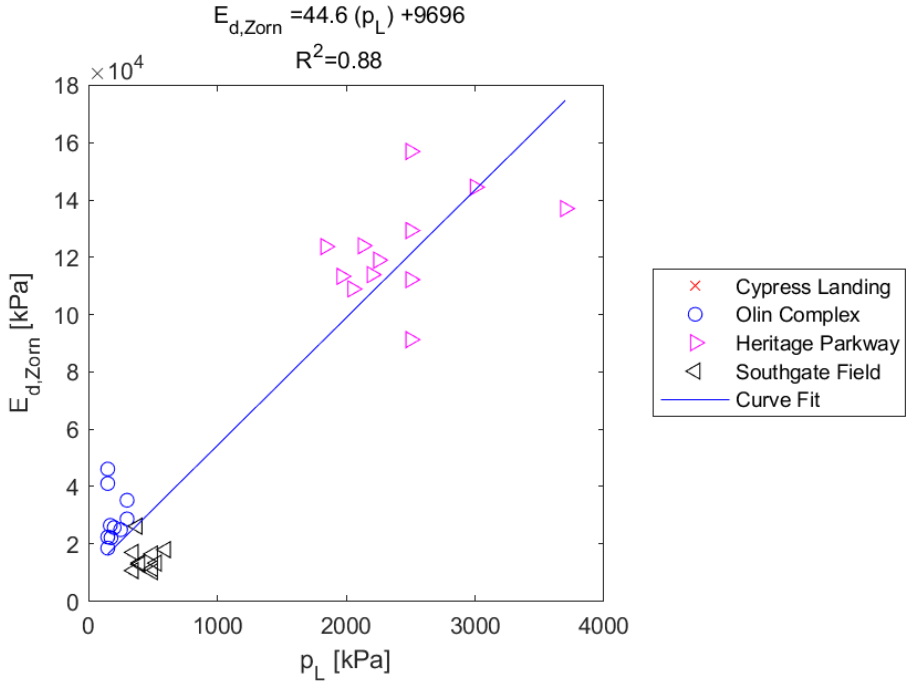

Figure E.66: Linear - Linear Model of $E_{d,zorn}$ versus p_L for SDPMT-6 Continuous Tests, All Sites

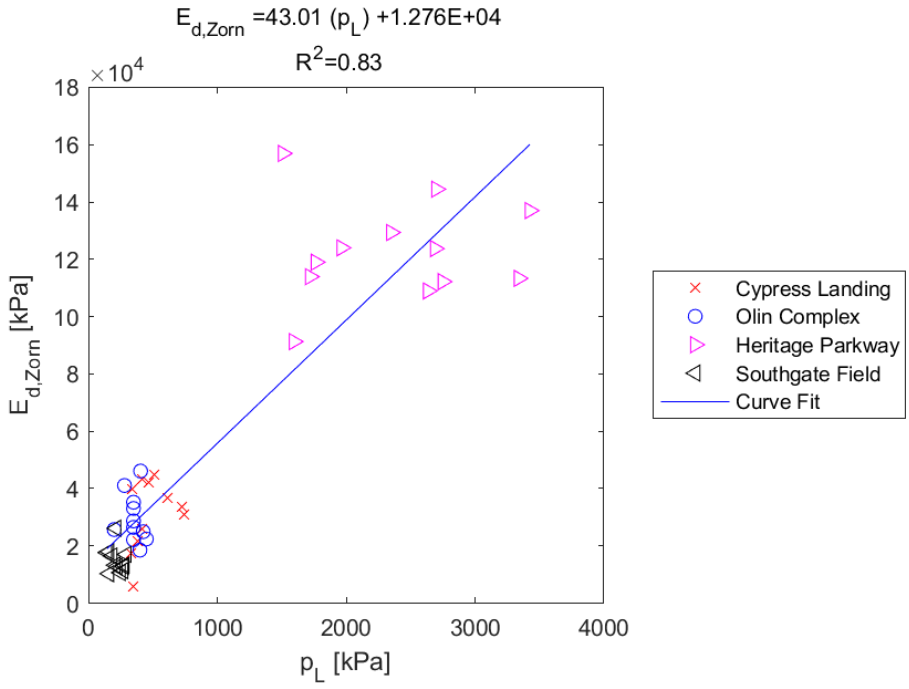

Figure E.67: Linear - Linear Model of $E_{d,zorn}$ versus p_L for SDPMT-12 Incremental Tests, All Sites

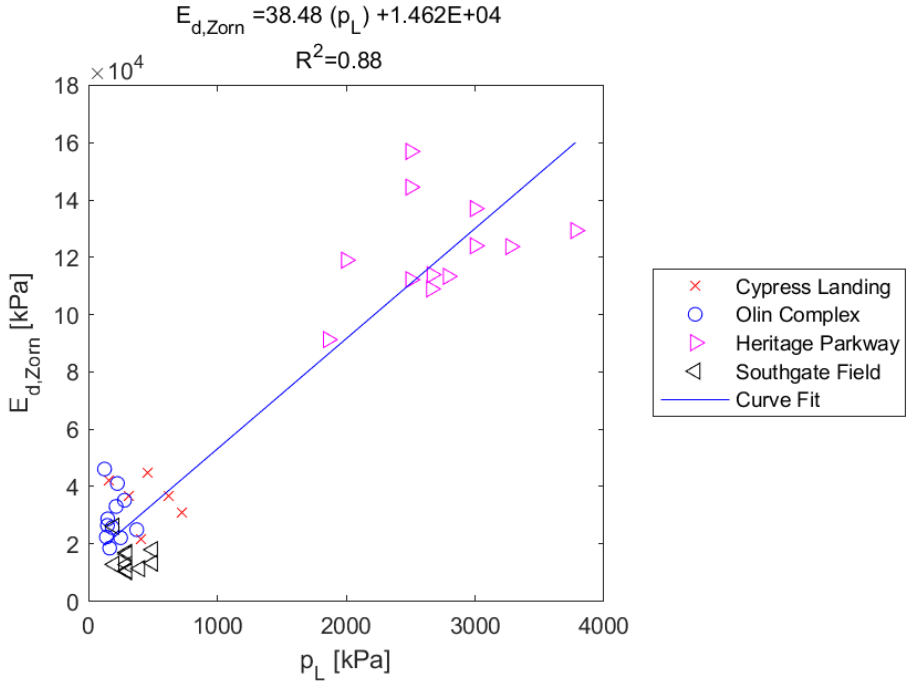

Figure E.68: Linear - Linear Model of $E_{d,zorn}$ versus p_L for SDPMT-12 Continuous Tests, All Sites

E.1.18 $\mathbf{E}_{d,zorn}$ versus $\mathbf{p}_0$

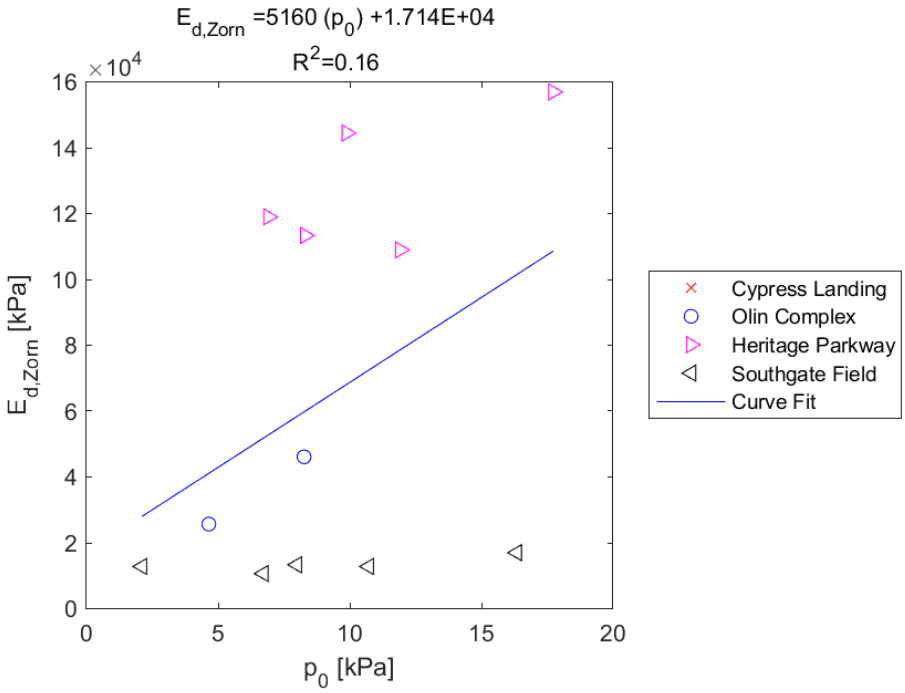

Figure E.69: Linear - Linear Model of $E_{d,zorn}$ versus p_0 for SDPMT-6 Incremental Tests, All Sites

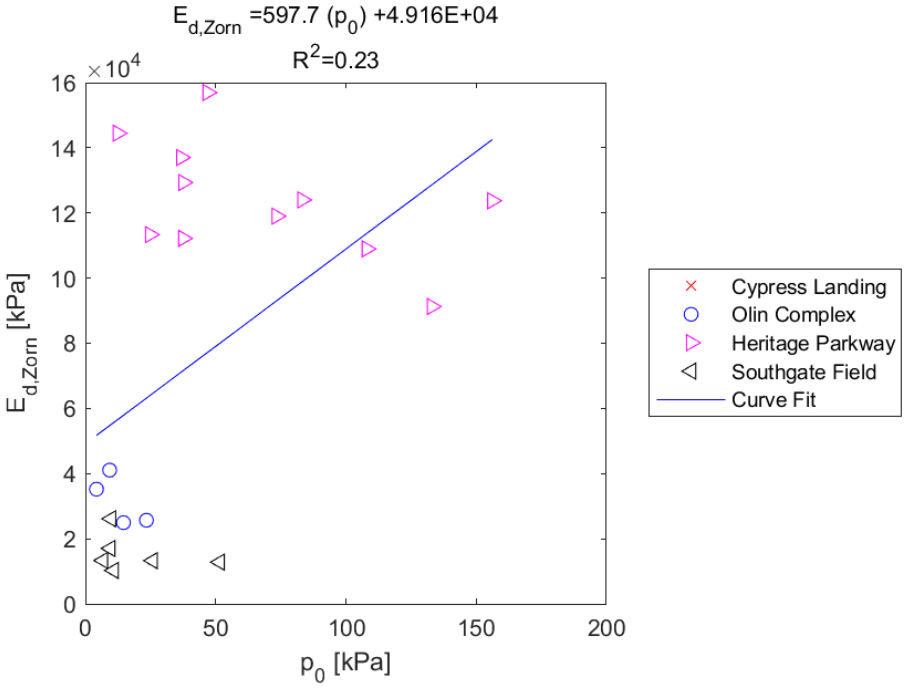

Figure E.70: Linear - Linear Model of $E_{d,zorn}$ versus p_0 for SDPMT-6 Continuous Tests, All Sites

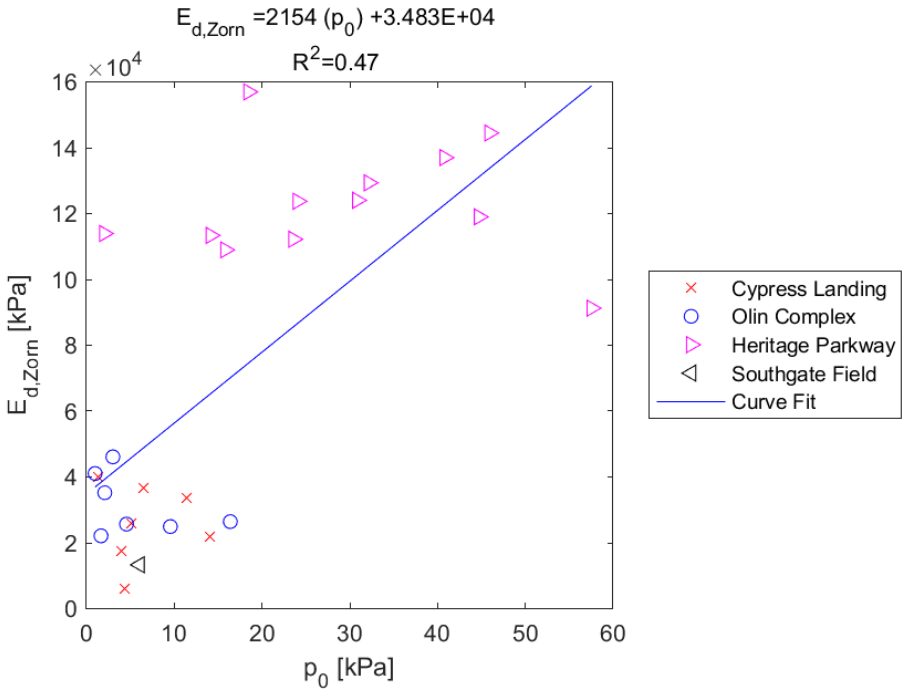

Figure E.71: Linear - Linear Model of $E_{d,zorn}$ versus p_0 for SDPMT-12 Incremental Tests, All Sites

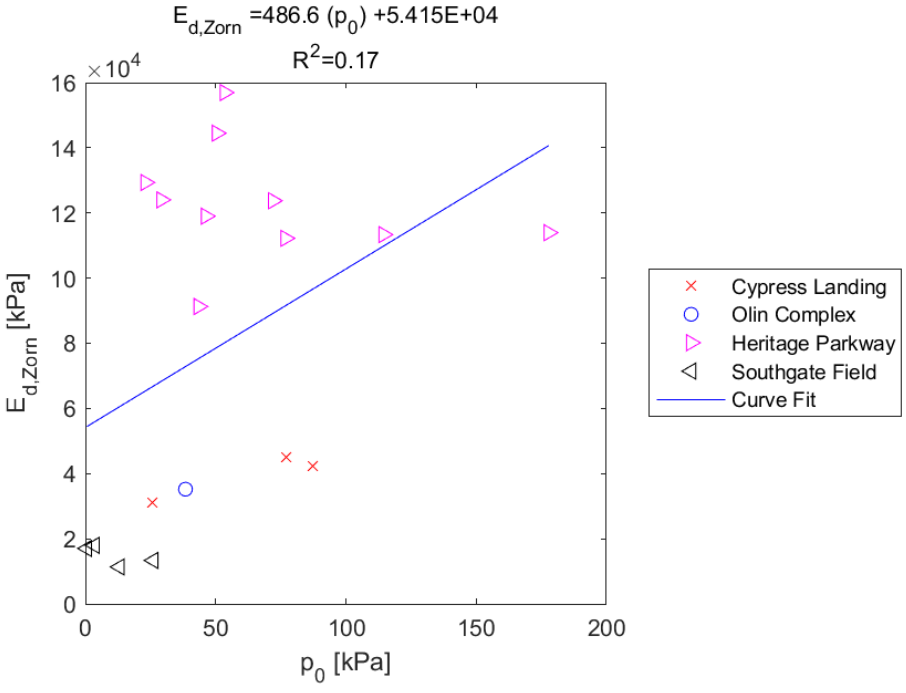

Figure E.72: Linear - Linear Model of $E_{d,zorn}$ versus p_0 for SDPMT-12 Continuous Tests, All Sites

E.1.19 $\mathbf{E}_{0,Dynatest}$ versus $\mathbf{E}_0$

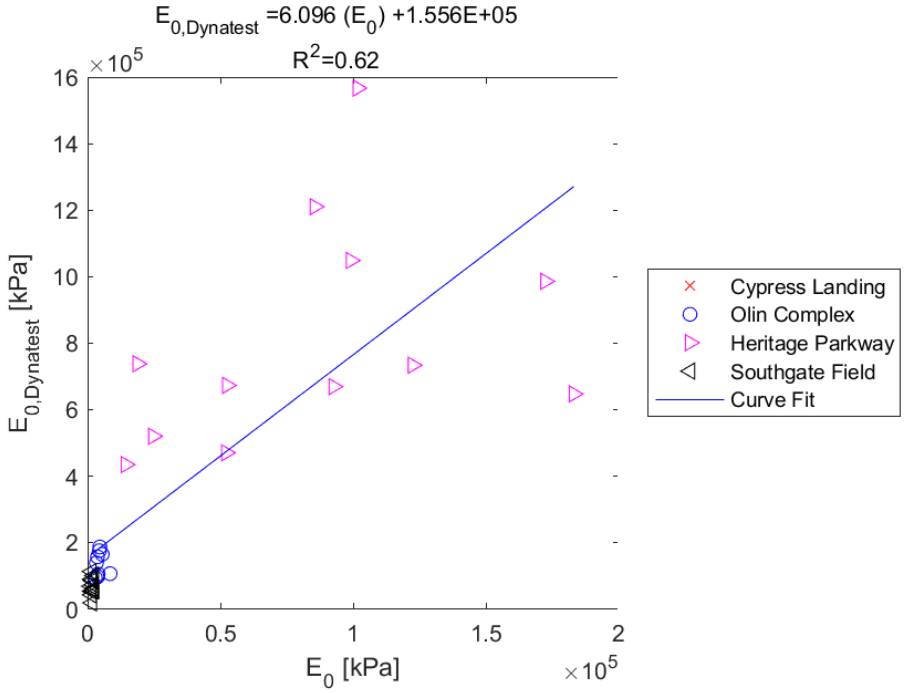

Figure E.73: Linear - Linear Model of $E_{0,Dynatest}$ versus E_0 for SDPMT-6 Incremental Tests, All Sites

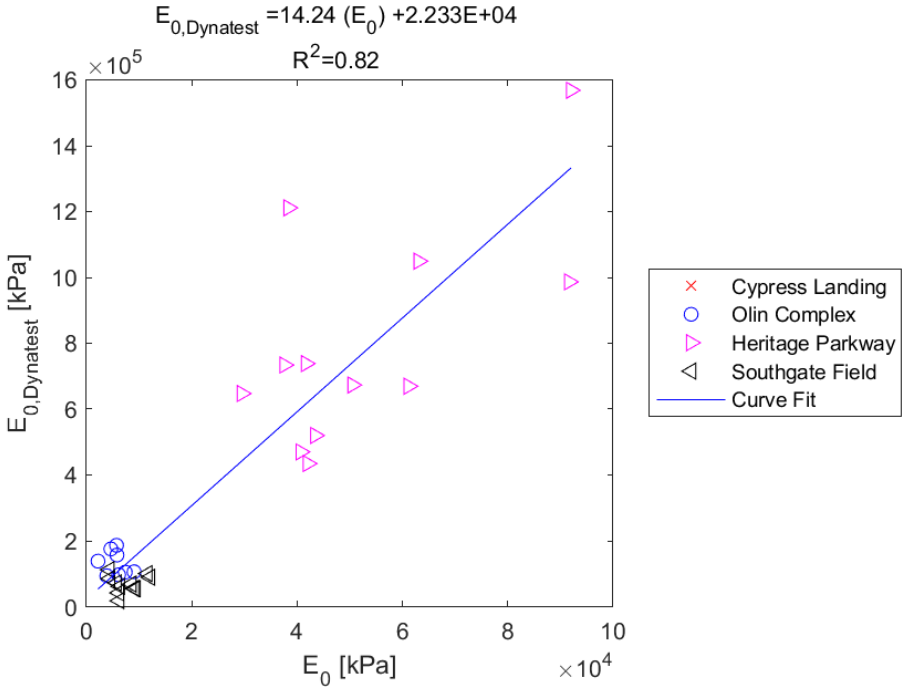

Figure E.74: Linear - Linear Model of $E_{0,Dynatest}$ versus E_0 for SDPMT-6 Continuous Tests, All Sites

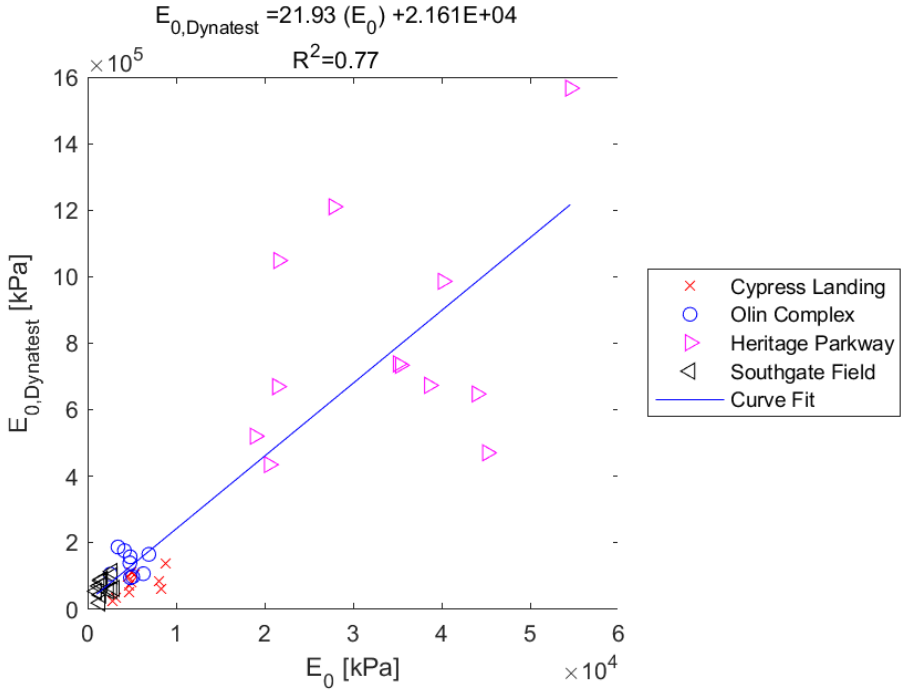

Figure E.75: Linear - Linear Model of $E_{0,Dynatest}$ versus E_0 for SDPMT-12 Incremental Tests, All Sites

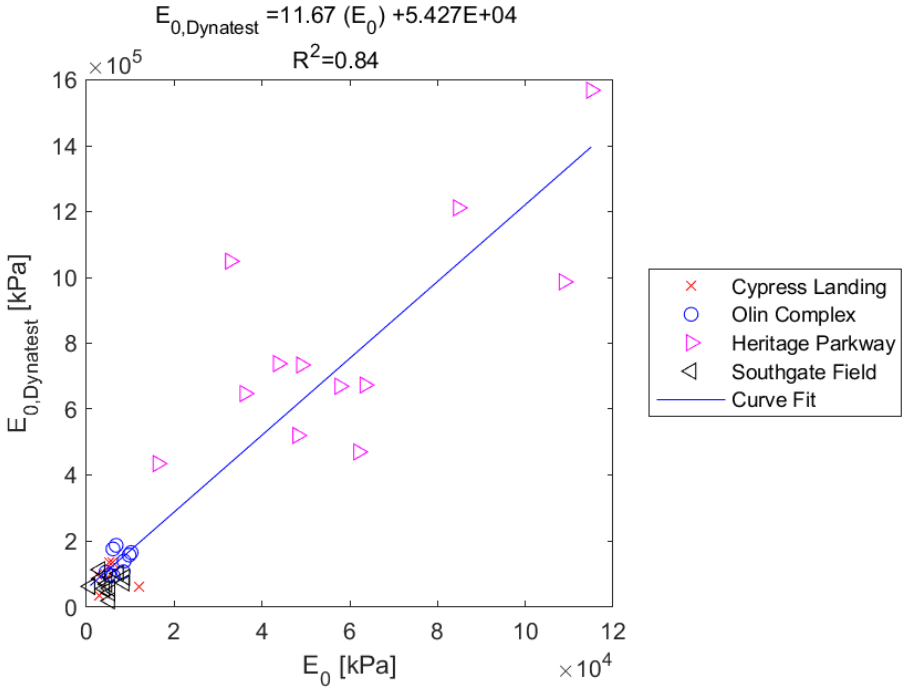

Figure E.76: Linear - Linear Model of $E_{0,Dynatest}$ versus E_0 for SDPMT-12 Continuous Tests, All Sites

E.1.20 $\mathbf{E}_{0,Dynatest}$ versus $\mathbf{p}_L$

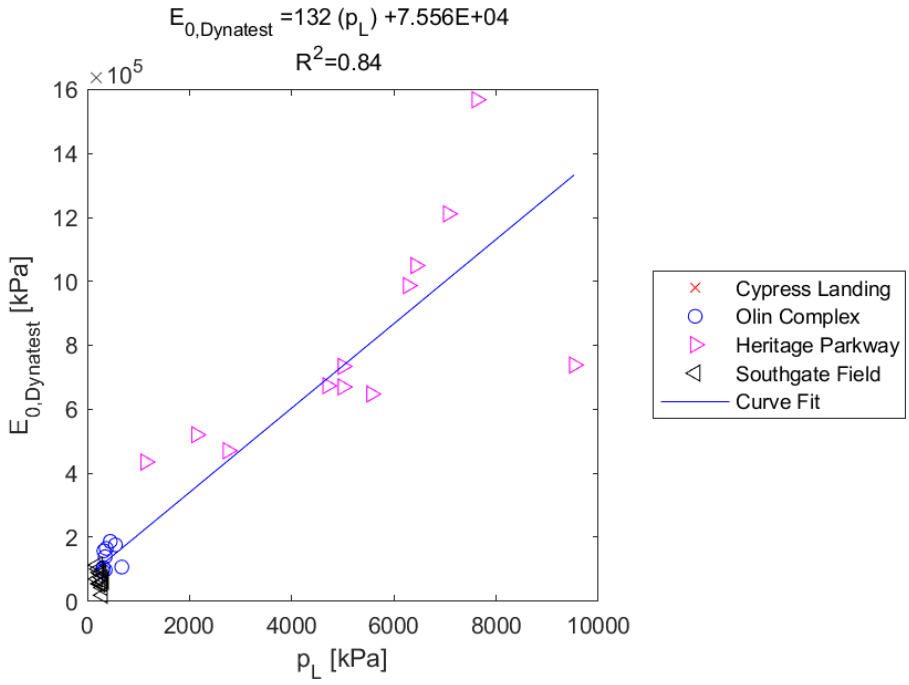

Figure E.77: Linear - Linear Model of $E_{0,Dynatest}$ versus p_L for SDPMT-6 Incremental Tests, All Sites

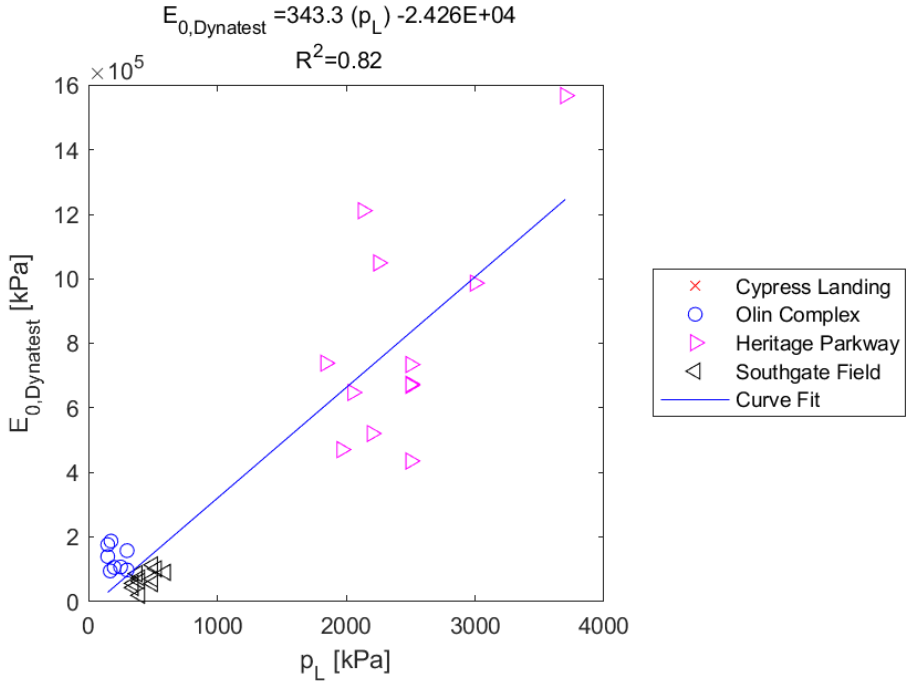

Figure E.78: Linear - Linear Model of $E_{0,Dynatest}$ versus p_L for SDPMT-6 Continuous Tests, All Sites

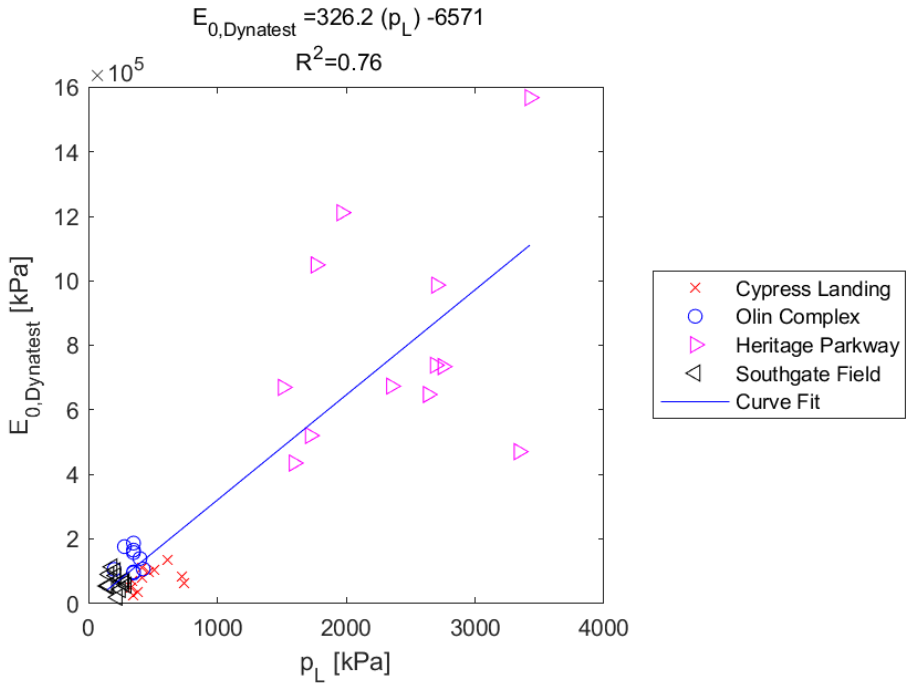

Figure E.79: Linear - Linear Model of $E_{0,Dynatest}$ versus p_L for SDPMT-12 Incremental Tests, All Sites

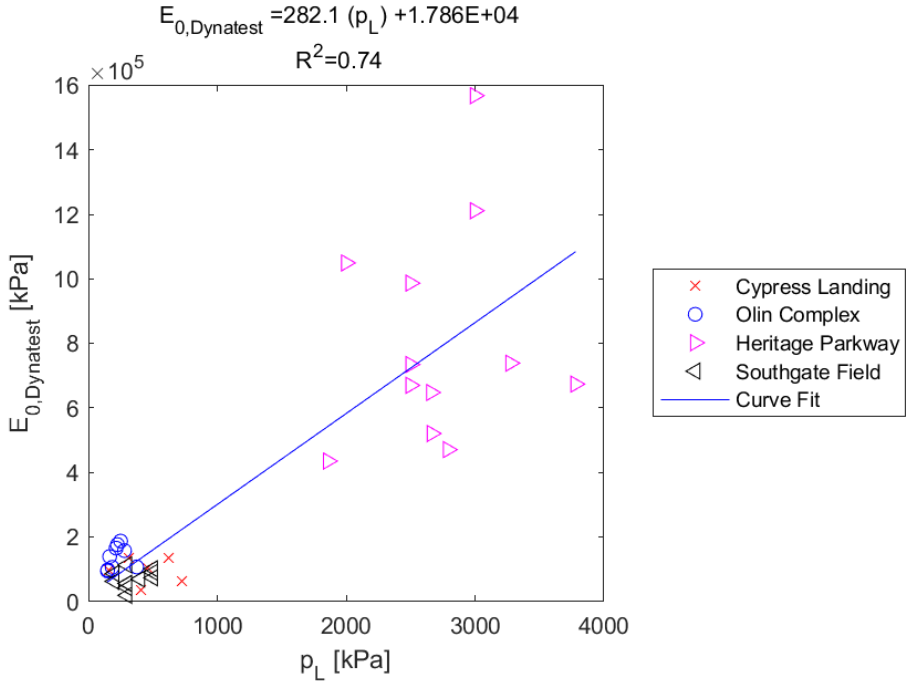

Figure E.80: Linear - Linear Model of $E_{0,Dynatest}$ versus p_L for SDPMT-12 Continuous Tests, All Sites

E.1.21 $\mathbf{E}_{0,Dynatest}$ versus $\mathbf{p}_0$

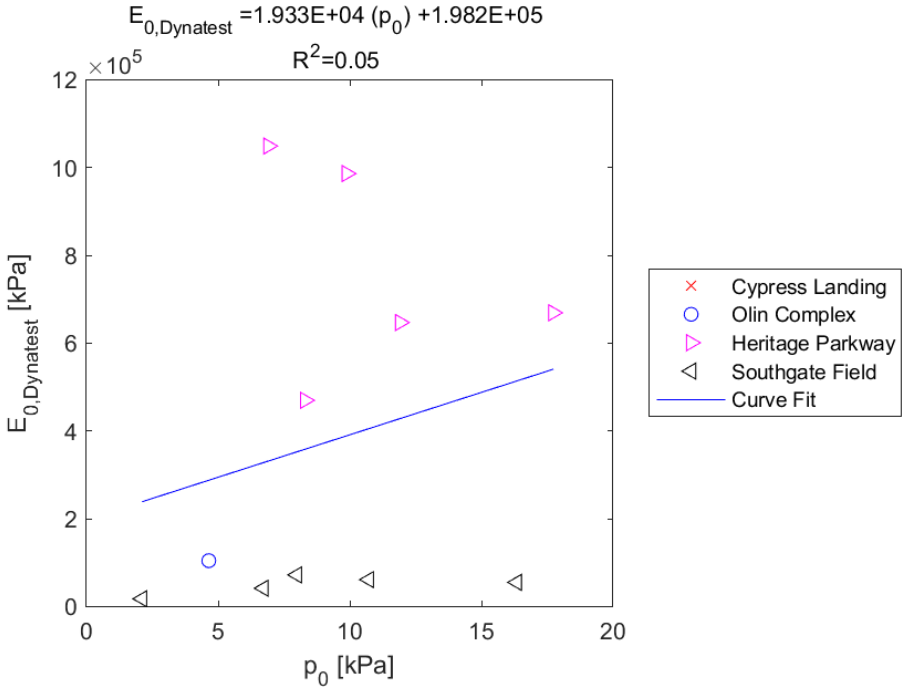

Figure E.81: Linear - Linear Model of $E_{0,Dynatest}$ versus p_0 for SDPMT-6 Incremental Tests, All Sites

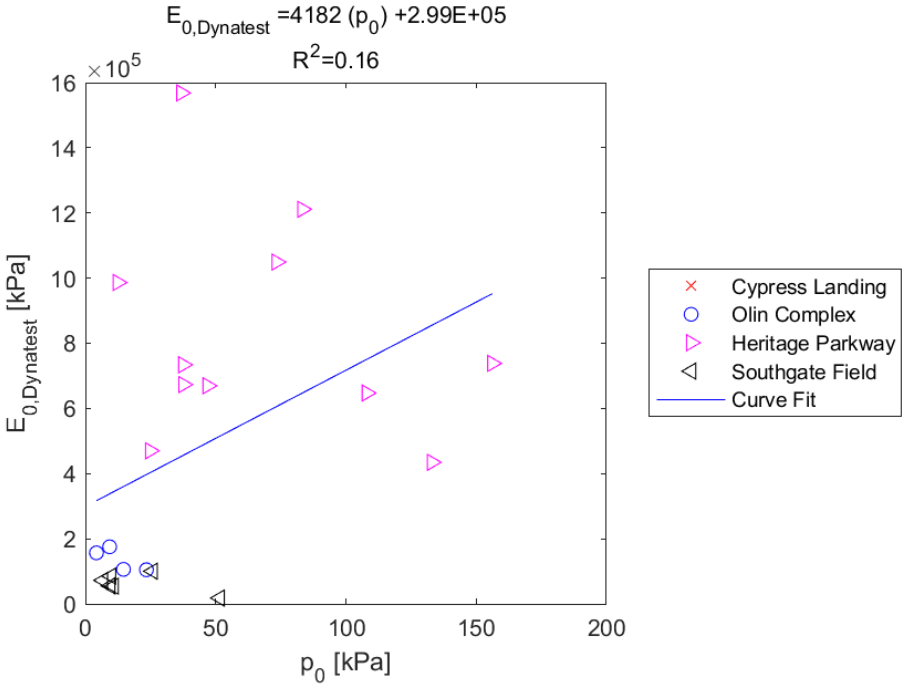

Figure E.82: Linear - Linear Model of $E_{0,Dynatest}$ versus p_0 for SDPMT-6 Continuous Tests, All Sites

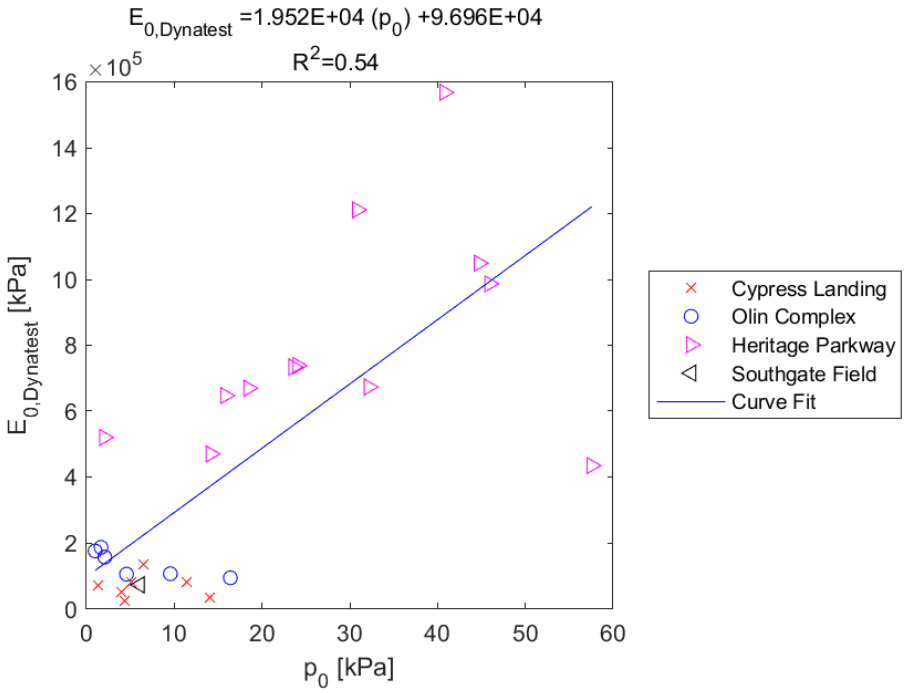

Figure E.83: Linear - Linear Model of $E_{0,Dynatest}$ versus p_0 for SDPMT-12 Incremental Tests, All Sites

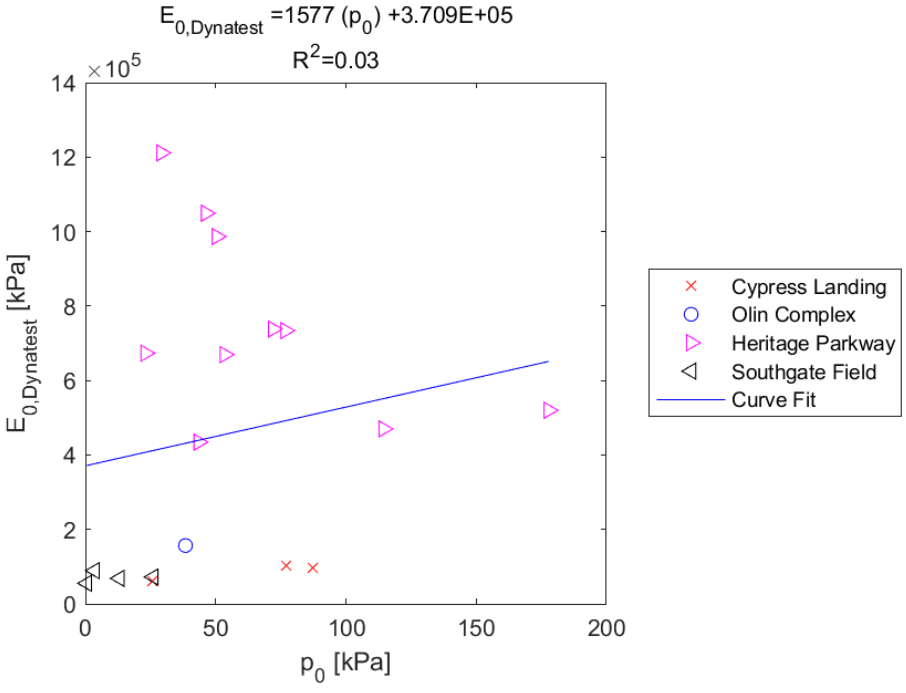

Figure E.84: Linear - Linear Model of $E_{0,Dynatest}$ versus p_0 for SDPMT-12 Continuous Tests, All Sites

E.1.22 CIV versus E_0

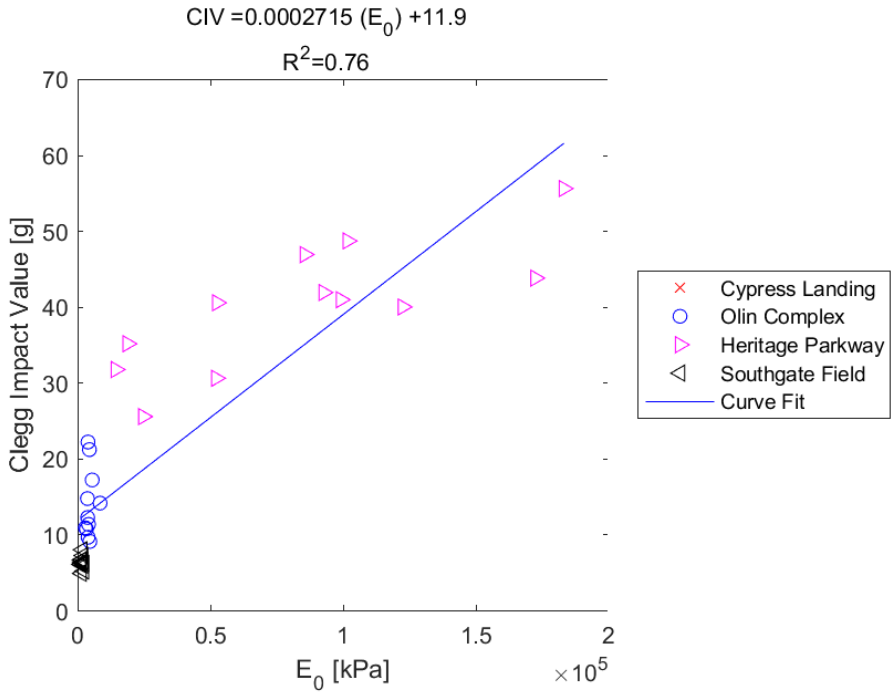

Figure E.85: Linear - Linear Model of CIV versus E_0 for SDPMT-6 Incremental Tests, All Sites

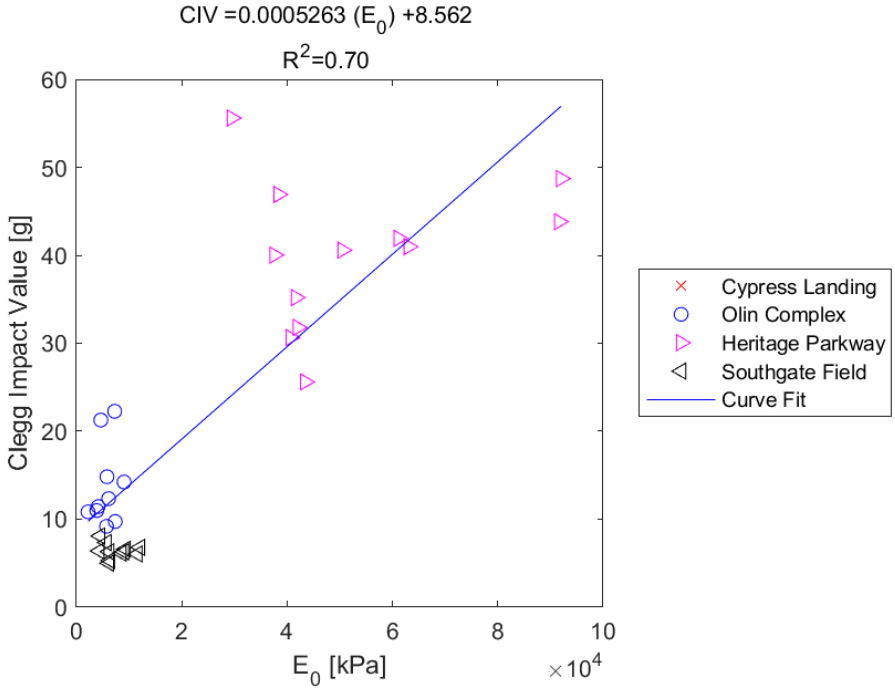

Figure E.86: Linear - Linear Model of CIV versus E_0 for SDPMT-6 Continuous Tests, All Sites

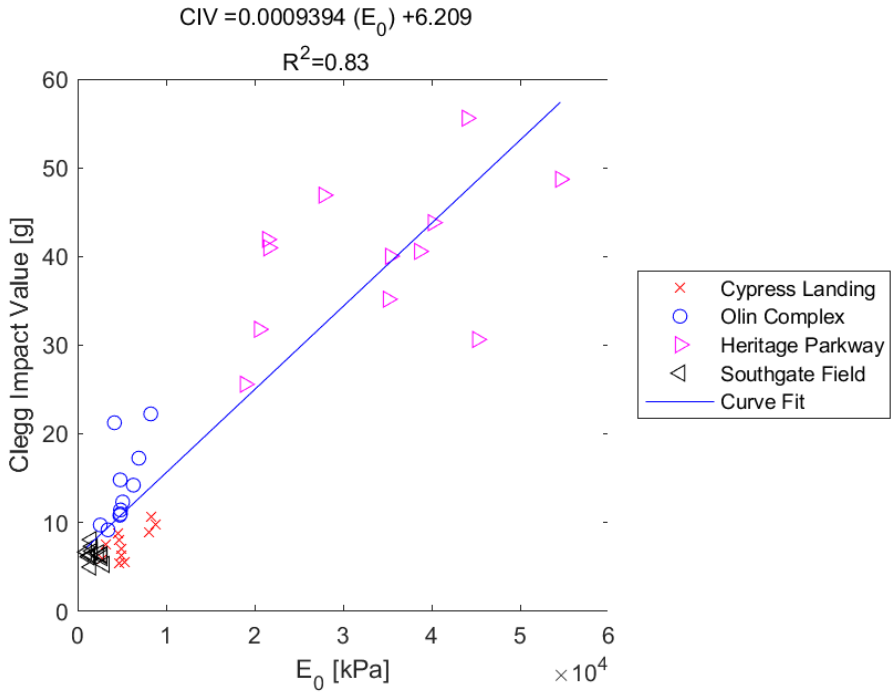

Figure E.87: Linear - Linear Model of CIV versus E_0 for SDPMT-12 Incremental Tests, All Sites

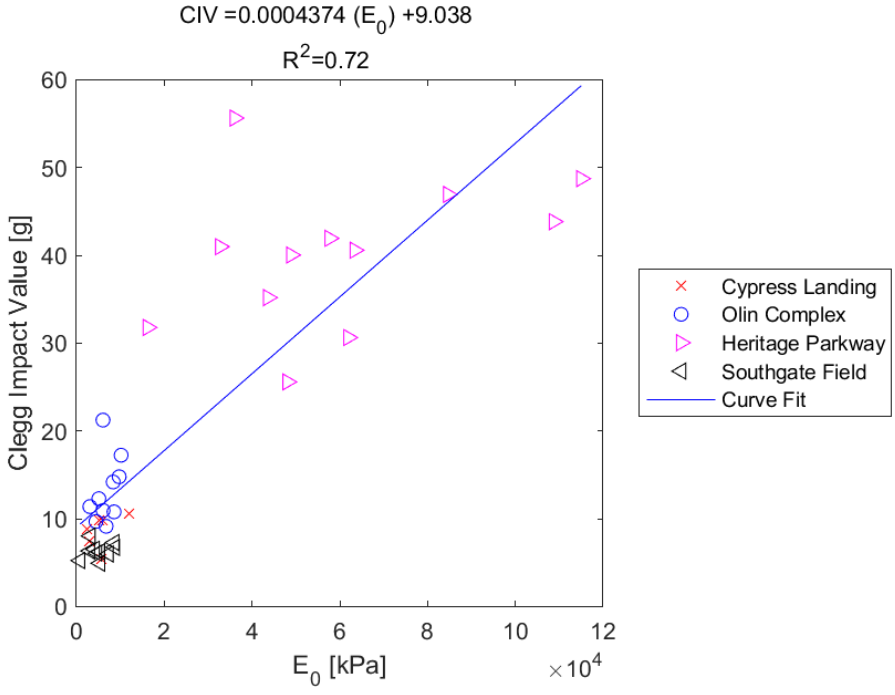

Figure E.88: Linear - Linear Model of CIV versus E_0 for SDPMT-12 Continuous Tests, All Sites

E.1.23 CIV versus $\mathbf{p}_L$

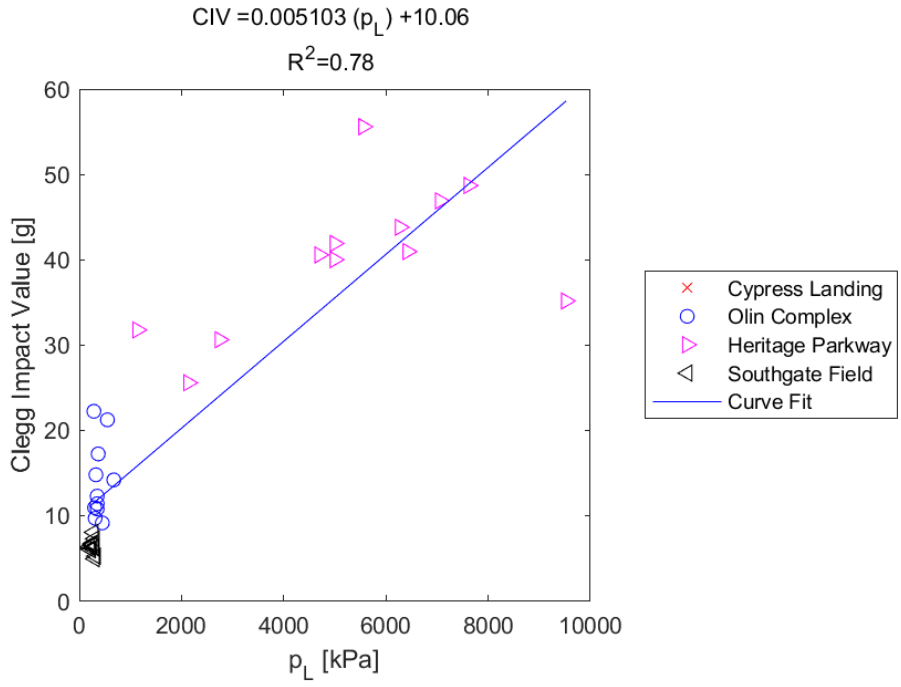

Figure E.89: Linear - Linear Model of CIV versus p_L for SDPMT-6 Incremental Tests, All Sites

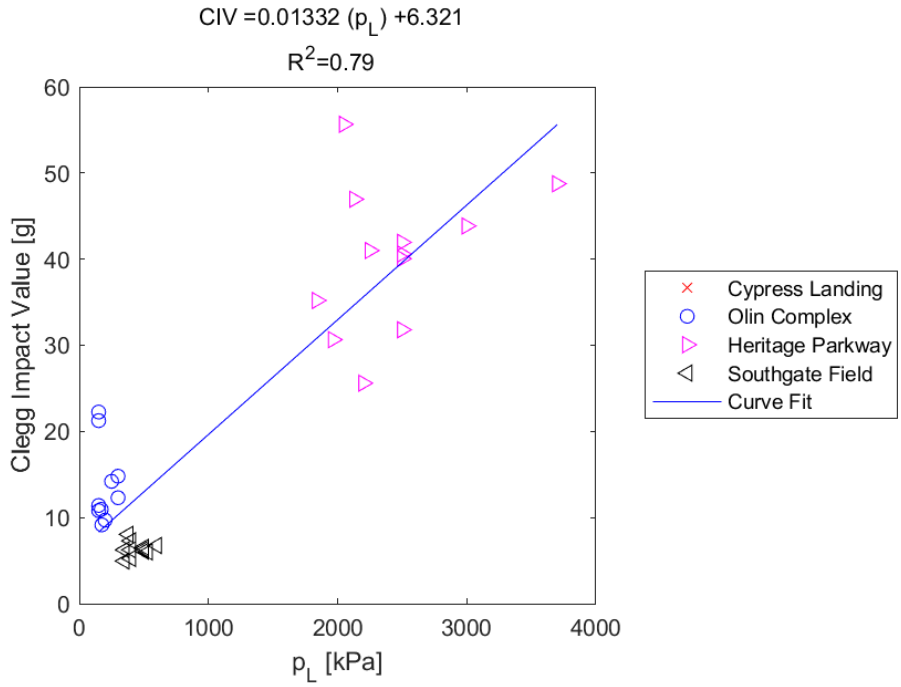

Figure E.90: Linear - Linear Model of CIV versus p_L for SDPMT-6 Continuous Tests, All Sites

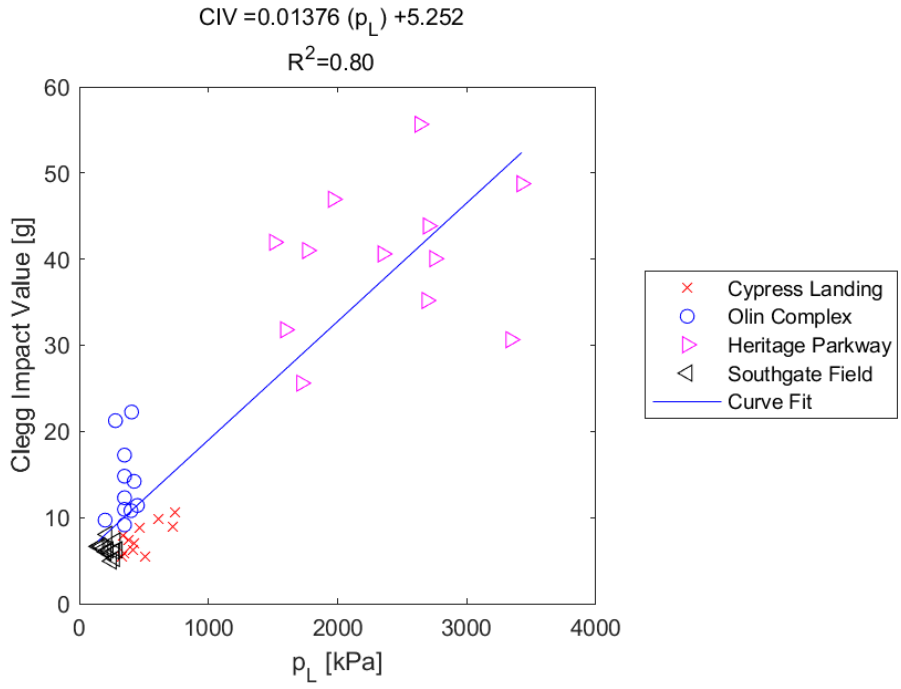

Figure E.91: Linear - Linear Model of CIV versus p_L for SDPMT-12 Incremental Tests, All Sites

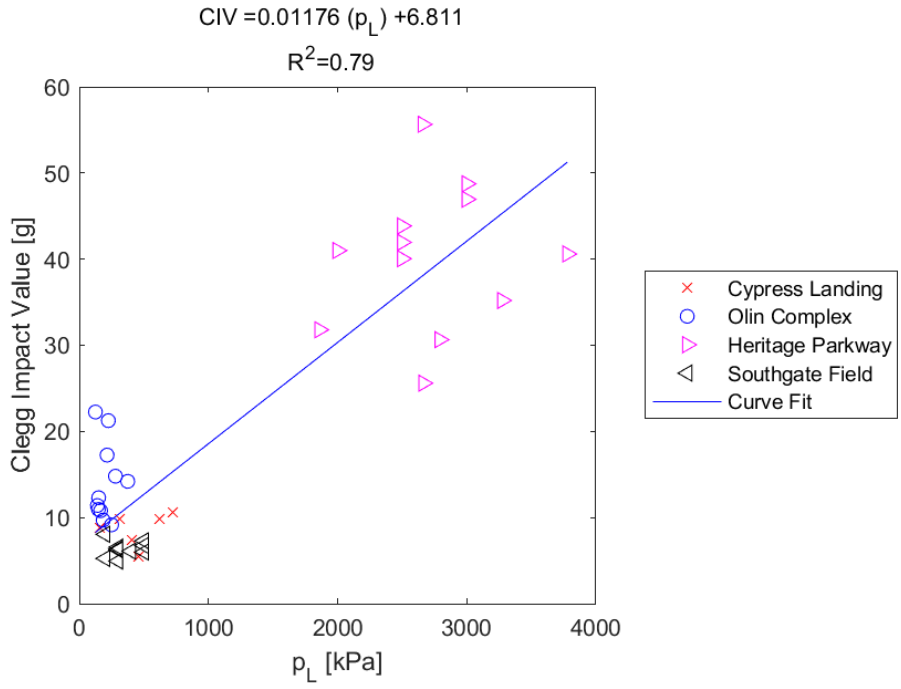

Figure E.92: Linear - Linear Model of CIV versus p_L for SDPMT-12 Continuous Tests, All Sites

E.1.24 CIV versus p_0

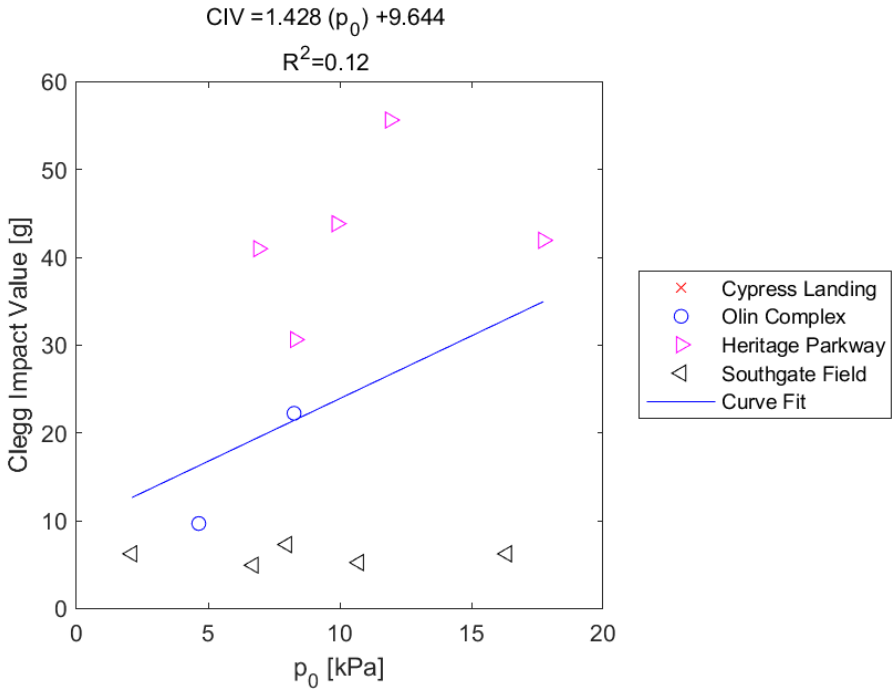

Figure E.93: Linear - Linear Model of CIV versus p_0 for SDPMT-6 Incremental Tests, All Sites

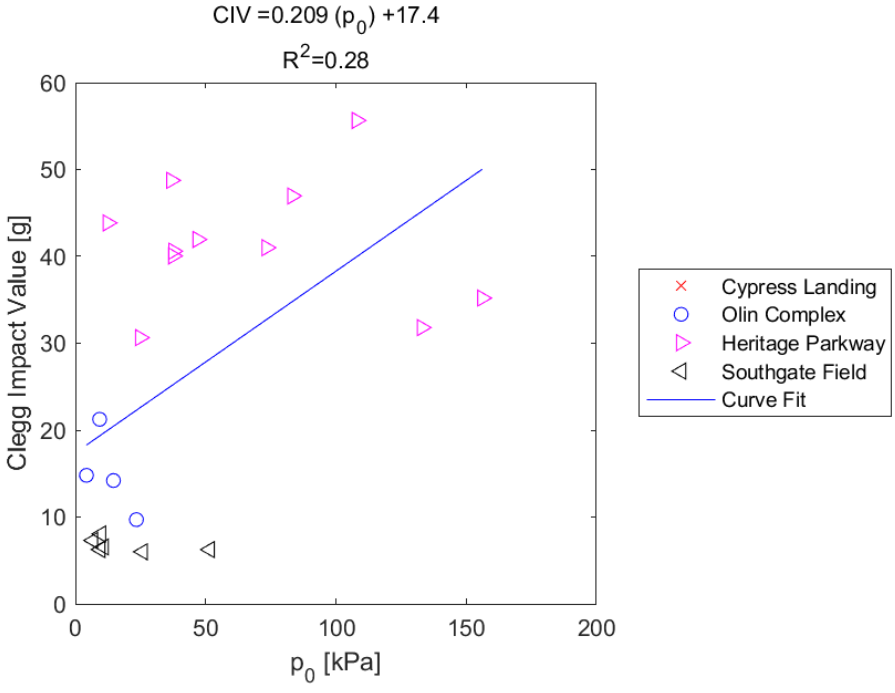

Figure E.94: Linear - Linear Model of CIV versus p_0 for SDPMT-6 Continuous Tests, All Sites

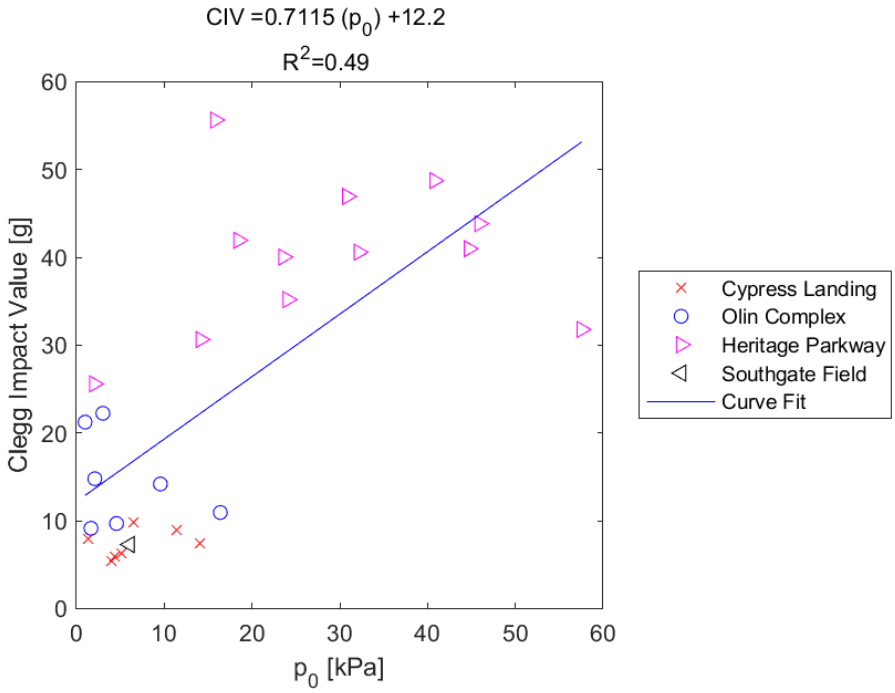

Figure E.95: Linear - Linear Model of CIV versus p_0 for SDPMT-12 Incremental Tests, All Sites

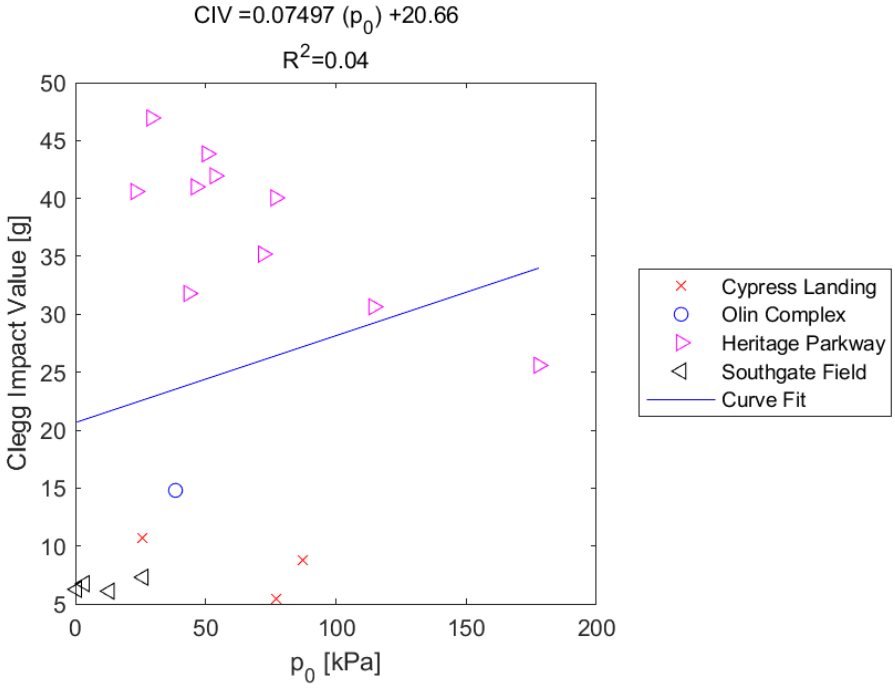

Figure E.96: Linear - Linear Model of CIV versus p_0 for SDPMT-12 Continuous Tests, All Sites

E.2 Log - Linear Models

E.2.1 SDPMT E_0 versus p_0

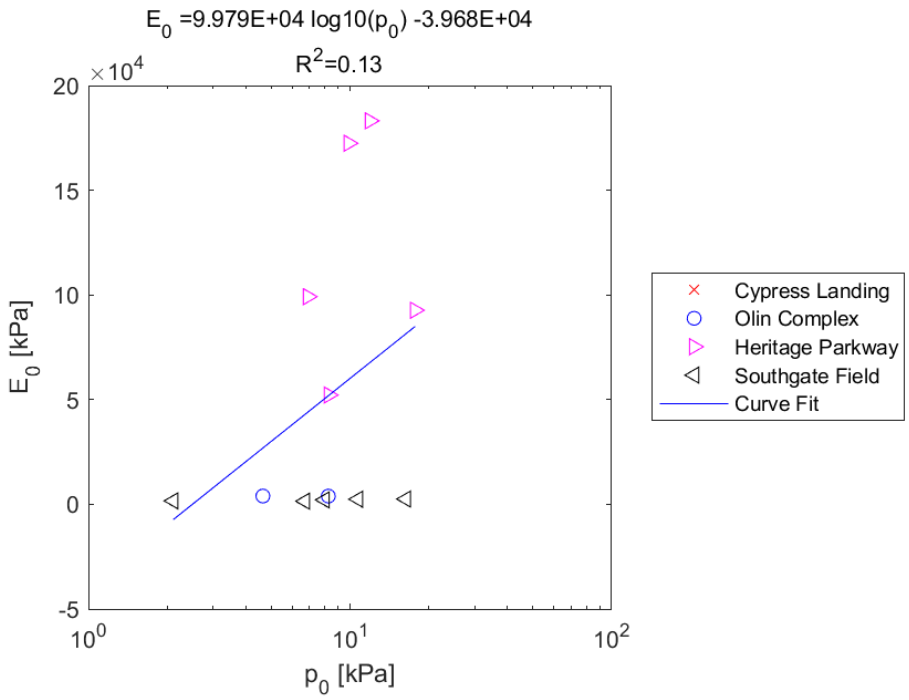

Figure E.97: Log - Linear Model of E_0 versus p_0 for SDPMT-6 Incremental Tests, All Sites

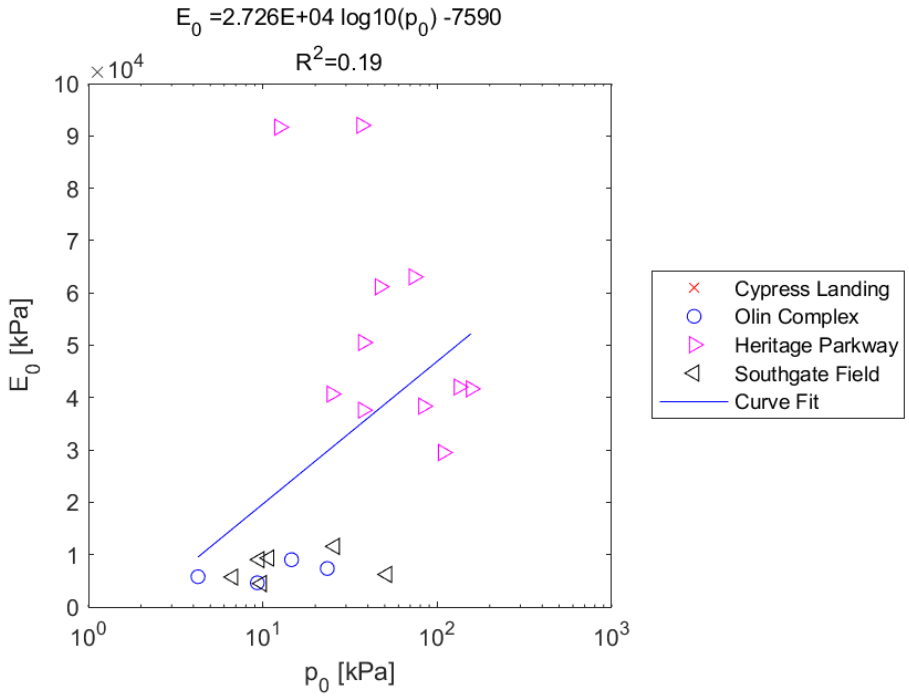

Figure E.98: Log - Linear Model of E_0 versus p_0 for SDPMT-6 Continuous Tests, All Sites

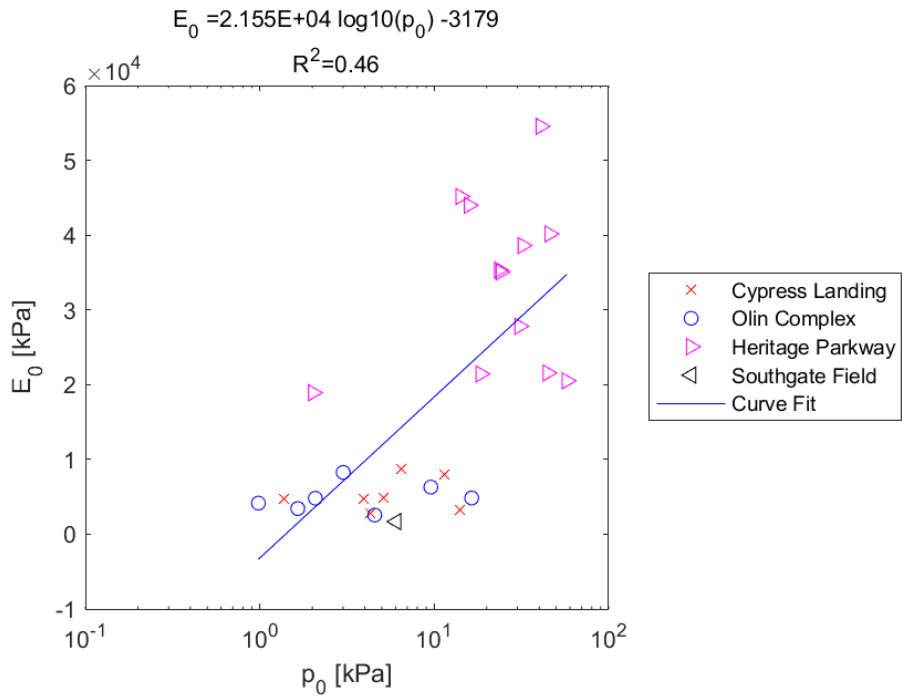

Figure E.99: Log - Linear Model of E_0 versus p_0 for SDPMT-12 Incremental Tests, All Sites

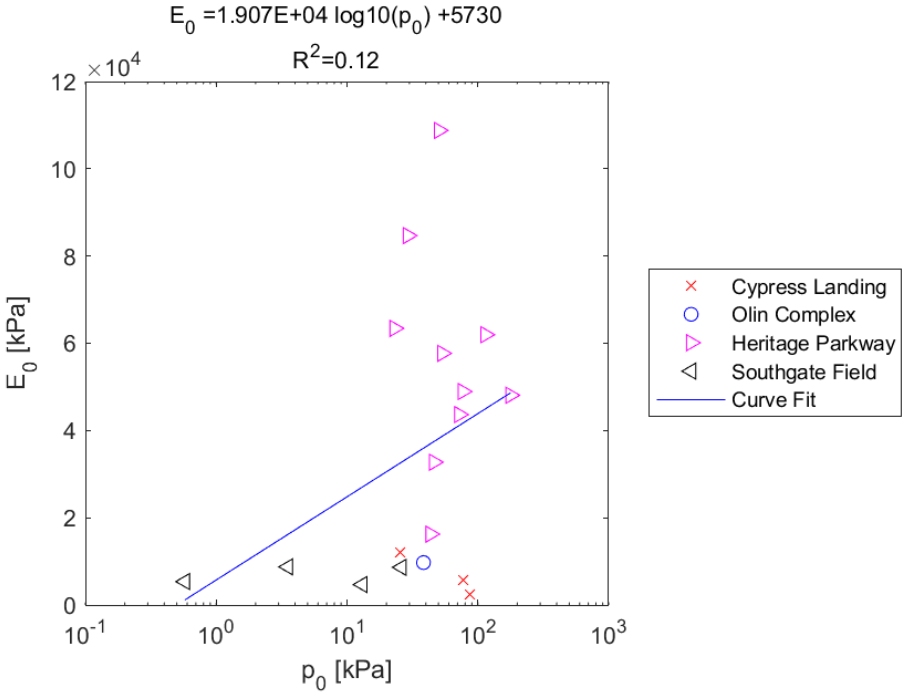

Figure E.100: Log - Linear Model of E_0 versus p_0 for SDPMT-12 Continuous Tests, All Sites

E.2.2 SDPMT p_0 versus E_0

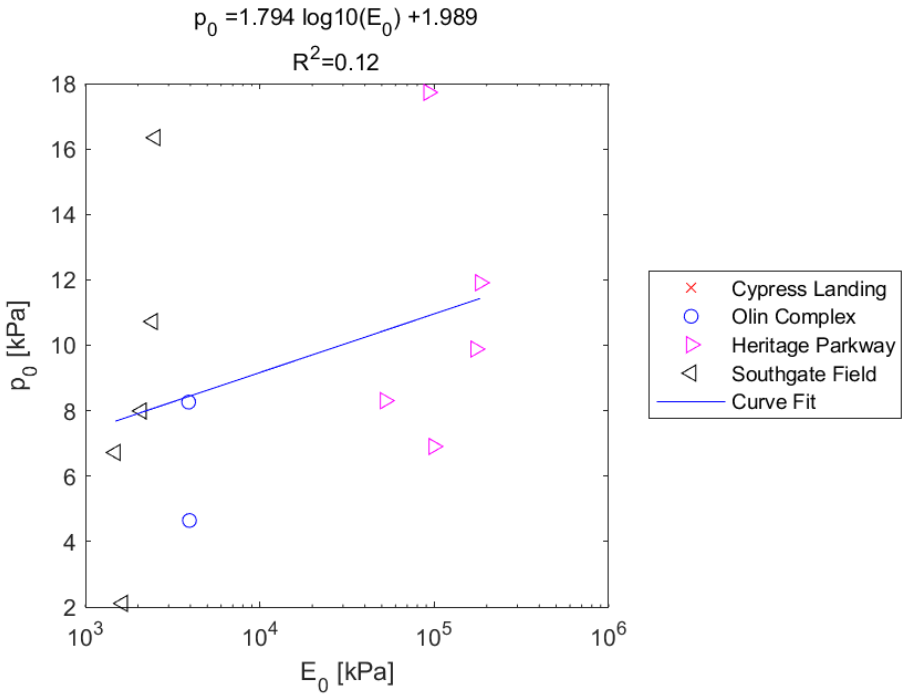

Figure E.101: Log - Linear Model of p_0 versus E_0 for SDPMT-6 Incremental Tests, All Sites

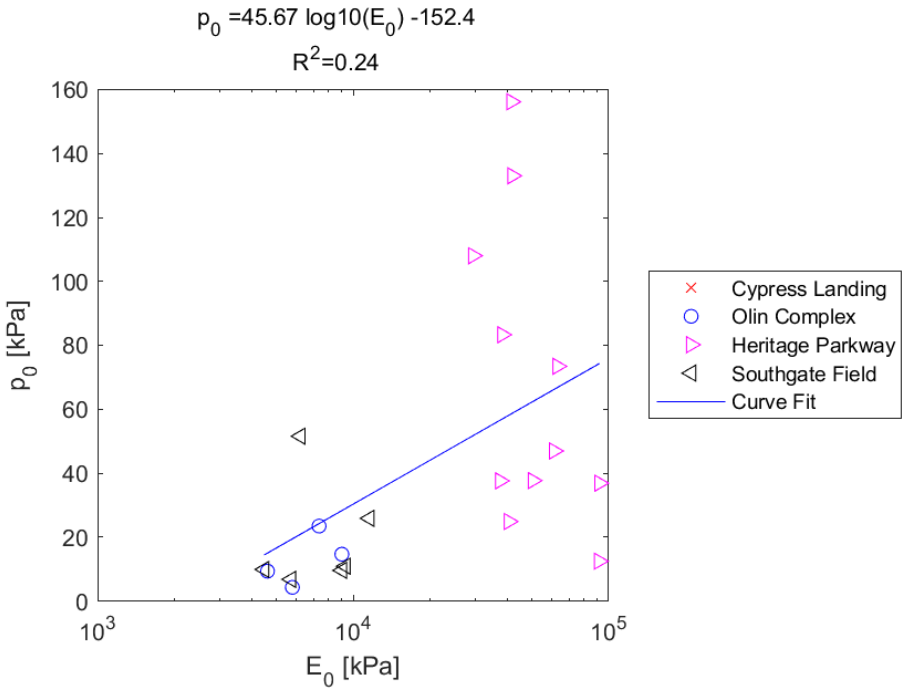

Figure E.102: Log - Linear Model of p_0 versus E_0 for SDPMT-6 Continuous Tests, All Sites

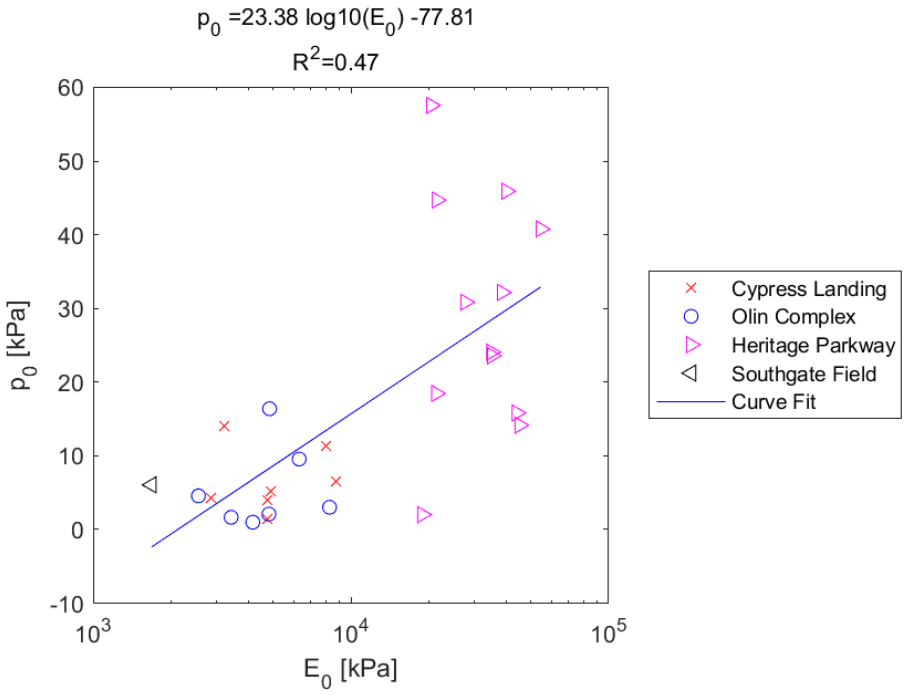

Figure E.103: Log - Linear Model of p_0 versus E_0 for SDPMT-12 Incremental Tests, All Sites

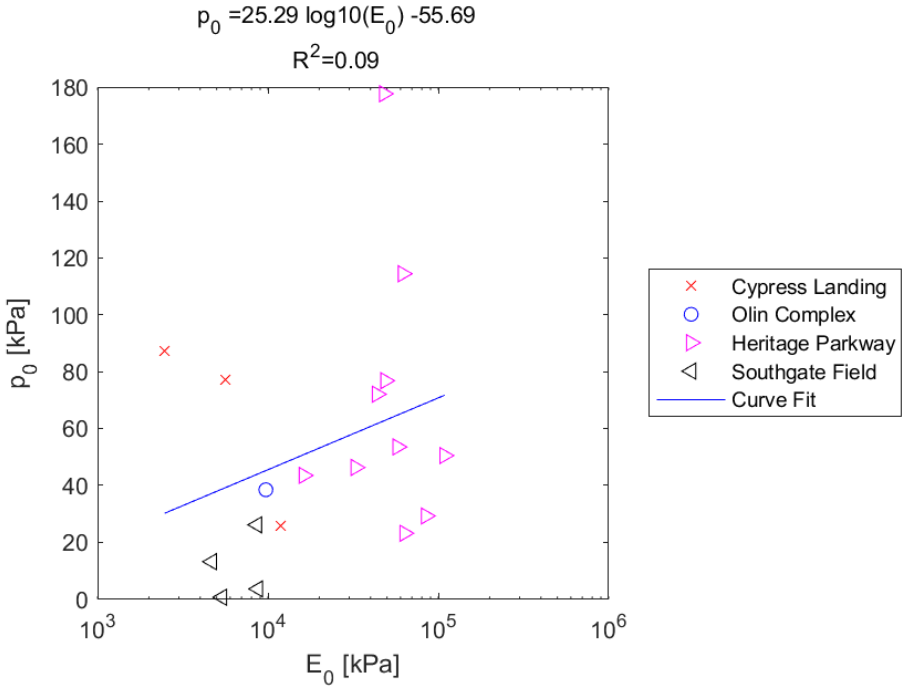

Figure E.104: Log - Linear Model of p_0 versus E_0 for SDPMT-12 Continuous Tests, All Sites

E.2.3 SDPMT $\mathbf{E}_0$ versus $\mathbf{p}_L$

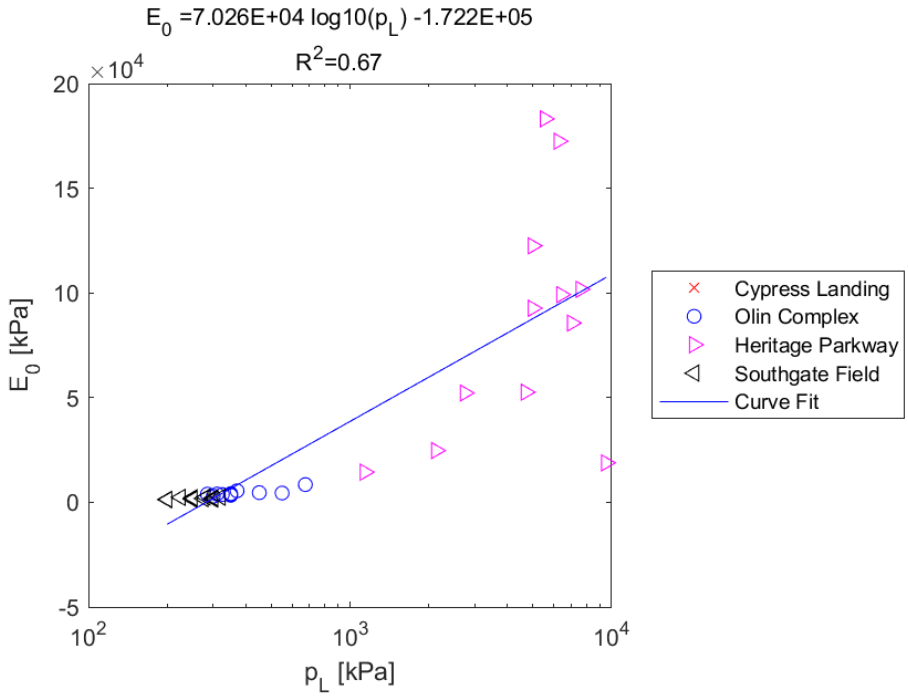

Figure E.105: Log - Linear Model of E_0 versus p_L for SDPMT-6 Incremental Tests, All Sites

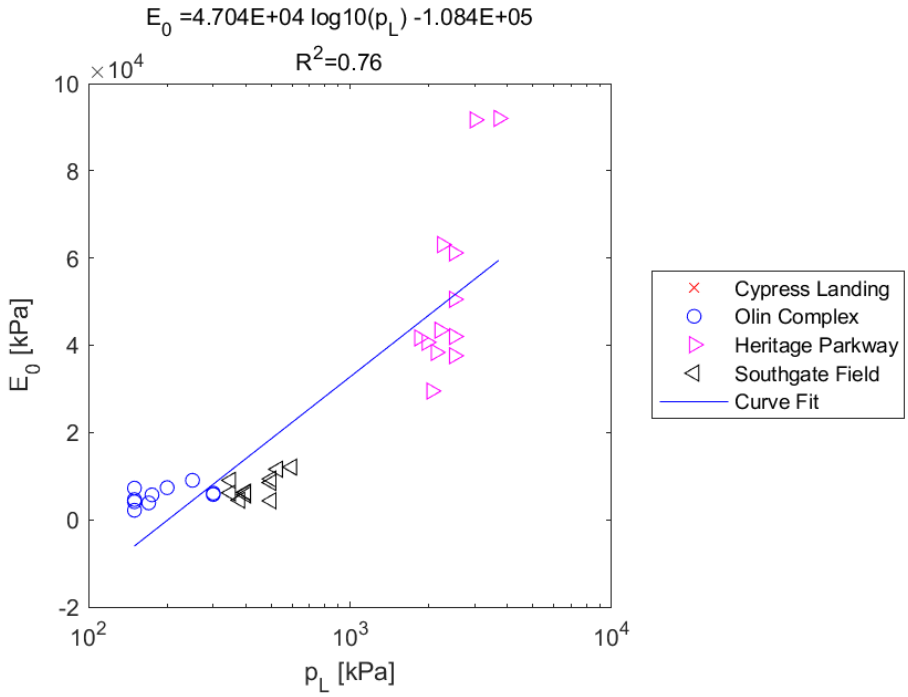

Figure E.106: Log - Linear Model of E_0 versus p_L for SDPMT-6 Continuous Tests, All Sites

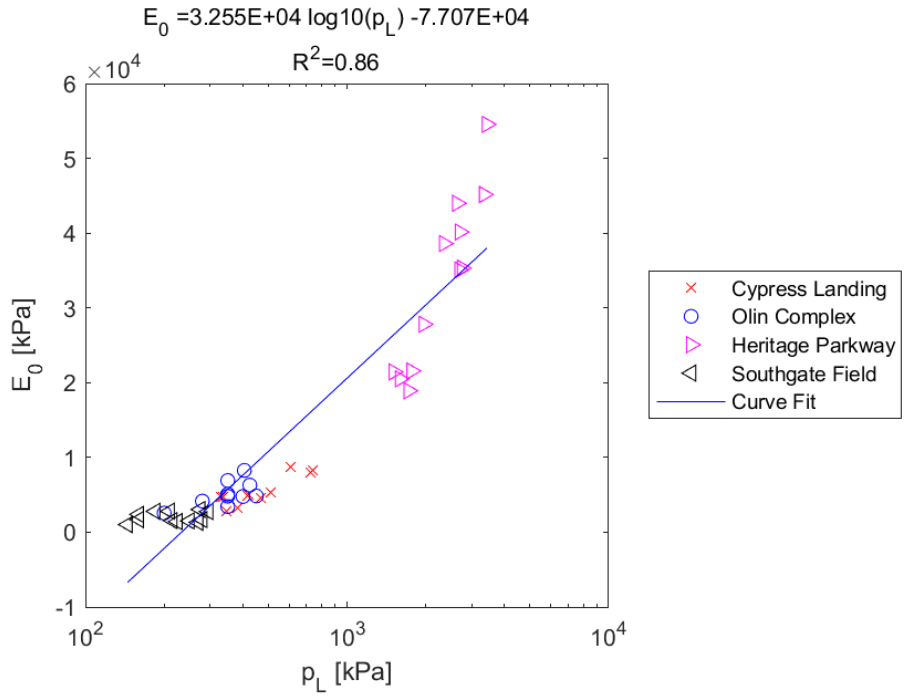

Figure E.107: Log - Linear Model of E_0 versus p_L for SDPMT-12 Incremental Tests, All Sites

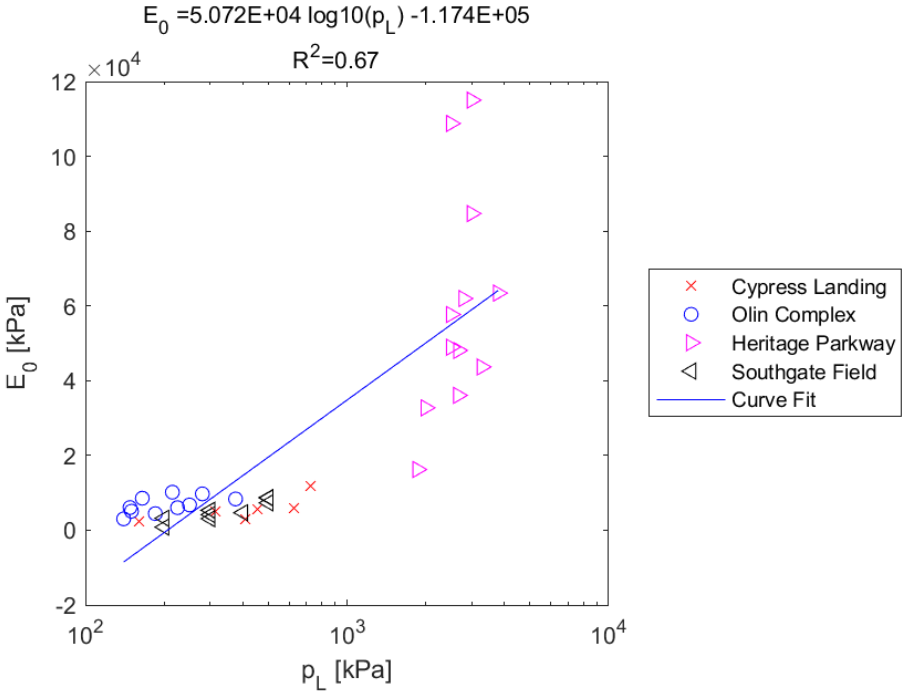

Figure E.108: Log - Linear Model of E_0 versus p_L for SDPMT-12 Continuous Tests, All Sites

E.2.4 SDPMT $\mathbf{p}_L$ versus $\mathbf{E}_0$

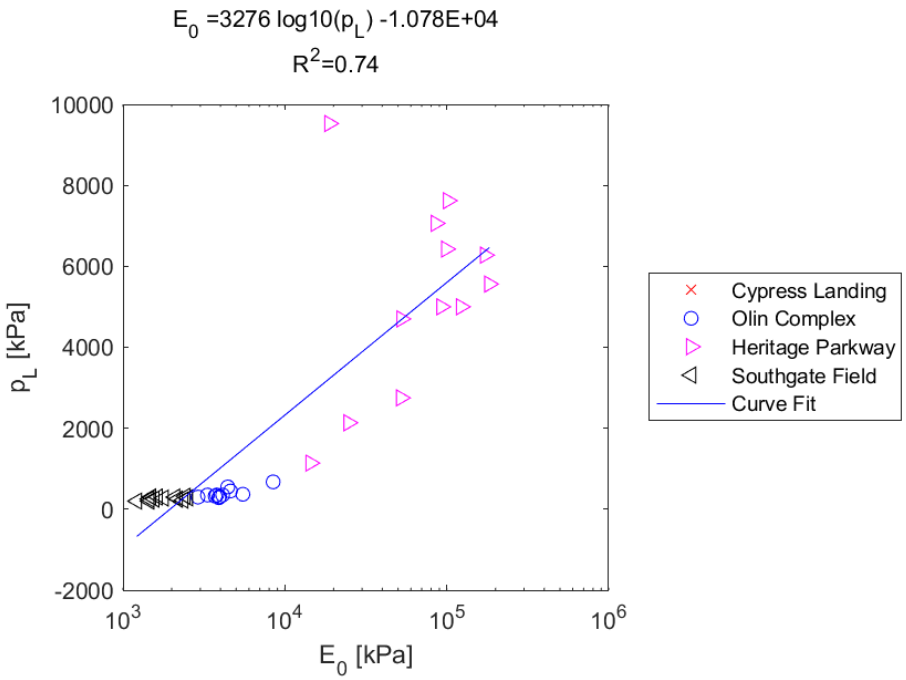

Figure E.109: Log - Linear Model of p_L versus E_0 for SDPMT-6 Incremental Tests, All Sites

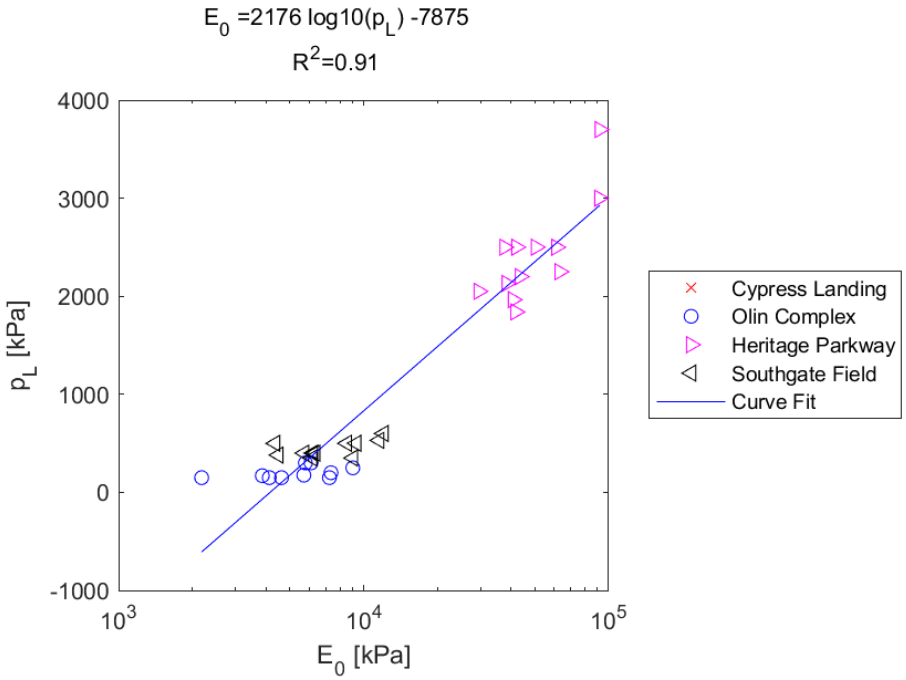

Figure E.110: Log - Linear Model of p_L versus E_0 for SDPMT-6 Continuous Tests, All Sites

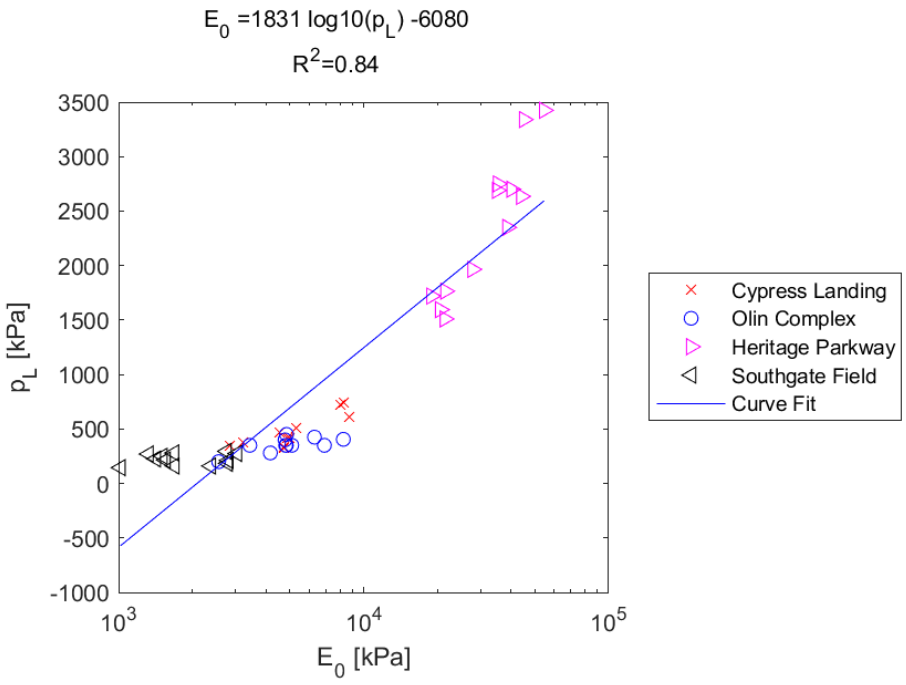

Figure E.111: Log - Linear Model of p_L versus E_0 for SDPMT-12 Incremental Tests, All Sites

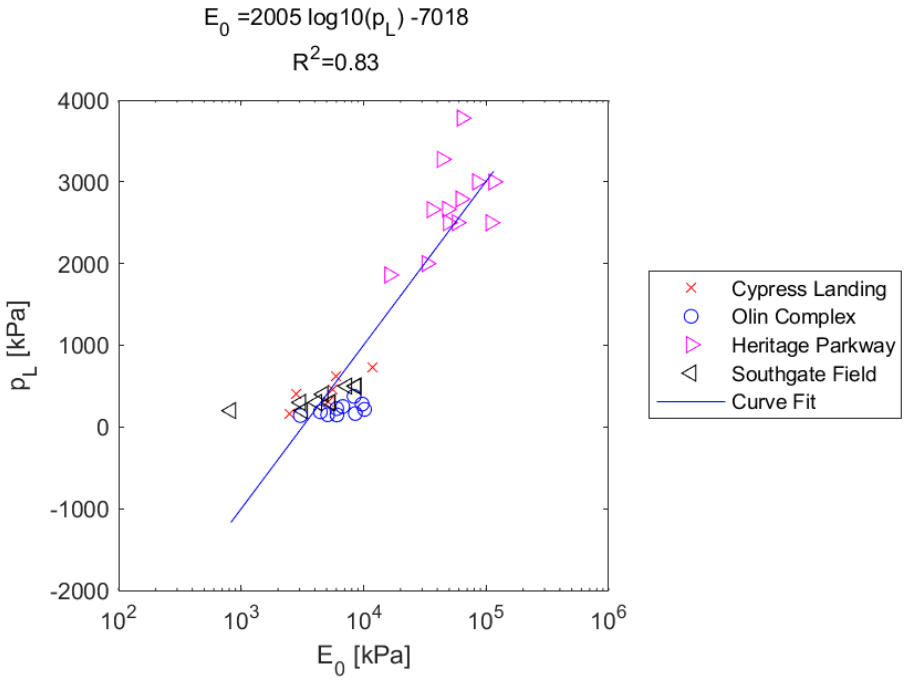

Figure E.112: Log - Linear Model of p_L versus E_0 for SDPMT-12 Continuous Tests, All Sites

E.2.5 SDPMT $\mathbf{p}_0$ versus $\mathbf{p}_L$

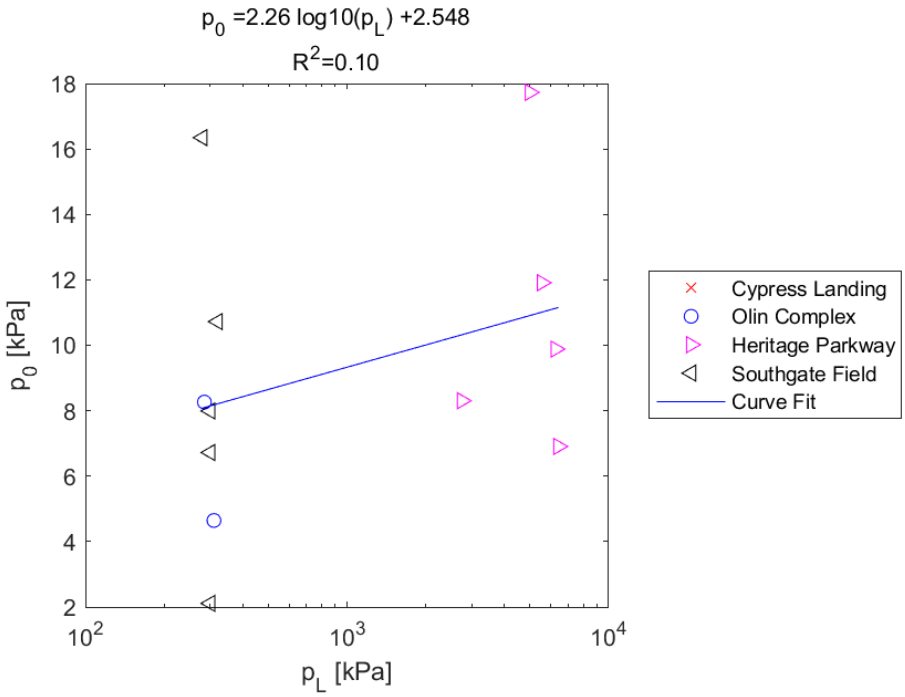

Figure E.113: Log - Linear Model of p_0 versus p_L for SDPMT-6 Incremental Tests, All Sites

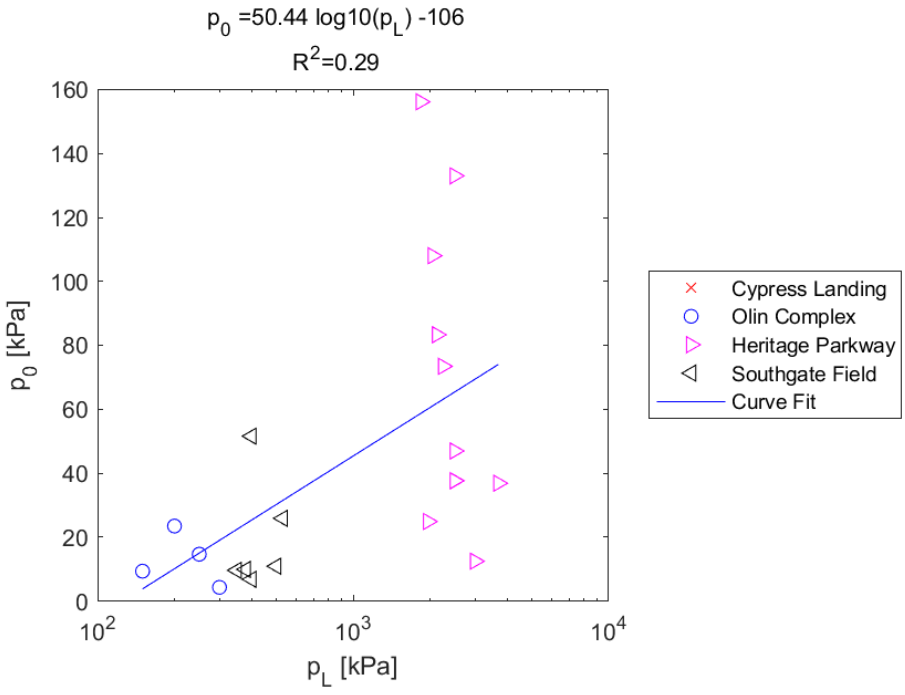

Figure E.114: Log - Linear Model of p_0 versus p_L for SDPMT-6 Continuous Tests, All Sites

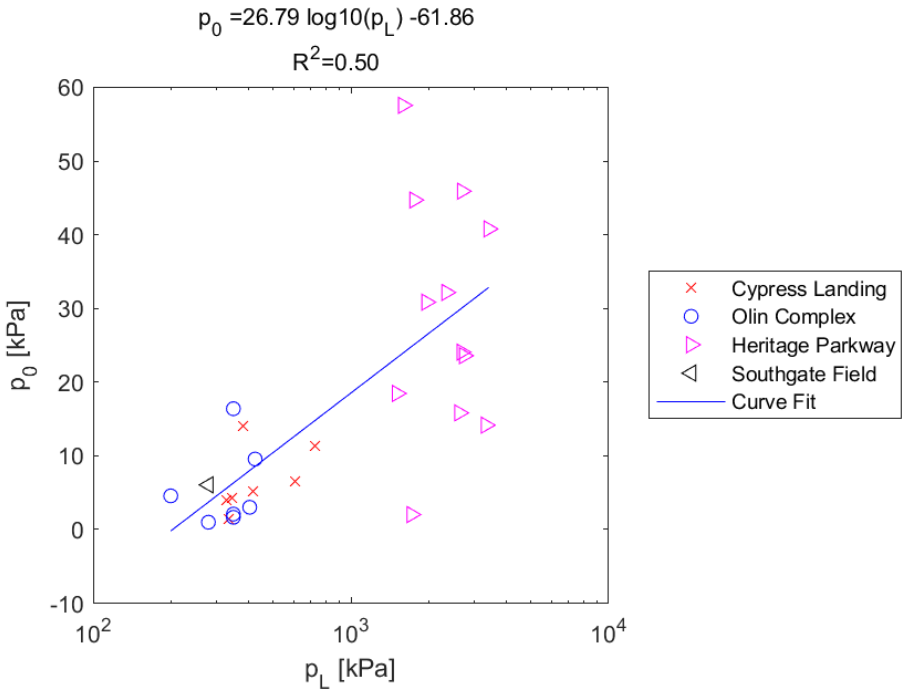

Figure E.115: Log - Linear Model of p_0 versus p_L for SDPMT-12 Incremental Tests, All Sites

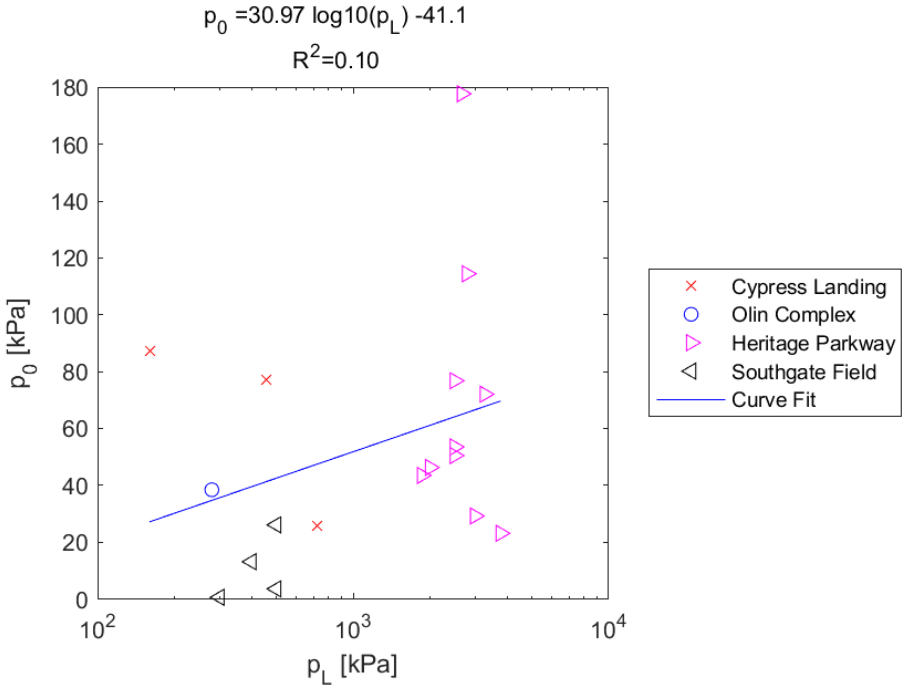

Figure E.116: Log - Linear Model of p_0 versus p_L for SDPMT-12 Continuous Tests, All Sites

E.2.6 SDPMT $\mathbf{p}_L$ versus $\mathbf{p}_0$

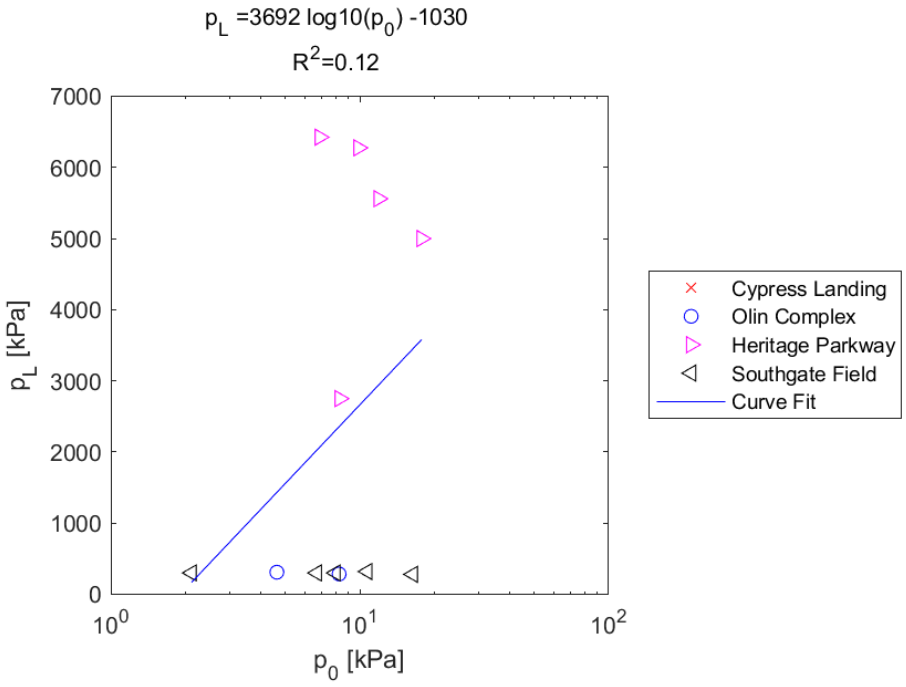

Figure E.117: Log - Linear Model of p_L versus p_0 for SDPMT-6 Incremental Tests, All Sites

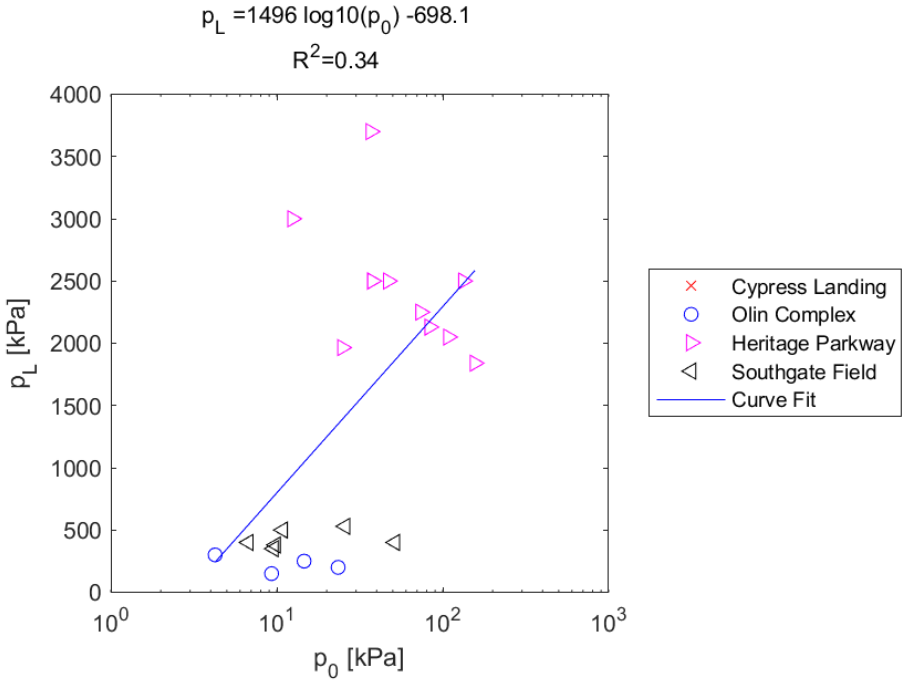

Figure E.118: Log - Linear Model of p_L versus p_0 for SDPMT-6 Continuous Tests, All Sites

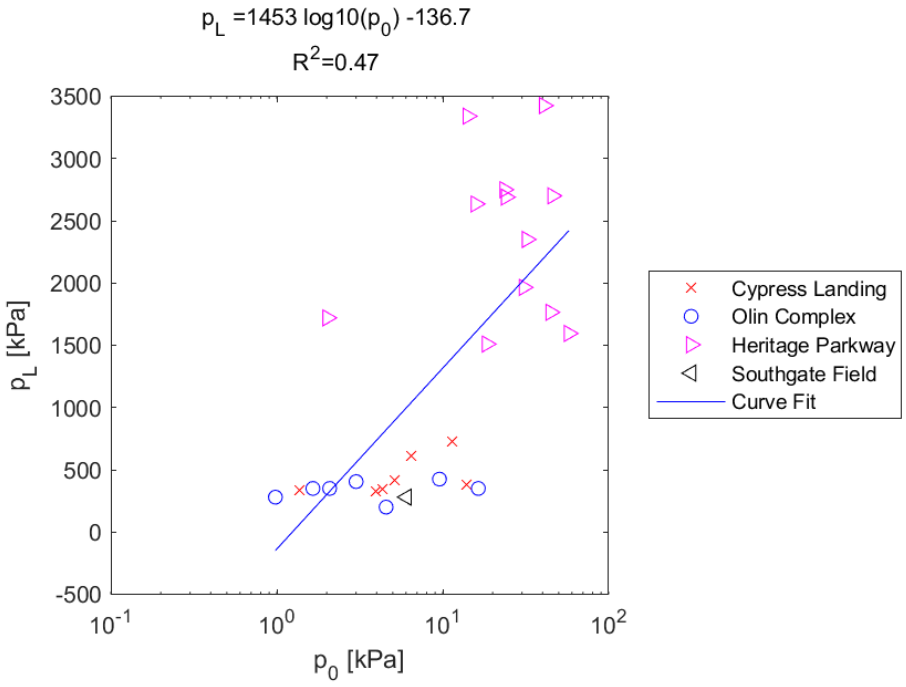

Figure E.119: Log - Linear Model of p_L versus p_0 for SDPMT-12 Incremental Tests, All Sites

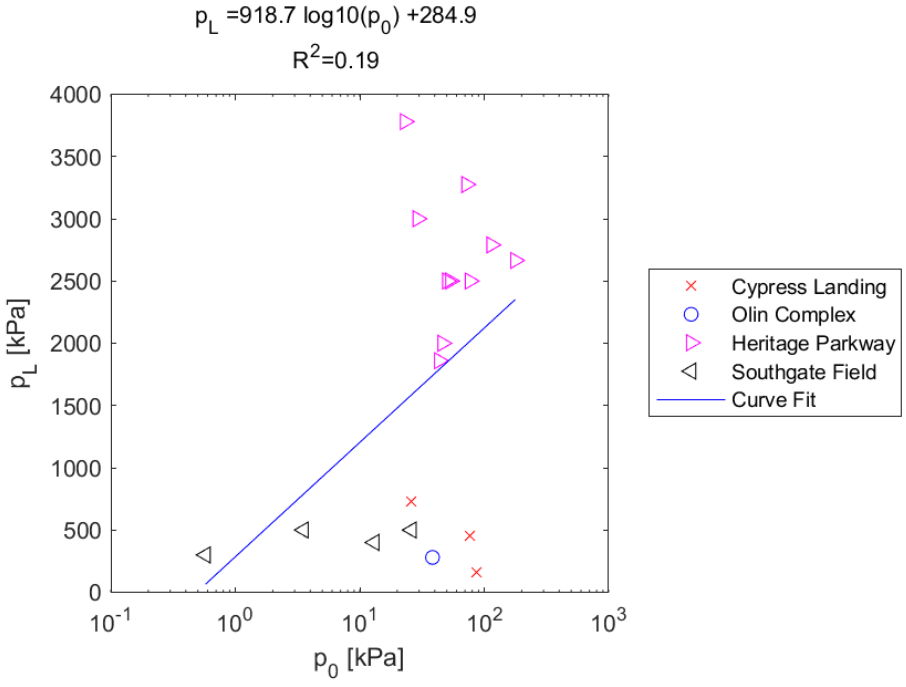

Figure E.120: Log - Linear Model of p_L versus p_0 for SDPMT-12 Continuous Tests, All Sites

E.2.7 γ_{wet} versus $\mathbf{E}_0$

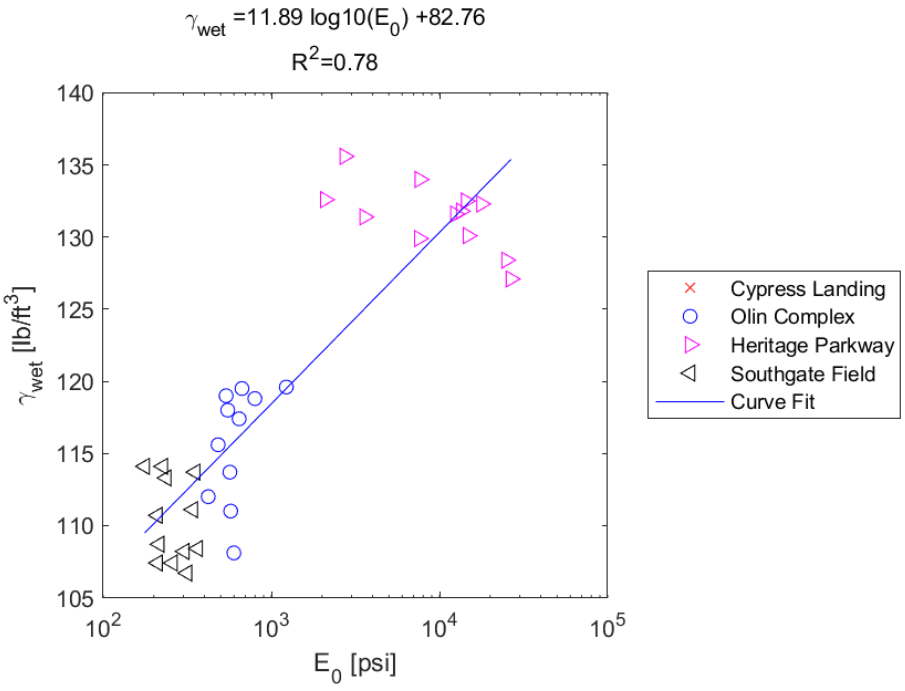

Figure E.121: Log - Linear Model of γ_{wet} versus E_0 for SDPMT-6 Incremental Tests, All Sites

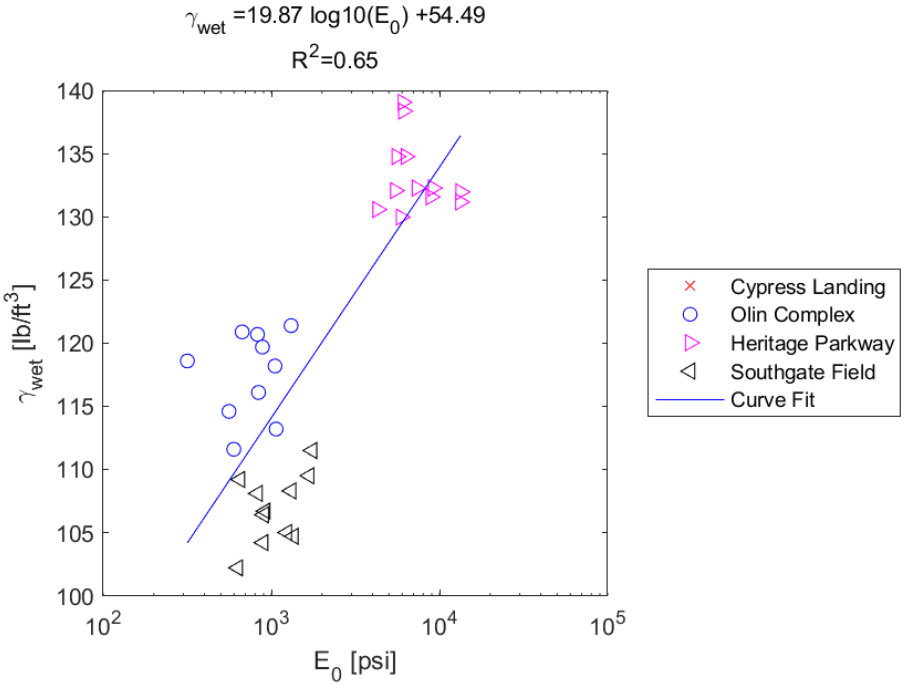

Figure E.122: Log - Linear Model of γ_{wet} versus E_0 for SDPMT-6 Continuous Tests, All Sites

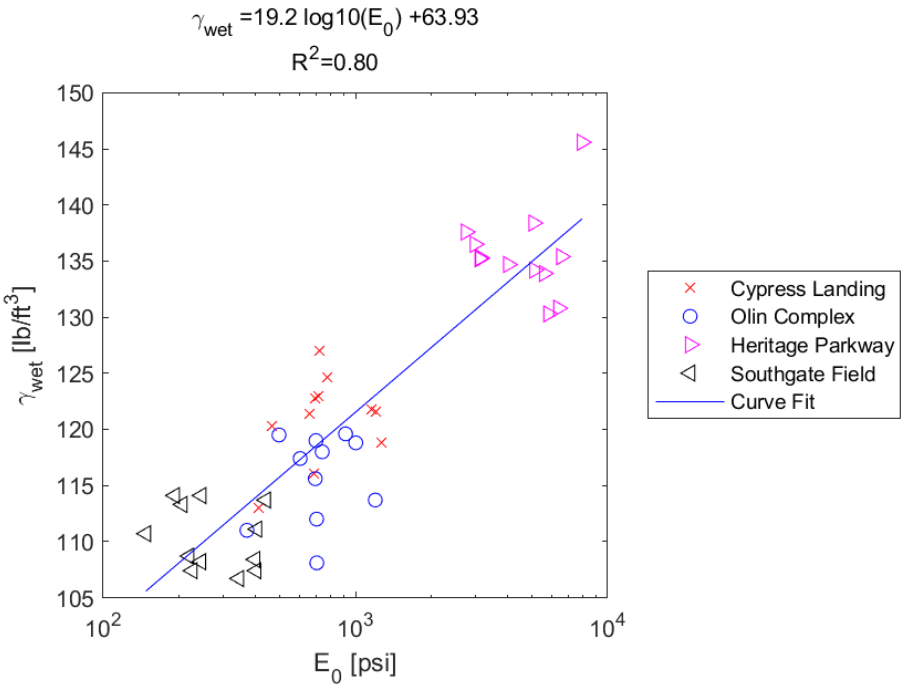

Figure E.123: Log - Linear Model of γ_{wet} versus E_0 for SDPMT-12 Incremental Tests, All Sites

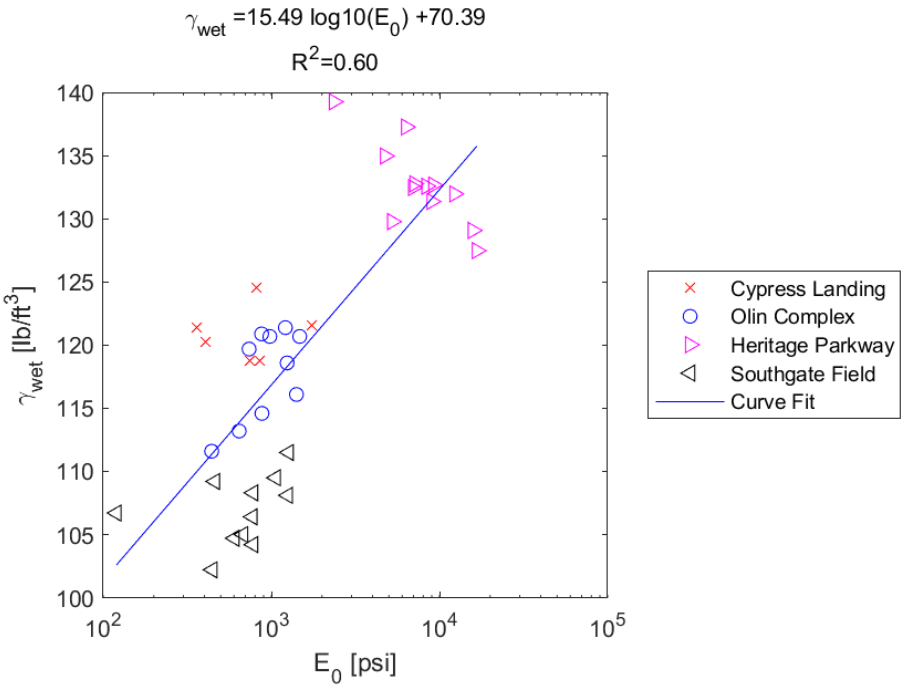

Figure E.124: Log - Linear Model of γ_{wet} versus E_0 for SDPMT-12 Continuous Tests, All Sites

E.2.8 γ_{wet} versus $\mathbf{p}_L$

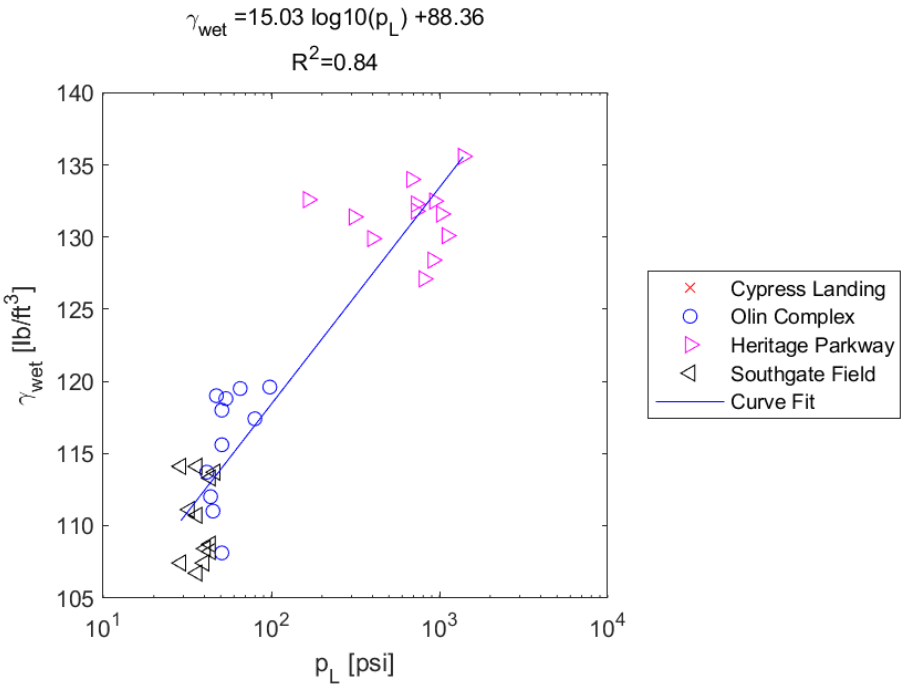

Figure E.125: Log - Linear Model of γ_{wet} versus p_L for SDPMT-6 Incremental Tests, All Sites

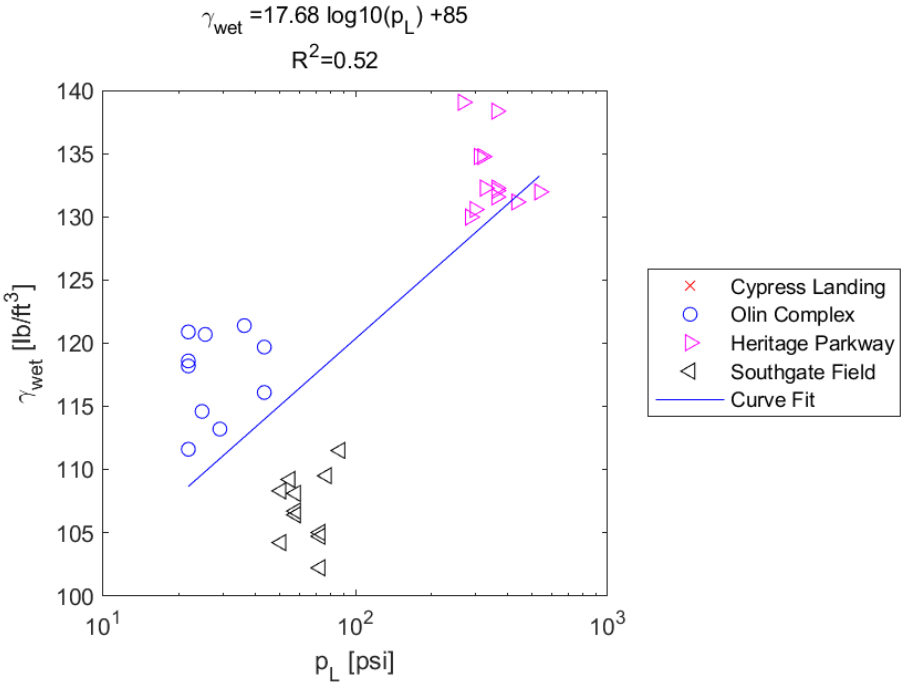

Figure E.126: Log - Linear Model of γ_{wet} versus p_L for SDPMT-6 Continuous Tests, All Sites

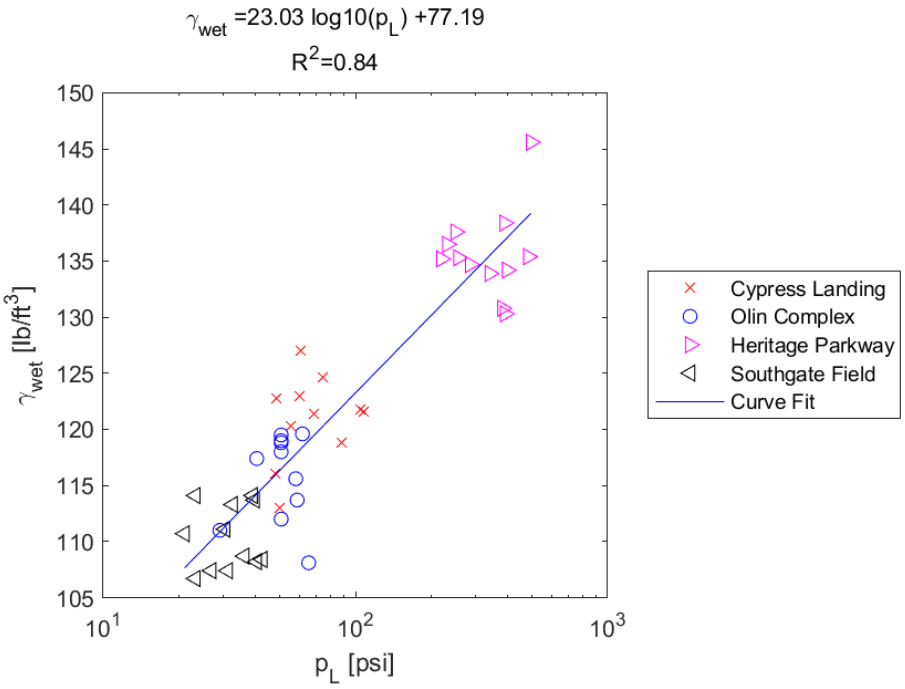

Figure E.127: Log - Linear Model of γ_{wet} versus p_L for SDPMT-12 Incremental Tests, All Sites

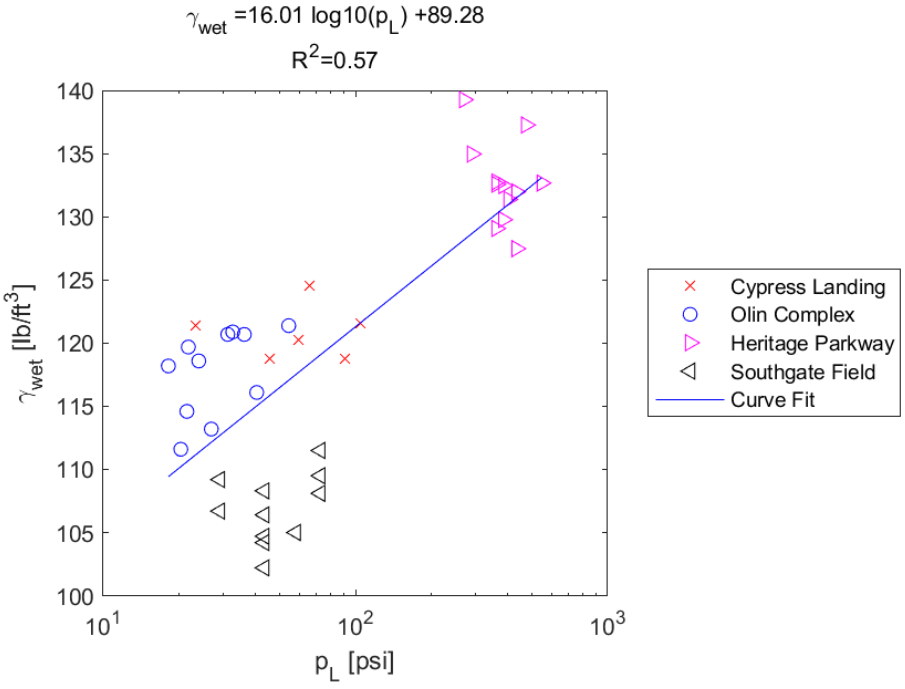

Figure E.128: Log - Linear Model of γ_{wet} versus p_L for SDPMT-12 Continuous Tests, All Sites

E.2.9 γ_{wet} versus $\mathbf{p}_0$

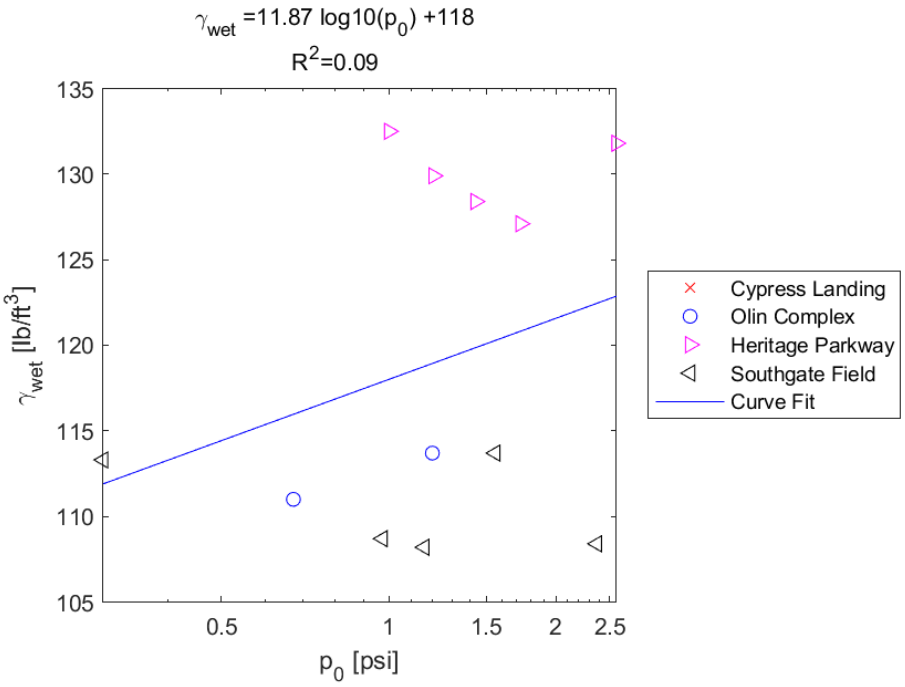

Figure E.129: Log - Linear Model of γ_{wet} versus p_0 for SDPMT-6 Incremental Tests, All Sites

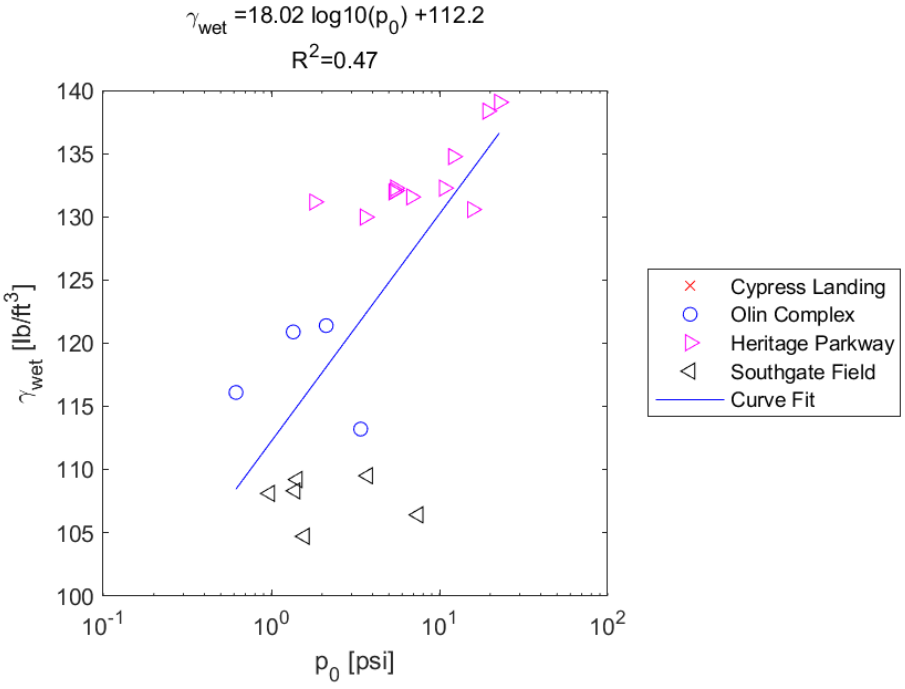

Figure E.130: Log - Linear Model of γ_{wet} versus p_0 for SDPMT-6 Continuous Tests, All Sites

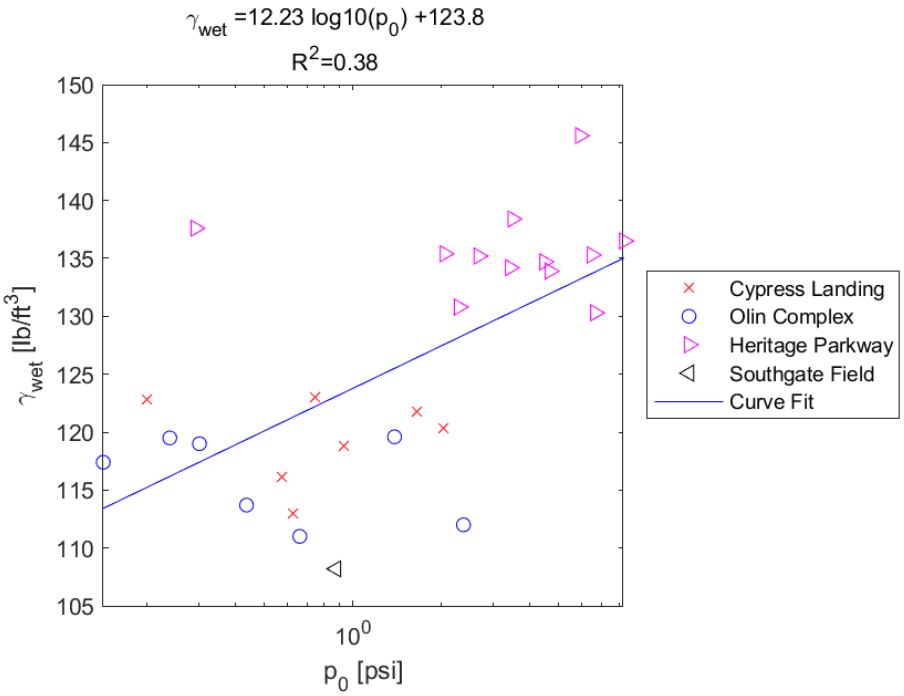

Figure E.131: Log - Linear Model of γ_{wet} versus p_0 for SDPMT-12 Incremental Tests, All Sites

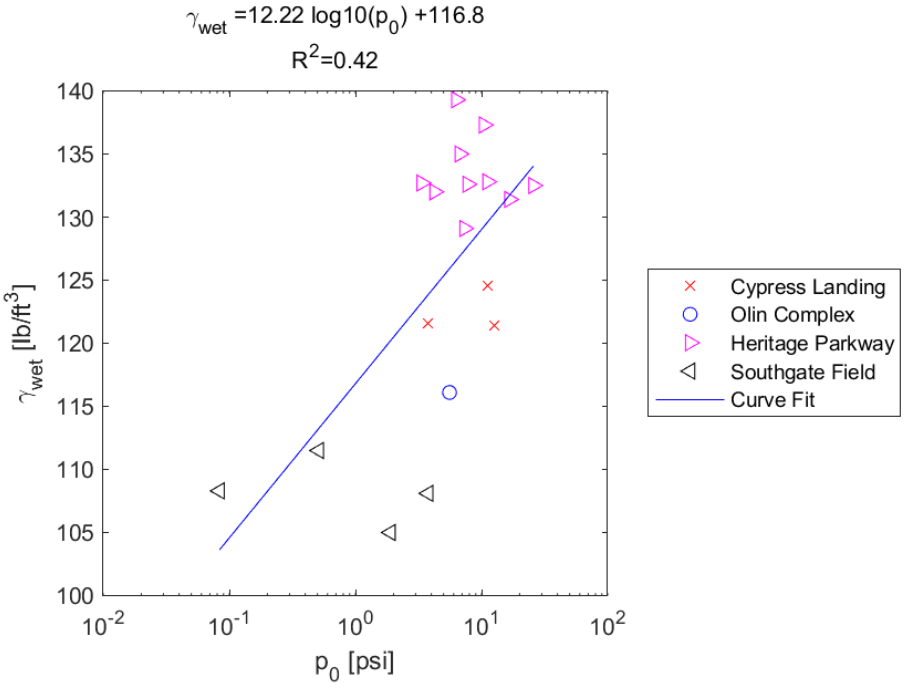

Figure E.132: Log - Linear Model of γ_{wet} versus p_0 for SDPMT-12 Continuous Tests, All Sites

E.2.10 γ_{dry} versus $\mathbf{E}_0$

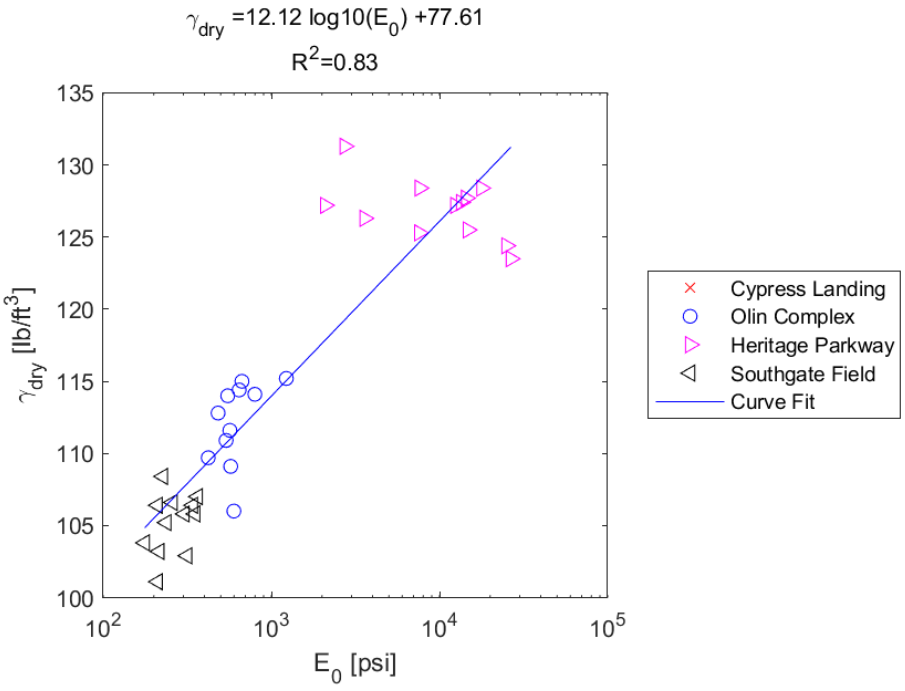

Figure E.133: Log - Linear Model of γ_{dry} versus E_0 for SDPMT-6 Incremental Tests, All Sites

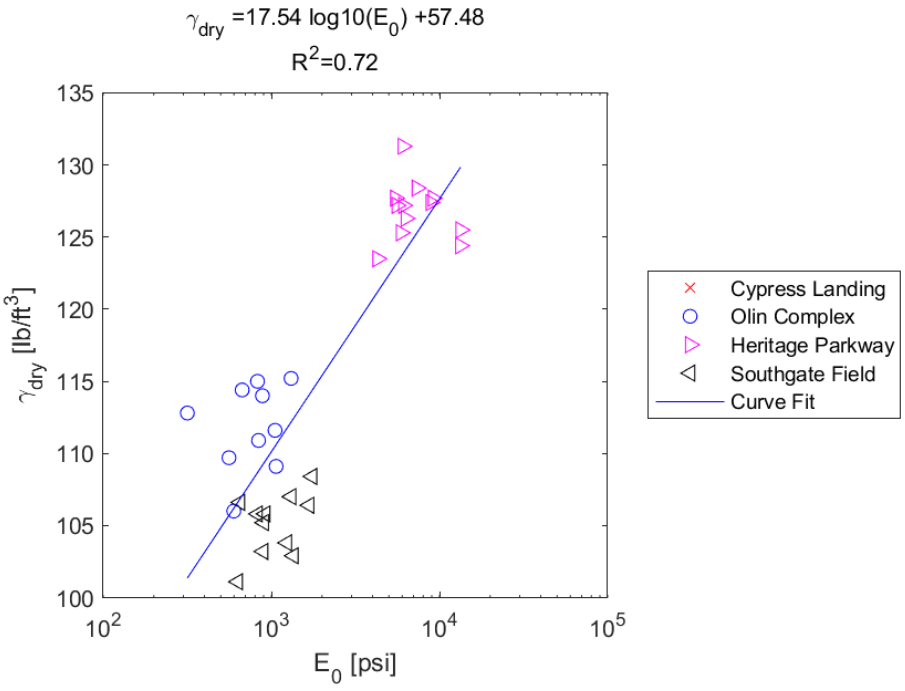

Figure E.134: Log - Linear Model of γ_{dry} versus E_0 for SDPMT-6 Continuous Tests, All Sites

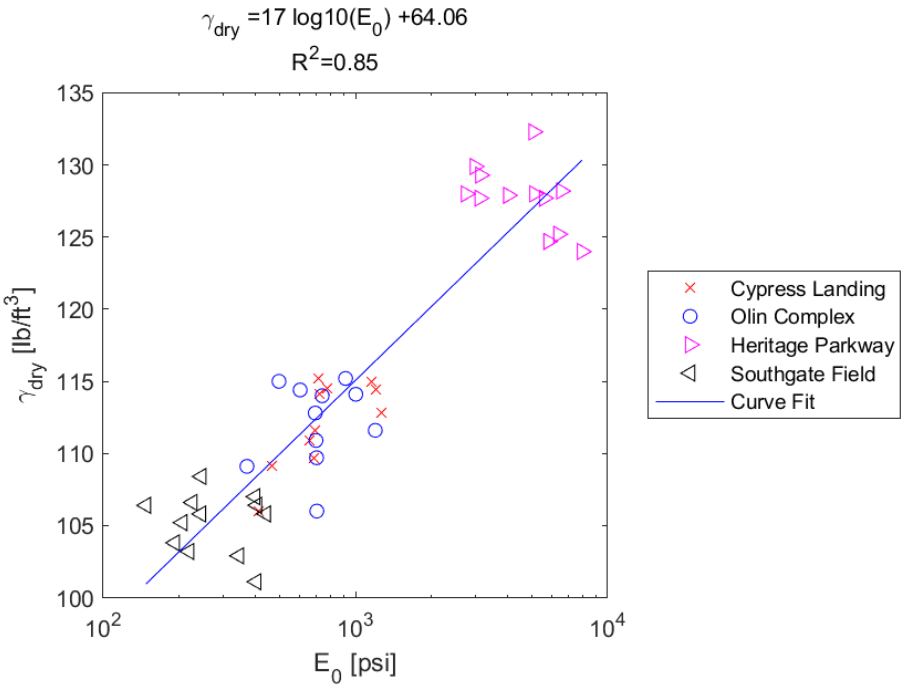

Figure E.135: Log - Linear Model of γ_{dry} versus E_0 for SDPMT-12 Incremental Tests, All Sites

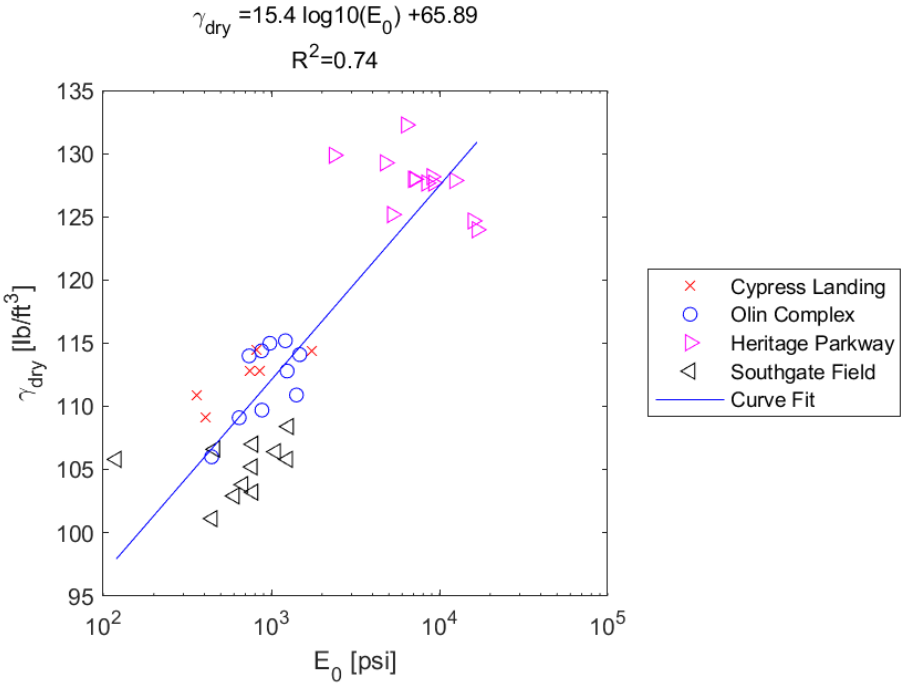

Figure E.136: Log - Linear Model of γ_{dry} versus E_0 for SDPMT-12 Continuous Tests, All Sites

E.2.11 γ_{dry} versus $\mathbf{p}_L$

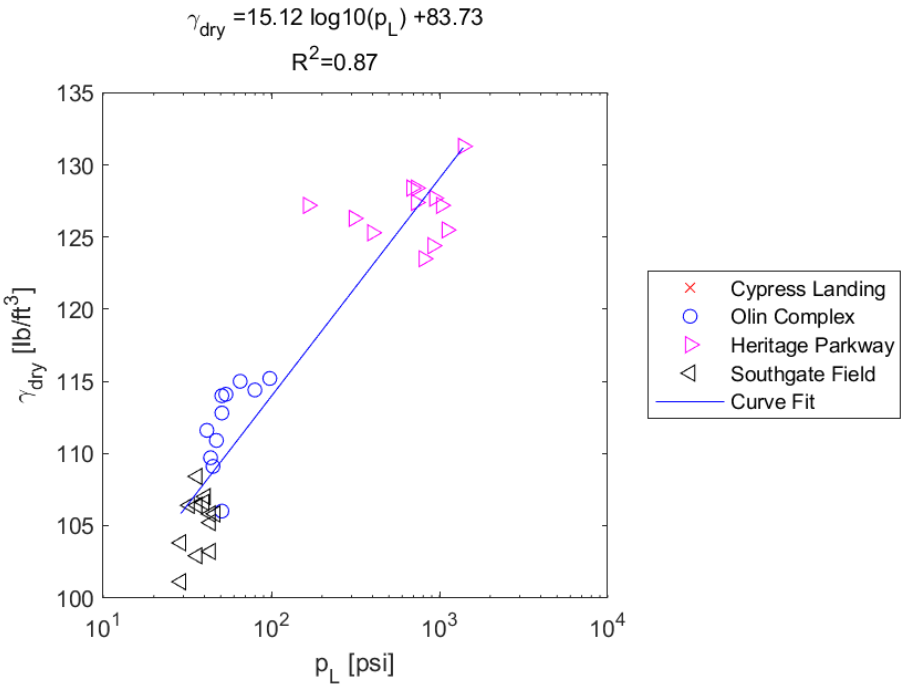

Figure E.137: Log - Linear Model of γ_{dry} versus p_L for SDPMT-6 Incremental Tests, All Sites

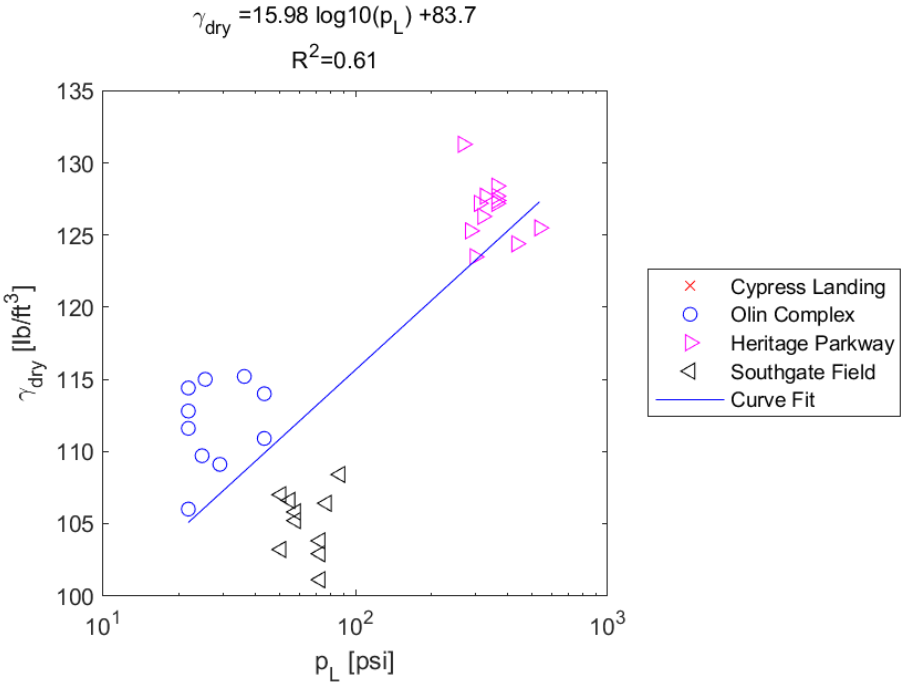

Figure E.138: Log - Linear Model of γ_{dry} versus p_L for SDPMT-6 Continuous Tests, All Sites

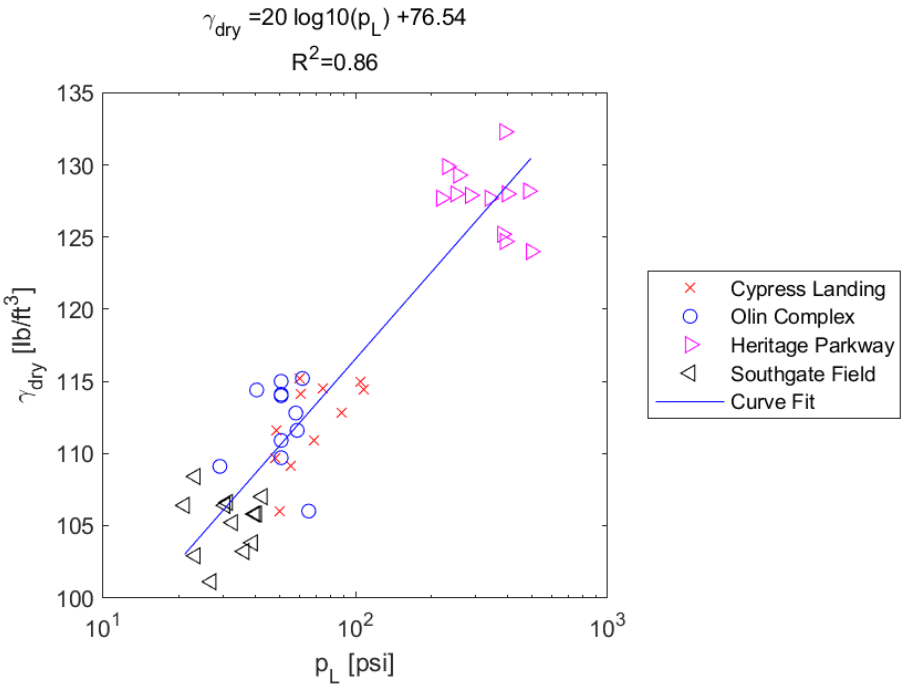

Figure E.139: Log - Linear Model of γ_{dry} versus p_L for SDPMT-12 Incremental Tests, All Sites

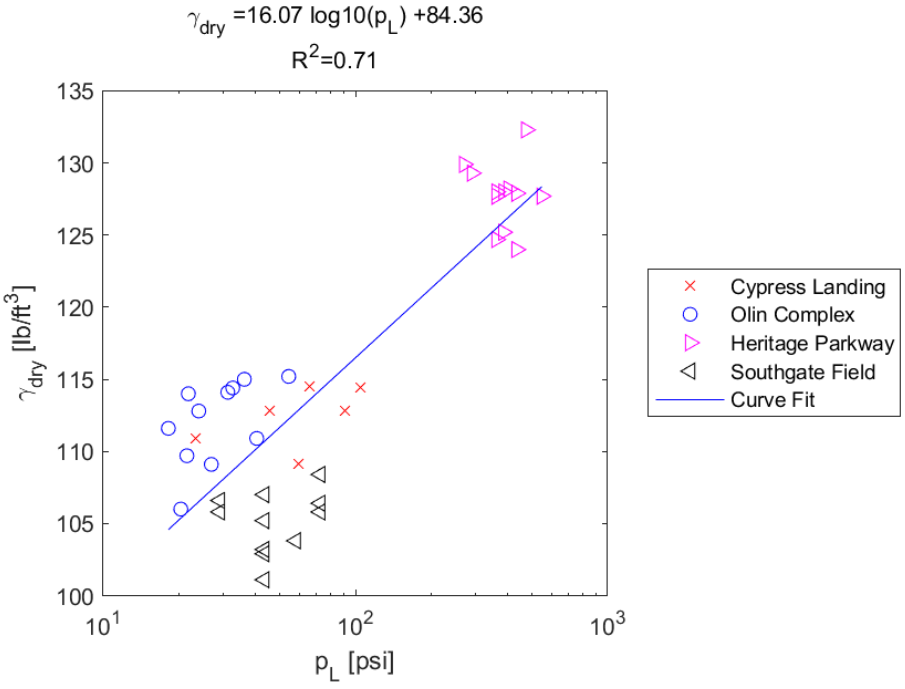

Figure E.140: Log - Linear Model of γ_{dry} versus p_L for SDPMT-12 Continuous Tests, All Sites

E.2.12 γ_{dry} versus $\mathbf{p}_0$

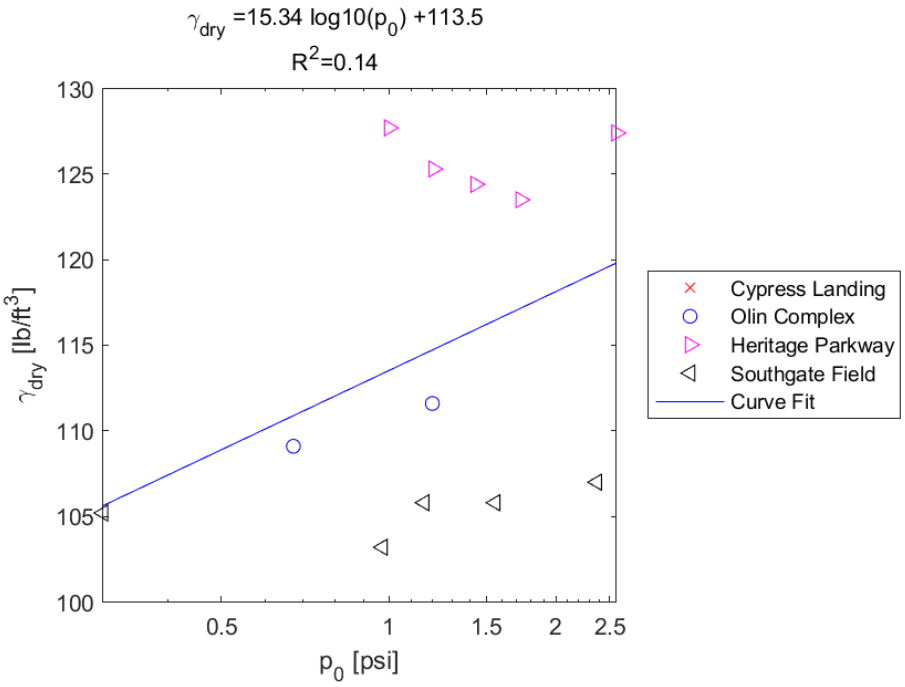

Figure E.141: Log - Linear Model of γ_{dry} versus p_0 for SDPMT-6 Incremental Tests, All Sites

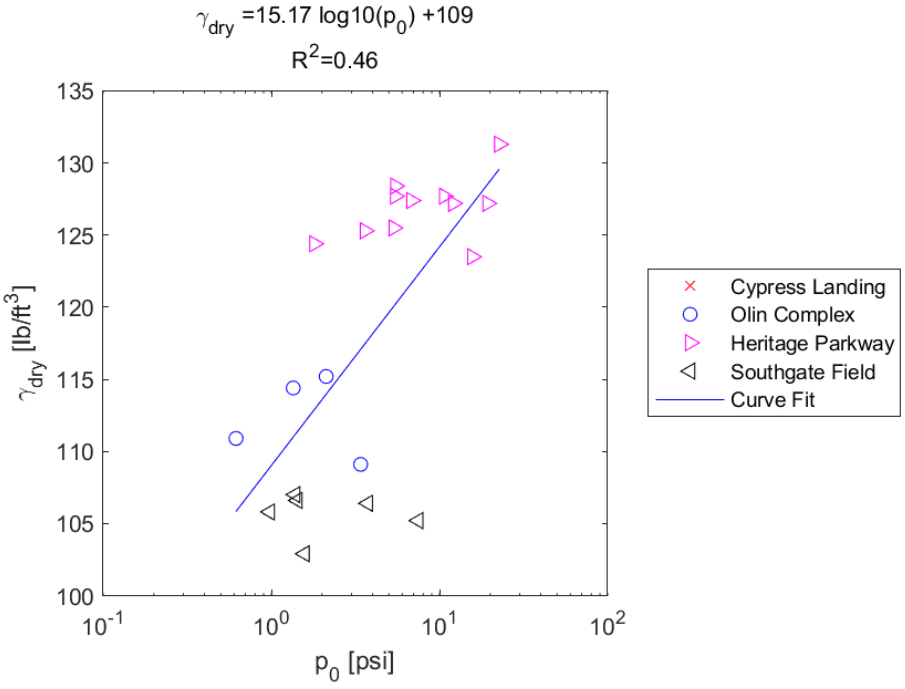

Figure E.142: Log - Linear Model of γ_{dry} versus p_0 for SDPMT-6 Continuous Tests, All Sites

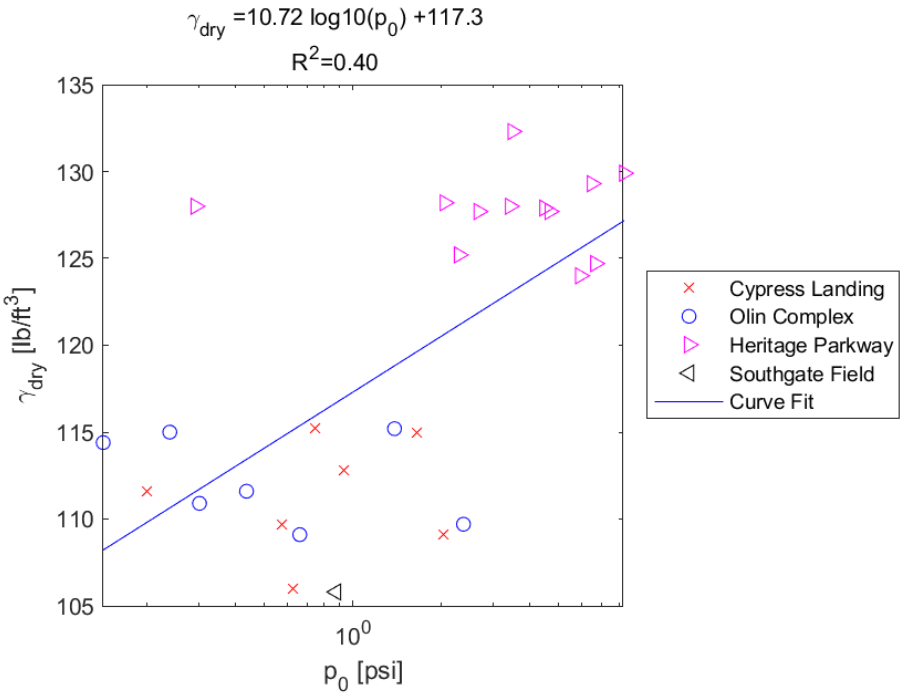

Figure E.143: Log - Linear Model of γ_{dry} versus p_0 for SDPMT-12 Incremental Tests, All Sites

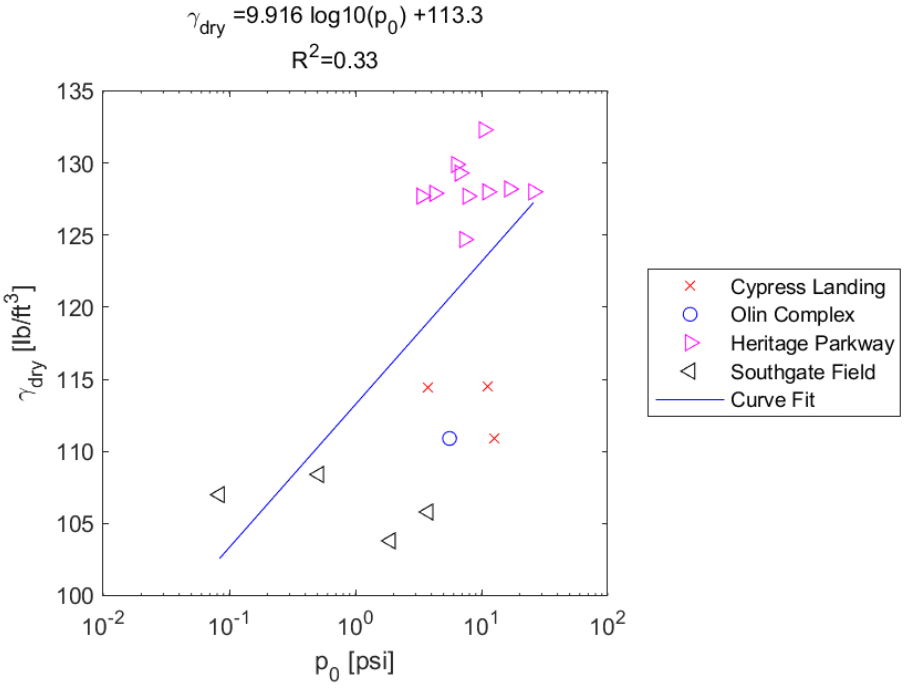

Figure E.144: Log - Linear Model of γ_{dry} versus p_0 for SDPMT-12 Continuous Tests, All Sites

E.2.13 DCP PI versus E_0

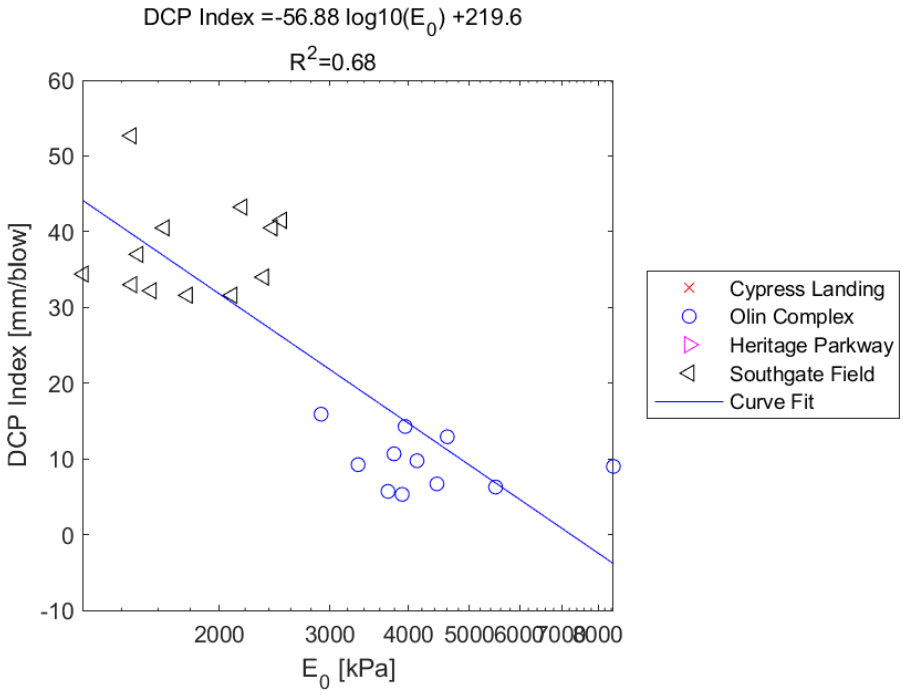

Figure E.145: Log - Linear Model of DCP PI versus E_0 for SDPMT-6 Incremental Tests, All Sites

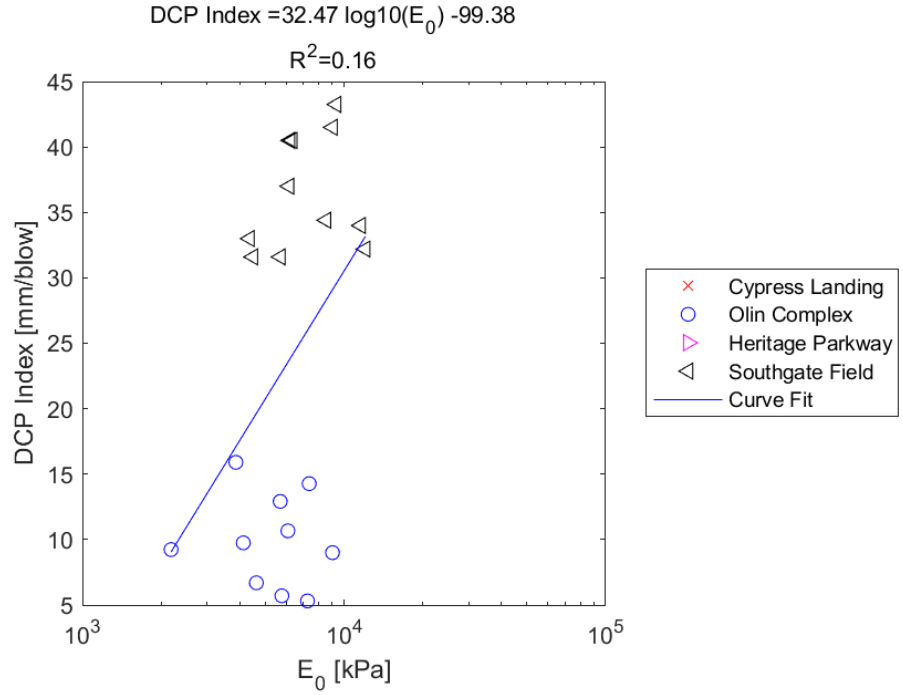

Figure E.146: Log - Linear Model of DCP PI versus E_0 for SDPMT-6 Continuous Tests, All Sites

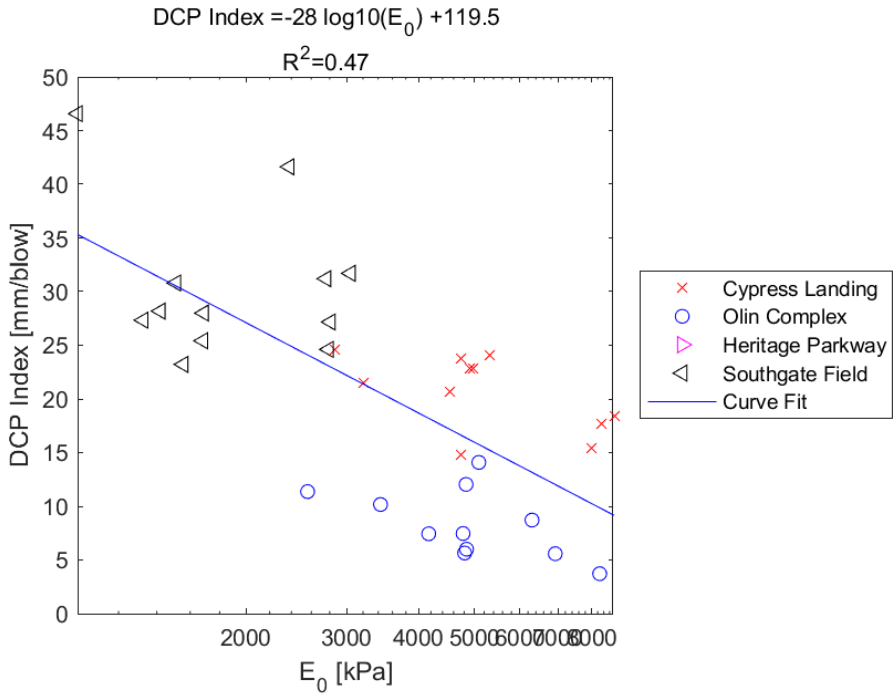

Figure E.147: Log - Linear Model of DCP PI versus E_0 for SDPMT-12 Incremental Tests, All Sites

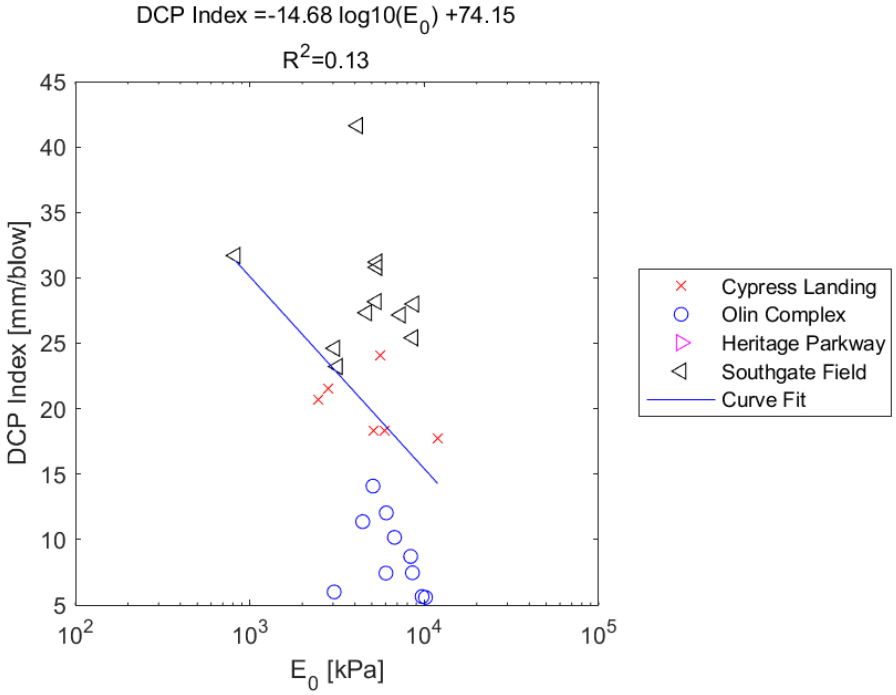

Figure E.148: Log - Linear Model of DCP PI versus E_0 for SDPMT-12 Continuous Tests, All Sites

E.2.14 DCP PI versus $\mathbf{p}_L$

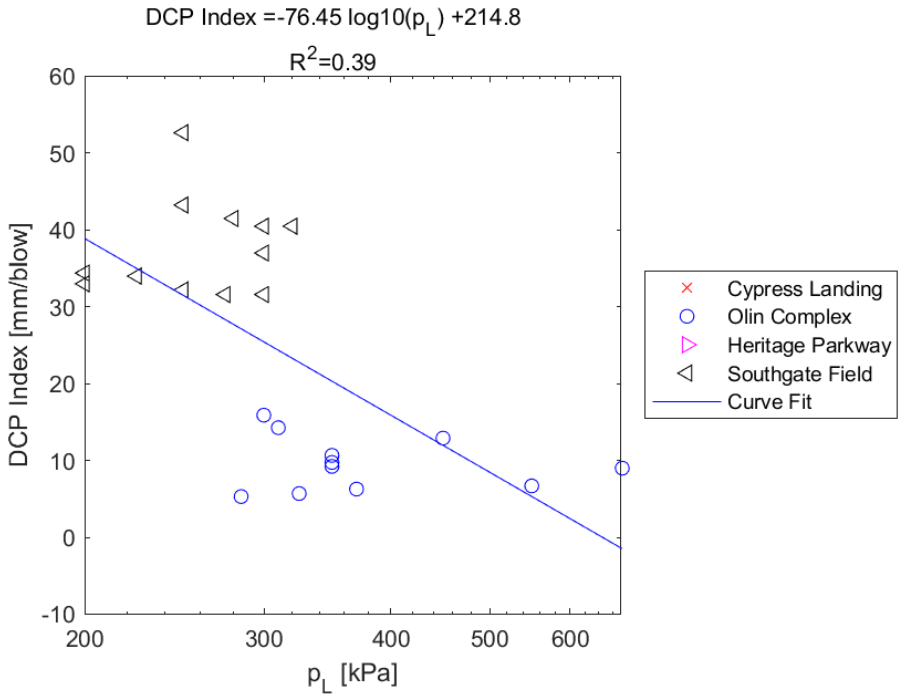

Figure E.149: Log - Linear Model of DCP PI versus p_L for SDPMT-6 Incremental Tests, All Sites

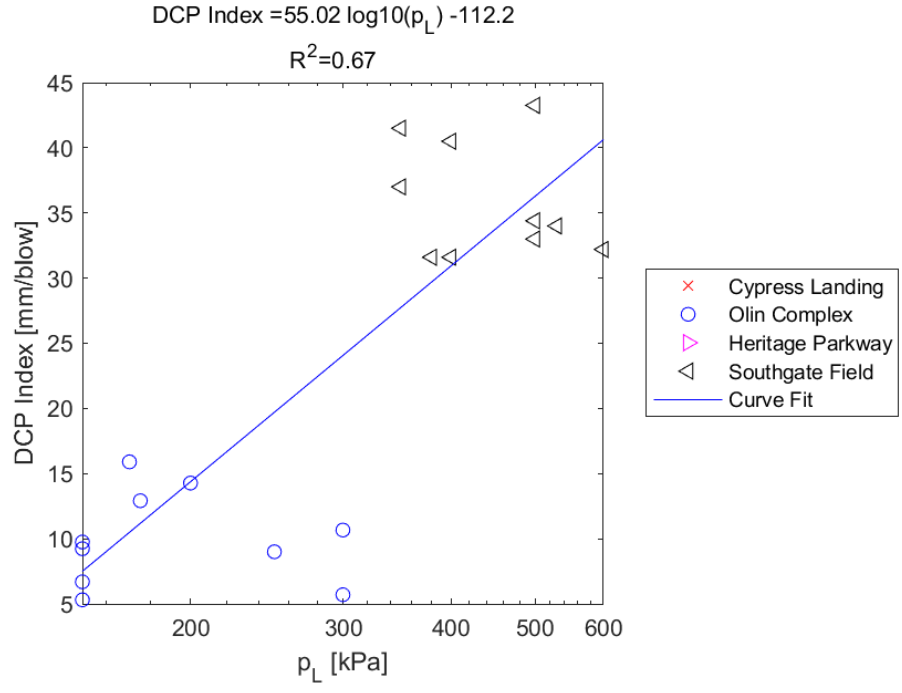

Figure E.150: Log - Linear Model of DCP PI versus p_L for SDPMT-6 Continuous Tests, All Sites

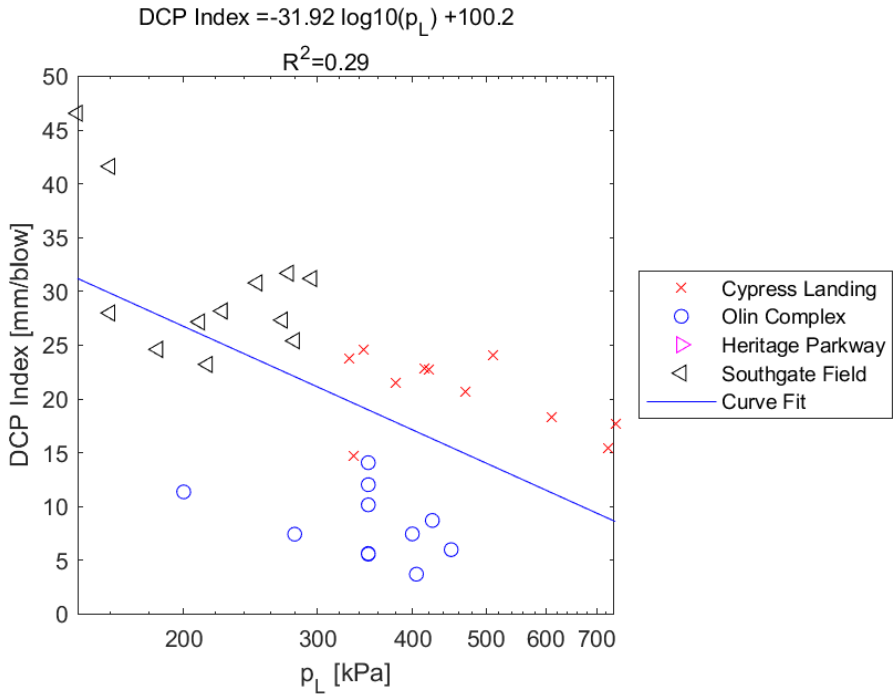

Figure E.151: Log - Linear Model of DCP PI versus p_L for SDPMT-12 Incremental Tests, All Sites

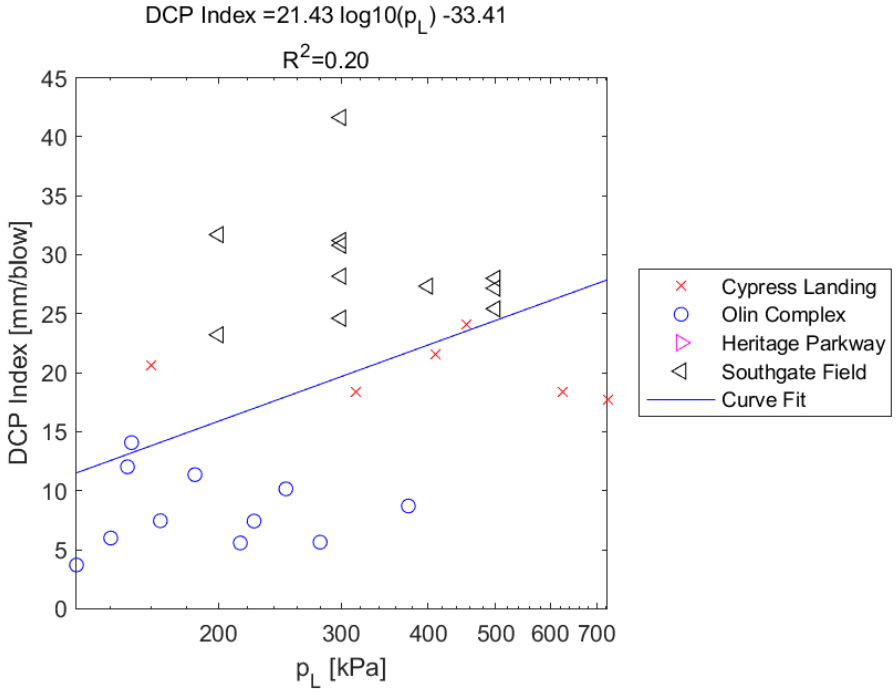

Figure E.152: Log - Linear Model of DCP PI versus p_L for SDPMT-12 Continuous Tests, All Sites

E.2.15 DCP PI versus $\mathbf{p}_0$

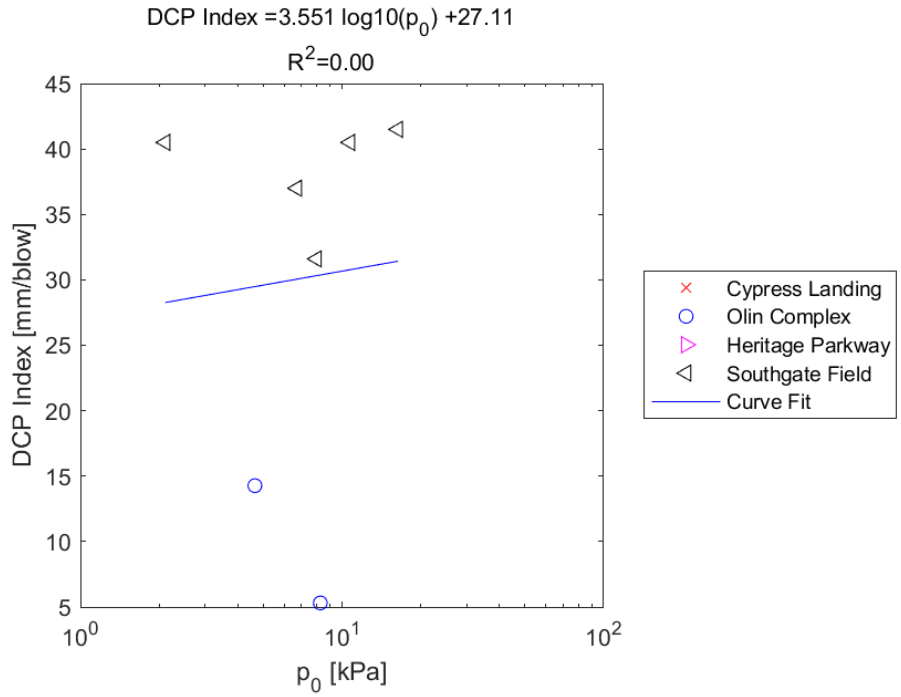

Figure E.153: Log - Linear Model of DCP PI versus p_0 for SDPMT-6 Incremental Tests, All Sites

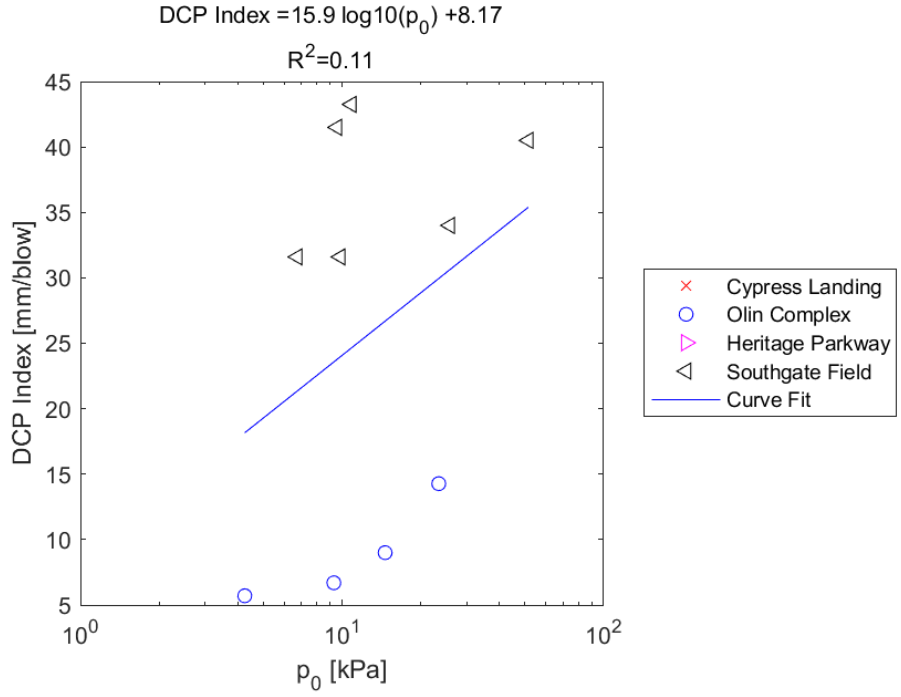

Figure E.154: Log - Linear Model of DCP PI versus p_0 for SDPMT-6 Continuous Tests, All Sites

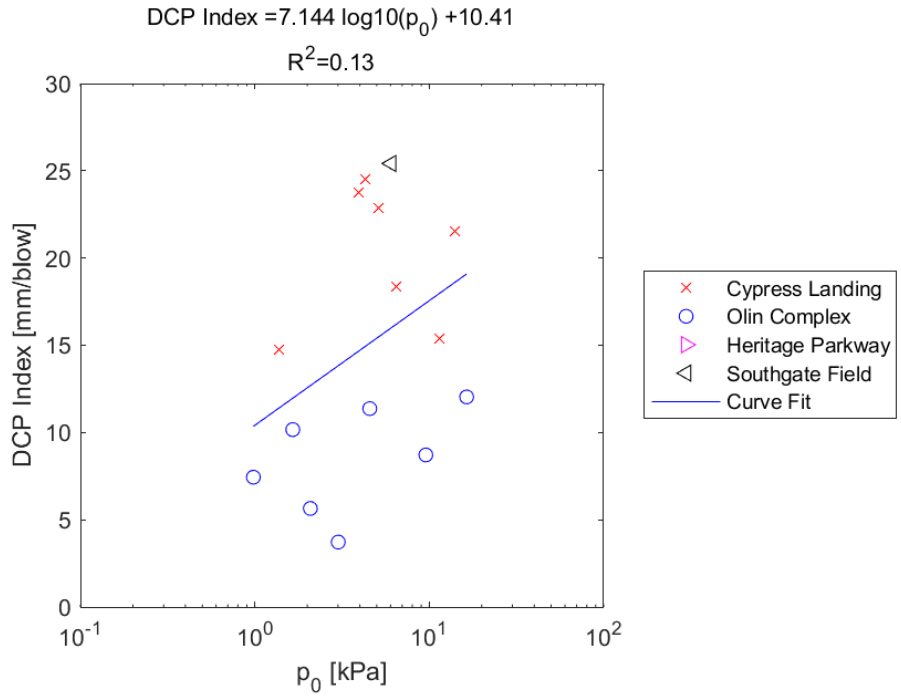

Figure E.155: Log - Linear Model of DCP PI versus p_0 for SDPMT-12 Incremental Tests, All Sites

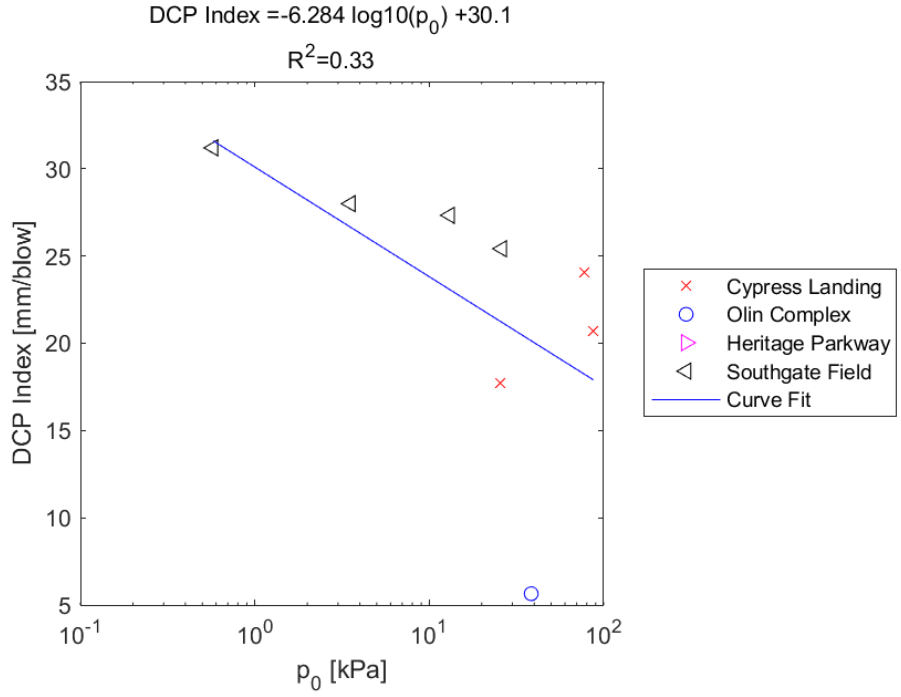

Figure E.156: Log - Linear Model of DCP PI versus p_0 for SDPMT-12 Continuous Tests, All Sites

E.2.16 $\mathbf{E}_{d,zorn}$ versus $\mathbf{E}_0$

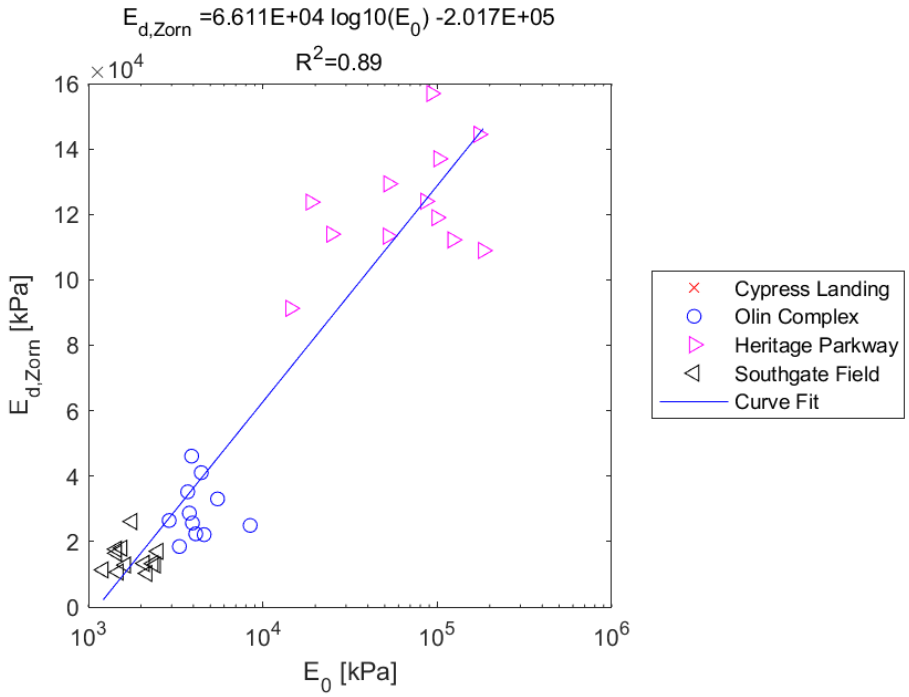

Figure E.157: Log - Linear Model of $E_{d,zorn}$ versus E_0 for SDPMT-6 Incremental Tests, All Sites

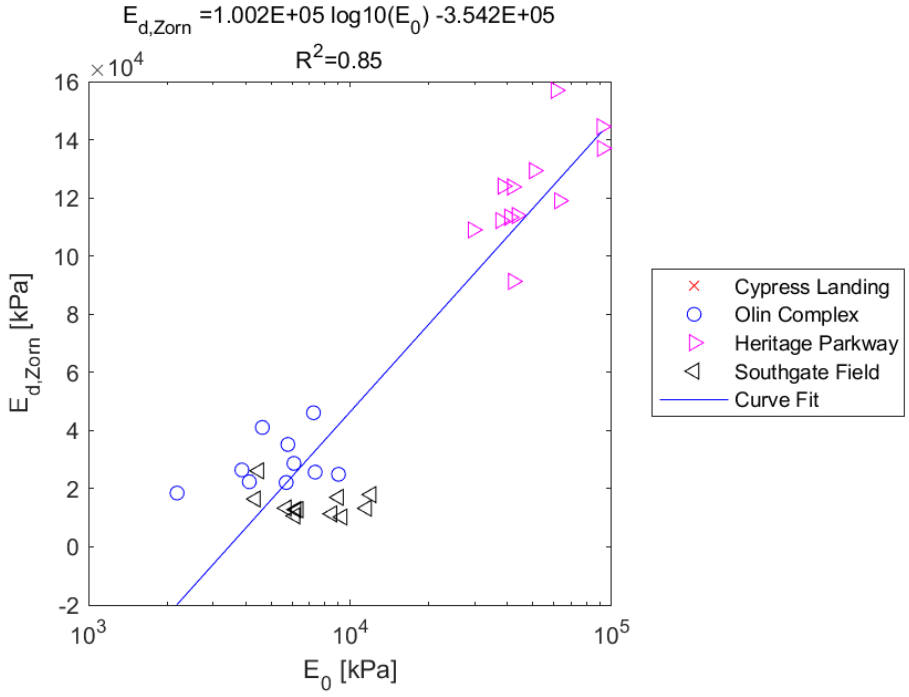

Figure E.158: Log - Linear Model of $E_{d,zorn}$ versus E_0 for SDPMT-6 Continuous Tests, All Sites

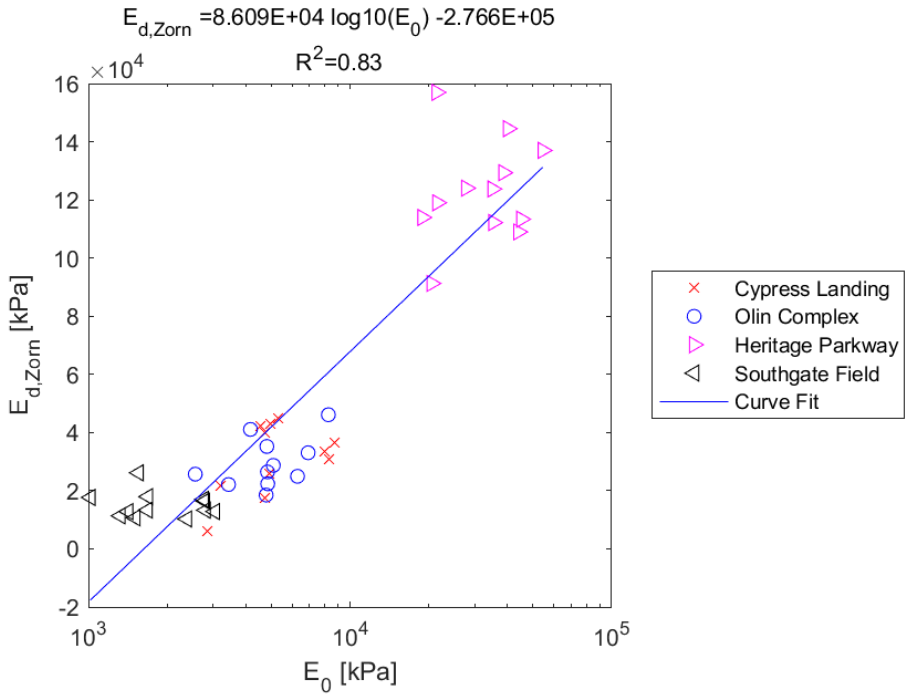

Figure E.159: Log - Linear Model of $E_{d,zorn}$ versus E_0 for SDPMT-12 Incremental Tests, All Sites

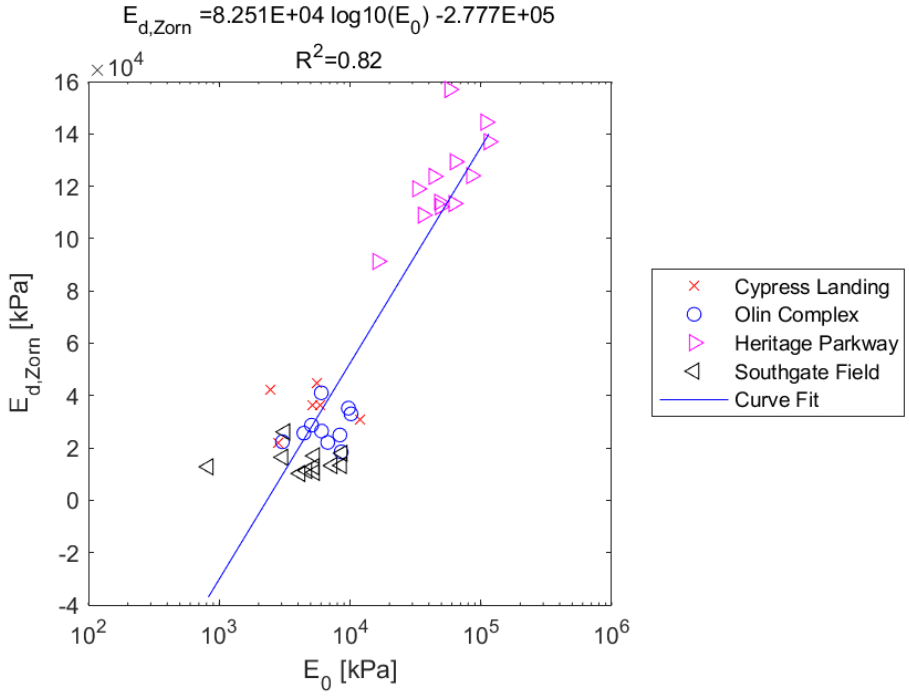

Figure E.160: Log - Linear Model of $E_{d,zorn}$ versus E_0 for SDPMT-12 Continuous Tests, All Sites

E.2.17 $\mathbf{E}_{d,zorn}$ versus $\mathbf{p}_L$

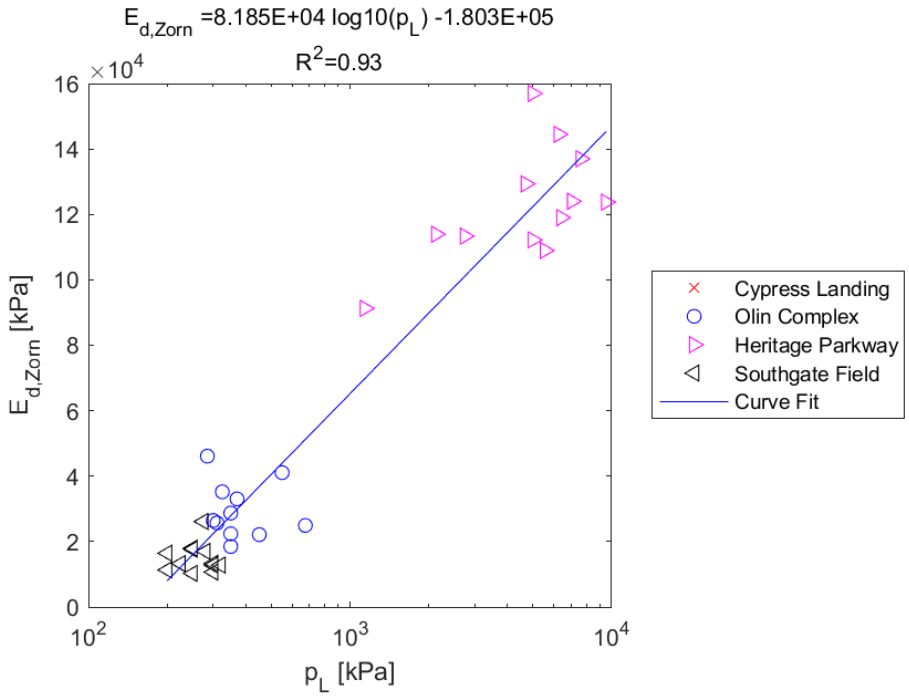

Figure E.161: Log - Linear Model of $E_{d,zorn}$ versus p_L for SDPMT-6 Incremental Tests, All Sites

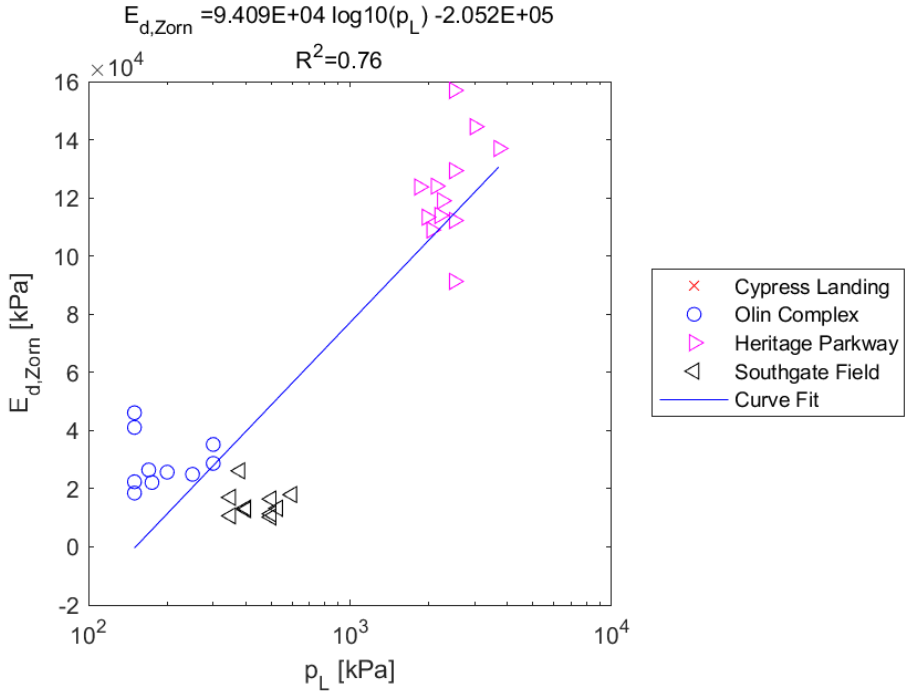

Figure E.162: Log - Linear Model of $E_{d,zorn}$ versus p_L for SDPMT-6 Continuous Tests, All Sites

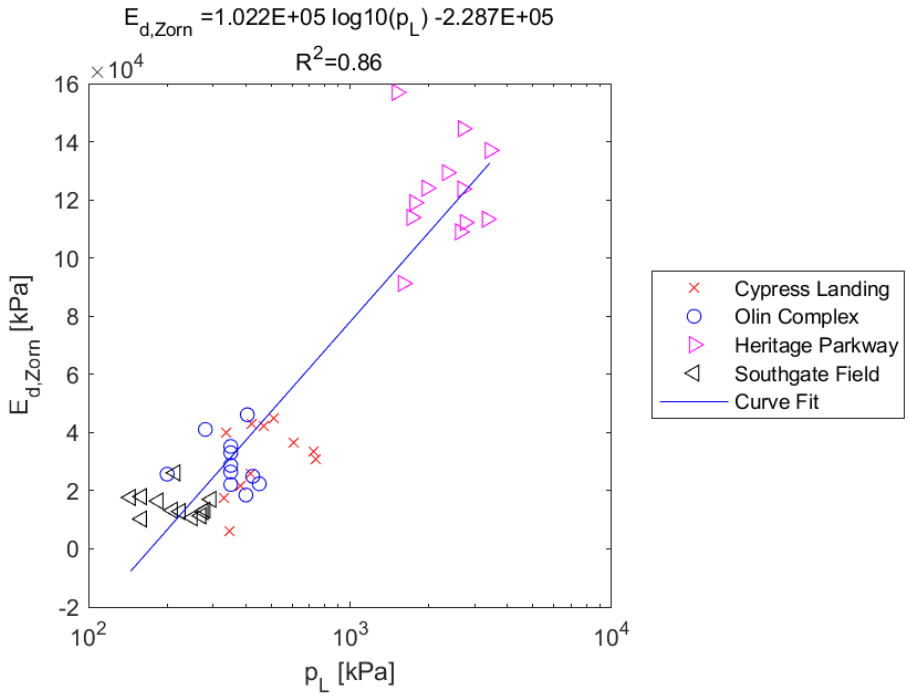

Figure E.163: Log - Linear Model of $E_{d,zorn}$ versus p_L for SDPMT-12 Incremental Tests, All Sites

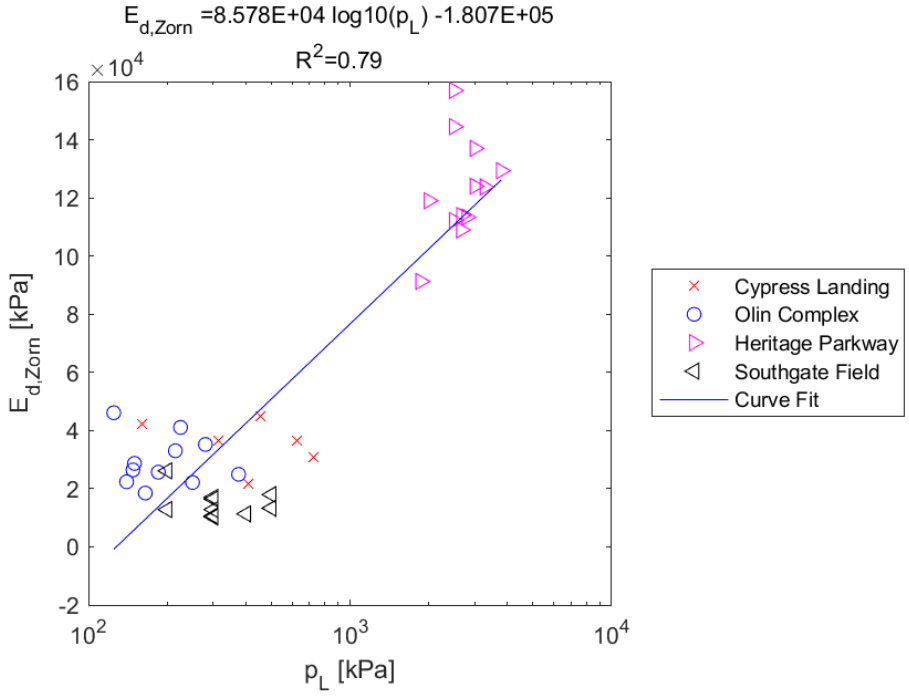

Figure E.164: Log - Linear Model of $E_{d,zorn}$ versus p_L for SDPMT-12 Continuous Tests, All Sites

E.2.18 $\mathbf{E}_{d,zorn}$ versus $\mathbf{p}_0$

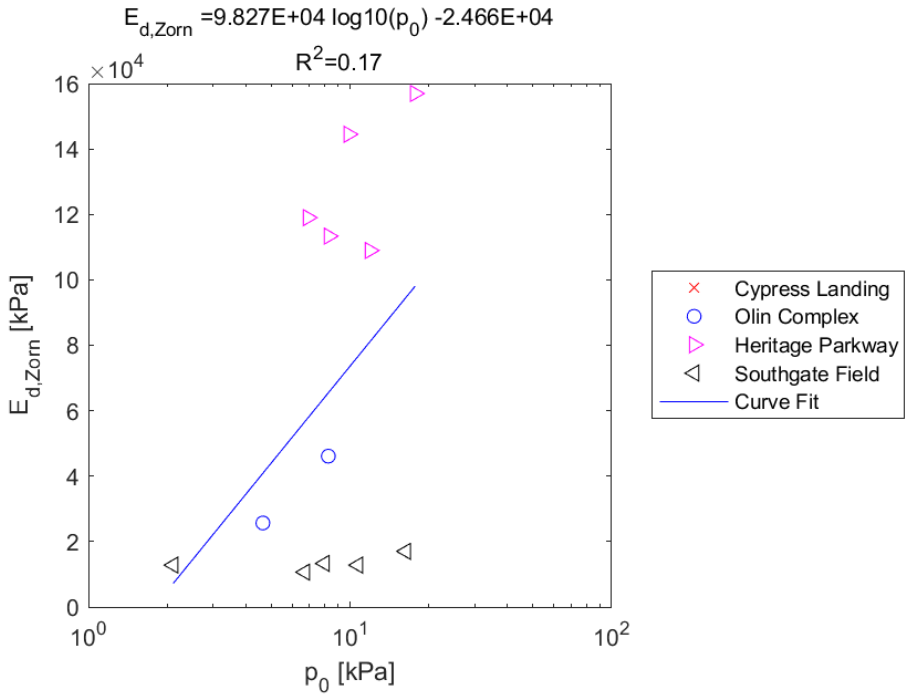

Figure E.165: Log - Linear Model of $E_{d,zorn}$ versus p_0 for SDPMT-6 Incremental Tests, All Sites

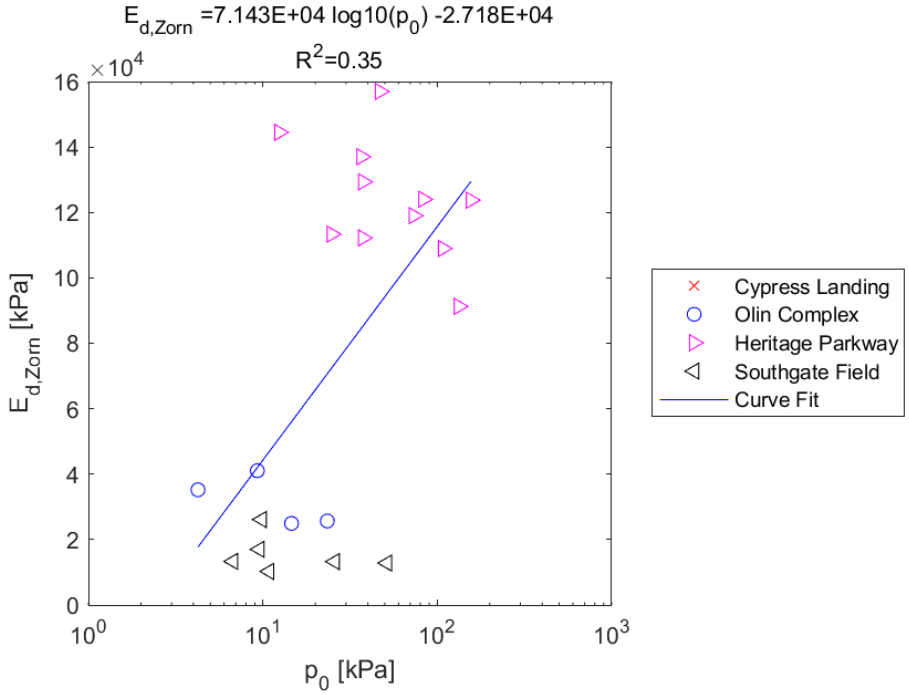

Figure E.166: Log - Linear Model of $E_{d,zorn}$ versus p_0 for SDPMT-6 Continuous Tests, All Sites

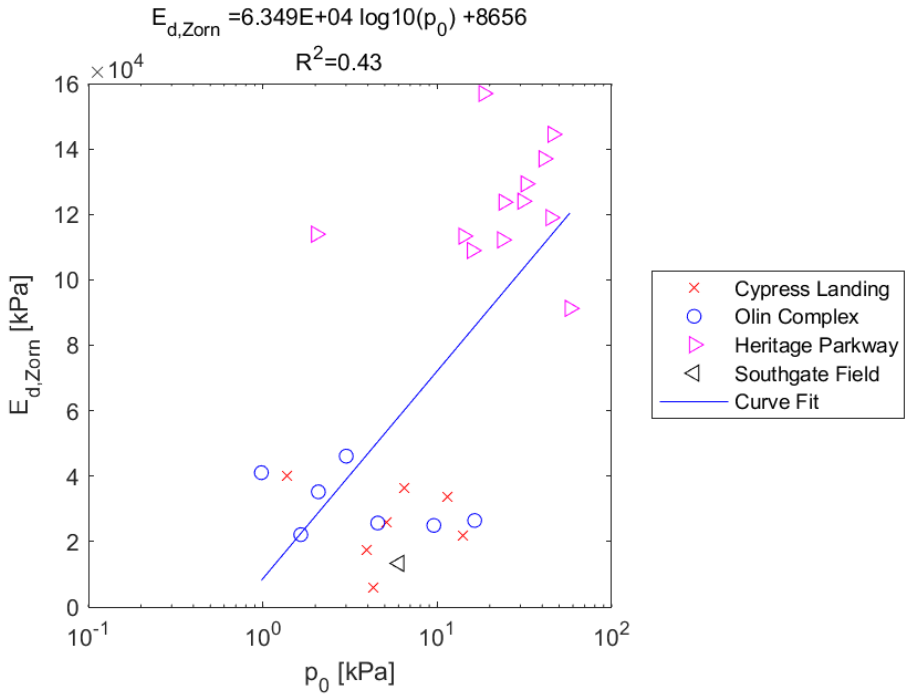

Figure E.167: Log - Linear Model of $E_{d,zorn}$ versus p_0 for SDPMT-12 Incremental Tests, All Sites

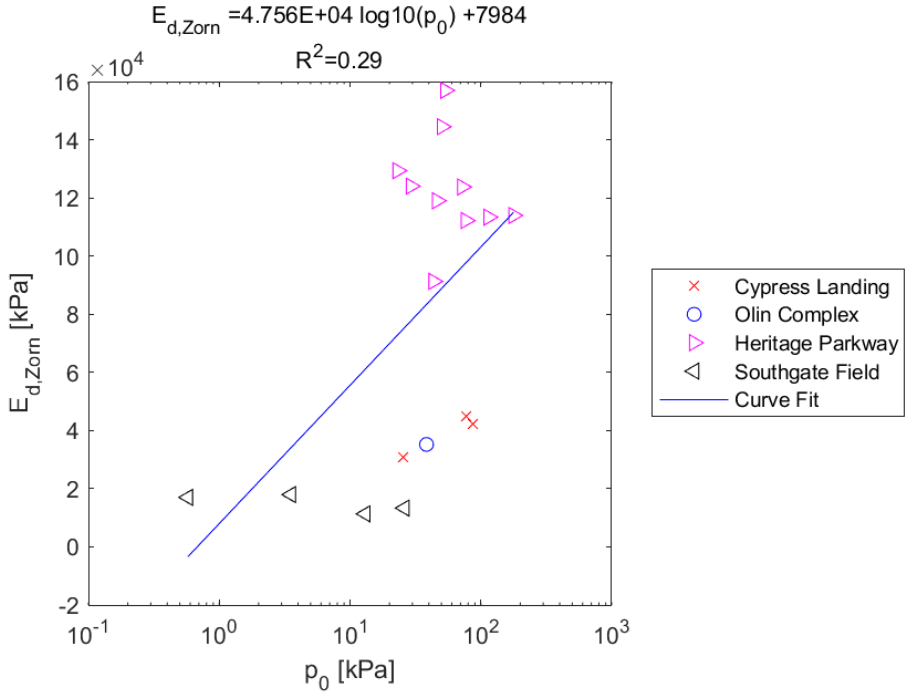

Figure E.168: Log - Linear Model of $E_{d,zorn}$ versus p_0 for SDPMT-12 Continuous Tests, All Sites

E.2.19 $\mathbf{E}_{0,Dynatest}$ versus $\mathbf{E}_0$

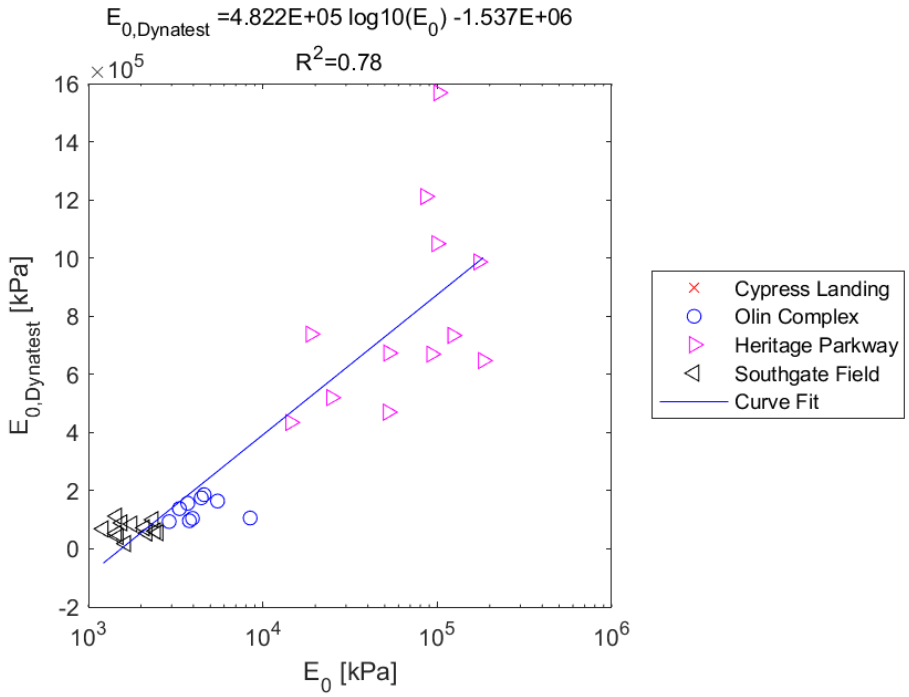

Figure E.169: Log - Linear Model of $E_{0,Dynatest}$ versus E_0 for SDPMT-6 Incremental Tests, All Sites

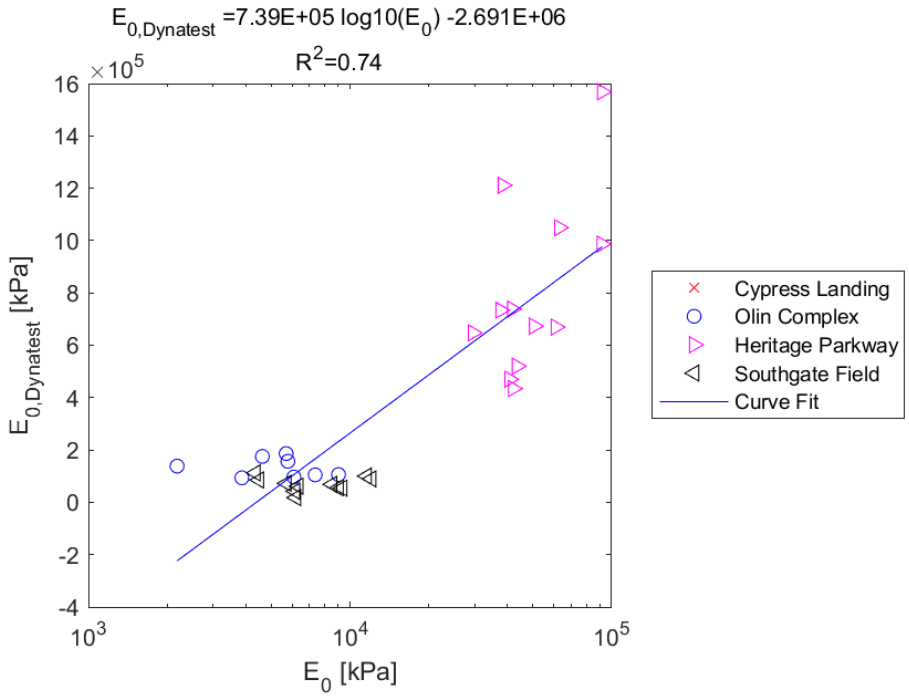

Figure E.170: Log - Linear Model of $E_{0,Dynatest}$ versus E_0 for SDPMT-6 Continuous Tests, All Sites

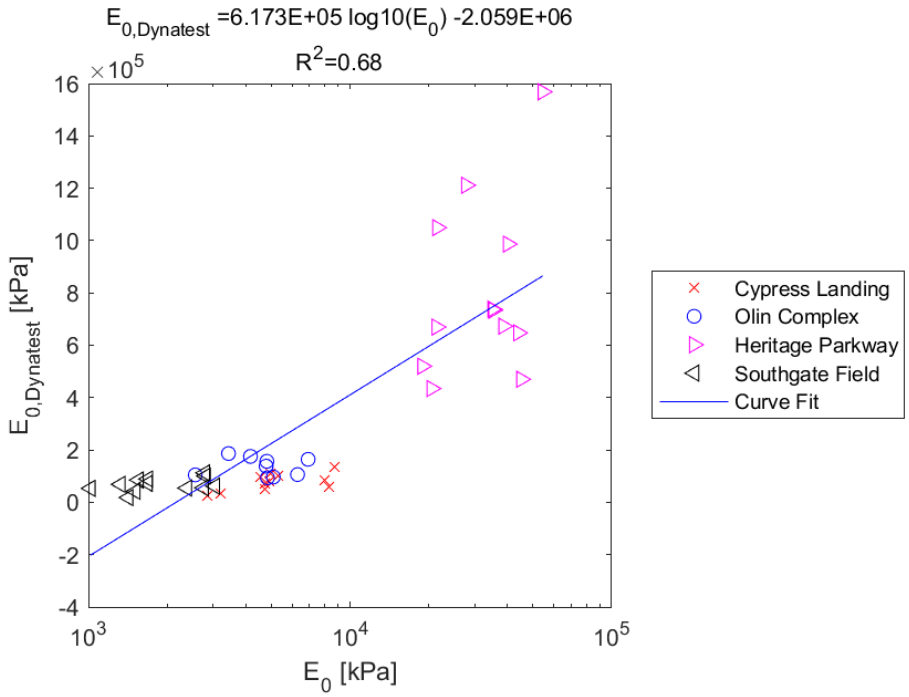

Figure E.171: Log - Linear Model of $E_{0,Dynatest}$ versus E_0 for SDPMT-12 Incremental Tests, All Sites

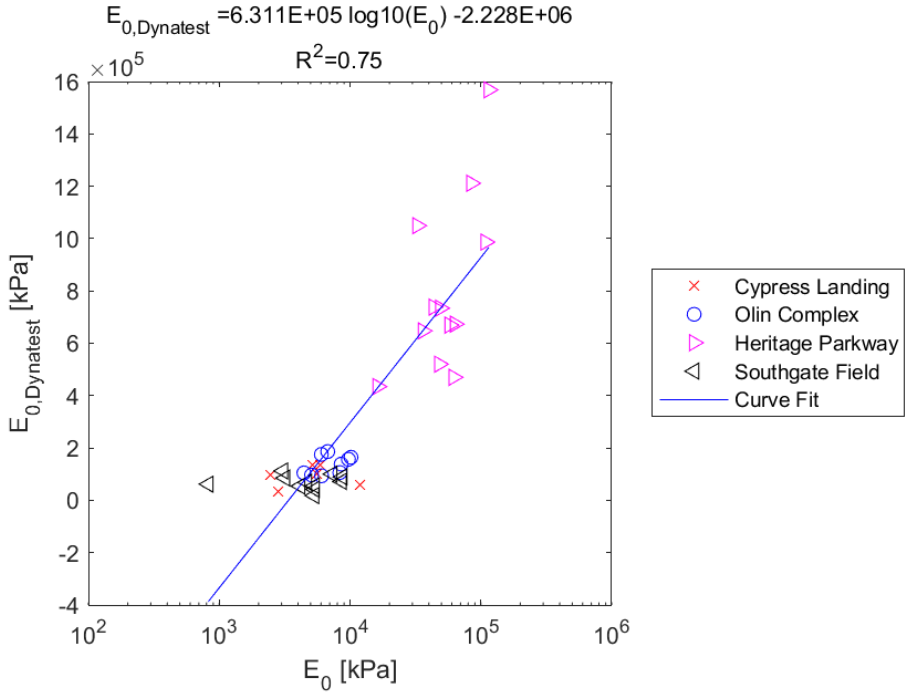

Figure E.172: Log - Linear Model of $E_{0,Dynatest}$ versus E_0 for SDPMT-12 Continuous Tests, All Sites

E.2.20 $\mathbf{E}_{0,Dynatest}$ versus $\mathbf{p}_L$

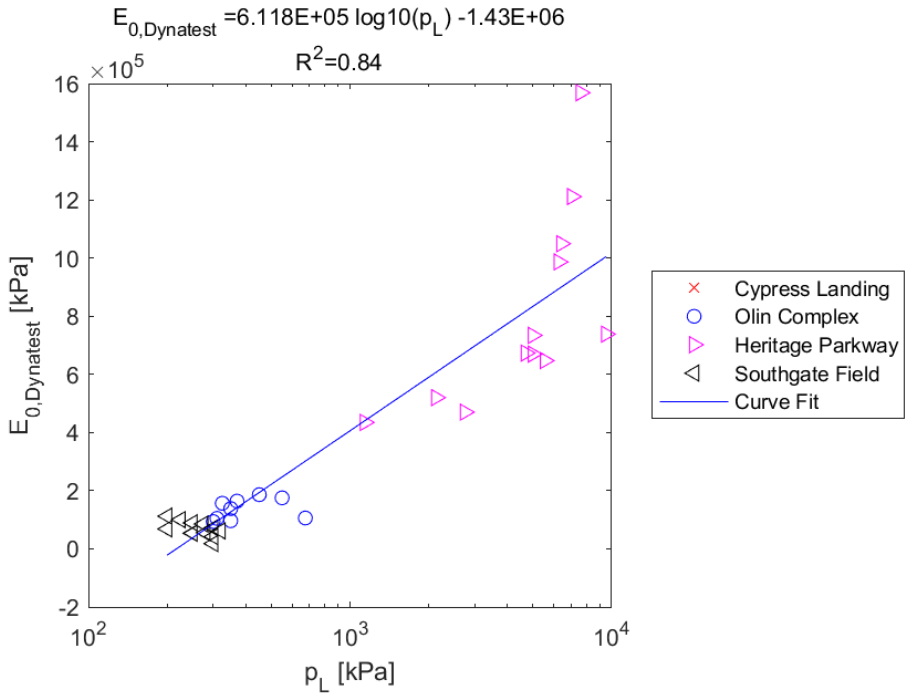

Figure E.173: Log - Linear Model of $E_{0,Dynatest}$ versus p_L for SDPMT-6 Incremental Tests, All Sites

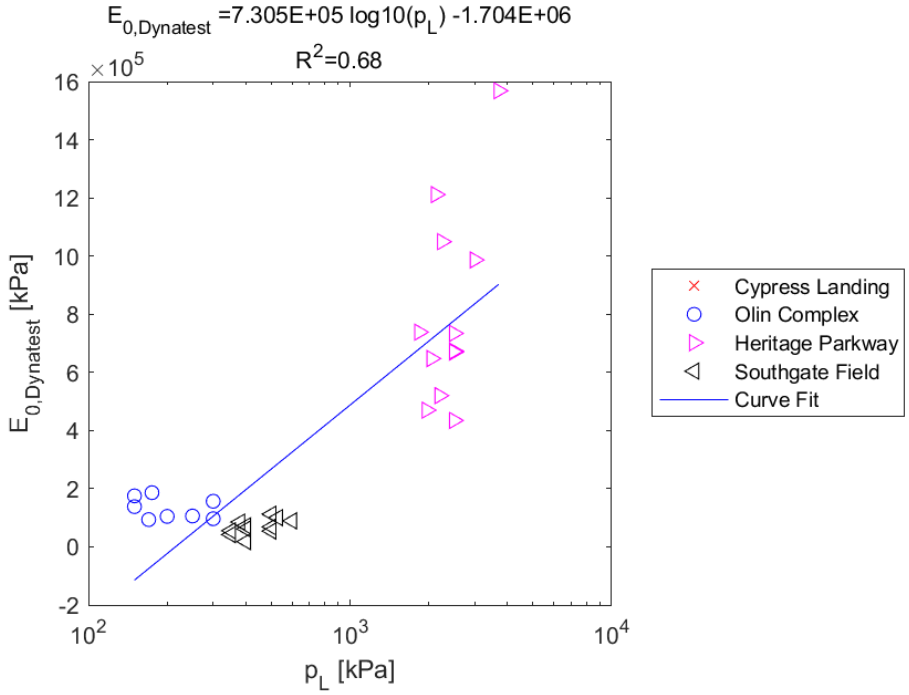

Figure E.174: Log - Linear Model of $E_{0,Dynatest}$ versus p_L for SDPMT-6 Continuous Tests, All Sites

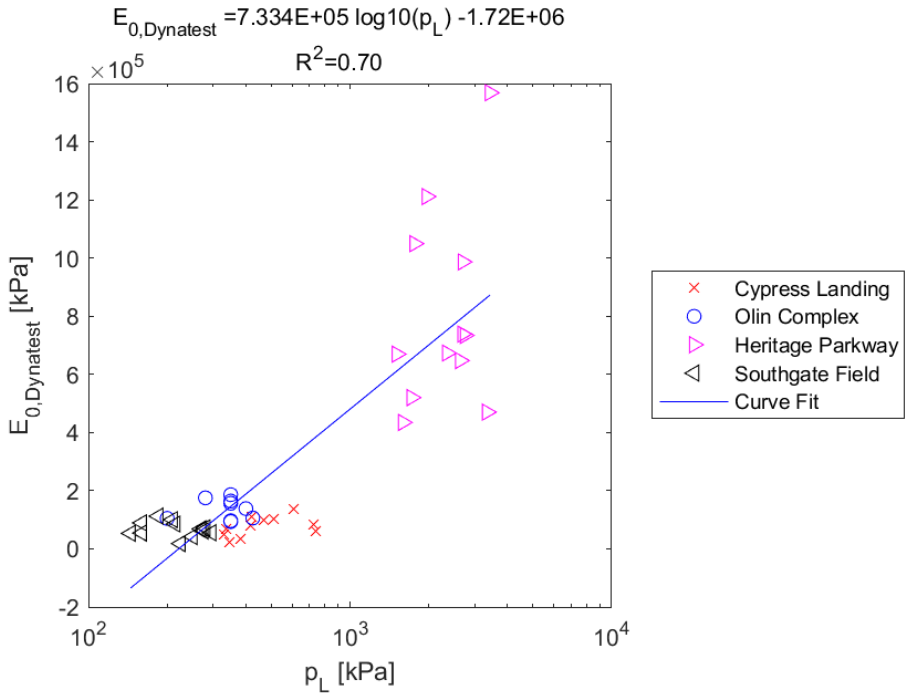

Figure E.175: Log - Linear Model of $E_{0,Dynatest}$ versus p_L for SDPMT-12 Incremental Tests, All Sites

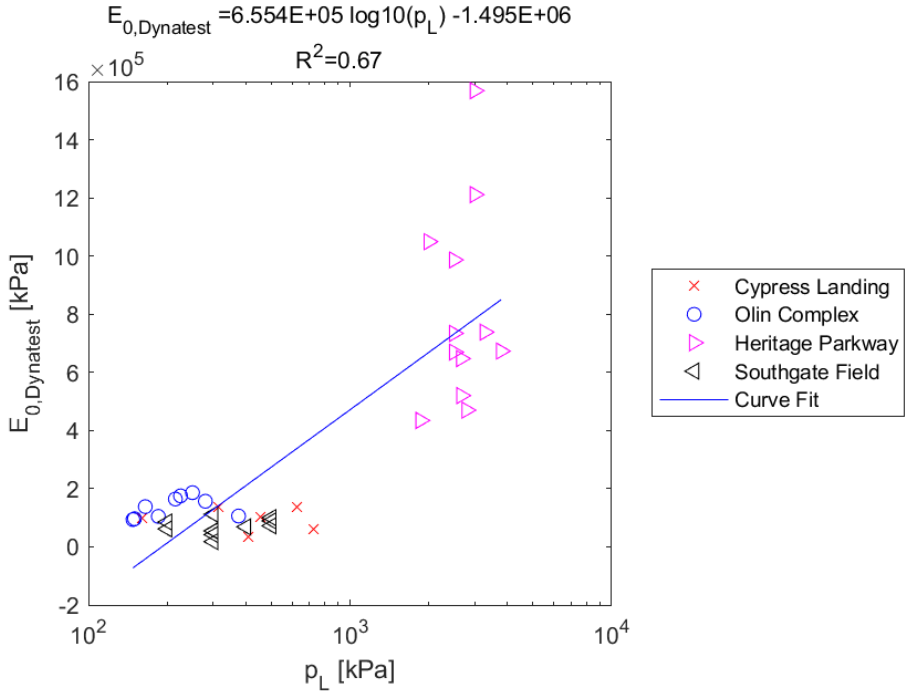

Figure E.176: Log - Linear Model of $E_{0,Dynatest}$ versus p_L for SDPMT-12 Continuous Tests, All Sites

E.2.21 $\mathbf{E}_{0,Dynatest}$ versus $\mathbf{p}_0$

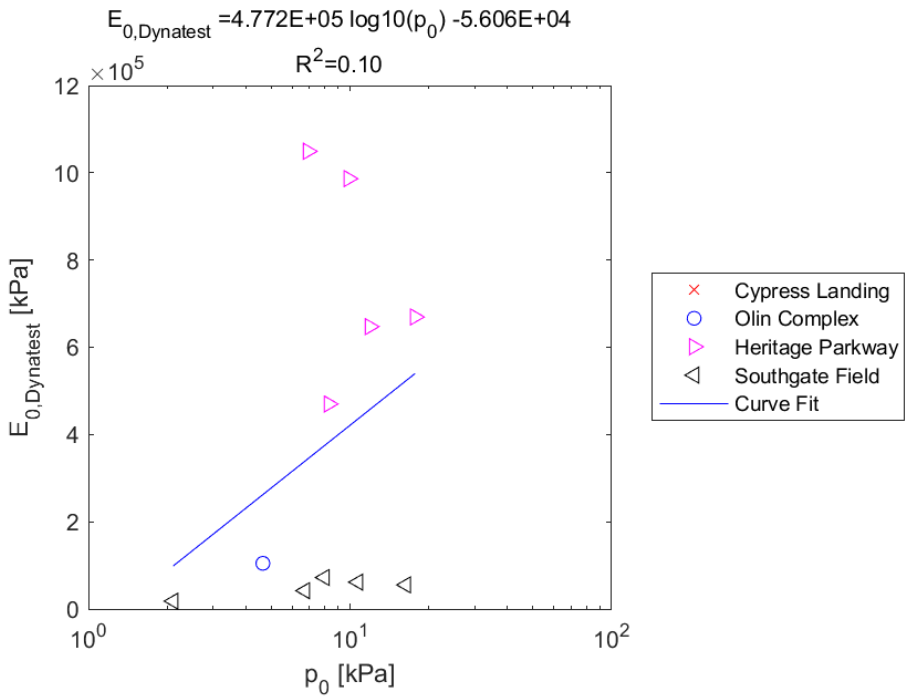

Figure E.177: Log - Linear Model of $E_{0,Dynatest}$ versus p_0 for SDPMT-6 Incremental Tests, All Sites

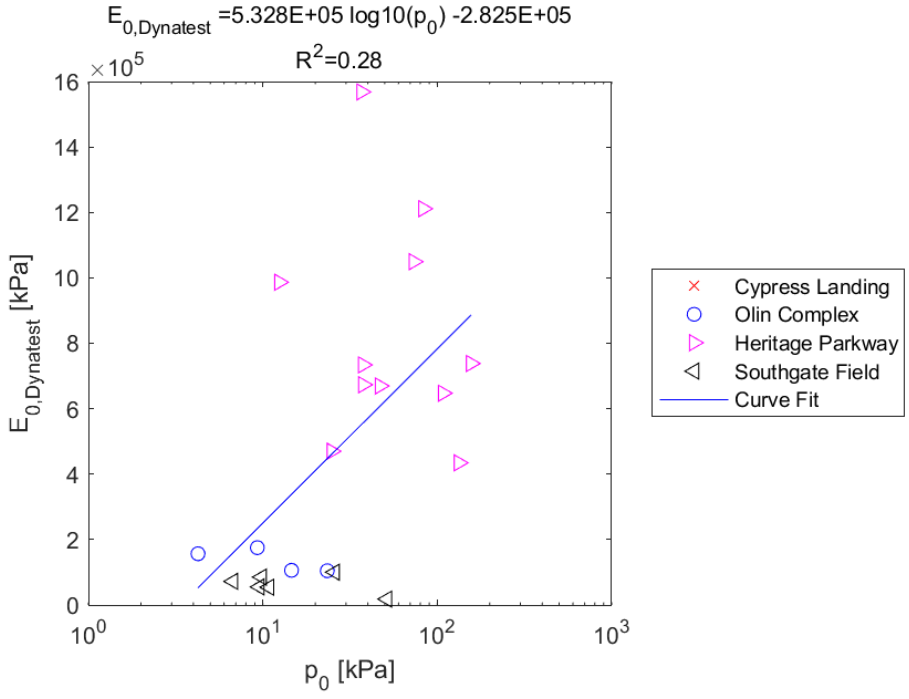

Figure E.178: Log - Linear Model of $E_{0,Dynatest}$ versus p_0 for SDPMT-6 Continuous Tests, All Sites

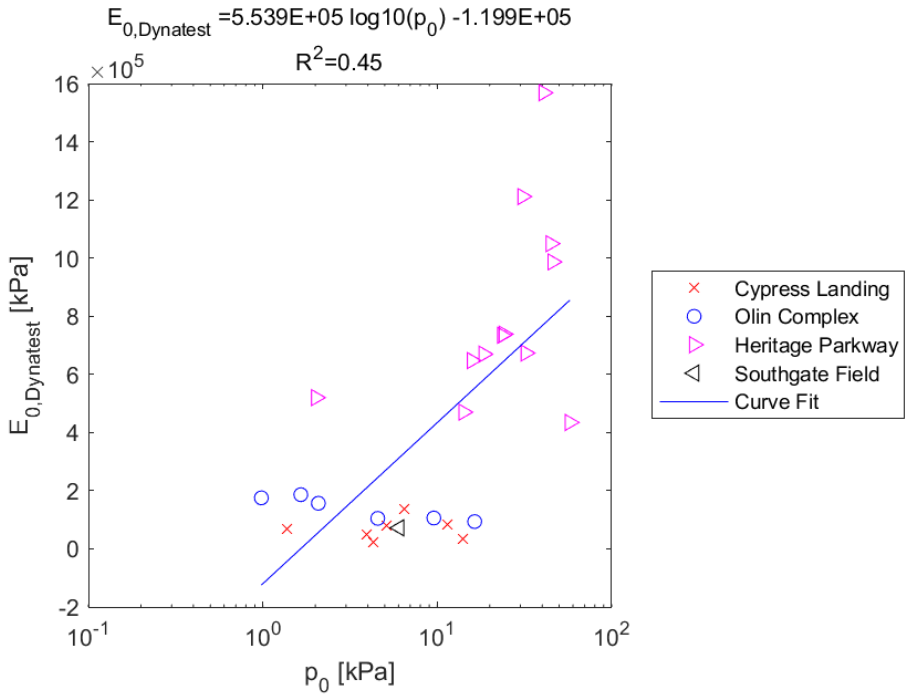

Figure E.179: Log - Linear Model of $E_{0,Dynatest}$ versus p_0 for SDPMT-12 Incremental Tests, All Sites

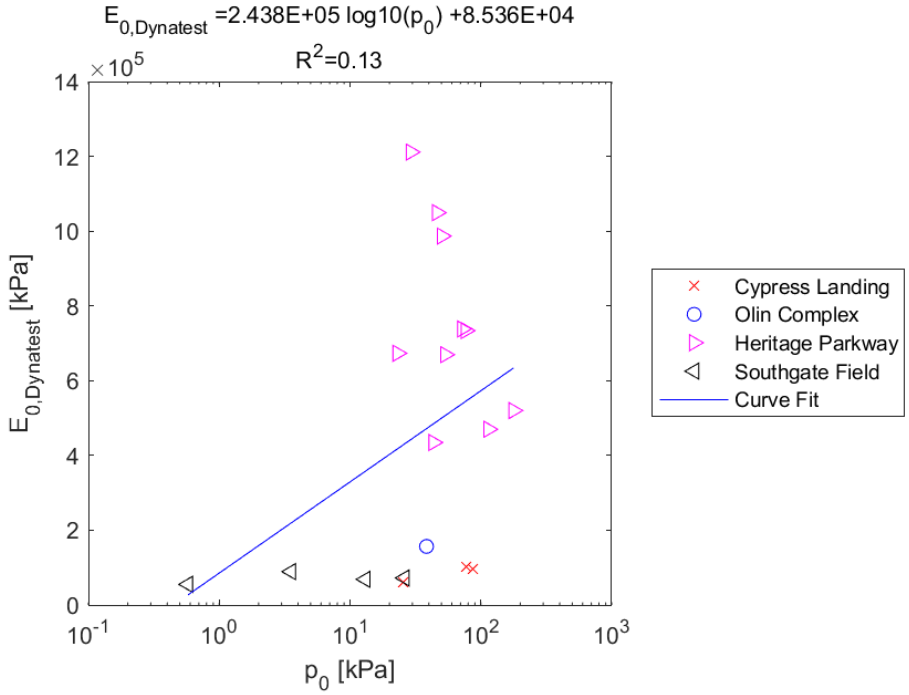

Figure E.180: Log - Linear Model of $E_{0,Dynatest}$ versus p_0 for SDPMT-12 Continuous Tests, All Sites

E.2.22 CIV versus E_0

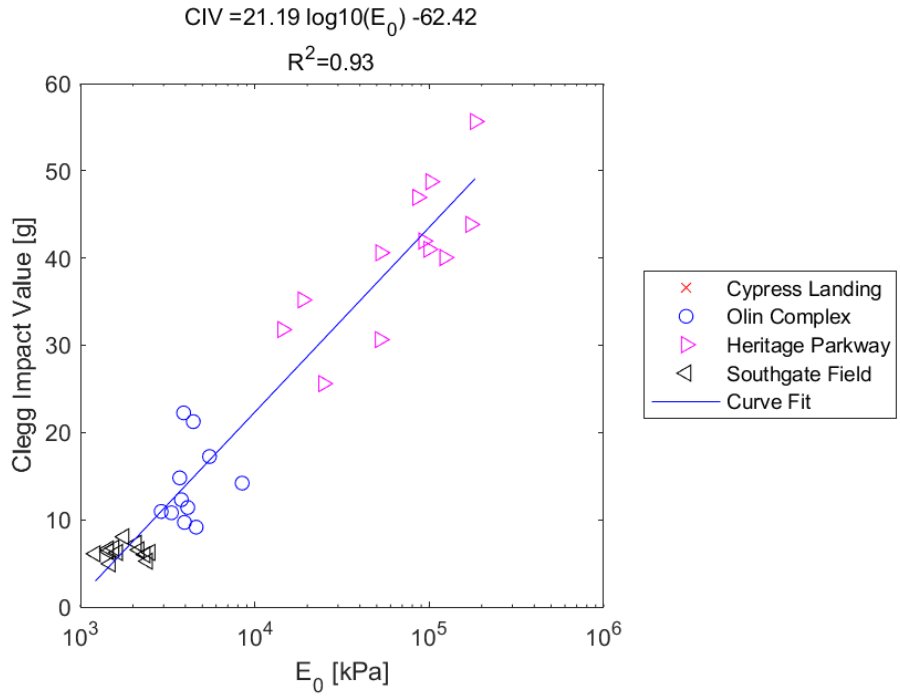

Figure E.181: Log - Linear Model of CIV versus E_0 for SDPMT-6 Incremental Tests, All Sites

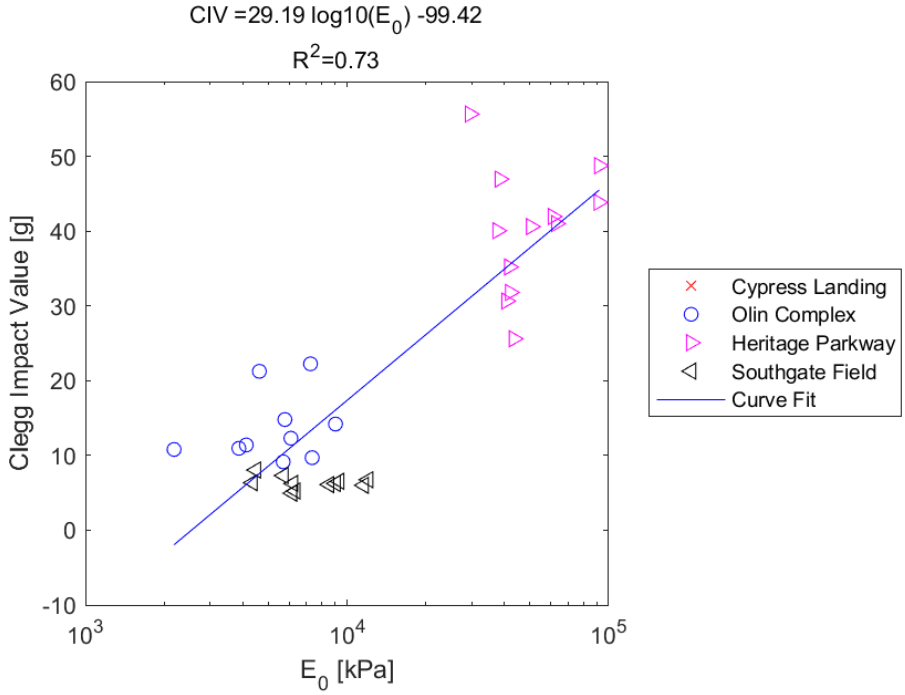

Figure E.182: Log - Linear Model of CIV versus E_0 for SDPMT-6 Continuous Tests, All Sites

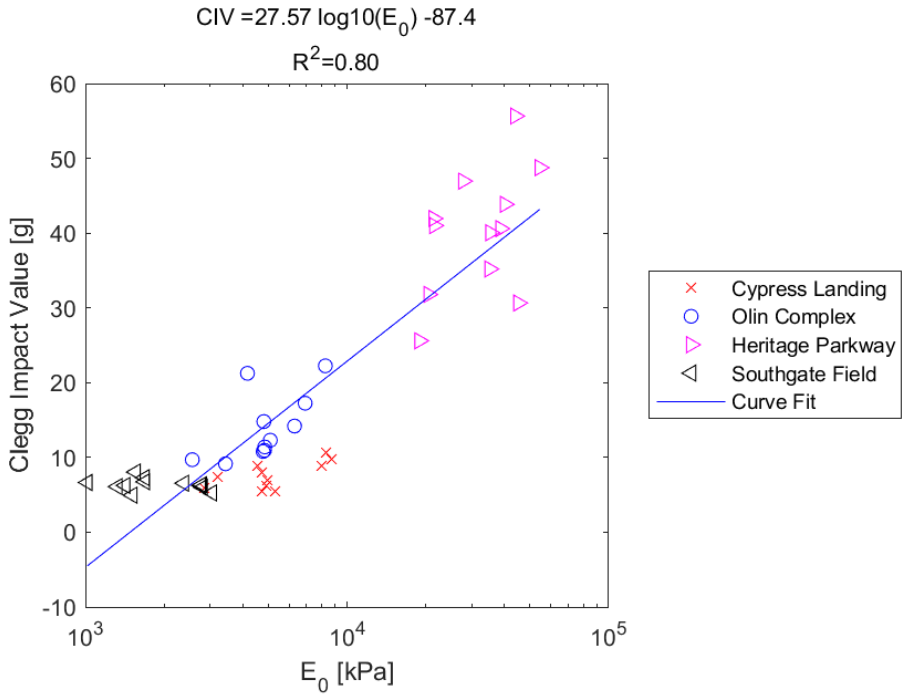

Figure E.183: Log - Linear Model of CIV versus E_0 for SDPMT-12 Incremental Tests, All Sites

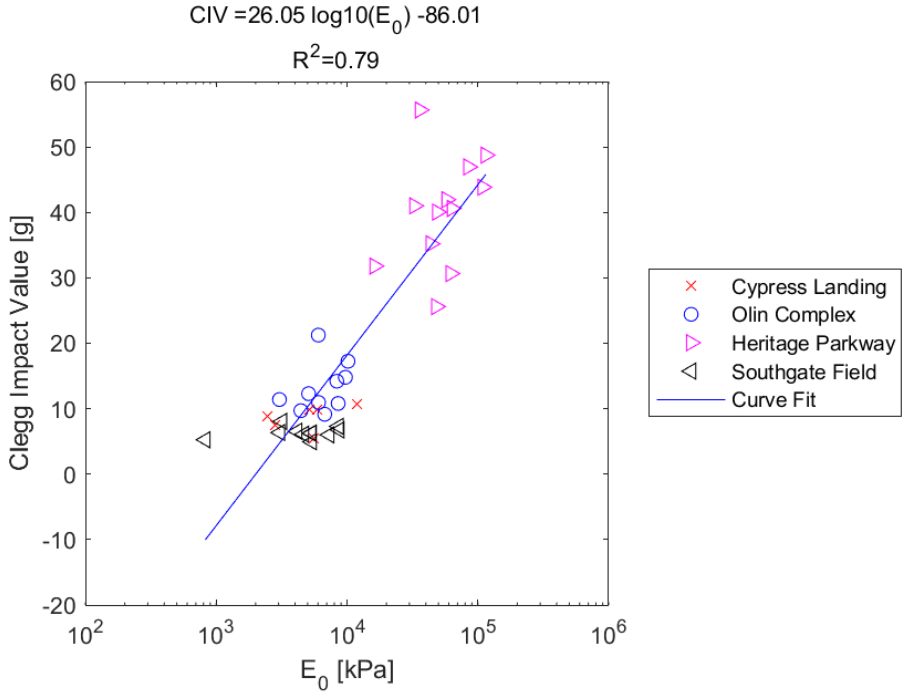

Figure E.184: Log - Linear Model of CIV versus E_0 for SDPMT-12 Continuous Tests, All Sites

E.2.23 CIV versus $\mathbf{p}_L$

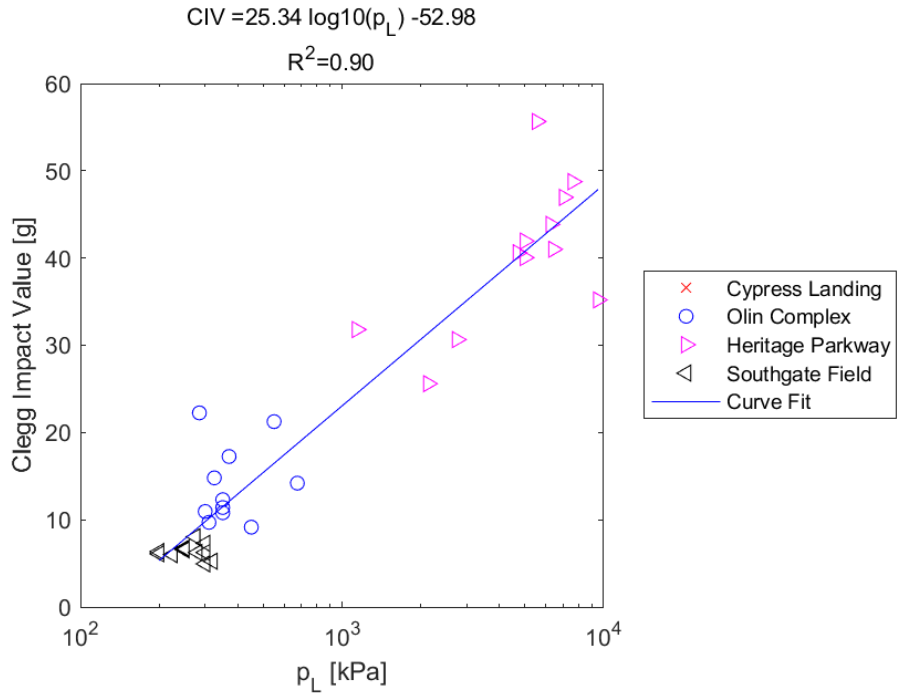

Figure E.185: Log - Linear Model of CIV versus p_L for SDPMT-6 Incremental Tests, All Sites

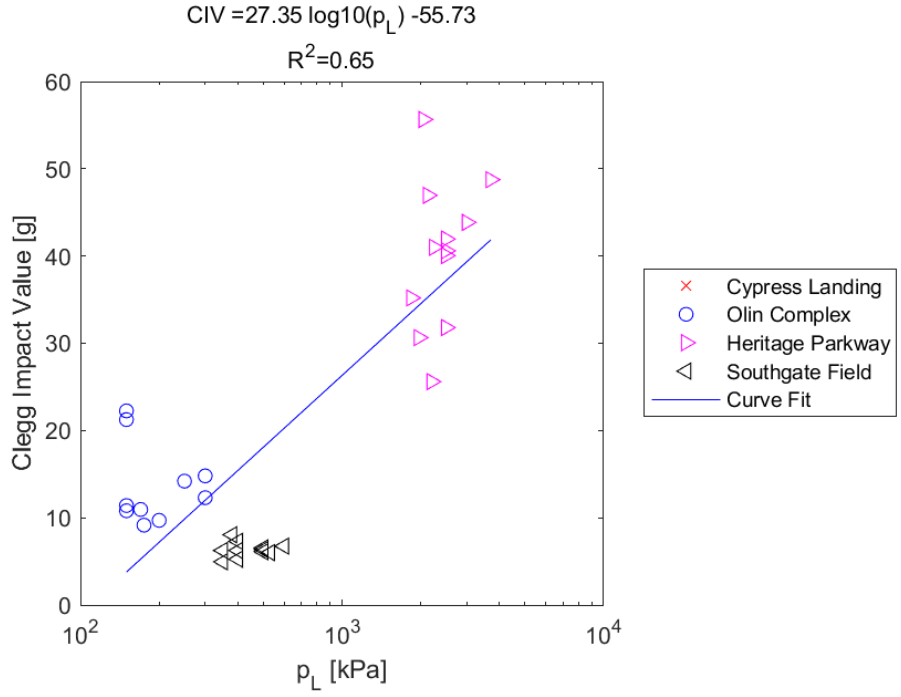

Figure E.186: Log - Linear Model of CIV versus p_L for SDPMT-6 Continuous Tests, All Sites

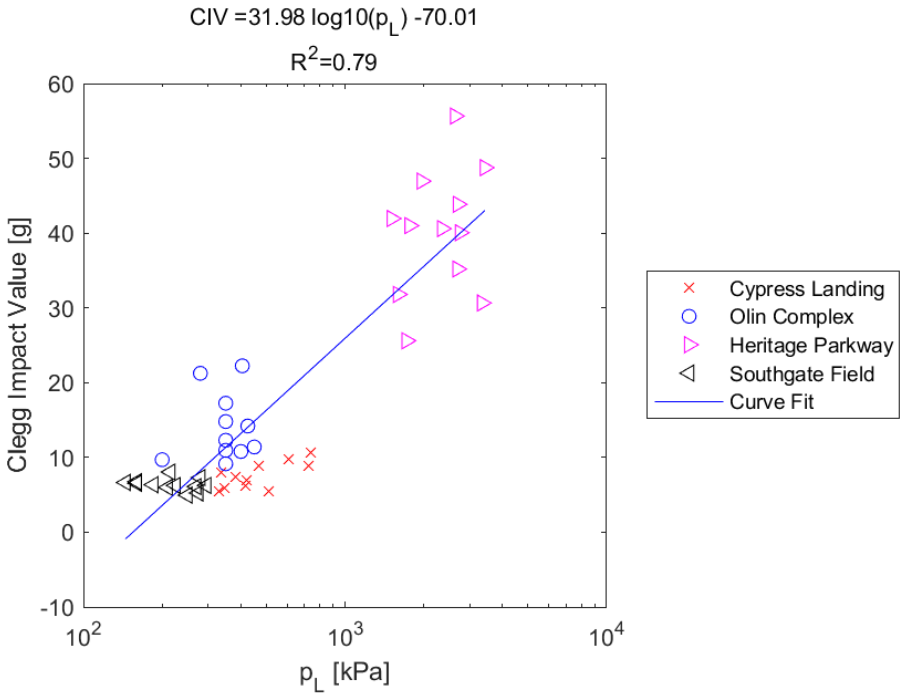

Figure E.187: Log - Linear Model of CIV versus p_L for SDPMT-12 Incremental Tests, All Sites

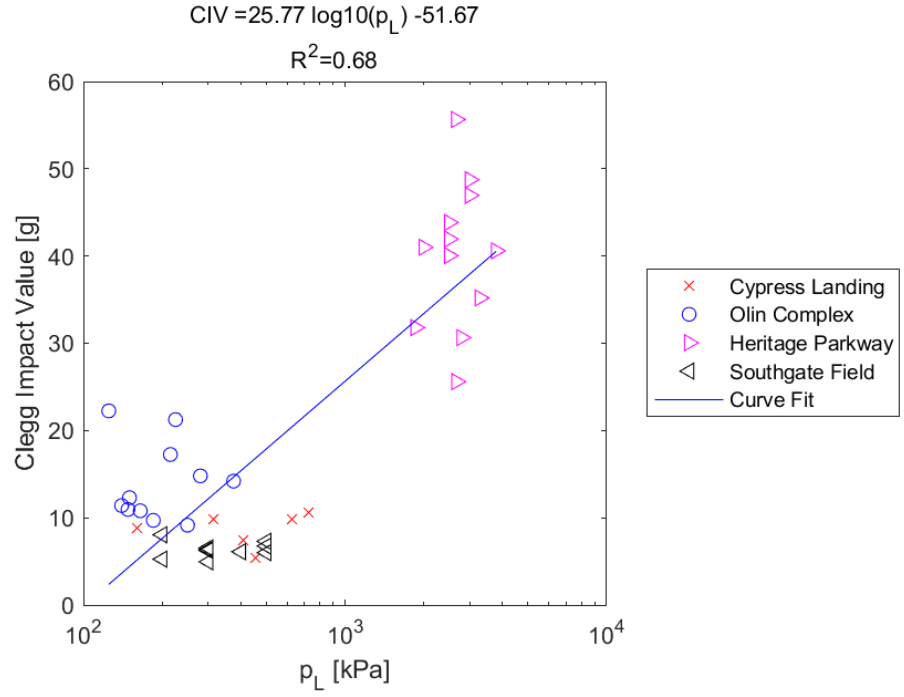

Figure E.188: Log - Linear Model of CIV versus p_L for SDPMT-12 Continuous Tests, All Sites

E.2.24 CIV versus p_0

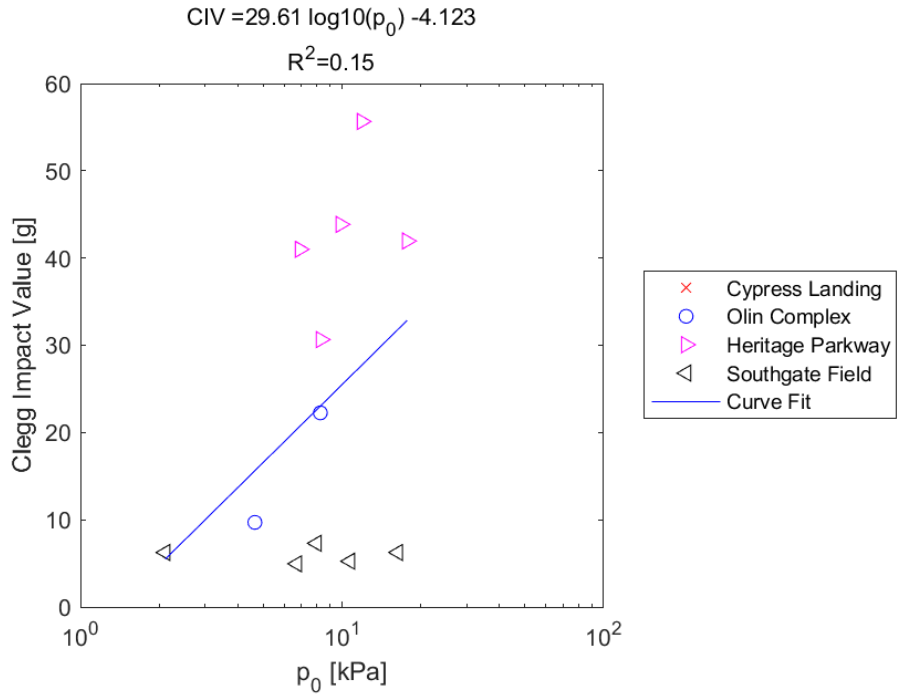

Figure E.189: Log - Linear Model of CIV versus p_0 for SDPMT-6 Incremental Tests, All Sites

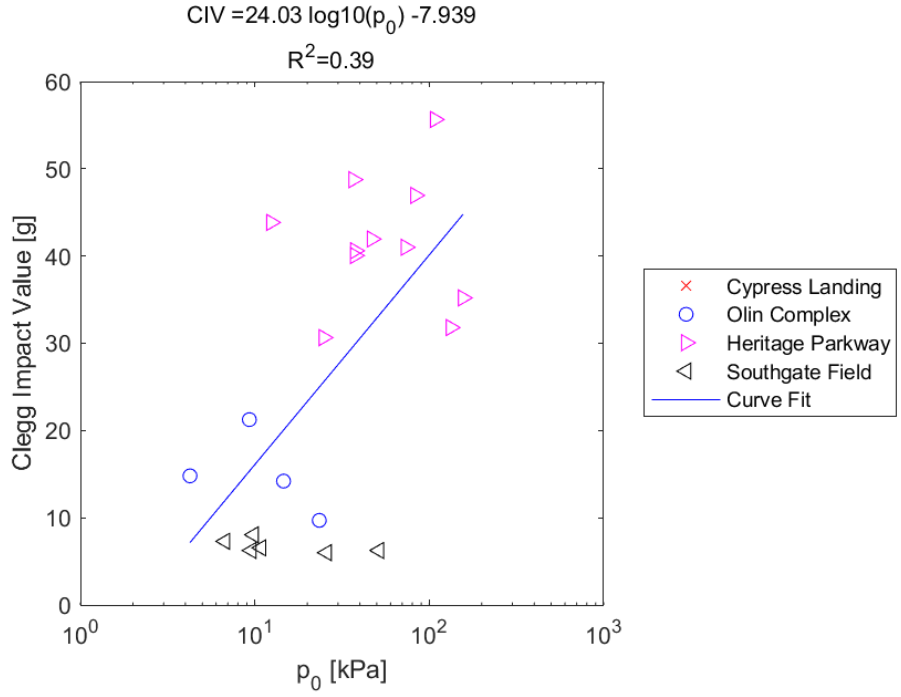

Figure E.190: Log - Linear Model of CIV versus p_0 for SDPMT-6 Continuous Tests, All Sites

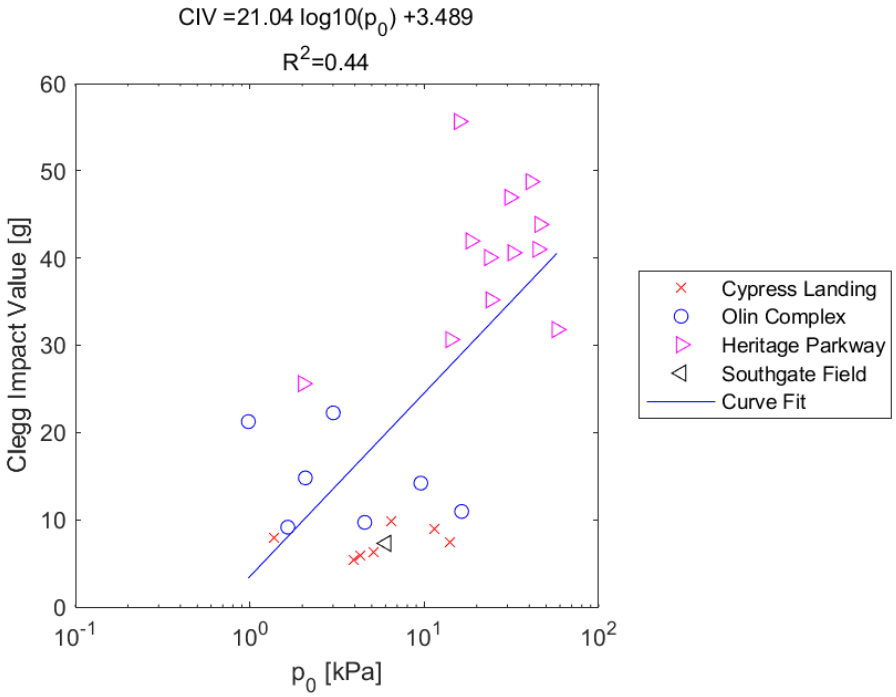

Figure E.191: Log - Linear Model of CIV versus p_0 for SDPMT-12 Incremental Tests, All Sites

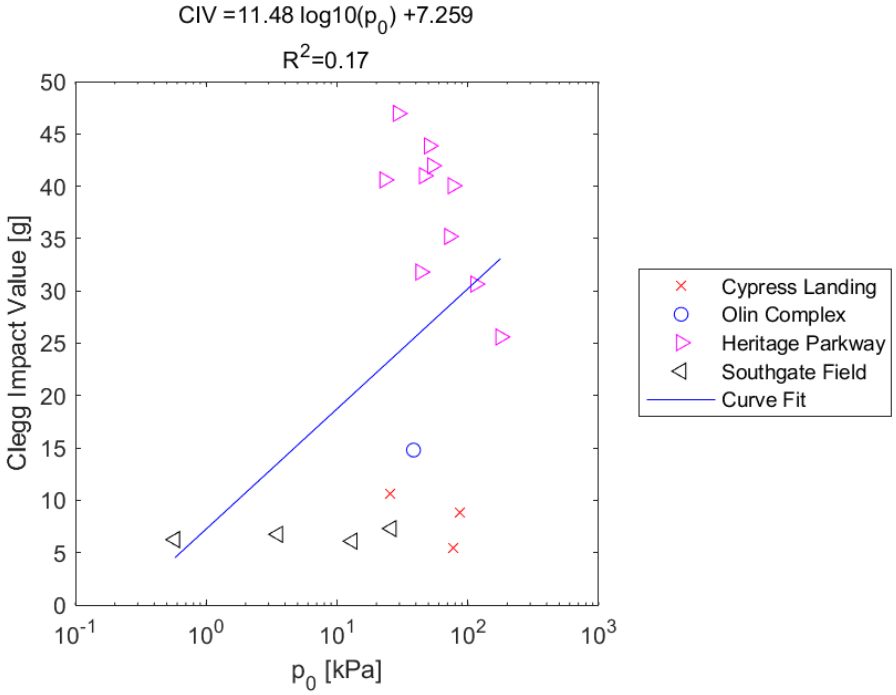

Figure E.192: Log - Linear Model of CIV versus p_0 for SDPMT-12 Continuous Tests, All Sites

E.3 Linear - Log Models

E.3.1 SDPMT E_0 versus p_0

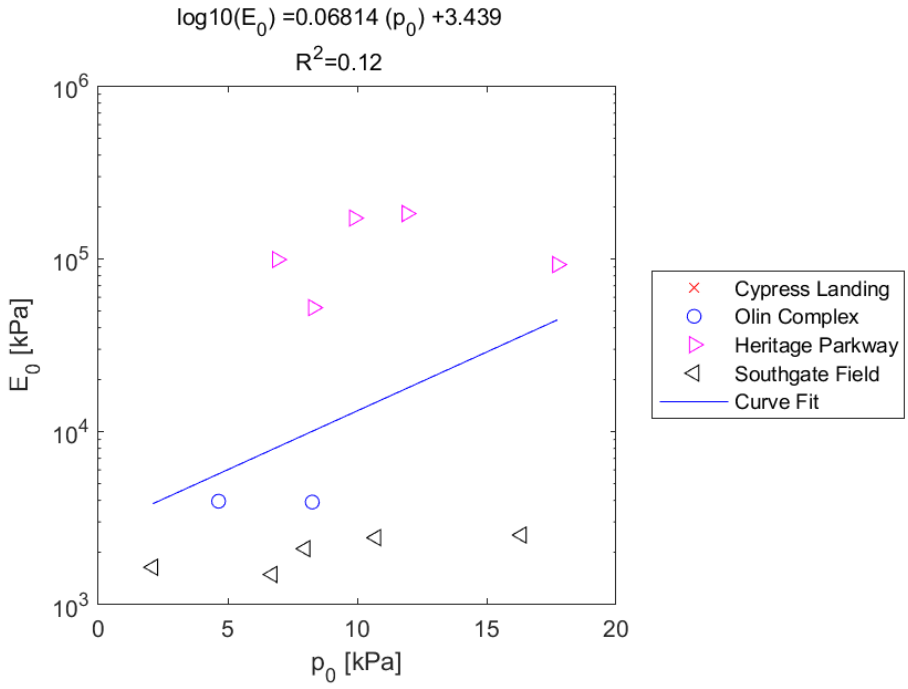

Figure E.193: Linear - Log Model of p_0 versus E_0 for SDPMT-6 Incremental Tests, All Sites

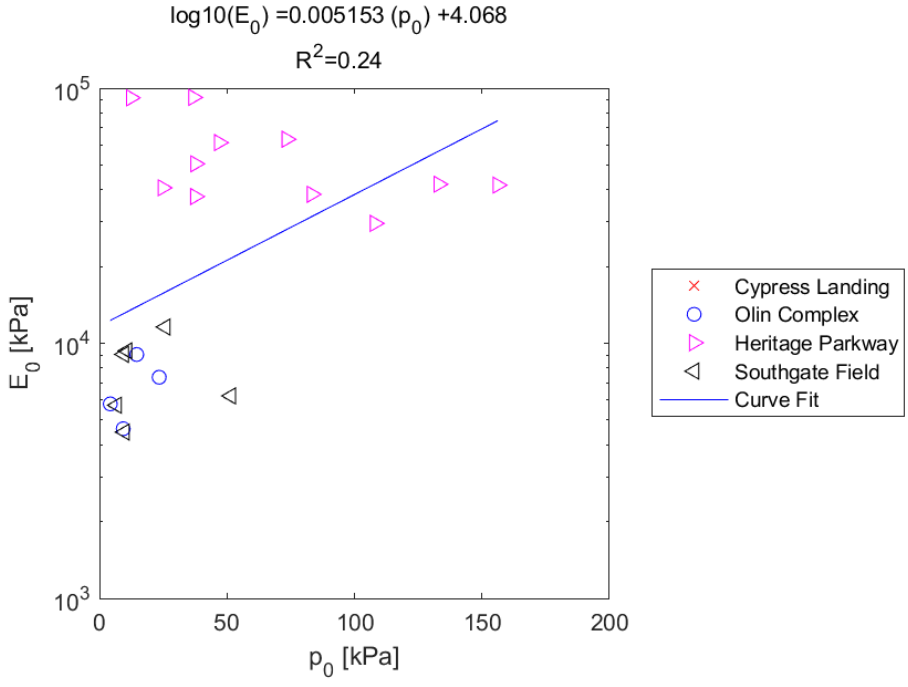

Figure E.194: Linear - Log Model of p_0 versus E_0 for SDPMT-6 Continuous Tests, All Sites

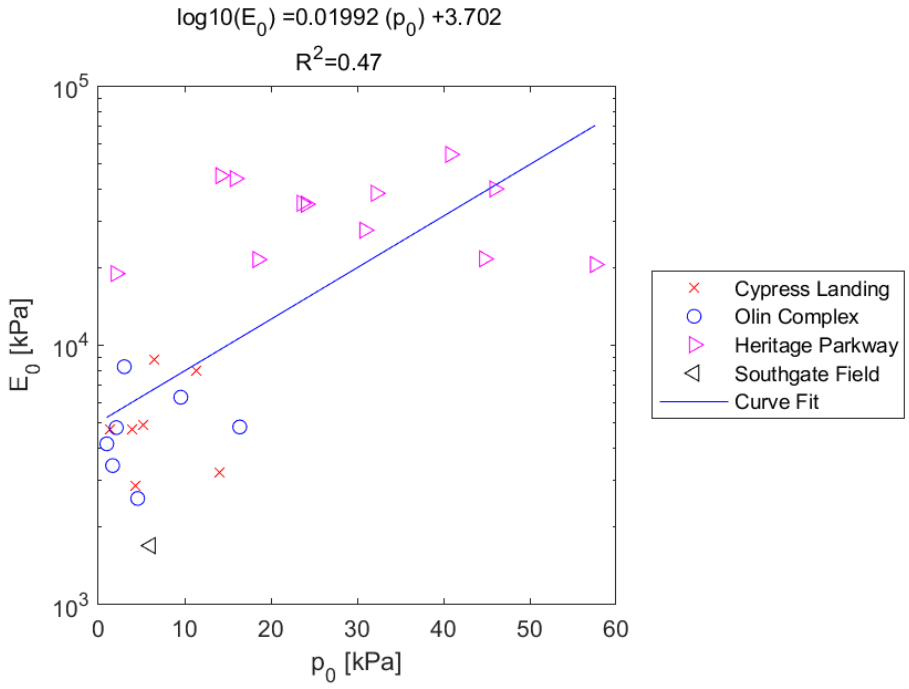

Figure E.195: Linear - Log Model of p_0 versus E_0 for SDPMT-12 Incremental Tests, All Sites

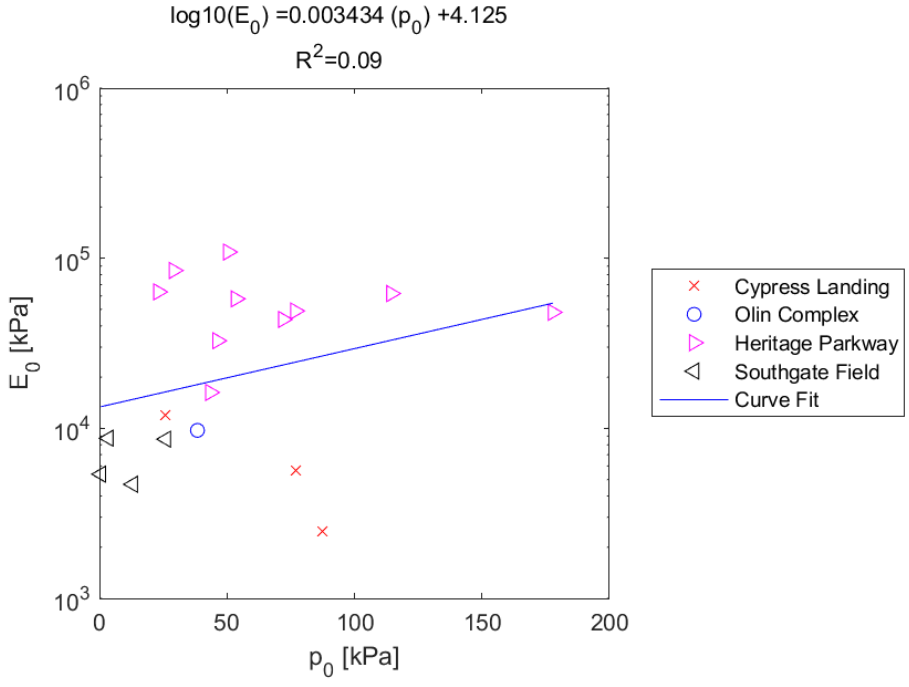

Figure E.196: Linear - Log Model of p_0 versus E_0 for SDPMT-12 Continuous Tests, All Sites

E.3.2 SDPMT p_0 versus E_0

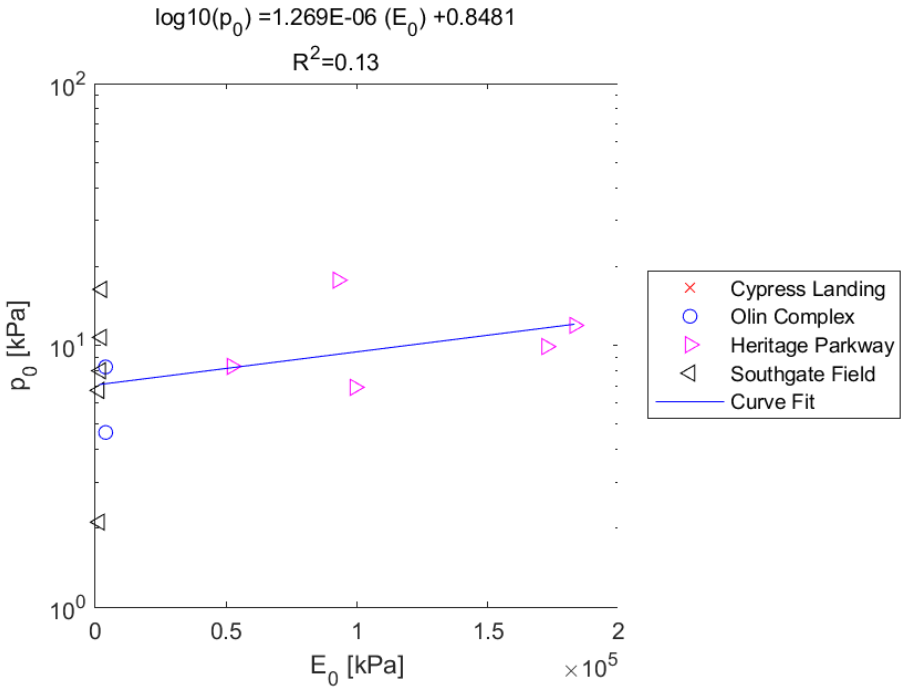

Figure E.197: Linear - Log Model of E_0 versus p_0 for SDPMT-6 Incremental Tests, All Sites

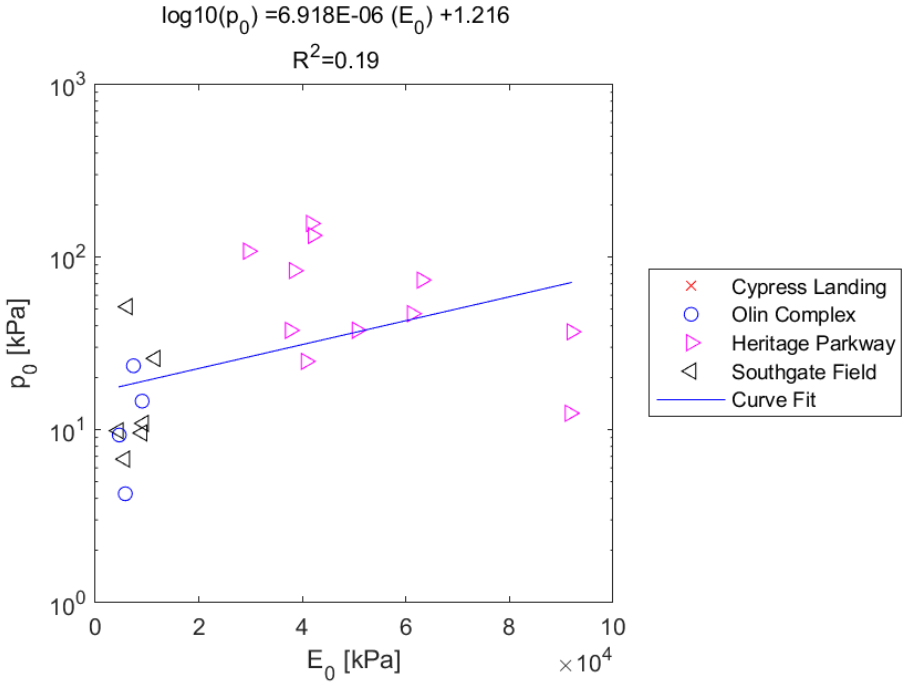

Figure E.198: Linear - Log Model of E_0 versus p_0 for SDPMT-6 Continuous Tests, All Sites

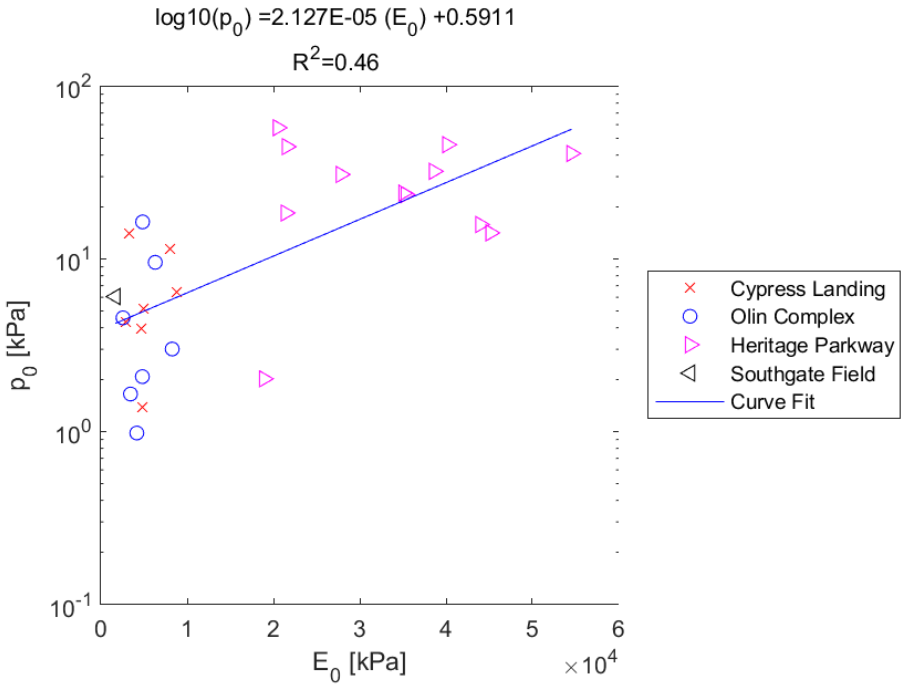

Figure E.199: Linear - Log Model of E_0 versus p_0 for SDPMT-12 Incremental Tests, All Sites

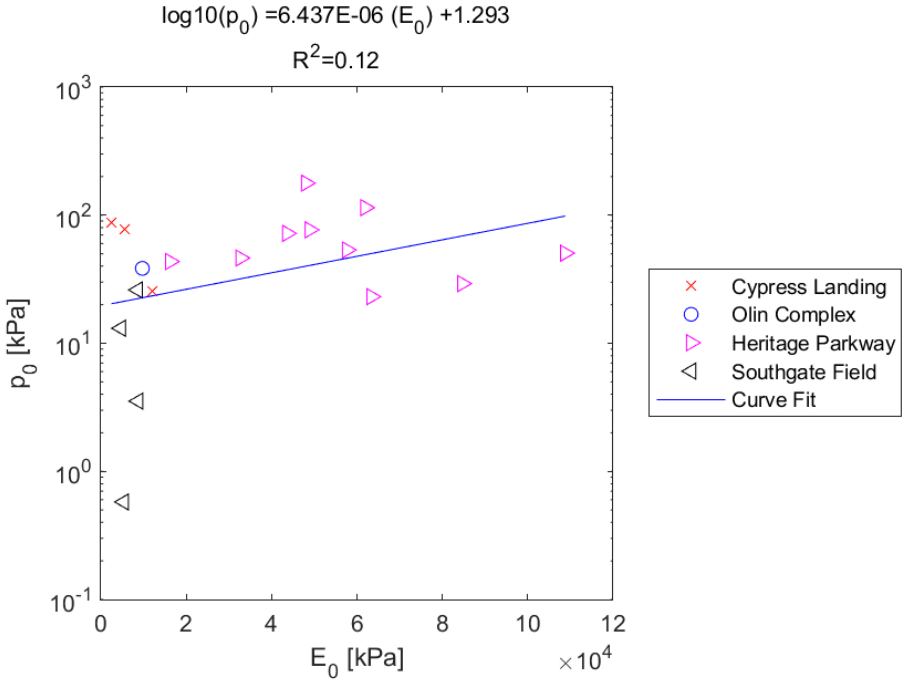

Figure E.200: Linear - Log Model of E_0 versus p_0 for SDPMT-12 Continuous Tests, All Sites

E.3.3 SDPMT $\mathbf{E}_0$ versus $\mathbf{p}_L$

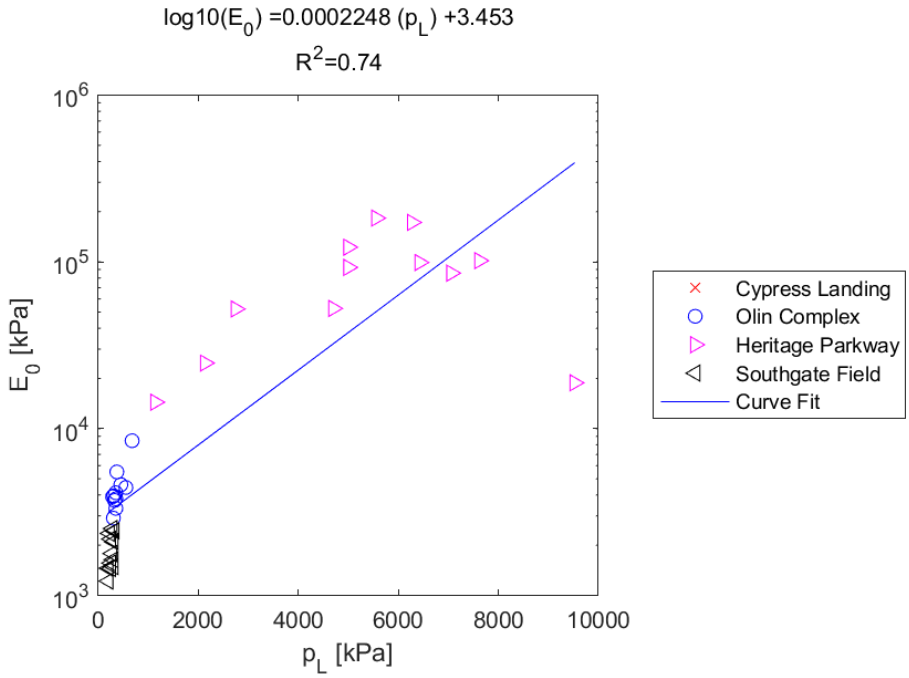

Figure E.201: Linear - Log Model of E_0 versus p_L for SDPMT-6 Incremental Tests, All Sites

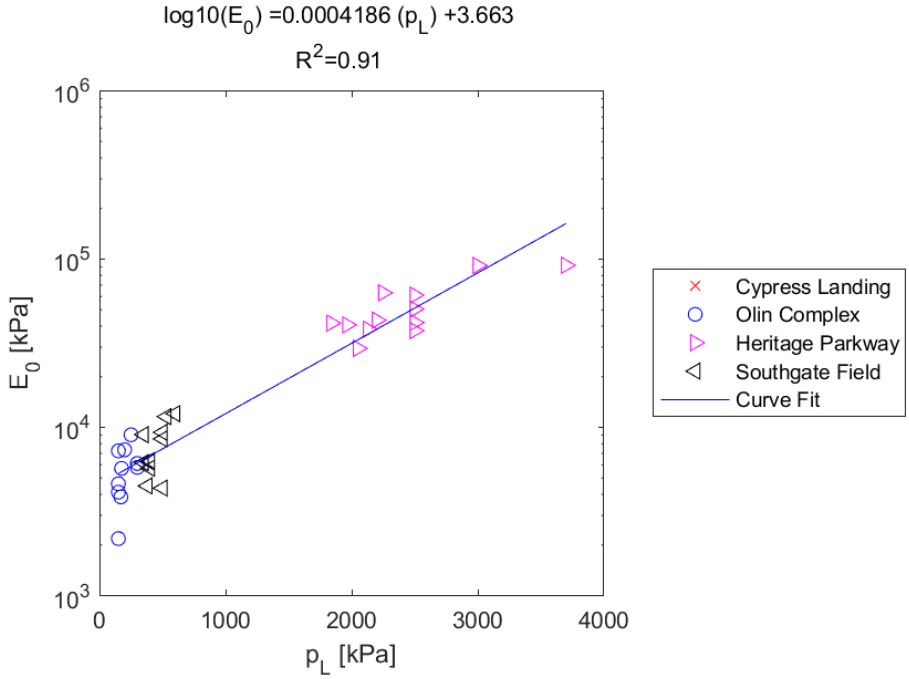

Figure E.202: Linear - Log Model of E_0 versus p_L for SDPMT-6 Continuous Tests, All Sites

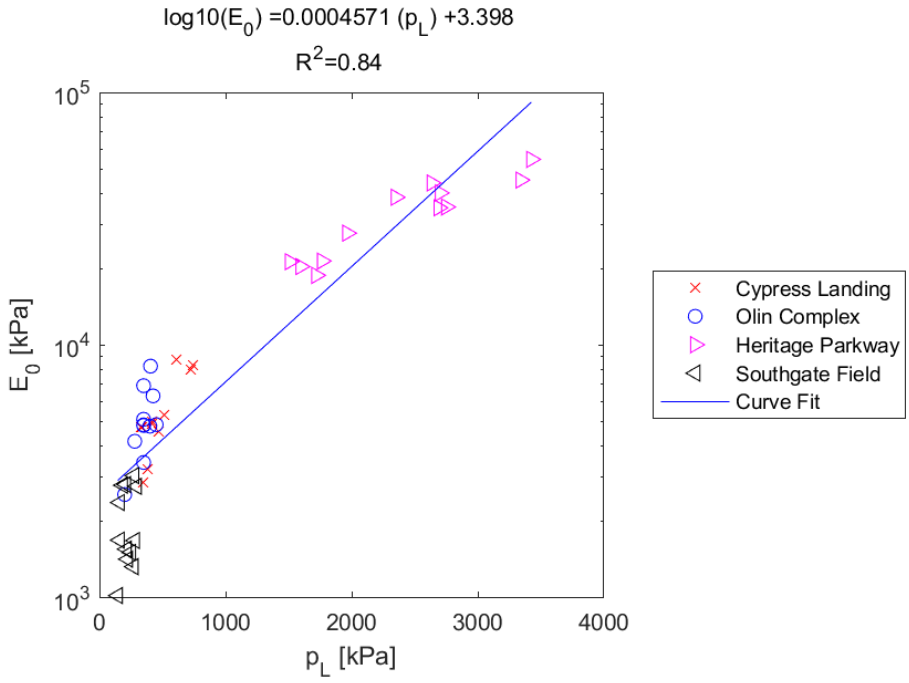

Figure E.203: Linear - Log Model of E_0 versus p_L for SDPMT-12 Incremental Tests, All Sites

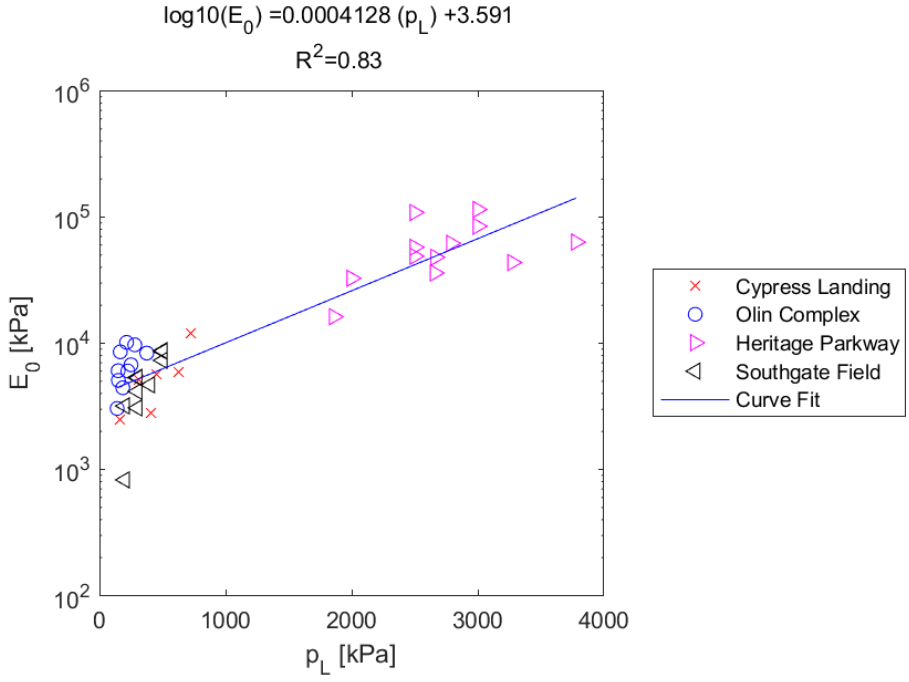

Figure E.204: Linear - Log Model of E_0 versus p_L for SDPMT-12 Continuous Tests, All Sites

E.3.4 SDPMT $\mathbf{p}_L$ versus $\mathbf{E}_0$

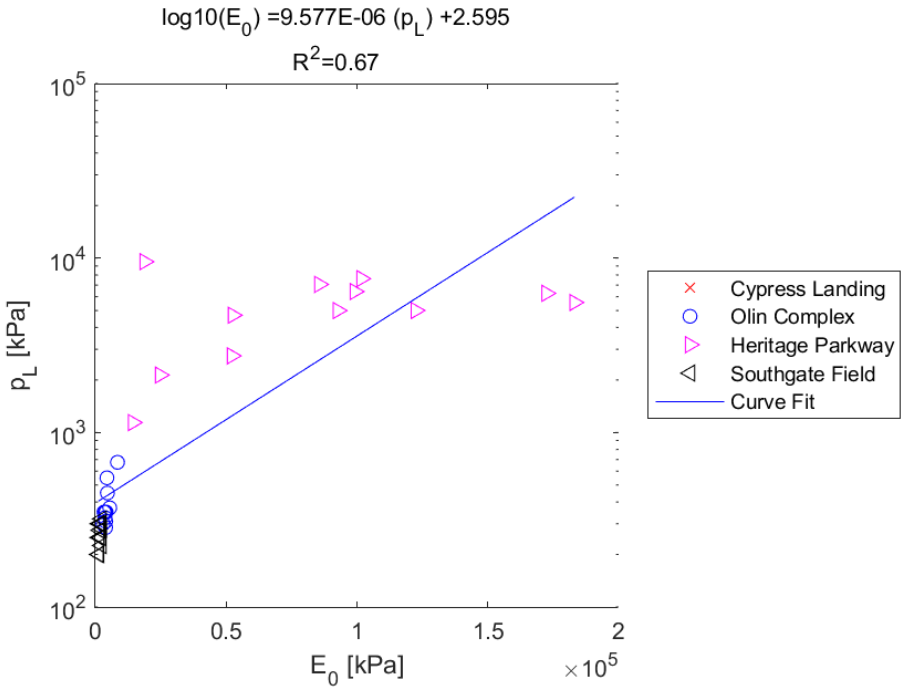

Figure E.205: Linear - Log Model of p_L versus E_0 for SDPMT-6 Incremental Tests, All Sites

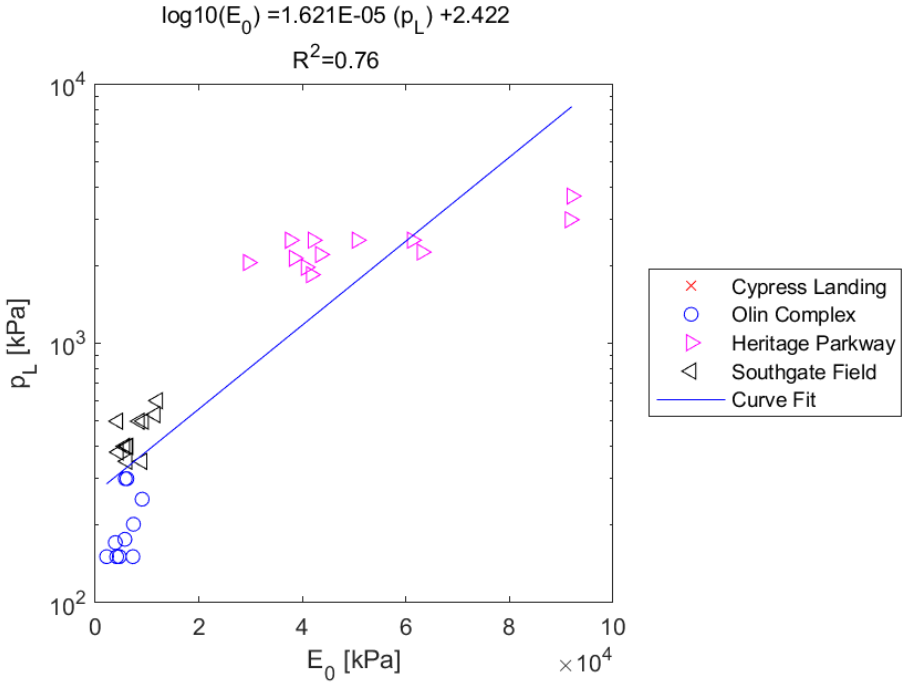

Figure E.206: Linear - Log Model of p_L versus E_0 for SDPMT-6 Continuous Tests, All Sites

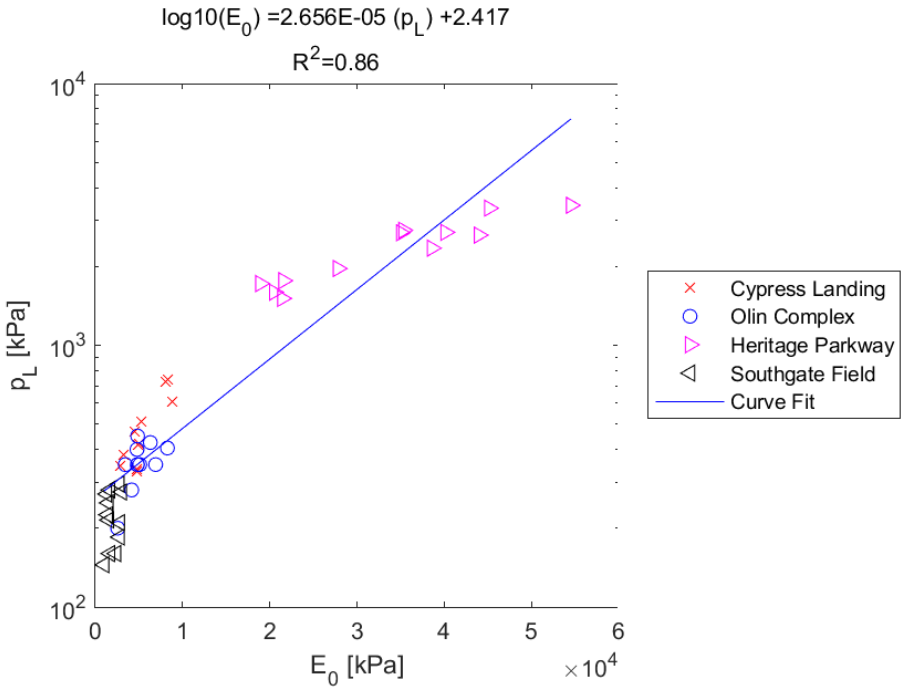

Figure E.207: Linear - Log Model of p_L versus E_0 for SDPMT-12 Incremental Tests, All Sites

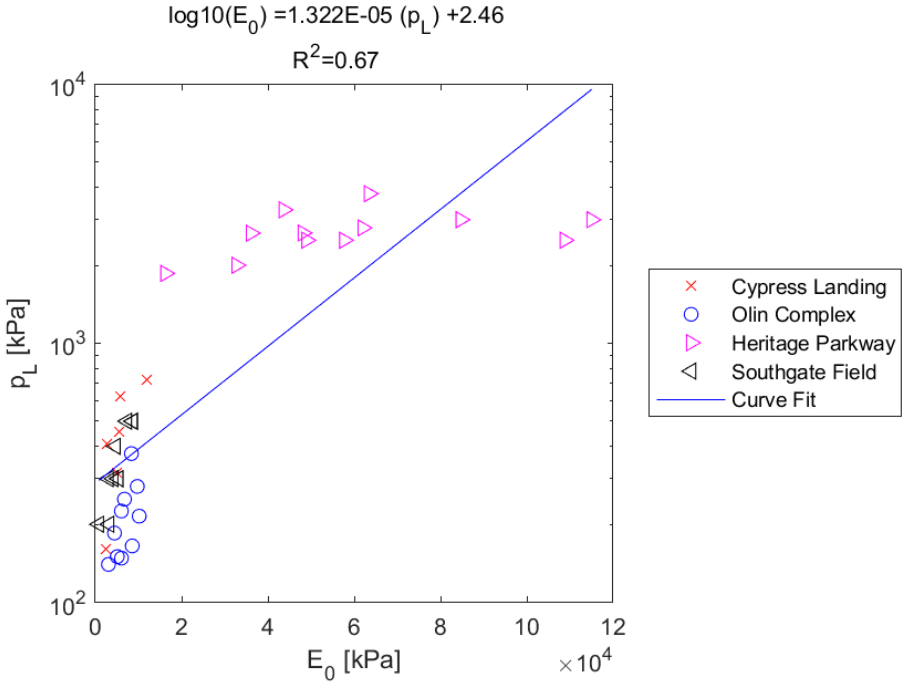

Figure E.208: Linear - Log Model of p_L versus E_0 for SDPMT-12 Continuous Tests, All Sites

E.3.5 SDPMT $\mathbf{p}_0$ versus $\mathbf{p}_L$

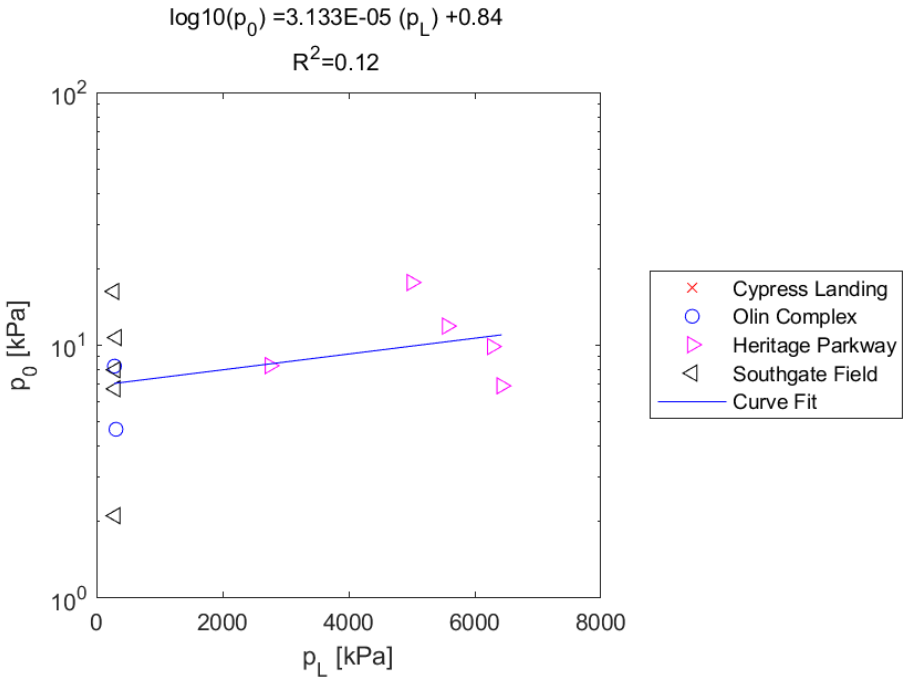

Figure E.209: Linear - Log Model of p_0 versus p_L for SDPMT-6 Incremental Tests, All Sites

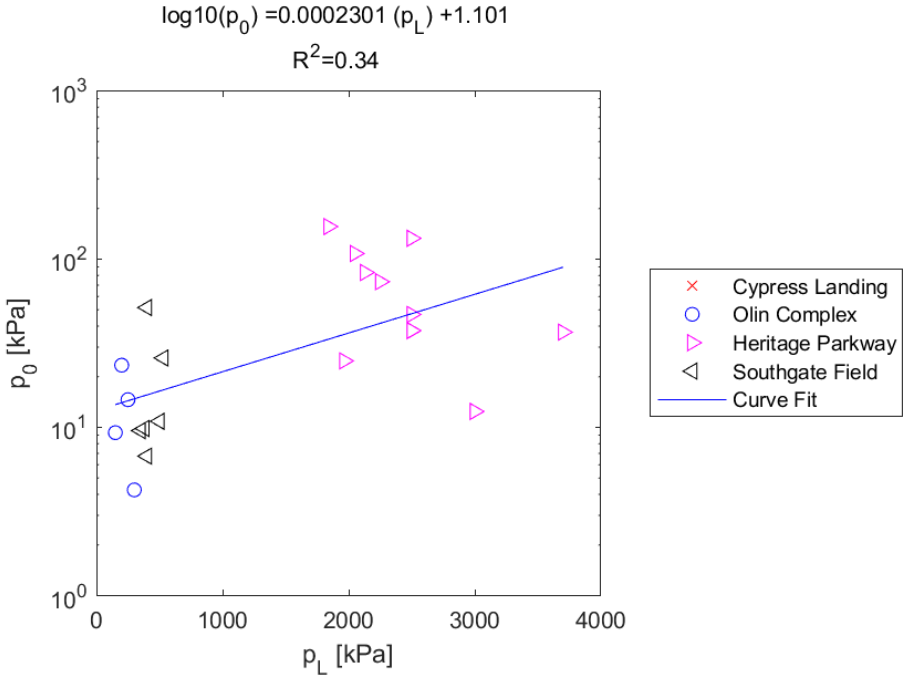

Figure E.210: Linear - Log Model of p_0 versus p_L for SDPMT-6 Continuous Tests, All Sites

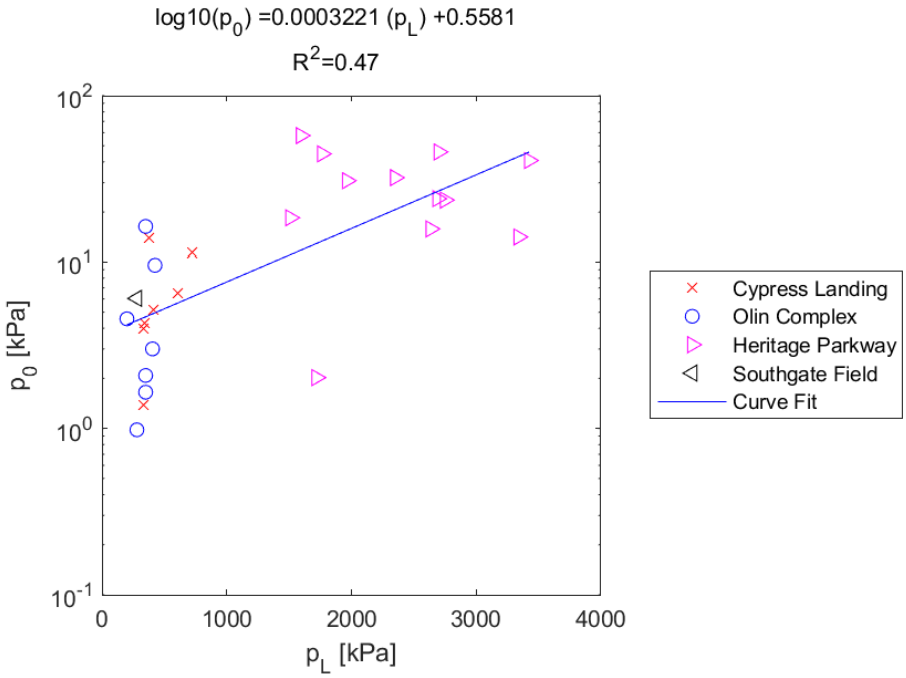

Figure E.211: Linear - Log Model of p_0 versus p_L for SDPMT-12 Incremental Tests, All Sites

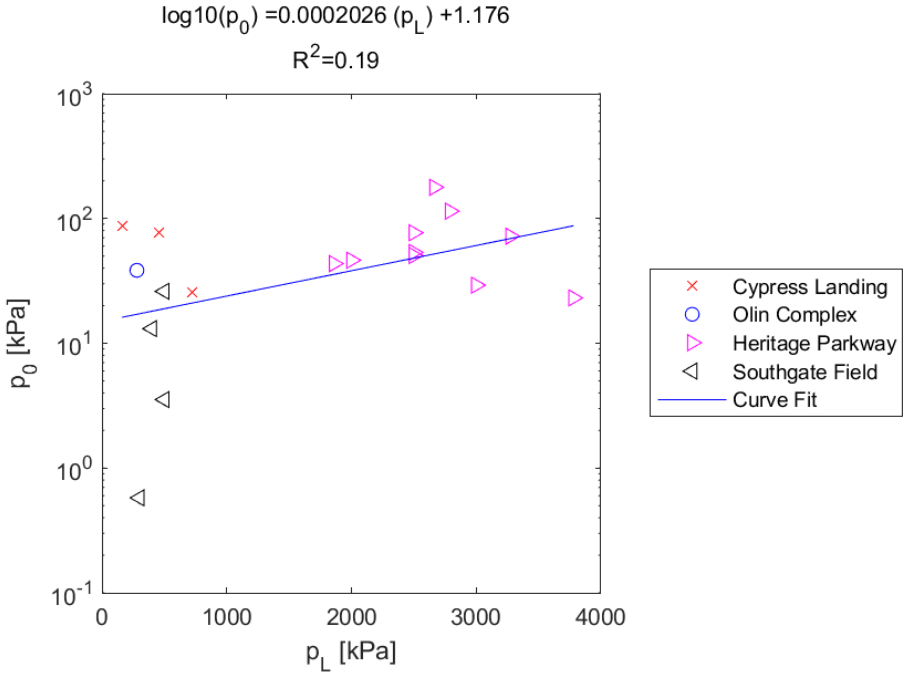

Figure E.212: Linear - Log Model of p_0 versus p_L for SDPMT-12 Continuous Tests, All Sites

E.3.6 SDPMT $\mathbf{p}_L$ versus $\mathbf{p}_0$

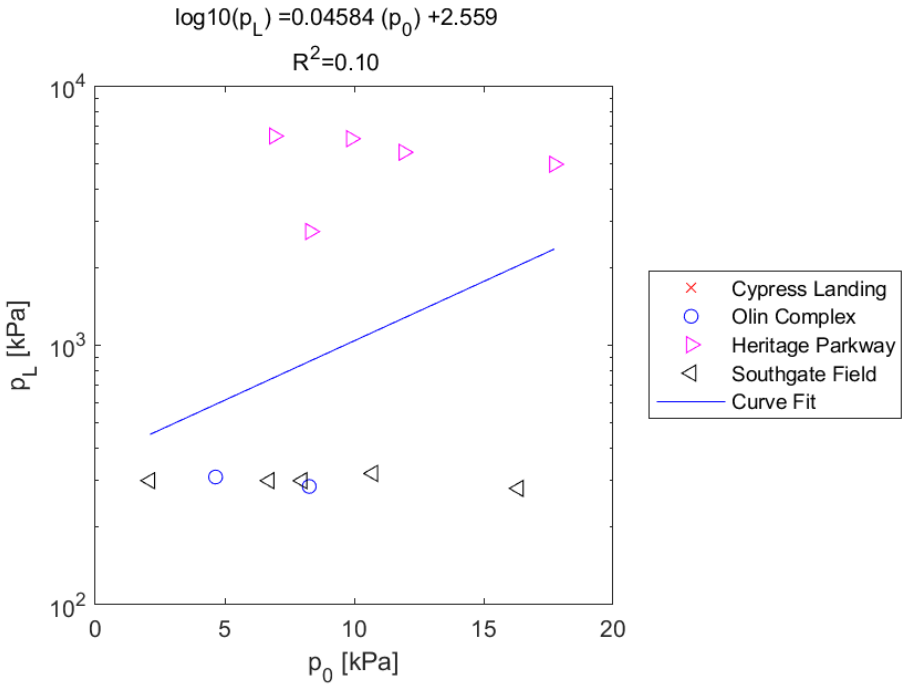

Figure E.213: Linear - Log Model of p_L versus p_0 for SDPMT-6 Incremental Tests, All Sites

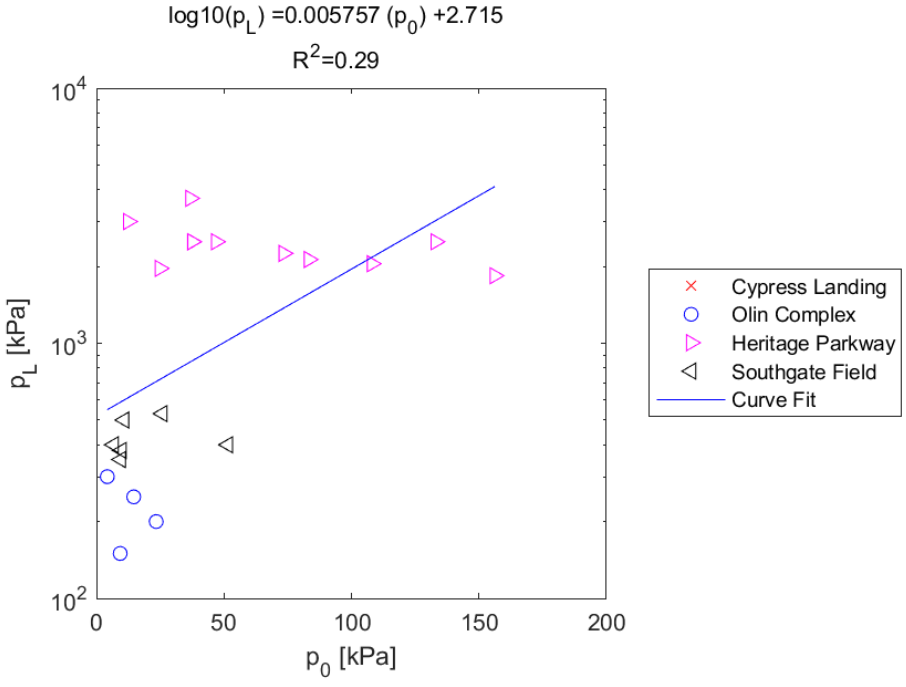

Figure E.214: Linear - Log Model of p_L versus p_0 for SDPMT-6 Continuous Tests, All Sites

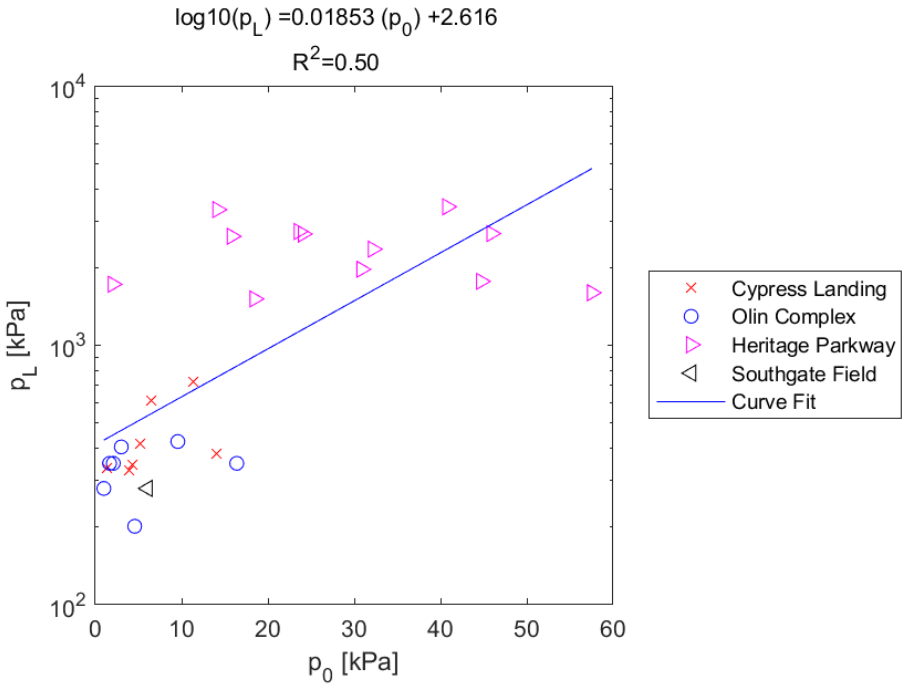

Figure E.215: Linear - Log Model of p_L versus p_0 for SDPMT-12 Incremental Tests, All Sites

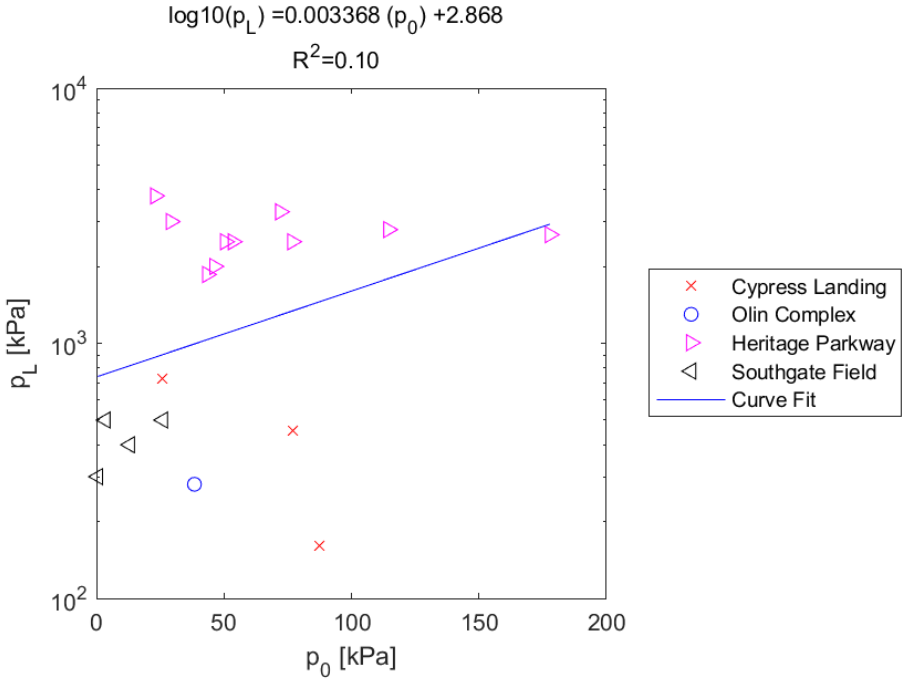

Figure E.216: Linear - Log Model of p_L versus p_0 for SDPMT-12 Continuous Tests, All Sites

E.3.7 γ_{wet} versus $\mathbf{E}_0$

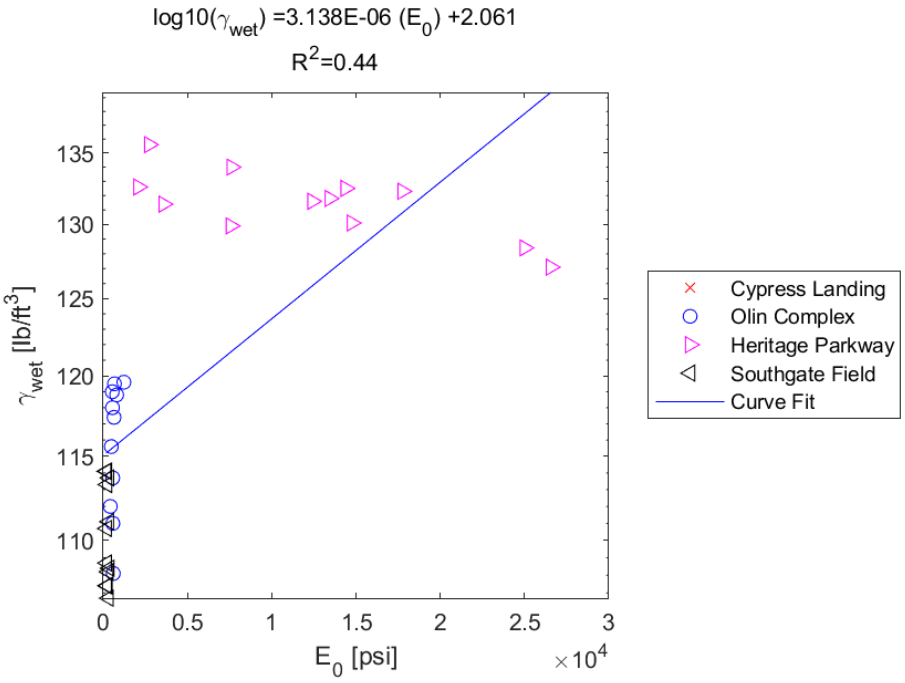

Figure E.217: Linear - Log Model of γ_{wet} versus E_0 for SDPMT-6 Incremental Tests, All Sites

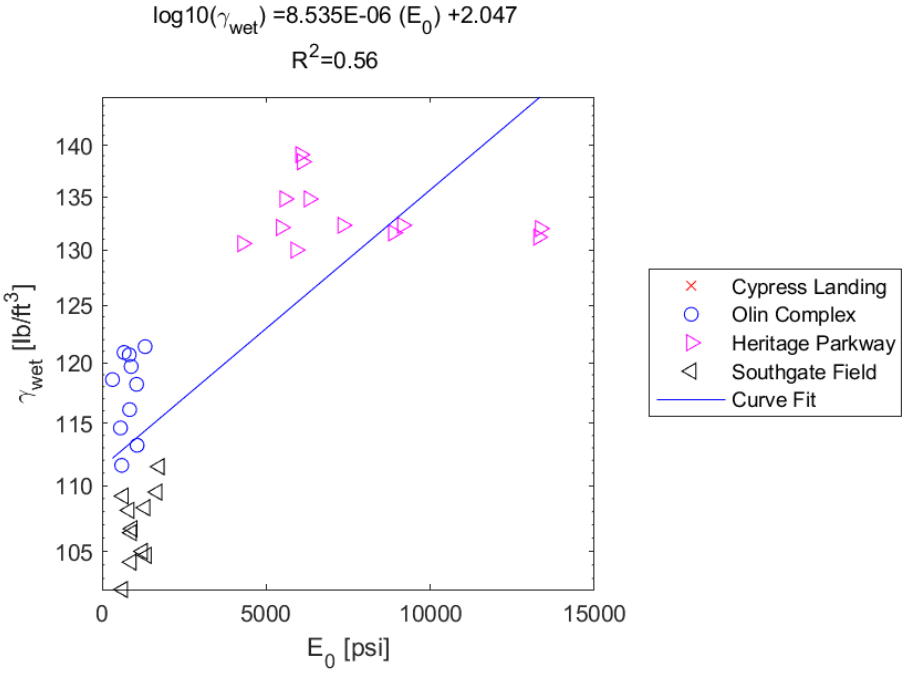

Figure E.218: Linear - Log Model of γ_{wet} versus E_0 for SDPMT-6 Continuous Tests, All Sites

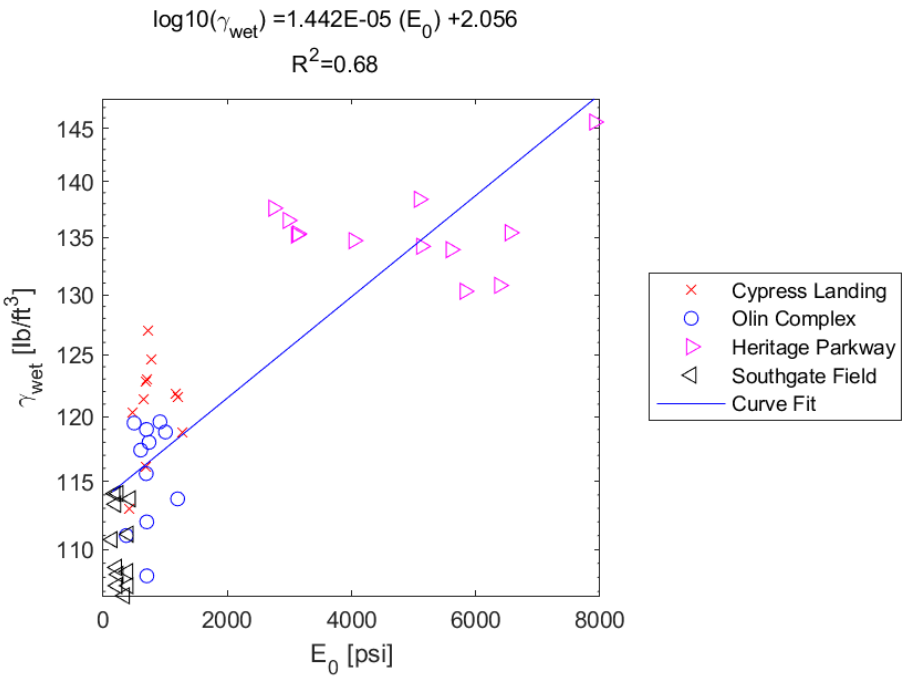

Figure E.219: Linear - Log Model of γ_{wet} versus E_0 for SDPMT-12 Incremental Tests, All Sites

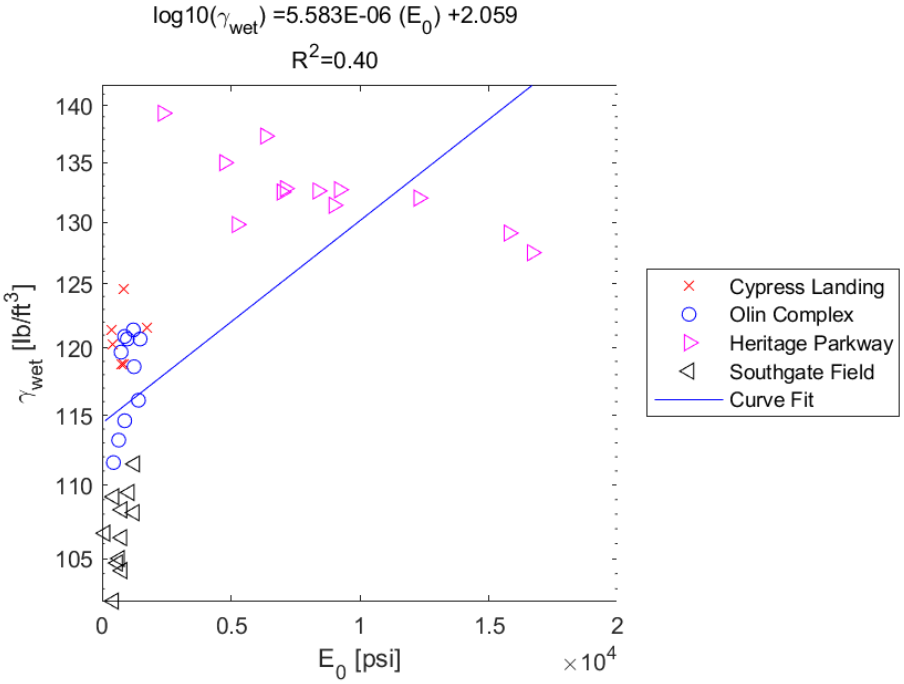

Figure E.220: Linear - Log Model of γ_{wet} versus E_0 for SDPMT-12 Continuous Tests, All Sites

E.3.8 γ_{wet} versus $\mathbf{p}_L$

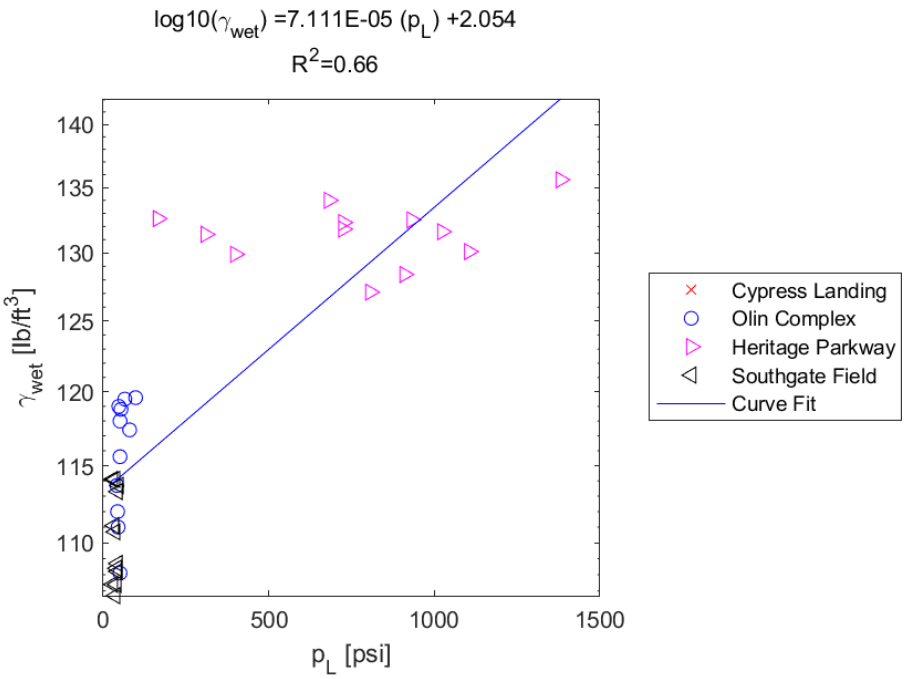

Figure E.221: Linear - Log Model of γ_{wet} versus p_L for SDPMT-6 Incremental Tests, All Sites

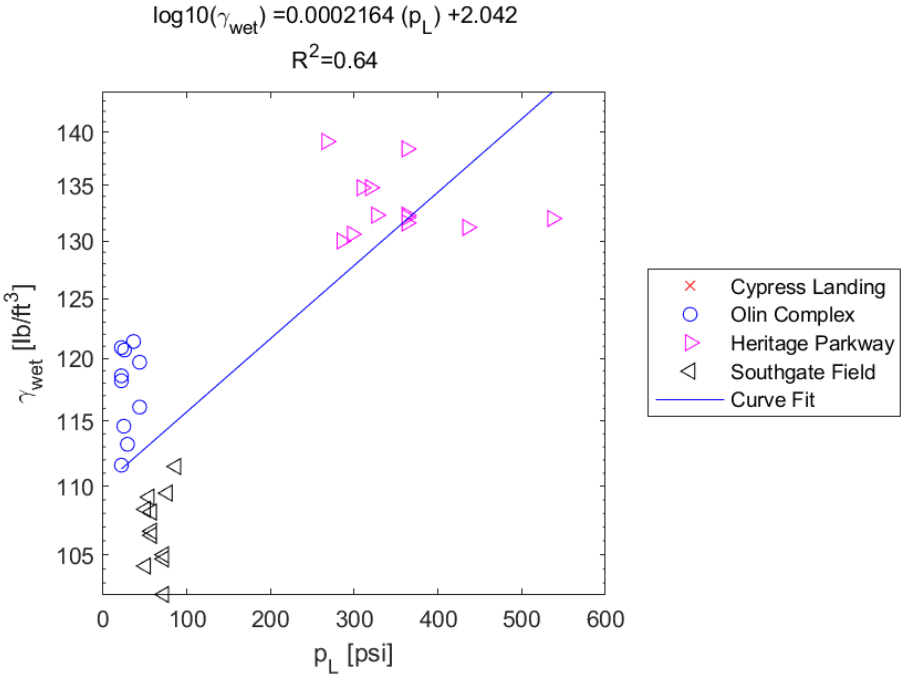

Figure E.222: Linear - Log Model of γ_{wet} versus p_L for SDPMT-6 Continuous Tests, All Sites

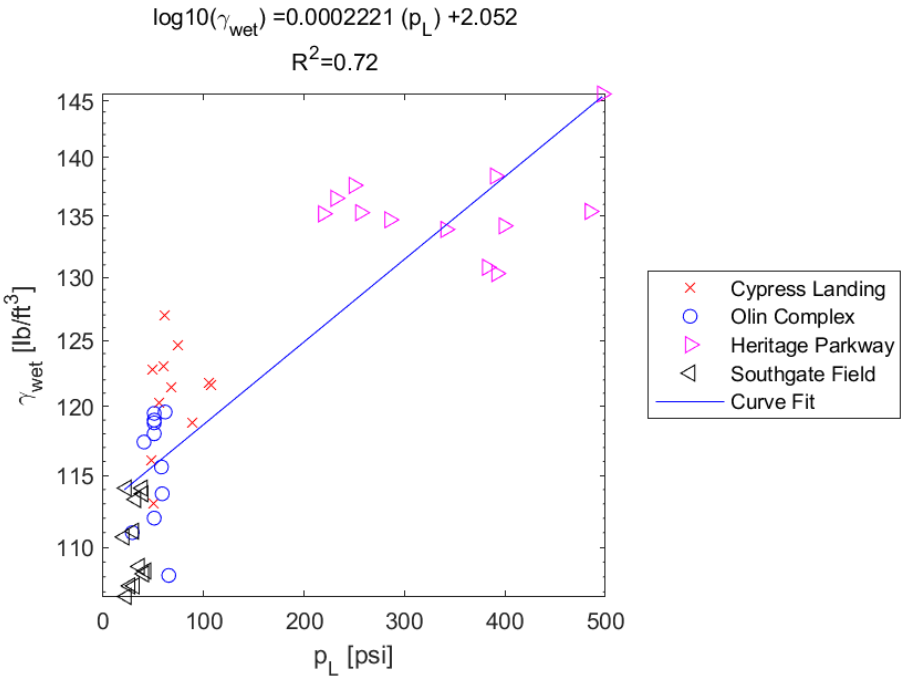

Figure E.223: Linear - Log Model of γ_{wet} versus p_L for SDPMT-12 Incremental Tests, All Sites

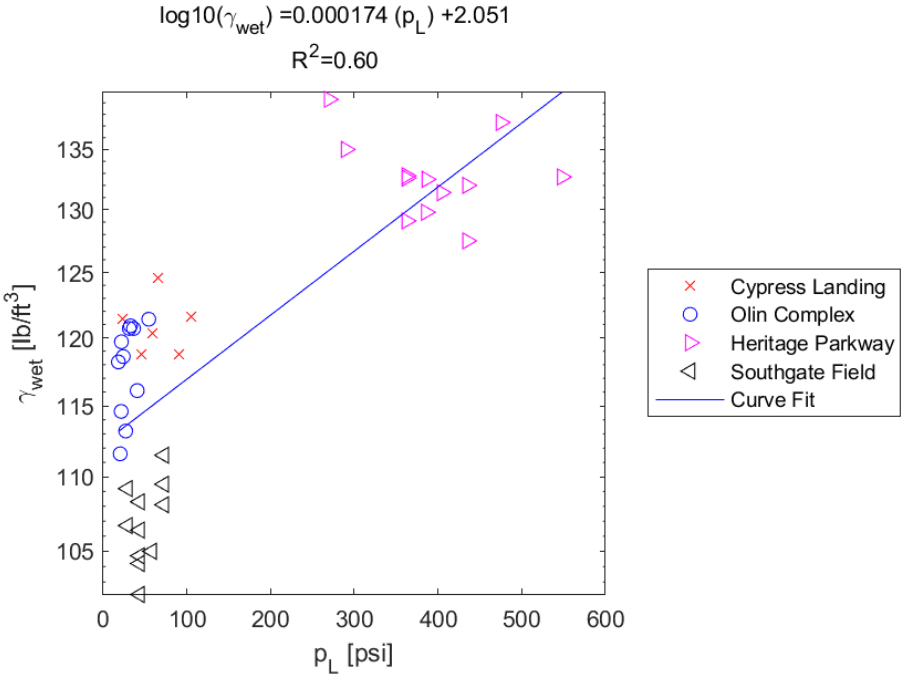

Figure E.224: Linear - Log Model of γ_{wet} versus p_L for SDPMT-12 Continuous Tests, All Sites

E.3.9 γ_{wet} versus $\mathbf{p}_0$

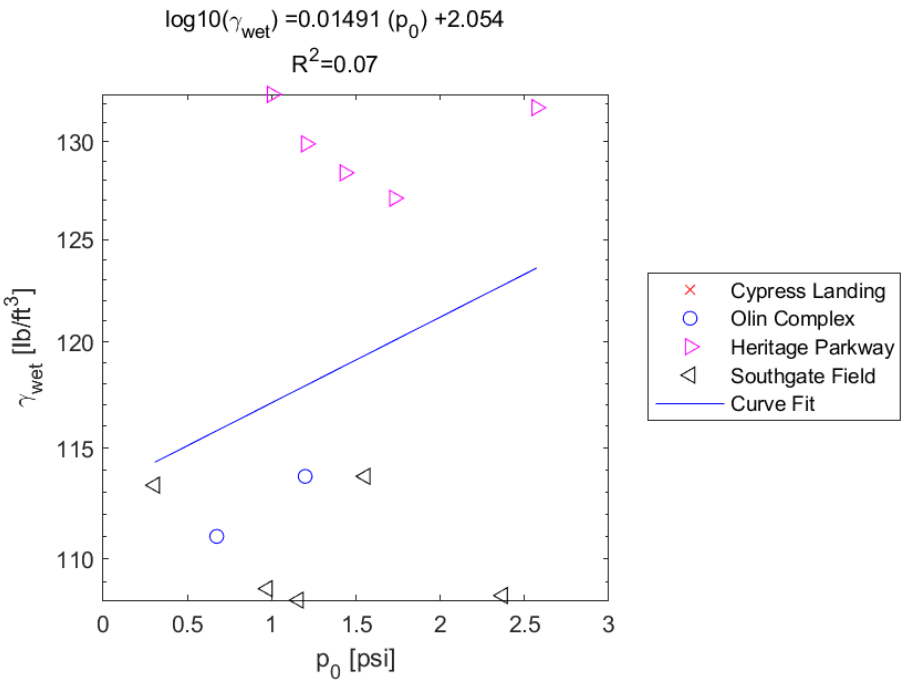

Figure E.225: Linear - Log Model of γ_{wet} versus p_0 for SDPMT-6 Incremental Tests, All Sites

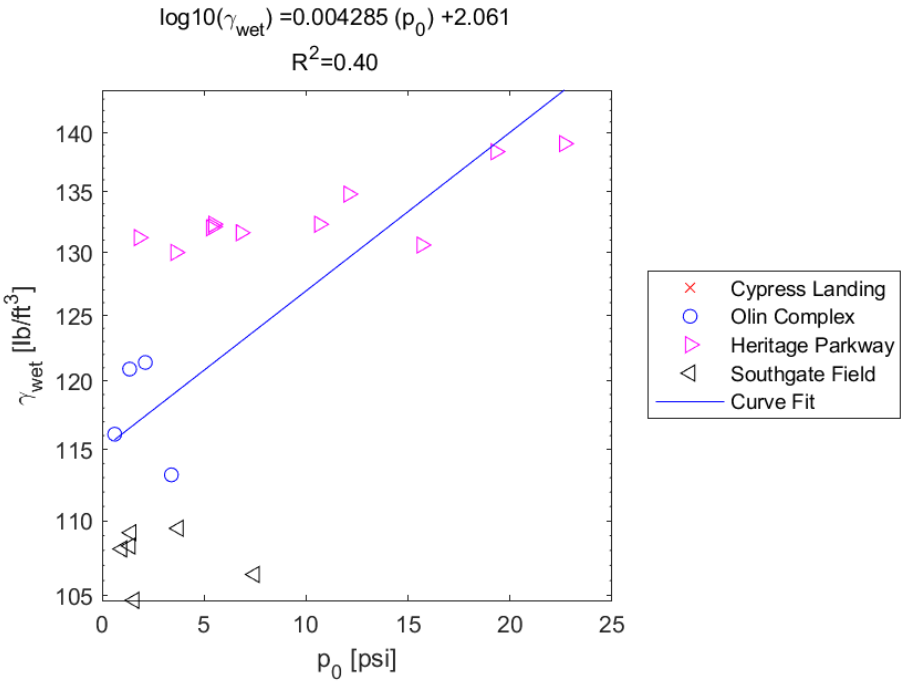

Figure E.226: Linear - Log Model of γ_{wet} versus p_0 for SDPMT-6 Continuous Tests, All Sites

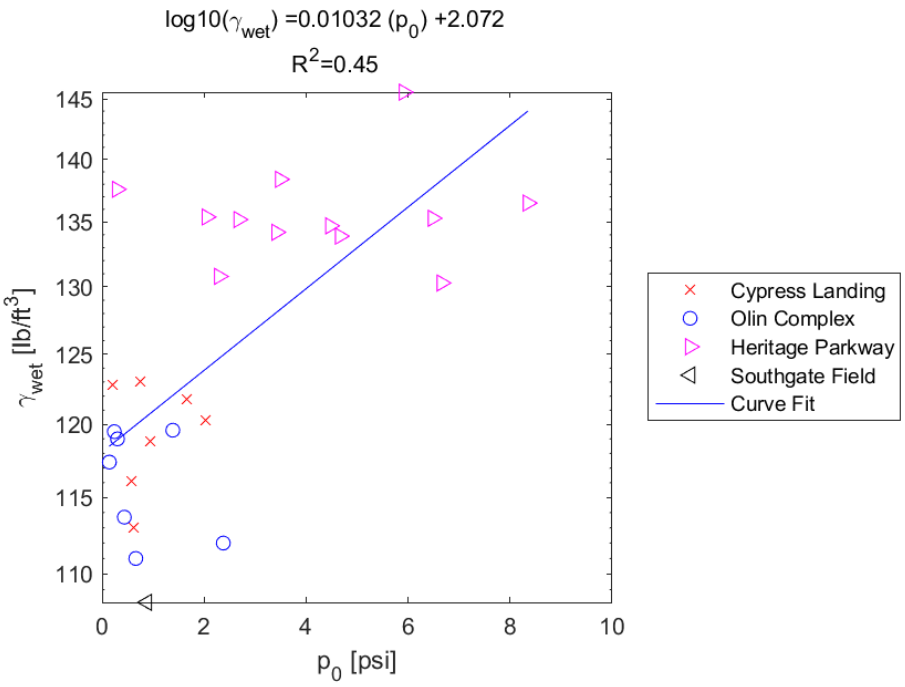

Figure E.227: Linear - Log Model of γ_{wet} versus p_0 for SDPMT-12 Incremental Tests, All Sites

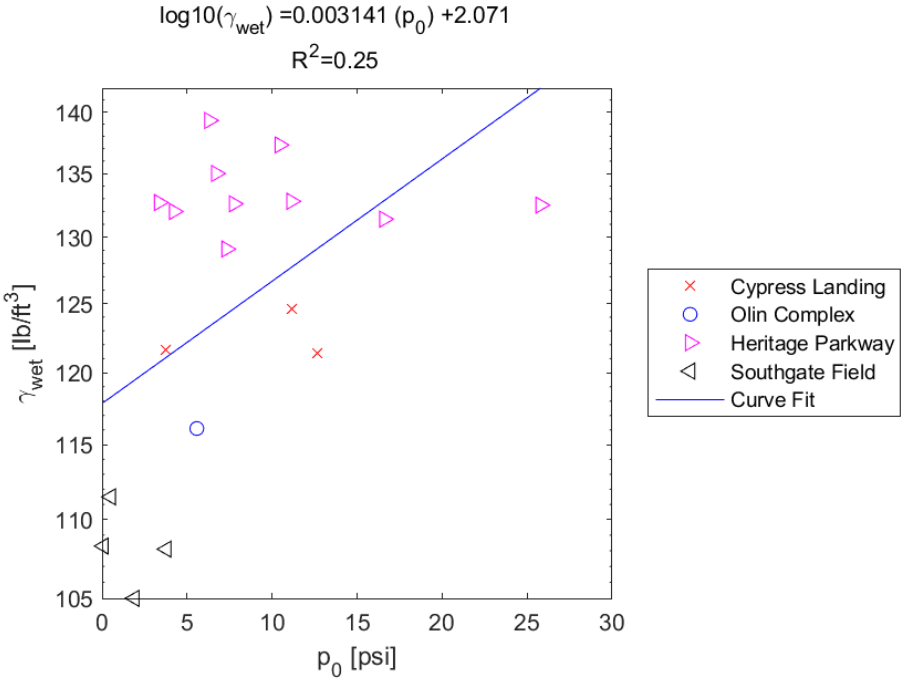

Figure E.228: Linear - Log Model of γ_{wet} versus p_0 for SDPMT-12 Continuous Tests, All Sites

E.3.10 γ_{dry} versus $\mathbf{E}_0$

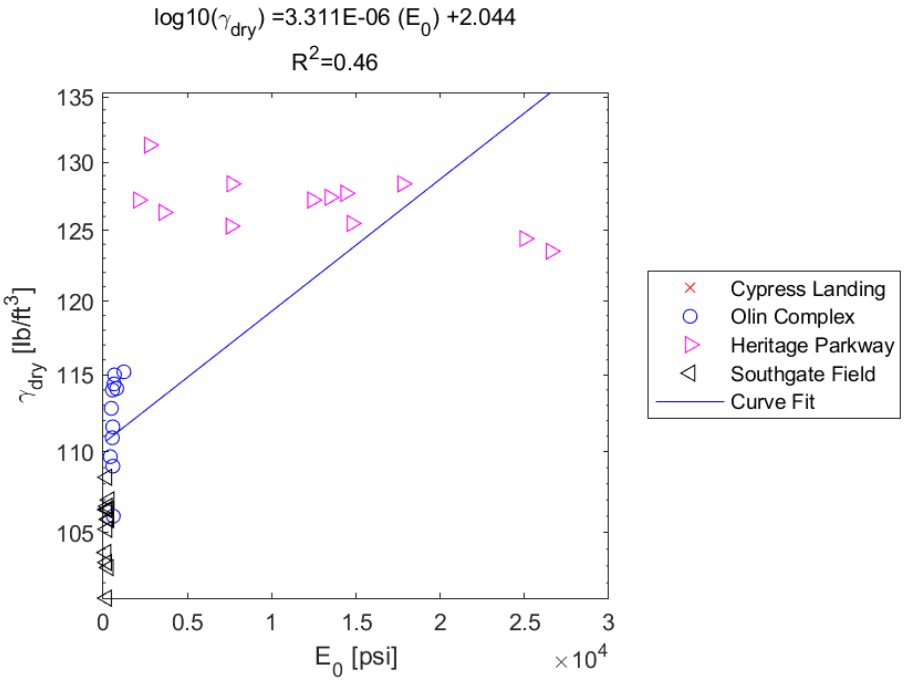

Figure E.229: Linear - Log Model of γ_{dry} versus E_0 for SDPMT-6 Incremental Tests, All Sites

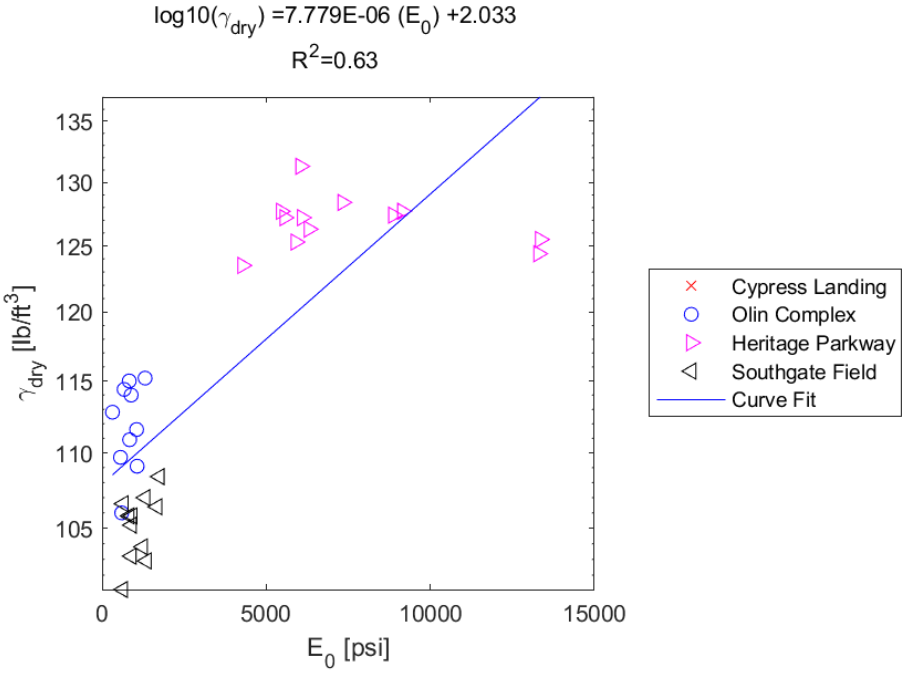

Figure E.230: Linear - Log Model of γ_{dry} versus E_0 for SDPMT-6 Continuous Tests, All Sites

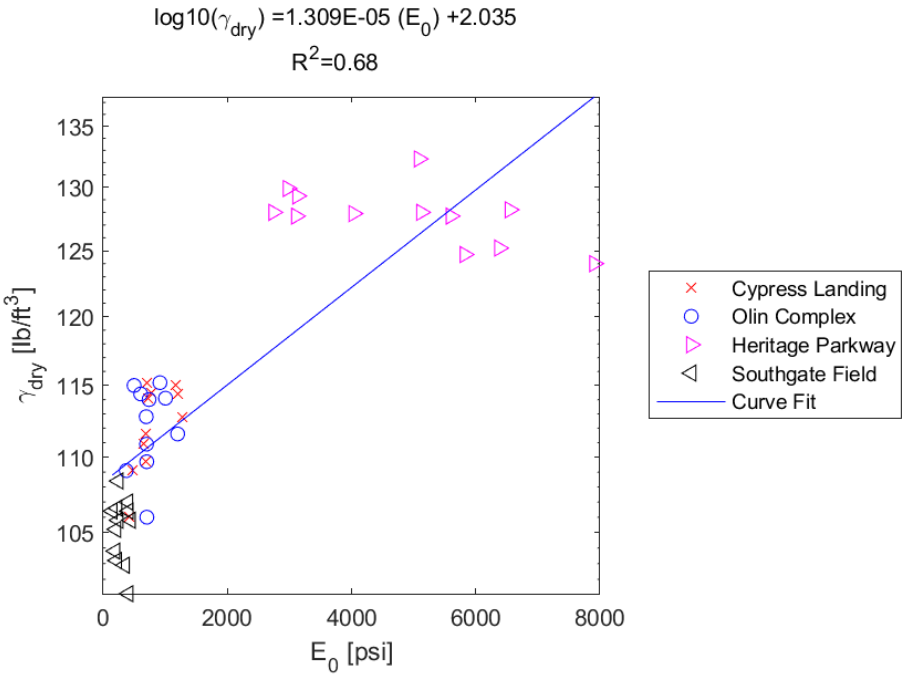

Figure E.231: Linear - Log Model of γ_{dry} versus E_0 for SDPMT-12 Incremental Tests, All Sites

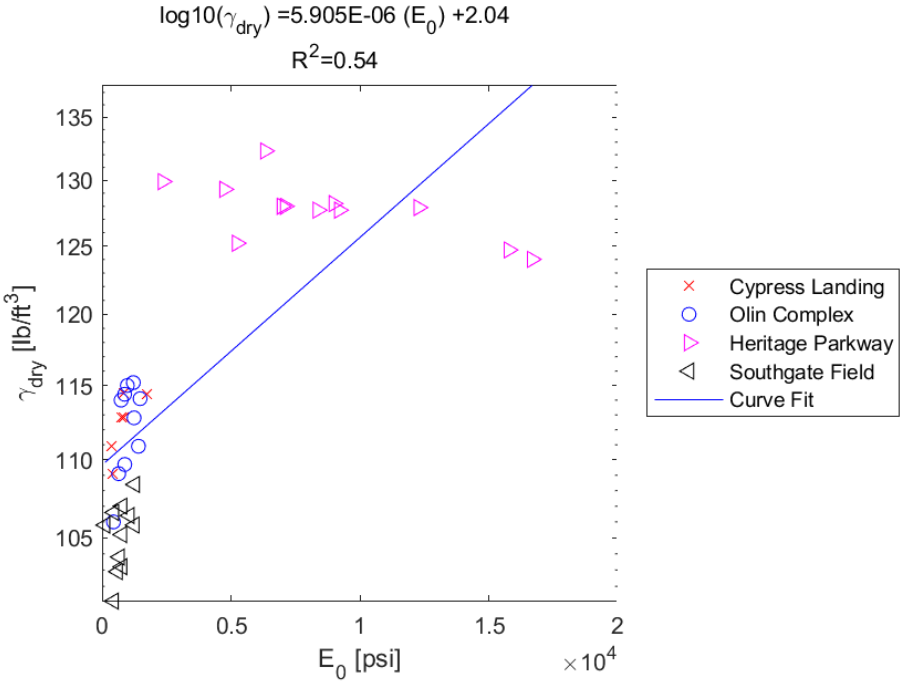

Figure E.232: Linear - Log Model of γ_{dry} versus E_0 for SDPMT-12 Continuous Tests, All Sites

E.3.11 γ_{dry} versus $\mathbf{p}_L$

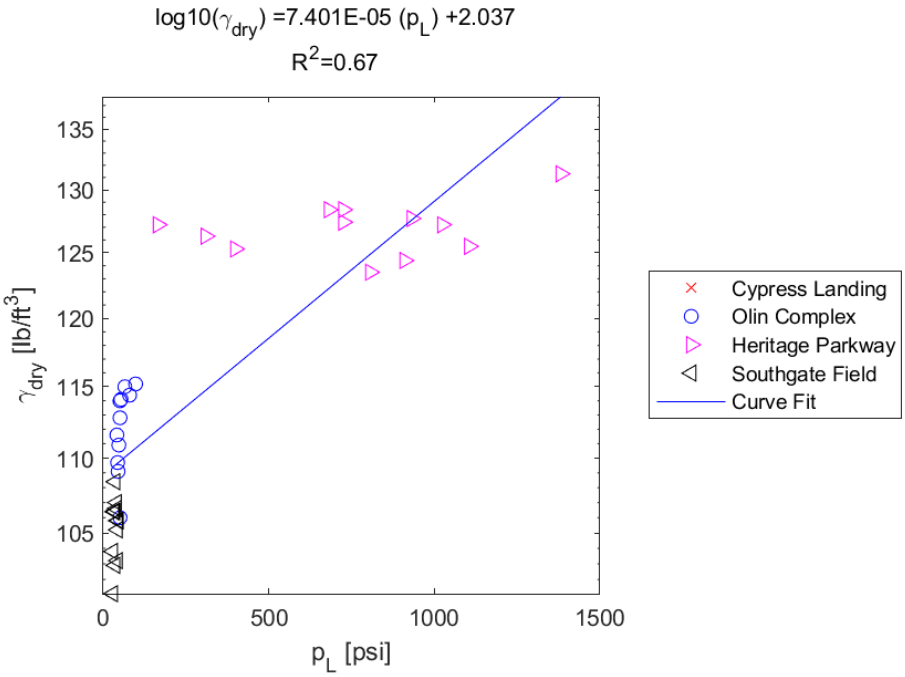

Figure E.233: Linear - Log Model of γ_{dry} versus p_L for SDPMT-6 Incremental Tests, All Sites

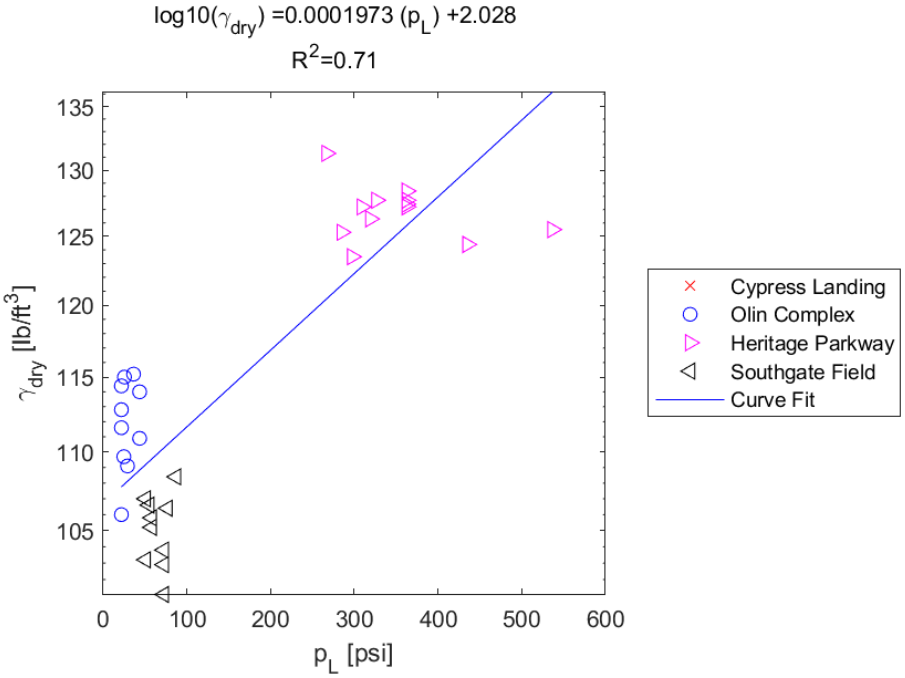

Figure E.234: Linear - Log Model of γ_{dry} versus p_L for SDPMT-6 Continuous Tests, All Sites

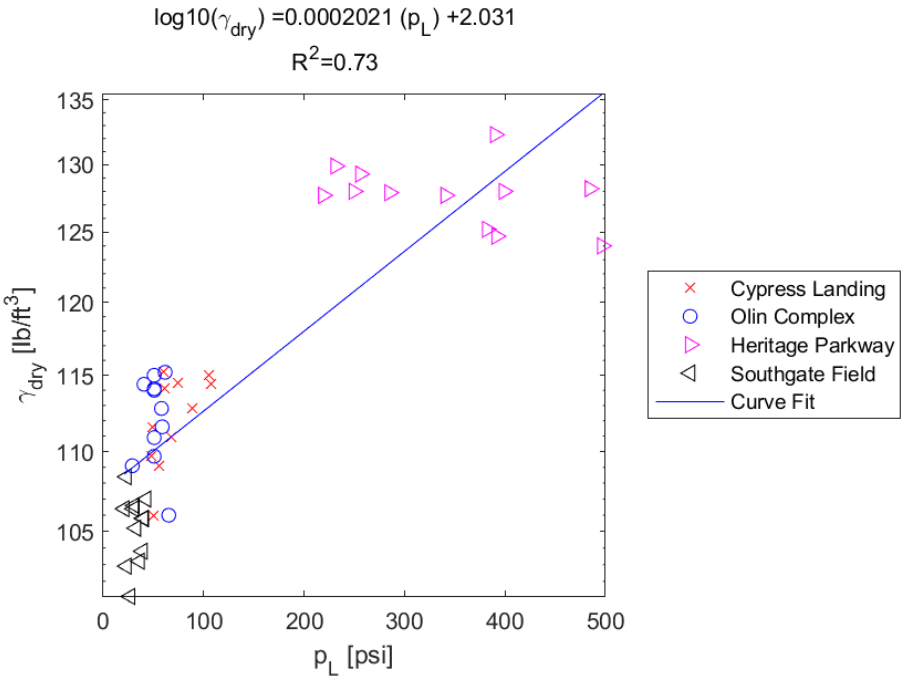

Figure E.235: Linear - Log Model of γ_{dry} versus p_L for SDPMT-12 Incremental Tests, All Sites

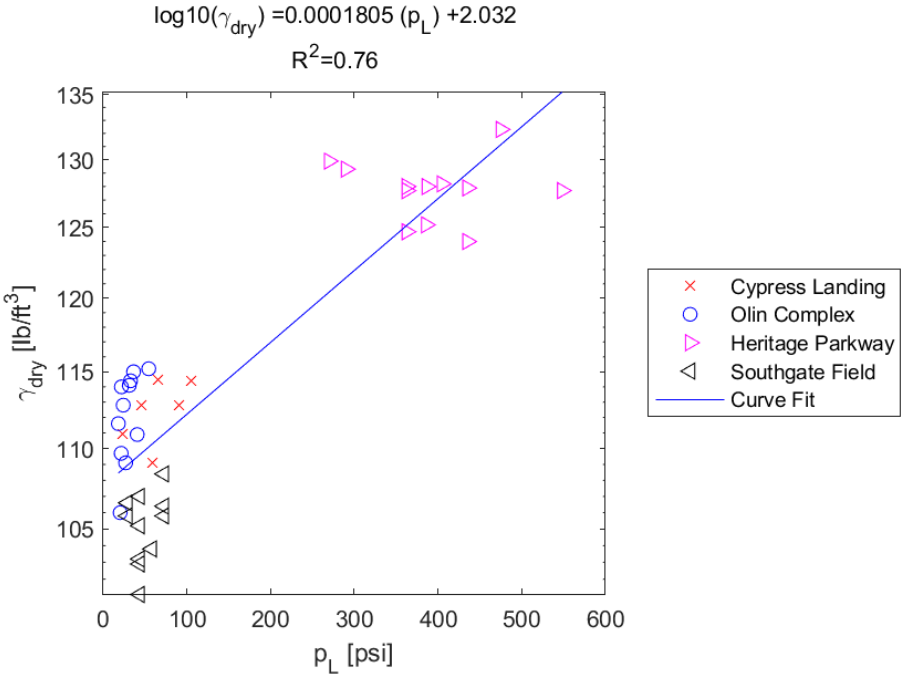

Figure E.236: Linear - Log Model of γ_{dry} versus p_L for SDPMT-12 Continuous Tests, All Sites

E.3.12 γ_{dry} versus $\mathbf{p}_0$

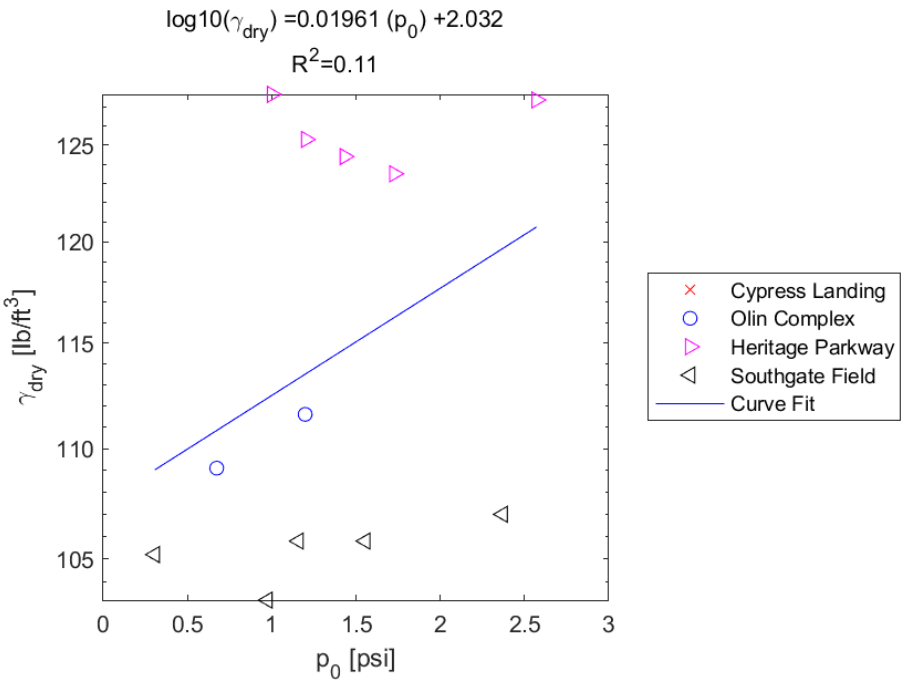

Figure E.237: Linear - Log Model of γ_{dry} versus p_0 for SDPMT-6 Incremental Tests, All Sites

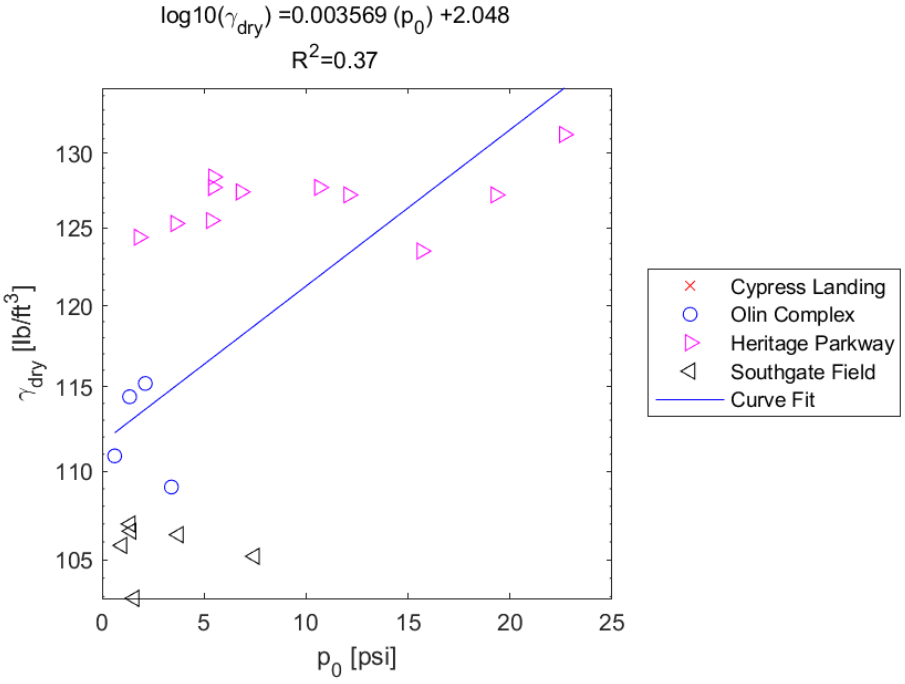

Figure E.238: Linear - Log Model of γ_{dry} versus p_0 for SDPMT-6 Continuous Tests, All Sites

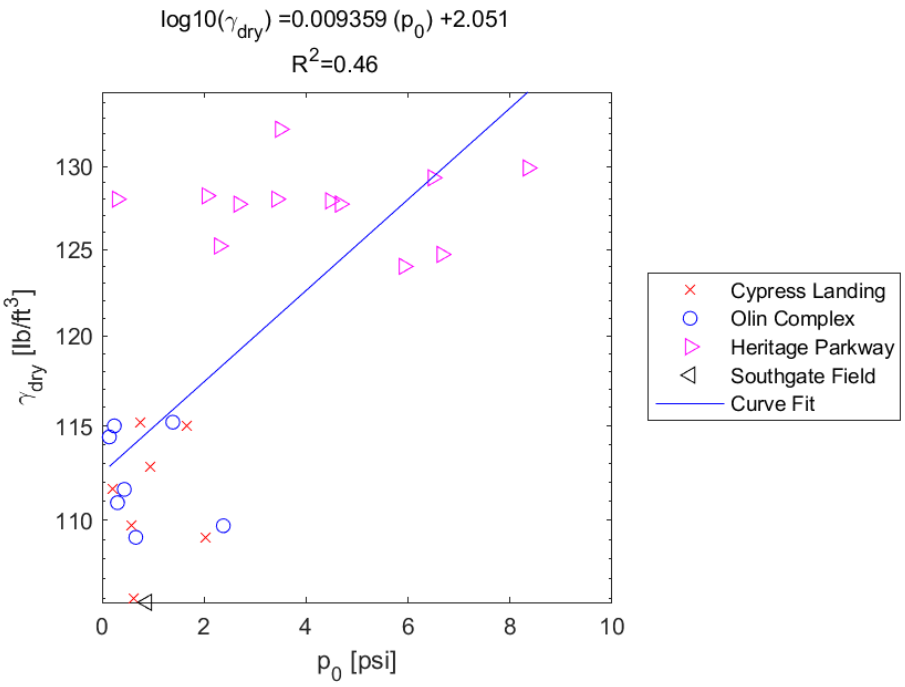

Figure E.239: Linear - Log Model of γ_{dry} versus p_0 for SDPMT-12 Incremental Tests, All Sites

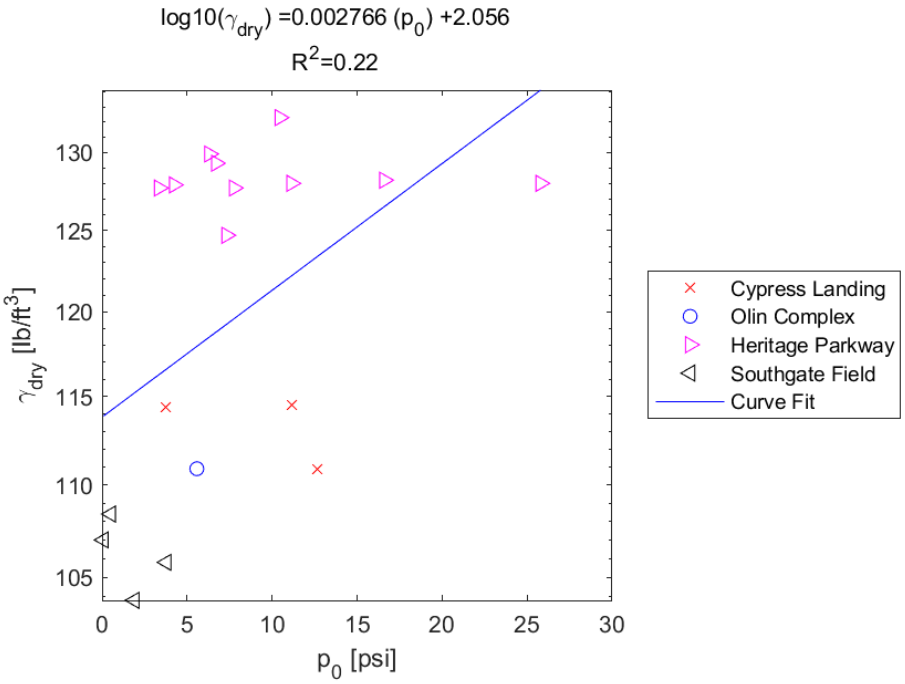

Figure E.240: Linear - Log Model of γ_{dry} versus p_0 for SDPMT-12 Continuous Tests, All Sites

E.3.13 DCP PI versus E_0

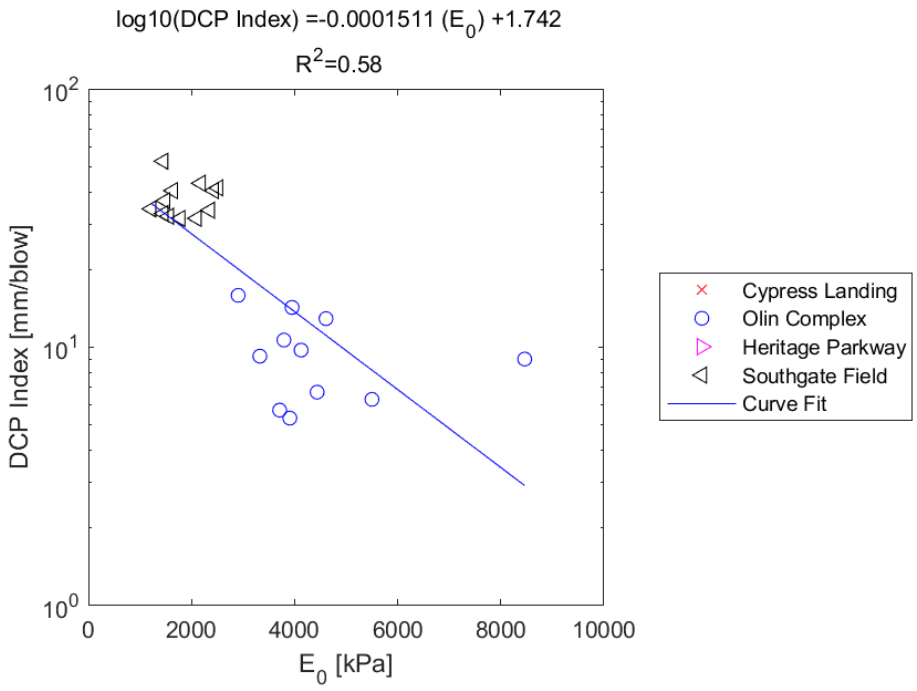

Figure E.241: Linear - Log Model of DCP PI versus E_0 for SDPMT-6 Incremental Tests, All Sites

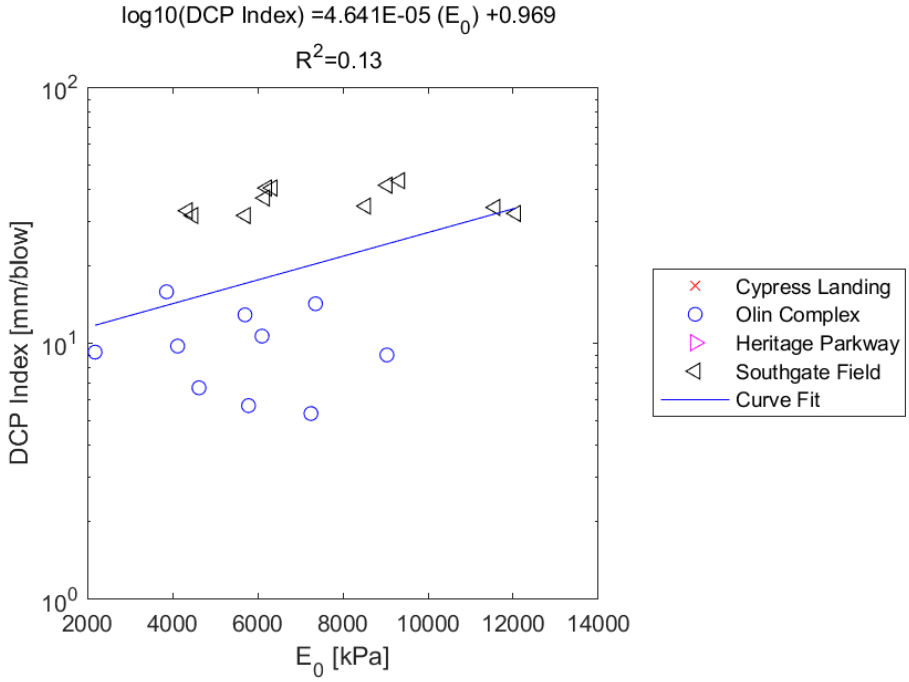

Figure E.242: Linear - Log Model of DCP PI versus E_0 for SDPMT-6 Continuous Tests, All Sites

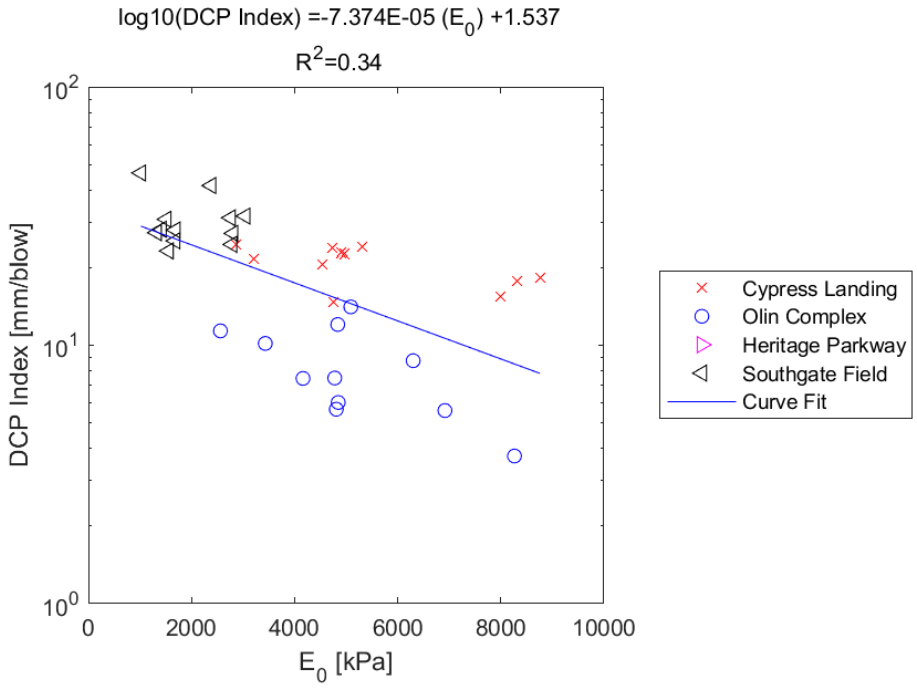

Figure E.243: Linear - Log Model of DCP PI versus E_0 for SDPMT-12 Incremental Tests, All Sites

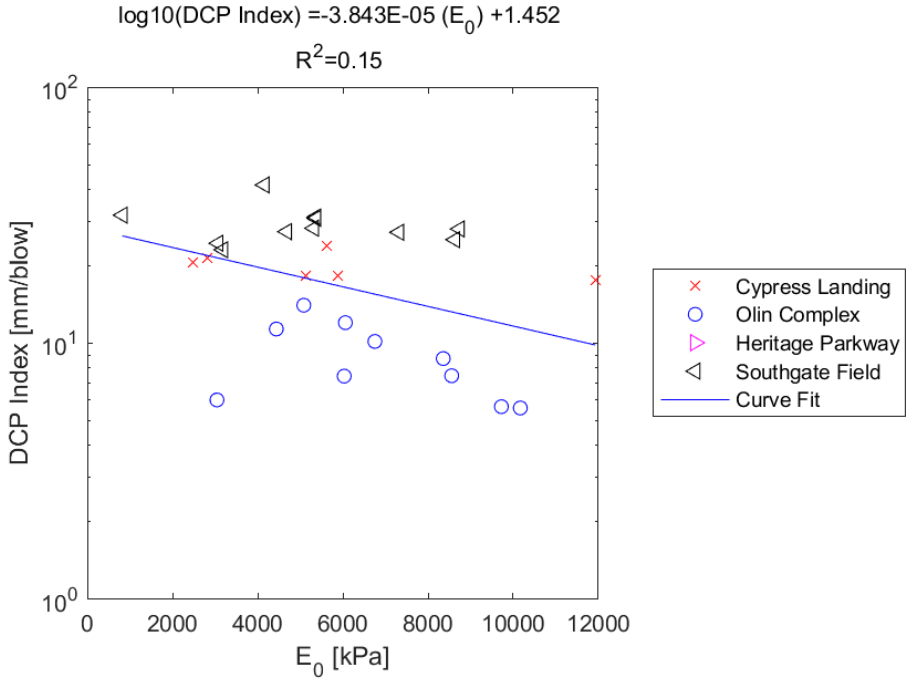

Figure E.244: Linear - Log Model of DCP PI versus E_0 for SDPMT-12 Continuous Tests, All Sites

E.3.14 DCP PI versus $\mathbf{p}_L$

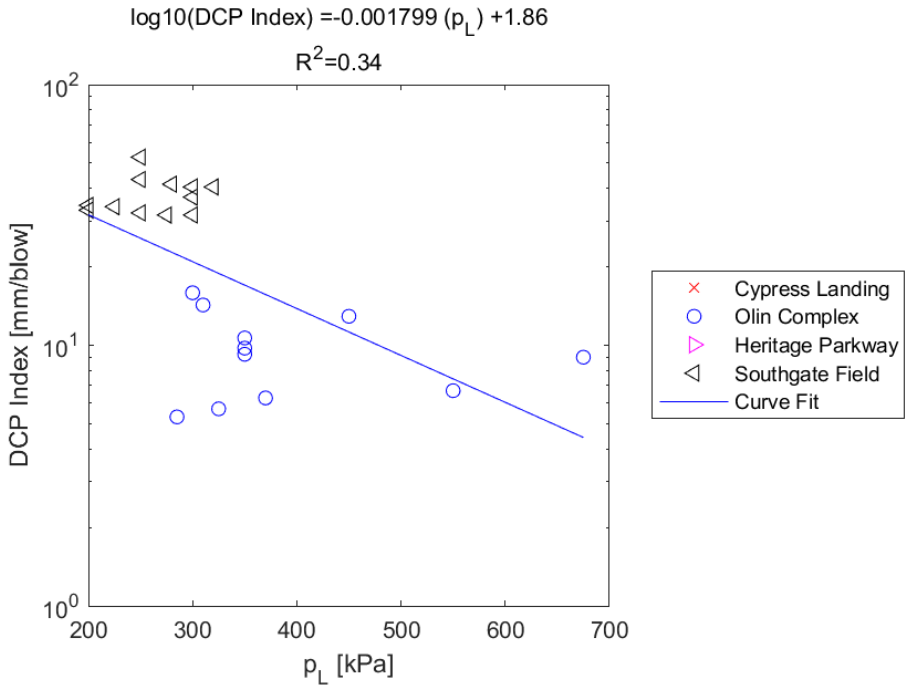

Figure E.245: Linear - Log Model of DCP PI versus p_L for SDPMT-6 Incremental Tests, All Sites

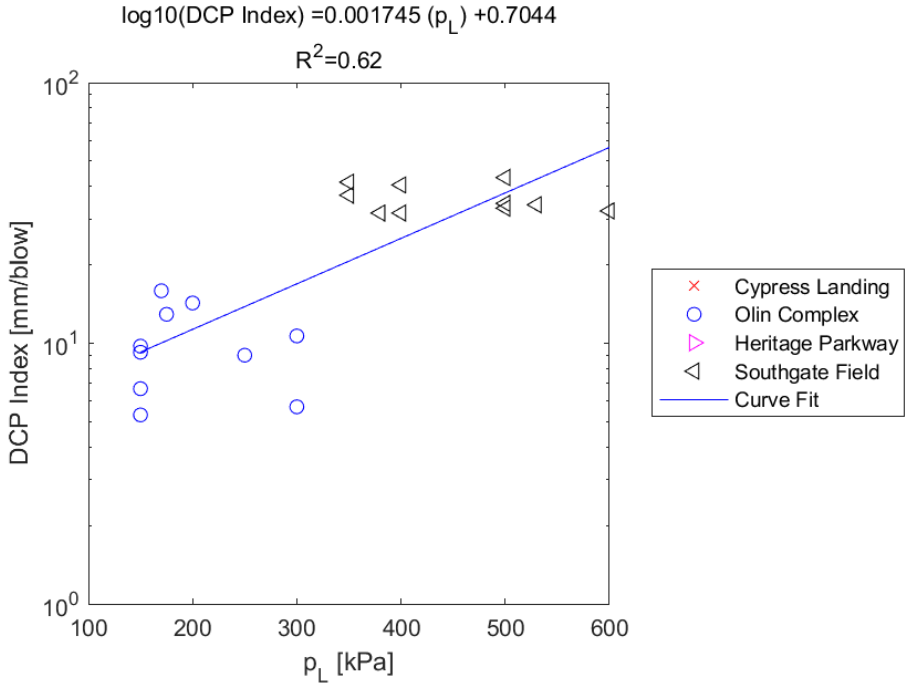

Figure E.246: Linear - Log Model of DCP PI versus p_L for SDPMT-6 Continuous Tests, All Sites

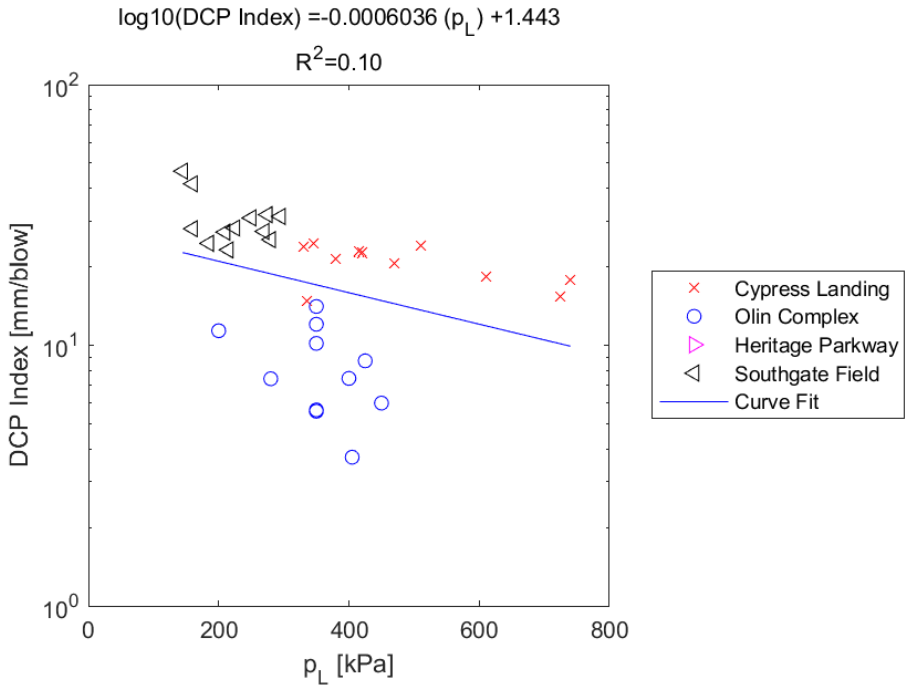

Figure E.247: Linear - Log Model of DCP PI versus p_L for SDPMT-12 Incremental Tests, All Sites

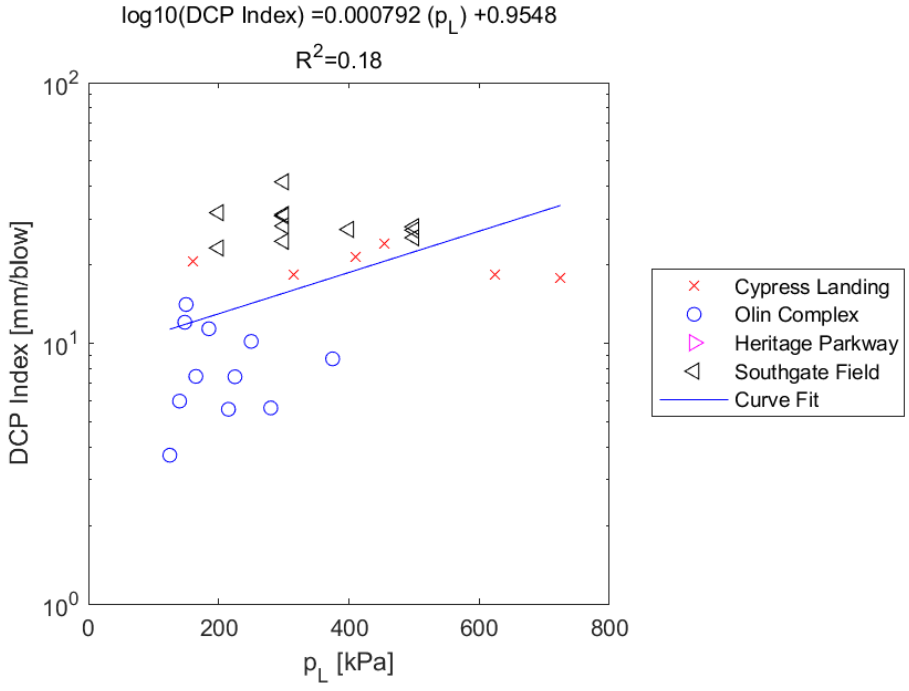

Figure E.248: Linear - Log Model of DCP PI versus p_L for SDPMT-12 Continuous Tests, All Sites

E.3.15 DCP PI versus $\mathbf{p}_0$

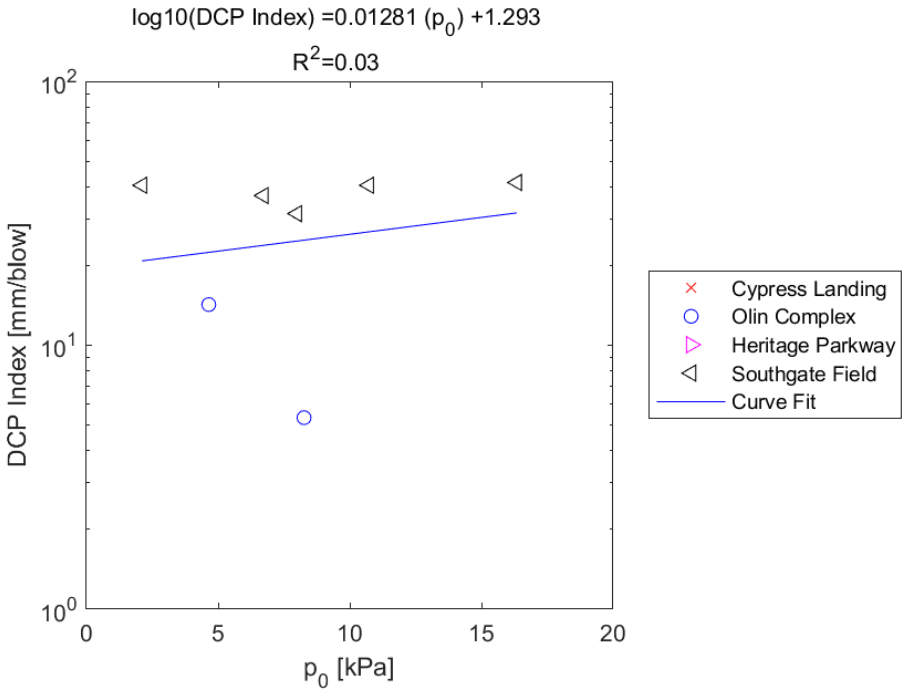

Figure E.249: Linear - Log Model of DCP PI versus p_0 for SDPMT-6 Incremental Tests, All Sites

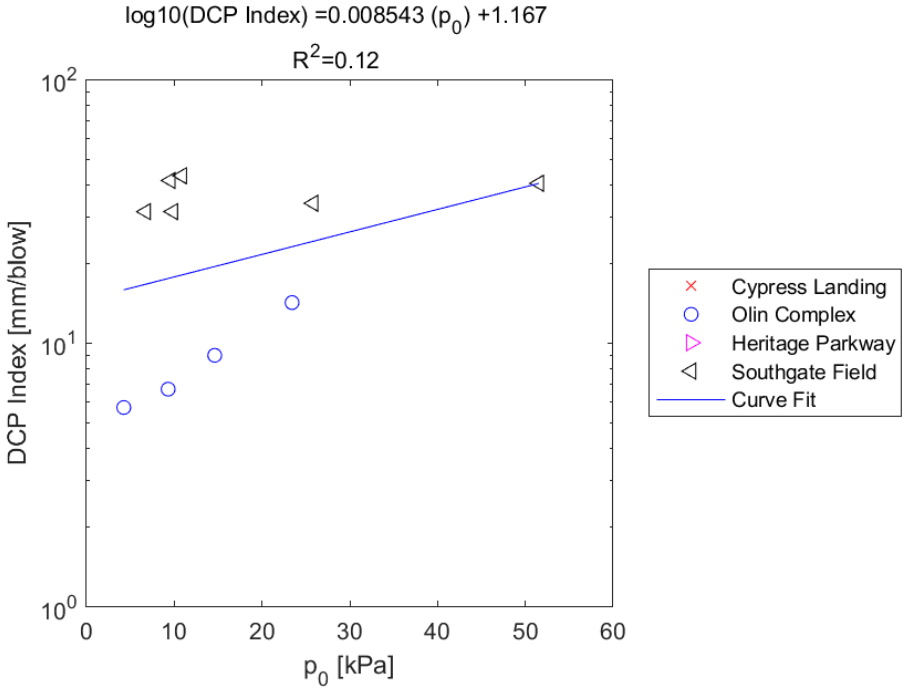

Figure E.250: Linear - Log Model of DCP PI versus p_0 for SDPMT-6 Continuous Tests, All Sites

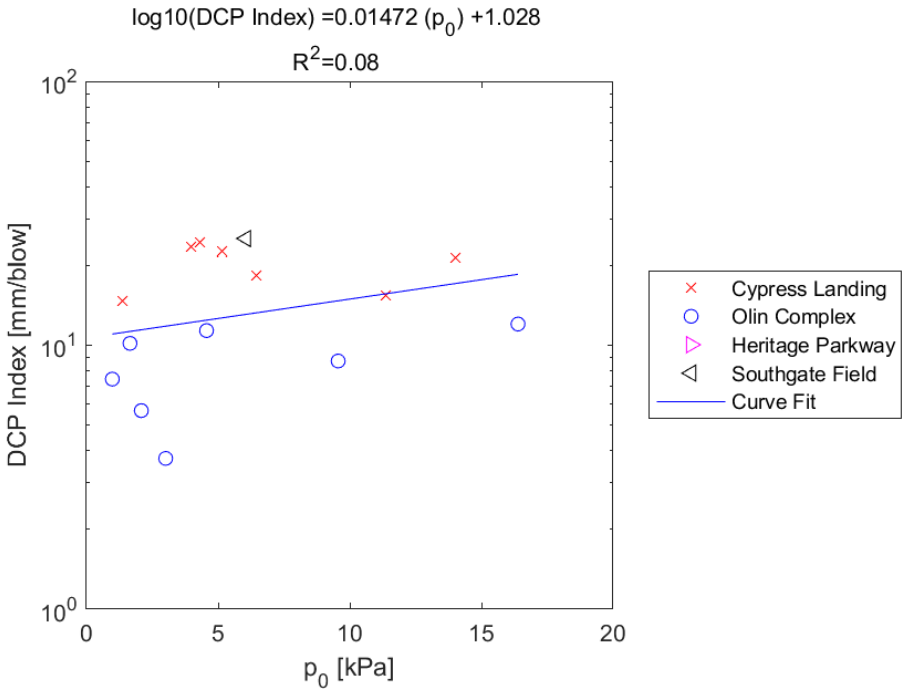

Figure E.251: Linear - Log Model of DCP PI versus p_0 for SDPMT-12 Incremental Tests, All Sites

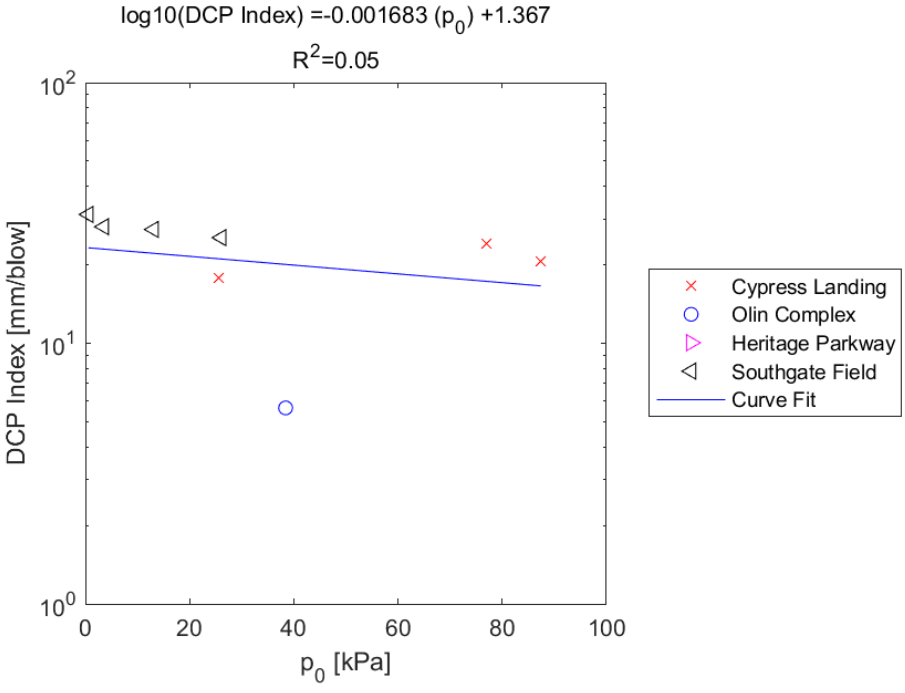

Figure E.252: Linear - Log Model of DCP PI versus p_0 for SDPMT-12 Continuous Tests, All Sites

E.3.16 $\mathbf{E}_{d,zorn}$ versus $\mathbf{E}_0$

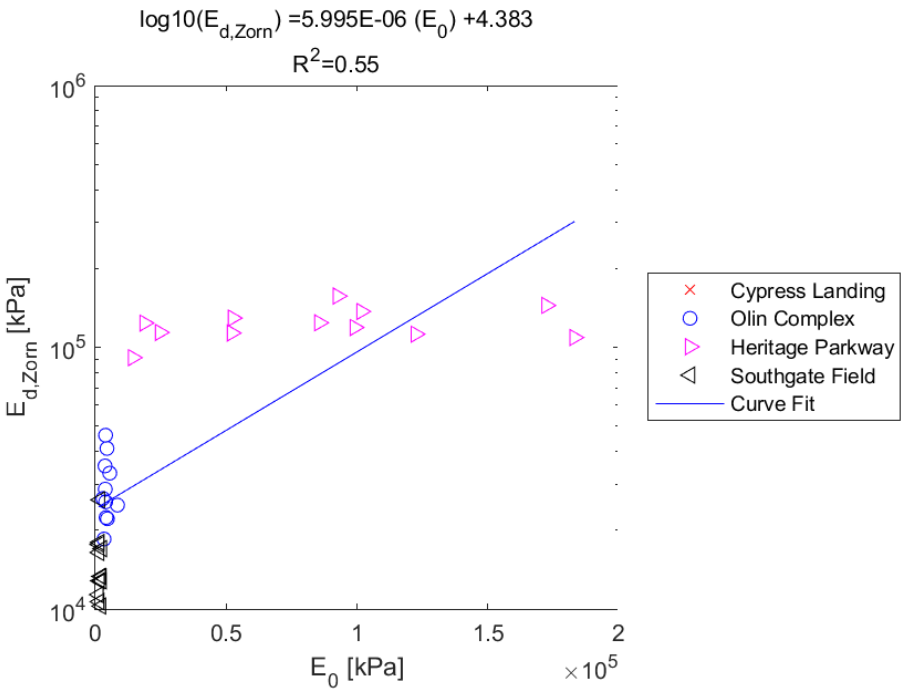

Figure E.253: Linear - Log Model of $E_{d,zorn}$ versus E_0 for SDPMT-6 Incremental Tests, All Sites

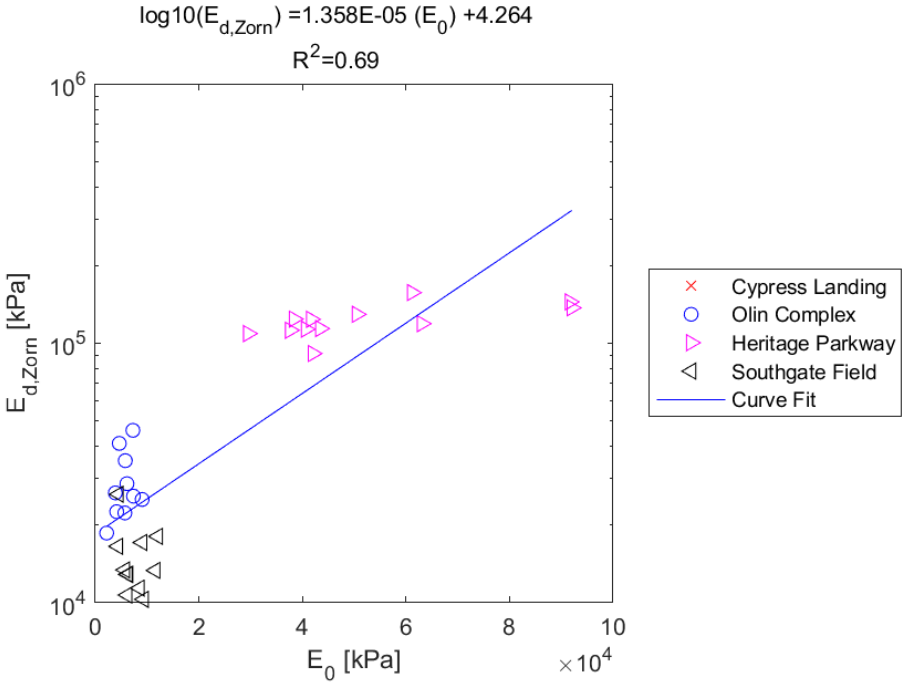

Figure E.254: Linear - Log Model of $E_{d,zorn}$ versus E_0 for SDPMT-6 Continuous Tests, All Sites

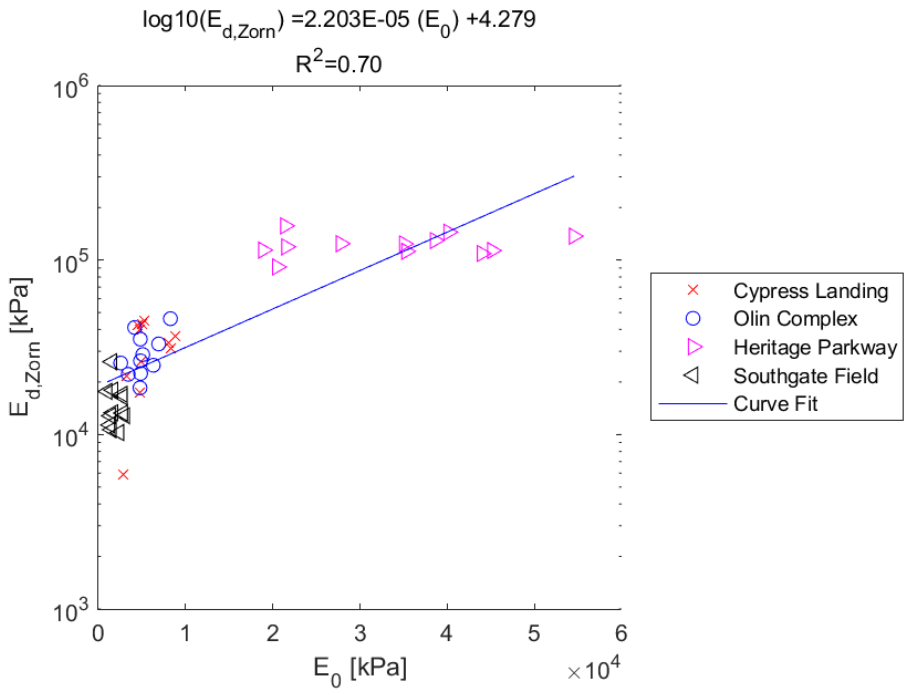

Figure E.255: Linear - Log Model of $E_{d,zorn}$ versus E_0 for SDPMT-12 Incremental Tests, All Sites

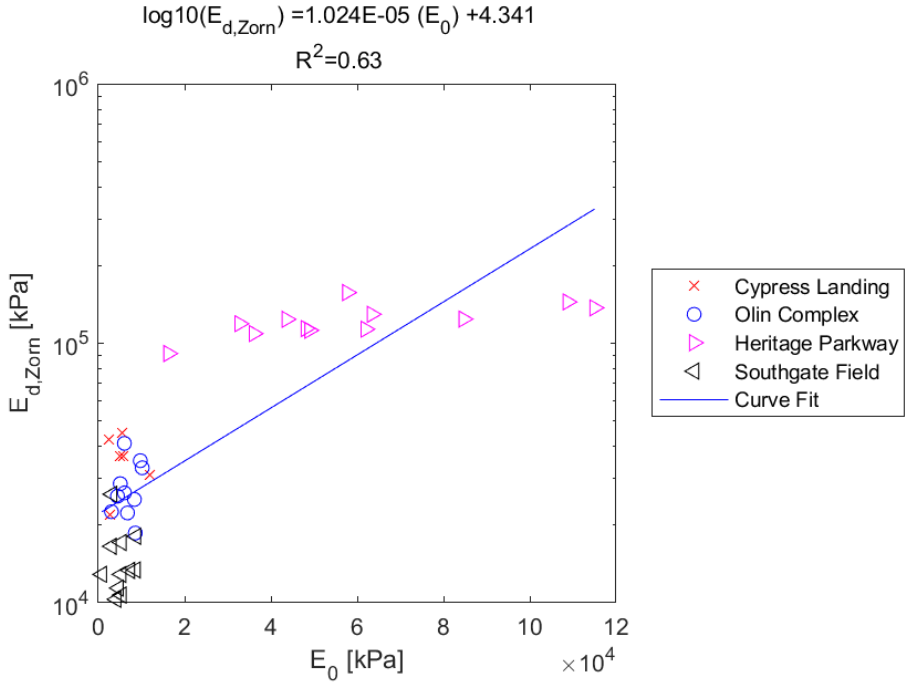

Figure E.256: Linear - Log Model of $E_{d,zorn}$ versus E_0 for SDPMT-12 Continuous Tests, All Sites

E.3.17 $\mathbf{E}_{d,zorn}$ versus $\mathbf{p}_L$

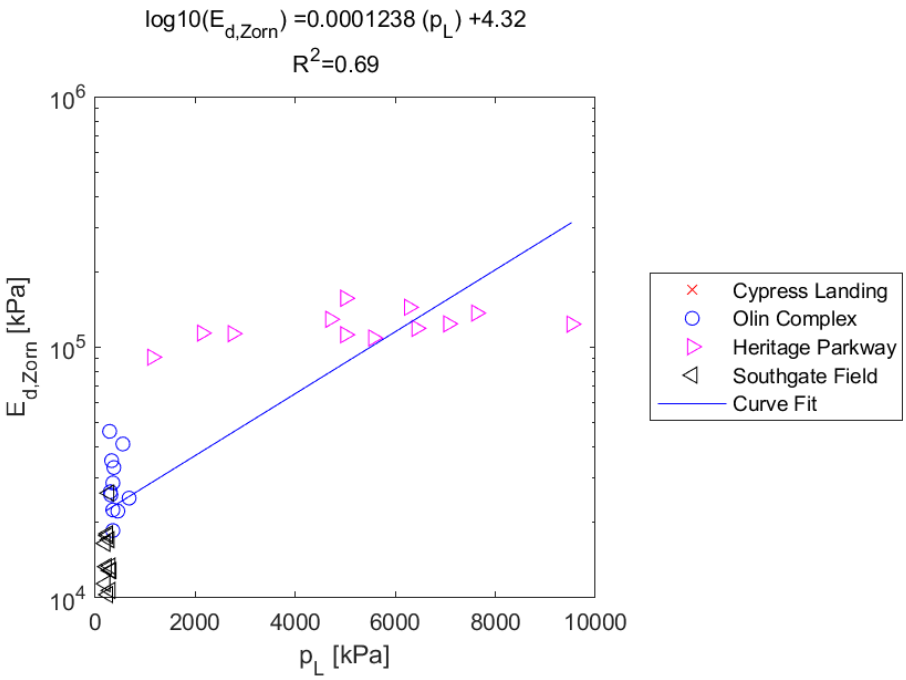

Figure E.257: Linear - Log Model of $E_{d,zorn}$ versus p_L for SDPMT-6 Incremental Tests, All Sites

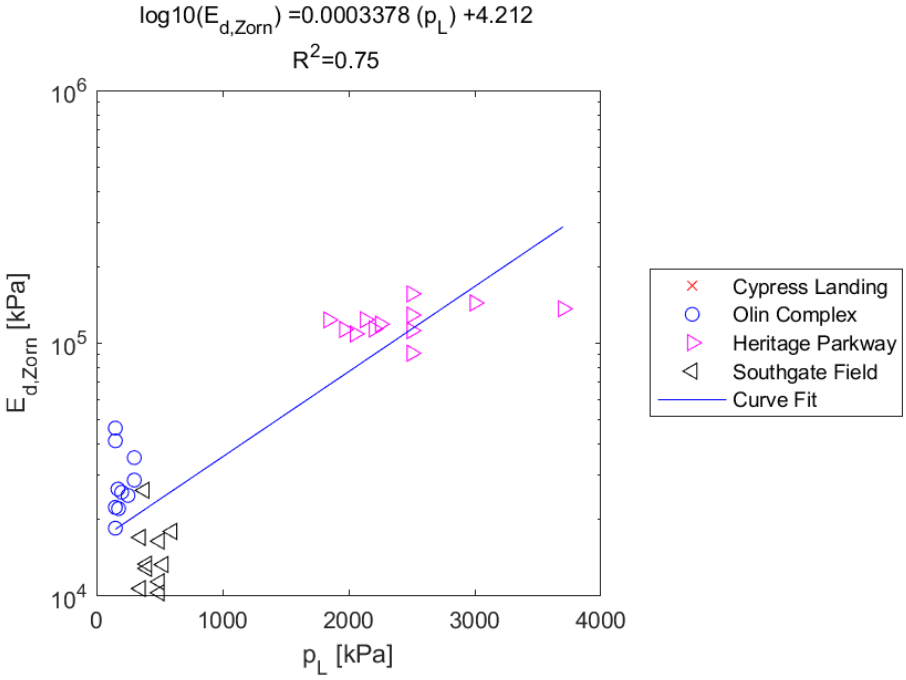

Figure E.258: Linear - Log Model of $E_{d,zorn}$ versus p_L for SDPMT-6 Continuous Tests, All Sites

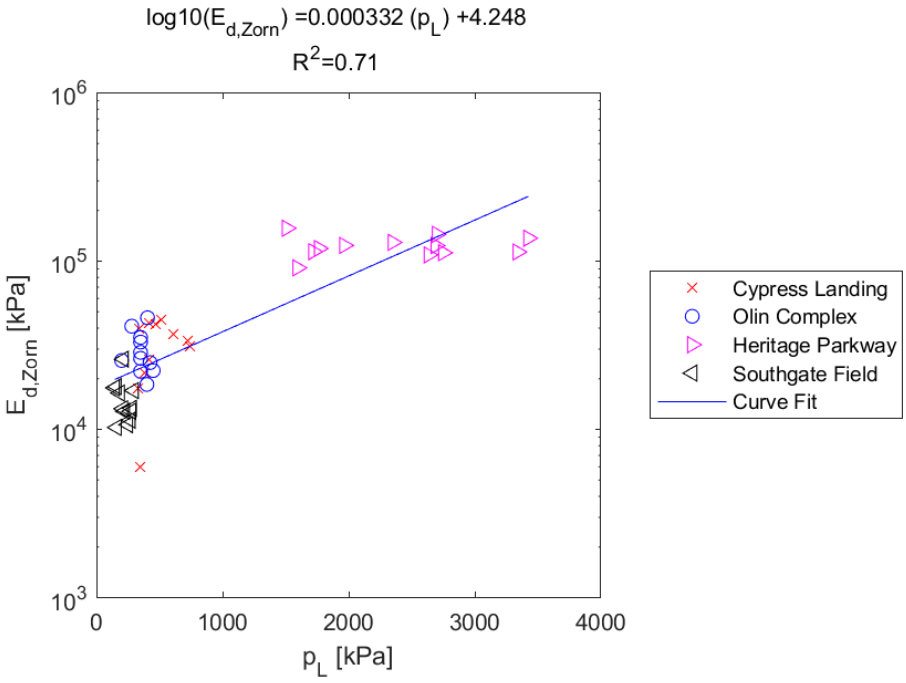

Figure E.259: Linear - Log Model of $E_{d,zorn}$ versus p_L for SDPMT-12 Incremental Tests, All Sites

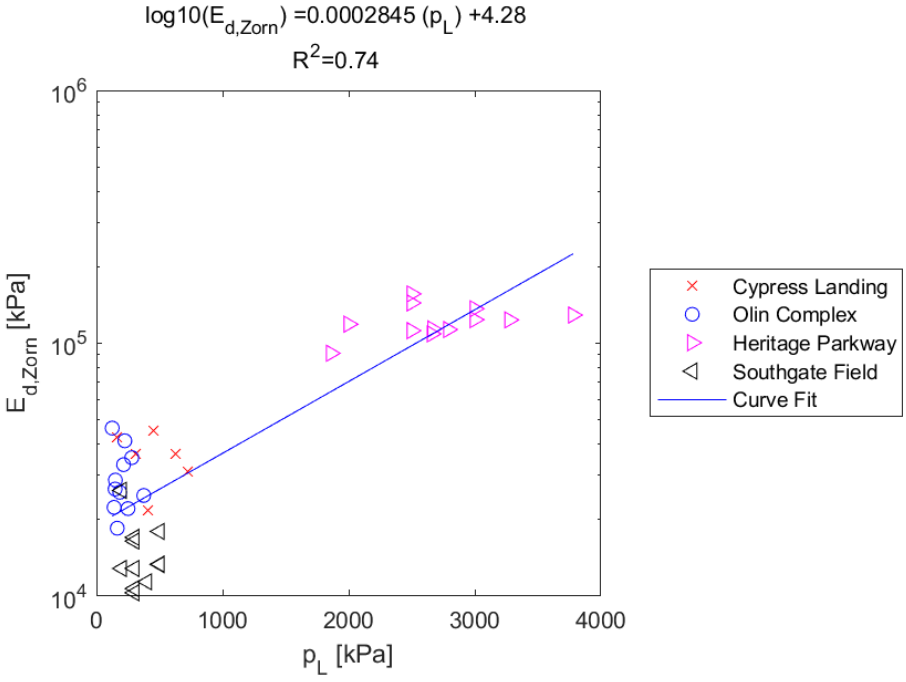

Figure E.260: Linear - Log Model of $E_{d,zorn}$ versus p_L for SDPMT-12 Continuous Tests, All Sites

E.3.18 $\mathbf{E}_{d,zorn}$ versus $\mathbf{p}_0$

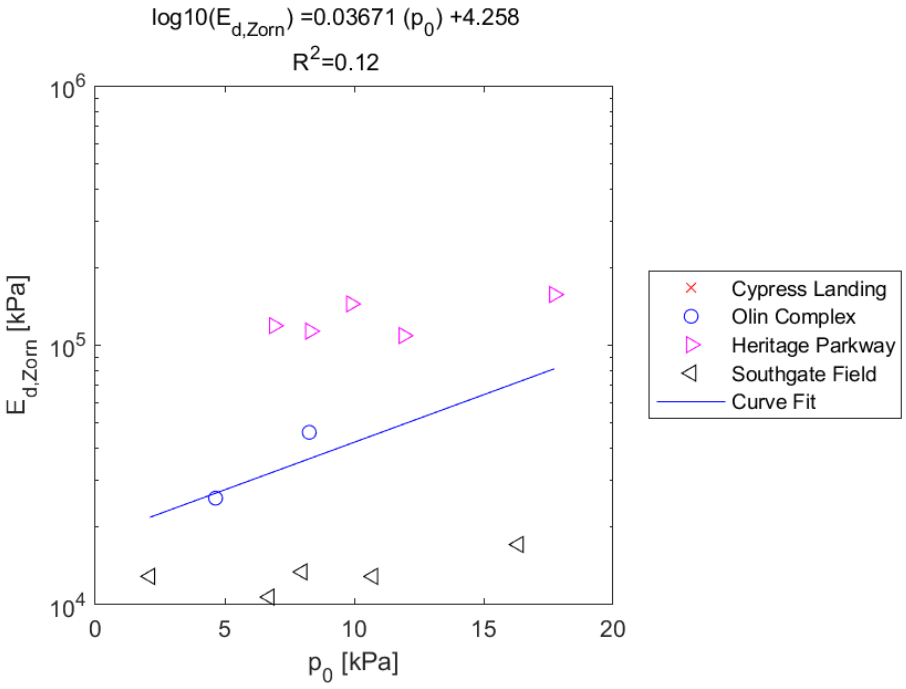

Figure E.261: Linear - Log Model of $E_{d,zorn}$ versus p_0 for SDPMT-6 Incremental Tests, All Sites

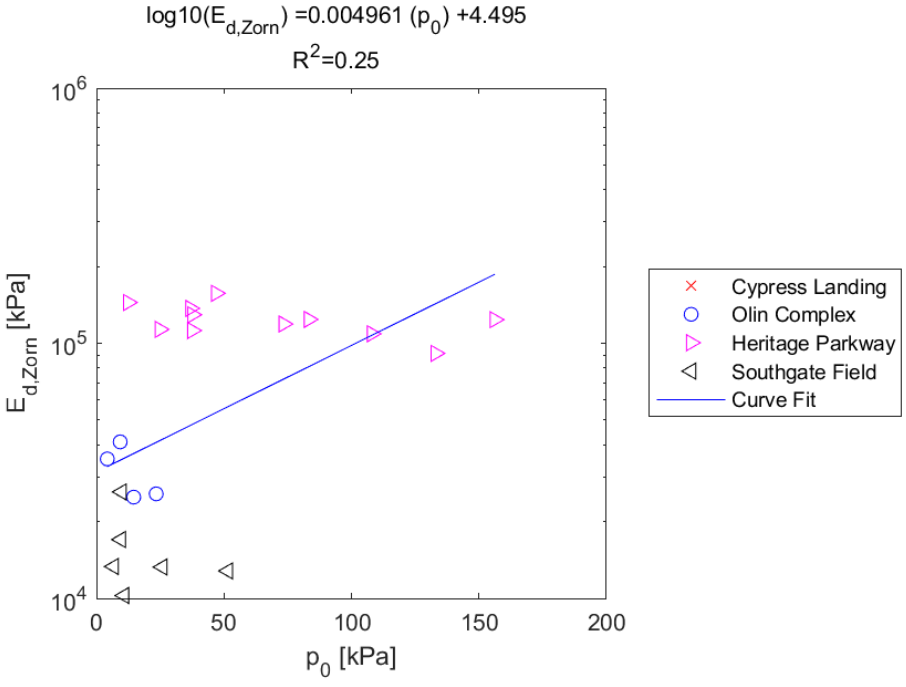

Figure E.262: Linear - Log Model of $E_{d,zorn}$ versus p_0 for SDPMT-6 Continuous Tests, All Sites

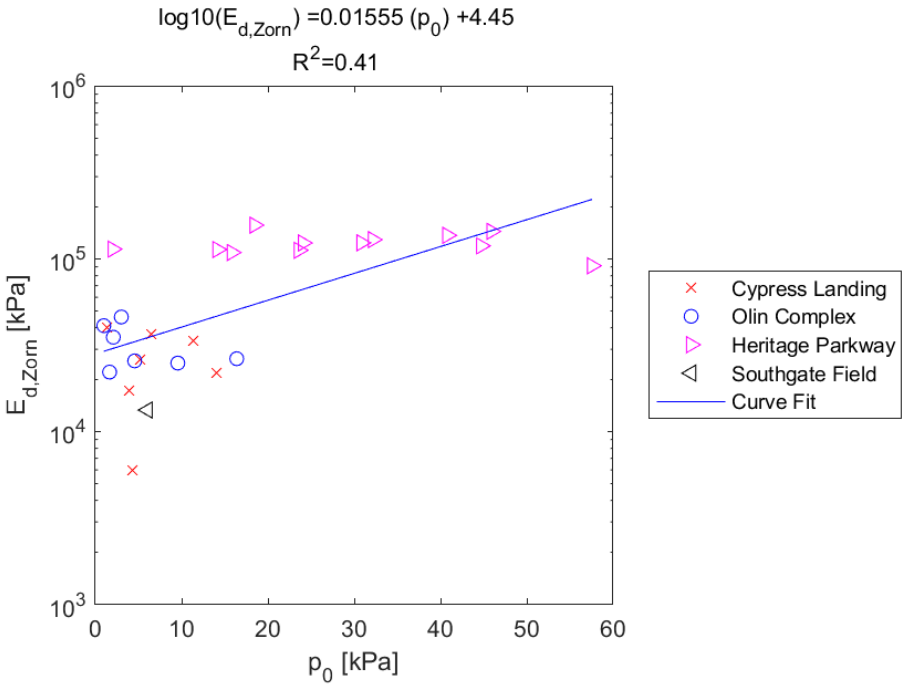

Figure E.263: Linear - Log Model of $E_{d,zorn}$ versus p_0 for SDPMT-12 Incremental Tests, All Sites

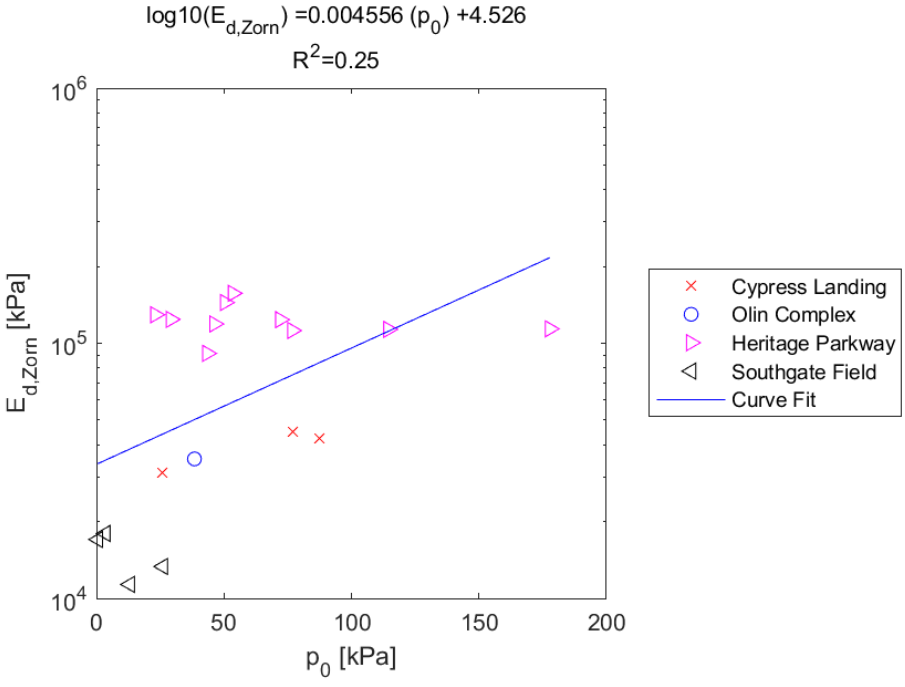

Figure E.264: Linear - Log Model of $E_{d,zorn}$ versus p_0 for SDPMT-12 Continuous Tests, All Sites

E.3.19 $\mathbf{E}_{0,Dynatest}$ versus $\mathbf{E}_0$

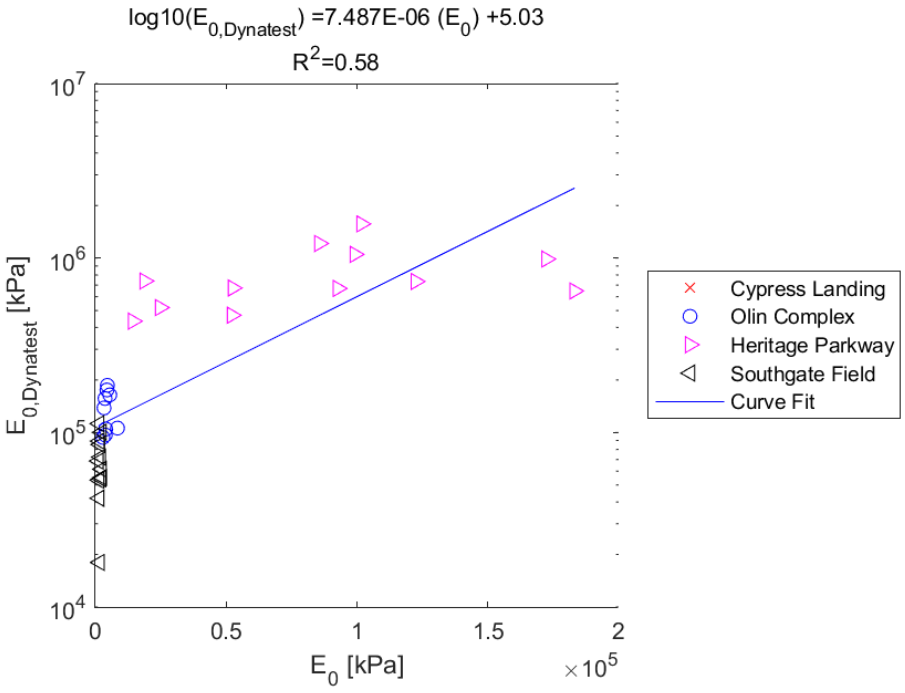

Figure E.265: Linear - Log Model of $E_{0,Dynatest}$ versus E_0 for SDPMT-6 Incremental Tests, All Sites

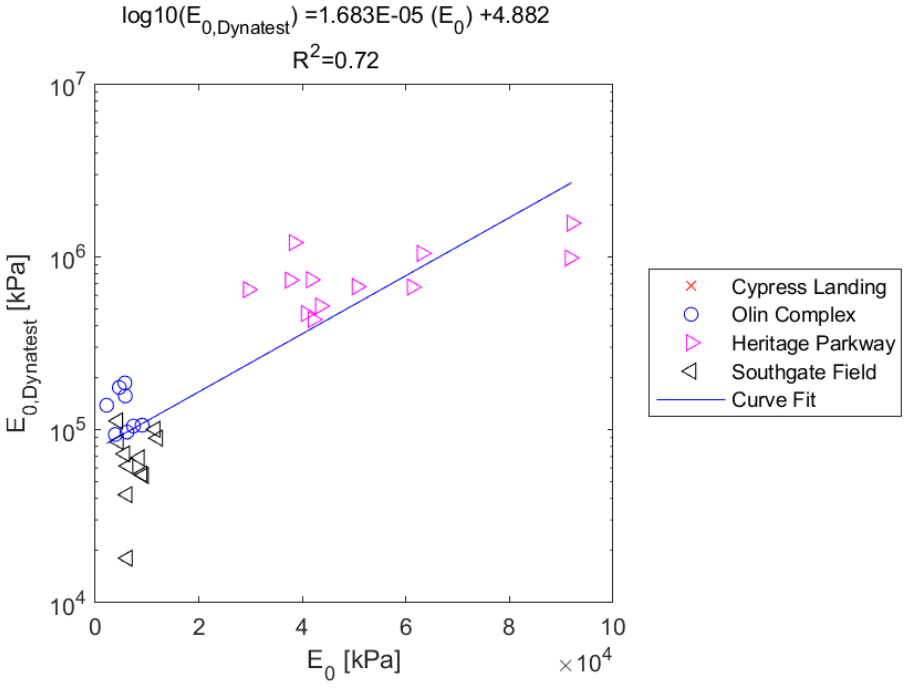

Figure E.266: Linear - Log Model of $E_{0,Dynatest}$ versus E_0 for SDPMT-6 Continuous Tests, All Sites

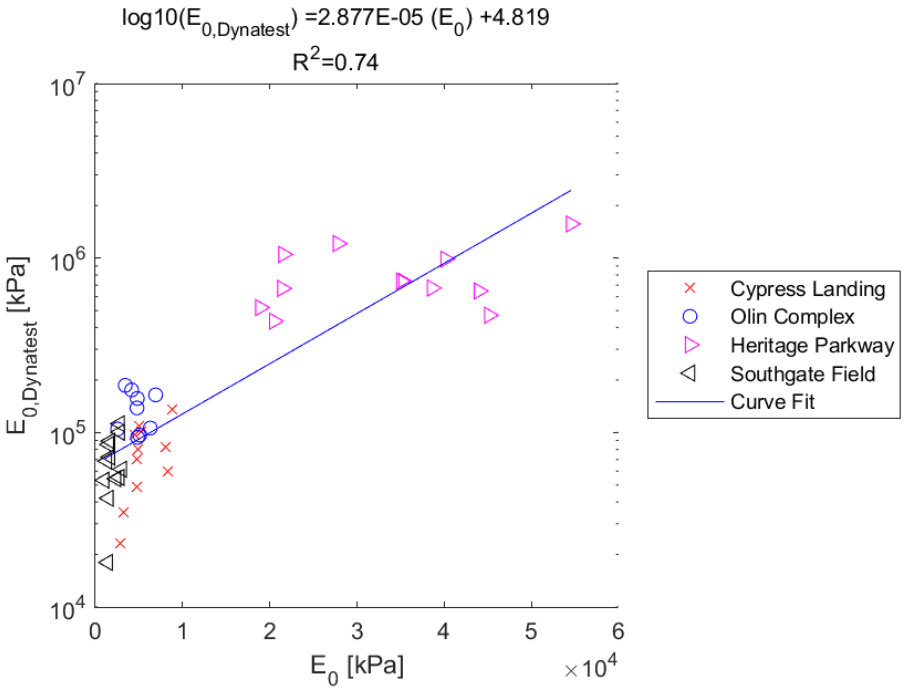

Figure E.267: Linear - Log Model of $E_{0,Dynatest}$ versus E_0 for SDPMT-12 Incremental Tests, All Sites

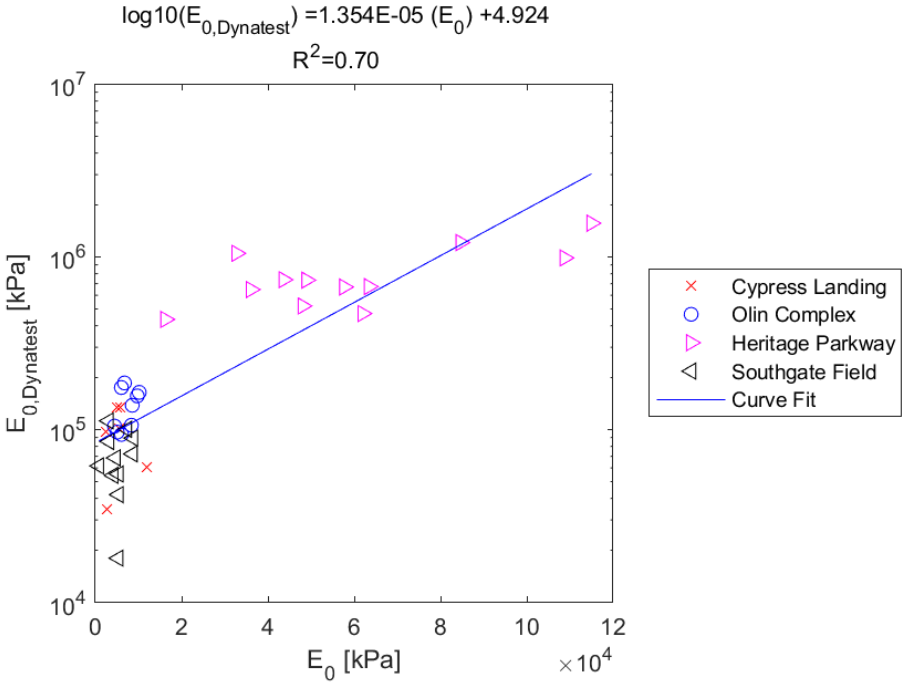

Figure E.268: Linear - Log Model of $E_{0,Dynatest}$ versus E_0 for SDPMT-12 Continuous Tests, All Sites

E.3.20 $\mathbf{E}_{0,Dynatest}$ versus $\mathbf{p}_L$

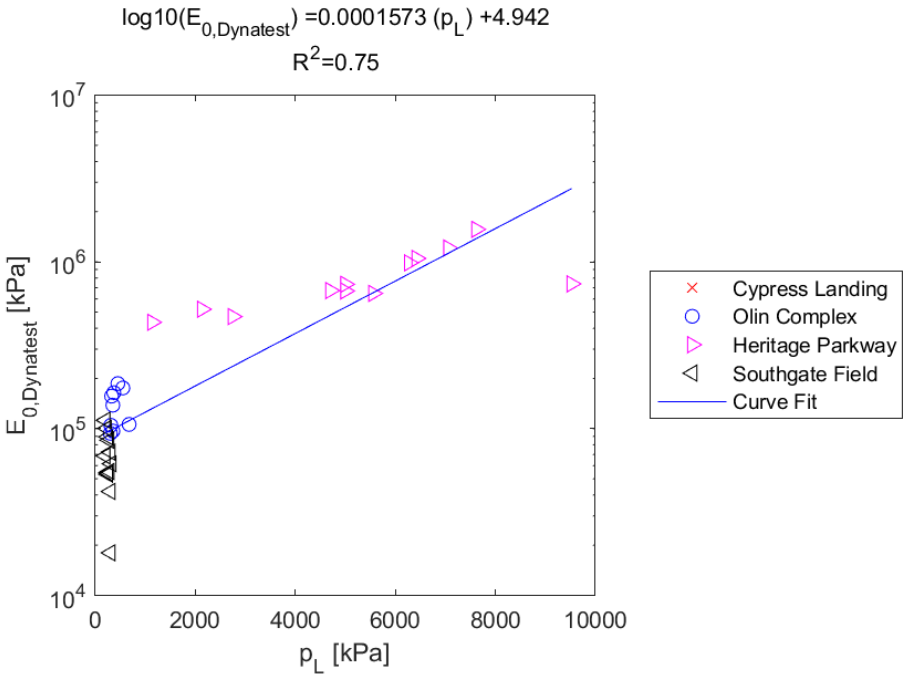

Figure E.269: Linear - Log Model of $E_{0,Dynatest}$ versus p_L for SDPMT-6 Incremental Tests, All Sites

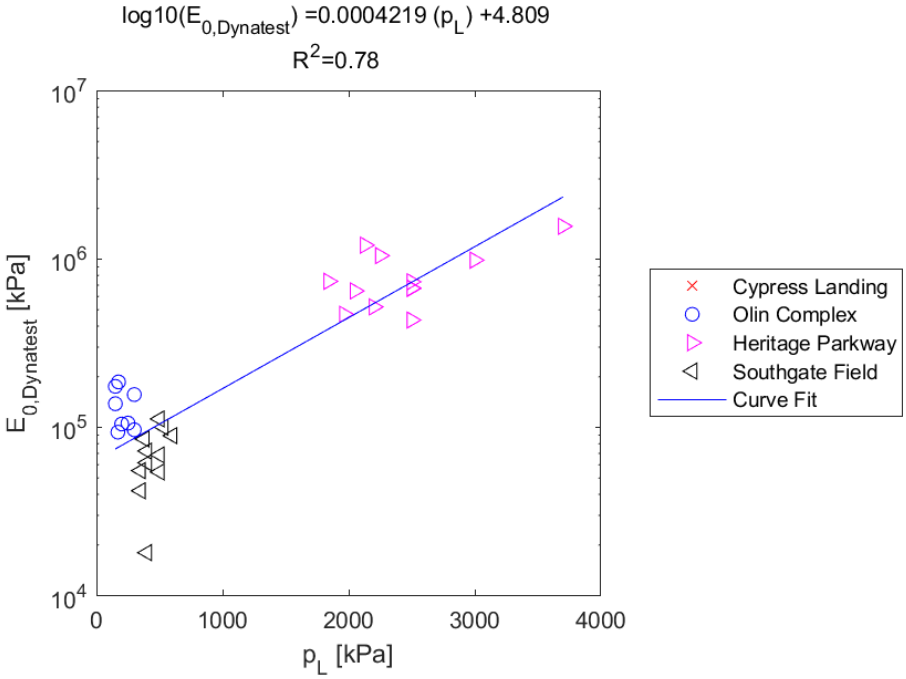

Figure E.270: Linear - Log Model of $E_{0,Dynatest}$ versus p_L for SDPMT-6 Continuous Tests, All Sites

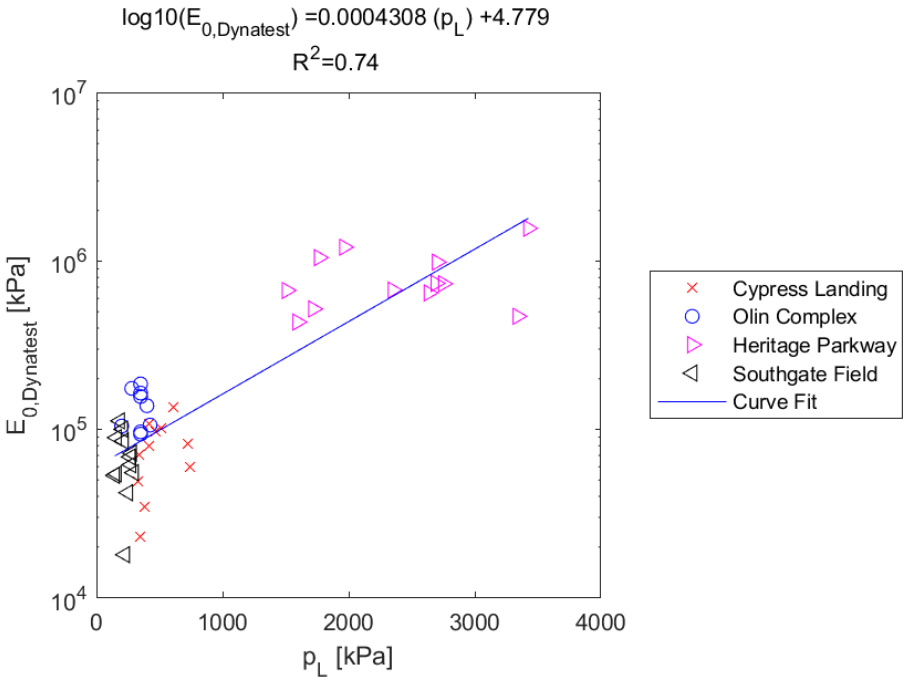

Figure E.271: Linear - Log Model of $E_{0,Dynatest}$ versus p_L for SDPMT-12 Incremental Tests, All Sites

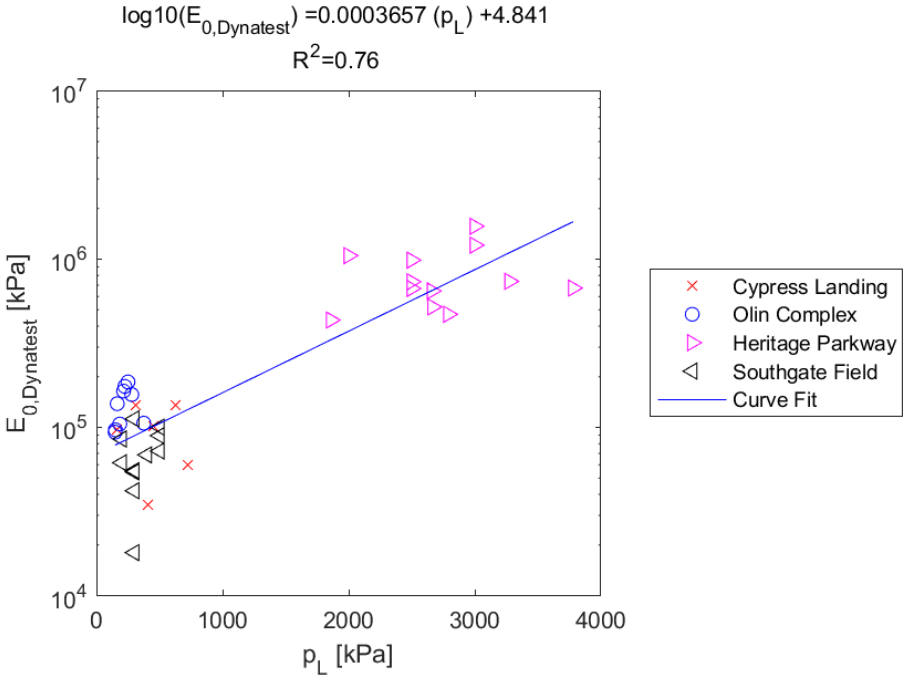

Figure E.272: Linear - Log Model of $E_{0,Dynatest}$ versus p_L for SDPMT-12 Continuous Tests, All Sites

E.3.21 $\mathbf{E}_{0,Dynatest}$ versus $\mathbf{p}_0$

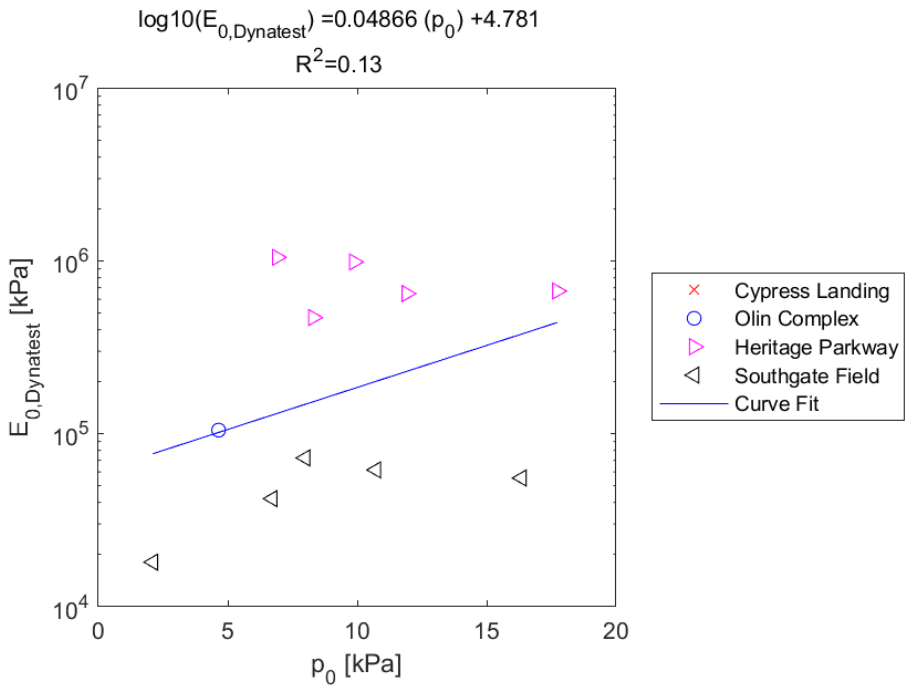

Figure E.273: Linear - Log Model of $E_{0,Dynatest}$ versus p_0 for SDPMT-6 Incremental Tests, All Sites

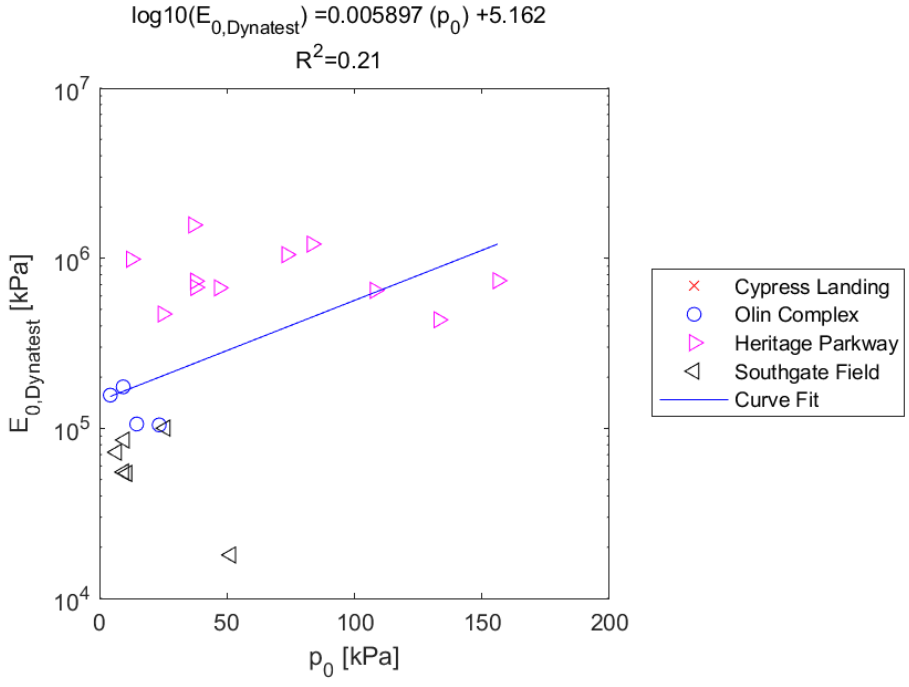

Figure E.274: Linear - Log Model of $E_{0,Dynatest}$ versus p_0 for SDPMT-6 Continuous Tests, All Sites

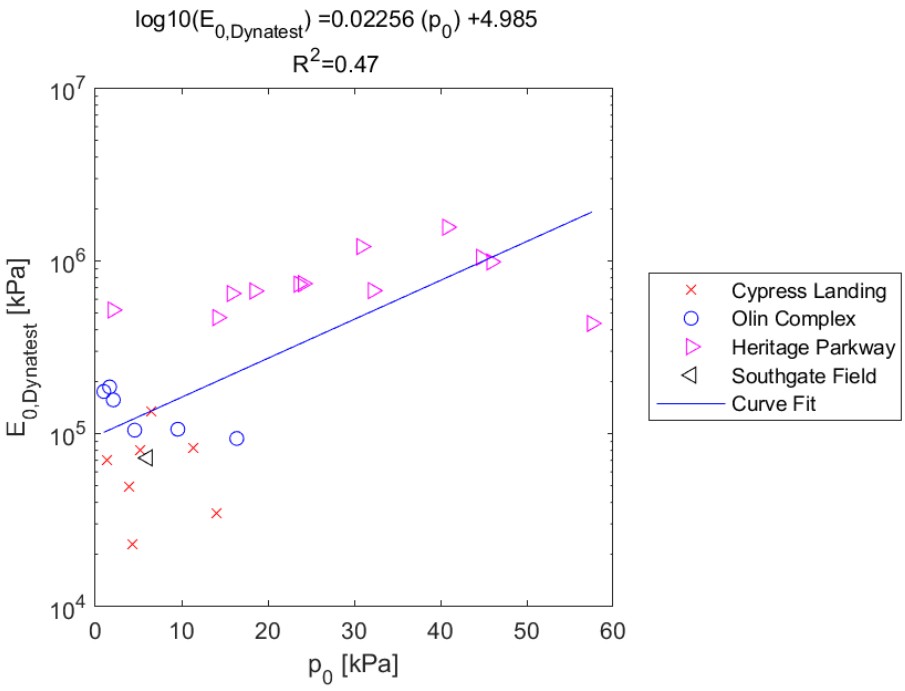

Figure E.275: Linear - Log Model of $E_{0,Dynatest}$ versus p_0 for SDPMT-12 Incremental Tests, All Sites

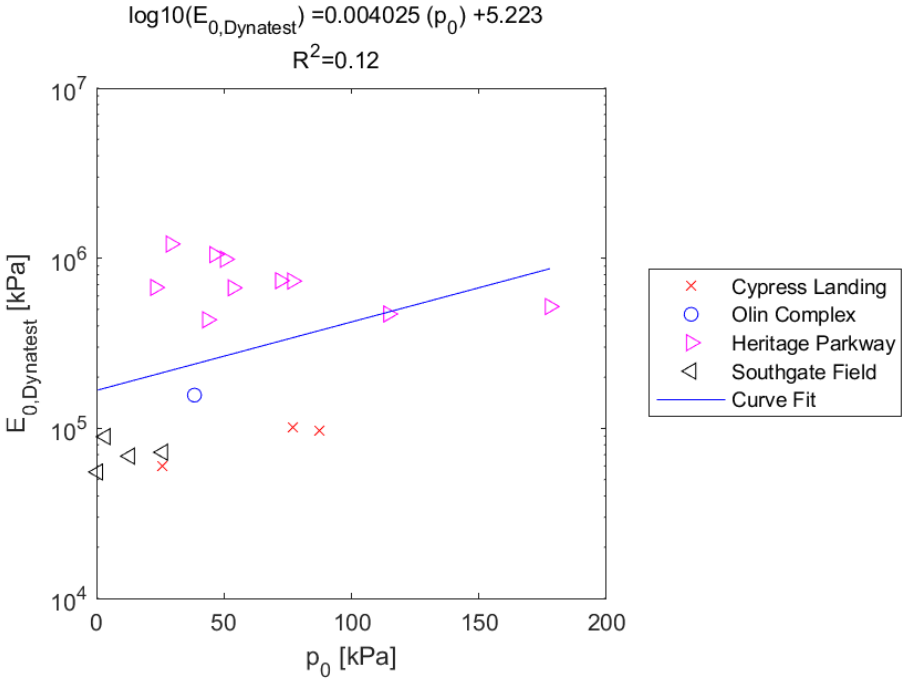

Figure E.276: Linear - Log Model of $E_{0,Dynatest}$ versus p_0 for SDPMT-12 Continuous Tests, All Sites

E.3.22 CIV versus E_0

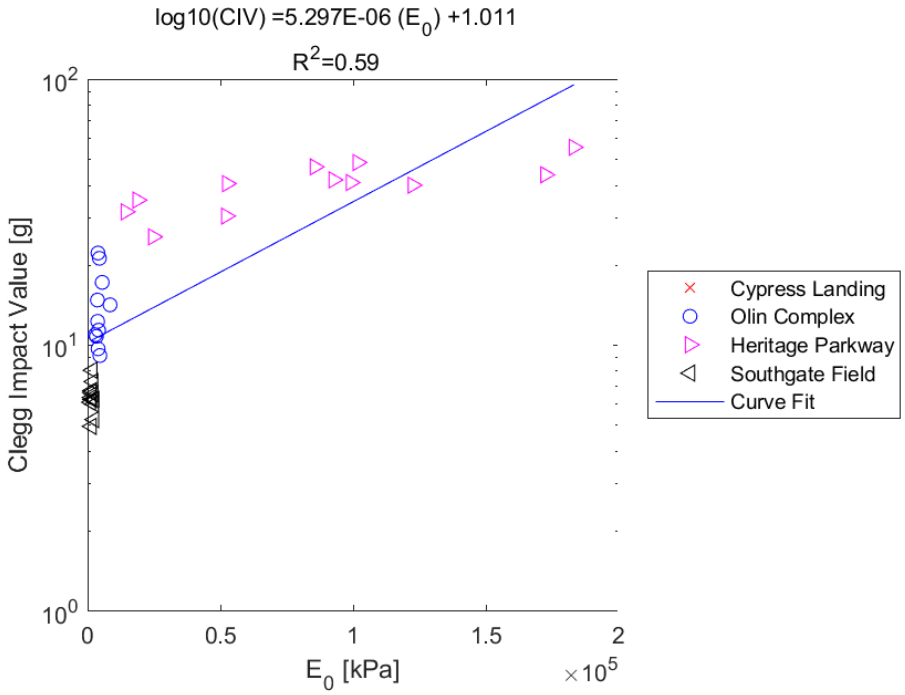

Figure E.277: Linear - Log Model of CIV versus E_0 for SDPMT-6 Incremental Tests, All Sites

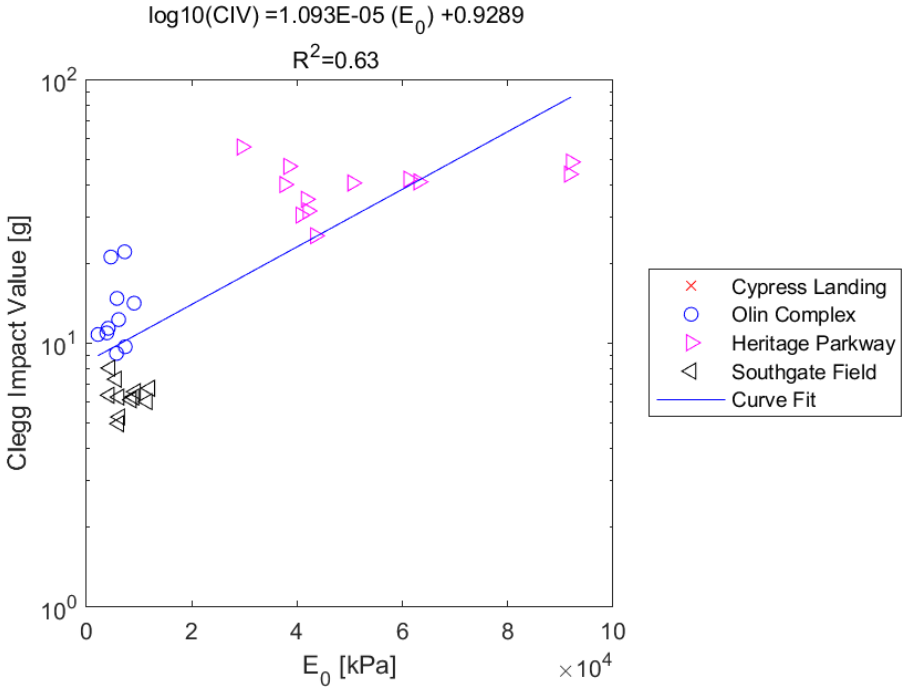

Figure E.278: Linear - Log Model of CIV versus E_0 for SDPMT-6 Continuous Tests, All Sites

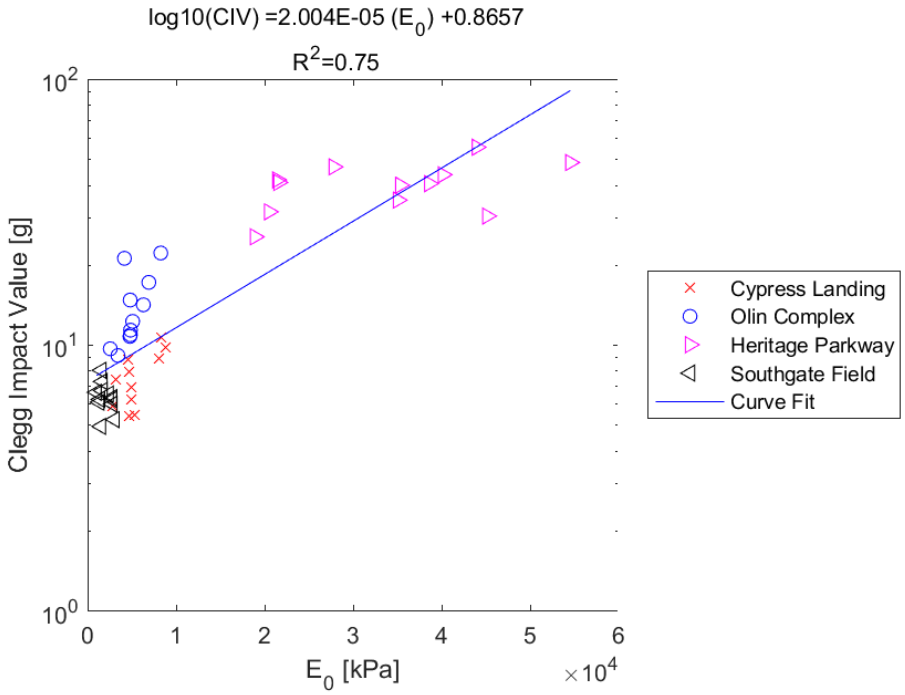

Figure E.279: Linear - Log Model of CIV versus E_0 for SDPMT-12 Incremental Tests, All Sites

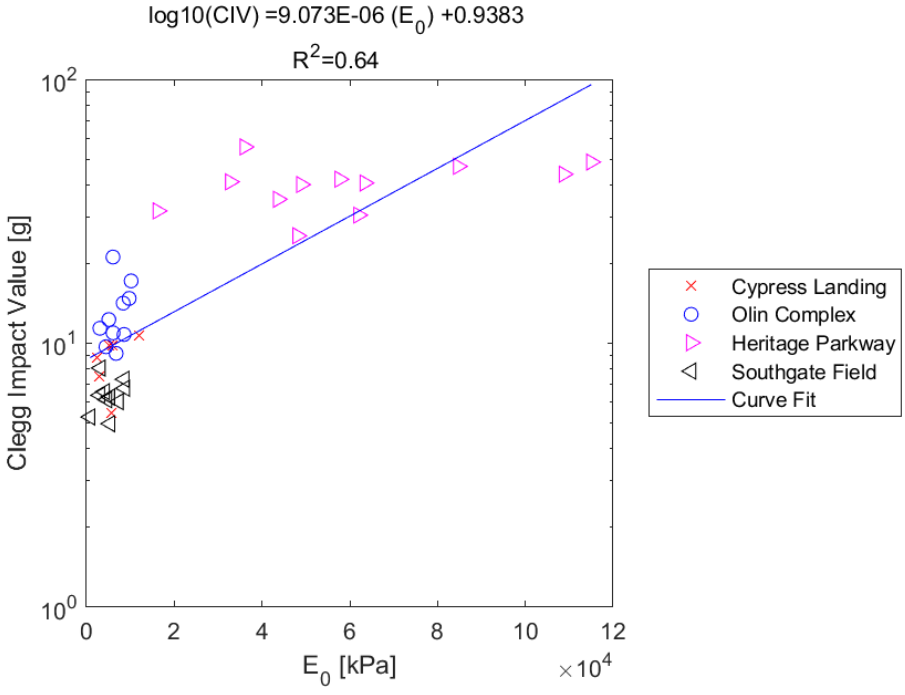

Figure E.280: Linear - Log Model of CIV versus E_0 for SDPMT-12 Continuous Tests, All Sites

E.3.23 CIV versus $\mathbf{p}_L$

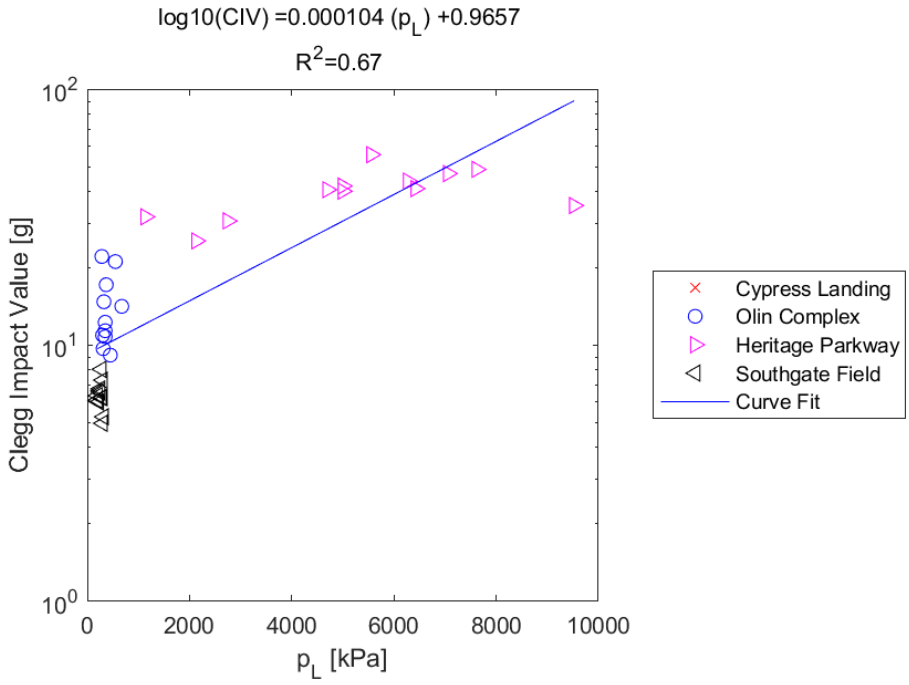

Figure E.281: Linear - Log Model of CIV versus p_L for SDPMT-6 Incremental Tests, All Sites

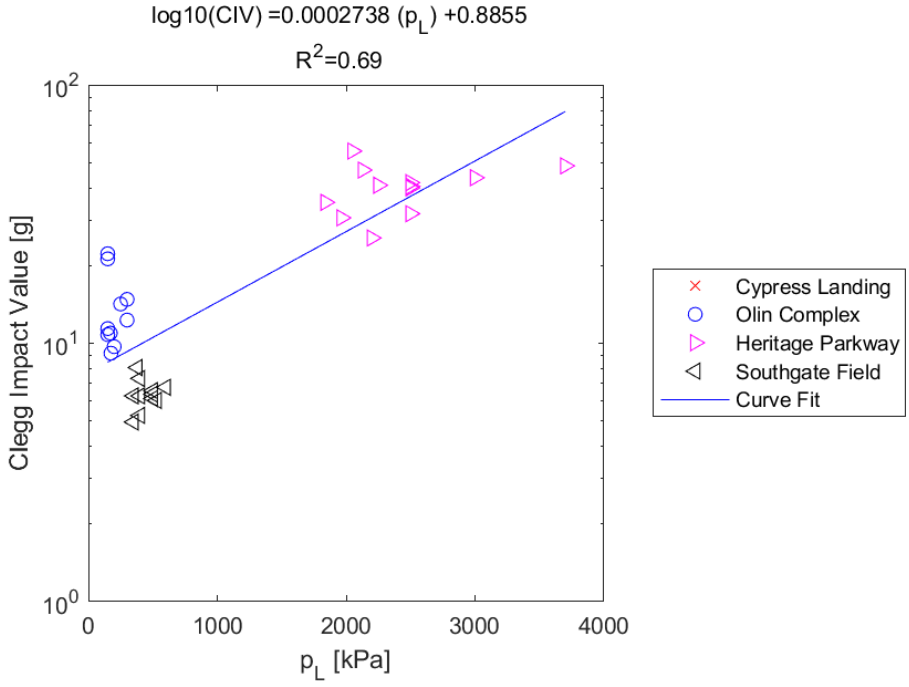

Figure E.282: Linear - Log Model of CIV versus p_L for SDPMT-6 Continuous Tests, All Sites

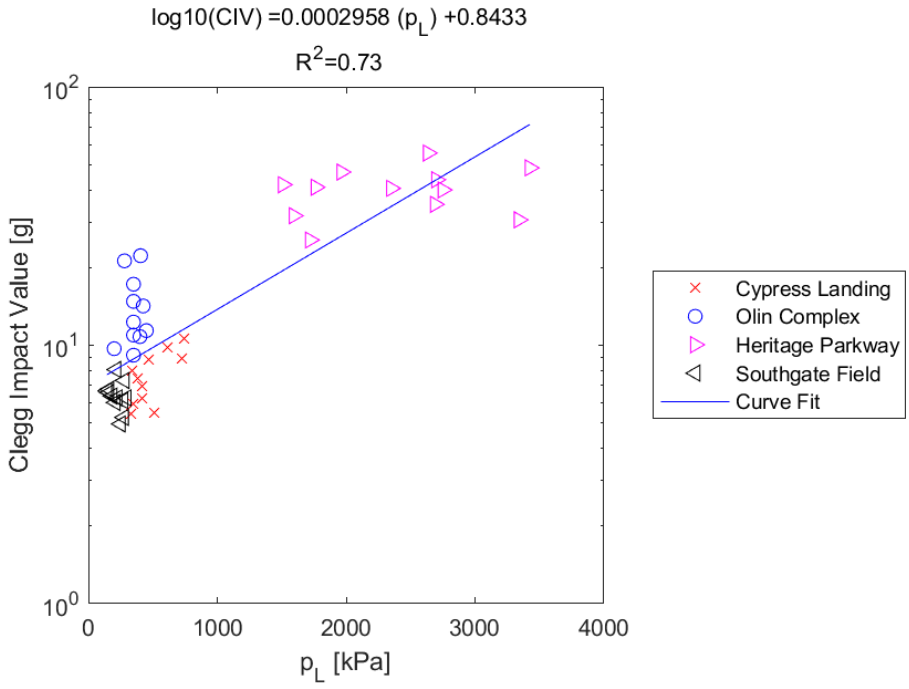

Figure E.283: Linear - Log Model of CIV versus p_L for SDPMT-12 Incremental Tests, All Sites

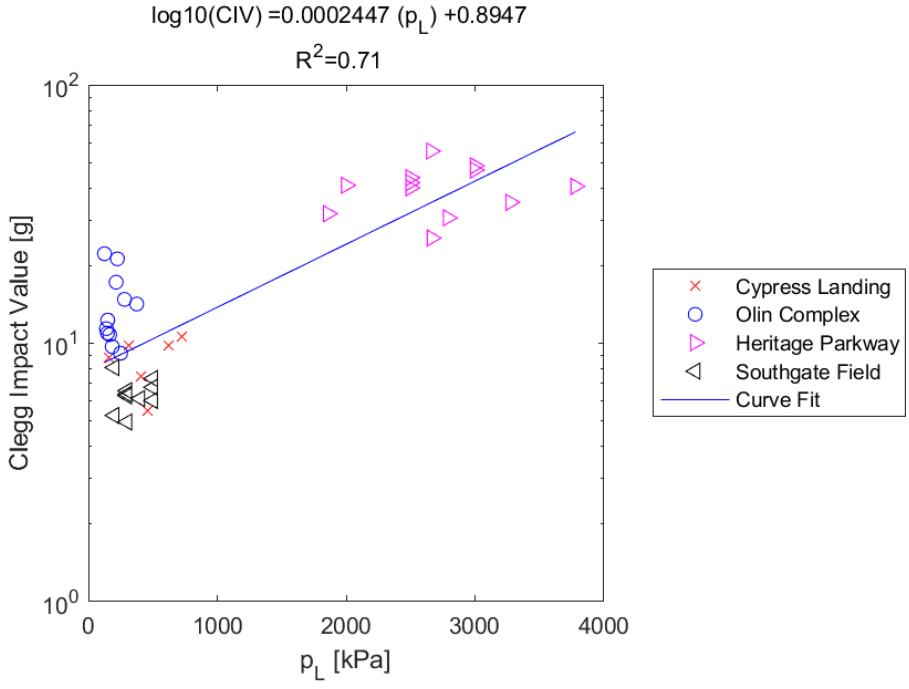

Figure E.284: Linear - Log Model of CIV versus p_L for SDPMT-12 Continuous Tests, All Sites

E.3.24 CIV versus p_0

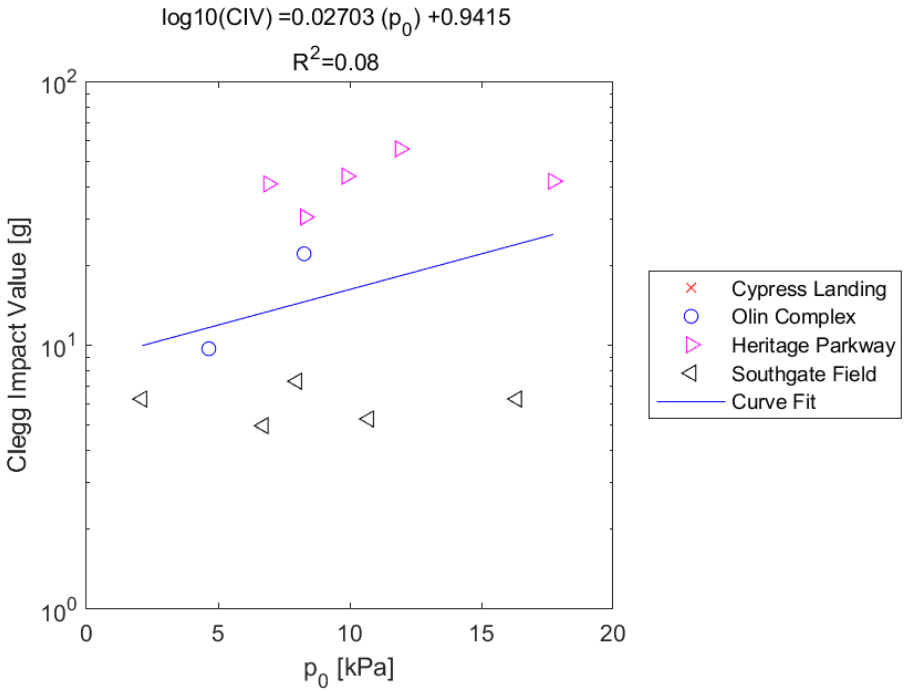

Figure E.285: Linear - Log Model of CIV versus p_0 for SDPMT-6 Incremental Tests, All Sites

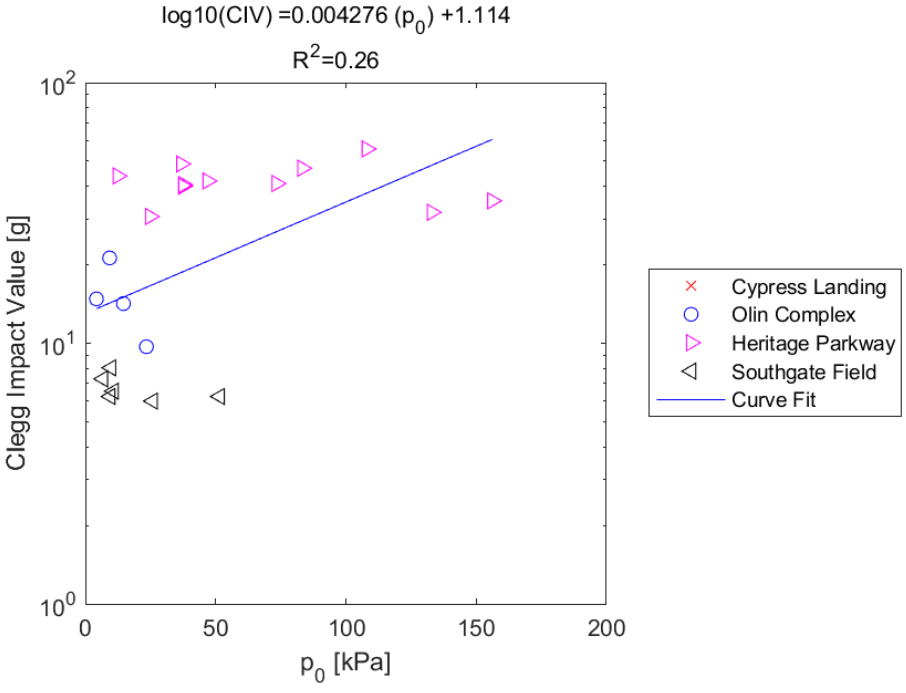

Figure E.286: Linear - Log Model of CIV versus p_0 for SDPMT-6 Continuous Tests, All Sites

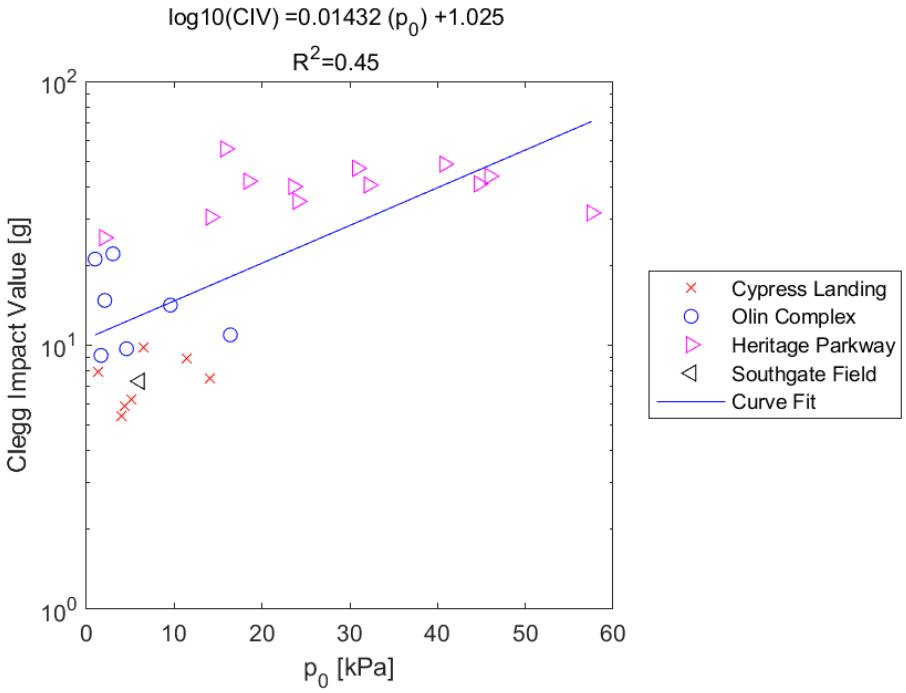

Figure E.287: Linear - Log Model of CIV versus p_0 for SDPMT-12 Incremental Tests, All Sites

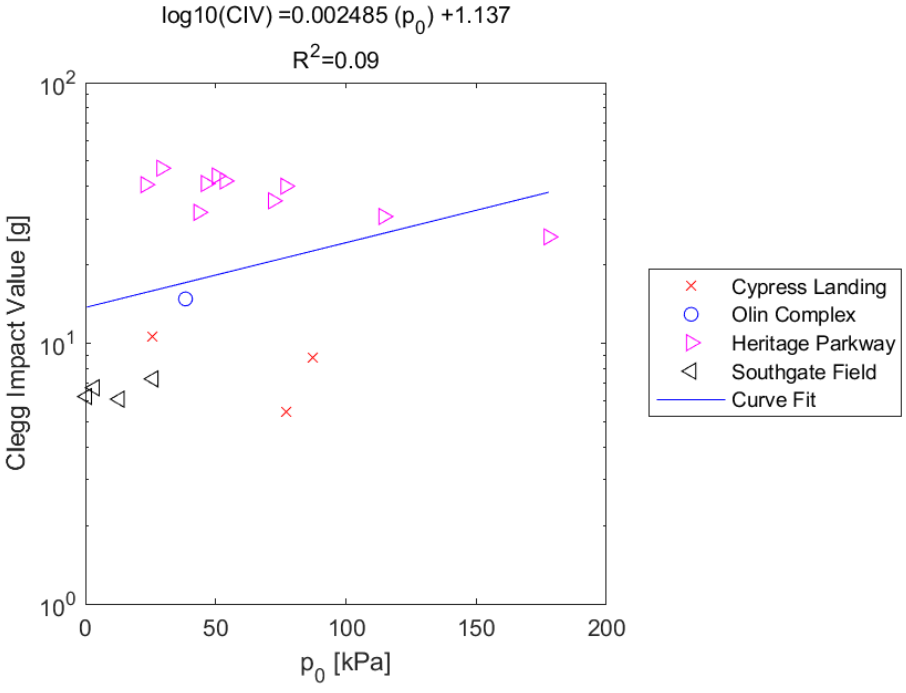

Figure E.288: Linear - Log Model of CIV versus p_0 for SDPMT-12 Continuous Tests, All Sites

E.4 Log - Log Models

E.4.1 SDPMT E_0 versus p_0

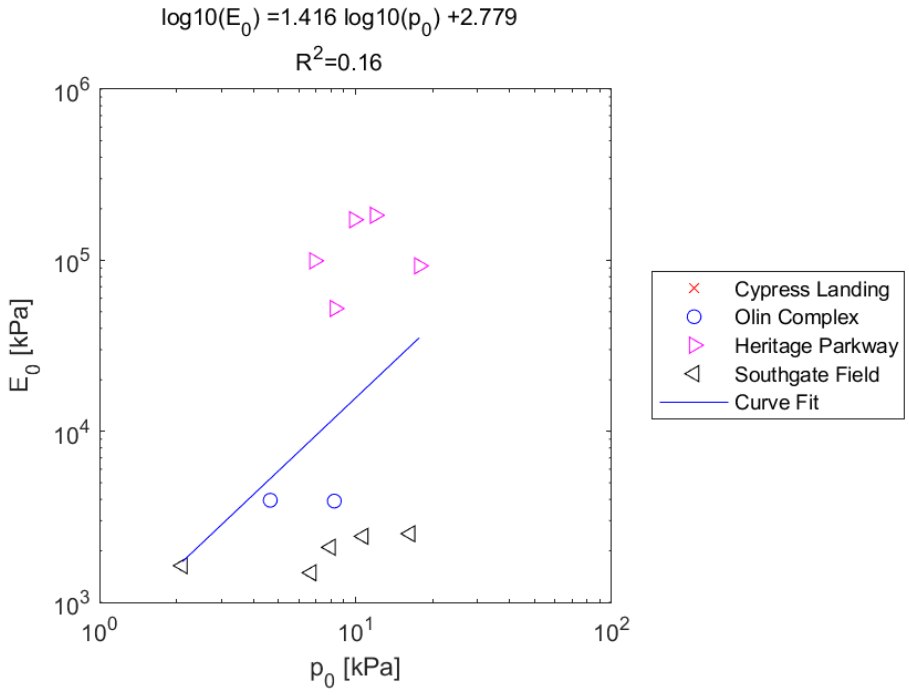

Figure E.289: Log - Log Model of E_0 versus p_0 for SDPMT-6 Incremental Tests, All Sites

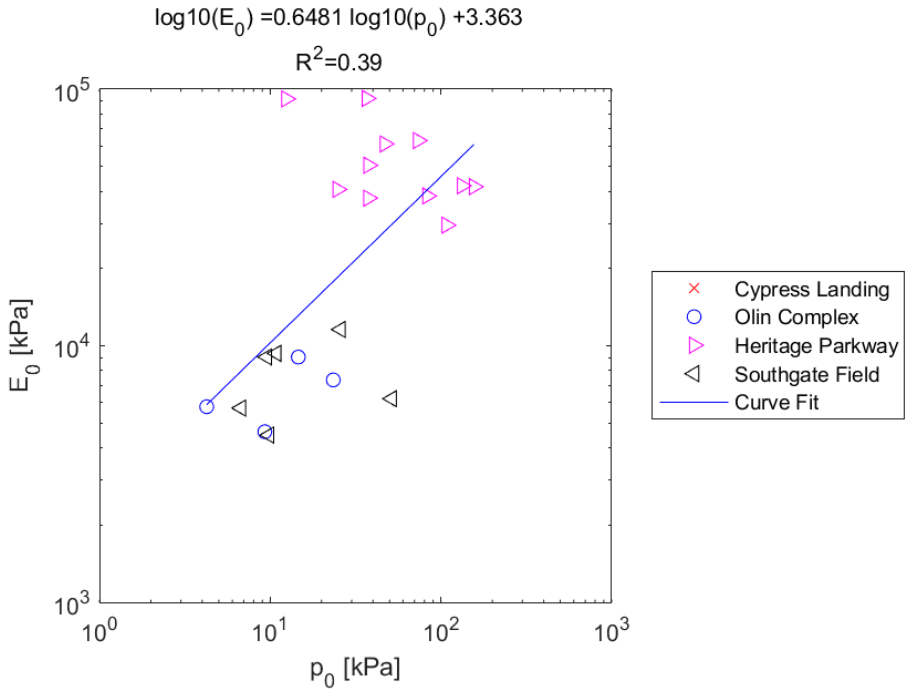

Figure E.290: Log - Log Model of E_0 versus p_0 for SDPMT-6 Continuous Tests, All Sites

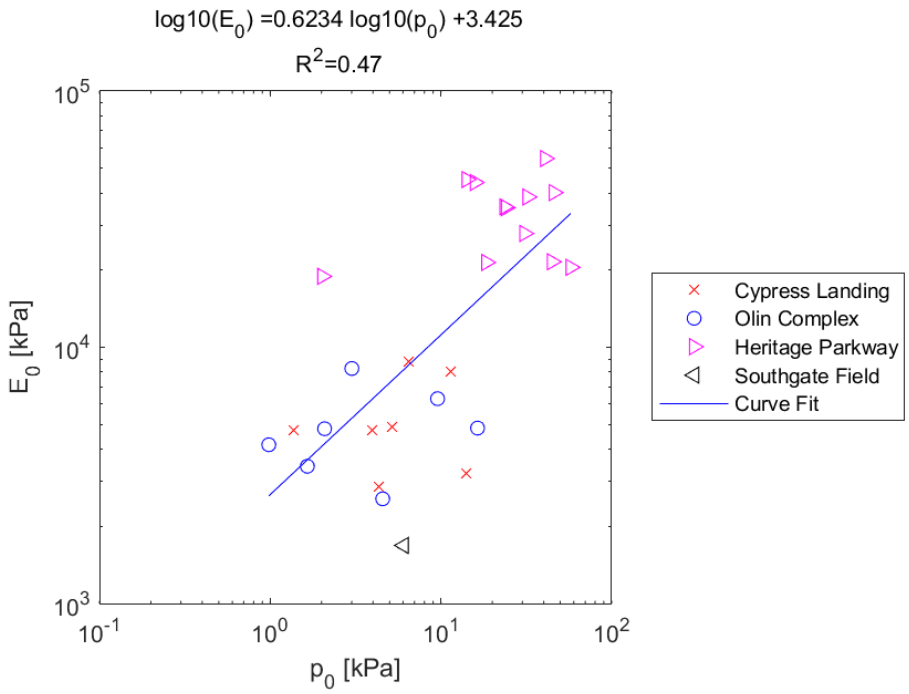

Figure E.291: Log - Log Model of E_0 versus p_0 for SDPMT-12 Incremental Tests, All Sites

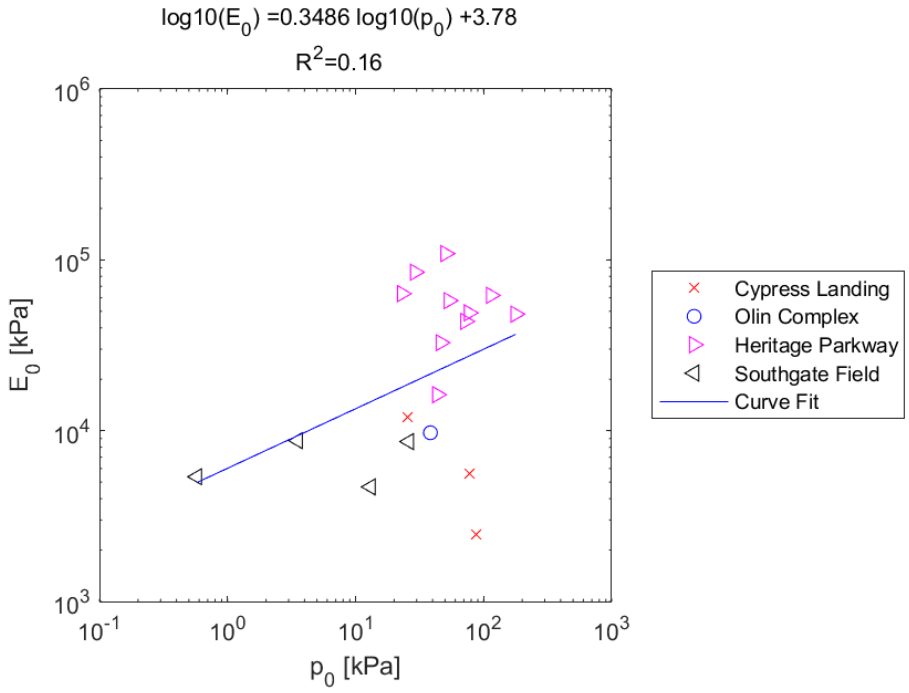

Figure E.292: Log - Log Model of E_0 versus p_0 for SDPMT-12 Continuous Tests, All Sites

E.4.2 SDPMT p_0 versus E_0

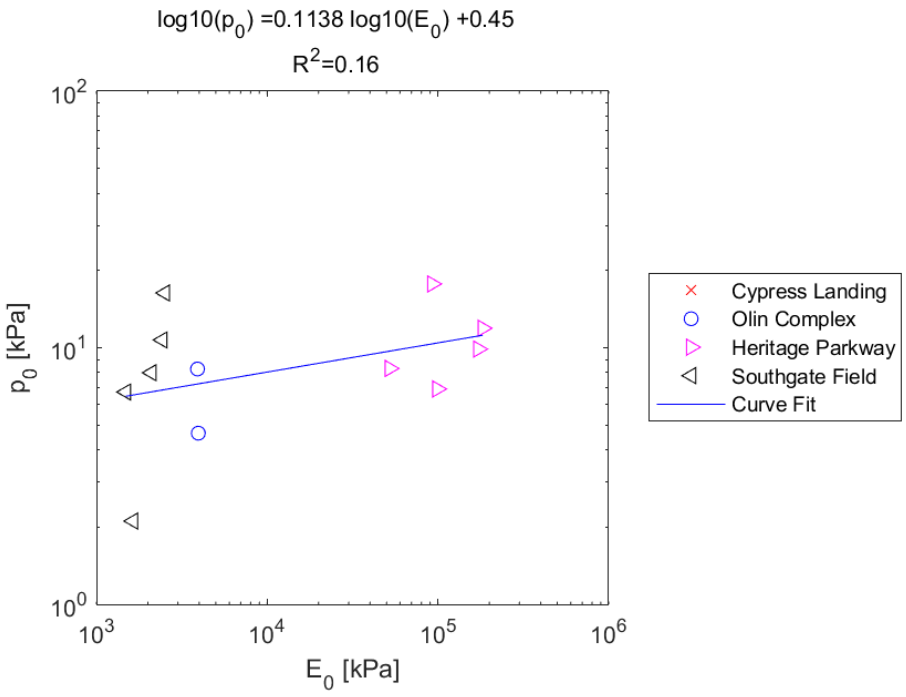

Figure E.293: Log - Log Model of p_0 versus E_0 for SDPMT-6 Incremental Tests, All Sites

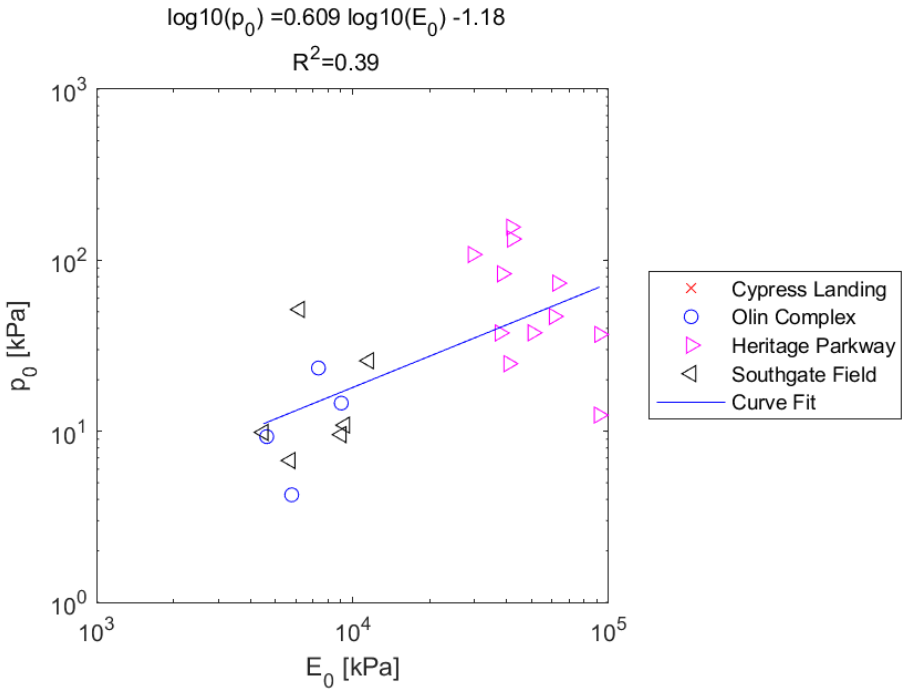

Figure E.294: Log - Log Model of p_0 versus E_0 for SDPMT-6 Continuous Tests, All Sites

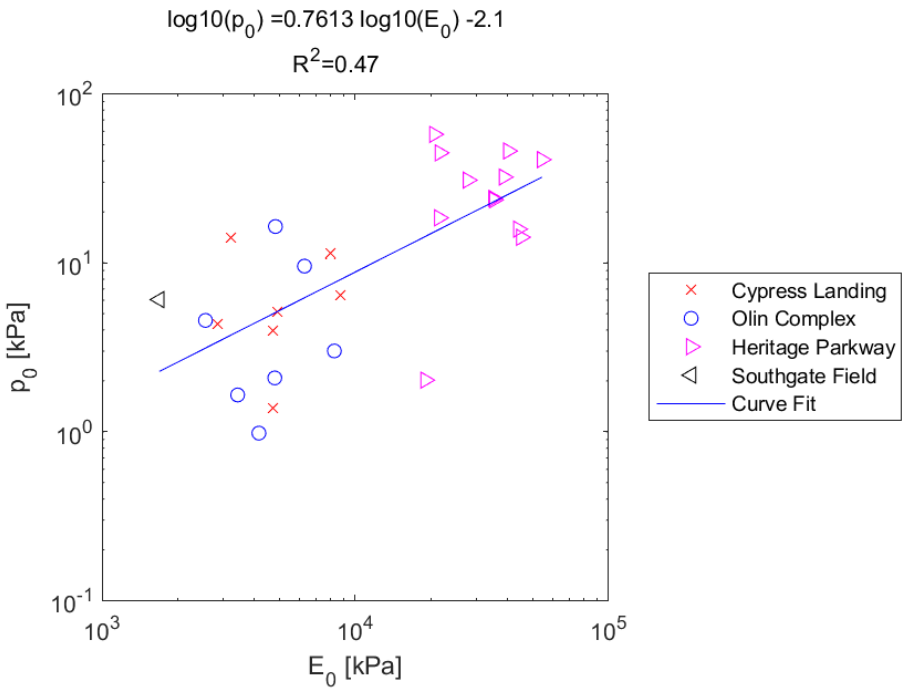

Figure E.295: Log - Log Model of p_0 versus E_0 for SDPMT-12 Incremental Tests, All Sites

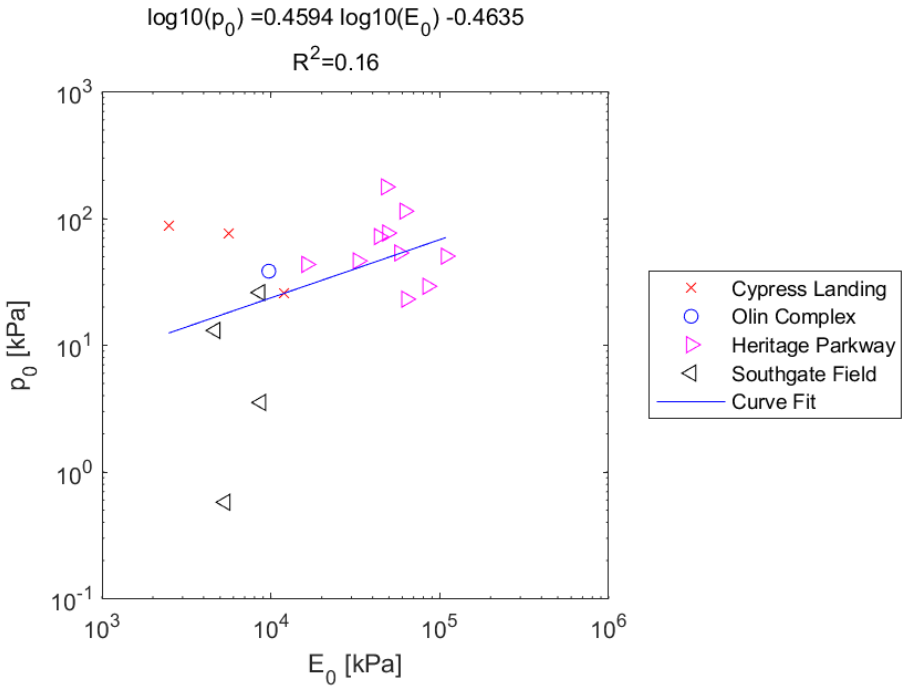

Figure E.296: Log - Log Model of p_0 versus E_0 for SDPMT-12 Continuous Tests, All Sites

E.4.3 SDPMT $\mathbf{E}_0$ versus $\mathbf{p}_L$

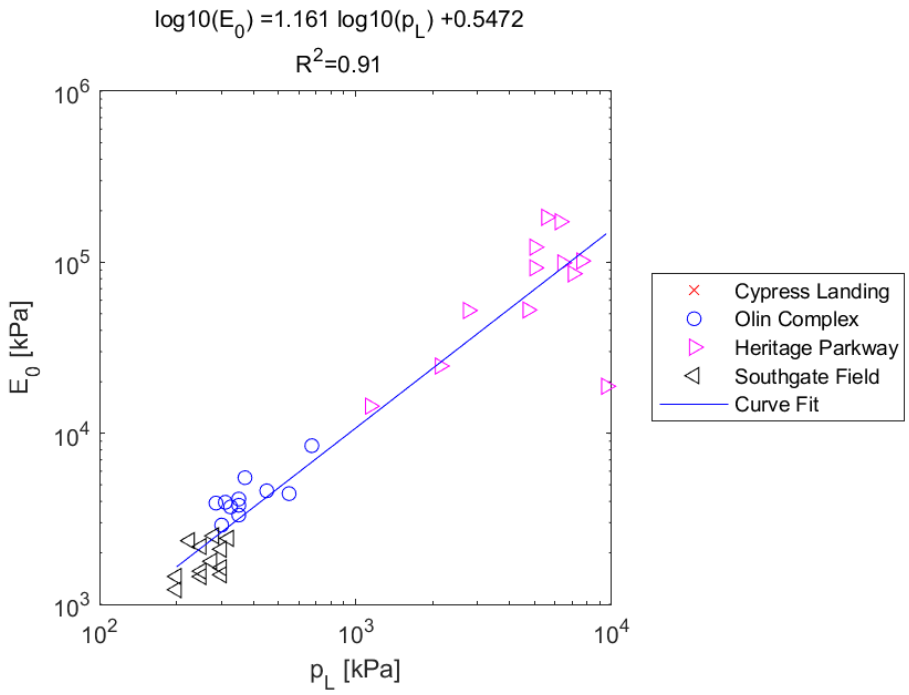

Figure E.297: Log - Log Model of E_0 versus p_L for SDPMT-6 Incremental Tests, All Sites

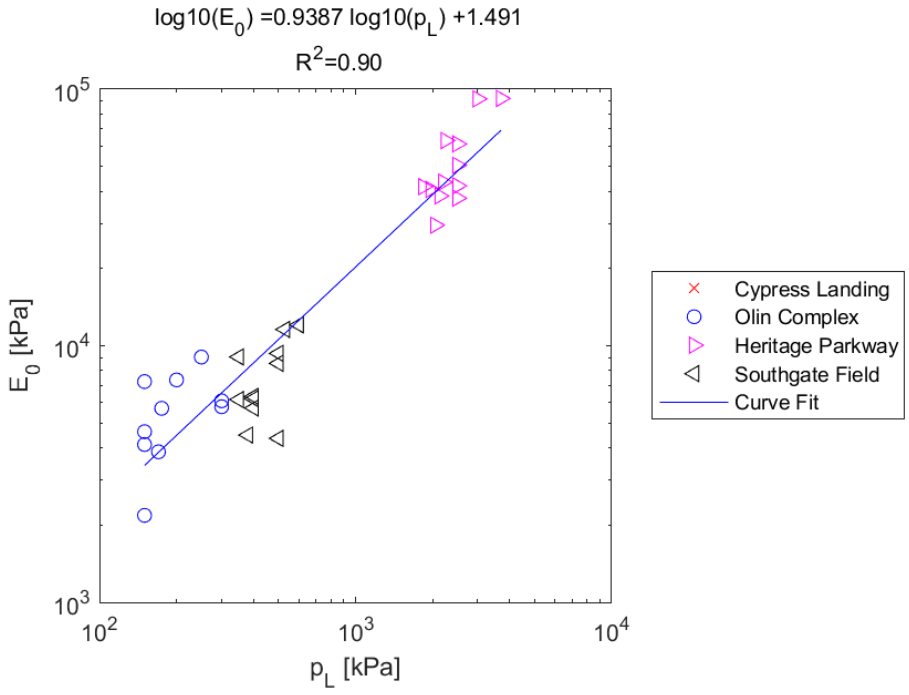

Figure E.298: Log - Log Model of E_0 versus p_L for SDPMT-6 Continuous Tests, All Sites

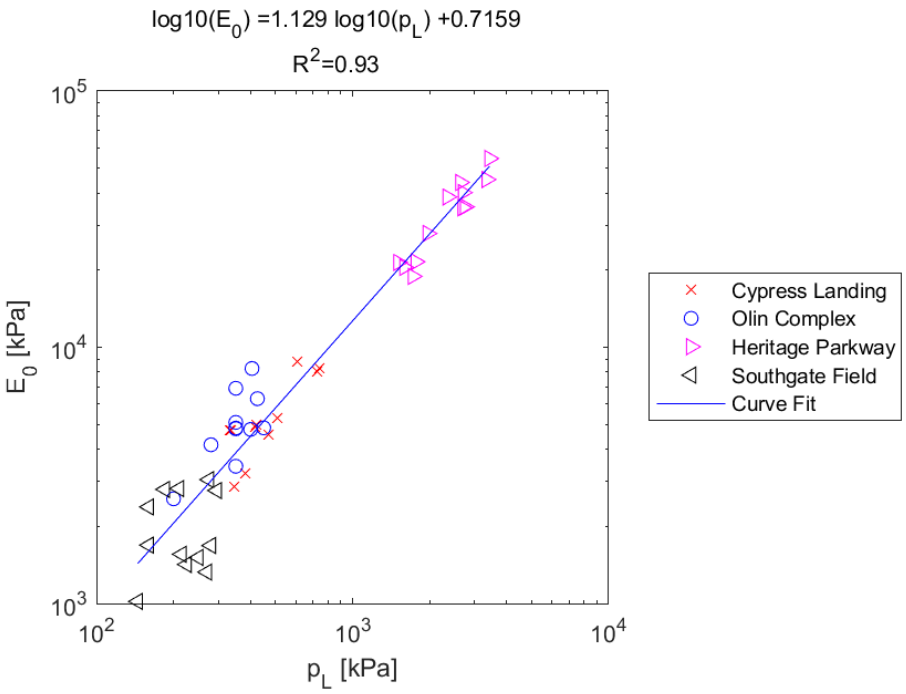

Figure E.299: Log - Log Model of E_0 versus p_L for SDPMT-12 Incremental Tests, All Sites

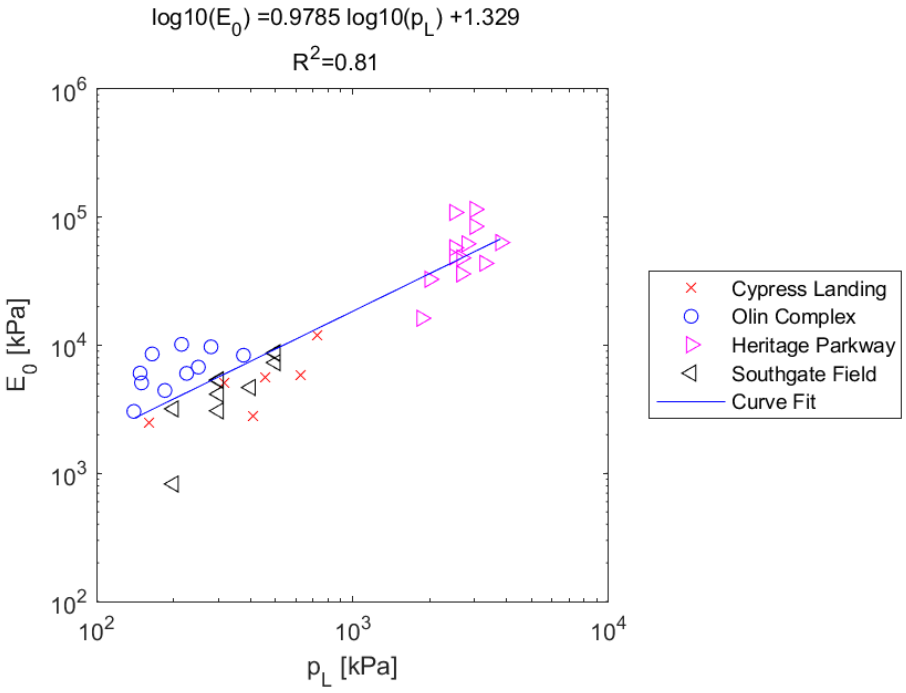

Figure E.300: Log - Log Model of E_0 versus p_L for SDPMT-12 Continuous Tests, All Sites

E.4.4 SDPMT $\mathbf{p}_L$ versus $\mathbf{E}_0$

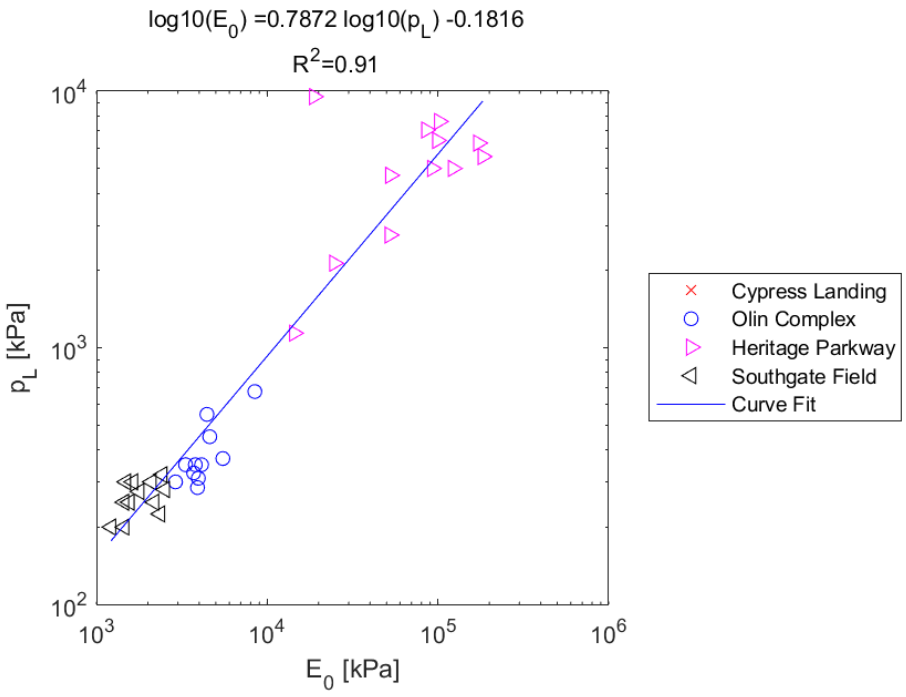

Figure E.301: Log - Log Model of p_L versus E_0 for SDPMT-6 Incremental Tests, All Sites

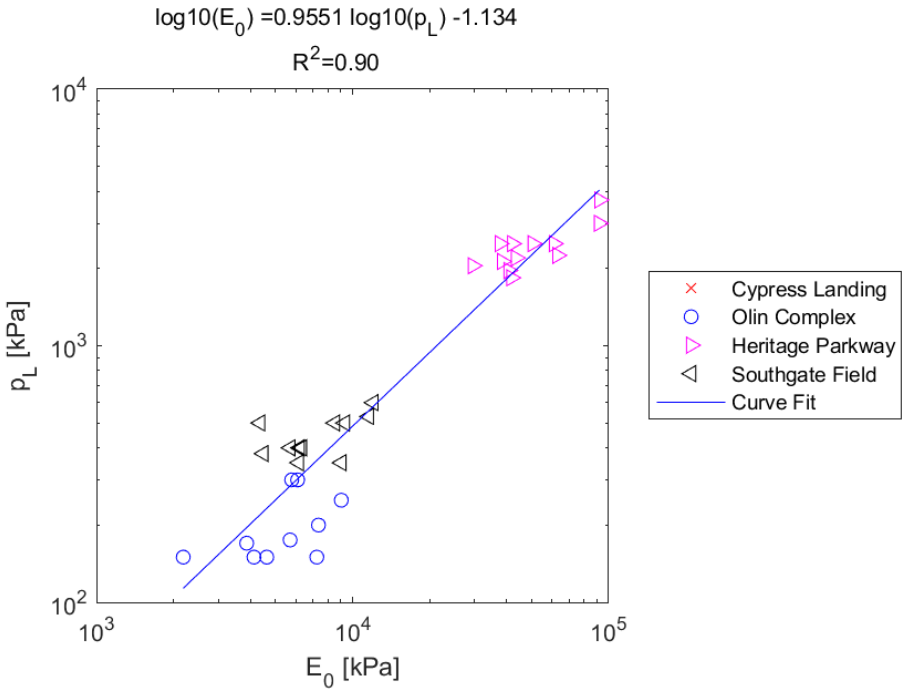

Figure E.302: Log - Log Model of p_L versus E_0 for SDPMT-6 Continuous Tests, All Sites

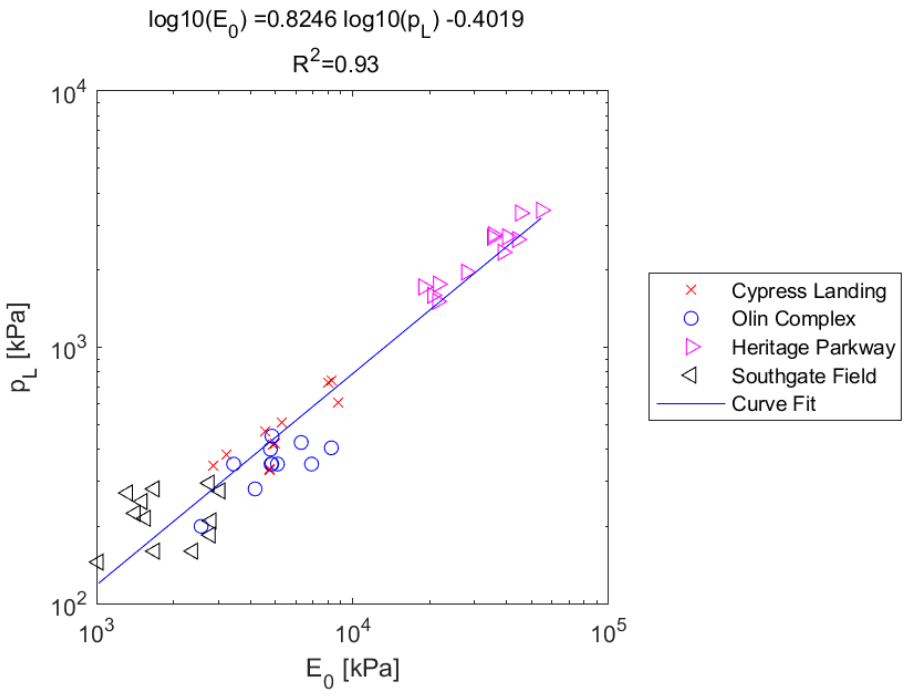

Figure E.303: Log - Log Model of p_L versus E_0 for SDPMT-12 Incremental Tests, All Sites

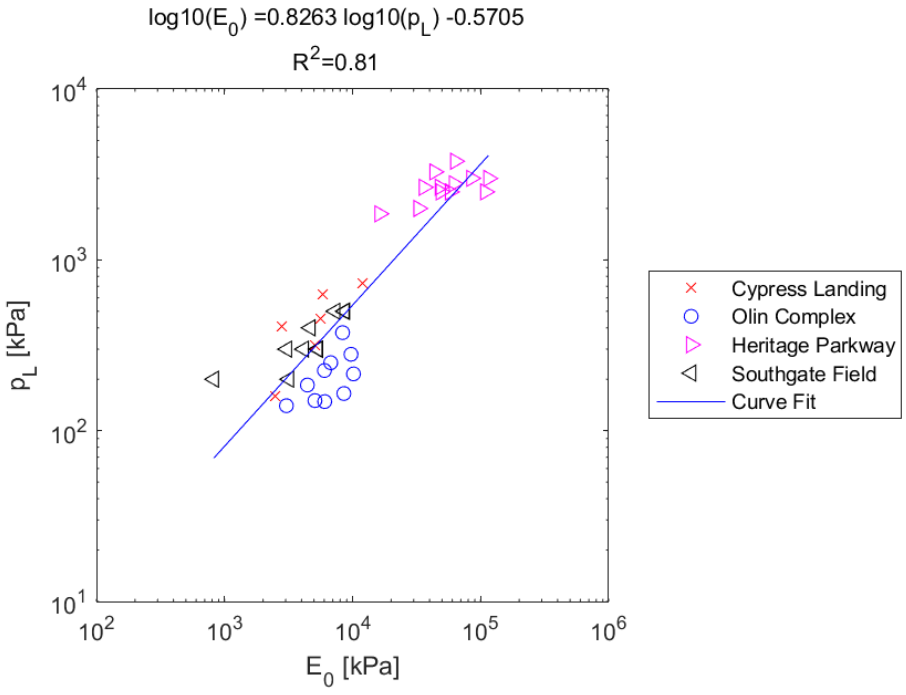

Figure E.304: Log - Log Model of p_L versus E_0 for SDPMT-12 Continuous Tests, All Sites

E.4.5 SDPMT $\mathbf{p}_0$ versus $\mathbf{p}_L$

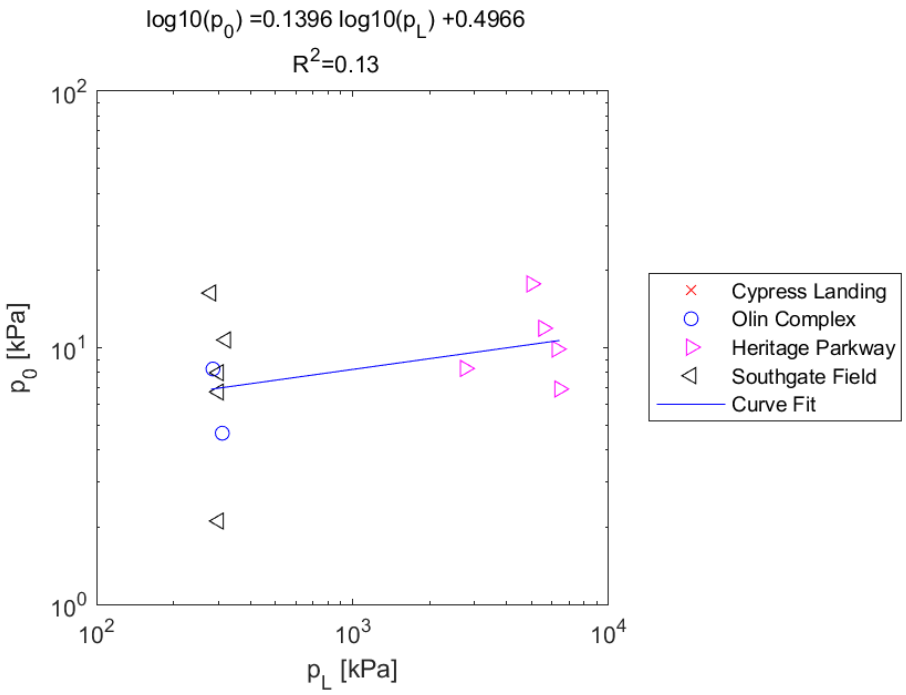

Figure E.305: Log - Log Model of p_0 versus p_L for SDPMT-6 Incremental Tests, All Sites

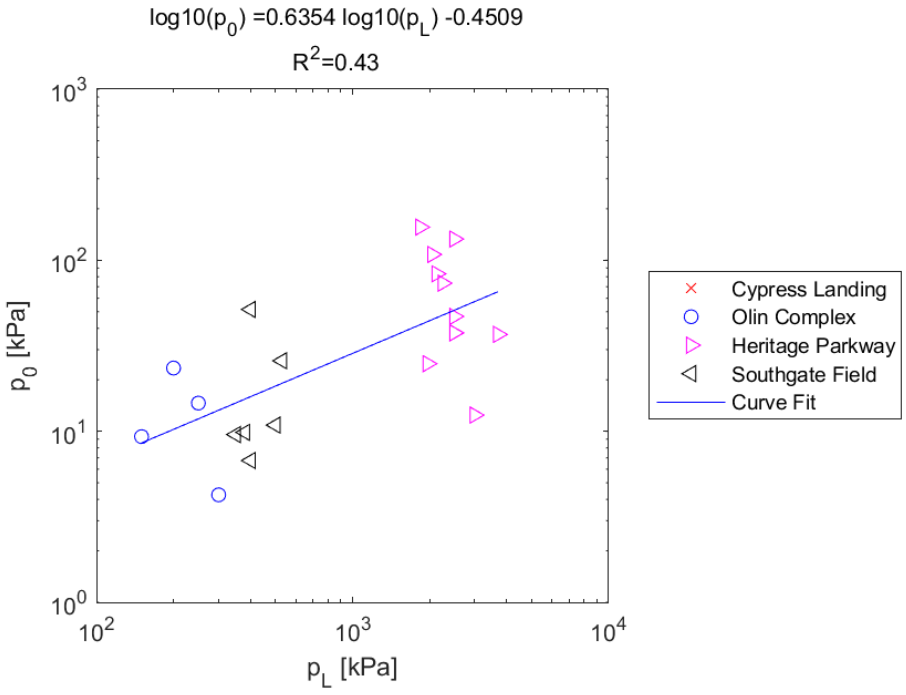

Figure E.306: Log - Log Model of p_0 versus p_L for SDPMT-6 Continuous Tests, All Sites

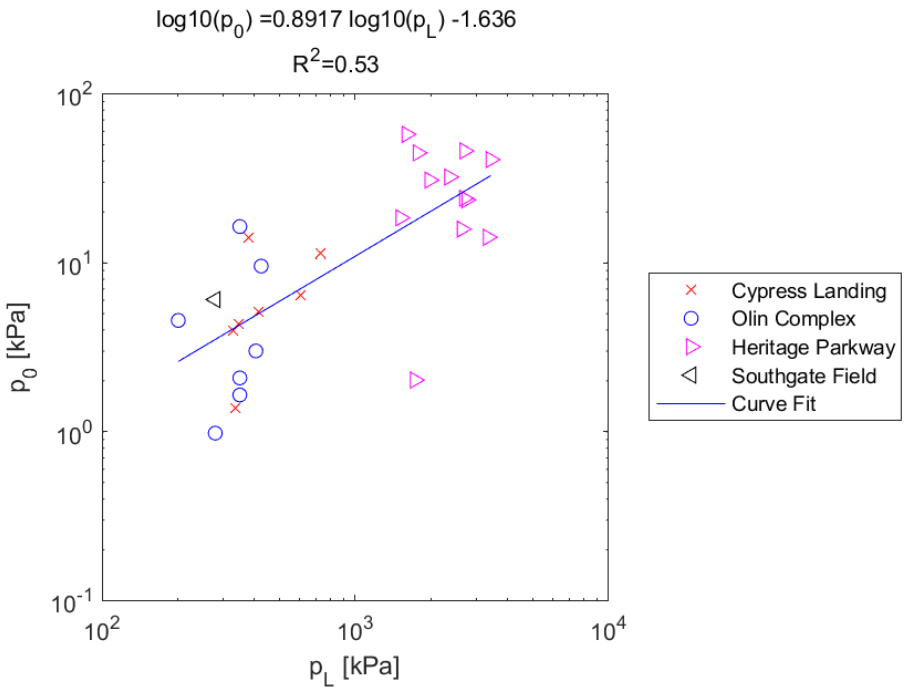

Figure E.307: Log - Log Model of p_0 versus p_L for SDPMT-12 Incremental Tests, All Sites

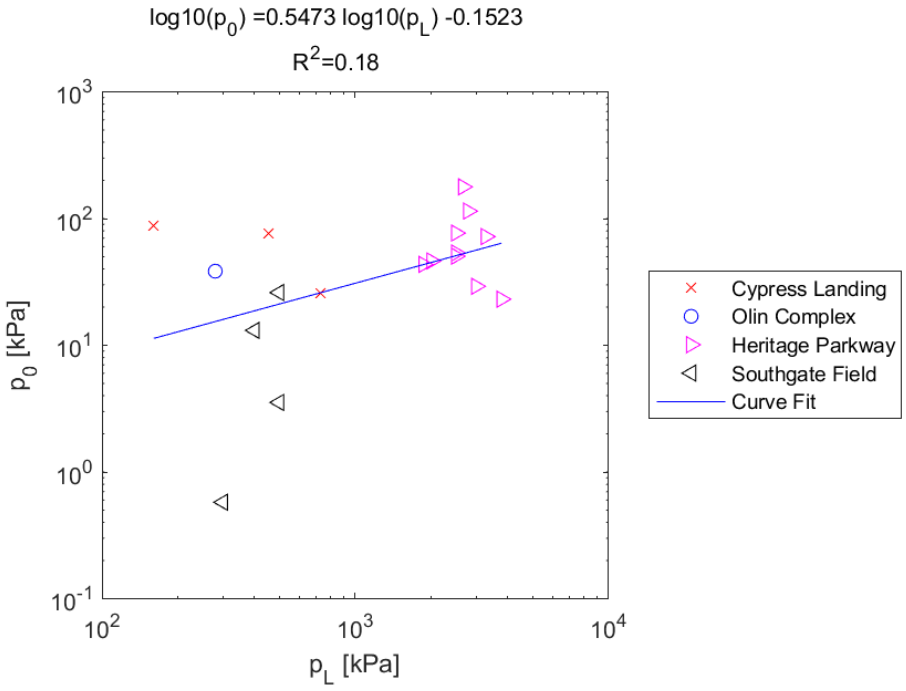

Figure E.308: Log - Log Model of p_0 versus p_L for SDPMT-12 Continuous Tests, All Sites

E.4.6 SDPMT $\mathbf{p}_L$ versus $\mathbf{p}_0$

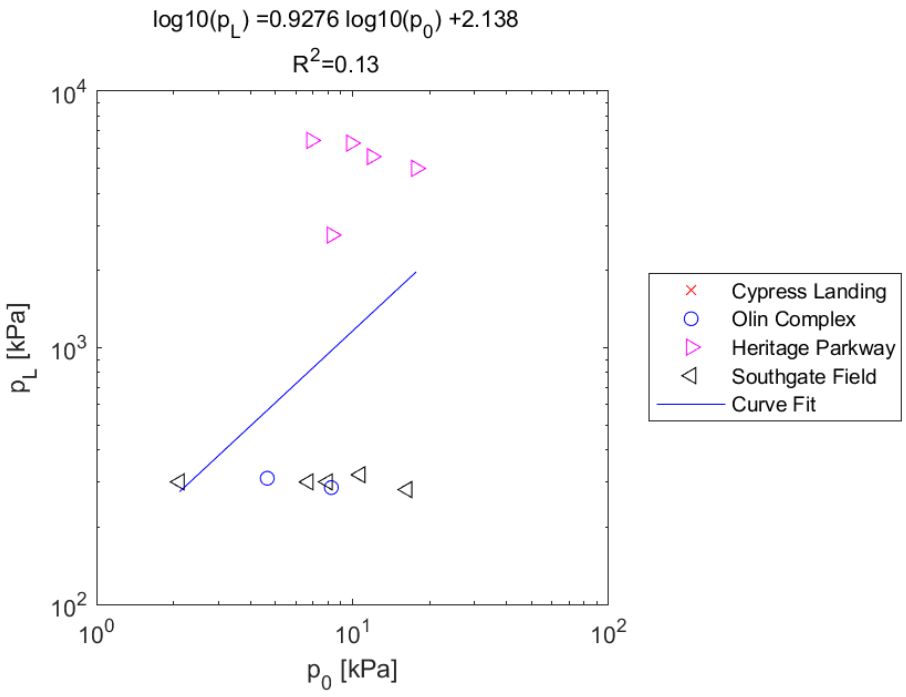

Figure E.309: Log - Log Model of p_L versus p_0 for SDPMT-6 Incremental Tests, All Sites

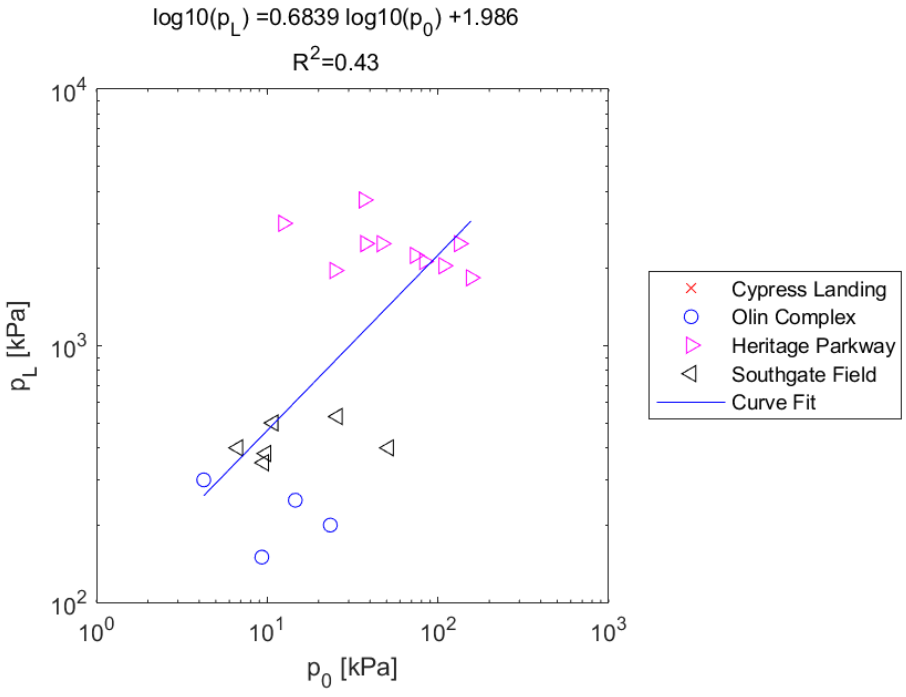

Figure E.310: Log - Log Model of p_L versus p_0 for SDPMT-6 Continuous Tests, All Sites

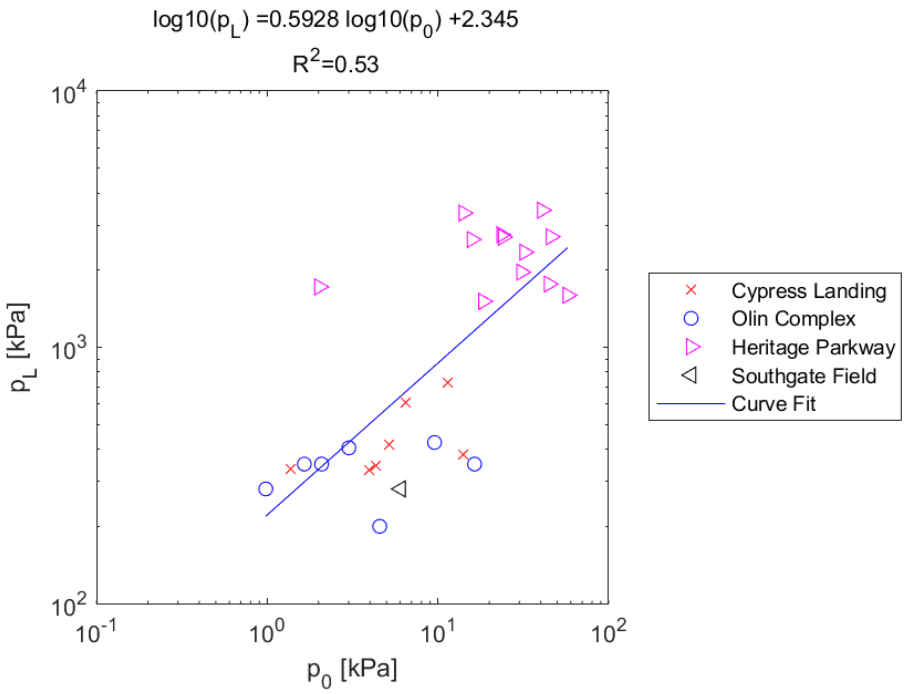

Figure E.311: Log - Log Model of p_L versus p_0 for SDPMT-12 Incremental Tests, All Sites

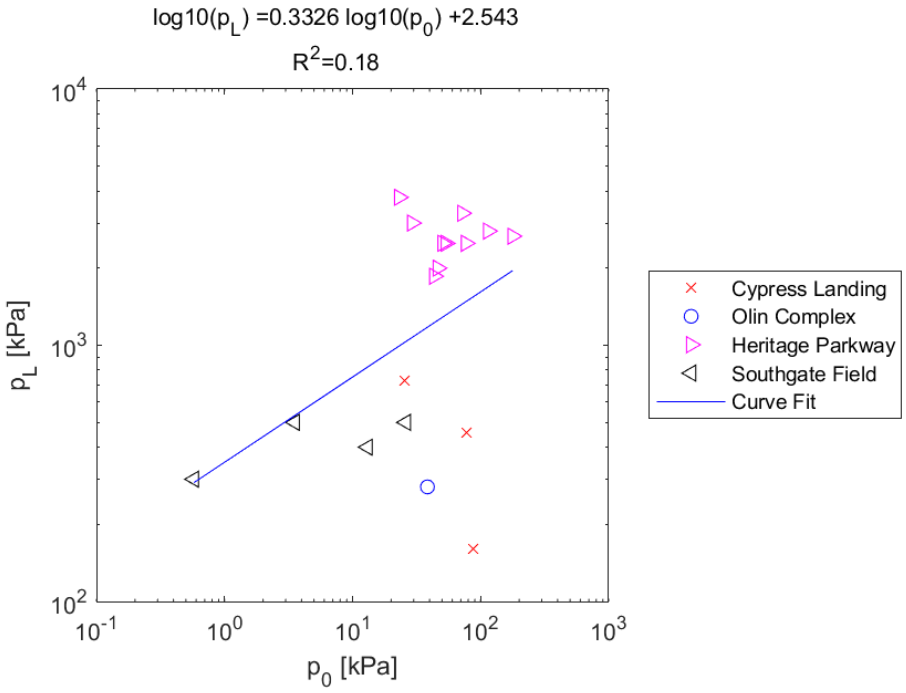

Figure E.312: Log - Log Model of p_L versus p_0 for SDPMT-12 Continuous Tests, All Sites

E.4.7 γ_{wet} versus $\mathbf{E}_0$

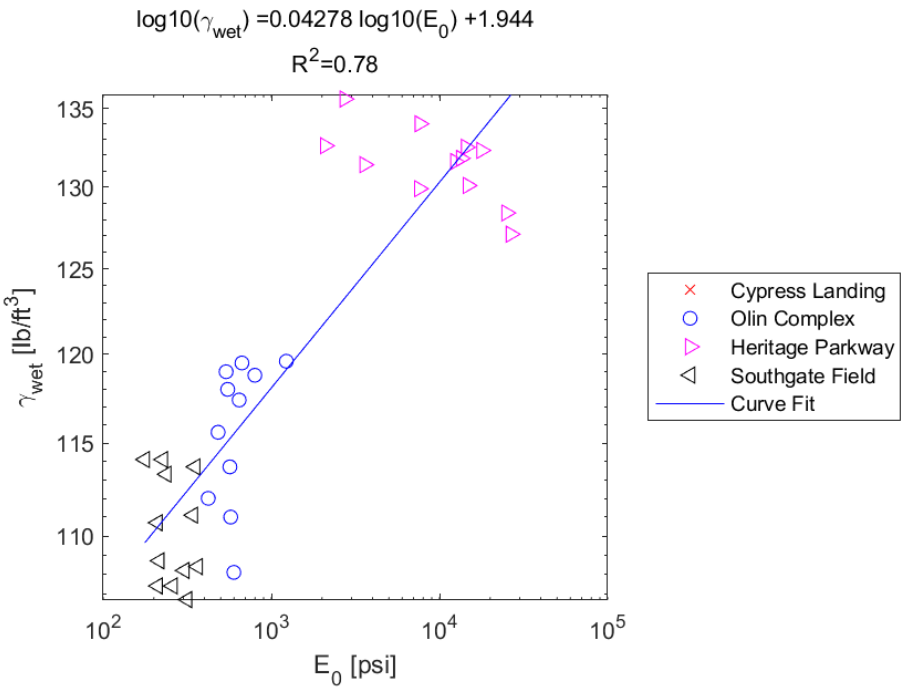

Figure E.313: Log - Log Model of γ_{wet} versus E_0 for SDPMT-6 Incremental Tests, All Sites

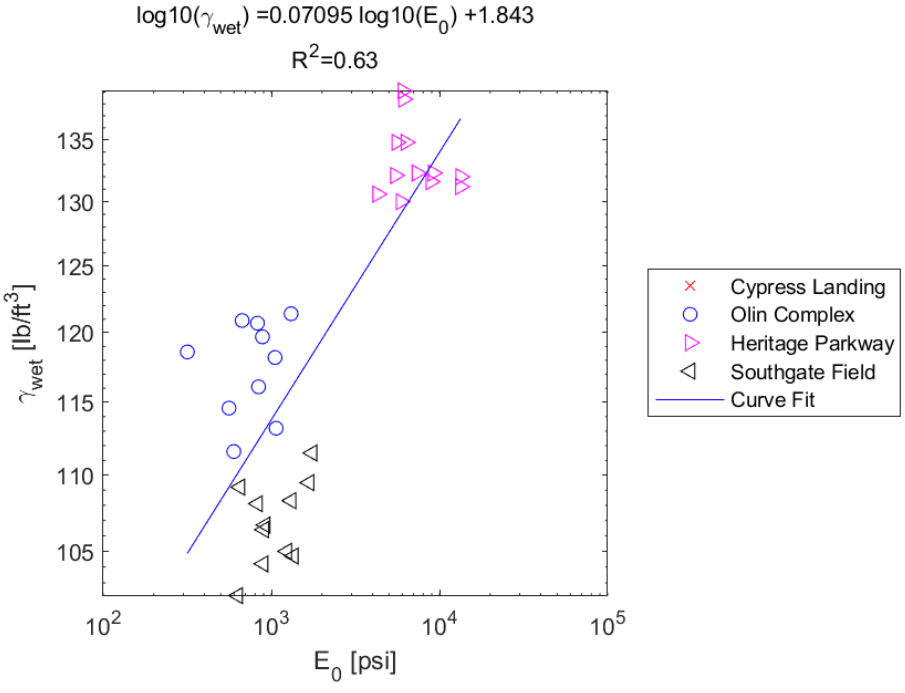

Figure E.314: Log - Log Model of γ_{wet} versus E_0 for SDPMT-6 Continuous Tests, All Sites

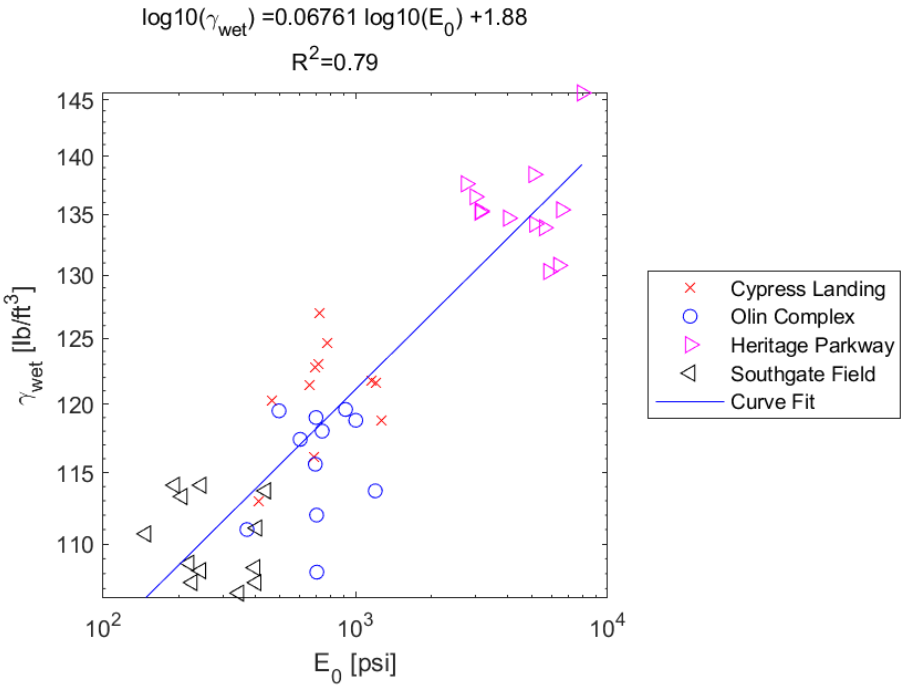

Figure E.315: Log - Log Model of γ_{wet} versus E_0 for SDPMT-12 Incremental Tests, All Sites

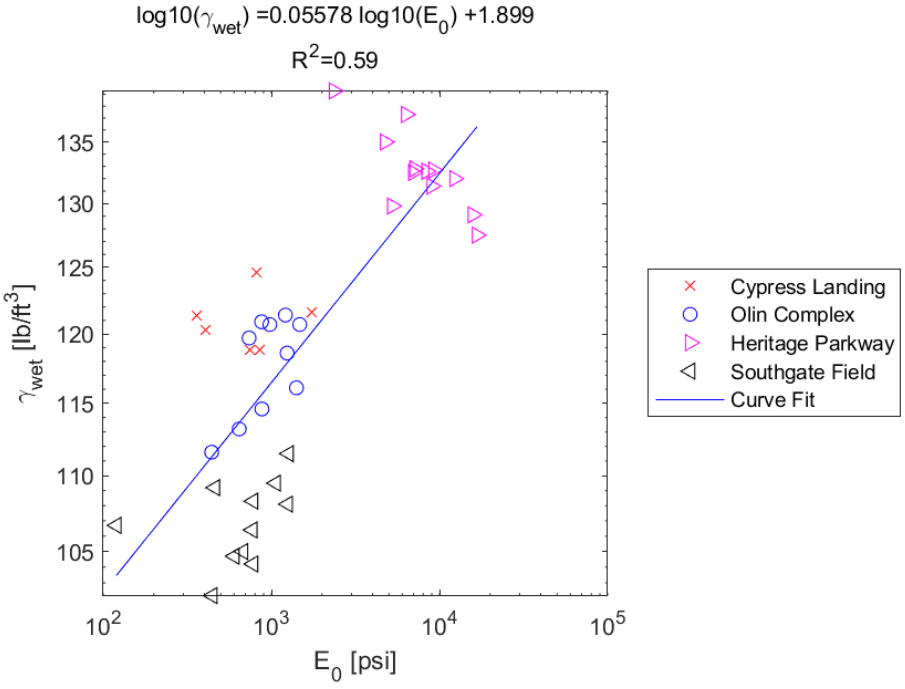

Figure E.316: Log - Log Model of γ_{wet} versus E_0 for SDPMT-12 Continuous Tests, All Sites

E.4.8 γ_{wet} versus $\mathbf{p}_L$

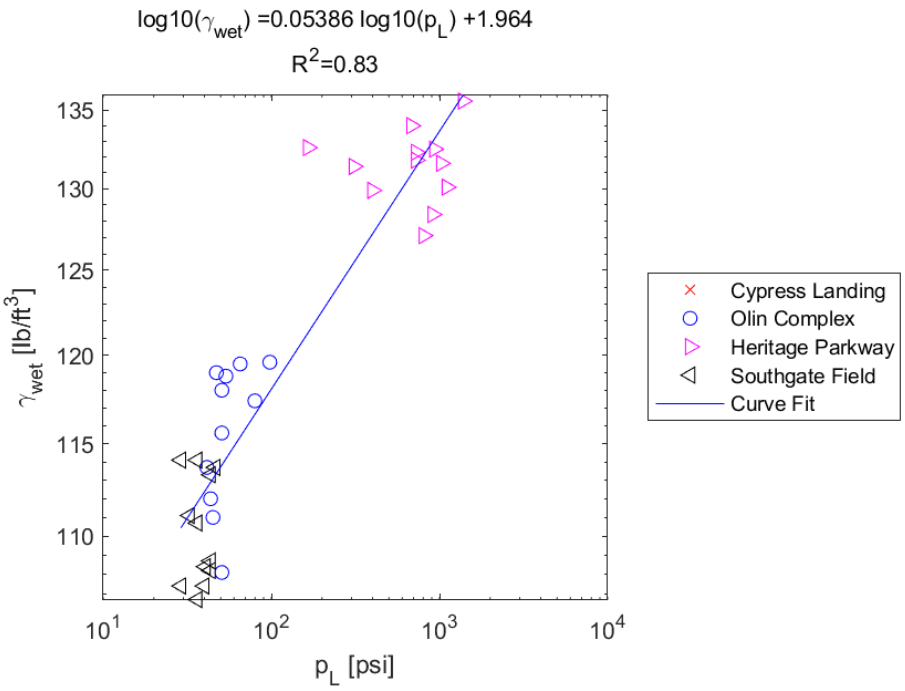

Figure E.317: Log - Log Model of γ_{wet} versus p_L for SDPMT-6 Incremental Tests, All Sites

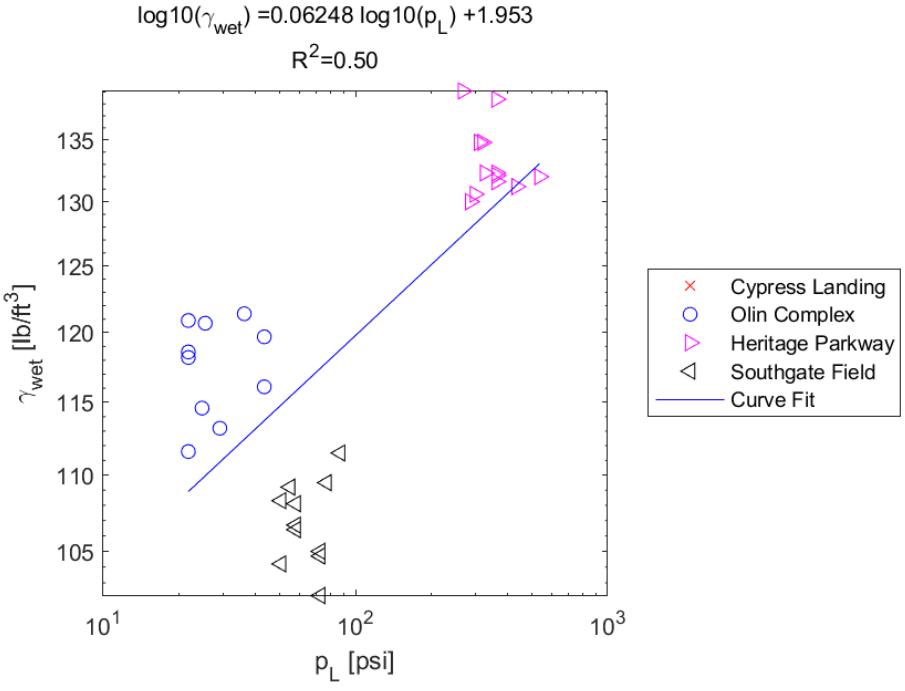

Figure E.318: Log - Log Model of γ_{wet} versus p_L for SDPMT-6 Continuous Tests, All Sites

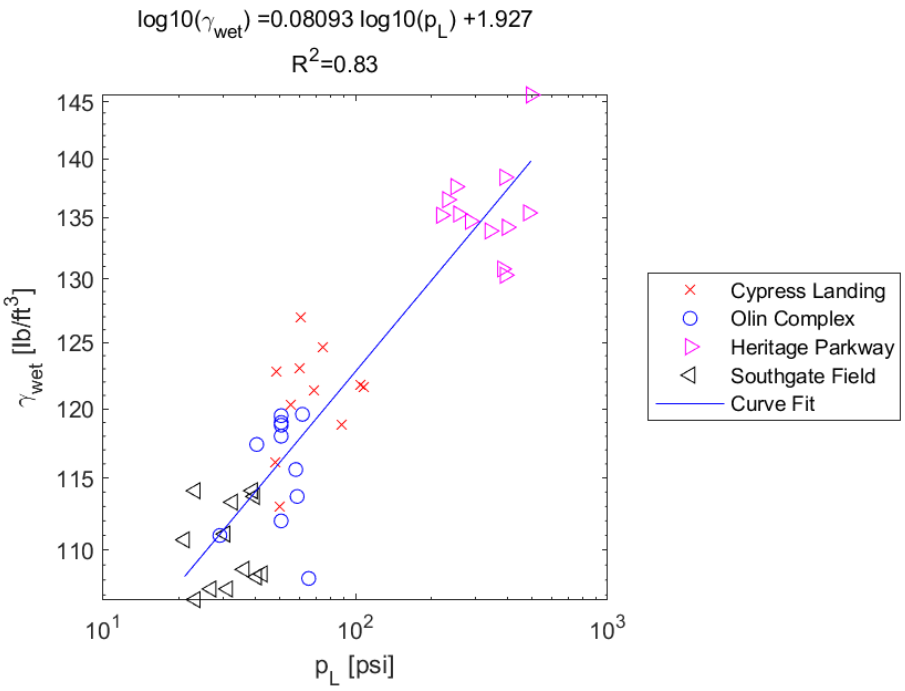

Figure E.319: Log - Log Model of γ_{wet} versus p_L for SDPMT-12 Incremental Tests, All Sites

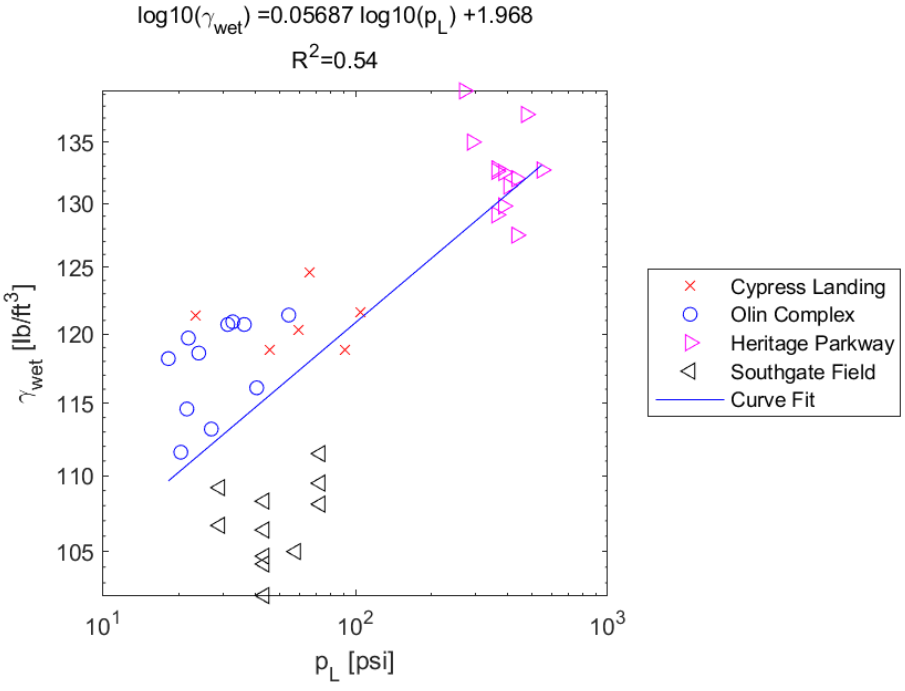

Figure E.320: Log - Log Model of γ_{wet} versus p_L for SDPMT-12 Continuous Tests, All Sites

E.4.9 γ_{wet} versus $\mathbf{p}_0$

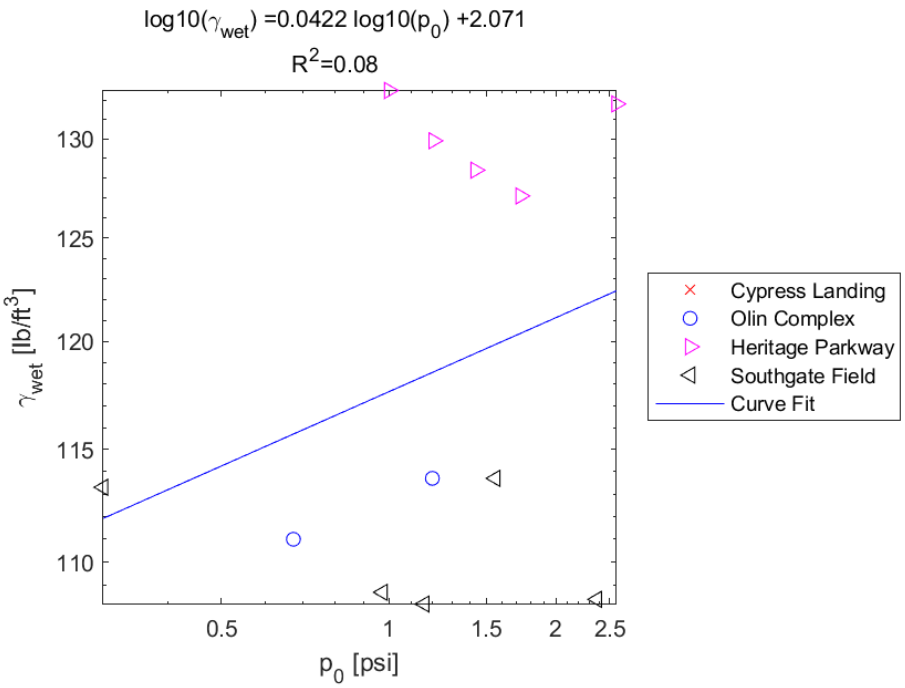

Figure E.321: Log - Log Model of γ_{wet} versus p_0 for SDPMT-6 Incremental Tests, All Sites

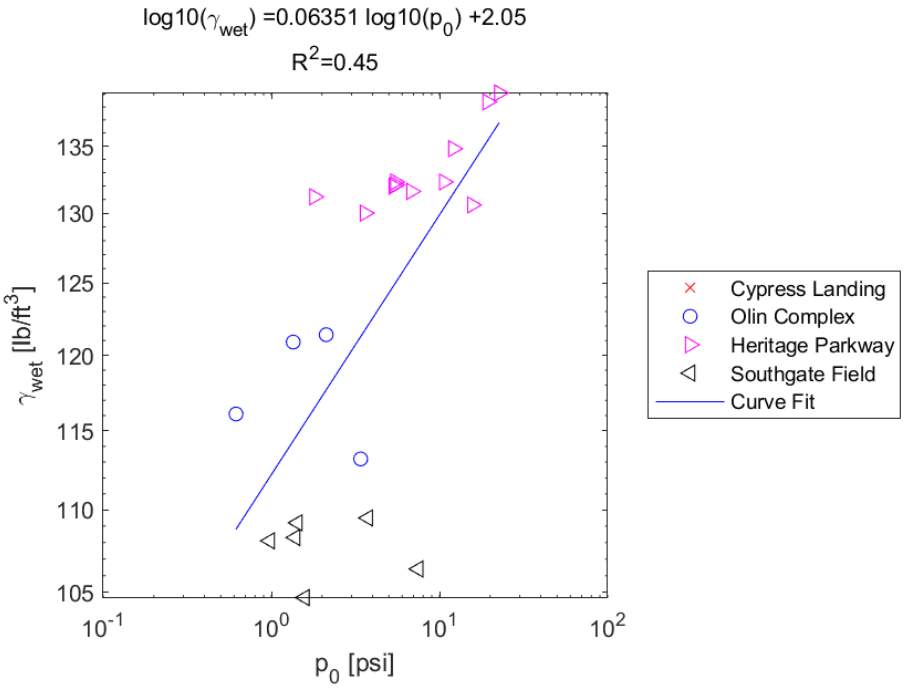

Figure E.322: Log - Log Model of γ_{wet} versus p_0 for SDPMT-6 Continuous Tests, All Sites

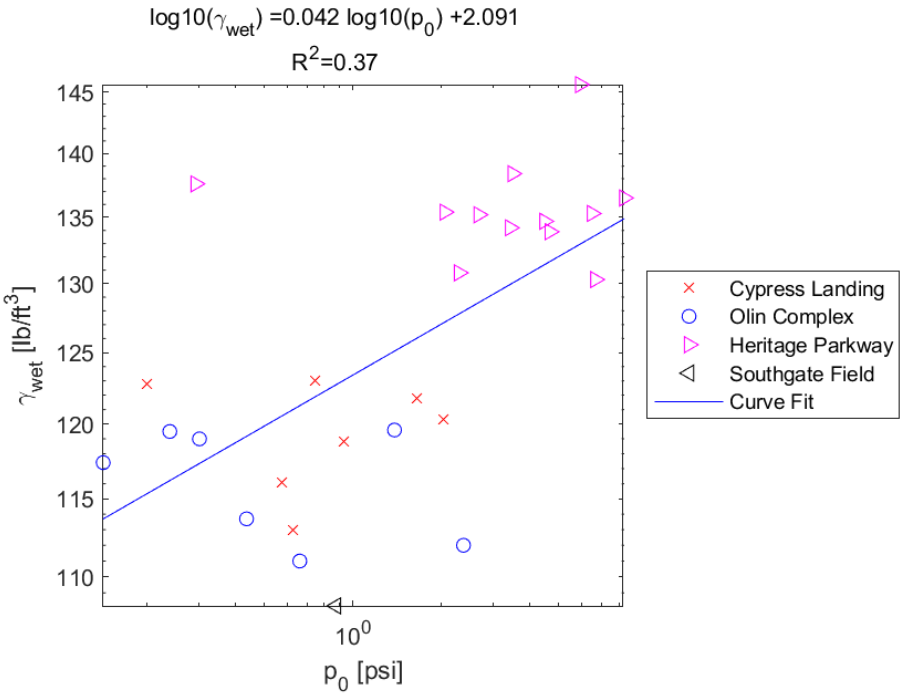

Figure E.323: Log - Log Model of γ_{wet} versus p_0 for SDPMT-12 Incremental Tests, All Sites

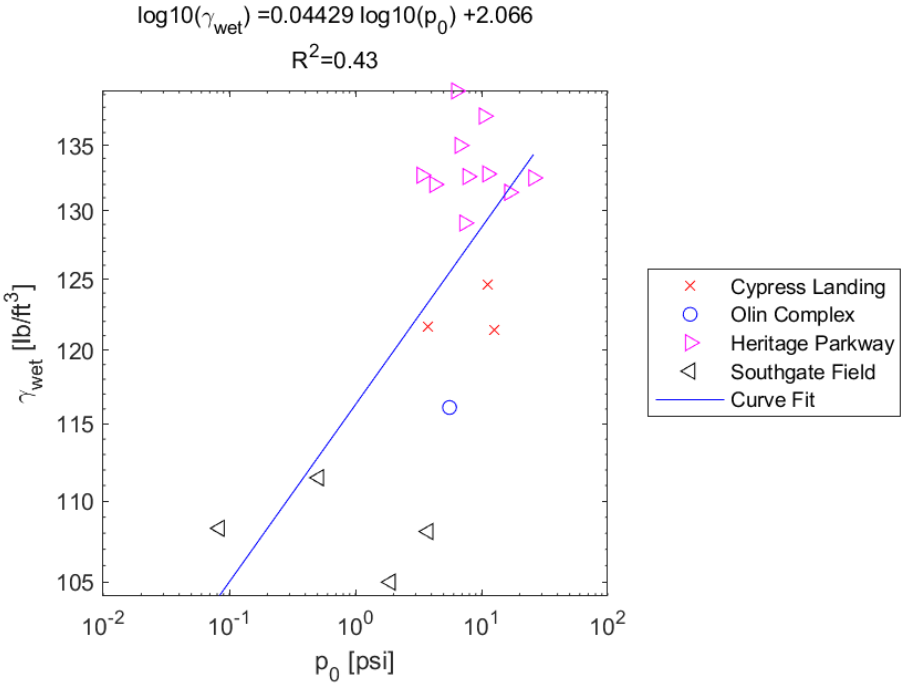

Figure E.324: Log - Log Model of γ_{wet} versus p_0 for SDPMT-12 Continuous Tests, All Sites

E.4.10 γ_{dry} versus $\mathbf{E}_0$

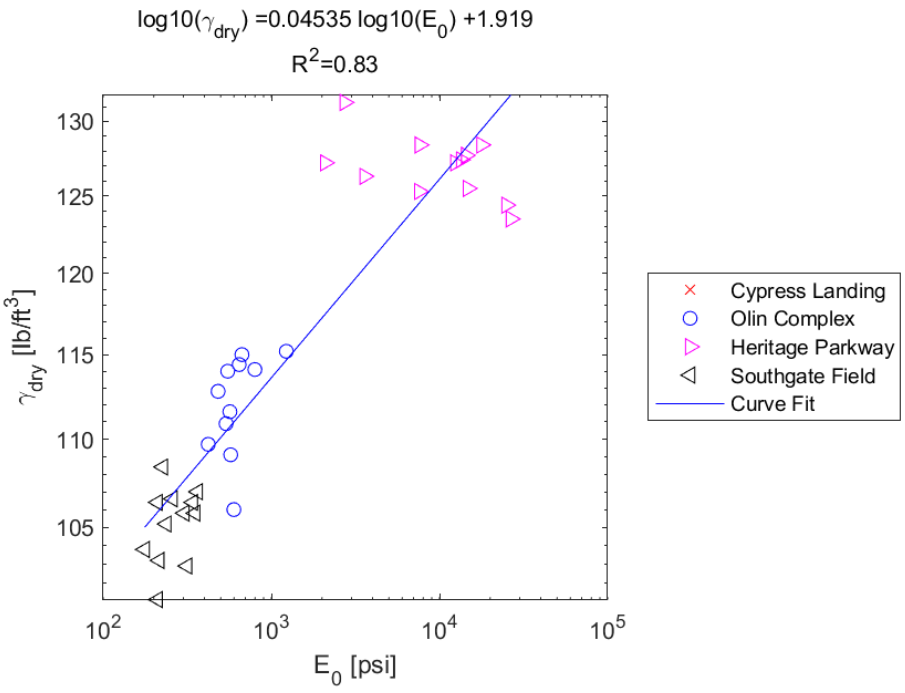

Figure E.325: Log - Log Model of γ_{dry} versus E_0 for SDPMT-6 Incremental Tests, All Sites

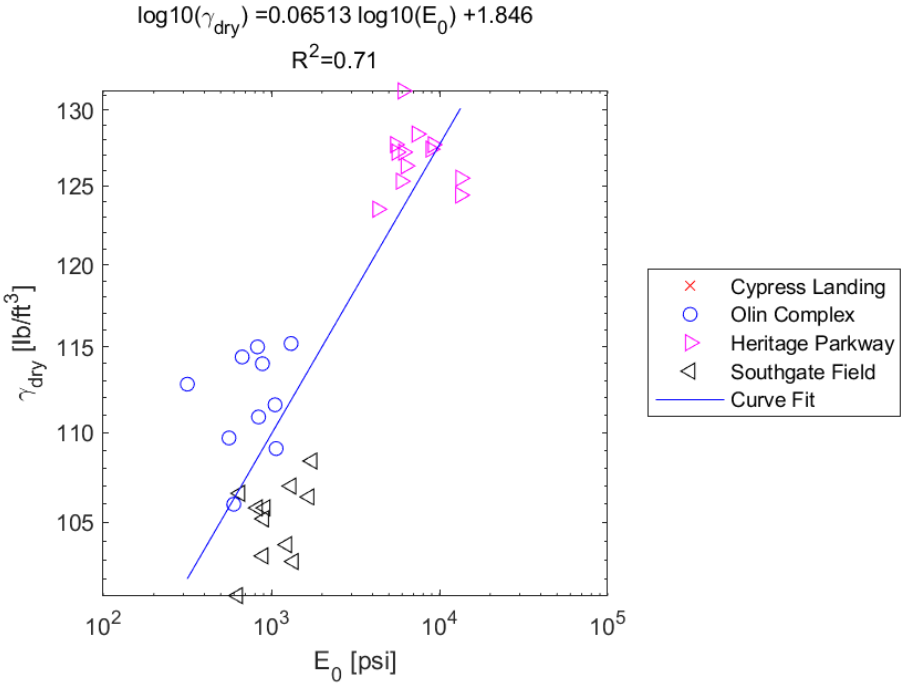

Figure E.326: Log - Log Model of γ_{dry} versus E_0 for SDPMT-6 Continuous Tests, All Sites

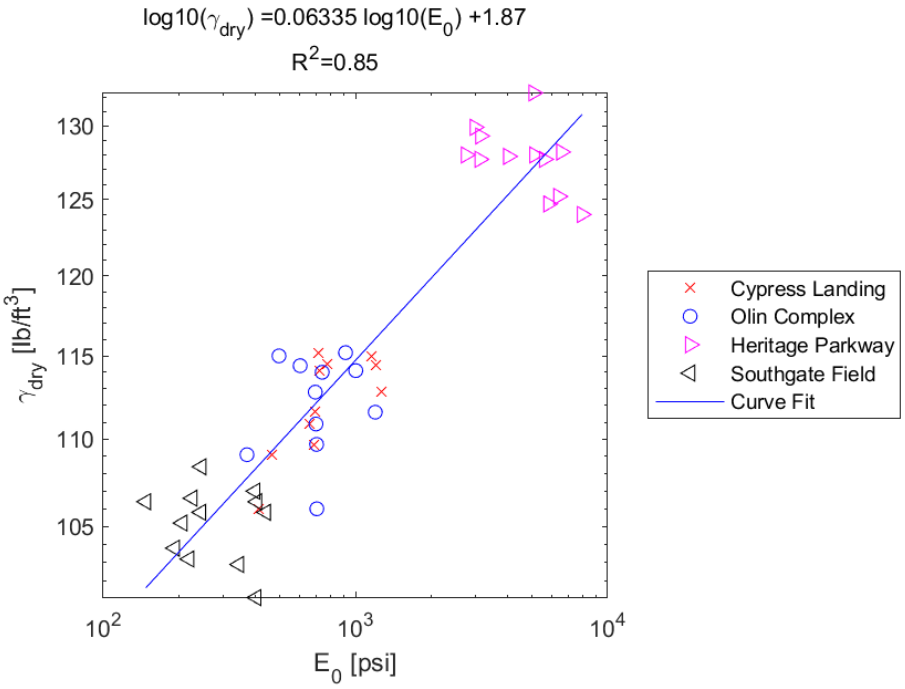

Figure E.327: Log - Log Model of γ_{dry} versus E_0 for SDPMT-12 Incremental Tests, All Sites

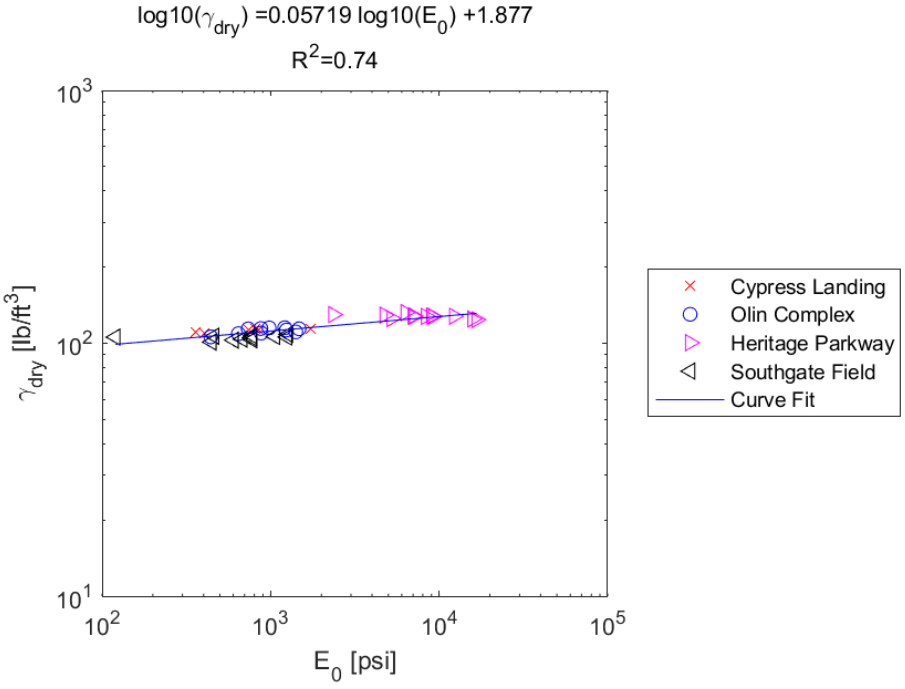

Figure E.328: Log - Log Model of γ_{dry} versus E_0 for SDPMT-12 Continuous Tests, All Sites

E.4.11 γ_{dry} versus $\mathbf{p}_L$

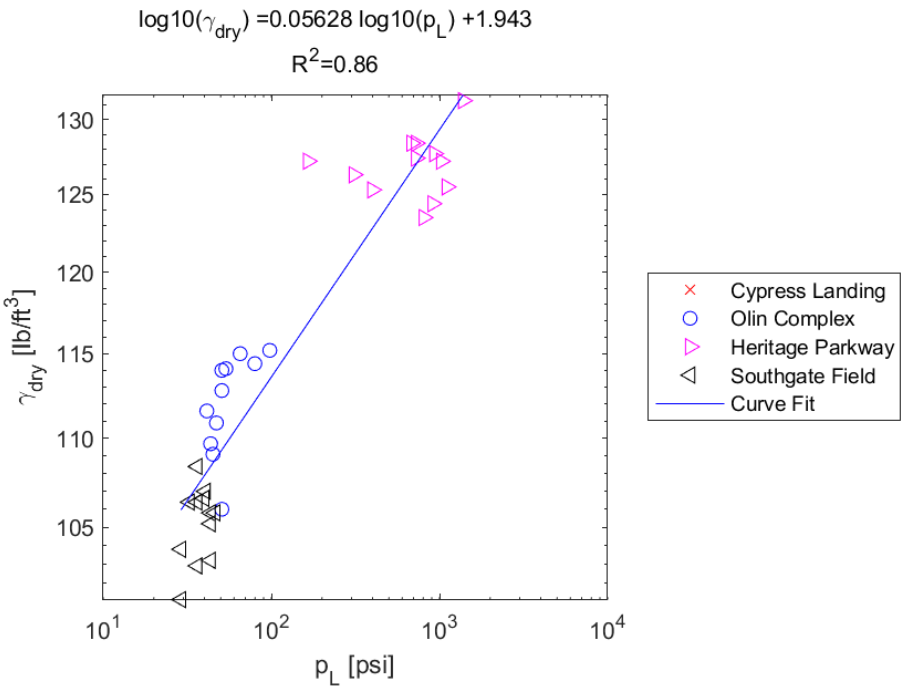

Figure E.329: Log - Log Model of γ_{dry} versus p_L for SDPMT-6 Incremental Tests, All Sites

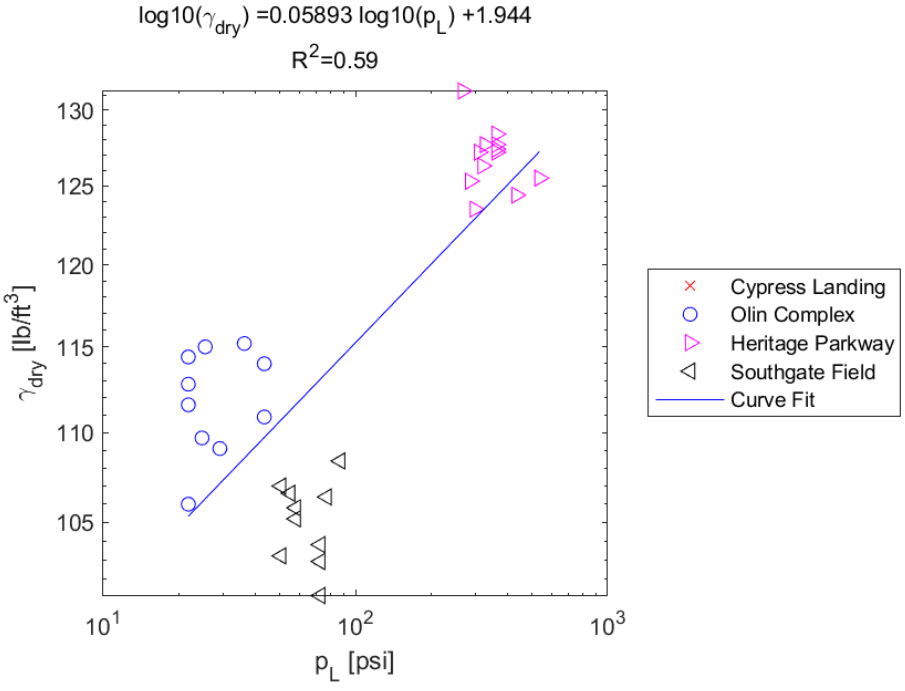

Figure E.330: Log - Log Model of γ_{dry} versus p_L for SDPMT-6 Continuous Tests, All Sites

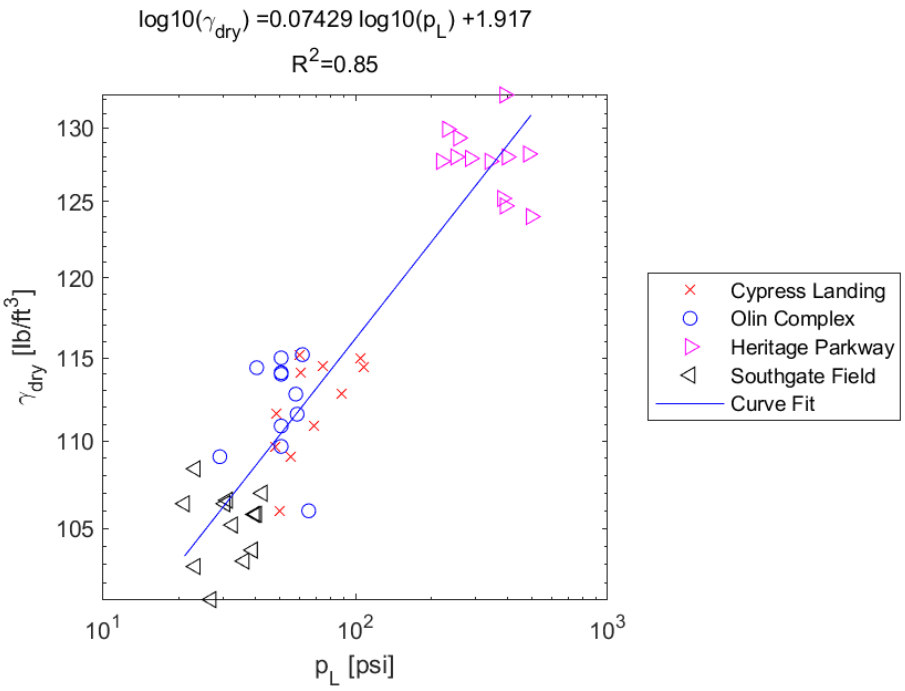

Figure E.331: Log - Log Model of γ_{dry} versus p_L for SDPMT-12 Incremental Tests, All Sites

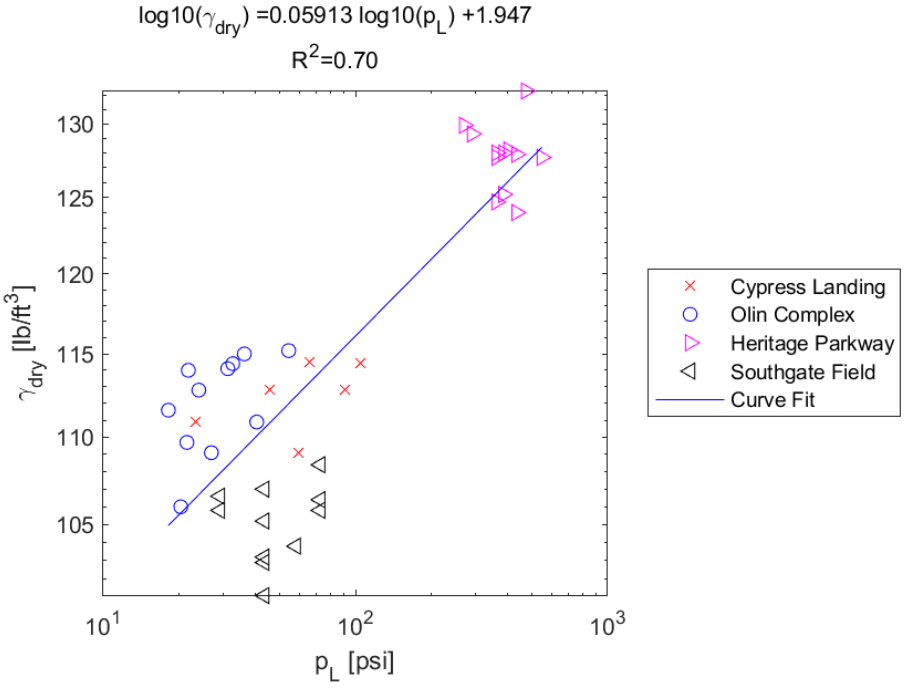

Figure E.332: Log - Log Model of γ_{dry} versus p_L for SDPMT-12 Continuous Tests, All Sites

E.4.12 γ_{dry} versus $\mathbf{p}_0$

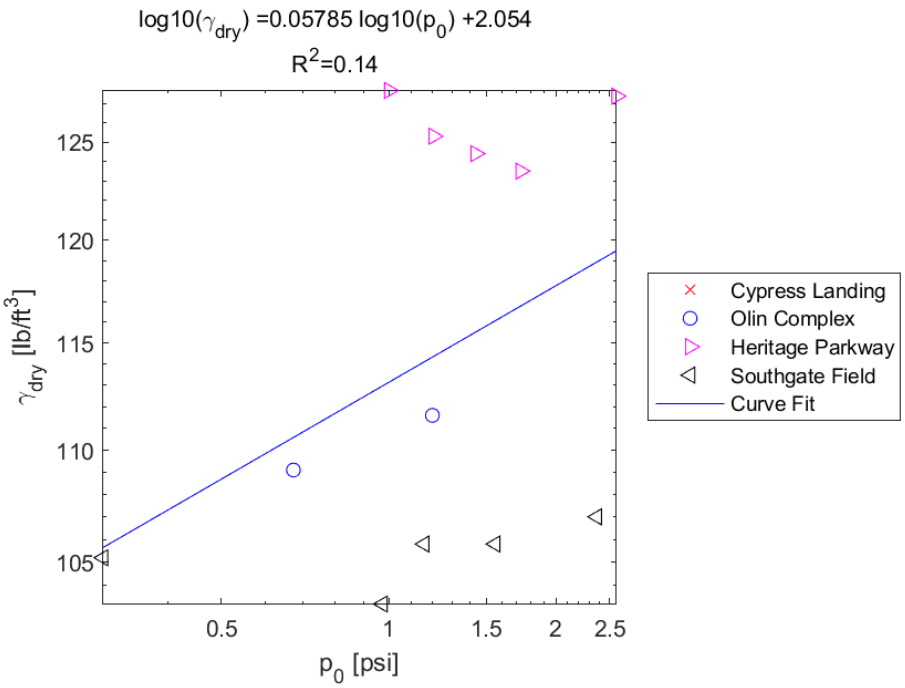

Figure E.333: Log - Log Model of γ_{dry} versus p_0 for SDPMT-6 Incremental Tests, All Sites

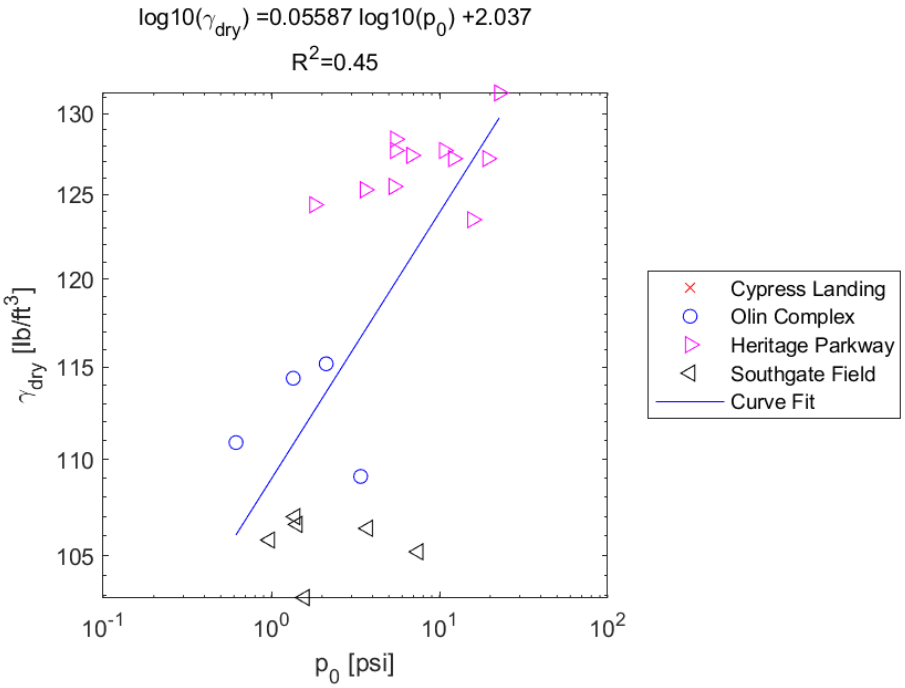

Figure E.334: Log - Log Model of γ_{dry} versus p_0 for SDPMT-6 Continuous Tests, All Sites

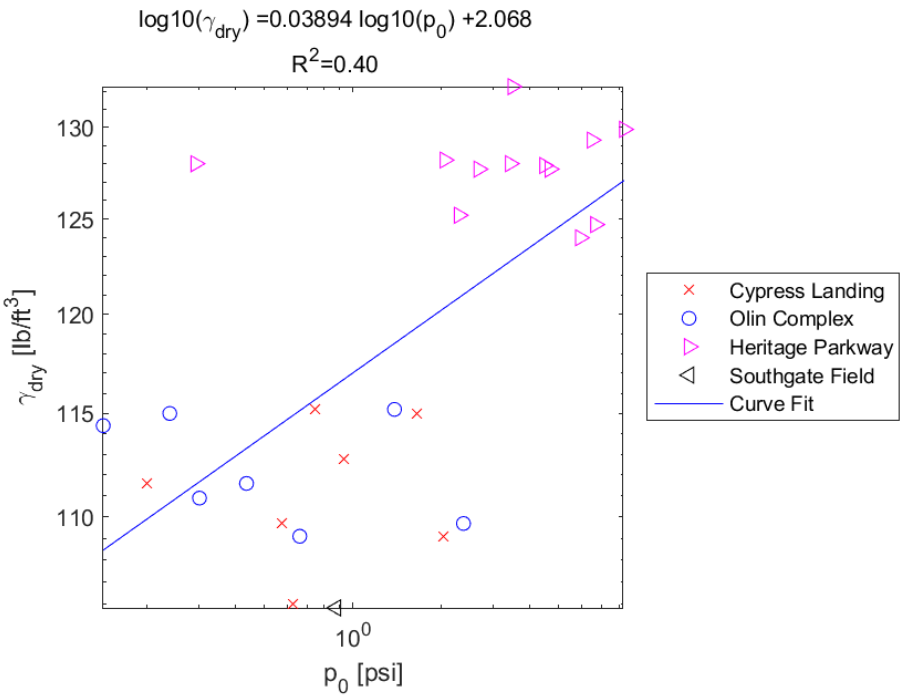

Figure E.335: Log - Log Model of γ_{dry} versus p_0 for SDPMT-12 Incremental Tests, All Sites

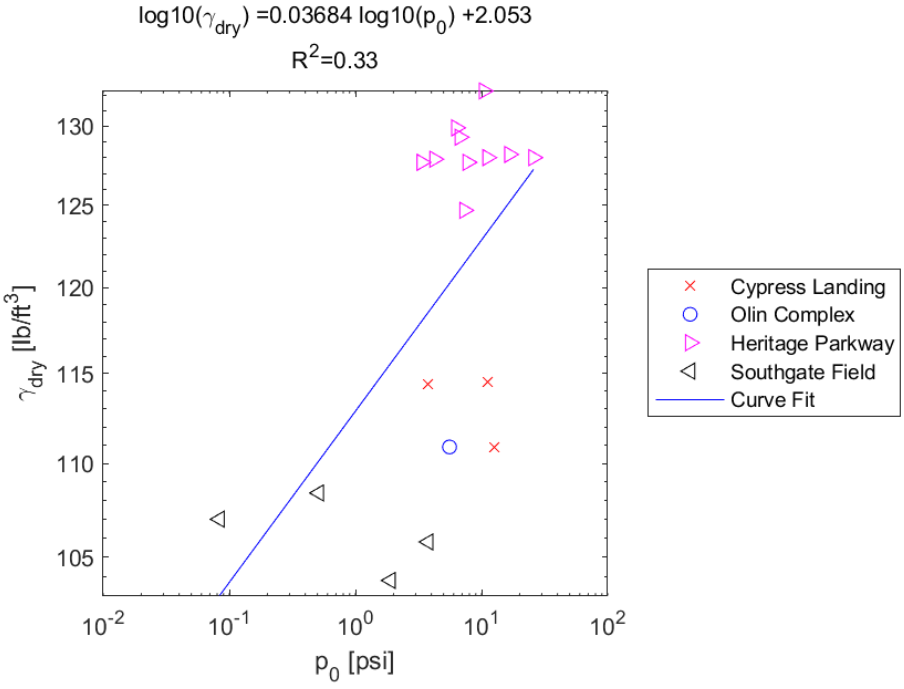

Figure E.336: Log - Log Model of γ_{dry} versus p_0 for SDPMT-12 Continuous Tests, All Sites

E.4.13 DCP PI versus E_0

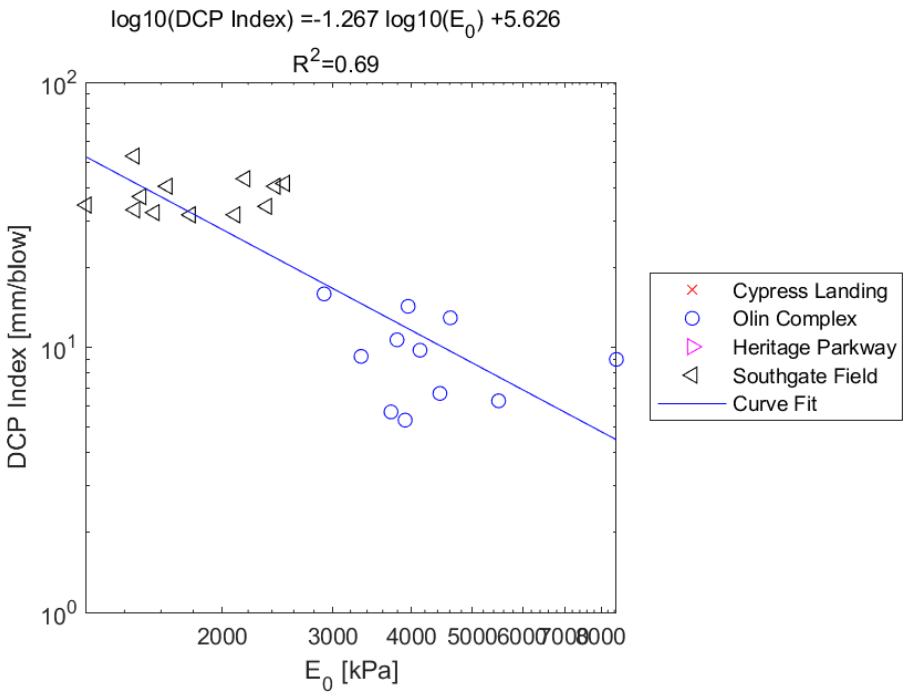

Figure E.337: Log - Log Model of DCP PI versus E_0 for SDPMT-6 Incremental Tests, All Sites

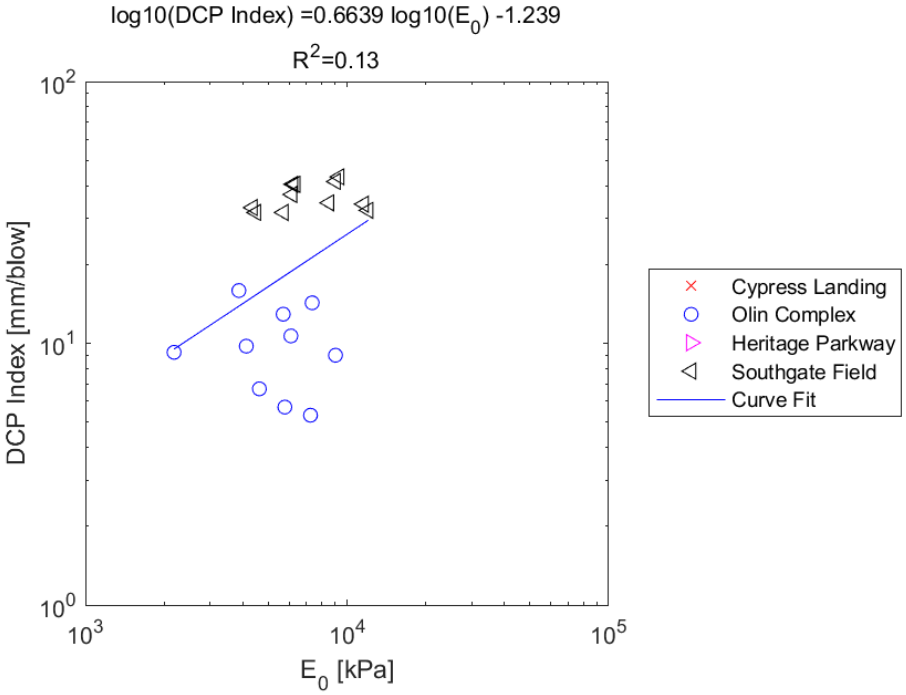

Figure E.338: Log - Log Model of DCP PI versus E_0 for SDPMT-6 Continuous Tests, All Sites

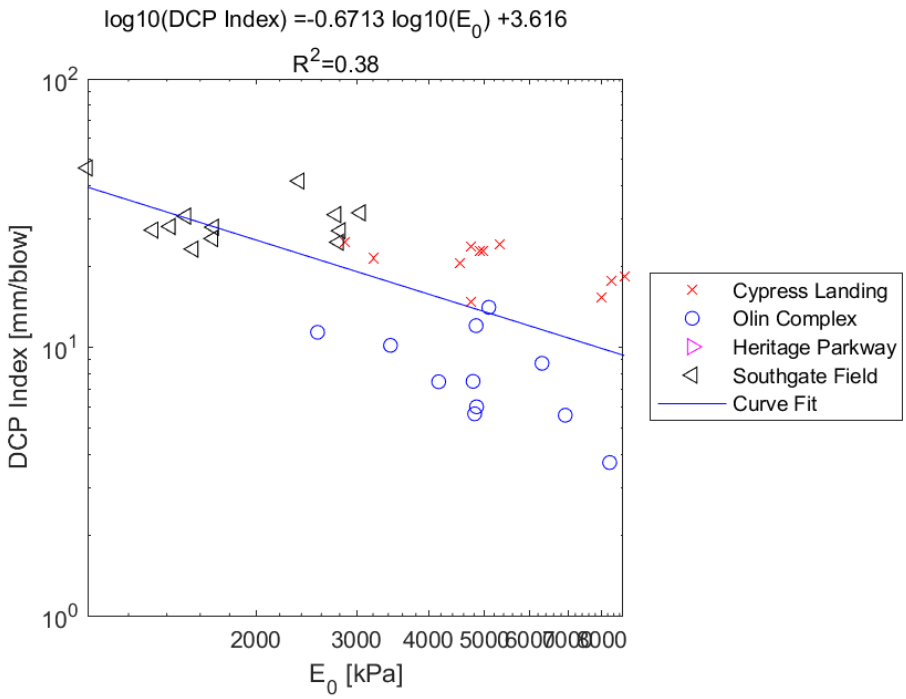

Figure E.339: Log - Log Model of DCP PI versus E_0 for SDPMT-12 Incremental Tests, All Sites

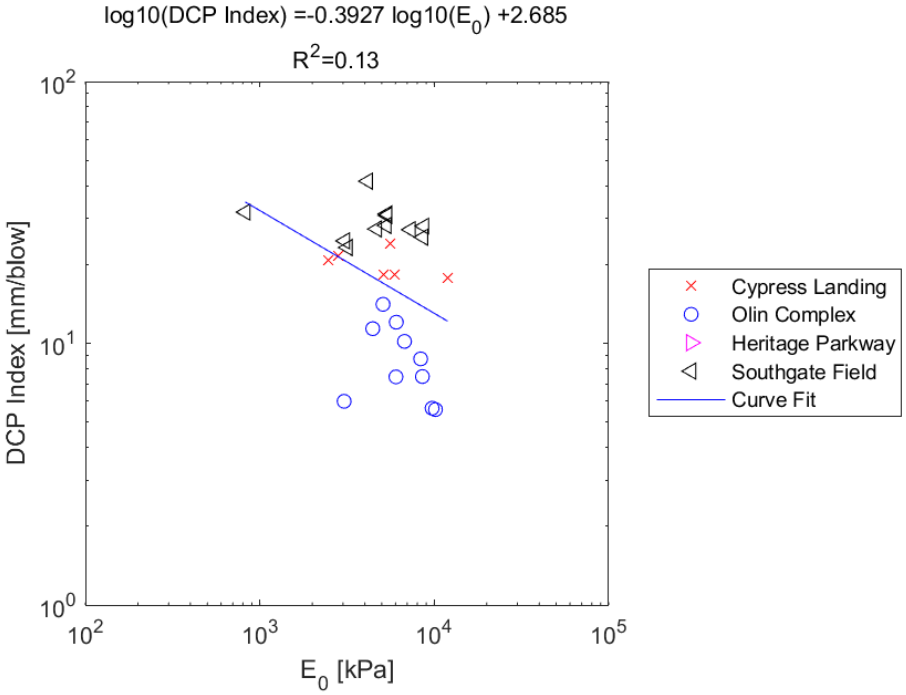

Figure E.340: Log - Log Model of DCP PI versus E_0 for SDPMT-12 Continuous Tests, All Sites

E.4.14 DCP PI versus $\mathbf{p}_L$

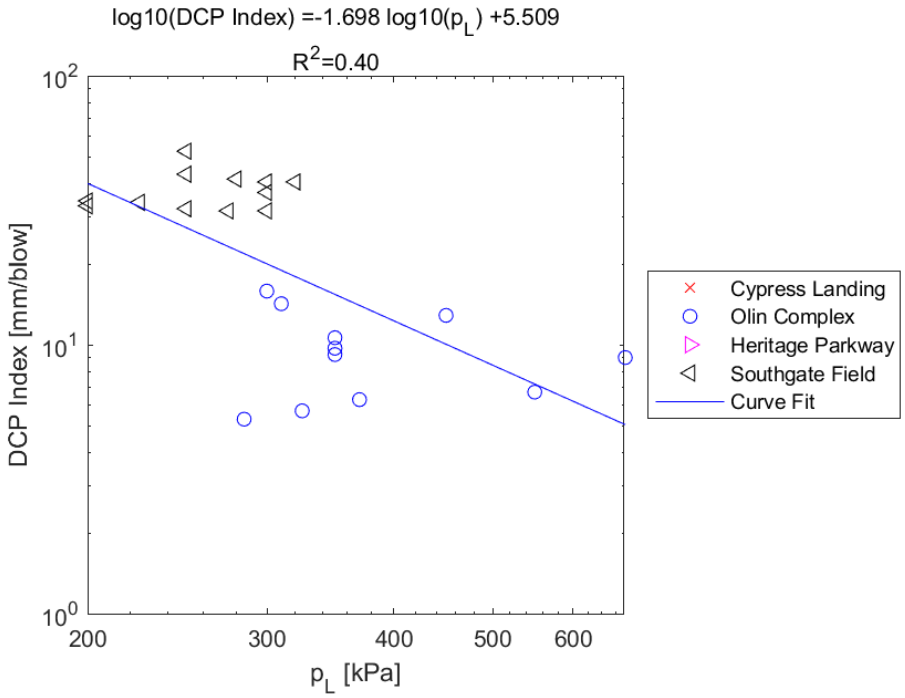

Figure E.341: Log - Log Model of DCP PI versus p_L for SDPMT-6 Incremental Tests, All Sites

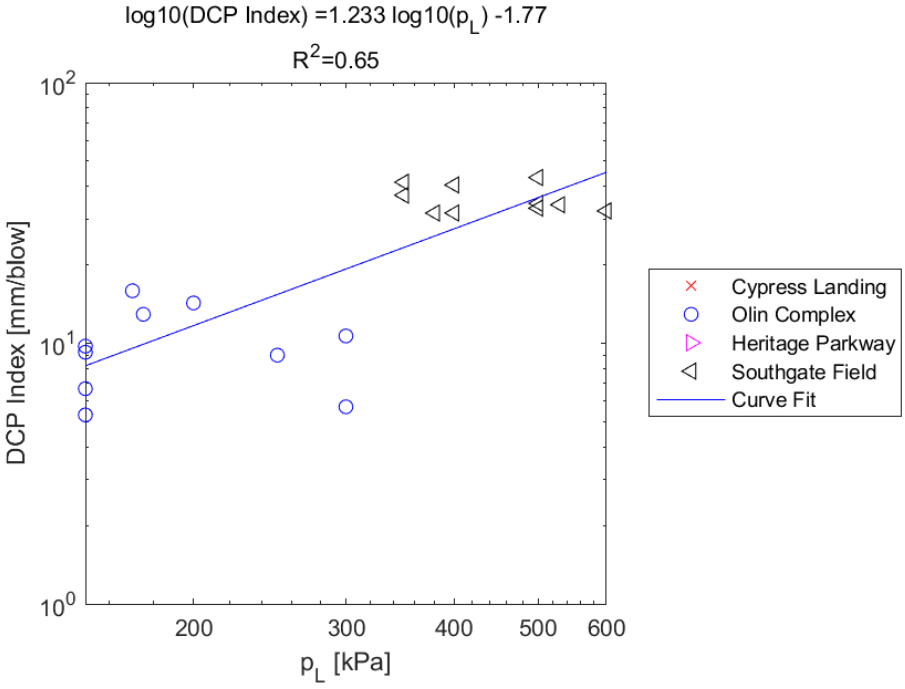

Figure E.342: Log - Log Model of DCP PI versus p_L for SDPMT-6 Continuous Tests, All Sites

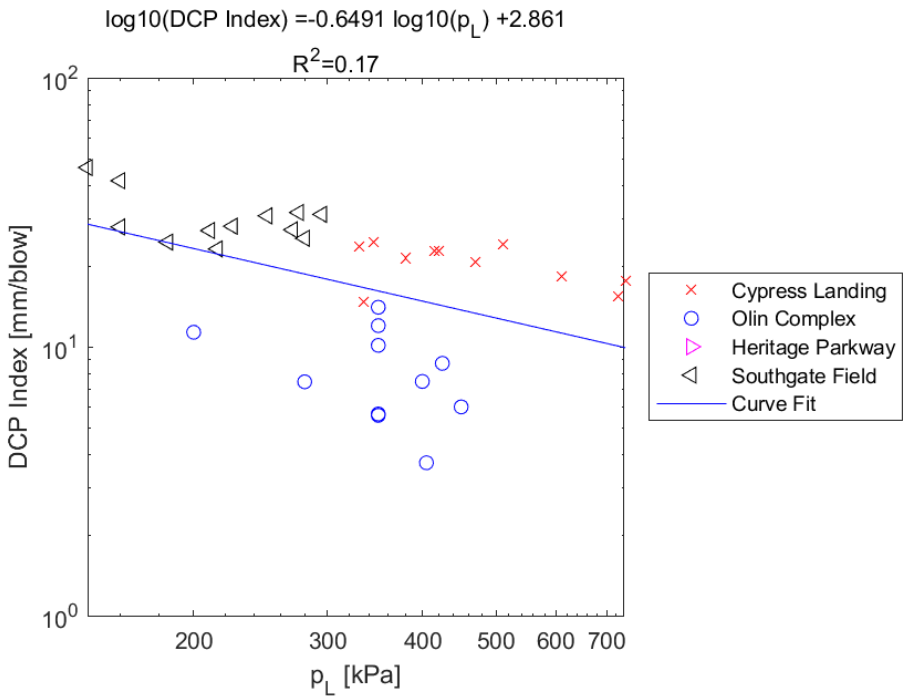

Figure E.343: Log - Log Model of DCP PI versus p_L for SDPMT-12 Incremental Tests, All Sites

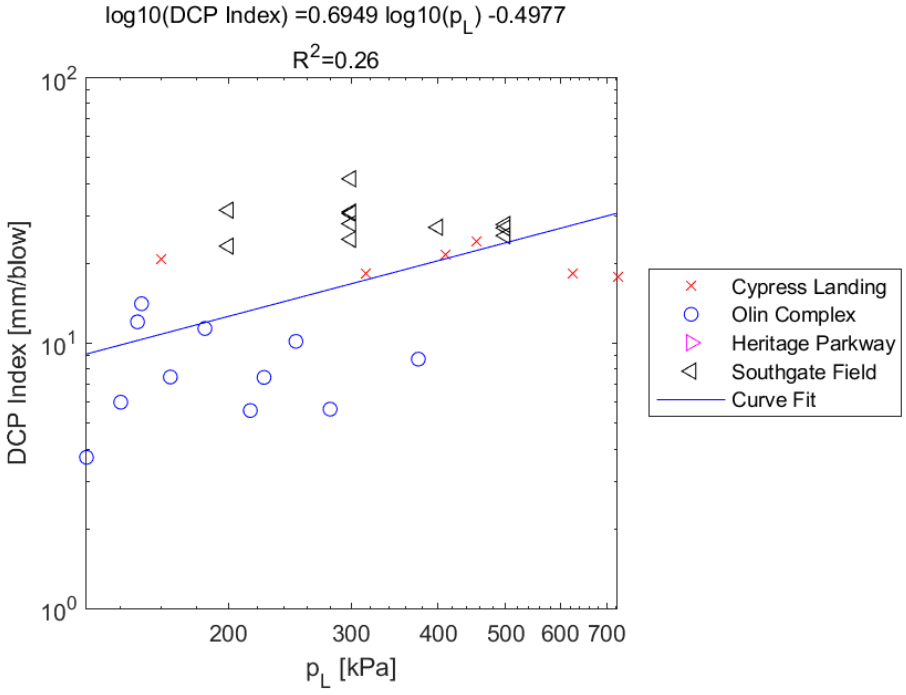

Figure E.344: Log - Log Model of DCP PI versus p_L for SDPMT-12 Continuous Tests, All Sites

E.4.15 DCP PI versus $\mathbf{p}_0$

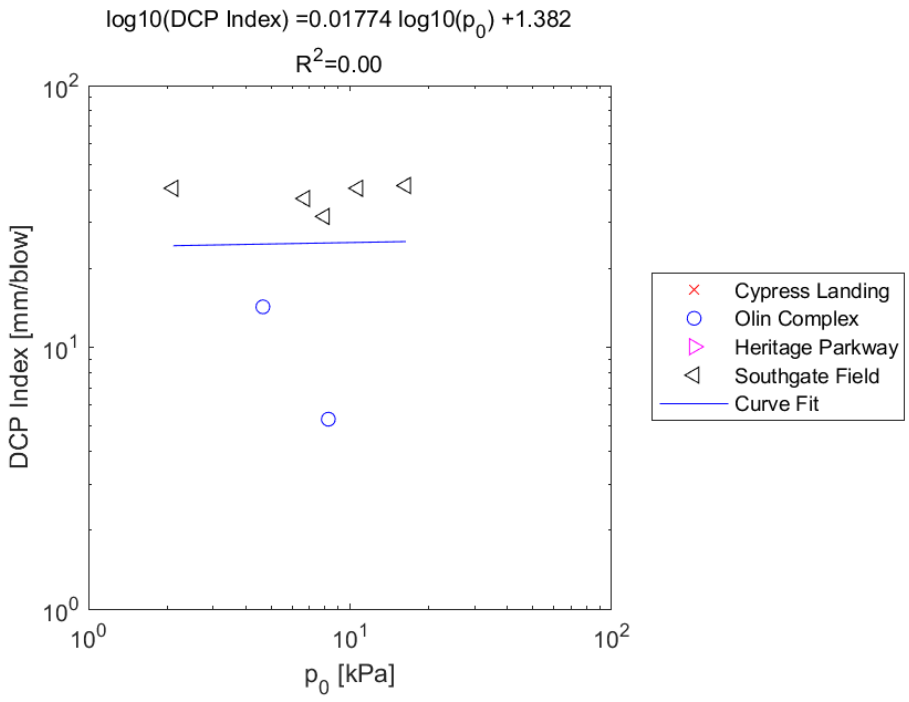

Figure E.345: Log - Log Model of DCP PI versus p_0 for SDPMT-6 Incremental Tests, All Sites

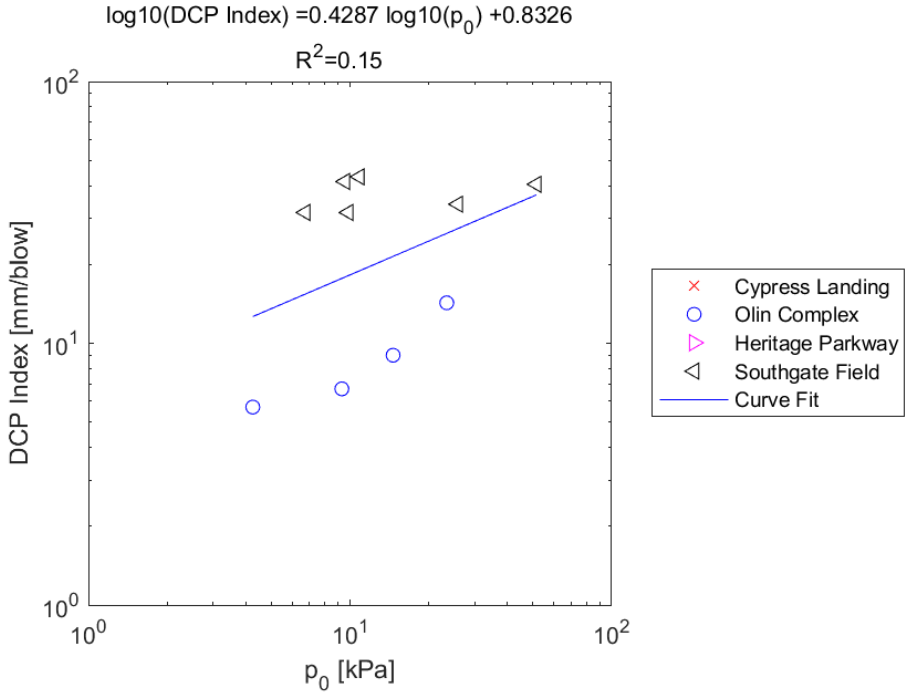

Figure E.346: Log - Log Model of DCP PI versus p_0 for SDPMT-6 Continuous Tests, All Sites

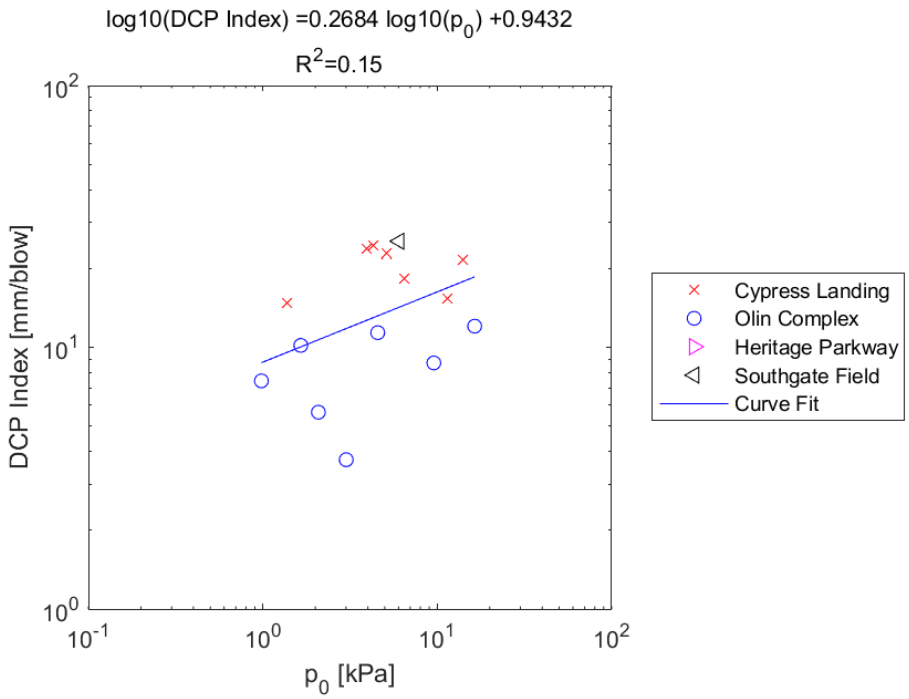

Figure E.347: Log - Log Model of DCP PI versus p_0 for SDPMT-12 Incremental Tests, All Sites

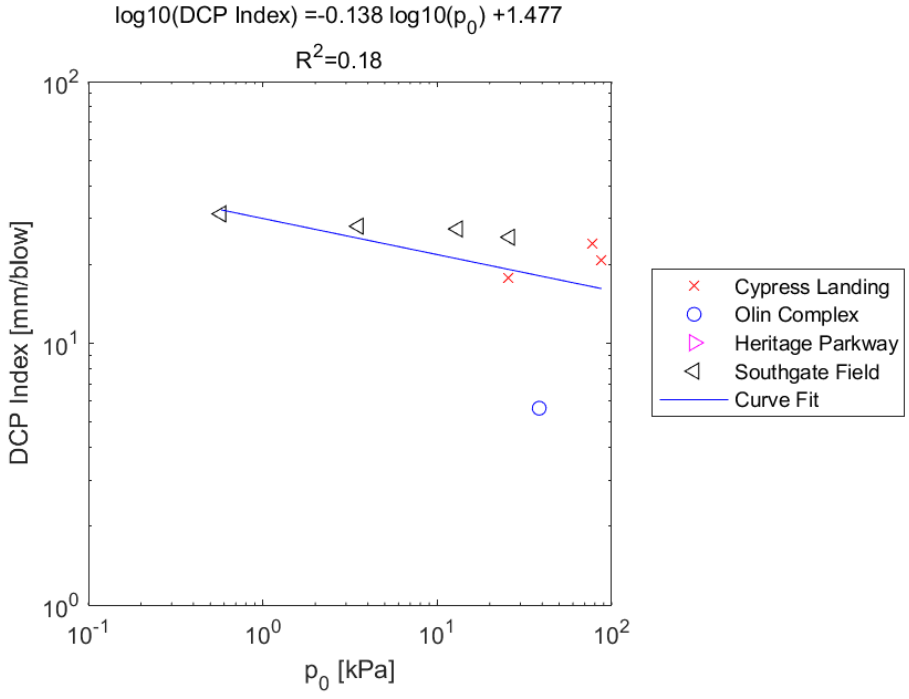

Figure E.348: Log - Log Model of DCP PI versus p_0 for SDPMT-12 Continuous Tests, All Sites

E.4.16 $\mathbf{E}_{d,zorn}$ versus $\mathbf{E}_0$

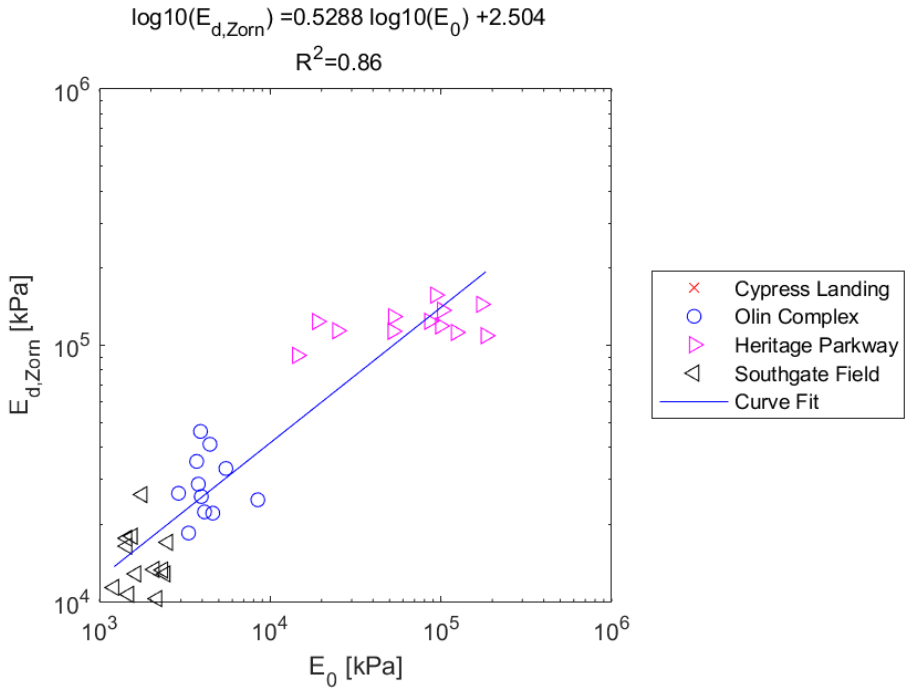

Figure E.349: Log - Log Model of $E_{d,zorn}$ versus E_0 for SDPMT-6 Incremental Tests, All Sites

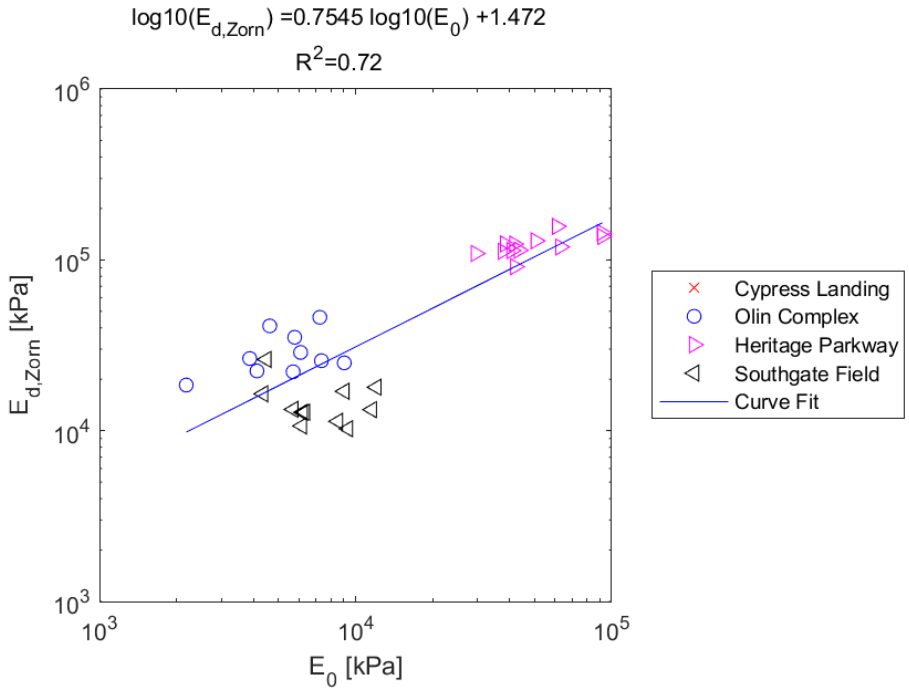

Figure E.350: Log - Log Model of $E_{d,zorn}$ versus E_0 for SDPMT-6 Continuous Tests, All Sites

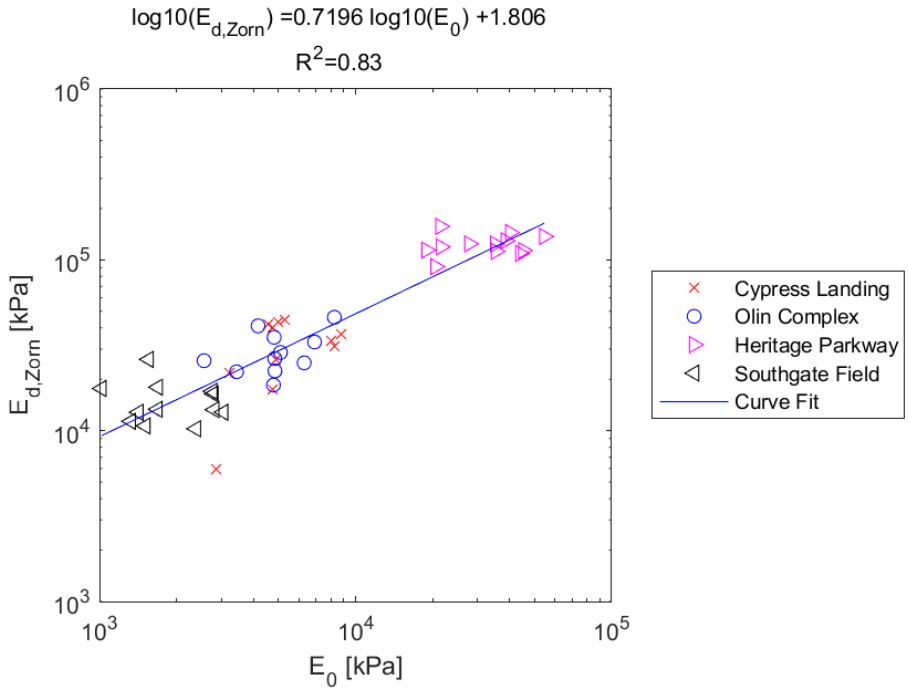

Figure E.351: Log - Log Model of $E_{d,zorn}$ versus E_0 for SDPMT-12 Incremental Tests, All Sites

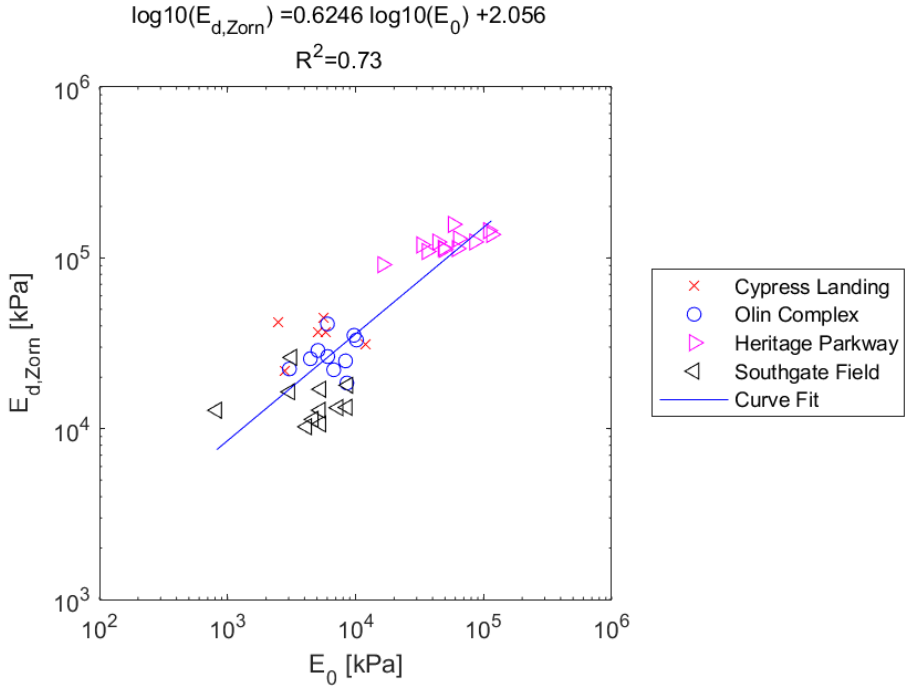

Figure E.352: Log - Log Model of $E_{d,zorn}$ versus E_0 for SDPMT-12 Continuous Tests, All Sites

E.4.17 $\mathbf{E}_{d,zorn}$ versus $\mathbf{p}_L$

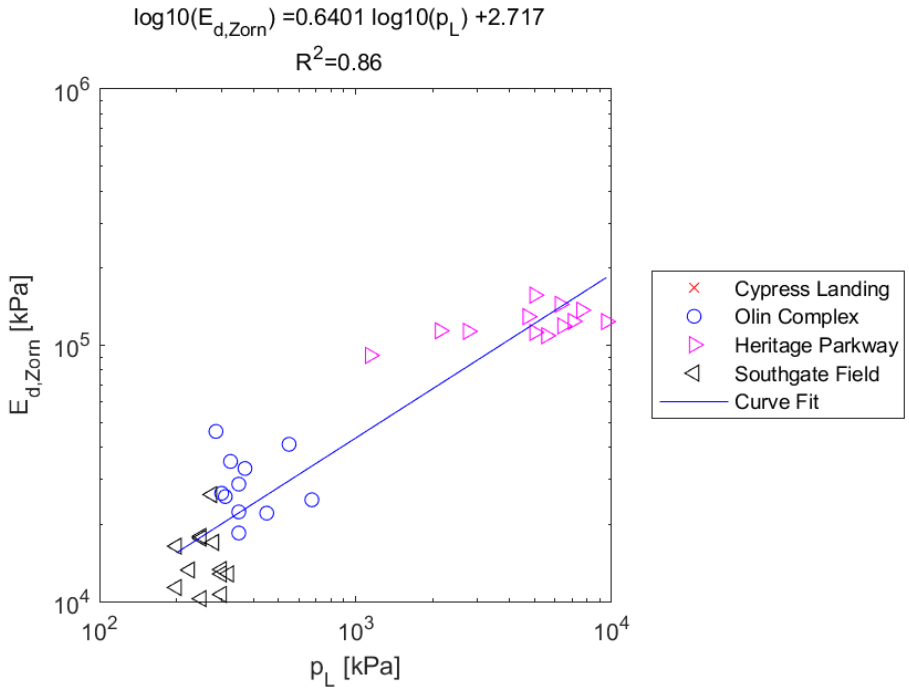

Figure E.353: Log - Log Model of $E_{d,zorn}$ versus p_L for SDPMT-6 Incremental Tests, All Sites

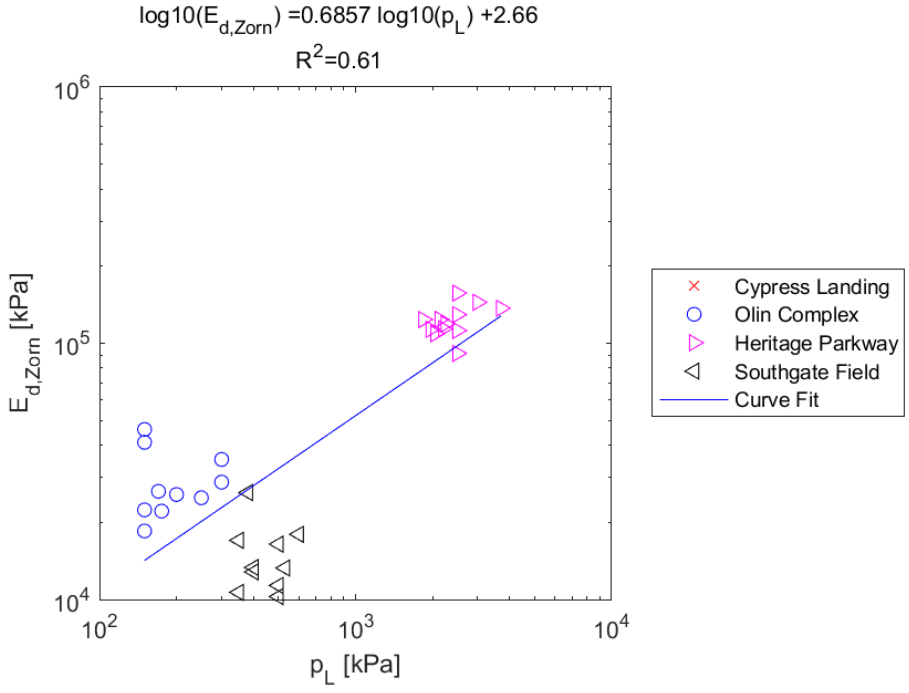

Figure E.354: Log - Log Model of $E_{d,zorn}$ versus p_L for SDPMT-6 Continuous Tests, All Sites

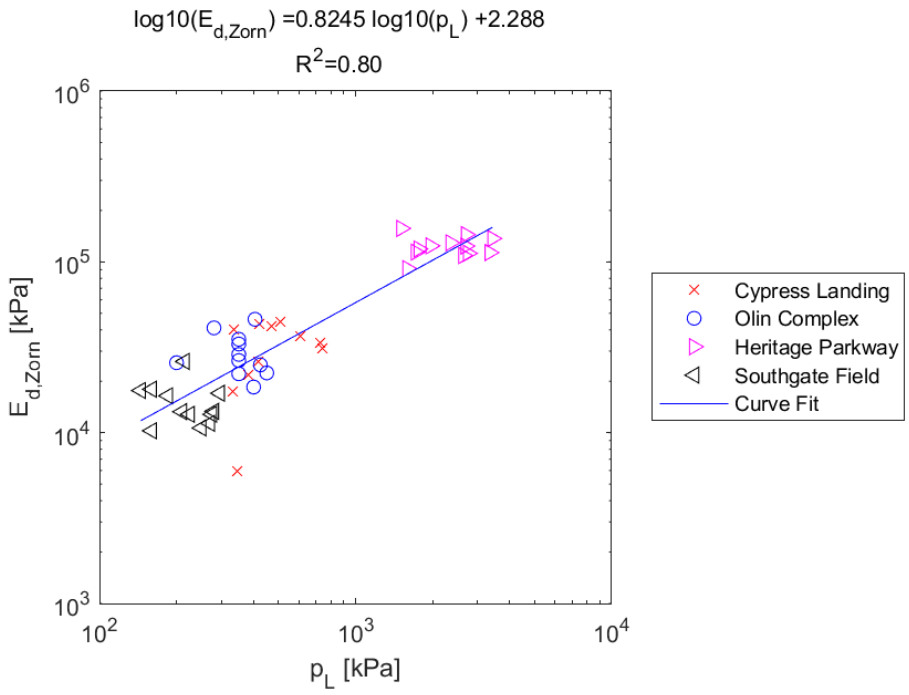

Figure E.355: Log - Log Model of $E_{d,zorn}$ versus p_L for SDPMT-12 Incremental Tests, All Sites

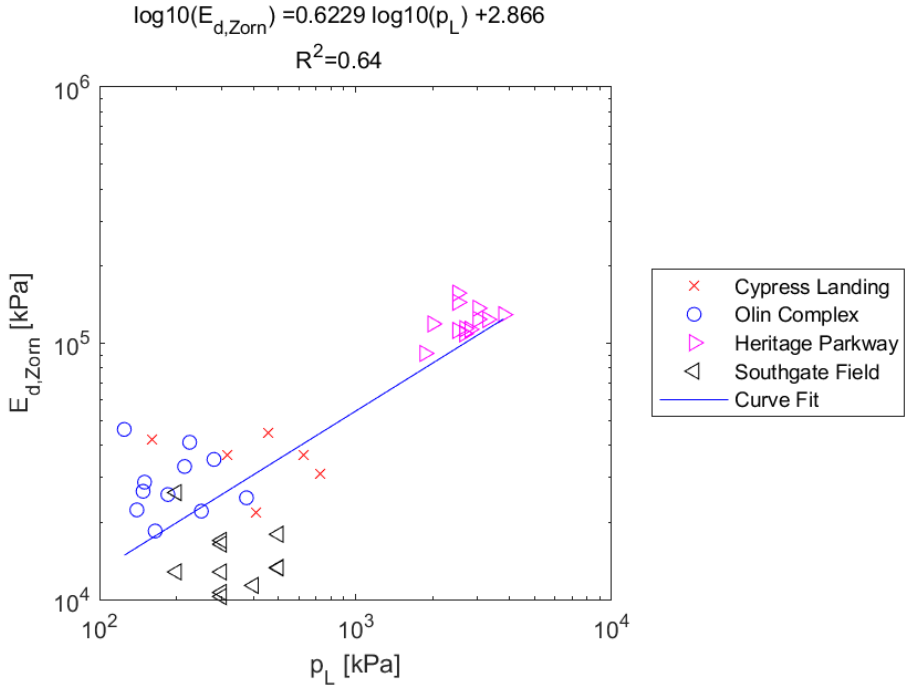

Figure E.356: Log - Log Model of $E_{d,zorn}$ versus p_L for SDPMT-12 Continuous Tests, All Sites

E.4.18 $\mathbf{E}_{d,zorn}$ versus $\mathbf{p}_0$

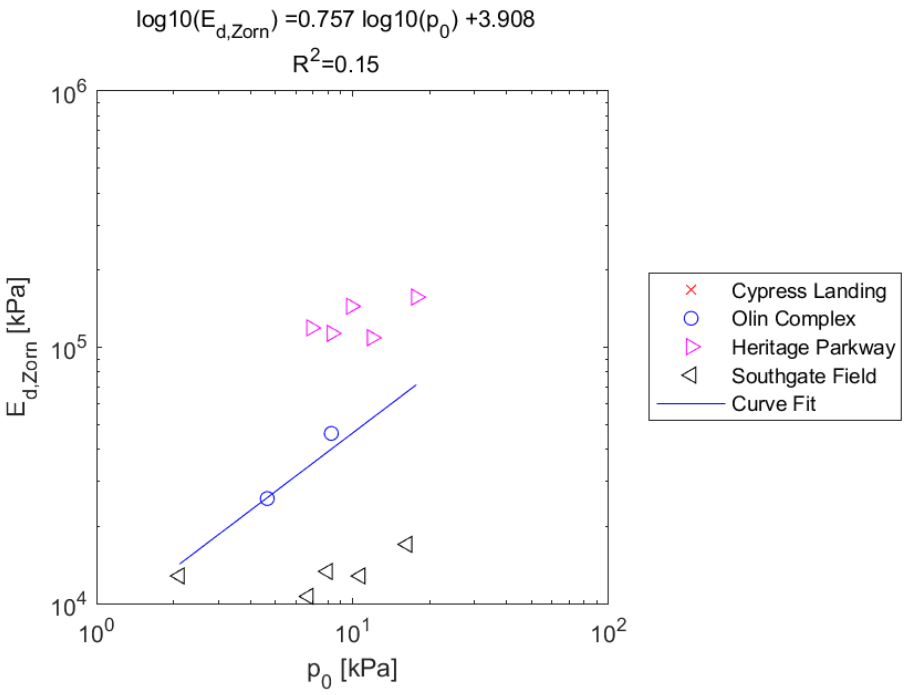

Figure E.357: Log - Log Model of $E_{d,zorn}$ versus p_0 for SDPMT-6 Incremental Tests, All Sites

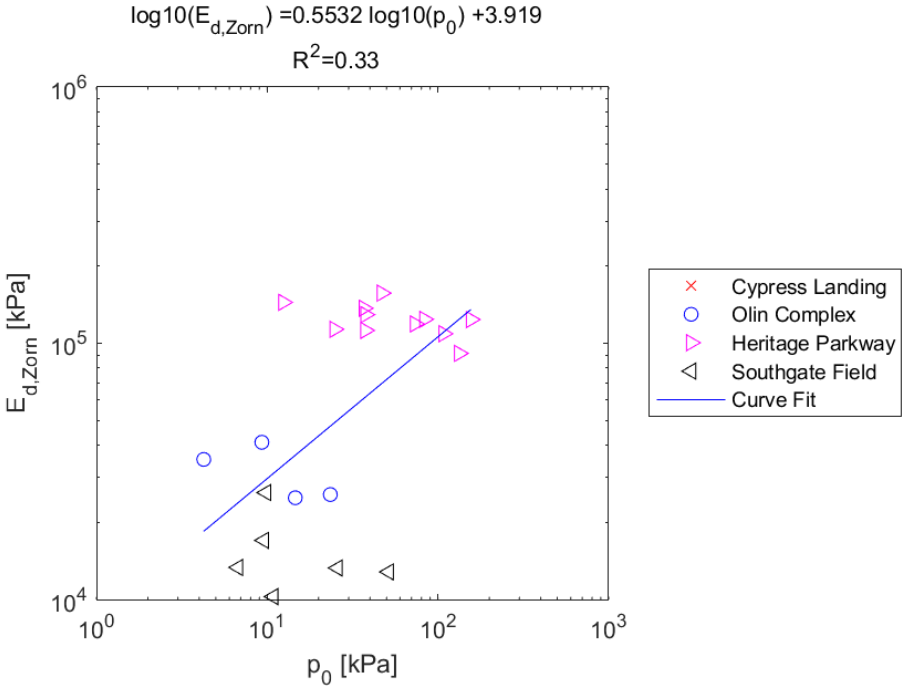

Figure E.358: Log - Log Model of $E_{d,zorn}$ versus p_0 for SDPMT-6 Continuous Tests, All Sites

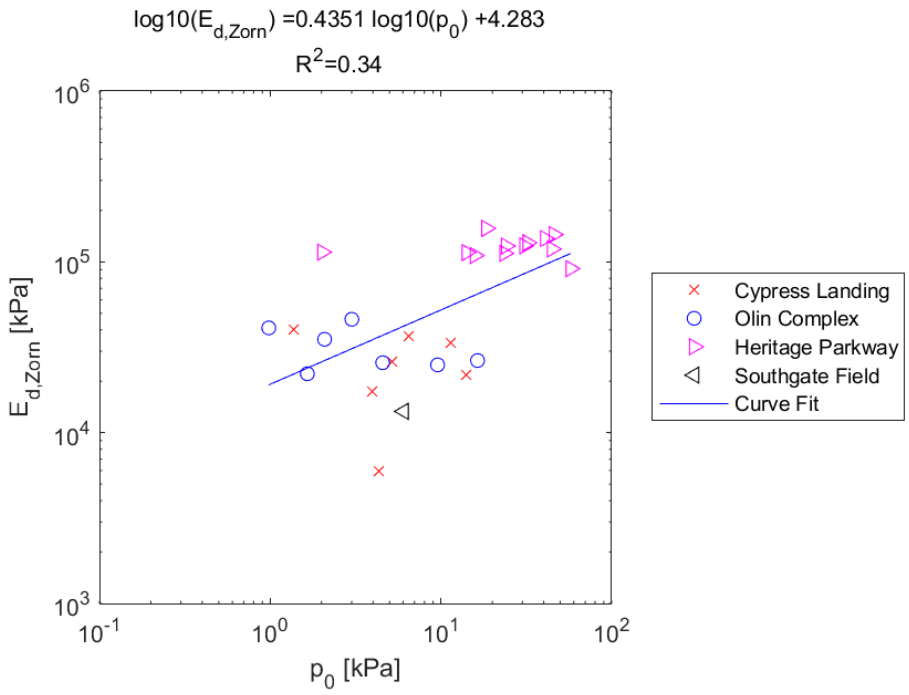

Figure E.359: Log - Log Model of $E_{d,zorn}$ versus p_0 for SDPMT-12 Incremental Tests, All Sites

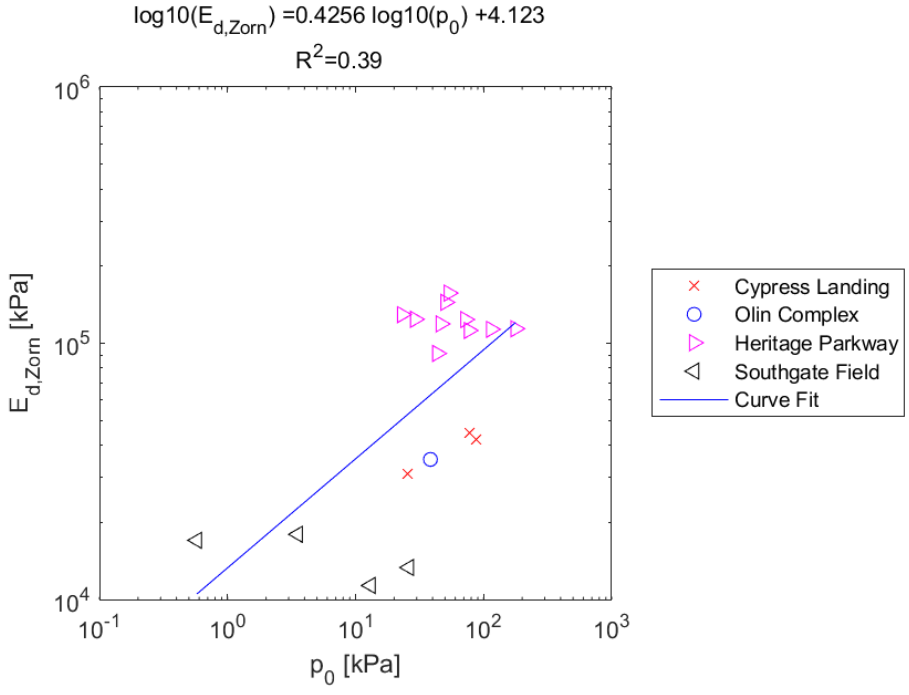

Figure E.360: Log - Log Model of $E_{d,zorn}$ versus p_0 for SDPMT-12 Continuous Tests, All Sites

E.4.19 $\mathbf{E}_{0,Dynatest}$ versus $\mathbf{E}_0$

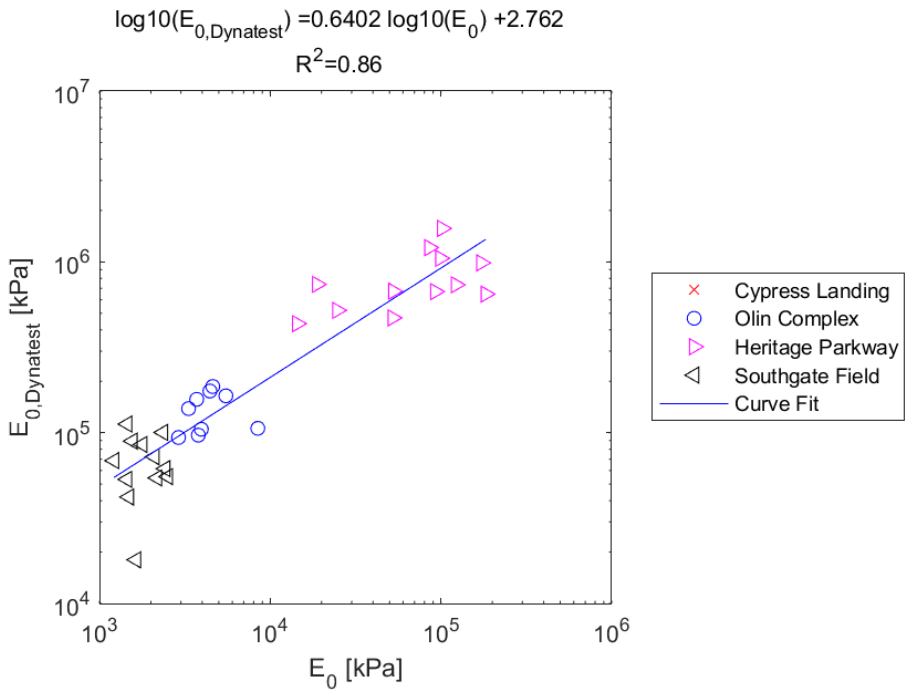

Figure E.361: Log - Log Model of $E_{0,Dynatest}$ versus E_0 for SDPMT-6 Incremental Tests, All Sites

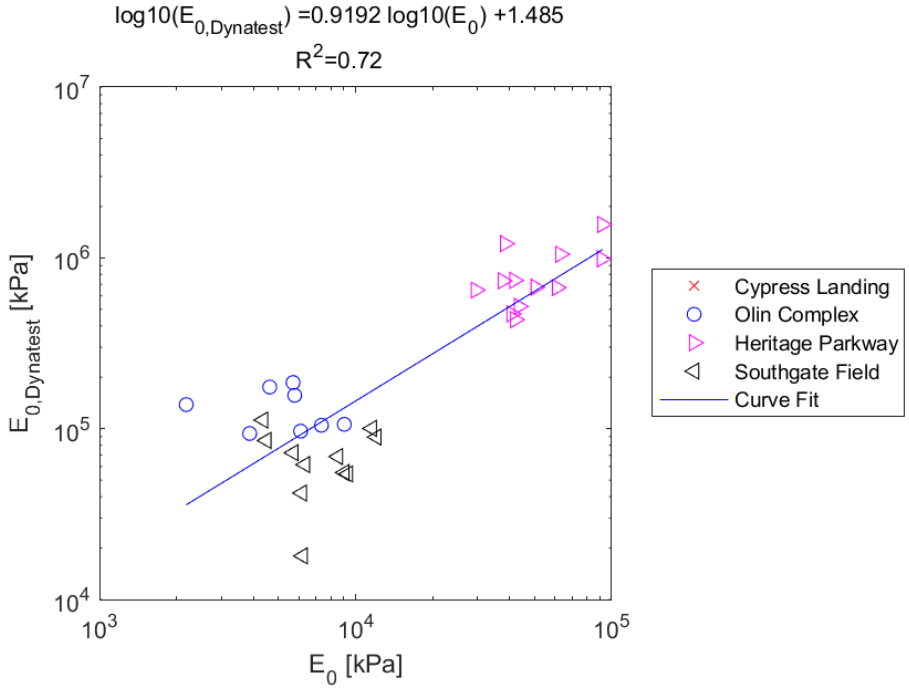

Figure E.362: Log - Log Model of $E_{0,Dynatest}$ versus E_0 for SDPMT-6 Continuous Tests, All Sites

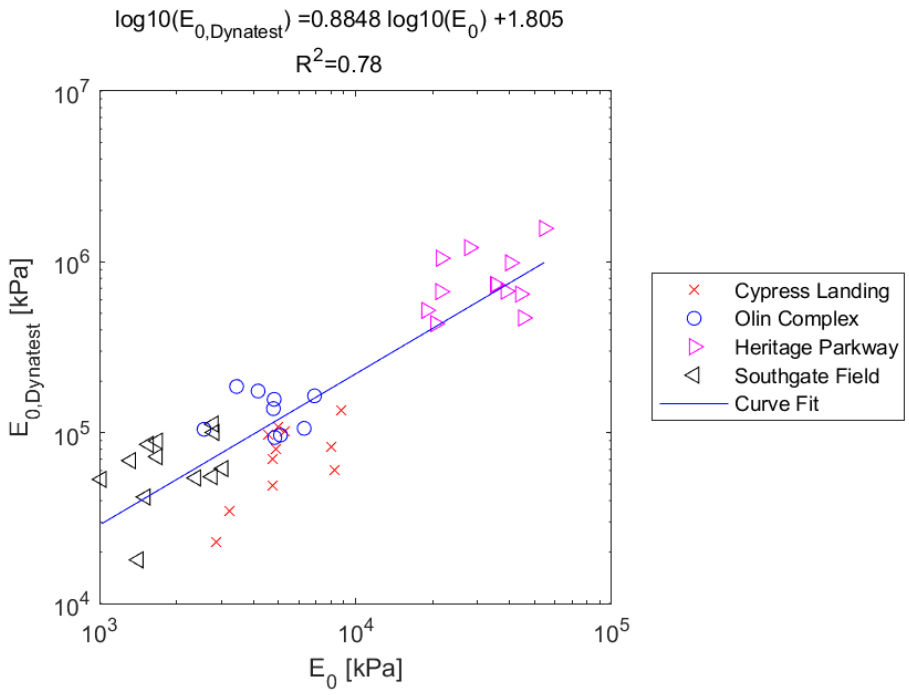

Figure E.363: Log - Log Model of $E_{0,Dynatest}$ versus E_0 for SDPMT-12 Incremental Tests, All Sites

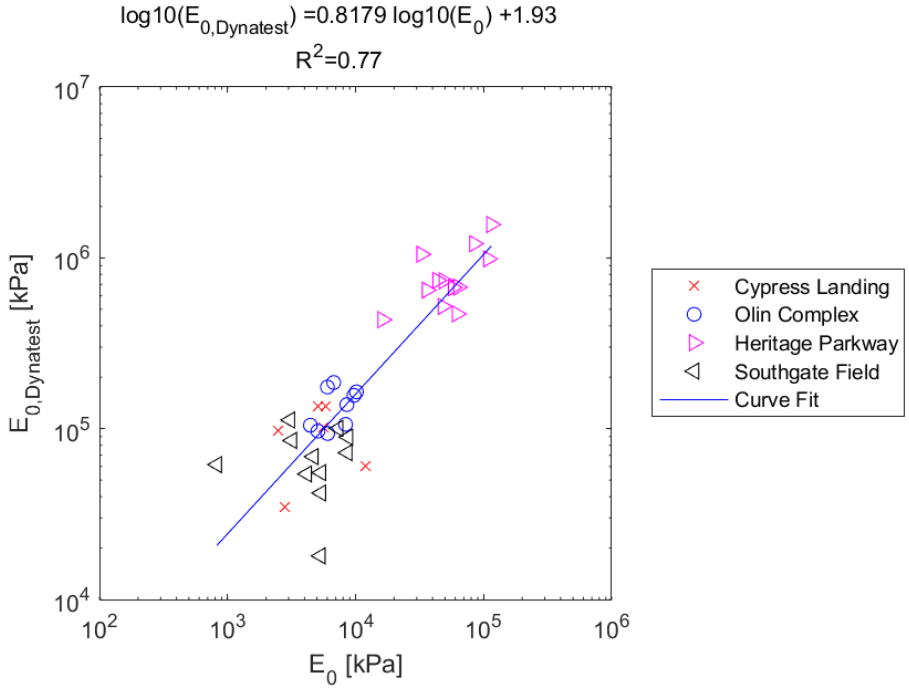

Figure E.364: Log - Log Model of $E_{0,Dynatest}$ versus E_0 for SDPMT-12 Continuous Tests, All Sites

E.4.20 $\mathbf{E}_{0,Dynatest}$ versus $\mathbf{p}_L$

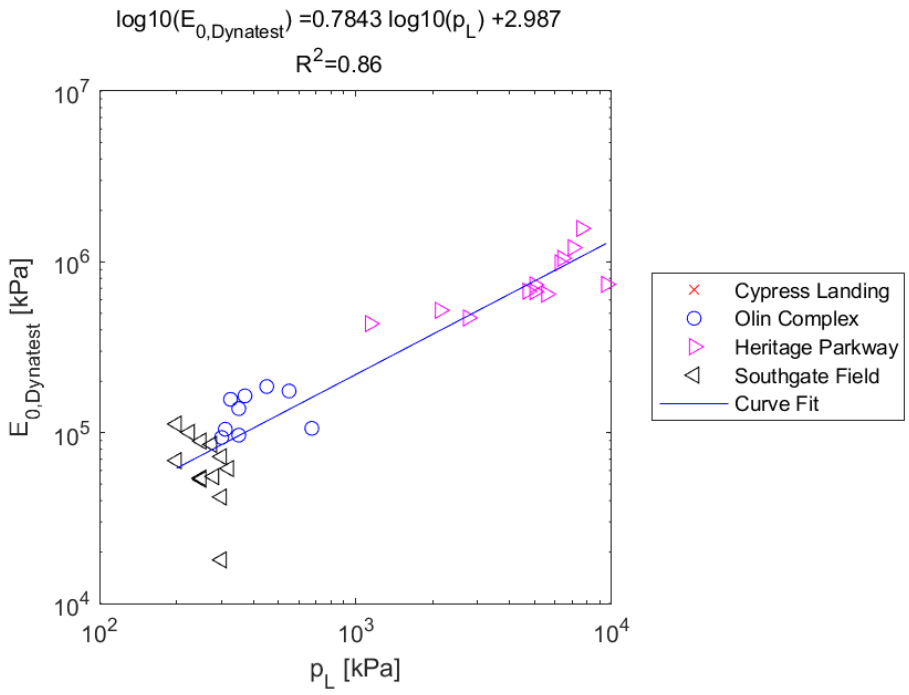

Figure E.365: Log - Log Model of $E_{0,Dynatest}$ versus p_L for SDPMT-6 Incremental Tests, All Sites

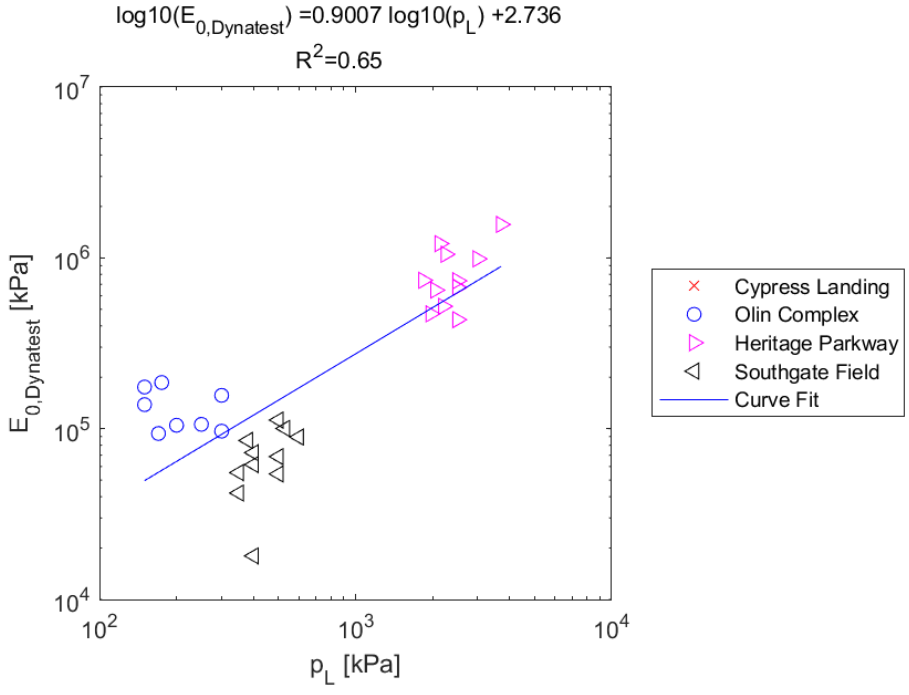

Figure E.366: Log - Log Model of $E_{0,Dynatest}$ versus p_L for SDPMT-6 Continuous Tests, All Sites

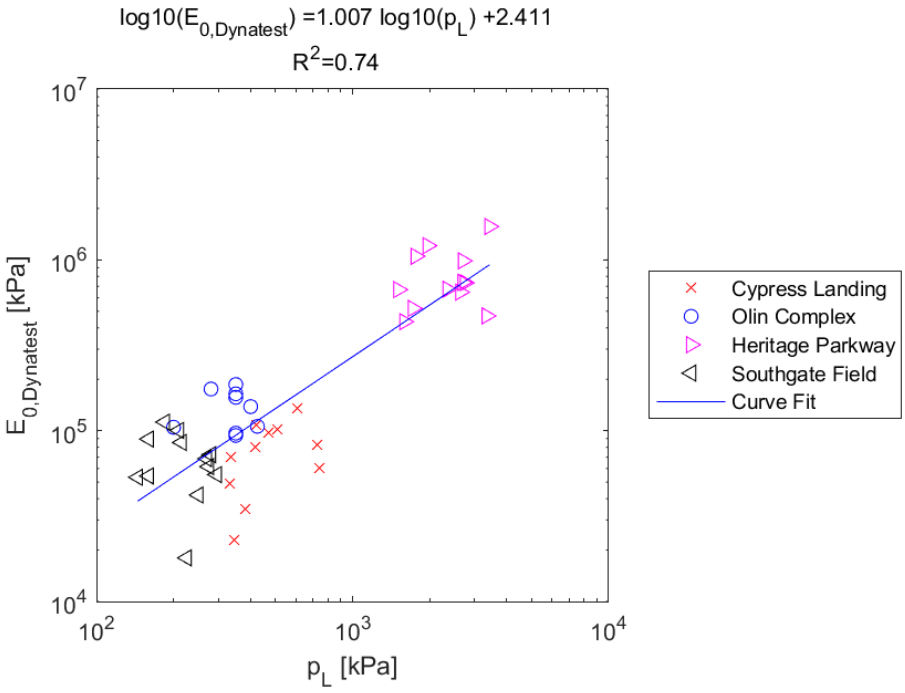

Figure E.367: Log - Log Model of $E_{0,Dynatest}$ versus p_L for SDPMT-12 Incremental Tests, All Sites

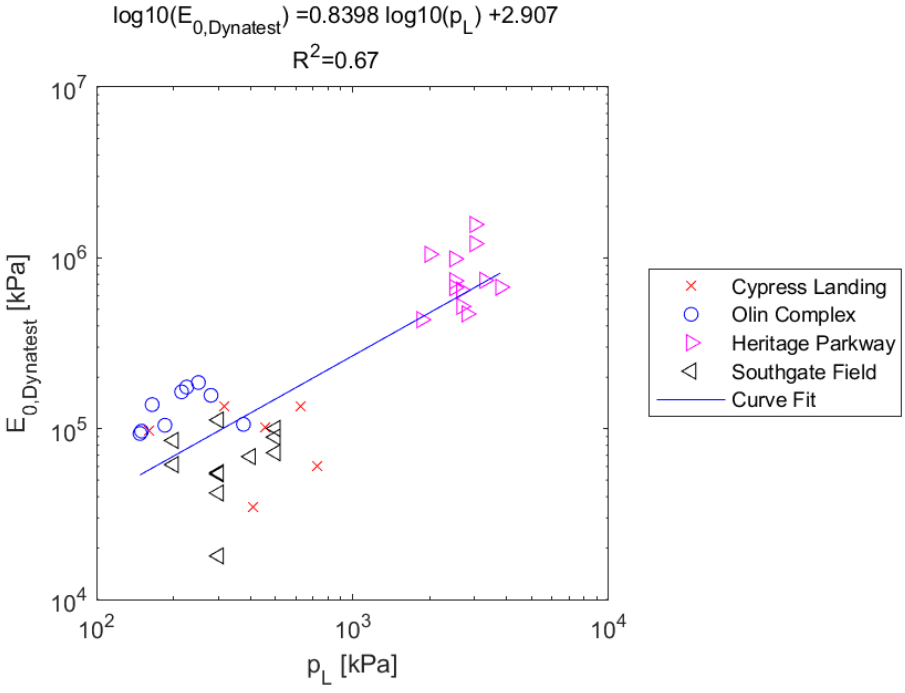

Figure E.368: Log - Log Model of $E_{0,Dynatest}$ versus p_L for SDPMT-12 Continuous Tests, All Sites

E.4.21 $\mathbf{E}_{0,Dynatest}$ versus $\mathbf{p}_0$

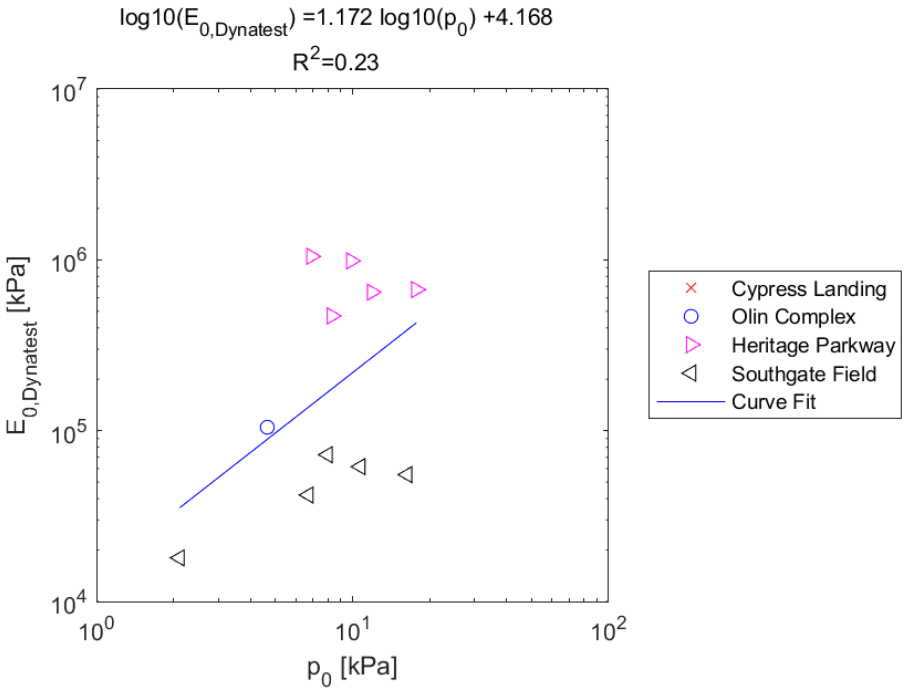

Figure E.369: Log - Log Model of $E_{0,Dynatest}$ versus p_0 for SDPMT-6 Incremental Tests, All Sites

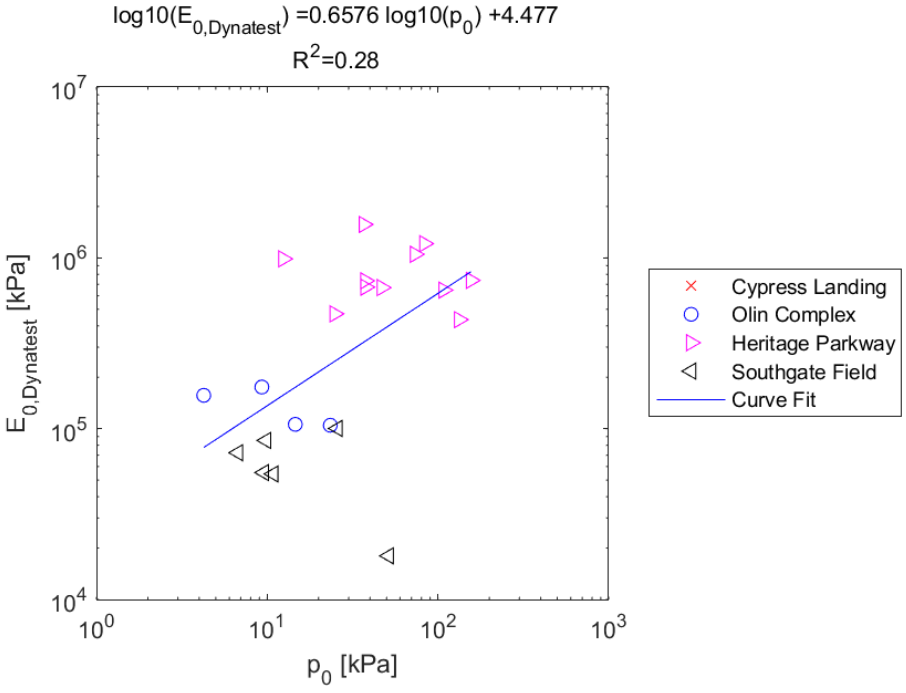

Figure E.370: Log - Log Model of $E_{0,Dynatest}$ versus p_0 for SDPMT-6 Continuous Tests, All Sites

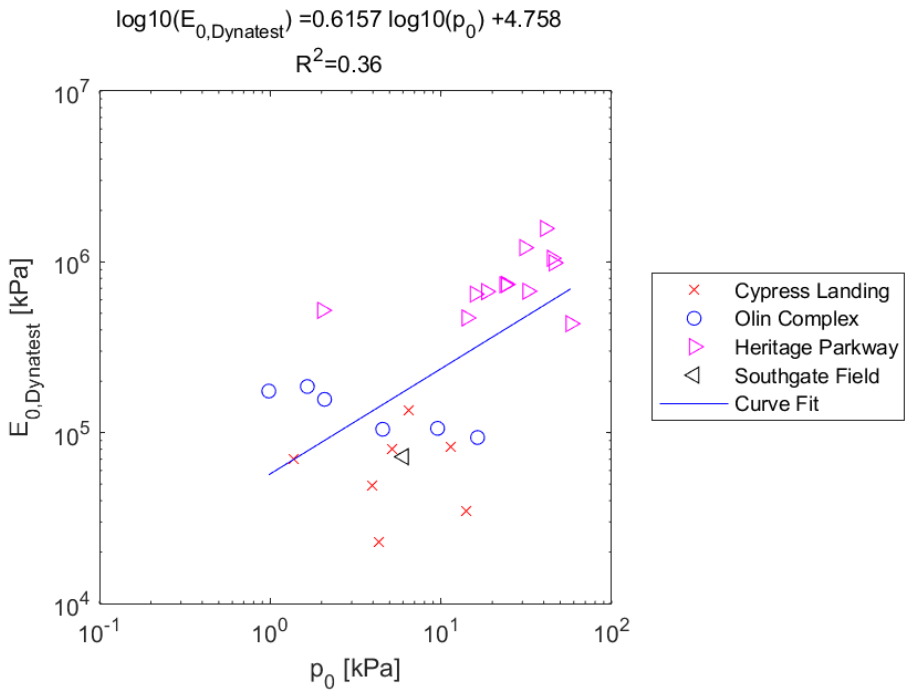

Figure E.371: Log - Log Model of $E_{0,Dynatest}$ versus p_0 for SDPMT-12 Incremental Tests, All Sites

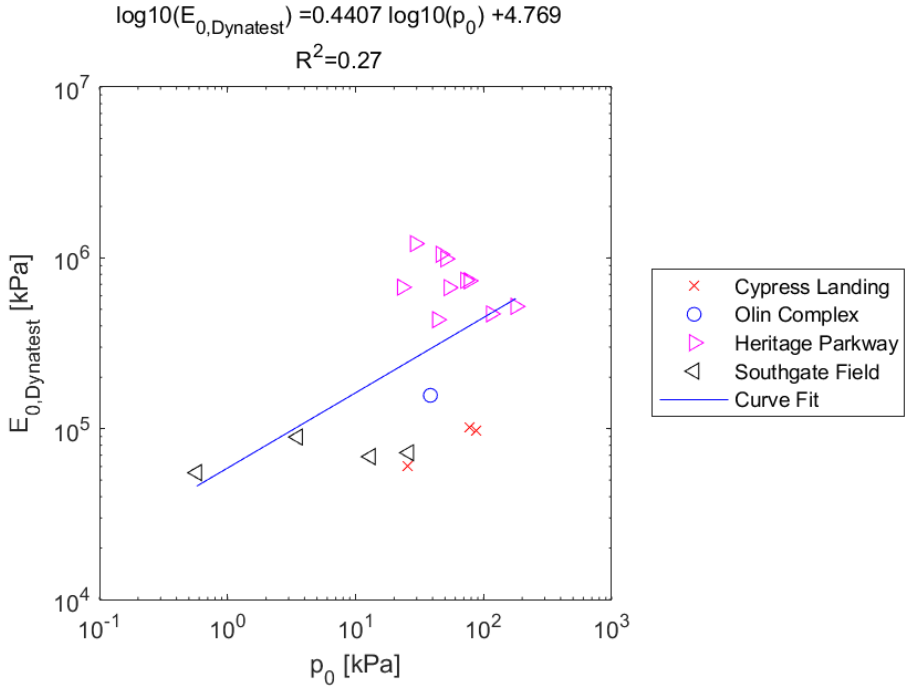

Figure E.372: Log - Log Model of $E_{0,Dynatest}$ versus p_0 for SDPMT-12 Continuous Tests, All Sites

E.4.22 CIV versus E_0

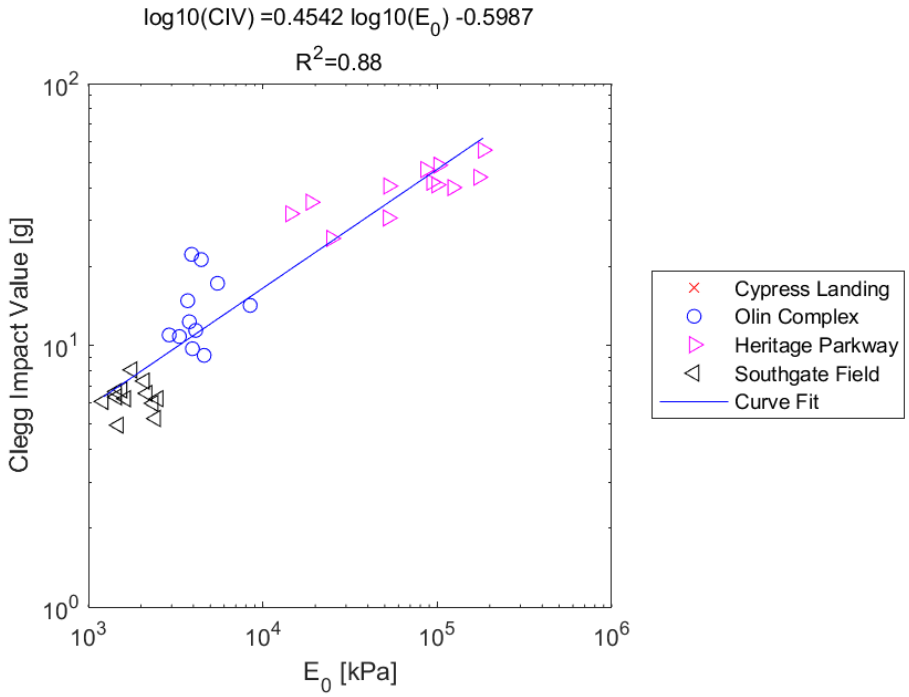

Figure E.373: Log - Log Model of CIV versus E_0 for SDPMT-6 Incremental Tests, All Sites

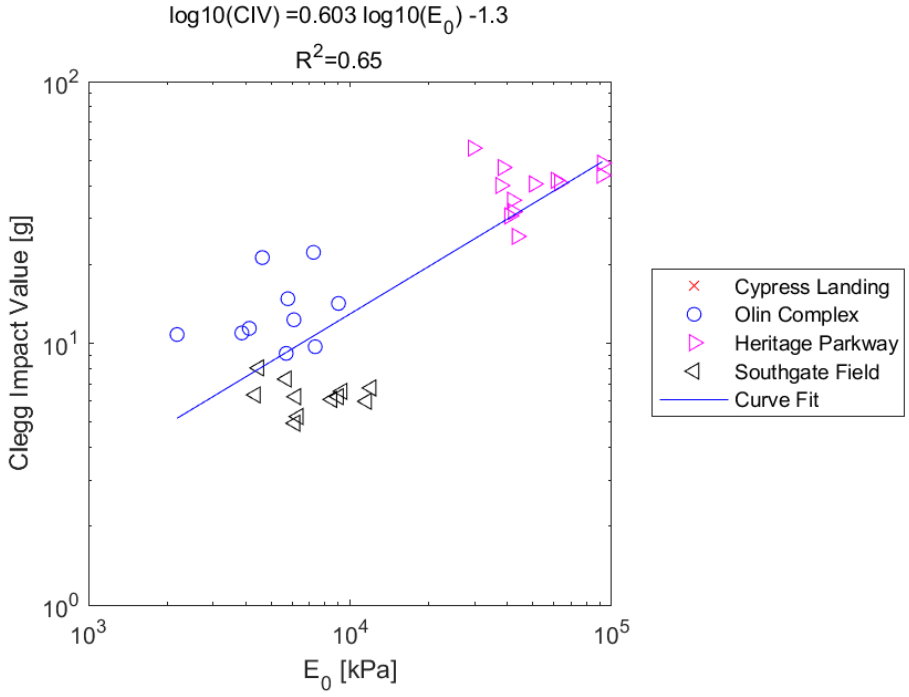

Figure E.374: Log - Log Model of CIV versus E_0 for SDPMT-6 Continuous Tests, All Sites

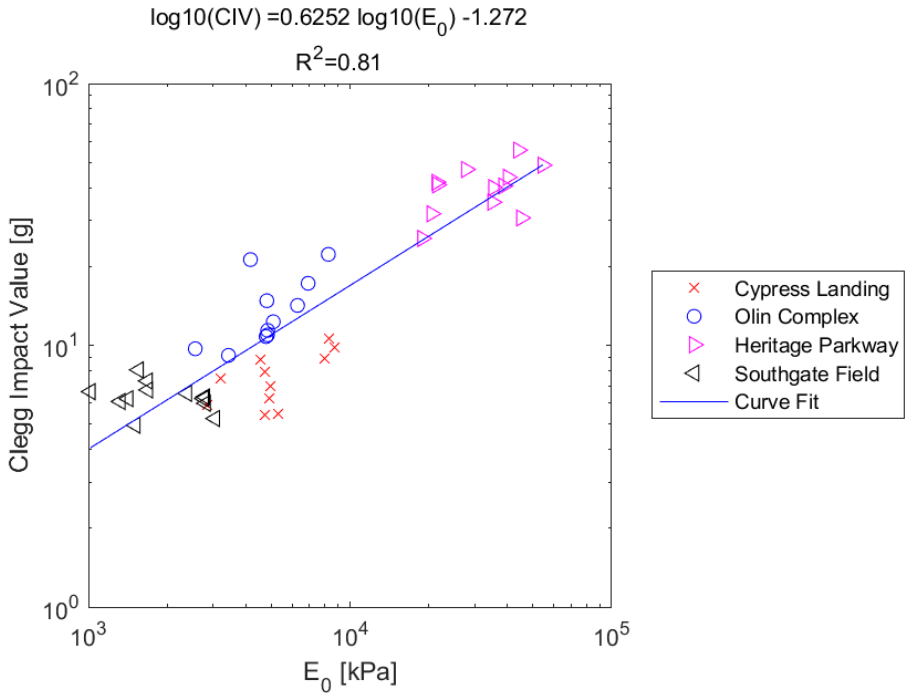

Figure E.375: Log - Log Model of CIV versus E_0 for SDPMT-12 Incremental Tests, All Sites

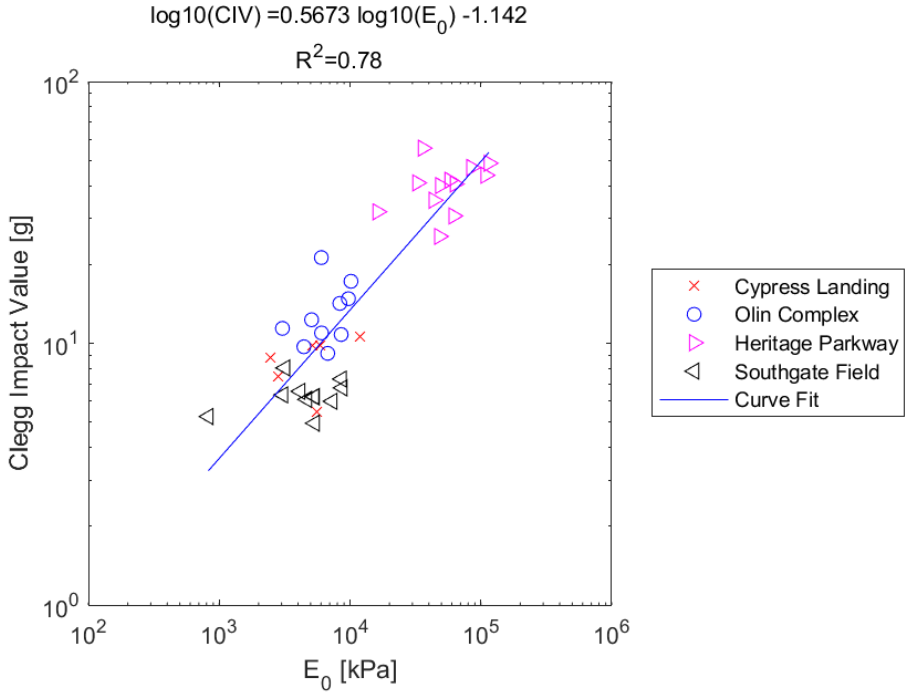

Figure E.376: Log - Log Model of CIV versus E_0 for SDPMT-12 Continuous Tests, All Sites

E.4.23 CIV versus $\mathbf{p}_L$

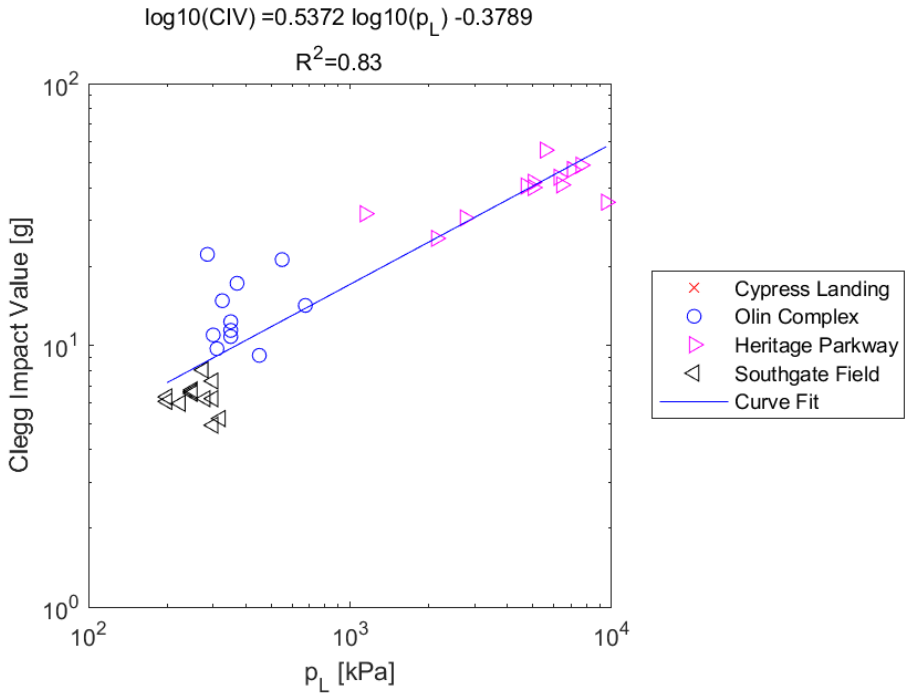

Figure E.377: Log - Log Model of CIV versus p_L for SDPMT-6 Incremental Tests, All Sites

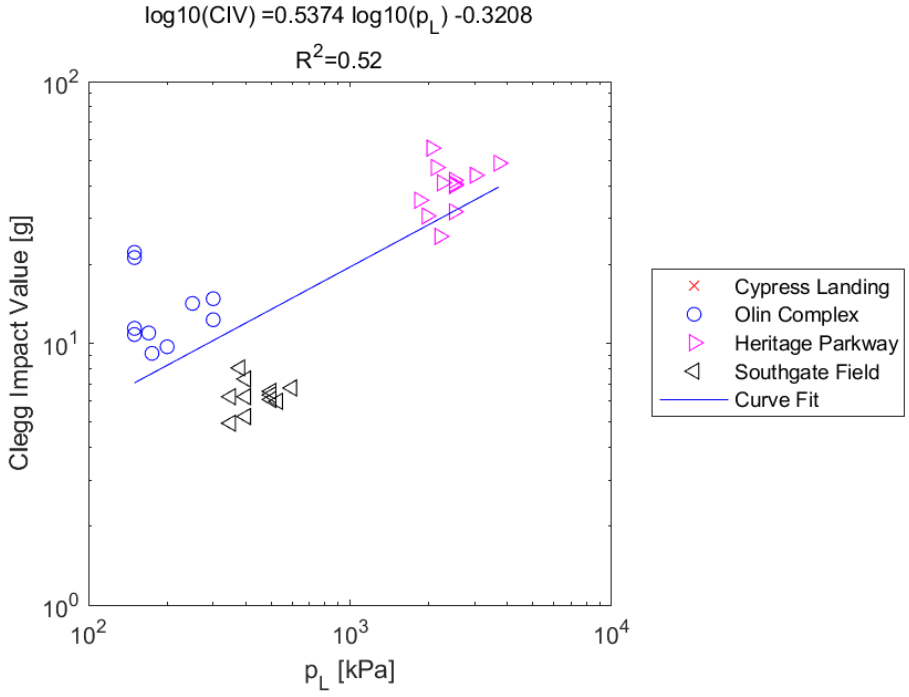

Figure E.378: Log - Log Model of CIV versus p_L for SDPMT-6 Continuous Tests, All Sites

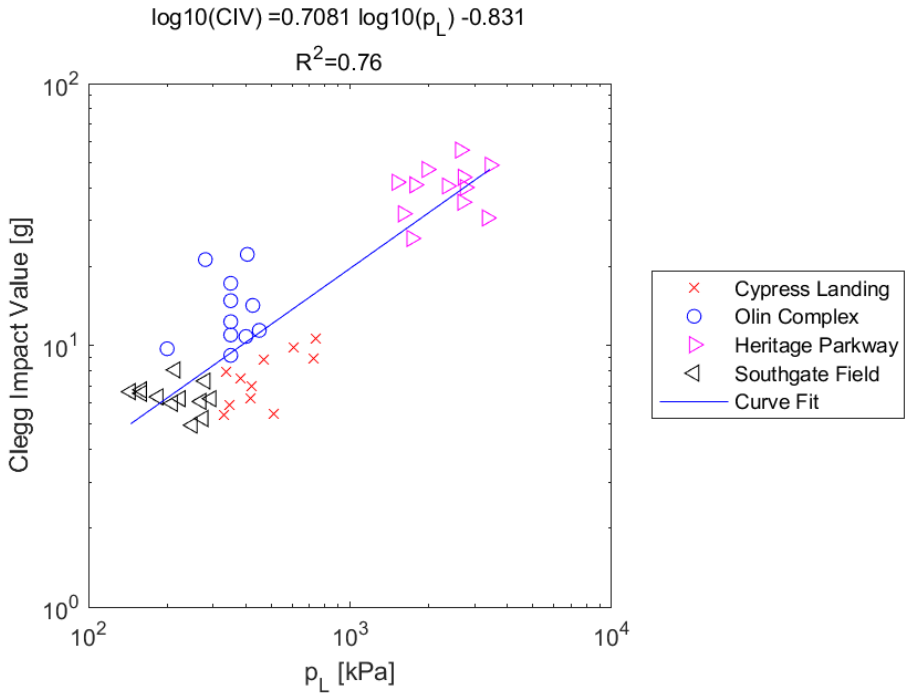

Figure E.379: Log - Log Model of CIV versus p_L for SDPMT-12 Incremental Tests, All Sites

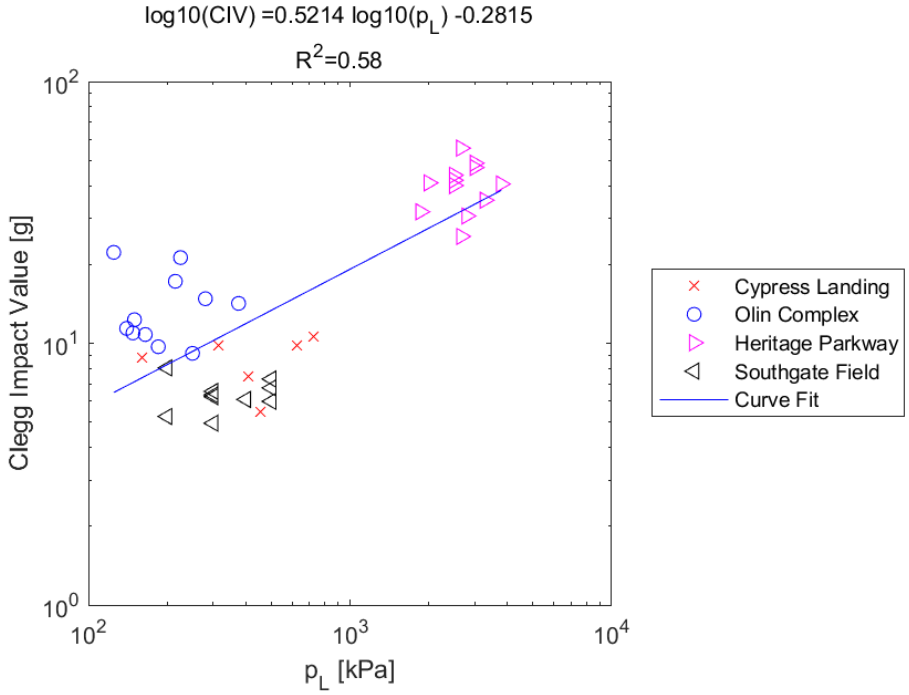

Figure E.380: Log - Log Model of CIV versus p_L for SDPMT-12 Continuous Tests, All Sites

E.4.24 CIV versus p_0

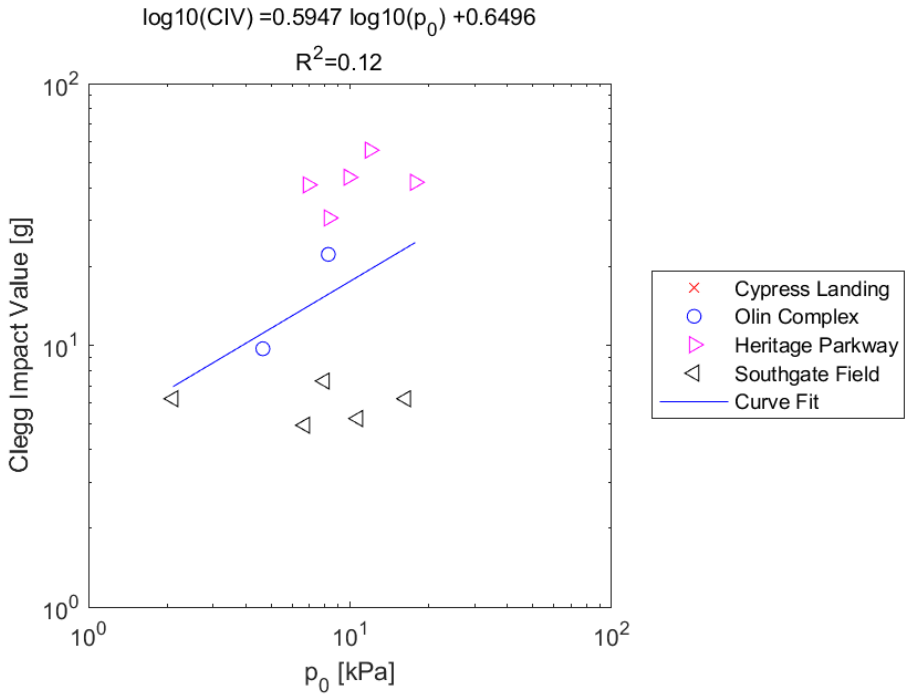

Figure E.381: Log - Log Model of CIV versus p_0 for SDPMT-6 Incremental Tests, All Sites

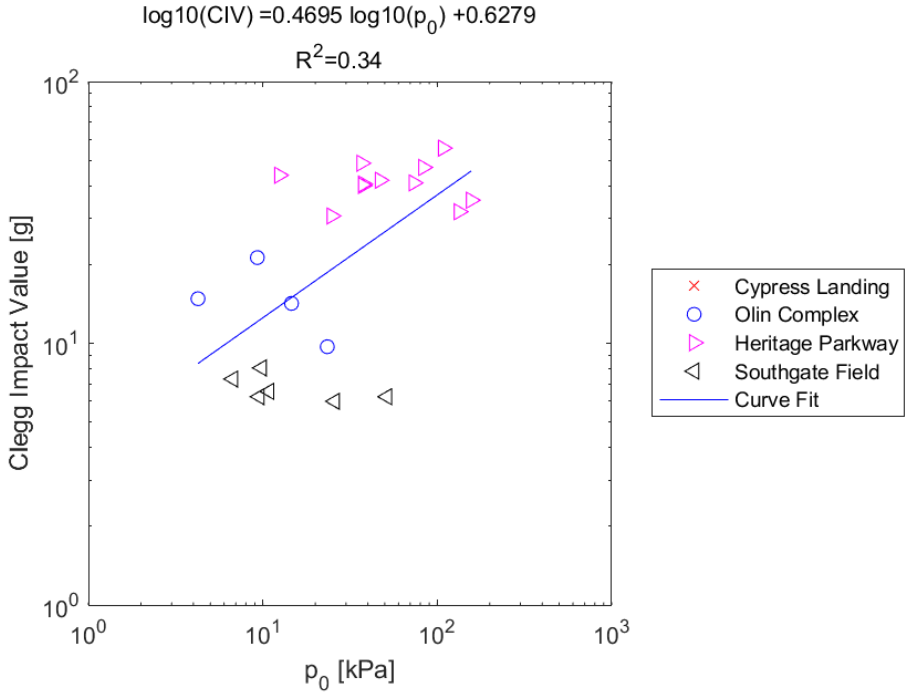

Figure E.382: Log - Log Model of CIV versus p_0 for SDPMT-6 Continuous Tests, All Sites

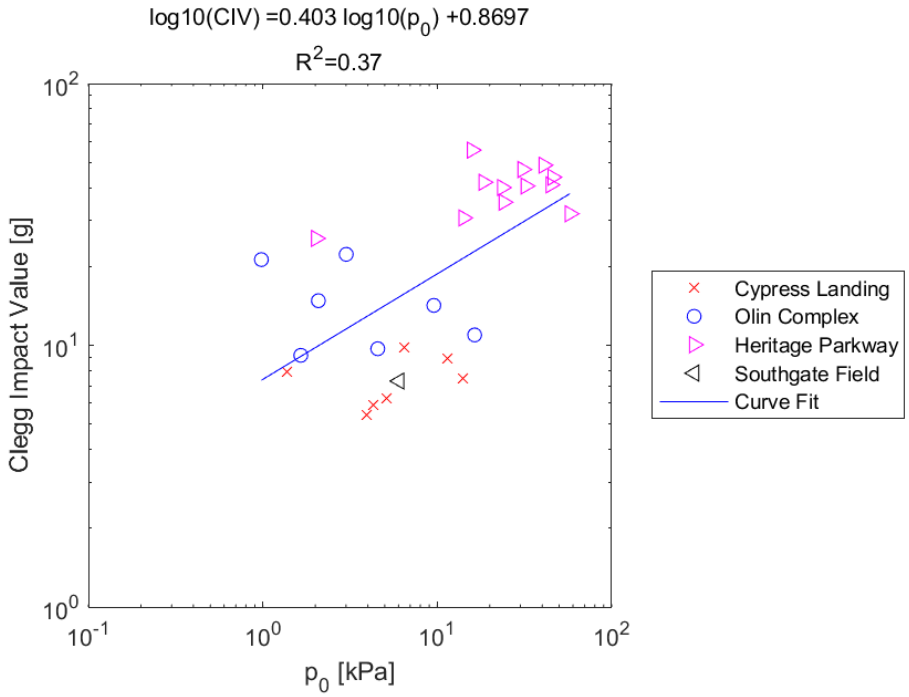

Figure E.383: Log - Log Model of CIV versus p_0 for SDPMT-12 Incremental Tests, All Sites

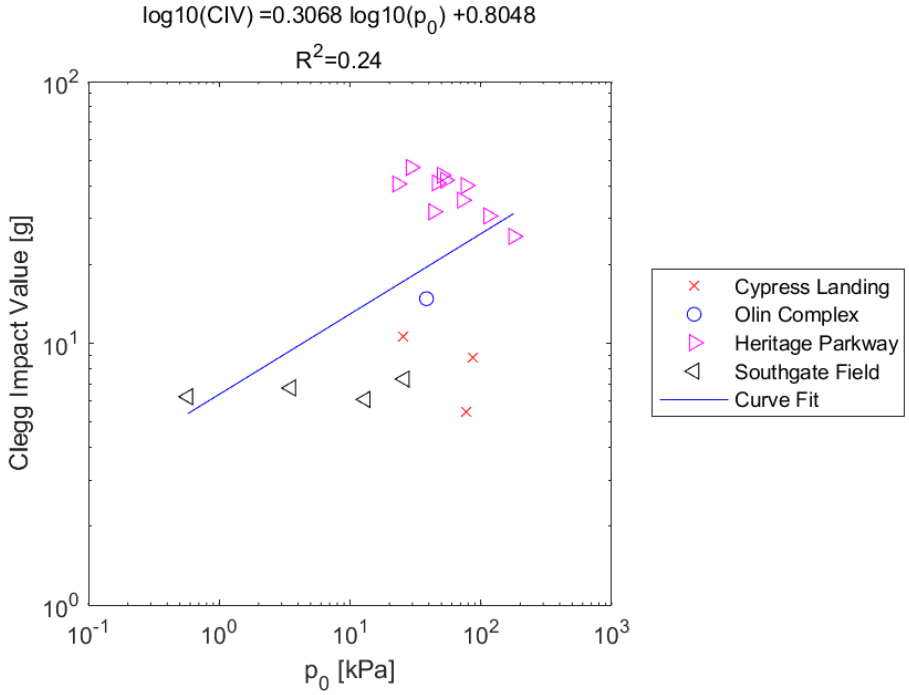

Figure E.384: Log - Log Model of CIV versus p_0 for SDPMT-12 Continuous Tests, All Sites

E.5 Exponential Models

E.5.1 SDPMT E_0 versus p_0

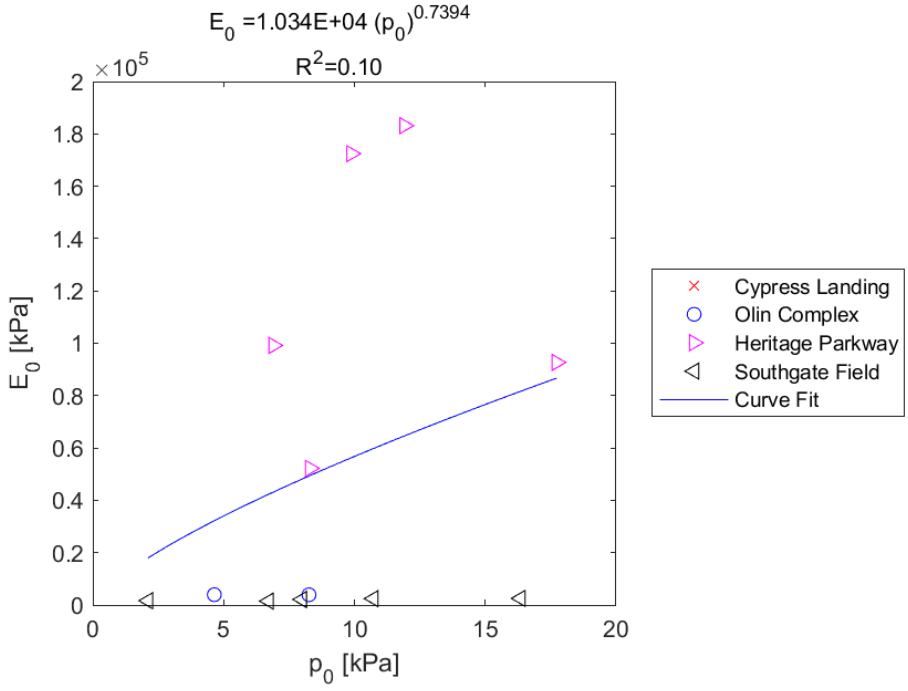

Figure E.385: Exponential Model of E_0 versus p_0 for SDPMT-6 Incremental Tests, All Sites

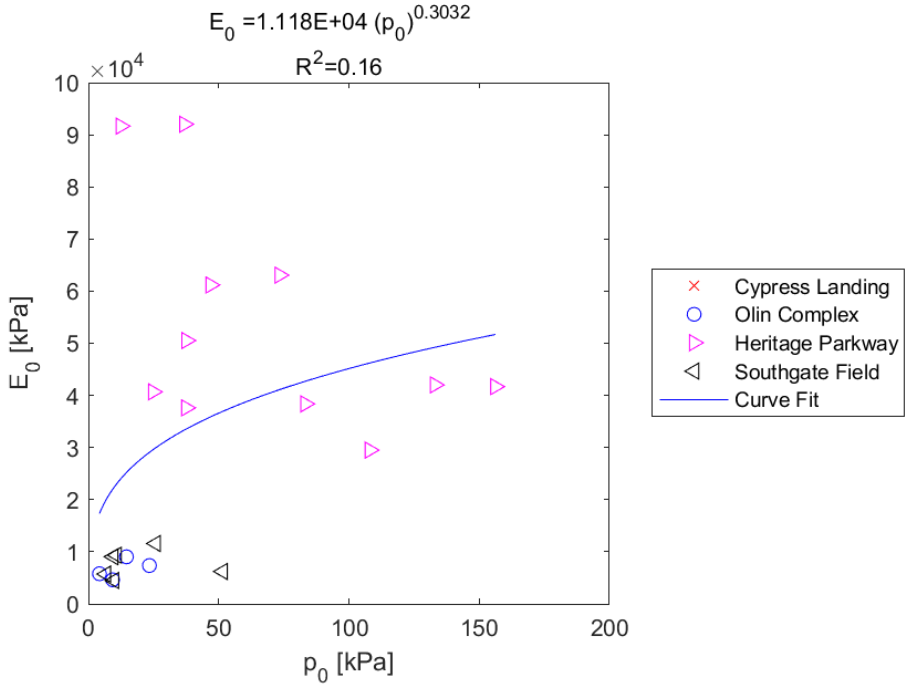

Figure E.386: Exponential Model of E_0 versus p_0 for SDPMT-6 Continuous Tests, All Sites

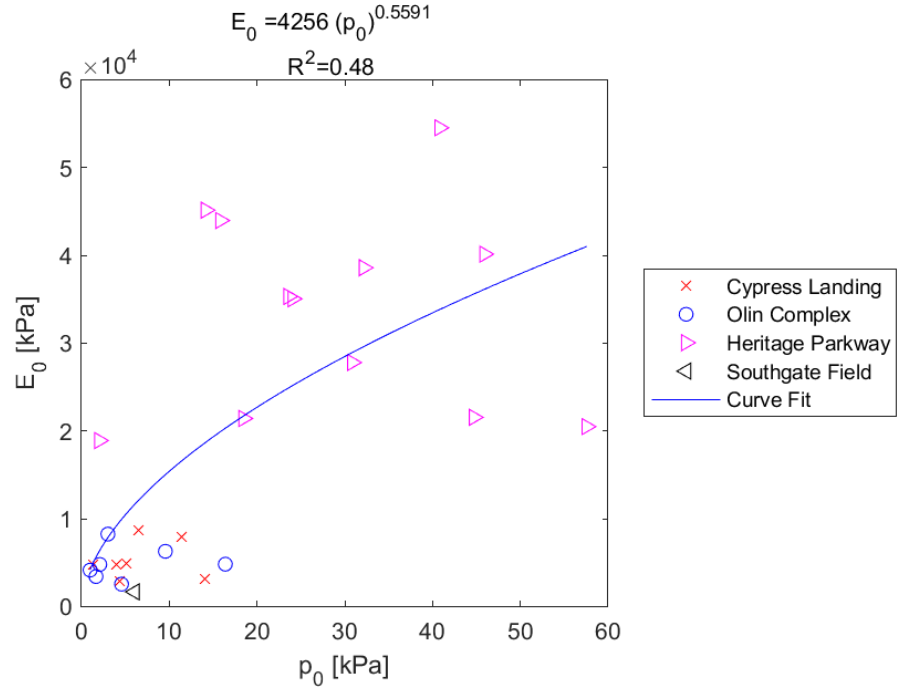

Figure E.387: Exponential Model of E_0 versus p_0 for SDPMT-12 Incremental Tests, All Sites

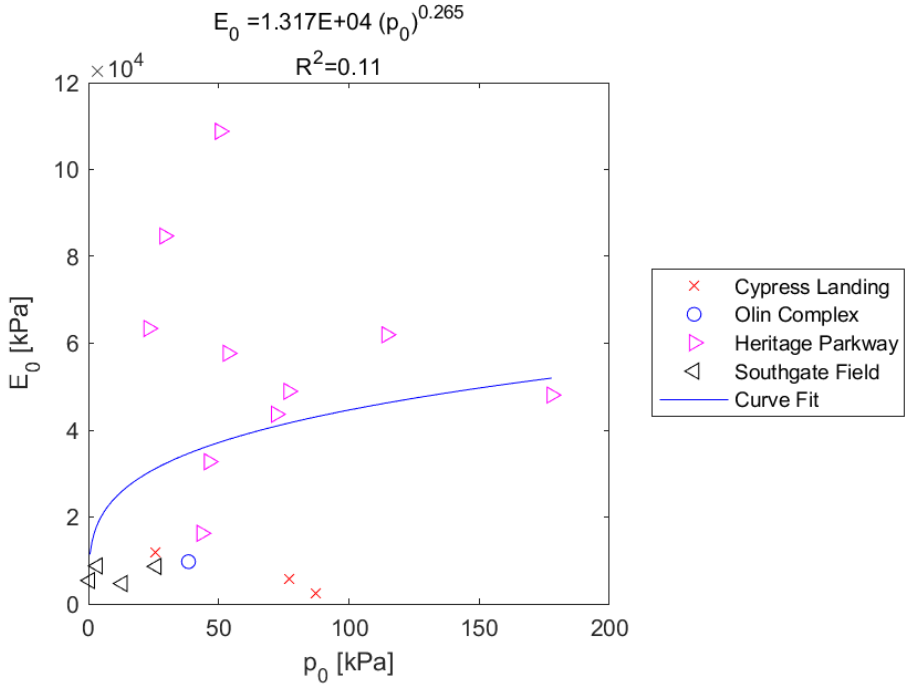

Figure E.388: Exponential Model of E_0 versus p_0 for SDPMT-12 Continuous Tests, All Sites

E.5.2 SDPMT p_0 versus E_0

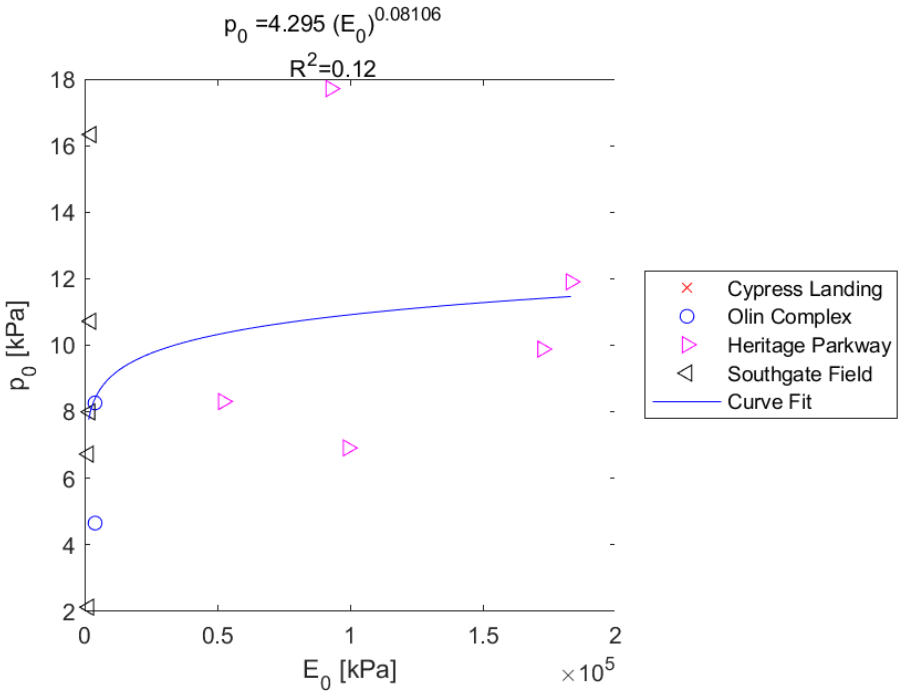

Figure E.389: Exponential Model of E_0 versus p_0 for SDPMT-6 Incremental Tests, All Sites

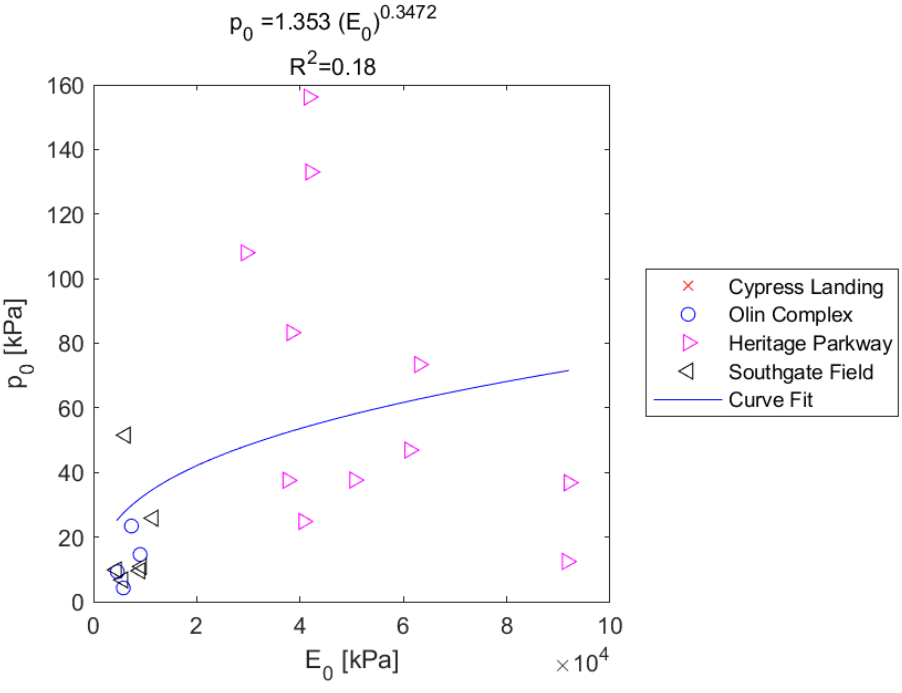

Figure E.390: Exponential Model of E_0 versus p_0 for SDPMT-6 Continuous Tests, All Sites

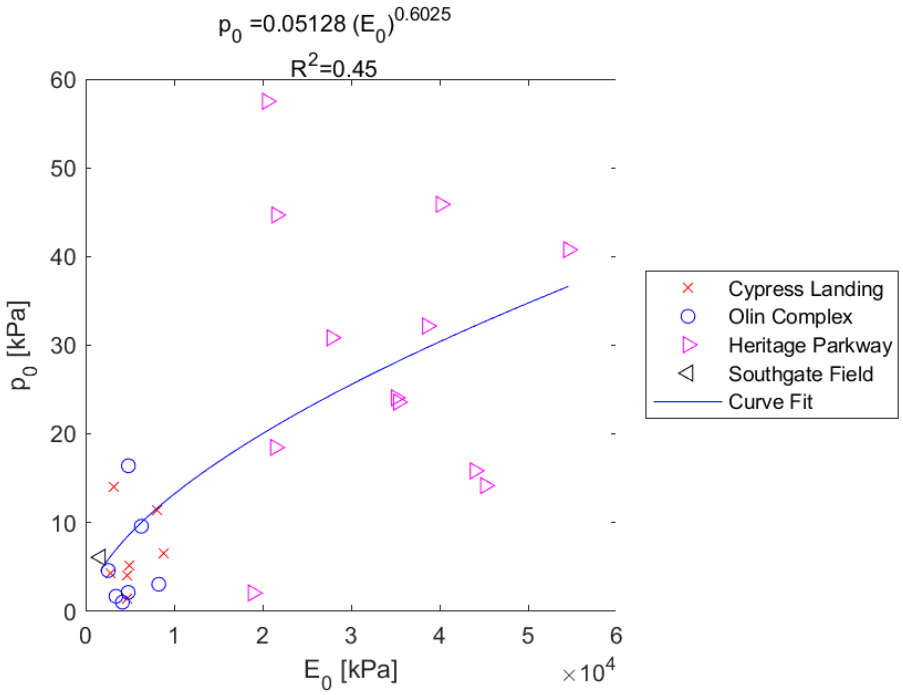

Figure E.391: Exponential Model of E_0 versus p_0 for SDPMT-12 Incremental Tests, All Sites

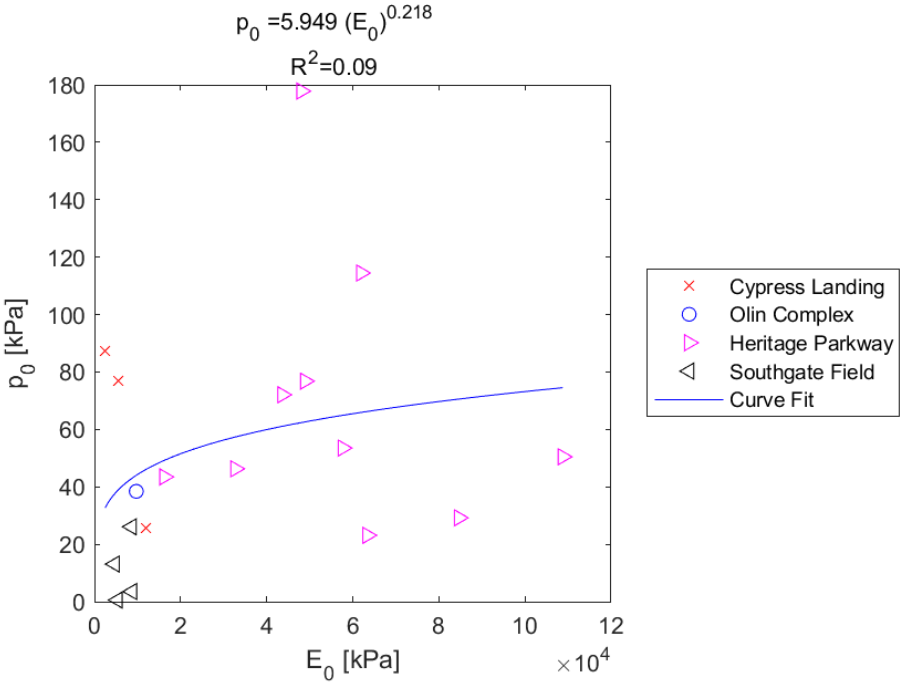

Figure E.392: Exponential Model of E_0 versus p_0 for SDPMT-12 Continuous Tests, All Sites

E.5.3 SDPMT $\mathbf{E}_0$ versus $\mathbf{p}_L$

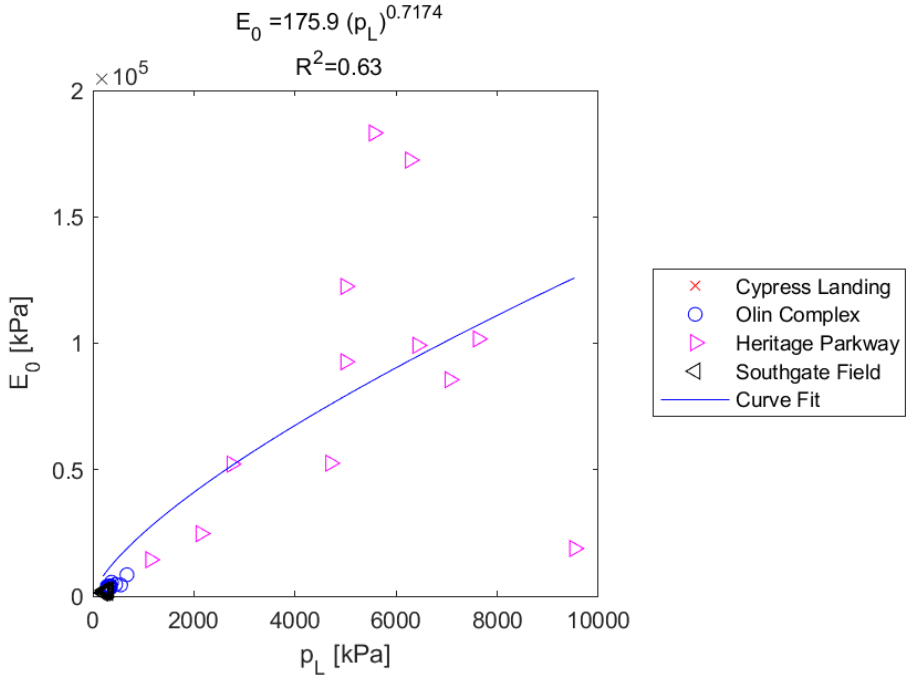

Figure E.393: Exponential Model of E_0 versus p_L for SDPMT-6 Incremental Tests, All Sites

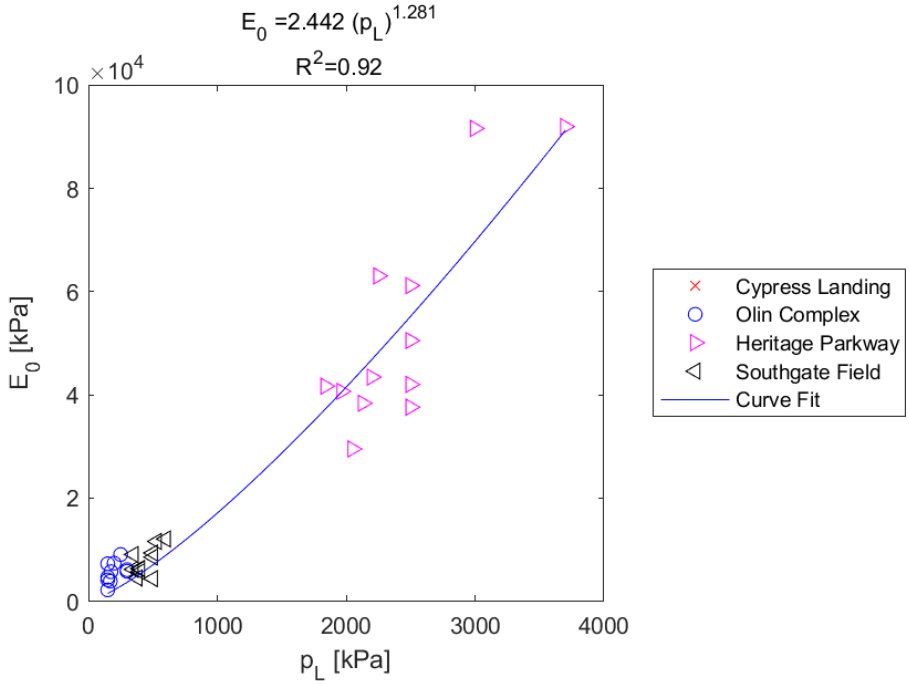

Figure E.394: Exponential Model of E_0 versus p_L for SDPMT-6 Continuous Tests, All Sites

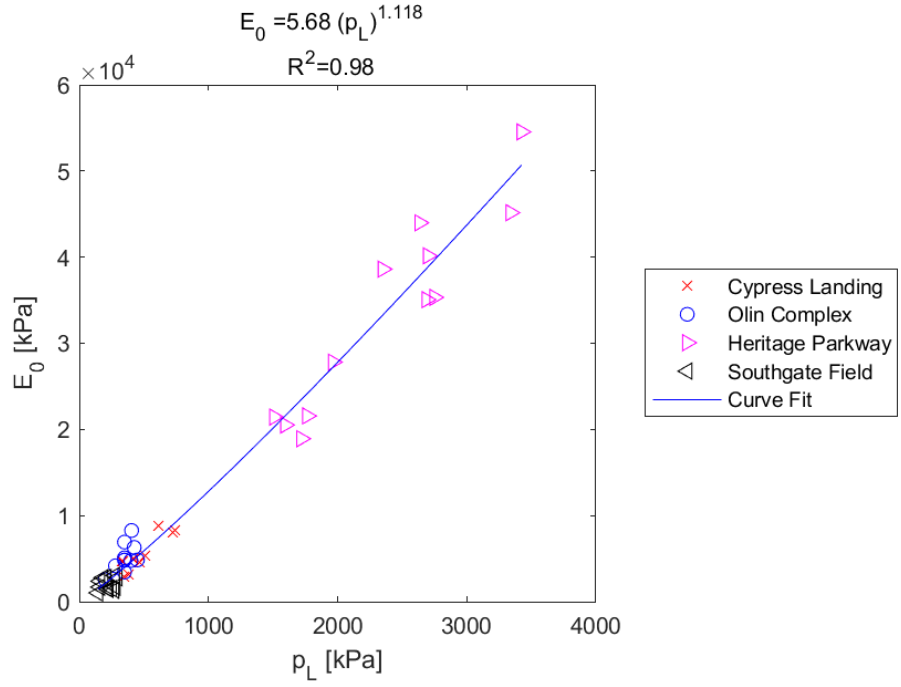

Figure E.395: Exponential Model of E_0 versus p_L for SDPMT-12 Incremental Tests, All Sites

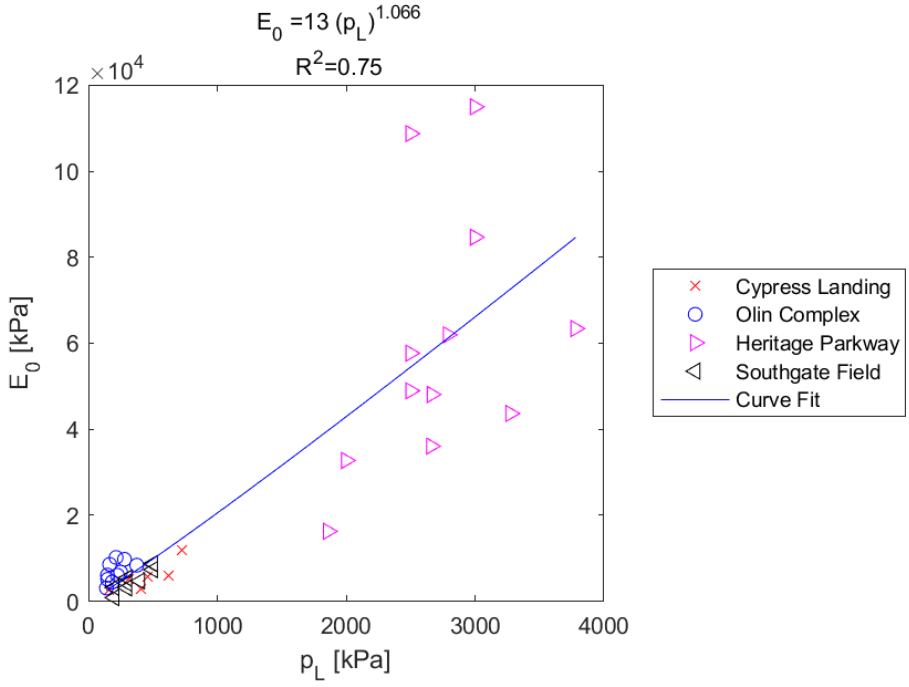

Figure E.396: Exponential Model of E_0 versus p_L for SDPMT-12 Continuous Tests, All Sites

E.5.4 SDPMT $\mathbf{p}_L$ versus $\mathbf{E}_0$

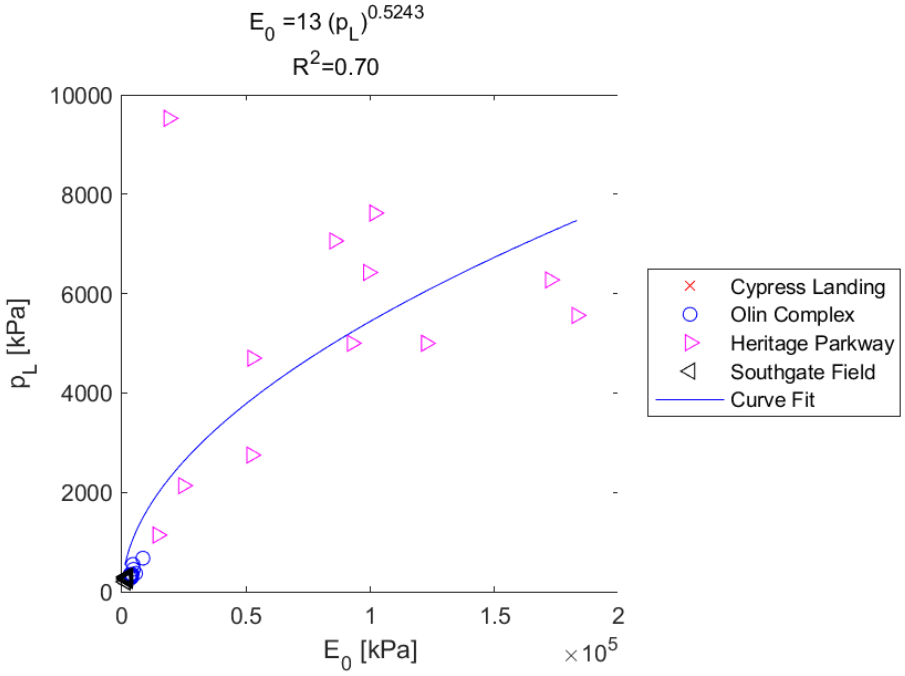

Figure E.397: Exponential Model of p_L versus E_0 for SDPMT-6 Incremental Tests, All Sites

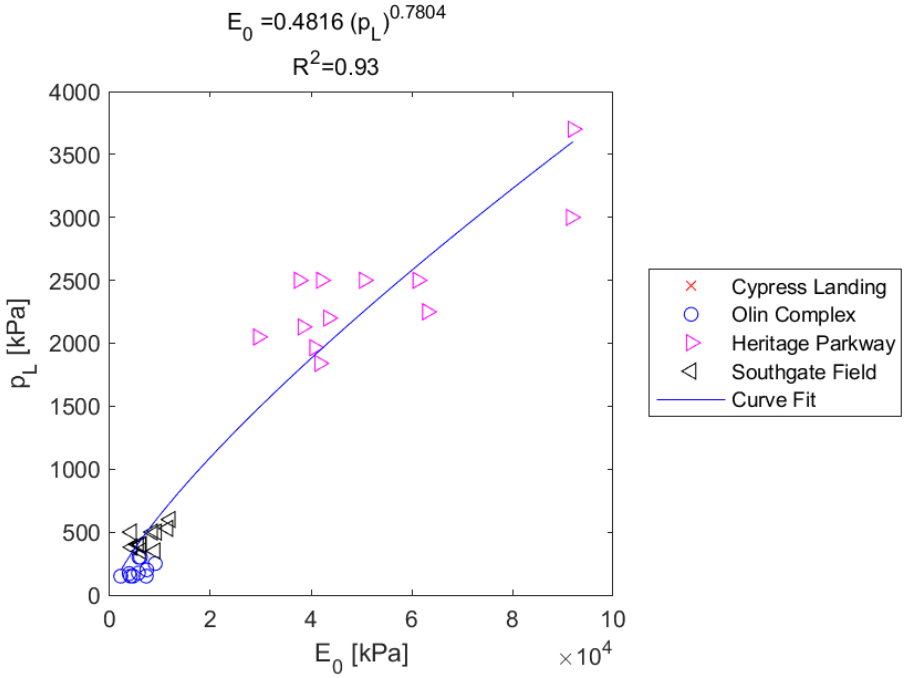

Figure E.398: Exponential Model of p_L versus E_0 for SDPMT-6 Continuous Tests, All Sites

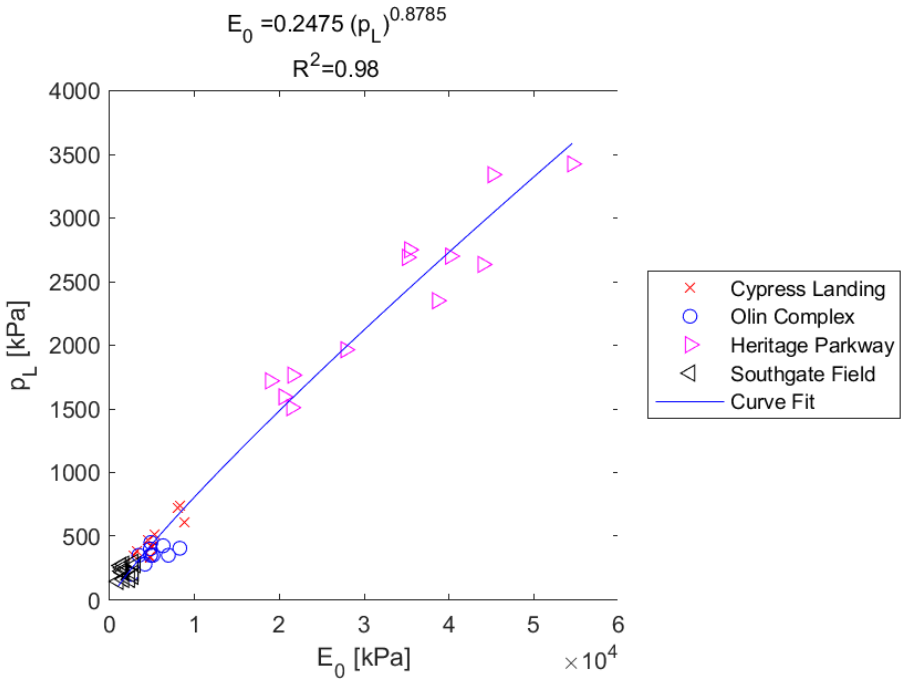

Figure E.399: Exponential Model of p_L versus E_0 for SDPMT-12 Incremental Tests, All Sites

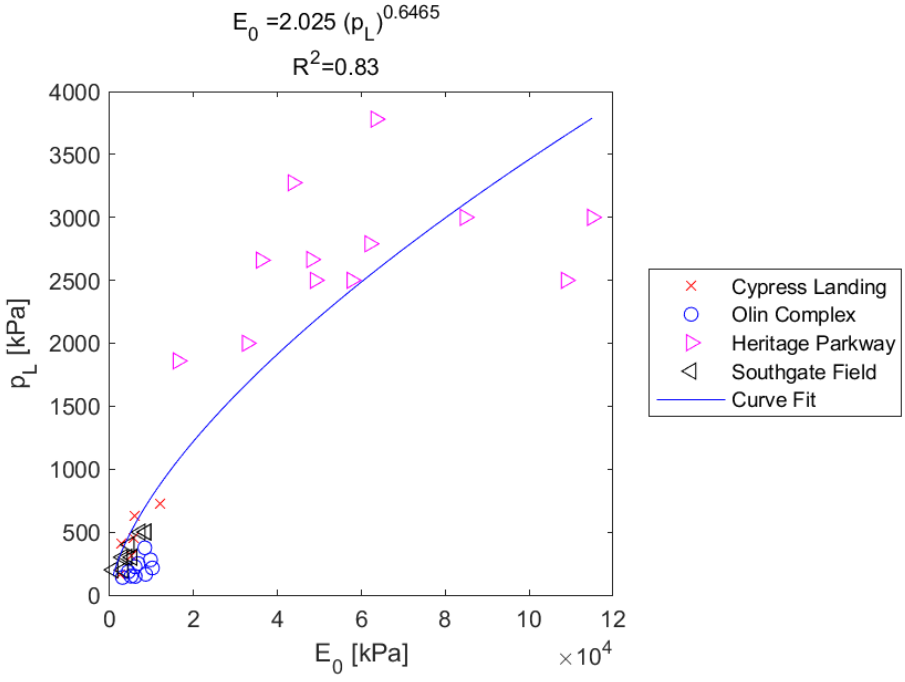

Figure E.400: Exponential Model of p_L versus E_0 for SDPMT-12 Continuous Tests, All Sites

E.5.5 SDPMT $\mathbf{p}_0$ versus $\mathbf{p}_L$

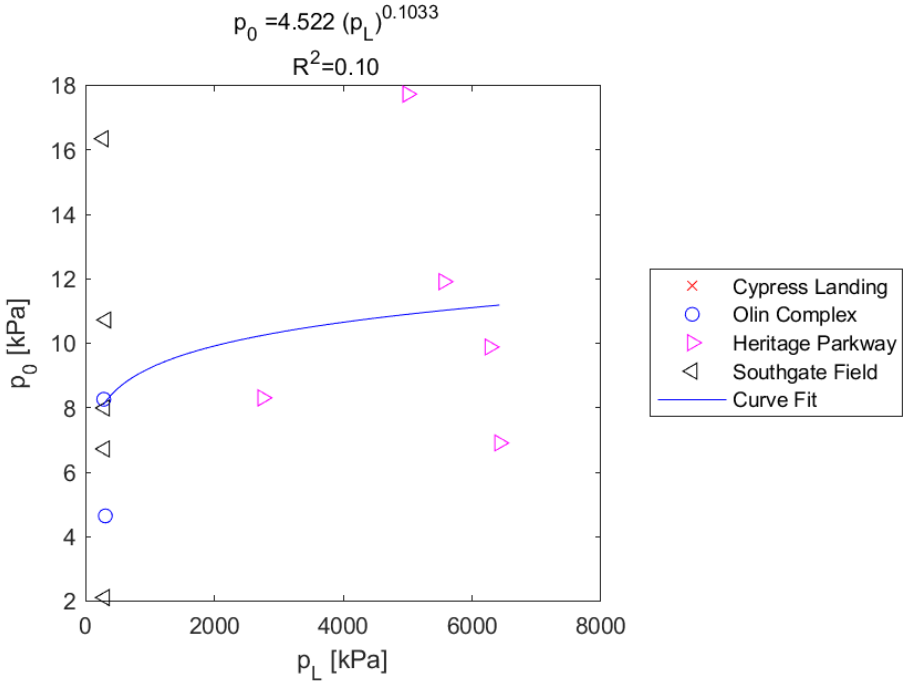

Figure E.401: Exponential Model of p_0 versus p_L for SDPMT-6 Incremental Tests, All Sites

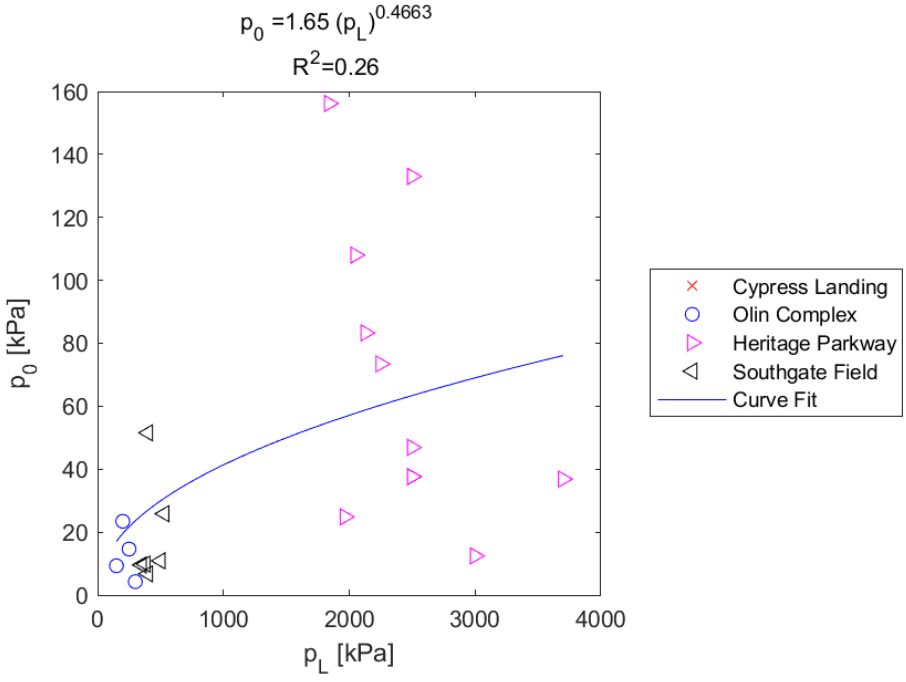

Figure E.402: Exponential Model of p_0 versus p_L for SDPMT-6 Continuous Tests, All Sites

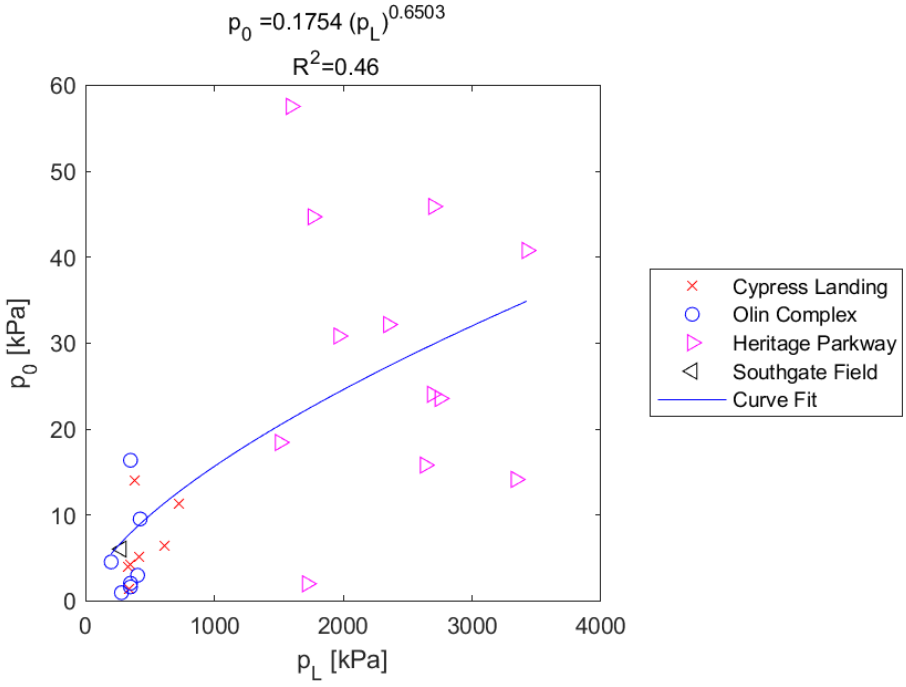

Figure E.403: Exponential Model of p_0 versus p_L for SDPMT-12 Incremental Tests, All Sites

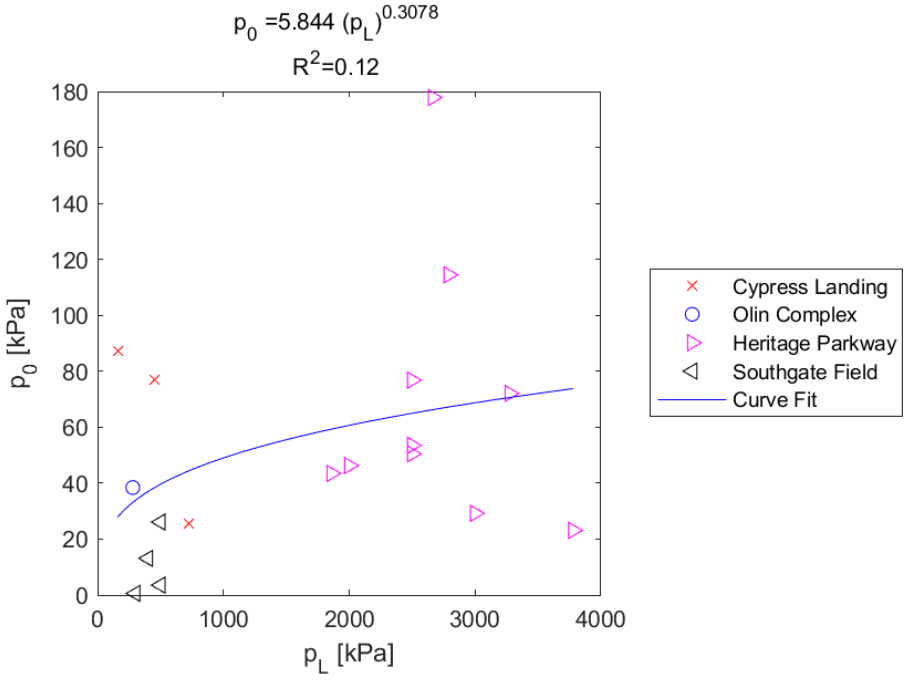

Figure E.404: Exponential Model of p_0 versus p_L for SDPMT-12 Continuous Tests, All Sites

E.5.6 SDPMT $\mathbf{p}_L$ versus $\mathbf{p}_0$

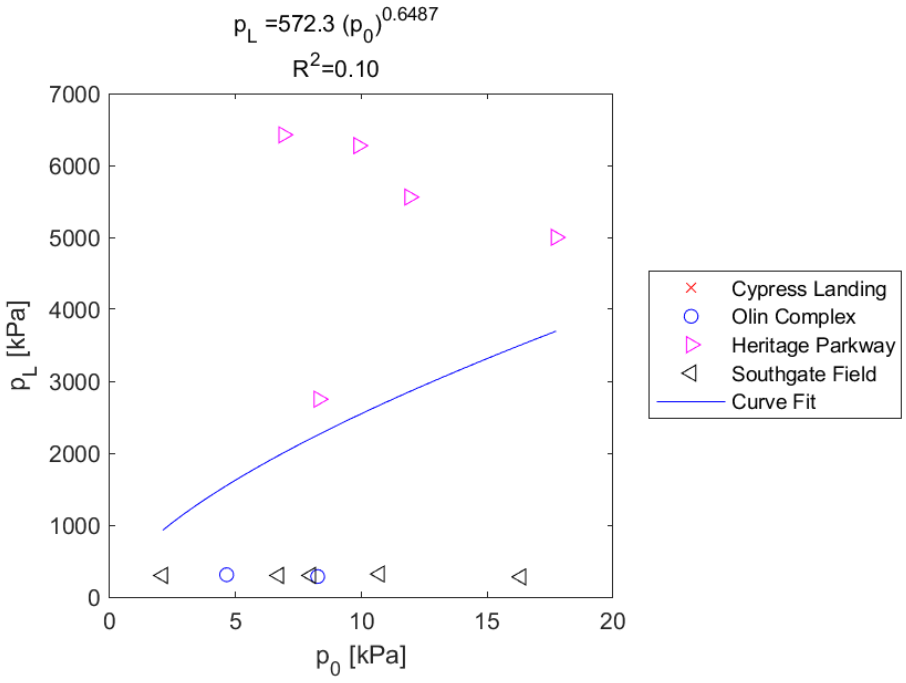

Figure E.405: Exponential Model of p_L versus p_0 for SDPMT-6 Incremental Tests, All Sites

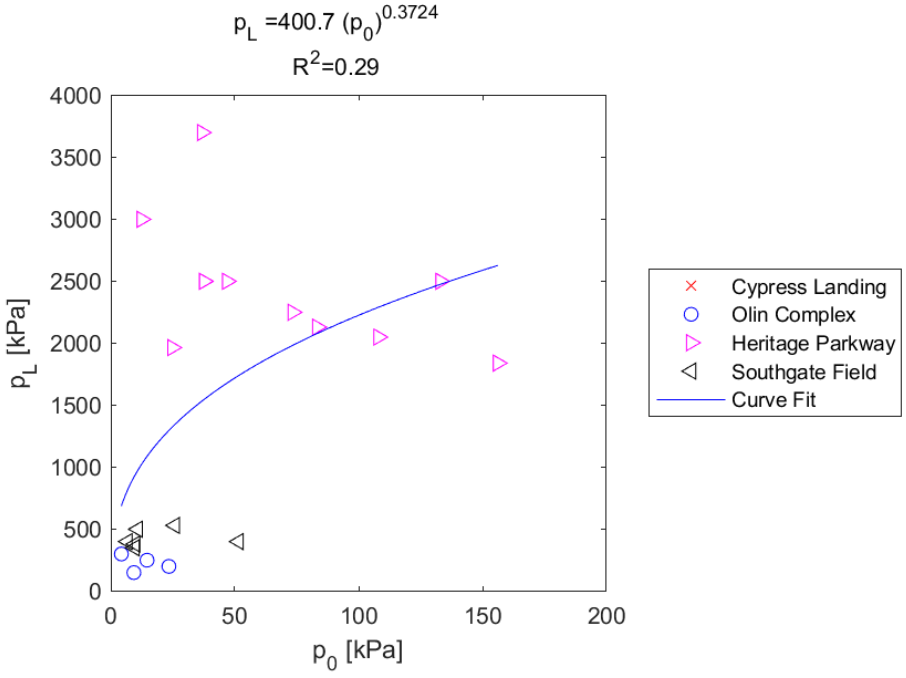

Figure E.406: Exponential Model of p_L versus p_0 for SDPMT-6 Continuous Tests, All Sites

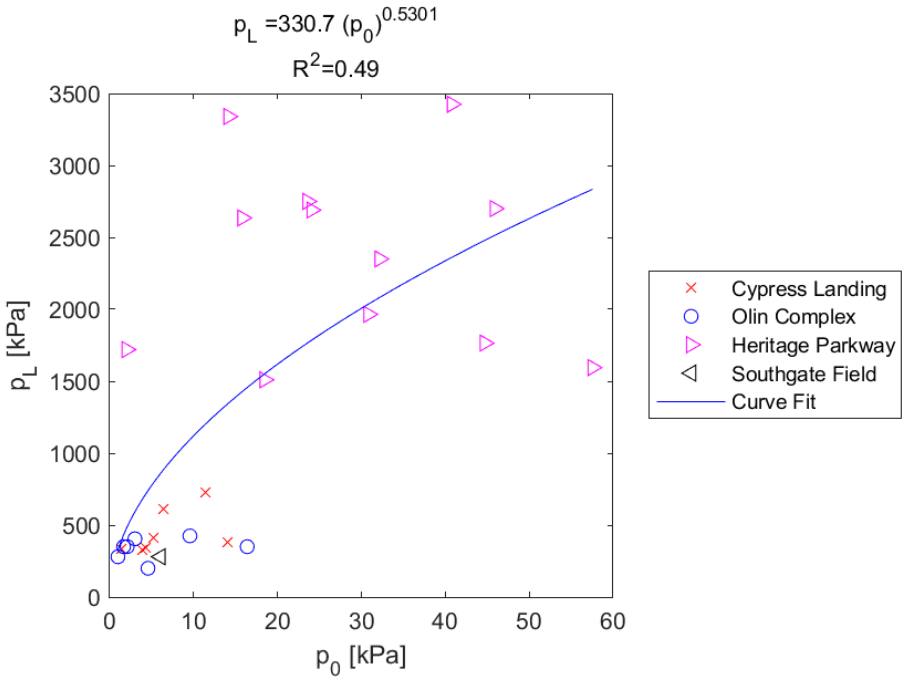

Figure E.407: Exponential Model of p_L versus p_0 for SDPMT-12 Incremental Tests, All Sites

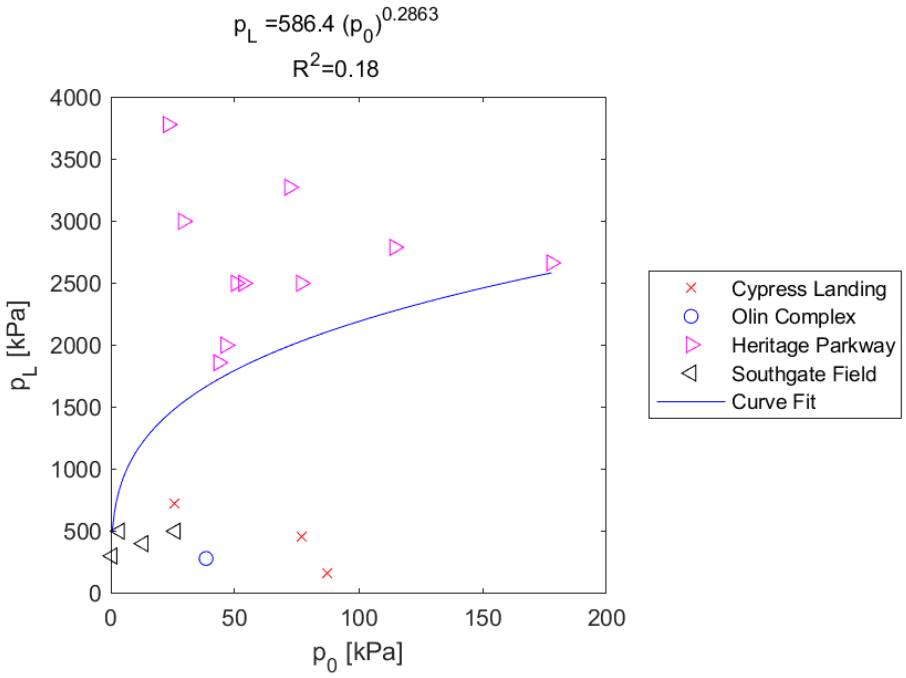

Figure E.408: Exponential Model of p_L versus p_0 for SDPMT-12 Continuous Tests, All Sites

E.5.7 γ_{wet} versus $\mathbf{E}_0$

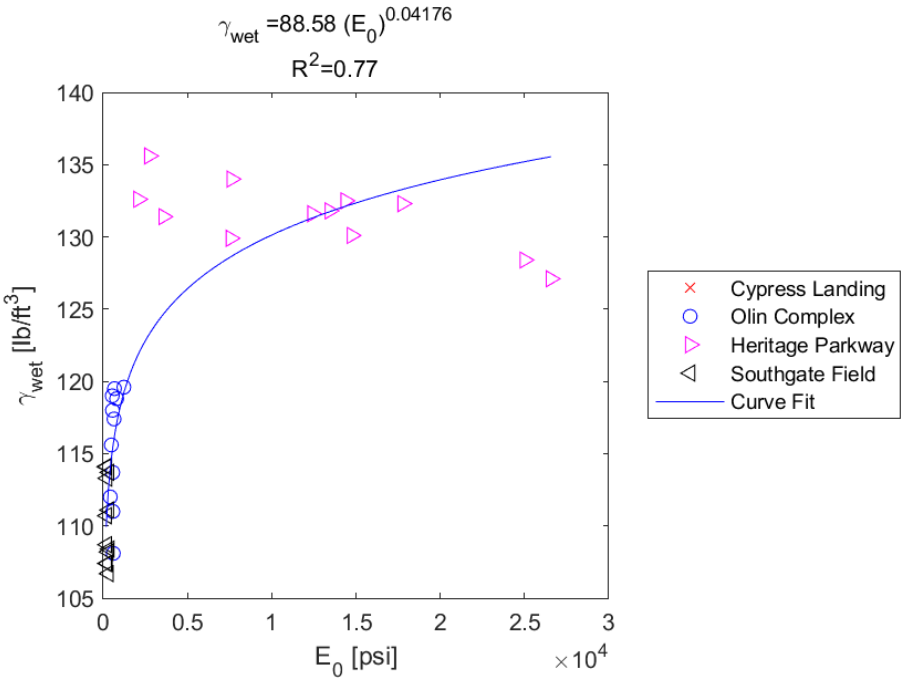

Figure E.409: Exponential Model of γ_{wet} versus E_0 for SDPMT-6 Incremental Tests, All Sites

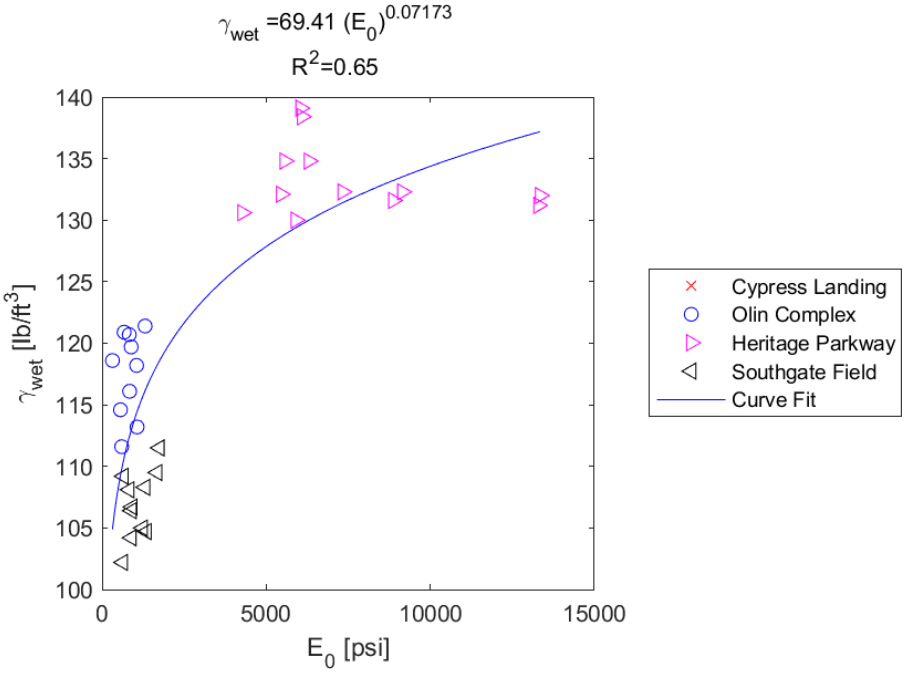

Figure E.410: Exponential Model of γ_{wet} versus E_0 for SDPMT-6 Continuous Tests, All Sites

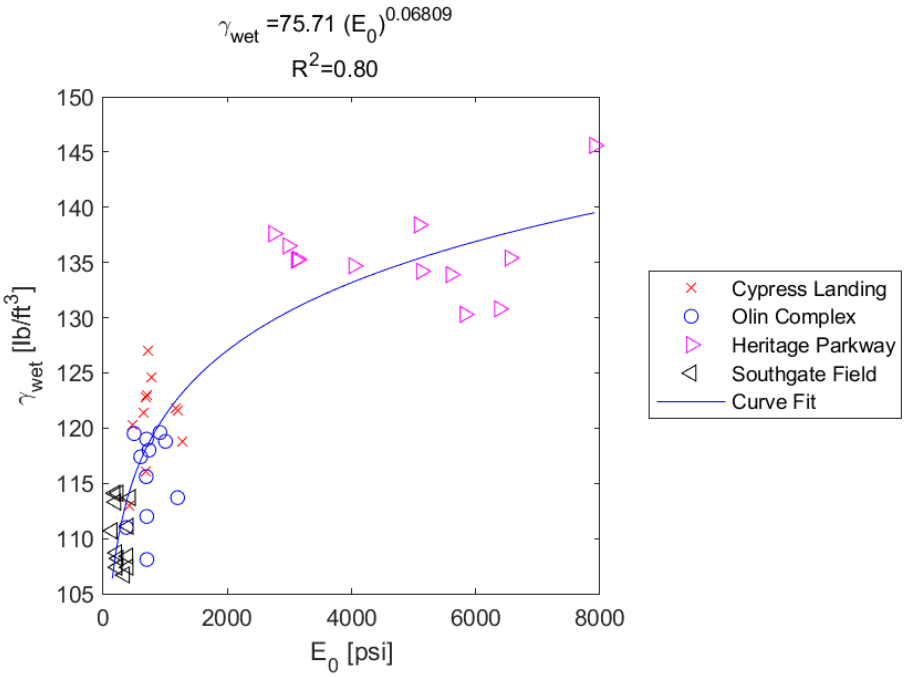

Figure E.411: Exponential Model of γ_{wet} versus E_0 for SDPMT-12 Incremental Tests, All Sites

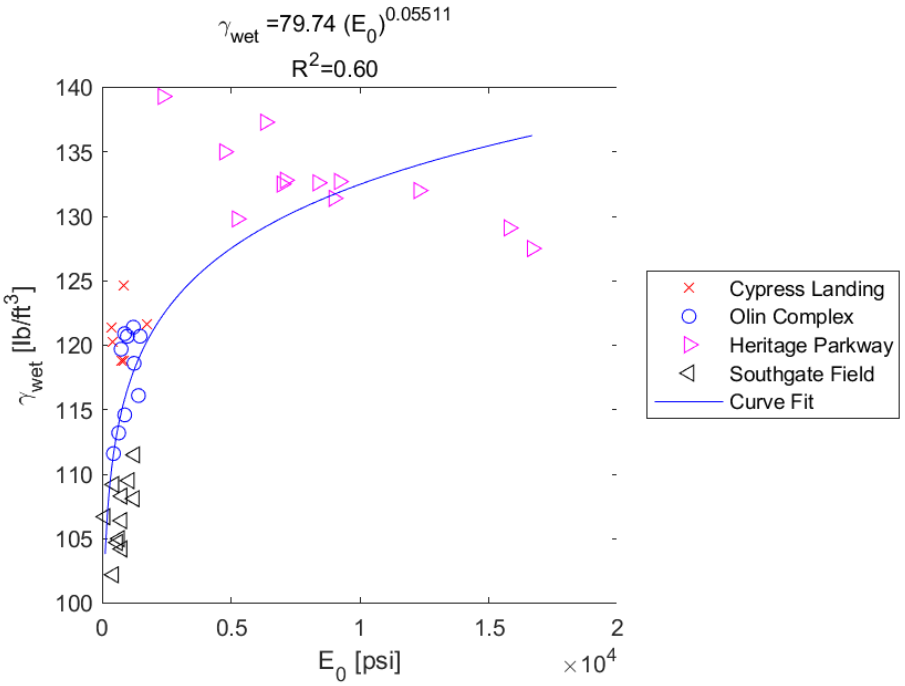

Figure E.412: Exponential Model of γ_{wet} versus E_0 for SDPMT-12 Continuous Tests, All Sites

E.5.8 γ_{wet} versus $\mathbf{p}_L$

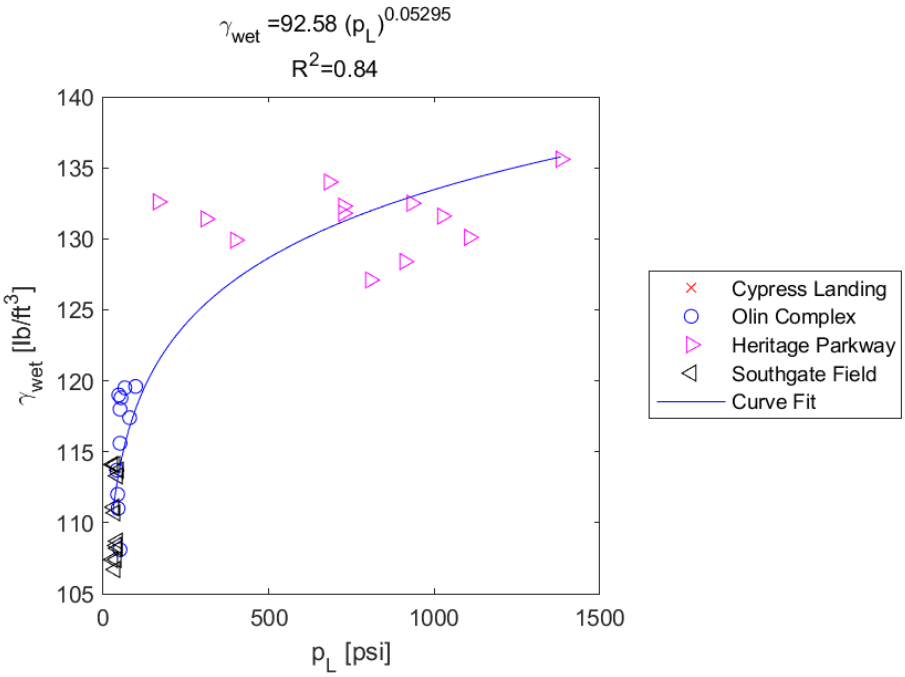

Figure E.413: Exponential Model of γ_{wet} versus p_L for SDPMT-6 Incremental Tests, All Sites

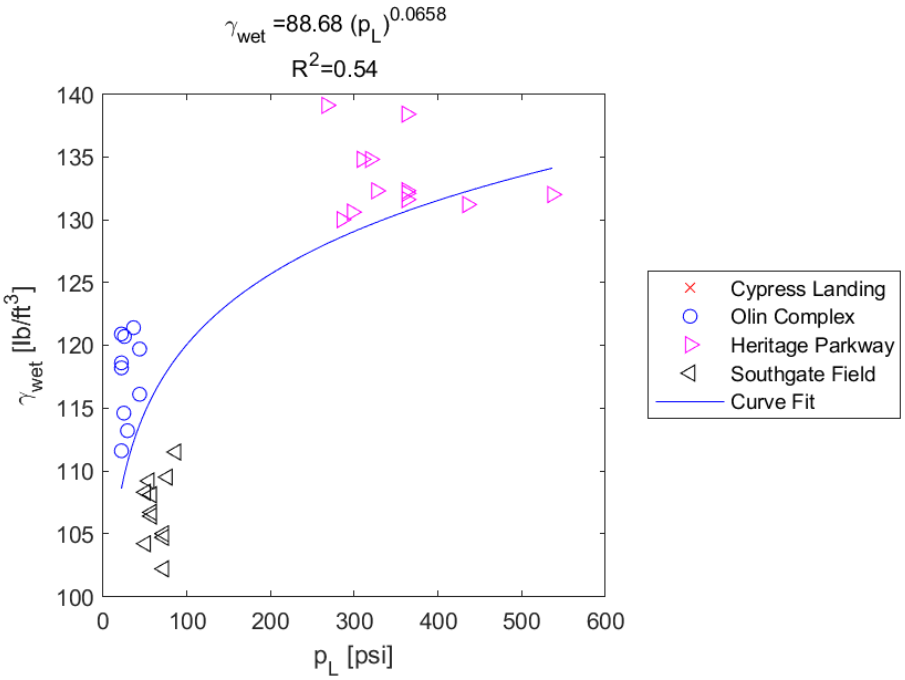

Figure E.414: Exponential Model of γ_{wet} versus p_L for SDPMT-6 Continuous Tests, All Sites

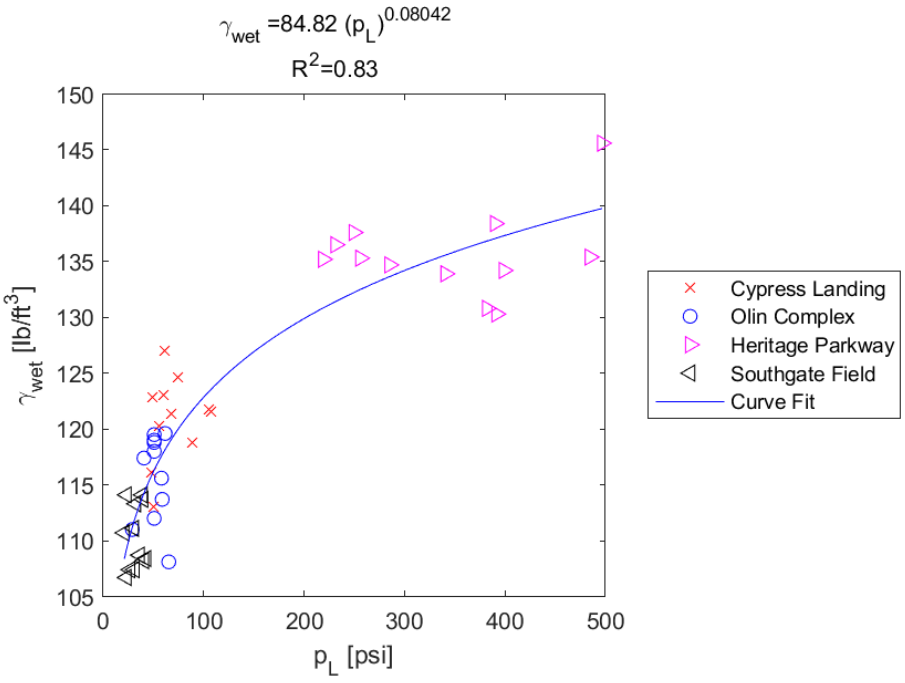

Figure E.415: Exponential Model of γ_{wet} versus p_L for SDPMT-12 Incremental Tests, All Sites

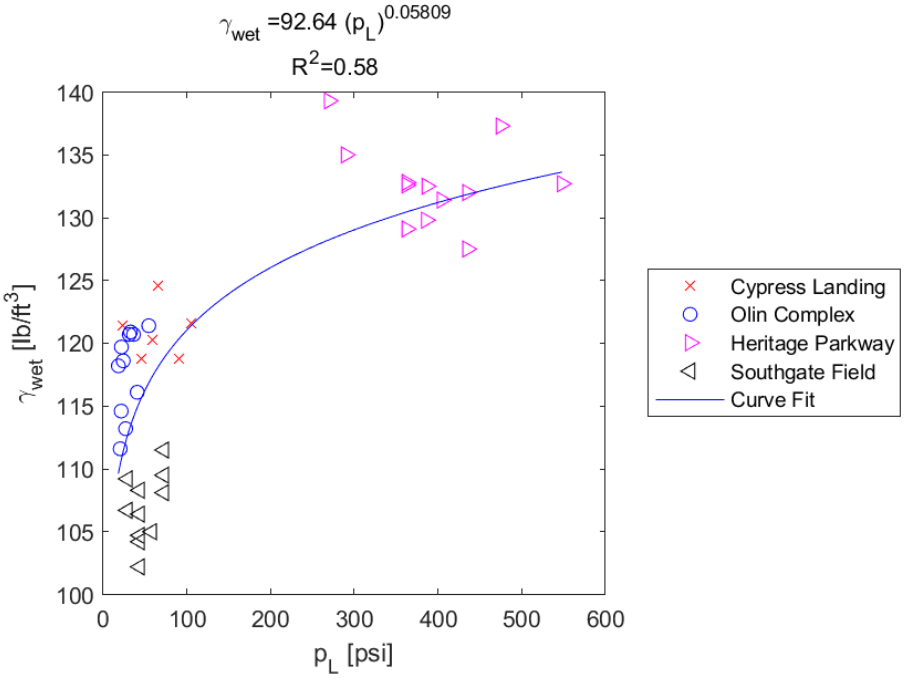

Figure E.416: Exponential Model of γ_{wet} versus p_L for SDPMT-12 Continuous Tests, All Sites

E.5.9 γ_{wet} versus $\mathbf{p}_0$

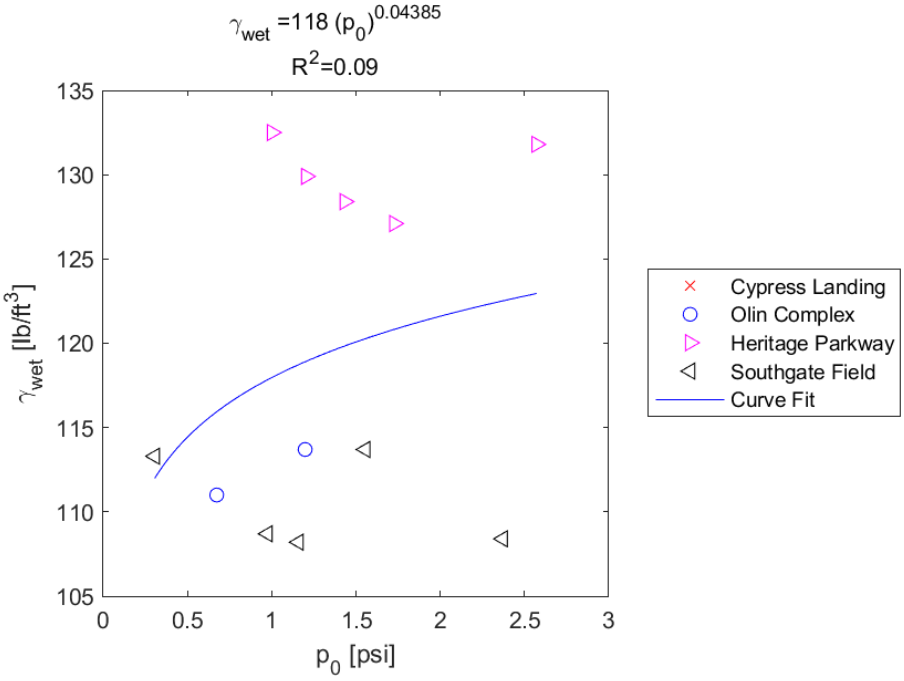

Figure E.417: Exponential Model of γ_{wet} versus p_0 for SDPMT-6 Incremental Tests, All Sites

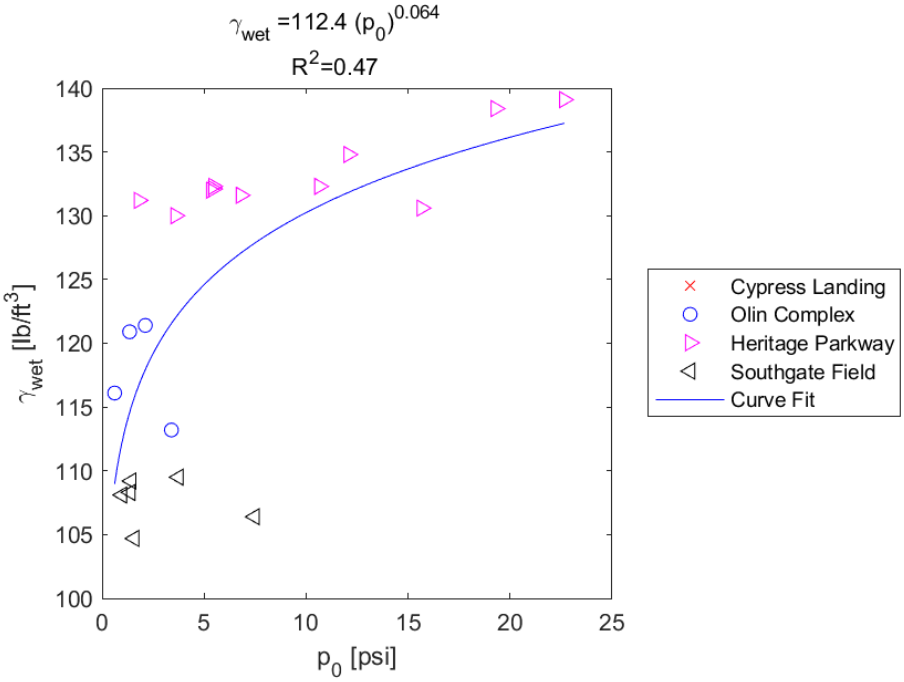

Figure E.418: Exponential Model of γ_{wet} versus p_0 for SDPMT-6 Continuous Tests, All Sites

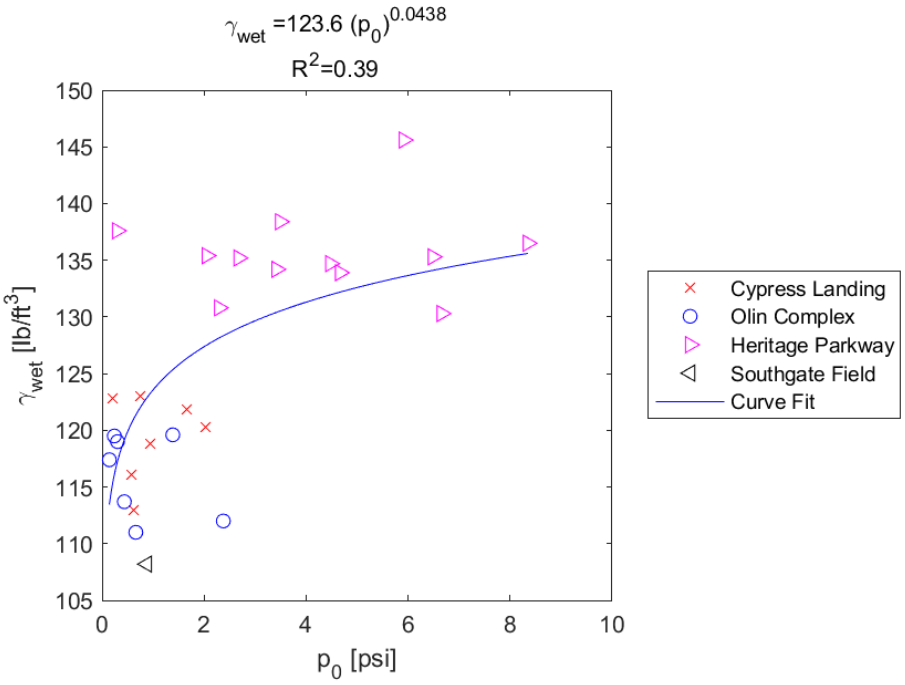

Figure E.419: Exponential Model of γ_{wet} versus p_0 for SDPMT-12 Incremental Tests, All Sites

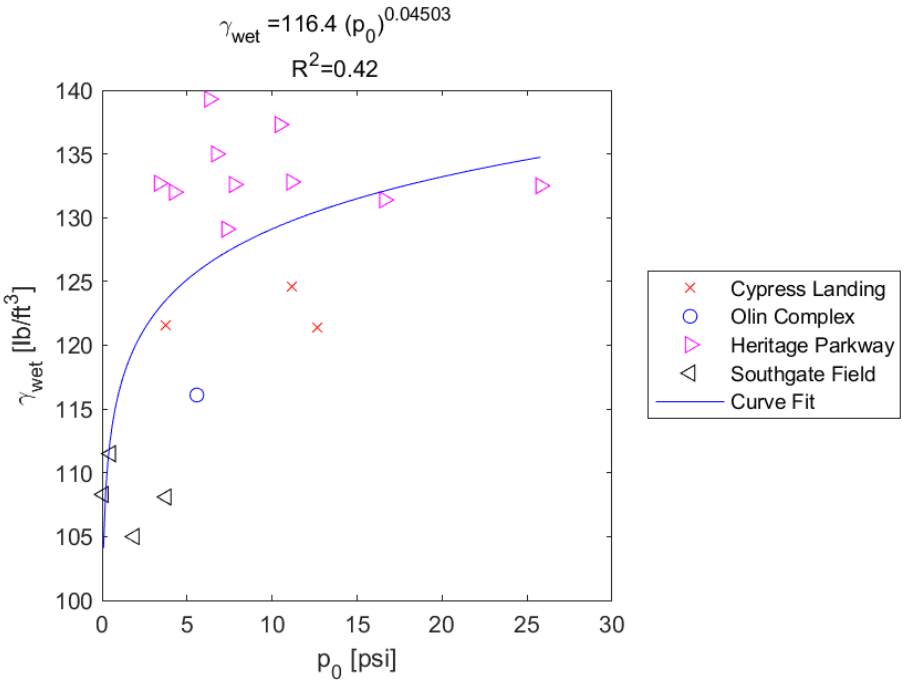

Figure E.420: Exponential Model of γ_{wet} versus p_0 for SDPMT-12 Continuous Tests, All Sites

E.5.10 γ_{dry} versus $\mathbf{E}_0$

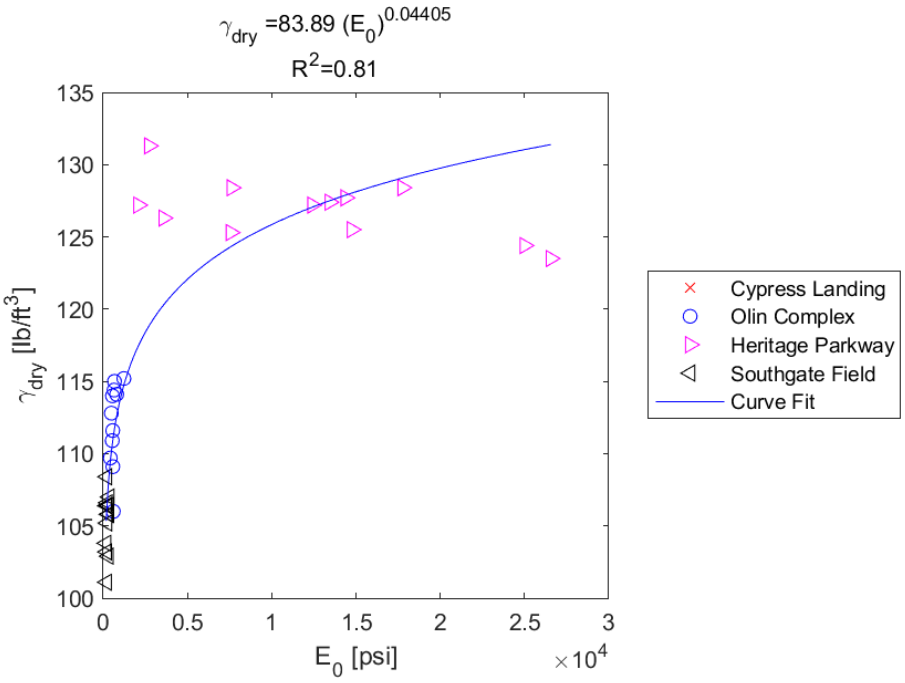

Figure E.421: Exponential Model of γ_{dry} versus E_0 for SDPMT-6 Incremental Tests, All Sites

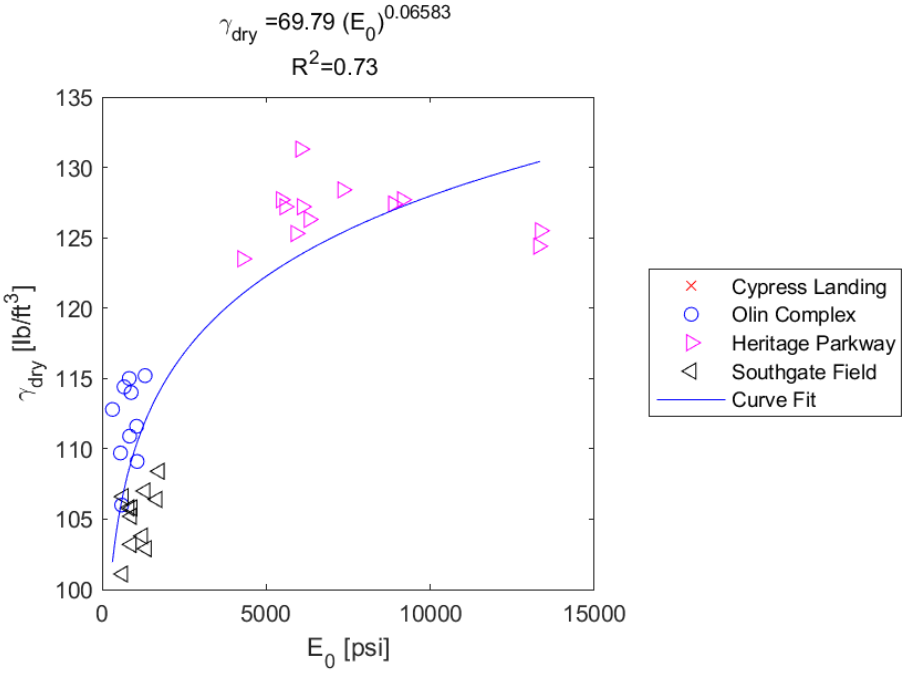

Figure E.422: Exponential Model of γ_{dry} versus E_0 for SDPMT-6 Continuous Tests, All Sites

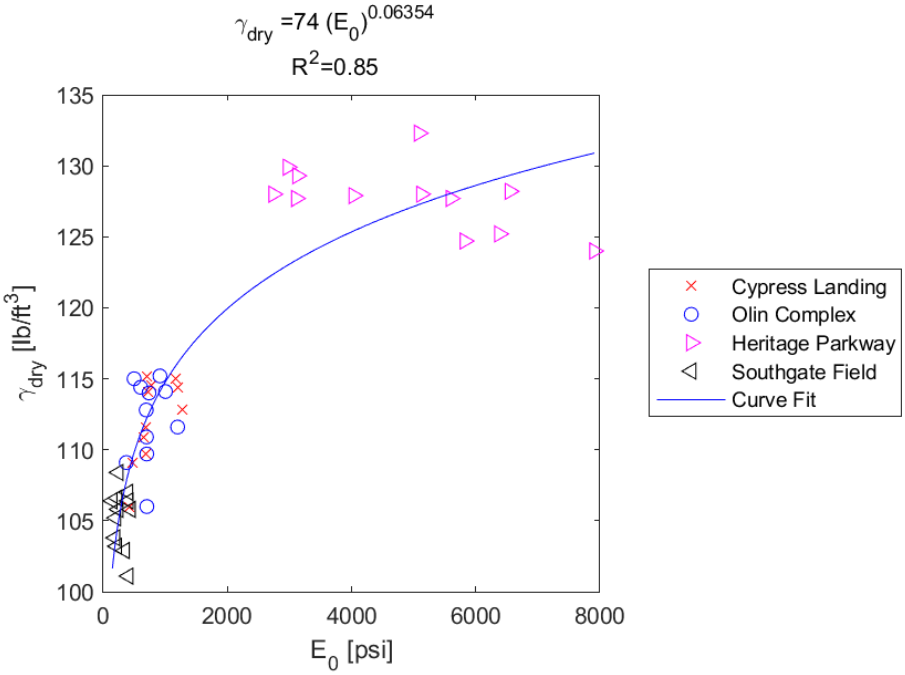

Figure E.423: Exponential Model of γ_{dry} versus E_0 for SDPMT-12 Incremental Tests, All Sites

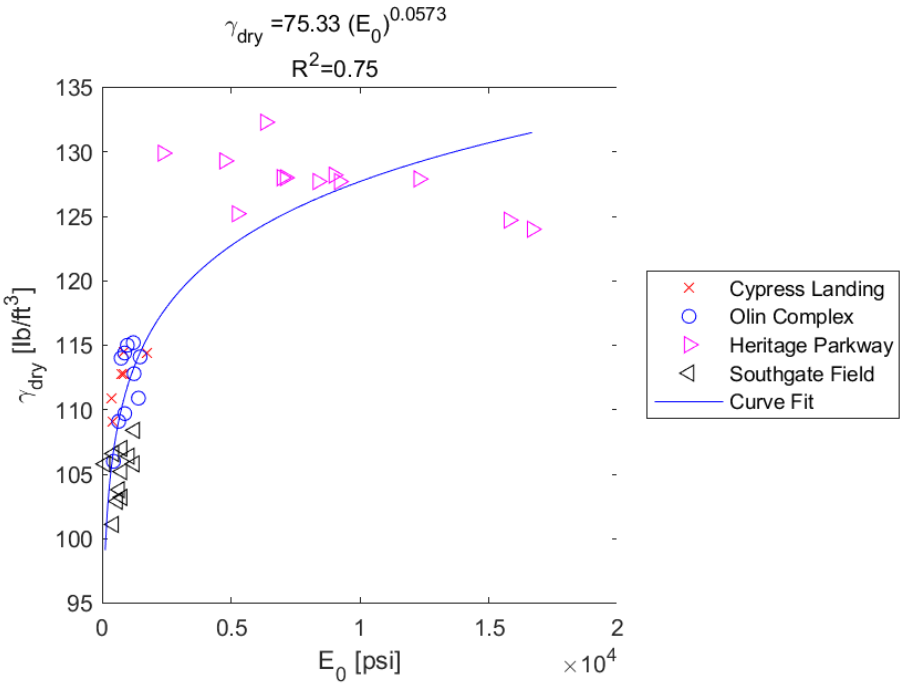

Figure E.424: Exponential Model of γ_{dry} versus E_0 for SDPMT-12 Continuous Tests, All Sites

E.5.11 γ_{dry} versus $\mathbf{p}_L$

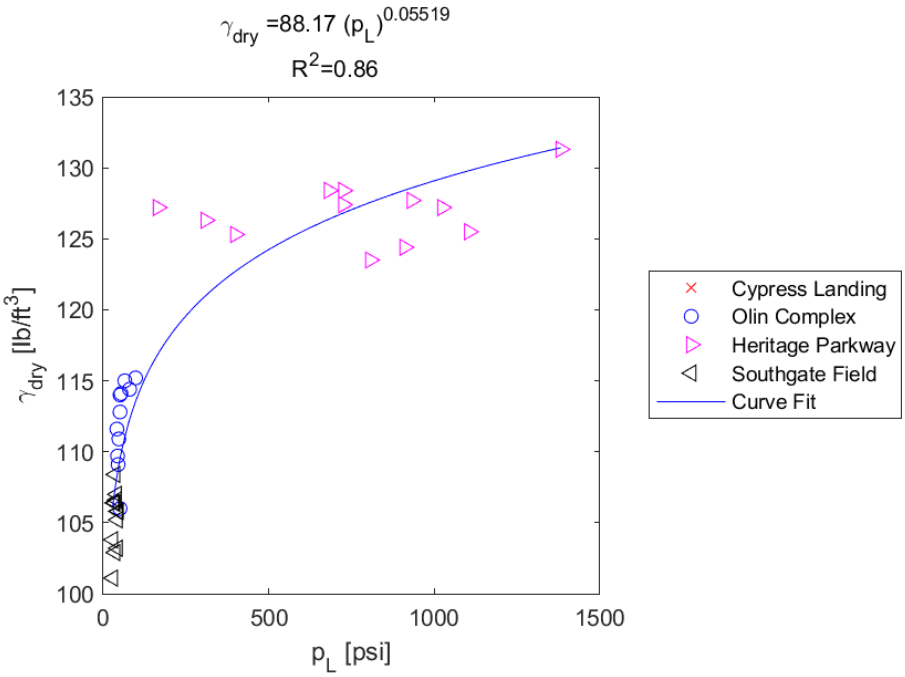

Figure E.425: Exponential Model of γ_{dry} versus p_L for SDPMT-6 Incremental Tests, All Sites

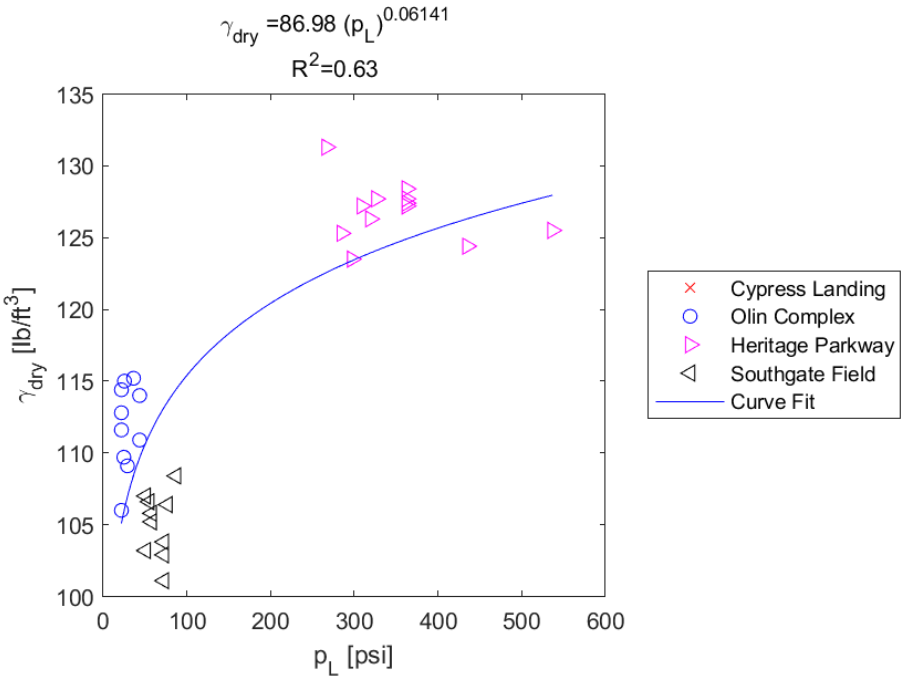

Figure E.426: Exponential Model of γ_{dry} versus p_L for SDPMT-6 Continuous Tests, All Sites

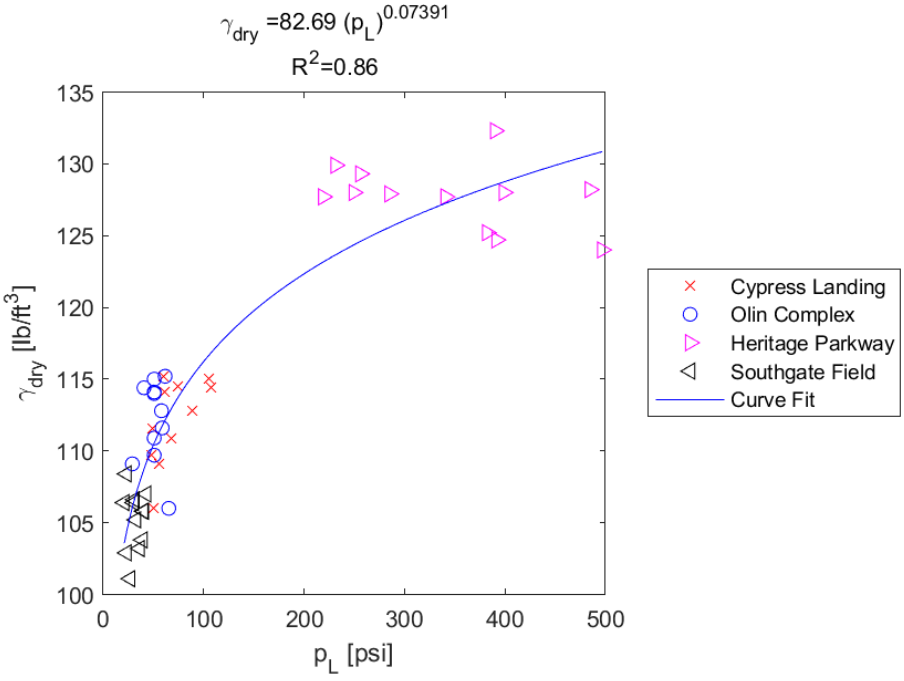

Figure E.427: Exponential Model of γ_{dry} versus p_L for SDPMT-12 Incremental Tests, All Sites

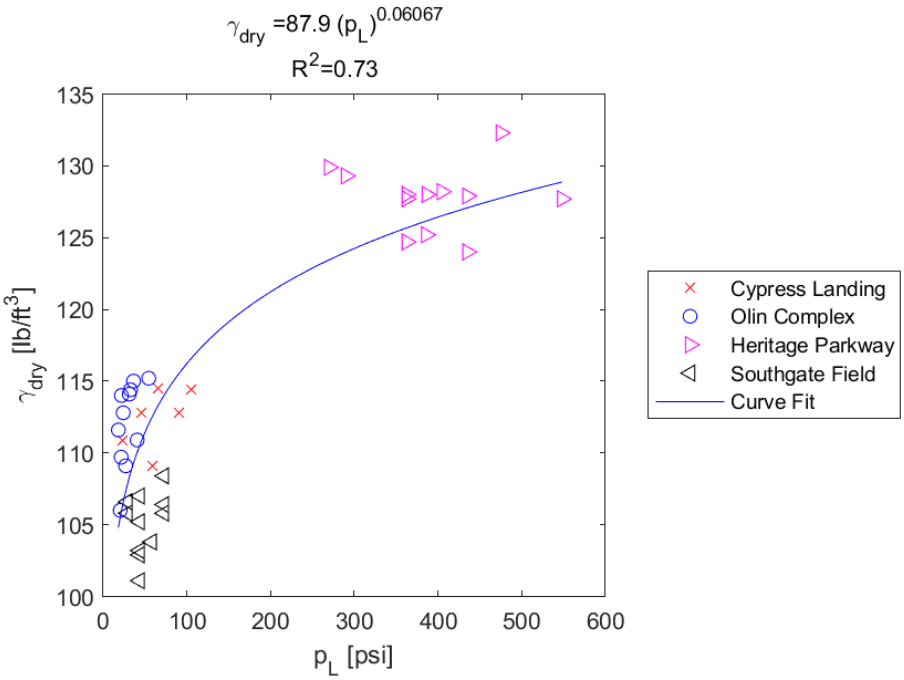

Figure E.428: Exponential Model of γ_{dry} versus p_L for SDPMT-12 Continuous Tests, All Sites

E.5.12 γ_{dry} versus $\mathbf{p}_0$

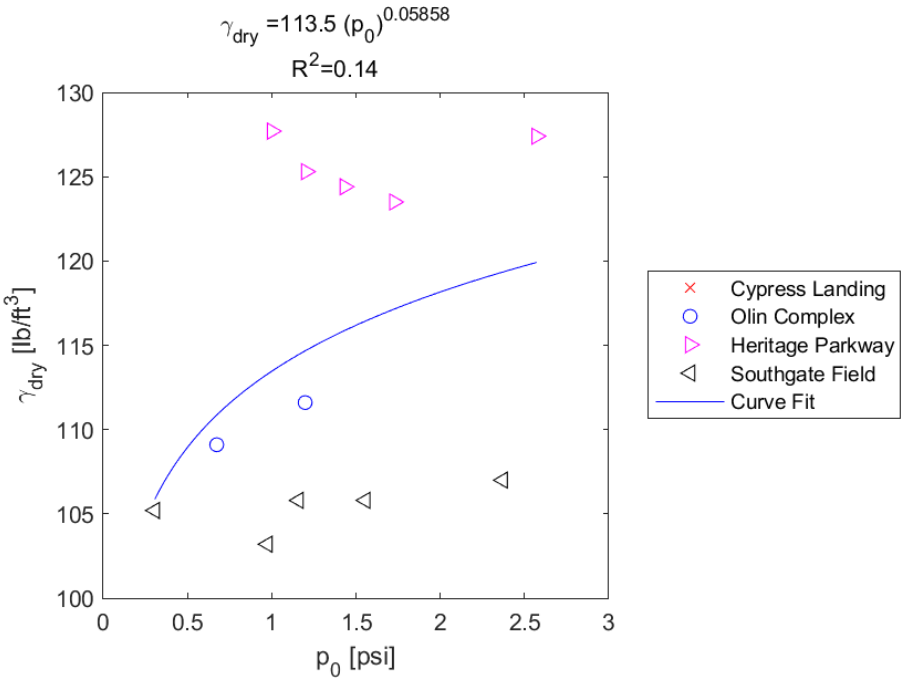

Figure E.429: Exponential Model of γ_{dry} versus p_0 for SDPMT-6 Incremental Tests, All Sites

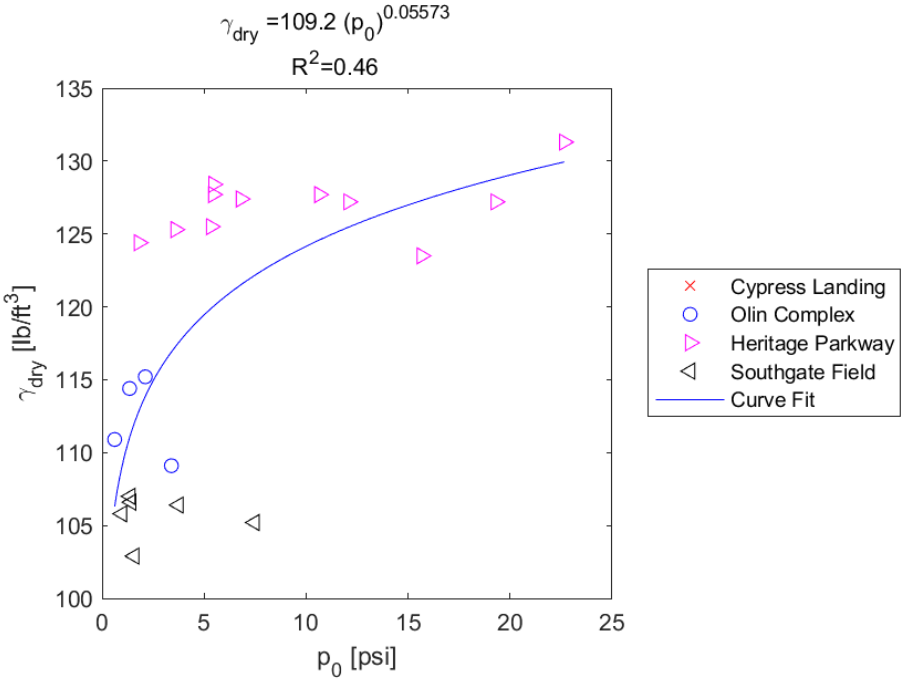

Figure E.430: Exponential Model of γ_{dry} versus p_0 for SDPMT-6 Continuous Tests, All Sites

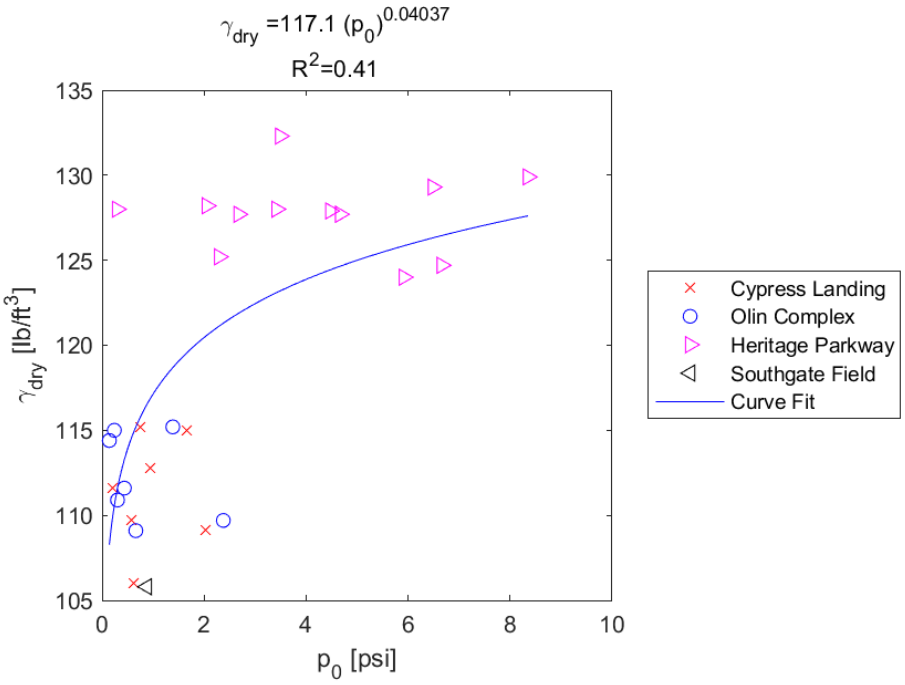

Figure E.431: Exponential Model of γ_{dry} versus p_0 for SDPMT-12 Incremental Tests, All Sites

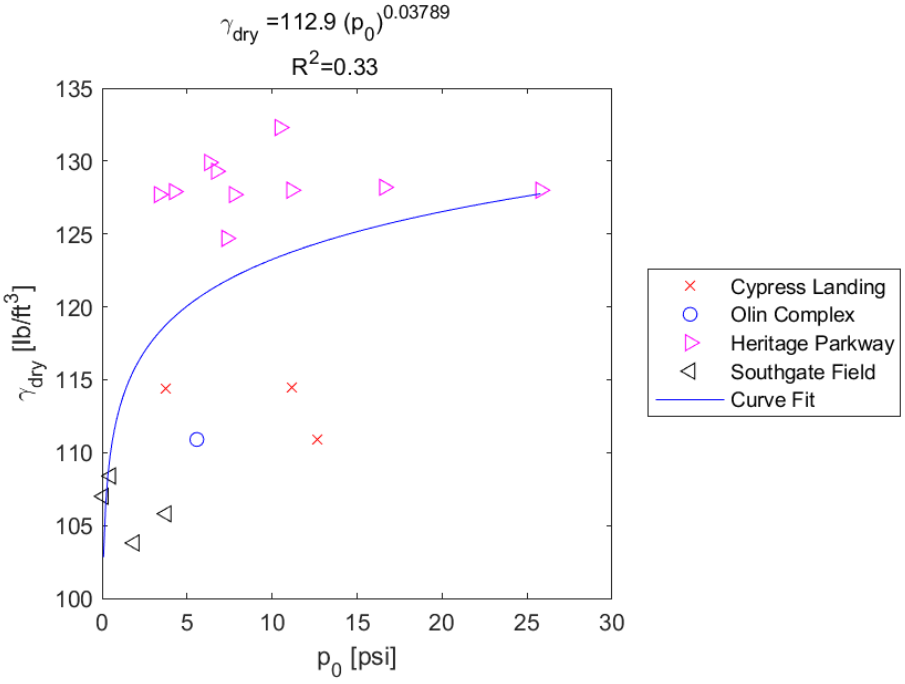

Figure E.432: Exponential Model of γ_{dry} versus p_0 for SDPMT-12 Continuous Tests, All Sites

E.5.13 DCP PI versus E_0

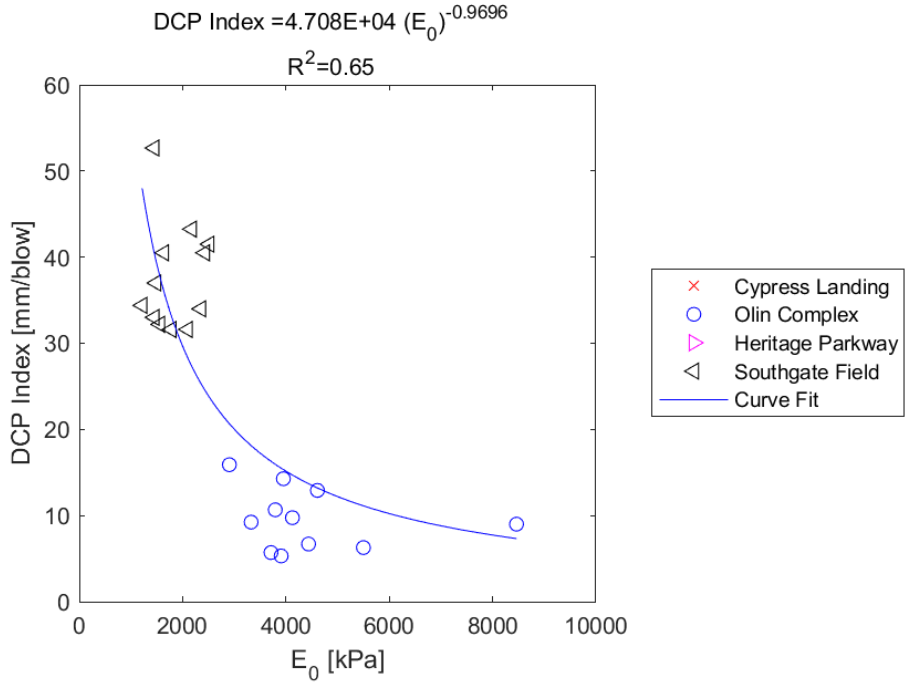

Figure E.433: Exponential Model of DCP PI versus E_0 for SDPMT-6 Incremental Tests, All Sites

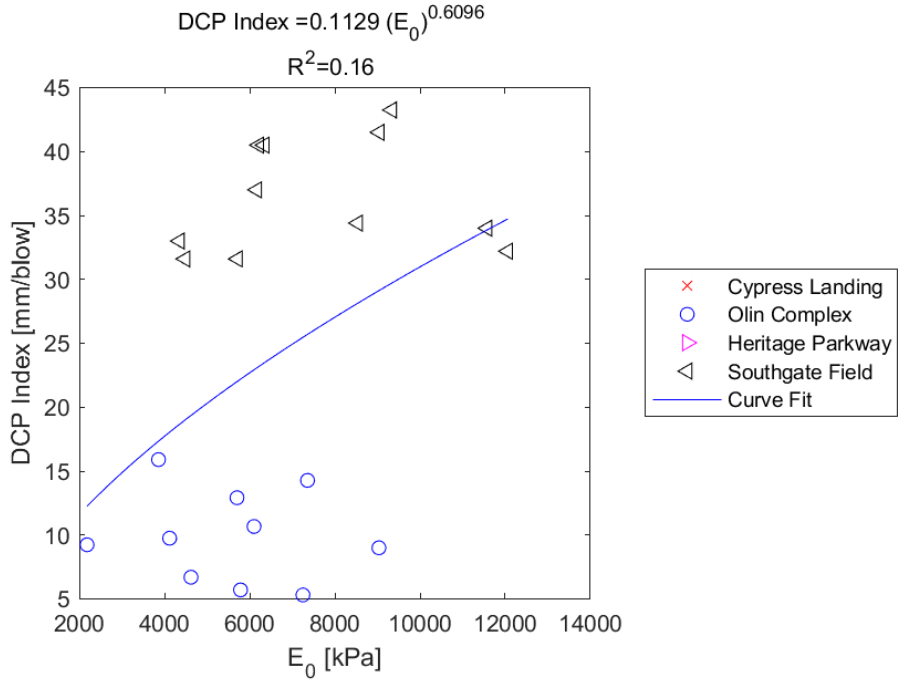

Figure E.434: Exponential Model of DCP PI versus E_0 for SDPMT-6 Continuous Tests, All Sites

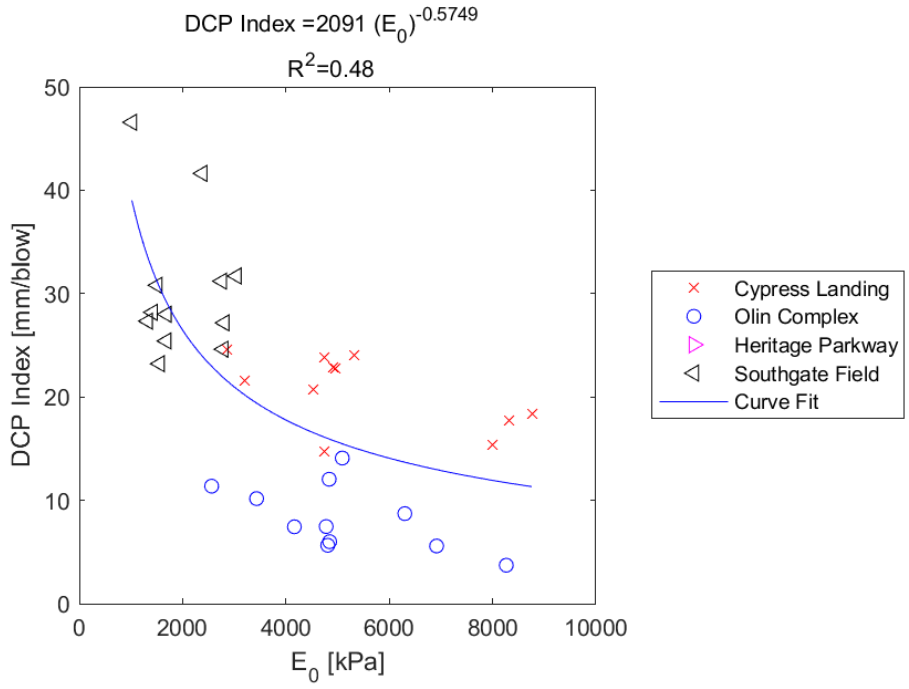

Figure E.435: Exponential Model of DCP PI versus E_0 for SDPMT-12 Incremental Tests, All Sites

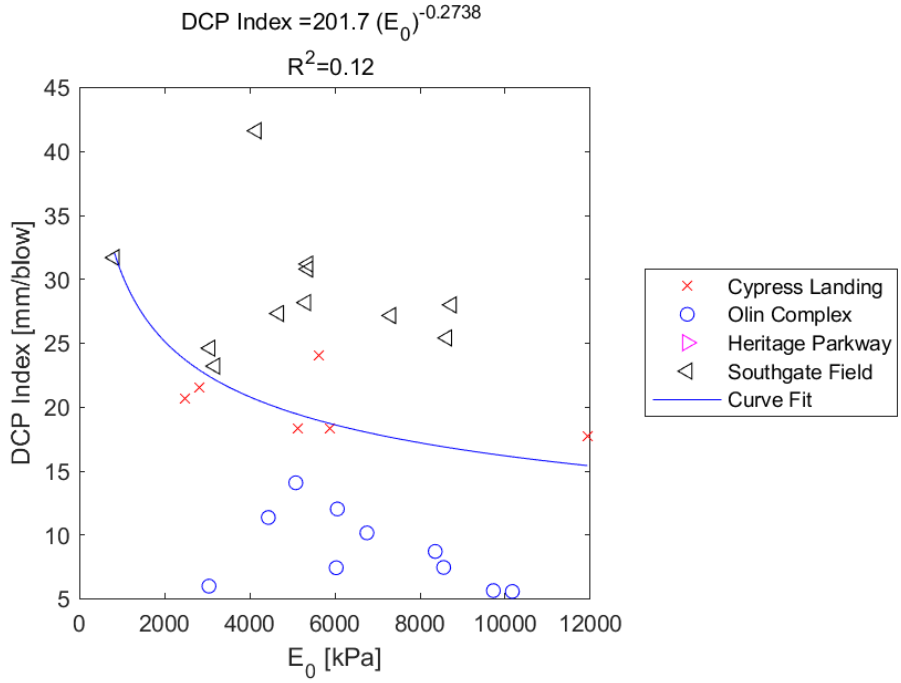

Figure E.436: Exponential Model of DCP PI versus E_0 for SDPMT-12 Continuous Tests, All Sites

E.5.14 DCP PI versus $\mathbf{p}_L$

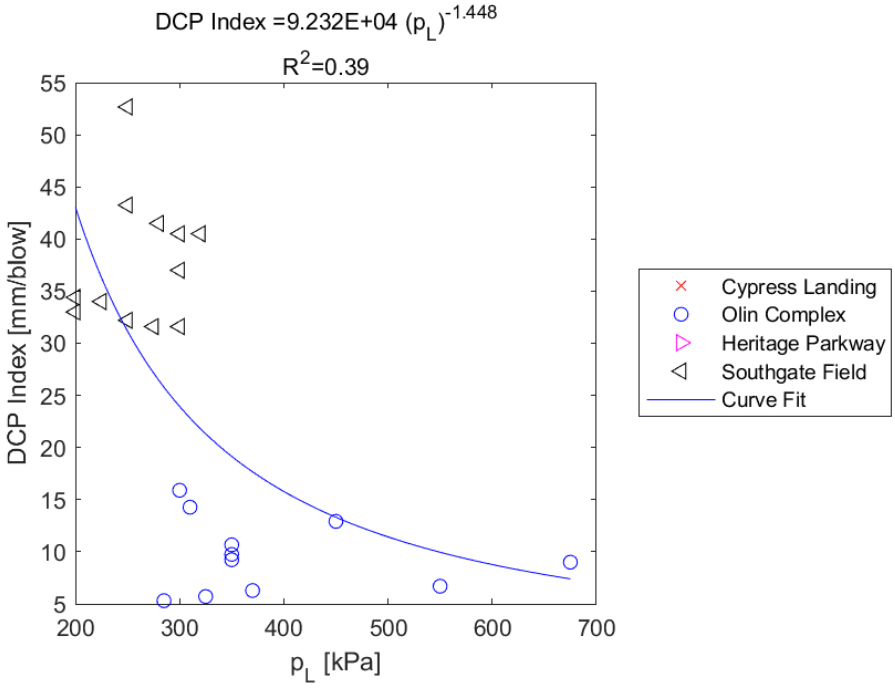

Figure E.437: Exponential Model of DCP PI versus p_L for SDPMT-6 Incremental Tests, All Sites

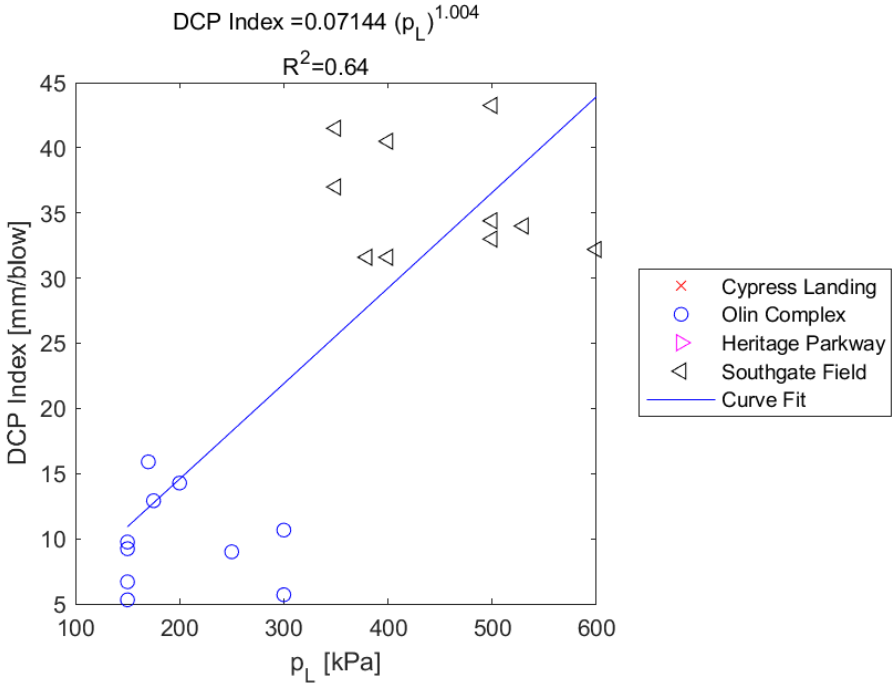

Figure E.438: Exponential Model of DCP PI versus p_L for SDPMT-6 Continuous Tests, All Sites

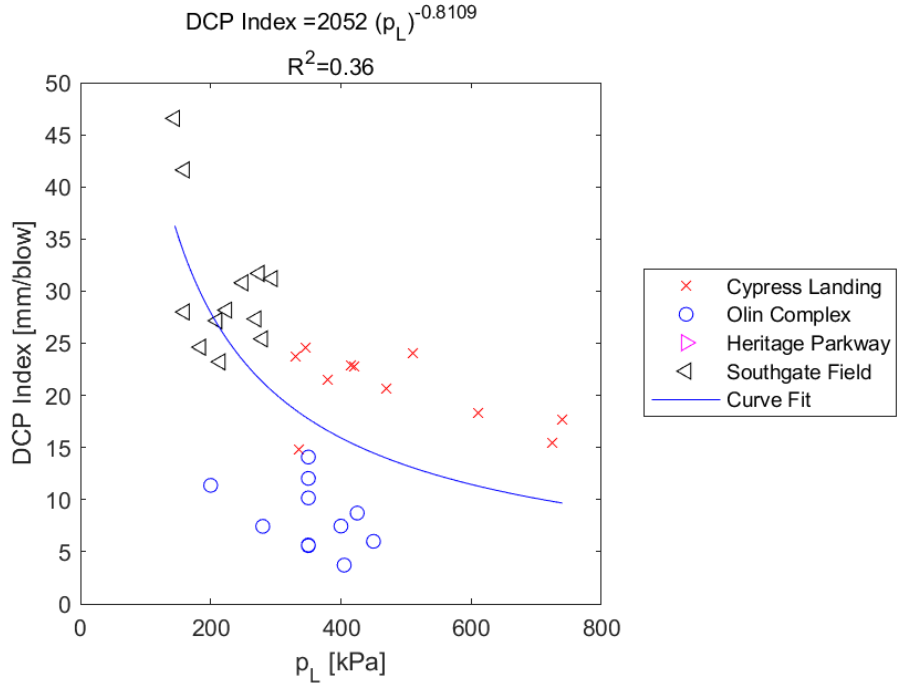

Figure E.439: Exponential Model of DCP PI versus p_L for SDPMT-12 Incremental Tests, All Sites

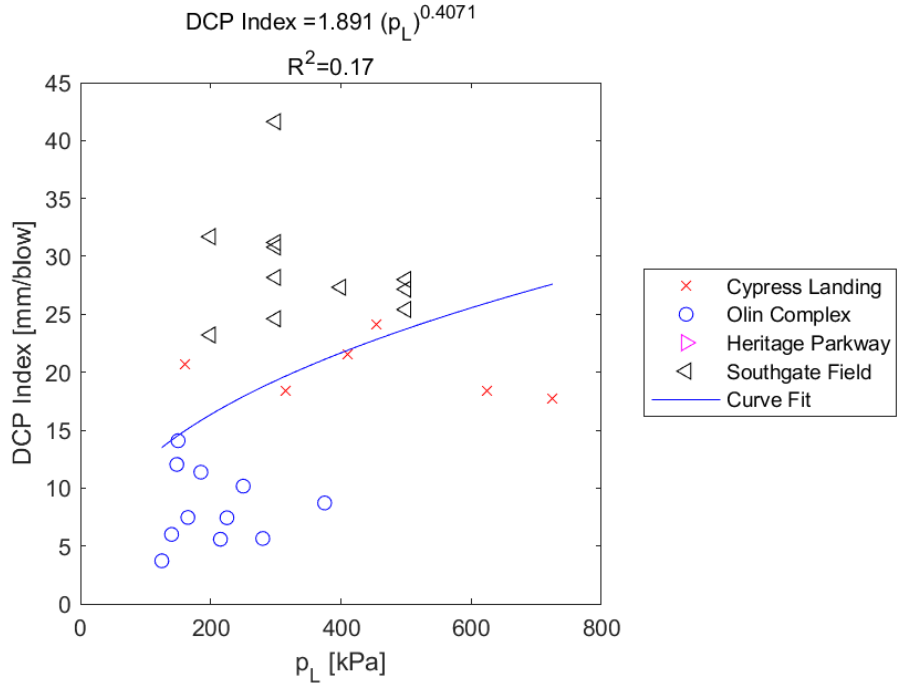

Figure E.440: Exponential Model of DCP PI versus p_L for SDPMT-12 Continuous Tests, All Sites

E.5.15 DCP PI versus $\mathbf{p}_0$

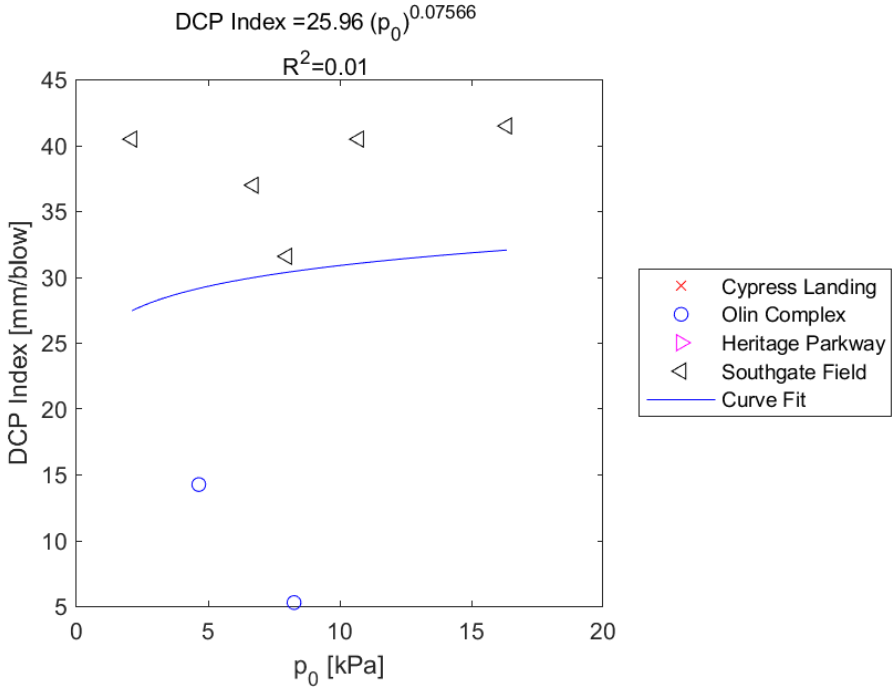

Figure E.441: Exponential Model of DCP PI versus p_0 for SDPMT-6 Incremental Tests, All Sites

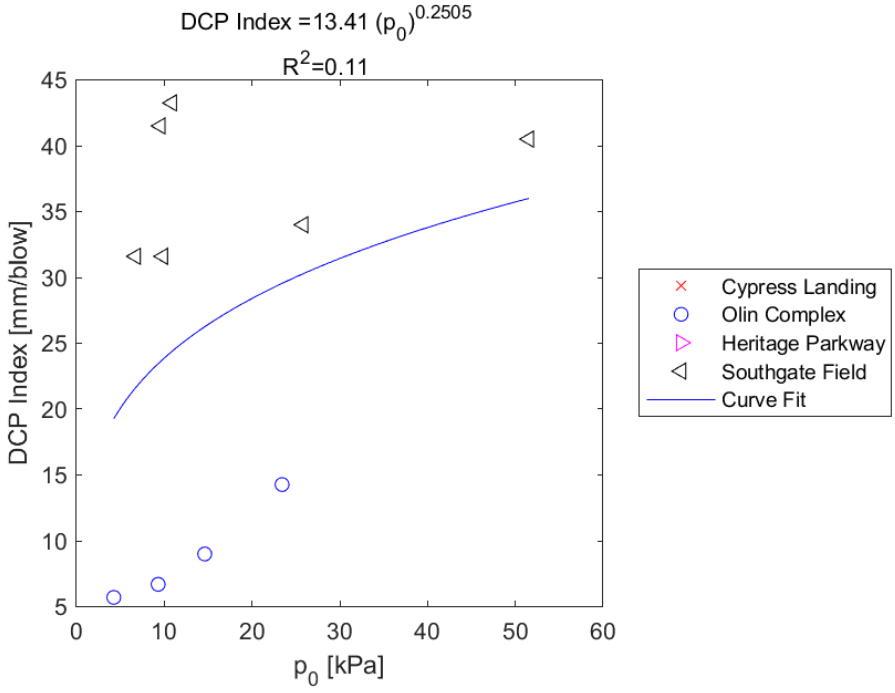

Figure E.442: Exponential Model of DCP PI versus p_0 for SDPMT-6 Continuous Tests, All Sites

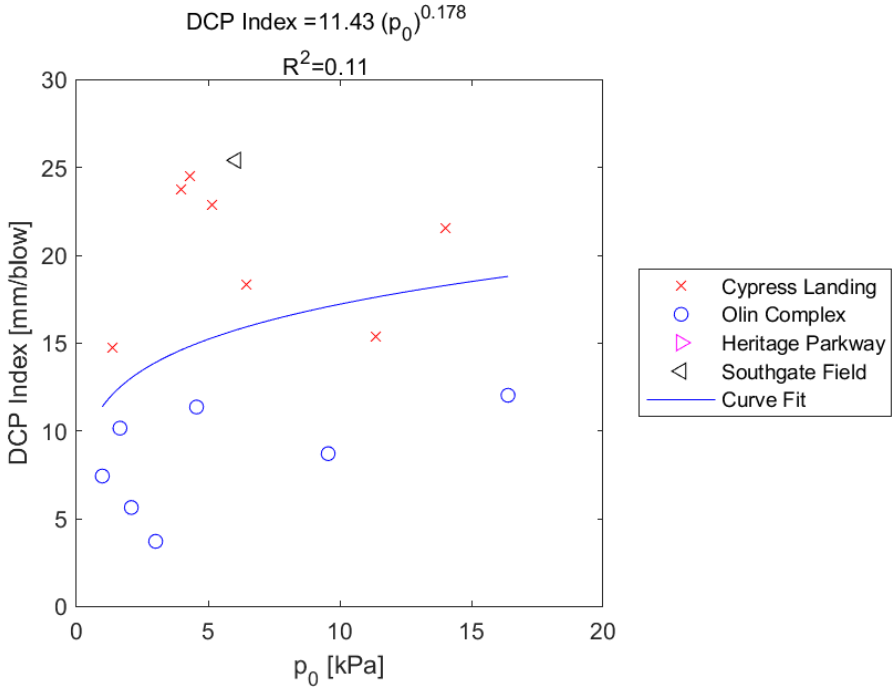

Figure E.443: Exponential Model of DCP PI versus p_0 for SDPMT-12 Incremental Tests, All Sites

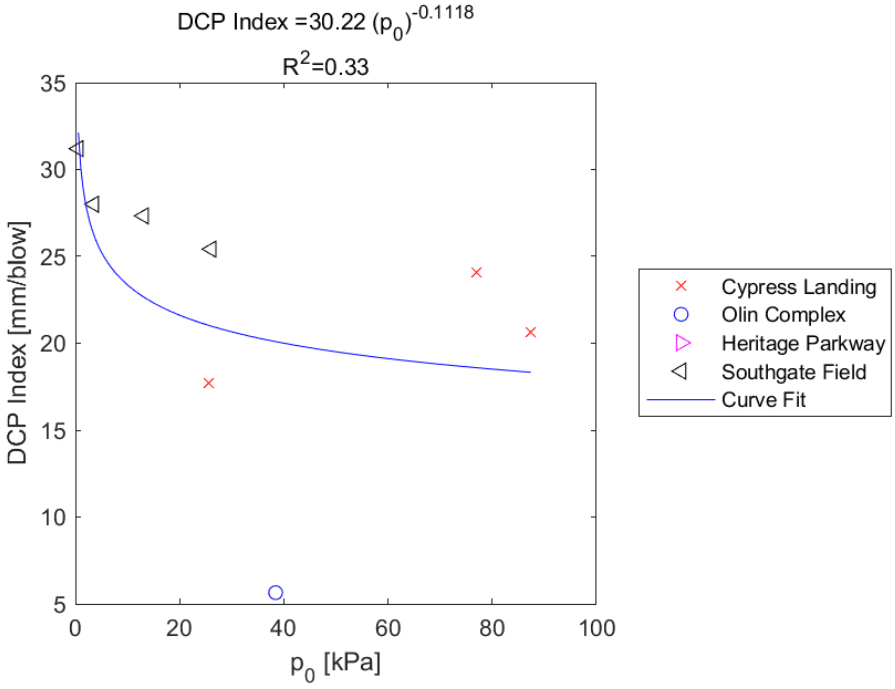

Figure E.444: Exponential Model of DCP PI versus p_0 for SDPMT-12 Continuous Tests, All Sites

E.5.16 $\mathbf{E}_{d,zorn}$ versus $\mathbf{E}_0$

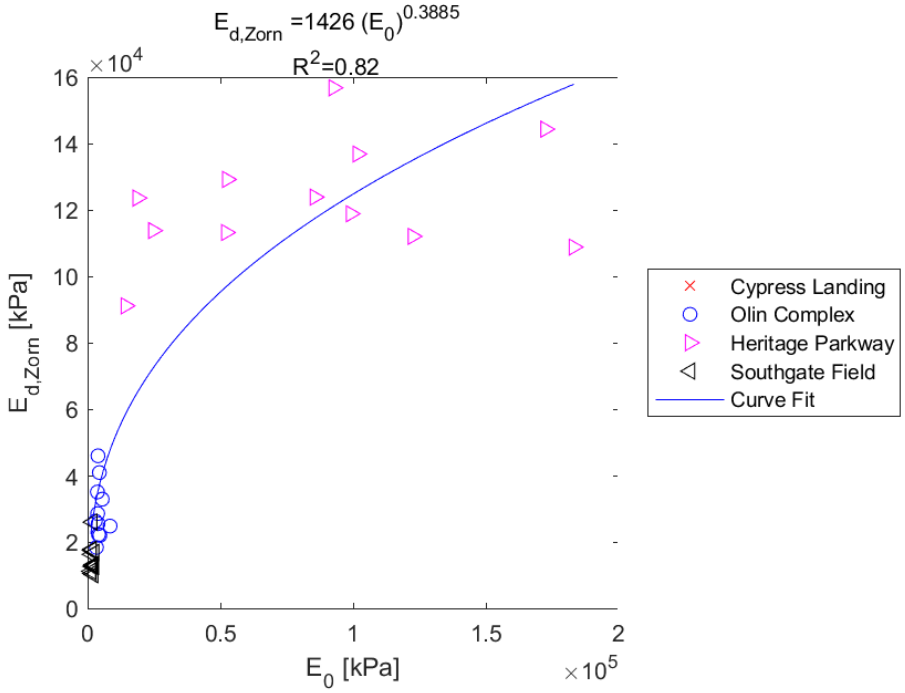

Figure E.445: Exponential Model of $E_{d,zorn}$ versus E_0 for SDPMT-6 Incremental Tests, All Sites

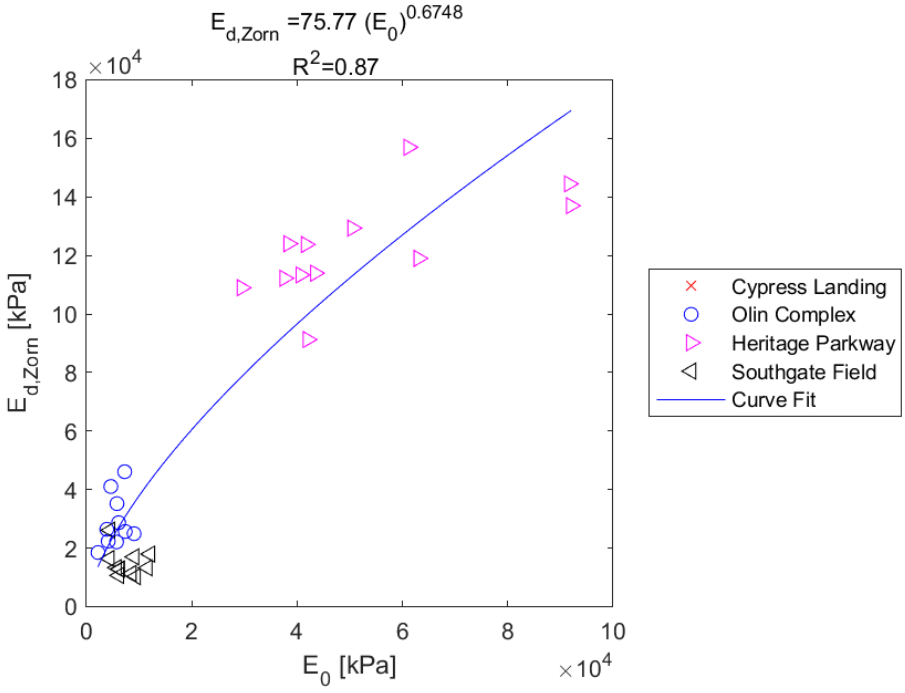

Figure E.446: Exponential Model of $E_{d,zorn}$ versus E_0 for SDPMT-6 Continuous Tests, All Sites

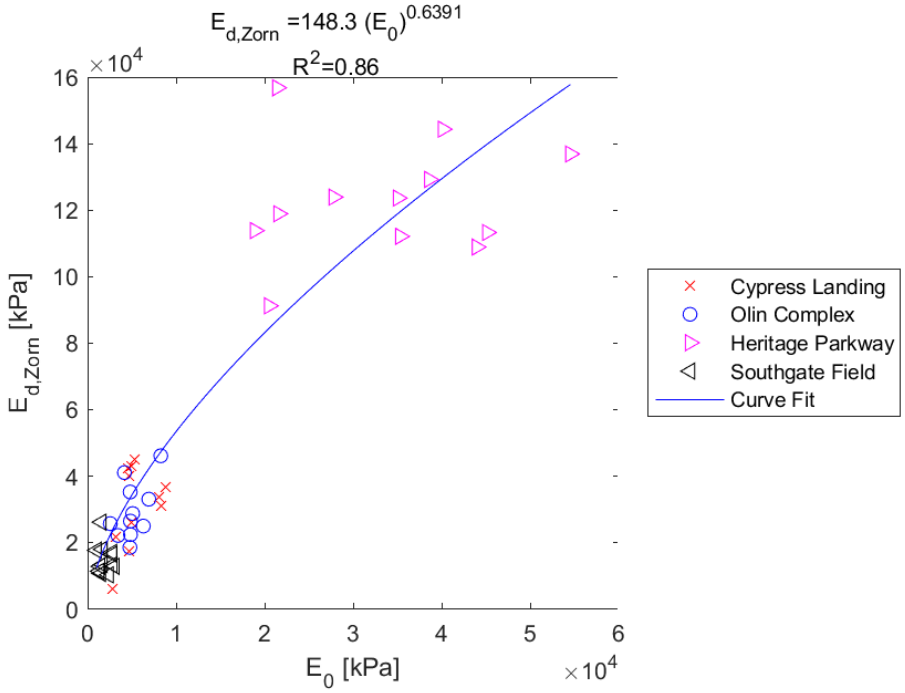

Figure E.447: Exponential Model of $E_{d,zorn}$ versus E_0 for SDPMT-12 Incremental Tests, All Sites

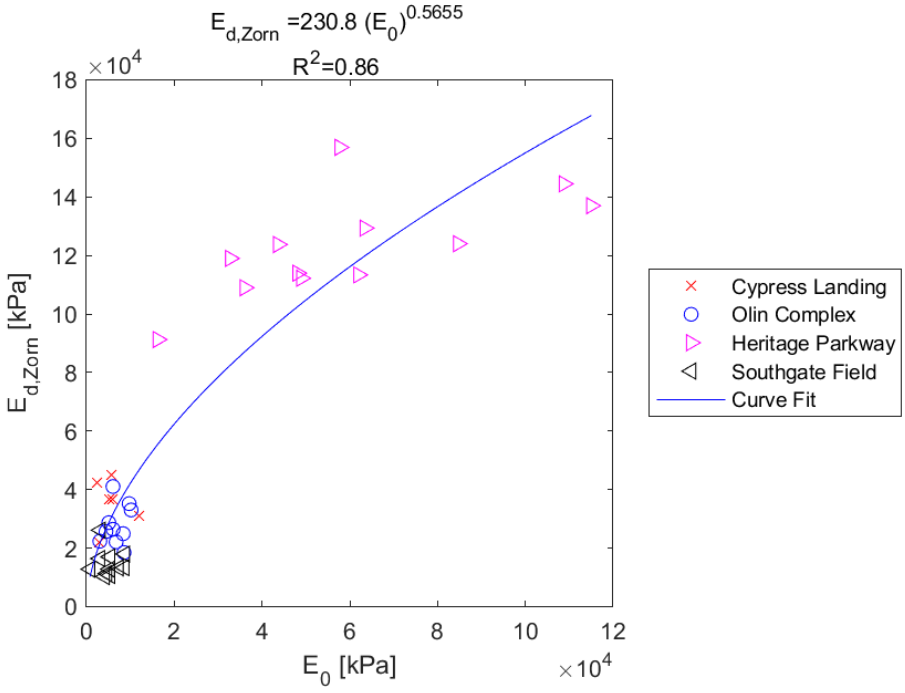

Figure E.448: Exponential Model of $E_{d,zorn}$ versus E_0 for SDPMT-12 Continuous Tests, All Sites

E.5.17 $\mathbf{E}_{d,zorn}$ versus $\mathbf{p}_L$

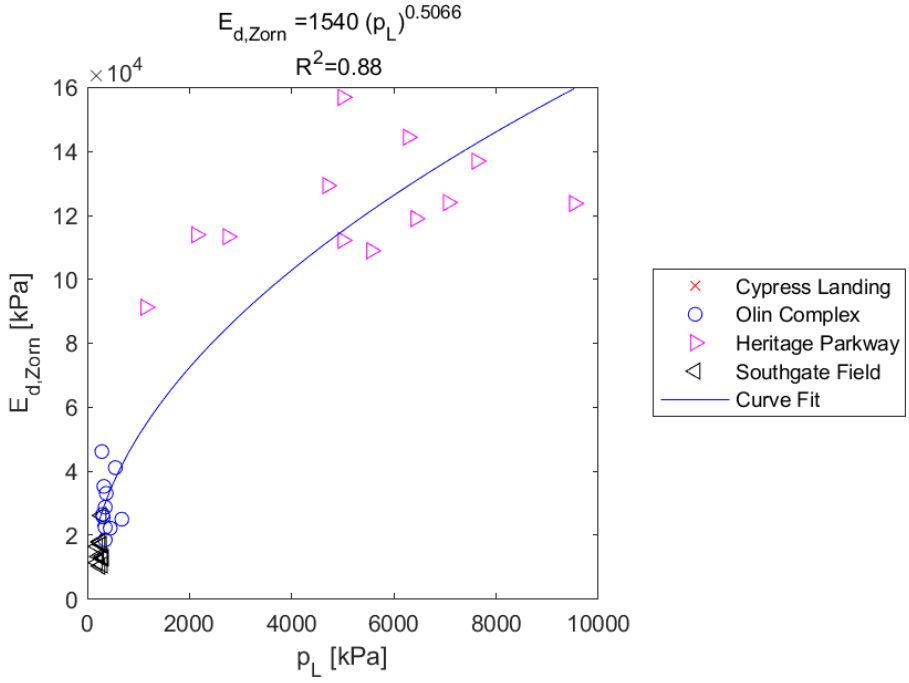

Figure E.449: Exponential Model of $E_{d,zorn}$ versus p_L for SDPMT-6 Incremental Tests, All Sites

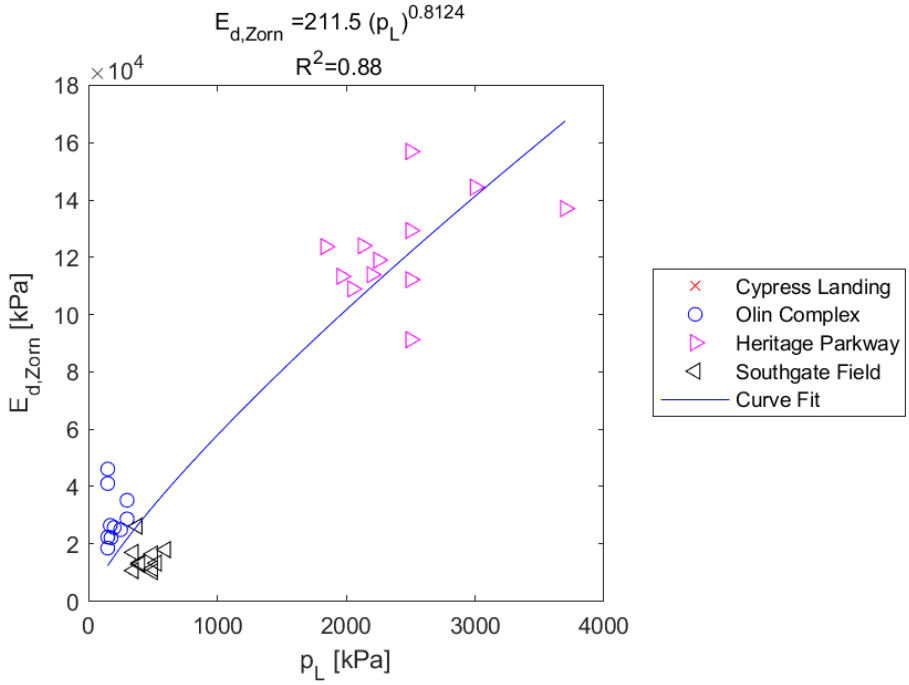

Figure E.450: Exponential Model of $E_{d,zorn}$ versus p_L for SDPMT-6 Continuous Tests, All Sites

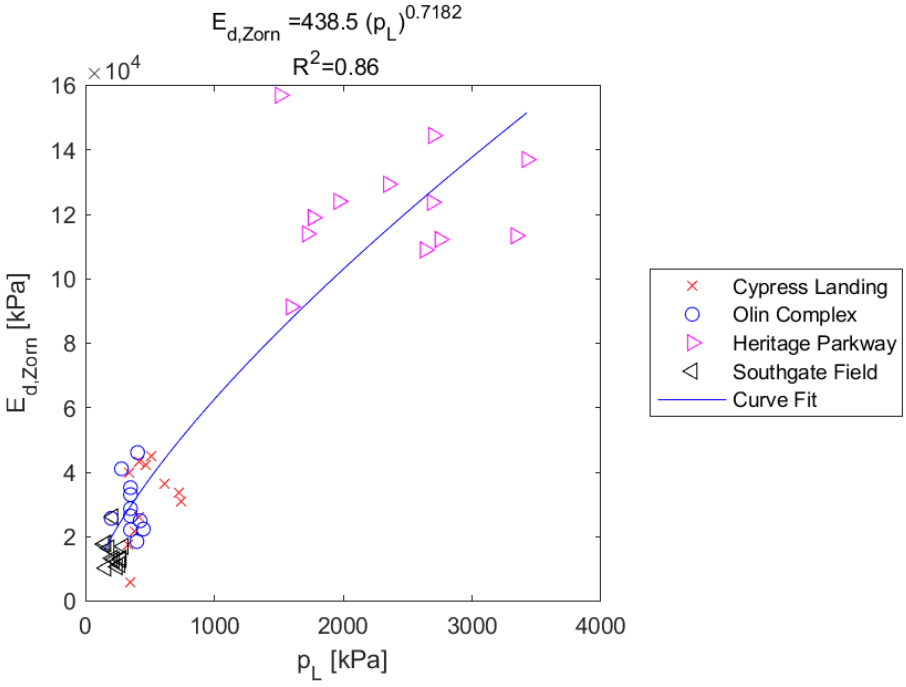

Figure E.451: Exponential Model of $E_{d,zorn}$ versus p_L for SDPMT-12 Incremental Tests, All Sites

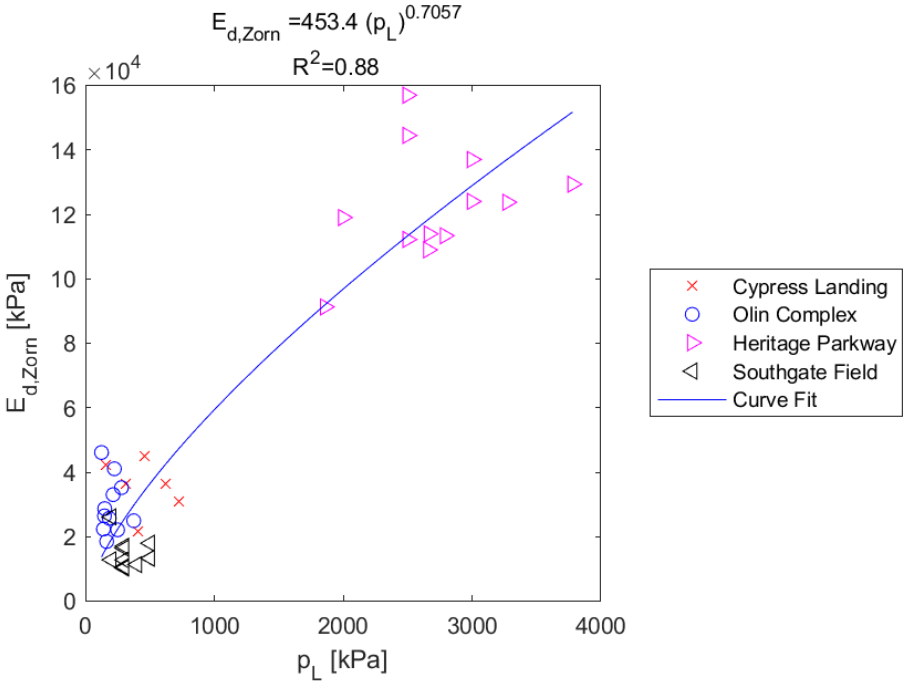

Figure E.452: Exponential Model of $E_{d,zorn}$ versus p_L for SDPMT-12 Continuous Tests, All Sites

E.5.18 $\mathbf{E}_{d,zorn}$ versus $\mathbf{p}_0$

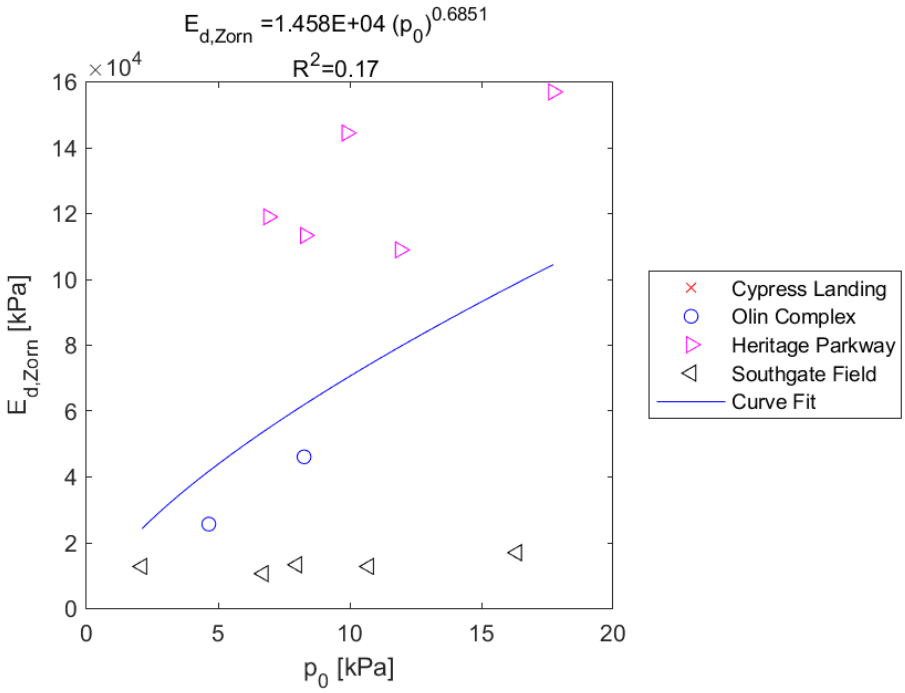

Figure E.453: Exponential Model of $E_{d,zorn}$ versus p_0 for SDPMT-6 Incremental Tests, All Sites

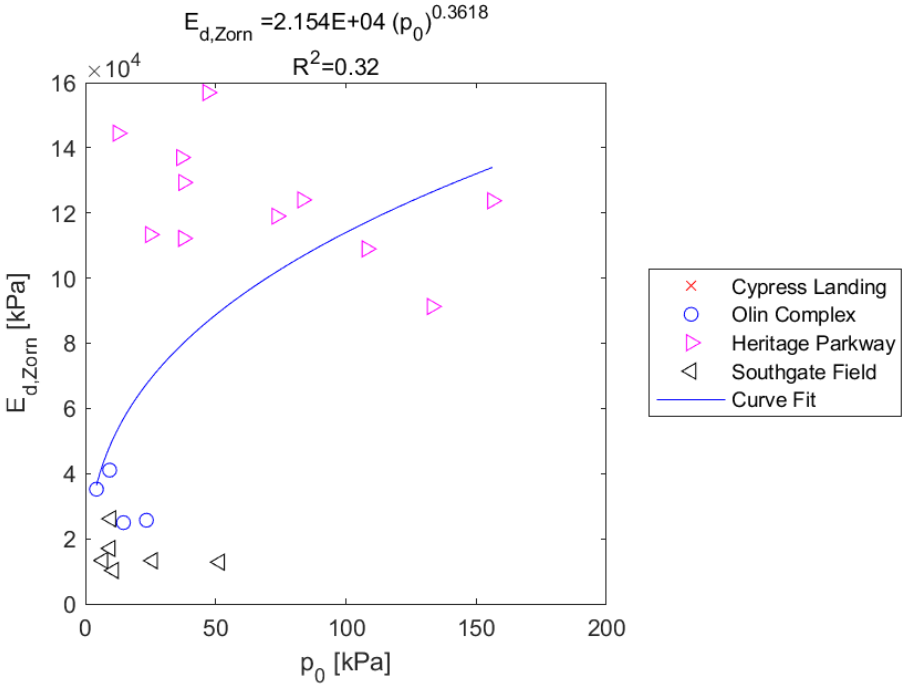

Figure E.454: Exponential Model of $E_{d,zorn}$ versus p_0 for SDPMT-6 Continuous Tests, All Sites

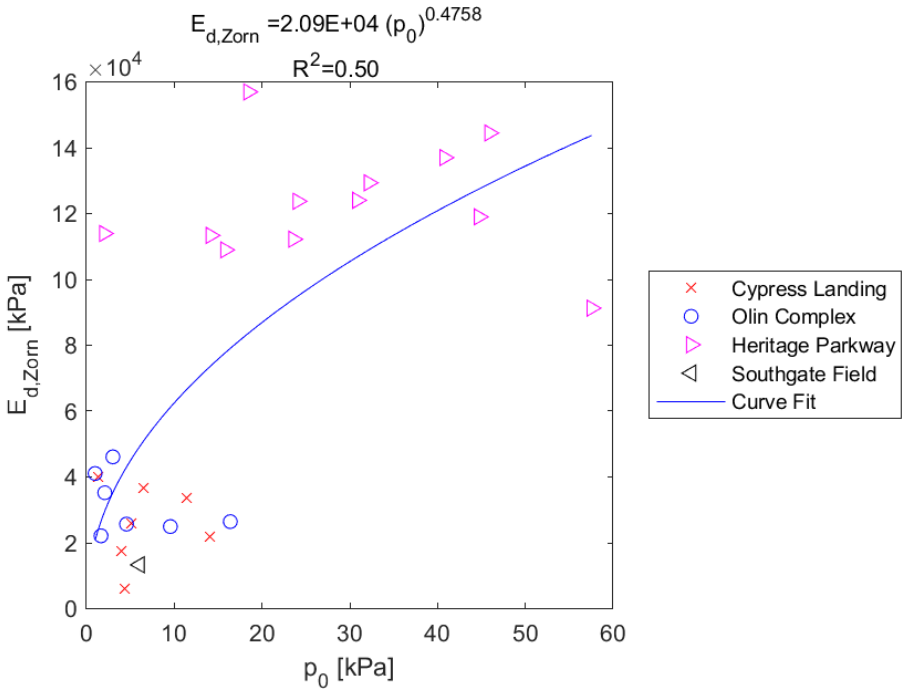

Figure E.455: Exponential Model of $E_{d,zorn}$ versus p_0 for SDPMT-12 Incremental Tests, All Sites

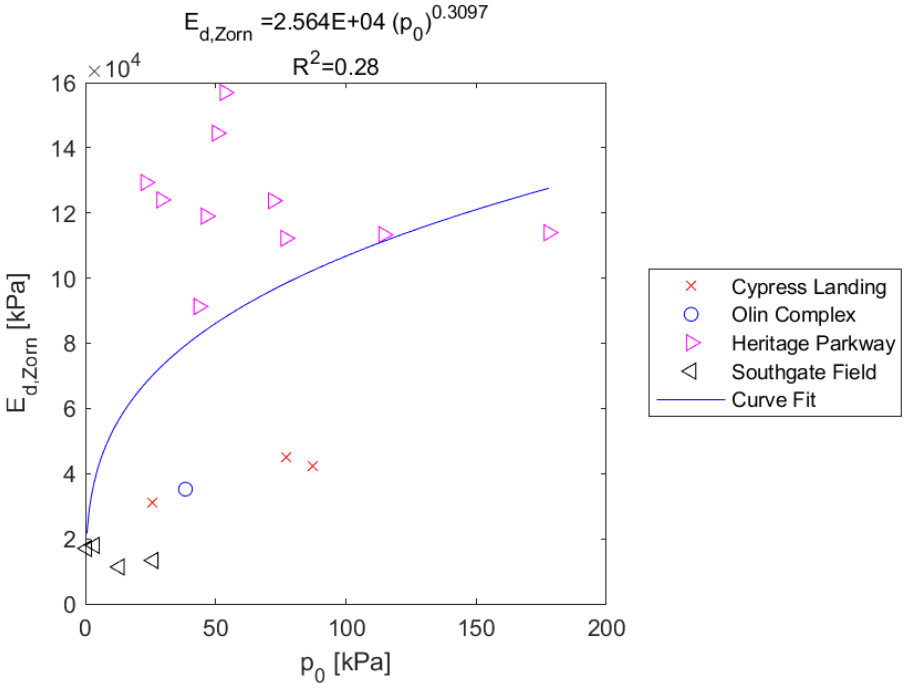

Figure E.456: Exponential Model of $E_{d,zorn}$ versus p_0 for SDPMT-12 Continuous Tests, All Sites

E.5.19 $\mathbf{E}_{0,Dynatest}$ versus $\mathbf{E}_0$

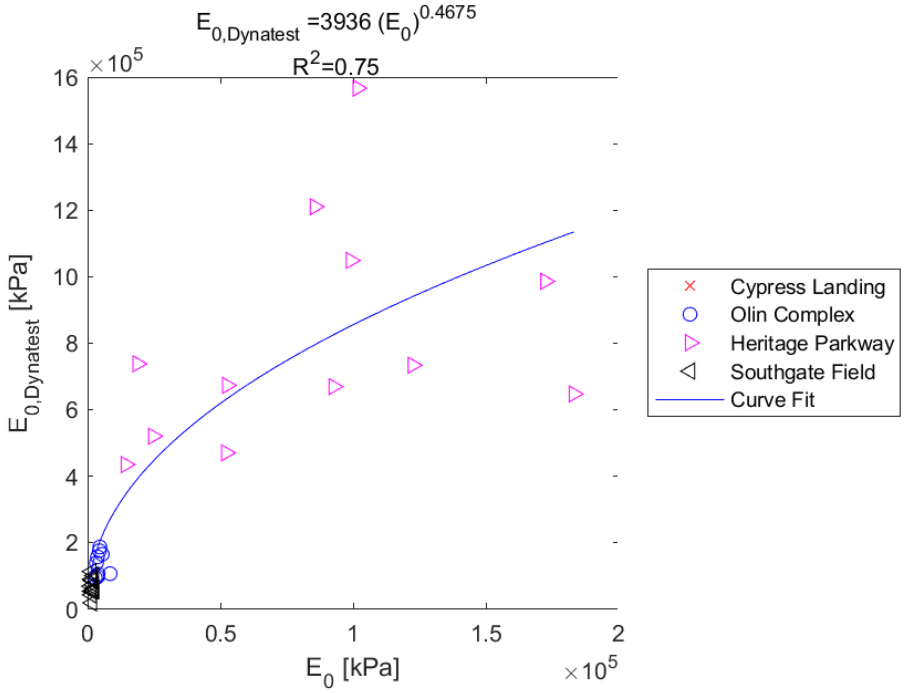

Figure E.457: Exponential Model of $E_{0,Dynatest}$ versus E_0 for SDPMT-6 Incremental Tests, All Sites

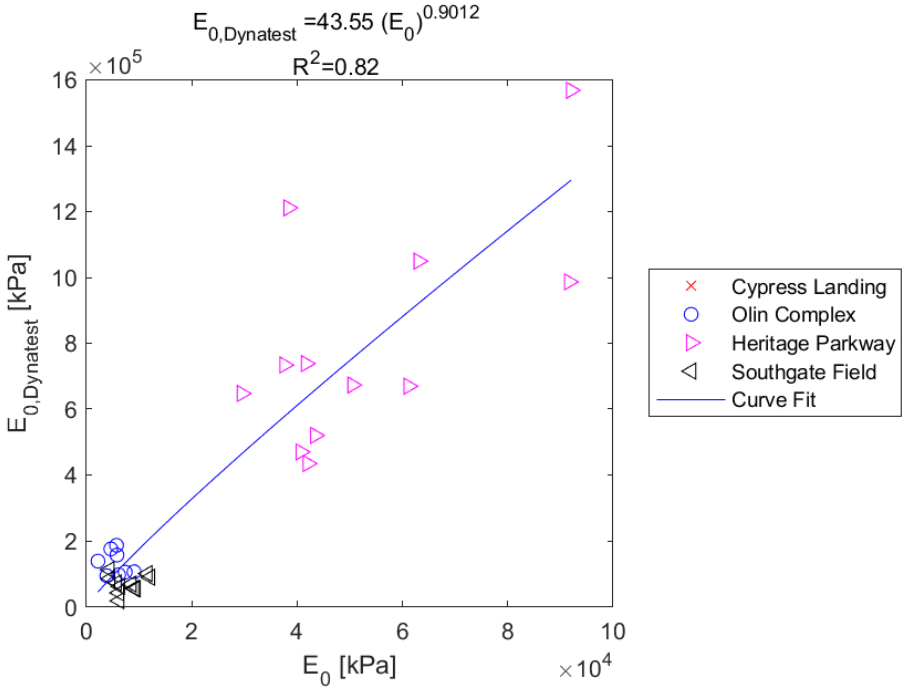

Figure E.458: Exponential Model of $E_{0,Dynatest}$ versus E_0 for SDPMT-6 Continuous Tests, All Sites

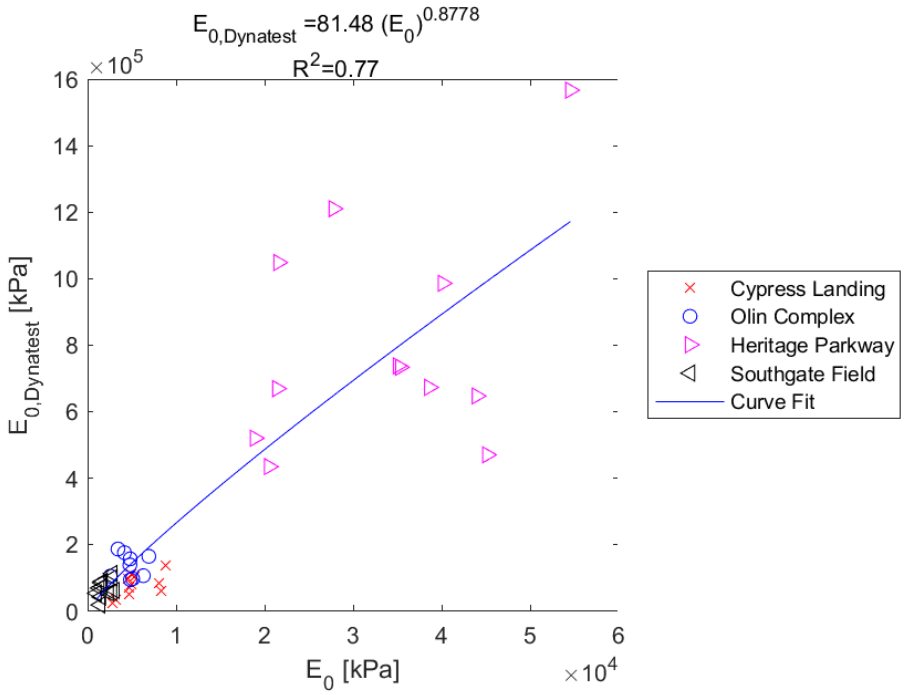

Figure E.459: Exponential Model of $E_{0,Dynatest}$ versus E_0 for SDPMT-12 Incremental Tests, All Sites

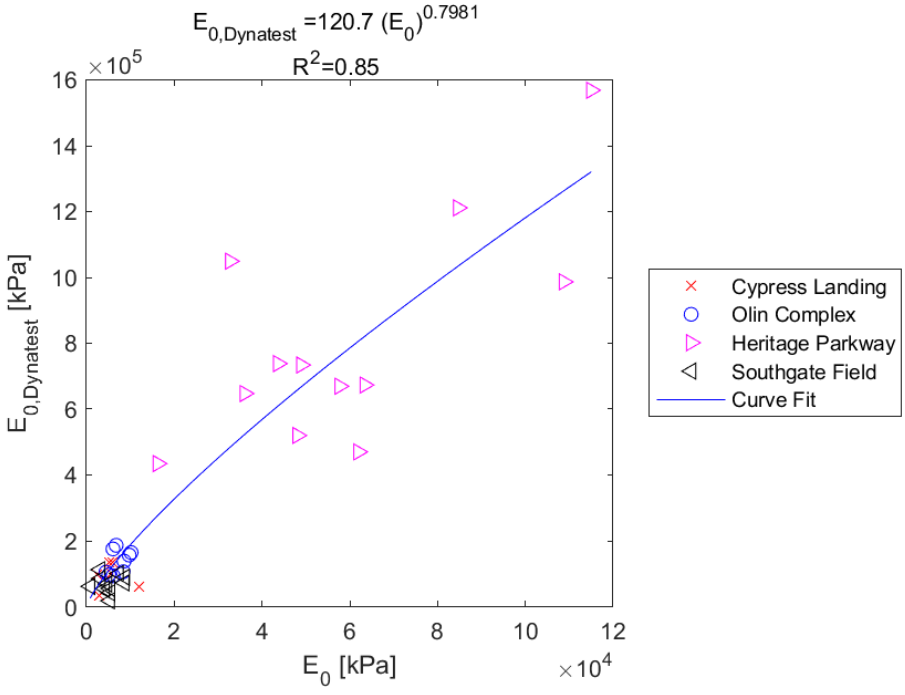

Figure E.460: Exponential Model of $E_{0,Dynatest}$ versus E_0 for SDPMT-12 Continuous Tests, All Sites

E.5.20 $\mathbf{E}_{0,Dynatest}$ versus $\mathbf{p}_L$

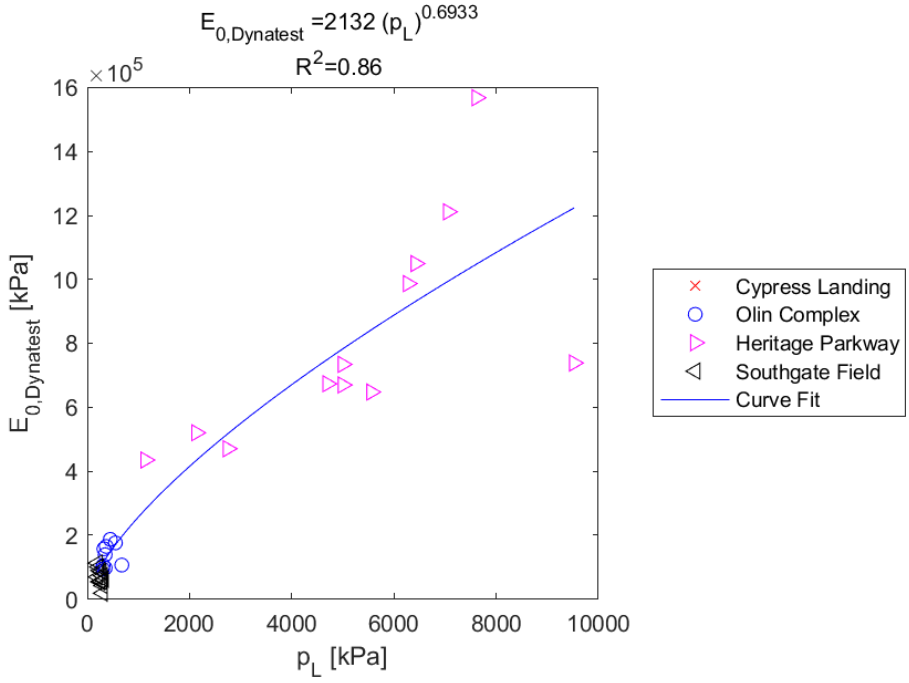

Figure E.461: Exponential Model of $E_{0,Dynatest}$ versus p_L for SDPMT-6 Incremental Tests, All Sites

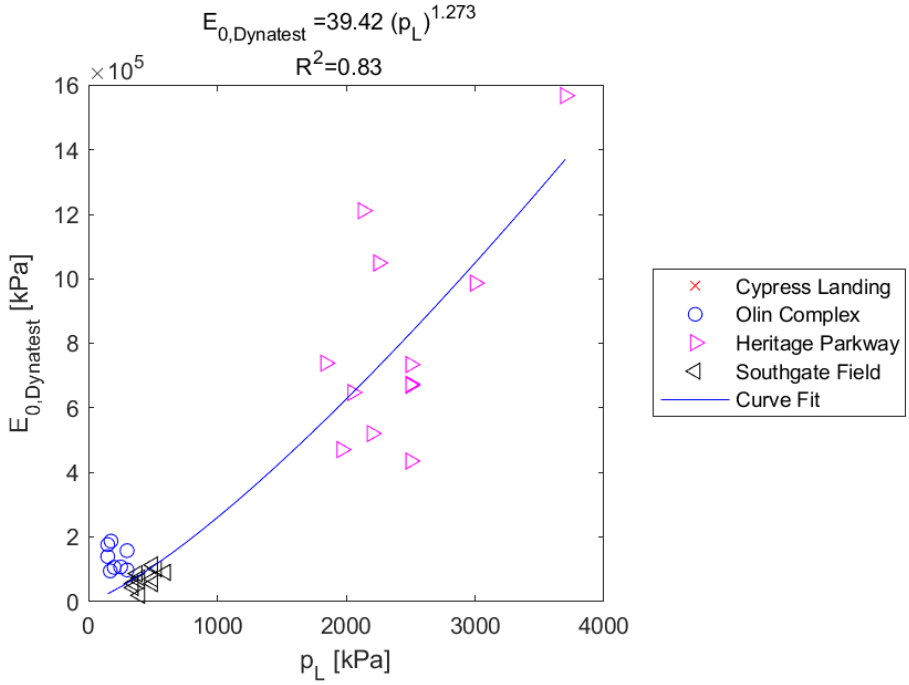

Figure E.462: Exponential Model of $E_{0,Dynatest}$ versus p_L for SDPMT-6 Continuous Tests, All Sites

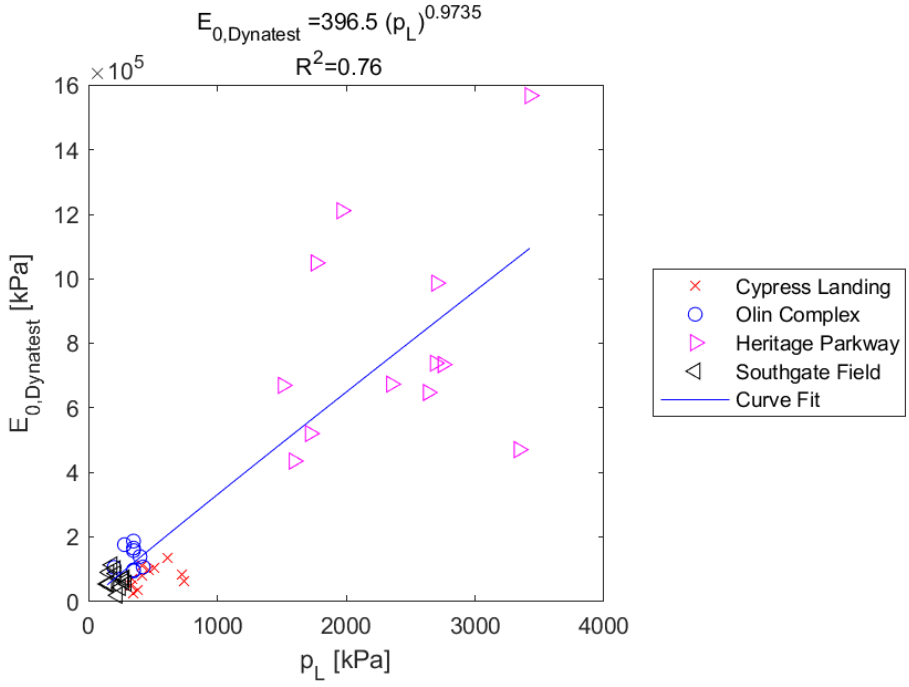

Figure E.463: Exponential Model of $E_{0,Dynatest}$ versus p_L for SDPMT-12 Incremental Tests, All Sites

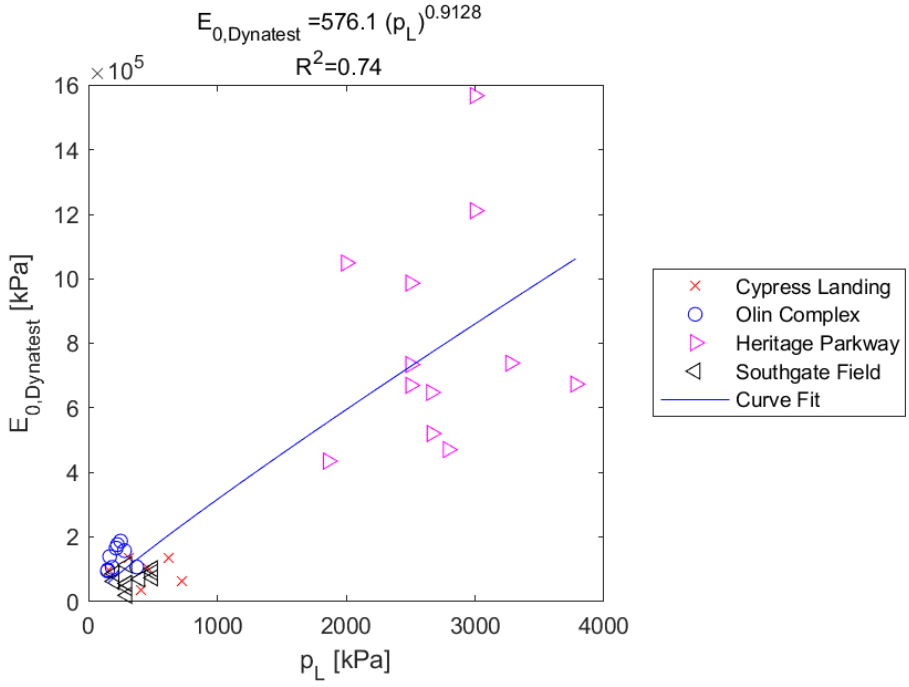

Figure E.464: Exponential Model of $E_{0,Dynatest}$ versus p_L for SDPMT-12 Continuous Tests, All Sites

E.5.21 $\mathbf{E}_{0,Dynatest}$ versus $\mathbf{p}_0$

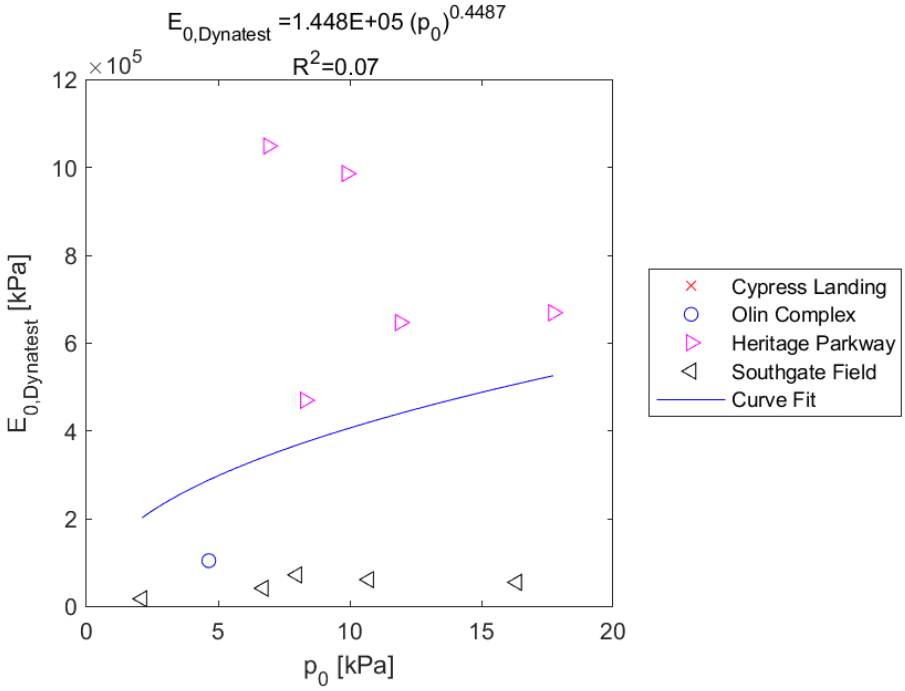

Figure E.465: Exponential Model of $E_{0,Dynatest}$ versus p_0 for SDPMT-6 Incremental Tests, All Sites

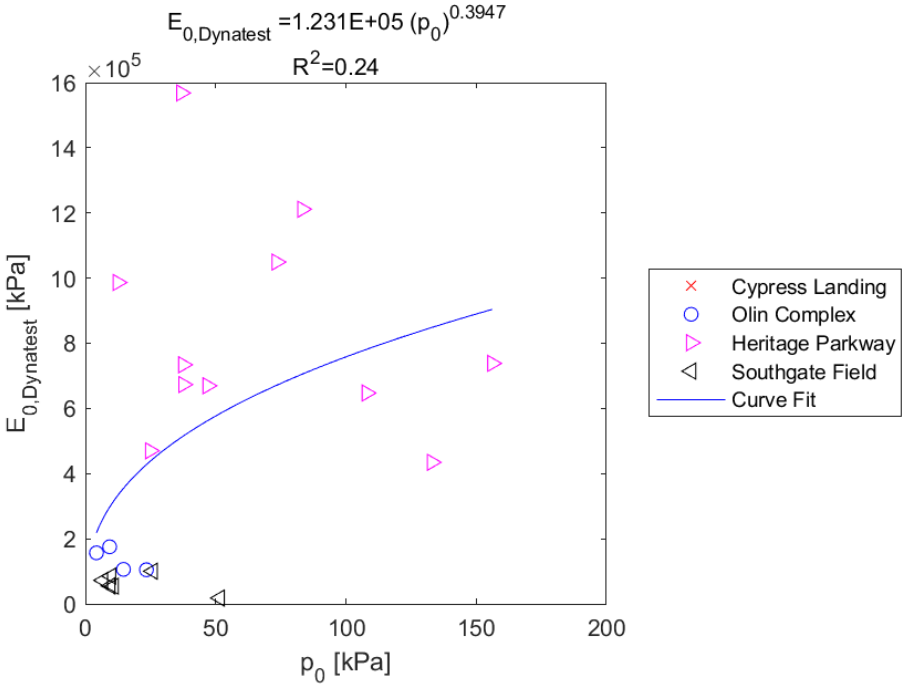

Figure E.466: Exponential Model of $E_{0,Dynatest}$ versus p_0 for SDPMT-6 Continuous Tests, All Sites

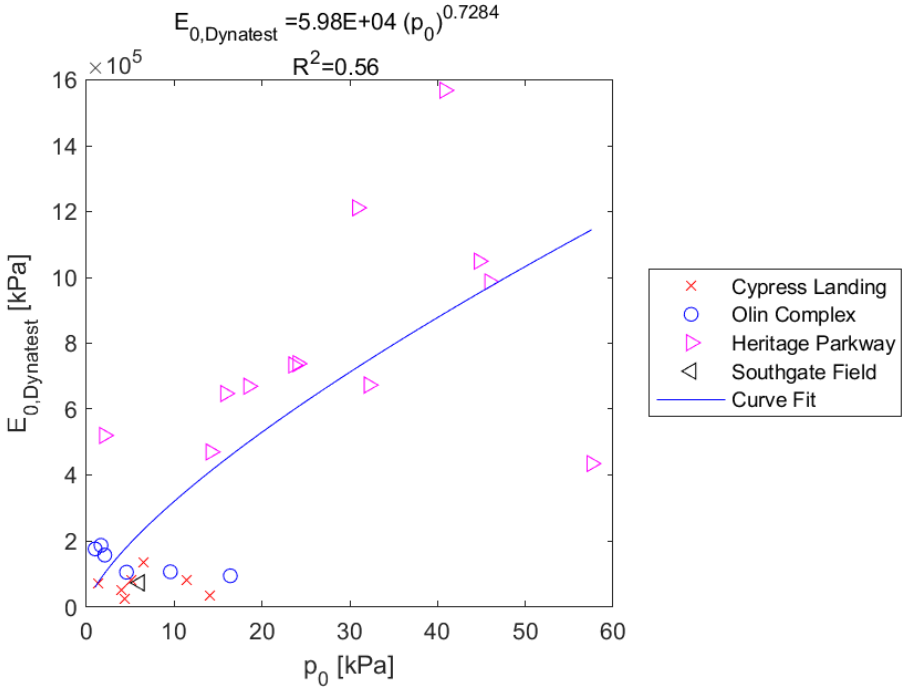

Figure E.467: Exponential Model of $E_{0,Dynatest}$ versus p_0 for SDPMT-12 Incremental Tests, All Sites

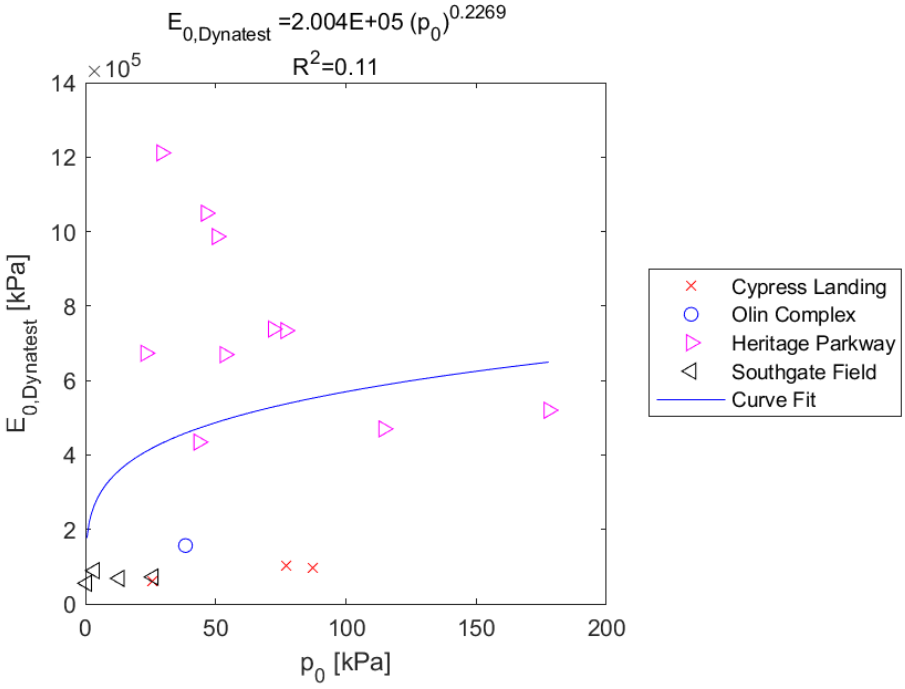

Figure E.468: Exponential Model of $E_{0,Dynatest}$ versus p_0 for SDPMT-12 Continuous Tests, All Sites

E.5.22 CIV versus E_0

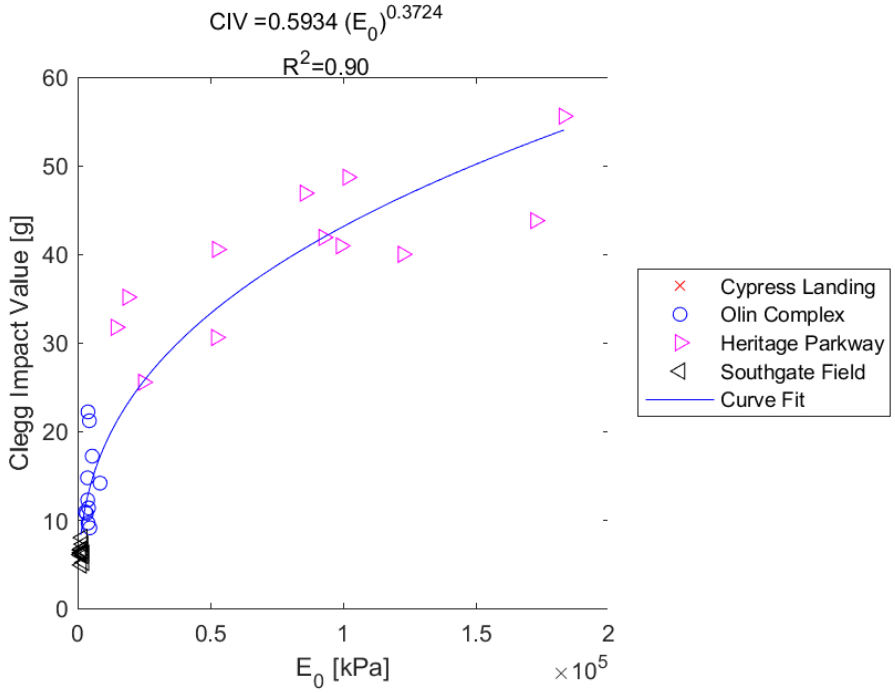

Figure E.469: Exponential Model of CIV versus E_0 for SDPMT-6 Incremental Tests, All Sites

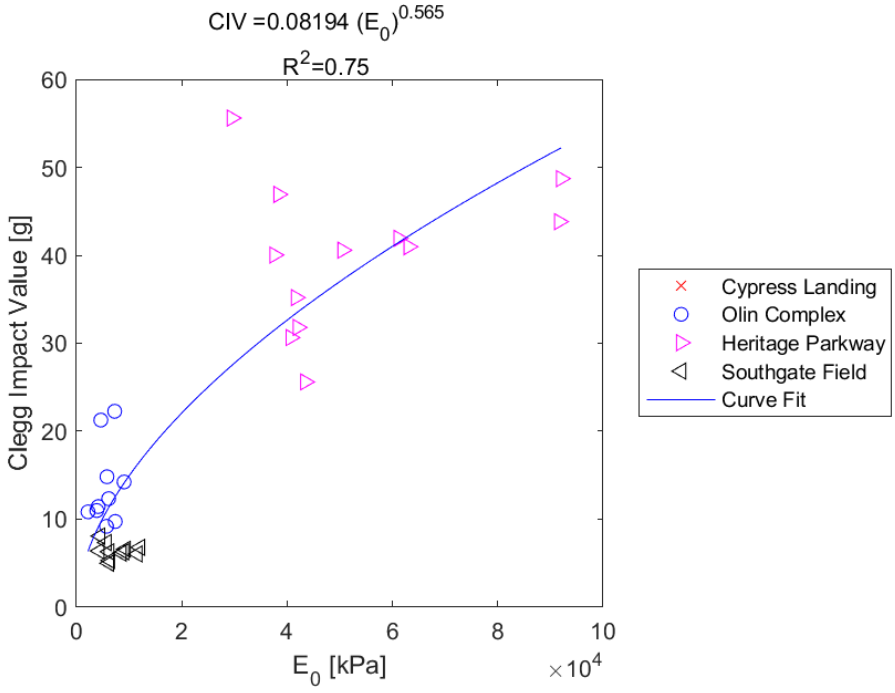

Figure E.470: Exponential Model of CIV versus E_0 for SDPMT-6 Continuous Tests, All Sites

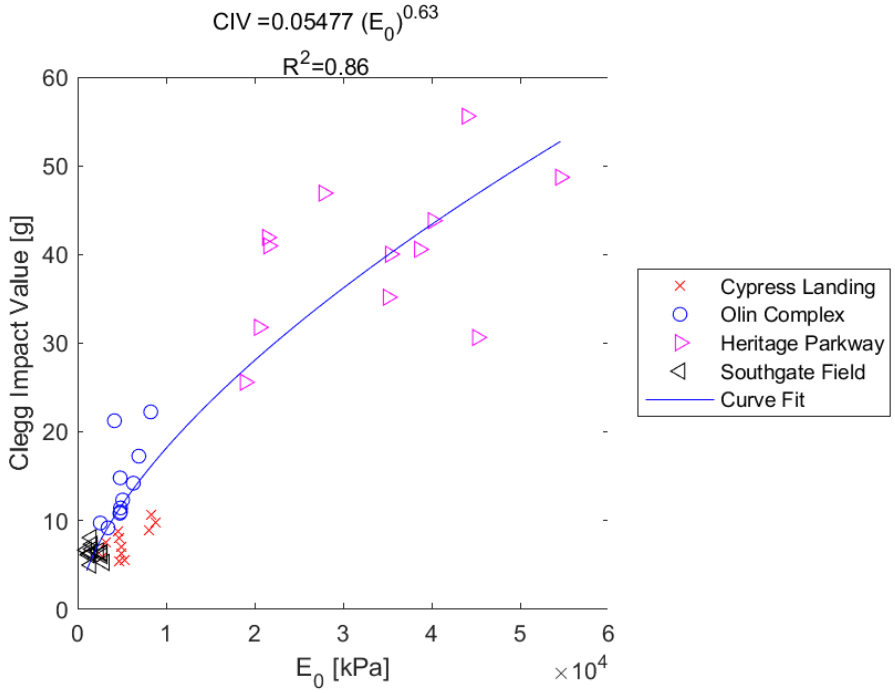

Figure E.471: Exponential Model of CIV versus E_0 for SDPMT-12 Incremental Tests, All Sites

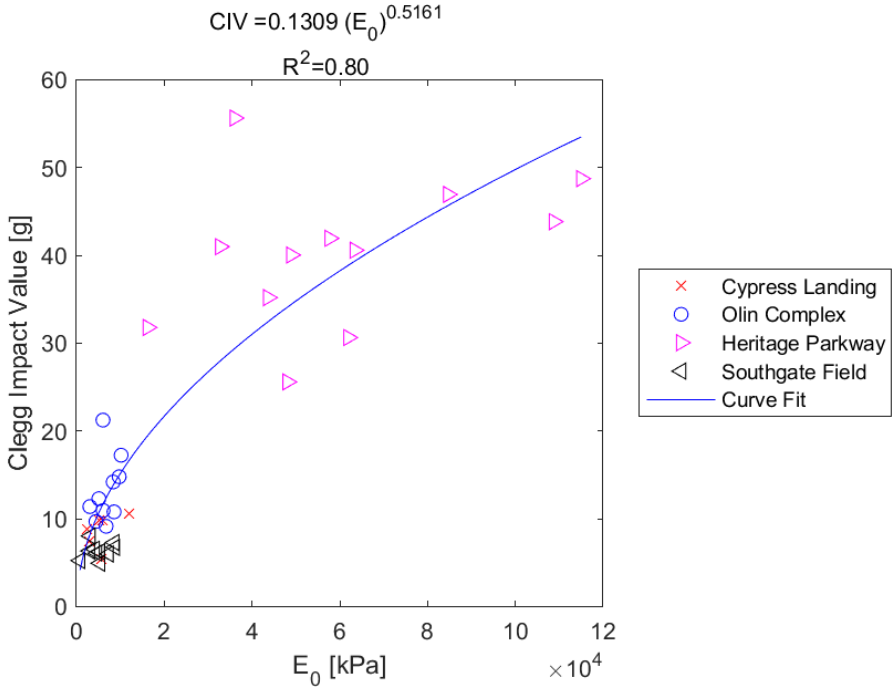

Figure E.472: Exponential Model of CIV versus E_0 for SDPMT-12 Continuous Tests, All Sites

E.5.23 CIV versus $\mathbf{p}_L$

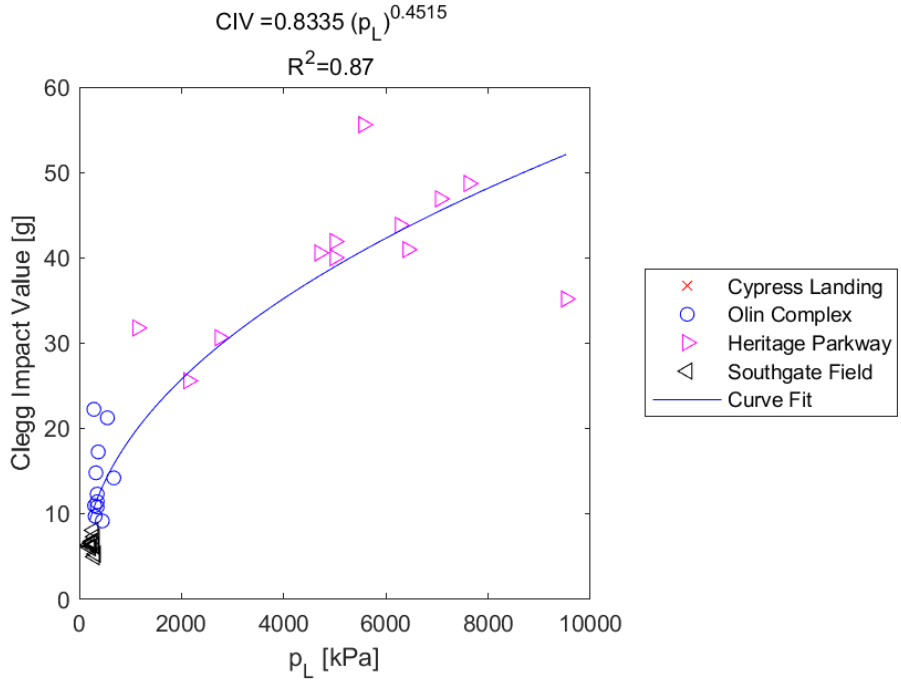

Figure E.473: Exponential Model of CIV versus p_L for SDPMT-6 Incremental Tests, All Sites

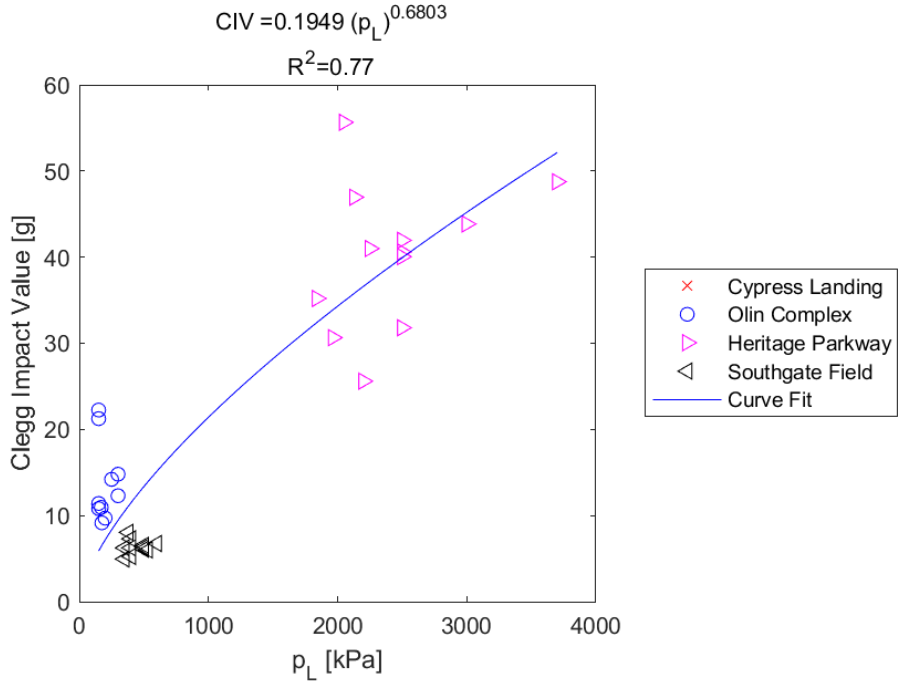

Figure E.474: Exponential Model of CIV versus p_L for SDPMT-6 Continuous Tests, All Sites

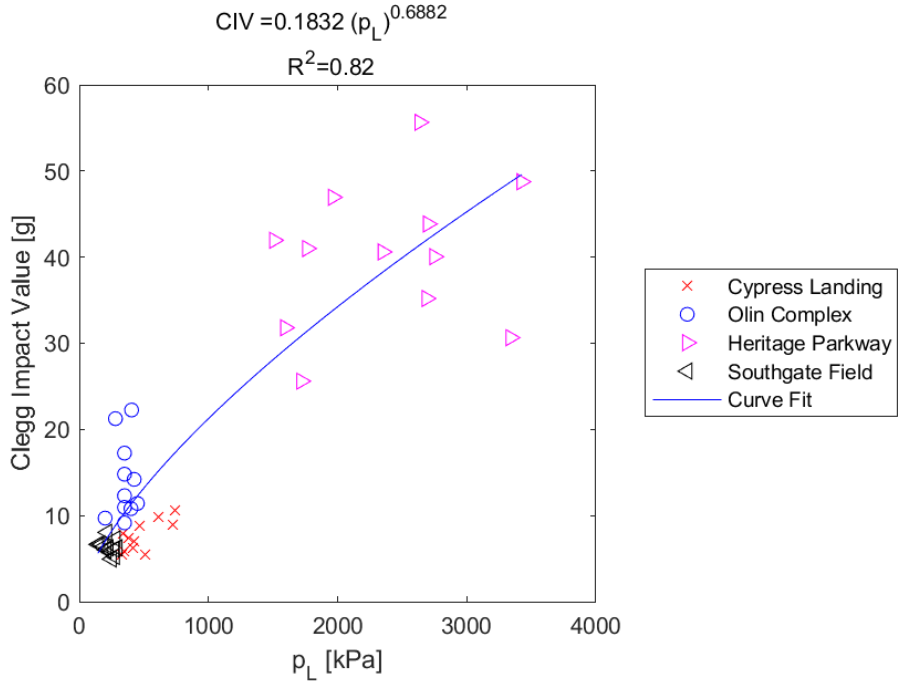

Figure E.475: Exponential Model of CIV versus p_L for SDPMT-12 Incremental Tests, All Sites

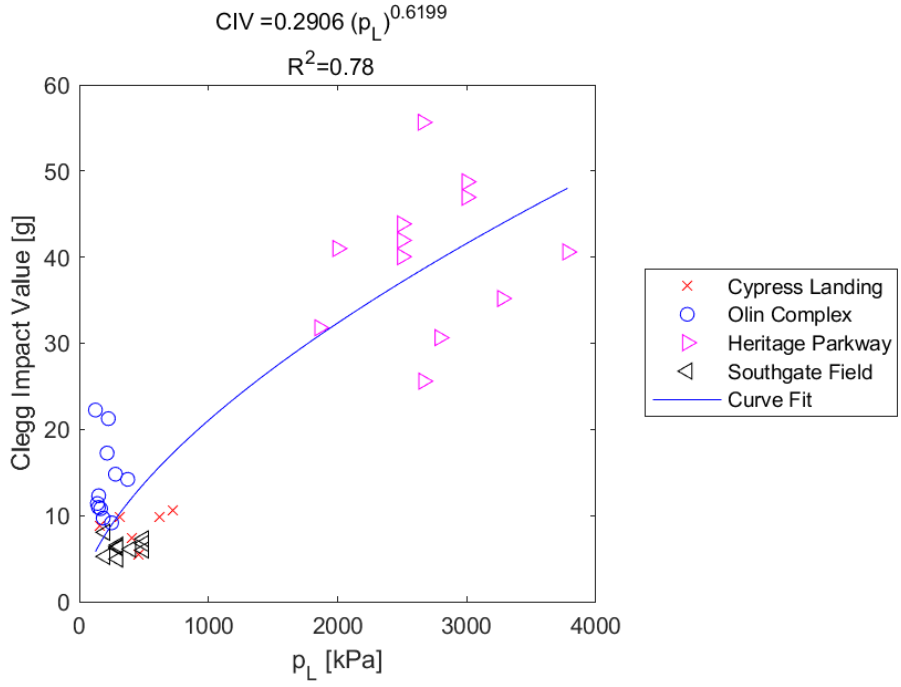

Figure E.476: Exponential Model of CIV versus p_L for SDPMT-12 Continuous Tests, All Sites

E.5.24 CIV versus p_0

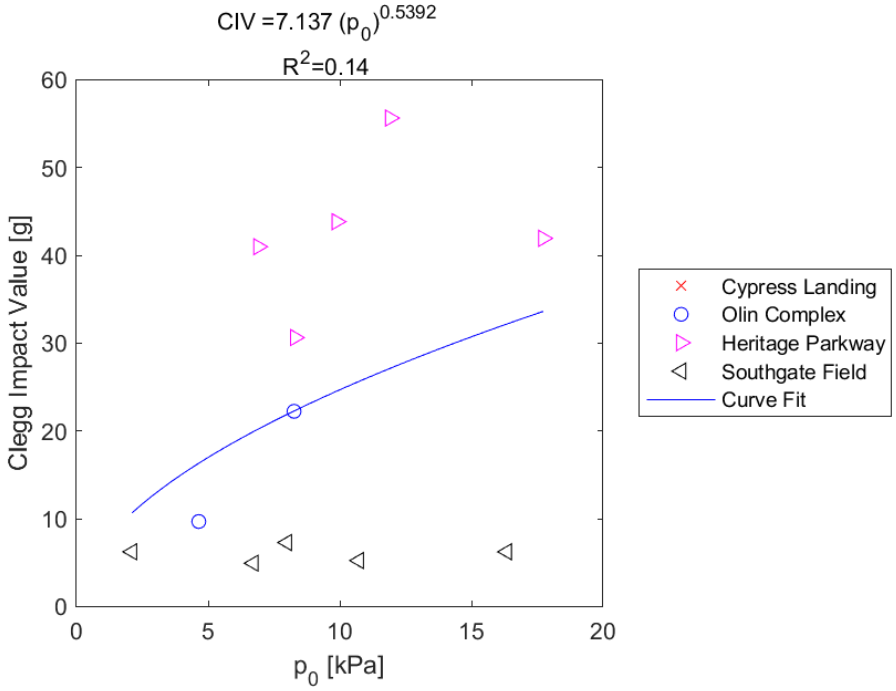

Figure E.477: Exponential Model of CIV versus p_0 for SDPMT-6 Incremental Tests, All Sites

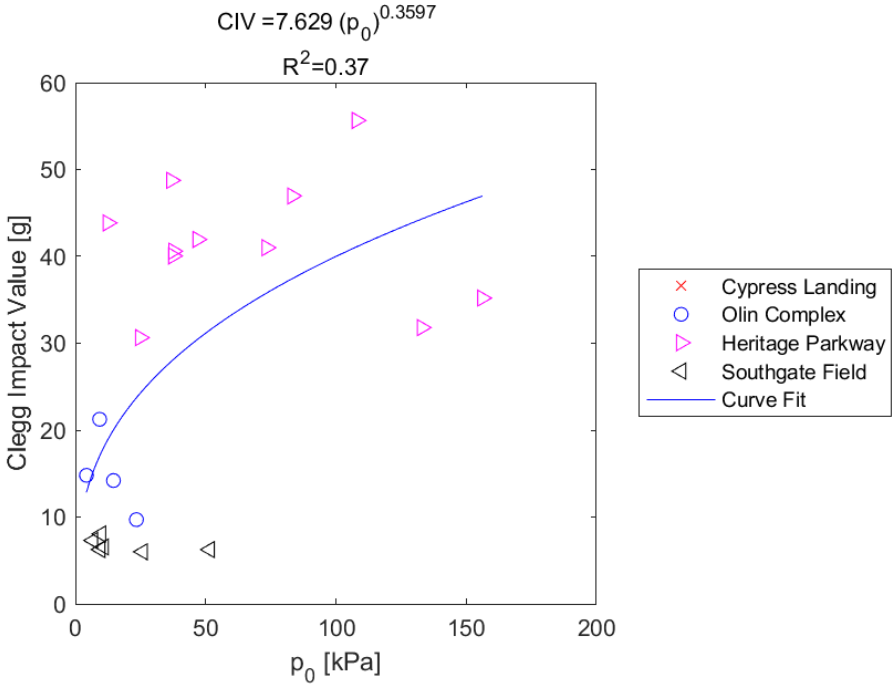

Figure E.478: Exponential Model of CIV versus p_0 for SDPMT-6 Continuous Tests, All Sites

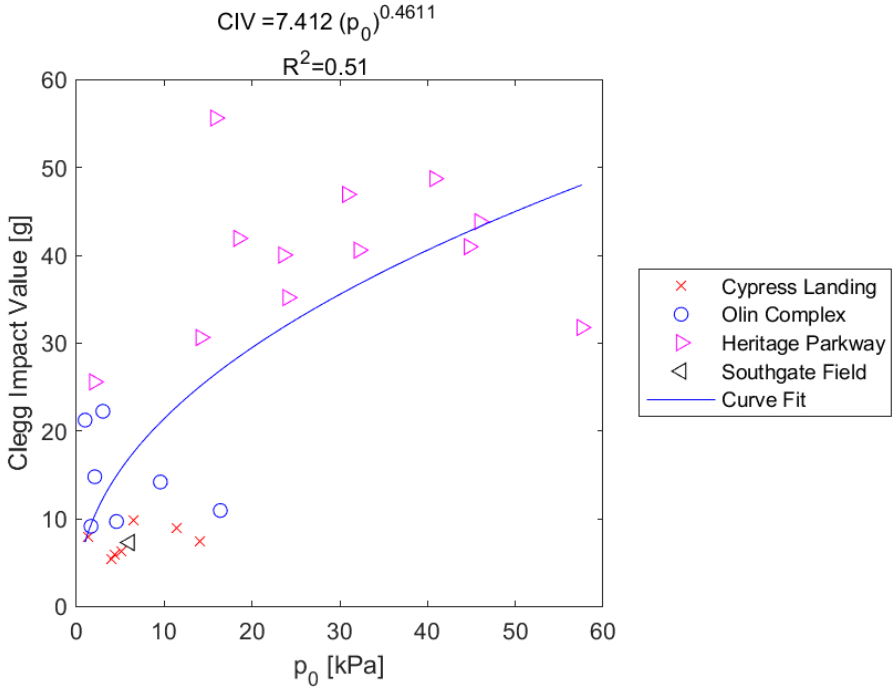

Figure E.479: Exponential Model of CIV versus p_0 for SDPMT-12 Incremental Tests, All Sites

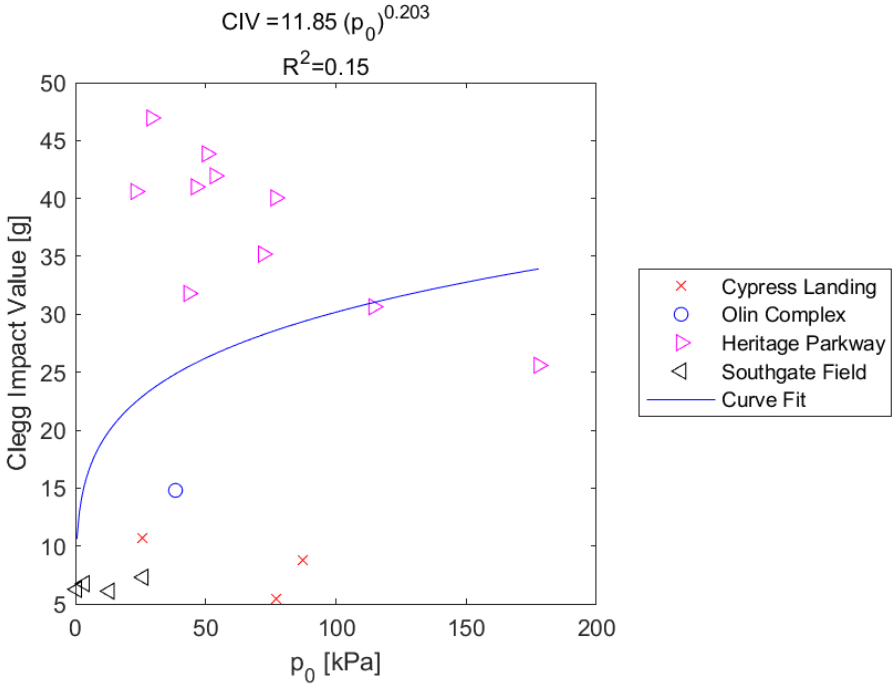

Figure E.480: Exponential Model of CIV versus p_0 for SDPMT-12 Continuous Tests, All Sites

Appendix F

SDPMT Kondner Strain Level Models

F.1 FIT Southgate Field

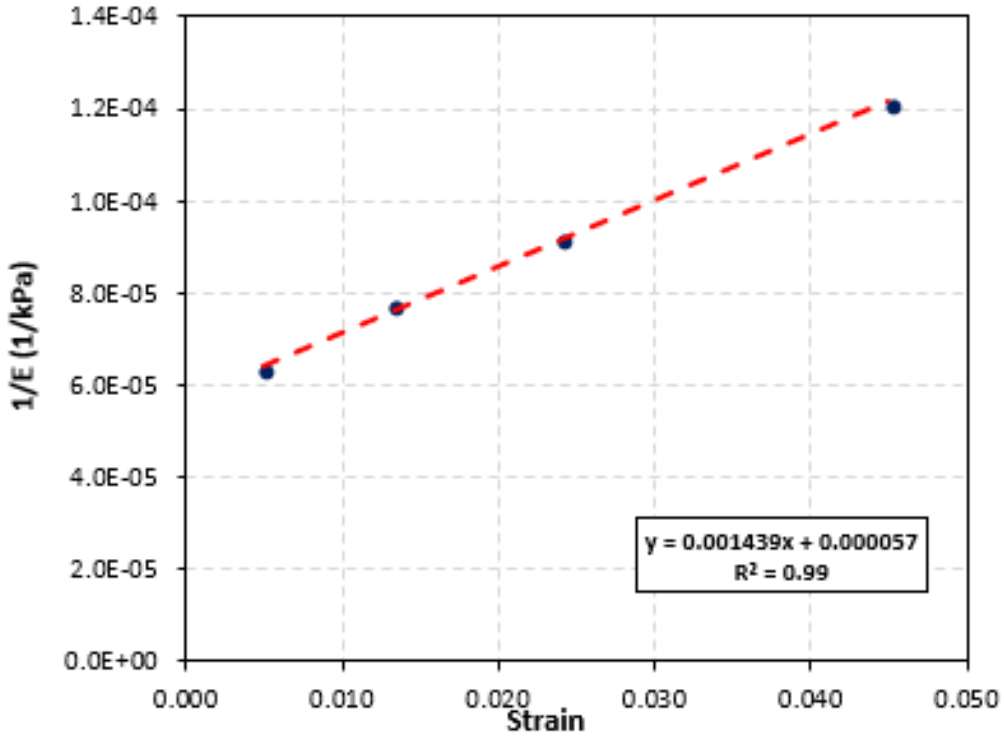

Figure F.1: Location 401 (SDPMT-6 Incremental)

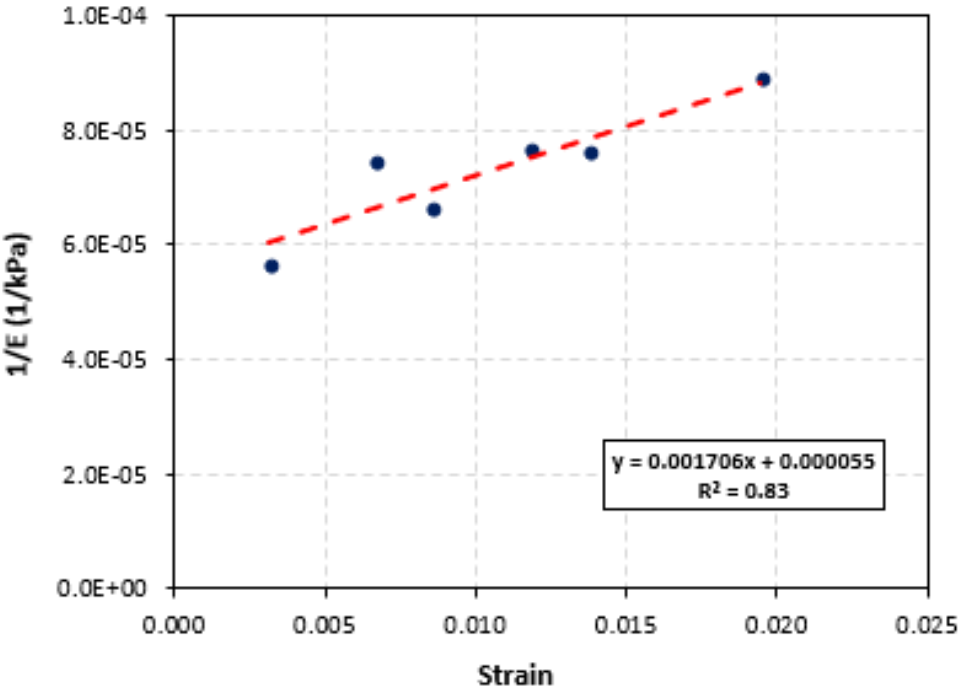

Figure F.2: Location 401 (SDPMT-12 Incremental)

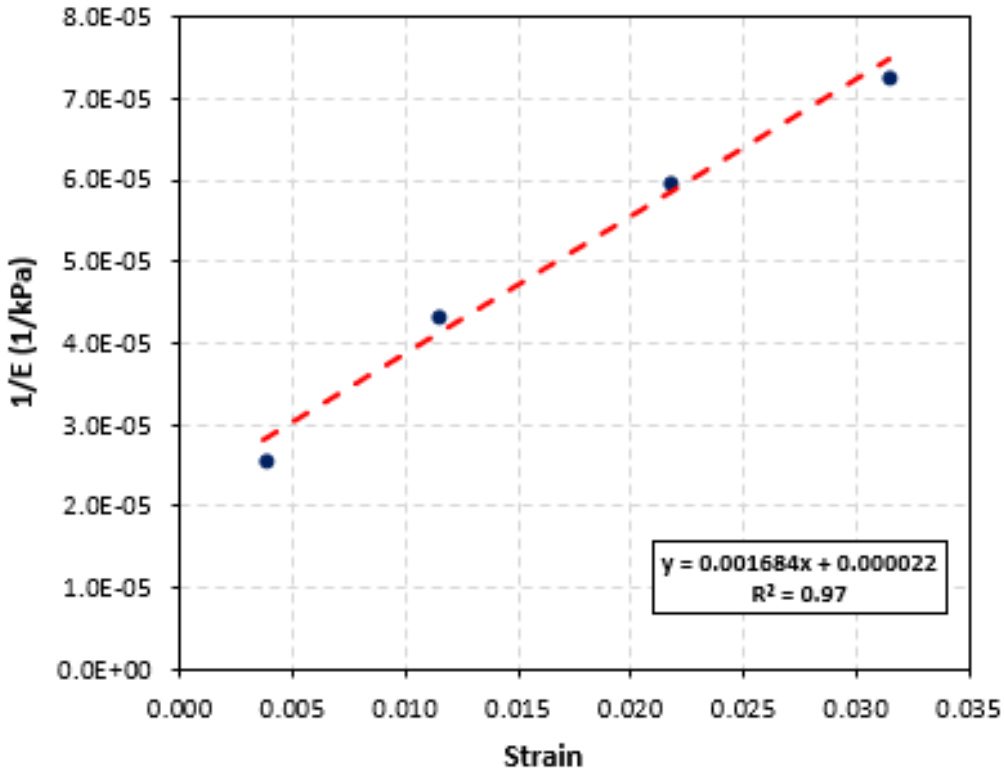

Figure F.3: Location 402 (SDPMT-6 Incremental)

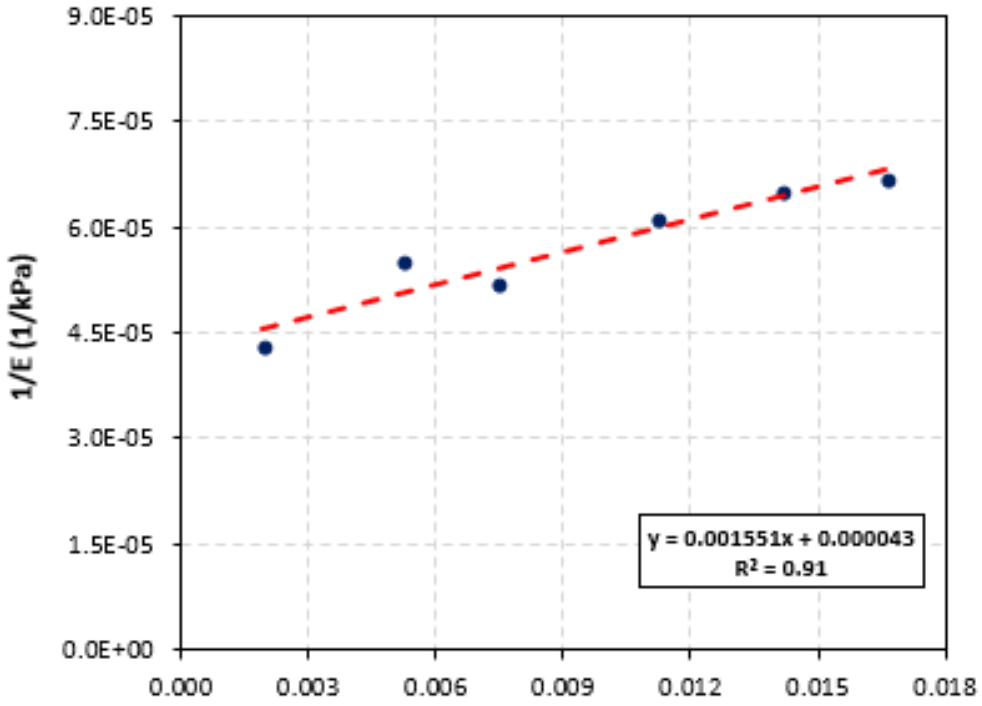

Figure F.4: Location 402 (SDPMT-12 Incremental)

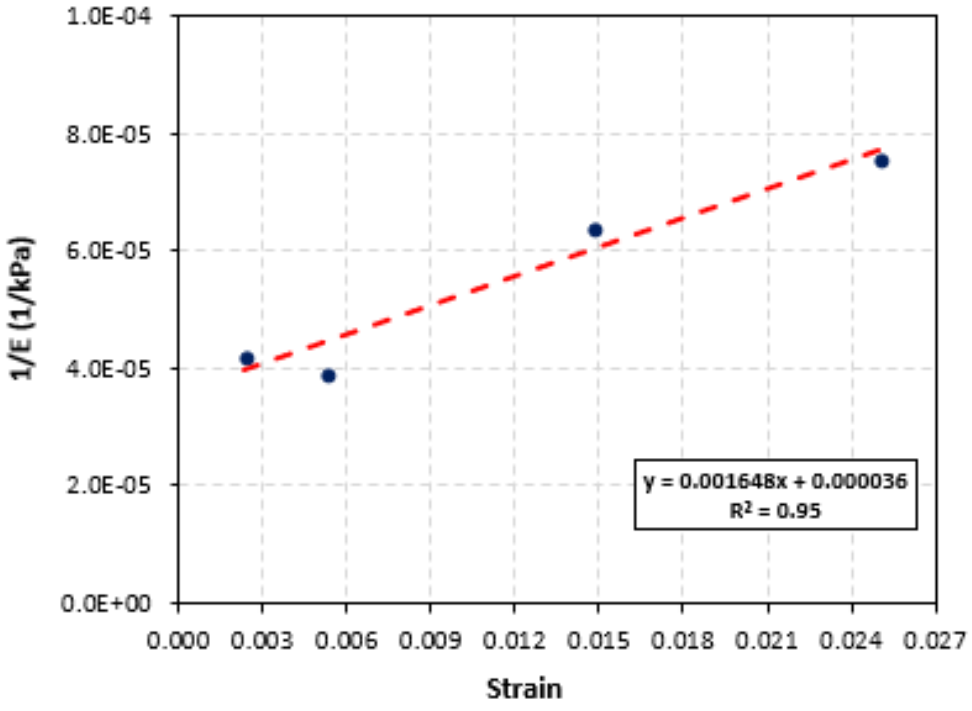

Figure F.5: Location 403 (SDPMT-6 Incremental)

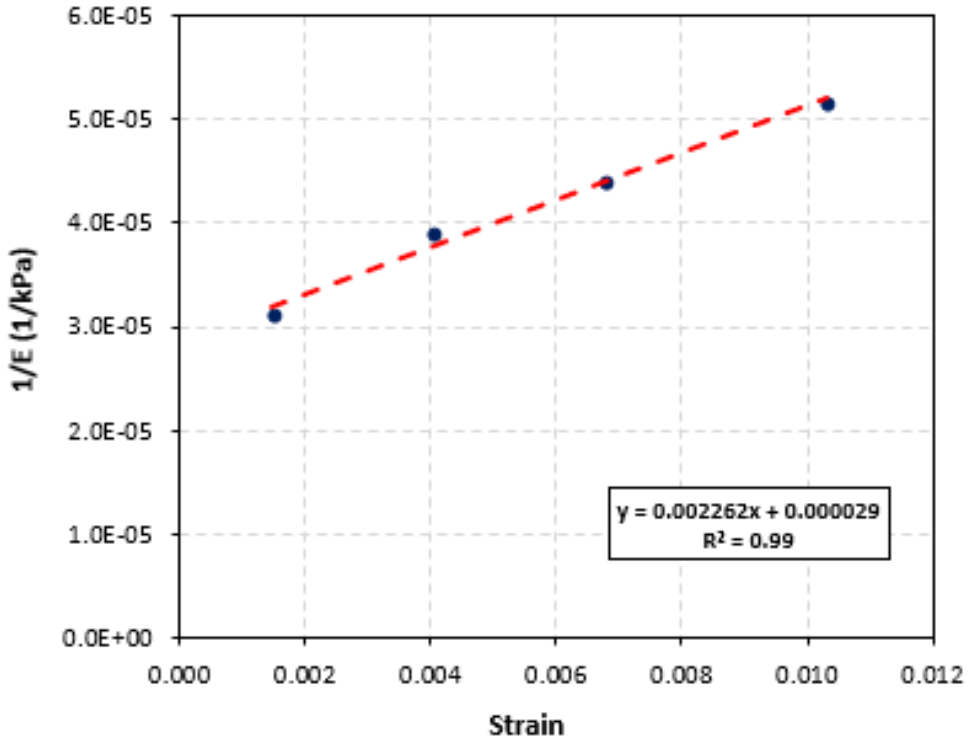

Figure F.6: Location 403 (SDPMT-12 Incremental)

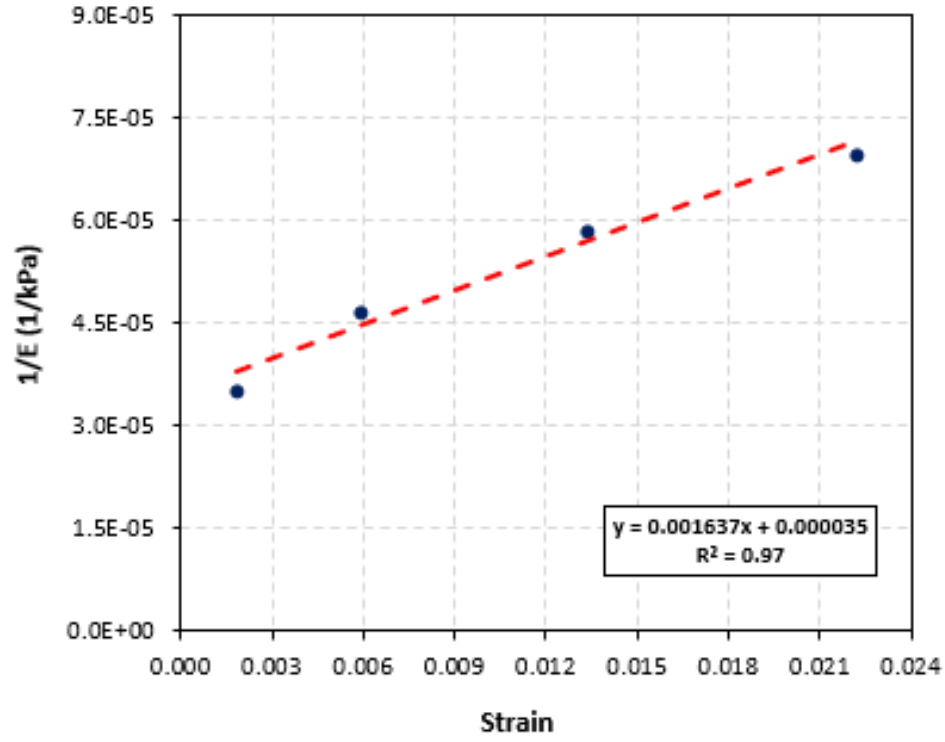

Figure F.7: Location 404 (SDPMT-6 Incremental)

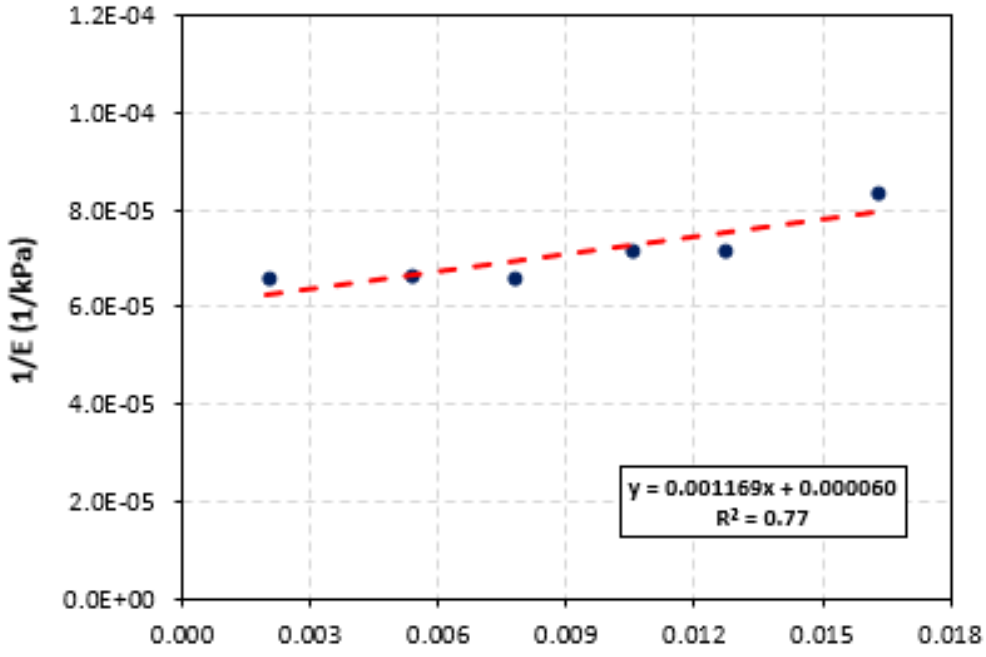

Figure F.8: Location 404 (SDPMT-12 Incremental)

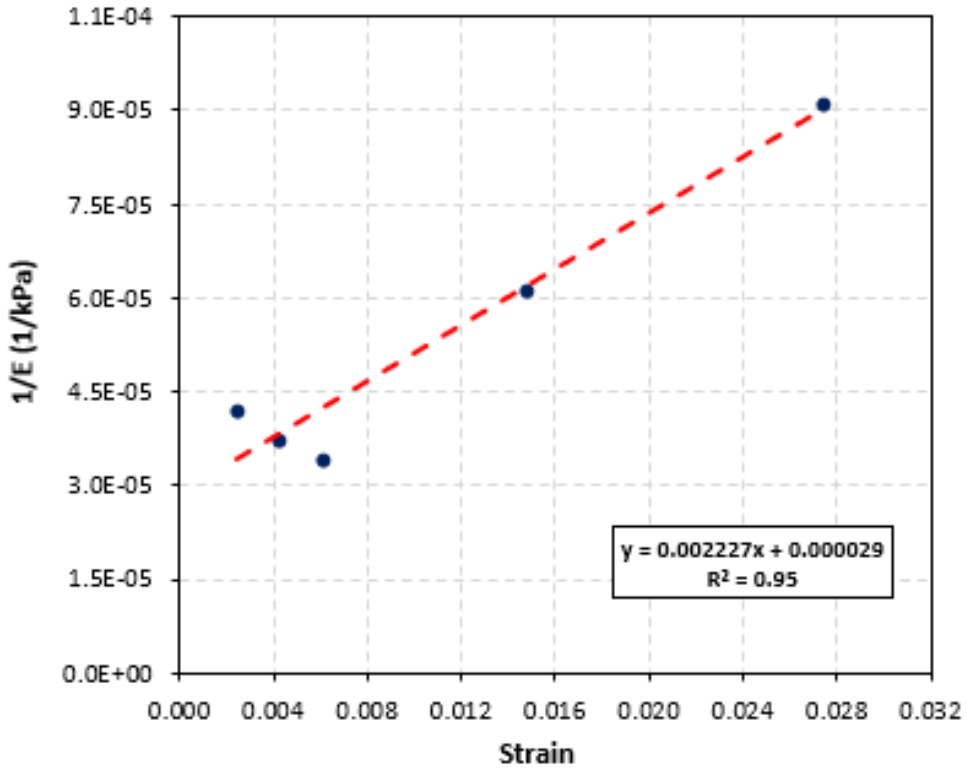

Figure F.9: Location 405 (SDPMT-6 Incremental)

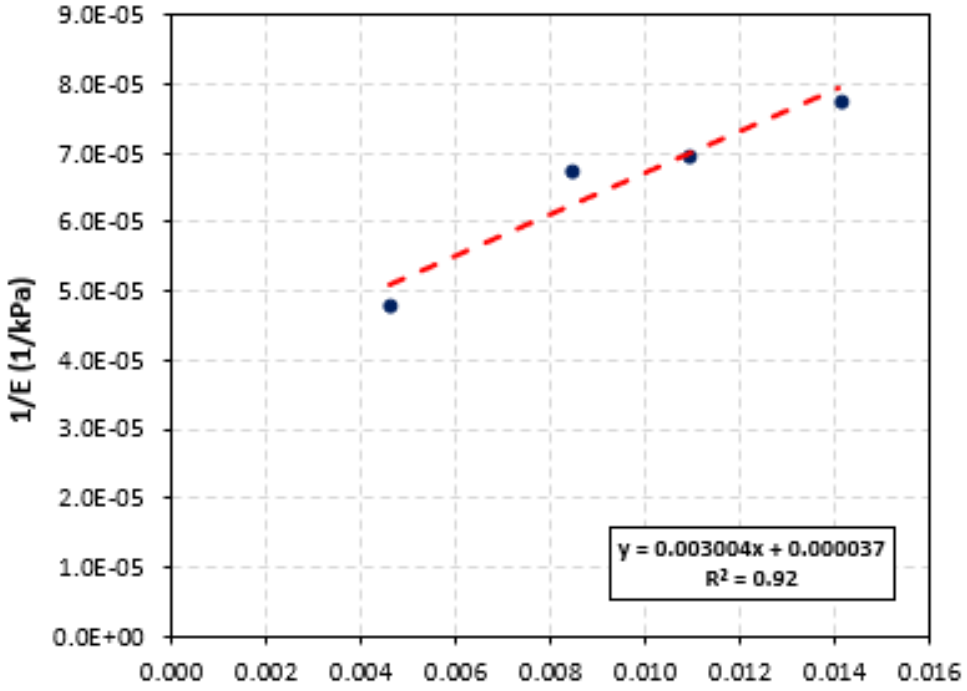

Figure F.10: Location 405 (SDPMT-12 Incremental)

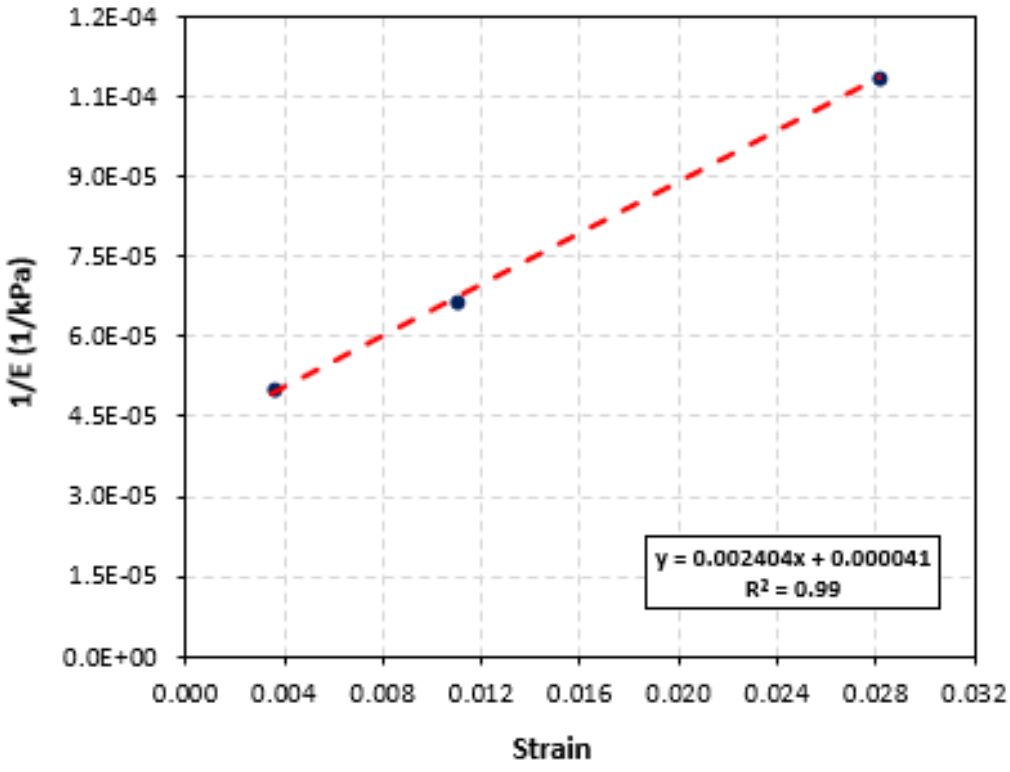

Figure F.11: Location 406 (SDPMT-6 Incremental)

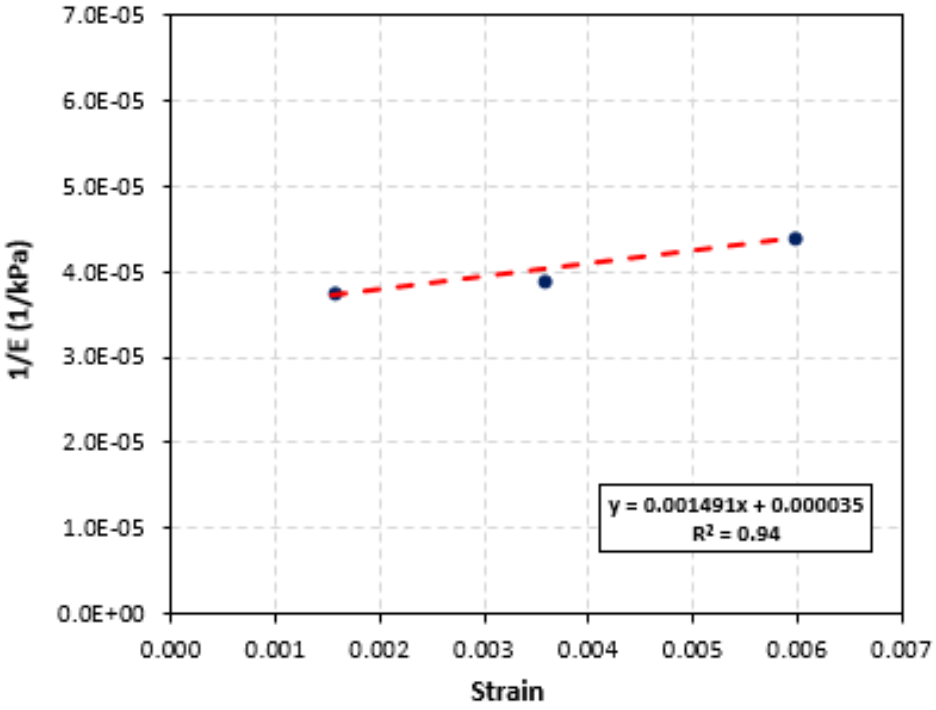

Figure F.12: Location 406 (SDPMT-12 Incremental)

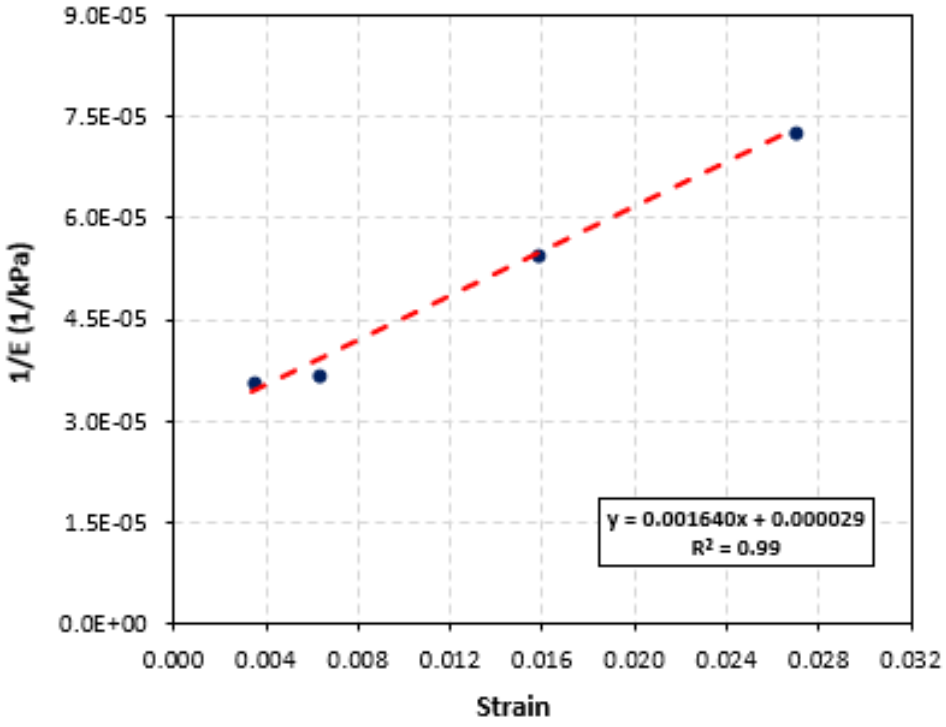

Figure F.13: Location 407 (SDPMT-6 Incremental)

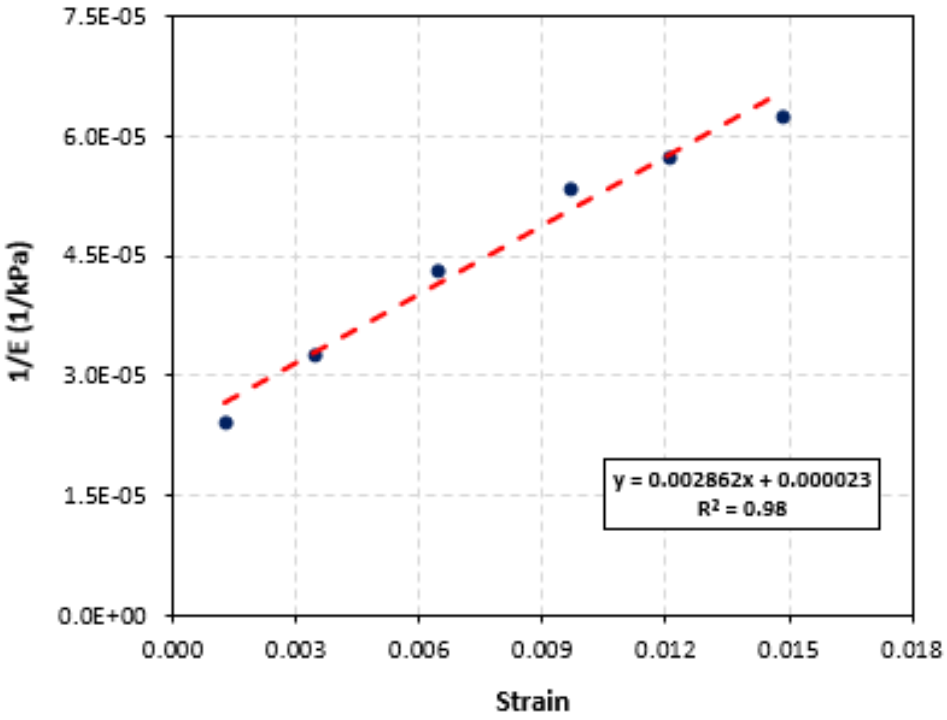

Figure F.14: Location 407 (SDPMT-12 Incremental)

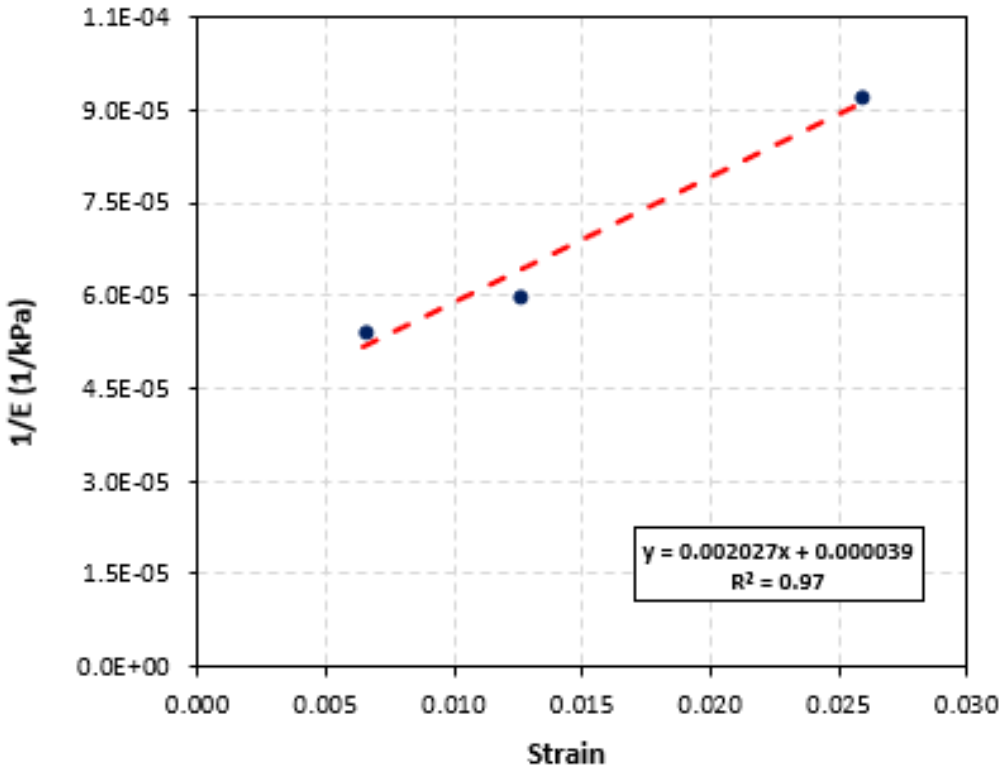

Figure F.15: Location 408 (SDPMT-6 Incremental)

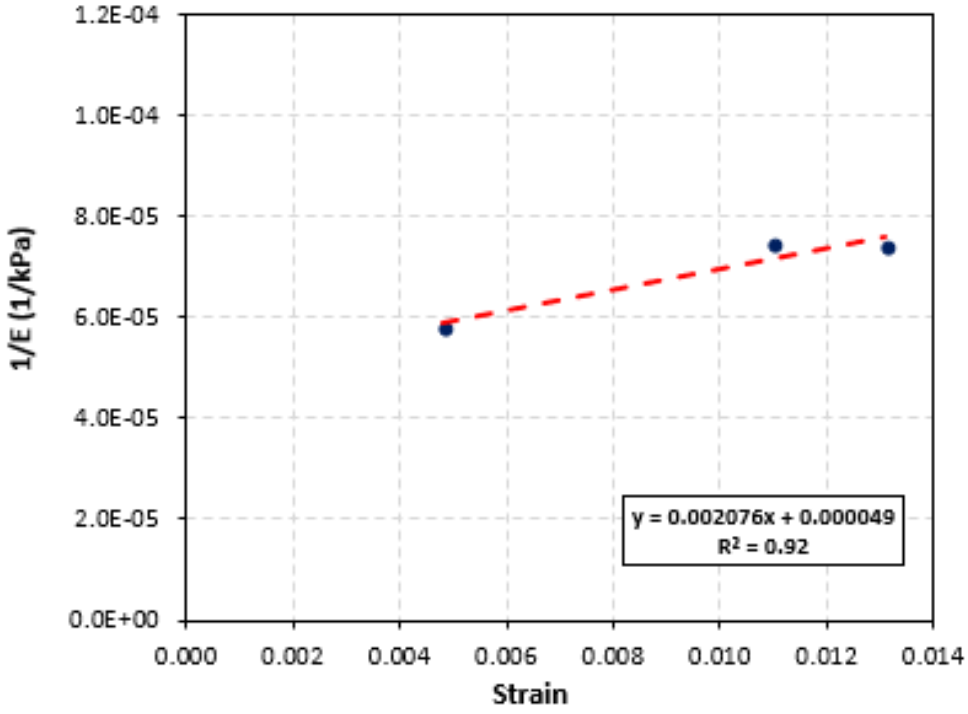

Figure F.16: Location 408 (SDPMT-12 Incremental)

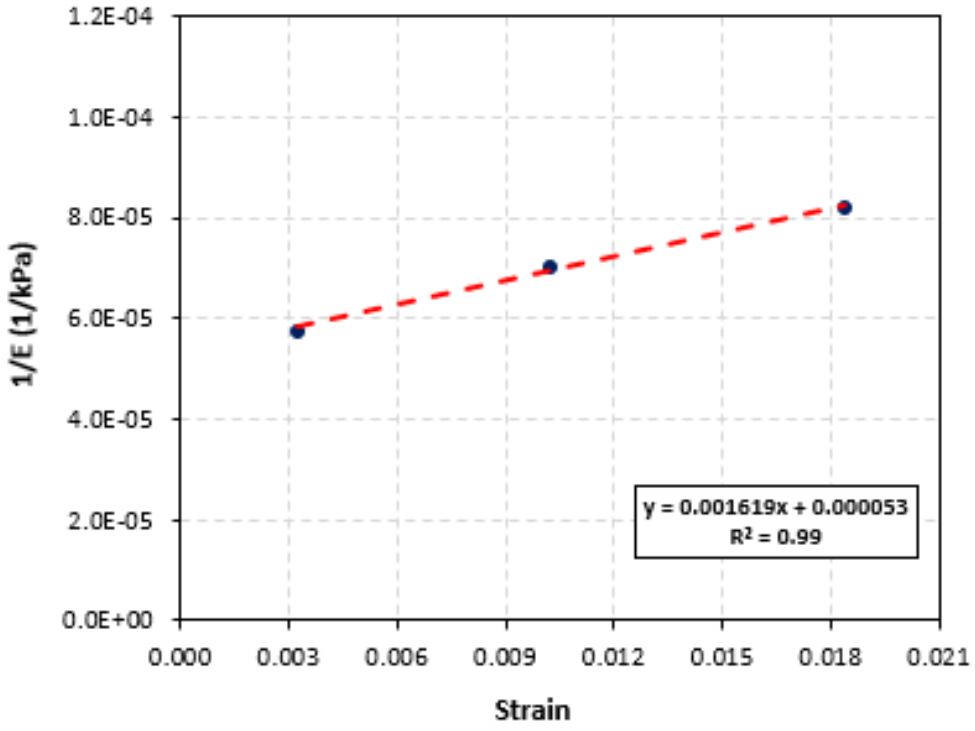

Figure F.17: Location 409 (SDPMT-6 Incremental)

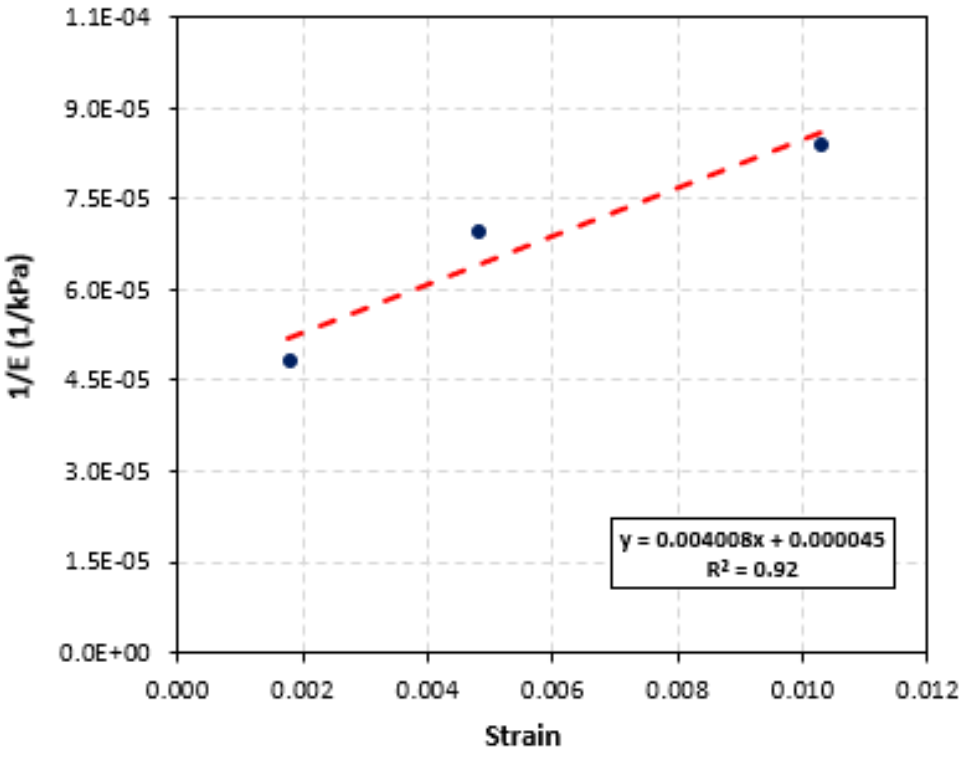

Figure F.18: Location 409 (SDPMT-12 Incremental)

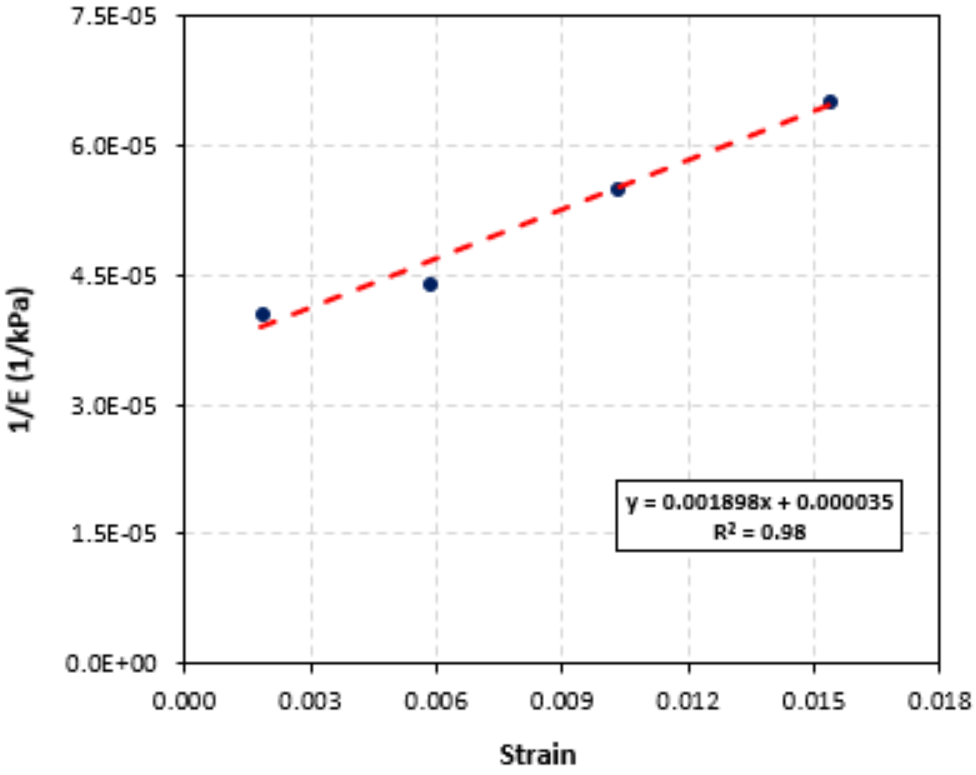

Figure F.19: Location 410 (SDPMT-6 Incremental)

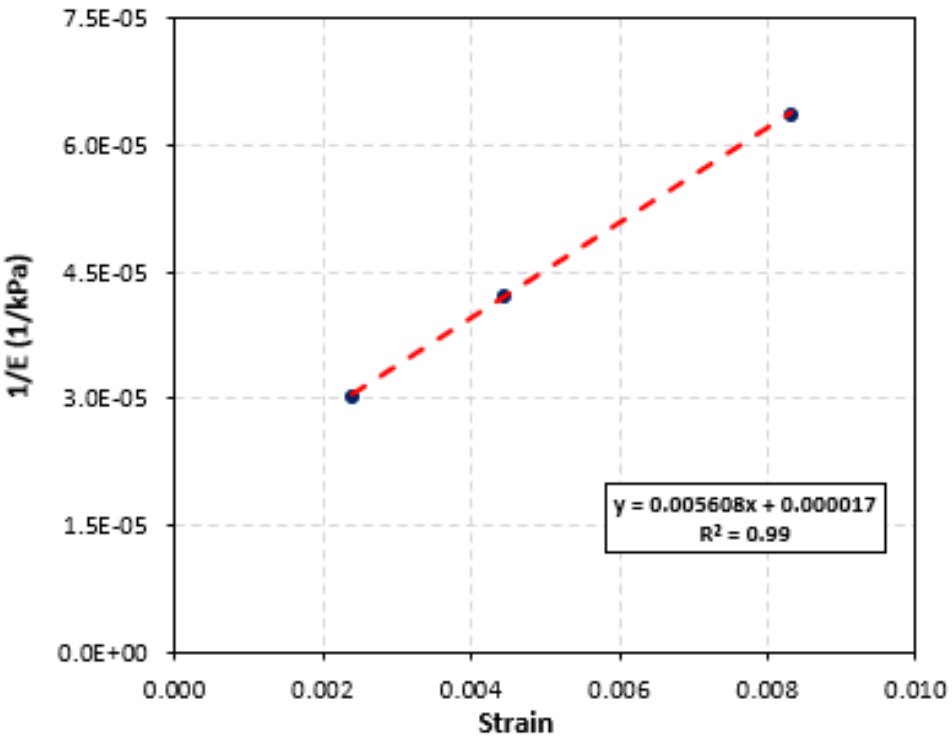

Figure F.20: Location 410 (SDPMT-12 Incremental)

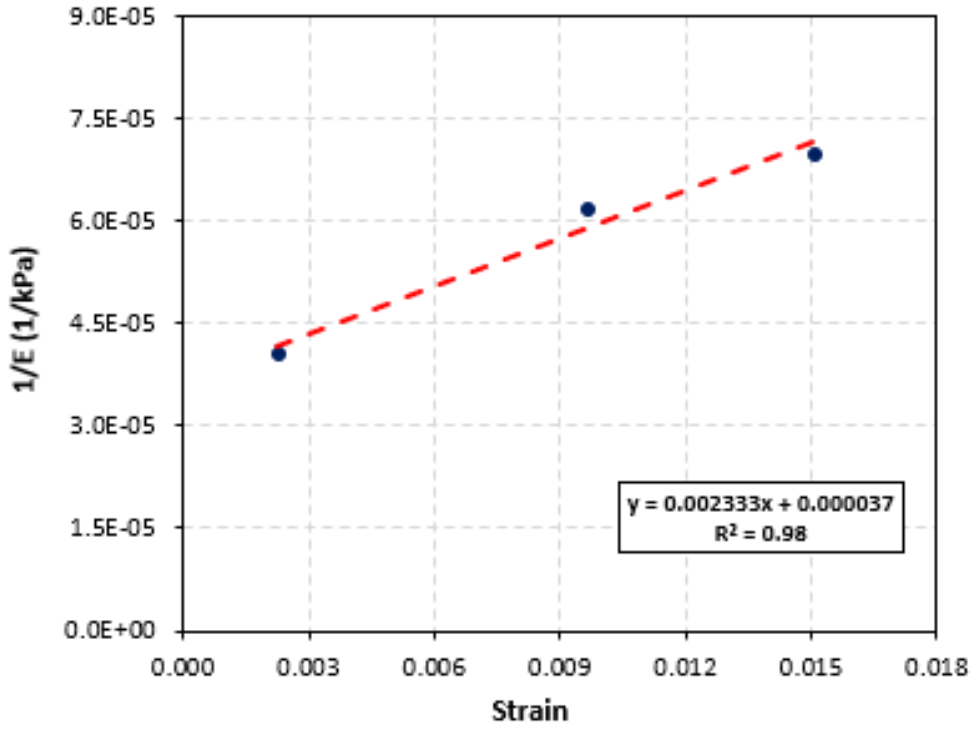

Figure F.21: Location 411 (SDPMT-6 Incremental)

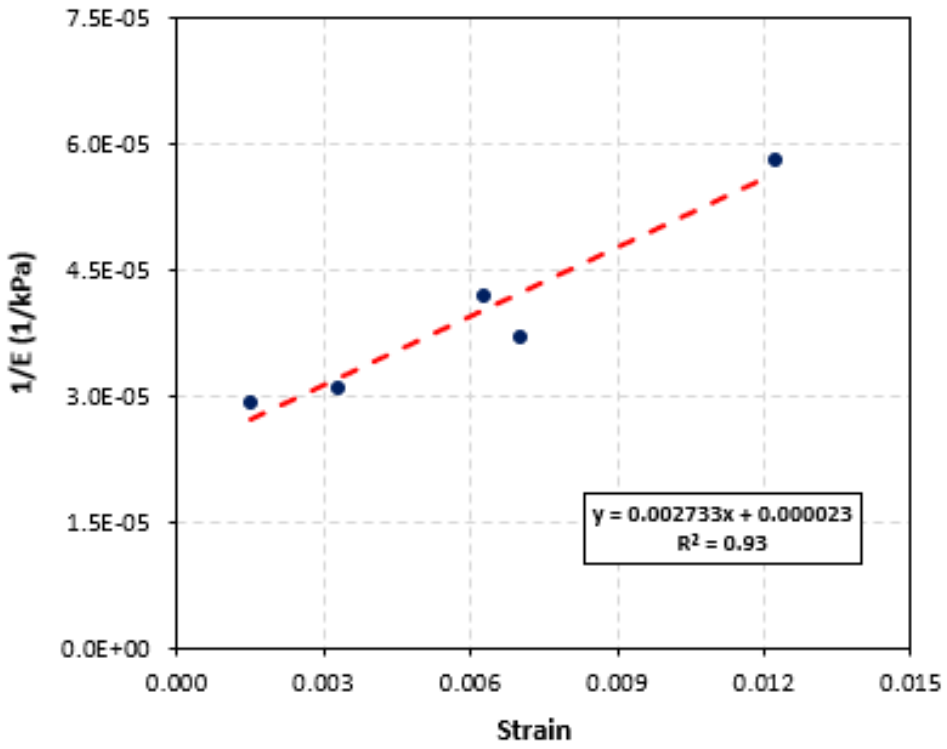

Figure F.22: Location 411 (SDPMT-12 Incremental)

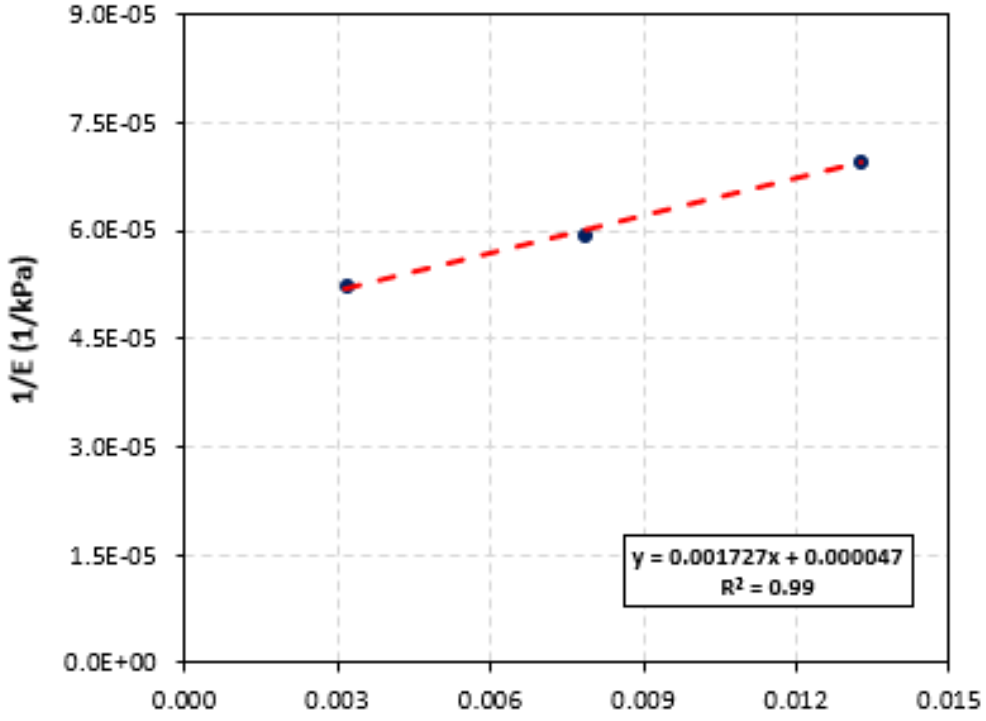

Figure F.23: Location 412 (SDPMT-6 Incremental)

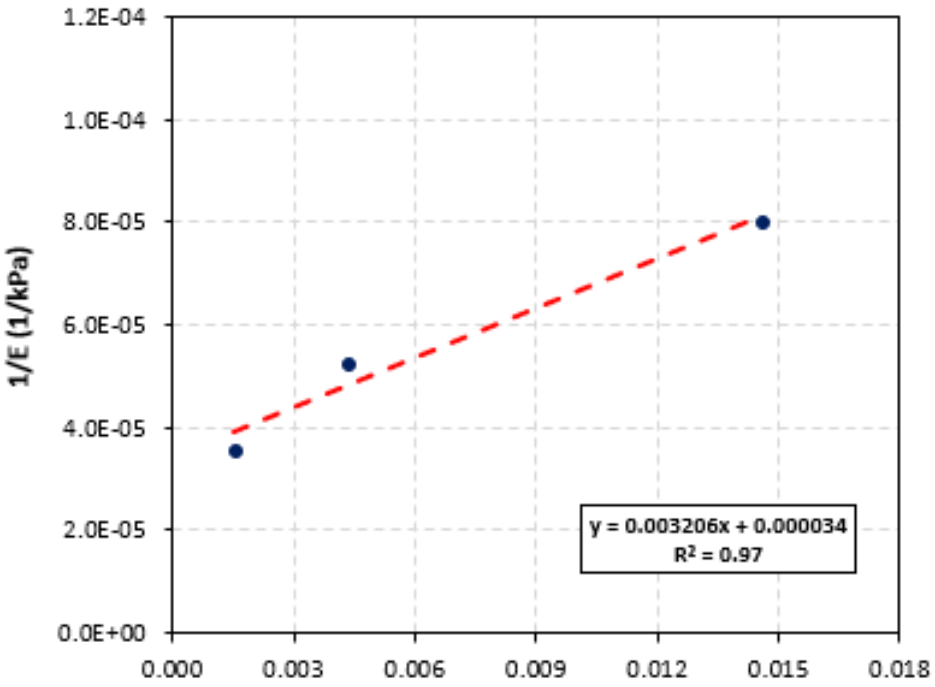

Figure F.24: Location 412 (SDPMT-12 Incremental)

F.2 FIT Olin Complex

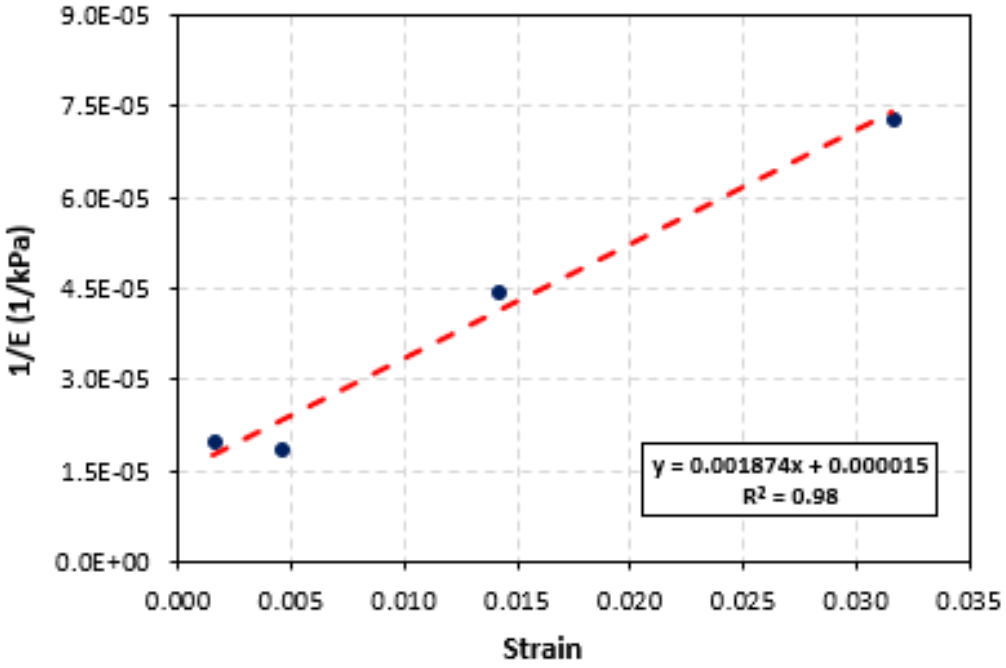

Figure F.25: Location 201 (SDPMT-6 Incremental)

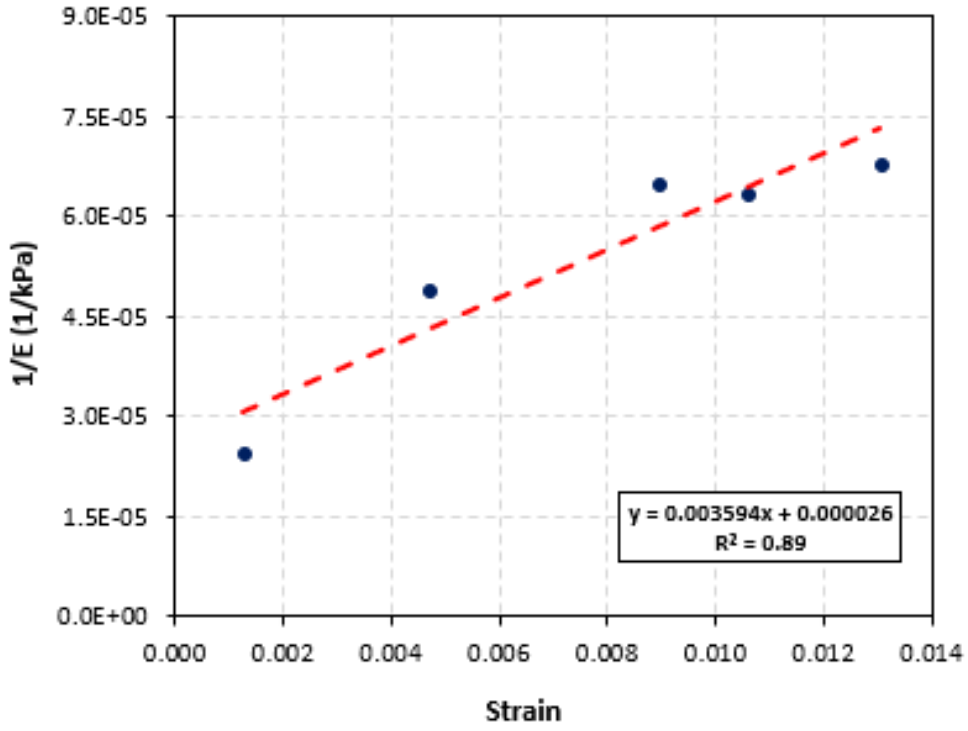

Figure F.26: Location 201 (SDPMT-12 Incremental)

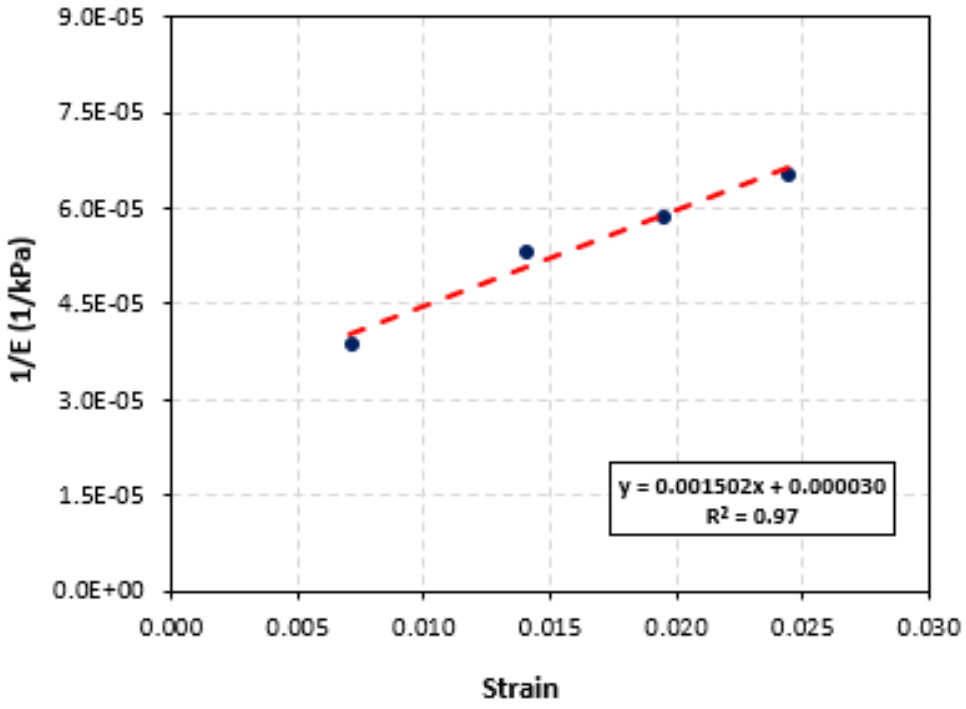

Figure F.27: Location 202 (SDPMT-6 Incremental)

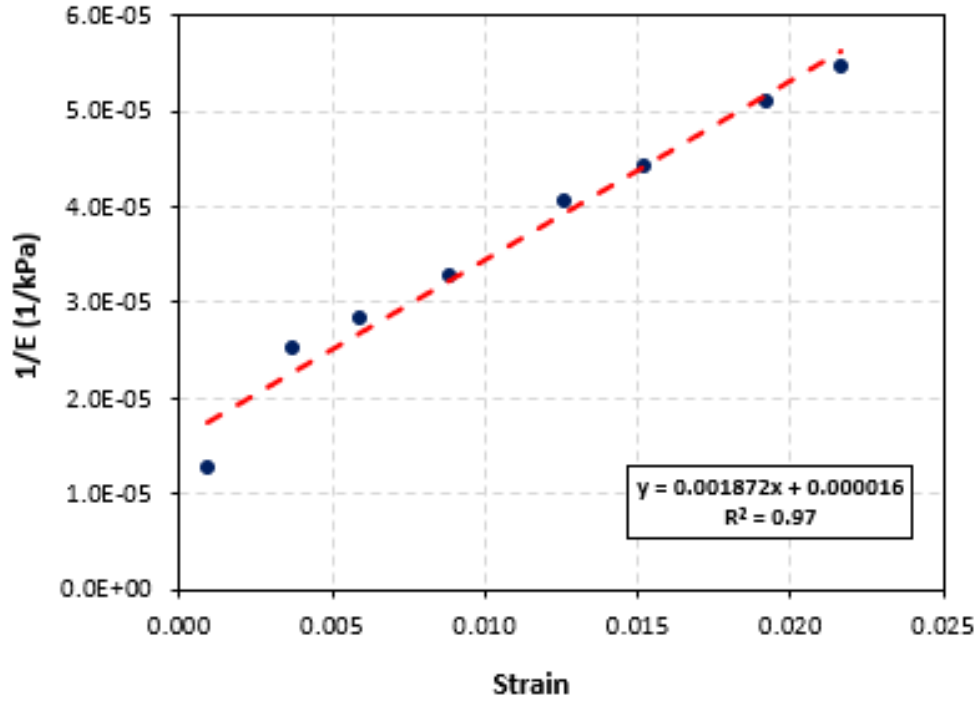

Figure F.28: Location 202 (SDPMT-12 Incremental)

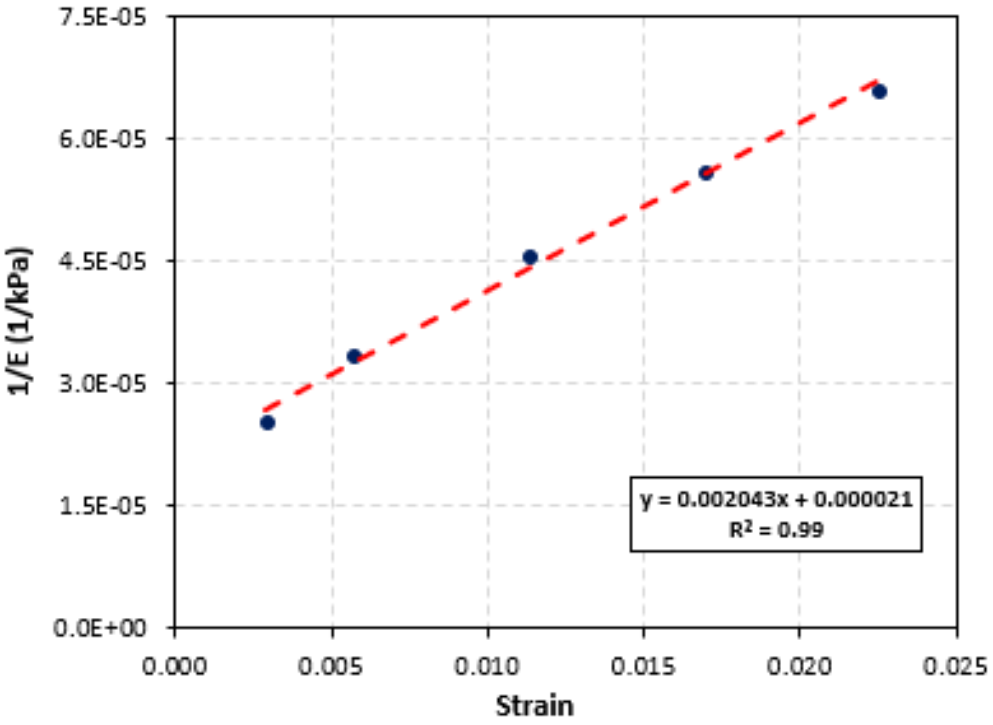

Figure F.29: Location 203 (SDPMT-6 Incremental)

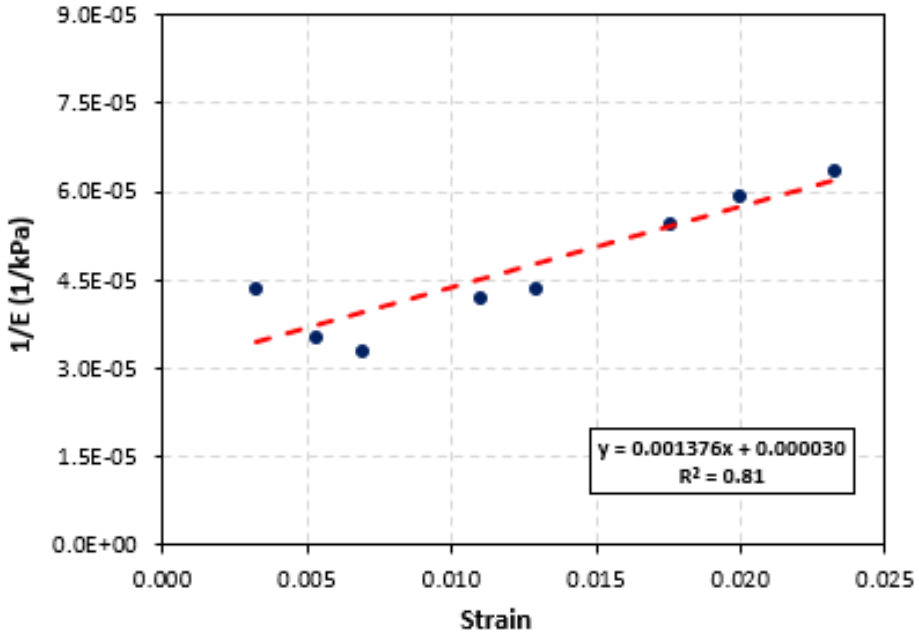

Figure F.30: Location 203 (SDPMT-12 Incremental)

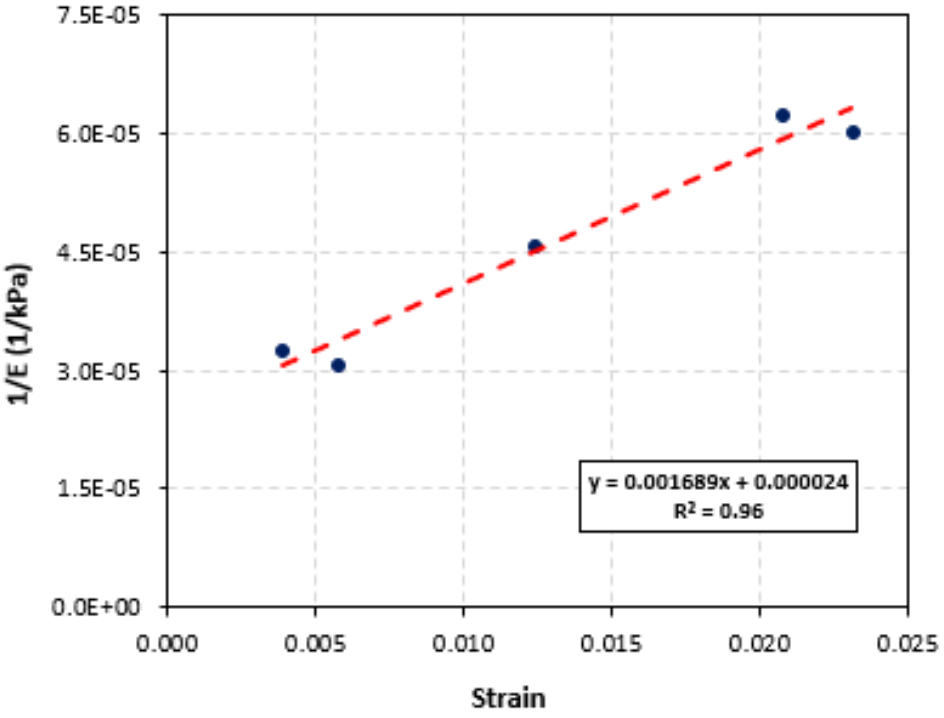

Figure F.31: Location 204 (SDPMT-6 Incremental)

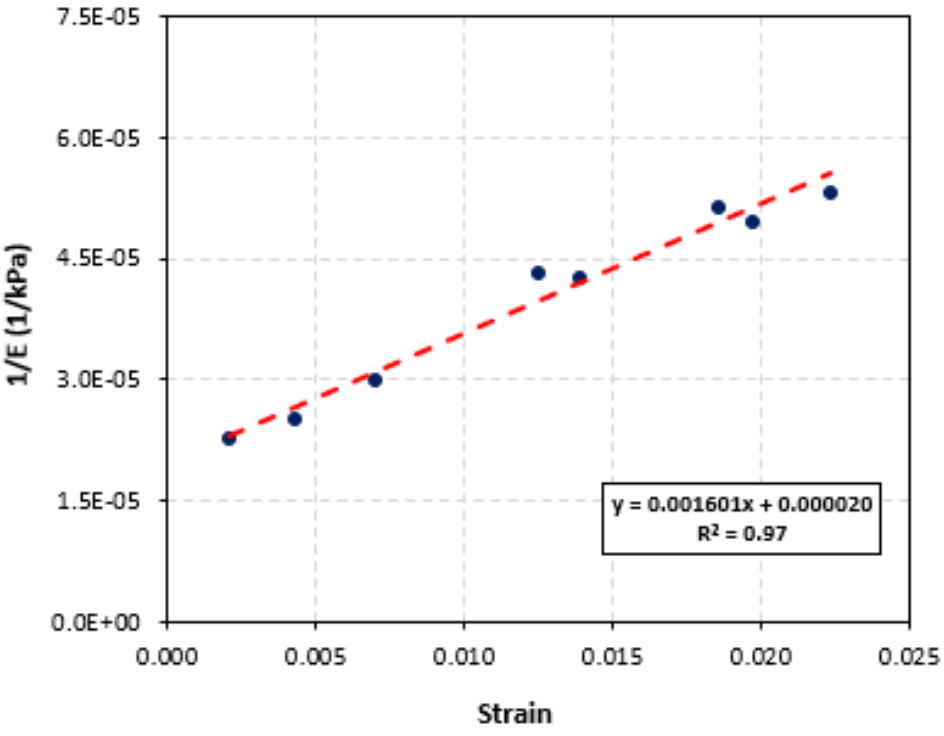

Figure F.32: Location 204 (SDPMT-12 Incremental)

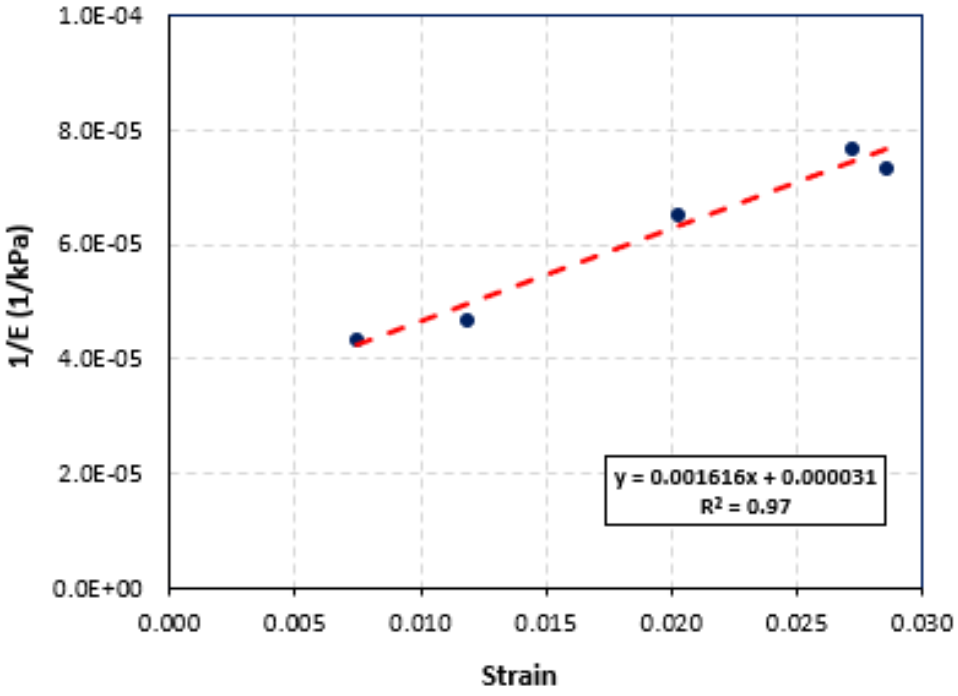

Figure F.33: Location 205 (SDPMT-6 Incremental)

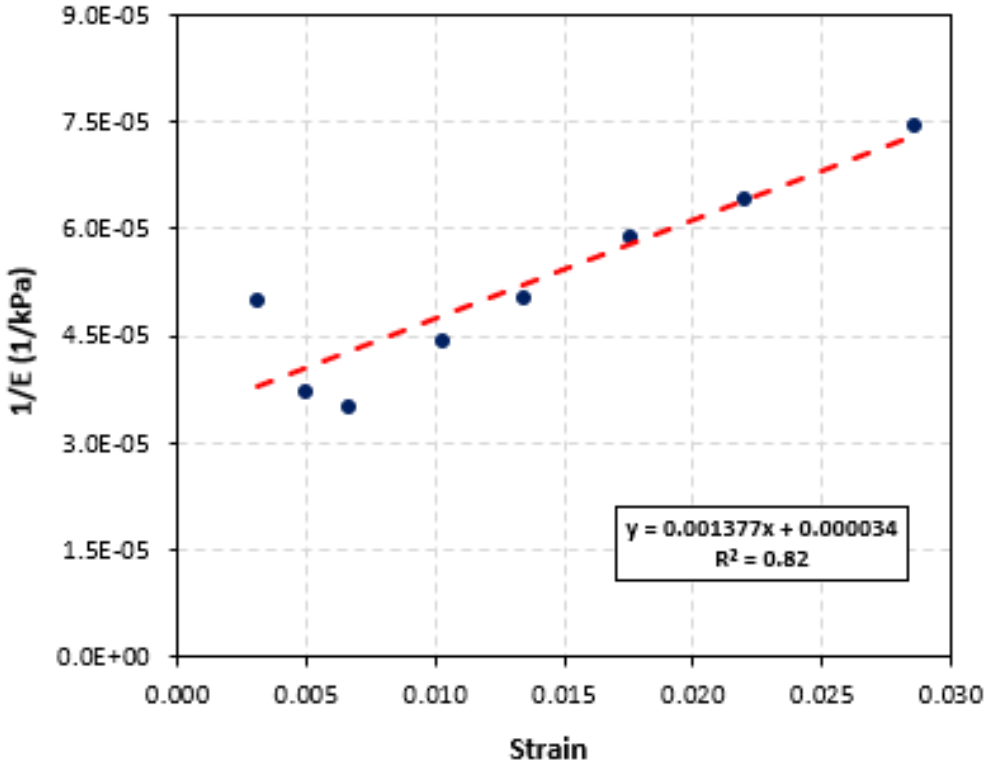

Figure F.34: Location 205 (SDPMT-12 Incremental)

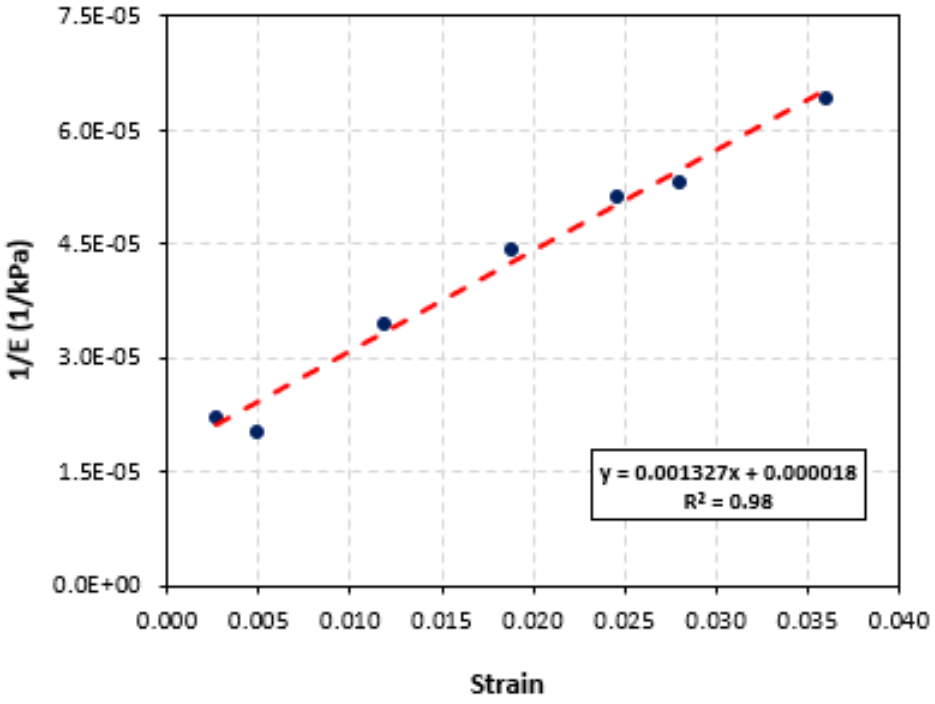

Figure F.35: Location 206 (SDPMT-6 Incremental)

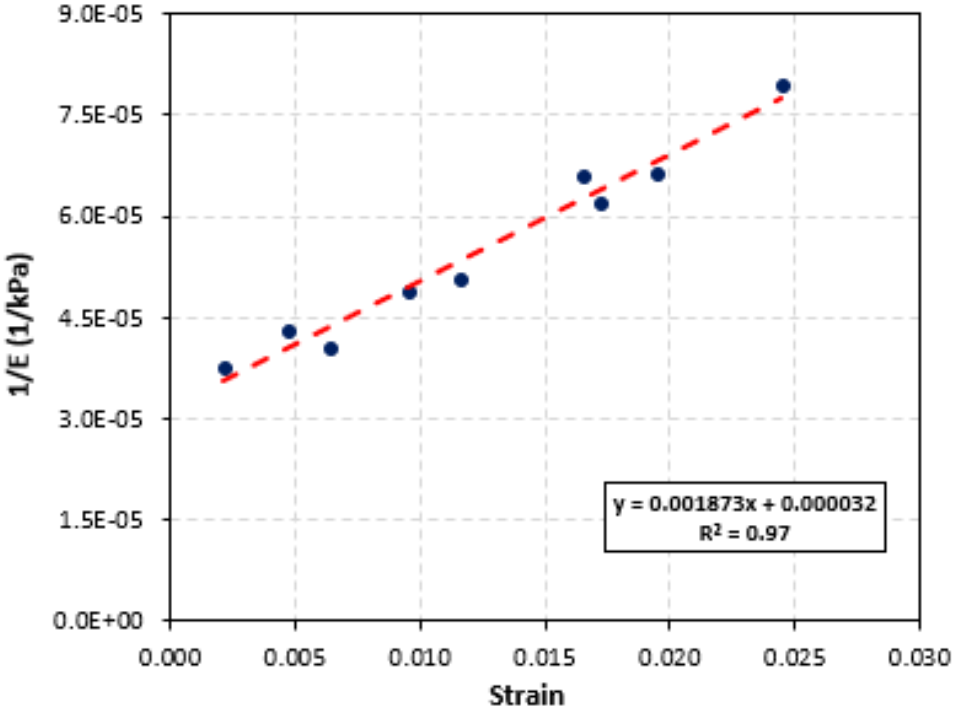

Figure F.36: Location 206 (SDPMT-12 Incremental)

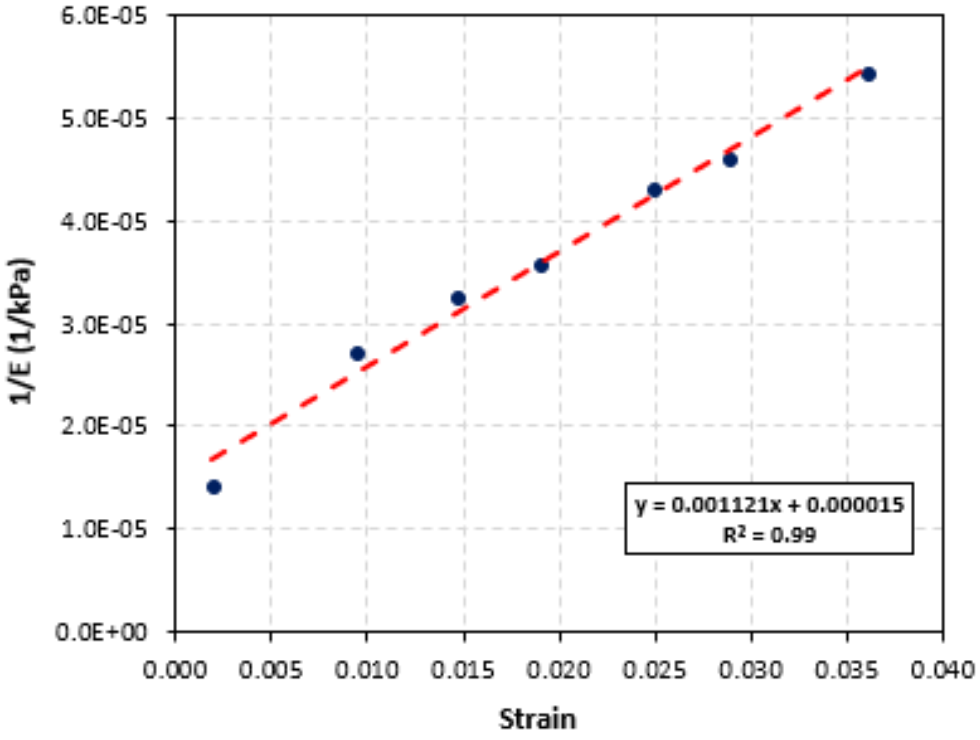

Figure F.37: Location 207 (SDPMT-6 Incremental)

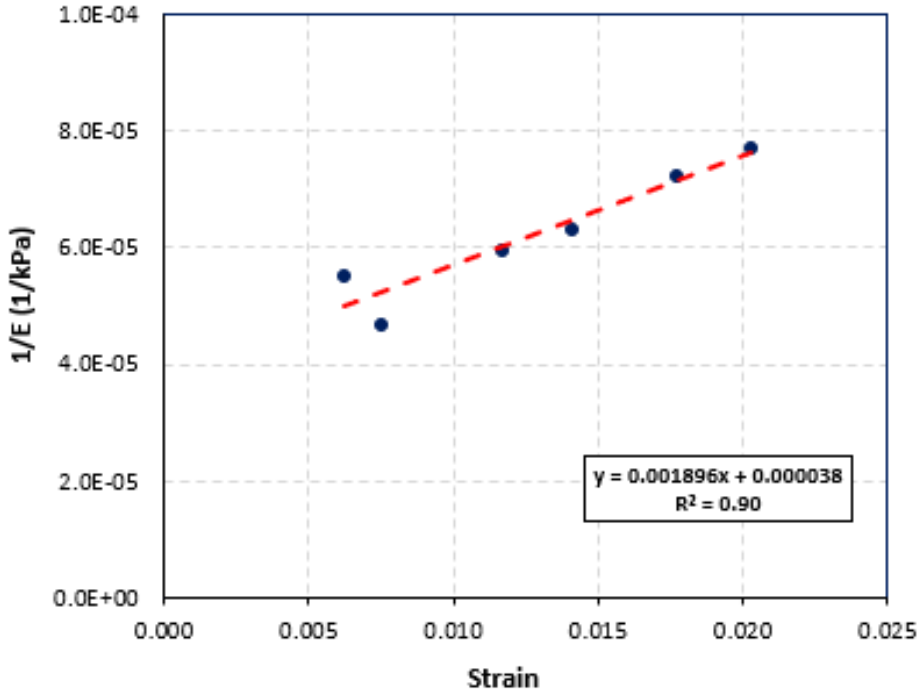

Figure F.38: Location 207 (SDPMT-12 Incremental)

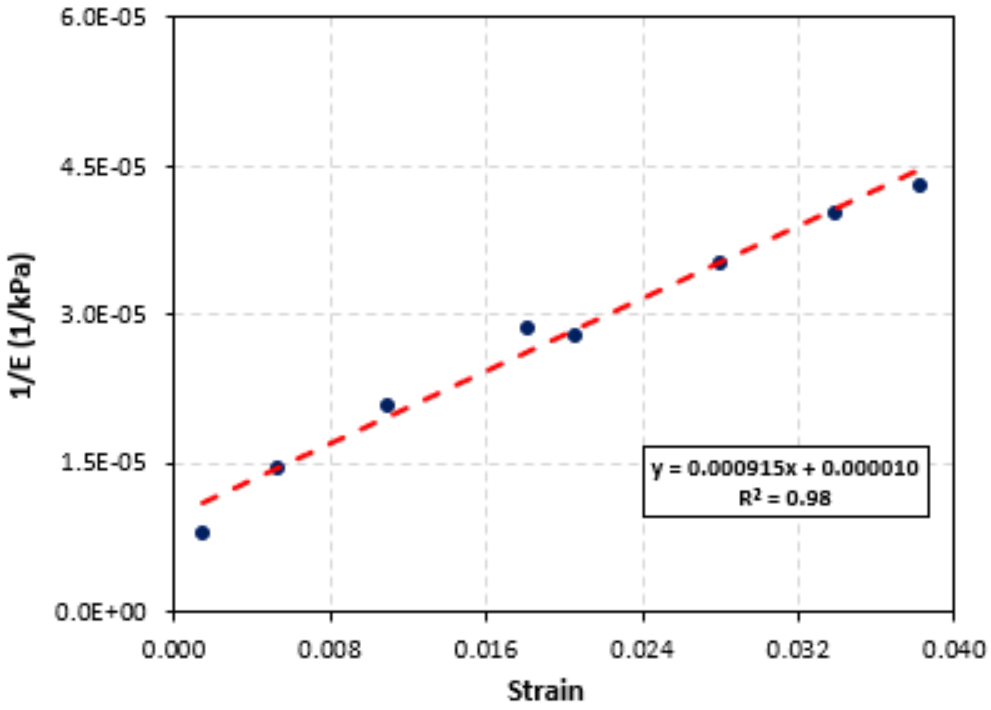

Figure F.39: Location 208 (SDPMT-6 Incremental)

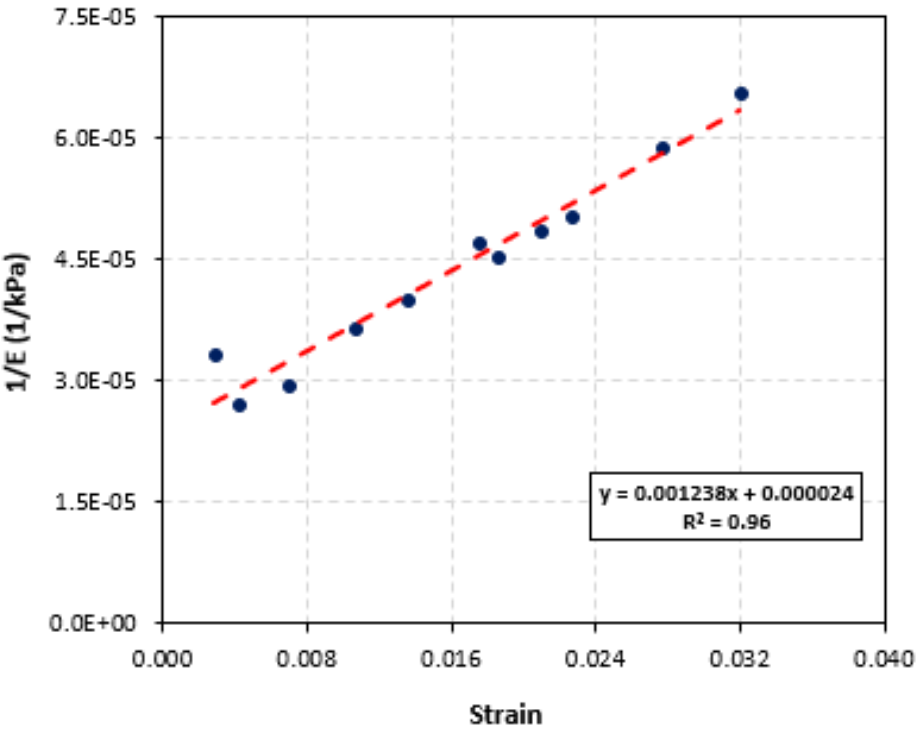

Figure F.40: Location 208 (SDPMT-12 Incremental)

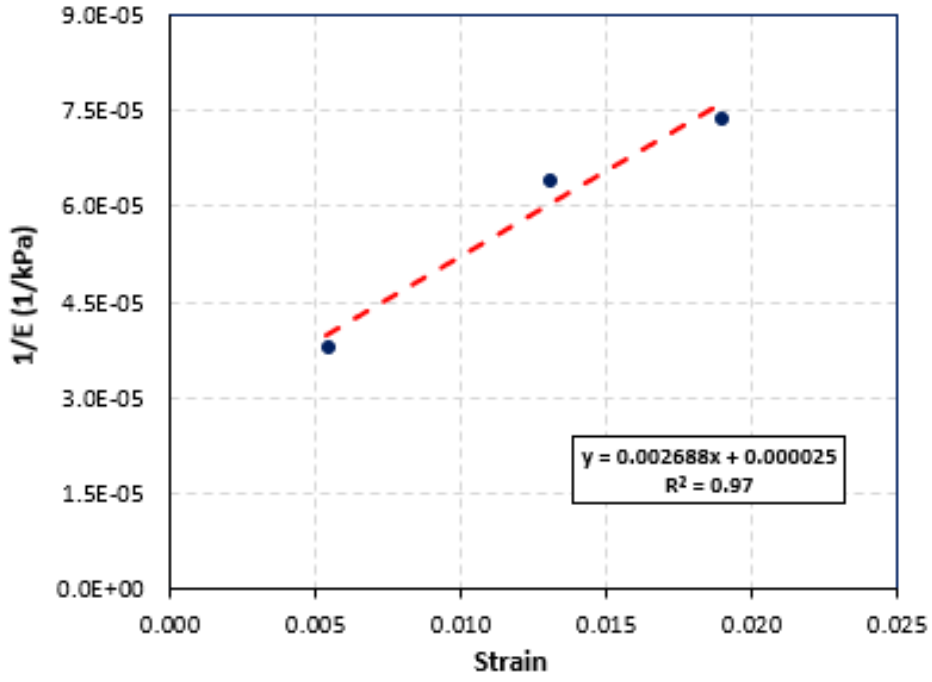

Figure F.41: Location 209 (SDPMT-6 Incremental)

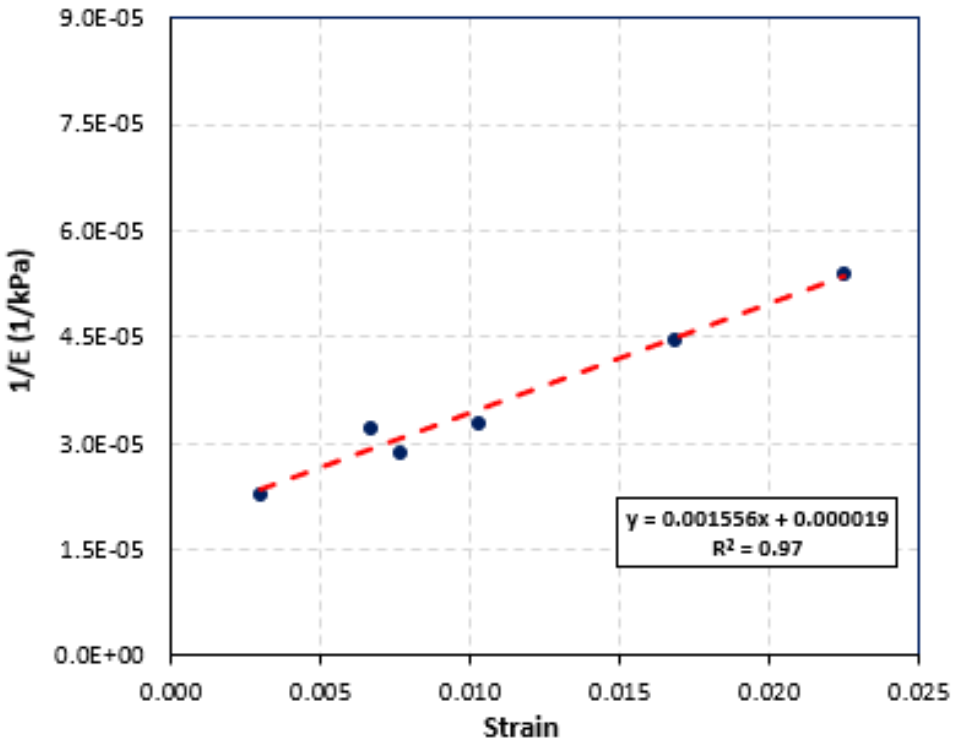

Figure F.42: Location 209 (SDPMT-12 Incremental)

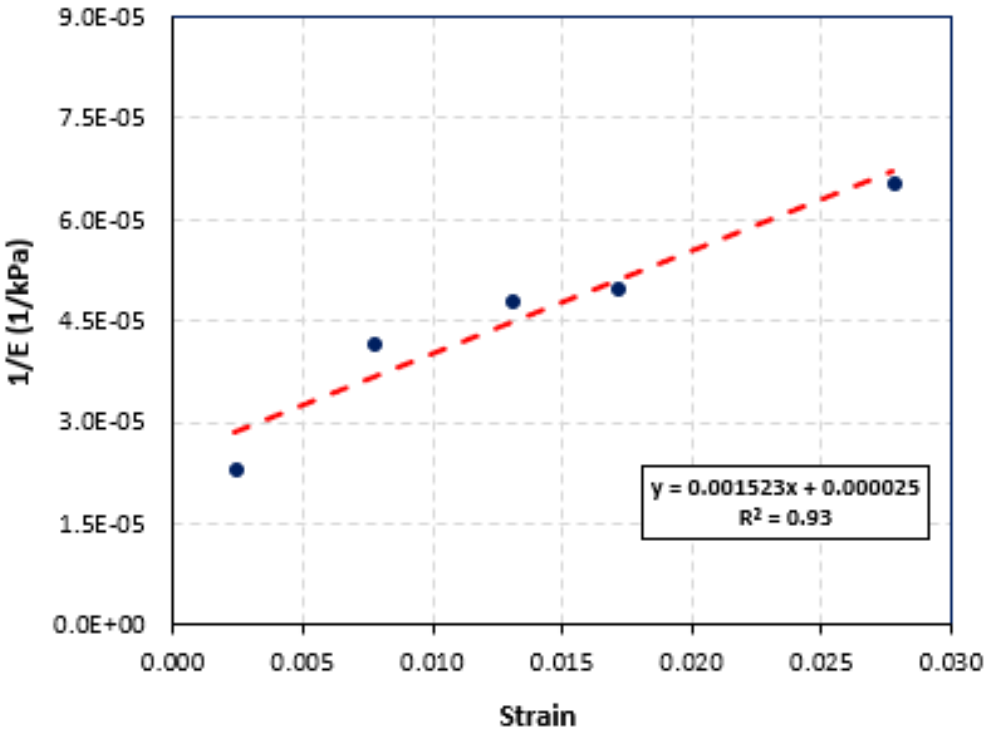

Figure F.43: Location 210 (SDPMT-6 Incremental)

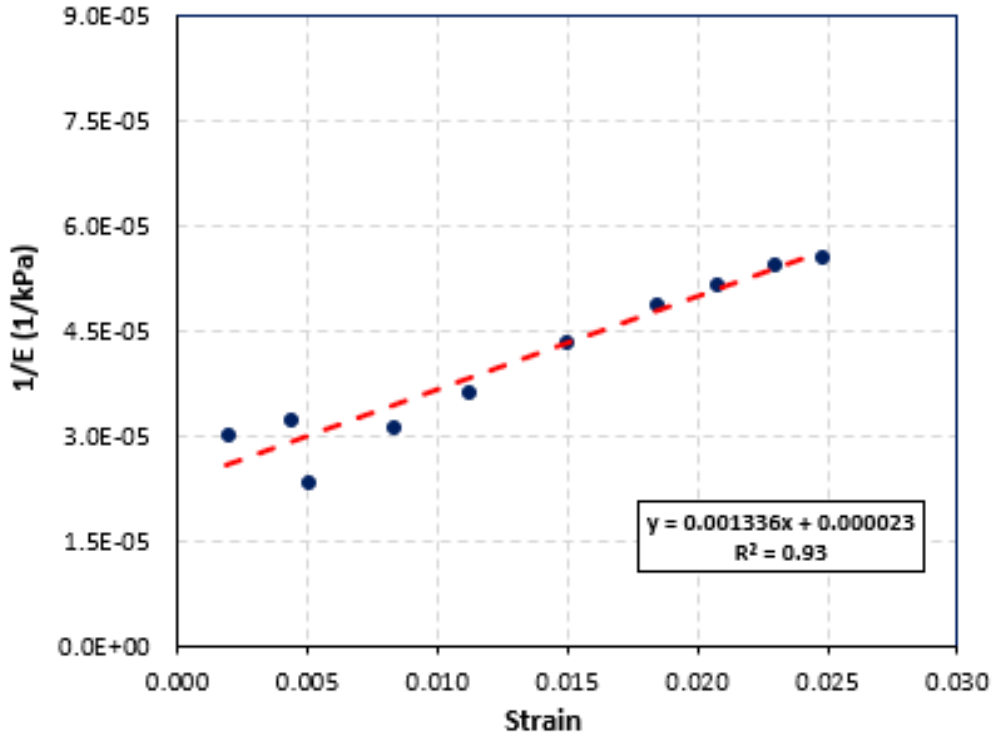

Figure F.44: Location 210 (SDPMT-12 Incremental)

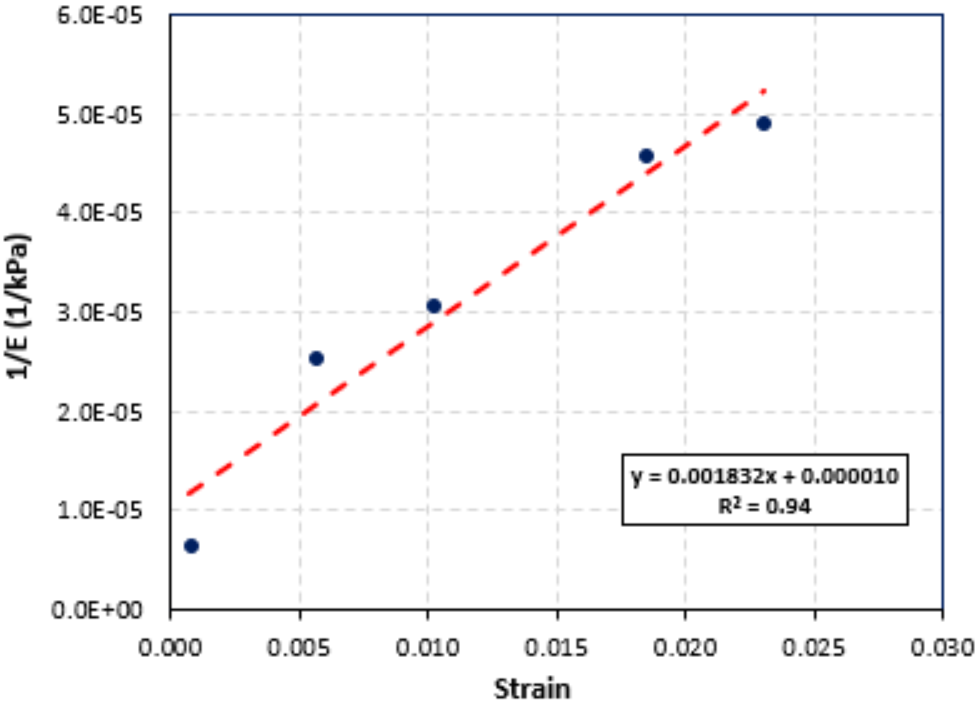

Figure F.45: Location 211 (SDPMT-6 Incremental)

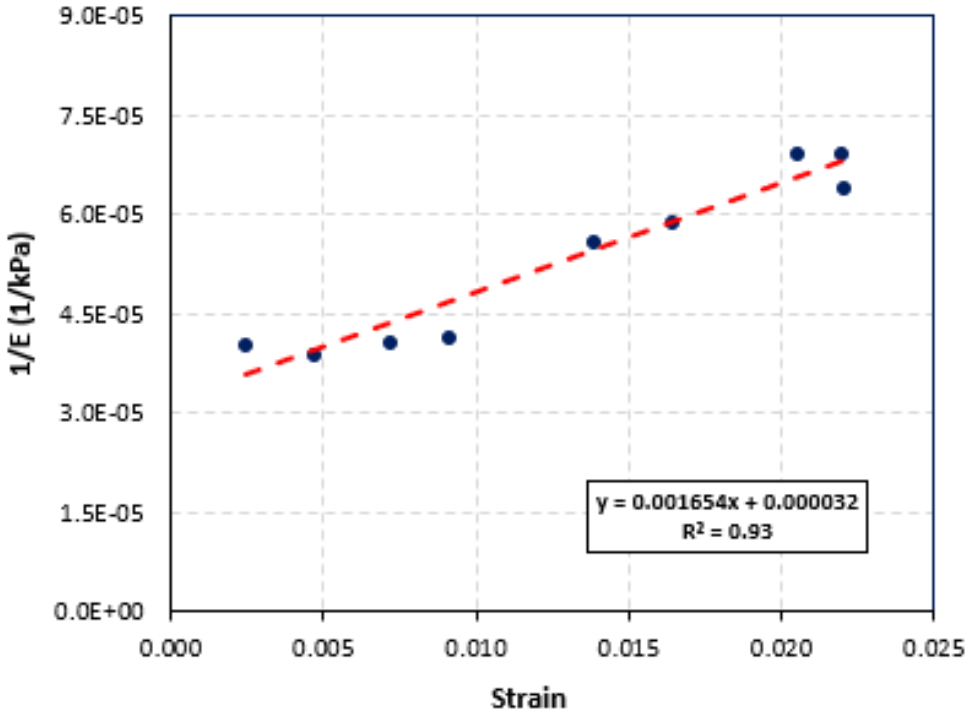

Figure F.46: Location 211 (SDPMT-12 Incremental)

F.3 Cypress Landing

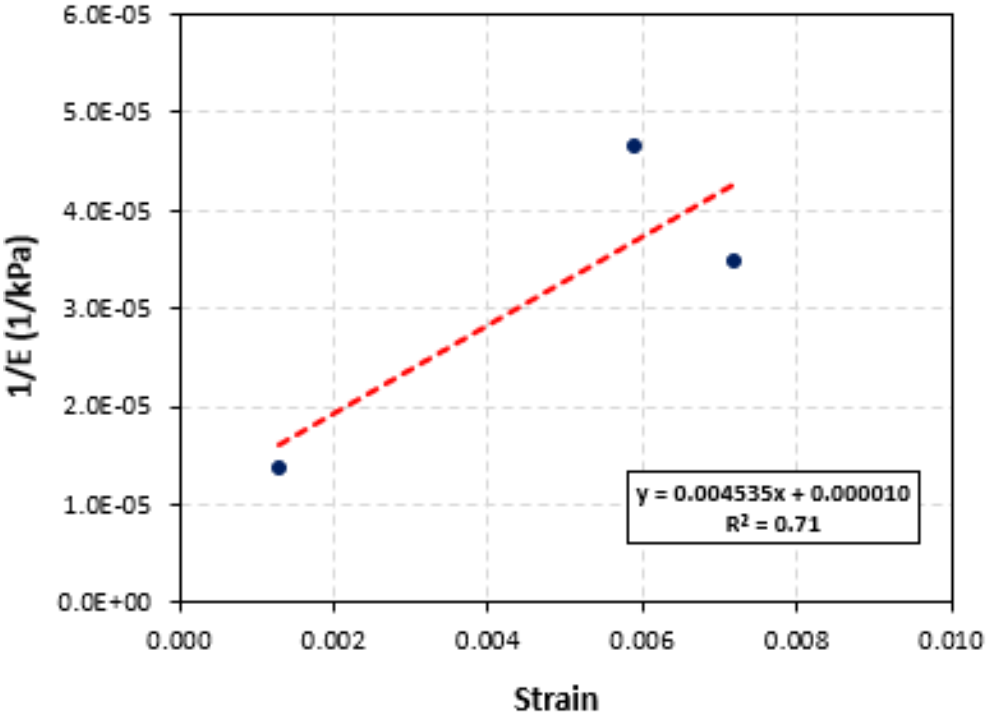

Figure F.47: Location 101 (SDPMT-12 Incremental)

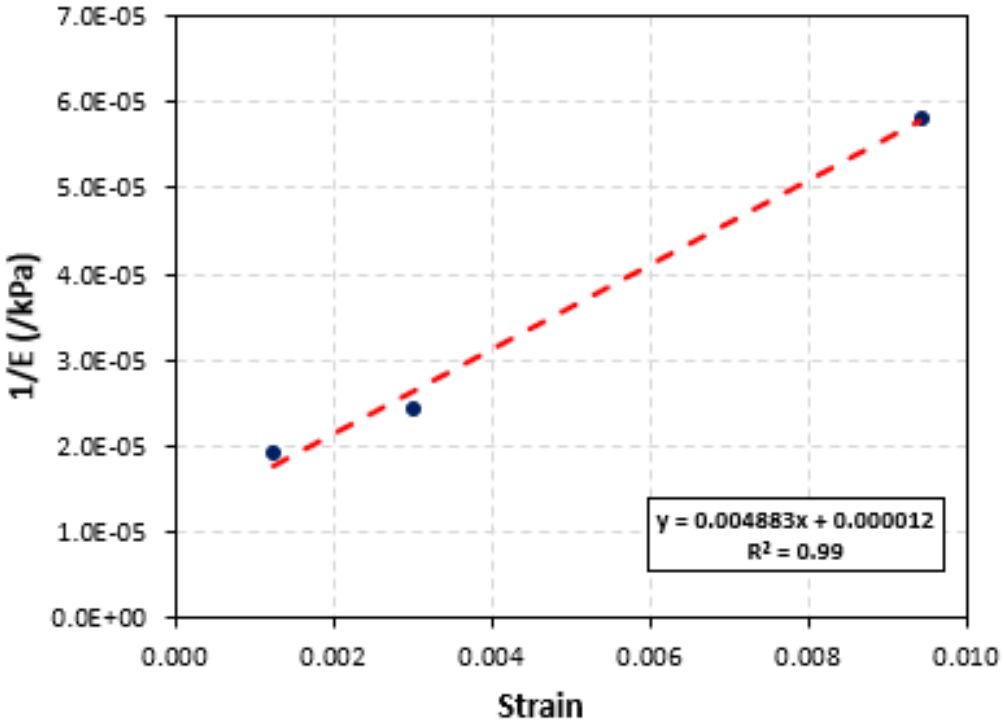

Figure F.48: Location 103 (SDPMT-12 Incremental)

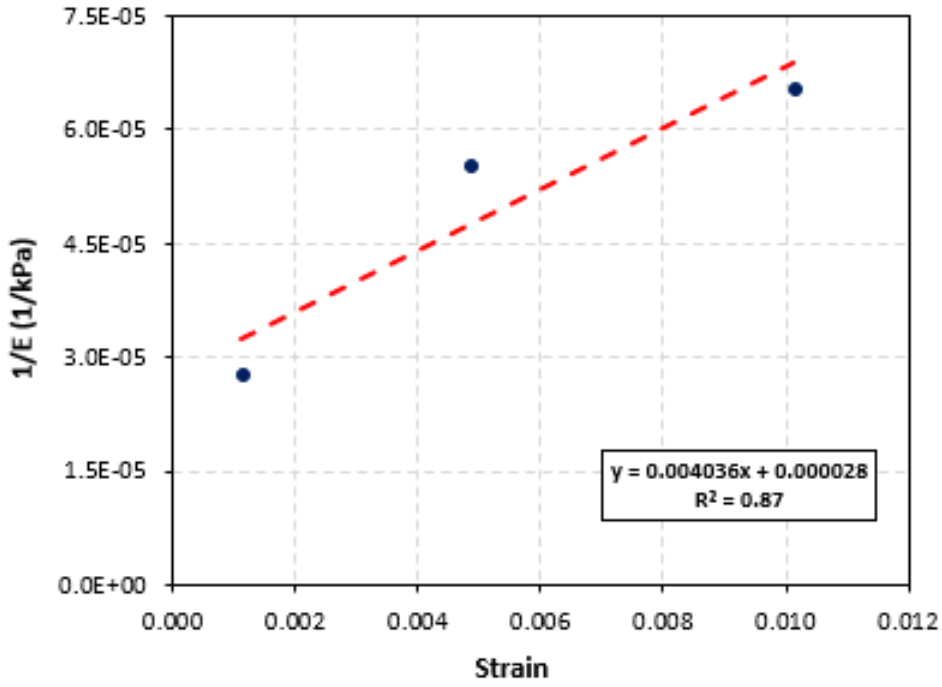

Figure F.49: Location 104 (SDPMT-12 Incremental)

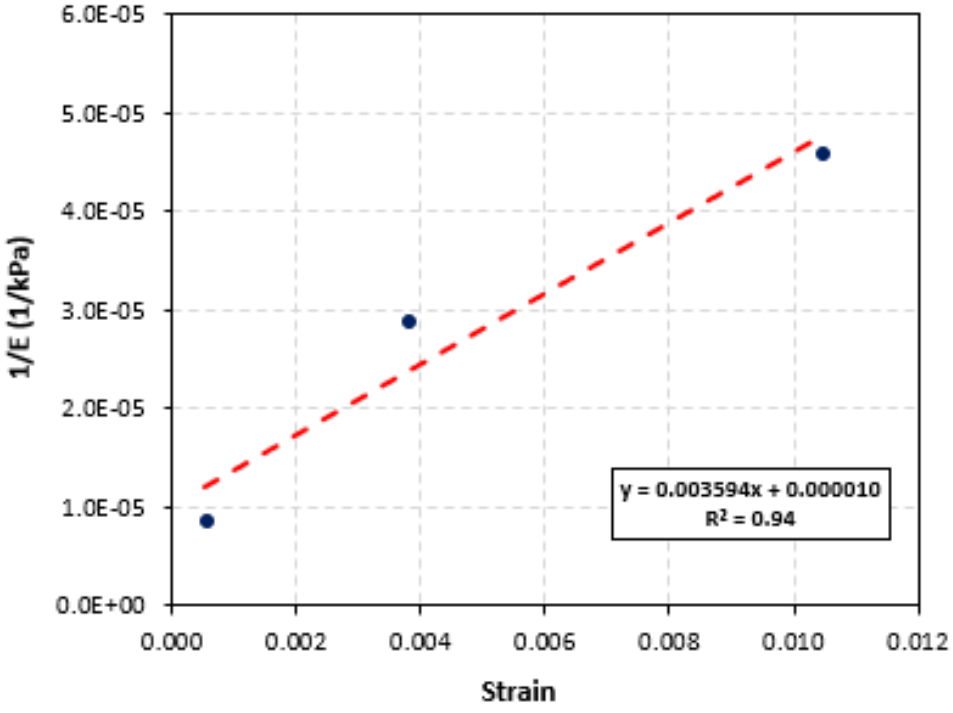

Figure F.50: Location 105 (SDPMT-12 Incremental)

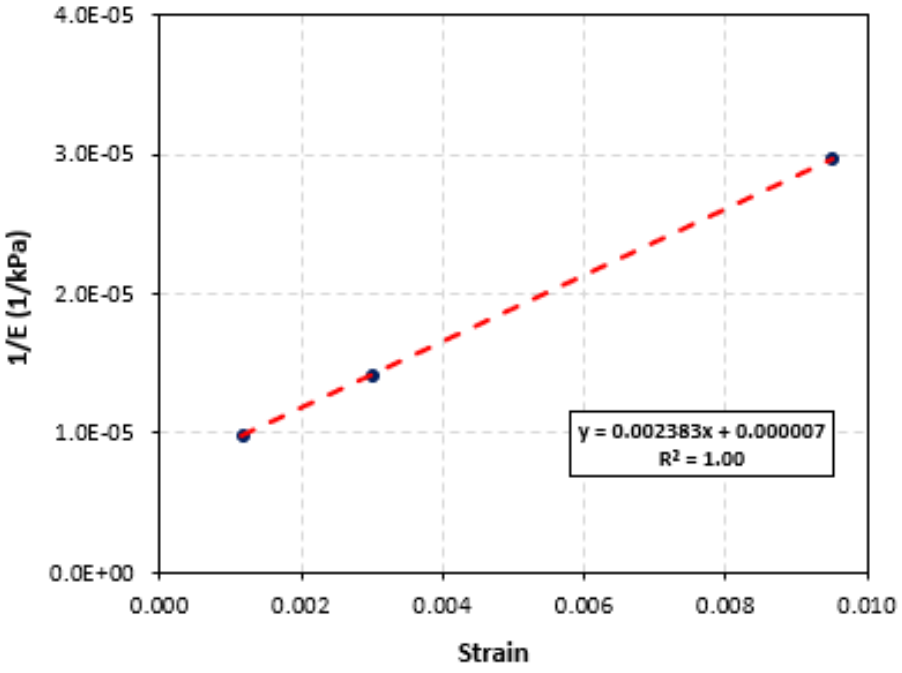

Figure F.51: Location 106 (SDPMT-12 Incremental)

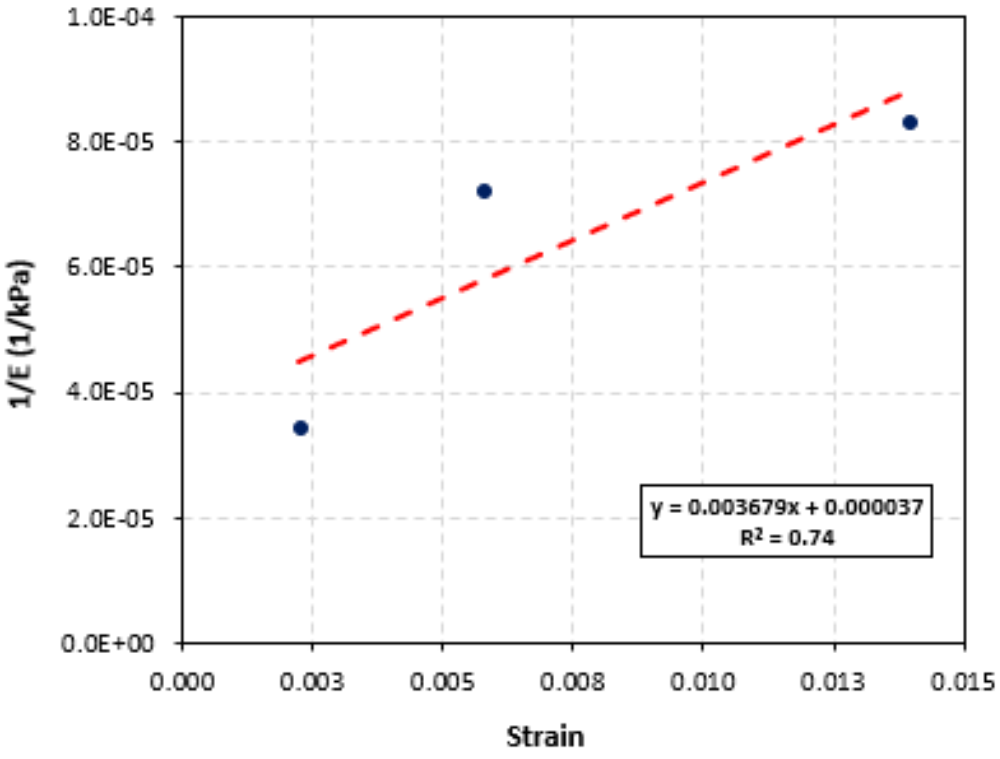

Figure F.52: Location 107 (SDPMT-12 Incremental)

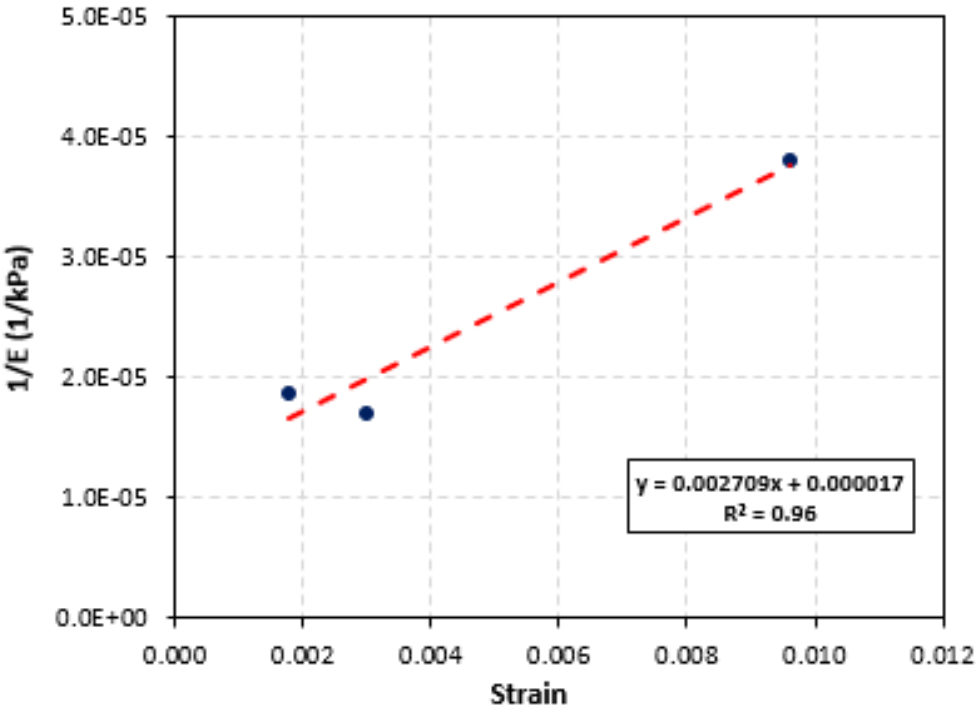

Figure F.53: Location 108 (SDPMT-12 Incremental)

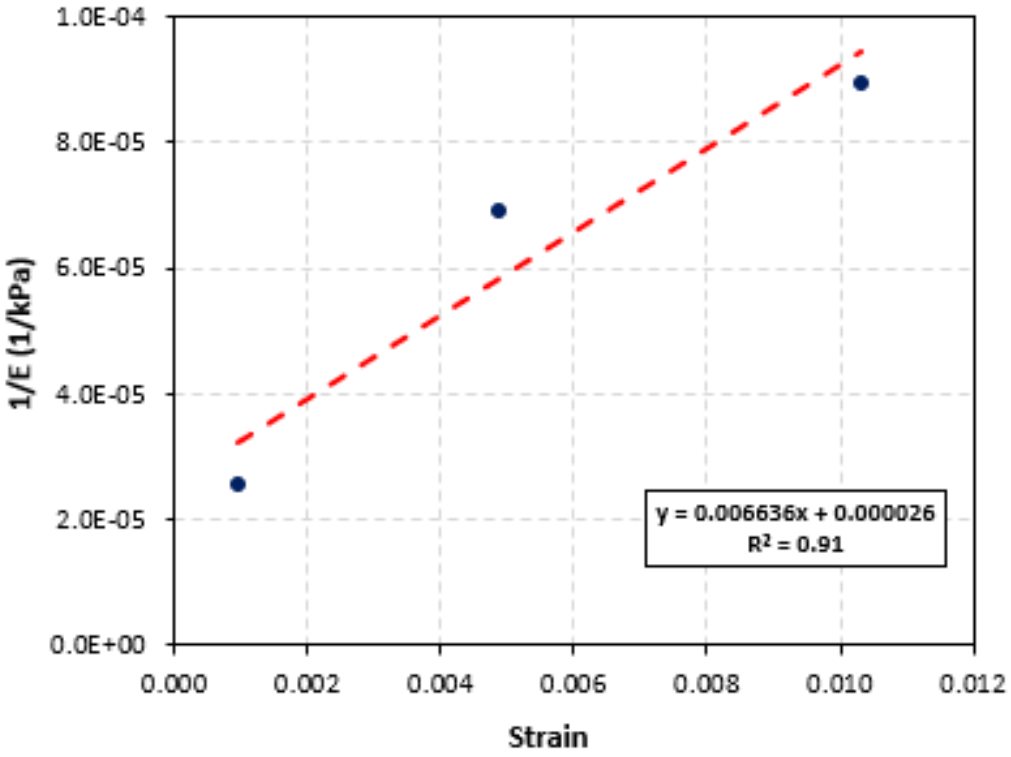

Figure F.54: Location 109 (SDPMT-12 Incremental)

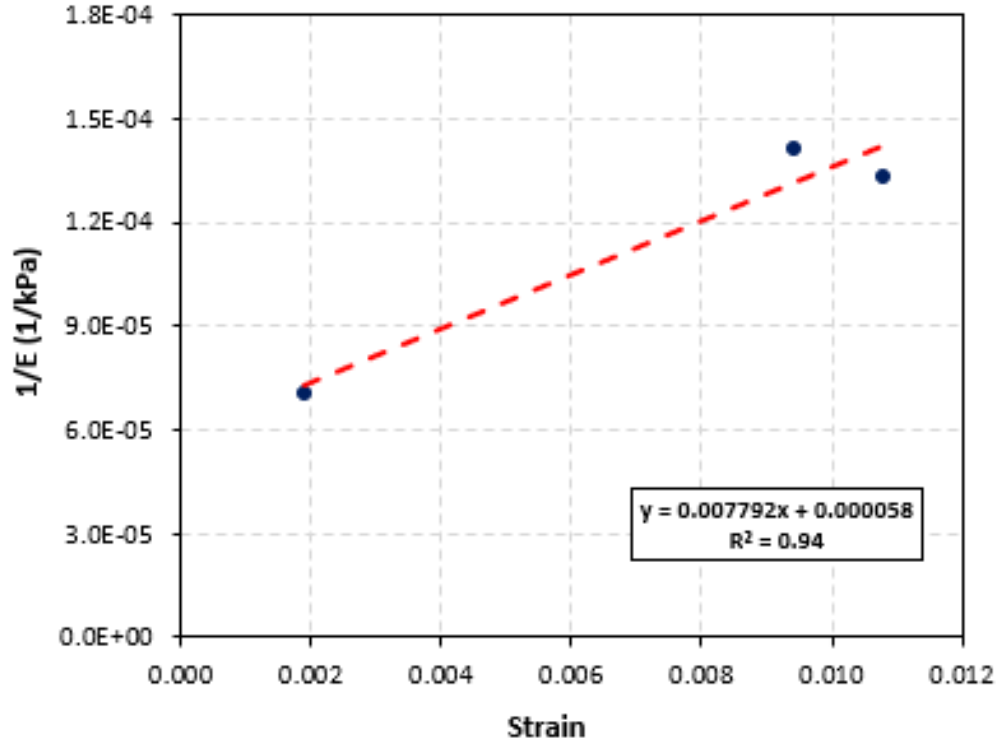

Figure F.55: Location 110 (SDPMT-12 Incremental)

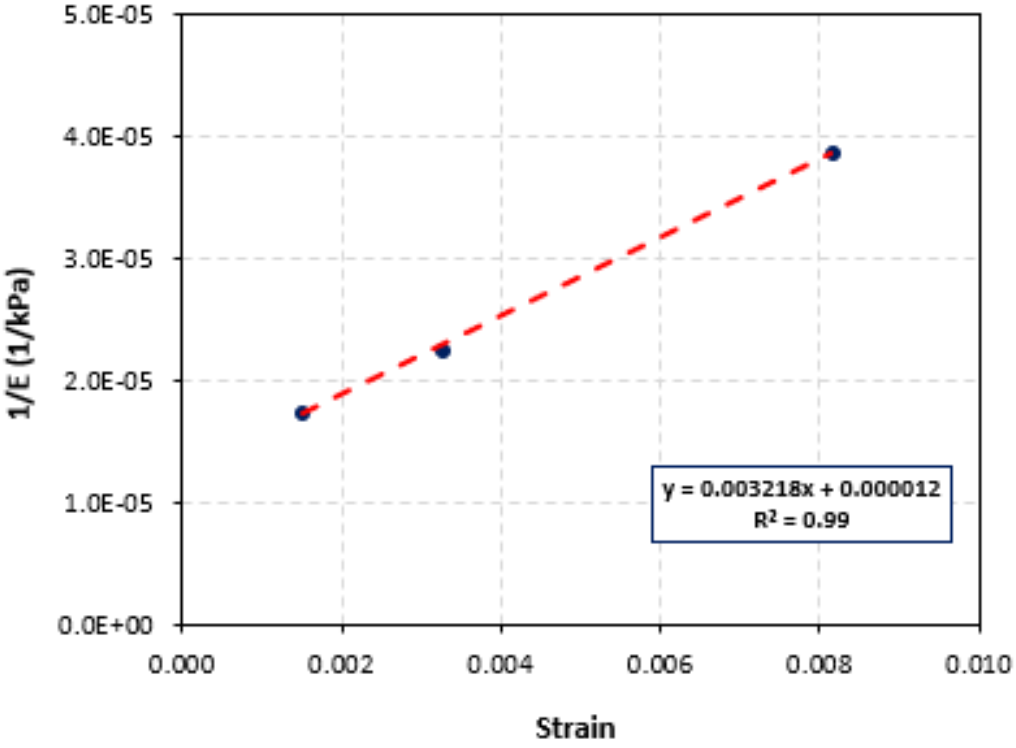

Figure F.56: Location 111 (SDPMT-12 Incremental)

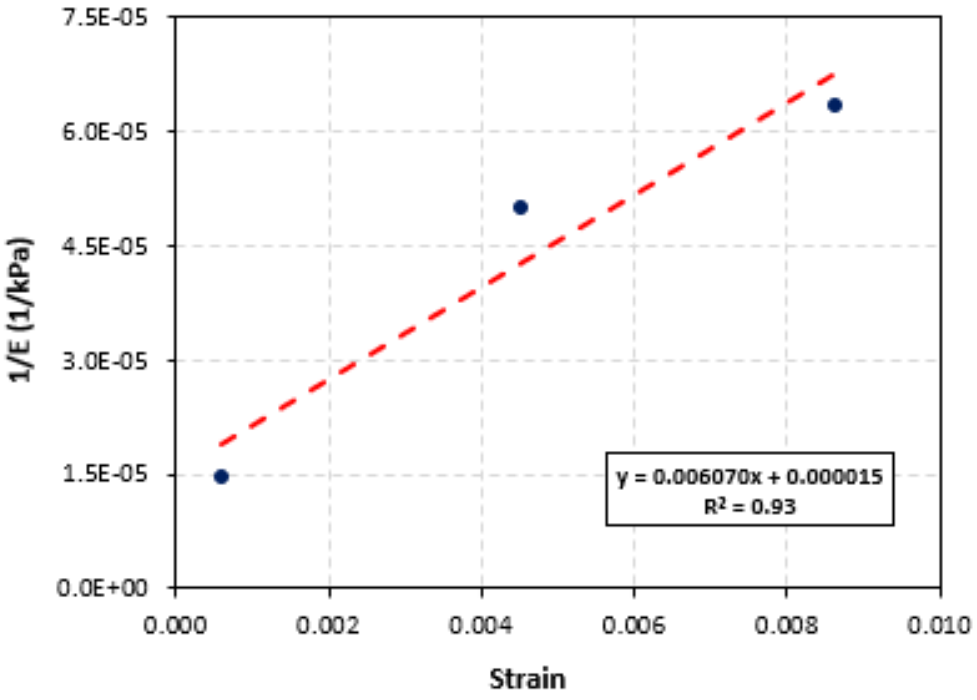

Figure F.57: Location 112 (SDPMT-12 Incremental)

F.4 Heritage Parkway

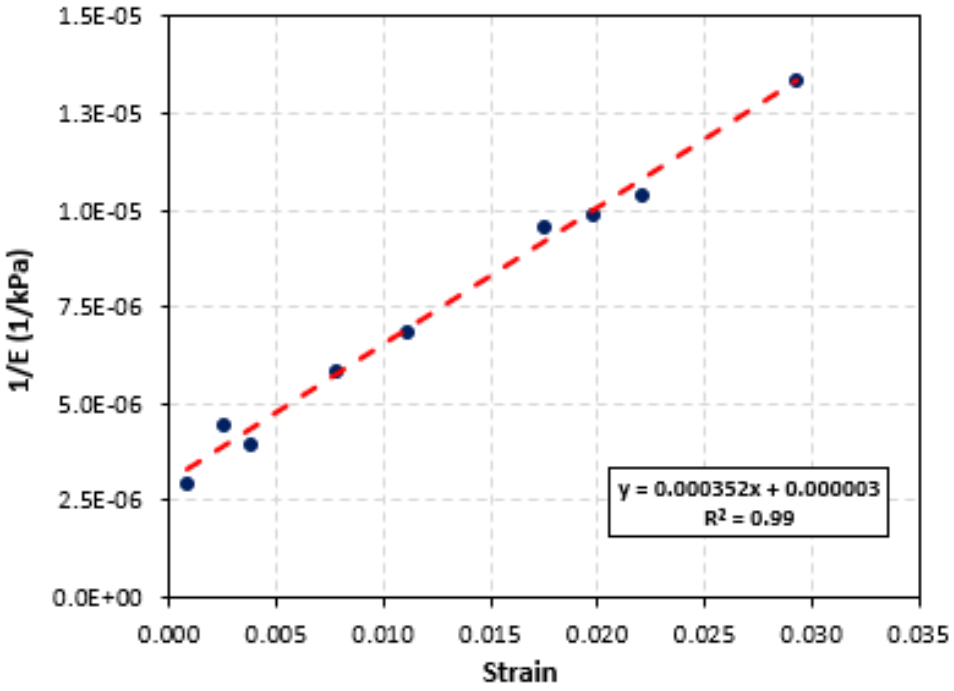

Figure F.58: Location 301 (SDPMT-6 Incremental)

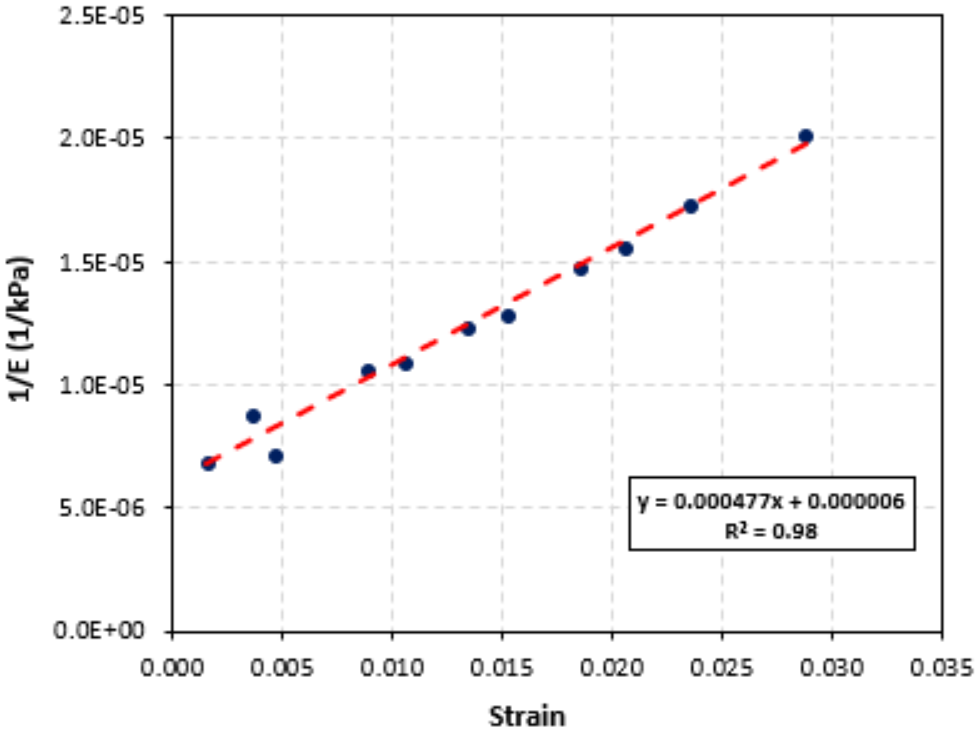

Figure F.59: Location 301 (SDPMT-12 Incremental)

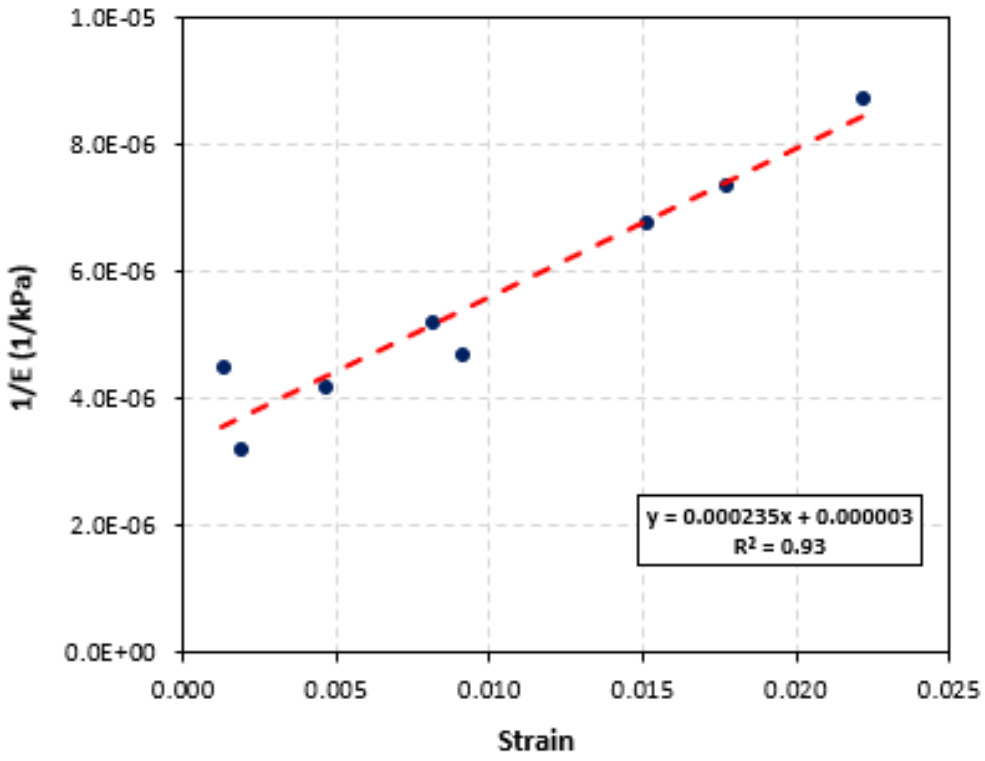

Figure F.60: Location 302 (SDPMT-6 Incremental)

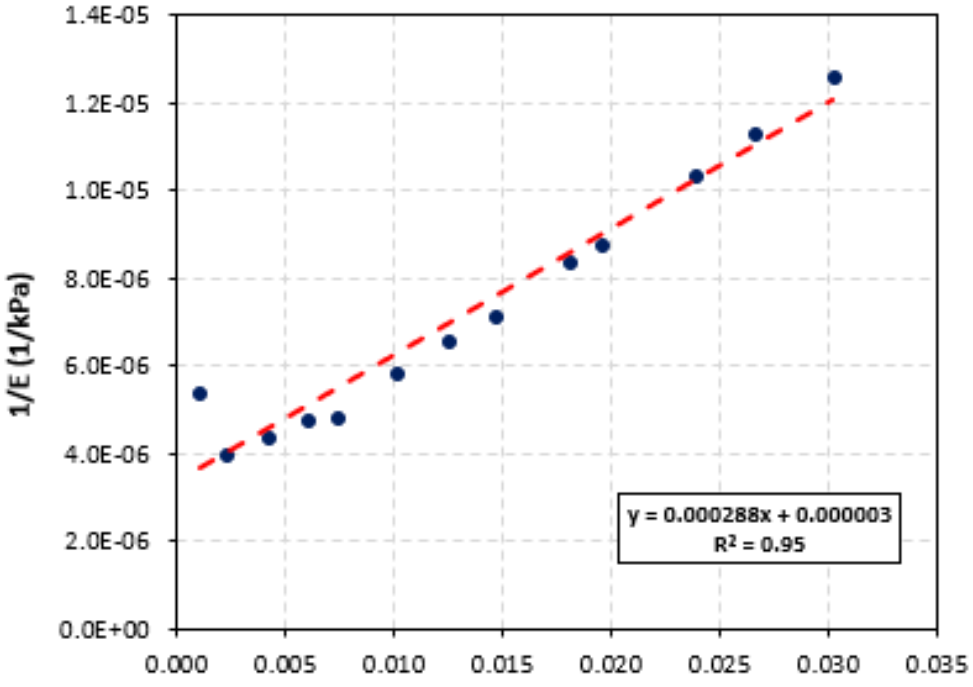

Figure F.61: Location 302 (SDPMT-12 Incremental)

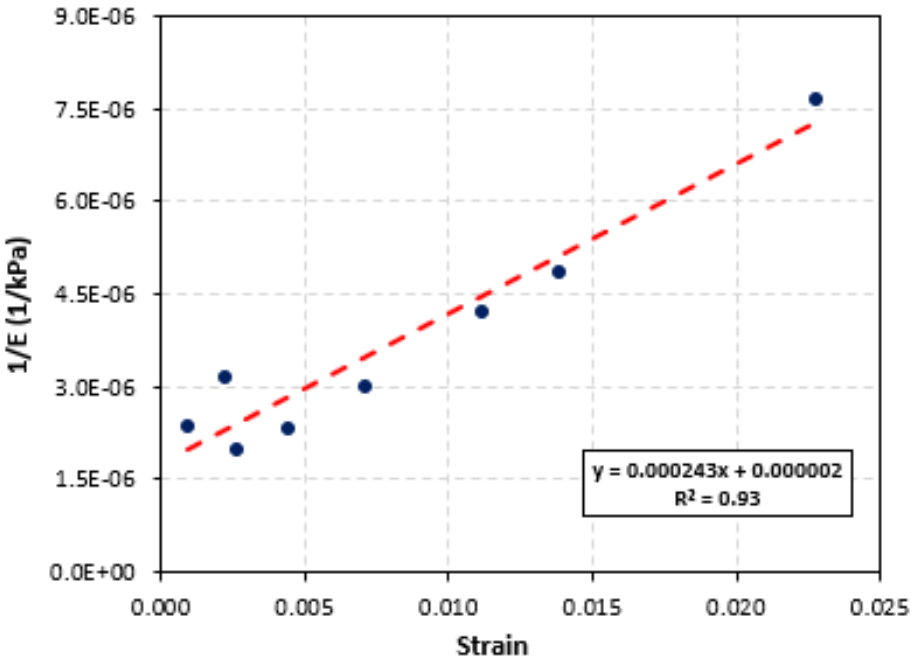

Figure F.62: Location 303 (SDPMT-6 Incremental)

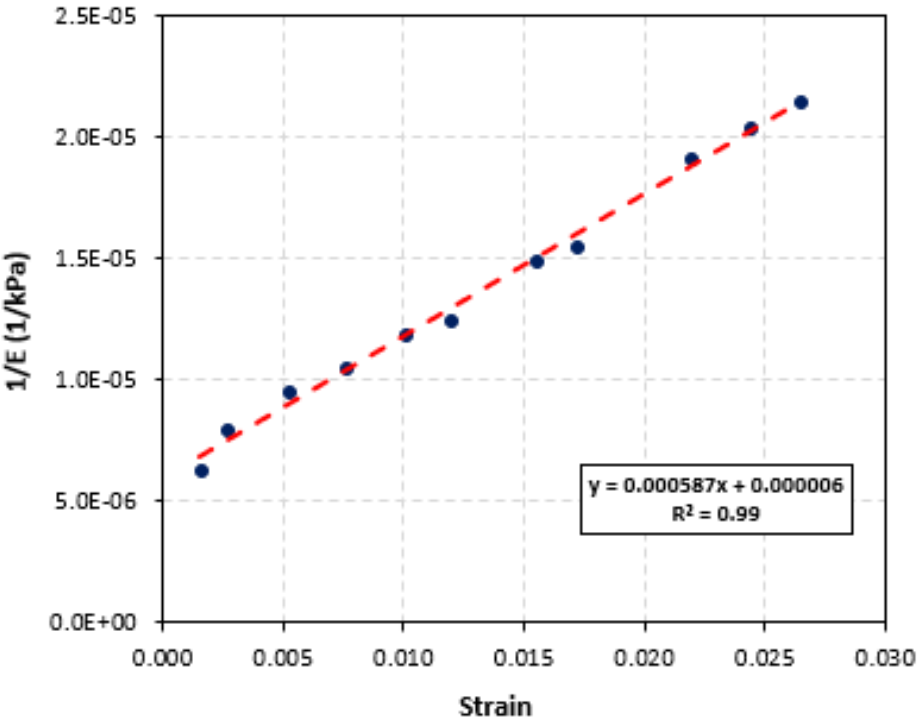

Figure F.63: Location 303 (SDPMT-12 Incremental)

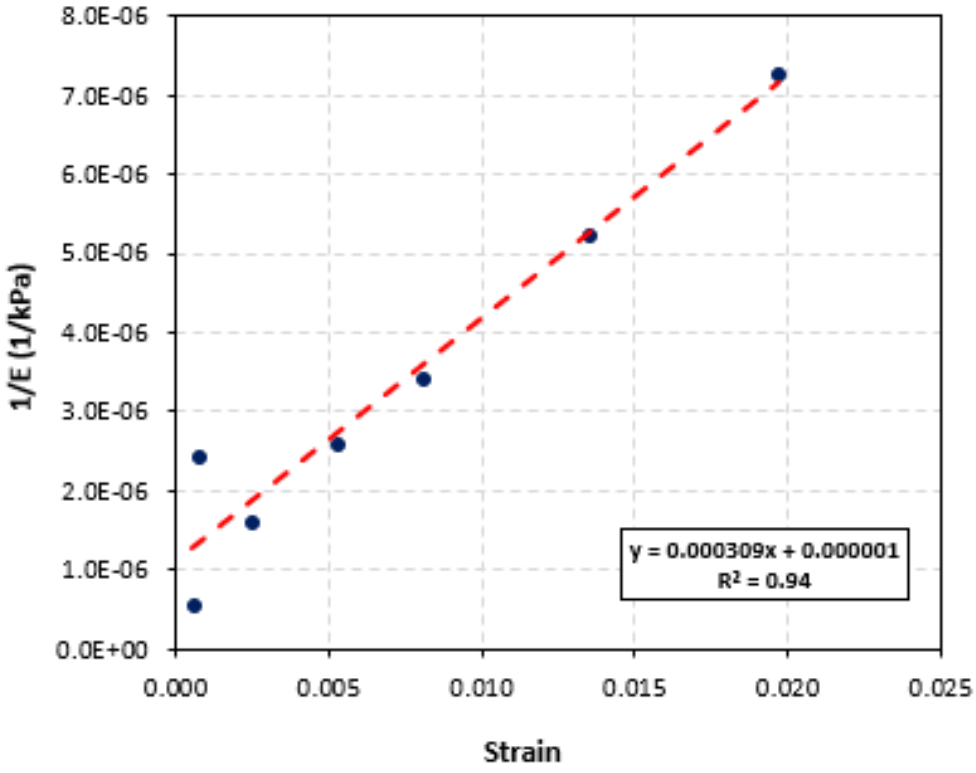

Figure F.64: Location 304 (SDPMT-6 Incremental)

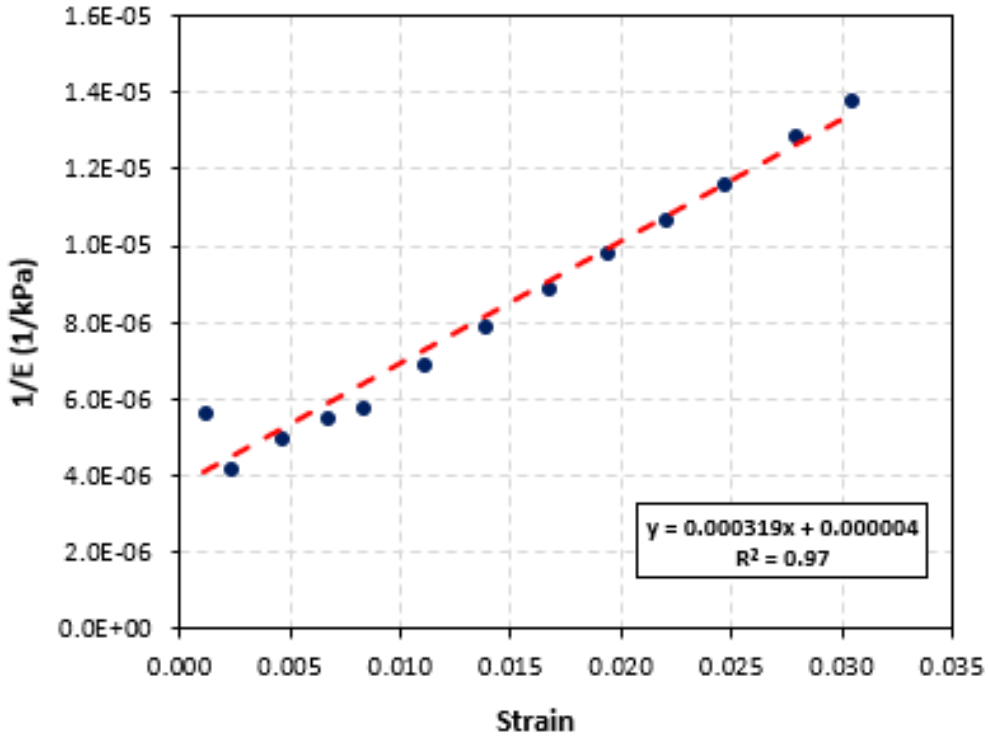

Figure F.65: Location 304 (SDPMT-12 Incremental)

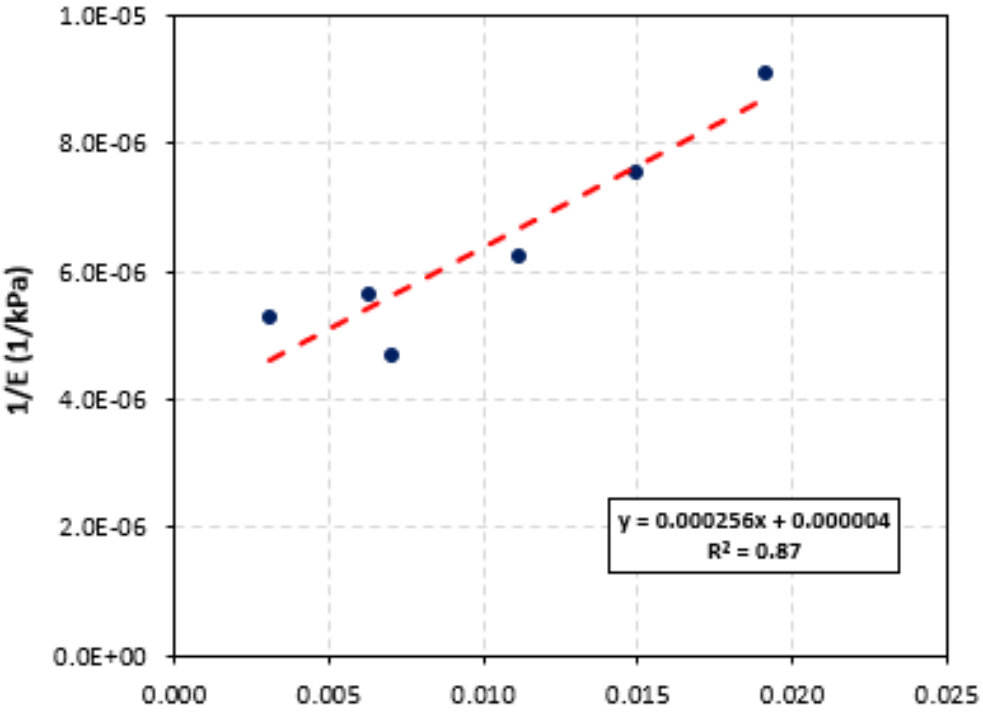

Figure F.66: Location 305 (SDPMT-6 Incremental)

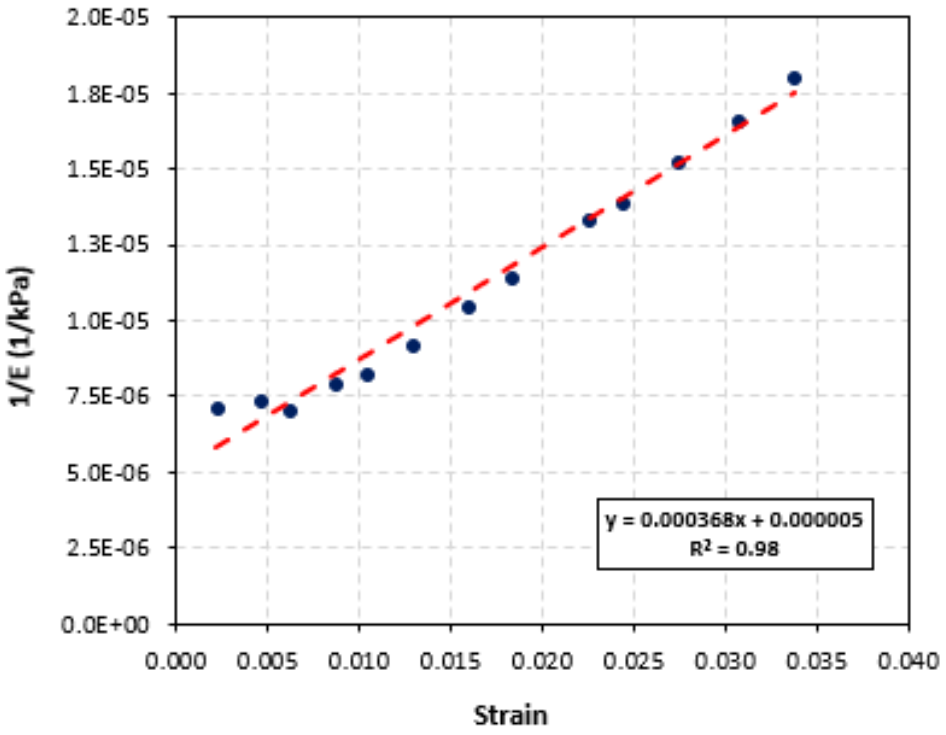

Figure F.67: Location 305 (SDPMT-12 Incremental)

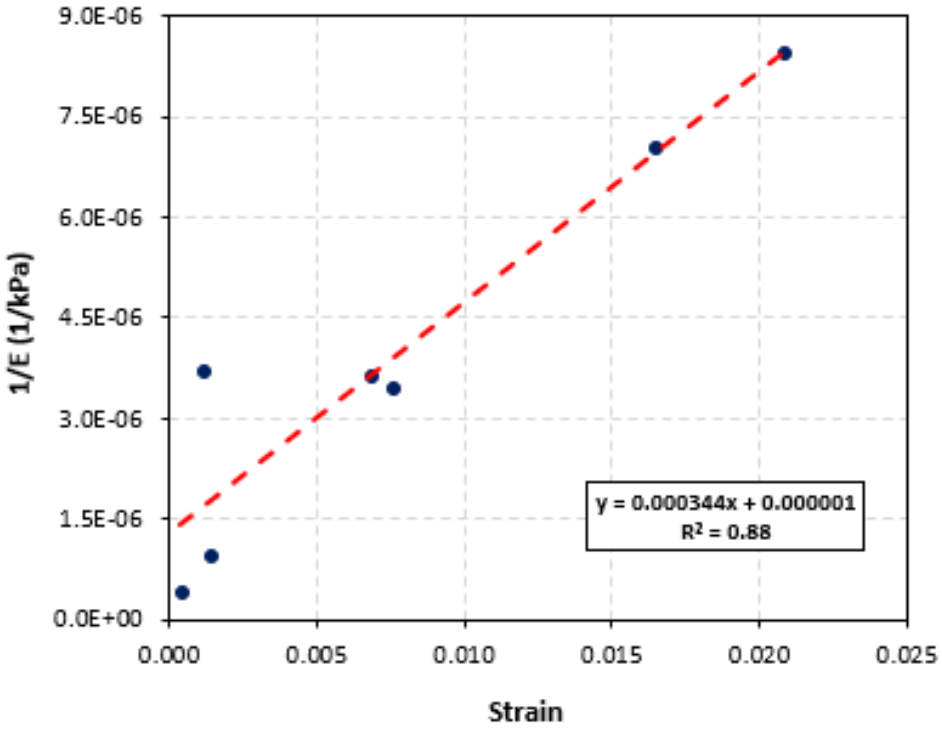

Figure F.68: Location 306 (SDPMT-6 Incremental)

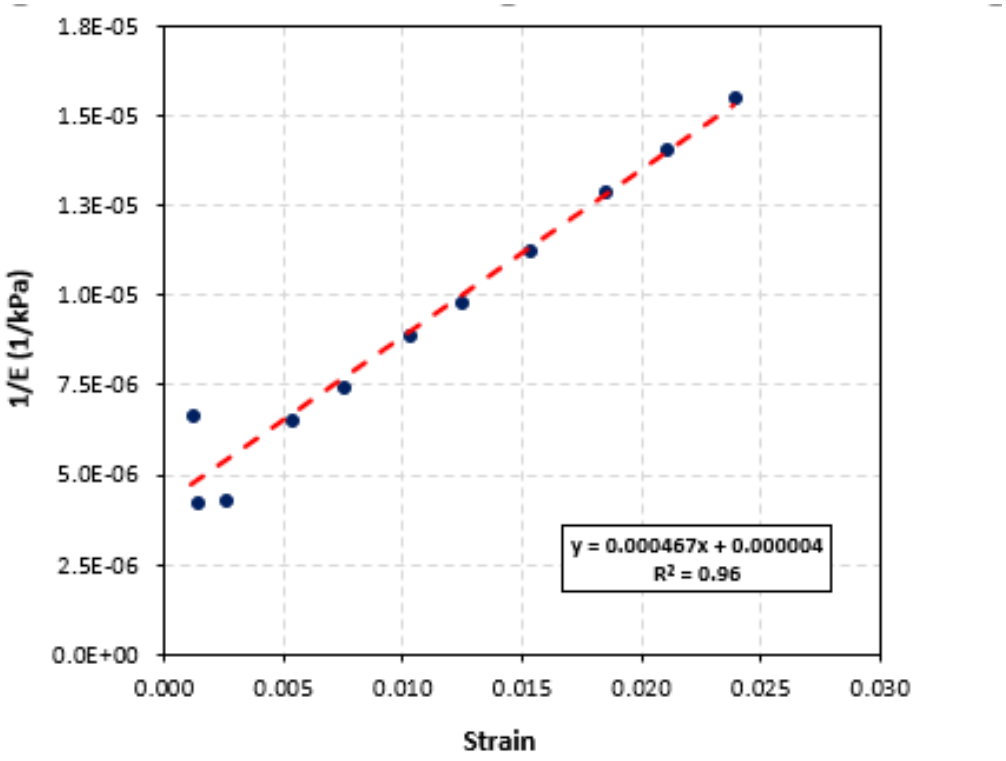

Figure F.69: Location 306 (SDPMT-12 Incremental)

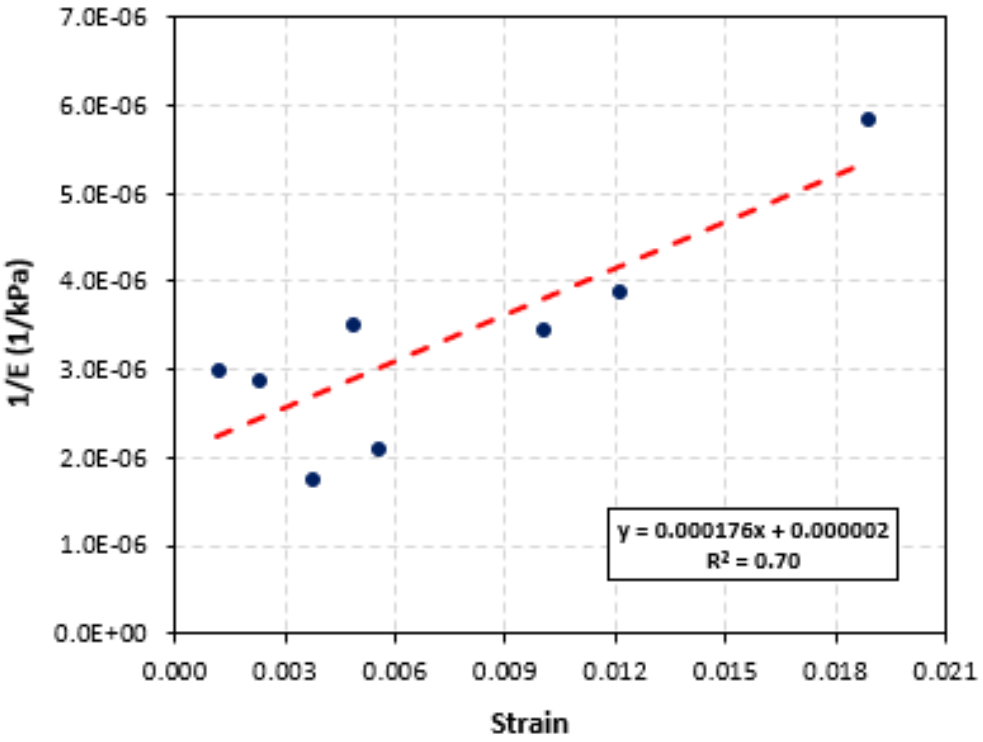

Figure F.70: Location 307 (SDPMT-6 Incremental)

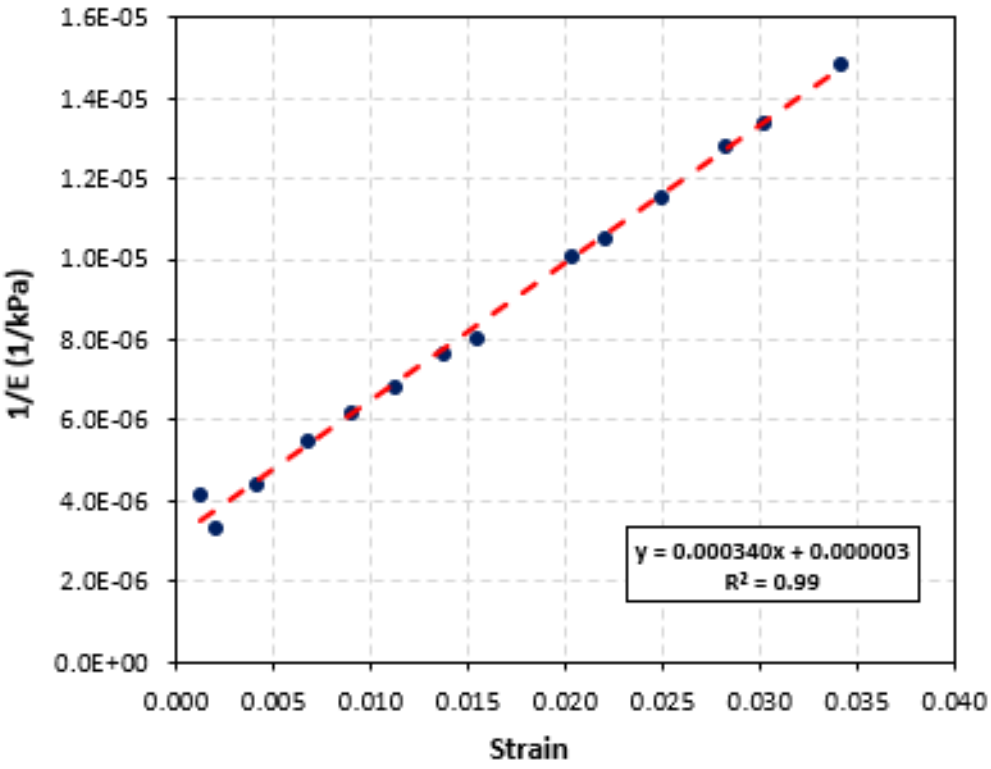

Figure F.71: Location 307 (SDPMT-12 Incremental)

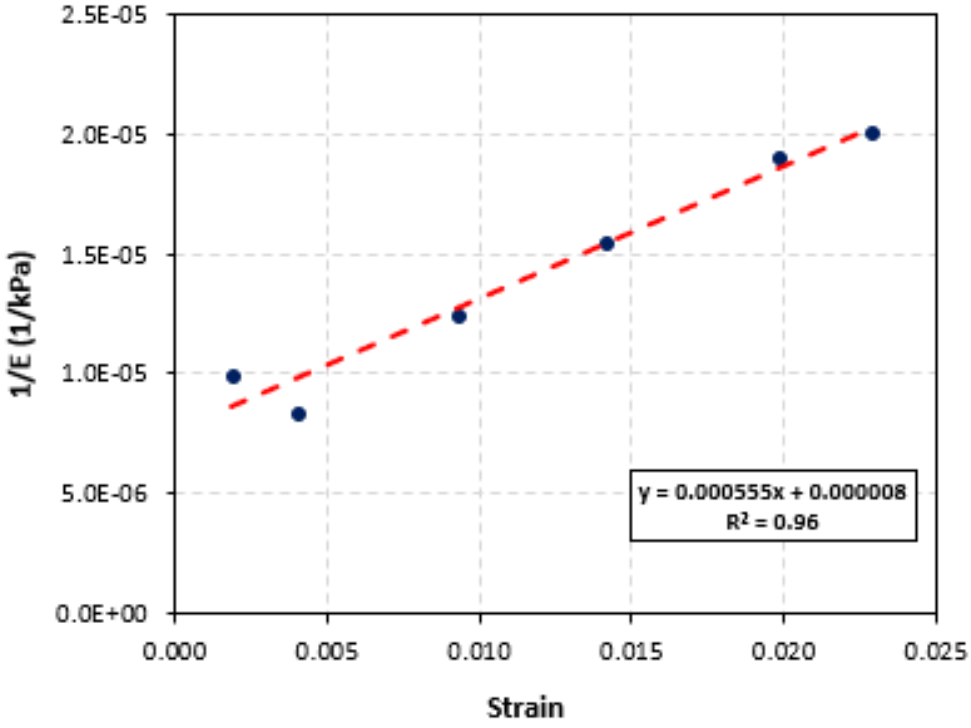

Figure F.72: Location 308 (SDPMT-6 Incremental)

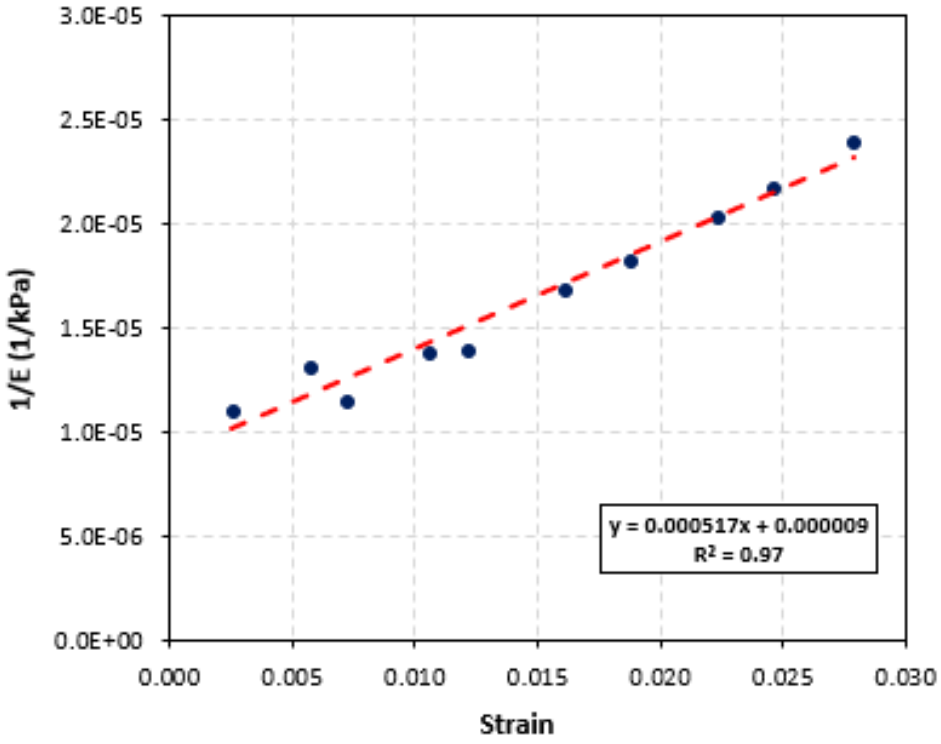

Figure F.73: Location 308 (SDPMT-12 Incremental)

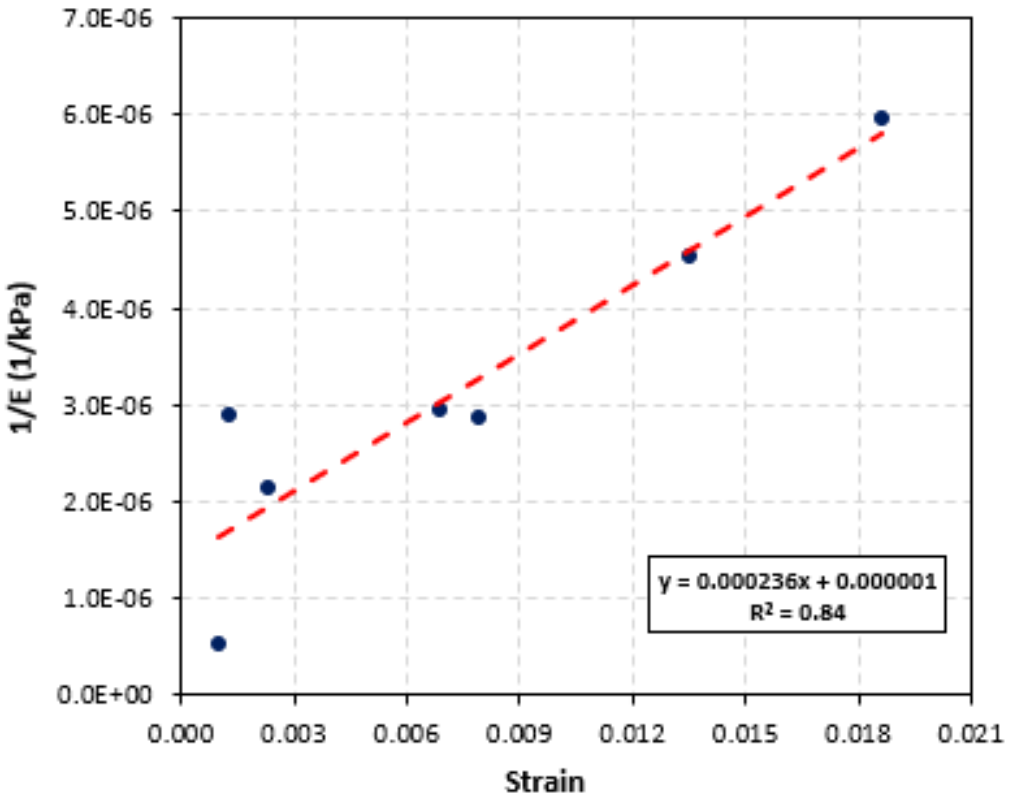

Figure F.74: Location 309 (SDPMT-6 Incremental)

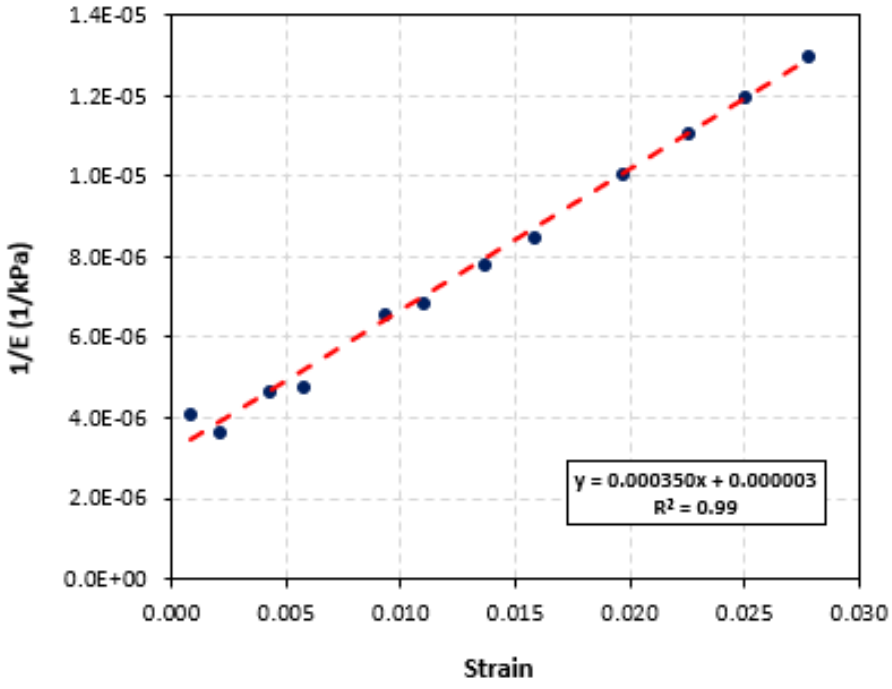

Figure F.75: Location 309 (SDPMT-12 Incremental)

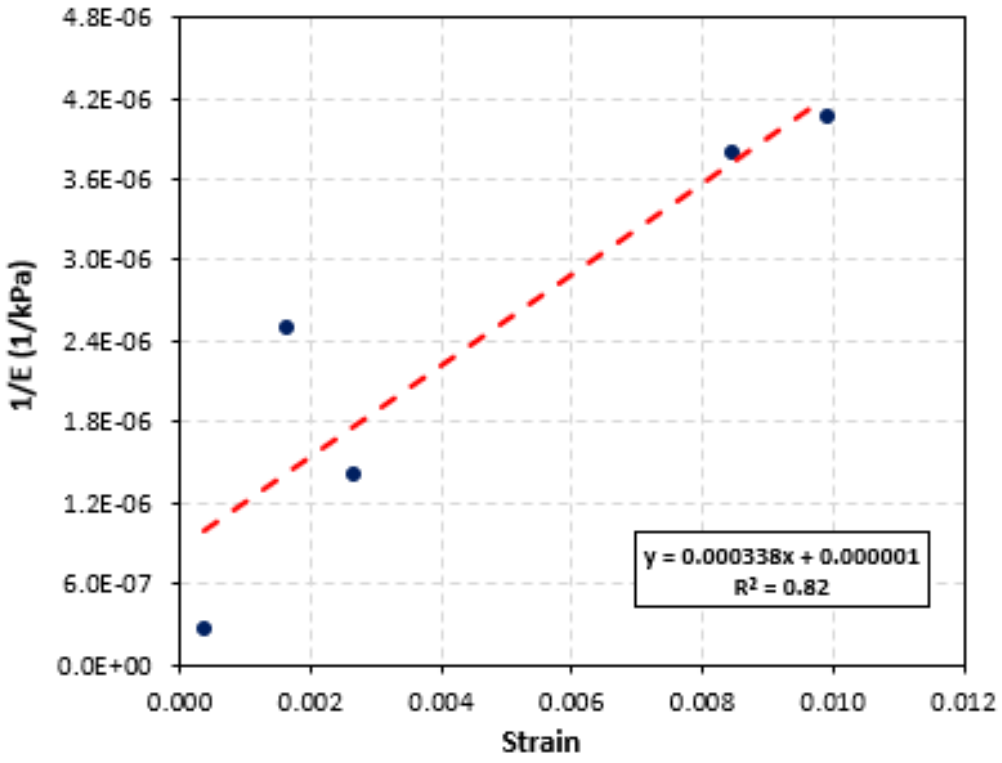

Figure F.76: Location 310 (SDPMT-6 Incremental)

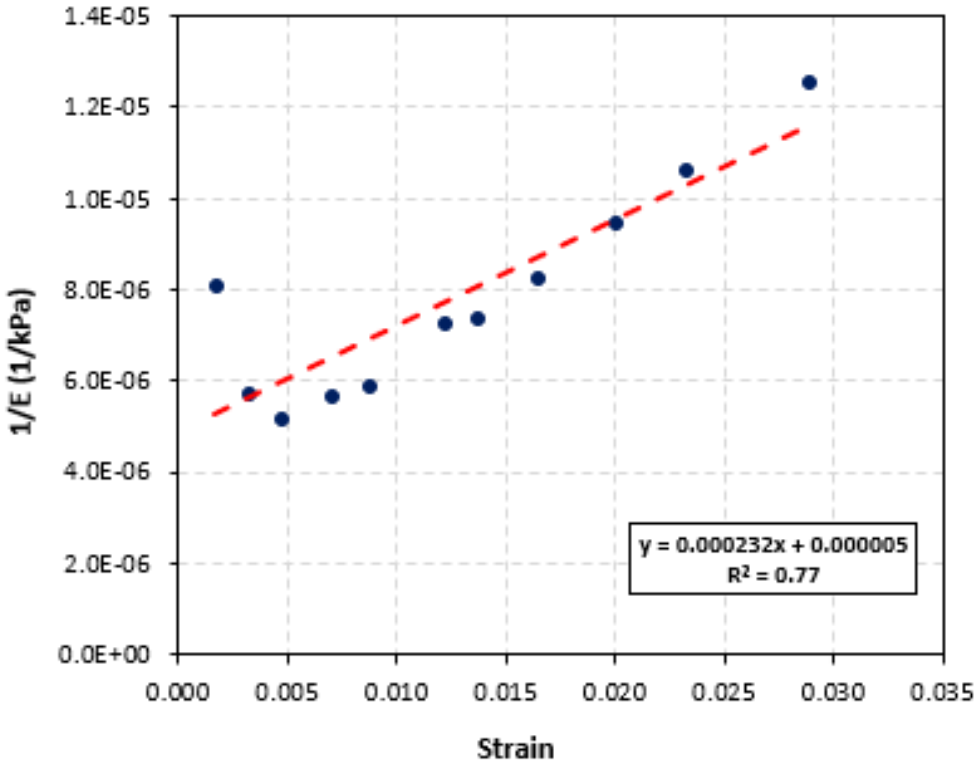

Figure F.77: Location 310 (SDPMT-12 Incremental)

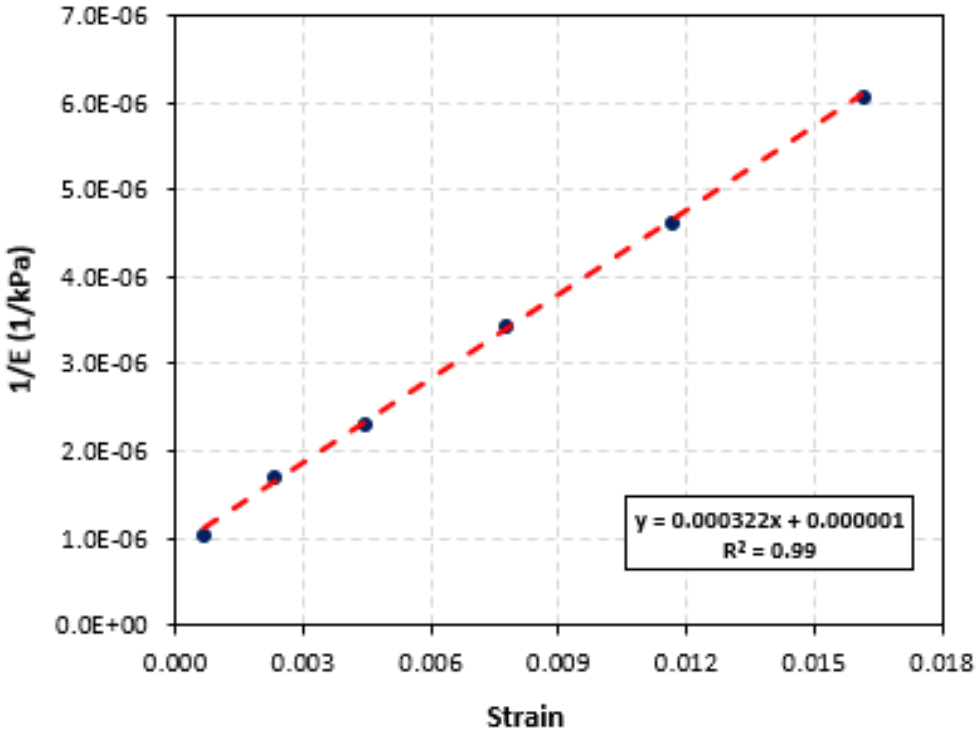

Figure F.78: Location 311 (SDPMT-6 Incremental)

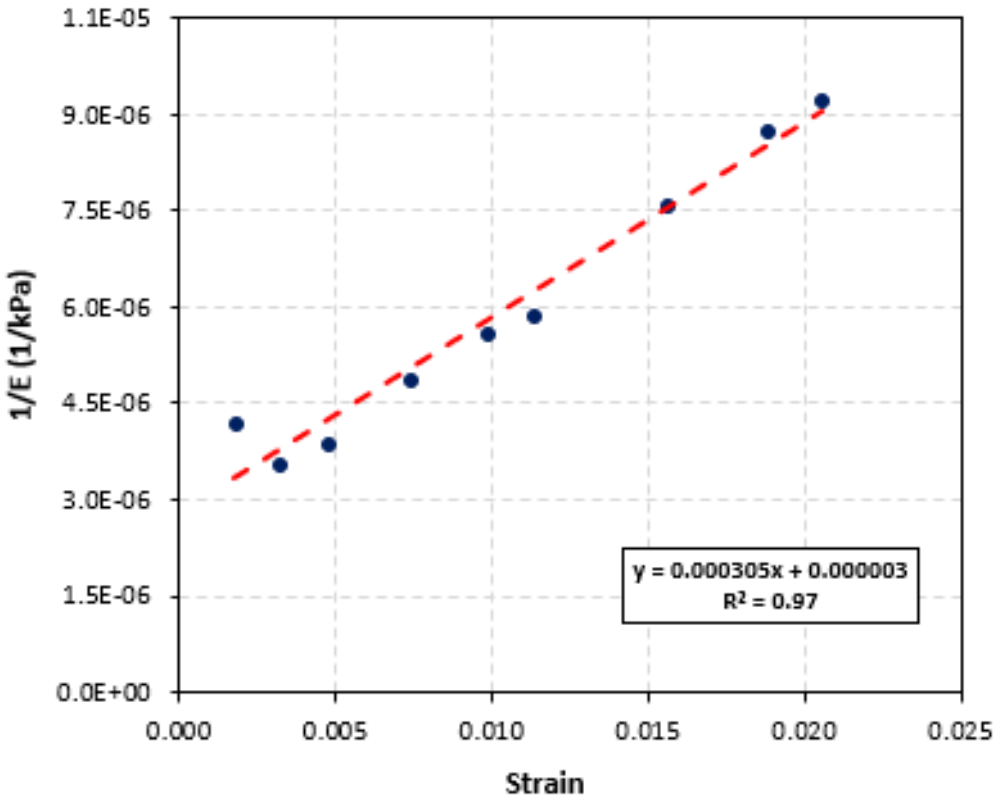

Figure F.79: Location 311 (SDPMT-12 Incremental)

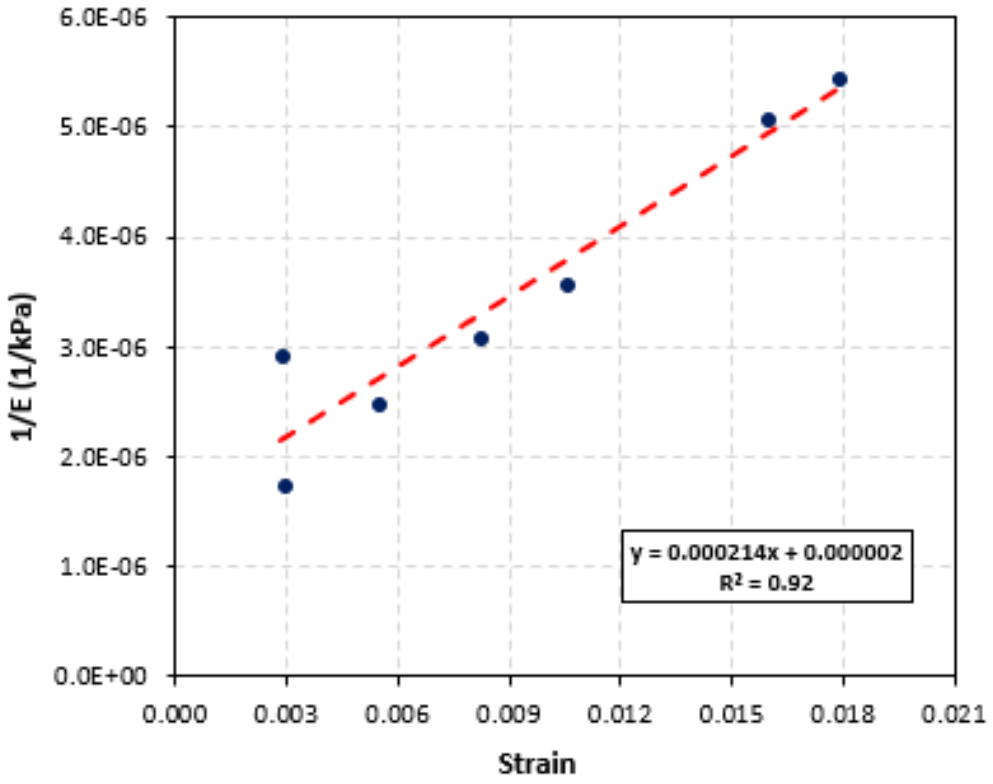

Figure F.80: Location 312 (SDPMT-6 Incremental)

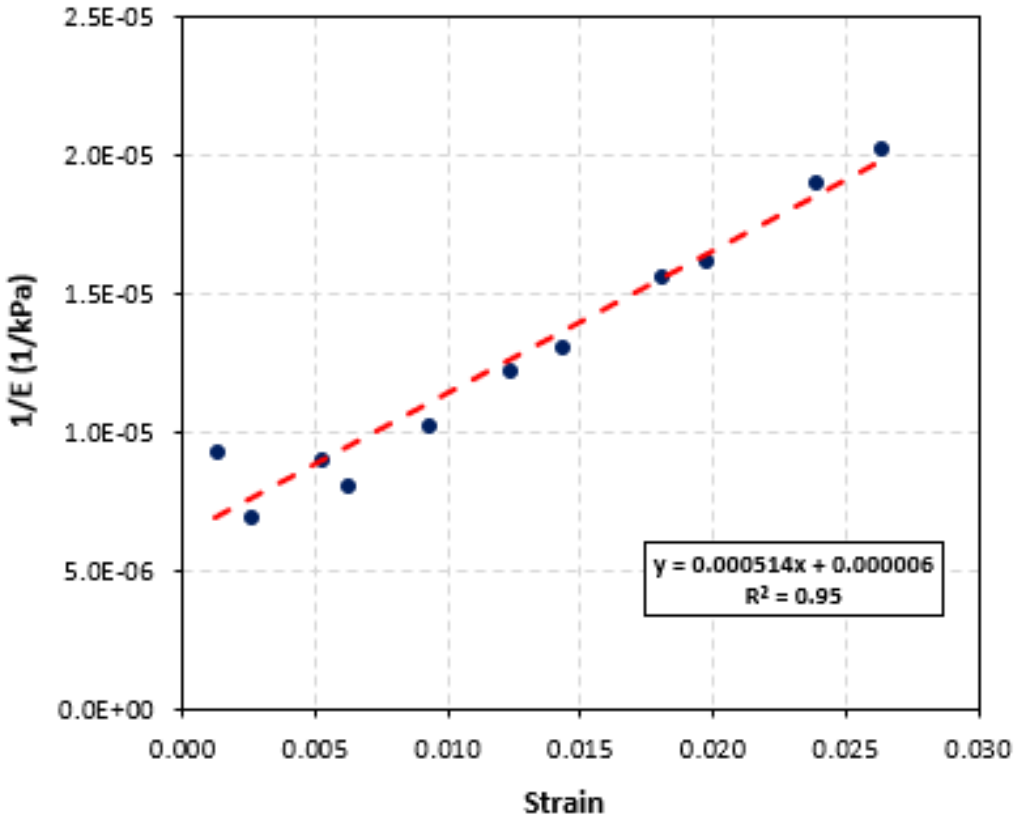

Figure F.81: Location 312 (SDPMT-12 Incremental)

Appendix G

Zorn LWD Time Deflection Data

G.1 FIT Southgate Field

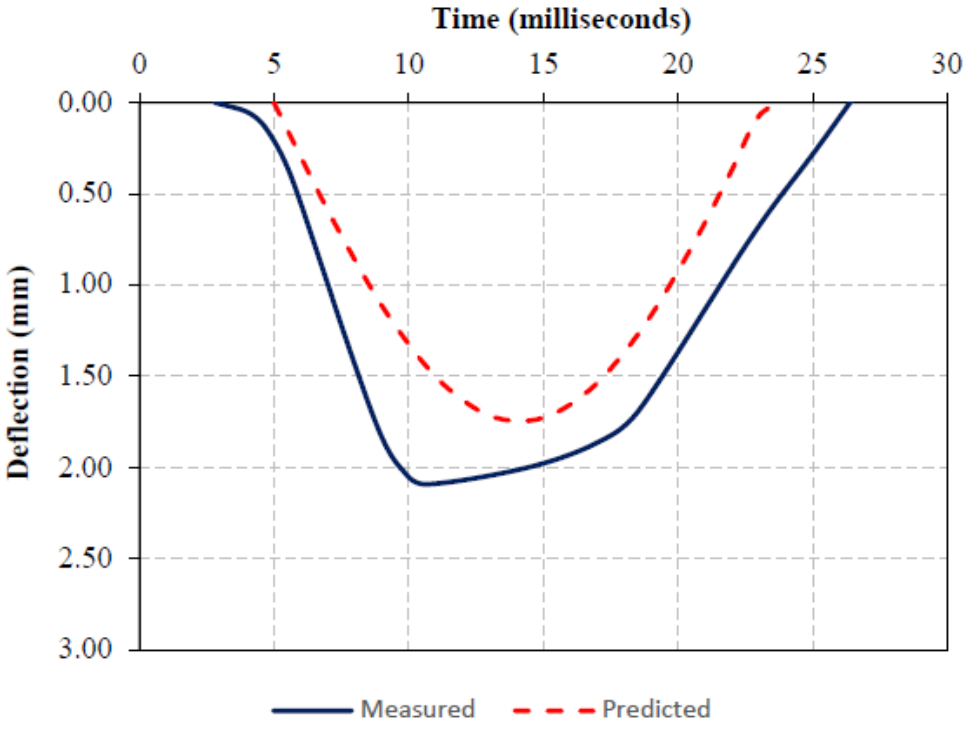

(a) 6-inch Results

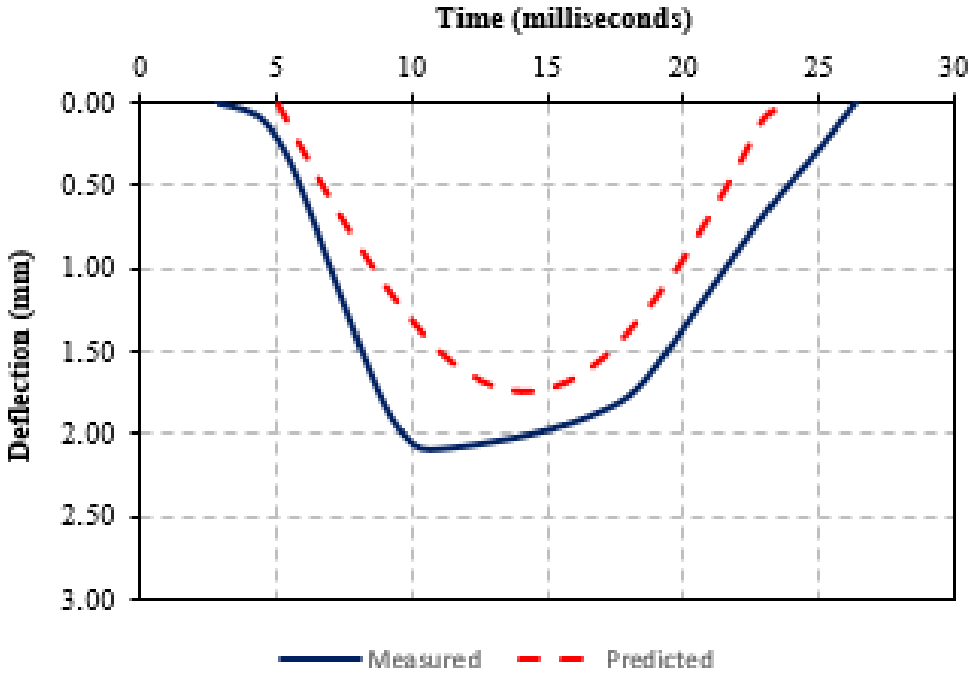

(b) 12-inch Results

Figure G.1: Measured and Predicted LWD Surface Deflections - Location 401

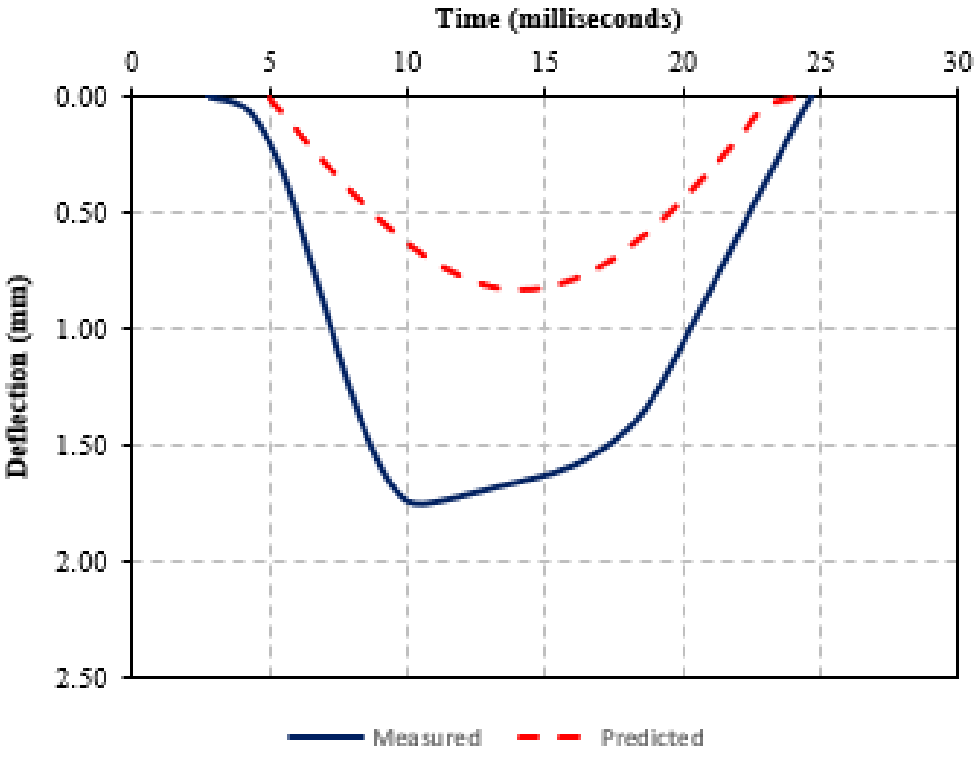

(a) 6-inch Results

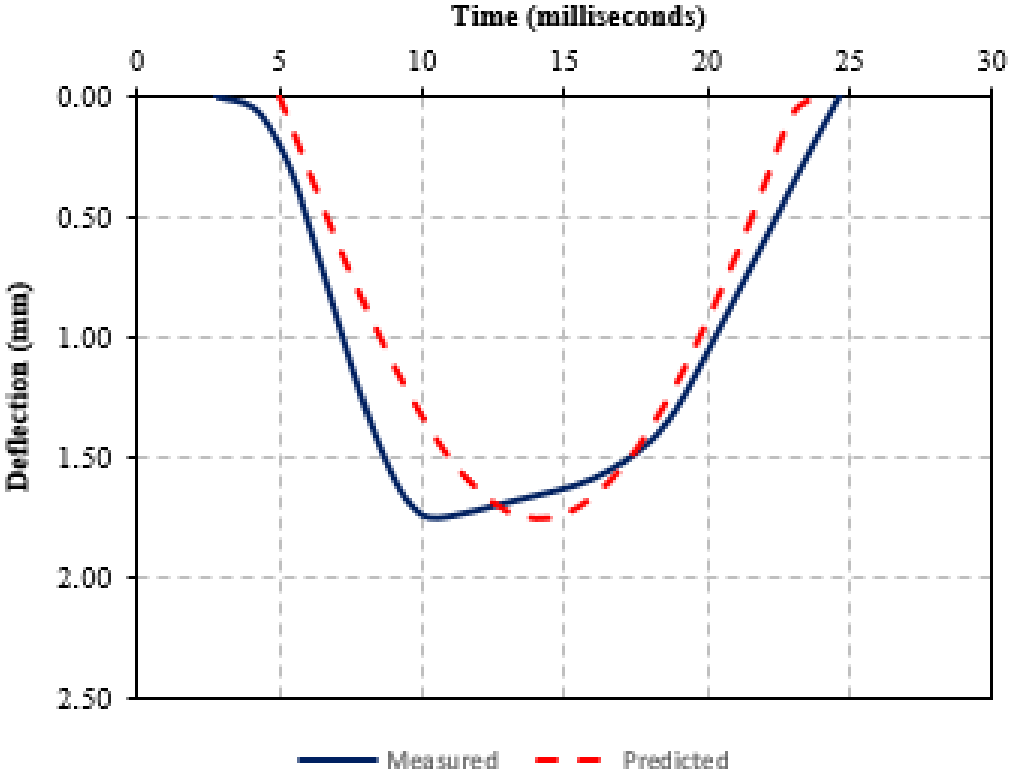

(b) 12-inch Results

Figure G.2: Measured and Predicted 9 kip FWD Surface Deflections - Location 402

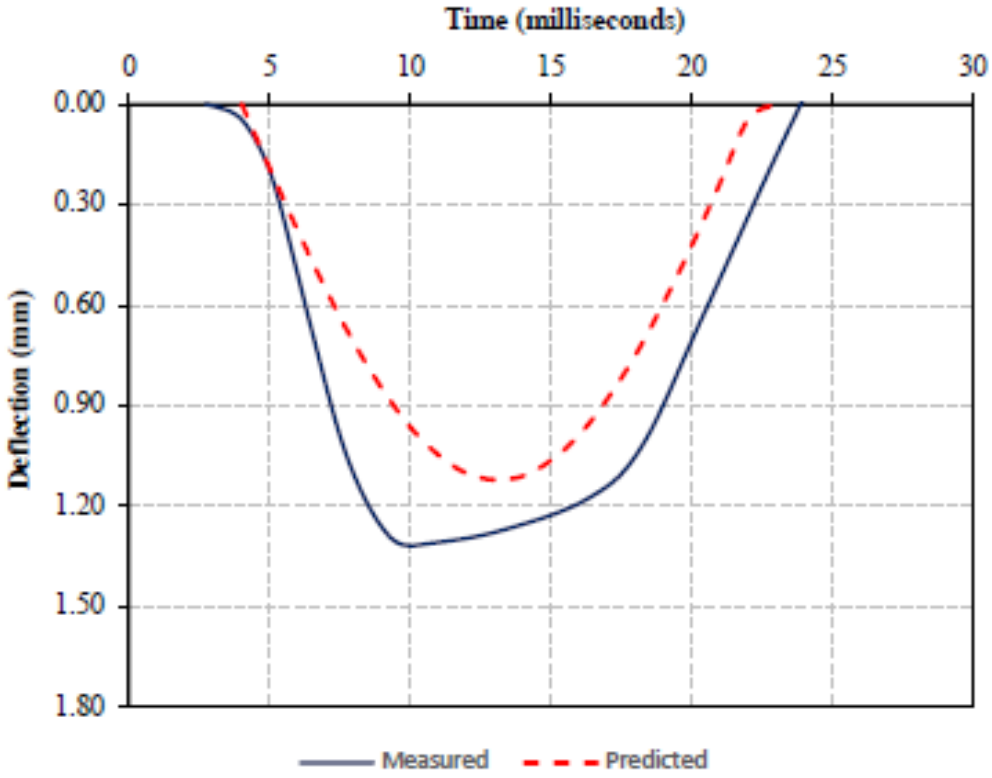

(a) 6-inch Results

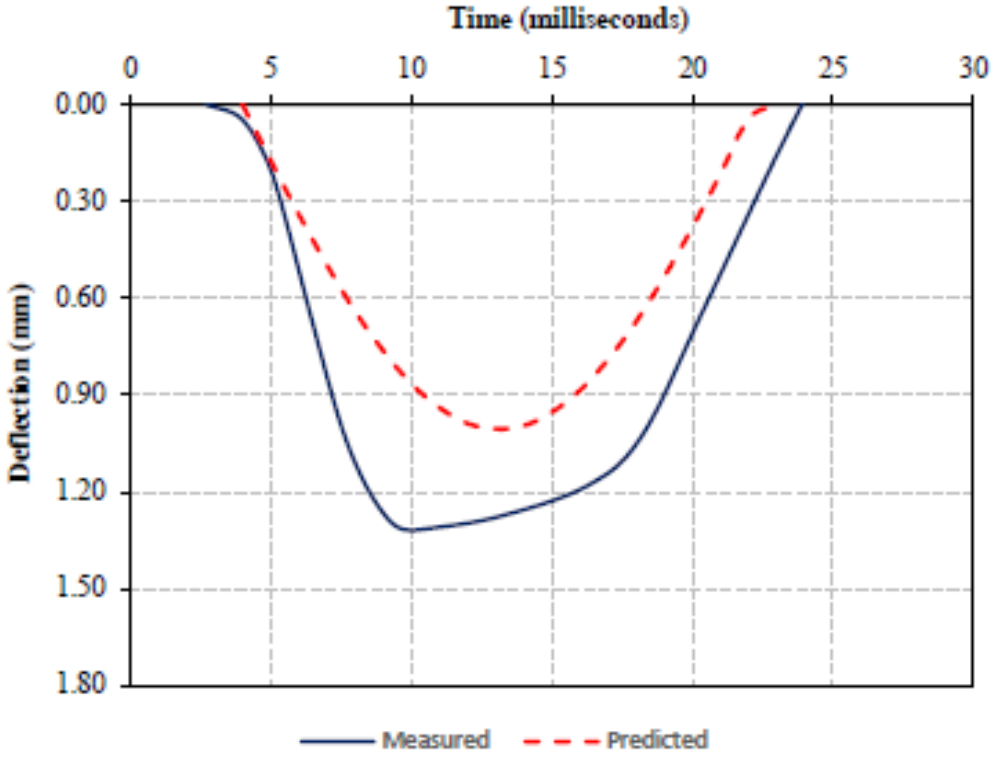

(b) 12-inch Results

Figure G.3: Measured and Predicted LWD Surface Deflections - Location 403 905

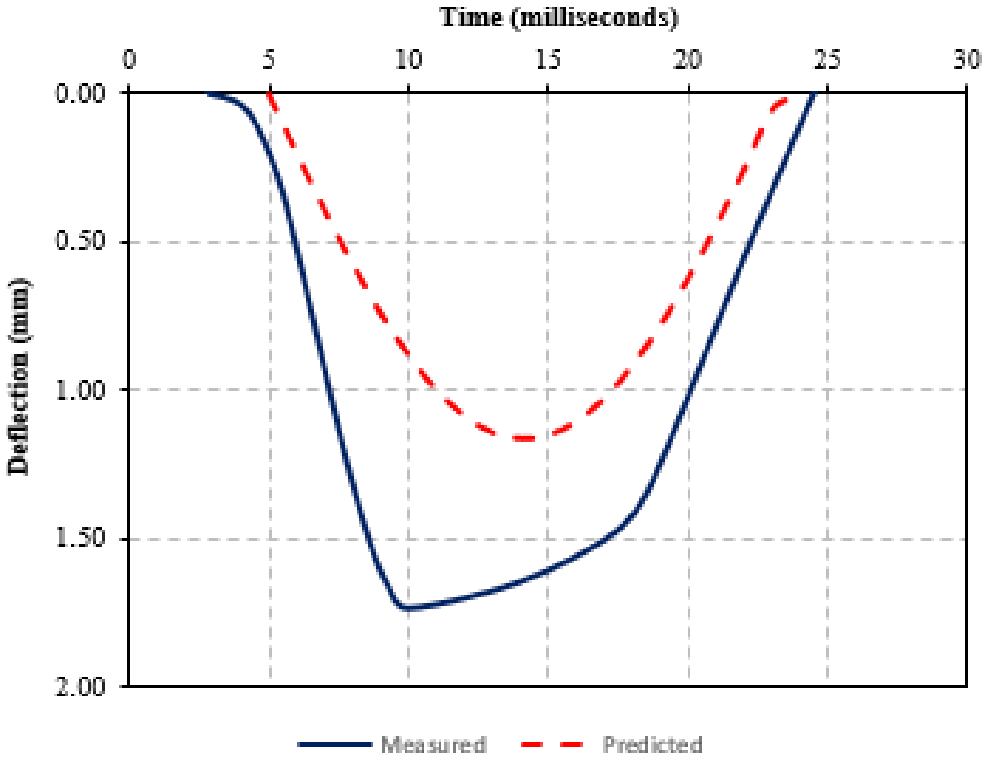

(a) 6-inch Results

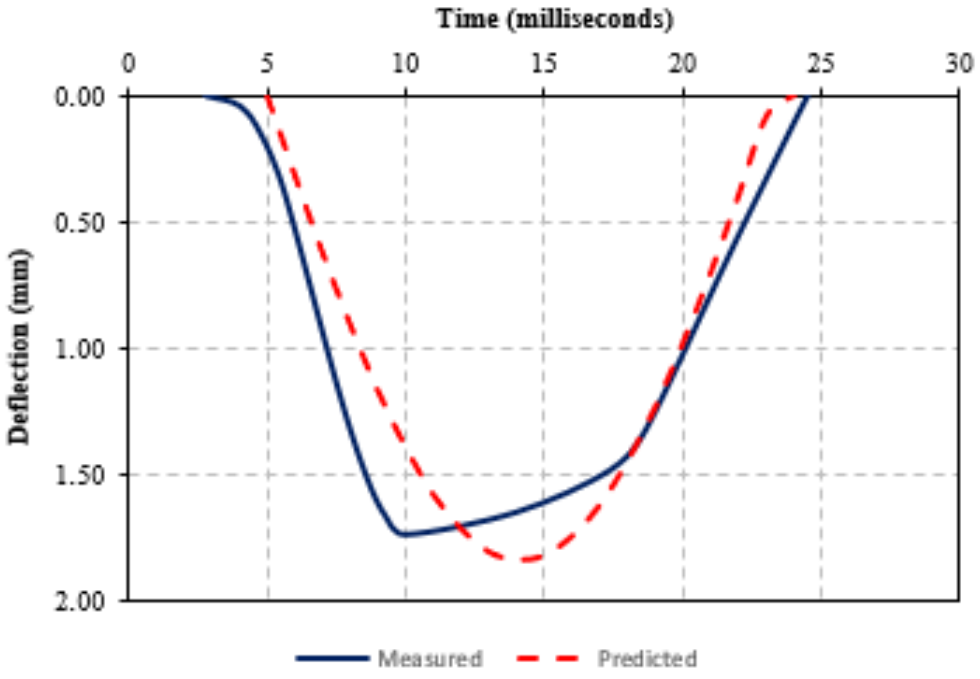

(b) 12-inch Results

Figure G.4: Measured and Predicted LWD Surface Deflections - Location 404

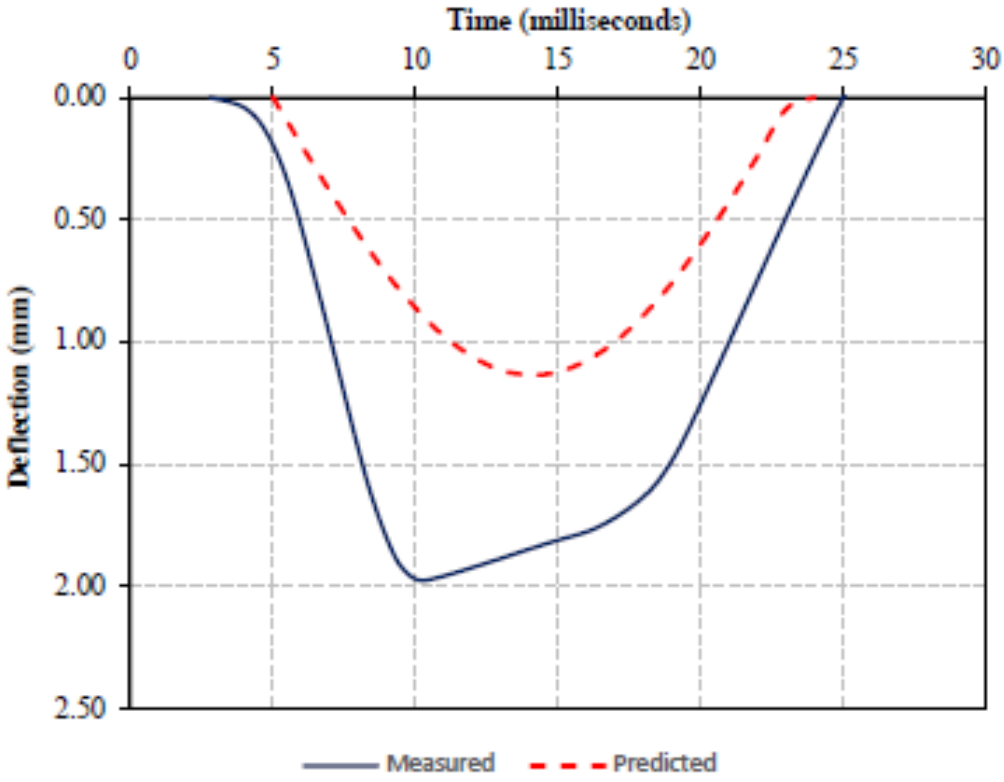

(a) 6-inch Results

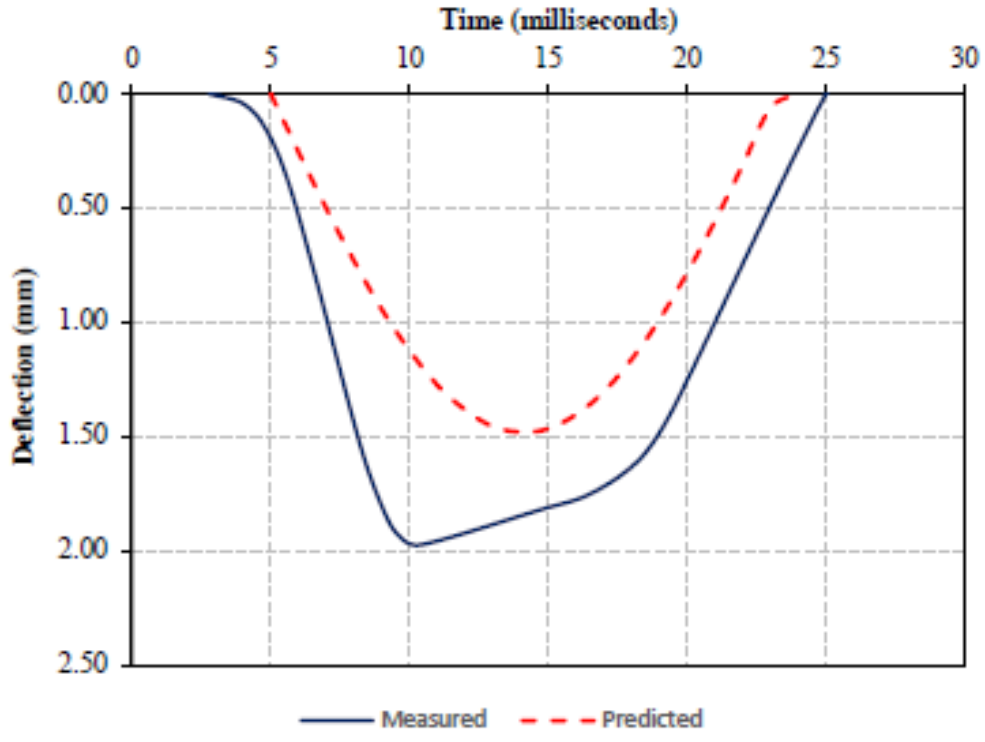

(b) 12-inch Results

Figure G.5: Measured and Predicted LWD Surface Deflections - Location 405

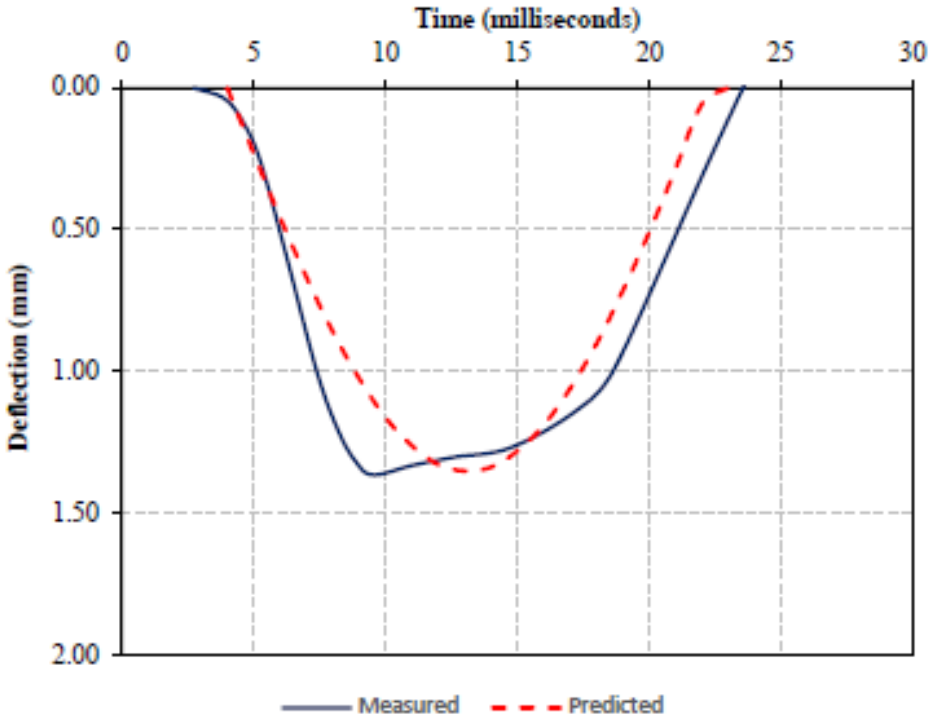

(a) 6-inch Results

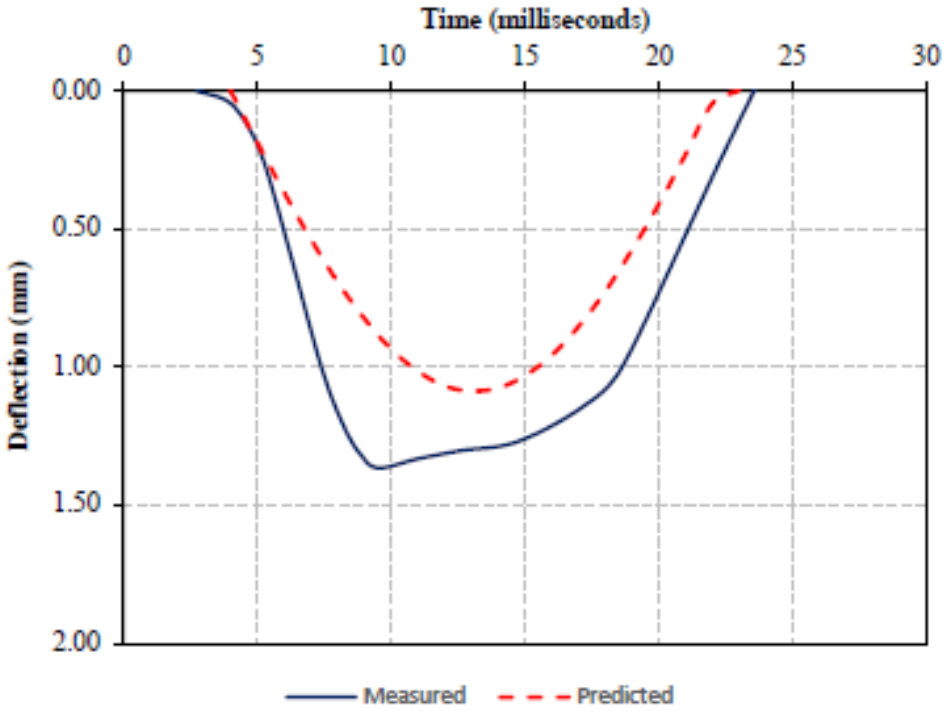

(b) 12-inch Results

Figure G.6: Measured and Predicted LWD Surface Deflections - Location 406

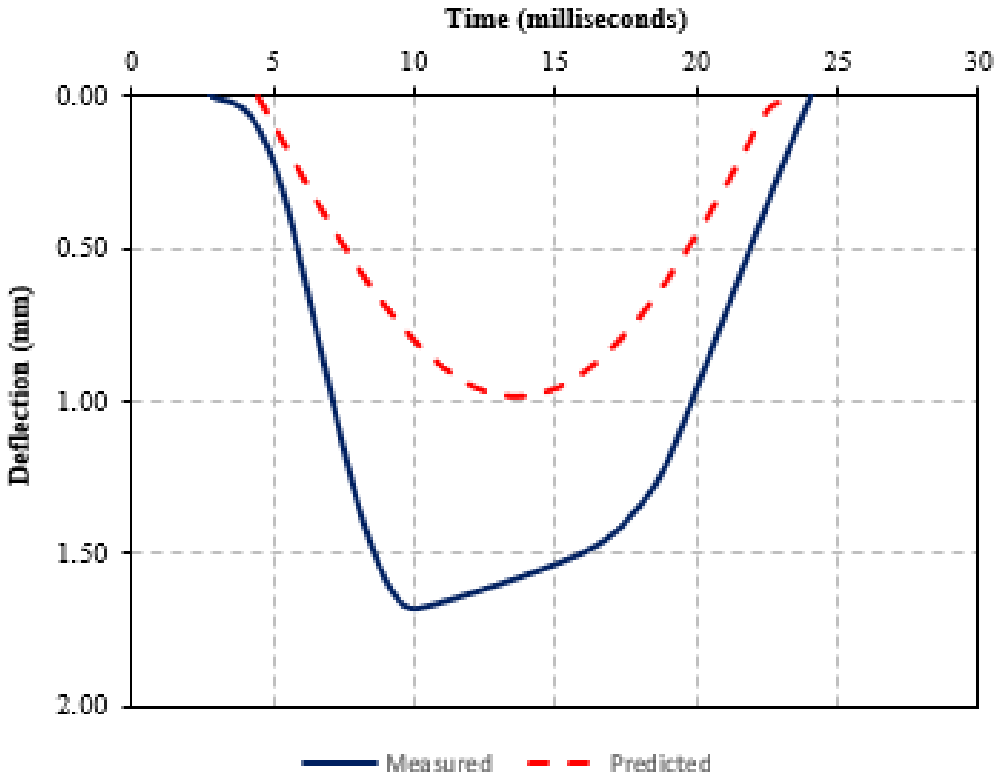

(a) 6-inch Results

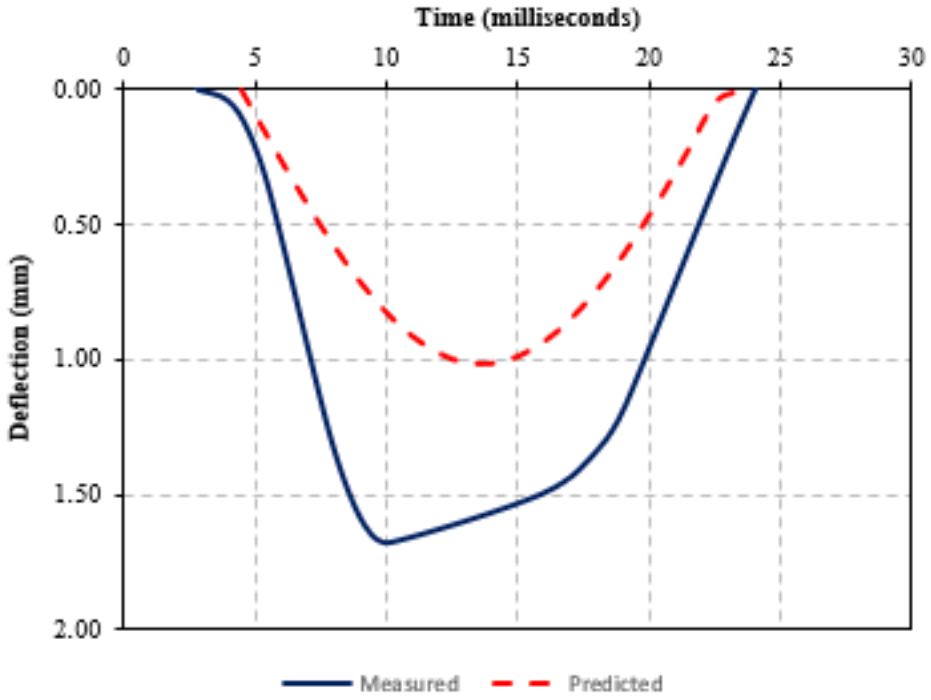

(b) 12-inch Results

Figure G.7: Measured and Predicted LWD Surface Deflections - Location 407

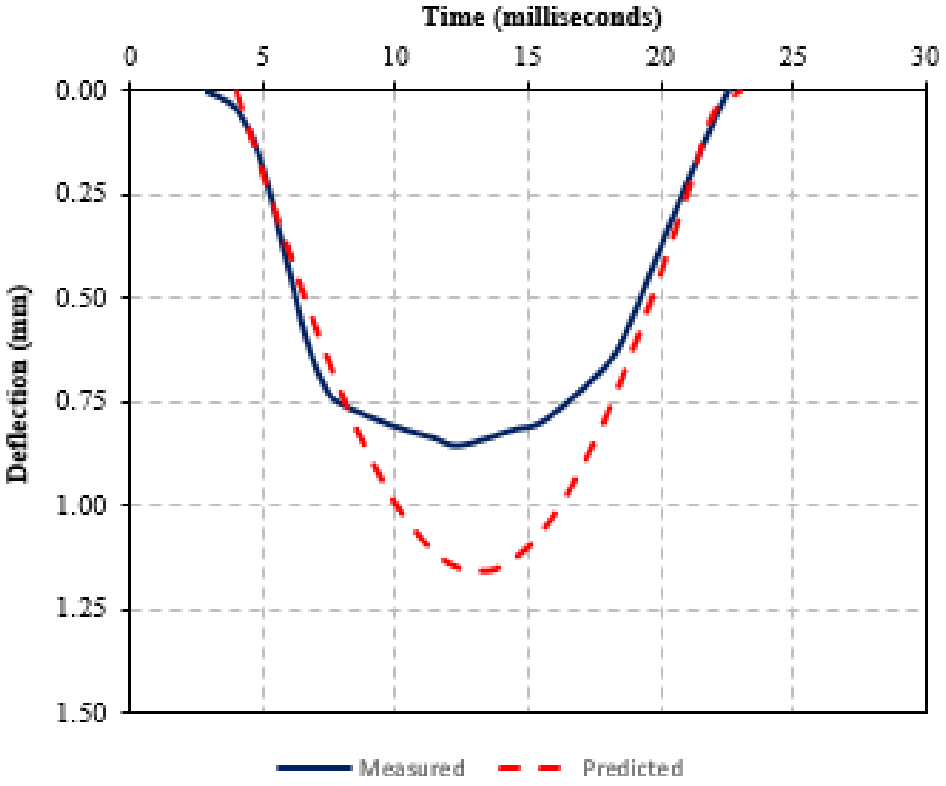

(a) 6-inch Results

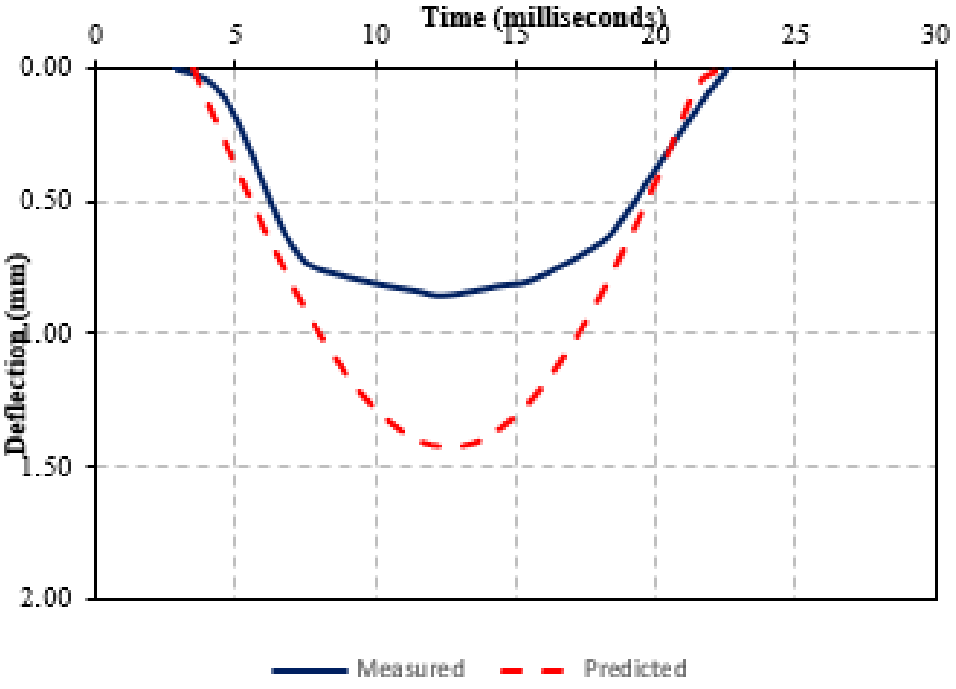

(b) 12-inch Results

Figure G.8: Measured and Predicted LWD Surface Deflections - Location 408

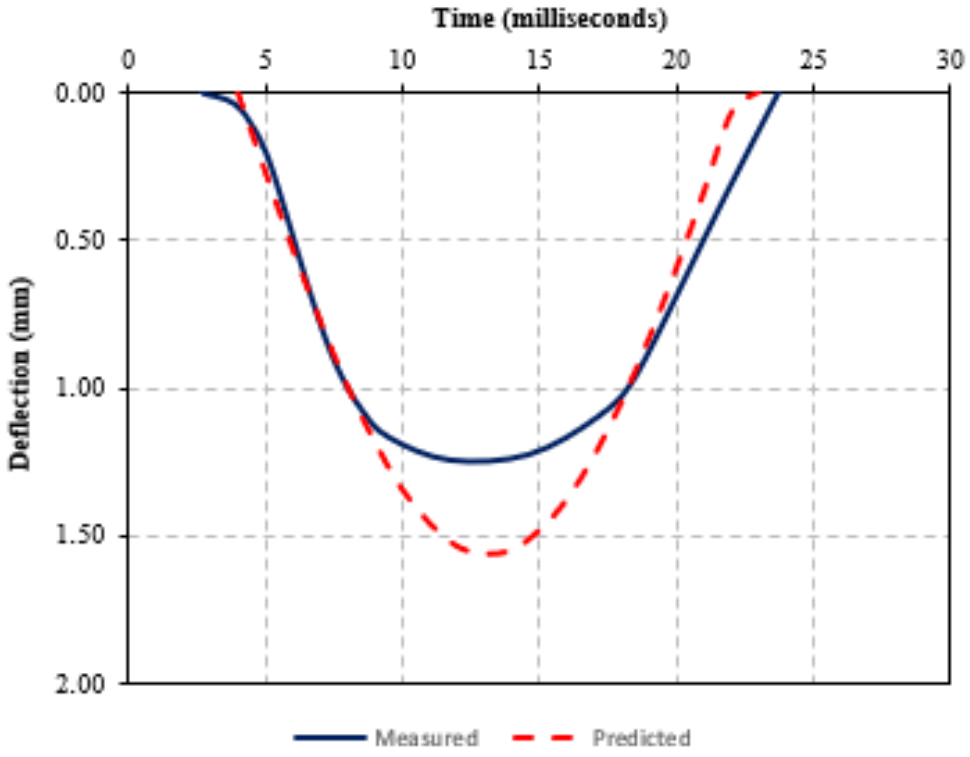

(a) 6-inch Results

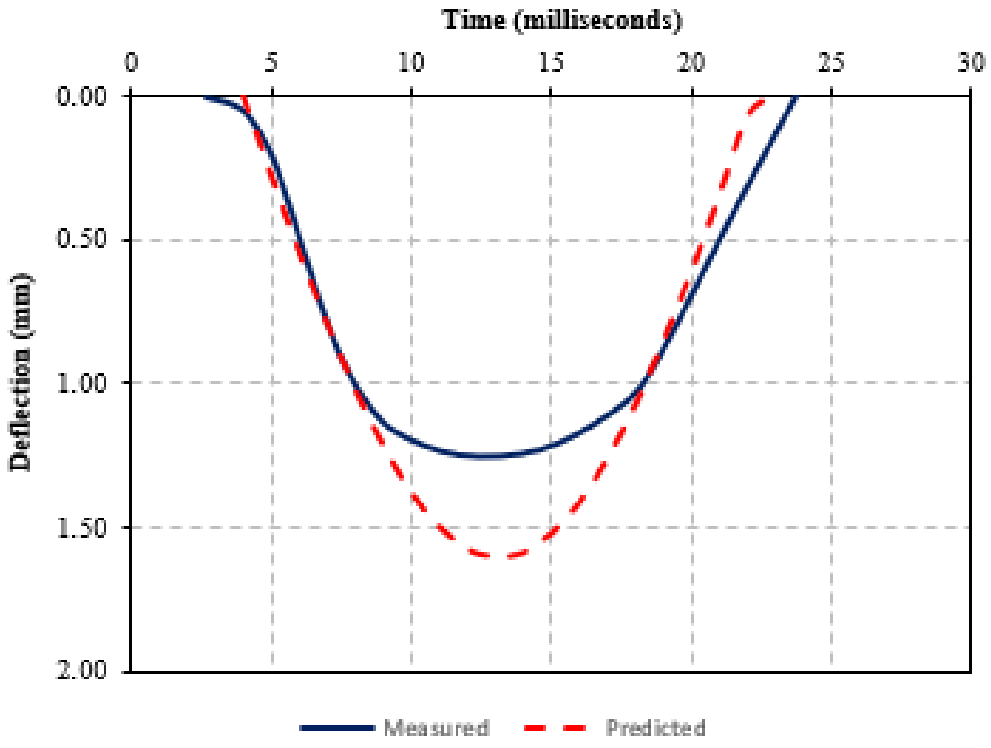

(b) 12-inch Results

Figure G.9: Measured and Predicted LWD Surface Deflections - Location 409

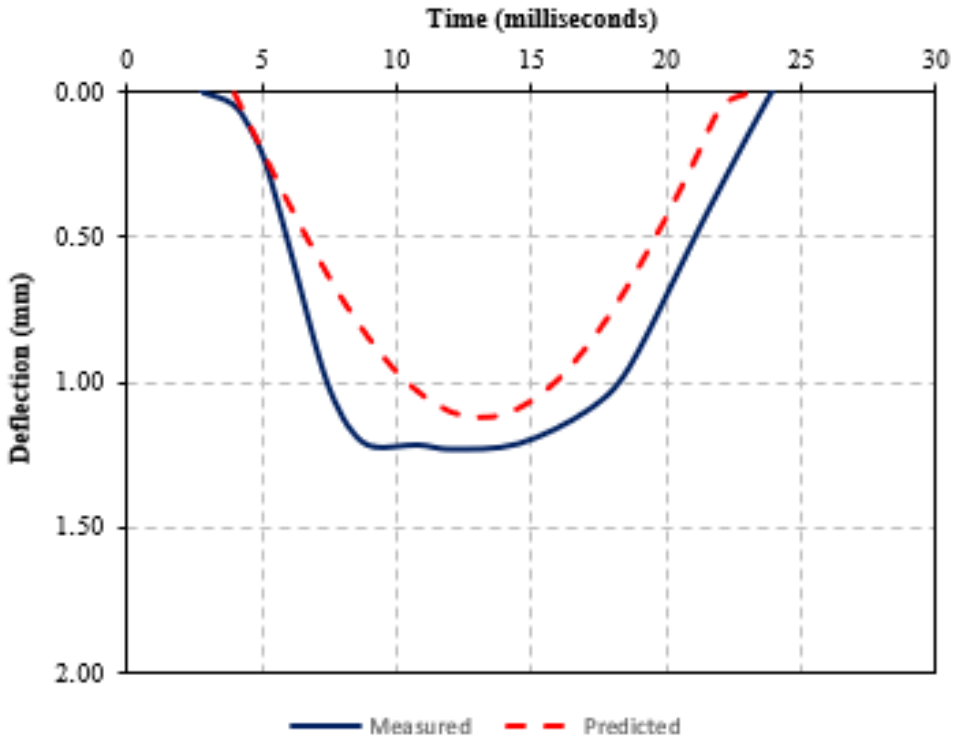

(a) 6-inch Results

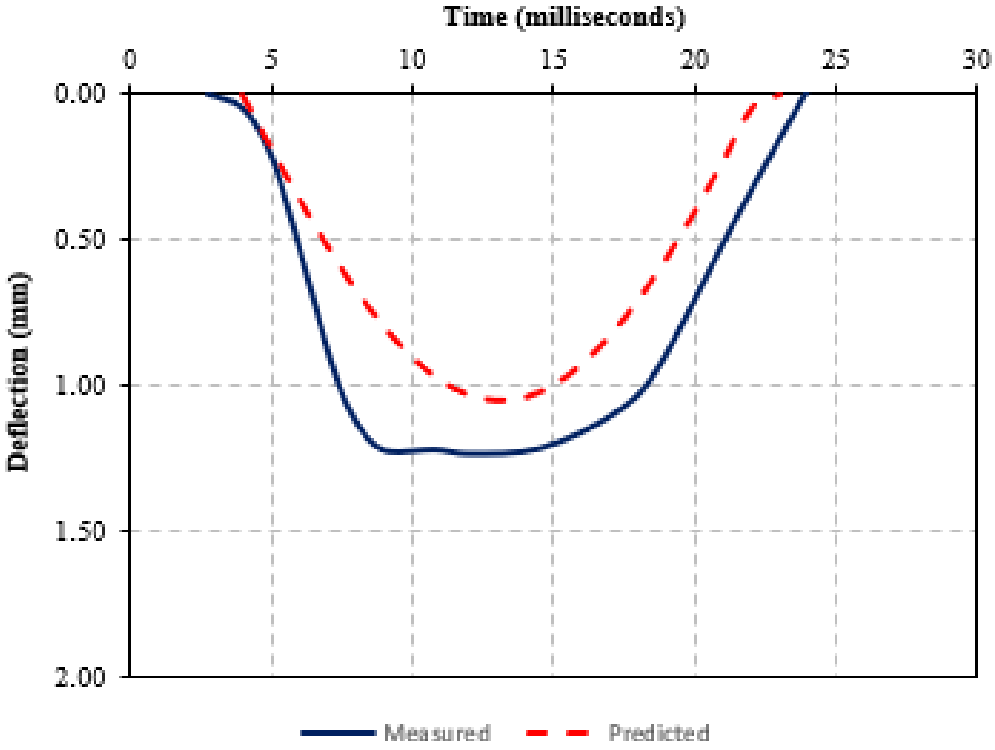

(b) 12-inch Results

Figure G.10: Measured and Predicted LWD Surface Deflections - Location 410

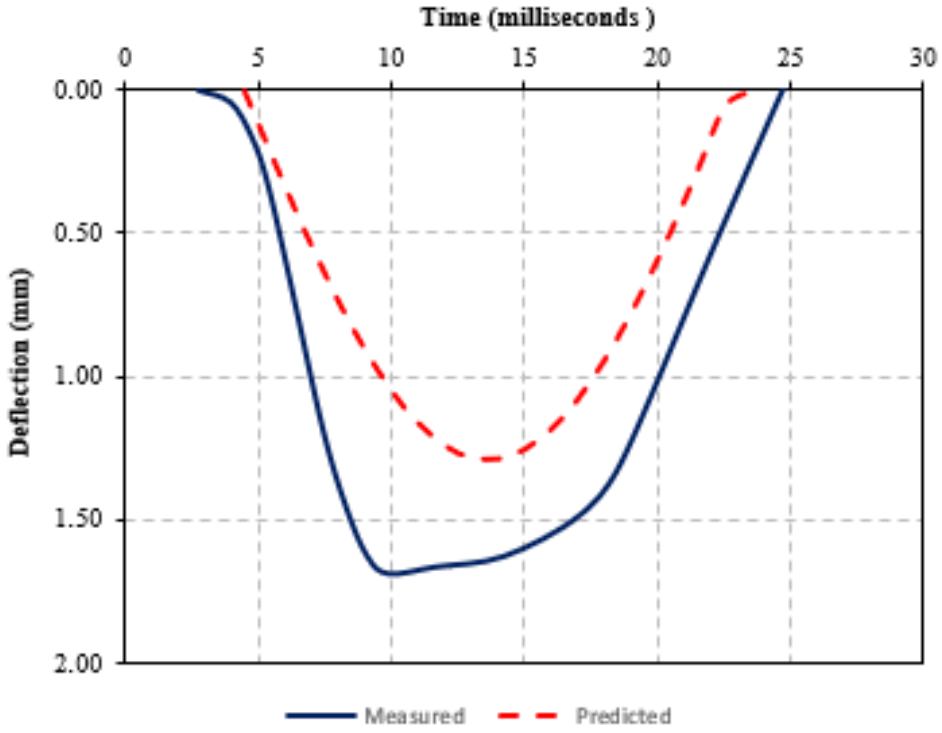

(a) 6-inch Results

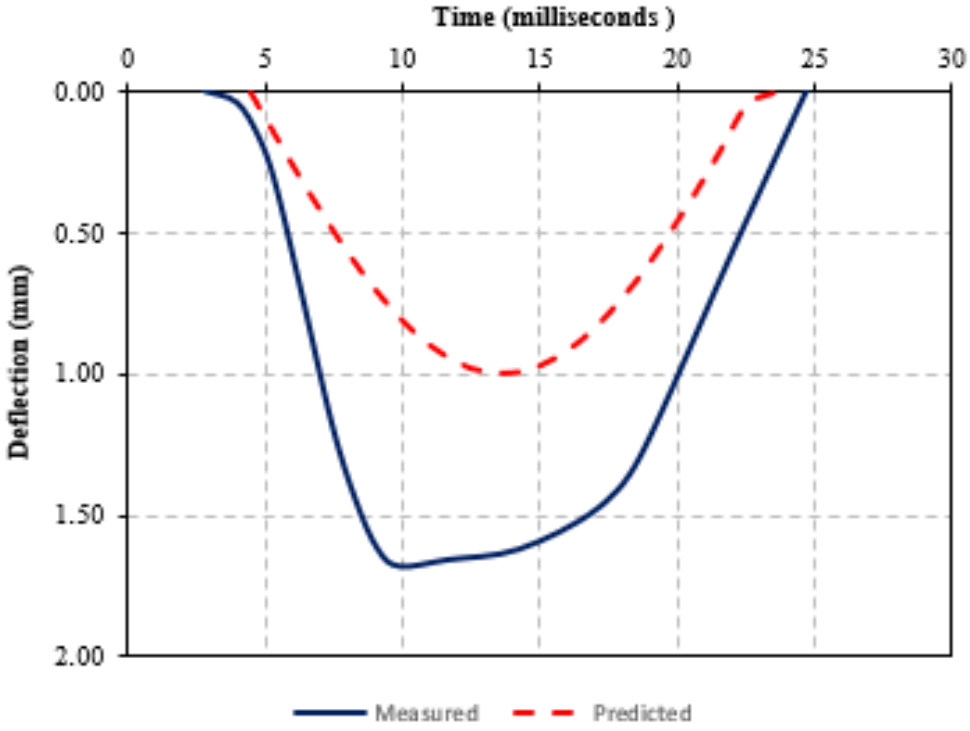

(b) 12-inch Results

Figure G.11: Measured and Predicted LWD Surface Deflections - Location 411

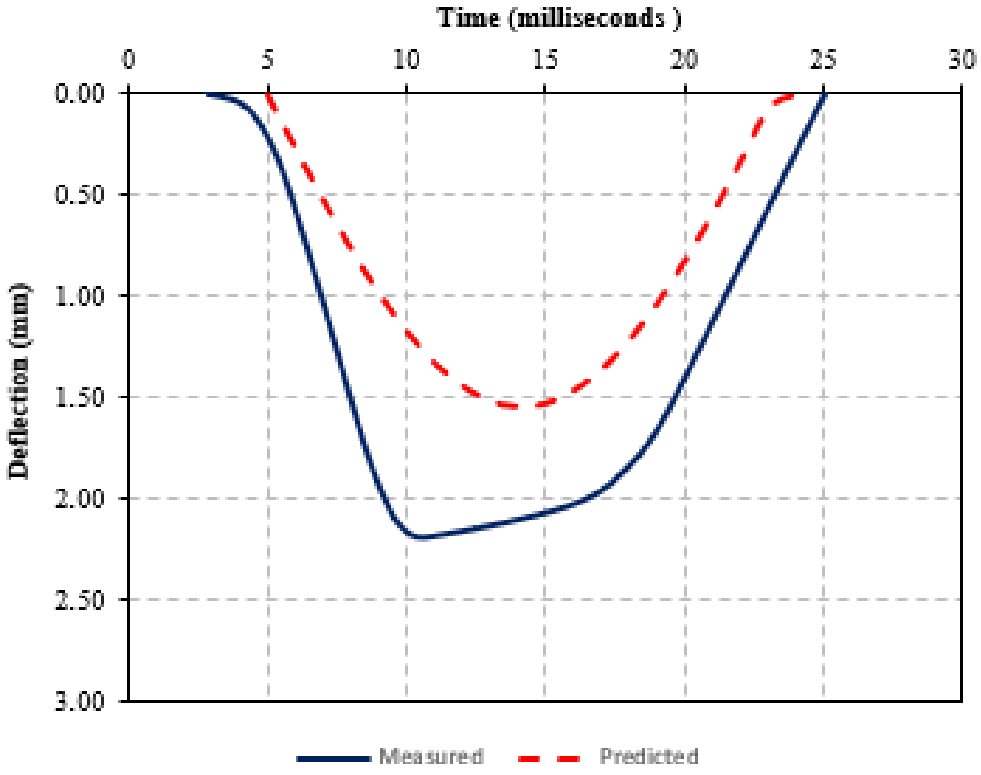

(a) 6-inch Results

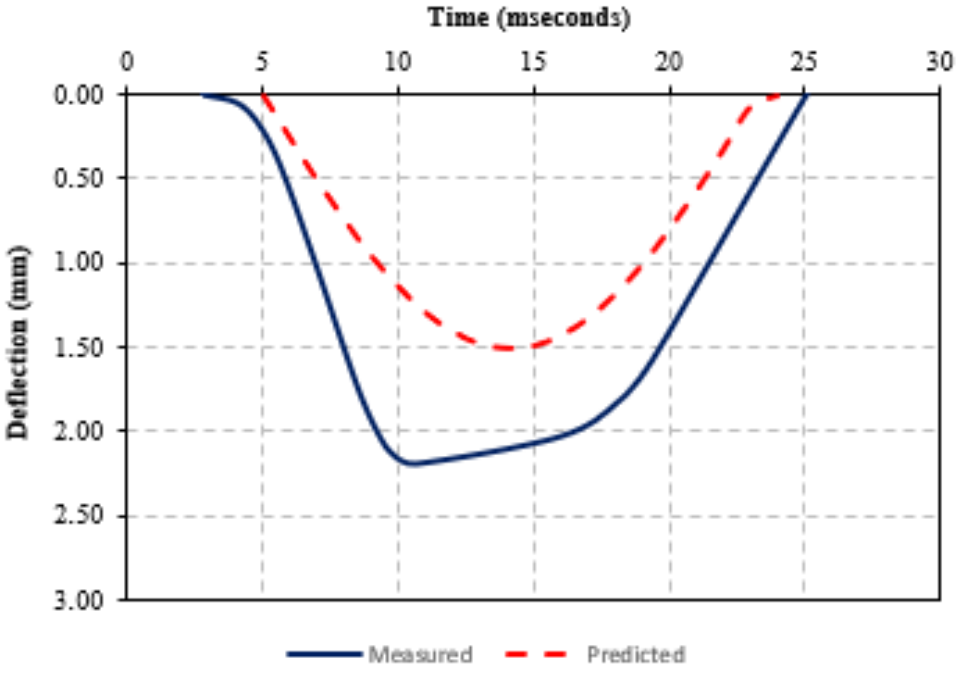

(b) 12-inch Results

Figure G.12: Measured and Predicted LWD Surface Deflections - Location 412

G.2 FIT Olin Complex

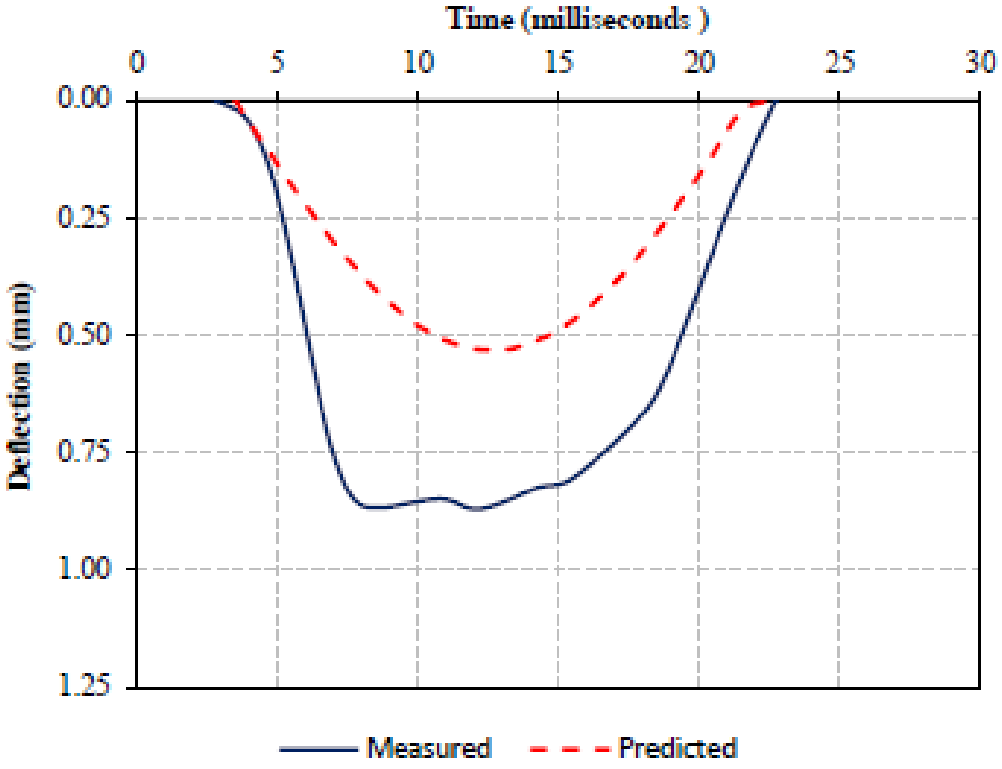

(a) 6-inch Results

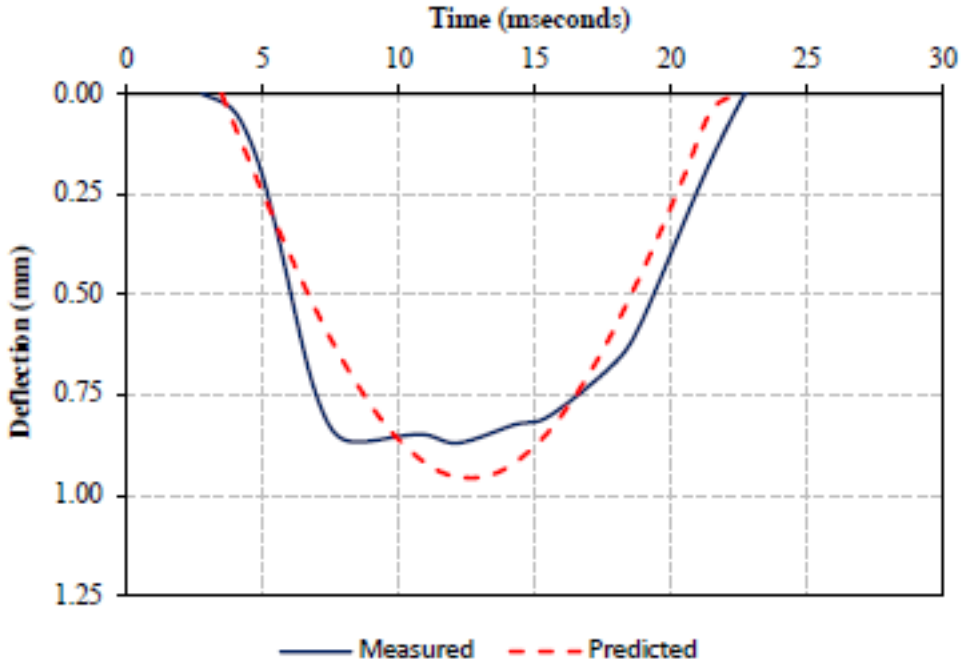

(b) 12-inch Results

Figure G.13: Measured and Predicted LWD Surface Deflections - Location 201

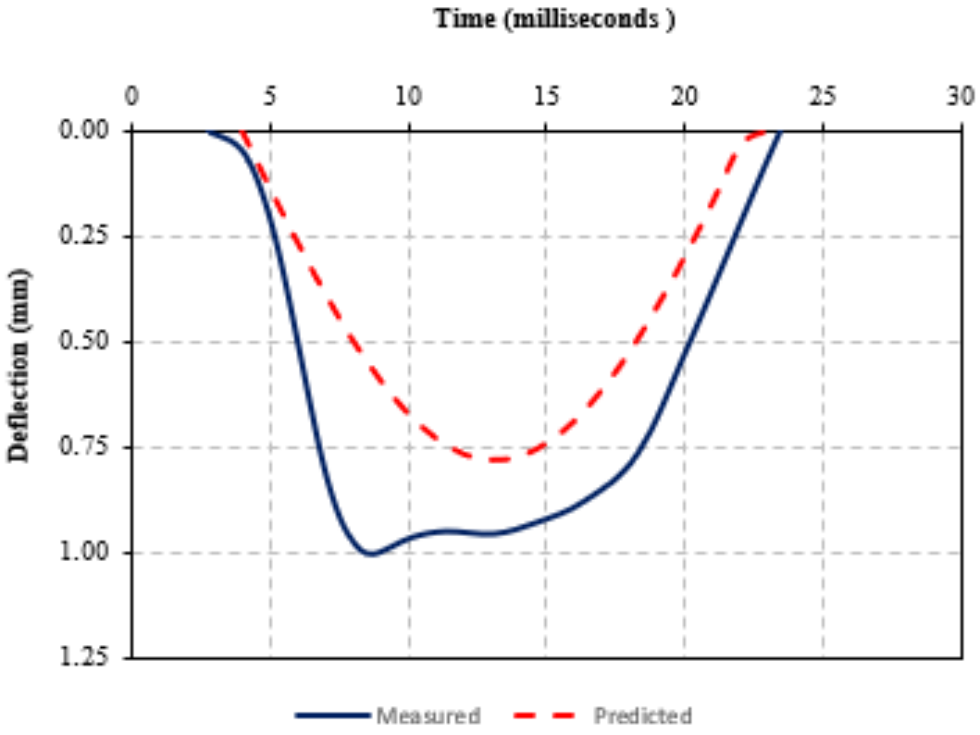

(a) 6-inch Results

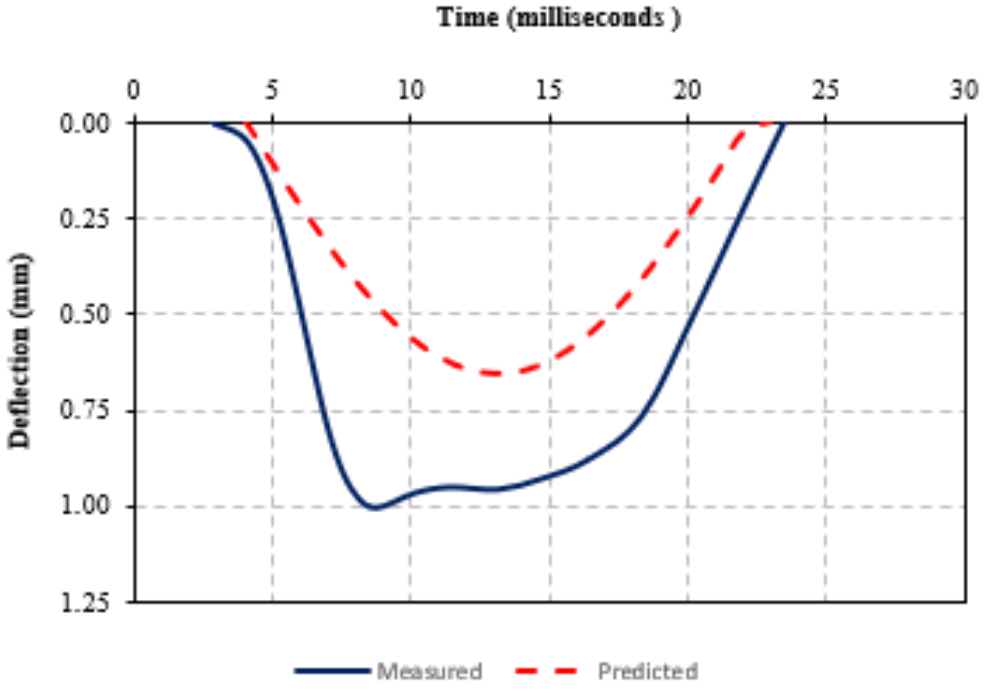

(b) 12-inch Results

Figure G.14: Measured and Predicted LWD Surface Deflections - Location 202

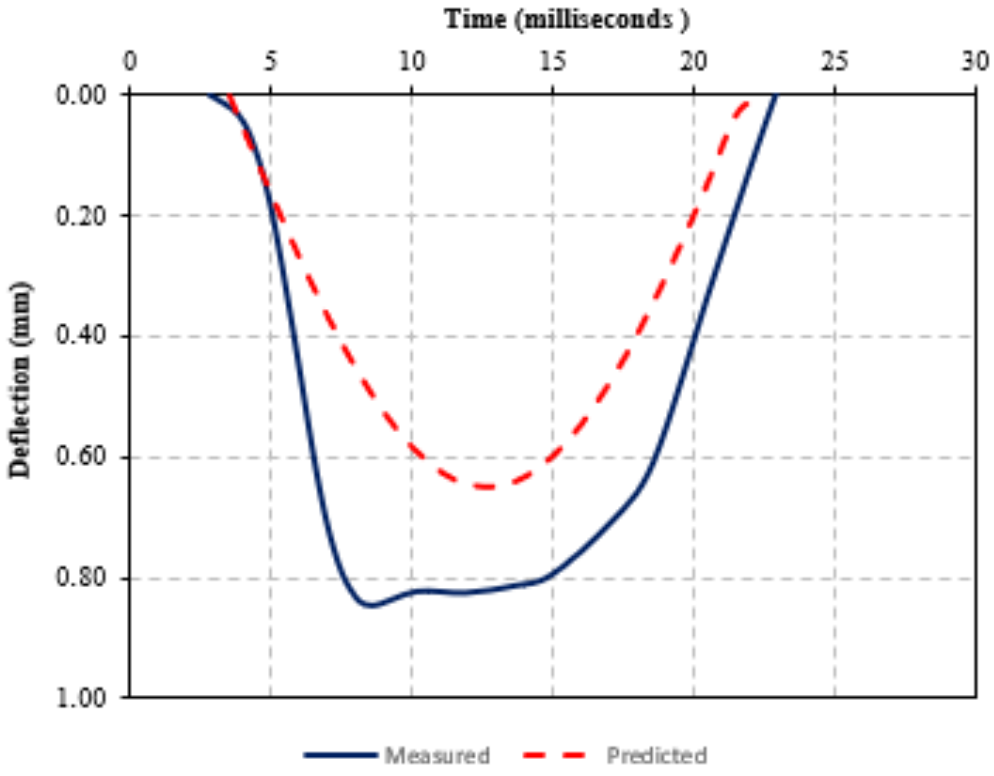

(a) 6-inch Results

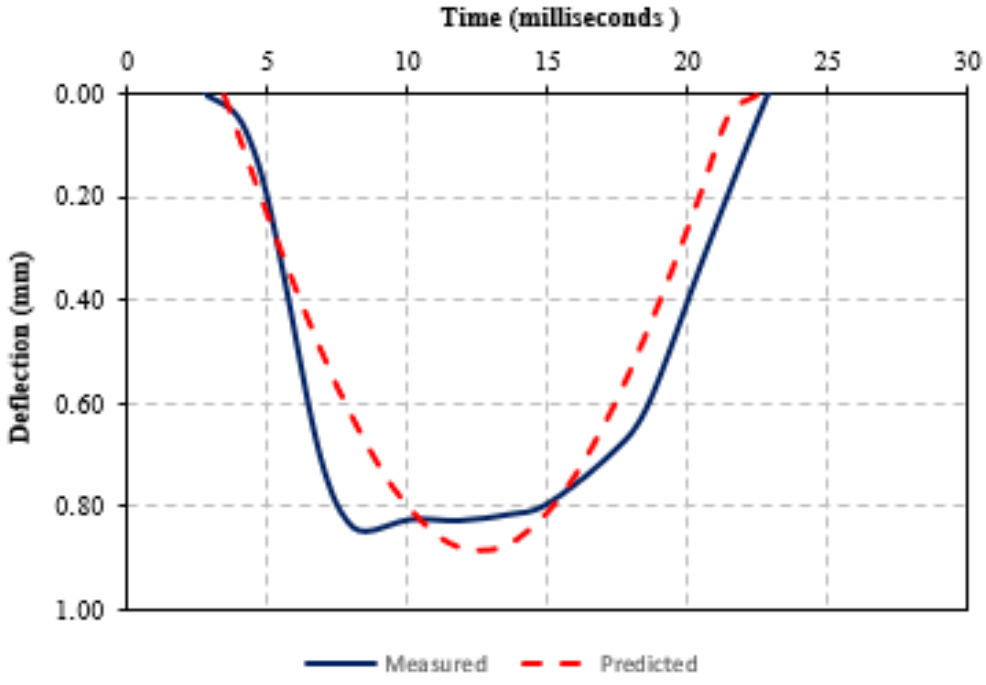

(b) 12-inch Results

Figure G.15: Measured and Predicted LWD Surface Deflections - Location 203 918

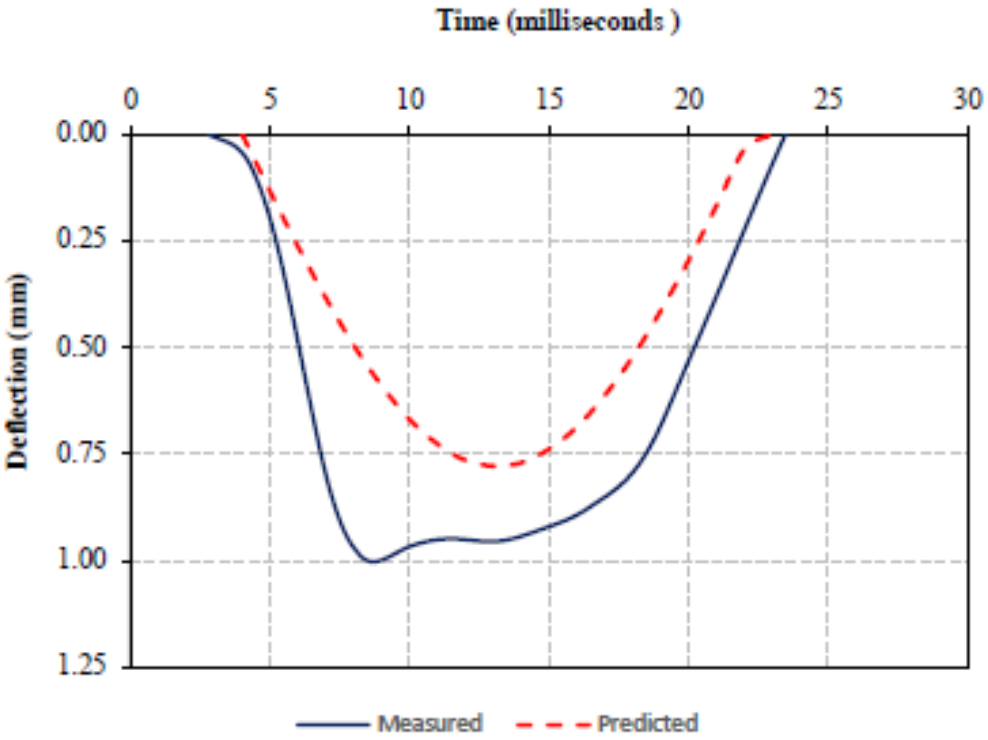

(a) 6-inch Results

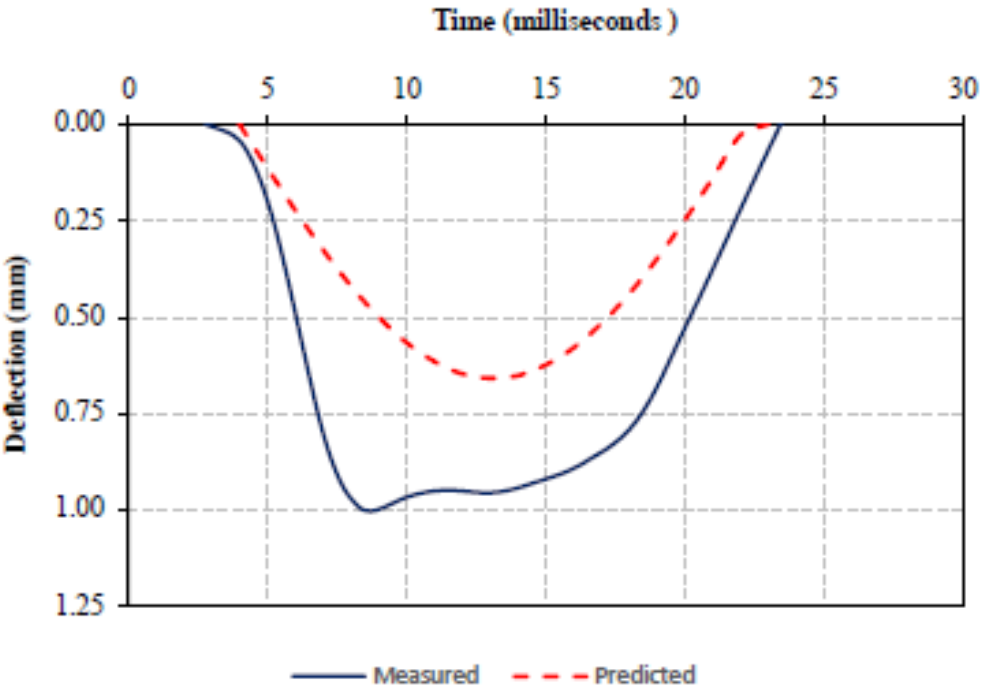

(b) 12-inch Results

Figure G.16: Measured and Predicted LWD Surface Deflections - Location 204

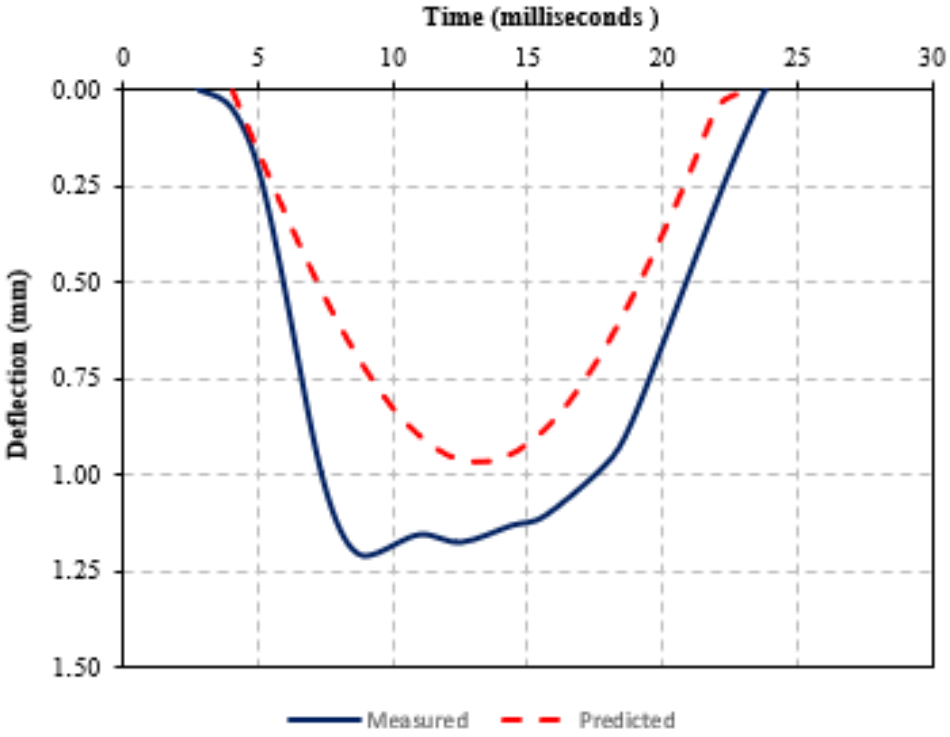

(a) 6-inch Results

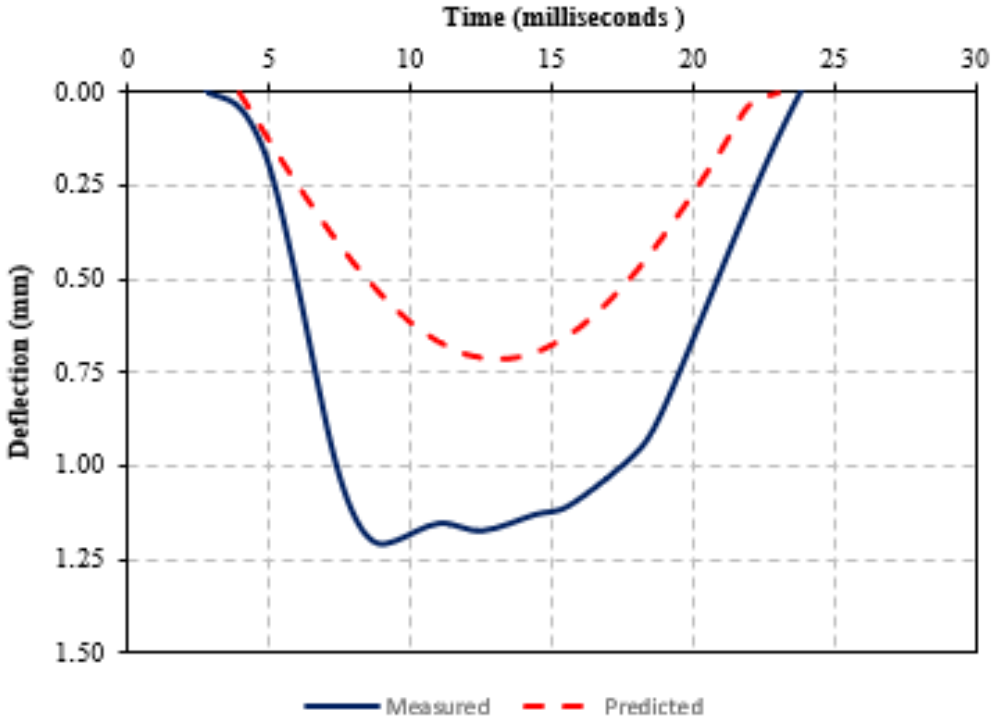

(b) 12-inch Results

Figure G.17: Measured and Predicted LWD Surface Deflections - Location 205

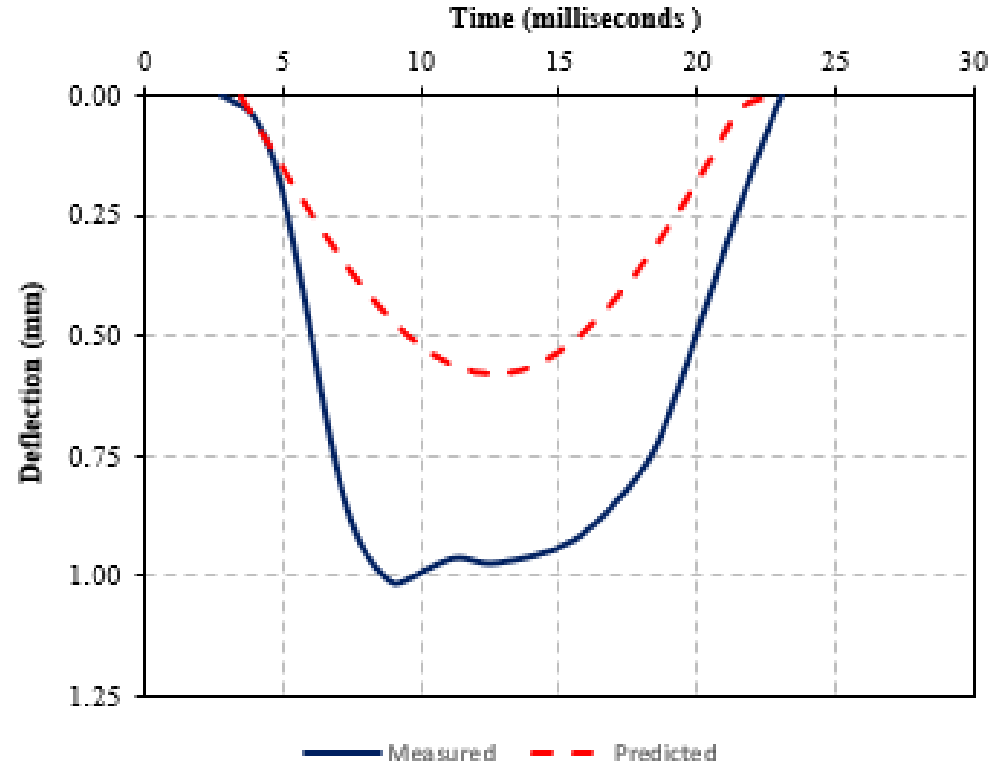

(a) 6-inch Results

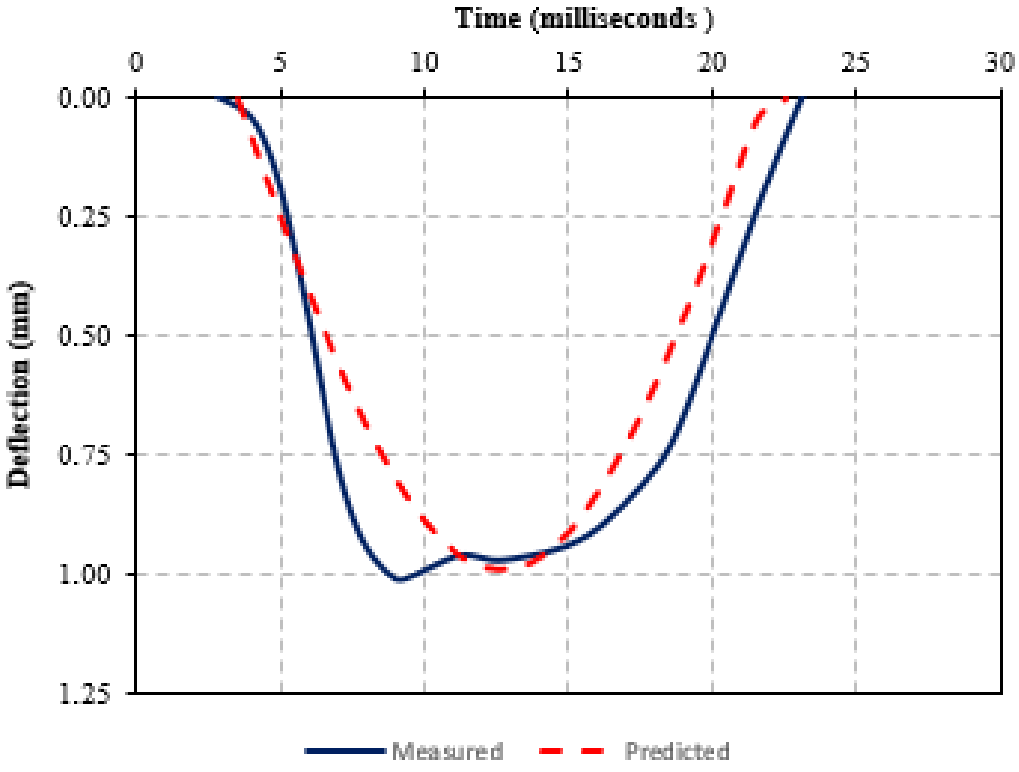

(b) 12-inch Results

Figure G.18: Measured and Predicted FWD Surface Deflections - Location 206

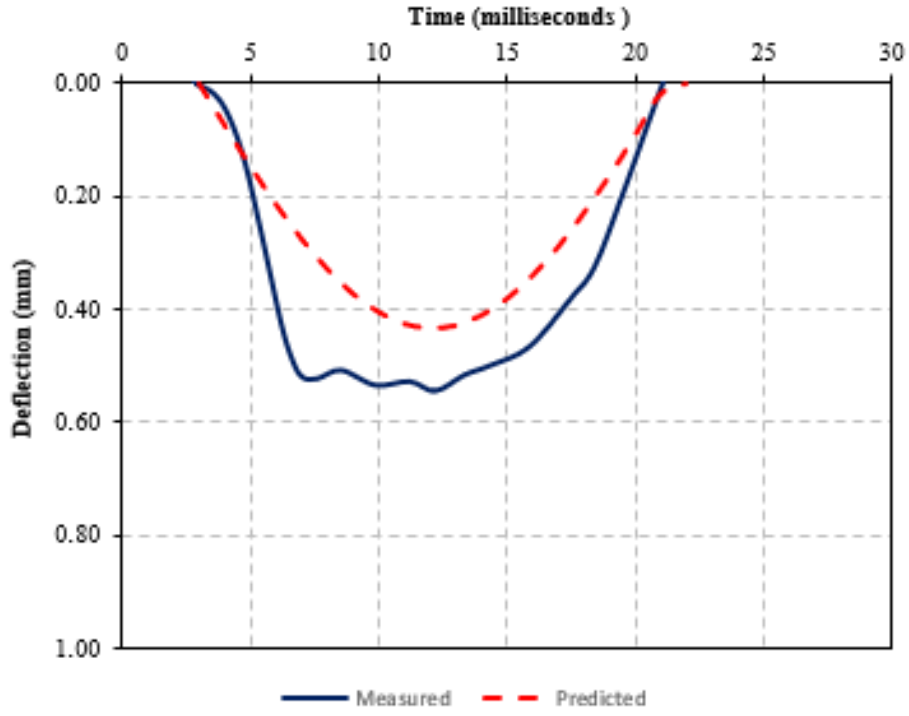

(a) 6-inch Results

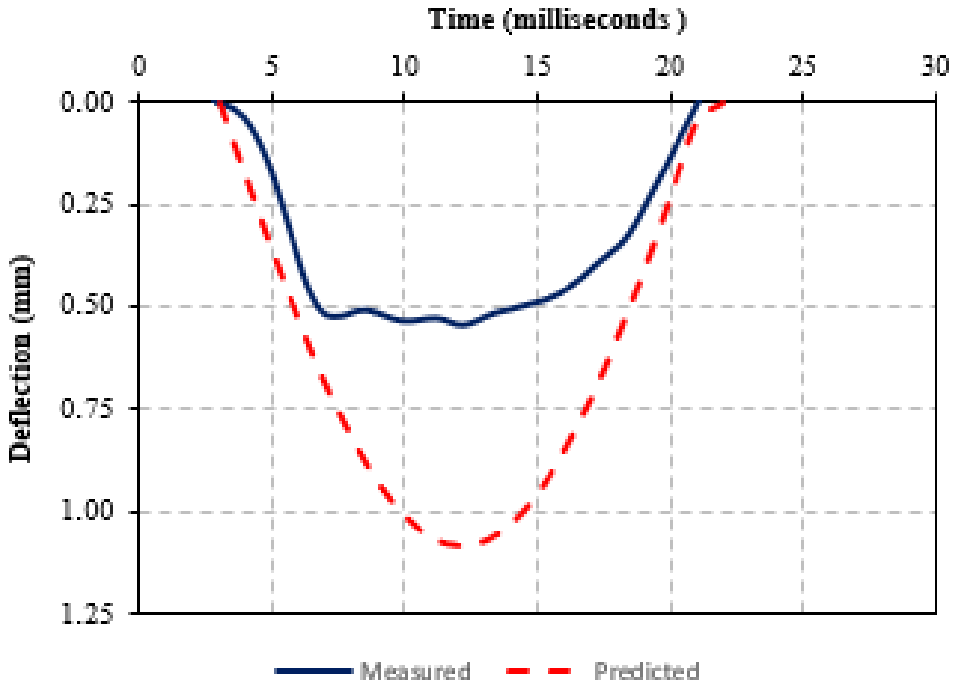

(b) 12-inch Results

Figure G.19: Measured and Predicted LWD Surface Deflections - Location 207

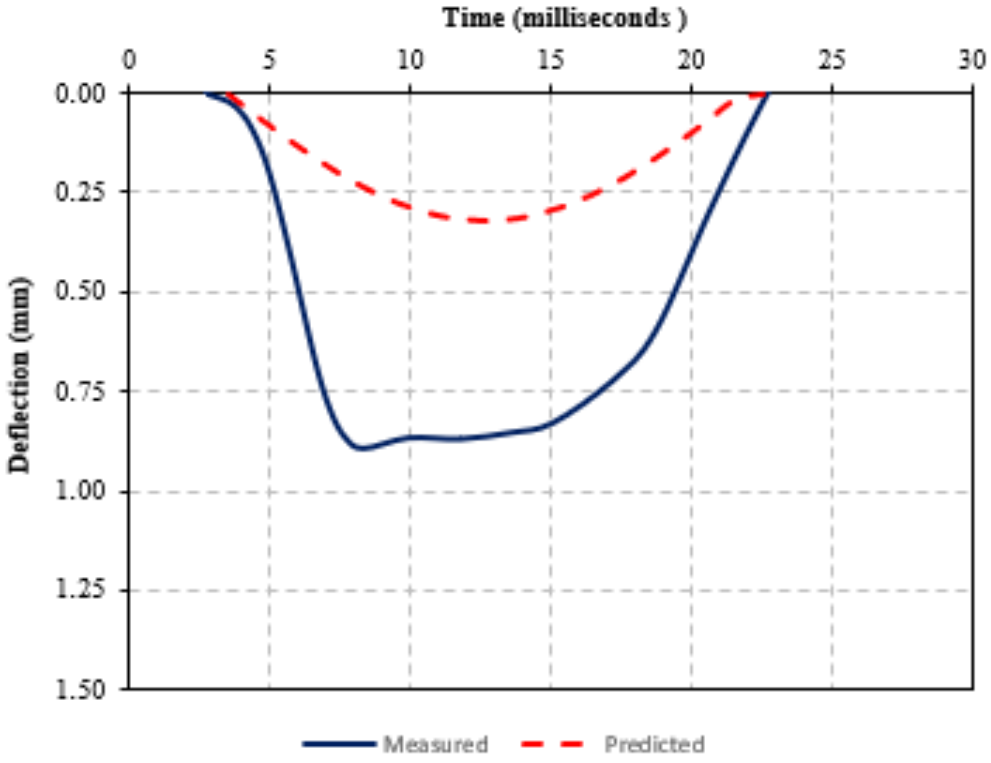

(a) 6-inch Results

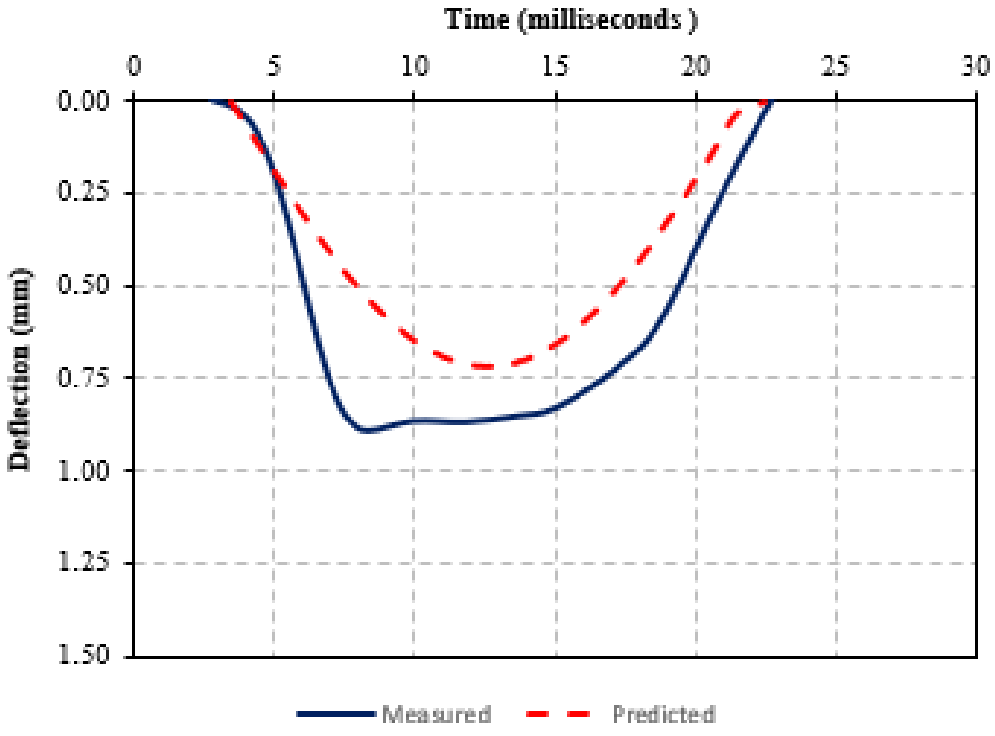

(b) 12-inch Results

Figure G.20: Measured and Predicted LWD Surface Deflections - Location 208

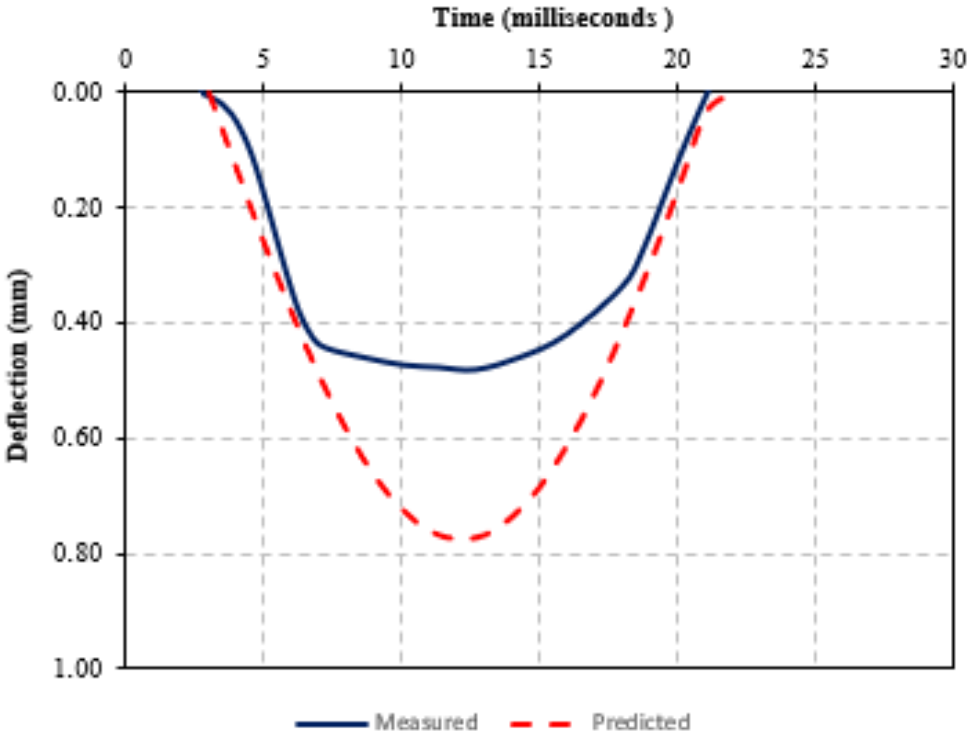

(a) 6-inch Results

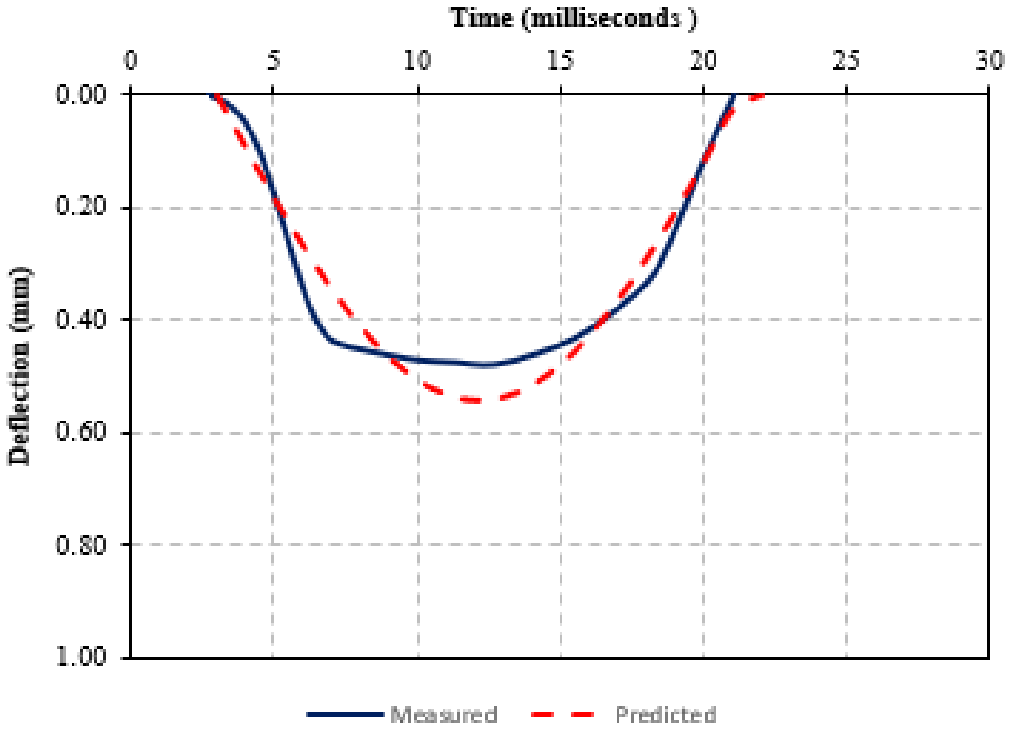

(b) 12-inch Results

Figure G.21: Measured and Predicted LWD Surface Deflections - Location 209

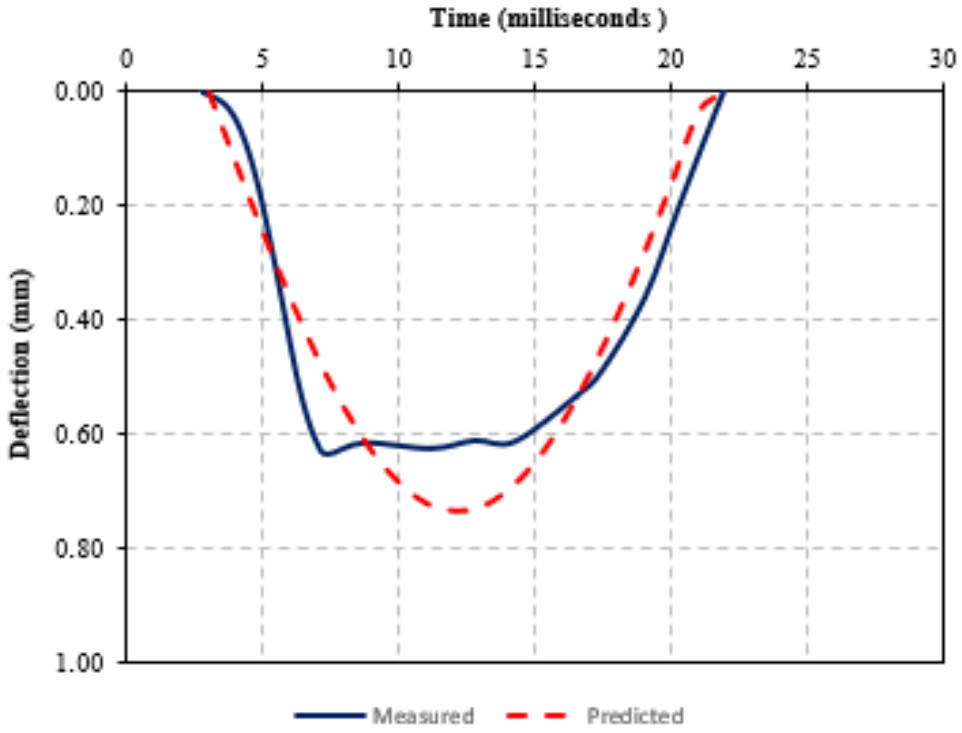

(a) 6-inch Results

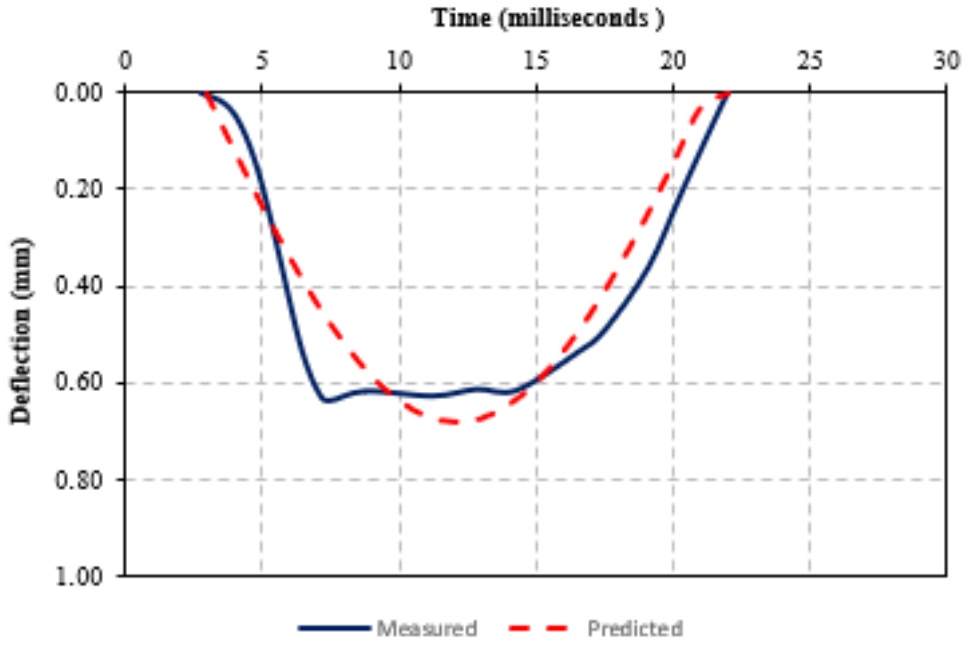

(b) 12-inch Results

Figure G.22: Measured and Predicted LWD Surface Deflections - Location 210

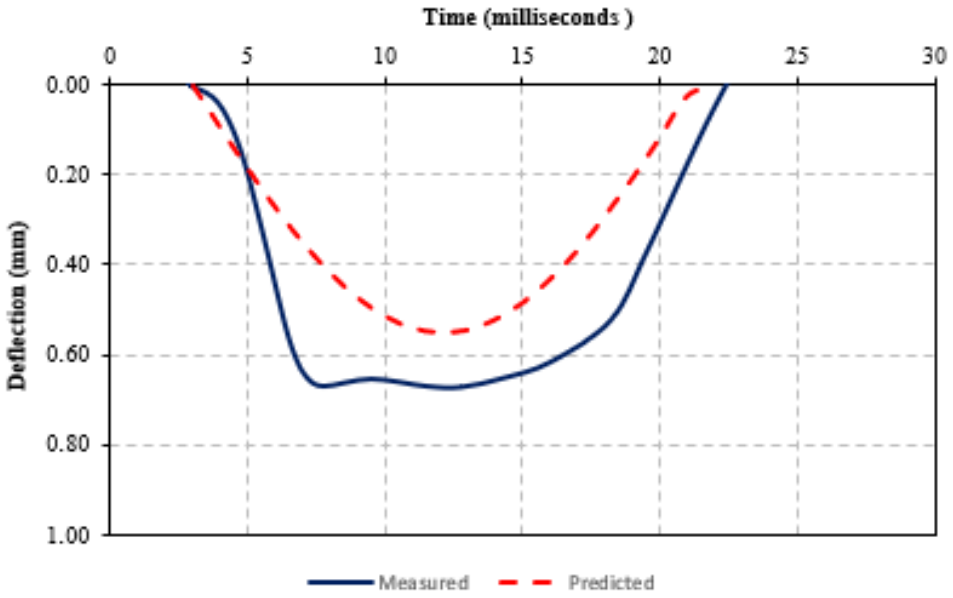

(a) 6-inch Results

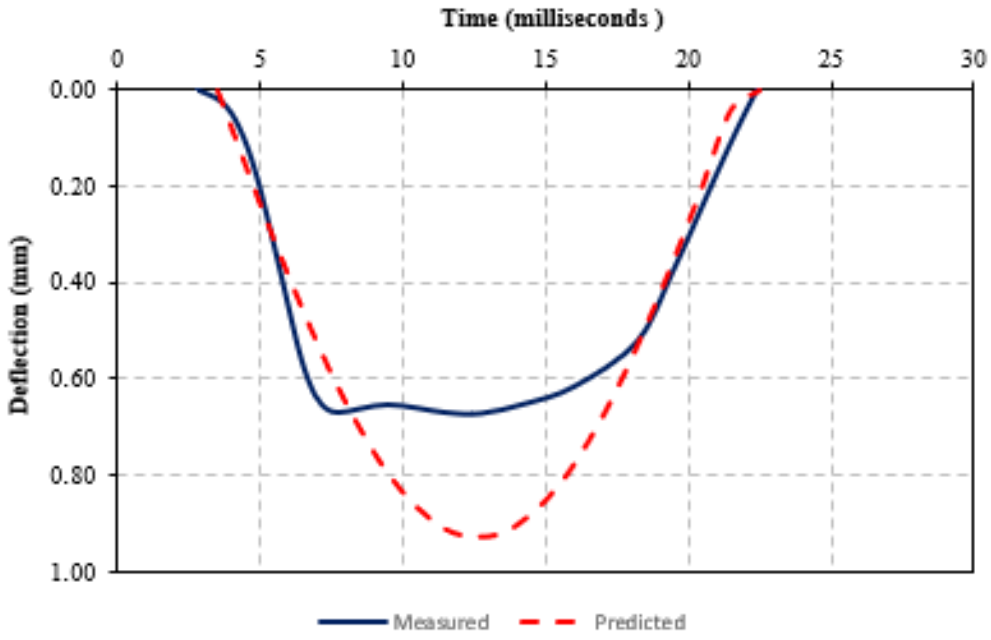

(b) 12-inch Results

Figure G.23: Measured and Predicted LWD Surface Deflections - Location 211

G.3 Cypress Landing

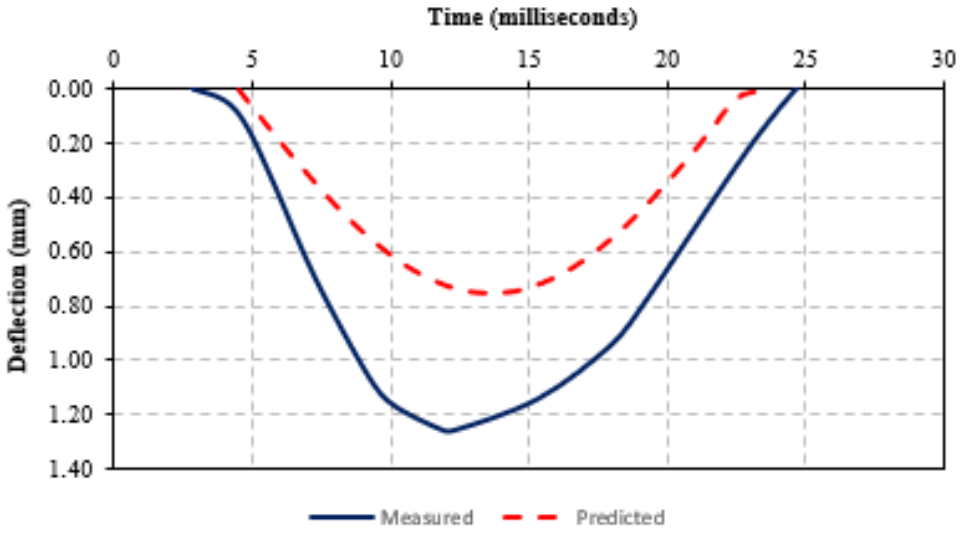

(a) 12-inch Results A

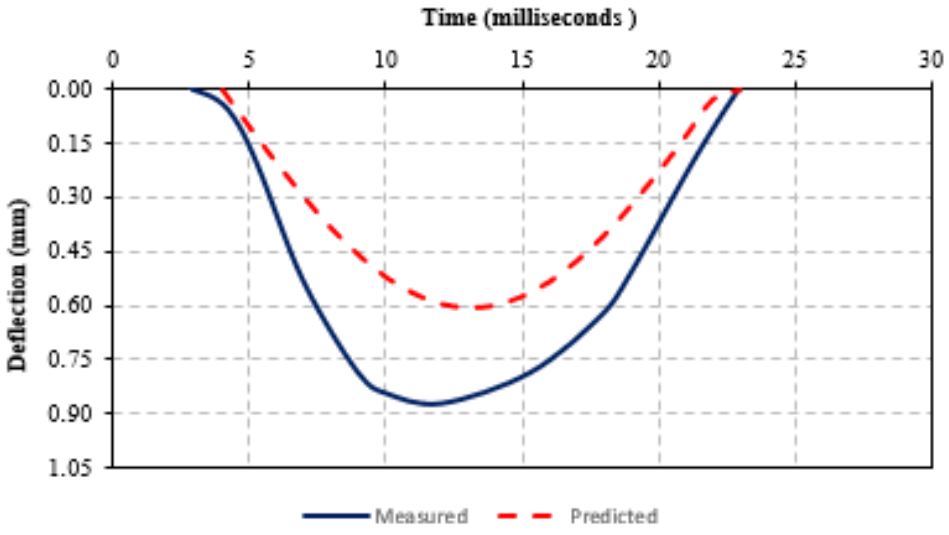

(b) 12-inch Results B

Figure G.24: Measured and Predicted LWD Surface Deflections - Location 101

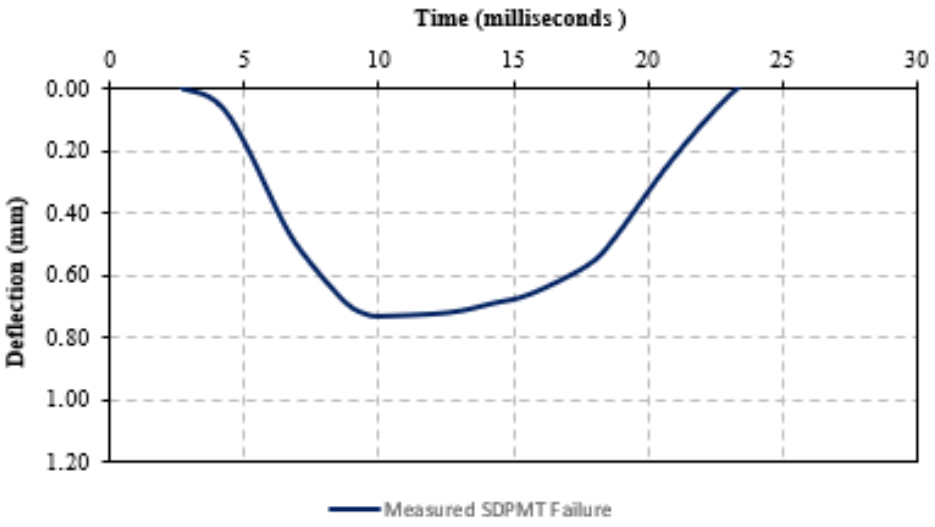

(a) 12-inch Results A

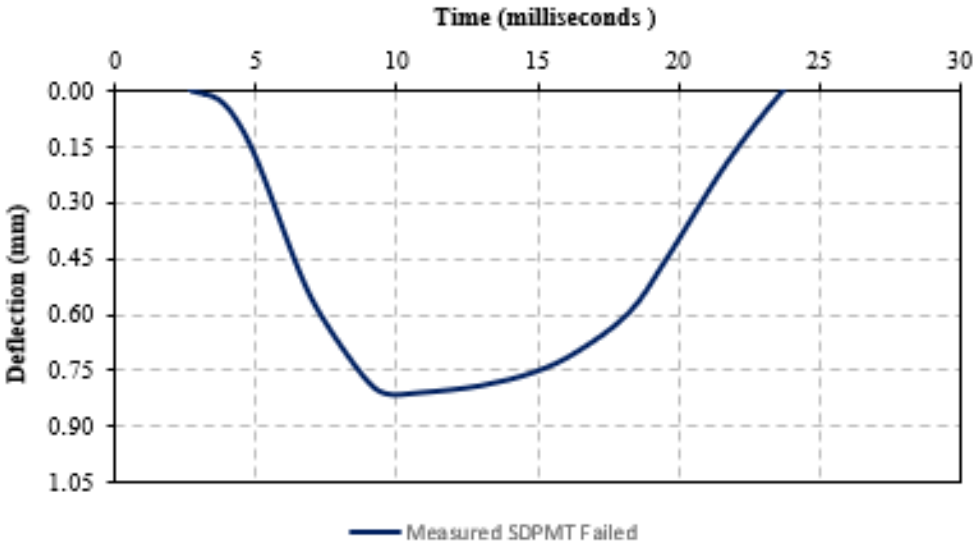

(b) 12-inch Results B

Figure G.25: Measured and Predicted LWD Surface Deflections - Location 102

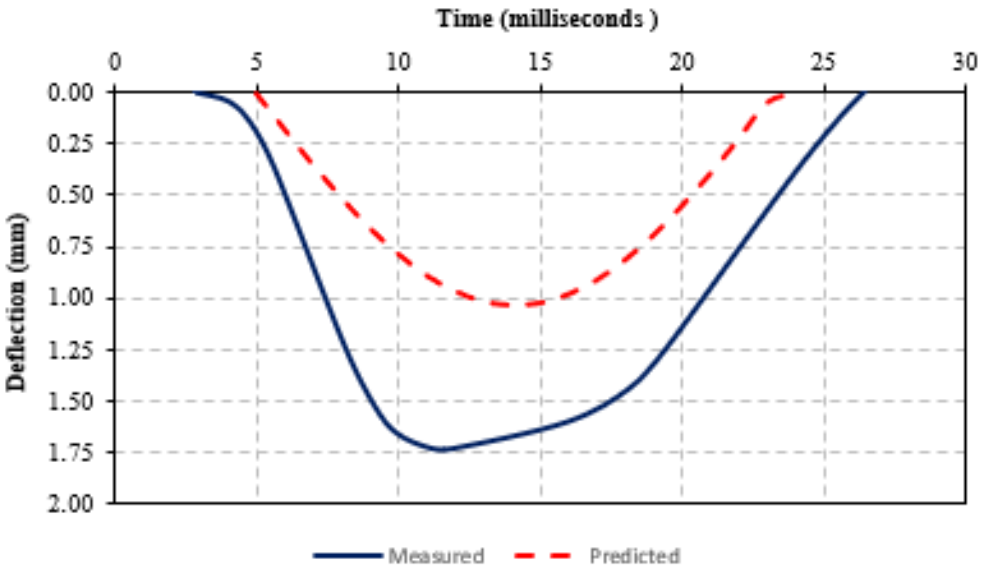

(a) 12-inch Results A

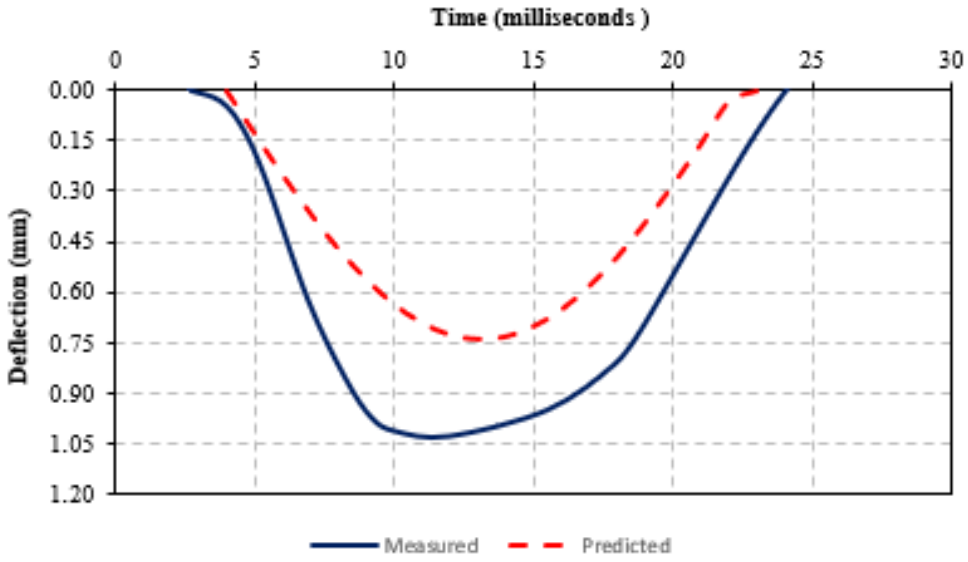

(b) 12-inch Results B

Figure G.26: Measured and Predicted LWD Surface Deflections - Location 103

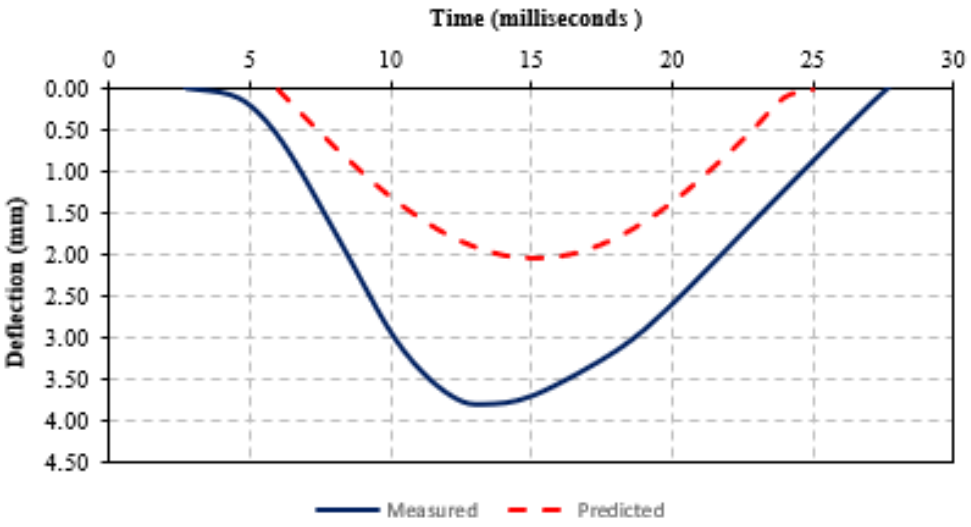

(a) 12-inch Results A

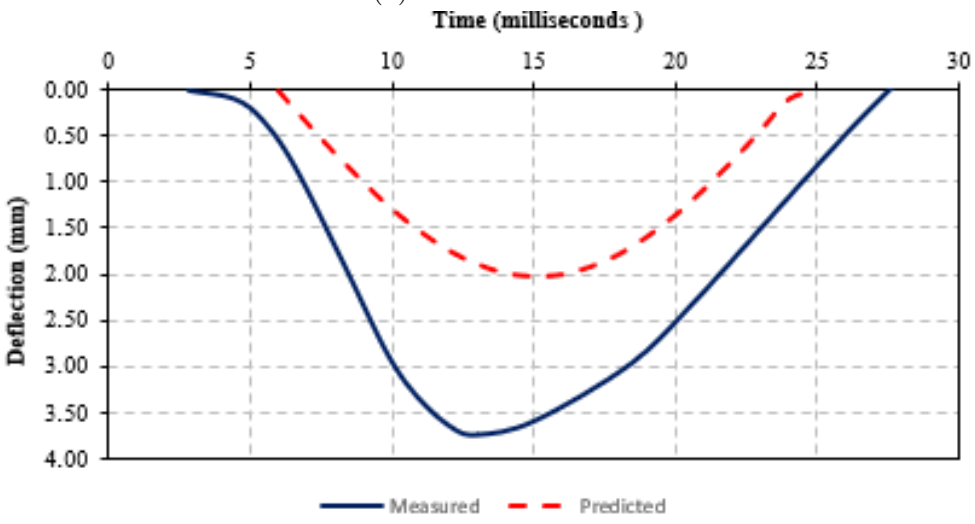

(b) 12-inch Results B

Figure G.27: Measured and Predicted LWD Surface Deflections - Location 104

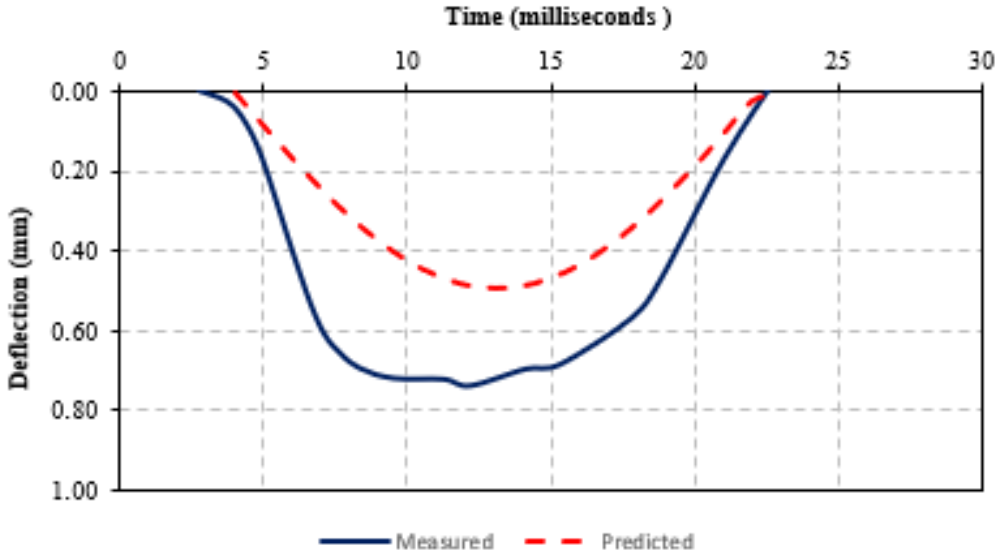

(a) 12-inch Results A

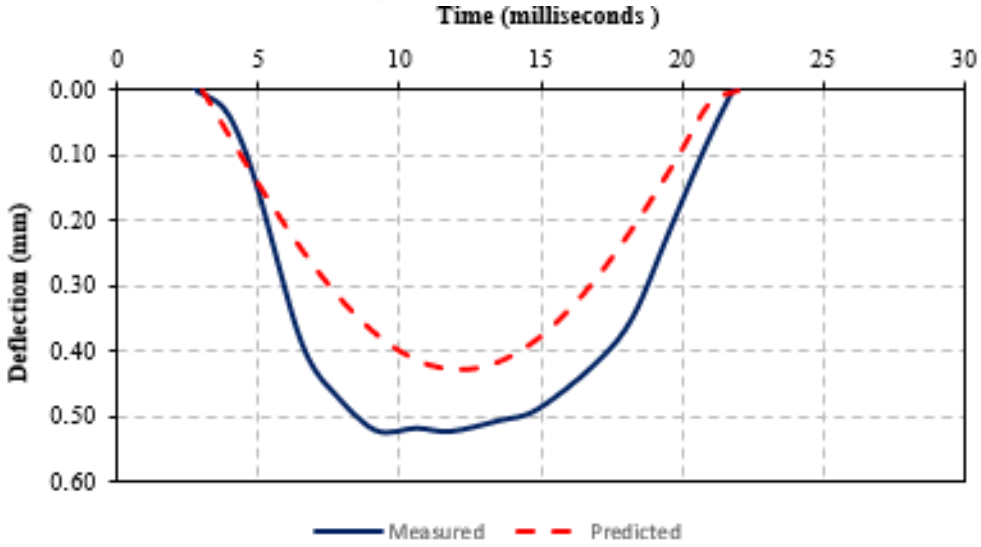

(b) 12-inch Results B

Figure G.28: Measured and Predicted LWD Surface Deflections - Location 105

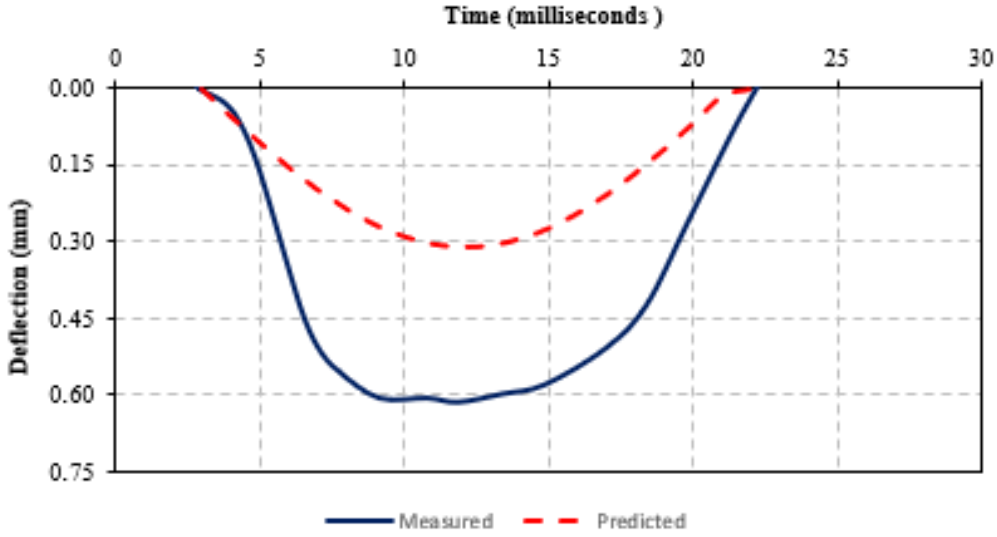

(a) 12-inch Results A

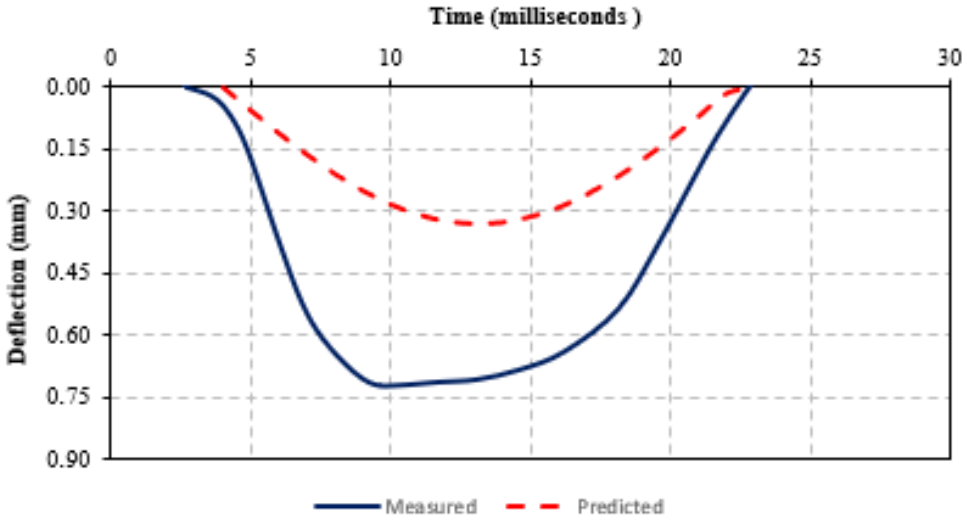

(b) 12-inch Results B

Figure G.29: Measured and Predicted LWD Surface Deflections - Location 106

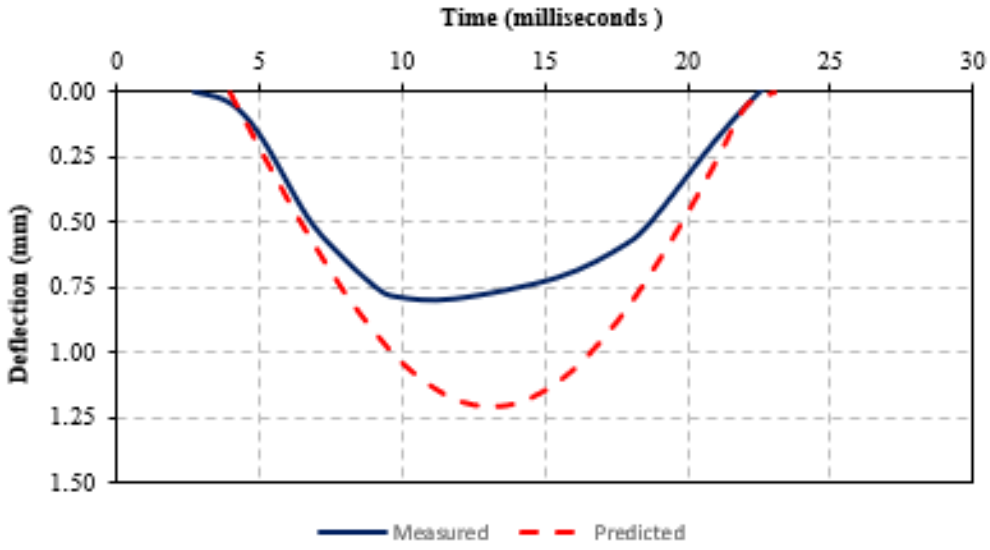

(a) 12-inch Results A

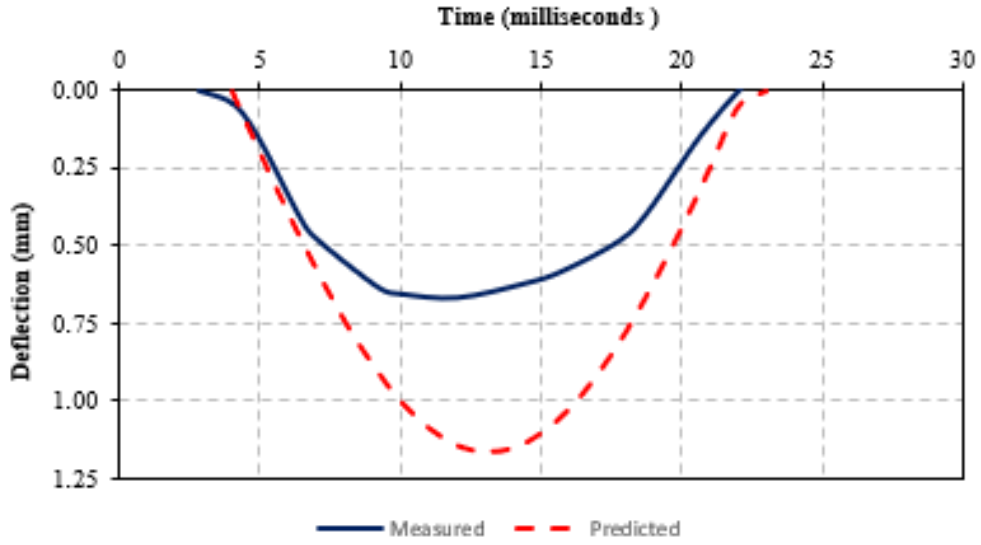

(b) 12-inch Results B

Figure G.30: Measured and Predicted LWD Surface Deflections - Location 107

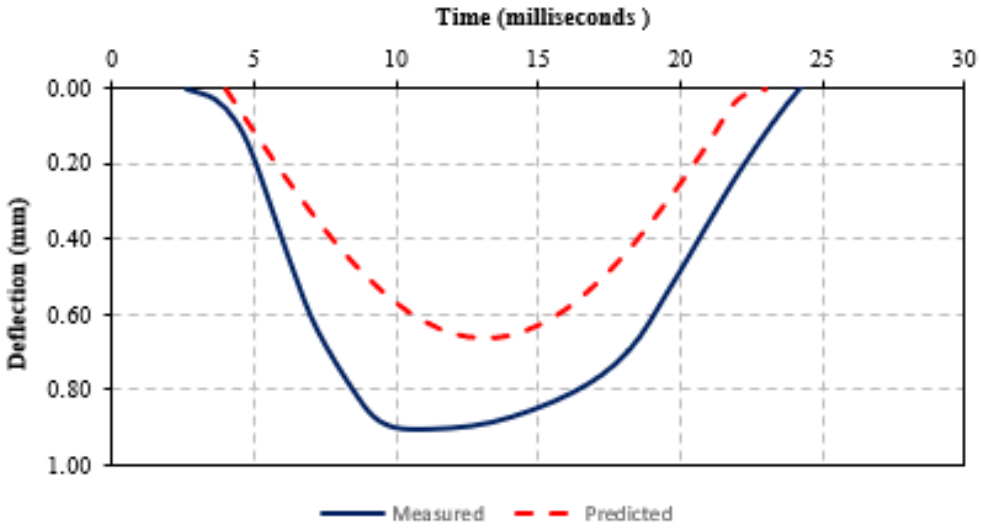

(a) 12-inch Results A

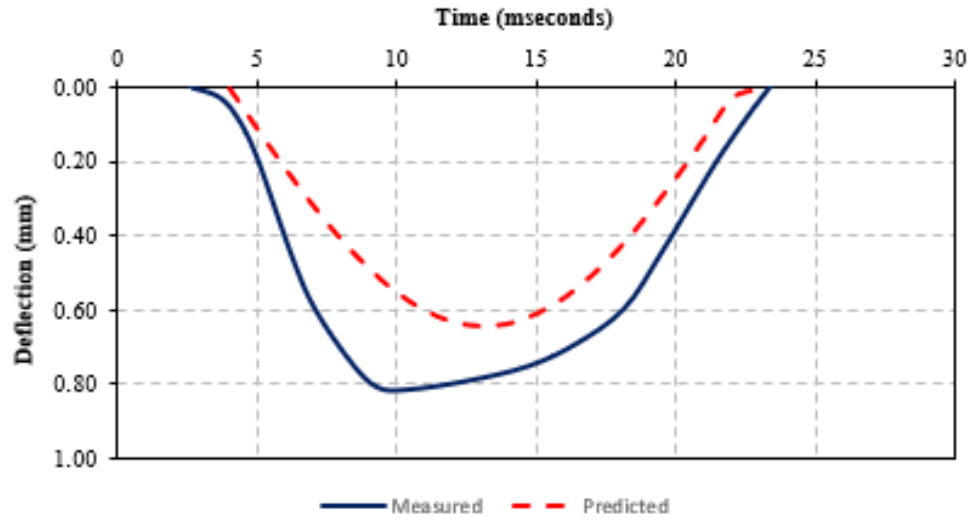

(b) 12-inch Results B

Figure G.31: Measured and Predicted LWD Surface Deflections - Location 108

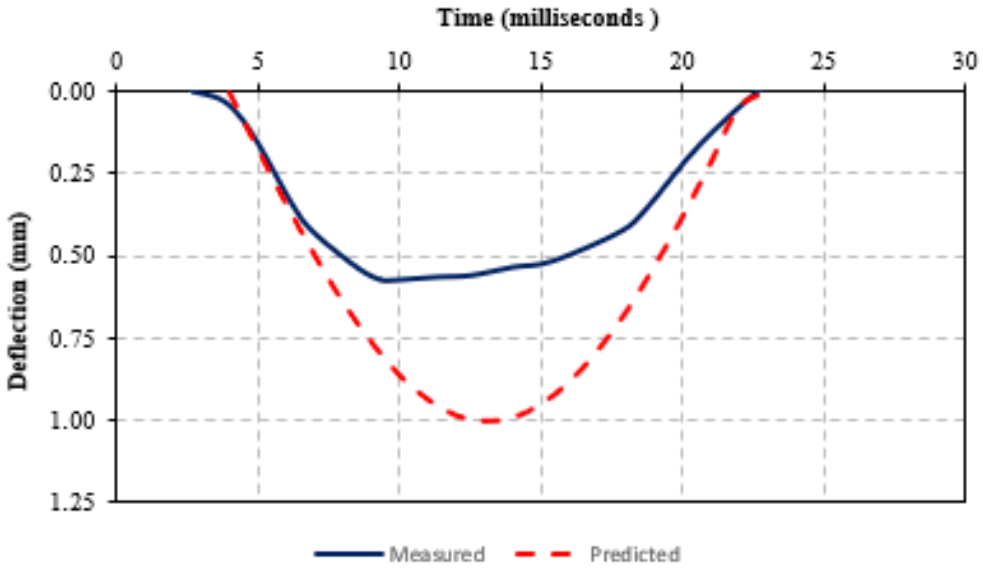

(a) 12-inch Results A

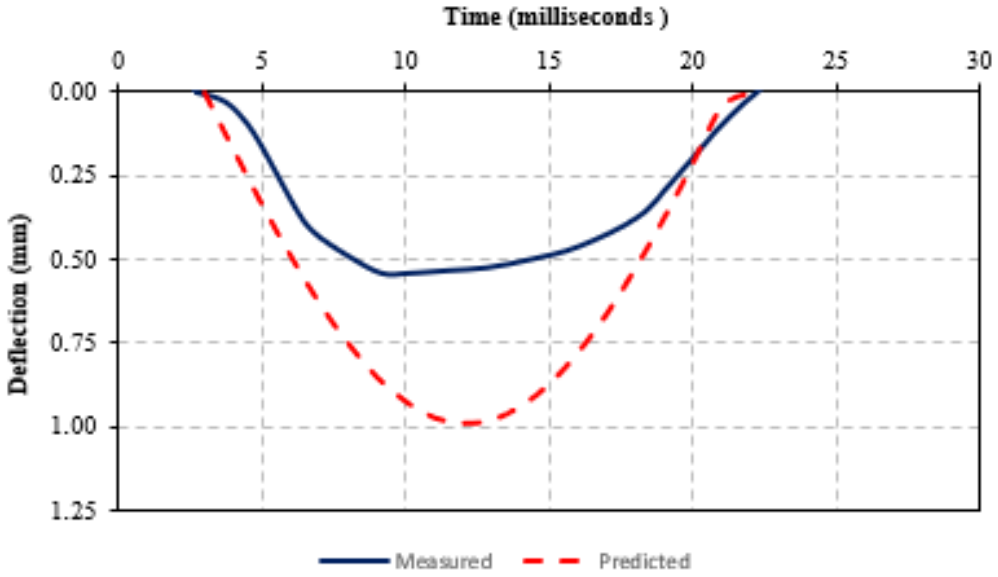

(b) 12-inch Results B

Figure G.32: Measured and Predicted LWD Surface Deflections - Location 109

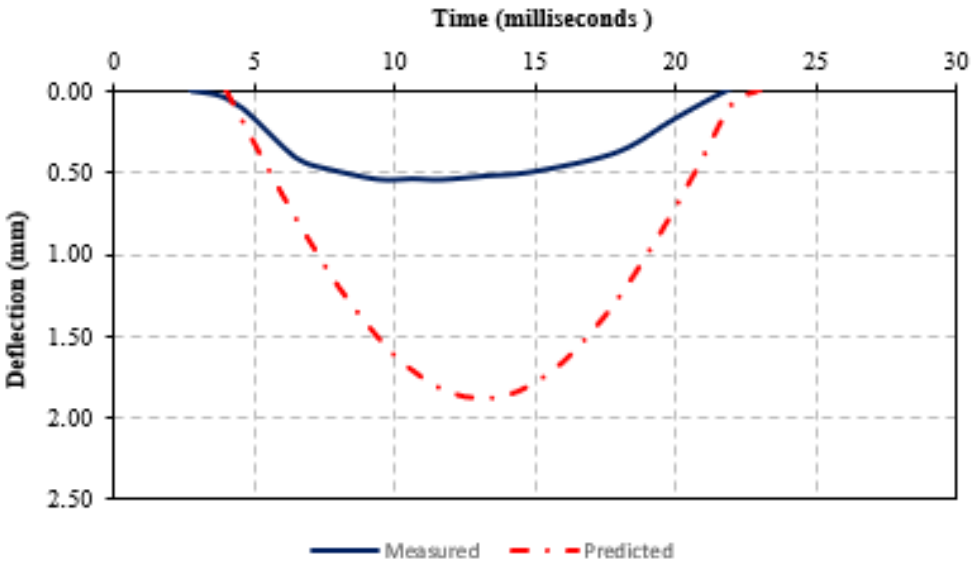

(a) 12-inch Results A

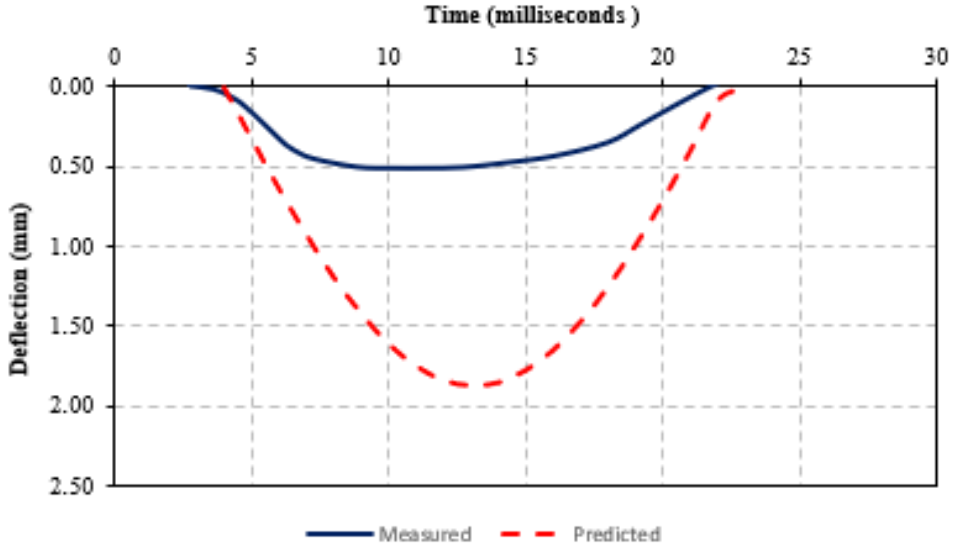

(b) 12-inch Results B

Figure G.33: Measured and Predicted LWD Surface Deflections - Location 110

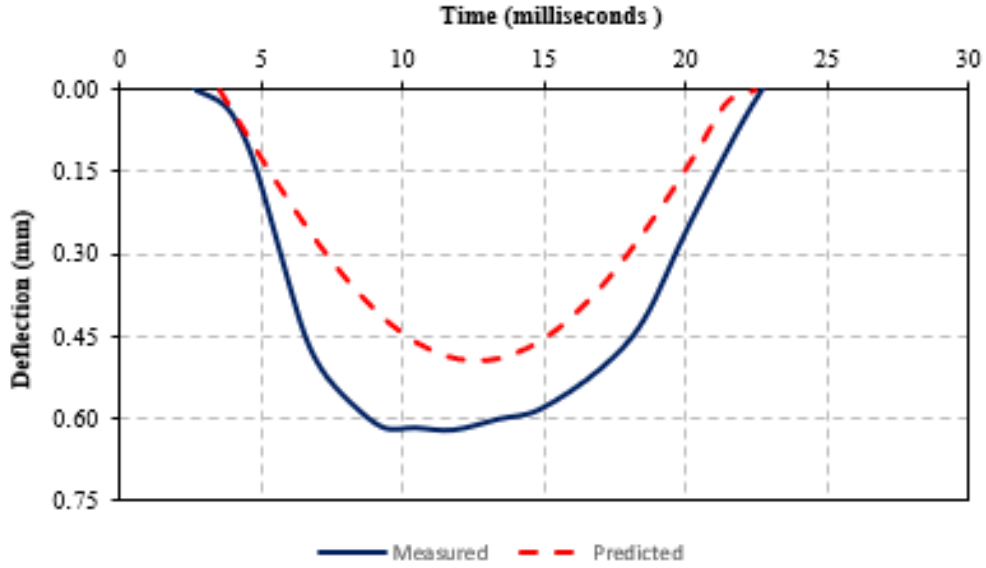

(a) 12-inch Results A

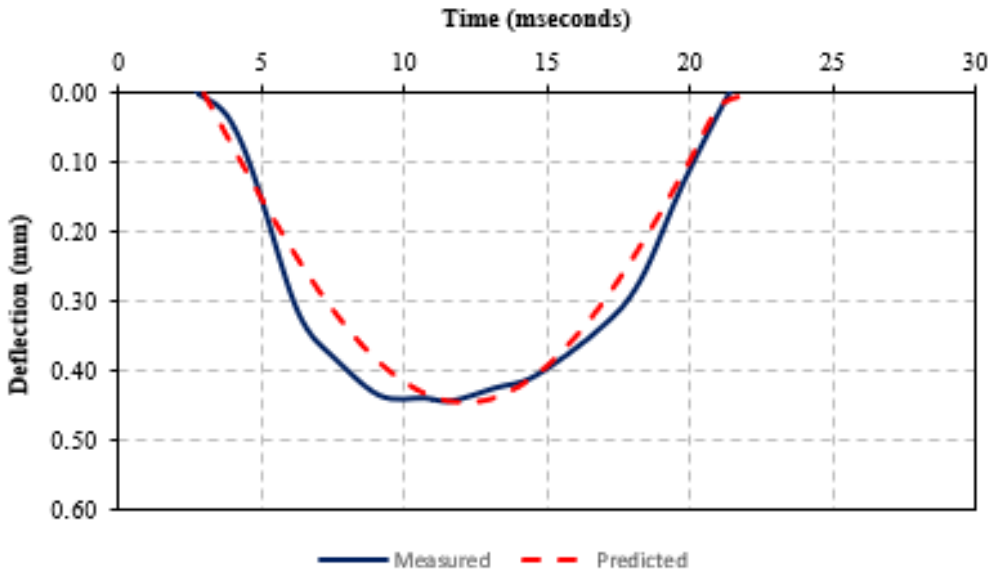

(b) 12-inch Results B

Figure G.34: Measured and Predicted LWD Surface Deflections - Location 111

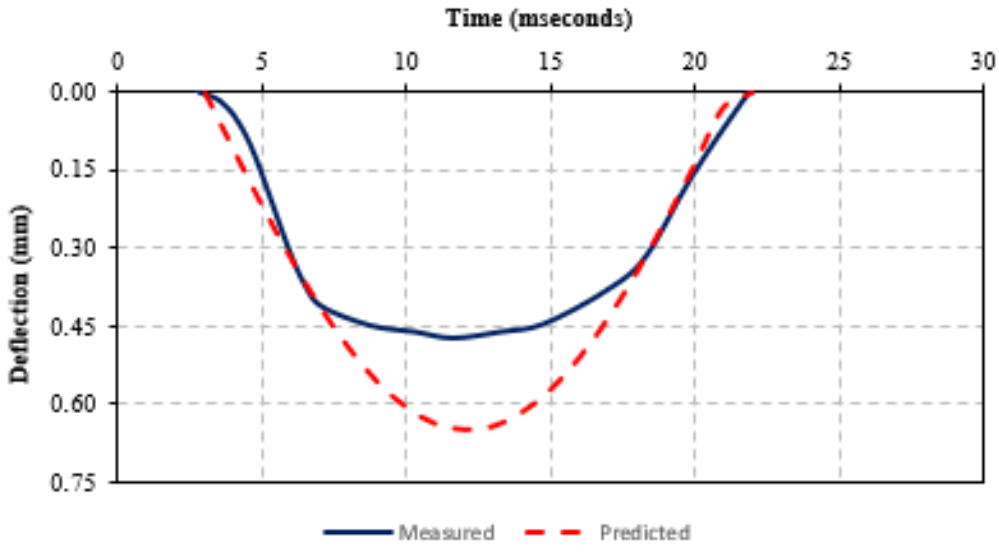

(a) 12-inch Results A

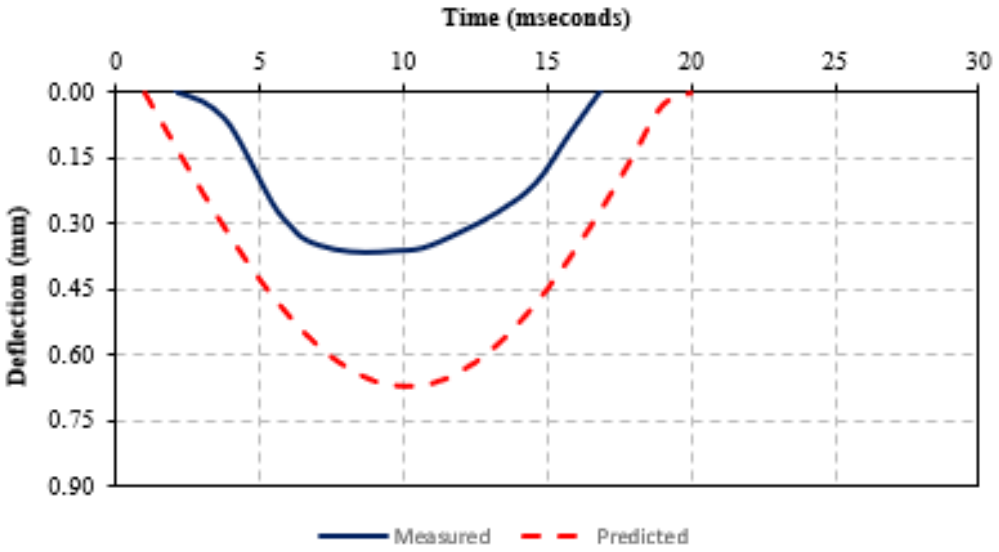

(b) 12-inch Results B

Figure G.35: Measured and Predicted LWD Surface Deflections - Location 112

G.4 Heritage Parkway

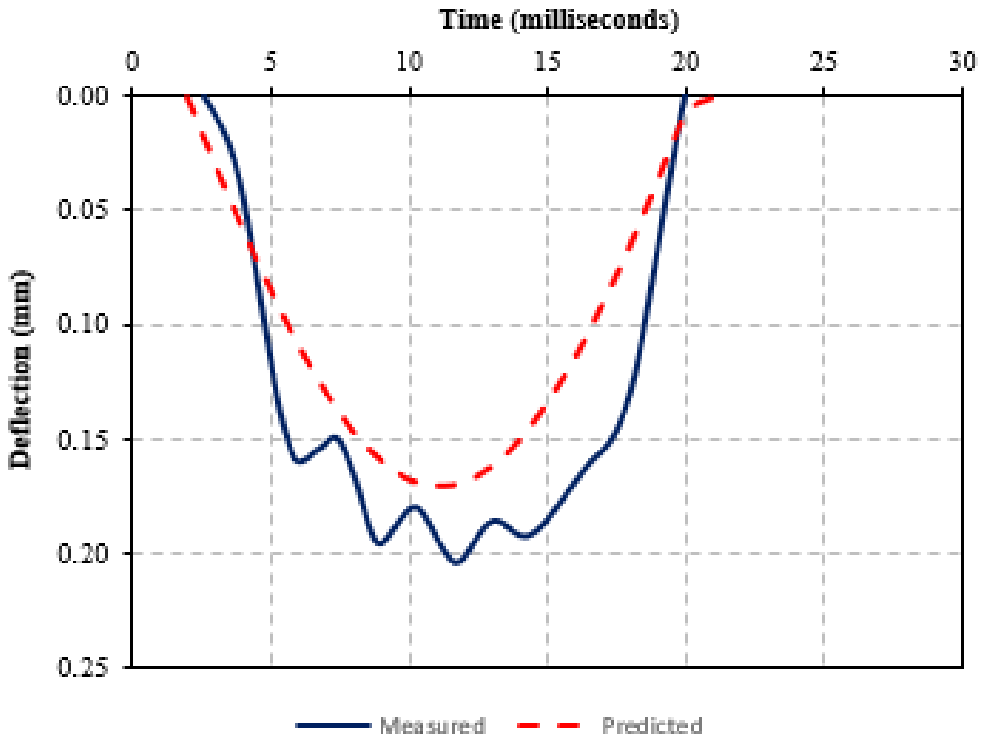

(a) 6-inch Results

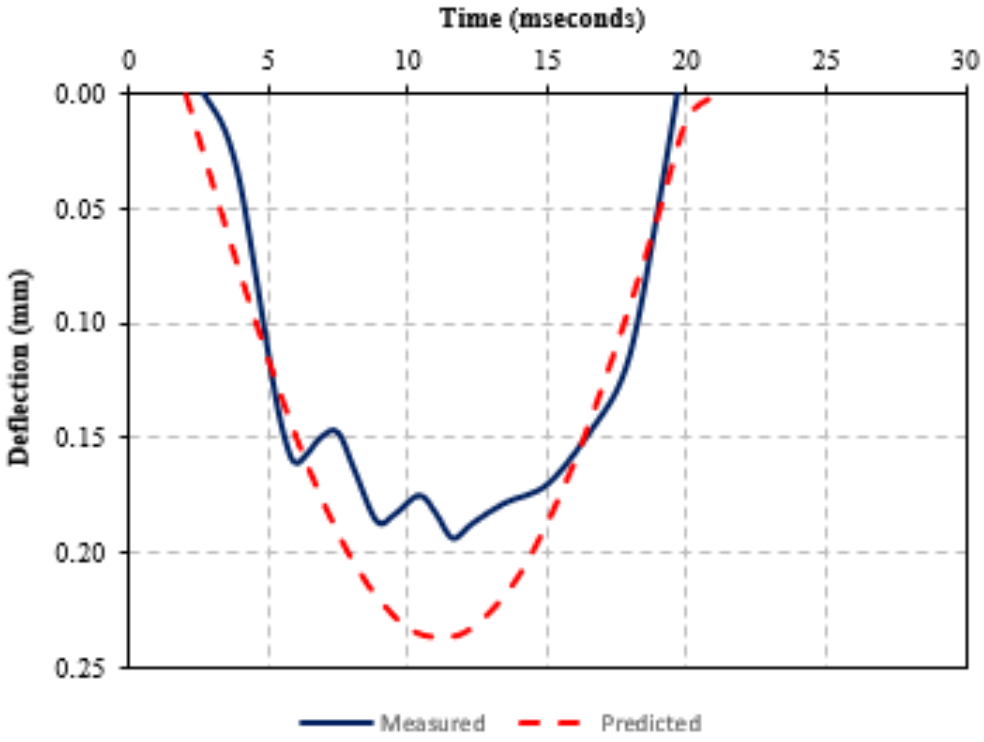

(b) 12-inch Results

Figure G.36: Measured and Predicted LWD Surface Deflections - Location 301

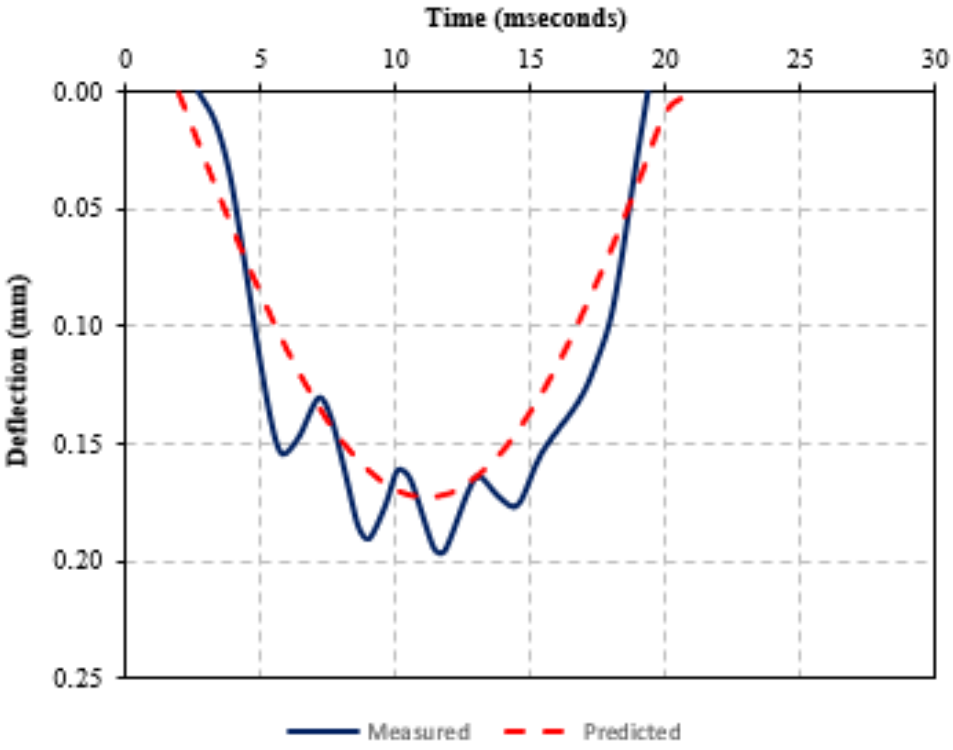

(a) 6-inch Results

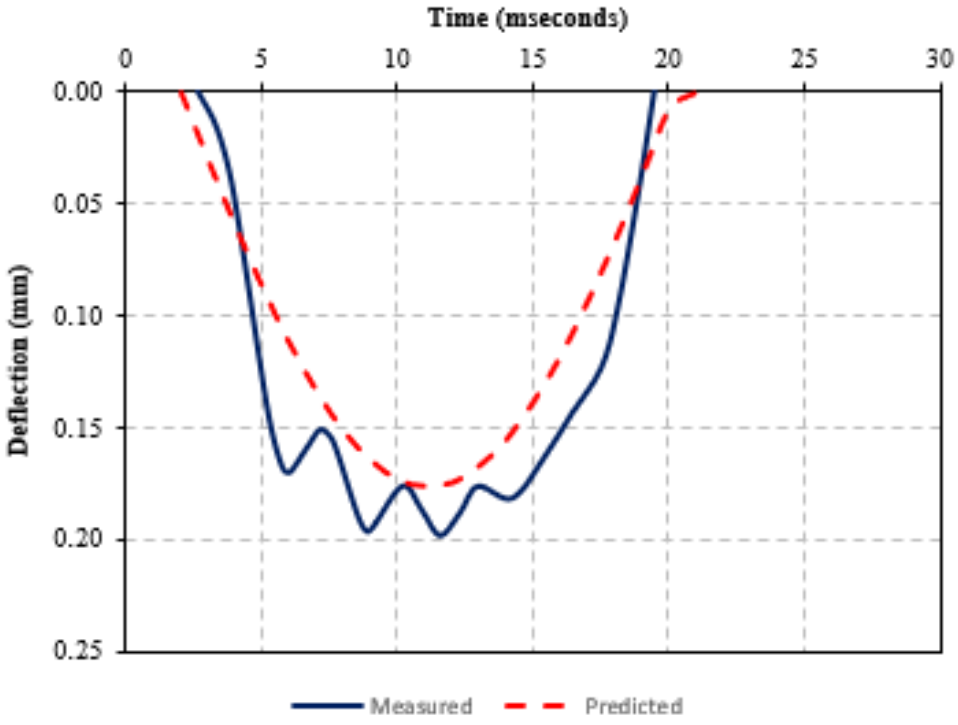

(b) 12-inch Results

Figure G.37: Measured and Predicted LWD Surface Deflections - Location 302

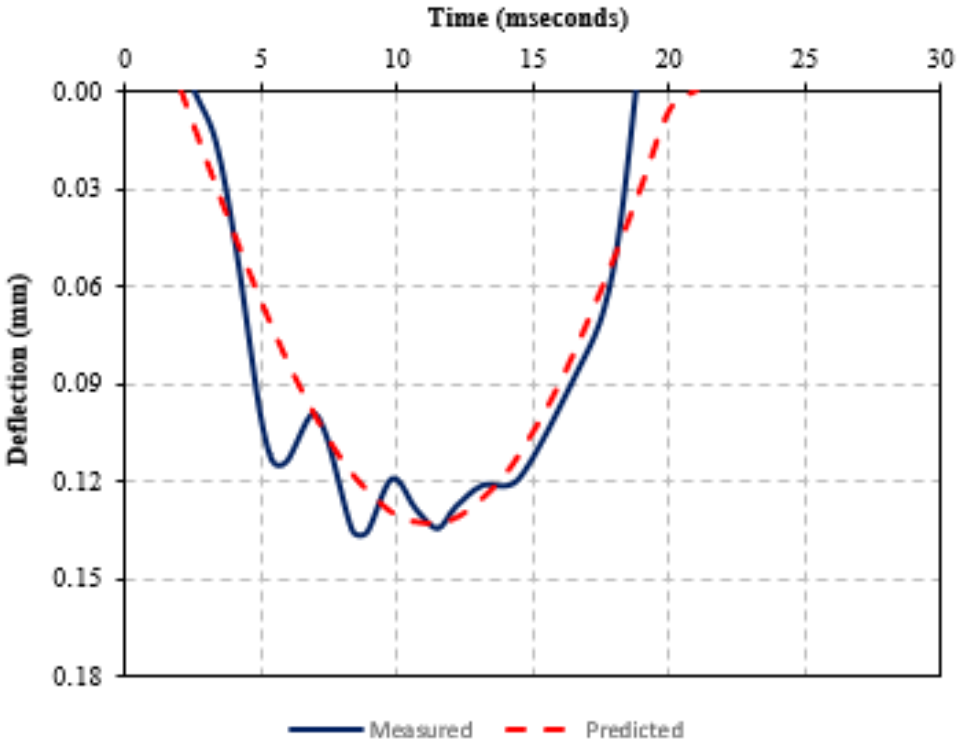

(a) 6-inch Results

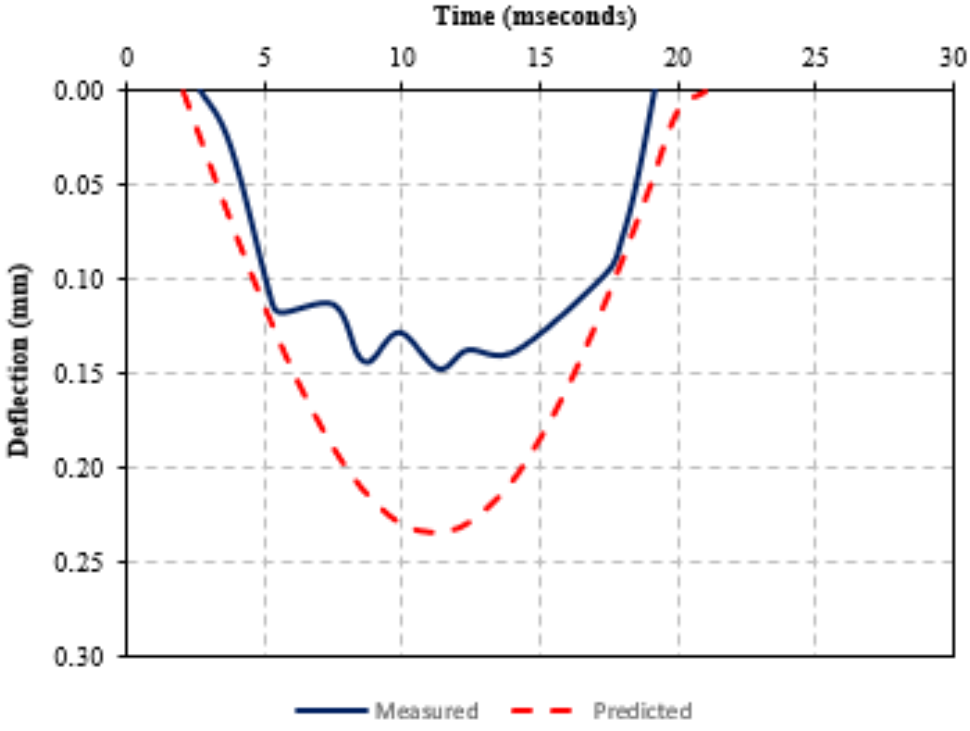

(b) 12-inch Results

Figure G.38: Measured and Predicted LWD Surface Deflections - Location 303 943

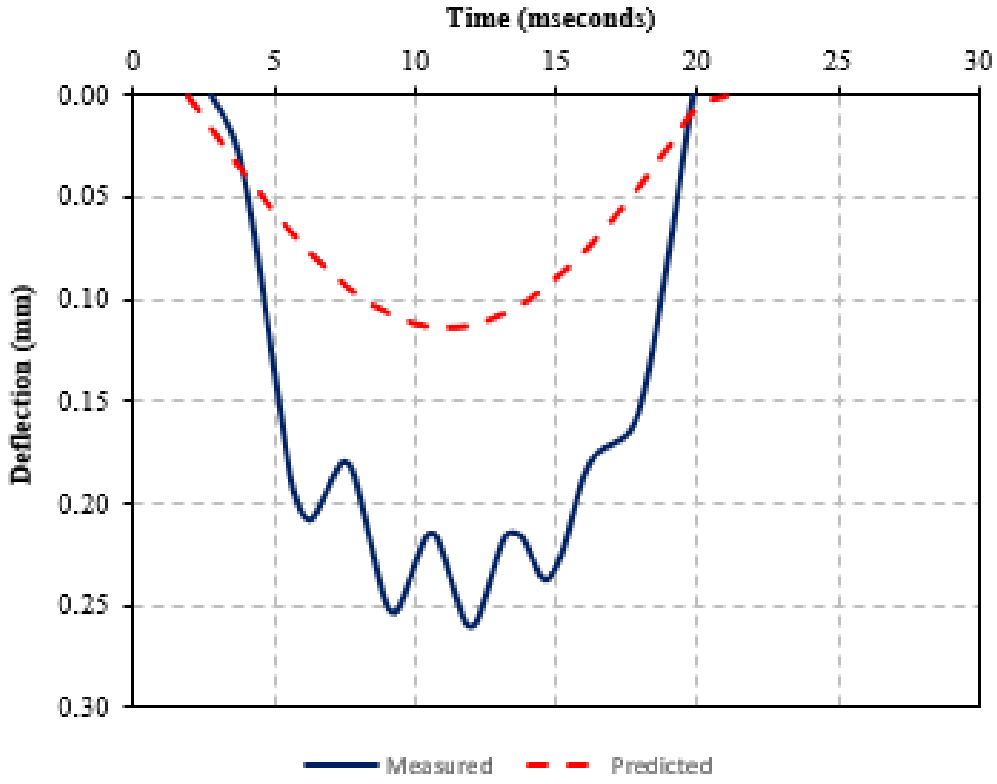

(a) 6-inch Results

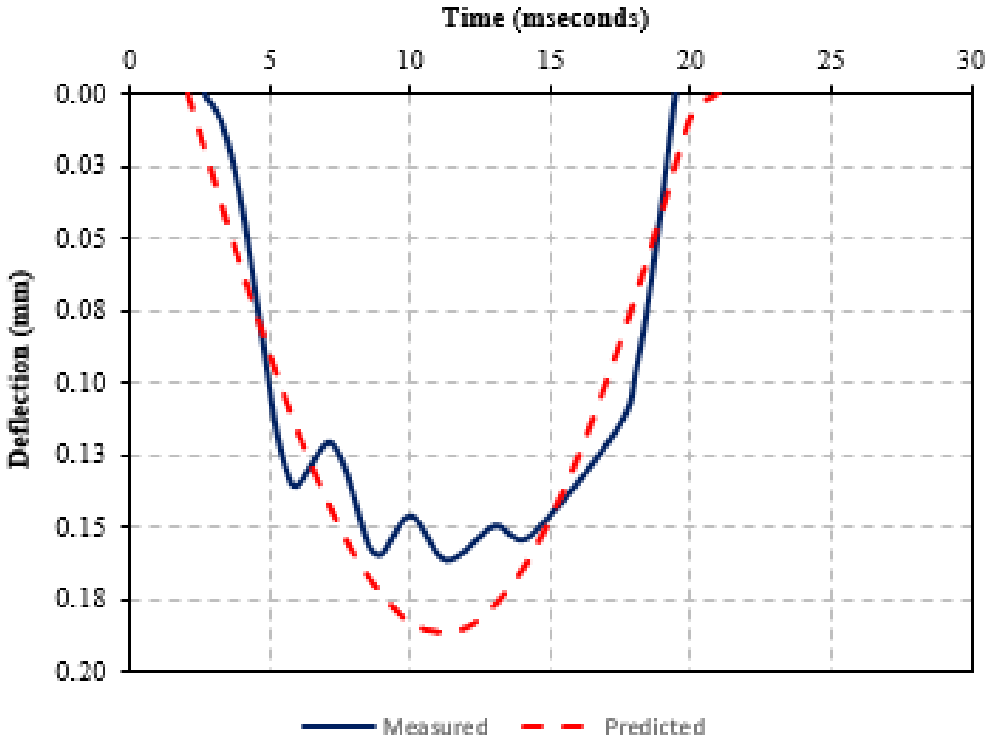

(b) 12-inch Results

Figure G.39: Measured and Predicted LWD Surface Deflections - Location 304

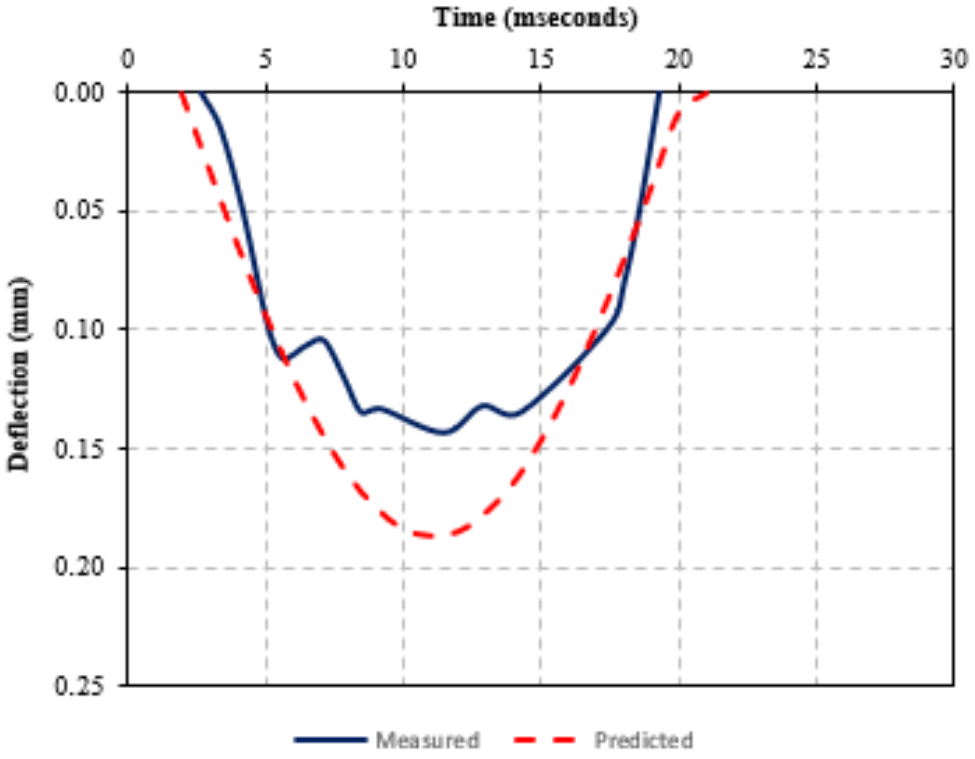

(a) 6-inch Results

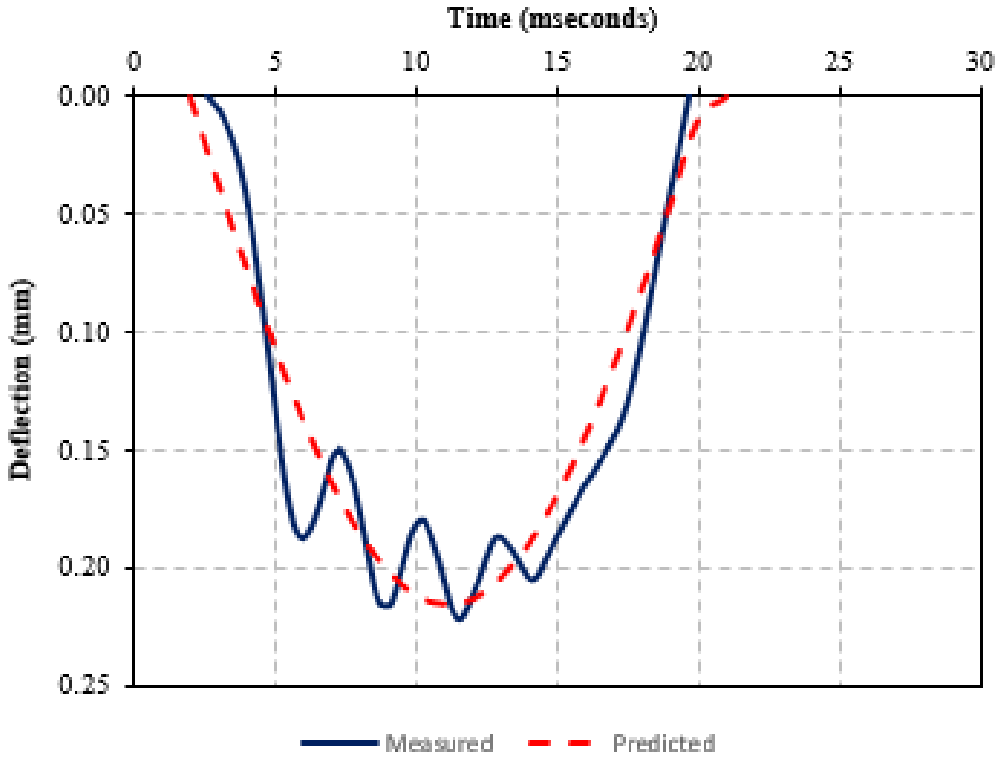

(b) 12-inch Results

Figure G.40: Measured and Predicted LWD Surface Deflections - Location 305

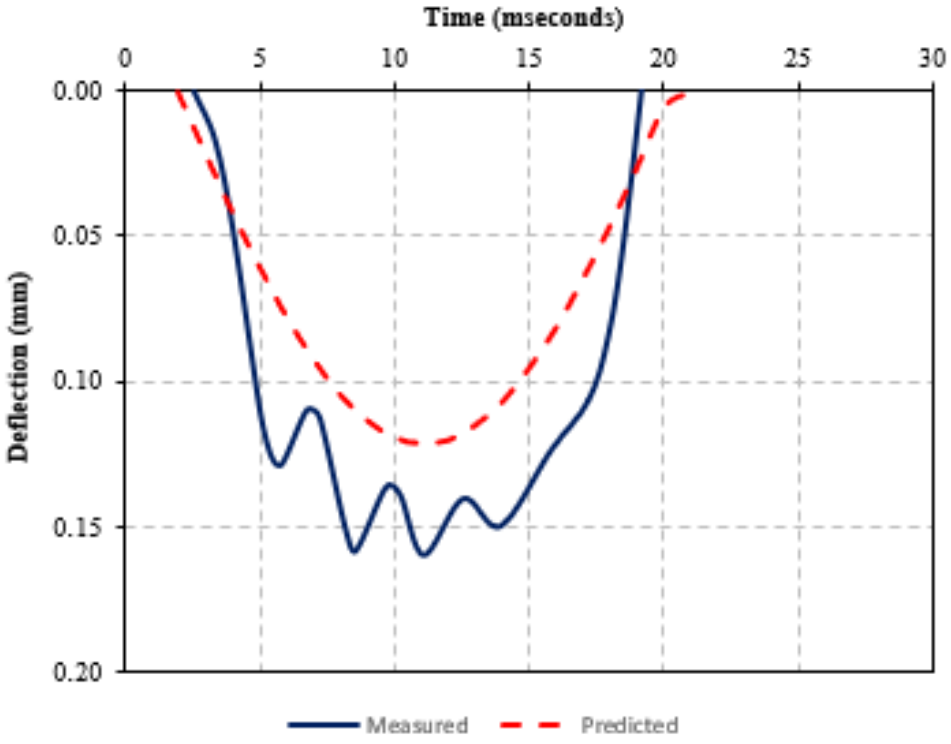

(a) 6-inch Results

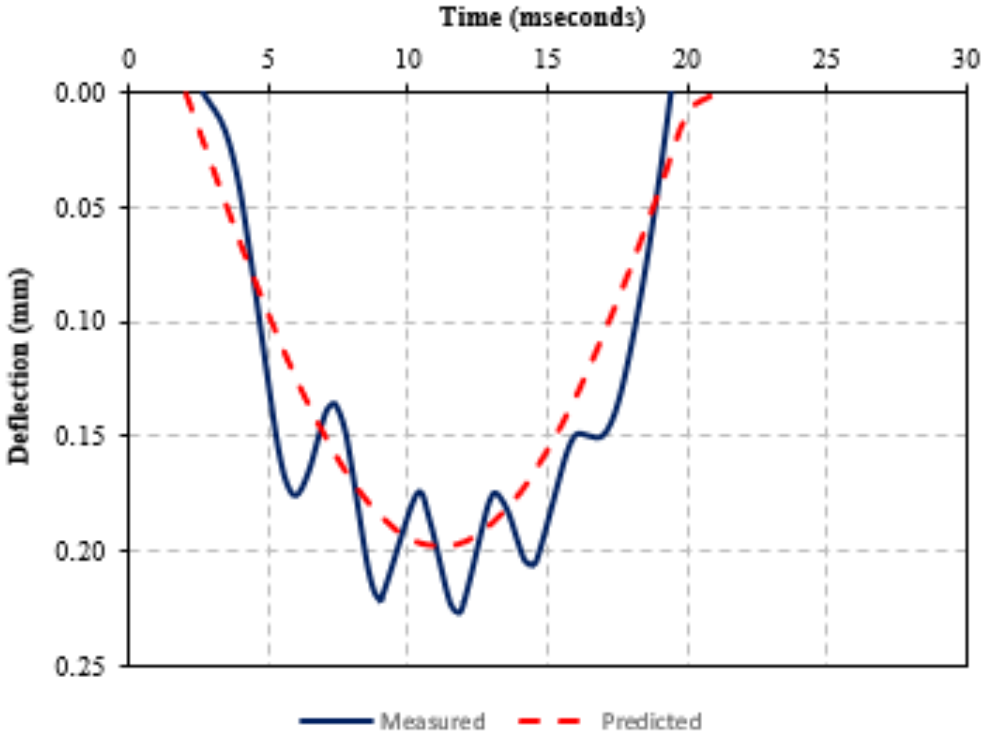

(b) 12-inch Results

Figure G.41: Measured and Predicted LWD Surface Deflections - Location 306

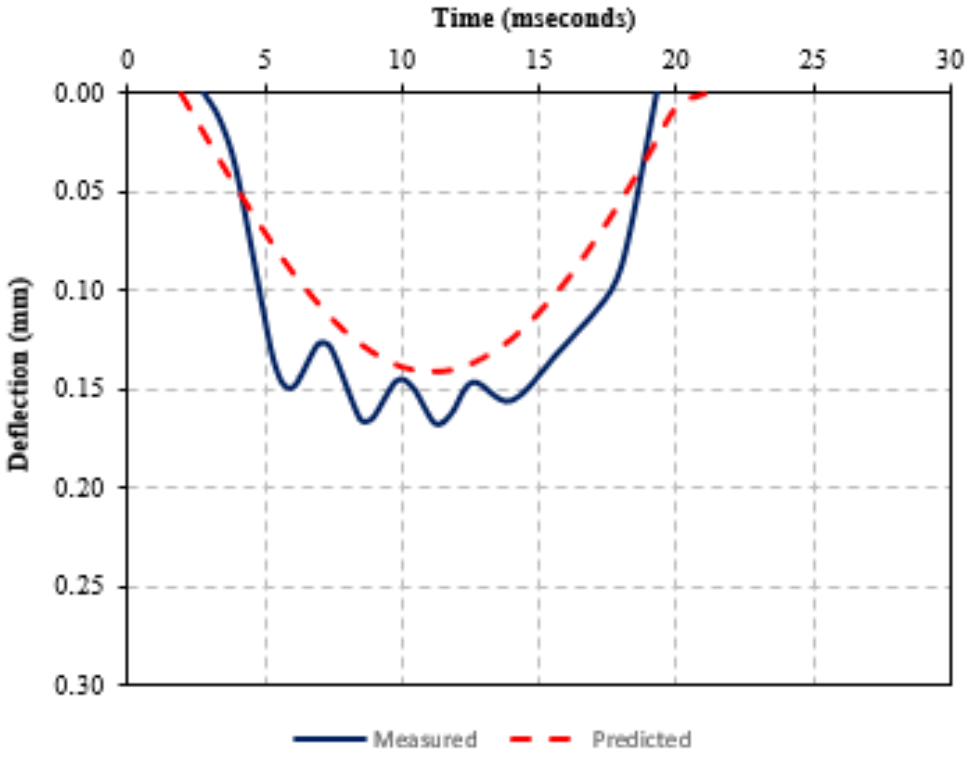

(a) 6-inch Results

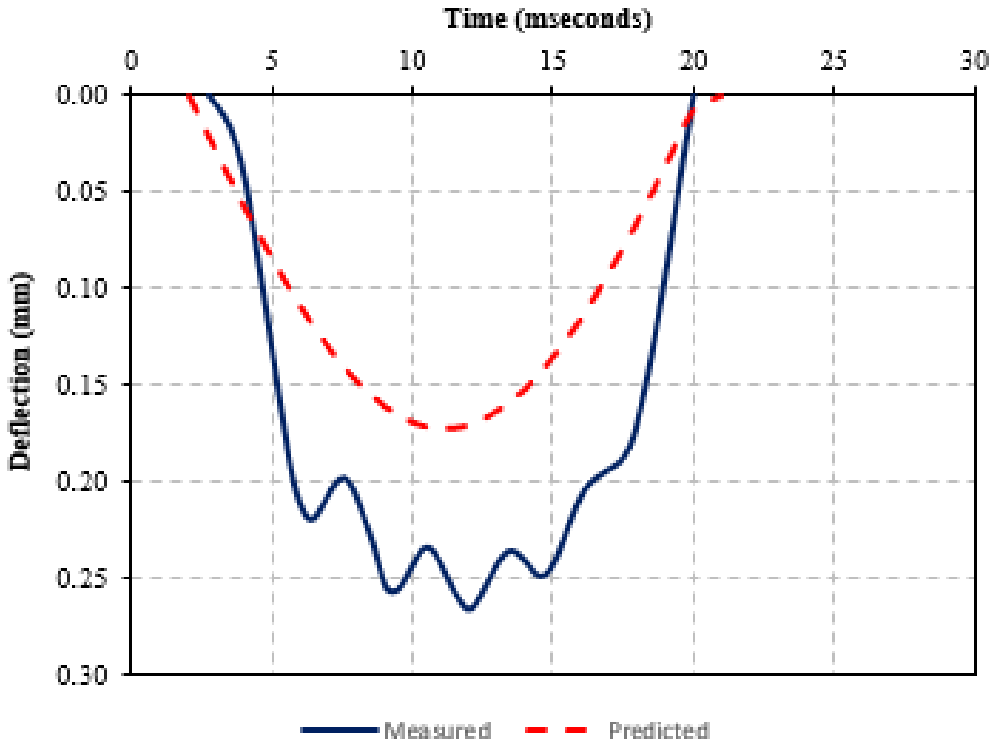

(b) 12-inch Results

Figure G.42: Measured and Predicted LWD Surface Deflections - Location 307

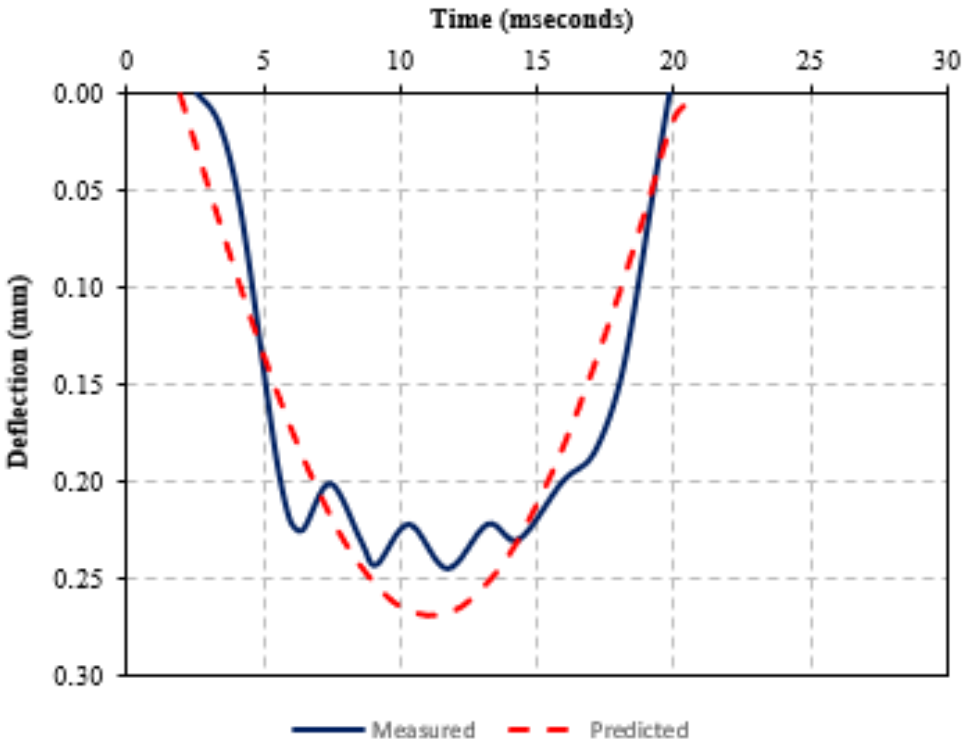

(a) 6-inch Results

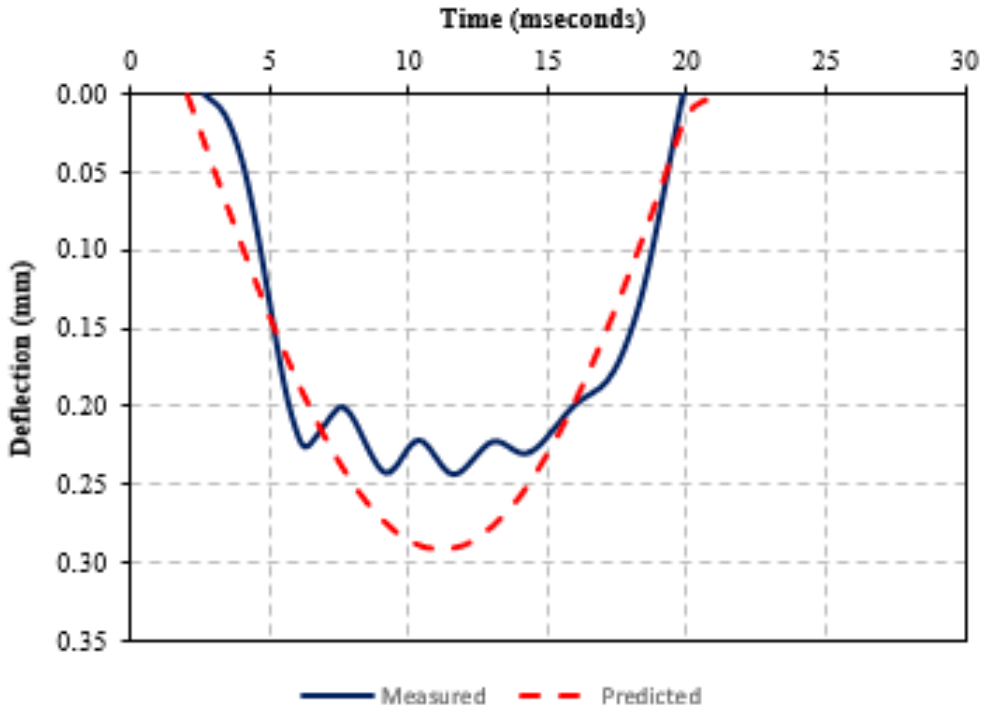

(b) 12-inch Results

Figure G.43: Measured and Predicted LWD Surface Deflections - Location 308

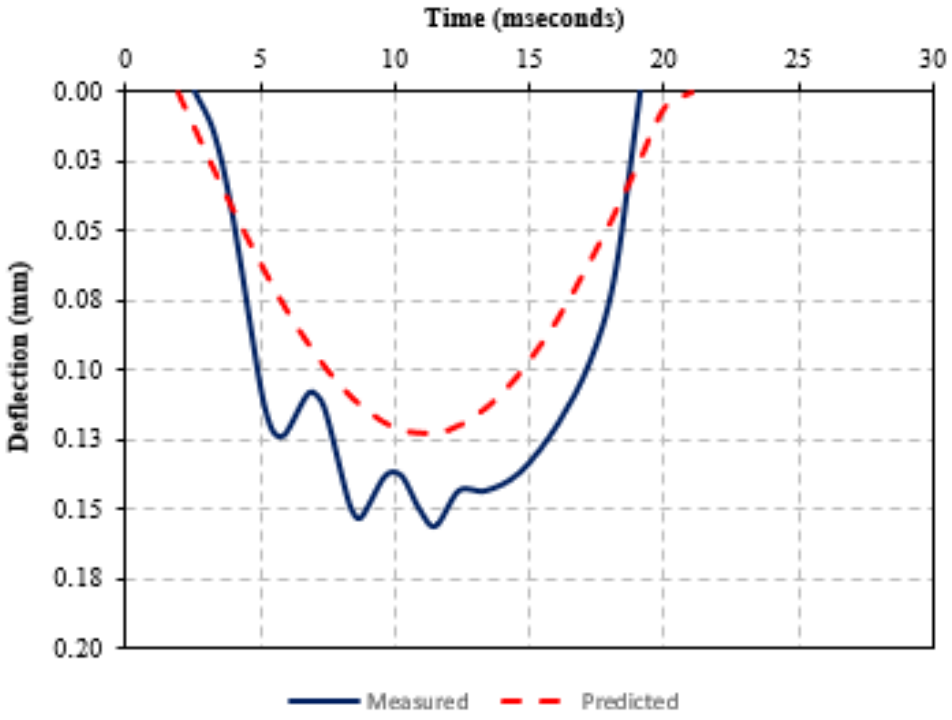

(a) 6-inch Results

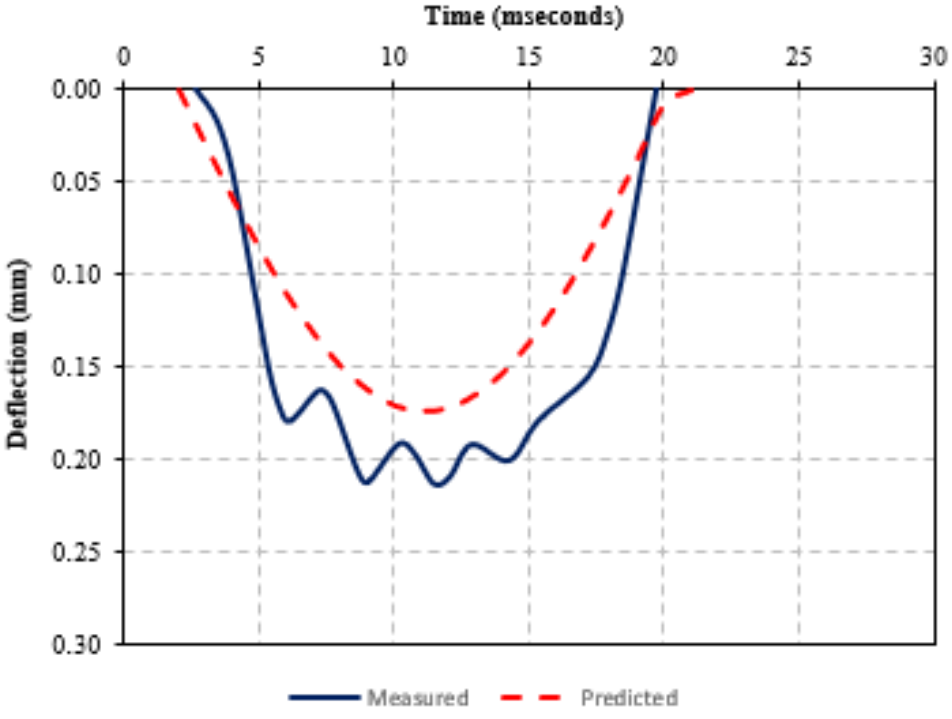

(b) 12-inch Results

Figure G.44: Measured and Predicted LWD Surface Deflections - Location 309

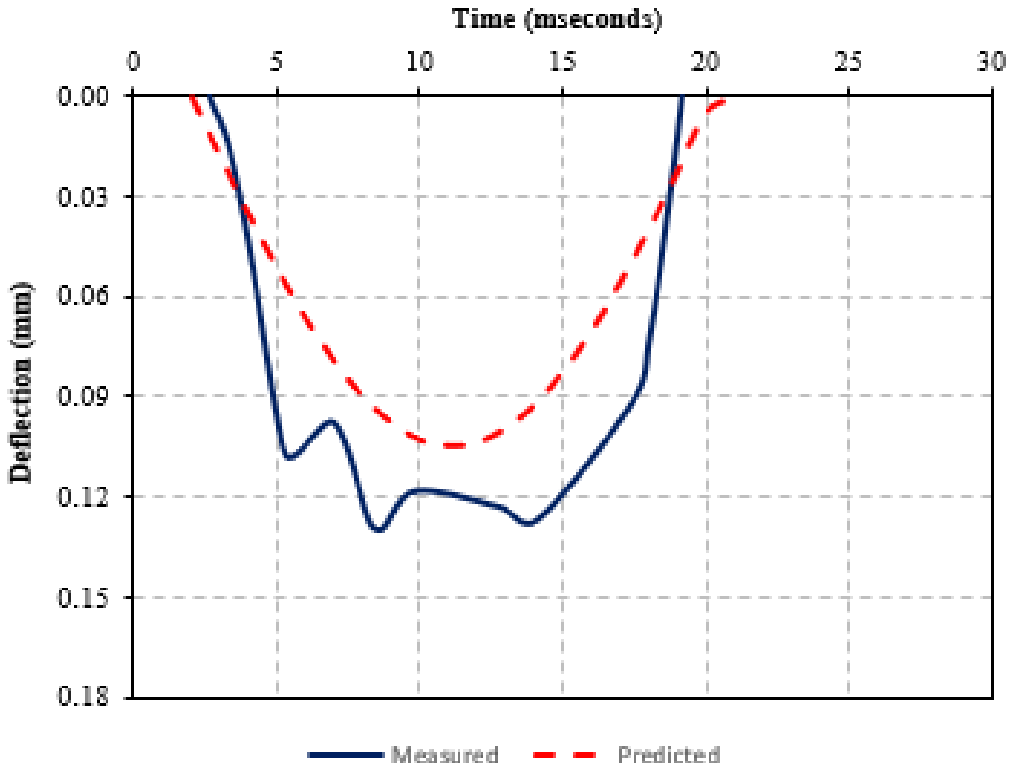

(a) 6-inch Results

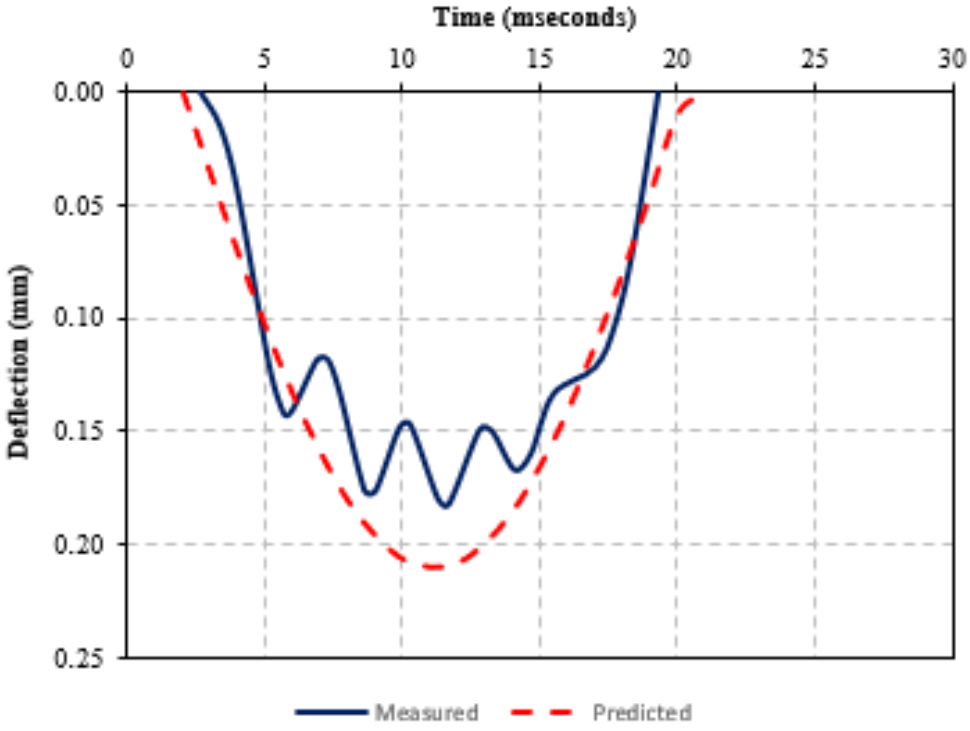

(b) 12-inch Results

Figure G.45: Measured and Predicted LWD Surface Deflections - Location 310

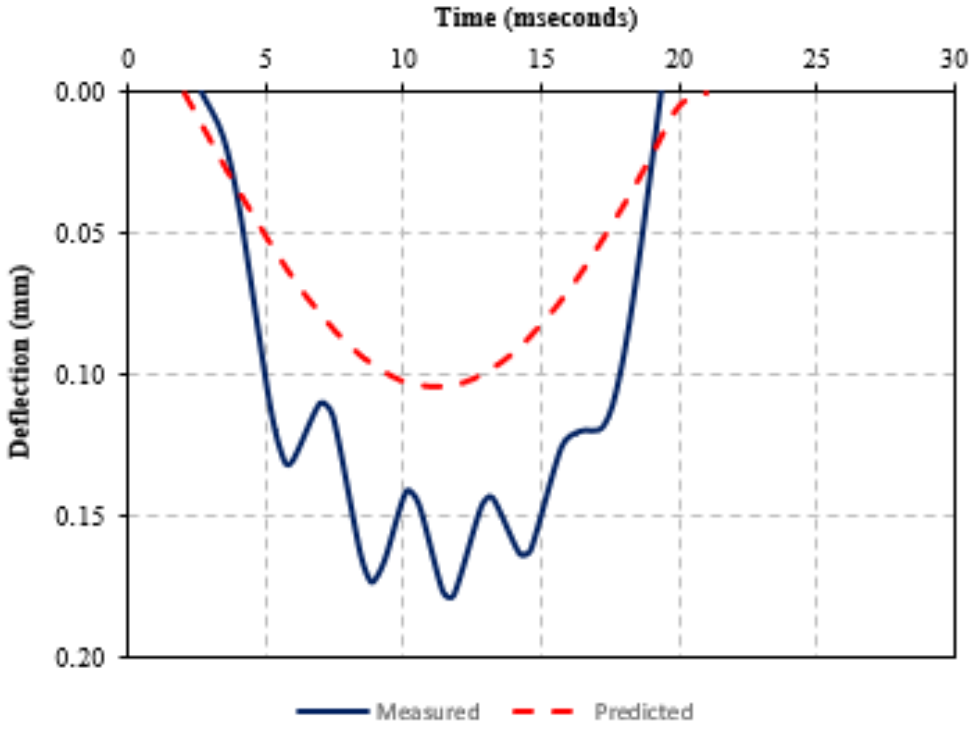

(a) 6-inch Results

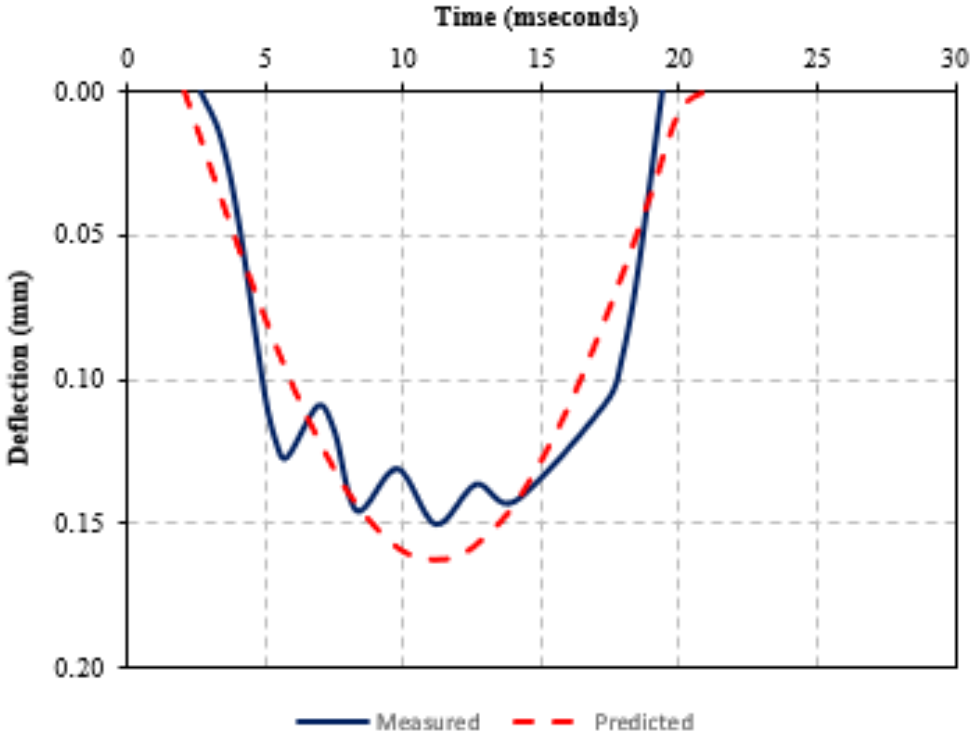

(b) 12-inch Results

Figure G.46: Measured and Predicted LWD Surface Deflections - Location 311

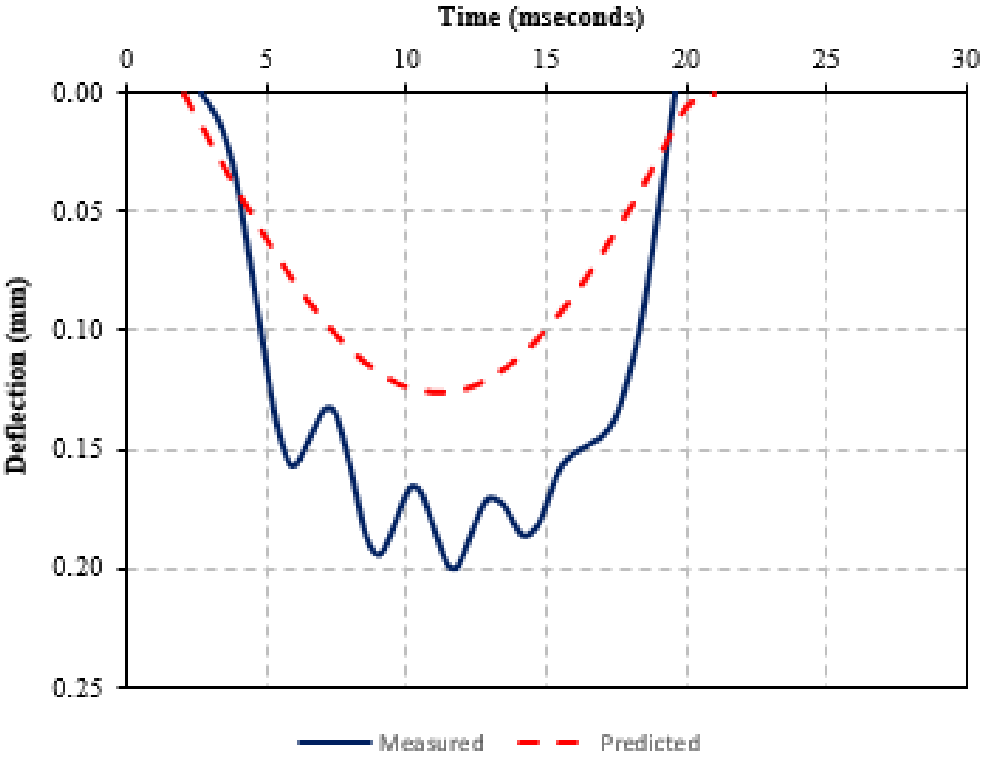

(a) 6-inch Results

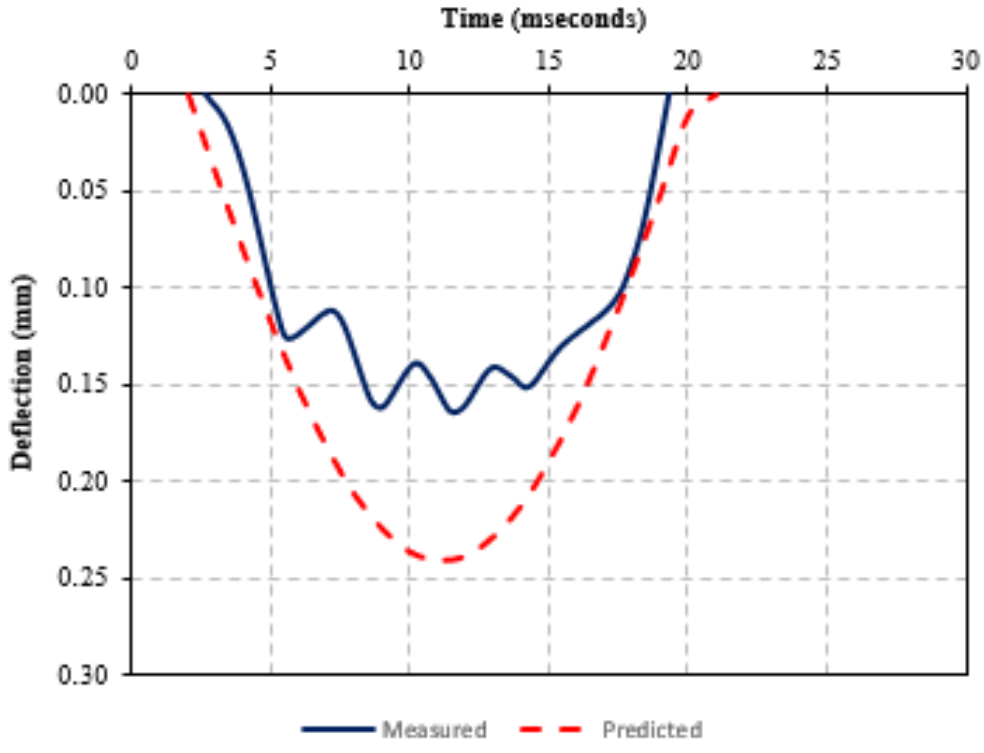

(b) 12-inch Results

Figure G.47: Measured and Predicted LWD Surface Deflections - Location 312

Appendix H

APMT Software Updates

In order to record data for the continuous SDPMT tests software modifications were necessary to allow for the new test profile. The updates consisted of updating the calibration module of the program and updating the testing module of the software. The updates are described here.

H.1 Update to Automated Calibration Module

There are two parts to the automated calibration module, the first is the volume calibration data collection system, and the second is the membrane calibration data collection system.

H.1.1 Update to Volume Calibration Data Collection System

In order to enable the ability to record a continuous volume calibration the software was updated from the operator needing to press a button in software to take a data point to automatically recording the data for the user. Figure H.1 shows the original data collection screen for collecting membrane calibration data, Figure H.2 shows the updated operator screen. The software has been configured to take volume calibration readings every 100 kPa up to 2400 kPa. The last two or three data points are used to determine the volume calibration slope that is used correct for system expansion.

H.1.2 Update to Membrane Calibration Data Collection System

The incremental module for membrane calibration data collection was updated to automatically collect calibration data points. Figure H.3 shows the incremental calibration data collection screen, Figure H.4 shows the updated membrane calibration screen for recording a continuous calibration. The update for this module removes the waiting to take data points, and replaces it with the user input fields for the control of

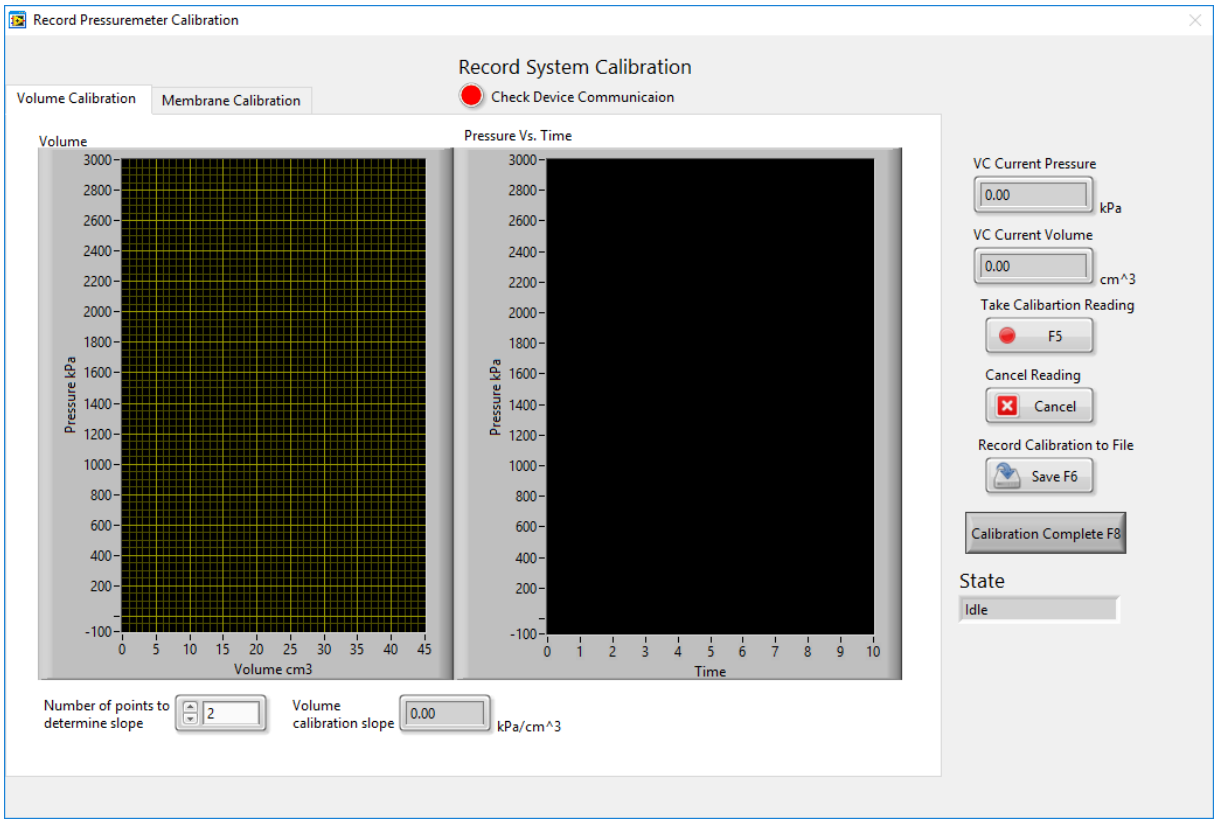

Figure H.1: Original APMT Calibration Module for recording Volume Calibration Data for Incremental Tests

the collection of data points for the membrane calibration curve. The first user input is the volume increment, this controls when data points are taken, a typical value for this is 2.5 cm^3 for a SDPMT test. The second new user input is the maximum injected volume, this is used to end the calibration, and this should be one volume increment beyond where a test will be run to, e.g. 35 cm^3.

H.2 Update to Testing APMT Module

The updates made to the APMT test module for incremental tests (Figure H.5 to allow for continuous testing included removing the Record Data Point and replacing it with start Triggered test. The start triggered test waits for the test operator to start turning the handle of the control unit. After the operator start turning the handle data points are recorded according to the volume increment and maximum injection values. When the operator reaches the maximum injected volume provided to the software the LED for Inflate probe turns off and the deflate Probe LED turns on; at this time the operator will turn the handle in the opposite direction, until all the injected fluid is removed; the test will end. The new screen layout is shown Figure H.6.

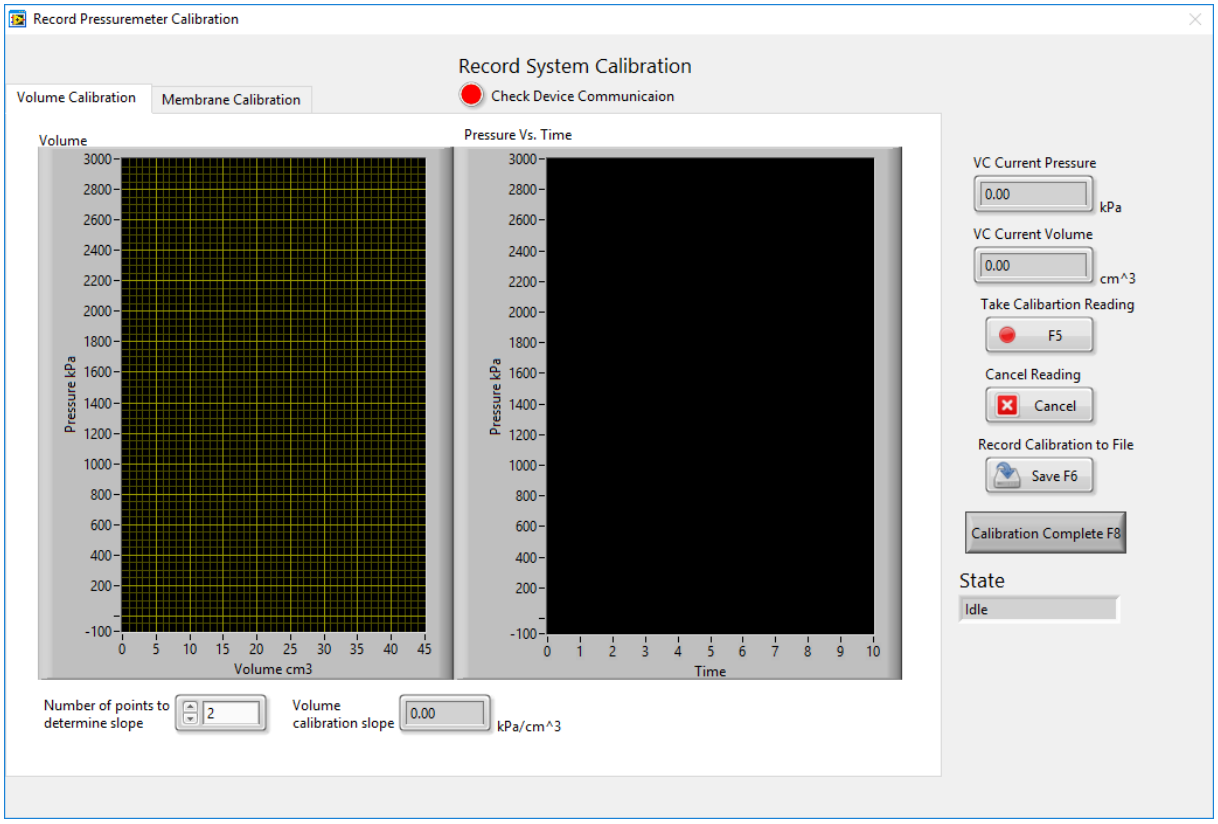

Figure H.2: New APMT Calibration Module for Recording Volume Calibration Data for Continuous Tests

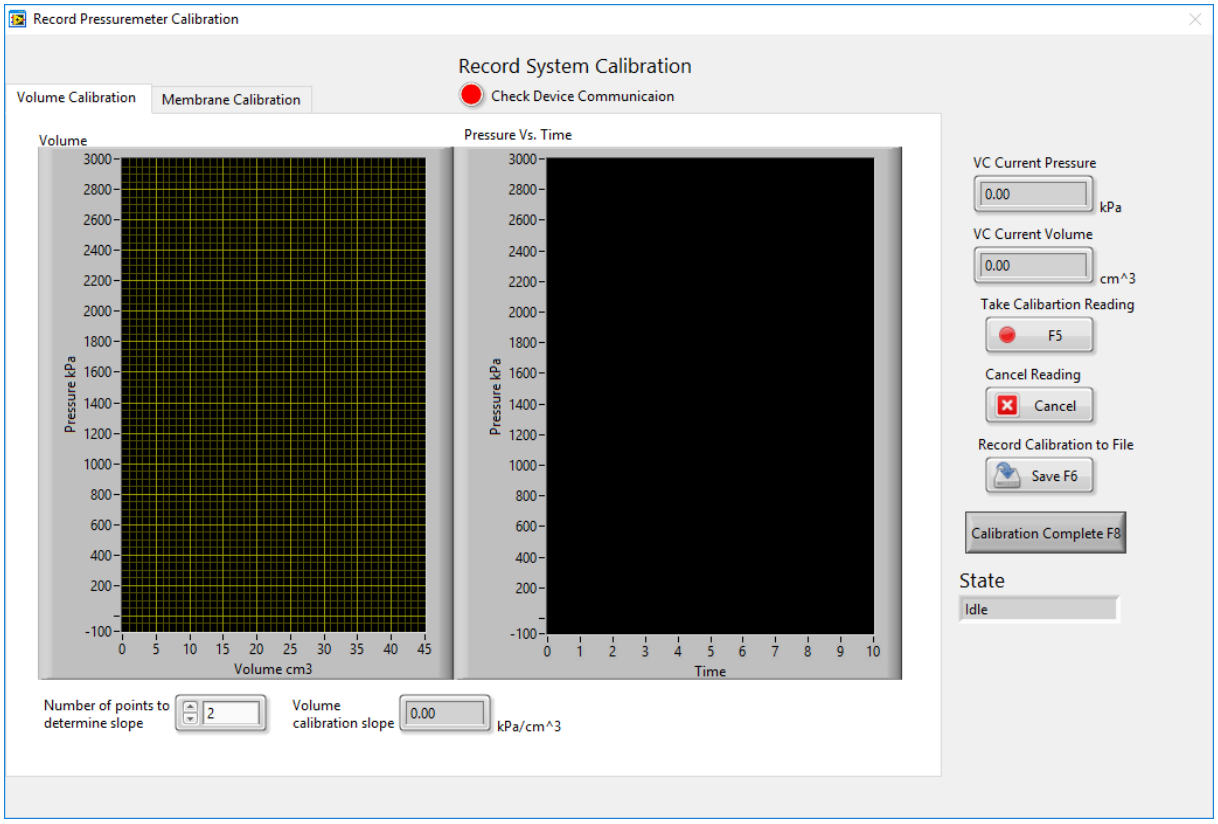

Figure H.3: Original APMT Membrane Calibration Data Collection Screen for Incremental Tests

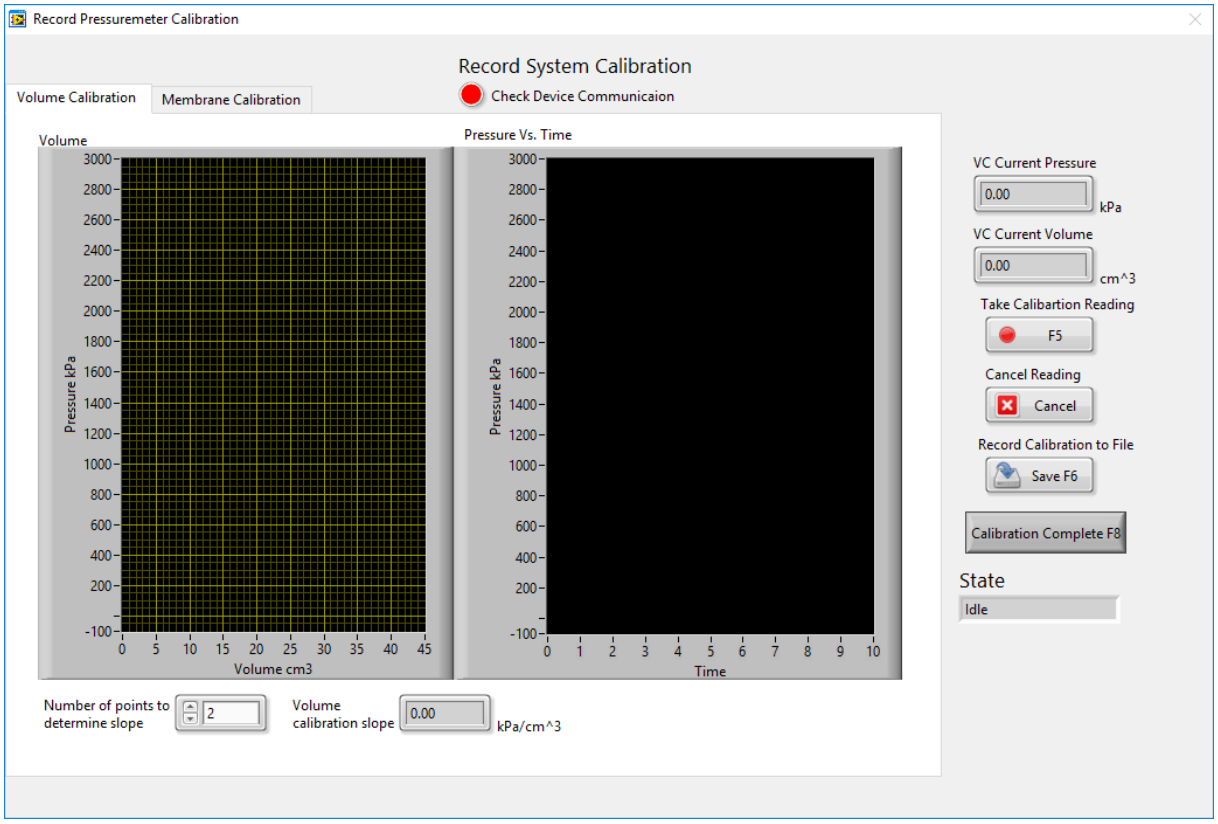

Figure H.4: New Membrane Calibration Data Collection Screen for use with Continuous Tests

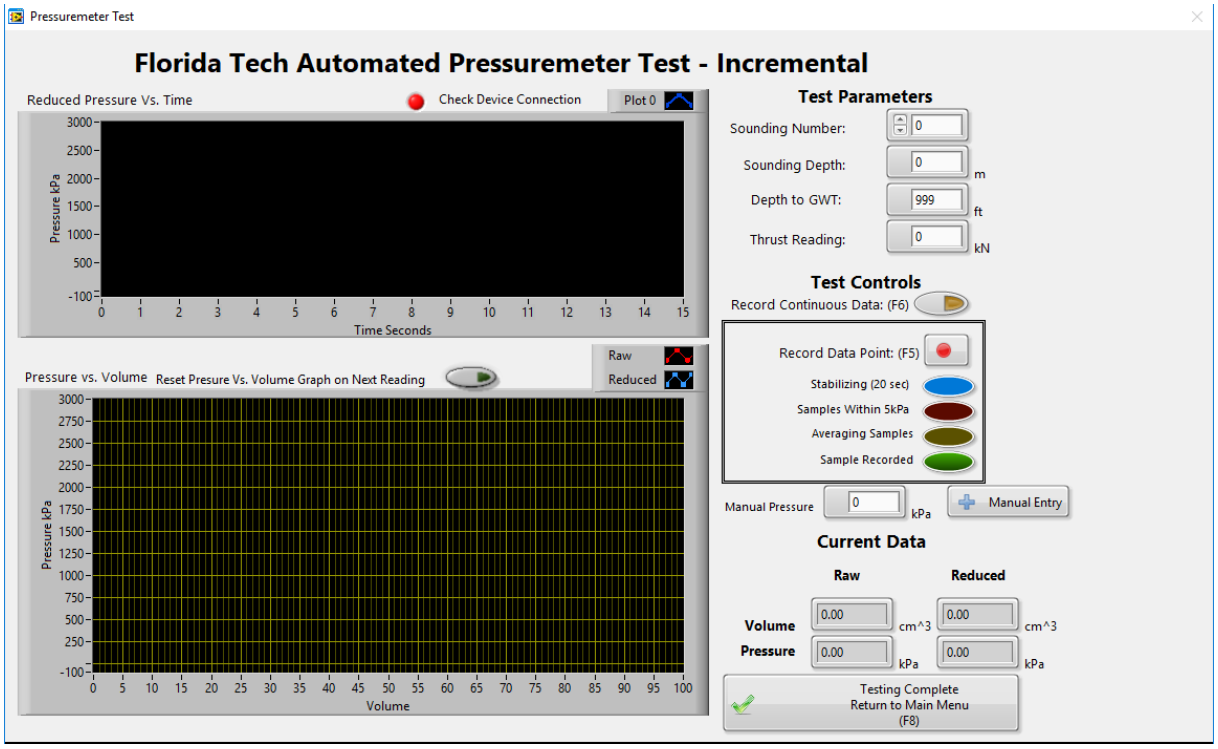

Figure H.5: Original APMT Screen for Incremental Test

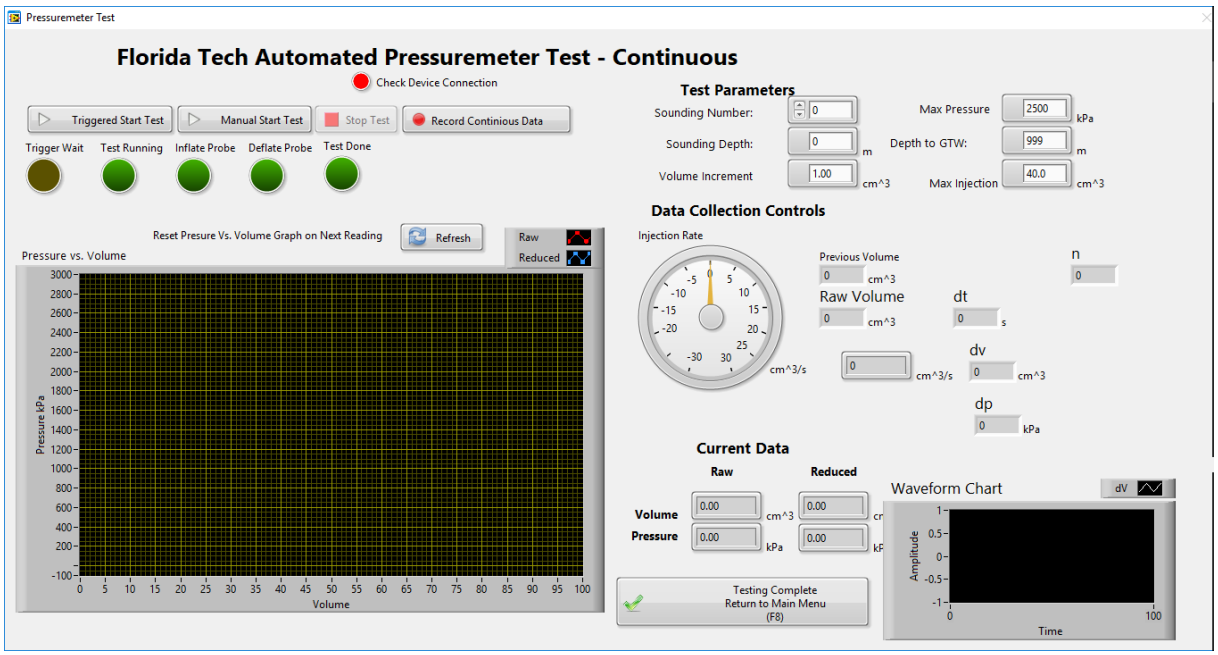

Figure H.6: New APMT Continuous Test Screen

Appendix I

DCP Test Results

I.1 Southgate Field DCP Tests

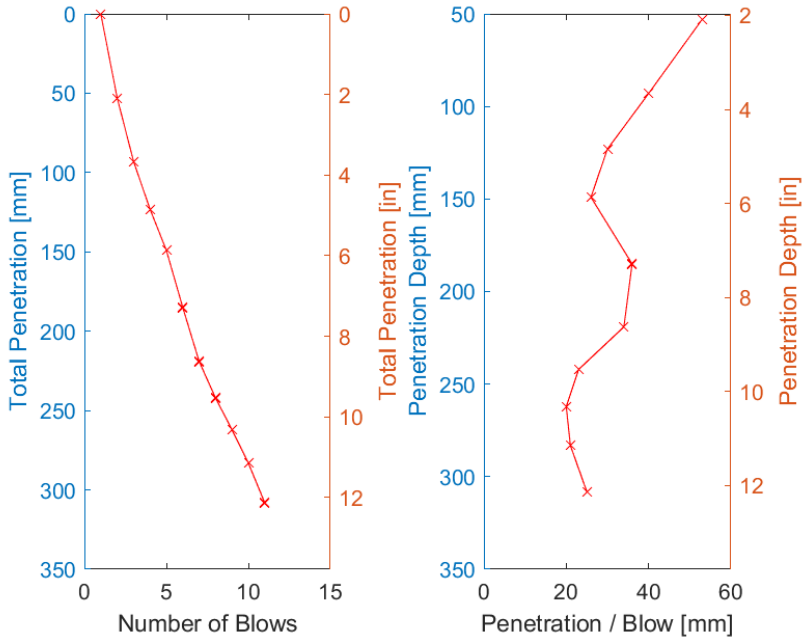

Figure I.1: FIT Southgate Field DCP Results Test Location 401

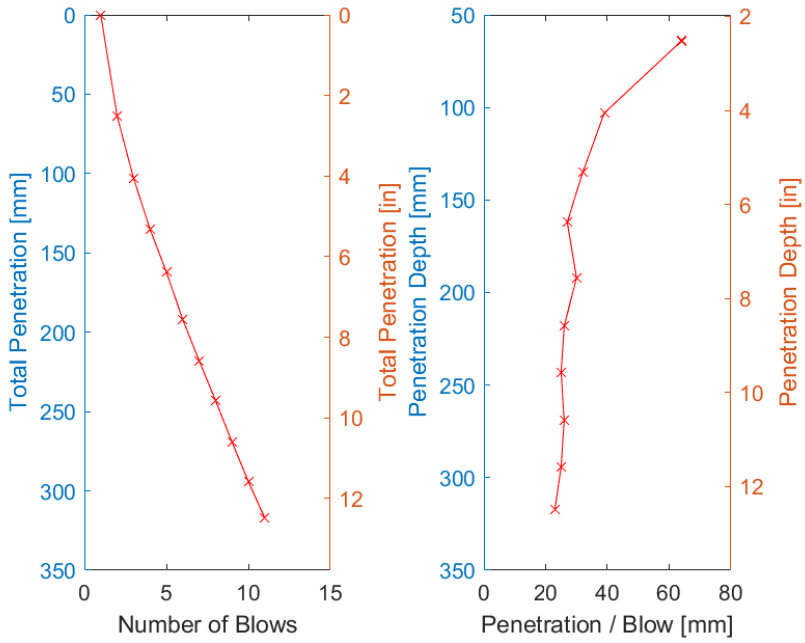

Figure I.2: FIT Southgate Field DCP Results Test Location 402

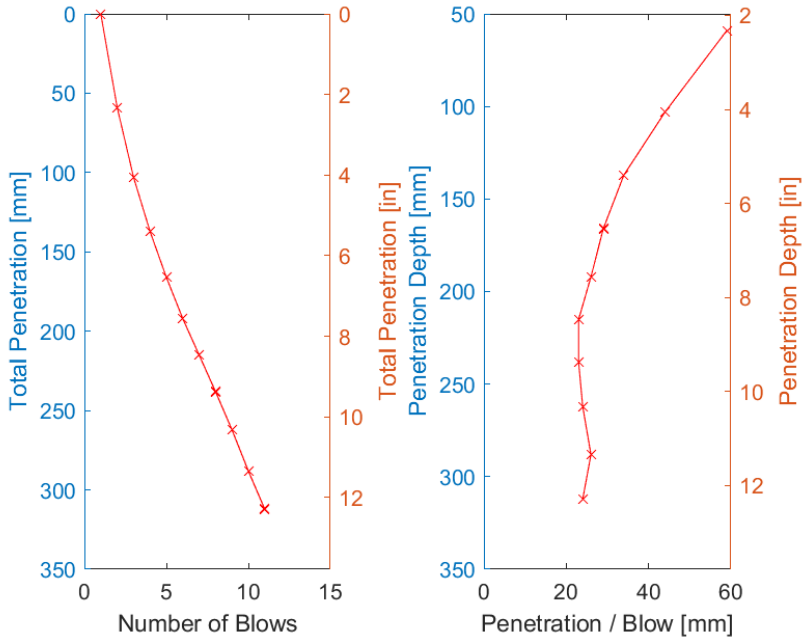

Figure I.3: FIT Southgate Field DCP Results Test Location 403

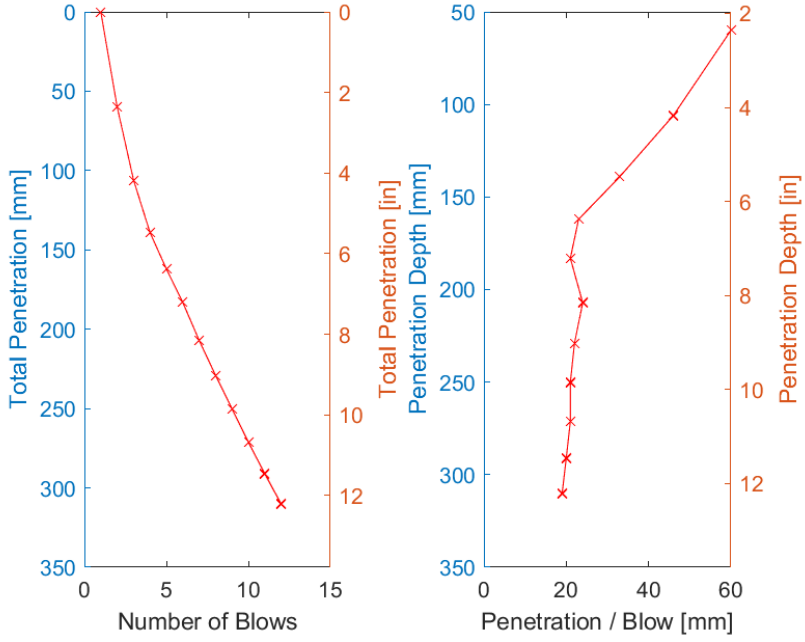

Figure I.4: FIT Southgate Field DCP Results Test Location 404

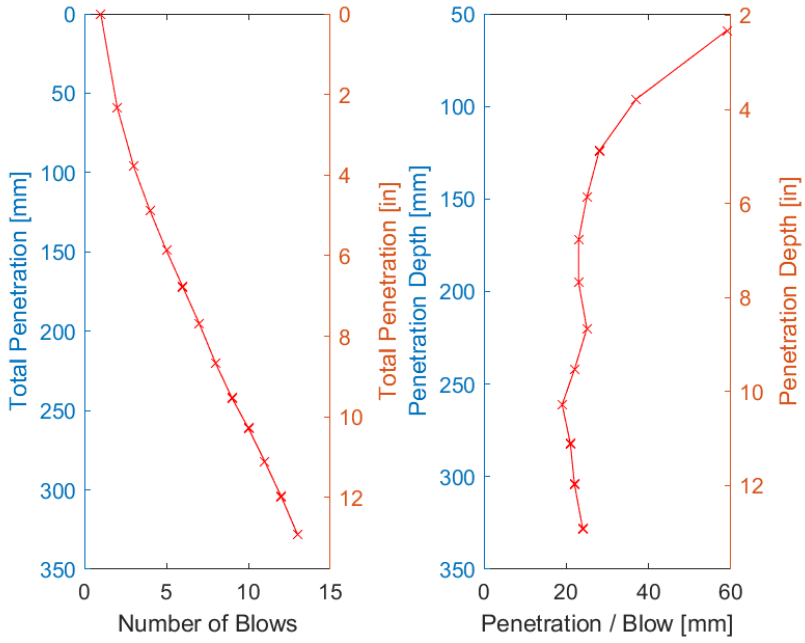

Figure I.5: FIT Southgate Field DCP Results Test Location 405

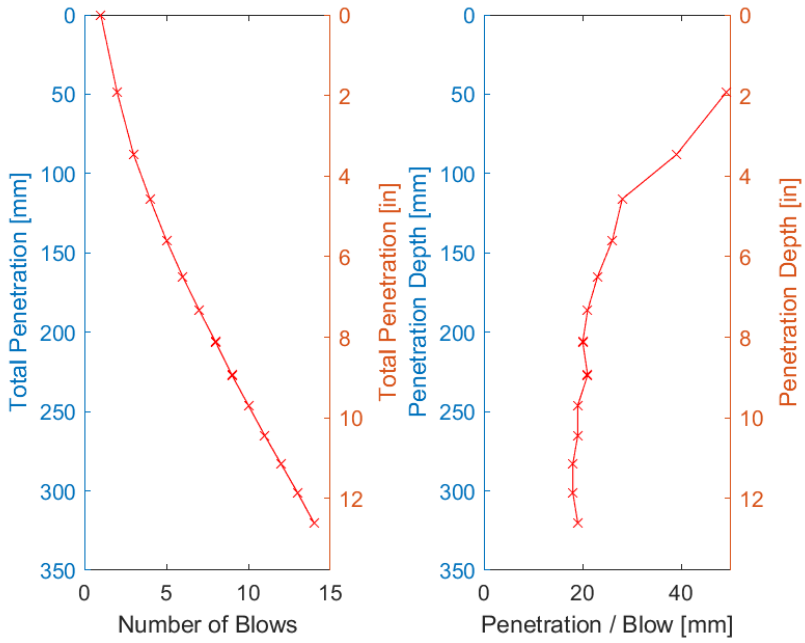

Figure I.6: FIT Southgate Field DCP Results Test Location 406

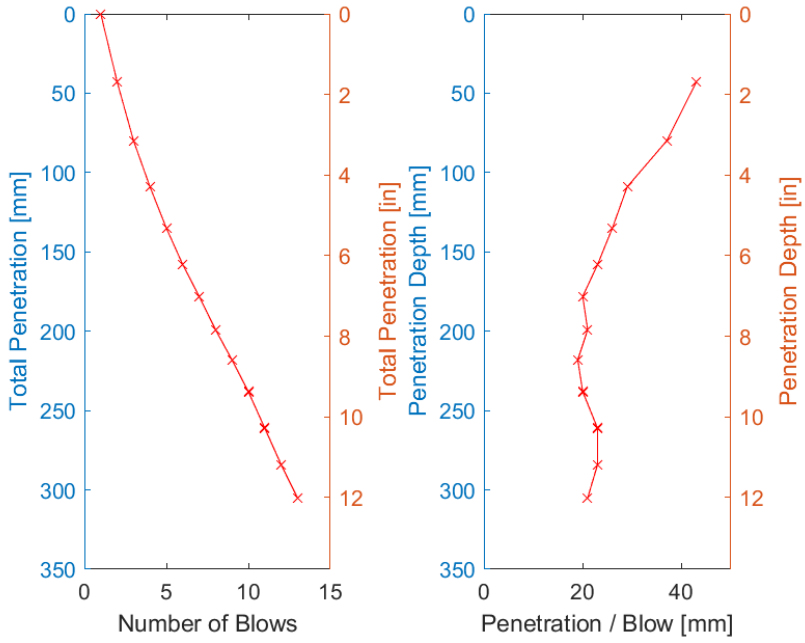

Figure I.7: FIT Southgate Field DCP Results Test Location 407

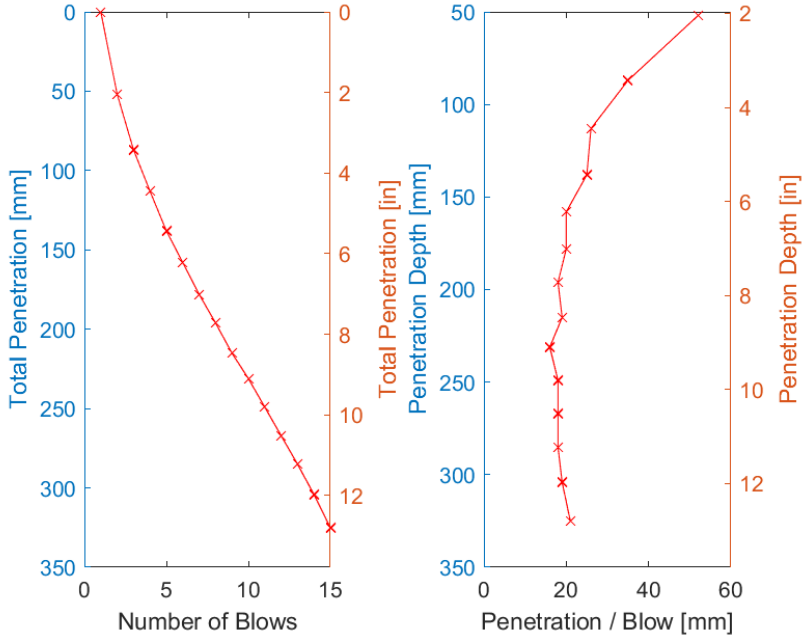

Figure I.8: FIT Southgate Field DCP Results Test Location 408

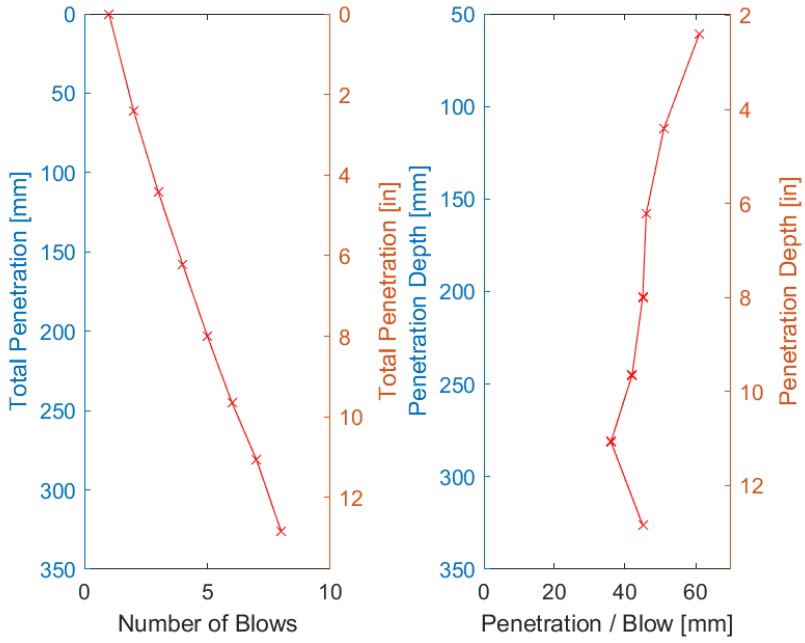

Figure I.9: FIT Southgate Field DCP Results Test Location 409

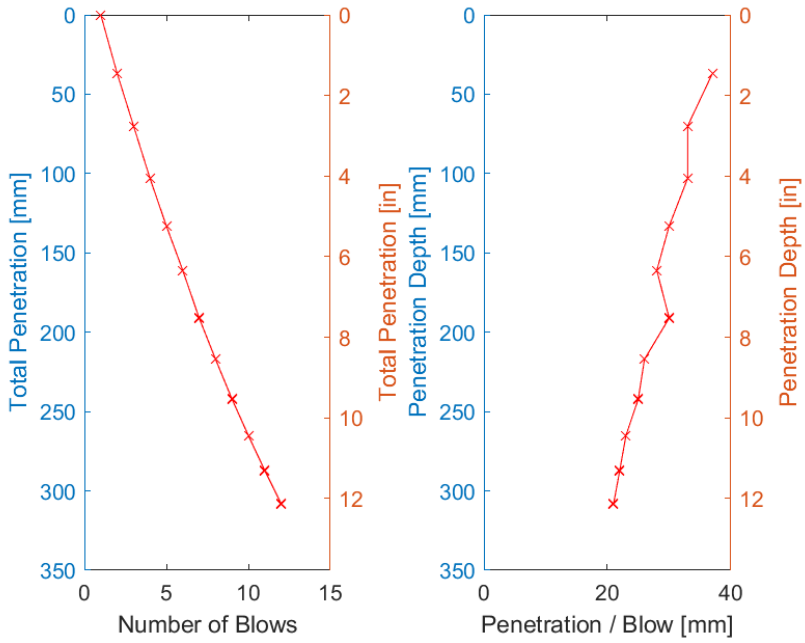

Figure I.10: FIT Southgate Field DCP Results Test Location 410

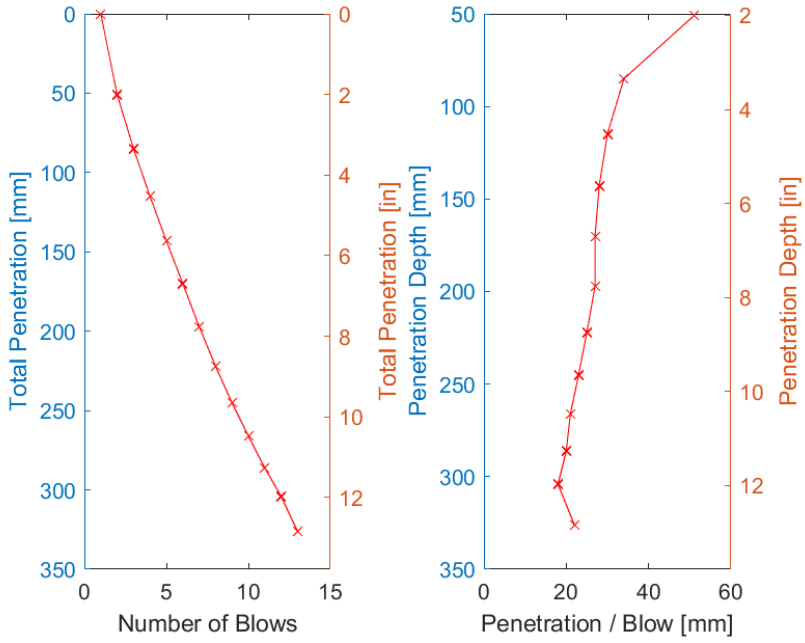

Figure I.11: FIT Southgate Field DCP Results Test Location 411

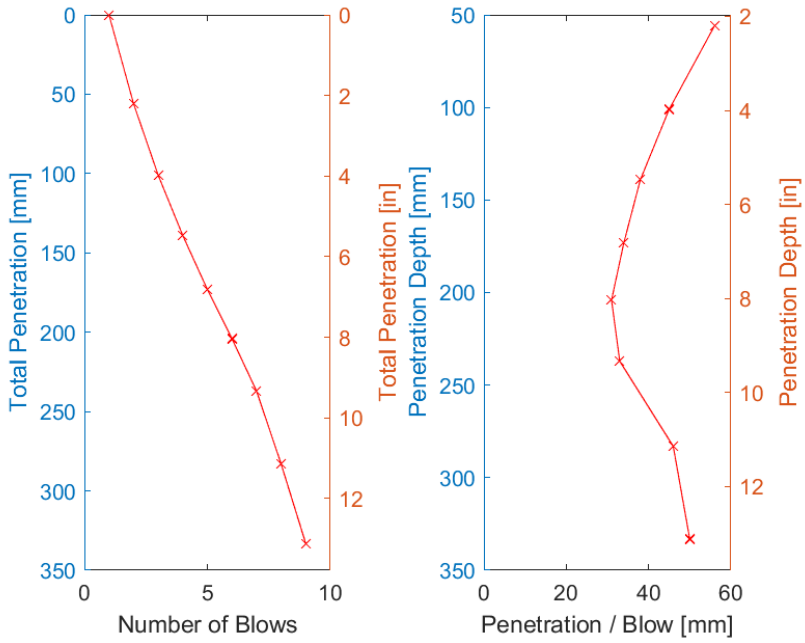

Figure I.12: FIT Southgate Field DCP Results Test Location 412

I.2 Olin Complex DCP Tests

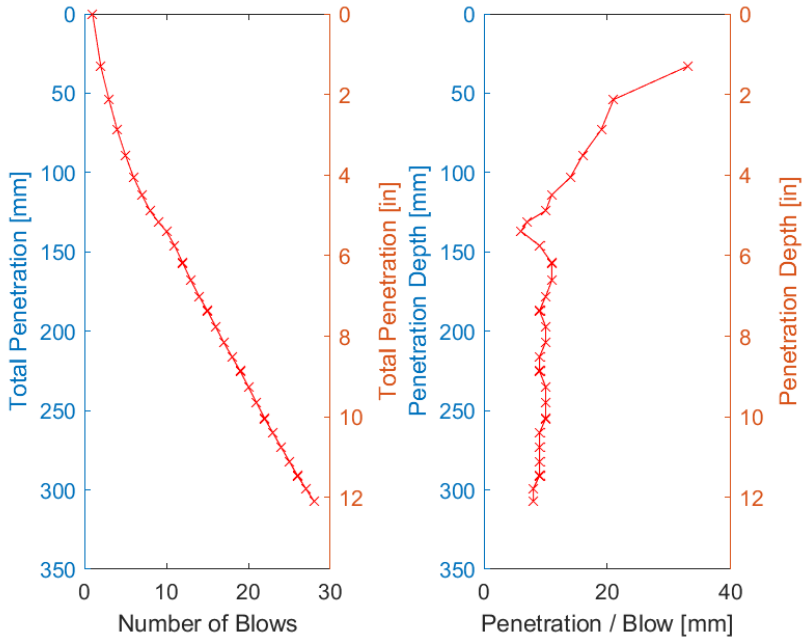

Figure I.13: Florida Tech Olin Overflow Parking Complex DCP Results Test Location 201

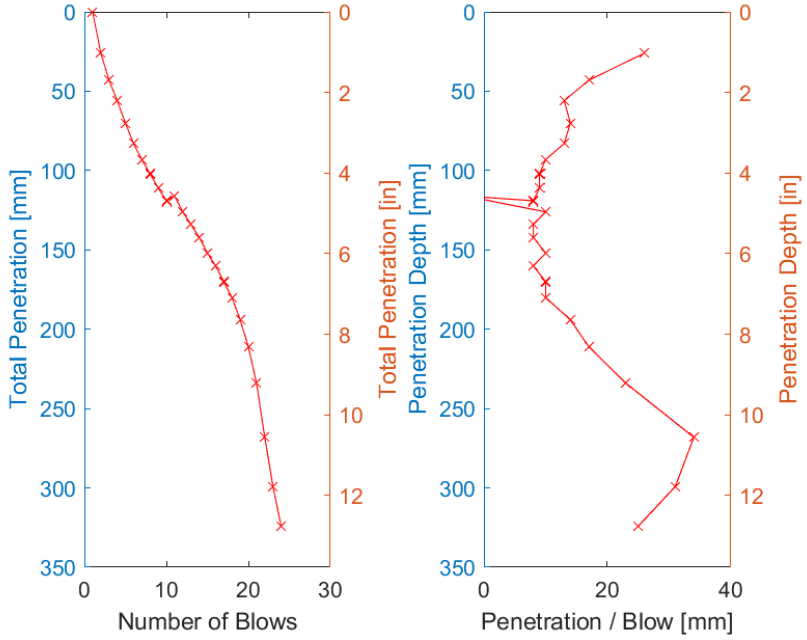

Figure I.14: Florida Tech Olin Overflow Parking Complex DCP Results Test Location 202

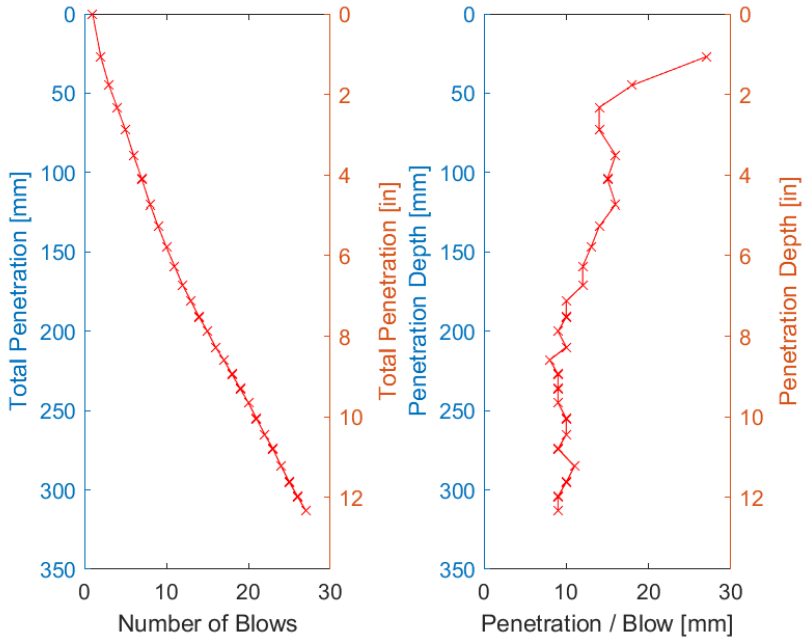

Figure I.15: Florida Tech Olin Overflow Parking Complex DCP Results Test Location 203

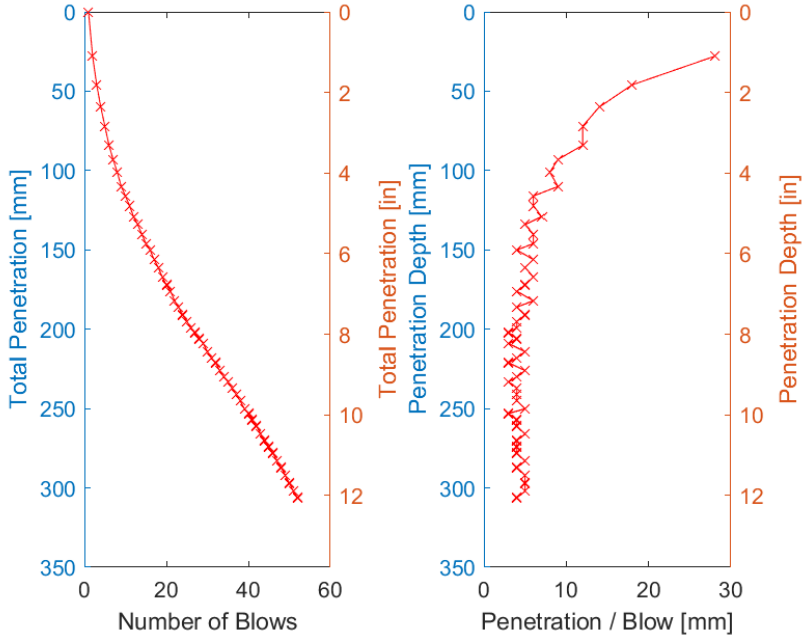

Figure I.16: Florida Tech Olin Overflow Parking Complex DCP Results Test Location 204

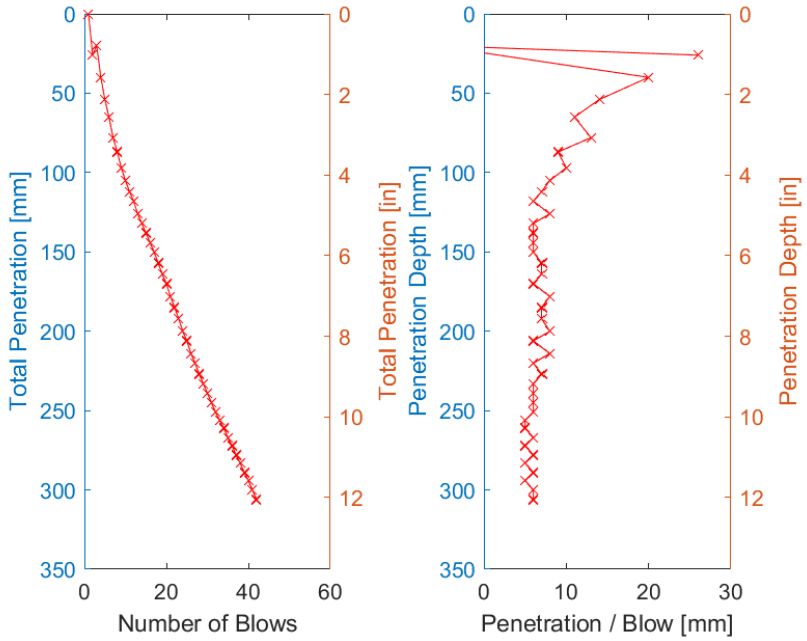

Figure I.17: Florida Tech Olin Overflow Parking Complex DCP Results Test Location 205

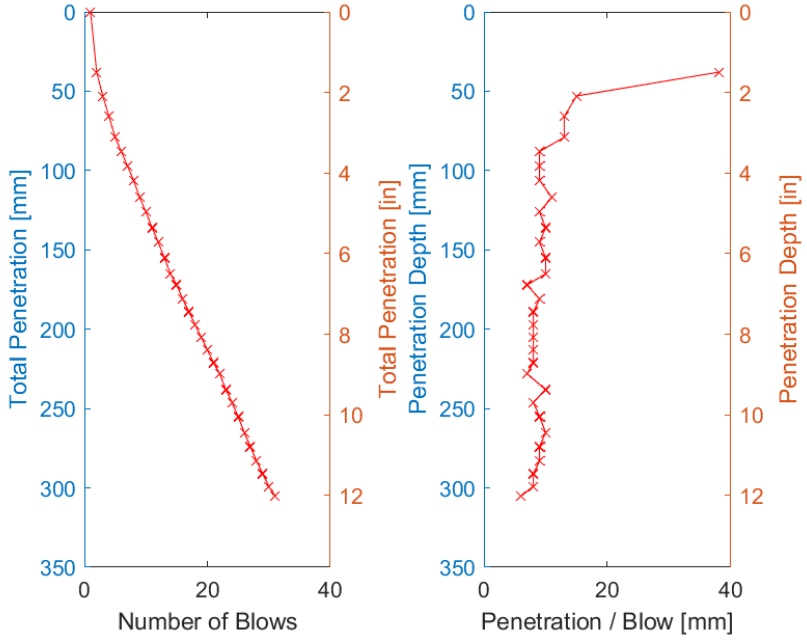

Figure I.18: Florida Tech Olin Overflow Parking Complex DCP Results Test Location 206

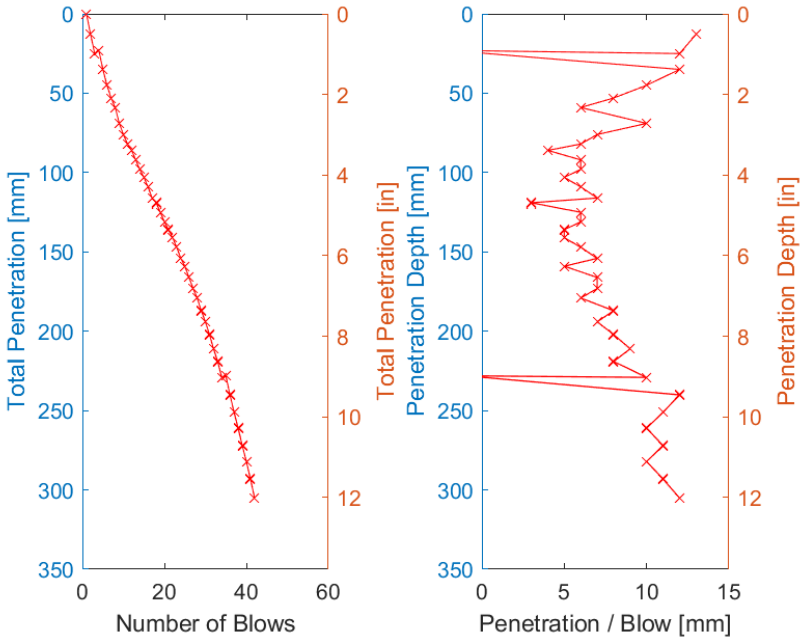

Figure I.19: Florida Tech Olin Overflow Parking Complex DCP Results Test Location 207

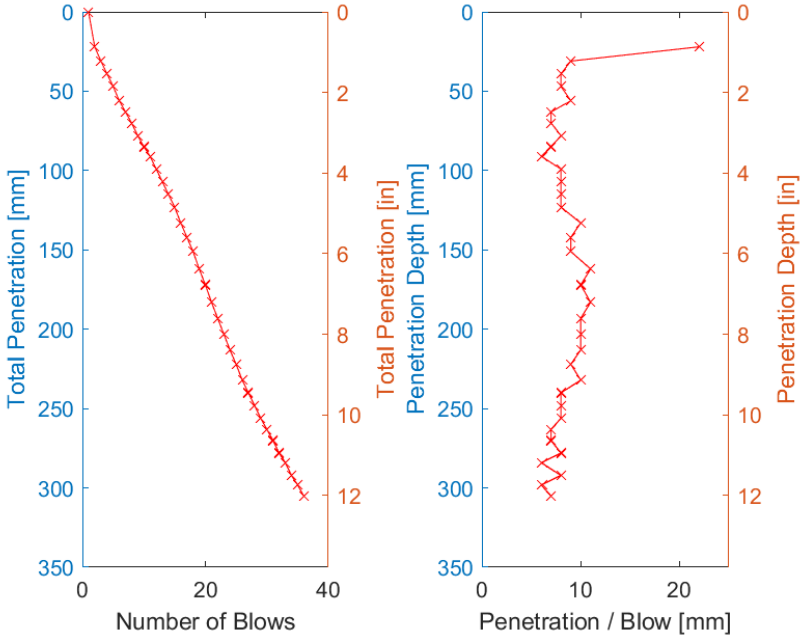

Figure I.20: Florida Tech Olin Overflow Parking Complex DCP Results Test Location 208

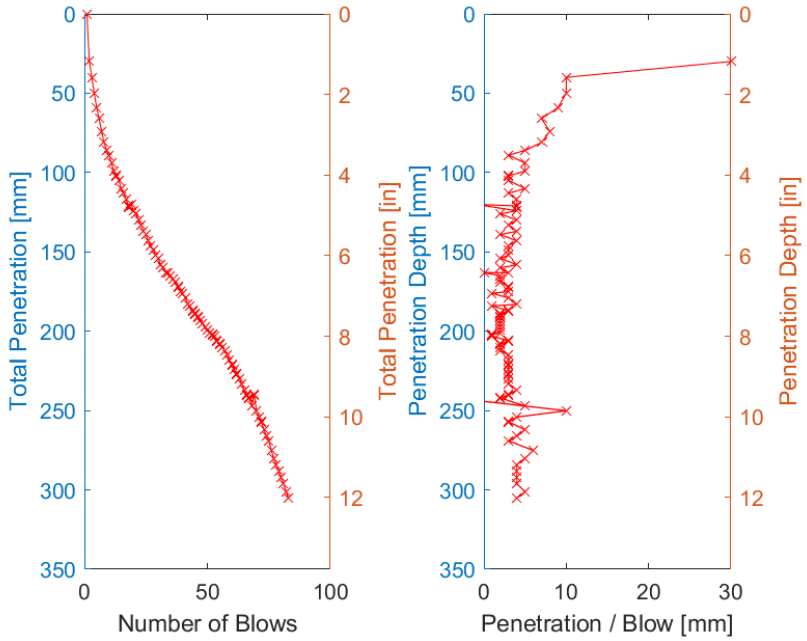

Figure I.21: Florida Tech Olin Overflow Parking Complex DCP Results Test Location 209

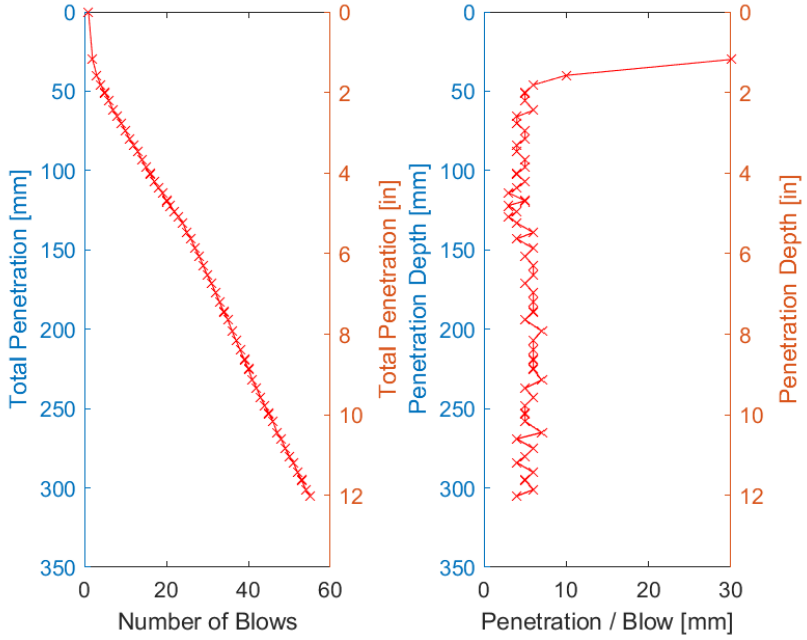

Figure I.22: Florida Tech Olin Overflow Parking Complex DCP Results Test Location 210

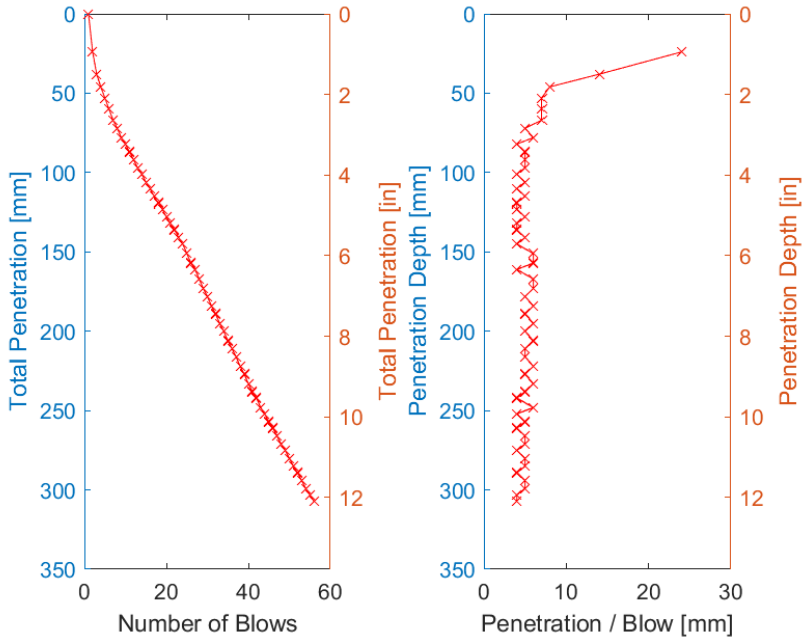

Figure I.23: Florida Tech Olin Overflow Parking Complex DCP Results Test Location 211

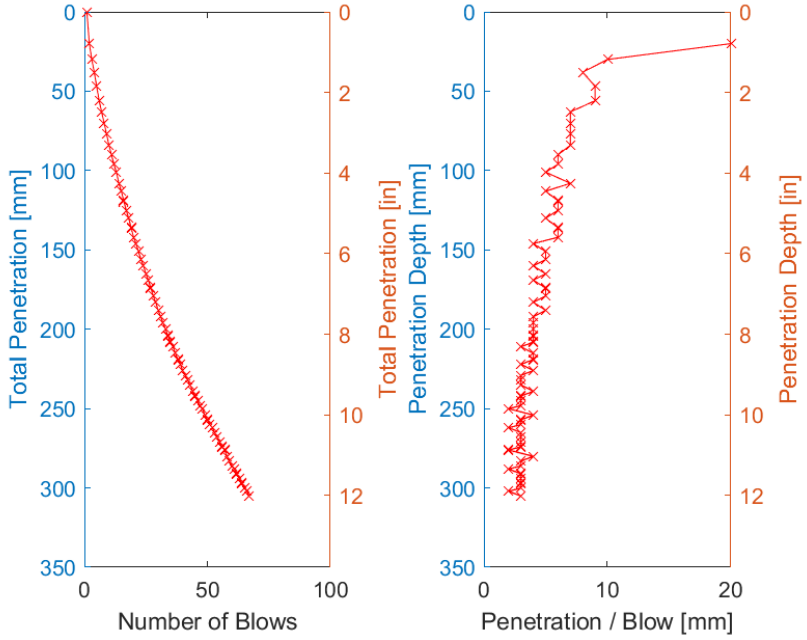

Figure I.24: Florida Tech Olin Overflow Parking Complex DCP Results Test Location 212

I.3 Cypress Landing DCP Tests

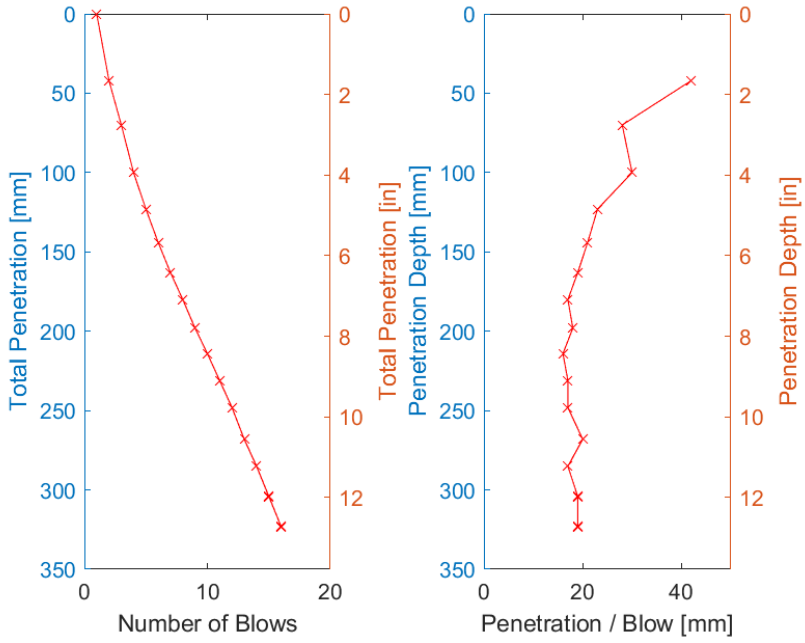

Figure I.25: Cypress Landing DCP Results Test Location 101

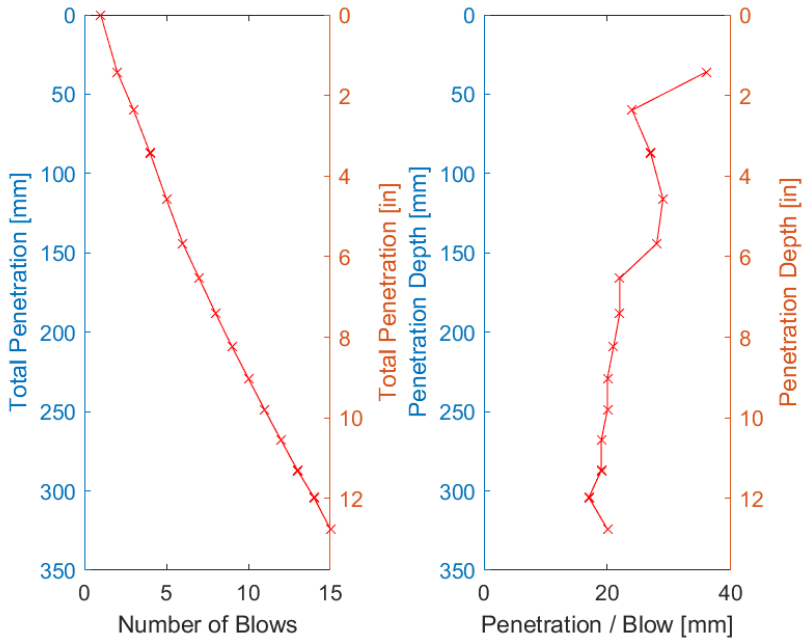

Figure I.26: Cypress Landing DCP Results Test Location 102

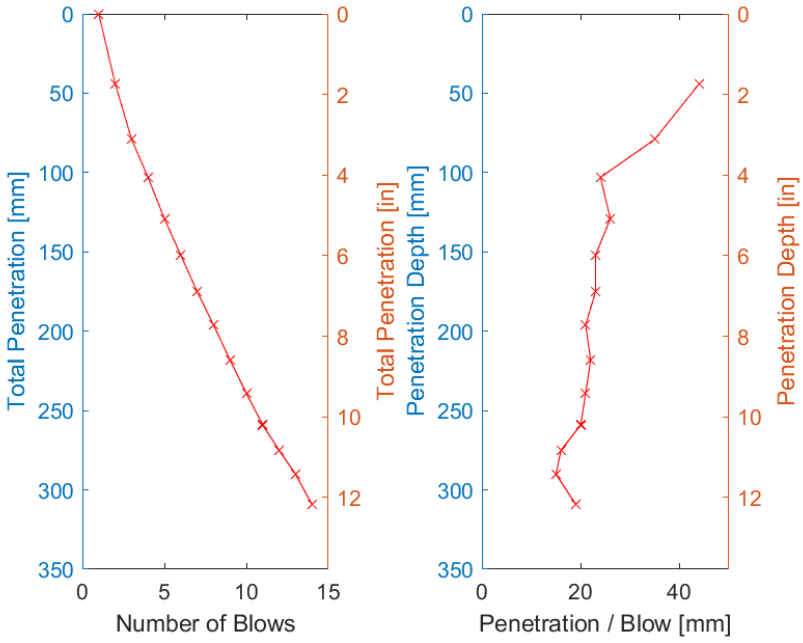

Figure I.27: Cypress Landing DCP Results Test Location 103

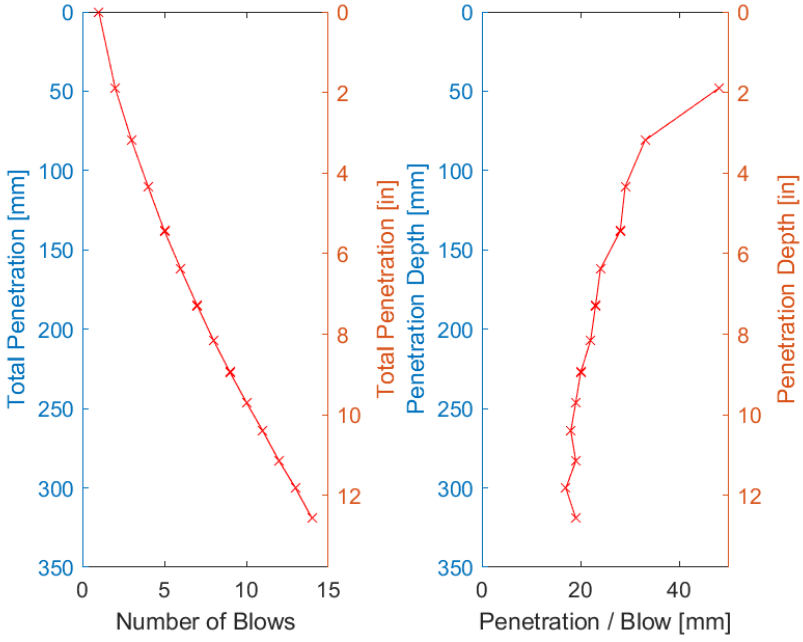

Figure I.28: Cypress Landing DCP Results Test Location 104

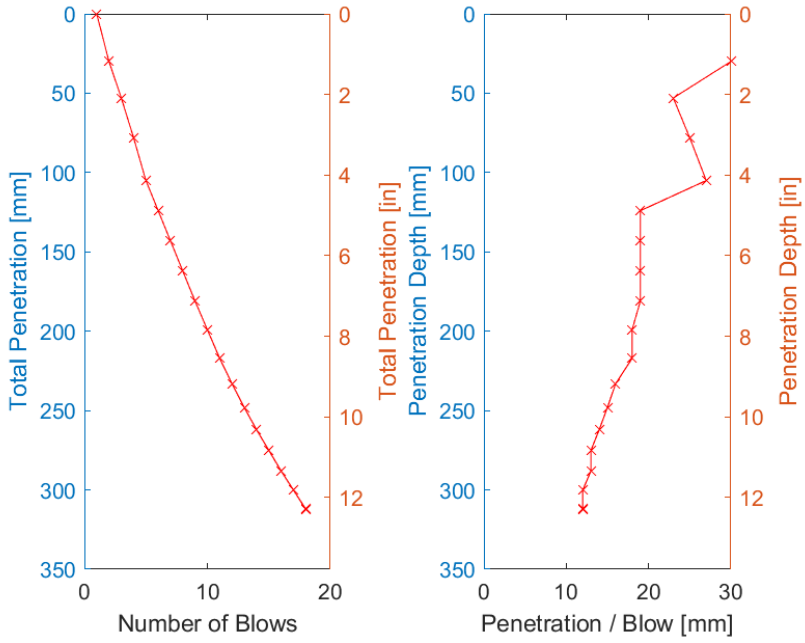

Figure I.29: Cypress Landing DCP Results Test Location 105

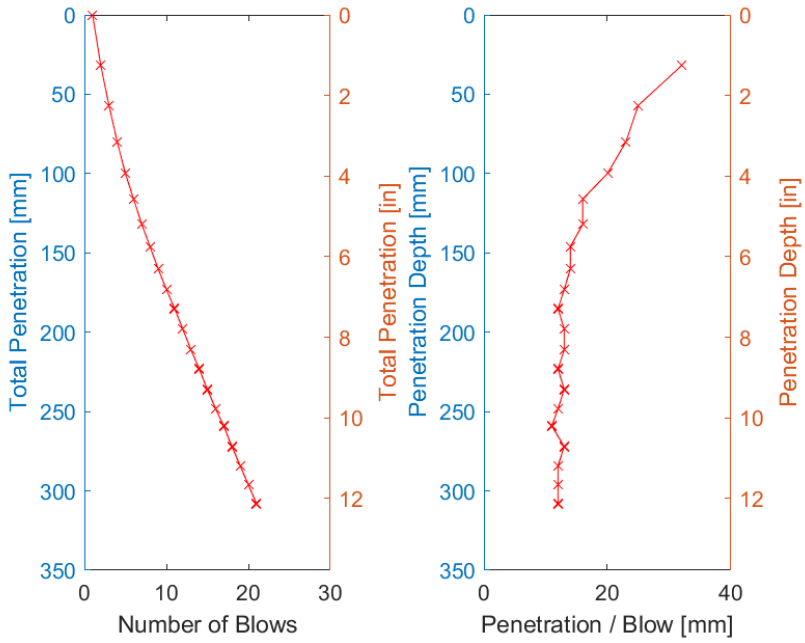

Figure I.30: Cypress Landing DCP Results Test Location 106

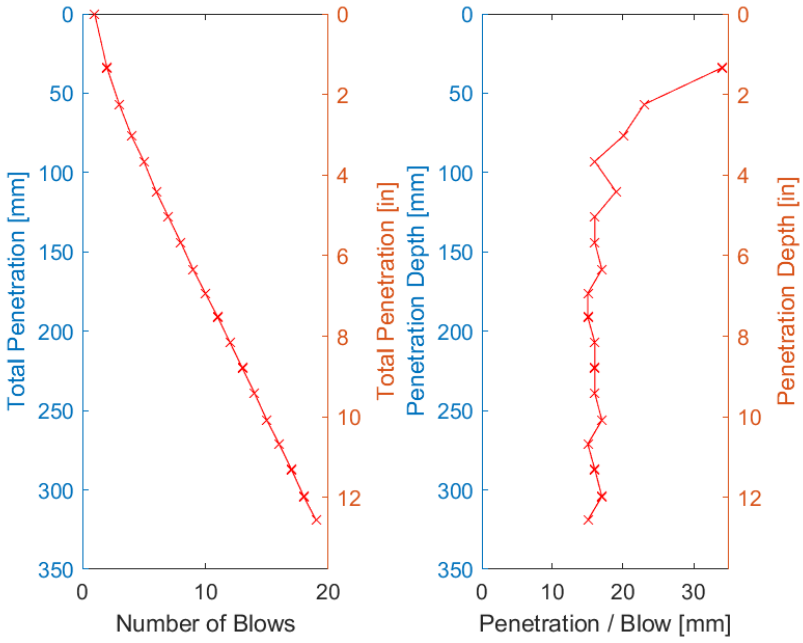

Figure I.31: Cypress Landing DCP Results Test Location 107

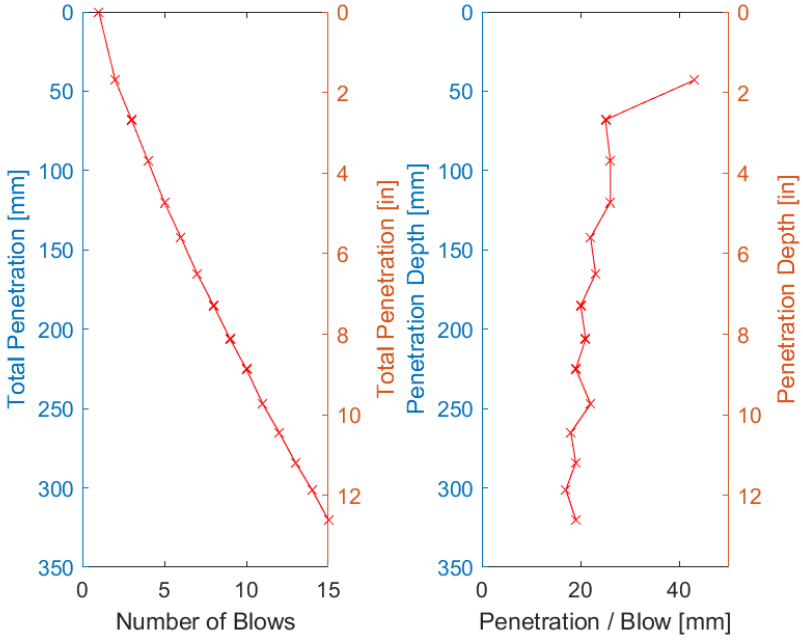

Figure I.32: Cypress Landing DCP Results Test Location 108

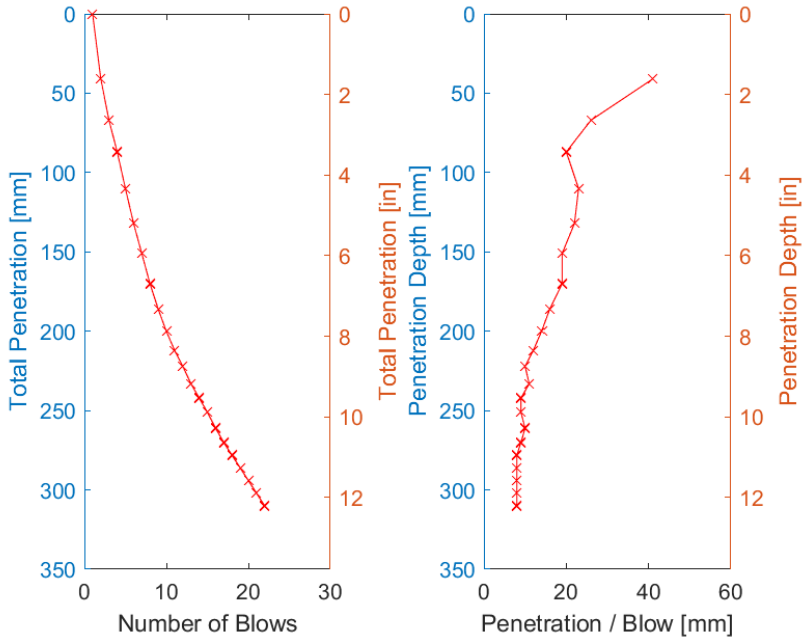

Figure I.33: Cypress Landing DCP Results Test Location 109

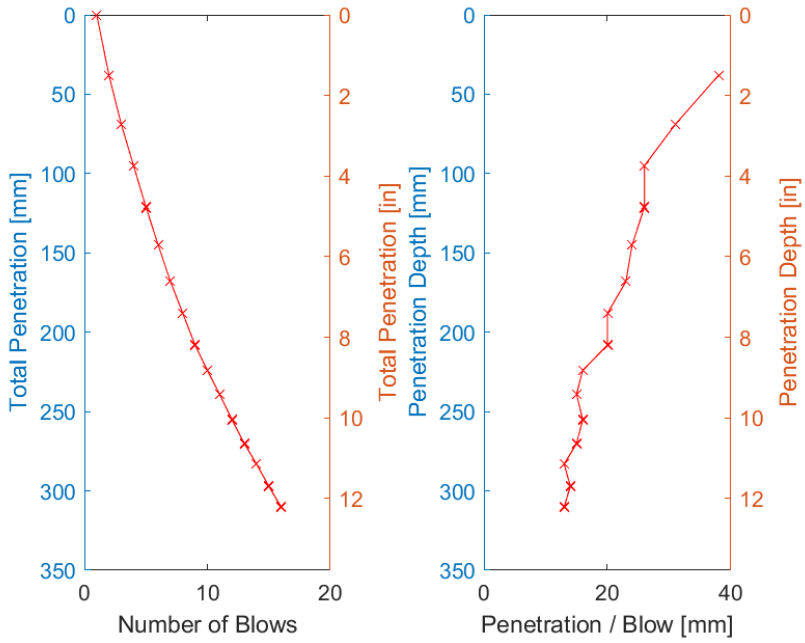

Figure I.34: Cypress Landing DCP Results Test Location 110

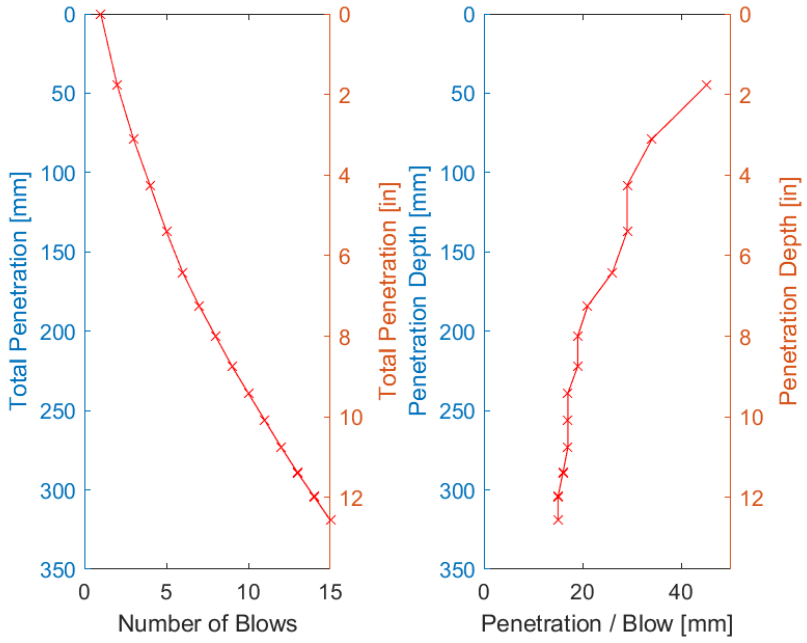

Figure I.35: Cypress Landing DCP Results Test Location 111

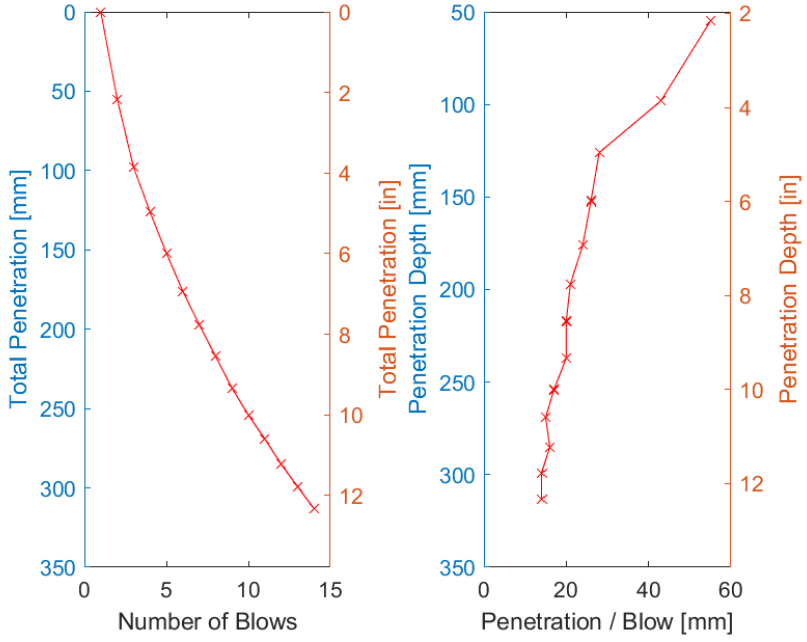

Figure I.36: Cypress Landing DCP Results Test Location 112